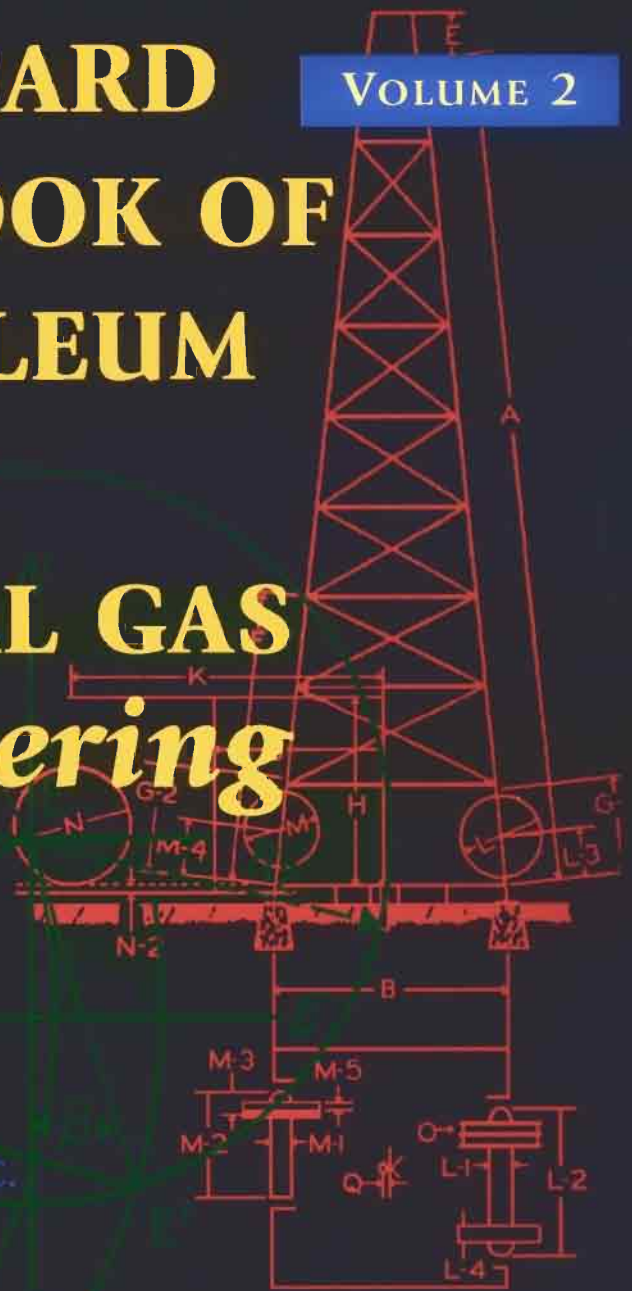


STANDARD HANDBOOK OF PETROLEUM & NATURAL GAS *Engineering*

VOLUME 2



$$\frac{1}{a} \sec^{-1} \left(\frac{u}{a} \right) + C = \frac{1}{a} \cos^{-1} \frac{a}{u} + C.$$

WILLIAM C. LYONS
EDITOR

$$F = \frac{M_{EB} \times D}{2I}$$

**STANDARD
HANDBOOK OF
PETROLEUM
&
NATURAL GAS
*Engineering***

VOLUME 2

**STANDARD
HANDBOOK OF
PETROLEUM
&
NATURAL GAS
*Engineering***

VOLUME 2

**WILLIAM C. LYONS, PH.D., P.E.
EDITOR**



Gulf Professional Publishing
an imprint of Butterworth-Heinemann

**STANDARD
HANDBOOK OF
PETROLEUM
&
NATURAL GAS
*Engineering***

VOLUME 2

Copyright © 1996 by Butterworth-Heinemann. All rights reserved.
Printed in the United States of America. This book, or parts thereof,
may not be reproduced in any form without permission of the
publisher.

Originally published by Gulf Publishing Company,
Houston, TX.

10 9 8 7 6 5 4 3 2

For information, please contact:

Manager of Special Sales
Butterworth-Heinemann
225 Wildwood Avenue
Woburn, MA 01801-2041
Tel: 781-904-2500
Fax: 781-904-2620

For information on all Butterworth-Heinemann publications available,
contact our World Wide Web home page at: <http://www.bh.com>

Library of Congress Cataloging-in-Publication Data

Standard handbook of petroleum and natural gas engineering /
[edited by William Lyons].

p. cm.

Includes bibliographical references and index.

ISBN 0-88415-642-7 (Vol. 1), ISBN 0-88415-643-5 (Vol. 2)

1. Petroleum engineering. 2. Natural gas. I. Lyons, William
(William C.)

TN870.S6233 1996

665.5—dc20

96-13965

CIP

ISBN 0-88415-643-5

Printed on Acid-Free Paper (∞)

Contents

Contributing Authors	vii
Preface	ix
5—Reservoir Engineering	1
Basic Principles, Definitions, and Data,	3
Formation Evaluation,	86
Pressure Transient Testing of Oil and Gas Wells,	214
Mechanisms and Recovery of Hydrocarbons by Natural Means,	225
Material Balance and Volumetric Analysis,	228
Decline-Curve Analysis,	244
Reserve Estimates,	249
Secondary Recovery,	259
Fluid Movement in Waterflooded Reservoirs,	269
Estimating Waterflood Residual Oil Saturation,	301
Enhanced Oil Recovery Methods,	319
References,	344
6—Production Engineering	363
Properties of Hydrocarbon Mixtures,	365
Flow of Fluids,	426
Natural Flow Performance,	533
Artificial Lift Methods,	594
Stimulation and Remedial Operations,	664
Surface Oil Production Systems,	702
Gas Production Engineering,	754

Corrosion and Scaling, 889	
Environmental Considerations, 939	
Offshore Operations, 964	
References, 971	
7—Petroleum Economics	985
Estimating Oil and Gas Reserves, 987	
Classification of Petroleum Products, 989	
Methods for Estimating Reserves, 990	
Non-Associated Gas Reservoirs, 997	
Production Stimulation, 1004	
Determining the Value of Future Production, 1010	
The Market for Petroleum, 1010	
Economics and the Petroleum Engineer, 1012	
Preparation of a Cash Flow, 1012	
Valuation of Oil and Gas Properties, 1023	
Risk Analysis, 1025	
References, 1030	
Appendix: Units and Conversions (SI)	1035
Index	1049

Contributing Authors

Robert M. Colpitts, P.G.
Consultant in Geology and Geophysics
Socorro, New Mexico

Micheal J. Economides, Ph.D.
Texas A & M University
College Station, Texas

Kazimierz Glowacki, Ph.D.
Consultant in Energy and Environmental Engineering
Krakow, Poland

Reza G. Kashmiri
International Lubrication and Fuel, Incorporated
Rio Rancho, New Mexico

Joseph V. LaBlanc
Consultant in Petroleum Engineering
Conroe, Texas

Julius P. Langlinais, Ph.D.
Louisiana State University
Baton Rouge, Louisiana

F. David Martin
New Mexico Institute of Mining and Technology
Socorro, New Mexico

Richard J. Miller
Richard J. Miller and Associates, Incorporated
Huntington Beach, California

Charles Nathan, Ph.D., P.E.
Consultant in Corrosion Engineering
Houston, Texas

Pudji Permadi, Ph.D.
Institut Teknologi Bandung
Bandung, Indonesia

Floyd W. Preston, Ph.D.
University of Kansas
Lawrence, Kansas

Chris S. Russell, P.E.
Consultant in Environmental Engineering
Grand Junction, Colorado

Oleg Salzberg
Consultant in Corrosion Engineering
Houston, Texas

Ardeshir K. Shahraki, Ph.D.
Dwight's Energy Data, Inc.
Richardson, Texas

Preface

This petroleum and natural gas engineering two-volume handbook is written in the spirit of the classic handbooks of other engineering disciplines. The two volumes reflect the importance of the industry its engineers serve (i.e., *Standard and Poor's* shows that the fuels sector is the largest single entity in the gross domestic product) and the profession's status as a mature engineering discipline.

The project to write these volumes began with an attempt to revise the old *Practical Petroleum Engineer's Handbook* that Gulf Publishing had published since the 1940's. Once the project was initiated, it became clear that any revision of the old handbook would be inadequate. Thus, the decision was made to write an entirely new handbook and to write this handbook in the classic style of the handbooks of the other major engineering disciplines. This meant giving the handbook initial chapters on mathematics and computer applications, the sciences, general engineering, and auxiliary equipment. These initial chapters set the tone of the handbook by using engineering language and notation common to all engineering disciplines. This common language and notation is used throughout the handbook (language and notation in nearly all cases is consistent with Society of Petroleum Engineers publication practices). The authors, of which there are 27, have tried (and we hope succeeded) in avoiding the jargon that had crept into petroleum engineering literature over the past few decades. Our objective was to create a handbook for the petroleum engineering discipline that could be read and understood by any up-to-date engineer.

The specific petroleum engineering discipline chapters cover drilling and well completions, reservoir engineering, production, and economics and valuation. These chapters contain information, data, and example calculations related to practical situations that petroleum engineers often encounter. Also, these chapters reflect the growing role of natural gas in industrial operations by integrating natural gas topics and related subjects throughout both volumes.

This has been a very long and often frustrating project. Throughout the entire project the authors have been steadfastly cooperative and supportive of their editor. In the preparation of the handbook the authors have used published information from both the American

Petroleum Institute and the Society of Petroleum Engineers. The authors thank these two institutions for their cooperation in the preparation of the final manuscript. The authors would also like to thank the many petroleum production and service companies that have assisted in this project.

In the detailed preparation of this work, the authors would like to thank Jerry Hayes, Danette DeCristofaro, and the staff of ExecuStaff Composition Services for their very competent preparation of the final pages. In addition, the authors would like to thank Bill Lowe of Gulf Publishing Company for his vision and perseverance regarding this project; all those many individuals that assisted in the typing and other duties that are so necessary for the preparation of original manuscripts; and all the families of the authors that had to put up with weekends and weeknights of writing. The editor would especially like to thank the group of individuals that assisted through the years in the overall organization and preparation of the original written manuscripts and the accompanying graphics, namely; Ann Gardner, Britta Larrson, Linda Sperling, Ann Irby, Anne Cate, Rita Case, and Georgia Eaton.

All the authors and their editor know that this work is not perfect. But we also know that this handbook had to be written. Our greatest hope is that we have given those that will follow us, in future editions of this handbook, sound basic material to work with.

William C. Lyons, Ph.D., P.E.
Socorro, New Mexico

**STANDARD
HANDBOOK OF
PETROLEUM
&
NATURAL GAS
*Engineering***

VOLUME 2

5

Reservoir Engineering

F. David Martin

New Mexico Institute of Mining and Technology
Socorro, New Mexico

Robert M. Colpitts, P.G.

Consultant, Geology and Geophysics
Socorro, New Mexico

Basic Principles, Definitions, and Data	3
Reservoir Fluids 3. Fluid Viscosities 7. Formation Volume Factors 12. Fluid Compressibilities 20. Estimating Fluid Properties Using Computers 27. Properties of Fluid-Containing Rocks 35. Porosity 35. Pore Volume 35. Permeability 36. Capacity 38. Transmissibility 38. Resistivity and Electrical Conductivity 38. Rock Compressibility 49. Properties of Rocks Containing Multiple Fluids 52. Total Reservoir Compressibility 52. Resistivity Index 53. Surface and Interfacial Tension 58. Wettability and Contact Angle 61. Capillary Pressure 68. Effective Permeabilities 72. Relative Permeabilities 76. Effect of Wettability on Fluid Rock Properties 79.	
Formation Evaluation	86
Coring and Core Analysis 86. Drill Stem Tests 108. Logging 109. Influences on Logs 118. Openhole Logs and Interpretation 122. Determination of Initial Oil and Gas in Place 208. Productivity Index 210.	
Pressure Transient Testing of Oil and Gas Wells	214
Definitions and Concepts 214. Important Pressure Transient Analysis Equations 222.	
Mechanisms and Recovery of Hydrocarbons by Natural Means	225
Petroleum Reservoir Definitions 225. Natural Gas Reservoirs 225. Primary Recovery of Crude Oil 225. Primary Recovery Factors in Solution-Gas-Drive Reservoirs 228.	
Material Balance and Volumetric Analysis	228
Material Balance for Gas Reservoirs 231. Material Balance Equations in Oil or Combination Reservoirs 233. Generalized Material Balance Equation 234. Material Balance for Solution-Gas-Drive Reservoirs 237. Predicting Primary Recovery in Solution-Gas-Drive Reservoirs 238. Predicting Primary Recovery in Water-Drive Reservoirs 240. Volumetric Calculations for Recovery of Gas and Oil 241.	
Decline-Curve Analysis	244
Exponential Decline 246. Hyperbolic Decline 247. Harmonic Decline 248. Production Type Curves 248.	
Reserve Estimates	249
Definition and Classification of Reserves 249. Methods of Estimating Reserves 254. Quality of Reserve Estimates 258.	
Secondary Recovery	259
Definitions 259. Gas Injection 260. Water Injection 262. Spacing of Wells and Well Patterns 262.	
Fluid Movement in Waterflooded Reservoirs	269
Displacement Mechanisms 269. Viscous Fingering 275. Mobility and Mobility Ratio 276. Recovery Efficiency 277. Displacement Sweep Efficiency 279. Volumetric Sweep Efficiency 279. Permeability Variation 284. Estimation of Waterflood Recovery by Material Balance 292. Prediction Methods 293. Performance Evaluation 293.	

2 Reservoir Engineering

Estimating Waterflood Residual Oil Saturation	301
Material Balance 301. Well Test Analyses 302. Coring and Core Testing 304. Tracer Tests for Determining Residual Oil 309. Geophysical Well Logging Techniques 312. Summary of Methods for Estimating Residual Oils 317. Recommended Methods for Assessing Residual Oil 318.	
Enhanced Oil Recovery Methods	319
Definition 319. Chemical Flooding 320. Gas Injection Methods 323. Thermal Recovery 326. Technical Screening Guides 327. Hydrocarbon Miscible Flooding 329. Nitrogen and Flue Gas Flooding 330. Carbon Dioxide Flooding 331. Surfactant/Polymer Flooding 332. Polymer Flooding 332. Alkaline Flooding 333. In-Situ Combustion 334. Steamflooding 335. Laboratory Design for Enhanced Recovery 342.	
References	344

5

Reservoir Engineering

Reservoir engineering covers a broad range of subjects including the occurrence of fluids in a gas or oil-bearing reservoir, movement of those or injected fluids, and evaluation of the factors governing the recovery of oil or gas. The objectives of a reservoir engineer are to maximize producing rates and to ultimately recover oil and gas from reservoirs in the most economical manner possible.

This chapter presents the basic fundamentals useful to practical petroleum engineers. Topics are introduced at a level that can be understood by engineers and geologists who are not expert in this field. Various correlations are provided where useful. Newer techniques for improving recovery are discussed.

The advent of programmable calculators and personal computers has dramatically changed the approach of solving problems used by reservoir engineers. Many repetitious and tedious calculations can be performed more consistently and quickly than was possible in the past. The use of charts and graphs is being replaced by mathematical expressions of the data that can be handled with portable calculators or personal computers. Programs relating to many aspects of petroleum engineering are now available. In this chapter, many of the charts and graphs that have been historically used are presented for completeness and for illustrative purposes. In addition, separate sections will be devoted to the use of equations in some of the more common programs suitable for programmable calculators and personal computers.

BASIC PRINCIPLES, DEFINITIONS, AND DATA

Reservoir Fluids

Oil and Gas

Reservoir oil may be saturated with gas, the degree of saturation being a function, among others, of reservoir pressure and temperature. If the reservoir oil has dissolved in it all the gas it is capable of holding under given conditions, it is referred to as saturated oil. The excess gas is then present in the form of a free gas cap. If there is less gas present in the reservoir than the amount that may be dissolved in oil under conditions of reservoir pressure and temperature, the oil is then termed undersaturated. The pressure at which the gas begins to come out of solution is called the saturation pressure or the bubble-point pressure. In the case of saturated oil, the saturation pressure equals the reservoir pressure and the gas begins coming out of solution as soon as the reservoir pressure begins to decrease. In the case of undersaturated oil, the gas does not start coming out of solution until the reservoir pressure drops to the level of saturation pressure.

Apart from its function as one of the propulsive forces, causing the flow of oil through the reservoir, the dissolved gas has other important effects on recovery of oil. As the gas comes out of solution the viscosity of oil increases and its gravity decreases. This makes more difficult the flow of oil through the reservoir toward the wellbore. Thus the need is quite apparent for production

practices tending to conserve the reservoir pressure and retard the evolution of the dissolved gas. Figure 5-1 shows the effect of the dissolved gas on viscosity and gravity of a typical crude oil.

The dissolved gas also has an important effect on the volume of the produced oil. As the gas comes out of solution the oil shrinks so that the liquid oil at surface conditions will occupy less volume than the gas-saturated oil occupied in the reservoir. The number of barrels of reservoir oil at reservoir pressure and temperature which will yield one barrel of stock tank oil at 60°F and atmospheric pressure is referred to as the formation volume factor or reservoir volume factor. Formation volume factors are described in a subsequent section. The solution gas-oil ratio is the number of standard cubic feet of gas per barrel of stock tank oil.

Physical properties of reservoir fluids are determined in the laboratory, either from bottomhole samples or from recombined surface separator samples. Frequently, however, this information is not available. In such cases, charts such as those developed by M.B. Standing and reproduced as Figures 5-2, 5-3, 5-4, and 5-5 have been used to determine the data needed [1,2]. The correlations on which the charts are based present bubble-point pressures, formation volume factors of bubble-point liquids, formation volume factors of gas plus liquid phases, and, density of a bubble-point liquid as empirical functions of gas-oil ratio, gas gravity, oil gravity, pressure, and temperature. More recent correlations will be presented subsequently.

Until recently, most estimates of PVT properties were obtained by using charts and graphs of empirically derived data. With the development of programmable calculators, graphical data are being replaced by mathematical expressions

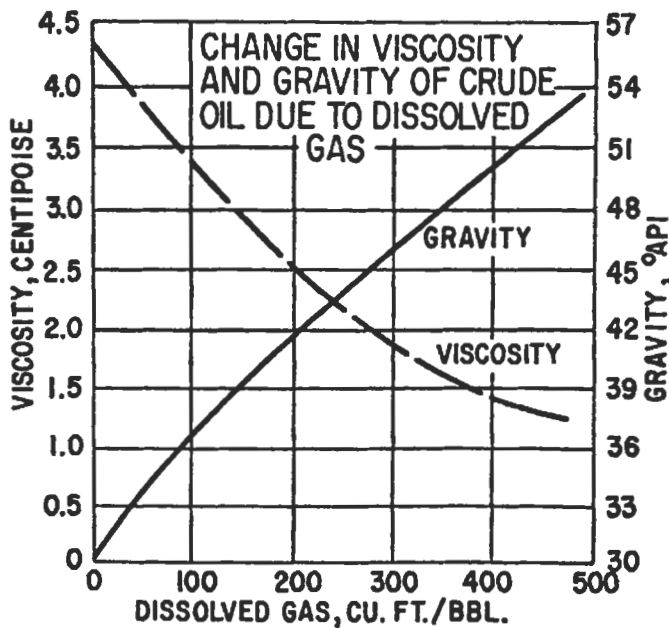


Figure 5-1. Change in viscosity and gravity of crude oil due to dissolved gas.

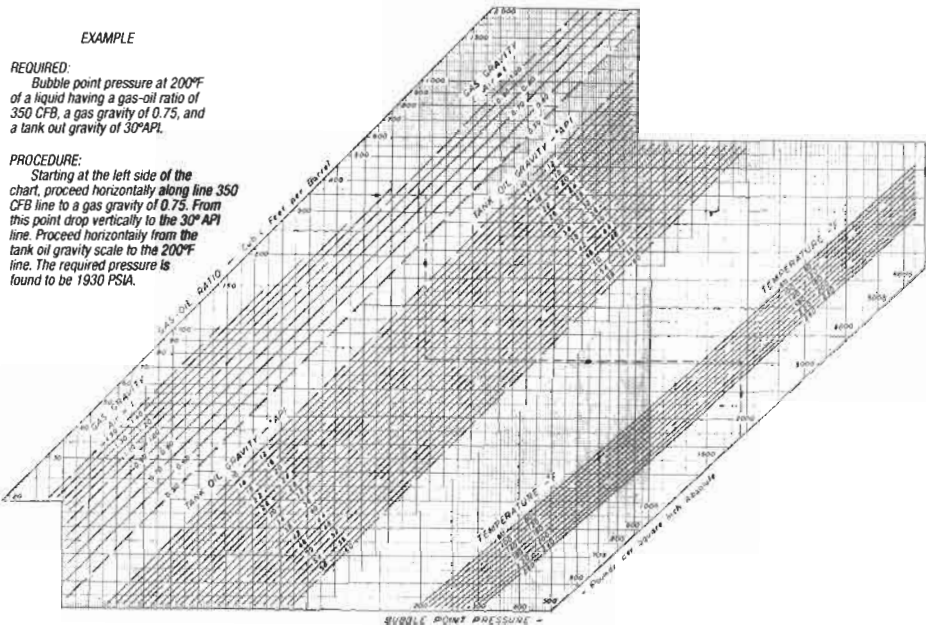


Figure 5-2. Properties of natural hydrocarbon mixtures of gas and liquid: bubble point pressure [1,2].

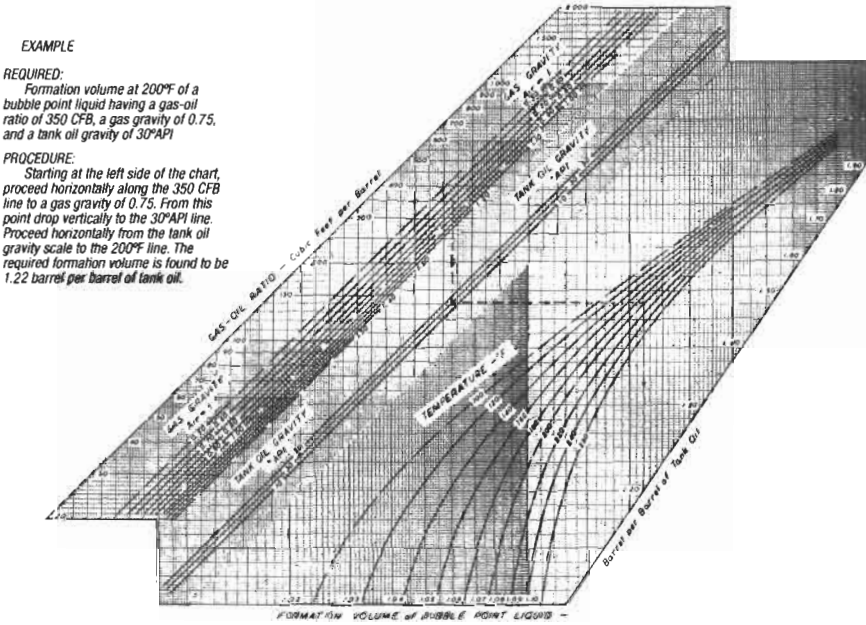


Figure 5-3. Properties of natural hydrocarbon mixtures of gas and liquid: formation volume of bubble point liquids [1,2].

6 Reservoir Engineering

EXAMPLE

REQUIRED:
Formation volume of the gas plus liquid phases of a 1500 CFB mixture, gas gravity = 0.80, tank oil gravity = 40°API, at 200°F and 1000 PSIA

PROCEDURE:
Starting at the left side of the chart proceed horizontally along the 1500 CFB line to the 0.80 gas gravity line. From this point drop vertically to the 40°API line. Proceed horizontally to 200°F and from that point drop to line 1000 PSIA pressure line. The required formation volume is found to be 5.0 barrels per barrel of tank oil.

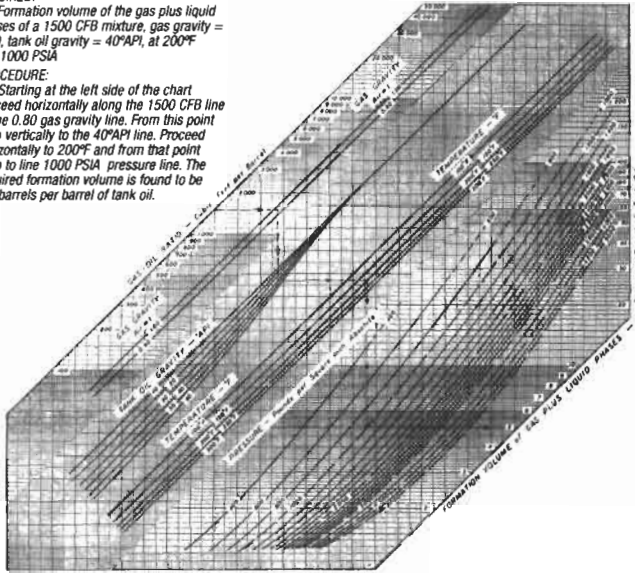


Figure 5-4. Properties of natural hydrocarbon mixtures of gas and liquid: formation volume of gas plus liquid phases [1,2].

EXAMPLE

REQUIRED:
Density at 200°F at a bubble point liquid having a gas-oil ratio at 350 CFB, a gas gravity of 0.75 on a tank oil gravity of 30° API.

PROCEDURE:
From Chart 3 determine formation volume of 1.22 barrels per barrel of tank oil. Starting a left side of chart proceed horizontally along the 350 CFB line to a gas gravity of 0.75. From this point drop vertically to the 30° API line. Proceed horizontally from the tank oil gravity scale to the formation volume of 1.22. The required density is found to be 47.5 pounds per cubic foot.

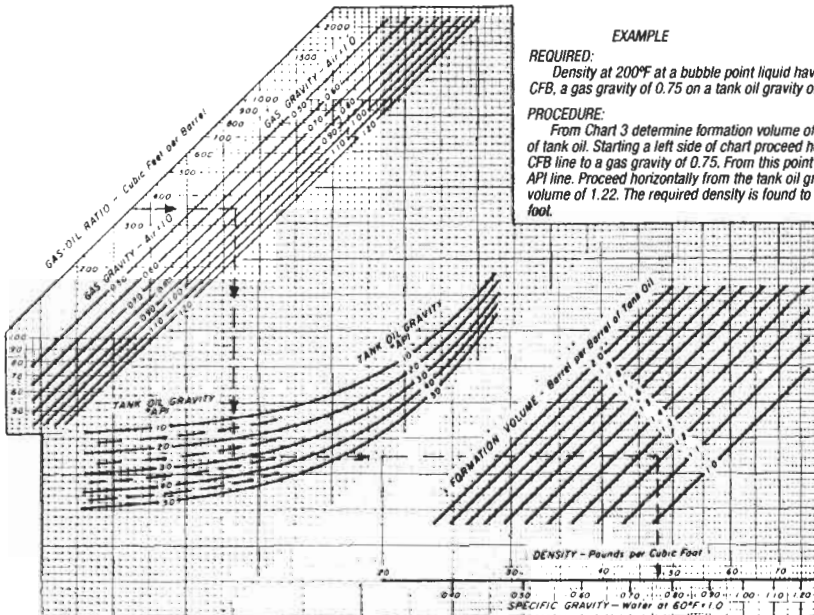


Figure 5-5. Properties of natural hydrocarbon mixtures of gas and liquid: density and specific gravity of mixtures [1,2].

suitable for computer use. In a later section, the use of such programs for estimating PVT properties will be presented. In the initial sections, the presentation of graphical data will be instructive to gaining a better understanding of the effect of certain variables.

Water

Regardless of whether a reservoir yields pipeline oil, water in the form commonly referred to as interstitial or connate is present in the reservoir in pores small enough to hold it by capillary forces.

The theory that this water was not displaced by the migration of oil into a water-bearing horizon is generally accepted as explanation of its presence.

The amount of the interstitial water is usually inversely proportional to the permeability of the reservoir. The interstitial water content of oil-producing reservoirs often ranges from 10% to 40% of saturation.

Consideration of interstitial water content is of particular importance in reservoir studies, in estimates of crude oil reserves and in interpretation of electrical logs.

Fluid Viscosities

Gas Viscosity. Viscosities of natural gases are affected by pressure, temperature, and composition. The viscosity of a specific natural gas can be measured in the laboratory, but common practice is to use available empirical data such as those shown in Figures 5-6 and 5-7. Additional data are given in the *Handbook of Natural Gas Engineering* [3]. Contrary to the case for liquids, the viscosity of a gas at low pressures increases as the temperature is raised. At high pressures, gas viscosity decreases as the temperature is raised. At intermediate pressures, gas viscosity may decrease as temperature is raised and then increase with further increase in temperature.

Oil Viscosity. The viscosity of crude oil is affected by pressure, temperature, and most importantly, by the amount of gas in solution. Figure 5-8 shows the effect of pressure on viscosities of several crude oils at their respective reservoir temperatures [4]. Below the bubble-point, viscosity decreases with increasing pressure because of the thinning effect of gas going into solution. Above the bubble-point, viscosity increases with increasing pressure because of compression of the liquid. If a crude oil is undersaturated at the original reservoir pressure, viscosity will decrease slightly as the reservoir pressure decreases. A minimum viscosity will occur at the saturation pressure. At pressures below the bubble-point, evolution of gas from solution will increase the density and viscosity of the crude oil as the reservoir pressure is decreased further.

Viscosities of hydrocarbon liquids decrease with increasing temperature as indicated in Figure 5-9 for gas-free reservoir crudes [5]. In cases where only the API gravity of the stock tank oil and reservoir temperature are known, Figure 5-9 can be used to estimate dead oil viscosity at atmospheric pressure. However, a more accurate answer can be obtained easily in the laboratory by simply measuring viscosity of the dead oil with a viscometer at reservoir temperature.

With the dead oil viscosity at atmospheric pressure and reservoir temperature (either measured or obtained from Figure 5-9), the effect of solution gas can be estimated with the aid of Figure 5-10 [6]. The gas-free viscosity and solution gas-oil ratio are entered to obtain viscosity of the gas-saturated crude at the bubble-point pressure. This figure accounts for the decrease in viscosity caused

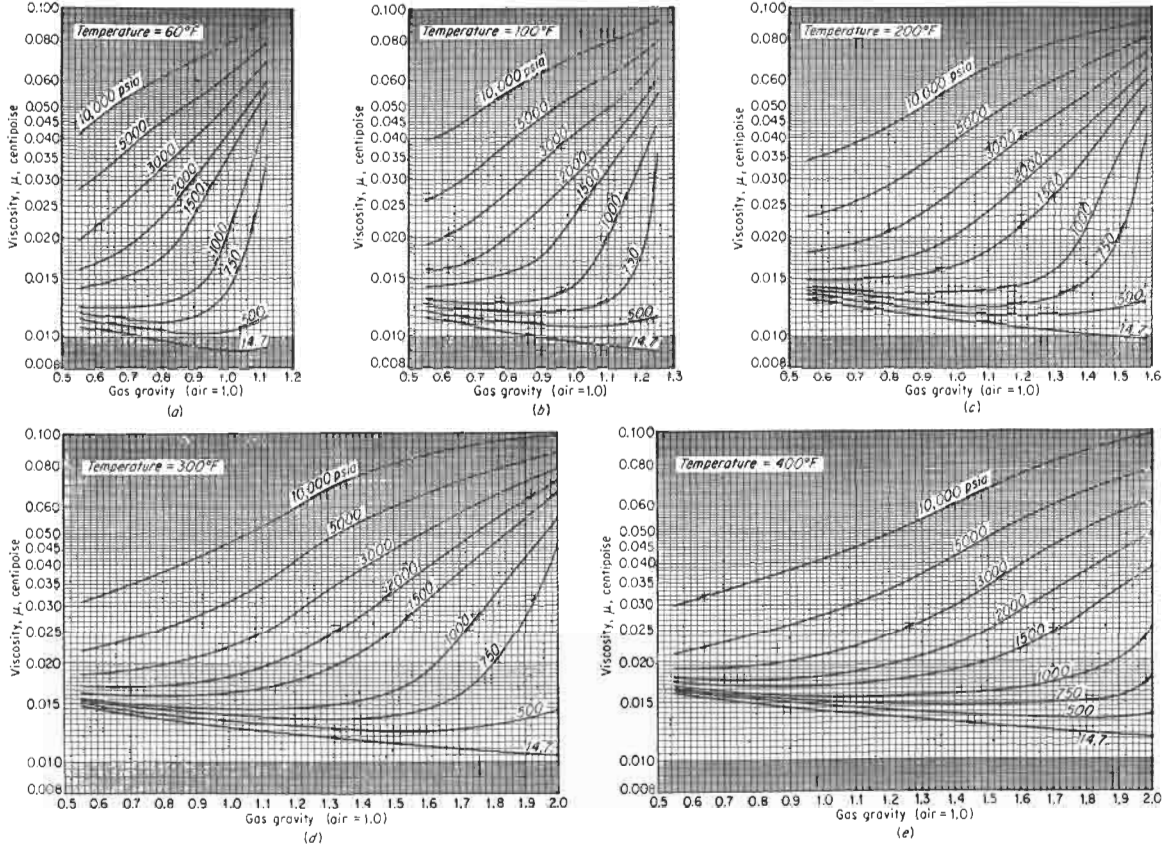


Figure 5-6. Viscosity of natural gases as a function of gravity at five temperatures [3].

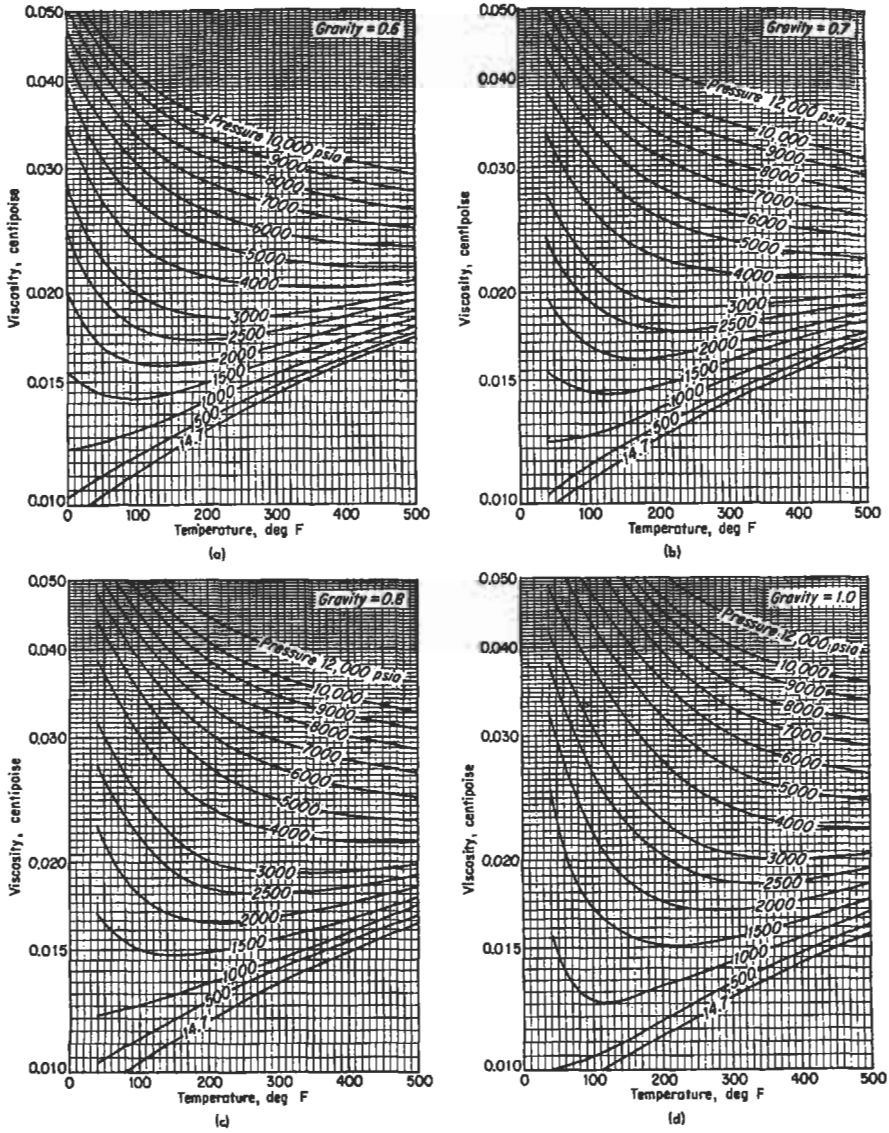


Figure 5-7. Viscosity of natural gases as a function of temperature at four gravities [3].

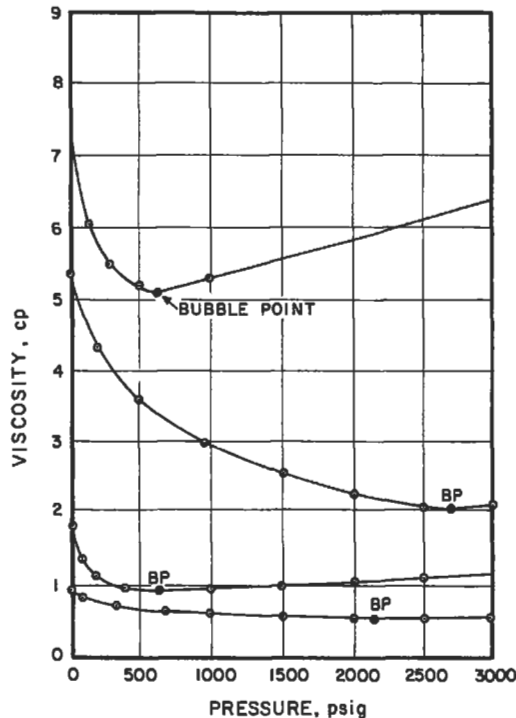


Figure 5-8. Effect of pressure on crude oil viscosities [4].

by gas going into solution as pressure is increased from atmospheric to the saturation pressure.

If the pressure is above the bubble-point pressure, crude oil viscosity in the reservoir can be estimated with Figure 5-11 [5]. This figure shows the increase in liquid viscosity due to compression of the liquid at pressures higher than the saturation pressure. Viscosity of the crude can be estimated from the viscosity at the bubble point pressure, and the difference between reservoir pressure and bubble-point pressure.

Recent correlations [7] were presented in equation form for the estimation of both dead oil and saturated oil viscosities. These correlations, which are presented in the section on programs for hand-held calculators, neglect the dependence of oil viscosity on composition of the crude. If compositional data are available, other correlations [8-10] for oil viscosity can be used.

Water Viscosity. In 1952, the National Bureau of Standards conducted tests [11] which determined that the absolute viscosity of pure water was 1.0019 cp as compared with the value of 1.005 cp that had been accepted for many years. Effective July 1, 1952, the value of 1.002 cp for the absolute viscosity of water was recommended as the basis for the calibration of viscometers and standard oil samples. Any literature values based on the old standard are in slight error. Water viscosity decreases as temperature is increased as shown in Table 5-1.

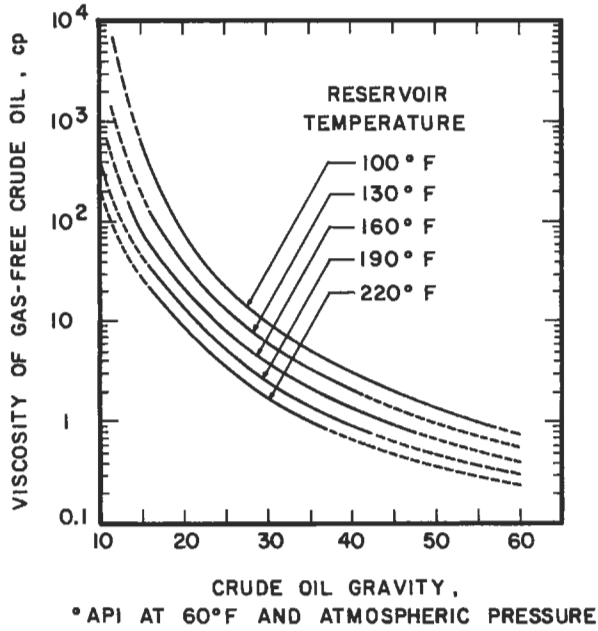


Figure 5-9. Crude oil viscosity as a function of API gravity [5].

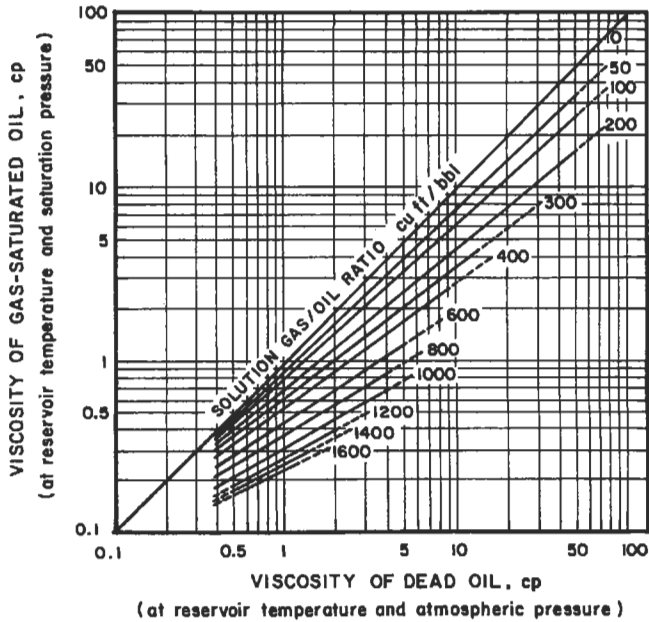


Figure 5-10. Viscosities of gas-saturated crude oils at reservoir temperature and bubble-point pressure [6].

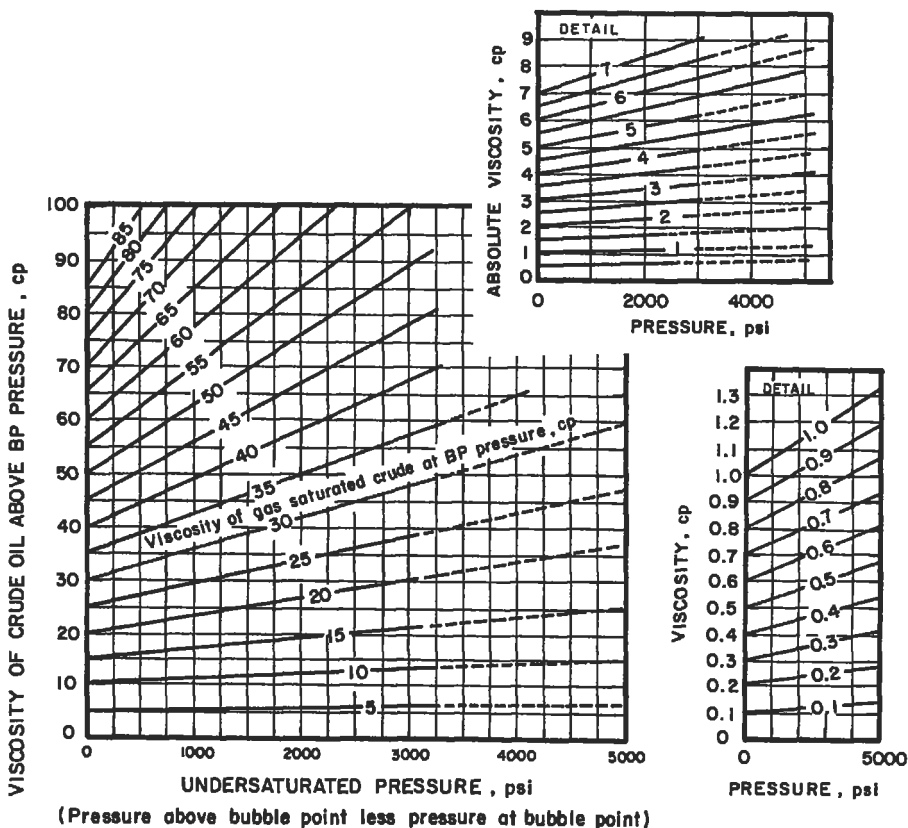


Figure 5-11. Increase in oil viscosity with pressure above bubble-point pressure [5].

Although the predominate effect on water viscosity is temperature, viscosity of water normally increases as salinity increases. Potassium chloride is an exception to this generality. Since most oilfield waters have a high sodium chloride content, the effect of this salt on viscosity of water is given in Table 5-2.

For temperatures of interest in oil reservoirs (>60°F), the viscosity of water increases with pressure but the effect is slight. Dissolved gas at reservoir conditions should reduce the viscosity of brines; however, the lack of data and the slight solubility of gas in water suggest that this effect is usually ignored. Figure 5-12 is the most widely cited data for the effect of sodium chloride and reservoir temperature on water viscosity [13].

Formation Volume Factors

These factors are used for converting the volume of fluids at the prevailing reservoir conditions of temperature and pressure to standard surface conditions of 14.7 psia and 60°F.

Table 5-1
Viscosity of Pure Water
at Various Temperatures

T, °C	T, °F	viscosity, cp
0	32	1.787
10	50	1.307
20	68	1.002
25	77	0.8904
30	86	0.7975
40	104	0.6529
50	122	0.5468
60	140	0.4665
70	158	0.4042
80	176	0.3547
90	194	0.3147
100	212	0.2818

From Reference 12.

Table 5-2
Viscosities of Sodium Chloride
Solutions at 68°F

NaCl (wt %)	Viscosity (cp)
0.1	1.004
0.3	1.008
0.5	1.011
1.0	1.020
1.5	1.028
2.0	1.036
3.0	1.052
4.0	1.068
5.0	1.085
10.0	1.193
15.0	1.351
20.0	1.557
25.0	1.902

From Reference 12.

Gas Formation Volume Factor. The behavior of gas can be predicted from:

$$pV = znRT \quad (5-1)$$

where p = absolute pressure
V = volume of gas
T = absolute temperature
n = number of moles of gas
R = gas constant
z = factor to correct for nonideal gas behavior

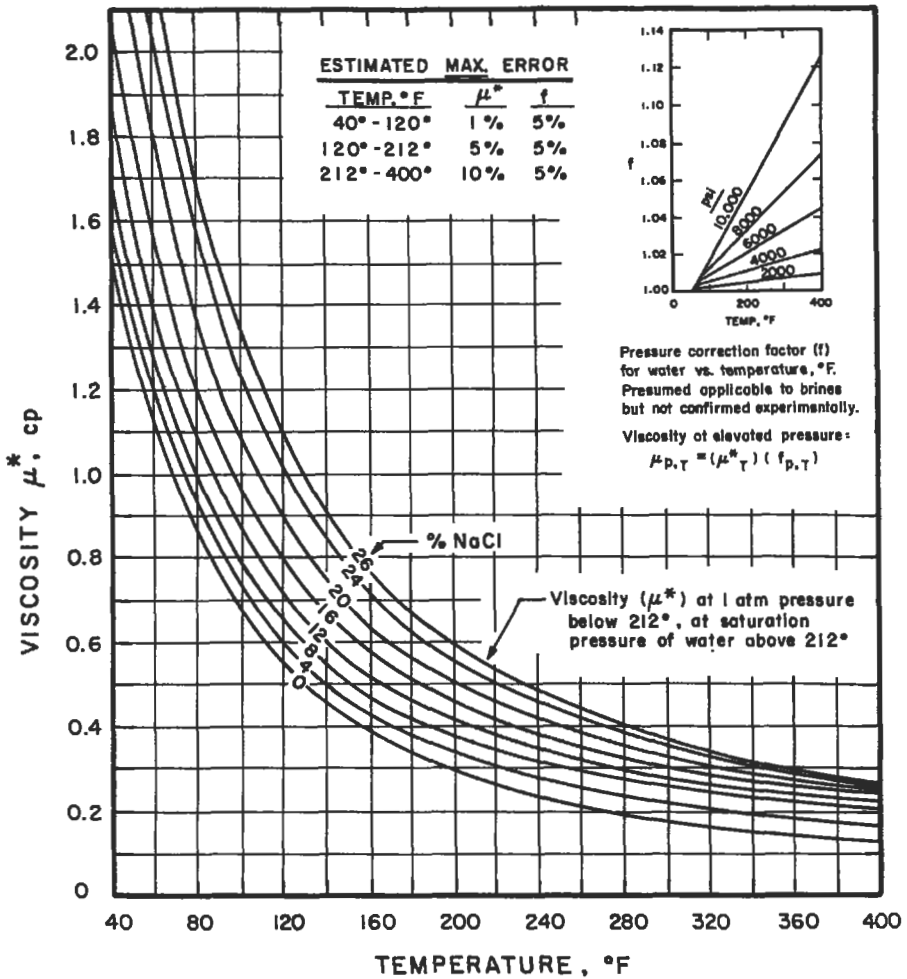


Figure 5-12. Water viscosities for various salinities and temperatures [13].

For conventional field units, p is in psia, V is in ft³, T is in °R (°F + 460), z is dimensionless, n is in lb moles, and R is 10.73 psia ft³/lb mole °R [14]. The gas formation volume factor, B_g, is the volume of gas in the reservoir occupied by a standard ft³ of gas at the surface:

$$B_g = \frac{V \text{ ft}^3}{5.615 \text{ ft}^3/\text{bbl}} = \frac{znR(T_R + 460)}{5.615} \tag{5-2}$$

where T_R is the reservoir temperature in °F.

Since one lb mole is equivalent to 379 ft³ at 60°F and 14.7 psia [15]:

$$B_g = \frac{1}{379} \times 10.73 \frac{zT_R}{p} = 0.00504 \frac{zT_R}{p} \quad (5-3)$$

In this expression, B_g will be in reservoir barrels per standard ft³ (RB/scf).

Gas formation volume factor can also be expressed in units of reservoir barrels per stock tank barrel or ft³ of gas at reservoir conditions per ft³ of gas at standard conditions:

$$B_g = 0.02827(460 + T_R) \frac{z}{p} \quad (5-4)$$

Because the gas formation volume factor can be expressed in so many different units (including the reciprocal of B_g), caution should be exercised when B_g is used. In much of the recent petroleum literature, notably SPE, B_g is expressed in RB/scf. If units of ft³/scf are given, B_g can be divided by 5.615 or multiplied by 0.1781 to get RB/scf.

Gas formation volume factors can be estimated by determining the gas deviation factor or compressibility factor, z , at reservoir pressure, p , and temperature T_R from the correlations of Standing and Katz [16] (Figure 5-13). To obtain the z factor, reduced pressure, p_r , and reduced temperature, T_r , are calculated:

$$p_r = \frac{p}{p_c} \quad (5-5)$$

where p_c is the critical pressure and

$$T_r = \frac{T}{T_c} \quad (5-6)$$

where T_c is the critical temperature. The critical pressure and temperature represent conditions above which the liquid and vapor phase are indistinguishable.

Compressibility factor and gas formation volume factor can be more conveniently estimated by the use of programs available for hand-held calculators. These programs will be subsequently discussed.

Oil Formation Volume Factor. The volume of hydrocarbon liquids produced and measured at surface conditions will be less than the volume at reservoir conditions. The primary cause is the evolution of gas from the liquids as pressure is decreased from the reservoir to the surface. When there is a substantial amount of dissolved gas, a large decrease in liquid volume occurs. Other factors that influence the volume of liquids include changes in temperature (a decrease in temperature will cause the liquid to shrink) and pressure (a decrease in pressure will cause some liquids to expand). All of these factors are included in the oil formation volume factor, B_o , which is the volume of oil in reservoir barrels, at the prevailing reservoir conditions of pressure and

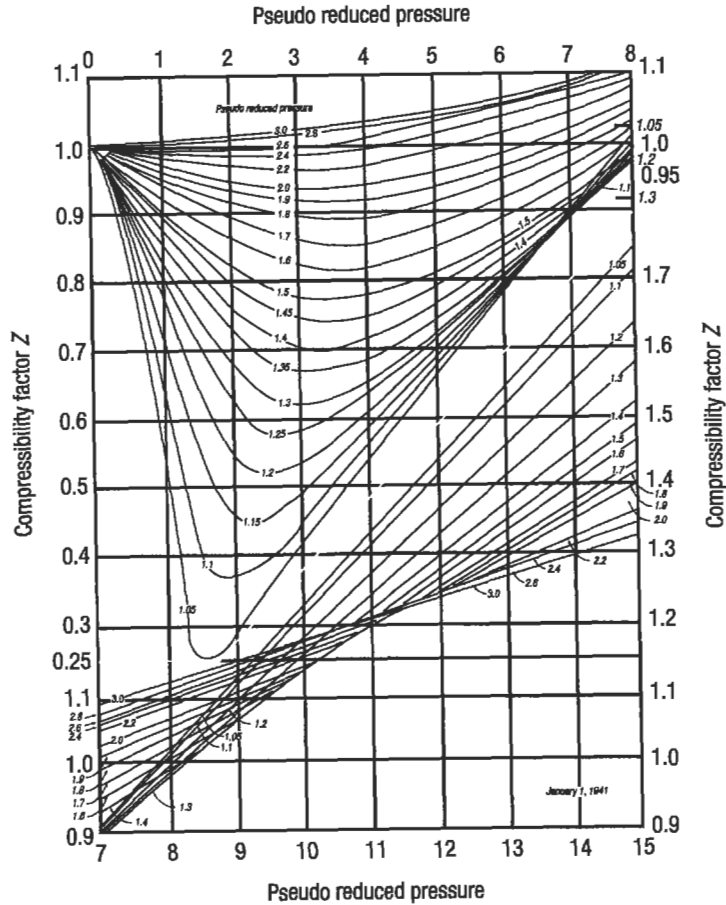


Figure 5-13. Compressibility factors [16].

temperature, occupied by a stock tank barrel of oil at standard conditions. The withdrawal of reservoir fluids can be related to surface production volumes by obtaining laboratory PVT data with reservoir fluids. Such data include B_g (the gas formation volume factor), B_o (the oil formation volume factor), and R_s (the solution gas-oil ratio which is the volume of gas in standard ft^3 that will dissolve in one stock tank barrel of oil at reservoir conditions).

The formation volume factor is used to express the changes in liquid volume accompanied by changes in pressure. Changes in formation volume factor with pressure for an undersaturated crude is displayed in Figure 5-14 [17]. As the initial reservoir pressure decreases, the all-liquid system expands and the formation volume factor increases until the bubble-point pressure is reached. As pressure decreases below the bubblepoint, gas comes out of solution, the volume of oil is reduced, thus, B_o decreases. For a saturated crude, the trend would be similar to that observed to the left of bubble-point pressure in Figure 5-14.

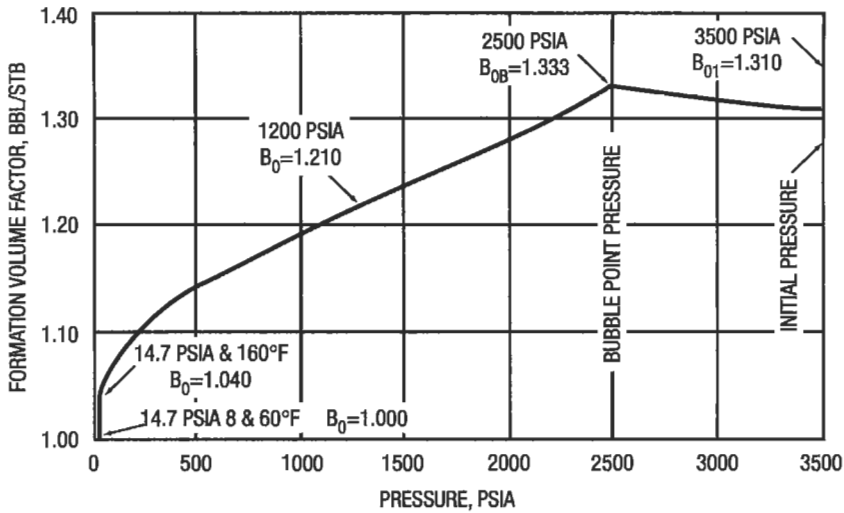


Figure 5-14. Formation volume factor of the Big Sandy Field reservoir oil, by flash liberation at reservoir temperature of 160°F. [17].

When two phases exist, the total formation volume factor or 2-phase formation volume factor is [17]:

$$B_t = B_o + B_g (R_{si} - R_s) \quad (5-7)$$

which includes the liquid volume, B_o , plus the gas volume times the difference in initial solution gas-oil ratio, R_{si} , and the solution gas-oil ratio at the specific pressure, R_s . At pressures above the bubblepoint, R_{si} equals R_s , and the single-phase and 2-phase formation volume factors are identical. At pressures below the bubblepoint, the 2-phase factor increases as pressure is decreased because of the gas coming out of solution and the expansion of the gas evolved.

For a system above the bubblepoint pressure, B_o is lower than the formation volume factor at saturation pressure because of contraction of the oil at higher pressure. The customary procedure is to adjust the oil formation volume factor at bubble-point pressure and reservoir temperature by a factor that accounts for the isothermal coefficient of compressibility such as [18]:

$$B_o = B_{ob} \exp [-c_o (p - p_b)] \quad (5-8)$$

where B_{ob} is the oil formation volume factor at bubblepoint conditions, p_b is the bubble-point pressure in psi, and c_o is oil compressibility in psi^{-1} .

The basic PVT properties (B_o , R_s , and B_g) of crude oil are determined in the laboratory with a high-pressure PVT cell. When the pressure of a sample of crude oil is reduced, the quantity of gas evolved depends on the conditions of liberation. In the flash liberation process, the gas evolved during any pressure reduction remains in contact with the oil. In the differential liberation process, the gas evolved during any pressure reduction is continuously removed from

contact with the oil. As a result, the flash liberation is a constant-composition, variable-volume process and the differential liberation is a variable-composition, constant-volume process. For heavy crudes (low volatility, low API gravity oils) with dissolved gases consisting primarily of methane and ethane, both liberation processes yield similar quantities and compositions of evolved gas as well as similar resulting oil volumes. However, for lighter, highly volatile crude oils containing a relatively high proportion of intermediate hydrocarbons (such as propane, butane, and pentane), the method of gas liberation can have an effect on the PVT properties that are obtained. An example of differences in formation volumes with flash and differential liberation processes can be seen in Figure 5-15 [19]. Actual reservoir conditions may be somewhere between these extremes because the mobility of the liberated gas is greater than the oil, the gas is produced at a higher rate, and the oil in the reservoir is in contact with all of the initial solution gas for only a brief period [20]. Since volatile oil situations are uncommon [20], many engineers feel the differential liberation process typifies most reservoir conditions [19]. For reservoir fluids at the bubblepoint when a well is put on production, the gas evolved from the oil as the pressure declines does not flow to the well until the critical gas saturation is exceeded. Since the greatest pressure drop occurs near the wellbore, the critical gas saturation occurs first near the well, especially if the pressure drop is large. In general, differential liberation data is applicable if the reservoir pressure falls considerably below the bubble-point pressure and the critical gas saturation is exceeded in the majority of the drainage area, as indicated by producing gas-oil ratios considerably in excess of the initial solution gas-oil ratio [17]. Flash liberation data may be applicable to reservoirs where there is only a moderate pressure decline below the bubblepoint, as indicated by producing gas-oil ratios

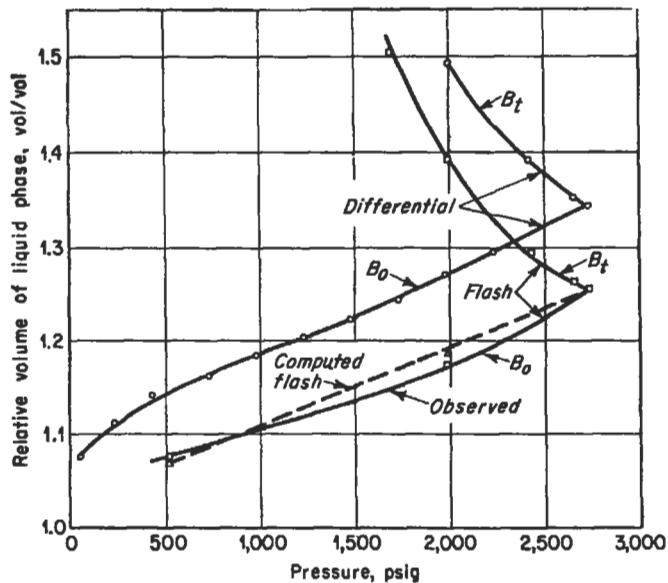


Figure 5-15. Comparison of measured and calculated composite oil volume [19].

not much higher than the initial solution gas-oil ratio, since the liberated gas stays in the reservoir in contact with the remaining oil [17].

Several correlations are available for estimating formation volume factors. Single-phase formation volume factors can be estimated from solution gas, gravity of solution gas, API gravity of the stock tank oil, and reservoir temperature by using the correlations of Standing [1,2]. Figure 5-3 provides Standing's empirical correlation of bubble-point oil formation volume factor as a function of the variables mentioned. Total formation volume factors of both solution gas and gas-condensate systems can be obtained from Standing's correlations given in Figure 5-4.

Empirical equations have been developed [21] from Standing's graphical data. These equations provide the oil formation volume factor and the solution gas-oil ratio as functions of reservoir pressure [21]:

$$B_o = a p^{1.17} + b \tag{5-9}$$

where *a* is a constant that depends on temperature, oil API gravity and gas gravity and *b* is a constant that depends on temperature. Values of both constants are given in Table 5-3; other values can be interpolated.

Solution gas-oil ratio can be estimated from:

$$R_s = y p^{1.17} \tag{5-10}$$

Table 5-3
Values of Constants for Equation 5-9

Oil gravity °API	Gas gravity:	Values of $a \times 10^5$					
		T = 120°F			T = 140°F		
		0.7	0.8	0.9	0.7	0.8	0.9
26		2.09	2.55	3.10	2.03	2.58	3.13
30		2.44	2.98	3.61	2.38	3.01	3.64
34		2.85	3.48	4.21	2.78	3.51	4.24
38		3.33	4.07	4.90	3.26	4.10	4.93
42		3.89	4.75	5.71	3.82	4.78	5.74
Oil gravity °API	Gas gravity:	T = 160°F			T = 180°F		
		0.7	0.8	0.9	0.7	0.8	0.9
26		2.02	2.47	3.02	1.95	2.38	2.91
30		2.33	2.85	3.48	2.27	2.78	3.39
34		2.69	3.29	4.01	2.65	3.24	3.96
38		3.10	3.80	4.62	3.09	3.79	4.61
42		3.58	4.38	5.33	3.60	4.42	5.38
		Values of <i>b</i>					
		T, °F			<i>b</i>		
		120			1.024		
		140			1.032		
		160			1.040		
		180			1.048		

From Reference 21.

where y is a constant that depends on temperature, gas gravity and oil gravity. Values of y are provided in Table 5-4.

Additional correlations suitable for use with programmable calculators are discussed in a later section of this chapter.

Water Formation Volume Factor. The factors discussed that affected B_o also affect the water formation volume factor, B_w . However, gas is only slightly soluble in water so evolution of gas from water has a negligible effect on B_w . Expansion and contraction of water due to reduction of pressure and temperature are slight and offsetting. Hence, B_w is seldom greater than 1.06 [18] and is usually near unity (see Table 5-5).

Several correlations for B_w are available, including the effect of gas saturation in pure water and the effect of salinity [23], and the effect of natural gas on B_w as a function of pressure and temperature [24]. However, since B_w is not greatly affected by these variables, only a simplified correction is presented [18]:

$$B_w = (1 + \Delta V_{wp})(1 + \Delta V_{wT}) \tag{5-11}$$

where ΔV_{wp} and ΔV_{wT} are the volume changes caused by reduction in pressure and temperature, respectively. Values of these corrections are given in Figures 5-16 and 5-17.

Fluid Compressibilities

Gas Compressibility. The compressibility of a gas, which is the coefficient of expansion at constant temperature, should not be confused with the compressibility factor, z , which refers to the deviation from ideal gas behavior. From the basic gas equation (see Equation 5-2), Muskat [25] provided an expression for the coefficient of isothermal compressibility:

Table 5-4
Values of Constant for Equation 5-10

Oil gravity °API	Gas gravity:	T = 120°F			T = 140°F		
		0.7	0.8	0.9	0.7	0.8	0.9
26		0.0494	0.0577	0.0645	0.0481	0.0563	0.0632
30		0.0568	0.0660	0.0737	0.0550	0.0635	0.0721
34		0.0654	0.0755	0.0842	0.0630	0.0736	0.0823
38		0.0752	0.0864	0.0962	0.0720	0.0841	0.0939
42		0.0865	0.0989	0.1099	0.0824	0.0961	0.1071
Oil gravity °API	Gas gravity:	T = 160°F			T = 180°F		
		0.7	0.8	0.9	0.7	0.8	0.9
26		0.0453	0.0519	0.0591	0.0426	0.0481	0.0543
30		0.0522	0.0597	0.0677	0.0492	0.0557	0.0629
34		0.0601	0.0686	0.0775	0.0567	0.0645	0.0728
38		0.0692	0.0788	0.0887	0.0654	0.0747	0.0842
42		0.0797	0.0906	0.1016	0.0755	0.0865	0.0975

From Reference 21.

Table 5-5
Formation Volumes of Water

Pressure psia	Formation volumes, bbl/bbl			
	100°F	150°F	200°F	250°F
Pure water				
5,000	0.9910	1.0039	1.0210	1.0418
4,000	0.9938	1.0067	1.0240	1.0452
3,000	0.9966	1.0095	1.0271	1.0487
2,000	0.9995	1.0125	1.0304	1.0523
1,000	1.0025	1.0153	1.0335	1.0560
Vapor pressure of water	1.0056	1.0187	1.0370	1.0598
Natural gas and water				
Saturation pressure				
5,000	0.9989	1.0126	1.0301	1.0522
4,000	1.0003	1.0140	1.0316	1.0537
3,000	1.0017	1.0154	1.0330	1.0552
2,000	1.0031	1.0168	1.0345	1.0568
1,000	1.0045	1.0183	1.0361	1.0584

From Reference 22.

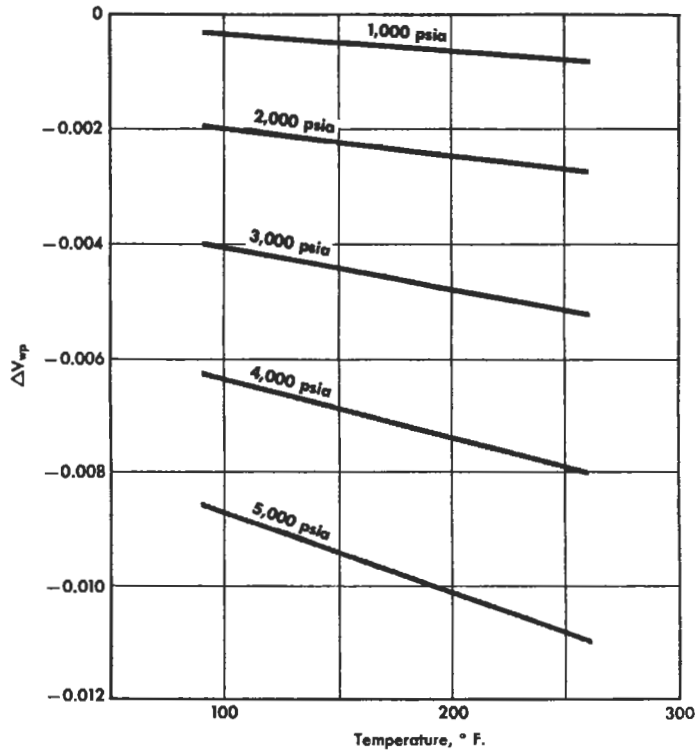


Figure 5-16. Change in water volume due to pressure reduction [18].

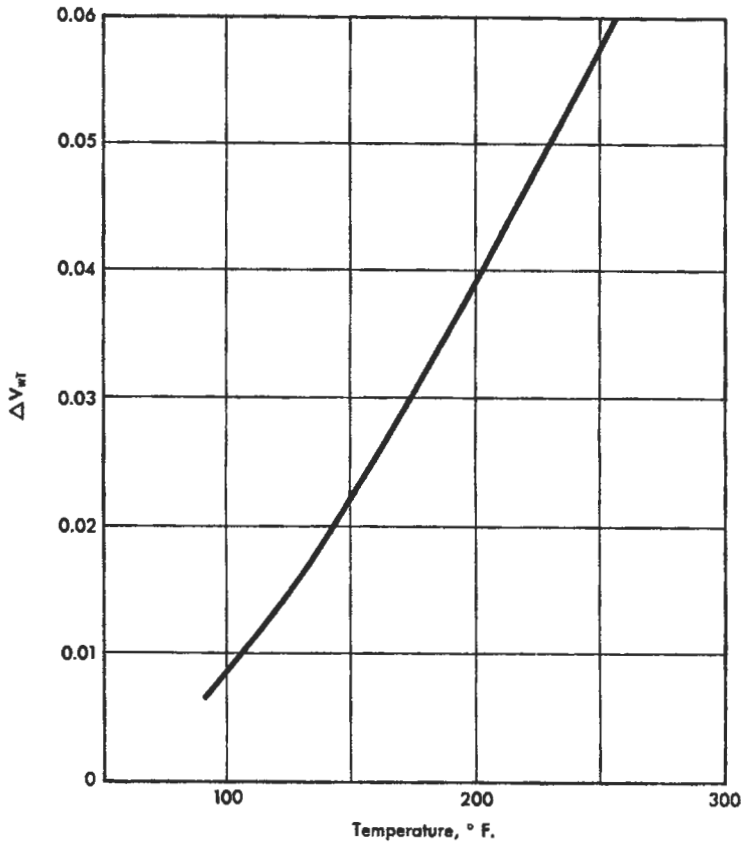


Figure 5-17. Change in water volume due to temperature reduction [18].

$$c_g = \frac{1}{p} - \frac{1}{z} \frac{dz}{dp} \quad (5-12)$$

For perfect gases ($z = 1$ and $dz/dp = 0$), c_g is inversely proportional to pressure. For example, an ideal gas at 1,000 psia has a compressibility of $1/1,000$ or $1,000 \times 10^{-6} \text{ psi}^{-1}$. However, natural hydrocarbon gases are not ideal gases and the compressibility factor, z , is a function of pressure as seen in Figure 5-18 [17]. At low pressures, z decreases as pressure increases and dz/dp is negative; thus, c_g is higher than that of an ideal gas. At high pressures, dz/dp is positive since z increases, and c_g is less than that of a perfect gas.

Compared to other fluids or to reservoir rock, the compressibility of natural gas is large; c_g ranges from about $1,000 \times 10^{-6} \text{ psi}^{-1}$ at 1,000 psi to about $100 \times 10^{-6} \text{ psi}^{-1}$ at 5,000 psi [27]. Compressibility of natural gases can be obtained from laboratory PVT data or estimated from the correlations given by Trube [27] (see Figures 5-19a and 5-19b). Trube defined the pseudo-reduced compressibility of a gas,

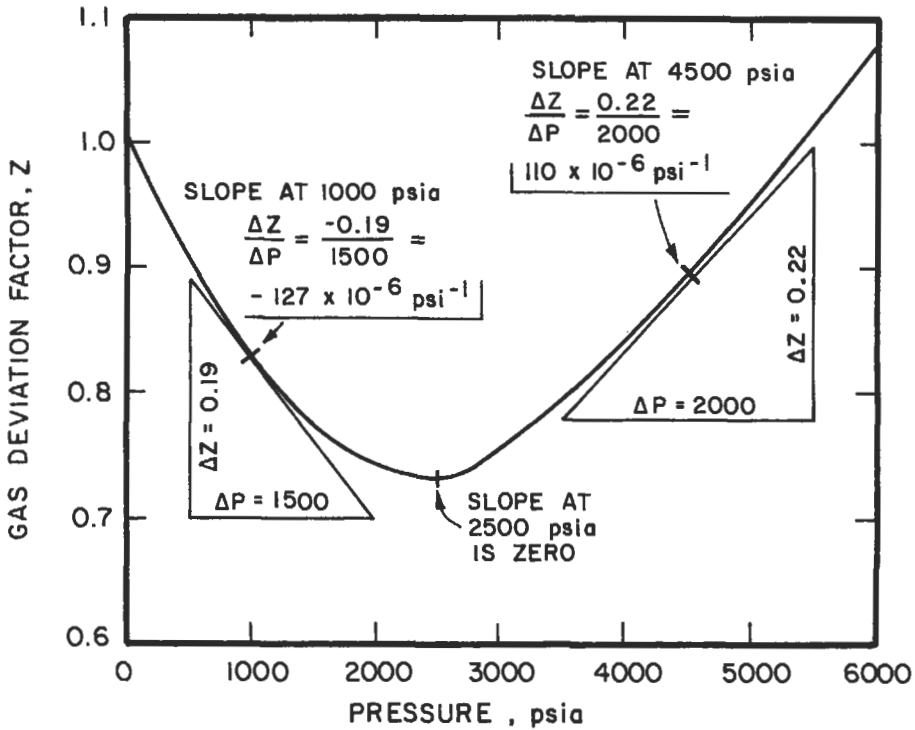


Figure 5-18. Gas compressibility from the gas deviation factor vs. pressure [17].

c_{pr} , as a function of pseudo-reduced temperature and pressure, T_{pr} and p_{pr} , respectively [27]:

$$c_g = \frac{1}{P_{pc}} \left[\frac{1}{P_{pr}} - \frac{1}{z} \left(\frac{dz}{dp_{pr}} \right) T_{pr} \right] \quad (5-13)$$

where p_{pc} is the pseudo-critical pressure (reduced and critical pressures have been defined earlier). Gas compressibility is computed for the pseudo-reduced compressibility from the appropriate figure:

$$c_g = \frac{c_{pr}}{P_{pr}} \quad (5-14)$$

Pseudo-critical pressures and temperatures can be calculated from the mole fraction of each component present in hydrocarbon gas mixture or estimated from Figure 5-20 [3].

Oil Compressibility. The compressibility of oil, c_o , can be obtained in the laboratory from PVT data. In the absence of laboratory data, Trube's correlation

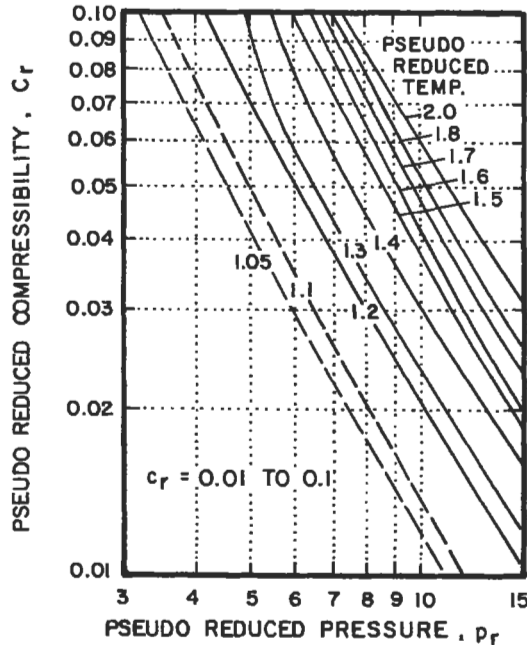
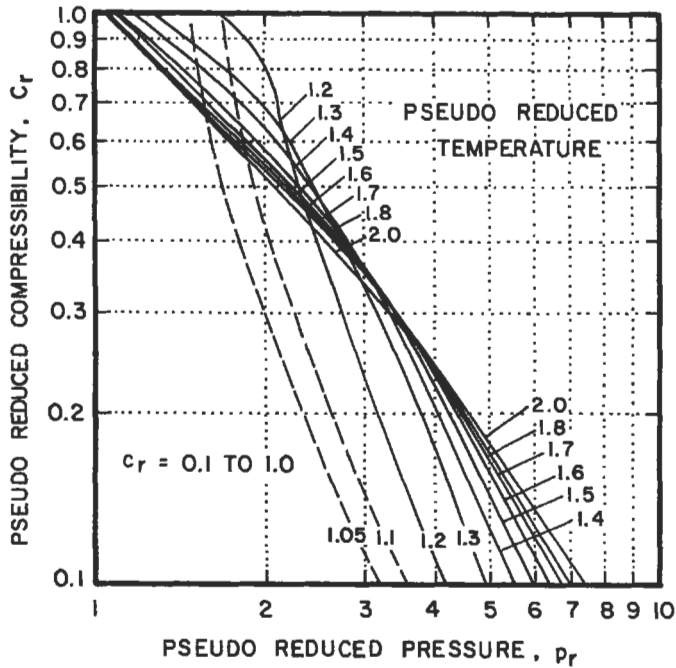


Figure 5-19 (a and b). Variation of reduced compressibility with reduced pressures for various fixed values of reduced temperature [27].

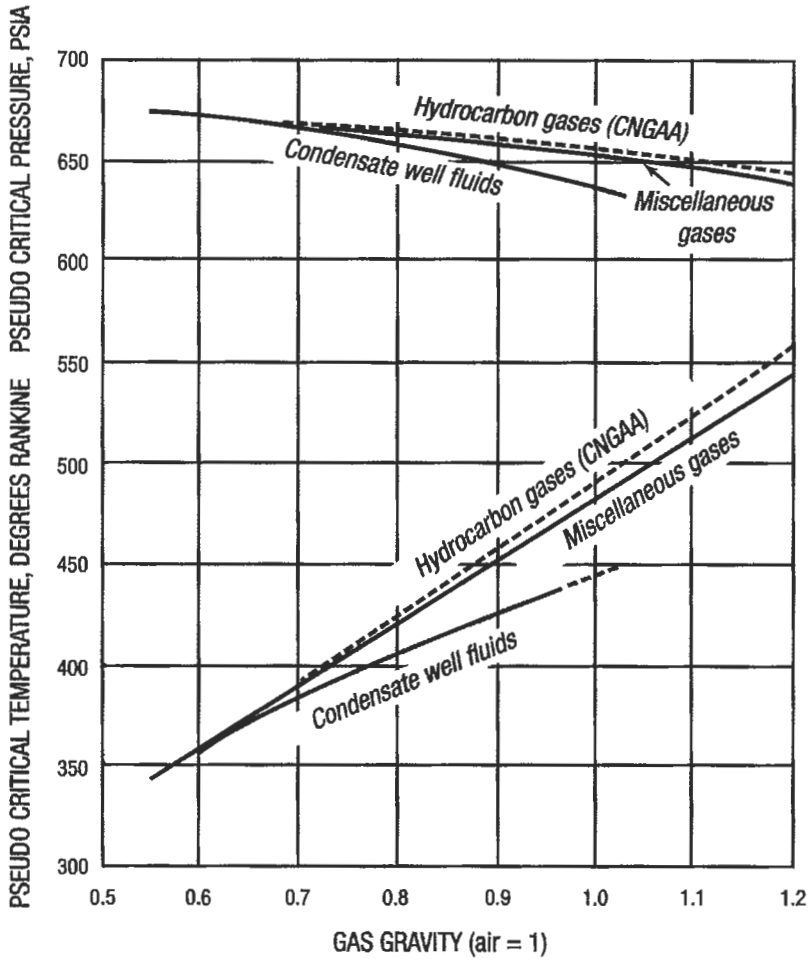


Figure 5-20. Pseudo-critical properties of natural gases [3].

[28] for compressibility of an undersaturated oil in Figure 5-21 can be used in a similar fashion as previously discussed for c_g . Pseudo-critical temperature and pressure can be estimated from Figure 5-22 or 5-23. With the pseudo-reduced compressibility from Figure 5-21, oil compressibility can be estimated:

$$c_o = \frac{c_{pr}}{P_{pc}} \tag{5-15}$$

For conditions below the bubblepoint, dissolved gas must be taken into account. In the absence of laboratory data, the changes in R_x and B_o with changes in

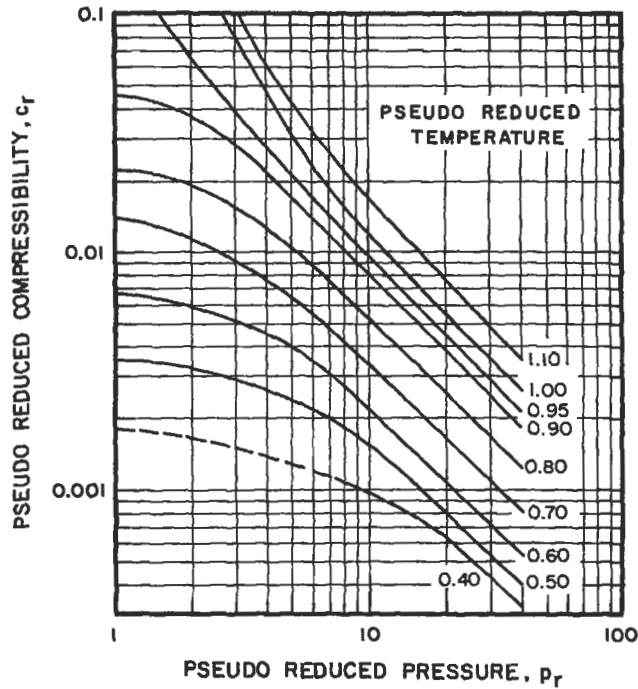


Figure 5-21. Variation of pseudo-reduced compressibility with pseudo-reduced pressures for various fixed values of pseudo-reduced temperature [28].

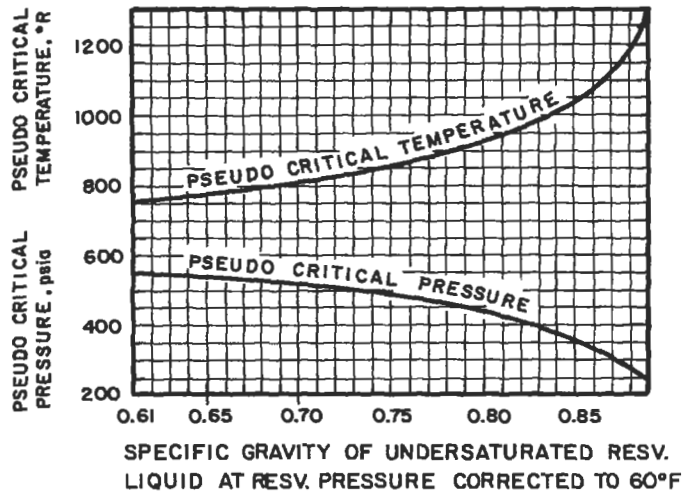


Figure 5-22. Approximate variation of pseudo-critical pressure and pseudo-critical temperature with specific gravity of liquid corrected to 60°F [28].

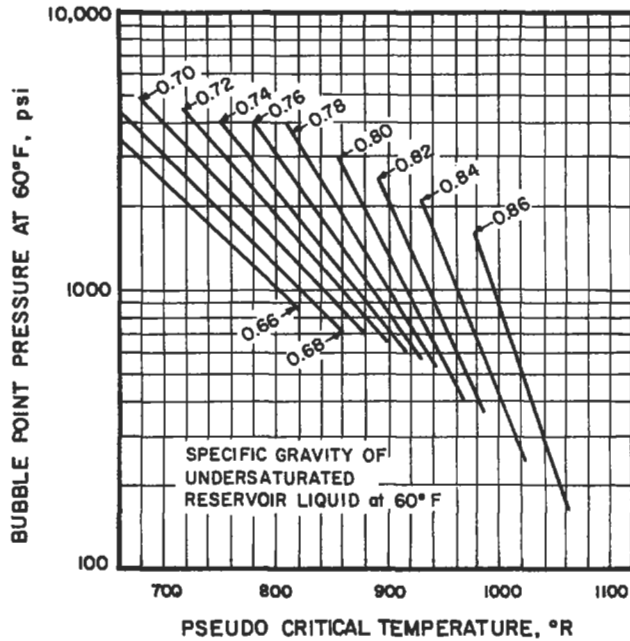


Figure 5-23. Variation of pseudo-critical temperature with specific gravity and bubble point of liquid corrected to 60°F [28].

pressure can be approximated from Figures 5-24 and 5-25 which were developed by Ramey [26] from Standing’s [1] data:

$$\left(\frac{\partial B_o}{\partial p}\right)_T = \left(\frac{\partial R_s}{\partial p}\right)_T \left(\frac{\partial B_o}{\partial R_s}\right)_T \tag{5-16}$$

B_o can be estimated from Figure 5-3, and gravities of both oil and gas must be known. Oil compressibility is often on the order of $10 \times 10^{-6} \text{ psi}^{-1}$.

Water Compressibility. Although the best approach is to obtain water compressibilities from laboratory PVT tests, this is seldom done and the use of correlations [22] such as are given in Figures 5-26 and 5-27 is often required. The compressibility of nongas-saturated water ranges from $2 \times 10^{-6} \text{ psi}^{-1}$ to $4 \times 10^{-6} \text{ psi}^{-1}$ and a value of $3 \times 10^{-6} \text{ psi}^{-1}$ is frequently used [13]. The compressibility of water with dissolved gas ranges from $15 \times 10^{-6} \text{ psi}^{-1}$ at 1,000 psi to $5 \times 10^{-6} \text{ psi}^{-1}$ at 5,000 psi [26].

Estimation of Fluid Properties with Programmable Calculators and Personal Computers

With the recent widespread use of hand-held programmable calculators and desk-top personal computers, engineers are no longer faced with estimating fluid properties from charts and graphs. Much of the data in the literature have been

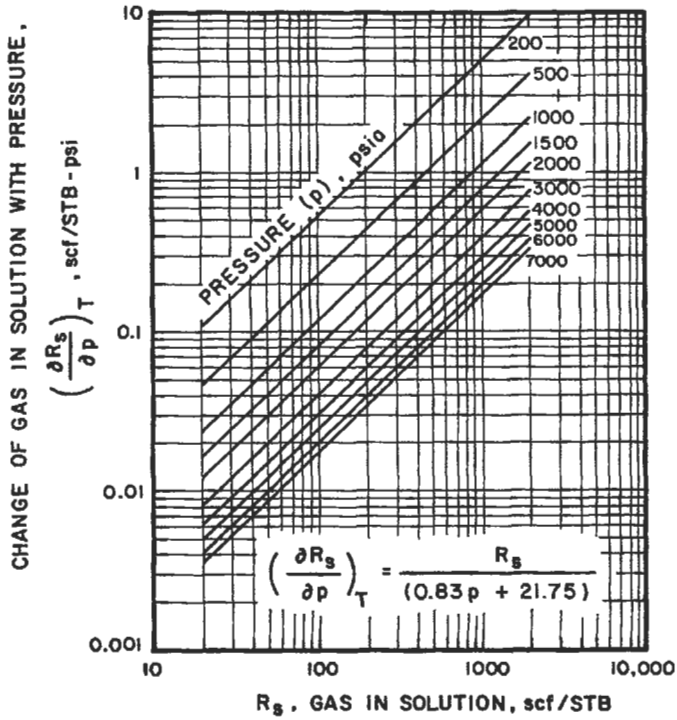


Figure 5-24. Change of gas solubility in oil with pressure vs. gas in solution [26].

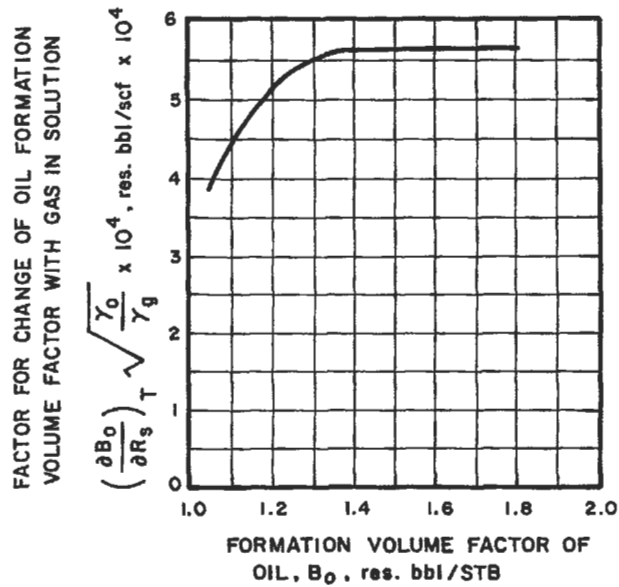


Figure 5-25. Change of oil formation volume factor with gas in solution vs. oil formation volume factor [26].

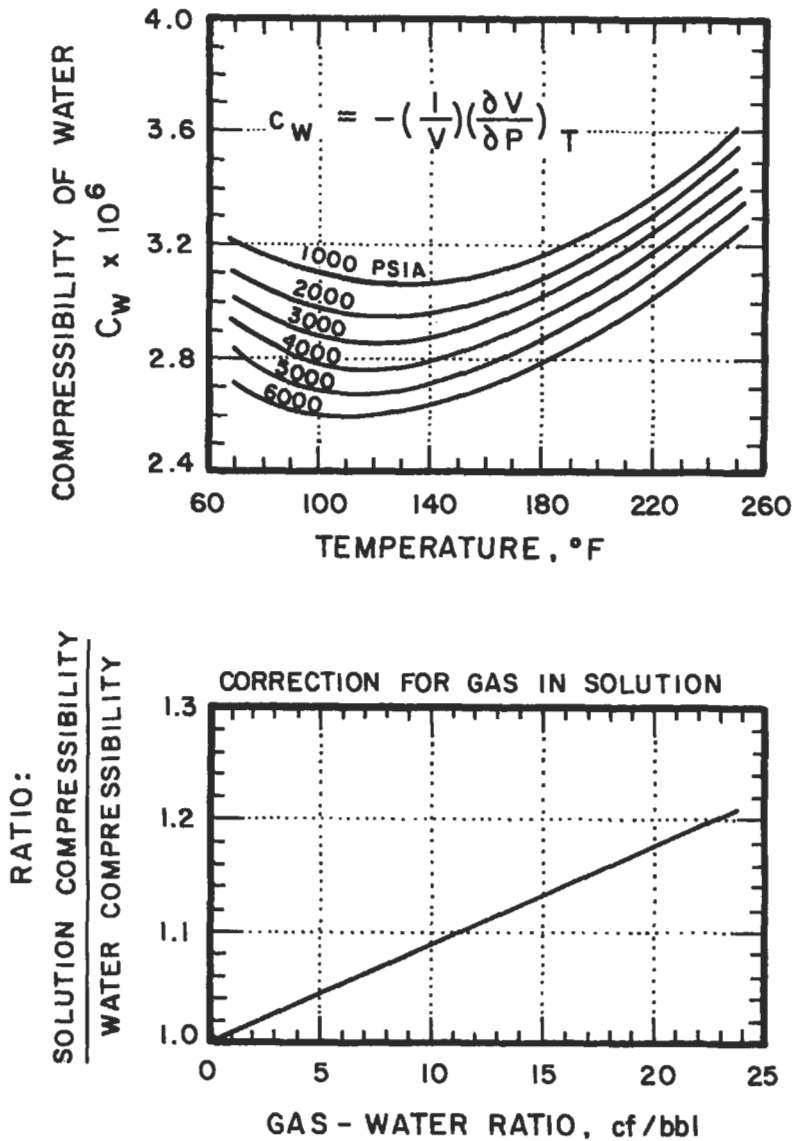


Figure 5-26. Effect of dissolved gas on the compressibility of water [22].

transmitted to empirical equations suitable for use with programmable calculators or personal computers. In some cases, improved empirical data have been presented recently. This section provides a number of the expressions available for computer use and also provides references for recent books devoted to programs for hand-held calculators. References to some of the software available for personal computers will be given.

Data from Figure 5-12 have been used to develop a correlation for water viscosity that can be used on programmable calculators [29]:

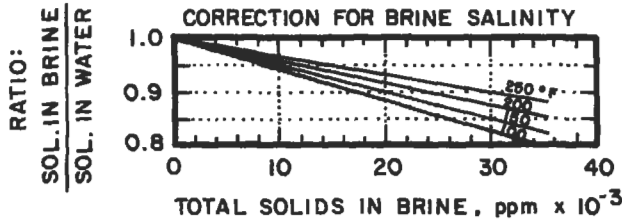
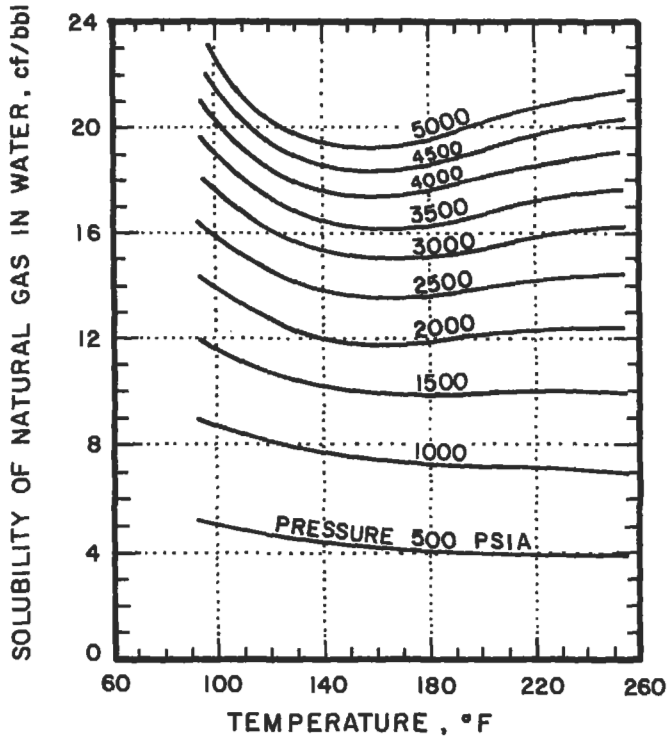


Figure 5-27. Solubility of natural gas in water [22].

$$\mu_w = \left(A + \frac{B}{T} \right) f_{pt} \tag{5-17}$$

where $A = -0.04518 + 0.009313 (\%NaCl) - 0.000393 (\%NaCl)^2$

$B = 70.634 + 0.09576 (\%NaCl)^2$

$T = \text{temperature, } ^\circ F$

$f_{pt} = 1 + [3.5 \text{ E} - 12 \text{ p}^2 (T - 40)]$

The correlation should only be used as an estimate and applies for pressures less than 10,000 psi, salinity less than 26% NaCl, and in a temperature range of 60° to 400°F.

In 1977, Standing's classic work [2] was reprinted [30] by the Society of Petroleum Engineers and an appendix was added by Standing that provides equations for several of the charts in the original work. Most of the equations were developed by simple curve fitting procedures. Some equations were based on computer solutions by other individuals; details of this will not be presented here and the reader is referred to Appendix 2 of Reference 30. Gas viscosity can be estimated from the correlations of Carr, Kobayashi, and Burrows [31] (the basis of Figures 5-6 and 5-7); first the atmospheric value of gas gravity at reservoir temperature, estimated from gravity and nonhydrocarbon content:

$$\mu_1 = (\mu_1 \text{ uncorrected}) + (\text{N}_2 \text{ correction}) + (\text{CO}_2 \text{ correction}) + (\text{H}_2\text{S correction}) \tag{5-18}$$

where $(\mu_1 \text{ uncorrected}) = [1.709(10^{-5}) - 2.062(10^{-6})\gamma_g]T + 8.188(10^{-3}) - 6.15(10^{-3}) \log \gamma_g$
 $(\text{N}_2 \text{ correction}) = y_{\text{N}_2}[8.48(10^{-3}) \log \gamma_g + 9.59(10^{-3})]$
 $(\text{CO}_2 \text{ correction}) = y_{\text{CO}_2}[9.08(10^{-3}) \log \gamma_g + 6.24(10^{-3})]$
 $(\text{H}_2\text{S correction}) = y_{\text{H}_2\text{S}}[8.49(10^{-3}) \log \gamma_g + 3.73(10^{-3})]$

is adjusted to reservoir conditions by a factor based on reduced temperature and pressure:

$$\ln \left[\left(\frac{\mu_g}{\mu_1} \right) (T_{pr}) \right] = a_0 + a_1 P_{pr} + a_2 P_{pr}^2 + a_3 P_{pr}^3 + T_{pr} (a_4 + a_5 P_{pr} + a_6 P_{pr}^2 + a_7 P_{pr}^3) + T_{pr}^2 (a_8 + a_9 P_{pr} + a_{10} P_{pr}^2 + a_{11} P_{pr}^3) + T_{pr}^3 (a_{12} + a_{13} P_{pr} + a_{14} P_{pr}^2 + a_{15} P_{pr}^3) \tag{5-19}$$

where $a_0 = - 2.462 \ 118 \ 20\text{E} - 00$	$a_8 = - 7.933 \ 856 \ 84\text{E} - 01$
$a_1 = 2.970 \ 547 \ 14\text{E} - 00$	$a_9 = 1.396 \ 433 \ 06\text{E} - 00$
$a_2 = - 2.862 \ 640 \ 54\text{E} - 01$	$a_{10} = - 1.491 \ 449 \ 25\text{E} - 01$
$a_3 = 8.054 \ 205 \ 22\text{E} - 03$	$a_{11} = 4.410 \ 155 \ 12\text{E} - 03$
$a_4 = 2.808 \ 609 \ 49\text{E} - 00$	$a_{12} = 8.393 \ 871 \ 78\text{E} - 02$
$a_5 = - 3.498 \ 033 \ 05\text{E} - 00$	$a_{13} = - 1.864 \ 088 \ 48\text{E} - 01$
$a_6 = 3.603 \ 730 \ 20\text{E} - 01$	$a_{14} = 2.033 \ 678 \ 81\text{E} - 02$
$a_7 = - 1.044 \ 324 \ 13\text{E} - 02$	$a_{15} = - 6.095 \ 792 \ 63\text{E} - 04$
	$(= 0.00 \ 060 \ 957 \ 9263)$

A reasonable fit to Beal's correlation (Figure 8 of Reference 5) of gas-free or dead oil viscosity (which is not very precise) is given by Standing:

$$\mu_{od} = \left[0.32 + \frac{1.8(10^7)}{^\circ\text{API}^{4.53}} \right] \left(\frac{360}{T + 200} \right)^a \tag{5-20}$$

where $a = \text{antilog} \left(0.43 + \frac{8.33}{^\circ\text{API}} \right)$

32 Reservoir Engineering

The dead oil viscosity can then be adjusted for dissolved gas with the correlation by Chew and Connally [6] (Figure 5-10) for saturated oil:

$$\mu_{ob} = A(\mu_{od})^b \quad (5-21)$$

where A and b are functions of solution gas-oil ratio.

Fit of A and b values given in Table 3 of Reference 6 are

$$A = \text{antilog}\{R_s[2.2(10^{-7})R_s - 7.4(10^{-4})]\}$$

$$b = \frac{0.68}{10^{8.62}(10^{-5})R_s} + \frac{0.25}{10^{1.1}(10^{-3})R_s} + \frac{0.062}{10^{3.74}(10^{-3})R_s}$$

The equation for compressibility factors of natural gases (Figure 5-13) is:

$$Z = A + (1 - A)/e^B + C p_{pr}^D \quad (5-22)$$

where $A = 1.39(T_{pr} - 0.92)^{0.5} - 0.36T_{pr} - 0.101$

$$B = (0.62 - 0.23T_{pr})P_{pr} + \left[\frac{0.066}{(T_{pr} - 0.86)} - 0.037 \right] P_{pr}^2 + \frac{0.32}{10^9(T_{pr}^{-1})} P_{pr}^6$$

$$C = (0.132 - 0.32 \log T_{pr})$$

$$D = \text{antilog} (0.3106 - 0.49T_{pr} + 0.1824T_{pr}^2)$$

T_{pr} is the dimensionless pseudo-reduced temperature, and p_{pr} is the dimensionless pseudo-reduced pressure. The relationship between formation volume factor of bubble-point liquids and gas-oil ratio, dissolved gas gravity, API oil gravity, and temperature (Figure 5-3) is [30]:

$$B_{ob} = 0.9759 + 12 (10^{-5})(CN)B_{ob} \quad (5-23)$$

$$\text{where } (CN)_{B_{ob}} = R_s \left(\frac{\gamma_g}{\gamma_o} \right)^{0.5} + 1.25T$$

where $(CN)_{B_{ob}}$ = bubble-point formation volume factor correlating number

R_s = solution gas-oil ratio in ft³/bbl

γ_g = gas gravity (air = 1)

γ_o = oil specific gravity (water = 1)

T = temperature in °F

The correlation of bubble-point pressure with dissolved gas-oil ratio, dissolved gas gravity, API oil gravity, and temperature (Figure 5-2) is [30]:

$$P_b = 18.2[(CN)_{pb} - 1.4] \quad (5-24)$$

$$\text{where } (CN)_{pb} = \left(\frac{R_s}{\gamma_g} \right)^{0.83} [10^{(0.00091T - 0.125^\circ \text{API})}]$$

where $(CN)_{pb}$ is the bubble-point pressure correlating number and the other terms have been previously defined.

Standing also presents equations for; density correction for compressibility of liquids; density correction for thermal expansion of liquids; apparent liquid densities of natural gases; effect of condensate volume on the ratio of surface gas gravity to well fluid gravity; pseudo-critical constants of gases and condensate fluids; pseudo-liquid density of systems containing methane and ethane; and pseudo-critical temperatures and pressures for heptane and heavier.

Beggs and Robinson [7] recently collected PVT data and presented a better estimate of the dead oil viscosity as a function of temperature and oil specific gravity:

$$\mu_{OD} = 10^X - 1 \tag{5-25}$$

where μ_{OD} = viscosity in cp of the gas-free oil at temperature, T, and $X = yT^{-1.168}$, $y = 10^Z$, and $Z = 3.0324 - 0.02023 \gamma_o$, with T in °F and the oil gravity γ in °API. An expression was also given for the saturated oil viscosity, μ , or live oil below the bubblepoint which results from a linear relationship between $\log \mu_{OD}$ and $\log \mu$ for a given value of dissolved gas, R_s :

$$\mu = A \mu_{OD}^B \tag{5-26}$$

where $A = 10.715 (R_s + 100)^{-0.515}$
 $B = 5.44(R_s + 150)^{-0.958}$
 $R_s = \text{scf/STB}$

In the first book specifically for hand-held calculators, Hollo and Fifadara [32] presented programs for estimating gas deviation factor (based on data of Standing and Katz):

$$Z = 1 + (A_1 + A_2/T_R + A_3/T_R^3)\rho R + (A_4 + A_5/T_R)\rho R^2 + A_6\rho R^2/T_R^3 \tag{5-27}$$

where $\rho R = 0.27 P_R/ZT_R$ $T_R = T/T_C$ $P_R = P/P_C$
 $A_1 = 0.31506$ $A_2 = - 1.0467$ $A_3 = - 0.5783$
 $A_4 = 0.5353$ $A_5 = - 0.6123$ $A_6 = 0.6815$

A program was also presented to calculate the single-phase formation volume factor using the correlation developed by Standing:

$$B_o = 0.972 + \frac{1.47}{10^4} \left[(R_s) \left(\frac{\gamma_g}{\gamma_o} \right)^{0.5} + 1.25T \right]^{1.175} \tag{5-28}$$

where γ_g = solution gas specific gravity
 γ_o = stock tank oil specific gravity (141.5/131.5 + °API)
 T = temperature, °F
 R_s = solution gas-oil ratio, scf/STB
 B_o = single-phase formation volume factor, RB/STB
 $^\circ\text{API}$ = stock tank oil gravity, °API

In 1980 Vazquez and Beggs [33] published improved empirical correlations for some of the commonly required crude oil PVT properties. Their study utilized a much larger database than was used in previous work so the results

are applicable to a wider range of oil properties. The empirical correlations, presented as a function of gas specific gravity, oil API gravity, reservoir temperature, and pressure, are particularly convenient to use with hand-held calculators. Gas gravity was found to be a strong correlating parameter. Since gas gravity depends on gas-oil separation conditions, Vazquez and Beggs chose 100 psig as a reference pressure, which resulted in a minimum oil shrinkage for the separator tests available. Thus, gas gravity must first be corrected to the value that would result from separation at 100 psig:

$$\gamma_g = \gamma_{gp} [1 + 5.912 \times 10^{-5}(\gamma_o)(T)\log(p/114.7)] \quad (5-29)$$

where γ_g = gas gravity (air = 1) that would result from separator conditions of 100 psig

γ_{gp} = gas gravity obtained at separator conditions of p and T
 p = actual separator pressure, psia
 T = actual separator temperature, °F
 γ_o = oil gravity, °API

For both dissolved gas and oil formation volume factor, improved correlations were obtained when the measured data were divided into two groups, with the division made at an oil gravity of 30°API. The expression for dissolved gas was presented:

$$R_s = C_1 \gamma_g p^{C_2} \exp\{C_3[\gamma_o/(T + 460)]\} \quad (5-30)$$

Values for the coefficients are as follows.

Coefficient	$\gamma_o \leq 30$	$\gamma_o > 30$
C_1	0.0362	0.0178
C_2	1.0937	1.1870
C_3	25.7240	23.9310

For saturated oils (reservoir pressure less than bubblepoint), oil formation volume factor was expressed as:

$$B_o = 1 + C_1 R_s + C_2 (T - 60)(\gamma_o/\gamma_g) + C_3 R_s (T - 60)(\gamma_o/\gamma_g) \quad (5-31)$$

The values for the coefficients depend on oil gravity and are given by the following:

Coefficient	$\gamma_o \leq 30$	$\gamma_o > 30$
C_1	4.677×10^{-4}	4.670×10^{-4}
C_2	1.751×10^{-5}	1.100×10^{-5}
C_3	-1.811×10^{-8}	1.337×10^{-9}

Since the oil formation volume of an undersaturated crude depends on the isothermal compressibility of the liquid, the oil formation volume as pressure is increased above bubble-point pressure was calculated from:

$$B_o = B_{ob} \exp[c_o(p - p_b)] \quad (5-32)$$

The correlation for compressibility of oil was given as:

$$c_o = (a_1 + a_2 R_s + a_3 T + a_4 \gamma_{gs} + a_5 \gamma_o) / a_6 p \quad (5-33)$$

where

$$\begin{aligned} a_1 &= -1,433.0 \\ a_2 &= 5.0 \\ a_3 &= 17.2 \\ a_4 &= -1,180.0 \\ a_5 &= 12.61 \\ a_6 &= 105 \end{aligned}$$

Vazquez and Beggs also presented an equation for viscosity of undersaturated crude oils that used the correlations of Beggs and Robinson:

$$\mu_o = \mu_{ob}(p/p_b)^m \quad (5-34)$$

where

$$\begin{aligned} m &= C_1 p^{C_2} \exp(C_3 + C_4 p) \\ C_1 &= 2.6 \\ C_2 &= 1.187 \\ C_3 &= -11.513 \\ C_4 &= -8.98 \times 10^{-5} \end{aligned}$$

The improved correlations of Vazquez and Beggs were incorporated by Meehan in the development of programs for hand-held calculators. These programs were presented in a series of articles in the *Oil and Gas Journal* [34-35]. Reference 34 contains the programs for calculating gas gravity, dissolved gas-oil ratio, oil formation volume factor and oil compressibility. Reference 35 contains the program for calculating oil viscosity.

See References 36-40 for a list of books devoted to the use of programs for handheld calculators and personal computers.

Properties of Fluid-Containing Rocks

Porosity

The porosity, ϕ , is equal to the void volume of the rock divided by the bulk volume and is expressed as a percent or fraction of the total bulk volume of the rock. Oil-bearing sandstones have porosities which often range from 15% to 30%. Porosities of limestones and dolomites are usually lower.

Differentiation must be made between absolute and effective porosity. Absolute porosity is defined as the ratio of the total pore volume of the rock to the total bulk volume of the rock whereas effective porosity is defined as the ratio of the interconnected pore volume of the rock to the total bulk volume of the rock.

Factors affecting porosity are compactness, character and amount of cementation, shape and arrangement of grains, and uniformity of grain size or distribution.

In problems involving porosity calculations it is convenient to remember that a porosity of one percent is equivalent to the presence of 77.6 barrels of pore space in a total volume of one acre-foot of sand.

Pore Volume

The pore volume of a reservoir is the volume of the void space, that is, the porosity fraction times the bulk volume. In conventional units, the pore volume, V_p , in reservoir barrels is:

$$V_p = 7758 V_b \phi = 7,758 A h \phi \quad (5-35)$$

where V_b is the bulk volume in ac-ft. A is the area in ft², h is the reservoir thickness in ft. and ϕ is the porosity expressed as a fraction.

Permeability

The permeability of a rock is a measure of the ease with which fluids flow through the rock. It is denoted by the symbol k and commonly expressed in units of darcies. Typical sandstones in the United States have permeabilities ranging from 0.001 to a darcy or more, and for convenience the practical unit of permeability is the millidarcy which equals 0.001 darcy. Some other useful conversion factors are given in Table 5-6.

Absolute Permeability

If a porous system is completely saturated with a single fluid, the permeability is a rock property and not a property of the flowing fluid (with the exception of gases at low pressure). This permeability at 100% saturation of a single fluid is termed the absolute permeability.

Darcy Equation

The Darcy equation relates the apparent velocity, v , of a homogeneous fluid in a porous medium to the fluid viscosity, μ , and the pressure gradient, $\Delta p/L$:

$$v = -\frac{k\Delta p}{\mu L} \quad (5-36)$$

This equation states that the fluid velocity is proportional to the pressure gradient and inversely proportional to fluid viscosity. The negative sign indicates that pressure decreases in the L direction when the flow is taken to be positive. The flow rate, q , is understood to be positive during production and negative during injection. As shown in Table 5-6, the Darcy equation can be written as:

$$k = \frac{q\mu L}{A\Delta p} \quad (5-37)$$

Linear Flow. In the Darcy equation for linear displacement:

$$q = \frac{kA(\Delta p)}{\mu L} \quad (5-38)$$

where q = fluid flow rate, cm³/sec

A = cross-sectional area of rock perpendicular to flow, cm²

p = pressure difference (in atm) across the distance L parallel to flow direction, cm

μ = viscosity of fluid, cp

A rock has permeability of one darcy if it permits the flow of one cc per second of a one-phase fluid having viscosity of one centipoise under the pressure

Table 5-6
Permeability Conversion Factors

1 darcy = 1,000 millidarcies; 1 millidarcy = 0.001 darcy
= 0.9869233 μm^2 (1 md $\equiv 10^{-3}$ μm^2)

$$k = \frac{q\mu}{(A)(\Delta p/L)}$$

$$\begin{aligned} 1 \text{ darcy} &= \frac{(\text{cc/sec})(\text{cp})}{(\text{cm}^2)(\text{atm})/\text{cm}} \\ &= 9.869 \times 10^{-9} \text{ cm}^2 \\ &= 1.062 \times 10^{-11} \text{ ft}^2 \\ &= 1.127 \frac{[\text{bb}/(\text{day})](\text{cp})}{(\text{ft}^2)(\text{psi})/\text{ft}} \\ &= 9.869 \times 10^{-7} \frac{(\text{cc/sec})(\text{cp})}{\text{cm}^2 [\text{dyne}/(\text{cm}^2)(\text{cm})]} \\ &= 7.324 \times 10^{-5} \frac{[\text{ft}^3/(\text{sec})](\text{cp})}{(\text{ft}^2)(\text{psi})/\text{ft}} \\ &= 9.679 \times 10^{-4} \frac{[\text{ft}^3/(\text{sec})](\text{cp})}{(\text{cm}^2)(\text{cm water})/\text{cm}} \\ &= 1.424 \times 10^{-2} \frac{[\text{gal}/(\text{min})](\text{cp})}{(\text{ft}^2)(\text{ft water})/\text{ft}} \end{aligned}$$

From Reference 19.

gradient of one atmosphere per centimeter. For liquid flow in a linear porous system, the flow rate q in barrels per day is [20]:

$$q = \frac{1.127kA(p_e - p_w)}{\mu L} \quad (5-39)$$

where k is in darcies, A is in ft^2 , μ is in cp, L is in ft, and pressures are in psia. For laminar gas flow in a linear system [20]:

$$q = \frac{0.112kA(p_e^2 - p_w^2)}{\mu zTL} \quad (5-40)$$

where q is in Mscf/D, T is in $^{\circ}\text{R}$ ($^{\circ}\text{F} + 460$), z is the dimensionless compressibility factor, and the other terms are in units consistent with Equation 5-39.

Radial Flow. Production from or injection into a reservoir can be viewed as flow for a cylindrical region around the wellbore. For the steady-state radial flow of an incompressible fluid [19]:

$$q = \frac{2\pi kh(p_e - p_w)}{\mu \ln(r_e/r_w)} \quad (5-41)$$

where q = volume rate of flow, cc/sec

k = permeability, darcies

h = thickness, cm

μ = viscosity, cp

p_e = pressure at external boundary, atm

p_w = pressure at internal boundary, atm

r_e = radius to external boundary, cm

r_w = radius to internal boundary, cm

\ln = natural logarithm, base e

For the flow rate, q , in the barrels per day of a liquid [19]:

$$q = \frac{7.08kh(p_e - p_w)}{\mu \ln(r_e/r_w)} \quad (5-42)$$

where k is in darcies, h is in ft. pressures are in psia, μ is in cp, and the radii are in consistent units, usually feet. For the laminar flow of a gas in MscfD [20]:

$$q = \frac{0.703kh(p_e^2 - p_w^2)}{\mu z T \ln(r_e/r_w)} \quad (5-43)$$

where T is in $^{\circ}\text{R}$, z is the dimensionless compressibility factor, and the other terms are as defined in Equation 5-42.

Capacity

Flow capacity is the product of permeability and reservoir thickness expressed in md ft. Since the rate of flow is proportional to capacity, a 10-ft thick formation with a permeability of 100 md should have the same production as a 100-ft thick formation of 10 md, if all other conditions are equivalent.

Transmissibility

Transmissibility is flow capacity divided by viscosity or kh/μ with units of md ft/cp. An increase in either reservoir permeability or thickness or a decrease in fluid viscosity will improve transmissibility of the fluid in the porous system.

Resistivity and Electrical Conductivity

Electrical conductivity, the electrical analog of permeability, is the ability of a material to conduct an electrical current. With the exception of certain clay minerals, reservoir rocks are nonconductors of electricity. Crude oil and gas are also nonconductors. Water is a conductor if dissolved salts are present so the conduction of an electric current in reservoir rocks is due to the movement of dissolved ions in the brine that occupies the pore space. Conductivity varies directly with the ion concentration of the brine. Thus, the electrical properties of a reservoir rock depend on the fluids occupying the pores and the geometry of the pores.

Resistivity, which is the reciprocal of conductivity, defines the ability of a material to conduct electric current:

$$R = \frac{rA}{L} \quad (5-44)$$

where R is the resistivity in ohm-meters, r is the resistance in ohms, A is the cross-sectional area in m^2 , and L is the length of the conductor in meters. As seen in Figure 5-28, resistivity of water varies inversely with salinity and temperature [41].

During flow through a porous medium, the tortuous flow paths cause the flowing fluid to travel an effective length, L_e , that is longer than the measured length, L . Some authors have defined this tortuosity, τ , as (L_e/L) while $(L_e/L)^2$ has been used by others.

Formation Resistivity Factor

The formation resistivity factor, F_R , is the ratio of the resistivity of a porous medium that is completely saturated with an ionic brine solution divided by the resistivity of the brine:

$$F_R = \frac{R_o}{R_w} \quad (5-45)$$

where R_o is the resistivity (ability to impede the flow electric current) of a brine-saturated rock sample in ohm-m, R_w is the resistivity of the saturating brine in ohm-m, and F_R is dimensionless. The formation resistivity factor, which is always greater than one, is a function of the porosity of the rock (amount of brine), pore structure, and pore size distribution. Other variables that affect formation factor include composition of the rock and confining pressure (overburden).

Archie [42] proposed an empirical formula that indicated a power-law dependence of F_R on porosity:

$$F_R = \phi^{-m} \quad (5-46)$$

where ϕ is porosity and m is a constant (commonly called the cementation factor) related to the pore geometry. The constant, m , was the slope obtained from a plot of F_R vs. porosity on log-log paper. For consolidated, shale free sandstones, the value of m ranged from 1.8 to 2. For clean, unconsolidated sands, m was found to be 1.3, and Archie speculated that m might vary from 1.3 to 2 for loosely or partly consolidated sands. Equations 5-45 and 5-46 were also combined by Archie to give:

$$R_o = R_w \phi^{-m} \quad (5-47)$$

so that a reasonable estimate of F_R or R_o can be made if the slope, m , is obtained.

Several other correlations [43-55], mostly empirical, between formation factor and porosity have been reported in the literature and these are summarized in Table 5-7.

From an analysis of about 30 sandstone cores from a number of different reservoirs throughout the United States, Winsauer et al. [45] presented what is now known as the Humble relation:

$$F_R = 0.62\phi^{-2.15} \quad (5-48)$$

(text continued on page 42)

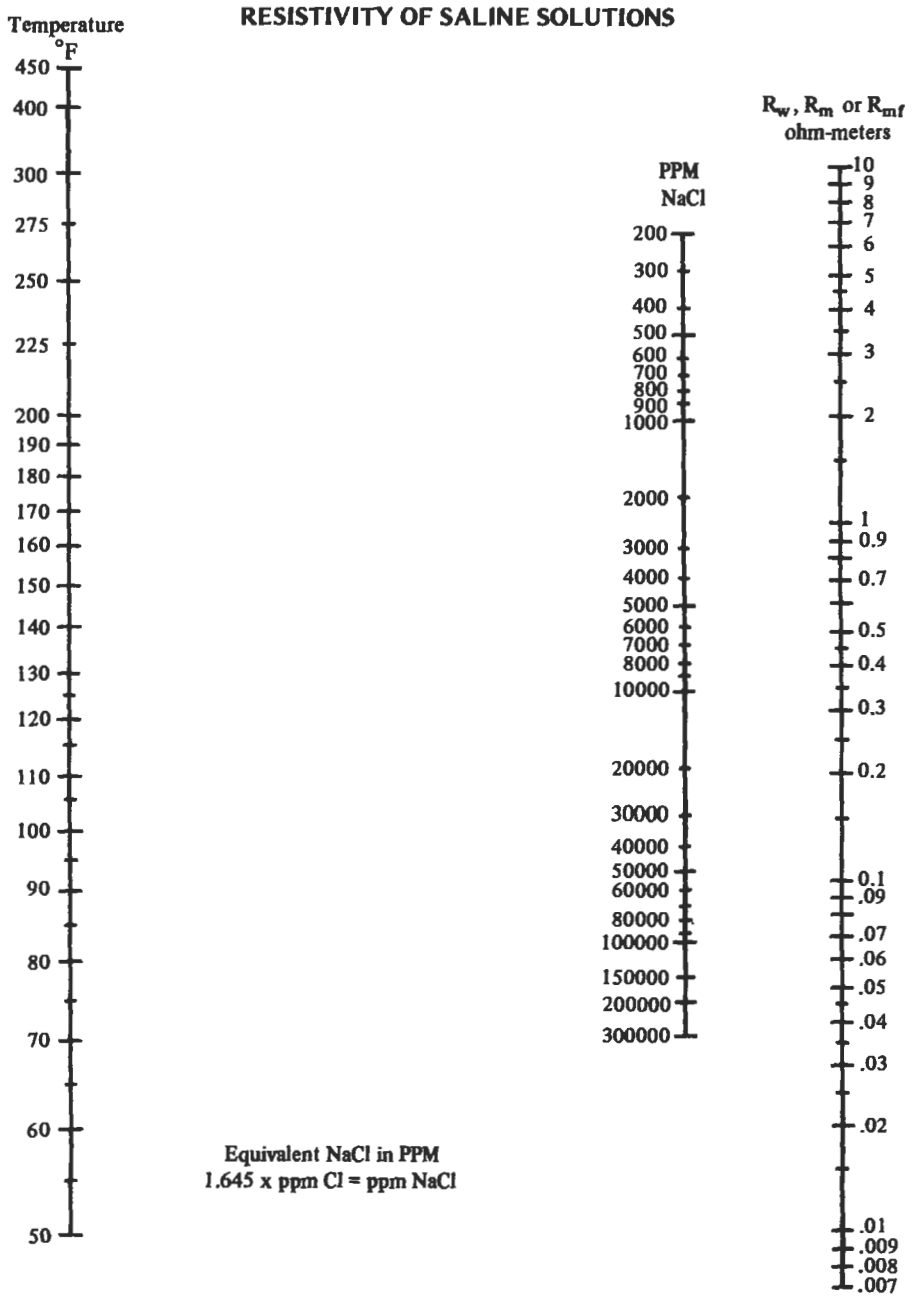


Figure 5-28. Resistivity of saline solutions [41].

Table 5-7
Correlations of Formation Resistivity Factor and Porosity

Source	Relation	Notes
Archie [42]	$F_R = \phi^{-m}$	For consolidated sands, $m = 1.8$ to 2.5. For unconsolidated sands, $m = 1.3$.
Wyllie and Rose [43]	$F_R = \frac{\tau^{V2}}{\phi}$	Tortuosity $\tau = L_o/L$
Tixier [44]	$F_R = \frac{1}{\phi^2}$	For limestone
Winsauer et al [45]	$F_R = \frac{\tau^2}{\phi}$	Theory
	$F_R = \frac{\tau^{1.67}}{\phi}$	Experimental (transport time of flowing ions)
	$F_R = 0.62 \phi^{-2.15}$	Sandstones containing varying amounts of clay
Wyllie/Gregory [46]	$F_R = a\phi^{-m}$	General form of Archie relation
Cornell and Katz [47]	$F_R = \frac{L_o^2}{\phi L}$	F_R directly proportional to length and inversely proportional to area
Owen [48]	$F_R = 0.68 \phi^{-2.23}$	Logs in dolomite, mud filtrate same resistivity as connate water
Hill and Milburn [49]	$F_R = 1.4\phi^{-1.78}$	Results of 450 sandstone and limestone cores with R_w of 0.01 ohm-m
	$F_R = \phi^{-1.93}$	When $a = 1$
Wyllie/Gardner [50]	$F_R = \frac{1}{\phi^2}$	Model of capillary bundle, for conducting wetting phase
Sweeney/Jennings [51]	$F_R = \phi^{-m}$	25 various carbonates
	$m = 1.57$	Water-wet
	$m = 1.92$	Intermediate wettability
	$m = 2.01$	Oil-wet
Carothers [52]	$F_R = 1.45 \phi^{-1.64}$	Sandstones
	$F_R = 0.85 \phi^{-2.14}$	Limestones
Porter/Carothers [53]	$F_R = 2.45 \phi^{-1.08}$	From California logs
	$F_R = 1.97 \phi^{-1.29}$	From Gulf Coast logs. All sandstones, $S_w = 100\%$
Timur [54]	$F_R = 1.13 \phi^{-1.73}$	Analysis of over 1,800 sandstone samples
Perez-Rosales [55]	$F_R = 1 + G(\phi^{-m} - 1)$	General theoretical relation
	$F_R = 1 + 1.03(\phi^{-1.73} - 1)$	Theoretical relation for sandstones

(text continued from page 39)

Wyllie and Gregory [46], citing their results and the results of Winsauer et al. [45], proposed that the data for consolidated porous media could be best described empirically by:

$$F_R = a\phi^{-m} \tag{5-49}$$

Results of a logging study in the Brown Dolomite formation, in which the resistivity of the mud filtrate was the same as the connate water, were used by Owen [48] to establish a relationship between the true formation factor and porosity. Shown in Figure 5-29 are the relationships obtained with the equations of Archie, Winsauer, et al., and Tixier.

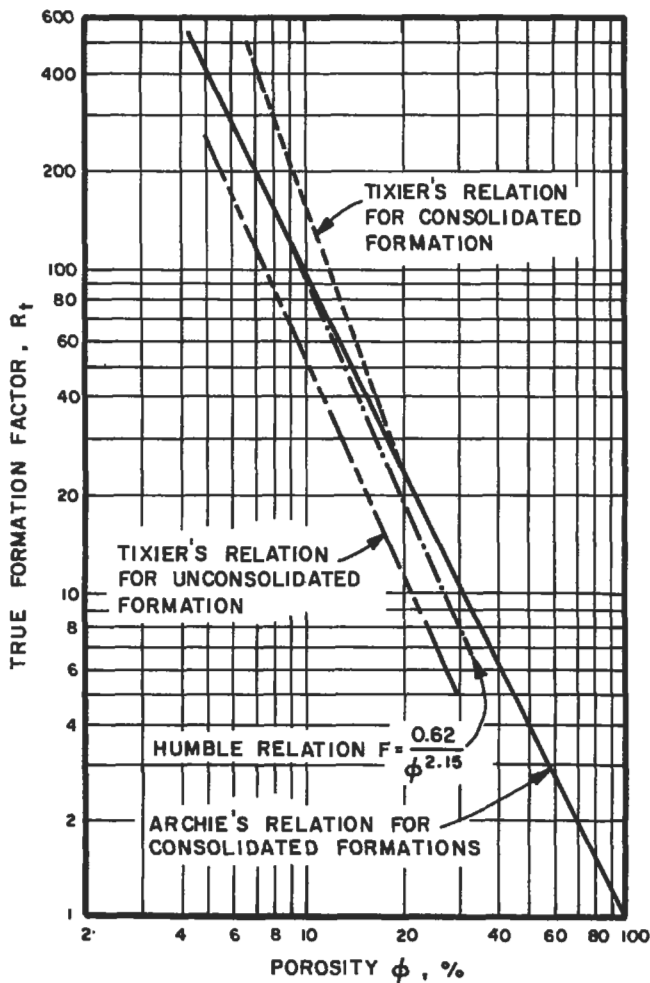


Figure 5-29. Formation factor vs. porosity from logs of Brown Dolomite formation [48].

Hill and Milburn [49] provided data from 450 core samples taken from six different sandstone formations and four different limestone reservoirs. The sandstone formations were described as ranging from clean to very shaly. The formation factor was determined at a water resistivity of 0.01 ohm-m since, at that value, the apparent formation factor approached the true formation factor when the rock contained low-resistivity water. From their data, the following equation was provided:

$$F_R = 1.4\phi^{-1.78} \quad (5-50)$$

An expression was also provided for the case in which the constant, a , in Equation 5-49 is taken as unity:

$$F_R = \phi^{-1.93} \quad (5-51)$$

Using 981 core samples (793 sandstone and 188 carbonate), Carothers [52] established a relationship for sands:

$$F_R = 1.45\phi^{-1.34} \quad (5-52)$$

and for limestones:

$$F_R = 0.85\phi^{-2.14} \quad (5-53)$$

As shown in Figure 5-30, a relationship was suggested for calcareous sands:

$$F_R = 1.45\phi^{-1.33} \quad (5-54)$$

and for shaly sands:

$$F_R = 1.65\phi^{-1.35} \quad (5-55)$$

Using these data, the nomograph in Figure 5-31 was constructed to solve the modified Archie expression (Equation 5-49) when it is desired to vary both constants.

Using 1,575 formation factors from California Pliocene well logs, Porter and Carothers [53] presented an in-situ relation:

$$F_R = 2.45\phi^{-1.08} \quad (5-56)$$

and a similar relation for 720 formation factors from Texas-Louisiana Gulf Coast logs:

$$F_R = 1.97\phi^{-1.29} \quad (5-57)$$

This investigation used well log data from sandstone formations known to have water saturations of 100%.

From an analysis of over 1,800 sandstone samples, Timur et al. [54] presented the following expression:

$$F_R = 1.13\phi^{-1.75} \quad (5-58)$$

(text continued on page 46)

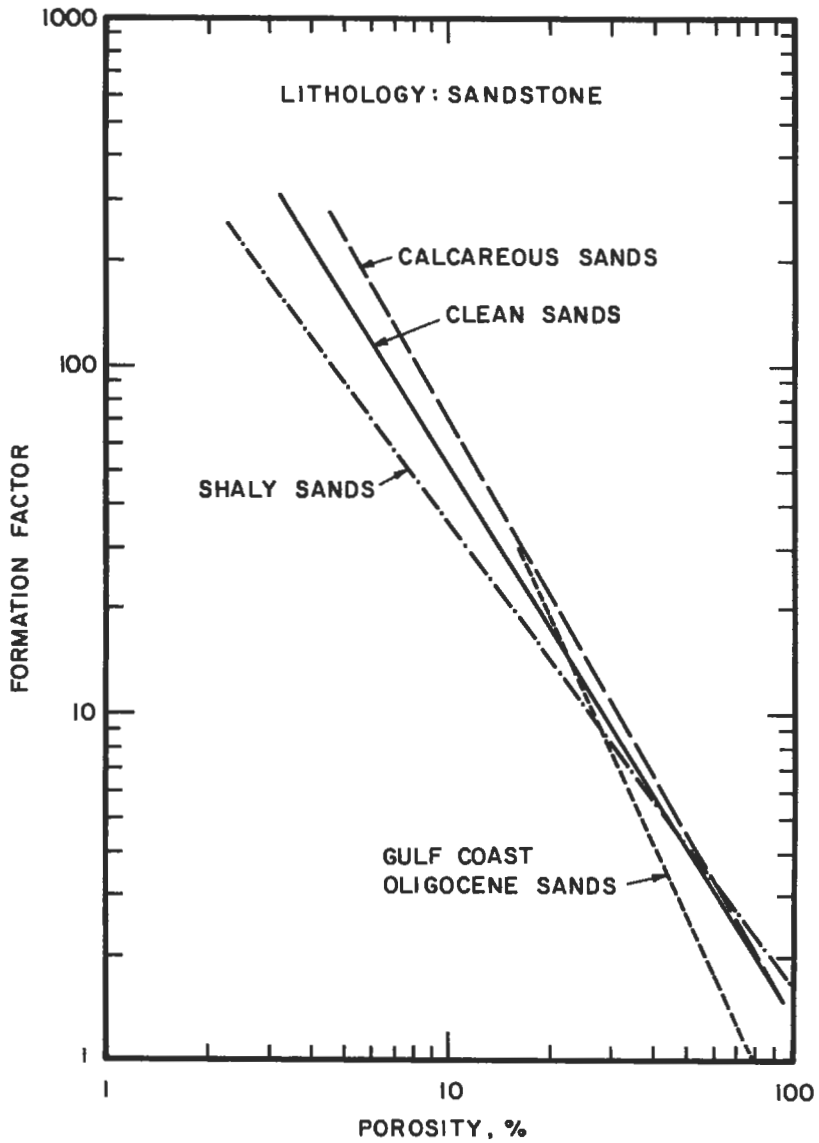


Figure 5-30. Formation factor vs. porosity for clean sands, shaly sands, and calcareous sands [52].

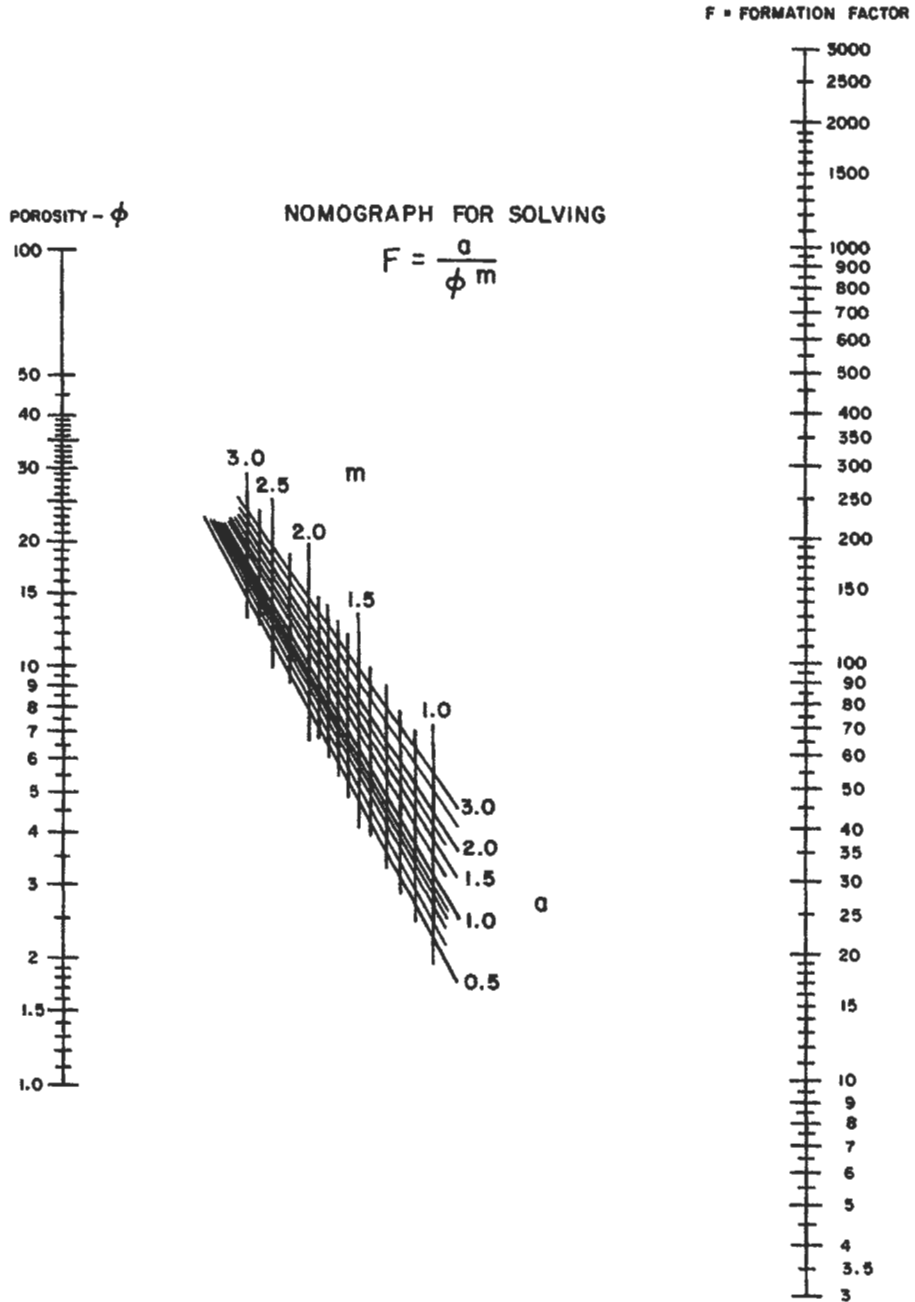


Figure 5-31. Nomograph for solving $F_R = a/\phi^m$ [52].

(text continued from page 43)

These samples included 569 core plugs (from Alaska, California, Louisiana, Colorado, Trinidad, Australia, and the Middle East) plus 28 samples from Winsauer et al. [45], 362 samples from Hill and Milburn [49], 788 from Carothers [52], and 85 samples from other sources [54].

In a recent paper [55], Perez-Rosales presented the following theoretical expression:

$$F_R = 1 + G(\phi^m - 1) \quad (5-59)$$

and a generalized equation for sandstones:

$$F_R = 1 + 1.03(\phi^{-1.73} - 1) \quad (5-60)$$

Perez-Rosales notes that the previous expressions are fundamentally incorrect since they do not satisfy the requirement that $F_R = 1$ when $\phi = 1$. A graphical comparison of expressions, provided by Perez-Rosales, is shown in Figure 5-32 for Equations 5-48, 5-58, and 5-60. In porosity ranges of practical interest, the three expressions yield similar results.

Coates and Dumanoir [56] listed values for the cementation exponent of the Archie equation for 36 different formations in the United States. These data are presented in the following section under "Resistivity Ratio."

In the absence of laboratory data, different opinions have existed regarding the appropriate empirical relationship. Some authors [57] felt that the Archie equation (Equation 5-46) with $m = 2$ or the Humble equation (Equation 5-48) yields results satisfactory for most engineering purposes, but Equation 5-50 may be more valid (these authors point out that the relationship used should be based on independent observations of interest). Another opinion was that, while the Humble relation is satisfactory for sucrosic rocks and the Archie equation with $m = 2$ is acceptable for chalky rocks, in the case of compact or oolitic rocks the cementation exponent in the Archie equation may vary from 2.2 to 2.5 [58]. Based on the more recent work of Timur et al. [54], it appears that Equation 5-58 may be more appropriate as a general expression for sandstones, if individual formation factor-porosity relationships are not available for specific cases.

Water in clay materials or ions in clay materials or shale act as a conductor of electrical current and are referred to as conductive solids. Results in Figure 5-33 show that clays contribute to rock conductivity if low-conductivity, fresh or brackish water is present [59,60]. The effect of clay on formation resistivity depends on the type, amount, and distribution of clay in the reservoir, as well as the water salinity. Values of m in Equation 5-49 for several clays are given in Table 5-8 [61].

Other variables that affect resistivity of natural reservoir rocks include overburden pressure and temperature during measurement. The value of the cementation exponent, m , is normally higher at overburden conditions [62], especially if porosity is low or with rocks that are not well-cemented. Thus, F_R increases with increasing pressure. Although the effect of temperature depends on clay content of the sample, F_R tends to increase with increasing temperature, but the effect is not as great as pressure [63,64]. At a fixed pressure, F_R may go through a minimum and then increase as temperature is increased; the combined increase of both temperature and pressure will cause an increase in F_R [64]. Factors that affect the exponent, m , and the coefficient, a , in the modified Archie expression (Equation 5-49) are summarized in Tables 5-9 and 5-10, respectively [65].

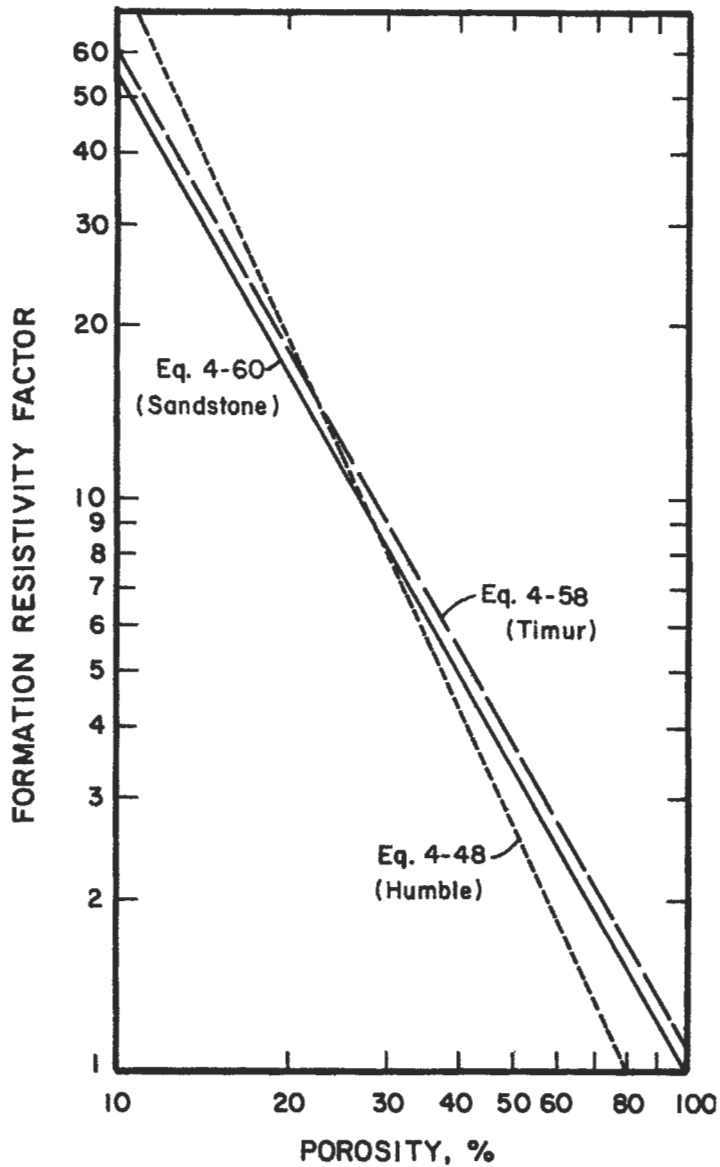


Figure 5-32. Graphical comparison of relationship between formation resistivity factor and porosity [55].

To summarize the general relationship between formation resistivity factor and porosity (refer to Equation 5-49), the normal range for the geometric term, a , is 0.6 to 1.4, and the range for the cementation exponent, m , is 1.7 to 2.5 for most consolidated reservoir rocks [62]. Since the exact values depend on pore geometry and composition of the rock, formation factors should be determined

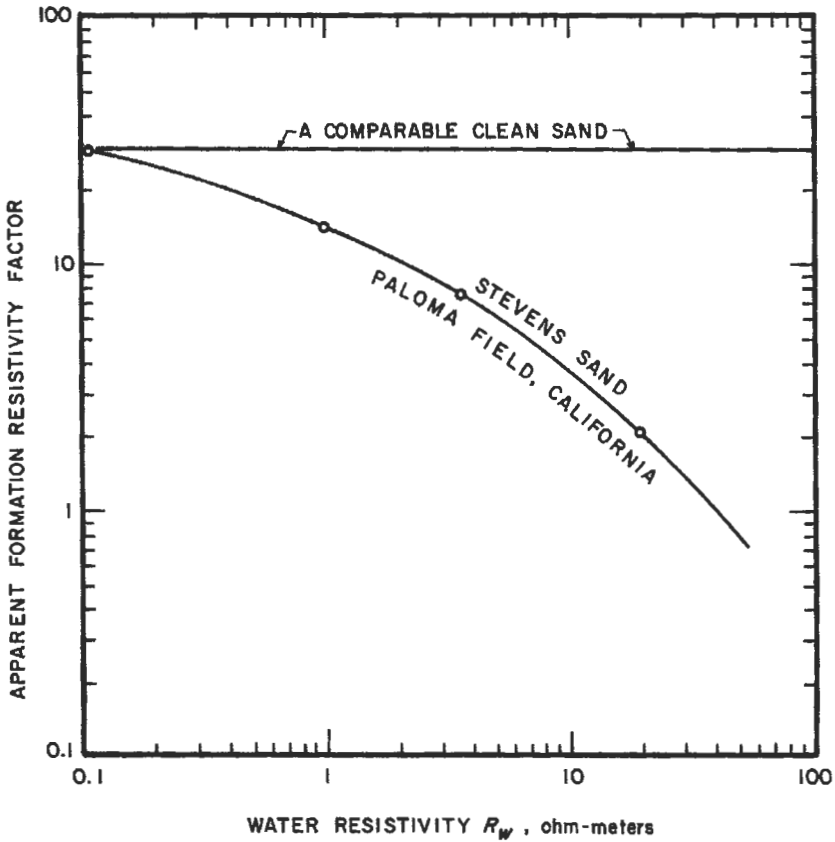


Figure 5-33. Effect of clays on formation resistivity factor [59,60].

with samples of the reservoir rock of interest, under the reservoir conditions of temperature and overburden pressure.

Based on core analyses of 793 sandstone and 188 carbonate samples, Carothers [52] observed different permeabilities and formation factors for samples from the same core even though porosity was identical. Furthermore, permeability generally decreased as formation factor increased. For permeabilities above 10 md, there appeared to be a relation between formation factor, permeability, and lithology. For sandstones, the general relationship was:

$$k = \frac{7 \times 10^8}{F_R^{4.5}} \tag{5-61}$$

and the relation for carbonates was:

$$k = \frac{4 \times 10^8}{F_R^{3.65}} \tag{5-62}$$

Carothers stated that more data are needed to confirm these observations. Any such relation should be used with caution.

Table 5-8
Values of Exponent in the Archie Equation for Clays

Mineral particle	Shape factor exponent
Sodium montmorillonite	3.28
Calcium montmorillonite	2.70
Muscovite	2.46
Attapulgitite	2.46
Illite	2.11
Kaolinite	1.87

From Reference 61

Table 5-9
Factors That Influence the m Exponent in Equation 5-49
for the Rock-Water Interface

1. Pore geometry.
 - a. Surface-area-to-volume ratio of the rock particle, angularity, sphericity.
 - b. Cementation.
 - c. Compaction.
 - d. Uniformity of mineral mixture.
2. Anisotropy.
3. Degree of electrical isolation by cementation.
4. The occurrence of an open fracture.

From Reference 65.

Table 5-10
Factors That Influence the a Coefficient In Equation 5-49

1. Surface conductance and ionic mobility occurring in water films adsorbed to solid surfaces.
 - a. The cation exchange capacity of particular solid materials.
 - b. The quantity of water adsorbed to clay particles in the rock framework or within the interstices.
2. Salinity of formation water.
3. Wettability relations between particular solid surfaces and hydrocarbons, as they influence cation exchange.
4. The presence and distribution of electrically conductive solid minerals.

From Reference 65.

Rock Compressibility

The isothermal rock compressibility is defined as the change in volume of the pore volume with respect to a change in pore pressure:

$$c_f = \frac{1}{V_p} \left(\frac{\partial V_p}{\partial p} \right)_T \quad (5-63)$$

where c_r is the formation (rock) compressibility with common units of psi^{-1} , V_p is pore volume, p is pressure in psi, and the subscript T denotes that the partial derivative is taken at constant temperature. The effective rock compressibility is considered a positive quantity that is additive to fluid compressibility; therefore, pore volume decreases as fluid pressure decreases [26,66]. Since overburden pressure of a reservoir is essentially constant, the differential pressure between the overburden pressure and the pore pressure will increase as the reservoir is depleted. Thus, porosity will decrease slightly, on the order of only one-half percent for a 1,000 psi change in internal fluid pressure [17]. For different reservoirs, porosities tend to decrease as overburden pressure (or depth) increases. Therefore, porosity under reservoir conditions may differ from values determined in the laboratory [67]. For sandstones with 15% to 30% porosity, reservoir porosity was found to be about 1% lower under reservoir conditions; for low porosity limestones, the difference was about 10% [68].

One of the commonly cited correlations between rock compressibility and porosity was developed by Hall [69] (Figure 5-34) for several sandstone and limestone reservoirs. All measurements were conducted with an external pressure of 3,000 psi and internal pressures from 0 to 1,500 psi. Fatt [67] found no correlation between compressibility and porosity, although the porosity range studied (10% to 15%) was very narrow. Van der Knapp [68], citing his measurements and those of Carpenter and Spencer [70], observed a general trend of increasing pore volume compressibility with decreasing porosity. For a particular limestone reservoir, Van der Knapp [68] found that pore compressibility and

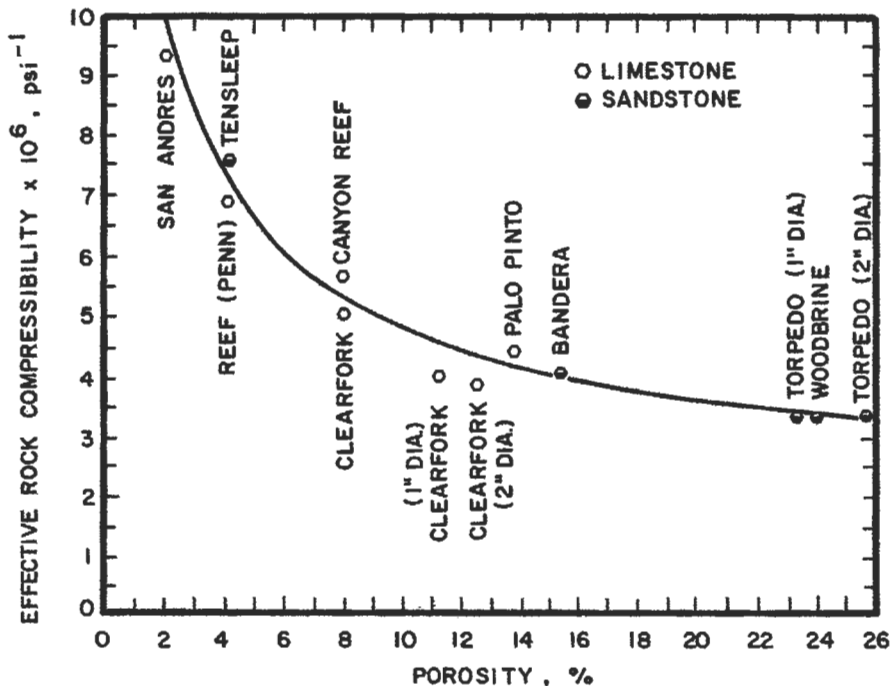


Figure 5-34. Effective rock compressibility vs. porosity [69].

porosity were related by a simple empirical formula. However, in a more extensive study, Newman [71] suggests that any correlation between pore volume compressibility and porosity does not apply to a wide range of reservoir rocks. As shown in Figure 5-35a, Newman's study in limestones showed poor agreement with the correlations of Hall and Van der Knapp. Figures 5-35b to 5-35d show

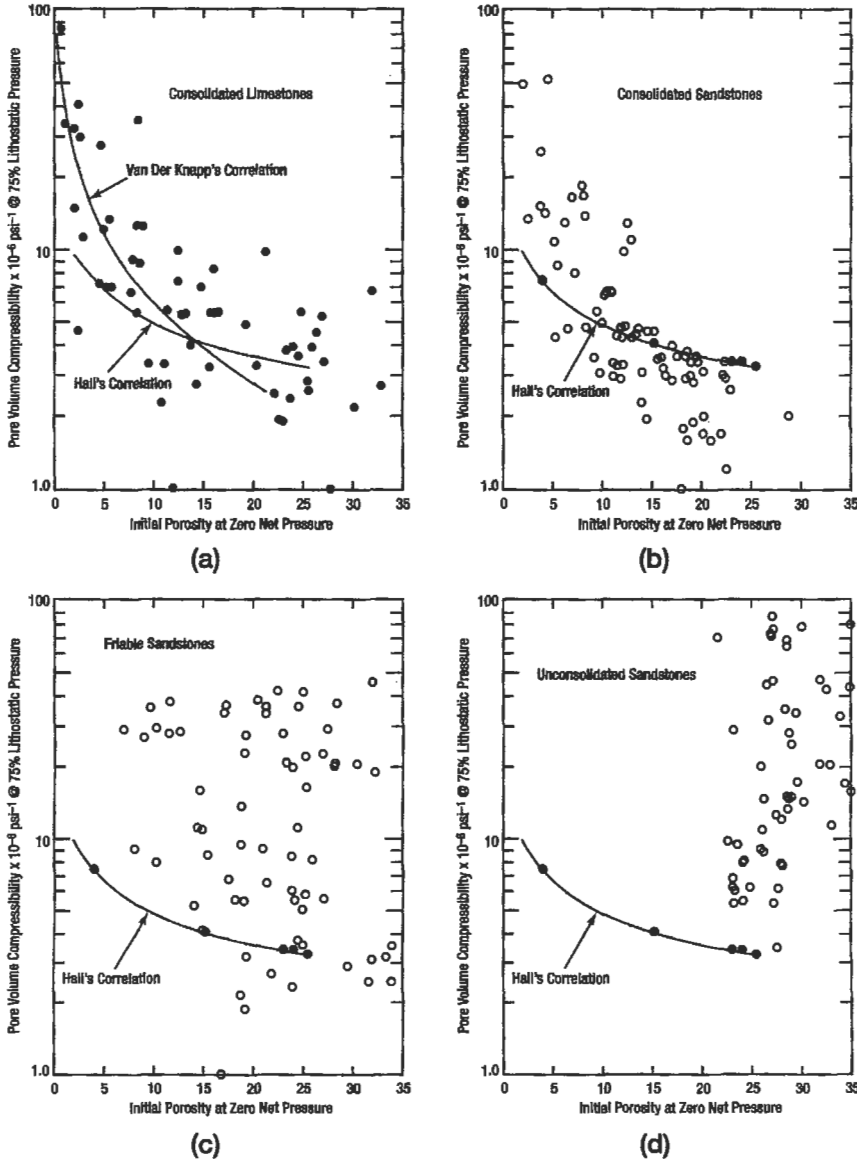


Figure 5-35. Pore-volume compressibility at 75% lithostatic pressure vs. sample porosity [71].

a comparison of Newman's data with Hall's correlation for consolidated sandstones, friable sandstones, and unconsolidated sandstones. While the general trend of Newman's data on consolidated sandstones (Figure 5-35b) is in the same direction as Hall's correlation, the agreement is again poor. Figure 5-35c shows no correlation for Newman's friable sandstones and Figure 5-35d for unconsolidated sandstones shows an opposite trend from the correlation presented by Hall. From Newman's data, ranges of compressibilities for various types of reservoir rocks are given in Table 5-11. Clearly, formation compressibility should be measured with samples from the reservoir of interest.

Table 5-11
Range of Formation Compressibilities

Formation	Pore volume compressibility, psi^{-1}
Consolidated sandstones	1.5×10^{-6} to 20×10^{-6}
Consolidated limestones	2.0×10^{-6} to 35×10^{-6}
Friable sandstones	2.5×10^{-6} to 45×10^{-6}
Unconsolidated sandstones	5.5×10^{-6} to 85×10^{-6}

From Reference 71.

Properties of Rocks Containing Multiple Fluids

Total Reservoir Compressibility

The total compressibility of oil- or gas-bearing reservoirs represents the combined compressibilities of oil, gas, water, and reservoir rock in terms of volumetric weighting of the phase saturations:

$$c_t = c_o S_o + c_w S_w + c_g S_g + c_f \quad (5-64)$$

where c_t is the total system isothermal compressibility in vol/vol/psi , c_o , c_w , c_g , and c_f are the compressibilities in psi^{-1} of oil, water, gas, and rock (pore volume), respectively, S is fluid saturation, and the subscripts o , w , and g refer to oil, water, and gas, respectively.

Based on the treatment by Martin [72], Ramey [26] has expressed volumes in terms of formation volume factors with consideration for gas solubility effects:

$$c_t = S_o \left[\frac{B_g}{B_o} \left(\frac{\partial R_s}{\partial p} \right) - \frac{1}{B_o} \left(\frac{\partial B_o}{\partial p} \right) \right] + S_w \left[\frac{B_g}{B_w} \left(\frac{\partial R_{sw}}{\partial p} \right) - \frac{1}{B_w} \left(\frac{\partial B_w}{\partial p} \right) \right] + S_g \left[- \frac{1}{B_g} \left(\frac{\partial B_g}{\partial p} \right) \right] + c_f \quad (5-65)$$

where p is pressure in psi , R_s is the solubility of gas in oil in scf/STB oil , R_{sw} is the solubility of gas in water in scf/STB water , and B_g , B_o , and B_w are the formation volume factors of gas, oil, and water, respectively.

Fluid and rock compressibilities have been discussed in prior sections of this chapter. Table 5-12 provides a summary of these data.

Table 5-12
Summary of Compressibility Values

	Compressibility, psi^{-1}	
	Range	Typical value
Consolidated rock*	2×10^{-6} to 7×10^{-6}	3×10^{-6}
Oil [17, 73]	5×10^{-6} to 100×10^{-6}	10×10^{-6}
Water (gas-free) [26]	2×10^{-6} to 4×10^{-6}	3×10^{-6}

	Compressibility, psi^{-1}	
	At 1,000 psi	At 5,000 psi
Gas [26]	$1,000 \times 10^{-6}$	100×10^{-6}
Water (with dissolved gas) [26]	15×10^{-6}	5×10^{-6}

* See Figure 5-35 (for most of samples having porosities of $20 \pm 10\%$ in Figures 5-35a and 5-35b).

The rock compressibilities in Table 5-12 represent a majority of the consolidated sandstone and limestone data from Newman [71] that have porosities in the range of 10% to 30%. Oil compressibility increases as a function of increasing API gravity, quantity of solution gas, or temperature [17]. As pointed out by Ramey [26], when the magnitude of water compressibility is important, the effect of solution gas in the water will be more important. Clearly, the magnitude of gas compressibility will dominate the total system compressibility if gas saturations are high.

In many gas reservoirs, only the gas terms in Equation 5-64 may be significant so that the total system compressibility becomes [26]:

$$c_t = c_g S_g \quad (5-66)$$

In certain cases of high pressure and high water saturation, rock and water compressibility may be significant so that Equation 5-65 must be used [26].

In oil reservoirs, gas saturations may be low and, even though gas compressibility is much larger than the other compressibilities, each term in Equation 5-64 or 5-65 should normally be considered [26]. In some cases, not all of the compressibility terms will be important. For example, if reservoir pressure is above the saturation pressure, the gas saturation will be zero [20]. However, if the gas saturation exceeds 2% or 3%, the gas compressibility term dominates the total system compressibility and the other terms become insignificant [20].

Resistivity Index

Since crude oil and natural gas are nonconductors of electricity, their presence in reservoir rock increases resistivity. The resistivity index or ratio, I , is commonly used to characterize reservoir rocks that are partially saturated with water and also contain oil and/or gas:

$$I = \frac{R_t}{R_o} \quad (5-67)$$

where R_t is the resistivity of the rock at some condition of partial water saturation, S_w , and R_o is the resistivity of the rock when completely saturated with water or brine.

Citing the work of Martin et al. [74], Jakosky and Hopper [75], Wyckoff and Botset [76], and Leverett [77], in which the variation in resistivity with water saturation was studied, Archie [42] plotted the resistivity ratio versus S_w on log-log paper (see Figure 5-36). For water saturations down to about 0.15 or 0.20, the following approximate equation appeared to hold, regardless of whether oil or gas was the nonconducting fluid:

$$S_w = \left(\frac{R_o}{R_t} \right)^{1/n} \tag{5-68}$$

where n has been commonly referred to as the saturation exponent. For clean sands and for consolidated sandstones, the value of n was close to 2.0, so the approximate relation was given by Archie as:

$$S_w = \left(\frac{R_o}{R_t} \right)^{1/2} \tag{5-69}$$

By substituting the equation for R_o (refer to Equation 5-47), Archie presented the relationship between water saturation, formation resistivity factor, brine resistivity, and the resistivity of the rock at the given S_w :

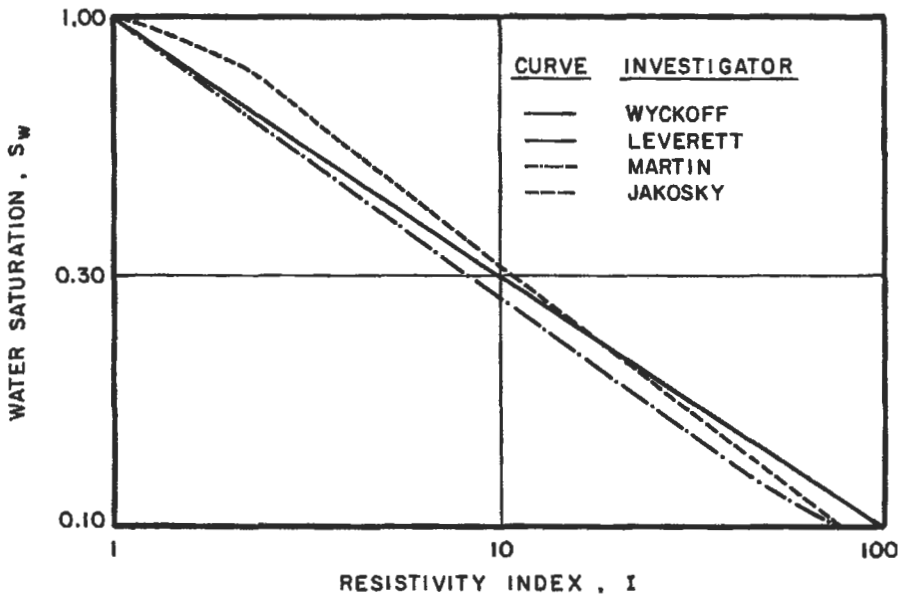


Figure 5-36. Variation of resistivity index with water saturation [42].

$$S_w = \left(\frac{F_R R_w}{R_t} \right)^{1/2} \tag{5-70}$$

The more general form of Equation 5-70, commonly used, is:

$$S_w = \left(\frac{F_R R_w}{R_t} \right)^{1/n} = \left(\frac{R_w \phi^{-m}}{R_t} \right)^{1/n} \tag{5-71}$$

An even more general form recognizes that the constant, a, in Equation 5-49 is not necessarily unity:

$$S_w = \left(\frac{a R_w}{\phi^m R_t} \right)^{1/n} \tag{5-72}$$

The foregoing equations are close approximations in clean formations having a regular distribution of porosity. The accuracy of the equations will not be as good in formations with vugs or fractures.

As shown in Figure 5-37, Patnode and Wyllie [59] found that the presence of clays affected the relationship between water saturation and resistivity index.

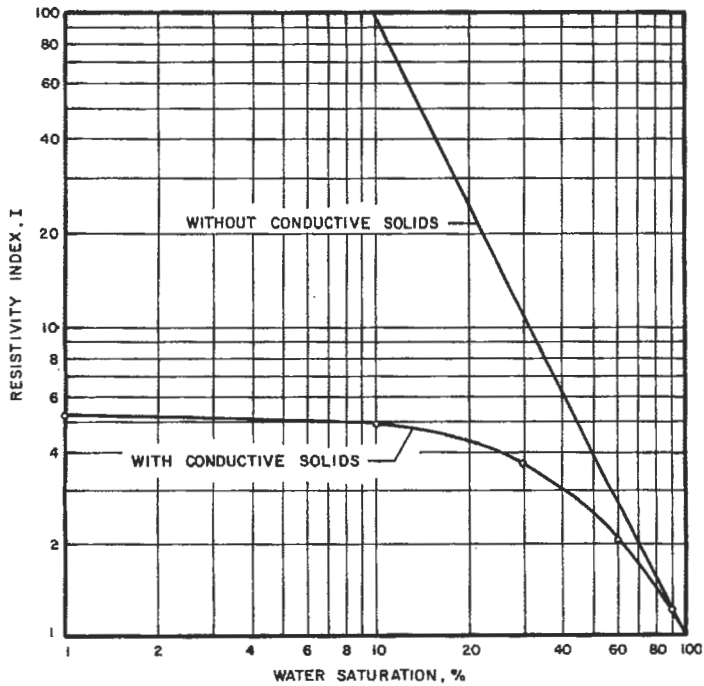


Figure 5-37. Effect of conductive solids on the relationship between resistivity index and water saturation [59].

As the water saturation is reduced toward zero, the resistivity approaches that of the clays rather than approaching infinity as with clean sands. Relationships between resistivities and fluid content in the presence of conductive solids have been presented in the literature [78,79].

Early investigations, using data from the Woodbine sand of east Texas, suggested that the saturation exponent, n , may range from 2.3 to 2.7 [80,81]. Wyllie and Spangler [82] presented data (see Figure 5-38) for several natural and synthetic porous media that showed a variation of the saturation exponent from 1.4 to 2.5. Other investigators found that the distribution of fluids within the core sample, at the same water saturation, could affect the resistivity index for both sandstones [83] and for limestones [84]. The exponent, n , was also found to vary depending upon the manner in which the conducting wetting phase saturation was varied [82,85].

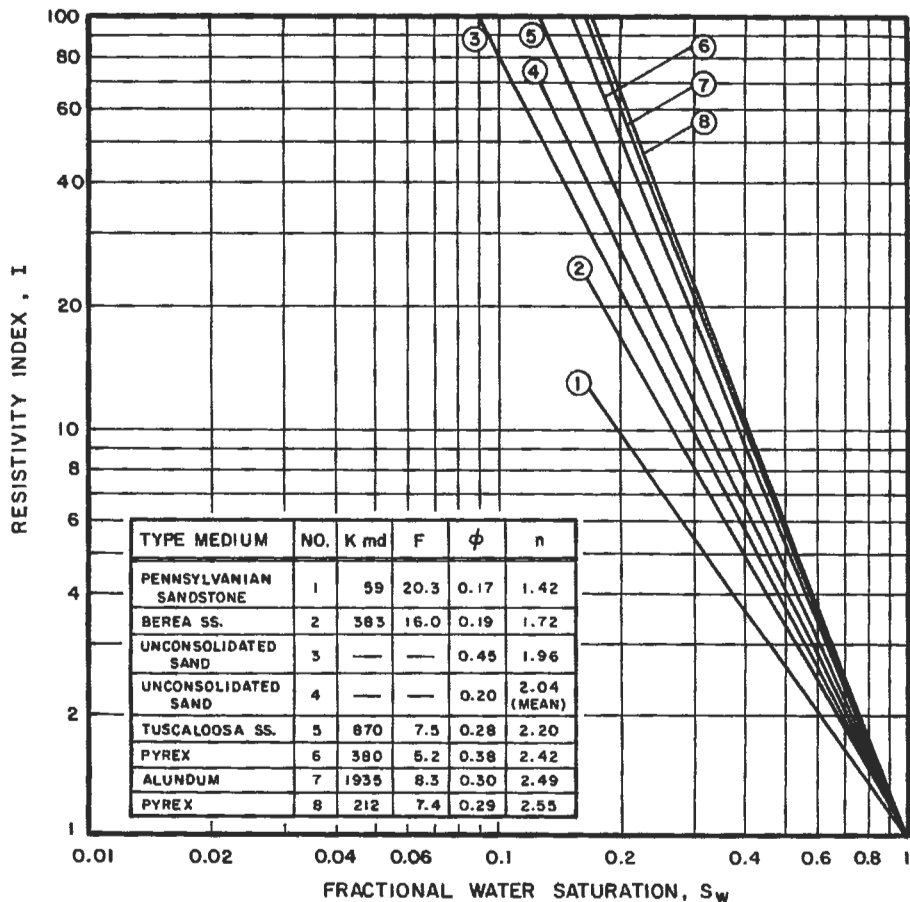


Figure 5-38. Relationship between resistivity index and water saturation for several media [82].

Data [56] from a number of different reservoirs for the values of m , the cementation or shape factor, and n , the saturation exponent, in Equation 5-71 are presented in Table 5-13.

Based on these data and other reasoning, Coats and Dumanoir [56] have proposed that the two exponents, m and n , can be assumed to be equal for water-wet, consolidated reservoirs. Ransome [65] has proposed that the saturation exponent may be a special case of the porosity exponent, and the two exponents may bear certain similarities but not necessarily the same value.

As recently pointed out by Dorfman [86], data in Table 5-13 strongly suggest that assuming a saturation exponent of 2 can result in serious errors in the

Table 5-13
Values of Constants in Equation 5-71

	Lithology	Avg. m	Avg. n
Ordovician Simpson, W. Texas and E. New Mexico	SS	1.6	1.6
Permian, W. Texas	SS	1.8	1.9
Ellenburger, W. Texas	LS and Dol.	2.0	3.8
Pennsylvanian, W. Texas	LS	1.9	1.8
Viola, Bowle Field, No. Texas	LS	1.77	1.15
Edwards, So. Texas	LS	2.0	2.8
Edwards Lime, Darst Creek, So. Texas	LS	1.94, 2.02	2.04, 2.08
Frio, So. Texas	SS	1.8	1.8
Frio, Agua Dulce, So. Texas	SS	1.71	1.66
Frio, Edinburgh, So. Texas	SS	1.82	1.47, 1.52
Frio, Hollow Tree, So. Texas	SS	1.80, 1.87	1.64, 1.69
Government Wells, So. Texas	SS	1.7	1.9
Jackson, Cole Sd., So. Texas	SS	2.01	1.66
Miocene, So. Texas	Cons. SS	1.95	2.1
	Uncons. SS	1.6	2.1
Navarro, Olmos, Delmonte, So. Texas	SS	1.89	1.49
Rodessa, E. Texas	LS	2.0	1.6
Woodbine, E. Texas	SS	2.0	2.5
Travis Peak and Cotton Valley, E. Texas and W. Louisiana	HD. SS	1.8	1.7
Wilcox, Gulf Coast	SS	1.9	1.8
Annona, No. Louisiana	Chalk	2.0	1.5
Cockfield, So. Louisiana	SS	1.8	2.1
Frio, Chocolate Bayou, Louisiana	SS	1.55-1.94	1.73-2.22
Sparta, So. Louisiana (Opelousas)	SS	1.9	1.6
Nacatoch, Arkansas	SS	1.9	1.3
Pennsylvanian, Oklahoma	SS	1.8	1.8
Bartlesville, Kansas	SS	2.0	1.9
Simpson, Kansas	SS	1.75	1.3
Muddy, Nebraska	SS	1.7	2.0
Lakota Sd., Crook Co., Wyoming	SS	1.52	1.28
Madison, No. Dakota	LS	1.9	1.7
Mississippian, Illinois	LS	1.9	2.0
Mississippian, Illinois	SS	1.8	1.9

After Reference 56.

estimation of water saturation. In low-porosity formations, such as the Cotton Valley sandstone, the saturation was found to vary greatly from the value of 2 [87]. If n is always assumed to be 2, Dorfman contends that many hydrocarbon zones will be overlooked and many water-producing zones could be tested. As related by Hilchie [88], most of the values for the saturation exponent have been obtained at atmospheric conditions and there is the need to obtain laboratory measurements under simulated reservoir pressure and temperature. At atmospheric pressure, the percentage of smaller pores is larger than at reservoir pressure [64], which results in the wrong saturation exponent and a higher value of water saturation [88].

Surface and Interfacial Tensions

The term interface indicates a boundary or dividing line between two immiscible phases. Types of interfaces include: liquid-gas, liquid-liquid, liquid-solid, solid-gas, and solid-solid. For fluids, molecular interactions at the interface result in a measurable tension which, if constant, is equal to the surface free energy required to form a unit area of interface. For the case of a liquid which is in contact with air or the vapor of that liquid, the force per unit length required to create a unit surface area is usually referred to as the surface tension. Interfacial tension is used to describe this quantity for two liquids or for a liquid and a solid. Interfacial tension between two immiscible liquids is normally less than the surface tension of the liquid with the higher tension, and often is intermediate between the individual surface tensions of the two liquids of interest. Common units of surface or interfacial tension are dynes per centimeter (or the identical ergs/cm²) with metric units in the equivalent milli-Newton per meter (mN/m).

The surface tension of pure water ranges from 72.5 dynes/cm at 70°F to 60.1 dynes/cm at 200°F in an almost linear fashion with a gradient of 0.095 dynes/cm/°F [25]. Salts in oilfield brines tend to increase surface tension, but surface active agents that may dissolve into the water from the oil can lower surface tension. At standard conditions, surface tensions of brines range from 59 to 76 dynes/cm [25]. As shown in Figure 5-39, dissolved natural gas reduces surface tension of water as a function of saturation pressure [89].

At a given temperature, surface tension of hydrocarbons in equilibrium with the atmosphere or their own vapor increases with increasing molecular weight (Figure 5-40) [90]. For a given hydrocarbon, surface tension decreases with increasing temperature. At 70°F, surface tensions of crude oils often range from 24 to 38 dyne/cm [25].

The presence of dissolved gases greatly reduces surface tension of crude oil as shown in Figure 5-41 [91]. Dissolved natural gas reduces surface tension of crude oil more than previously noted for water, but the amount and nature of gas determines the magnitude of the reduction. The direct effect of a temperature increase on reduction of surface tension more than counterbalances the decreased gas solubility at elevated temperatures. Thus, surface tension at reservoir temperature and pressure may be lower than indicated by Figure 5-41 [25].

Under reservoir conditions, the interfacial interaction between gas and oil involves the surface tension of the oil in equilibrium with the gas. Similarly, the interaction between oil and water determines the interfacial tension between the crude and brine. Listed in Table 5-14 are the surface and interfacial tensions for fluids from several Texas fields [92].

The effect of temperature on interfacial tensions for some oil-water systems is shown in Figure 5-42 [92]; the reduction in interfacial tension with increasing

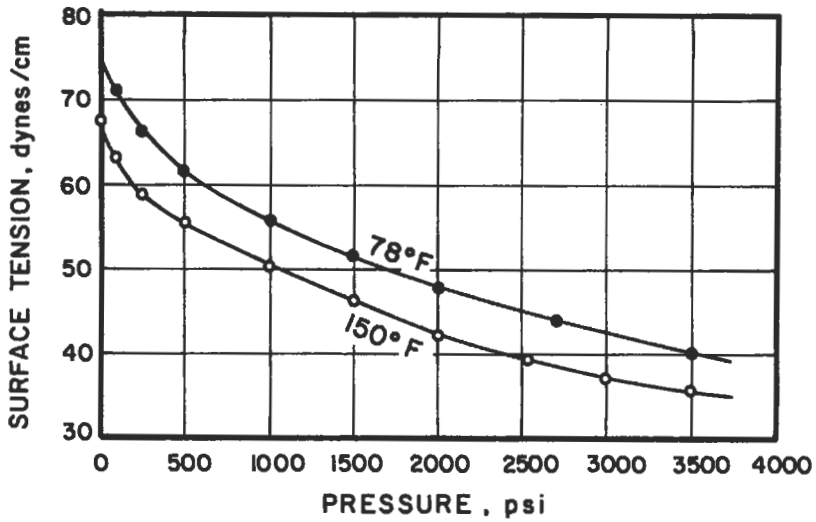


Figure 5-39. Surface tension between water and natural gas as a function of saturation pressure [89].

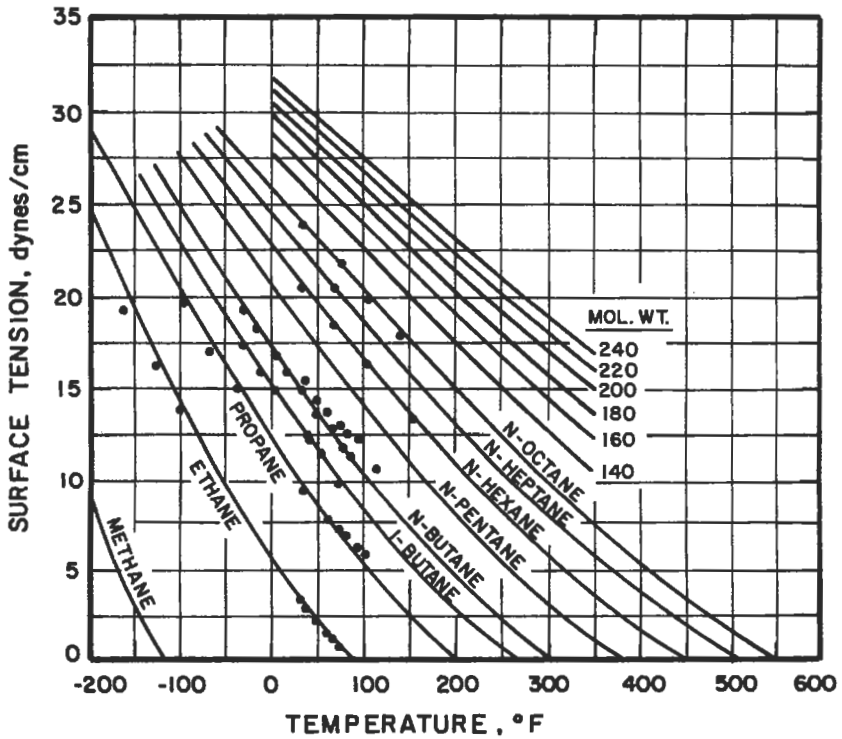


Figure 5-40. Surface tension of several hydrocarbons [90].

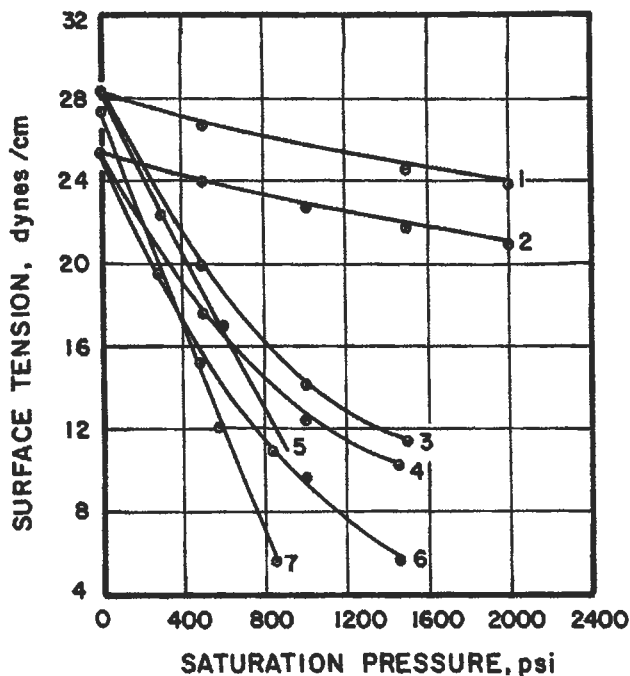


Figure 5-41. Surface tension of several crude oils [91].

temperature is usually somewhat more pronounced than is observed for surface tension. Although no quantitative relation is observed, the general trend suggests lower interfacial tensions for the higher API gravity crudes. However, in studies with a crude oil containing large amounts of resins and asphaltenes, different effects of temperature on interfacial tension were observed when measurements made at aerobic conditions were compared to anaerobic tests [93]. Interfacial tension between the crude and reservoir brine showed a decrease with an increase in temperature under aerobic conditions, whereas at anaerobic conditions, interfacial tension increased with increasing temperatures. This difference in behavior was attributed to oxidation of the stock tank oil in the aerobic tests. At conditions of reservoir temperature and pressure, interfacial tension of the live reservoir oil was higher than the stock tank oil. The study concluded that live reservoir crude should be used in measurements of interfacial properties and that if stock tank oil is used, at least the temperature should correspond to reservoir conditions.

Figure 5-43 shows the effect of dissolved gas and pressure on the interfacial tension of three oil-water systems [89]. For each system, interfacial tension increases as the amount of dissolved gas increases, but drops slightly as pressure is increased above the bubblepoint.

Surface and interfacial tensions are important in governing the flow of fluids in the small capillaries present in oil-bearing reservoirs. The capillary forces in oil or gas reservoirs are the result of the combined effect of surface and interfacial tensions, pore size distribution, pore shape, and the wetting properties of the hydrocarbon/rock system.

Table 5-14
Surface and Interfacial Tensions for Several Texas Fields

Field	Formation	Depth, ft	Oil Gravity, °API	Surface tension, dynes/cm		Oil-water interfacial tension, dynes/cm		
				Oil	Water	70°F	100°F	130°F
Breckenridge	Marble Falls	3,200	38.2	28.8	67.6	19.0	10.9	
South Bend	Strawn	2,300	36.1	29.9	61.5	29.1	21.4	
Banyon	Austin	2,135	37.0	29.3	72.5	24.4	17.4	9.6
South Bend	Marble Falls	3,900	25.5	31.8	71.4	24.5	16.9	
Banyon	Austin	2,255	37.9	28.9	72.1	16.9	13.6	12.9
Salt Flats	Edwards	2,700	34.9	30.0	73.0	23.0	16.9	16.7
Driscoll	Catahoula	3,929	26.0	32.4	61.4	20.4	16.0	15.5
Wortham	Woodbine	2,800	38.3	29.2	63.2	13.6	7.3	
Wortham	Corsicana	2,200	22.4	33.2	59.6	25.1	16.7	13.2
Mexia	Woodbine	3,000	36.4	30.0	66.2	21.4	19.0	17.6
Powell	Woodbine	3,000	22.9	30.0	66.2	22.6	15.0	
Wortham	Woodbine	2,800	22.2	33.3	66.0	25.8	15.6	
Mexia	Woodbine	3,000	36.6	30.2	66.6	15.0	9.2	
Breckenridge	Marble Falls	3,200	37.7	28.9	70.1	16.2	8.5	10.0
Breckenridge	Marble Falls	3,200	36.6	29.4	74.1	15.5	11.3	
South Bend	Marble Falls	4,200	38.6	28.9	68.1	14.8	10.8	10.1
Van	Woodbine	2,710	33.9	29.0	61.7	18.1	16.2	
Raccoon Bend	Cockfield	3,007	34.1	31.6	69.8	24.7	14.6	14.3
Tomball	Cockfield	5,541	41.6	28.5	62.0	14.1	13.6	
Van	Woodbine	2,710	35.0	28.8	64.1	17.9	15.0	7.8
Saxet	Catahoula	4,308	26.2	32.0	65.2	17.2	11.5	10.8
Saxet	Catahoula	4,308	27.1	32.3	66.5	20.9	16.5	14.1
Pierce Junction	Frio	4,325	29.4	31.0	62.0	16.9	13.9	8.7
Pierce Junction	Frio	4,335	22.2	32.6	64.1	20.7	12.9	2.1
East Texas	Woodbine	3,660	36.5	28.2	68.6	19.7	10.9	9.6
East Texas	Woodbine	3,660	39.5	27.5	70.2	31.4	17.9	13.9
Goose Creek	Pliocene	1,470	14.2	34.1	63.7	24.4	19.5	
Goose Creek	Pliocene	2,040	21.1	33.6	63.5	18.8	15.3	12.5
Goose Creek	Mio-Pliocene	2,560	21.2	33.3	64.2	18.1	12.9	12.5
Talco	Glen Rose	5,000	23.0	31.9	73.9	20.5	18.8	14.8
Big Lake	Ordovician	8,300	42.6	28.5	63.3	18.1	14.8	12.5
Big Lake	Permian	3,000	38.0	27.9	66.2	27.3	18.3	15.7
Crane	Permian	3,500	31.1	29.5	68.2	18.6	14.8	7.8
Echo	Frye (Pa.)	1,950	38.4	27.8	49.5	34.3	24.6	18.6

From Reference 92.

Wettability and Contact Angle

The contact angle (θ_c), existing between two fluids in contact with a solid and measured through the more dense phase, is a measure of the relative wetting or spreading by a fluid on a solid. A contact angle of zero indicates complete wetting by the more dense phase, an angle of 180° indicates complete wetting of the less dense phase, and an angle of 90° means that neither fluid preferentially wets the solid.

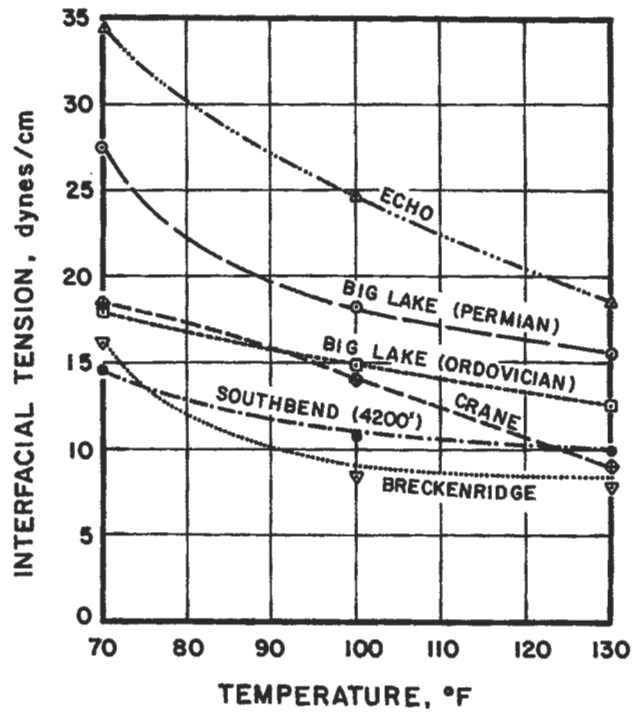


Figure 5-42. Influence of temperature on interfacial tensions for crude oil water systems [92].

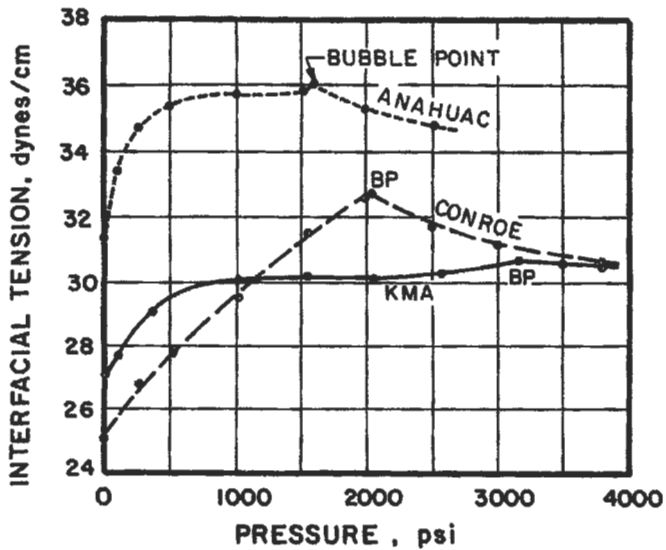


Figure 5-43. Effect of dissolved gas and pressure on interfacial tension between crude oil water [89].

From a combination of Dupre's equation for wetting tension and Young's equation [94], the adhesion tension (τ_A) can be given as [19,95-97]:

$$\tau_A = \sigma_{os} - \sigma_{ws} = \sigma_{wo} \cos \theta_{wo} \tag{5-73}$$

where σ_{os} is the interfacial tension between the solid and the less dense fluid phase, σ_{ws} is the interfacial tension between the solid and the more dense phase, and σ_{wo} is the interfacial tension between the fluids of interest. With gas-oil systems, oil is the more dense phase and is always the wetting phase [96]. With oil-water systems water is almost always the more dense phase, but either can be the wetting phase. For oil and water, a positive adhesion tension ($\theta_c < 90^\circ$) indicates a preferentially water-wet surface, whereas a negative adhesion tension ($\theta_c > 90^\circ$) indicates a preferentially oil-wet surface. For a contact angle of 90° , an adhesion tension of zero indicates that neither fluid preferentially wets the solid. Examples of various contact angles are depicted in Figure 5-44 [96].

The importance of wettability on crude oil recovery has been recognized for many years. This subject is discussed in a subsequent section of this chapter. Although Nutting [98] observed that some producing formations were oil-wet, many early workers considered most oil reservoirs to be water-wet (e.g., References 23, 99, and 100; discussion and comments in Reference 96). From a thermodynamic standpoint, it was felt that pure, clean silica must be wetted by water in preference to any hydrocarbon. In one study [101], no crude oils were tested that had a greater adhesion than pure water. Other results [102] tended to support this contention: capillary pressure tests suggested that all cores tested were water-wet with contact angles ranging from 31° to 80° . However, there are two reasons why these results were obtained [103]: (1) the cores were extracted with chloroform prior to the tests which could have affected the natural wettability, and (2) only receding (decrease in wetting phase saturation) contact angles were measured during the capillary pressure tests. As with capillary pressures, there is a hysteresis in the receding and advancing (increase in wetting) pressures.

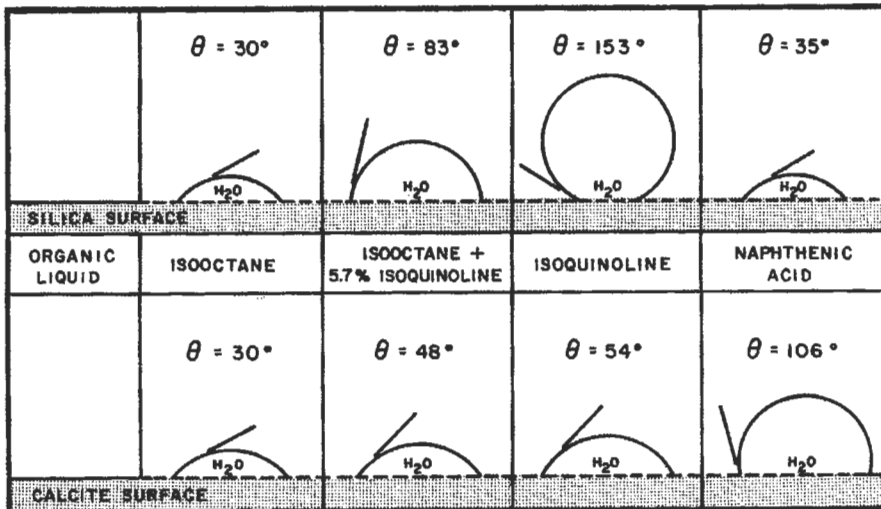


Figure 5-44. Examples of contact angles [96].

phase saturation) contact angles; receding angles are smaller than advancing angles [97]. Bartell and coworkers [95-97] were among some of the first investigators to measure contact angles with crude oil systems that suggested the possibility that oil reservoirs may not be water-wet. Furthermore, they concluded that spontaneous displacement of oil by water should occur only when both advancing and receding angles are less than 90° , and no spontaneous imbibition should occur if the two angles are on opposite sides of 90° [97].

A common technique for measuring advancing contact angles using polished mineral crystals is described in the literature [104]. For many crude oil systems, a considerable amount of time may be required before an equilibrium contact angle on a pure mineral is obtained. As shown in Figure 5-45 [104], some systems that initially appear to be preferentially water-wet become more oil-wet. Small amounts of polar compounds in some crude oils can adsorb on the rock surfaces and change wettability from preferentially water-wet to more oil-wet [96]. A detailed study on how crude oil components affect rock wettability has been made by Denekas et al. [105]. Imbibition tests have been described to examine wettability of reservoir cores [106,107]. A preferred technique of inferring reservoir wetting from core samples is the Amott method [108] which involves spontaneous imbibition and forced displacement tests; ratios of spontaneous displacement volumes to total displacement volumes are used as an index of wettability. Based on the correlation suggested by Gatenby and Marsden [109], Donaldson et al. [110-112] developed a quantitative indication of wettability,

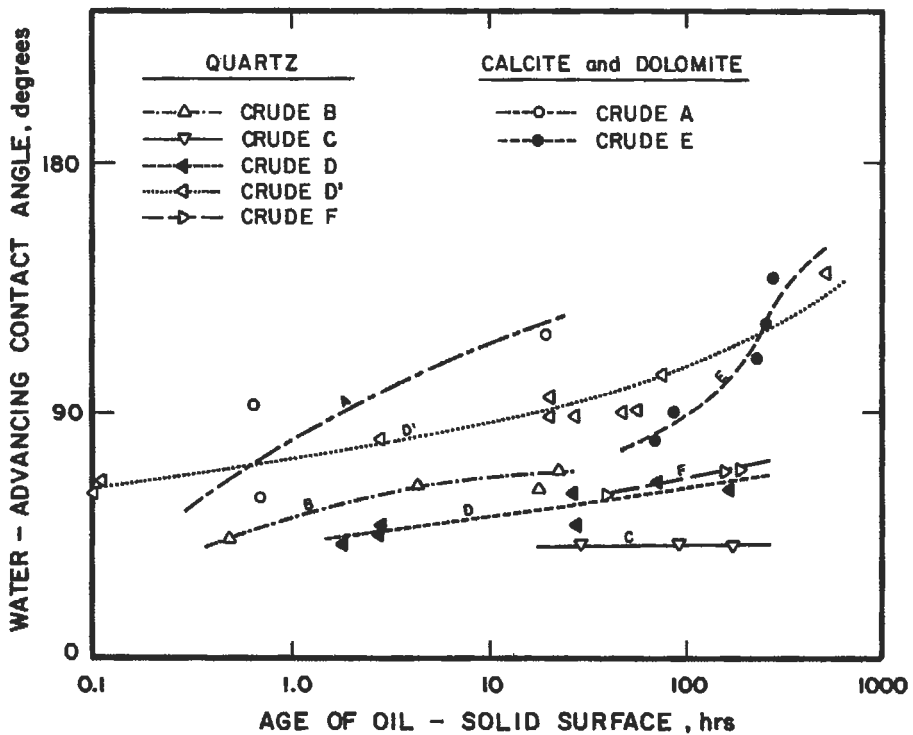


Figure 5-45. Change in contact angles with time [104].

called the U.S. Bureau of Mines (USBM) test, by measuring the areas under capillary pressure curves. The USBM method has the advantage of working well in the intermediate wettability region. A multitude of techniques for the qualitative indication of wettability that have been proposed will not be described but have been discussed in the literature [133].

In a fairly extensive examination of 55 different reservoirs, Treiber, Archer and Owens [114] arbitrarily assigned water-wet conditions for contact angles of 0° to 75° and oil-wet conditions for contact angles of 105° to 180° with contact angles of 75° to 105° representing an intermediate (referred to as neutral by others) wettability. With these designations, 27% of the samples were water-wet, 66% were oil-wet, and the remaining 7% were of intermediate wettability. Subsequently, Morrow [115] has defined an intermediate wettability when neither fluid spontaneously imbibes in a "squatters' rights" situation. Morrow found that for contact angles less than 62° , the wetting phase would spontaneously imbibe, and for contact angles above 133° , the nonwetting phase would spontaneously imbibe; therefore, the intermediate wettability condition would be operative for contact angles from 62° to 133° . Using Morrow's guidelines, the data of Treiber, Archer and Owens indicate that 47% of the samples were of intermediate wettability, 27% were oil-wet, and 26% were water-wet. The distribution in wettability according to lithology is given in Table 5-15. In either case, it is apparent that a majority of the samples were not water-wet.

Using 161 core samples representing various carbonate reservoirs, Chilingar and Yen [116] found that 8% were water-wet ($\theta_c > 80^\circ$), 12% were intermediate ($\theta_c = 80^\circ - 100^\circ$), 65% were oil-wet ($\theta_c = 100^\circ - 160^\circ$), and 15% were strongly oil-wet ($\theta_c = 160^\circ - 180^\circ$). The arbitrary definitions of wettability differ from Treiber et al. [114] and Morrow [115], but the distributions appear to be similar to the carbonate data in Table 5-15.

In the previous discussion, it was implied that pore surfaces within a reservoir rock are uniformly wetted. The concept whereby a portion of the reservoir surfaces are preferentially oil-wet while other portions are preferentially water-wet was termed fractional wettability by Brown and Fatt [117] and Fatt and Klikoff [118]. Fractional wetting was believed to be a result of the varying amount of adsorption of crude oil components on the different minerals present in a reservoir. Other evidence [119,120] supported the existence of a heterogeneous wetting (also called spotted or Dalmation wettability in the literature). Salathiel [121] introduced the concept of a mixed-wettability condition, a special case of fractional wetting, in which the fine pores and grain contacts are

Table 5-15
Wettability of 55 Reservoir Rock Samples

	Water-wet ($\theta_c < 75^\circ$)*	Intermediate ($\theta_c = 75^\circ - 105^\circ$)*	Oil-wet ($\theta_c > 105^\circ$)*
Sandstones	43%	7%	50%
Carbonate	8%	8%	84%
Total samples	27%	7%	66%
	Water-wet ($\theta_c < 62^\circ$ **)	Intermediate ($\theta_c = 62^\circ - 133^\circ$ **)	Oil-wet ($\theta_c > 133^\circ$ **)
Total samples**	26%	47%	27%

*Based on contact angle/wettability relation suggested by Treiber, Archer and Owens [114].

**Based on contact angle/wettability relation suggested by Morrow [115].

preferentially water-wet and the large pore surfaces are strongly oil-wet. Salathiel concluded that the oil-wet paths can be continuous to provide a means for oil to flow even at very low oil saturations; these results were offered to explain the very good oil recovery noted in some field projects. More recently, Morrow, Lim, and Ward [122] introduced the concept of a speckled wettability in which a rationale is presented whereby oil tends to be trapped in pore throats rather than pore bodies. Speckled wettability mimics behavior of strongly water-wet conditions observed during waterflooding: water breakthrough is abrupt, relative permeability to water at residual oil saturation is low, water is imbibed spontaneously, and oil is not imbibed spontaneously.

When cores are obtained for laboratory tests where wettability is important, precautions must be taken to ensure the wetting preference of the formation is not altered during coring. Mud additives, such as dispersants, weighting agents, lost circulation materials, thinners or colloids, that possess surface-active properties may drastically change core wettability. Surface active agents should be avoided so that the core samples have the same wettability as the reservoir rock. Listed in Table 5-16 are the effects of various mud additives on wettability of water-wet and oil-wet cores [107].

In the case of water-wet sandstone or limestone cores, rock-salt, bentonite, carboxymethylcellulose (CMC), and barite had no effect on wettability. However, oil-wet sandstone cores were reversed to a water-wet condition when exposed to CMC, bentonite, or lime solutions. Additional tests with bentonite solutions indicated that wettability of oil-wet cores is not reversed if the solution pH is lowered to a neutral or slightly acidic value. These results suggest that from a wettability standpoint, the best coring fluid is water (preferably formation brine); if bentonite is used, mud pH should be neutral or slightly acidic. If appreciable hydrogen sulfide is suspected in the interval being cored, it may be undesirable to lower pH. In fact, a very alkaline mud (pH 10–12) may be used to keep the sulfide in the ionized state for safety and corrosion considerations. Subsequent work [123] suggests the preferred system to obtain fresh cores is a natural water-base mud with no additives, or a bland mud consisting of bentonite, salt, and CMC. However, recent results [124] conclude that bland muds may not, in fact, be bland. While none of the bland additives altered wettability of water-wet rock

Table 5-16
Effect of Water-Base Mud Additives on the Wettability of Cores

Component	Wettability of Test Cores after Exposure to Filtrate		
	Water-Wet Limestone	Water-Wet Sandstone	Oil-Wet Sandstone
Rock-salt	No change	No change	No change
Starch	Slightly less water-wet	Slightly less water-wet	—
CMC	No change	No change	Water-wet
Bentonite	No change	No change	Water-wet
Tetrasodium pyrophosphate	No change	Less water-wet	—
Calcium lignosulfonate	No change	Less water-wet	—
Lime	No change	Slightly more water-wet	Water-wet
Barite	No change	No change	—

From Reference 107.

samples, all of the components with the exception of bentonite made oil-wet samples significantly less oil-wet. The bland additives that were tested included bentonite, pregelatinized starch, dextrid (an organic polymer), drispac (a polyanionic cellulose polymer), hydroxyethylcellulose, xanthan gum polysaccharide, and CMC. All of the drilling mud components considered to be bland decreased the amount of oil imbibed into a core and increased the amount of water imbibed.

Preventing wettability changes in core material, after it has been recovered at the surface, is equally important so that subsequent laboratory measurements are representative of reservoir conditions. Changes in wettability of core material that occur during handling or storage are usually caused by oxidation of the crude oil, evaporation of volatile components, or decreases in temperature or pressure which cause the deposition of polar compounds, asphaltenes, or heavy hydrocarbon compounds [107,125]. Because of the complexity of the mechanisms involved, the magnitude and direction of changes in wetting conditions, when reservoir cores are preserved, are not fully understood. Weathering of water-wet cores has been reported to frequently cause the grain surfaces to become oil-wet [107]. In other experiments [126] oil-wet cores changed to water-wet upon contact with air. Therefore it is necessary to preserve core samples at the well-site to ensure that wettability is not altered by contamination, oxidation, or evaporation. Two methods of preserving conventional cores, immediately after they have been removed from the core barrel, will prevent changes in wettability for several months [107]. One method consists of immersing the core in deoxygenated formation brine or suitable synthetic brine (i.e., drilling mud filtrate) and keeping the sample in suitable nonmetallic containers that can be

Table 5-17
Empirical Relative Permeability Equations

I. Oil-gas relative permeabilities
(for drainage cycle relative to oil)

$$S^* = \frac{S_o}{(1 - S_{iw})}$$

where S_{iw} is the irreducible water saturation.

	k_{ro}	k_{rg}
A. Unconsolidated sand—well sorted	$(S^*)^{3.0}$	$(1 - S^*)^3$
B. Unconsolidated sand—poorly sorted	$(S^*)^{3.5}$	$(1 - S^*)^2(1 - S^{*1.5})$
C. Cemented sand, oolitic lime, and vugular lime	$(S^*)^{4.0}$	$(1 - S^*)^{2.0}(1 - S^{*2.0})$

II. Water-oil relative permeabilities
(for drainage cycle relative to water)

$$S^* = \frac{S_w - S_{iw}}{(1 - S_{iw})}$$

where S_{iw} is the irreducible water saturation.

	k_{ro}	k_{rw}
A. Unconsolidated sand—well sorted	$(1 - S^*)^{3.0}$	$(S^*)^{3.0}$
B. Unconsolidated sand—poorly sorted	$(1 - S^*)^2(1 - S^{*1.5})$	$(S^*)^{3.5}$
C. Cemented sand, oolitic lime, and vugular lime	$(1 - S^*)^2(1 - S^{*2.0})$	$(S^*)^{4.0}$

From Reference 20.

sealed to prevent leakage and the entrance of oxygen. In a second method, the cores are wrapped in Saran or polyethylene film and aluminum foil, and then coated with wax or strippable plastic. Cores obtained by either of these methods are referred to as preserved, native-state, or fresh cores, and are preferred for many laboratory tests.

For certain laboratory tests, it may be possible to clean reservoir cores with solvents and resaturate with reservoir fluids to restore the original wetting conditions. Details of preparing such restored-state or extracted cores are discussed subsequently in the section "Coring and Core Analysis." The concept of the method is to clean the core thoroughly until it is water-wet, saturate with reservoir brine, flush with crude oil, and age for over 1,000 hours at reservoir temperature.

Regardless of the method of core handling employed, the rock samples used in the laboratory should have a surface state as close as possible to that present in the reservoir. If preserved cores are used, it is essential they be stored under air-free conditions because exposure to air for as little as 6–8 hours can cause water evaporation and other changes in core properties. If extracted cores are used, drying of the cores can be very critical when hydratable minerals, capable of breaking down at low temperatures are present. Contamination from core holders that contain certain types of rubber sleeves can be prevented by using an inner liner of tubular polyethylene film. Because of the instability of many oilfield waters, it is usually desirable to prepare synthetic brines to prevent core plugging caused by deposition of insolubles.

When possible, tests should be made under reservoir conditions of temperature and pressure using live reservoir oil. This is an improvement over room condition techniques where tests are made at atmospheric conditions with refined laboratory oils. Use of the live crude exposes the rock to compounds present in the oil that might influence wettability, and establishes an environment as close as possible to reservoir conditions. Cores evaluated at atmospheric conditions may be more oil-wet than similar tests at reservoir conditions because of the decreased solubility of wettability-altering compounds at lower temperatures and pressures [107,123]. In a recent contact angle study [93] with calcium carbonate crystals and a crude oil containing 27.3% resins and 2.2% asphaltenes, a complete reversal from a predominantly oil-wet system at lower temperatures to a predominantly water-wet system at higher temperatures was found. While pressure alone had little effect on the wettability of the system, the study speculated that the addition of gas-in-solution with increasing pressure should favor a more water-wet situation than would be indicated from laboratory tests at atmospheric conditions. Even when all precautions have been taken, there is no absolute assurance that reservoir wettability has been duplicated.

Capillary Pressure

Curvature at an interface between wetting and nonwetting phases causes a pressure difference that is called capillary pressure. This pressure can be viewed as a force per unit area that results from the interaction of surface forces and the geometry of the system.

Based on early work in the nineteenth century of Laplace, Young, and Plateau (e.g., Reference 94), a general expression for capillary pressure, P_c , as a function of interfacial tension, σ , and curvature of the interface is [19]:

$$P_c = \sigma \left(\frac{1}{r_1} + \frac{1}{r_2} \right) \quad (5-74)$$

where r_1 and r_2 are the principal radii of curvature at the interface. These radii are not usually measured, and a mean radius of curvature is given by the capillary pressure and interfacial tension.

For a cylindrical vertical capillary, such as a small tube, the capillary pressure for a spherical interface is [19]:

$$P_c = \frac{2\sigma \cos \theta_c}{r} = gh(\rho_1 - \rho_2) \tag{5-75}$$

where r is the radius of the tube, θ_1 is the contact angle measured through the more dense phase that exists between the fluid and the wall of the tube, g is the gravitational constant, ρ is density, h is column height, and the subscripts refer to the fluids of interest. For a fluid that wets the wall of a capillary tube, the attraction between the fluid and the wall causes the fluid to rise in the tube. The extent of rise in the capillary is proportional to the interfacial tension between the fluids and the cosine of the contact angle and is inversely proportional to the tube radius.

An analogous situation can occur during two-phase flow in a porous medium. For example if capillary forces dominate in a water-wet rock, the existing pressure differential causes flow of the wetting fluid to occur through the smaller capillaries. However, if viscous forces dominate, flow will occur through the larger capillaries (from Pouiselle's law, as a function of the 4th power of the radius).

Figure 5-46 depicts a typical capillary pressure curve for a core sample in which water is the wetting phase. Variation of capillary pressure is plotted as a function of water saturation. Initially, the core is saturated with the wetting phase (water). The nonwetting phase, oil in this case, is used to displace the

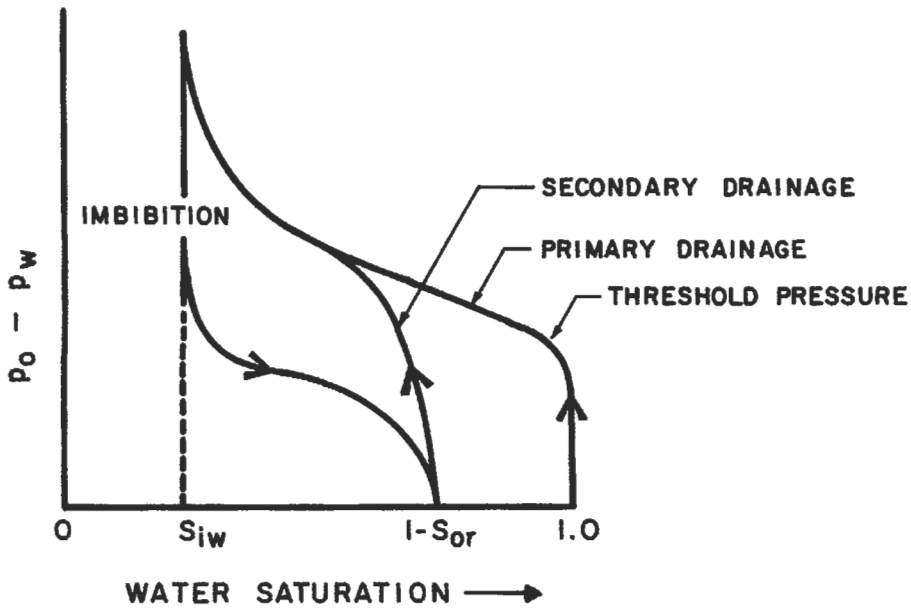


Figure 5-46. Example capillary pressure curves.

water. As shown in the figure, a threshold pressure must be overcome before any oil enters the core. The initial (or primary) drainage curve represents the displacement of the wetting phase from 100% saturation to a condition where further increase in capillary pressure causes little or no change in water saturation. This condition is commonly termed the irreducible saturation, S_{w_i} . The imbibition curve reflects the displacement of the nonwetting phase (oil) from the irreducible water saturation to the residual oil saturation. Secondary drainage is the displacement of the wetting phase from the residual oil saturation to the irreducible water saturation. A hysteresis is always noted between the drainage and imbibition curves. Curves can be obtained within the hysteresis loop by reversing the direction of pressure change at some intermediate point along either the imbibition or secondary drainage curve. The nonuniform cross-section of the pores is the basic cause of the hysteresis in capillary pressure observed in porous media. Therefore, capillary pressure depends on pore geometry, interfacial tension between the fluids, wettability of the system (which will be discussed later in this chapter), and the saturation history in the medium.

Leverett [100] introduced a reduced capillary pressure function (subsequently termed the Leverett J function by Rose and Bruce [127]) that was suggested for correlating capillary pressure data:

$$J(S_w) = \frac{P_c}{\sigma \cos \theta_c} \left(\frac{k}{\phi} \right)^{1/2} \quad (5-76)$$

where $J(S_w)$ = the correlating group consisting of the terms of Equation 5-75
 k = the permeability
 ϕ = porosity of the sample

The J function was originally proposed as means of converting all capillary pressure data for clean sand to a universal curve. A series of capillary pressure curves are shown as a function of permeability in Figure 5-47 [20]. An example of the J function curve generated from these data is shown in Figure 5-48 [20]. While the J function sometimes correlates capillary pressure data from a specific lithology within the same formation, significant variations can be noted for different formations.

Common laboratory methods of measuring capillary pressure include [19]: mercury injection, porous diaphragm or plate (restored state), centrifuge method, and steady-state flow in a dynamic method. While the restored state test is generally considered the most accurate, mercury injection is routinely used. However, it is necessary to correct the mercury injection data for wetting conditions before comparison to results from the restored state test.

A very valuable use of capillary pressure data is to indicate pore size distribution. Since the interfacial tension and contact angle remain constant during a test such as already described, pore sizes can be obtained from capillary pressures. For rocks with more uniform pore sizes, capillary pressure curves will be close to horizontal. The slope of the capillary pressure curve will generally increase with broader pore-size distribution.

If laboratory capillary pressure data are corrected to reservoir conditions, the results can be used for determining fluid saturations. Figure 5-49 shows a close agreement in water saturations obtained from capillary pressure and electric logs [48].

Capillary pressure data are helpful in providing a qualitative assessment of the transition zones in the reservoir. A transition zone is defined as the vertical

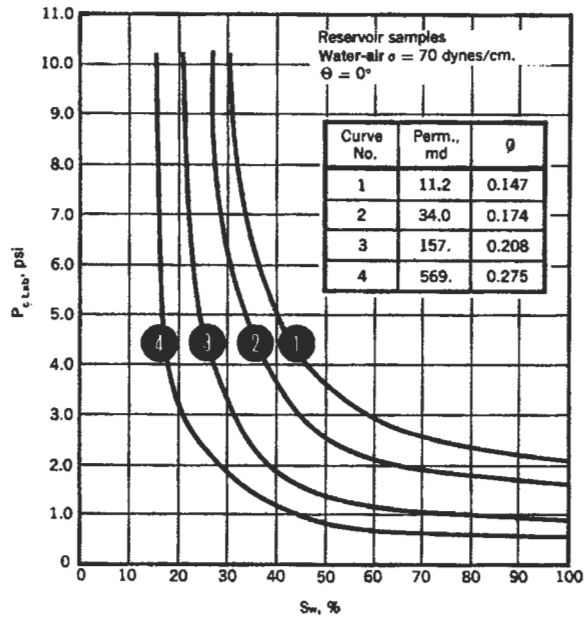


Figure 5-47. Capillary pressures of different permeability core samples [20].

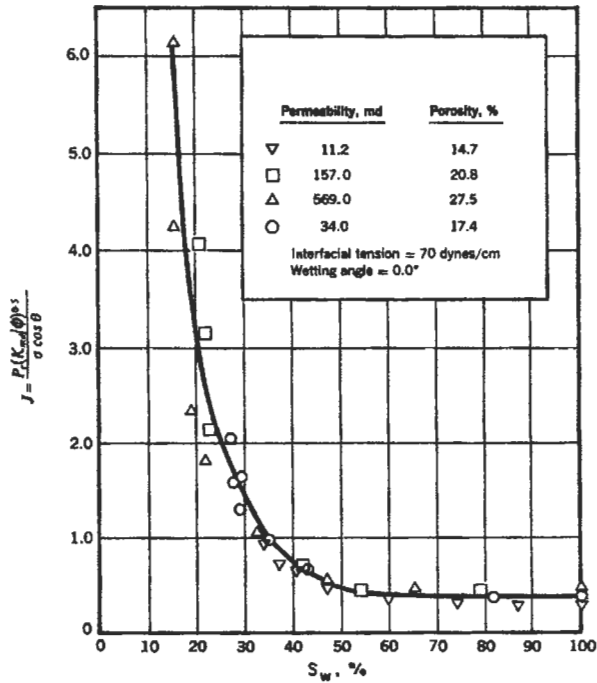


Figure 5-48. J function plot for data in Figure 5-47 [20].

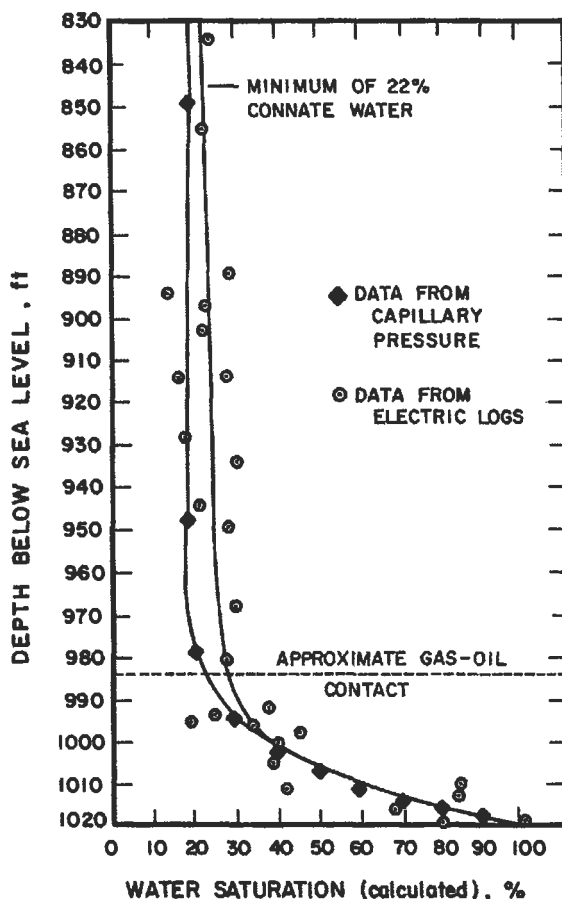


Figure 5-49. Comparison of water saturations from capillary pressure and electric logs [48].

thickness where saturation changes from 100% water to irreducible water for a water-oil contact, or from 100% liquid to an irreducible water saturation for a gas-oil contact.

Effective Permeabilities

In the previous section, "Absolute Permeability," it was stated that permeability at 100% saturation of a fluid (other than gases at low pressure) is a characteristic of the rock and not a function of the flowing fluid. Of course, this implies that there is no interaction between the fluid and the rock (such as interaction between water and mobile or swelling clays). When permeabilities to gases are measured, corrections must be made for gas slippage which occurs when the capillary openings approach the mean free path of the gas. Klinkenberg [128] observed that gas permeability depends on the gas composition and is approximately a linear function of the reciprocal mean pressure. Figure 5-50

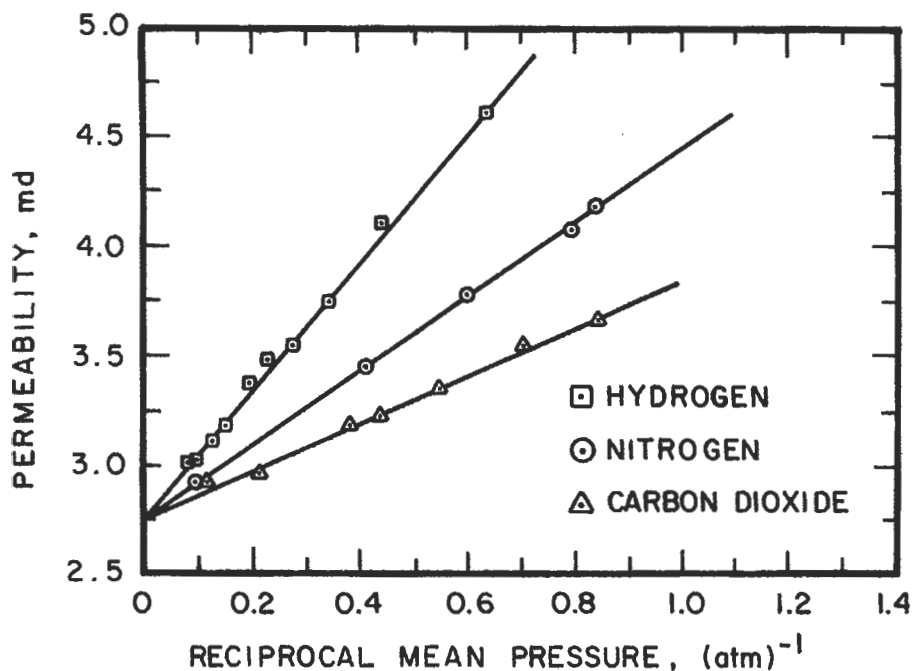


Figure 5-50. Gas slippage in core [128].

shows the variation in permeability as a function of mean pressure for hydrogen, nitrogen, and carbon dioxide. Klinkenberg found that by extrapolating all data to infinite mean pressure, the points converged at an equivalent liquid permeability (k_e), which was the same as the permeability of the porous medium to a nonreactive single-phase liquid. From plots of this type, Klinkenberg showed that the equivalent liquid permeability could be obtained from the slope of the data, m , the measured gas permeability, k_g , at a mean flowing pressure \bar{p} , at which k_g was observed:

$$k_e = \frac{k_g}{1 + (b/\bar{p})} = k_g - \frac{m}{\bar{p}} \quad (5-77)$$

where b is a constant for a given gas in a given medium and is equal to m divided by k_e . The amount of correction, known as the Klinkenberg effect, varies with permeability and is more significant in low permeability formations.

In recent studies [129,130] with very low permeability sandstones, liquid permeabilities were found to be less than gas permeabilities at infinite mean pressure, which is in contrast with the prior results of Klinkenberg. Furthermore, it has been shown [130] that liquid permeabilities decreased with increasing polarity of the liquid. For gas flow or brine flow in low-permeability sandstones, permeabilities were independent of temperature at all levels of confining pressure [130]. The data [130] showed that for a given permeability core sample at a given confining pressure, the Klinkenberg slip factors and slopes of the

Klinkenberg plots were proportional to the product of viscosity and the square root of absolute temperature.

As shown in Figure 5-51 permeability of reservoir rocks can decrease when subjected to overburden pressure [131]. When cores are retrieved from a reservoir, the confining forces are removed and the rock can expand in all directions which can increase the dimensions of the available flow paths. In reservoirs where this is significant, it is imperative that permeability measured in the laboratory be conducted at the confining pressure that represents the overburden pressure of the formation tested.

As a general trend, air permeability decreases with increasing connate water saturation. Relationships between air permeability and connate water saturation in Figure 5-52 show a linear decrease in the logarithm of permeability as a function of water saturation that depends on the individual field [132].

The fluid system of an oil reservoir consists usually of gas, oil, and water. In the case of such a heterogeneous system, flow of the different phases is a function of fluid saturation in the reservoir by the different phases. The lower the saturation of a certain liquid, as compared to other liquids, the lower the permeability to that liquid. This type of permeability is termed effective permeability and is defined as permeability of the rock to one liquid under conditions of saturation when more than one liquid is present. Typical permeability-saturation relations for oil and gas and for oil and water are shown in Figure 5-53.

From the practical point of view, permeability may be considered as a measure of productivity of the producing horizon. Knowledge of permeability is useful in a number of reservoir problems. The concept of effective permeability is of particular importance since it emphasizes a need for production practices, which tend to maintain good permeability of the reservoir to oil.

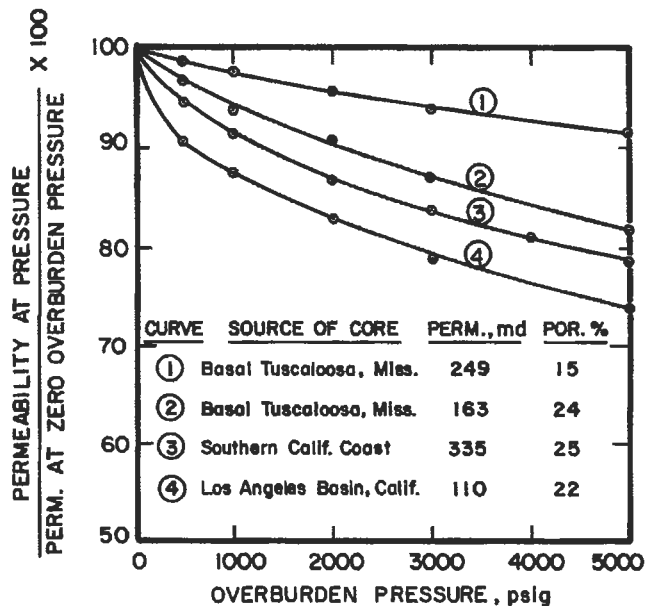


Figure 5-51. Air permeability at different overburden pressures [131].

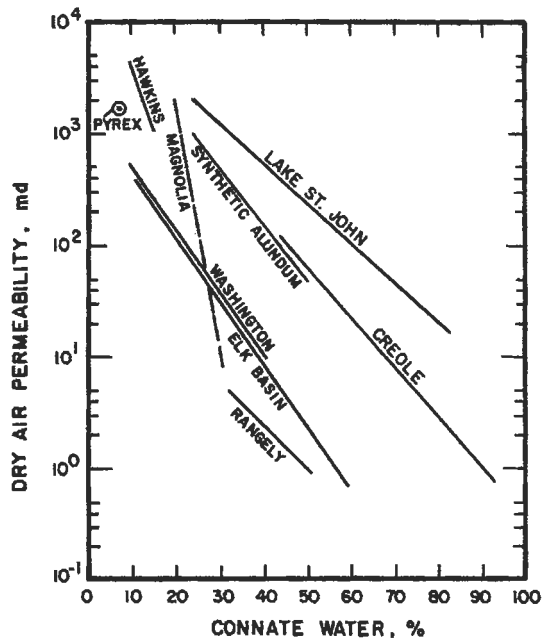


Figure 5-52. Relationship between air permeability and connate water saturation [132].

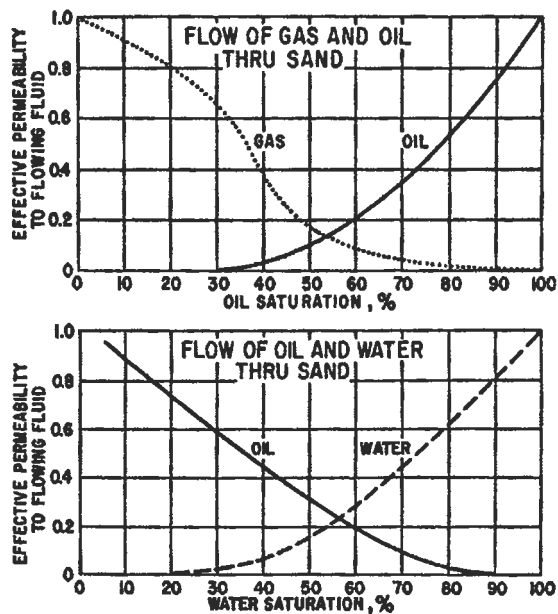


Figure 5-53. Effective permeabilities.

Thus, the absolute permeability is the permeability measured when the medium is completely saturated with a single fluid. Effective permeability is the permeability to a particular fluid when another fluid is also present in the medium. For example, if both oil and water are flowing, the effective permeability to oil is k_o and that to water is k_w . The sum of the effective permeabilities is always less than the absolute permeability [17]. As noted in the previous section, permeability is commonly expressed in millidarcies (md).

Relative Permeabilities

If the effective permeabilities are divided by a base permeability (i.e., the absolute permeability), the dimensionless ratio is referred to as the relative permeability, namely k_{rg} for gas, k_{ro} for oil, and k_{rw} for water:

$$k_{rg} = \frac{k_g}{k}; \quad k_{ro} = \frac{k_o}{k}; \quad k_{rw} = \frac{k_w}{k} \quad (5-78)$$

where k_g , k_o , and k_w are the effective permeabilities to gas, oil, and water, respectively, and k is some base permeability that represents the absolute permeability. For gas-oil two-phase relative permeabilities, the base permeability is often the equivalent liquid permeability. For oil-water two-phase relative permeabilities, three different base permeabilities are often used [133]:

1. The permeability to air with only air present.
2. The permeability to water at 100% S_w .
3. The permeability to oil at irreducible water saturation.

Wyckoff and Botset [76] are generally credited with performing the first gas and liquid relative permeabilities which were conducted in unconsolidated sandpacks in 1936. In these early experiments, a relationship was observed between the liquid saturation of a sand and the permeability to a liquid or gas phase [76,134]. At about the same time, Hassler, Rice, and Leeman [135] measured relative air permeabilities in oil-saturated cores. In 1940, relative permeability measurements were extended to consolidated cores by Botset [136]. Since then, a number of dynamic (fluid displacement or fluid drive) methods [83,137-143] and static (or stationary-phase) methods [144-150] have been proposed to determine relative permeabilities in core samples. In the latter methods, only the nonwetting phase is allowed to flow by the use of a very low pressure drop across the core; hence, this method is applicable only to the relative permeability of the nonwetting phase. The dynamic methods include: (1) steady-state methods in which fluids are flowed simultaneously through a core sample at a fixed gas-oil or water-oil ratio until equilibrium pressure gradients and saturations are achieved, and (2) unsteady-state methods in which an oil-saturated core is flooded with either gas or water at a fixed pressure drop or flow rate so that the average fluid saturation changes result in a saturation gradient. The most popular steady-state procedure is the Penn State method [83], but the most common dynamic test is the unsteady-state method because of the reduced time requirement. The various methods have been evaluated [139,151] and generally provide similar results.

Based on the initial work of Leverett [100] and Buckley and Leverett [152], Welge [153] was the first to show how to calculate relative permeability ratios in the absence of gravity effects. Subsequently, Johnson, Bossler, and Naumann

[154] showed that each of the relative permeabilities could be calculated even when gravity is not neglected. Other calculations of relative permeabilities have been proposed by Higgins [155], Guerrero and Stewart [156,157], and a graphical technique has been presented by Jones and Rozelle [158].

An example water-oil relative permeability plot vs. water saturation is given in Figure 5-54. Several features will be described that pertain to generating relative permeability curves from cores in the laboratory. If a clean, dry core is completely saturated with water, the permeability at 100% S_w should be similar to the equivalent liquid permeability obtained from gas flow measurements at 100% S_g . Exceptions to this generality include some low-permeability systems and other cores that contain clays or minerals that interact with the water used. If a clean core is used, it will probably be strongly water-wet when saturated with brine. As crude oil is injected into the core, the relative permeability to water decreases during the drainage cycle (decreases in wetting phase) while the relative permeability to oil increases. Some water that resides in the nooks and crannies of the pore space cannot be displaced by the oil, regardless of the throughput volume. This water saturation, which does not contribute significantly to occupying the flow paths, is called the irreducible water saturation, S_{iw} . With the core at S_{iw} , there is 100% relative permeability to oil (only

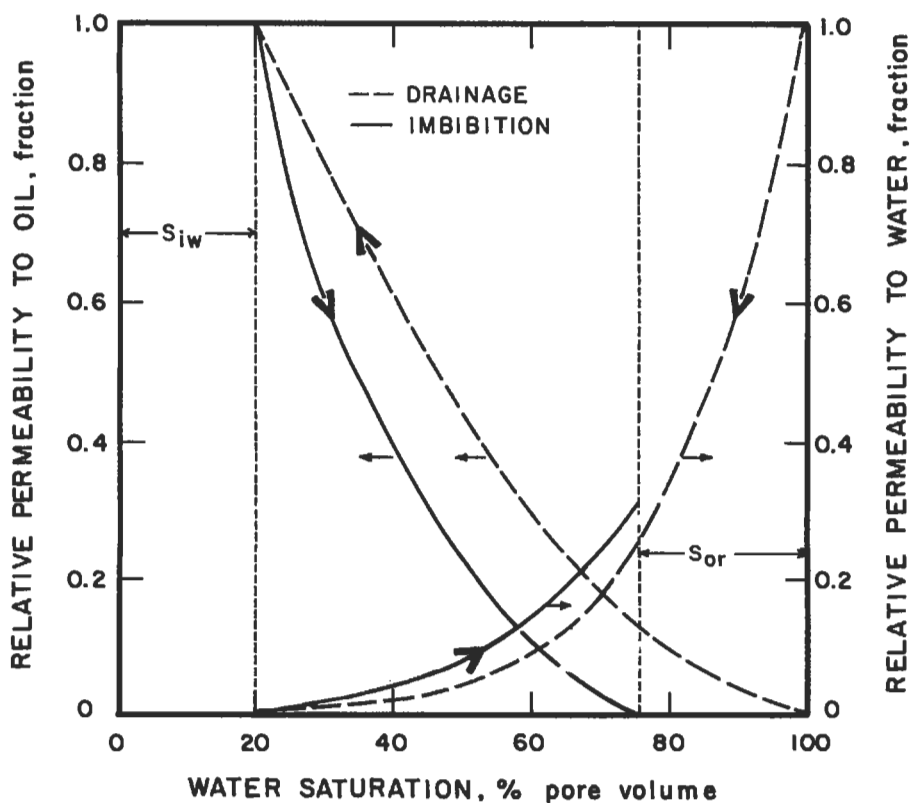


Figure 5-54. Example of water-oil relative permeability data.

oil is flowing) and no permeability to water. At this point, the core can be closed in for about 1,000 hours to allow sufficient time for wettability changes to occur. Then the core is flooded with water in an unsteady-state test, or fixed ratios of water and oil are injected in the steady-state test. If water continues to be the wetting phase, the relative permeability to water (which will be only a function of saturation) will be the same during the drainage and imbibition cycles. (The importance of wettability on relative permeabilities will be discussed in the next section of this chapter.) As the water is injected into the oil-flooded core, k_{rw} increases while k_{ro} decreases. Not all of the oil can be displaced from the core, regardless of the water throughput (at modest flow rates or pressure drops), and this is referred to as the waterflood residual oil saturation, S_{or} .

Similar observations apply to gas-oil relative permeability data as displayed in Figure 5-55. Typically, the gas-oil relative permeabilities are plotted against the total liquid saturation, which includes not only the oil but also any connate water that may be present. In the presence of gas, the oil (even if connate water is present) will be the wetting phase in preference to gas. As a result, the k_{ro} curve from gas-oil flow tests resembles the drainage k_{rw} curve from oil-water flow tests. As seen in Figure 5-55, the irreducible gas saturation (also called the equilibrium or critical gas saturation) is usually very small. When gas

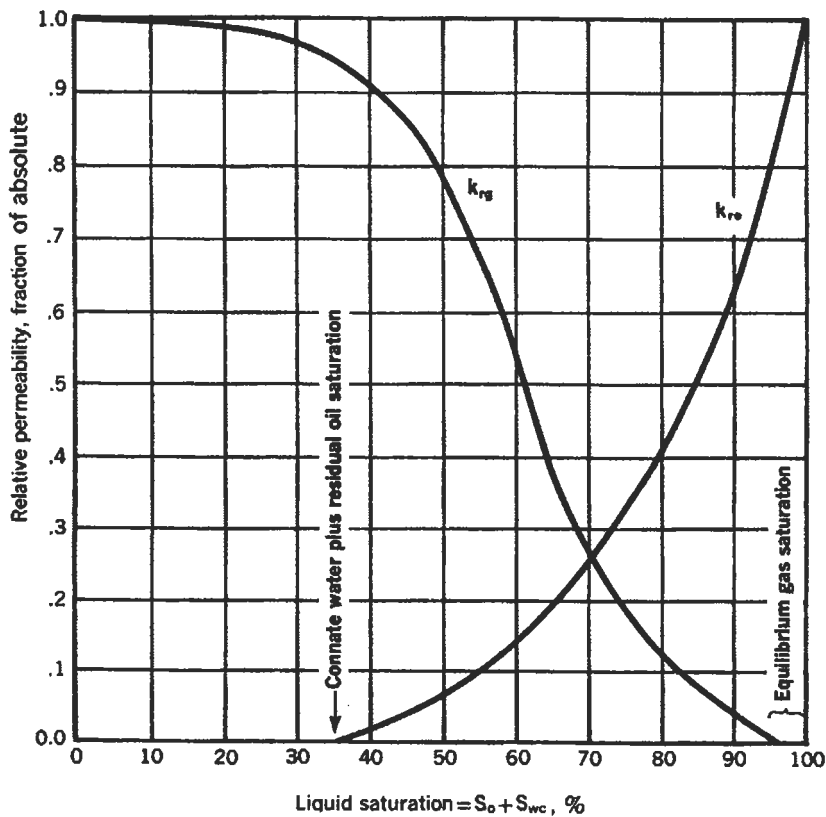


Figure 5-55. Gas-oil relative permeability data [20].

saturation is less than the critical value, gas is not mobile but does impede oil flow and reduces k_{ro} .

Three-phase relative permeabilities pertaining to simultaneous flow of gas, oil, and water have been provided in the literature [19,50]. Since the occurrence of such three-phase flow in a reservoir is limited [20], relative permeabilities for these conditions will not be discussed in this chapter, and the reader is referred to other sources [19,20,137,140,159,160].

Based on the work of Corey [150] and Wyllie [23,50], empirical equations have been summarized by Slider [20] to estimate relative permeabilities. These equations permit the estimation of k_{ro} from measurements of k_{rg} . Other empirical equations for estimating two-phase relative permeabilities in consolidated rocks are available in the literature [161].

Early work in unconsolidated sands showed that fluid viscosity or the range of permeability had negligible effects on the relationship between relative permeability and fluid saturation [76,100]. Geffen et al. [141] confirmed that relative permeabilities in cores are not affected by fluid properties provided wettability is not altered. However, others [162,163] have found that viscosity ratio influences relative permeability data when the displacing fluid is non-wetting. For constant wettability conditions, the higher the viscosity of one of the liquids, the lower is the relative permeability of the other liquid [163].

Geffen et al. [141] did cite a number of factors, in addition to fluid saturations, that affect relative permeability results. Because of capillary hysteresis, saturation history was important in that fluid distribution in the pores was altered. Flow rates during laboratory tests need to be sufficiently high to overcome capillary end effects (retention of the wetting phase at the outlet end of the core) [141]. According to Wyllie [23], relative permeability varies because of varying geometry of the fluid phases present, which is controlled by effective pore size distribution, method of obtaining the saturation (saturation history); heterogeneity of the core sample, and wettability of the rock-fluid system.

Controversy continues to exist regarding the effect of temperature on relative permeabilities (for example see the discussion and prior citations in References 164 and 165). Miller and Ramey [164] observed no change in relative permeability with temperatures for clean systems, and speculated that for reservoir fluid/rock systems, effects such as clay interactions or pore structure would need to be considered. Honarpour et al. [165] summarized the effects of temperature on two-phase relative permeabilities as measured by various researchers. In field situations, the larger overburden pressure associated with greater depths may be more important in affecting relative permeabilities than the associated temperature increases. As with many other tests, relative permeability measurements should be conducted at reservoir conditions of overburden pressure and temperature with crude oil and brine representative of the formation under study.

Effect of Wettability on Fluid-Rock Properties

Oil Recovery and Fluid Saturations. Since a reservoir rock is usually composed of different minerals with many shapes and sizes, the influence of wettability in such systems is difficult to assess fully. Oil recovery at water breakthrough in water-wet cores is much higher than in oil-wet cores [106,110,166-169], although the ultimate recovery after extensive flooding by water may be similar, as shown in Figure 5-56. These authors have shown that oil recovery, as a function of water injected, is higher from water-wet cores than from oil-wet cores at economical water-oil ratios. In 1928, Uren and Fahmy [170] observed better recovery of oil from unconsolidated sands that had an intermediate wettability,

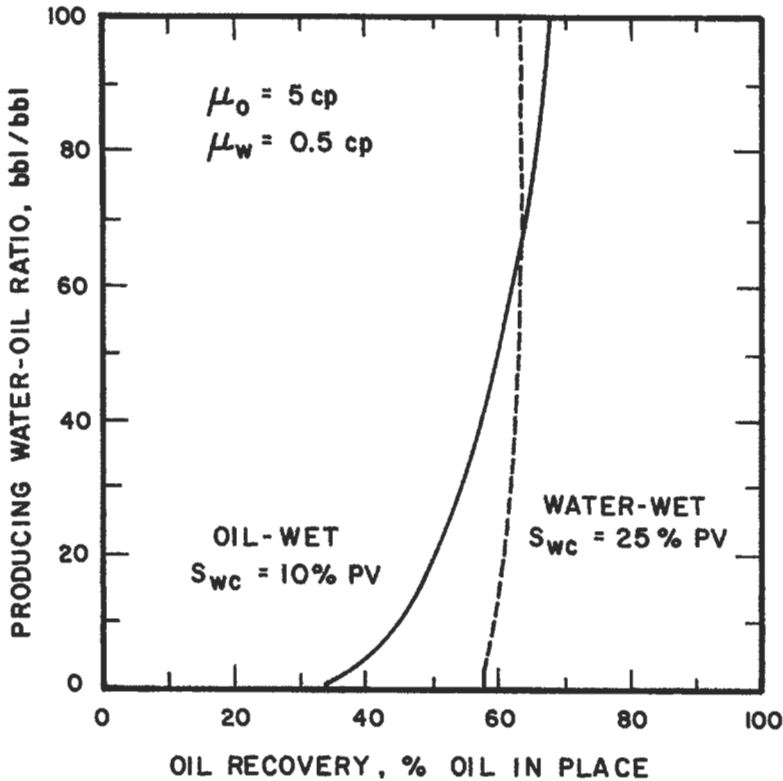


Figure 5-56. Comparison of oil recovery for oil-wet and water-wet cores [133].

and several investigators have suggested better oil recovery from cores of intermediate or mixed wettability [106,108,121,123,171]. More recent evidence by Morrow [172] and Melrose and Brandner [173] suggests that mobilization of trapped oil is more difficult in the intermediate wettability region, but the prevention of oil entrapment should be easier for advancing contact angles slightly less than 90° .

With water-wet cores in laboratory waterfloods, the oil production at water breakthrough ceases abruptly and water production increases sharply. With systems that are not water-wet, water breakthrough may occur earlier, but small fractions of oil are produced for long periods of time at high water cuts. In strongly water-wet systems, the residual oil that is permanently trapped by water resides in the larger pores, whereas in oil-wet systems trapping occurs in the smaller capillary spaces [106,133].

Relative Permeability Characteristics. For a system having a strong wetting preference for either oil or water, relative permeability of the wetting phase is a function of fluid saturation only [76,137,160]. Details of the effect of wettability on relative permeabilities have been discussed by several authors [113, 133,174,175]. In a detailed study using fired Torpedo (outcrop sandstone) cores, Owens and Archer [174] changed wettability by adding surface active agents to either the oil or water. Firing of the cores stabilized any clay minerals present

and provided more constant internal conditions. Both gas-oil and water-oil relative permeabilities were obtained. Some of the water-oil relative permeability data, all started at the same water saturation and obtained with the Penn State steady-state method, are reproduced in Figure 5-57. As the contact angle was increased to create more oil-wet conditions the effective permeability to oil decreased. Because of the differences in flow paths for the different wettability conditions, oil-wet systems had lower k_{ro} and higher k_{rw} when compared to water-wet conditions at the same water saturation. As the level of oil-wetting increased, k_{ro} at any saturation decreased whereas k_{rw} increased.

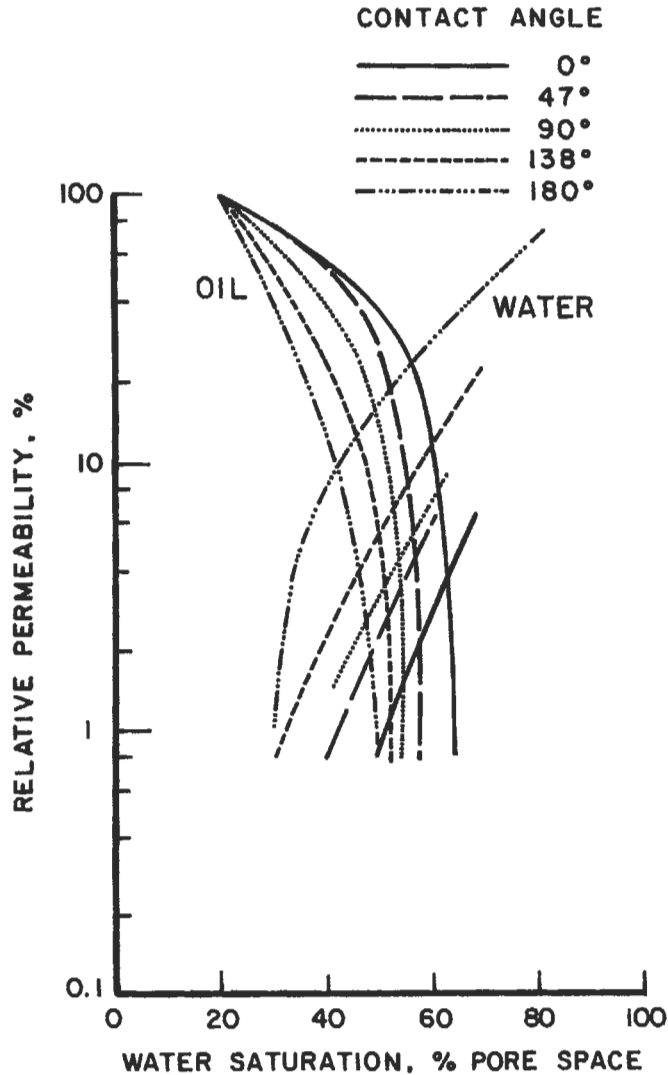


Figure 5-57. Effect of wettability on water-oil relative permeabilities [174].

Craig [133] has presented typical relative permeability curves, such as given in Figure 5-58, to point out differences in strongly water-wet and strongly oil-wet conditions. Craig suggests that several rules of thumb can help in distinguishing wetting preferences; typical characteristics of water-oil relative permeability curves are given in Table 5-18 [133]. Additionally, the strongly oil-wet relative permeability curves tend to have more curvature. Craig suggests the generality that relative permeability curves of intermediate wettability systems will have some of the characteristics of both water-wet and oil-wet conditions.

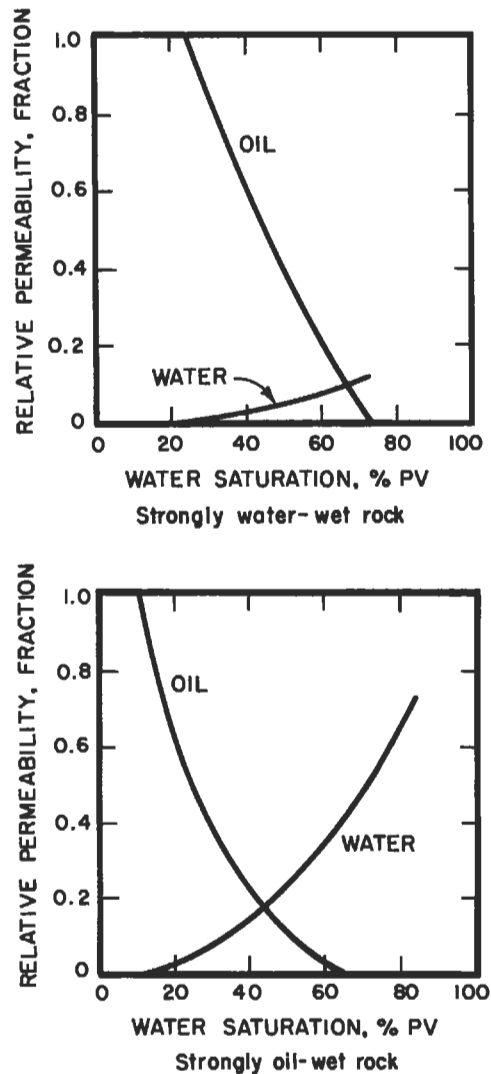


Figure 5-58. Strongly water-wet and strongly oil-wet relative permeability curves [133].

Table 5-18
Typical Water-Oil Relative Permeability Characteristics

	Strongly Water-Wet	Strongly Oil-Wet
Connate water saturation.	Usually greater than 20% to 25% PV.	Generally less than 15% PV, frequently less than 10%.
Saturation at which oil and water relative permeabilities are equal.	Greater than 50% water saturation.	Less than 50% water saturation.
Relative permeability to water at maximum water saturation; i.e., floodout.	Generally less than 30%.	Greater than 50% and approaching 100%.

From Reference 133.

However, as mentioned earlier in the section "Wettability and Contact Angle," a speckled wettability form of intermediate wetting mimics the relative permeability characteristics of strongly water-wet conditions [122].

Capillary Pressure Curves. By convention, oil-water capillary pressure, P_c , is defined as the pressure in the oil phase, p_o , minus the pressure in the water phase, p_w :

$$P_c = p_o - p_w \quad (5-79)$$

Depending on wettability and history of displacement, capillary pressure can be positive or negative. Figure 5-59 presents the effect of wettability on capillary pressure as related by Killins, Nielsen, and Calhoun [176]. Drainage and imbibition curves can have similarities, but the capillary pressure values are positive for strongly water-wet and negative for strongly oil-wet conditions. In the intermediate wettability case shown in Figure 5-59, the small positive value of threshold pressure during the drainage cycle suggests the sample was moderately water-wet [133]. After the drainage cycle, the sample spontaneously imbibed water until the capillary pressure was zero at a water saturation of 55%. Then, as water pressure was applied, the maximum water saturation of about 88% was achieved. As discussed previously, capillary pressure curves can be used as a criterion of wettability.

Resistivity Factors and Saturation Exponents. As shown previously in Table 5-7, Sweeney and Jennings [51] found that the formation resistivity factor changed when wettability was altered. However, the naphthenic acid they used to alter wettability may have also reduced porosity which could account for the increase in the saturation exponent in Equation 5-46. Other investigators [177,178] have found no significant effect of wettability on formation factors. Because of the scarcity of data and the difficulty of altering wettability without affecting other properties, the effect of wettability on formation resistivity remains unclear.

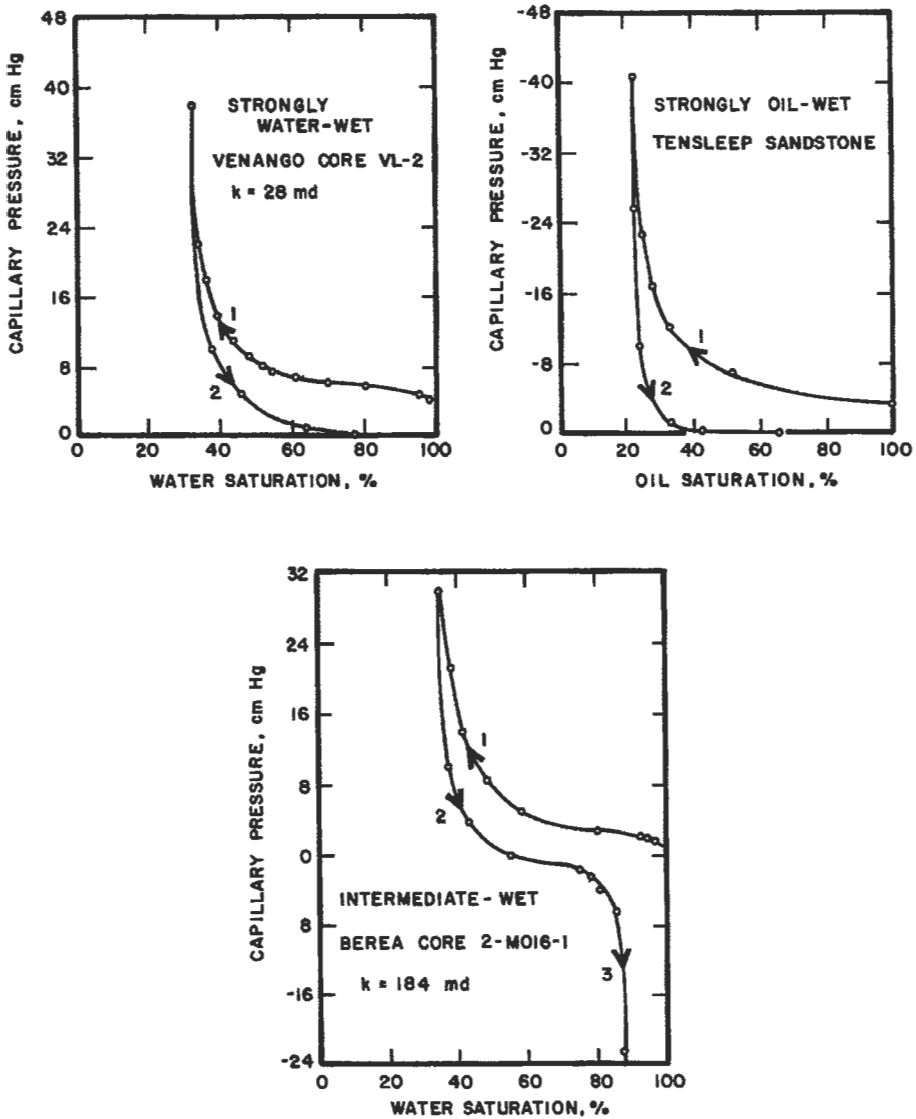


Figure 5-59. Effect of wettability on capillary pressure [176].

As related by Mungan and Moore [178], three assumptions are made in the Archie saturation expression (Equation 5-68): all of the brine contributes to electrical flow: the saturation exponent, n , is constant for a given porous media; and only one resistivity is measured for a given saturation. Since the saturation exponent depends on the distribution of the conducting phase, which is dependent on wettability, the foregoing assumptions are valid only for strongly water-wet conditions. When wettability is altered, the differences in fluid distribution cause variations in the cross-sectional areas of conductive paths and in the

tortuous path lengths. These variations affect resistivity, which results in different resistivity-saturation relationships such as were presented for carbonate cores by Sweeney and Jennings [51] in Figure 5-60. The saturation exponent, which is the slope of the lines, was about 1.6 for water-wet cores, about 1.9 for neutral-wet cores, and about 8 for oil-wet cores [51]. Similar data in sandstone cores were provided by Rust [177]; saturation exponents were about 1.7 and 13.5 for water-wet and oil-wet conditions respectively. These differences in oil-wet rocks most likely occur because of the isolation of trapped brine in dendritic fingers or dead-end pores which do not contribute to electrical conductivity.

Table 5-19, presenting data given by Mungan and Moore [178], shows that the effect of wettability on saturation exponent becomes more important at low brine saturations. Morgan and Pirson [179] conducted tests on fractionally wetted bead packs in which portions of the beads were water-wet and portions

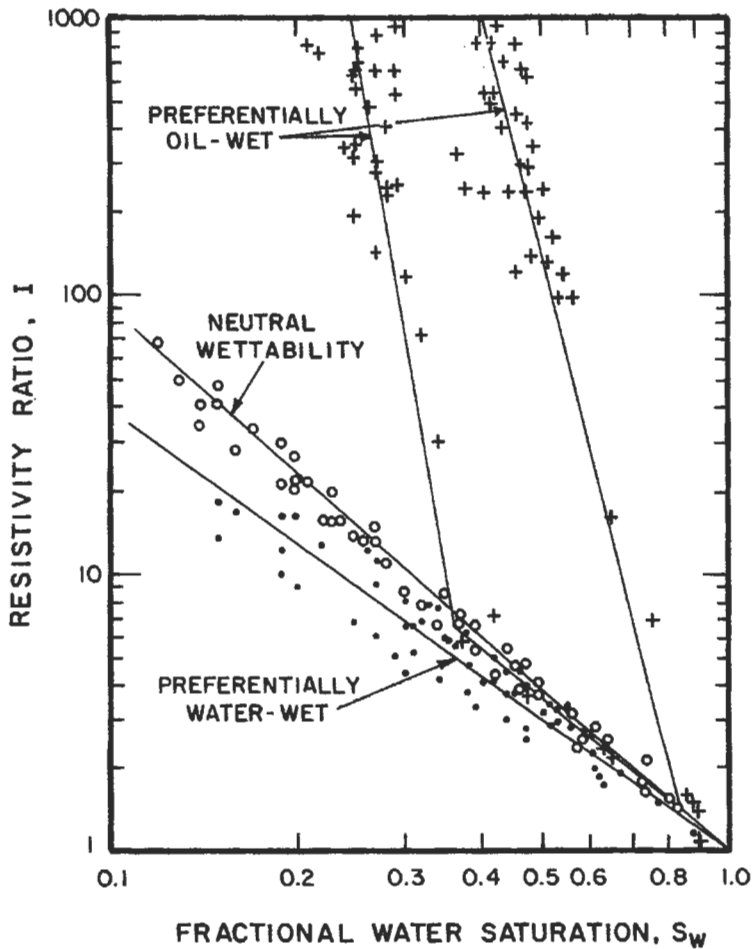


Figure 5-60. Resistivity-saturation relationships for different wettability carbonate cores [51].

Table 5-19
Saturation Exponents in Teflon Cores Partially Saturated
with Nonwetting Conducting Liquid

Air-NaCl solution		Oil-NaCl solution	
Brine saturation % PV	n	Brine saturation % PV	n
66.2	1.97	64.1	2.35
65.1	1.98	63.1	2.31
63.2	1.92	60.2	2.46
59.3	2.01	55.3	2.37
51.4	1.93	50.7	2.51
43.6	1.99	44.2	2.46
39.5	2.11	40.5	2.61
33.9	4.06	36.8	2.81
30.1	7.50	34.3	4.00
28.4	8.90	33.9	7.15
		31.0	9.00

From Reference 178.

were treated so that they were mildly oil-wet. From their data, plotted in Figure 5-61, the saturation exponent increased as the extent of oil-wetting increased.

The foregoing data suggest that unless the reservoir is known to be water-wet, the saturation exponent should be measured with native-state (preferably) or restored cores. If the reservoir is oil-wet and clean cores are used that may be water-wet, the saturation exponents that are obtained can lead to an underestimate of connate water saturation in the formation tested.

FORMATION EVALUATION

Formation evaluation, as applied to petroleum reservoirs, consists of the quantitative and qualitative interpretation of formation cores, geophysical well logs, mud logs, flow tests, pressure tests, and samples of reservoir fluids. The goal of the interpretation is to provide information concerning reservoir lithology, fluid content, storage capacity, and producibility of oil or gas reservoirs. The final analysis includes an economic evaluation of whether to complete an oil or gas well and, once completed, an ongoing analysis of how to produce the well most effectively. These interpretations and analyses are affected by geological complexity of the reservoir, rock quality, reservoir heterogeneity, and, from a logistical standpoint, the areal extent and location of the project of interest. In the early stages of development, the purpose of formation evaluation is to define reservoir thickness and areal extent, reservoir quality, reservoir fluid properties, and ranges of rock properties. The key rock properties are porosity, permeability, oil, gas, and water saturations. Because of space limitations and the importance of these properties, methods of measuring porosity, permeability, and fluid saturations will be emphasized.

Coring and Core Analysis

Routine or conventional core analyses refer to common procedures that provide information on porosity, permeability, resident fluids, lithology, and

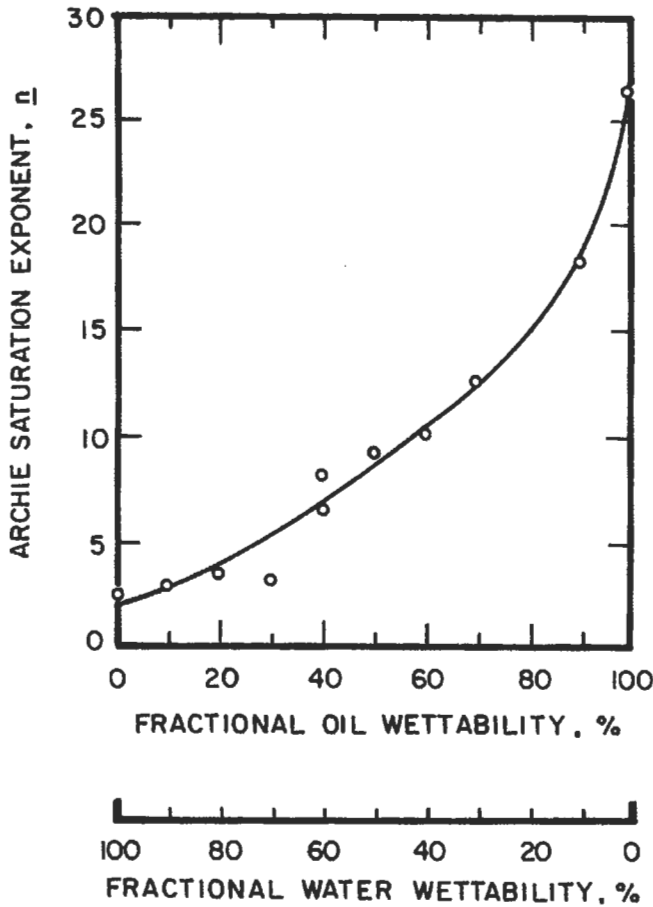


Figure 5-61. Influence of wettability on saturation exponent [179].

texture of petroleum reservoirs. Table 5-20 [180] lists the types of analyses that are obtained and how the results of each analysis are used. Specialized core analyses, such as are listed in Table 5-21, are done less often, but are important for specific applications. Routine core analyses can be performed on whole cores or on small plugs that are cut from a larger core. With the exception of petrographic analyses (thin sections, x-ray; scanning electron microscopy, etc.), special core analyses are normally done with core plugs. After a well is drilled and logs are available to identify zones of interest, very small portions of the reservoir can be obtained with percussion sidewall or sidewall drilled cores. Sidewall cores are less expensive and are valuable for petrographic analyses, but are generally not suitable for special core analyses.

The subject of coring and core analysis was summarized recently in a series of articles [181-189]. An overview article [190] described how core analyses can aid reservoir description. A handbook [191] is available that describes procedures and tools for conventional coring as well as methods for routine core analysis. Procedures for routine core analysis and methods of preserving cores have been

Table 5-20
Routine Core Analysis Tests

Type of analysis	Use of results
Porosity	A factor in volume and storage determinations.
Permeability—horizontal and vertical	Defines flow capacity, crossflow, gas and water coning and relative profile capacity of different zones, pay and nonpay zones.
Saturations	Defines presence of hydrocarbons, probable fluid recovery by test, type of recovery, fluid contacts, completion interval.
Lithology	Rock type, fractures, vugs, laminations, shale content used in log interpretation, recovery forecasts, capacity estimates.
Core-gamma ray log	Relates core and log depth.
Grain density	Used in log interpretation and lithology.

From Reference 180.

recommended by the American Petroleum Institute [192]. Some of the information available in these sources will be highlighted.

Coring

Well coring refers to the process of obtaining representative samples of the productive formation in order to conduct a variety of laboratory testing. Various techniques are used to obtain core samples: conventional diamond-bit coring, rubbersleeve coring, pressure coring, sidewall coring, and recovery of cuttings generated from the drilling operation. Conventional coring is normally done in competent formations to obtain full-diameter cores. Rubber sleeve-coring improves core recovery in softer formations. Pressure coring, although relatively expensive, is used to obtain cores that have not lost any fluids during lifting of the core to the surface.

A common problem with all of these techniques is to decide when to core. In many instances, cores from the interval of interest are not obtained because of abrupt stratigraphic changes. A second problem is that, typically, non-productive intervals of the desired strata are obtained. These intervals did not initially contain a significant amount of hydrocarbon.

Core Preservation

The importance of not altering wettability with drilling mud filtrate has been discussed in this chapter in the section entitled "Wettability and Contact Angle." Preventing wettability changes in core material, after it has been recovered at the surface, can be equally important so that subsequent laboratory measurements are representative of formation conditions.

Cores obtained with drilling muds that minimize wettability alteration, and that are protected at the well-site to prevent evaporation or oxidation, are called preserved cores. They are also referred to as fresh cores or native-state cores.

Table 5-21
Special Core Analysis Tests

Type of test	Use of results
Capillary pressure	Defines irreducible fluid content, contacts.
Rock compressibility	Volume change caused by pressure change.
Permeability and porosity vs. pressure	Corrects to reservoir conditions.
Petrographic studies	
mineral	Used in log interpretation.
diagenesis	Origin of oil and source bed studies.
clay identification	Origin of oil and log analysis.
sieve analysis	Selection of screens, sand grain size.
Wettability	Used in capillary pressure interpretation and recovery analysis-relative permeability.
Electrical	
formation factor	Used in log interpretation.
resistivity index	
Acoustic velocity	Log and seismic interpretation.
Visual inspection	Rock description and geological study.
Thin sections, slabs	
Air, water, and other liquid permeability	Evaluates completion, workover, fracture and injection fluids; often combined with flood-pot test.
Flood-pot test and waterflood evaluation	Results in values for irreducible saturations, values for final recovery with special recovery fluids such as surfactants, water, and polymers.
Relative permeability	Relative permeability is used to obtain values for effective permeability to each fluid when two or more fluids flow simultaneously; relative permeability enables the calculation of recovery versus saturation and time while values from flood-pot test give only end-point results.
gas-oil	
gas-water	
water-oil	
oil-special fluids	
thermal	

From Reference 180.

Cores that are cleaned with solvents and resaturated with reservoir fluids are called restored-state cores or extracted cores. The restoring process is often performed on nonpreserved or weathered cores, but the same technique could apply to cores that had been preserved.

Two methods of preserving conventional cores, immediately after they have been removed from the core barrel, will prevent changes in wettability for several months. One method consists of immersing the core in deoxygenated formation brine or suitable synthetic brine (i.e., drilling mud filtrate) and keeping the samples in suitable containers that can be sealed to prevent leakage and the entrance of oxygen. In the second method, the cores are wrapped in Saran or polyethylene film and aluminum foil and then coated with wax or strippable plastic. The second method is preferred for cores that will be used for laboratory determination of residual oil content, but the first method may be preferred for laboratory displacement tests. Plastic bags are often recommended for short-term (2-4 days) storage of core samples. However, this method will not ensure unaltered rock wettability. Air-tight metal cans are not recommended because of the possibility of rust formation and potential leakage.

Cores taken with a pressure core barrel are often frozen at the well-site for transportation to the laboratory. (Cores are left in the inner core barrel.) Normally, the inner barrel containing the cores is cut into lengths convenient for transport. Because of the complexity of the operation, the pressure core barrel is not used as extensively as the conventional core barrel. An alternate procedure involves bleeding off the pressure in the core and core barrel while the produced liquids are collected and measured. Analysis of the depressured core is done by conventional techniques. Fluids collected from the barrel during depressuring are proportionately added to the volumes of liquid determined from core analysis. In this manner a reconstructed reservoir core saturation is provided.

Core Preparation

Depending on the type of core testing to be done, core samples may be tested as received in the laboratory or they may be cleaned to remove resident fluids prior to analysis. Details for cutting, cleaning, and preparing core plugs can be found in API RP-40: Recommended Practice for Core-Analysis Procedure [192], available from API Production Department, 211 North Ervay, Suite 1700, Dallas, TX 75201.

Core Analysis

Conventional core analysis procedures are described in detail in API RP-40 and elsewhere [191]. A good discussion on core analysis procedures is in the textbook written by Amyx, Bass, and Whiting [19].

Porosity. A number of methods [192] are suitable for measuring porosity of core samples. In almost all the methods, the sample is cleaned by solvent extraction and dried to remove liquid. Porosity can be determined by saturating the dry core with brine and measuring the weight increase after saturation. Another common method includes compressing a known volume of gas (usually helium) at a known pressure into a core that was originally at atmospheric pressure. Several other techniques have been used; one of the more common methods is the mercury porosimeter in which pressure on the core plug is reduced and the volume of the expanded air or gas is measured accurately. A summation of fluids technique, which measures and sums the oil, gas and water volumes in a freshly recovered reservoir core sample, is often used for plugs or sidewall samples of non-vuggy consolidated rocks that contain minimum amounts of clay [188].

Equations commonly used for calculation of porosity by gas expansion or compression include:

$$\phi = \left(\frac{V_p}{V_b} \right) 100 \quad (5-80)$$

$$\phi = \left(\frac{V_b - V_g}{V_b} \right) 100 \quad (5-81)$$

where ϕ = porosity expressed as a percent

V_p = pore volume
 V_b = bulk volume
 V_{gr} = grain volume

All volumes should be in consistent units, commonly cm^3 . If pore volume is measured directly in cores that contain vugs (such as some carbonates), Equation 5-80 may give erroneously high porosity because the bulk volume may be erroneously low [188]. If bulk volume of vuggy cores is determined by submerging the core in mercury or water, Equation 5-81 may yield erroneously low porosity [188]. Thus valid porosity values can only be obtained if bulk volume and grain volume measurements are accurate.

Permeability. The permeability of core plugs is determined by flowing a fluid (air gas, or water) through a core sample of known dimensions. If the absolute permeability is to be determined, the core plug is cleaned so that permeability is measured at 100% of the saturating fluid. Methods of measuring permeability of core plugs are described in API RP-27: Recommended Practice for Determining Permeability of Porous Media [193]. Equation 5-36 can be used to calculate permeability of core plugs.

Fluid Saturations. Coring procedures usually alter the fluid content of the reservoir rock during the coring process. Drilling fluid is jetted against the formation rock ahead of the coring bit and the core surface as it enters the core barrel; as a result of this flushing action by the drilling mud filtrate, most free gas and a portion of the liquid are displaced from the core. When water base drilling fluid is used, the mud filtrate may displace oil until a condition of residual oil saturation is obtained. Also, this flushing action may result in the fluid content of the core being predominately that of the drilling fluid. When oil base drilling fluid is used, the core sample that is obtained may be driven to an irreducible water saturation.

Factors Affecting Oil Displaced During Coring. During the coring operation, it is important to avoid extreme flushing conditions that could cause mobilization of residual oil [194]. Some of the variables that control the amount of oil flushed from a core by mud filtrate are: borehole-to-formation differential pressure (overbalance), coring penetration rate, core diameter, type of drill bit, drilling mud composition (including particle size distribution), depth of invasion of mud particles into the core, rate of filtrate production (both spurt loss and total fluid loss), interfacial tension of mud filtrate, permeability of the formation (both horizontal and vertical), and nature of the reservoir (uniformity, texture, etc.). In one type of system investigated in the laboratory [195], the amount of oil stripped from cores varied directly with the overbalance pressure, filtration production rate, core diameter and core permeability; it varied inversely with penetration rate. In that system, the overbalance pressure exerted more influence than the other factors. When large pressure gradients exist near the core bit, unintentional displacement of residual oil may occur in coring operations. In this region close to the bit, high velocities caused by this high pressure may mobilize some of the residual oil. Drilling mud composition can affect subsequent laboratory oil displacement tests in core samples by: changing wettability of the reservoir rock, altering interfacial tension of the mud filtrate, being penetrated by mud particles into the zone of interest, and yielding undesirable fluid loss properties. Since fluids with lower interfacial tension contribute to

additional oil recovery, whenever possible, the use of mud additives that lower interfacial tension should be avoided. Greater amounts of residual oil are displaced from cores as the filtrate production rate is increased. Higher API filter loss or smaller core diameters will generally lead to larger amounts of flushing, but a key factor in the amount of mobilized residual oil is the spurt loss (the rapid loss to the formation that occurs before an effective filter cake is formed). As stated previously, uniformity of the formation being cored will influence the amount of oil that will be displaced. Identical drilling conditions may yield varying results with changes in lithology or texture of the reservoir. In particular, drastic differences may be observed in reservoirs that contain both sandstone and carbonate oil-bearing strata.

Factors Affecting Oil Saturation Changes During Recovery of Cores. Surface oil saturations should be adjusted to compensate for shrinkage and bleeding [123]. Shrinkage is the term applied to the oil volume decrease caused by a temperature change or by a drop in pressure which causes dissolved gases to escape from solution. Shrinkage of reservoir fluids is measured in the laboratory by differentially liberating the samples at reservoir temperature. The formation volume factors are used to adjust surface oil volume back to reservoir temperature and pressure. Gases coming out of solution can cause some oil to flow out of the core even though it may have been flushed to residual oil by mud filtrate. Bleeding is the term applied to this decrease in oil saturation as the core is brought to the surface. Calculations have been proposed [123] to account for shrinkage and bleeding (see the discussion in this chapter entitled "Estimation of Waterflood Residual Oil Saturation").

Measurement of Fluid Saturations. There are two primary methods of determining fluid content of cores; these methods are discussed in API RP-40: Recommended Practice for Core-Analysis Procedure [192]. In the retort or vacuum distillation method, a fluid content still is used to heat and vaporize the liquids under controlled conditions of temperature and pressure. Prior to testing, the gas space in the core is displaced with water. The fluids produced from the still are condensed and measured, and the fluid saturations are calculated. Normally the percent oil and water are subtracted from 100% to obtain the gas saturation; however, considerable error may be inherent in this assumption. The second common method is the distillation-extraction method in which water in the core is distilled, condensed, and accumulated in a calibrated receiving tube. Oil in the core is removed by solvent extraction and the oil saturation is calculated from the weight loss data and the water content data.

Conventional core samples have oil content determined by atmospheric distillation. The oil distilled from a sample is collected in a calibrated receiving tube where the volume is measured. Temperatures up to 1,200°F (about 650°C) are used to distill the oil from the sample which causes some coking and cracking of the oil and the loss of a small portion of the oil. An empirically derived correction is applied to the observed volume to compensate for the loss. Calibration tests are made on each type of oil.

Whole core samples have oil content determined by vacuum distillation. This technique is used to remove oil from the sample without destroying the minerals of the sample. A maximum temperature of 450°F is used. The oil distilled from the sample is collected in a calibrated receiving tube which is immersed in a cold bath of alcohol and dry ice at about -75°C. This prevents the oil from being drawn into the vacuum system. As in the atmospheric distillation method, corrections must be applied to the measured volumes.

The oil content (V_o) divided by the pore volume (V_p) yields the oil saturation (S_o) of a sample in percent of pore space:

$$S_o = \left(\frac{V_o}{V_p} \right) 100 \quad (5-82)$$

Two sources of error are inherent in the retort method. At the high temperatures employed, water of crystallization within the rock is driven off which causes the water saturation to appear to be higher than the actual value. Another error results from the cracking of the oil and subsequent deposition of coke within the pore structure. Thus, a calibration curve should be prepared on various gravity crudes to compensate for the oil lost from the cracking and coking. Both of the above errors will result in a measured oil saturation that is lower than the actual saturation in the rock. Another possible source of error is the liberation of carbon dioxide from carbonate material in the core at elevated temperatures; this would cause a weight loss that can be interpreted as a change in saturation. The solvent extraction method has the disadvantage in that it is an indirect method since only the water removed from the core is measured. However the extraction method has the advantage that the core is usually not damaged and can be used for subsequent tests.

Grain Density and Core Description. Grain density and lithologic descriptions are often provided in data for routine core analysis. Grain density depends on the lithology and composition of the reservoir of interest. Densities of some common minerals found in reservoir rocks are listed in Table 5-22 [41].

Results of Core Analyses from Various Reservoirs. Typical core analyses [23] of different formations from various states and regions of the U.S. are listed in Table 5-23a to 5-23i. In addition to ranges in permeability, porosity, oil saturation, connate water saturation, the depth and thickness of the productive intervals are given.

(text continued on page 108)

Table 5-22
Densities of Common Minerals
in Reservoir Rocks

Material	Matrix density* (gm/cm³)
Sand (consolidated)	2.65
Sand (unconsolidated)	2.65
Limestone	2.71
Dolomite	2.8-2.9
Shale	1.8-2.7
Gypsum	2.32
Anhydrite	2.9-3.0
Halite	2.16

From Reference 41.

* These figures are averages and may vary from area to area, depending on types and abundance of secondary minerals.

Table 5-23
Typical Core Analyses from Various Reservoirs [23]
(a) Arkansas

Formation	Fluid prod.	Range of prod. depth, ft	Avg. prod. depth, ft	Range of prod. thickness, ft	Avg. prod. thickness, ft	Range of perm. K, md	Avg. perm. K, md	Range of porosity, %	Avg. porosity, %	Range of oil satn., %	Avg. oil satn., %	Range of calc. connate water satn., %	Avg. calc. connate water satn., %
Blossom	C/O*	2,190–2,655	2,422	3–28	15	1.6– 8,900	1,685	15.3–40	32.4	1.2–36	20.1	24–55	32
Cotton Vally	C/O	5,530–8,020	6,774	4–79	20	0.6– 4,820	333	11.3–34	20.3	0.9–37	13.1	21–43	35
Glen Rose†	O	2,470–3,835	3,052	5–15	10	1.6– 5,550	732	17.3–38	23.4	4.0–52	21.0	28–50	38
Graves	C/O	2,400–2,725	2,564	2–26	11	1.2– 4,645	1,380	9.8–40	34.9	0.3–29	16.8	19–34	30
Hogg	O	3,145–3,245	3,195	12–33	17	6.5– 5,730	1,975	14.4–41	30.9	2.6–56	19.9	26–34	27
Meakin	G/C/O*	2,270–2,805	2,485	2–20	11	3.0– 6,525	1,150	17.1–40	31.8	0.6–43	12.9	24–63	43
Nacatoch	C/O	1,610–2,392	2,000	8–45	20	0.7– 6,930	142	9.9–41	30.5	0.2–52	4.9	41–70	54
Paluxy	O	2,850–4,890	3,868	6–17	12	5–13,700	1,213	15.1–32	26.9	7.5–49	21.2	28–43	35
Pettit	O	4,010–5,855	4,933	4–19	11	0.1– 698	61	6.2–28	15.4	9.1–29	12.7	25–44	30
Rodessa‡	O	5,990–6,120	6,050	8–52	16	0.1– 980	135	5.1–28	16.5	0.7–26	14.8	25–38	31
Smackover§	G/C/O	6,340–9,330	8,260	2–74	16	0.1–12,600	850	1.1–34	14.2	0.7–41	12.8	21–50	31
Tokio	C/O	2,324–2,955	2,640	2–19	13	0.5–11,550	2,100	13.6–42	32.1	0.9–57	25.8	17–43	27
Travis Peak	C/O	2,695–5,185	3,275	3–25	10	0.4– 6,040	460	9.4–36	24.3	0.5–36	14.3	16–48	36
Tuscaloosa	C/O	3,020–3,140	3,080	4–25	15	0.4– 3,760	506	15.6–39	27.3	0.3–53	14.0	31–63	45

From Reference 23.

* Indicates fluid produced: G—gas; C—condensate; O—oil.

† Specific zone not identified locally.

‡ Includes data from Mitchell and Gloyd zones.

§ Includes data from Smackover Lime and Reynolds zones.

(b) East Texas Area

Formation	Fluid prod.	Range of prod. depth, ft	Avg. prod. depth, ft	Range of prod. thickness, ft	Avg. prod. thickness, ft	Range of perm. K, md	Avg. perm. K, md	Range of porosity, %	Avg. porosity, %	Range of oil satn., %	Avg. oil satn., %	Range of calc. connate water satn., %	Avg. calc. connate water satn., %
Bacon	C/O	6,685-7,961	7,138	3-24	11	0.1- 2,040	113	1.5-24.3	15.2	2.7-20.6	8.6	9-22	16
Cotton Vally	C	8,448-8,647	8,458	7-59	33	0.1- 352	39	6.9-17.7	11.7	1.1-11.6	2.5	13-32	25
Fredericksburg	O	2,330-2,374	2,356	5- 8	7	0.1- 4.6	1.2	11.9-32.8	23.1	3.3-39.0	20.8	35-43	41
Gloyd	C/O	4,812-6,971	5,897	3-35	19	0.1- 560	21	8.0-24.0	14.9	tr-24.3	8.2	16-45	31
Henderson	G/C/O	5,976-6,082	6,020	3-52	12	0.1- 490	19	7.0-26.2	15.2	0.8-23.3	10.6	21-44	27
Hill	C/O	4,799-7,668	5,928	3-16	9	0.1- 467	70	6.4-32.2	15.6	0.9-26.7	12.2	23-47	33
Mitchell	O	5,941-6,095	6,010	3-43	21	0.1- 487	33	7.2-29.0	15.5	1.8-25.9	12.5	15-47	29
Mooringsport	O	3,742-3,859	3,801	4-12	8	0.4- 55	5	5.3-19.6	14.6	2.8-26.6	13.8	29-48	40
Nacatoch*	O	479-1,091	743	2-21	12	1.9- 4,270	467	13.4-40.9	27.1	0.6-37.4	14.5	24-55	41
Paluxy	O	4,159-7,867	5,413	7-46	27	0.1- 9,600	732	6.3-31.1	21.6	2.2-48.7	24.1	22-47	30
Pecan Gap	O	1,233-1,636	1,434	5-20	13	0.5- 55	6	16.3-38.1	26.6	3.5-49.8	12.9	30-56	46
Pettit†	G/C/O	5,967-6 379	7,173	2-23	11	0.1- 3,670	65	4.5-25.8	14.7	0.9-31.6	9.8	10-35	23
Rodessa	C/O	4,790-8 756	6,765	4-42	17	0.1- 1,180	51	2.3-29.0	14.5	tr-25.3	5.3	6-42	23
Sub-Clarksville‡	O	3,940-5,844	4,892	3-25	12	0.1- 9,460	599	8.2-38.0	24.8	1.4-34.6	17.9	12-60	33
Travis Peak‡	C/O	5,909-8,292	6,551	2-30	11	0.1- 180	42	5.6-25.8	15.0	0.1-42.8	12.5	17-38	28
Wolfe City	O	981-2,054	1,517	6-22	13	0.3- 470	32	17.1-38.4	27.9	1.5-37.4	15.6	23-68	46
Woodbine	C/O	2,753-5,993	4,373	2-45	14	0.1-13,840	1,185	9-7-38.2	25.5	0.7-35.7	14.5	14-65	35
Young	C	5,446-7,075	8,261	4-33	17	0.1- 610	112	4.4-29.8	19.7	tr-4.5	0.8	13-27	21

* Small amount of Navarro data combined with Nacatoch.

† Data for Pittsburg, Potter, and Upper Pettit combined with Pettit.

‡ Small amount of Eagleford data combined with Sub-Clarksville.

§ Data for Page combined with Travis Peak.

Table 5-23
(continued)
(c) North Louisiana Area

Formation	Fluid prod.	Range of prod. depth, ft	Avg. prod. depth, ft	Range of prod. thickness, ft	Avg. prod. thickness, ft	Range of perm. K, md	Avg. perm. K, md	Range of porosity, %	Avg. porosity, %	Range of oil satn., %	Avg. oil satn., %	Range of calc. connate water satn., %	Avg. calc. connate water satn., %
Annona Chalk	O	1,362– 1,594	1,480	15–69	42	0.1– 2.5	0.7	14.3–36.4	26.8	6.0–40	22	24–40	37
Buckrange	C/O	1,908– 2,877	2,393	2–24	13	0.1–2,430	305	13.4–41	31.4	0.7–51	22.6	29–47	35
Cotton Valley ^a	G/C/O	3,650– 9,450	7,450	4–37	20	0.1–7,350	135	3.5–34	13.1	0.0–14	3.1	11–40	24
Eagleford ^b	C	8,378– 8,417	8,397	9–11	10	3.5–3,040	595	12.8–28	22.9	1.6–28	4.3	...	36
Fredericksburg	G/C	6,610– 9,880	8,220	8– 6	7	1.6– 163	90	12.8–23.1	19.9	1.7–4.3	2.7	35–49	41
Haynesville	C	10,380–10,530	10,420	22–59	40	0.1– 235	32	5.5–23.1	13.4	1.1–14.5	5.1	31–41	38
Hosston	C/O	5,420– 7,585	6,480	5–15	12	0.4–1,500	140	8.8–29	18.6	0.0–35	8.8	18–37	28
Nacatoch	O	1,223– 2,176	1,700	6–12	8	27–5,900	447	25.8–40	31.4	2.5–33	19.5	45–54	47
Paluxy	C/O	2,195– 3,240	2,717	2–28	16	0.2–3,080	490	9.6–39	27.2	0.1–48	11.8	23–55	35
Pettit ^c	C/O	3,995– 7,070	5,890	3–30	14	0.1– 567	26	4.5–27	14.3	0.1–59	15.6	10–43	29
Pine Island ^d	O	4,980– 5,080	5,010	5–13	9	0.2–1,100	285	8.5–27	20.8	13.3–37	24.1	16–30	22
Rodessa ^e	G/C/O	3,625– 5,850	4,880	6–52	18	0.1–2,190	285	5.1–34	19.1	0.0–31	2.9	21–38	30
Schuler ^f	G/C/O	5,500– 9,190	8,450	4–51	19	0.1–3,180	104	3.6–27.4	15.0	0.0–24	4.8	6–51	25
Sligo ^g	C/O	2,685– 5,400	4,500	3–21	7	0.1–1,810	158	7.3–35	21.1	0.6–27	9.8	12–47	31
Smackover	C/O	9,980–10,790	10,360	6–55	24	0.1–6,190	220	3.4–23	12.9	1.1–22	7.2	9–47	25
Travis Peak ^h	C/O	5,890– 7,900	6,895	7–35	18	0.1–2,920	357	7.0–27	19.4	0.1–35	8.8	26–38	31
Tuscaloosa	G/C/O	2,645– 9,880	5,164	4–44	24	0.1–5,750	706	10.7–36	27.6	0.0–37	8.5	31–61	43

^a Data reported where member formations of Cotton Valley group not readily identifiable.

^b Data reported as Eutaw in some areas.

^c Includes data reported as Pettit, Upper Pettit, and Mid Pettit. Sometimes considered same as Sligo.

^d Sometimes referred to as Woodruff.

^e Includes data reported locally for Jeter, Hill, Kilpatrick, and Fowler zones.

^f Includes data reported locally for Bodcaw, Vaughn, Doris, McFerrin, and Justiss zones.

^g Includes data reported as Birdsong-Owens.

^h Frequently considered same as Hosston.

(d) California

Formation	Area	Fluid prod.	Range of prod. depth, ft	Ave. prod. depth, ft	Range of prod. thickness, ft	Ave. prod. thickness, ft	Range of perm. K, md	Ave. perm. K, md	Range of porosity, %	Ave. porosity, %	range of oil satn., %	Avg. oil satn., %	Range of total water satn., %	Ave. total water satn., %	Range of calc. water satn., %	Ave. calc. connete water satn., %	Range of grav-ity, °API	Ave. grav-ity, °API
Eocene, Lower	San Joaquin Valley ^a	O	6,820-8,263	7,940	—	—	35-2,000	518	14-26	20.7	8-23	14.1	16-51	35	15-49	35	28-34	31
Miocene	Los Angeles Basin and Coastal ^b	O	2,870-9,530	5,300	60- 450	165	10-4,000	300	15-40	28.5	6-65	18.8	25-77	50	15-72	36	15-32	26
Miocene, Upper	San Joaquin Valley ^c	O	1,940-7,340	4,210	10-1,200	245	4-7,500	1,000	17-40	28.2	9-72	32 ^x	20-68 ^x	50 ^x	12-62	30	13-34	23
	Los Angeles Basin and Coastal ^d	O	2,520-6,660	4,100	5-1,040	130	86-5,000	1,110	19.5-39	30.8	10-55	25	22-72	44	12-61	30	11-33	21
Miocene, Lower	San Joaquin Valley ^e	O	2,770-7,590	5,300	30- 154	76	15-4,000	700	20-38	28.4	4-40	19	25-80	51	14-67	36	15-40	34
	Los Angeles Basin and Coastal ^f	O	3,804-5,610	4,430	20- 380	134	256-1,460	842	21-29	24.3	13-20	15.8	32-67	63	27-60	37	34-36	35
Oligocene	San Joaquin Valley ^g	O	4,589-4,717	4,639	—	—	10-2,000	526	19-34	26.3	12-40	22	2-60	43	3-45	30	37-36	38
	Coastal ^h	O	5,838-6,170	6,090	—	—	20- 400	107	15-22	19.5	6-17	11.8	19-56	46	15-52	42	—	25
Pliocene	San Joaquin Valley ⁱ	O	2,456-3,372	2,730	5- 80	33	279-9,400	1,260	30-38	34.8	7-43 ^j	24.1 ^j	33-84	54	10-61	34	18-44	24
	Los Angeles Basin and Coastal ^k	O	2,050-3,450	2,680	—	100	25-4,500	1,410	24-11	35.6	15-80	45	19-54	36	10-40	21	12-23	15

^a Mainly data from Gatchell zone.

^b Includes Upper and Lower Terminal, Union Pacific, Ford, "237," and Sesnon zones.

^c Includes Kernco, Republic, and "26 R" zones.

^d Includes Jones and Main zones.

^e Includes "JV," Olcese, and Phacoides zones.

^f Mainly data from Vaqueros zone.

^g Mainly data from Oceanic zone.

^h Mainly data from Sespe zone.

ⁱ Includes Sub Mulinia and Sub Scaletz No. 1 and No. 2 zones.

^j Includes Ranger and Tar zones.

^k Oil-base data show high oil saturation (avg. 61 percent) and low water (3-54 percent, avg. 15 percent).

^l Oil-base data show range 27.6 to 52.4 and avg. of 42.3 percent—not included in above "oil-saturation" values.

Table 5-23
(continued)
(e) Texas Gulf Coast—Corpus Christi Area*

Formation	Fluid prod.	Range of prod. depth, ft	Avg. prod. depth, ft	Range of prod. thickness, ft	Avg. prod. thickness, ft	Range of perm. K, md	Avg. perm. K, md	Range of porosity, %	Avg. porosity, %	Range of oil satn., %	Avg. oil satn., %	Range of calc. connate water satn., %	Avg. calc. connate water satn., %	Range of gravity, °API	Avg. gravity, °API
Catahoula	O	3,600–4,800	3,900	1–18	8	45–2,500	670	17–36	30	1–30	14	30–44	36	23–30	29
Frio	C/O	1,400–9,000	6,100	3–57	13	5–9,000	460	11–37	27	2–38	13	20–59	34	23–48	41
Jackson	O	600–5,000	3,100	2–23	9	5–2,900	350	16–38	27	3–32	15	21–70	45	22–48	37
Marginulina	C	6,500–7,300	7,000	5–10	7	7– 300	75	14–30	24	1–4	2	20–48	34	55–68	60
Oakville	O	2,400–3,100	2,750	5–35	22	25–1,800	700	21–35	28	9–30	18	32–48	44	23–26	25
Vicksburg	C/O	3,000–9,000	6,200	4–38	12	4–2,900	220	14–32	24	1–17	7	26–54	38	37–65	48
Wilcox	C	6,000–8,000	7,200	30–120	60	1– 380	50	15–25	19	0–10	1	22–65	37	53–63	58
Yegua	O	1,800–4,000	3,000	3–21	7	6–1,900	390	22–38	29	4–40	17	14–48	36	20–40	32

* Includes counties in Texas Railroad Commission District IV: Jim Wells, Brooks, Hidalgo, Aransas, San Patricio, Nueces, Willacy, Duval, Webb, Jim Hog, and Starr.

(f) Texas Gulf Coast-Houston Area

Formation	Fluid prod.	Range of prod. depth, ft	Avg. prod. depth, ft	Range of prod. thickness, ft	Avg. prod. thickness, ft	Range of perm. K, md	Avg. perm. K, md	Range of porosity, %	Ave. porosity, %	Range of oil satn., %	Ave. oil satn., %	Range of total water satn., %	Ave. total water satn., %	Range of calc. connate water satn., %	Avg. calc. connate water satn., %	Range of gravity, °API	Avg. gravity °API
Frio	C	4,000-11,500	8,400	2-50	12.3	18- 9,200	810	18.3-38.4	28.8	0.1- 6.0	1.0	34-72	54	20-63	34		
	O	4,600-11,200	7,800	2-34	10.4	33- 9,900	1,100	21.8-37.1	29.8	4.6-41.2	13.5	24-79	52	12-61	33	25-42	38
Marginulina	C	7,100- 8,300	7,800	4-28	17.5	308- 3,870	2,340	35-37	35.9	0.2- 0.8	0.5	33-61	48	14-31	21		
	O	4,700- 6,000	5,400	4-10	5.7	355- 1,210	490	28.5-37.3	32.8	8.1-21.8	15.3	48-68	59	25-47	36	25-30	28
Miocene	C	2,900- 6,000	4,000	3- 8	5.5	124-13,100	2,970	28.6-37.8	33.2	0.2- 1.5	0.5	55-73	66	23-53	38		
	O	2,400- 8,500	3,700	2-18	7.2	71- 7,660	2,140	23.5-38.1	35.2	11-29	18.8	45-69	58	21-55	34	21-34	25
Vicksburg	C	7,400- 8,500	8,100	1- 6	2.0	50- 105	88	28.5-31.0	27.1	0- 1.5	0.2	66-78	74	53-61	56		
	O	8,900- 8,200	7,400	3-18	8.3	190- 1,510	628	28.5-31.8	30.4	14.4-20.3	15.3	45-55	53	26-36	35	22-37	35
Wilcox	C	5,800-11,500	9,100	5-94	19.1	3.0- 1,860	96	14.5-27.4	19.6	0.2-10.0	1.5	27-62	46	20-54	36		
	O	2,300-10,200	7,900	3-29	10.0	9.0- 2,460	195	16.2-34.0	21.9	4.6-20.5	9.7	32-72	47	20-50	37	19-42	34
Woodbine	O	4,100- 4,400	4,300	6-13	6.2	14- 680	368	23.5-26.7	25.5	10.7-27.4	20.1	34.4-72.7	46	24-59	36	26-28	27
Yegua	G/C	4,400- 8,700	6,800	3-63	11.0	24- 5,040	750	23.4-37.8	30.7	0.1-15.5	1.2	26-74	57	17-59	33		
	O	3,700- 9,700	6,800	2-59	8.5	23- 4,690	903	22.9-38.5	31.6	3.5-21.6	11.4	31-73	57	17-53	34	30-46	37
Louisiana Gulf Coast-Lafayette Area																	
Miocene	C	5,200-14,900	11,200	3-96	20.2	36- 6,160	1,010	15.7-37.8	27.3	0.1- 4.7	1.5	37-79	53	20-74	35		
	O	2,700-12,700	9,000	3-32	11.0	45- 9,470	1,630	18.3-39.0	30.0	6.5-26.9	14.3	30-72	51	18-50	32	25-42	36
Oligocene	C	7,300-14,800	9,800	2-80	14.8	16- 5,730	920	16.7-37.6	27.7	0.5- 6.9	2.3	33-71	51	19-57	32		
	O	6,700-12,000	9,400	2-39	6.3	64- 5,410	1,410	22.1-36.2	29.0	5.2-20.0	11.1	34-70	54	23-60	35	29-44	38

**Table 5-23
(continued)
(g) Oklahoma-Kansas Area**

Formation	Fluid prod.	Range of prod. depth, ft	Avg. prod. depth, ft	Range of thick-ness, ft	Avg. prod. thick-ness, ft	Range of perm. K, md	Avg. perm. K, md	Range of perm. K _{sp} , md	Avg. perm. K _{sp} , md	Range of porosity, %	Avg. porosity, %	Range of oil satn., %	Avg. oil satn., %	Range of total water satn., %	Avg. total water satn., %	Range of calc. connate water satn., %	Avg. calc. connate water satn., %	Range of grav-ity, °API	Avg. grav-ity, °API
Arbuckle	G	2,700- 5,900	4,500	5.0-37	18.3	3.2- 544	131	—	—	9.0-20.9	14.4	0.7- 9.4	3.7	34.5-62.7	43.1	28-82	40		
	O	500- 6,900	3,500	1.0-65.5	11.8	0.2-1,530	140	0.1-1,270	67.8	2.1-24.3	12.0	5.2-42.3	17.7	20.6-79.3	52.4	20-79	47	29-44	37
	T ^a	800-11,600	3,600	2.0-33	14.3	0.1- 354	57	0.1-135	21.8	3.7-23.1	9.2	0 -23.8	7.1	37.2-91.9	69.2	37-91	52	42	42
Atoka ^a	G	3,700- 3,800	3,700	1.0- 9.0	4.0	1.3- 809	174	—	—	8.5-17.3	12.9	0 - 8.1	2.0	36.4-65.2	47.2	32-85	45		
	O	500- 4,500	2,600	3.0-16	7.8	0.3- 920	144	0.6-2.6	1.7	5.9-28.6	14.5	5.1-35.1	20.7	16.4-61.5	38.7	19-61	37	31-42	38
Bartlesville	T	300- 3,700	2,100	2.0-10	6.5	9 - 168	87.3	—	—	11.9-18.6	14.9	5.8-21.1	12.1	42.7-55.4	47.0	40	40		
	G	700- 7,400	2,600	1.5-42	11.4	0.2- 36	10.4	5.5	5.5	8.4-21.1	15.6	0 -11.1	4.7	23.4-70	54.1	23-68	48		
	O	200- 5,700	1,500	1.0-72	14.0	0.2- 537	32.7	1.5	1.5	8.5-26.8	17.8	3.3-60.6	18.2	17.4-85.2	44.4	17-72	40	28-42	34
Bois D'Arc	T	500- 2,800	1,200	4 - 40	14.5	0.1- 83	18.2	0.07	0.07	8.5-20.1	14.6	0.9-35.7	12.2	43.9-88	63.6	43-67	54	35	35
	G	4,800- 5,100	5000	4 - 46	19	0.1- 43	24.4	—	—	3.8-19.8	12.2	0 - 8.7	4.3	32.9-62.4	42.8	26-62	40		
Booch	O	3,700- 7,800	6,500	2.3-59.8	37.9	0.3- 664	36.0	0.1-2.2	0.45	1.2-19.3	7.2	3.3-25.8	15.0	14.6-58.5	32.4	15-59	32	32-42	40
	G	2,600- 3,200	2,900	5 - 8	8.5	1.4- 8.6	4.0	—	—	11.9-14.8	13.4	4.8- 8.6	8.7	50 -51.3	50.7	50	50		
	O	1,000- 3,800	2,800	2 -28.6	8.8	0.3- 160	19.3	—	—	8.3-21.4	15.6	4.8-49.7	21.5	15.3-60	40.0	15-59	37	29-42	35
Burgess	T	2,700- 3,300	3,000	4 - 5	4.5	3.1- 13	6.0	—	—	18.9-16.1	17.5	7.4- 7.8	7.6	47.3-65.2	51.3	44	44		
	G	—	1,600	—	20	—	142	—	—	—	14.2	—	8.3	—	37.3	—	35		
First Bromide ^d	O	300- 2,800	1,800	2.5- 9	5.8	0.2- 104	19	22	22	8.1-22.8	13.2	16.2-33	21.5	19.3-65.4	42.2	19-58	40	31-38	36
	G	6,600- 7,600	7,200	3.0-19.5	11.3	0.6- 62	31.3	0.4	0.40	1.5- 6.5	4.0	0 - 7.6	3.8	35.7-71.8	53.8	38-72	54		
Second Bromide ^d	O	3,700-13,800	6,600	2.0-82	16.7	0.1-2,260	175	0.2-7.4	2.23	1.4-15.7	9.6	3.1-24	11	12.8-67.2	35.4	12-67	34	31-42	40
	T	6,000-13,200	11,500	15 -161.3	65.1	0.9- 40	18.3	1.40	1.40	1.5-10.9	6.5	0.4- 8.8	2.2	29.5-78.8	48.3				
Burbank	G	6,900-16,200	12,600	20 - 53.8	37.9	3.4- 72	21.4	0.3-0.9	0.60	3.5-14.5	6.8	0 - 6.9	4.0	26.2-45.7	37.9	28-45	32	42	42
	O	4,500-11,200	9,000	3.0- 8.9	18.2	2.0- 585	118	—	—	5.8-11.7	9.3	2.4-24.2	11.5	6.9-44.9	25.1	8-44	25	37-42	41
Chester	T	4,400-13,300	9,700	5 - 44.5	18.4	0.8- 42	12.9	—	—	5.8-11.4	7.4	0 -13.8	4.8	21.1-57.8	43.5	40			
	O	1,300- 4,500	2,800	3 - 48	17.3	0.1- 226	8.64	—	—	8.4-21.6	15.7	9.3-26.6	15.3	31.5-73.4	47.2	31-73	43.	35-41	39
Cleveland ^f	T	2,800- 3,700	3,000	3 - 19	9.1	0.1- 4.8	1.53	—	—	7.1-17.0	13.7	2.0-15.7	11.2	45.7-80.7	57.8	45-81	51		
	G	4,200- 6,700	5,700	2 - 45	10.9	0.1- 269	33.0	0.9-3.5	1.87	2.6-20.7	12.2	0 - 7.5	1.1	20.9-80.7	46.8	19-81	43		
Deese ^g	O	4,700- 6,700	5,700	2 - 23	8.6	0.1- 81	9.11	0-0.5	0.21	2.3-18.0	10.1	7.2-35.9	19.1	17.7-80.8	42.1	17-81	33	38-42	40
	T	4,800- 6,100	5,700	4 - 20.5	10.0	0.1- 13	2.36	0.1-5.0	1.18	3.2-17.6	7.7	0 -11.1	1.2	40.9-89.2	61.7	40-89	61		
Deese ^g	G	2,200- 5,700	3,500	2 - 17	9.0	2.5- 338	50.8	—	—	9.8-23.5	16.9	0 - 7.1	4.1	40 -64.4	48.9	30-64	42		
	O	300- 6,400	3,200	1 - 70	13.4	0.1- 135	15.4	1.4-2.3	1.85	7.4-24.6	15.2	5.8-35.5	13.1	10.2-74.0	46.7	10-74	44	27-58	42
Deese ^g	T	1,900- 3,900	3,100	3 - 22	7.7	0.1- 112	12.9	—	—	11.0-20.4	15.6	0 -21.1	7.6	32.9-77.2	55.3	32-77	49		
	G	4,300-11,800	6,500	5 - 55	19.3	7.8- 232	94.1	0.80	0.80	9.8-22.6	16.7	2.2- 8.3	3.6	19.1-54.9	42.1	19-49	37		
Deese ^g	O	800-10,000	5,200	2 - 80.3	11.7	0.4- 694	62.8	1.10	1.10	4.7-26.4	17.4	5.9-46.4	20.4	14.0-56.6	37.8	13-57	33	17-42	32

Hoover	G	2,200-6,800	4,000	4 -49	16.6	1.9-	200	61.8	—	—	11.7-23.4	18.3	0 - 7.0	0.6	41.1-77.1	53.8	19-76	45
	O	1,800-2,100	2,000	3 -37	11.9	1.3-	974	288	—	—	12.7-24.1	18.7	12.6-23.1	18.0	14.8-48.5	40.2	14-47	36
	T	1,900-2,000	2,000	2 -17	8.4	55 -	788	372	—	—	16.7-22.5	20.5	6.6-17.1	14.5	34.8-50.7	42.9	31-42	36
Hoxbar	G	3,800-8,880	8,300	9 -11	10.0	8.4-	61	33.7	—	—	13.9-18.2	16.1	0.7- 4.4	2.6	40.1-40.8	40.4	34-39	37
	O	1,000-10,300	4,200	2 -83	14.4	0.1-1,820	277	—	—	3.1-29.7	18.5	3.2-48.7	21.4	13.8-68.5	45.1	13-68	39	
	T	2,900-3,000	3,000	3 -13	9.3	0.5-	31	14.4	—	—	14.3-22.7	18.5	3.3-11.4	6.8	50.5-69.8	57.9		34
Hunton	O	1,800-9,600	4,800	2 -77.3	14.0	0.1-	678	34.5	0-77.0	5.24	1 -33.8	10.9	1.6-34.5	15.3	16.7-83.4	48.6	17-93	46
	T	2,500-8,700	4,900	2 -73	14.7	0.1-	48	5.3	0.1-7.9	2.04	1 -19.5	7.3	0 -61.1	10.6	16.0-88.7	54.5	16-89	48
	O	1,900-5,600	3,800	3 -16.2	8.5	0.3-	390	101	0.3-182	52.3	6.4-16.0	12.2	6.5-28.9	18.1	37.4-68.6	51.9	28-69	49
Lansing	T	—	3,300	—	22.0	—	14	—	—	8.7	—	7.2	—	12.8	—	75.5		37
	G	700-6,100	3,900	4 -18	9.3	0.2-	210	26.3	—	—	5.1-25.9	14.5	0 - 7.8	2.4	36.2-83.7	54.1	34-83	47
	O	500-6,300	2,900	1 -57	10.3	0.3-	280	54.1	05-162	23.3	4.6-27.2	17.8	1.6-37.3	15.3	28 -76.3	45.5	23-76	41
Marmatom	T	1,800-5,700	3,200	3 -15.5	7.4	1.1-	143	23.6	—	—	14.2-21.3	17.1	0 -14.3	6.9	33.2-68.4	45.9	31-69	43
	O	4,300-4,600	4,400	1.5- 7.5	4.7	24 -	105	46.4	0.20	0.20	1.8-21.4	14.0	6.4-16.1	11.7	42.8-66.4	55.5	42-66	53
	G	8,100	8,100	3 -14	8.5	37 -	171	104	—	—	11.0-12.1	11.8	2.1- 2.3	2.2	19.8-22.9	21.4	18-22	20
Milner	O	2,600-6,500	4,300	2 -58.5	10.6	0.1-	603	89.7	0-2.1	0.62	2.1-20.9	11.9	4.1-41.8	14.6	16.9-88.7	41.5	14-87	38
	T	4,900-6,200	6,000	8 -21	15.8	0.1-	120	41.8	—	—	1.9-11.3	8.1	0 - 8.2	4.7	21.4-51.7	33.0	20-51	32
	G	1,800-5,100	4,000	2 -34.4	16.1	0.4-	516	33.5	0.2-74	13.9	6.5-37.8	21.0	0 - 6.8	2.4	60.3-93.4	76.7	60-93	77
Mississippi Chat	O	800-5,200	3,100	2 -48.1	12.2	0.1-	361	21.9	0-216	13.7	5.7-39.3	22.3	1.4-30.0	12.9	27.1-94.8	64.0	27-95	58
	T	1,200-5,200	3,900	1 -43	10.9	0.2-	229	21.3	0-163	14.2	1.5-38.0	16.7	1.1-16.3	7.6	47.4-84.9	71.5	43-85	63
	G	900-6,800	4,600	3 -27.1	13.3	0.1-	129	22.2	0.1-89	13.2	1.5-23.6	10.3	0 - 9.3	2.8	22.6-93.5	63.2	22-83	53
Mississippi Lime	O	600-6,800	4,100	1.5-95.3	12.0	0.1-1,210	43.5	0.1-165	9.44	1.3-34.1	13.4	2.1-56.5	15.0	16.9-65.3	50.7	16-85	46	
	T	400-7,200	4,000	4 -70.1	17.4	0.1-	135	7.5	0.1-38	4.23	1.1-26.1	9.3	0 -41.2	6.9	32.9-94.0	67.6	32-94	61
	G	3,600-17,000	10,100	14 -58	35.3	12 -	98	48.0	—	—	2.8- 9.8	6.7	4.0-14.7	7.8	19.3-76.5	43.9	19-77	44
McLish	O	1,600-11,200	8,100	3 -42	12.2	0.7-	157	39.0	—	—	5.5- 1.5	11.0	5.1-27.7	13.2	14.8-52.2	32.1	14-52	31
	G	4,300-9,700	6,100	2 -84	11.0	0.1-1,460	115	6.2-8.8	7.5	4.2-24.4	14.8	0 -33.0	4.3	29.0-77.0	46.5	16-77	36	
	O	4,100-7,500	5,700	2 -37	9.8	0.2-1,840	117	0.3-55	23.1	57-23.2	14.6	0.7-44.5	15.1	23.9-75.5	42.1	18-54	35	
Morrow	T	5,500-8,900	6,100	3 -30	9.5	0.1-	410	34.4	0.1-48	26.0	5.5-16.2	11.3	0 -15.2	5.0	31.1-90.1	57.2	31-90	36
	G	7,100-14,000	10,900	14 -149	48.3	0.1-	132	32.0	—	—	6.1-13.5	9.0	0 - 6.5	1.6	12.5-40.8	25.2	12-40	24
	O	5,100-11,700	8,300	3 -71	12.6	0.1-	615	131	0.2-230	75.6	1.8-23.9	13.1	1.3-29.5	13.0	14.2-76.4	39.1	14-76	34
Oil Greek	T	8,400-13,700	12,300	8 -27	15.0	0.1-	87	22.1	—	—	5.2-16.1	10.9	0 - 5.6	2.6	21.7-74.9	48.6	21-74	
	G	4,500-4,800	4,800	6 - 9	8.5	2.4-	151	76.7	—	—	12.0-17.3	14.7	5.1- 8.4	5.8	39.8-55.5	47.7	34-55	45
	O	300-6,300	3,600	3.8-34.1	12.3	0.2-	296	27.3	0.1-66	9.24	2.8-21.6	10.1	0 -27.1	15.0	16.2-73.4	41.5	15-73	37
Oawego	T	1,200-5,600	3,300	2 -21	10.6	0.1-	117	27.0	0-41	11.5	4.7-20.9	8.7	0 -14.5	5.8	41.7-89.7	63.4	42-89	57
	G	1,200-5,300	3,100	4 -17	9.6	3.1-	42	15.0	—	—	12.3-17.5	15.6	0.1- 7.9	4.1	44.3-59.4	52.5	44-58	51
	O	200-3,200	1,200	2 -42	12.4	0.2-	284	20.6	—	—	12.7-33.8	18.7	8.7-36.8	14.7	34.4-73.1	50.6	28-73	44
Peru	T	700-2,500	1,500	4 -21	10.3	1.7-	804	205	—	—	13.6-24.4	19.2	2.8-25.5	12.0	38.0-60.4	50.7	36-56	51
	G	3,000-6,600	4,000	5 -22	13.6	0.7-	42	18.3	—	—	13.6-22.4	17.8	2.3- 9.1	5.5	31.4-53.4	42.2	26-49	37
	O	800-5,700	3,100	2 -81	14.6	0.1-	254	22.6	—	—	7.6-23.8	17.0	4.7-34.1	16.9	24.4-73.1	41.8	20-72	38
Prus	T	3,000-5,400	3,700	3 -18	11.7	0.5-	133	42.8	—	—	9.8-23.4	17.5	3.7-34.3	19.0	40.7-80.9	47.1	32-80	36
	O	4,200-7,400	4,500	3 -30	14.8	7.4-	500	192	51-286	179	12.3-18.8	16.7	10.1-27.2	20.0	31.4-58.1	41.5	16-50	29
	T	—	4,200	—	4.8	—	195	—	—	166	—	17.8	—	13.6	—	56.2		41

**Table 5-23
(continued)
(g) Oklahoma-Kansas Area**

Formation	Fluid prod.	Range of depth, ft	Avg. prod. depth, ft	Range of prod. thick-ness, ft	Avg. prod. thick-ness, ft	Range of perm. K, md	Avg. perm. K, md	Range of perm. K_{ro} , md	Avg. perm. K_{ro} , md	Range of porosity, %	Avg. porosity, %	Range of oil satn., %	Avg. oil satn., %	Range of total water satn., %	Avg. total water satn., %	Range of calc. connate water satn., %	Avg. calc. connate water satn., %	Range of grav-ity, °API	Avg. grav-ity, °API
Reagan	G	3,500- 3,600	3,600	2 - 13	7.4	1.1- 173	39.3	—	—	9.3-12.7	10.8	1.1- 7.9	4.2	28.4-68.4	44.4	28-86	40	41	41
	O	2,100- 3,700	3,600	1 - 32	11.0	0.2-2,740	255	—	—	8.9-21.5	13.3	3.0-42.0	14.2	17.5-72.9	32.9	12-72	31	24-43	38
	T	3,600	3,600	5 - 7	8.0	19.0- 37	38.0	—	—	10.8-12.8	11.7	1.8-10.5	6.2	33.3-48.7	40.0	29-45	29		
Redfork	G	2,900- 7,400	4,900	4 - 19	7.9	0.1- 160	23.4	—	—	3.6-21.2	14.5	0 -21.7	4.7	18.2-63.8	45.8	16-69	39		
	O	300- 7,600	3,100	1 - 83	10.5	0.1- 868	14.2	—	—	8.6-26.1	16.2	5.4-30.8	18.9	29.5-57.7	43.7	27-55	41	32-48	37
	T	1,200- 3,600	3,100	2 - 9	5.3	0- 23	8.3	—	—	10.1-18.8	15.3	0.3-38.3	9.9	41.4-89.7	52.8	41-89	49		
Skinner	G	1,000 - 5,900	3,700	4 - 29	11.8	0.1- 127	27.7	—	—	13.3-19.8	15.7	0 - 9.9	4.2	30.6-48	40.8	26-47	36		
	O	1,000- 5,800	3,200	1 - 42.5	9.2	0.1- 255	20.8	2-8.6	3.30	7.4-21.7	15.3	2.5-29.7	20.1	14.3-78.7	40.3	14-78	38	30-46	36
	T	2,400- 4,600	3,400	6 - 35.9	11.5	0.3- 18	6.0	2.40	2.40	11.7-19.0	15.5	4.9-18.2	8.5	39.9-71.1	52.4	39-71	39		
Strawn	G	—	1,100	—	12.0	—	71.0	—	—	—	21.3	—	9.9	—	61.8	—	38		
	O	1,000- 7,400	3,500	2 - 40.5	12.4	0.1- 599	58.1	—	—	8.2-23.5	16.8	5.7-31.1	15.1	28.5-61.5	45.8	22-58	41	31-44	40
Sycamore	O	2,600- 8,700	4,600	2 - 84	26.4	0.1- 3.1	0.87	0.13	0.50	7.2-18.4	13.3	9.2-33.5	21.1	36.0-61.8	45.5	32-62	43	33-38	35
Tonkawa	G	5,000- 7,100	5,800	4.42-27.5	9.8	0.3- 283	46.7	—	—	11.7-21.4	16.4	0 - 8.1	2.0	31.8-58.3	44.5	27-58	41		
	O	2,400- 5,700	4,800	4.42-28.5	8.7	1.4- 278	98.8	8-22	15.0	13.2-22.9	18.4	7.5-18.5	12.5	36.1-76.0	45.0	31-78	38	40-45	43
	T	2,300- 3,100	2,700	4 - 9	7.0	1.3- 408	108	—	—	15.4-18.9	17.1	8.9-17.3	11.4	45.1-52.8	49.0	44-52	45		
Tucker	O	1,900- 2,900	2,200	2 - 14	7.8	2.1- 123	36	—	—	12.4-20.3	15.8	7.3-29.8	18.0	35.6-50.1	40.7	33-43	36	29-40	36
Tucker	T	2,700- 2,900	2,800	8.9-18	12.5	4.3- 252	128	53	53	11.8-19.5	15.7	7.1-10.9	9.0	58 -64.3	61.2	52-62	52		
Tulip Creek	G	7,200-18,700	13,400	21 -288.4	78.1	0.9- 24	7.83	0.5-1.0	0.40	2.0-11.9	8.1	0 - 6.6	4.1	23.7-54.8	33.2	23-55	34	49.5	49.5
	O	700-18,800	8,000	2 -138	15.3	0.1-1,470	154	0.2-1.8	0.80	2.5- 25.0	11.8	3.0-44.5	12.2	10.0-63.0	34.9	9-63	33	32-50	40
	T	1,400-12,900	8,800	3 - 86.5	20	2.0- 143	44.8	0.40	0.40	0.7-28.0	11.0	0.7- 7.7	2.8	15.9-62.8	45.7	15-62	46		

Viola	G	4,300- 7,300	5,400	3 -73	39.1	3.6- 23	10.8	3.40	3.40	8.1-10.1	9.3	1.7- 9.4	5.0	19.7-37.2	30.7	19-37	30		
	O	2,100-11,100	4,900	2 -111.7	17.2	0.1-1,150	52.3	0.2-188	18.3	1.0-16.1	8.4	3.2-41.0	15.5	24.1-85.5	54.4	24-86	51	28-48	37
	T	2,600-10,300	4,600	2 -117	19.6	0.1- 997	45.1	0.3-49	4.38	0.6-18.8	7.1	0 -33.7	8.6	39.0-90.8	65.7	39-90	58		
Wayside	O	300- 2,800	800	3.1-34	10.8	0.2- 133	22.2	—	—	13.2-24.9	18.6	8.1-33.8	18.6	29.4-68.0	51.3	28-67	47	29-42	35
First Wilcox	G	2,800- 5,400	4,300	2 -35	11.3	0.7- 145	72.1	—	—	5.2-15.8	10.8	0.7- 8.3	3.6	29.7-80.5	43.9	29-60	44		
	O	2,800- 7,400	4,900	2 -28	10.0	0.2- 445	91.3	—	—	5.4-20.5	12.0	3.6-40.5	11.7	15.0-58.2	32.0	14-58	31	33-50	42
	T	3,200- 8,100	3,900	1.9-29	7.7	0.3- 418	84.1	0.80	0.80	6.8-17.7	10.9	0 -16.9	7.9	24.8-83.8	41.7				
Second Wilcox	G	5,000-10,000	8,700	5 -28	13.4	0.2- 154	76.2	—	—	5.0-15.1	11.2	0 - 3.8	1.5	17.7-45.8	30.9	17-43	29		
	O	3,700- 8,400	6,500	1.3-32	11.3	0.4-2,960	214	—	—	4.2-20.6	12.4	2.9-19.2	10.2	19.0-56.3	36.9	18-56	34	34-42	40
	T	4,700- 7,500	6,000	1.5- 5	4.4	0.4- 756	246	—	—	1.9-20.4	12.9	0 - 8.4	6.1	41.4-80.5	42.5	40-60	43		
Woodford	O	4,100- 5,000	4,800	2.6-30.4	16.2	1.4- 250	87.1	2.4-156	79.2	1.9- 6.6	4.4	8.3-16.7	11.8	43.0-87.9	60.1	43-87	60	41	41

^a General geologic sections taken at different points in Oklahoma-Kansas areas indicate some variations in the properties and an appreciable variations in the occurrence and relative depths of many of the more important oil- and/or gas-producing zones, formations, geologic groups, and their members. The general identification of core samples from these producing intervals reflect local conditions or activities significantly. In the development of the average data values, an attempt has been made to combine data originally reported for locally named zones into more generally recognized formations or geologic groups. In some instances (i.e., Deese, Cherokee) data are reported for a major geologic group as well as for some of its individual members. The values designated by the major group name represent areas where the general characteristics permit identification as to the geologic group but not as to group members. In other areas the group members or zones are readily identifiable. The combinations of data and the use of local rather than regional geologic names in some instances are explained in the footnotes.

^b T Represents transition zone or production of both water and either gas or oil.

^c Includes data reported as Domick Hills and Dutcher.

^d Includes Bromide First and Second as reported on McClain County area.

^e Data reported locally as Bromide Third, Bromide Upper third, and Bromide Lower have been considered as part of the Tulip Creek.

^f Includes data reported as Cleveland Sand, Cleveland, Lower, and Cleveland Upper.

^g Includes the numerous zones (Deese First, Second, Third, Fourth, Fifth, Zone A, Zone B, Zone C, and Zone D) reported locally for the Anadarko, Ardmore, and Marietta Basin areas. In northwest Oklahoma, these different zones are normally referred to as Cherokee. In other areas the zones are frequently identifiable and properties are reported as for Redfork, Bartlesville, etc.

Table 5-23
(continued)
(h) Rocky Mountain Area

Formation	Fluid prod.	Range of prod. depth, ft	Avg. prod. depth, ft	Range of prod. thickness, ft	Avg. prod. thickness, ft	Range of perm. K, md	Avg. perm. K, md	Range of perm. K_{sp} , md	Avg. perm. K_{sp} , md	Range of porosity, %	Avg. porosity, %	Range of oil satn., %	Avg. oil satn., %	Range of total water satn., %	Avg. total water satn., %	Range of calc. con-nate water satn., %	Avg. calc. con-nate water satn., %	Range of grav-ity, °API	Avg. grav-ity, °API
Aneth	O	5,100- 5,300	5,200	3.8-23.1	14.0	0.7- 34	9.35	0.2-23	6.10	4.4-10.5	8.1	14.5-35.9	25.0	12.5-30.5	23.6	13-31	24	41	41
Boundary	G	5,500- 5,800	5,600	8-27	17.5	0.1- 2.0	1.05	—	—	4.3- 6.5	4.7	4.7	4.7	23.8-35.0	29.4	23-35	29		
butte	O	5,400- 5,900	5,600	2-68	16.2	0.1- 114	13.3	0.2-33	12.5	5.4-21.6	11.0	4.8-26.7	12.5	9.3-48.8	28.3	7-45	27	40-41	41.1
Cliffhouse	G	3,600- 5,800	4,800	2-58	13.7	0.1- 3.7	0.84	—	—	7.0-16.2	11.3	0 -19.8	4.5	10.2-60.3	38.9	10-59	36		
D Sand	O	4,350- 5,050	5,800	7-33	15.0	0 - 900	192	—	—	8.6-29.5	21.6	8.4-39.5	13.2	—	—	9-46	23	36-42	38
Dakota	G	500- 7,100	5,700	2-24	9.5	0.1- 710	28.6	0.08	0.08	7.3-19.6	11.2	0 - 7.8	3.5	14.8-55.3	40.6	15-52	38		
	O	3,400- 7,200	5,600	4-19	7.9	0.1- 186	22.3	33.0	33	5.0-23.3	11.2	13.8-35.9	24.4	11.6-44.3	31.0	11-44	29	38-43	40
Desert	O	5,400- 5,500	5,500	11.6-18.3	14.9	1.0- 11	4.4	0.4-2.4	1.13	11.9-13.8	12.7	13.4-16.8	15.2	14.8-24.7	19.2	14-25	19	41	41
Frontier sands	O	265- 8,295	2,950	8-100	46	0 - 534	105	—	—	6.3-29.8	20.0	7.6-37.6	14.9	—	—	28-45	33	31-50	41
Gallop	G	1,500- 6,900	5,000	5-25	11.6	0.1- 324	26.5	0.3-20	10.2	8.5-20.8	13.3	0 -26.6	5.7	20.7-59.2	40.0	20-54	37	39	39
	O	500- 6,400	4,800	2-43	12.4	0.1-2,470	48.2	0.1-3.2	0.7	6.9-23.1	12.5	8.5-43.7	25.3	17.2-76.9	35.7	14-77	34	36-42	39
Hermosa	G	4,900- 7,700	5,800	5-30	14.1	0.1- 91	18.6	45.0	45.0	5.5-18.5	10.2	0 - 6.5	3.0	14.2-46.3	32.7	12-45	32		
	O	5,300- 6,000	5,600	3-38.2	15.1	0.1- 37	7.32	0-26	4.26	2.7-17.9	8.3	3.9-29.1	10.8	11.6-60.0	35.6	12-50	35	41-42	40

Hospa	G	4,800- 7,100	5,500	3-17	10.5	0.1-	70	18.2	—	—	7.4-11.9	10.5	0.5-23.8	7.5	8.7-49.7	36.1	8-49	37		
	O	4,600- 5,100	4,800	8-18	13.3	0.7-	25	8.69	—	—	6.8-14.8	11.3	20.4-29.8	25.0	32.3-44.8	36.0	31-45	35	40	40
J Sand	O	4,470- 5,480	4,900	15-82	25	0	-1,795	330	—	—	8.8-32.7	19.6	8.8-46.5	13.9	—	—	6-42	20	36-42	38
Madison lime†	O	3,400- 6,200	4,900	41-450	186	0	-1,460	13	—	—	1.8-26.4	11.9	6.0-43.5	17.4	—	—	22-33	27	21.6-30	26
Menefee	G	5,200- 5,700	5,400	7-25	12.7	0.1-	20	5.03	—	—	8.7-13.5	11.2	0.3- 5.3	1.8	14.5-45.1	27.5	15-43	27		
Mesa Verde	G	1,500- 8,100	4,700	2-22	10.0	0.1-	17	3.57	—	—	10.0-19.6	14.6	0 - 6.8	3.3	14.5-88.4	42.0	15-84	40		
	O	"	300	—	4.0	—	—	60	—	—	—	—	—	8.3	—	61.0	—	44		
Morrison	O	1,800- 6,900	4,500	24-54	40	0	-1,250	43	—	—	9.9-25.5	17.5	5.0-26.0	13.1	—	—	15-41	35	29-56	42
Muddy	O	930- 8,747	1,845	7-75	20	0	-2,150	173	—	—	2.3-32.9	22.3	7.6-48.5	30.8	—	—	5-47	19	26-42	38
Paradox	G	5,100- 9,500	6,900	4-44.2	12.2	0.2-	42	11.6	0.1-28	4.43	1.4-19.4	7.4	0 -10.1	3.1	9.9-57.9	34.7	10-58	34		
	O	5,300- 8,100	5,700	2-66	14.8	0.1-	119	10.4	0-57	4.57	3.3-21.8	10.5	3.6-38.7	12.4	10.8-80.5	33.6	10-61	33	40-43	41
Phosphoria (formerly Embar)	O	700-10,500	4,600	5-100	64	0	- 128	3.7	—	—	2.0-25.0	8.9	3.0-40.0	22.5	—	—	5-30	21	15-42.3	28.4
Picture Cliffs	G	1,800- 5,800	3,400	3-43	16.8	0.1-	7.68	1.12	—	—	8.5-25.5	15.7	0 -21.1	2.6	23.6-67.5	46.7	23-53	43	55	55
	O	"	2,900	—	23.0	—	—	0.5	—	—	—	—	—	23.3	—	49.1	—	49		
Point Lookout	G	4,300 -6,500	5,500	2-101	22.9	0.1-	16	1.74	—	—	5.8-21.8	10.9	0 - 9.1	2.9	11.9-55.8	36.7	12-55	36		
	O	"	4,700	—	7.0	—	—	2.90	—	2.40	—	13.3	—	23.8	40	40.9	—	41	—	39
Sundance	O	1,100- 5,860	3,100	5-100	44	0	-1,250	100	—	—	15.0-25.0	19.0	8.0-25.0	17.0	—	—	20-49	35	22-63	39
Tensleep	O	800-11,800	4,700	10-200	118	0	-2,950	120	—	—	5.0-27.0	13.6	6.0-30.0	23.3	7.0-59	25.7	5-50	19	17-58.5	26.2
Tocito	G	"	7,900	—	7	—	—	230	—	—	—	—	—	4.0	—	51.8	—	43		
	O	1,400- 5,100	4,600	4-58	17.3	0	- 31	3.36	—	—	12.8-17.8	14.7	11.9-26.6	21.3	40.6-65	46.3	40-55	46	36-40	38

* Not enough wells to justify range of variations.

† Data limited to Big Horn Basin

(I) West Texas-Southeastern New Mexico Areas

Formation	Group*	Range Area ^b	Fluid prod. depth prod.	Range of prod. depth, ft	Avg. prod. depth, ft	Range of prod. thickness, ft	Ave. prod. thickness, ft	Range of perm. K, md	Ave. perm. K, m ^d	Range of perm. K90, md	Ave. perm. K90, md	Range of porosity, %	Ave. porosity, %	Range of oil satn., %	Ave. oil satn., %	Range of total water satn., %	Ave. total water satn., %	Range of connate water satn., %	Ave. connate water satn., %	Range of gravity *API	Ave. gravity *API	
Bend conglomerate	1	1, 2, 4 5, 8, 8	O	6,000- 6,100	6,000	3 - 22	13.2	4 - 311	150	—	—	13.8-16.9	15.0	8.1- 8.8	8.3	43-64	52	42-62	50	40-42	14	
	2	3	O	10,900-10,500	10,400	10 - 28	20.0	1.8- 11	5.7	0.0- 5.1	2.2	4.0-15.7	10.8	9.5-16.1	11.5	21-41	33	21-39	32	41-45	43	
Bilneby	—	8	G	5,383- 5,575	5,480	23 - 50	36	1.8- 3.8	2.4	—	—	10.7-14.8	12.7	2.1- 9.1	4.9	34-40	36	31-33	33	—	—	
			O	5,282- 5,950	5,610	4 - 95	43	0.1- 5.3	1.8	0.2- 4.2	1.4	3.1-12.5	7.8	9.8-19.3	12.8	29-57	40	27-58	39	39-42	40	
Cambrian	—	3	O	5,500- 8,300	5,900	2.0- 95	30.3	0.9-1,190	173	—	—	4.1-16.8	12.0	6.9-21.2	11.8	22-71	39	22-71	36	44-51	46	
Canyon Reef	—	2, 3, 4 5, 8, 7	O	4,200-10,400	7,100	4.0-222	36.8	0.8- 746	42	0.3- 249	17	3.0-21.5	8.9	3.8-39.2	11.6	18.3-73	44	18-73	43	30-47	42	
Canyon Sand	—	2, 3, 4, 7	G	—	5,000	—	8.0	—	1.7	—	—	—	15.1	—	5.8	—	46	—	44	—	—	
Clearfork	1	3, 4, 7 2 (part) 5, 6	O	3,000-10,000	5,500	3.0- 57	18.9	0.1- 477	38	—	—	5.5-22.1	14.3	4.8-27.7	13.7	21-72	48	21-72	41	37-43	40	
			G	—	2,400	—	85	—	11	—	7.8	—	—	13.5	—	5.7	—	50	—	50	—	—
2	—	2 (part) 5, 6	O	1,500- 8,800	4,400	4.0-180	41	0.1- 48	4.8	<0.1- 24	2.5	4.1-20.5	9.2	7.5-31.4	15.8	18-84	54	18-84	53	23-42	28	
			G	5,400- 8,300	8,600	3.0-259	3.3	<0.1- 136	5.8	<0.1- 109	3.1	1.9-19.4	5.8	5.8-27.1	16.5	22-99	47	21-69	47	28-40	32	
Dean	—	2, 4, 7	O	7,700- 9,100	8,200	6.0- 88	26.2	<0.1- 0.3	0.12	—	—	7.5-12.7	10.3	22 -44	33.7	20-52	34	19-51	33	37-40	39	
Delaware	—	1 ^a	G	4,700- 5,000	4,800	5.2- 39	19.8	1.1- 33	12.9	—	—	13.8-21.8	17.9	2.0-10.3	8.0	45-86	53	36-63	49	—	—	
			O	3,500- 5,100	4,200	3.0- 52	14.5	0.8- 84	24.5	—	—	—	15.2-25.4	21.0	3.9-16.8	11.2	33-65	49	31-64	42	35-42	40
Devonian	1	2, 5 ^d	G	11,200-11,800	11,400	14 -117	54	0.5- 36	10.5	0.1- 1.3	0.5	1.7- 5.3	3.3	2.1- 6.8	3.7	37-68	53	37-68	53	—	—	
			O	11,300-12,300	11,800	8 -299	99	0.2- 23	4.0	0.1- 5.8	0.8	1.3- 8.8	4.3	3.3-18.7	9.2	19-53	33	19-53	33	48-52	49	
2	—	2, 5 ^d	G	—	9,200	—	17	—	0.4	—	—	—	8.7	—	5.7	—	82	—	81	—	—	
			O	5,500- 9,900	7,700	8 -113	34	2.5- 50	14.9	0.2- 19	7.0	5.5-27.7	15.2	6.8-22.9	11.0	41-78	51	41-78	51	35-48	42	
3	—	2, 3, 4, 5, 8, 7, 8 ^e	C	11,000-11,200	11,100	19 - 34	27	<0.1- 2.2	1.1	<0.1- 0.9	0.5	2.2- 7.7	5.0	3.1- 4.8	4.0	45-89	57	45-89	57	—	—	
			O	7,800-12,800	11,200	8.5-954	89	1.0-2,840	177	0.3-1,020	37	1.8-25.2	6.0	5.3-24.8	12.9	22-85	46	22-85	46	36-49	42	
Ellenburger	—	All	C	4,100-10,800	7,400	11 - 18	14.3	203 - 248	225	1.4- 54	27.7	3.7- 4.5	4.2	0.8- 7.8	4.2	47-87	57	47-87	57	—	—	
			O	5,500-16,800	10,100	3.0-347	55	0.1-2,250	75	<0.1- 396	22.9	1.3-13.8	3.8	1.0-19.2	8.4	40-84	61	40-84	60	37-52	47	
Fuselman	—	All	C	6,700-12,700	10,300	18 - 51	34	1.2- 26	8.4	0.3- 1.3	0.9	2.6- 3.7	3.3	0.2- 3.9	1.7	32-47	40	32-47	40	—	—	
			O	9,500-12,500	12,000	8 - 49	32	0.6- 25	10.3	0.2- 17	3.9	1.4-10.7	3.3	5.2-18	10.4	25-64	42	24-64	38	47-50	48	
Glorietta (Paddock) ^f	—	All	G	2,200- 2,800	2,400	3 - 44	18.3	4.8- 12	5.8	—	—	9.3	14 -18.2	15.0	3.9- 4.4	3.7	39-80	51	37-90	50	—	—
			O	2,300- 8,000	4,300	3 -103	22.3	0.4- 223	11.5	0.2- 128	6.1	5.2-20.9	13.8	3.1-22.1	15.4	24-72	48	24-71	47	28-40	33	
Granite wash	—	3, 4, 6, 7	G	3,000- 8,800	4,700	4 - 8	5.1	11 -2,890	477	—	—	53	12.1-20.4	14.4	2.9- 8.7	5.2	39-96	55	39-96	53	—	—
			O	2,300- 3,400	3,000	2 - 81	15.8	5 -3,280	609	—	30	3.5-26.1	17.7	4.8-22.5	14.7	42-71	54	35-88	49	40-45	42	

Grayburg	1	8	G	3,600- 4,200	3,800	3.0- 5.0	4.2	1.8- 9.3	6.5	—	—	11.1-14.3	12.4	7.1-42	16.8	22-53	39	22-52	38			
			O	2,400- 4,500	4,100	3.0-123	27.4	0.5- 159	13.7	0.2- 48	5.2	7.0-20.0	11.3	6.2-37.9	17.8	26-88	38	25-55	35	31-41	38	
	2	4, 5, 6, 7	G	4,400	4,400	12 - 26	20.8	0.6- 3.7	2.5	0.3- 2.1	1.3	8.3- 6.6	6.4	2.4- 7.1	4.7	55-68	80	55-88	80			
			O	3,000- 4,800	4,400	6 -259	45	0.2- 118	5.5	0.1- 110	2.7	2.7-16.2	7.9	4.8-22.1	13.9	32-84	55	32-84	55	23-40	32	
	3	1, 2, 3	O	1,300- 3,900	2,700	4.5-182	50	0.3-1,430	37.7	0.1- 228	14.3	5.3-24.3	11.9	6.3-34	18.2	31-78	56	31-78	56	28-36	31	
			O	4,100-11,400	9,100	1.7- 77	22.3	0.3- 482	34.9	0.1- 188	14.7	2.7-13.9	7.7	4.7-18.8	9.7	28-58	42	28-58	41	36-47	41	
Pennsylvanian sand (Morrow) ^a																						
Queen (Penrose) ^a																						
	—	All	G	3,000- 3,200	3,100	4.0- 29	9.9	10 - 318	84	—	—	10.7-22.2	16.5	2.8- 7.8	7.4	36-82	48	36-58	45			
			O	800- 4,900	3,500	1.5- 38	10.2	0.2-4,190	123	—	—	1.0	5.7-27.0	17.2	4.2-34.7	15.8	32-88	49	30-66	45	30-42	33
San Andres	1	8	O	3,900- 4,700	4,500	6 - 39	18.6	0.3- 481	81	0.1- 482	53	3.2-14.0	8.5	6.9-33.9	18.7	21-49	36	19-49	36	34-38	37	
			O	4,100- 5,300	4,500	4.7-124	40.1	0.3- 295	6.9	0.1- 208	3.8	3.1-12.8	7.1	4.9-30.8	14.7	28-89	52	25-69	51	30-37	33	
			O	1,500- 8,100	3,300	3.0-197	30.2	0.2- 593	9.7	0.2- 510	8.4	3.3-25.1	15.5	3.5-24.2	13.2	38-74	56	37-74	56	26-37	32	
Seven Rivers																						
	—	1, 2, 5, 6	G	3,600- 4,100	3,900	3.0- 8.0	5.8	0.8- 23	12.2	—	—	0.3	15.5-18.8	16.0	3.4- 9.5	6.4	51-86	58	48-85	64		
			O	800- 4,000	2,800	4.0-138	16.5	0.4- 426	51.4	—	—	8.0	5.9-28.9	18.5	4.2-41.7	16.2	39-70	54	38-81	50	28-38	32
Sprayberry	1.	4.7	O	4,800- 8,500	7,100	2.0- 69	21.7	0.2- 71	6.3	—	—	4.0	10.1-23.3	15.8	7.0-24.5	15.3	32-66	45	30-67	43	36-42	39
Strawn Lime																						
	—	All	G	—	5,800	11 - 57	34.4	4.5- 310	179	27 - 189	108	10.9-14.8	12.9	5.5- 8.3	6.9	38-39	39	38-39	38	39-47	41	
			O	5,200- 8,700	5,900	2.0-101	36.7	1.9- 186	43	0.8- 148	19.1	31-12.8	7.2	4.8-26.3	11.2	15-86	44	15-86	43	39-47	41	
Strawn Sand																						
	—	2, 3, 4, 7	G	3,800-10,500	7,600	3.0- 39	16.8	0.3- 42	11.4	0.1- 0.4	0.2	2.1-14.2	6.9	1.7- 5.2	3.0	48-80	52	48-80	52			
			O	1,100-11,300	5,200	2.0- 78	15.1	0.2- 716	47	0.1- 136	11.7	1.0-20.3	12.8	2.7-27.9	12.2	23-77	43	23-77	41	29-48	42	
Others ^b																						
	—	1, 2, 5, 8	O	918- 7,368	3,838	6 - 21	14	1.0- 400	45	—	—	8.0-27	16.2	5.0-27	14.1	25-90	43	23-59	41			
			O	5,100- 7,300	8,500	15 - 43	33.5	0.2- 135	27.6	0.1- 1.1	0.5	2.5- 7.1	4.9	8.5-25.3	12.9	37-64	54	37-64	54	38	38	
Tubb																						
Wolfcamp (Abo) ^c																						
	1	2	O	—	9,800	—	10.8	—	2.3	—	—	0.4	—	4.3	—	19.6	—	25	—	25	42	42
			O	6,400- 9,200	8,800	13 -129	41.7	2.3-9,410	419	1.5-6,210	274	4.9-18.5	9.9	6.8-16.8	9.7	32-86	44	31-56	44	36-45	40	
	2	4, 5, 6, 7	O	2,500- 4,100	3,600	4.0-119	22.5	0.1-1,380	57	—	—	3.4	7.2-24.5	15.3	0.5-18.1	4.6	30-84	48	28-84	45		
			O	2,400- 4,100	3,500	2.0-114	26.0	1.0-1,270	80	—	—	4.3	5.4-26.3	15.5	1.8-28.8	14.3	32-85	48	29-84	44	40-50	46
	3	3 (part)	G	9,000-10,600	9,700	4.5-204	59	0.2- 147	20.4	0.2- 38	5.4	2.6-12.6	8.1	5.3-23.8	14.4	28-56	39	28-56	39	40-44	42	
			O	1,400- 3,500	2,800	3.0- 53	10.8	0.2- 145	19.3	—	—	—	12.1-27.4	17.9	1.3-17.0	5.8	43-79	59	38-78	53		
Yates	—	1, 2, 5, 8	G	1,400- 4,000	2,300	3.0- 86	16.5	1.0-4,000	42.7	—	—	27.8	2.4-27.0	18.8	3.7-37.3	16.0	31-75	53	31-75	47	27-41	32
			O	—	—	—	—	—	—	—	—	—	—	—	—	—	—	—	—	—	—	—

^a More than one group indicates distinct differences in formation as found in different areas.

^b Area numbers refer to map of Figure 24-1.

^c Plus Ward, Pecos, and Southwestern Lea County.

^d Midland and Ector counties only.

^e Crane, Ward, Winkler, and Pecos counties only.

^f Except counties in 4 and 5 above.

^g Names in parentheses are those commonly used in New Mexico, Area 8.

^h Archer, Baylor, Clay, Jack, Montague, Wichita, Wise, and Young counties.

(text continued from page 93)

Special Core Analysis Tests. Special core analysis testing is done when specifically required. Visual inspection and some petrographic studies are frequently done. For sandstones and conglomerates, particle size is often obtained by disaggregating and sieving reservoir rock material. Fractions of the various sizes of grains are determined and described according to the nomenclature in Table 5-24. Larger grain size is associated with higher permeability, and very small grain sizes include silt and clay fractions that are associated with lower permeabilities.

Table 5-24
Particle Size Definitions

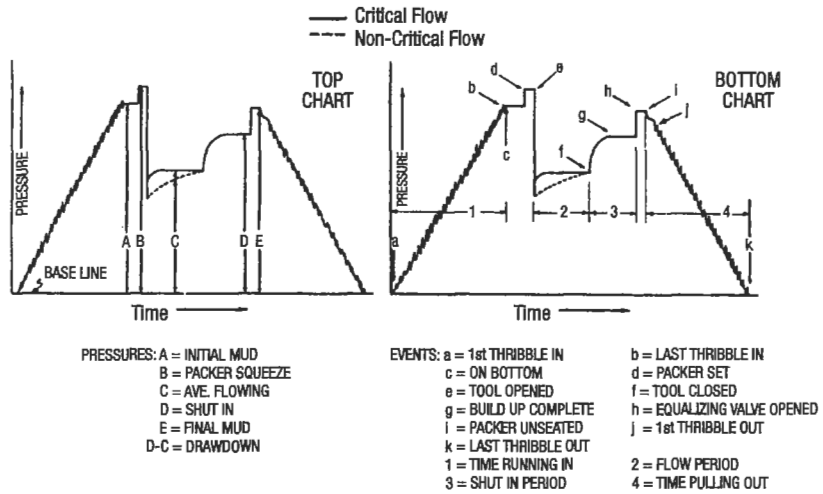
Material	Particle size, μm	U.S. standard sieve mesh no.
Coarse sand	>500	<35
Medium sand	250-500	35-60
Fine sand	125-250	60-120
Very fine sand	62.5-125	120-230
Coarse silt	31-62.5	—
Medium silt	15.6-31	—
Fine silt	7.8-15.6	—
Very fine silt	3.9-7.8	—
Clay	<2	—

Drill Stem Tests

A drill stem test (DST) is some form of temporary completion of a well that is designed to determine the productivity and fluid properties prior to completion of the well. Although a DST can be performed in uncased hole (open hole) or in cased hole (perforation tests), the open hole test is more common. The tool assembly which consists of a packer, a test valve, and an equalizing valve, is lowered on the drill pipe to a position opposite the formation to be tested. The packer expands against the hole to segregate the mud-filled annular section from the interval of interest, and the test valve allows formation fluids to enter the drill pipe during the test. The equalizing valve allows pressure equalization after the test so the packer can be retrieved. Details of the DST and DST assemblies are described elsewhere [13,19,66] and will only be summarized here. By closing the test valve, a build up in pressure is obtained; by opening the test valve, a decline in pressure is obtained. (Pressure buildup and falloff analyses are discussed subsequently in this section of the chapter.) During the DST, both pressures and flow rates are measured as a function of time.

Interpretation of DST results is often regarded as an art rather than a science. Certainly, a DST can provide a valuable indication of commercial productivity from a well, provided engineering judgment and experience are properly utilized. Interpretations of various pressure charts are shown in Figure 5-62 [13,196] and 5-63 [180]; details of interpreting DST data are described in the literature [66,197].

(text continued on page 116)



LEGEND: ——— Top Chart (or Bottom Charts)
 - - - Bottom Chart
 (Critical Flow)

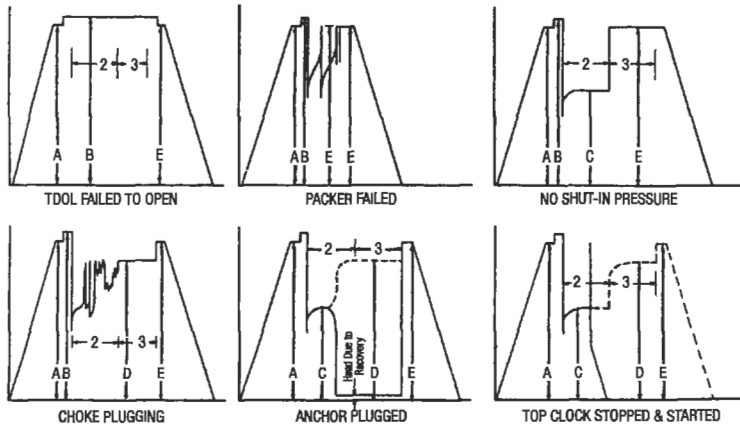
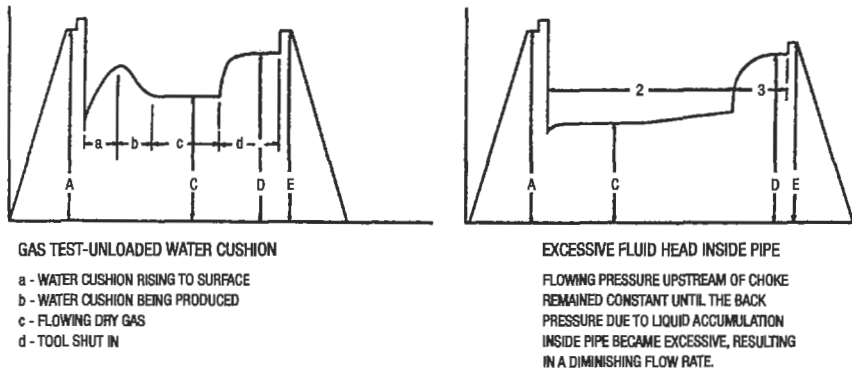
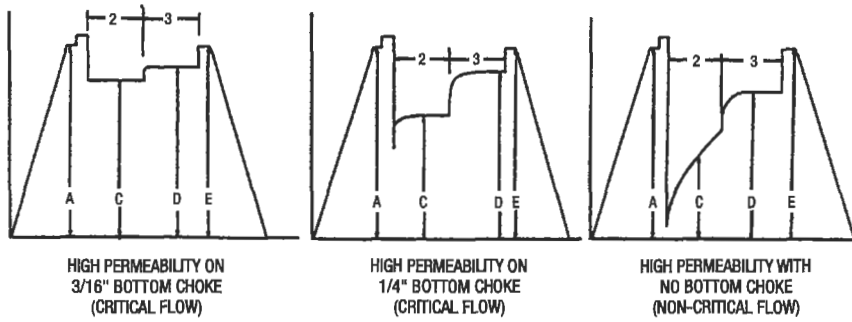
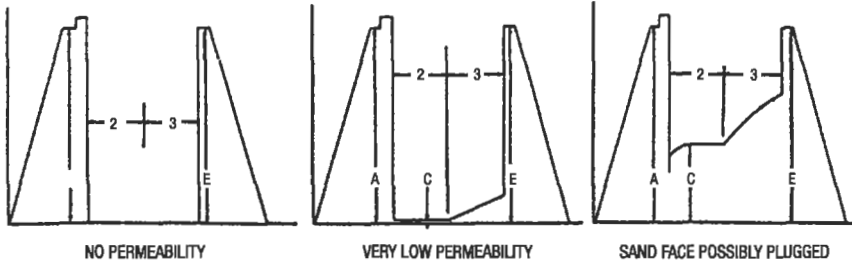


Figure 5-62.



NOTE: THE RUNNING IN AND PULLING OUT PERIODS ON THESE CHARTS ARE SHOWN COMPRESSED ON TIME SCALE FOR CLARITY.

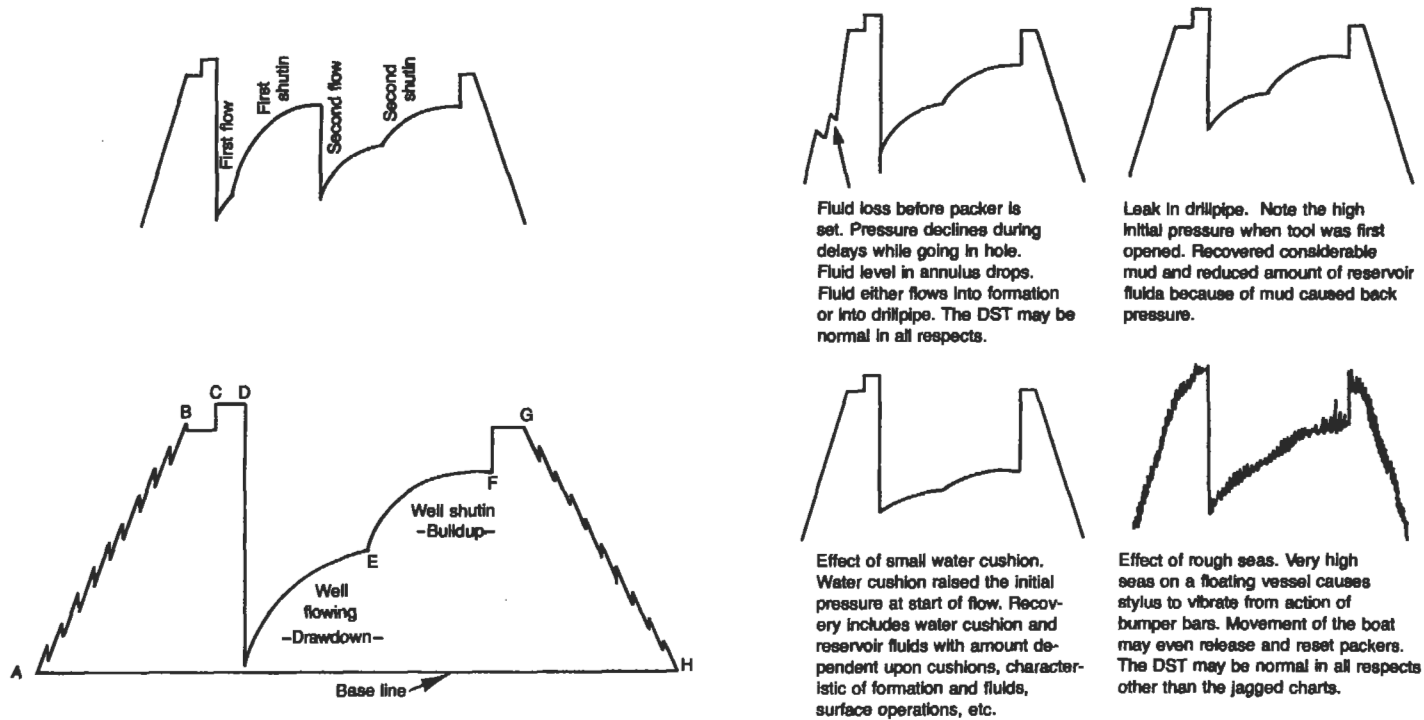


Figure 5-63.

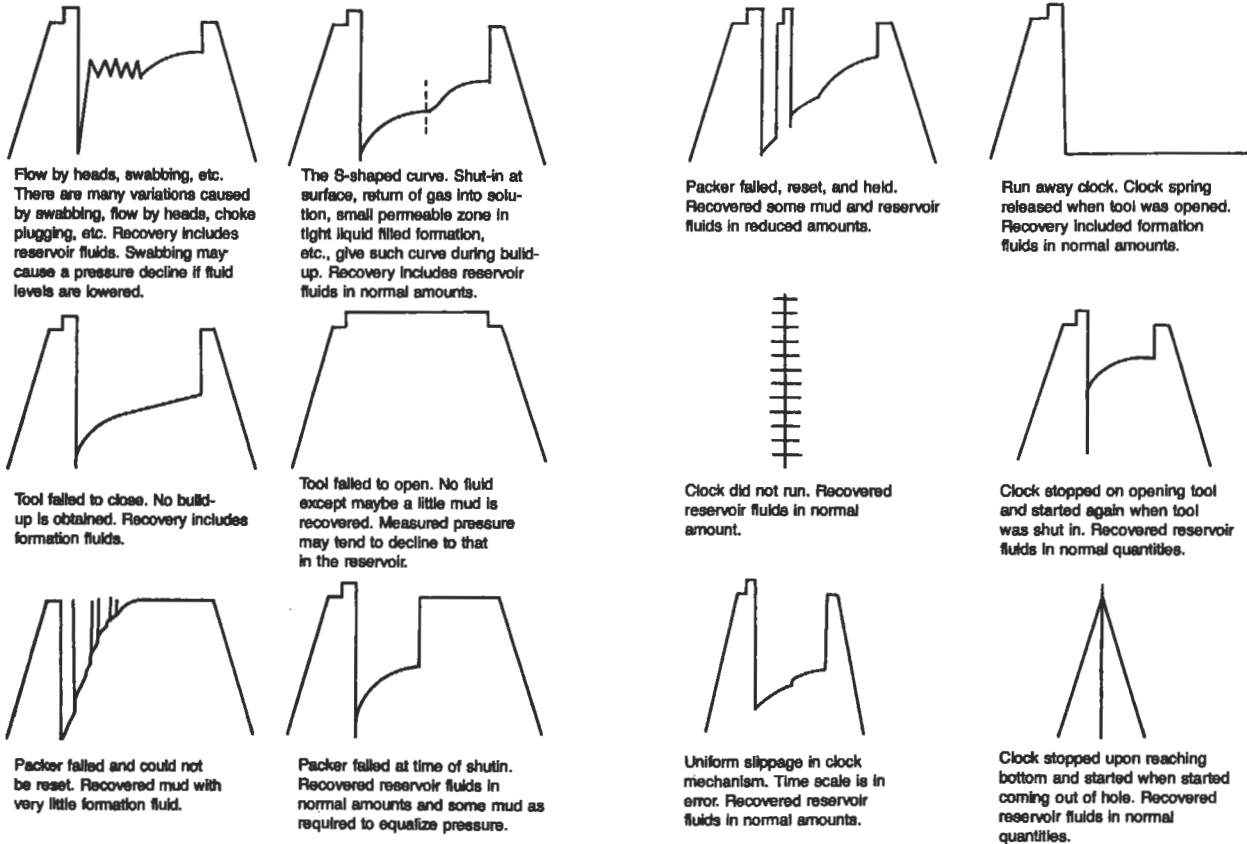


Figure 5-63. Continued.

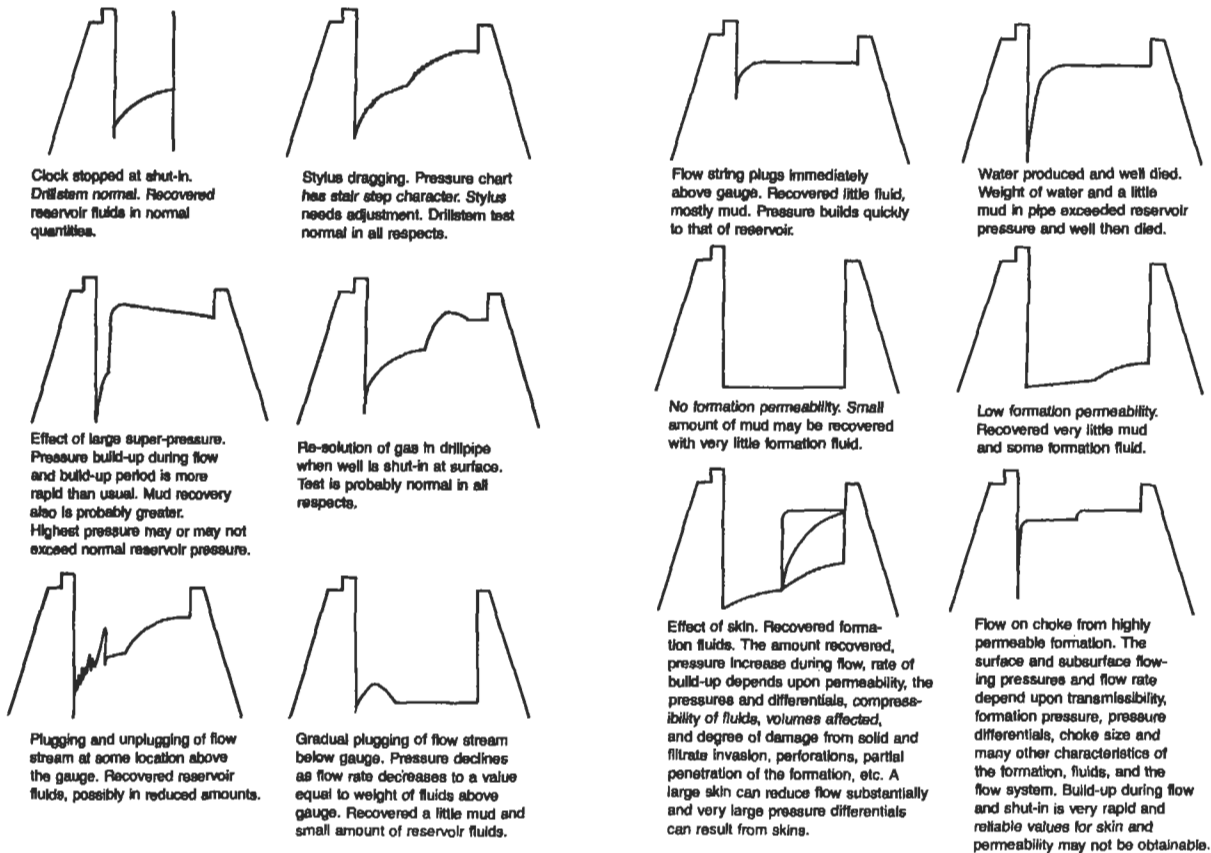


Figure 5-63. Continued.

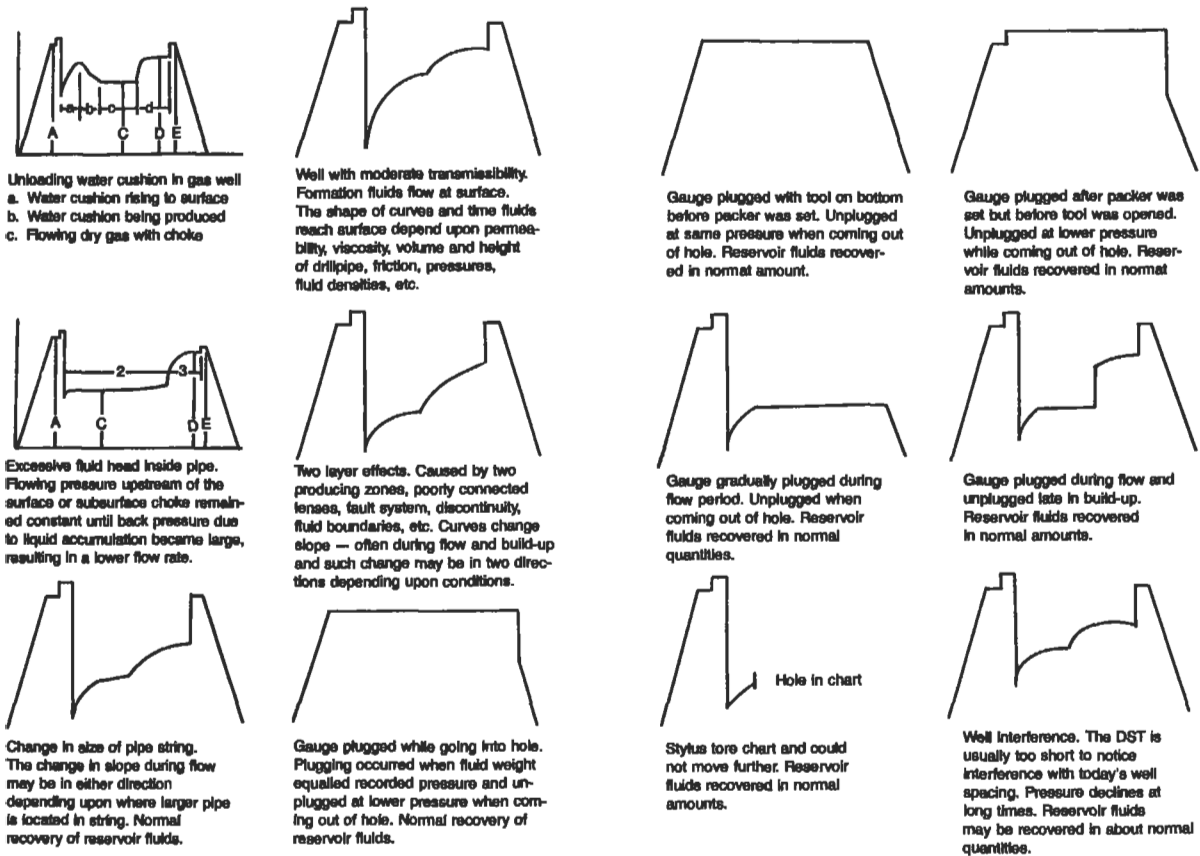


Figure 5-63. Continued.



Two tests with the same gauge. Second build-up extrapolated pressure is lower than that of first build-up. Depletion of a small reservoir might be suggested.



Single test with two gauges. Left gauge suggests highly permeable formation with little or no skin — maybe negative — while right curve indicates gauge which plugged upon reaching bottom and unplugged when starting out of hole. If right gauge was at bottom, it was probably stuck in debris at bottom of hole.



Two tests with the same gauge. Character of the curves for the second test differs appreciably from that of the first test. Skin or other parameter in the flow and build-up equations which might be sensitive to flow or shut-in has changed between the two tests. Since some fluid entered drillstring during first test, initial pressure of second test will be higher than that of first test by the weight of this fluid column.



Single test with two gauges. Left gauge shows gradual plugging below gauge while right gauge shows actual behavior of the reservoir. Left gauge measures weight of fluids above gauge rather than reservoir characteristics. The two are not identical because a plug in the flow string has removed the connection between the two pressure sources which are in balance in the normal test.



Single test with two gauges. The two sets of curves should be identical except for the small difference in pressure related to location of the gauges within the flow string. This is the normal condition to be expected if both gauges are operating properly and no plugging, etc., is occurring.



Single test with two gauges. Left gauge measures reservoir characteristics while right gauge plugged while going into the well and did not unplug until inspected at surface.

Figure 5-63. Continued.

(text continued from page 108)

Logging

Introduction

This section deals with the part of formation evaluation known as well logging. Well logs are a record versus depth of some physical parameter of the formation. Parameters such as electrical resistance, naturally occurring radioactivity, or hydrogen content may be measured so that important producing characteristics such as porosity, water saturation, pay thickness, and lithology may be determined. Logging instruments (called *sondes*) are lowered down the borehole on armored electrical cable (called a *wireline*). Readings are taken while the tool is being raised up the hole. The information is transmitted uphole via the cable where it is processed by an on-board computer and recorded on magnetic tape and photographic film. In older logging units, downhole signals are processed by analog circuits before being recorded.

Well logging can be divided into two areas: open hole and cased hole. Open hole logging is done after drilling, before casing is set. The purpose of open hole logging is to evaluate all strata penetrated for the presence of oil and gas. Open hole logs give more reliable information on producing characteristics than cased hole logs. Cased hole logs provide information about cement job quality, casing corrosion, fluid flow characteristics, and reservoir performance. In areas where the geologic and producing characteristics of a reservoir are well known, as in development wells, cased hole logs are used for correlation. In recent years, many new open- and cased-hole logs and services have become available, including fluid samplers, sidewall cores, fracture height log, and seismic services. These products, in conjunction with new computer processing techniques, provide the engineer and geologist with an enormous amount of data for any well.

Parameters that Can Be Calculated or Estimated from Logs

Porosity. Porosity is defined as the ratio of volume of pores to the total volume of the rock. It occurs as primary (depositional) or secondary (diagenetic or solution) porosity. Primary and secondary porosity can be read directly from neutron, density, and sonic logs. These tools do not measure pore volume directly, rather they measure physical parameters of the formation and relate them to porosity mathematically or empirically. Since the sonic tool only records primary (or matrix) porosity, it can be combined with total porosity tools, such as density or a combined neutron and density, to determine secondary porosity:

$$\phi_{\text{secondary}} = \phi_{\text{total}} - \phi_{\text{sonic}} \quad (5-83)$$

where $\phi_{\text{secondary}}$ = porosity due to vugs and fractures
 ϕ_{total} = total porosity as determined from cores, density log, neutron-density crossplot, or local knowledge
 ϕ_{sonic} = porosity determined from sonic log.

No distinction between effective and total porosity can be made with present logging methods.

Water Saturation. Connate water saturation (S_w) and flushed zone water saturation (S_{xo}) can be calculated from information supplied by well logs.

Connate water saturation is the fraction of pore volume in an undisturbed formation filled with connate water.

$$S_w = \frac{\text{volume of water}}{\text{volume of pores}} \quad (5-84)$$

Flushed zone saturation (S_{xo}) is the fraction of the pore volume filled with flushing agent (normally drilling fluid).

$$S_{xo} = \frac{\text{volume of flushing agent}}{\text{volume of pores}} \quad (5-85)$$

Prior to penetration by a drill bit, only two fluids are assumed to be present in the formation—water and hydrocarbons. Therefore, all pore space that is not occupied by water is occupied by hydrocarbons. With this assumption hydrocarbon saturation can be calculated:

$$S_h = 1 - S_w \quad (5-86)$$

where S_h = hydrocarbon saturation.

Pay Thickness. The thickness of a hydrocarbon-bearing formation (h_{pay}) is easily determined from well logs once ϕ and S_w cutoffs are established. The S_w cutoff is the maximum value for S_w for a given rock type. The ϕ cutoff is the minimum value for ϕ below which hydrocarbons cannot be produced. For example:

Depth	ϕ	S_w	Comment
3,668–3,670	1%	53%	ϕ too low
3,666–3,668	2%	50%	ϕ too low
3,664–3,666	6%	38%	possible hydrocarbons
3,662–3,664	6%	36%	possible hydrocarbons
3,660–3,662	8%	31%	possible hydrocarbons
3,658–3,660	7%	74%	too wet
3,656–3,658	8%	100%	too wet

In this case, the water saturation cutoff is a maximum of 60% and the porosity cutoff is a minimum of 3%, so this well will have 6 feet of pay ($h_{\text{pay}} = 6$ ft). Other factors that may reduce h_{pay} include shaliness, shale streaks, low permeability, and low reservoir pressure. Porosity and water saturation cutoffs are usually established for specific regions or reservoirs based on detailed production and geologic information.

Lithology. It is often necessary to know the rock type in order to properly design downhole assemblies, casing programs, and completion techniques. Data from well logs can provide the geologist or engineer with an estimate of the lithologic makeup of any formation. The accuracy of this estimate is a function of the complexity of the formation (mineralogic makeup and fluid types) and the kinds of tools used to investigate the rocks. More tools are needed to accurately determine compositions of complex formations. Simple lithologies (three or less

minerals, or gas) can be determined with combined neutron, density, and sonic logs. This technique will be discussed later. More complex lithologies can be determined with the aid of special logging tools and computers.

Since well logs infer lithology from physical and chemical parameters, certain rocks will look the same on logs though they differ in their geologic classification. Sandstone, quartz, and chert are all SiO_2 and appear the same on porosity logs. The same is true of limestone and chalk. Dolomite, anhydrite, and salt have very distinct characteristics and are easily distinguished from other rock types. Shales are composed of clay minerals. The type and amount of different clay minerals, which vary widely between shales, can affect their bulk properties.

Permeability. Permeability is one of the essential properties used in evaluation of a potentially producing formation. Unfortunately there are no logging devices that read permeability. This is because permeability is a dynamic property. Most logging tools spend only a few seconds in front of any one point of a formation, therefore it is impossible to measure any time-dependent parameter. There are methods to estimate permeability from well logs, but they are based on general assumptions. From a practical standpoint, log parameters only provide an "order of magnitude" approximation. Several methods of inferring permeability with well logs are discussed where applicable in each section.

Two relationships between porosity and irreducible water saturation (S_{iw}) are used to estimate permeability:

1. The Timur relationship [198] (Figure 5-64) for granular rocks (sandstones and oolitic limestones), which generally gives a more conservative estimate of permeability.
2. The Wyllie and Rose relationship [43] modified by Schlumberger [199] (Figure 5-65), which generally gives a higher estimate of permeability.

To enter these charts, porosity and irreducible water saturation (S_{iw}) must be known. Porosity can be obtained from cores or any porosity device (sonic, neutron, or density). Irreducible water saturation must be found from capillary pressure curves or it can be estimated. The permeabilities from these charts should be considered "order of magnitude" estimates.

Influences on Logs

The purpose of well logging is to determine what fluids are in the formation and in what quantity. Unfortunately the drilling process alters the fluid saturations by flushing the pores near the borehole and filling them with the fluid fraction of the drilling mud (mud filtrate). To correct for these influences, the invasion profile must be identified. Figure 5-66, an idealized cross-sectional view of the borehole and formations, shows an invasion profile and the appropriate symbols for each part of that profile [199].

Mud Relationships. Since the borehole is filled with mud and the adjacent portion of the formation is invaded with mud filtrate, mud properties must be accurately known so they can be taken into account. Mud has a minor influence on most porosity tools; however, it can have a large effect on the resistivity tools. In general:

$$R_{mc} > R_m > R_{mf} \quad (5-87)$$

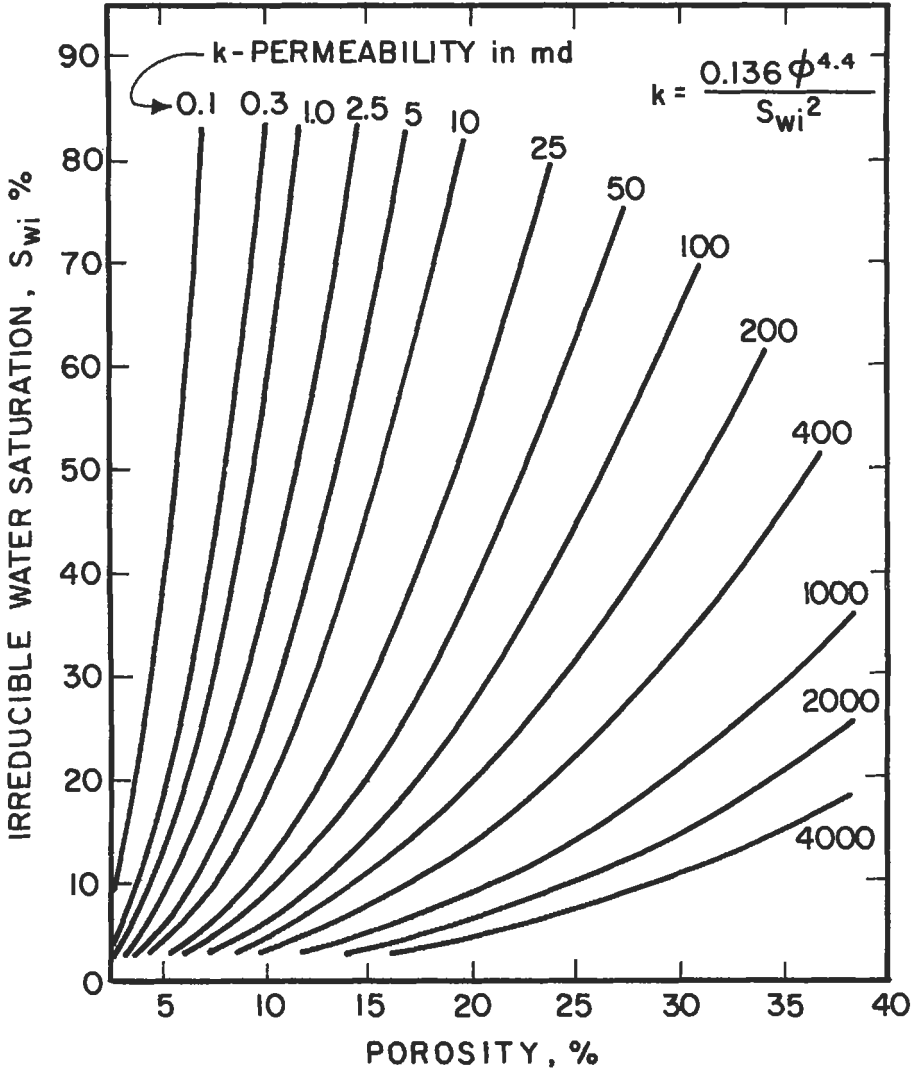


Figure 5-64. Timur chart for estimating permeability [198].

This is because the mudcake is mostly clay particles and has very little water associated with it. The clay particles in the mudcake tend to align themselves parallel to the borehole wall, developing a high horizontal resistivity, R_h (Figure 5-67). Since the mud filtrate is composed only of fluid and has no solids, it will have a lower resistivity. If the resistivity of the mud (R_m) is known, R_{mc} and R_{mf} can be estimated with the following equations:

$$R_{mf} = K_m (R_m)^{1.07} \tag{5-88}$$

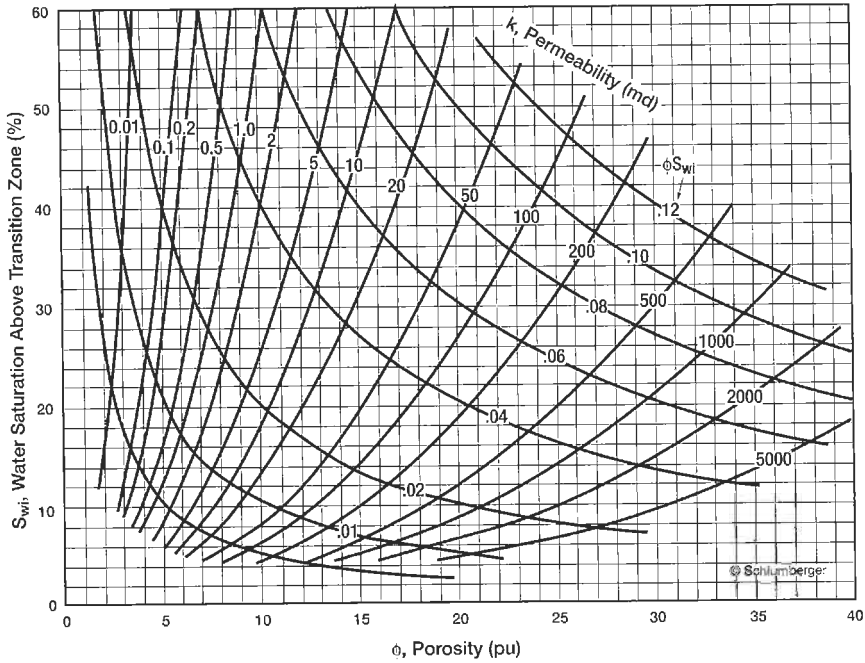


Figure 5-65. Schlumberger chart (after Wyllie and Rose) for estimating permeability [199].

$$R_{mc} = 0.69(R_{mf}) \left(\frac{R_m}{R_{mf}} \right)^{2.65} \tag{5-89}$$

where $K_m =$

0.847	for 10 lb/gal
0.708	11 lb/gal
0.584	12 lb/gal
0.488	13 lb/gal
0.412	14 lb/gal
0.380	16 lb/gal
0.350	18 lb/gal

These relationships work well for most muds (except lignosulfonate) with resistivities between 0.1 Ω -m and 10 Ω -m.

Another approximation that works well for salt muds is:

$$R_{mf} = 0.75R_m \tag{5-90}$$

$$R_{mf} = 1.5R_m \tag{5-91}$$

Temperature Relationships. Mud resistivity is a function of temperature and ion concentration. Since temperature increases with depth due to geothermal gradient, the mud resistivity is lower at the bottom of the hole than at the surface (pits). The temperature of a formation can be found with an equation suggested by Hilchie [200]:

- — Resistivity of the zone
- — Resistivity of the water in the zone
- △ — Water saturation in the zone

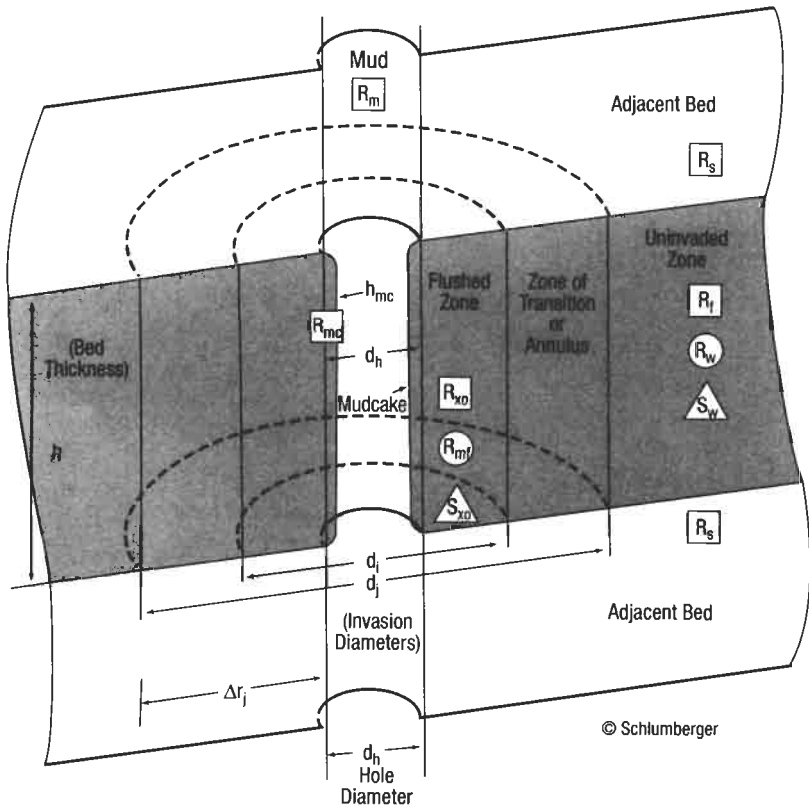


Figure 5-66. Diagram of the borehole environment showing the various zones and their parameters [199].

$$T_f = (T_{TD} - T_s) \frac{D_f}{D_{TD}} + T_s \tag{5-92}$$

- where T_f = formation temperature ($^{\circ}$ F)
- T_{TD} = temperature at total depth (BHT)($^{\circ}$ F)
- T_s = average surface temperature ($^{\circ}$ F)
- D_f = formation depth (ft)
- D_{TD} = total depth (ft)

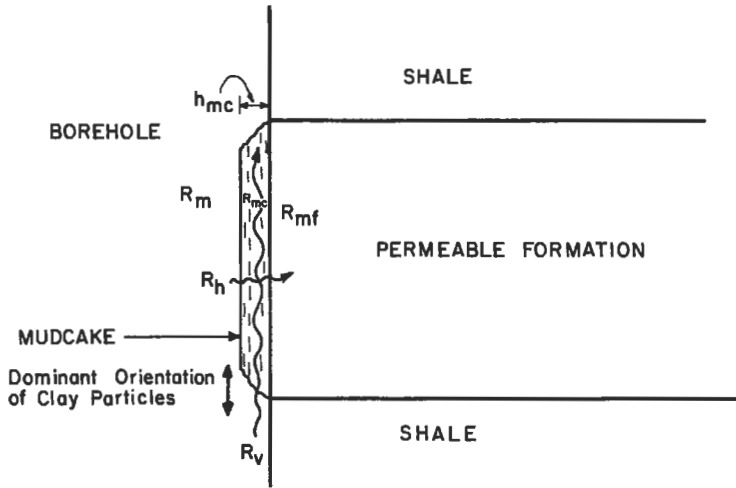


Figure 5-67. Resistivity components on mud cake that develop opposite a permeable formation.

Average surface temperatures in various oilfield areas are:

Alberta	40°F
California	65°F
Colorado-Northern New Mexico	55°F
Gulf Coast	80°F
Oklahoma	65°F
Permian Basin	65°F
Wyoming	45°F

Figure 5-68 solves this equation graphically [199].

Fluid resistivity at any formation depth can be found using the Arps Equation if the resistivity at any temperature and formation temperature are known [199]:

$$R_2 = R_1 \frac{T_1 + 6.77}{T_2 + 6.77} \tag{5-93}$$

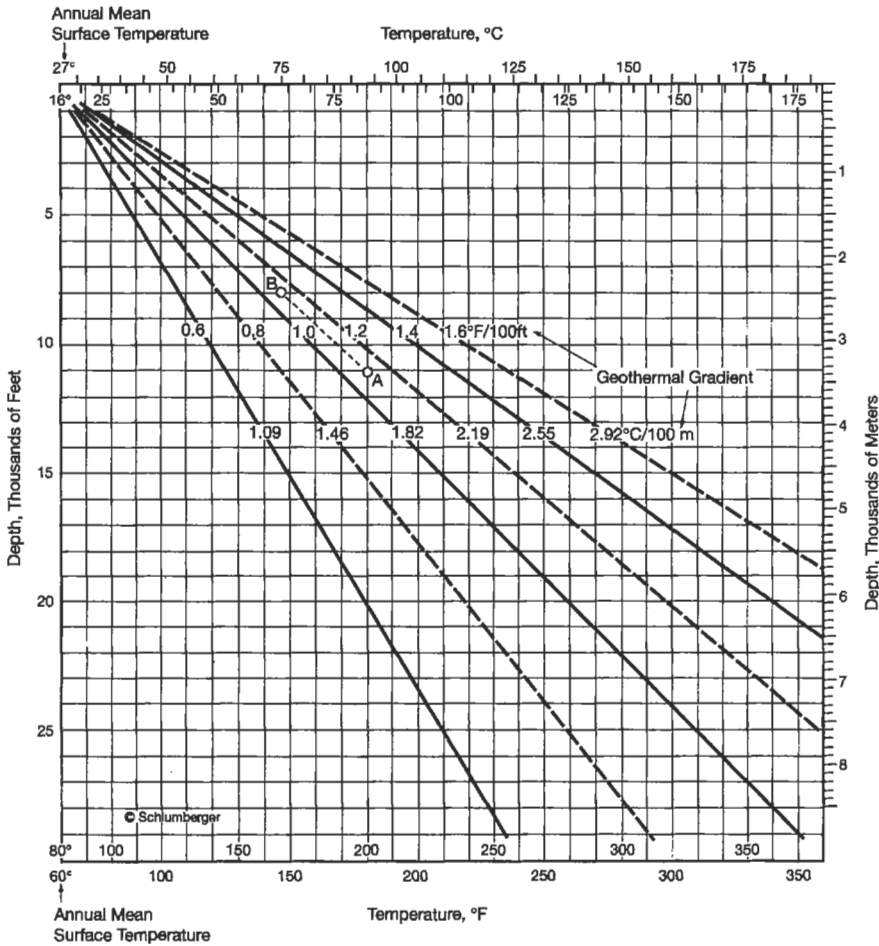
where R_2 = fluid resistivity at formation temperature, Ω -m
 R_1 = fluid resistivity at some temperature, Ω -m
 T_2 = formation temperature, °F
 T_1 = temperature R_1 was measured at, °F

A nomograph that solves this equation graphically is presented in Figure 5-69 [199].

Openhole Logs and Interpretation

SP (Spontaneous Potential). The SP log has 4 basic uses: (1) recognition of permeable zones, (2) correlation of beds, (3) determination of R_w , and (4) qualitative indication of shaliness. The SP can only be used in fresh mud and

Temperature Gradient Conversions: $1^{\circ}\text{F}/100\text{ ft} = 1.823^{\circ}\text{C}/100\text{ m}$
 $1^{\circ}\text{C}/100\text{ m} = 0.5486^{\circ}\text{F}/100\text{ ft}$



EXAMPLE: Bottom hole temperature, BHT, is 200°F at 11,000 ft (Point A).
 Temperature at 8,000 ft is 167°F (Point B).

Figure 5-68. Chart for estimating formation temperature [199].

is run with several resistivity tools. The curve is presented in Track 1 and is scaled in millivolts (mV).

The SP log is a record of the naturally occurring electrical currents created in the borehole. These currents or circuits usually occur at bed boundaries and are created by the interaction between fresh drilling mud and salty formation water. The curve represents the potential difference between a stationary electrode on the surface (ground) and a moving electrode in the borehole.

Theory. The total potential (E_t) can be separated into two components: the electrochemical (E_c) and the electrokinetic (E_k). The electrokinetic component is generally very small and is often ignored. It is created when an electrolyte (mud

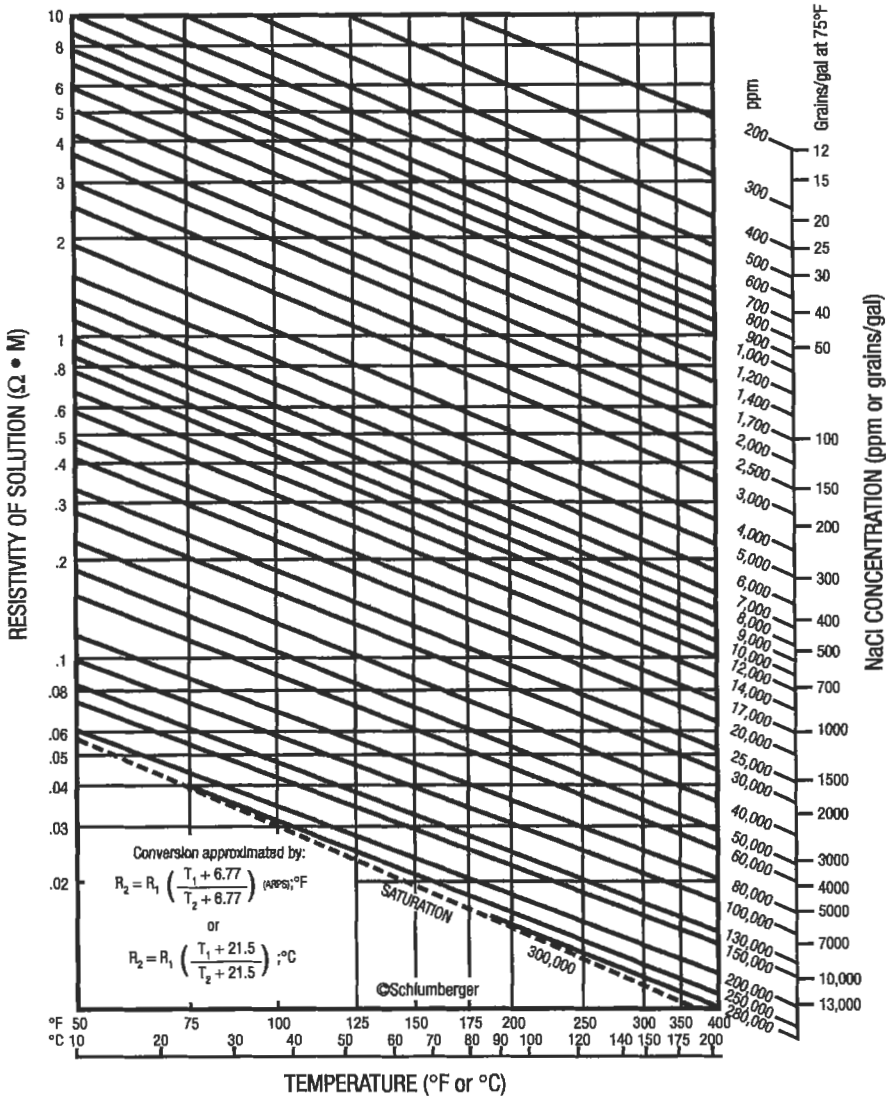


Figure 5-69. Chart for determining salinity, solution resistivity and for converting resistivity to formation temperature [199].

filtrate) flows through a nonmetallic permeable material. The magnitude of E_k is a function of the pressure drop across the material and the resistivity of the electrolyte. The electrokinetic (or streaming) potential is most significant in low pressure (depleted) formations, overbalanced mud conditions and opposite low permeability formations. See Doll's classic paper [201] for more detailed information.

The electrochemical component (E_c) is the sum of the liquid-junction potential (E_l) and the membrane potential (E_m). The liquid junction potential occurs at

the interface between fresh mud filtrate and salty formation water. This interface is usually a few inches to a few feet away from the borehole. Only two ions are assumed to be in solution in the mud and formation water: Na⁺ and Cl⁻. Chloride ions are concentrated in the formation water, and being more mobile than Na⁺ ions, move toward lower concentrations in the borehole (Figure 5-70). This creates a net negative charge near the borehole and a current flows toward the undisturbed formation. The liquid-junction potential accounts for about 20% of the electrochemical component.

The membrane (E_m) potential is created at the bed boundary between a permeable bed (sand) and an impermeable bed (shale). The shale acts as an ion-selective membrane, allowing only the smaller Na⁺ ion to move through the clay crystal structure from the salty formation water toward the fresh drilling fluid in the bore. This creates a net positive charge along the shale. It also creates a large concentration of negative charges associated with the Cl⁻ ion in the permeable bed. This phenomena is also shown in Figure 5-70. The membrane potential accounts for about 80% of the electrochemical potential. The total effect of these two potentials is a net negative charge within the permeable zone when the connate water is saltier than the mud filtrate.

Interpretation. The total electrochemical component of the total potential is what the SP records. It can be calculated with the following equation:

$$E_c = -K \log \frac{a_w}{a_{mf}} \tag{5-94}$$

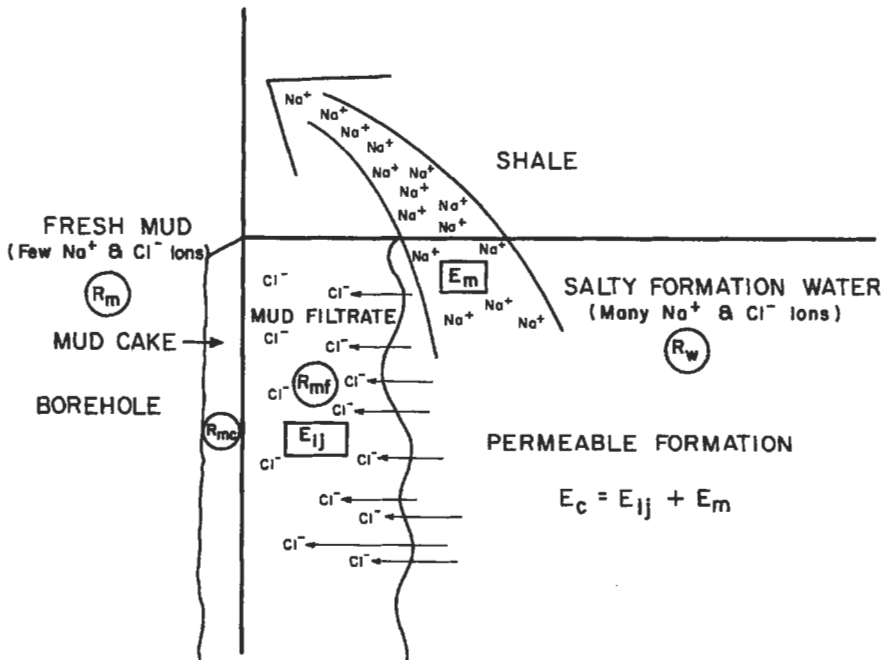


Figure 5-70. Ionic movement that contributes to the development of an SP curve.

where $-K = -(0.133T + 61)(T \text{ in } ^\circ\text{F})$

a_w = chemical activity of formation water

a_{mf} = chemical activity of drilling mud filtrate

Since the chemical activity of a solution cannot be used, it must be converted to its equivalent electrical resistivity. Chemical activity of a fluid is approximately equal to the inverse of its equivalent electrical resistivity. Conversion to equivalent resistivities makes the equation:

$$E_c = -K \log \frac{R_{mf\text{eq}}}{R_{w\text{eq}}} \quad (5-95)$$

Since E_c is equal to the maximum SP deflection recorded on a log (SSP), Equation 5-95 can be rewritten to read:

$$\text{SSP} = -K \log \frac{R_{mf\text{eq}}}{R_{w\text{eq}}} \quad (5-96)$$

where SSP is the static (or maximum) spontaneous potential recorded opposite a permeable formation. Since the purpose of an SP log is to find $R_{w\text{eq}}$ and then R_w , if we know SSP we can solve Equation 5-96 for $R_{w\text{eq}}$:

$$R_{w\text{eq}} = \frac{R_{mf\text{eq}}}{10^{(-\text{SSP}/K)}} \quad (5-97)$$

Once $R_{w\text{eq}}$ is known, it is converted to R_w using the chart shown in Figure 5-71 [199]. SSP can come directly from the log if the bed is thick and the SP curve reaches a constant value and develops a "flat top." If the curve is pointed or rounded, it must be corrected for bed thickness.

The shape and amplitude of the SP are affected by:

1. Thickness and resistivity of the permeable bed (R_f).
2. Diameter of invasion and resistivity of flushed zone (R_{xo}).
3. Resistivity of the adjacent shales (R_s).
4. Resistivity of the mud (R_m).
5. Borehole diameter (d_h).

All of these must be accounted for when examining the SP, and any necessary corrections should be made. To find the magnitude of the SP, take the maximum deflection from the average shale value (shale baseline) to the most negative value. (Figure 5-72 shows a curve that needs correction and one that does not.) Bed thickness corrections can be made from Figure 5-73 and should *always* increase the magnitude of the SP.

Another use for the SP log is finding permeable zones. Any negative deflection of the curve indicates a potentially permeable zone. The magnitude of the deflection has no relation to the amount of permeability (in millidarcies); it merely indicates that the rock has ionic permeability. No quantitative information on this parameter can be derived from the SP. Figure 5-74 shows an example of permeable and impermeable zones on an SP log.

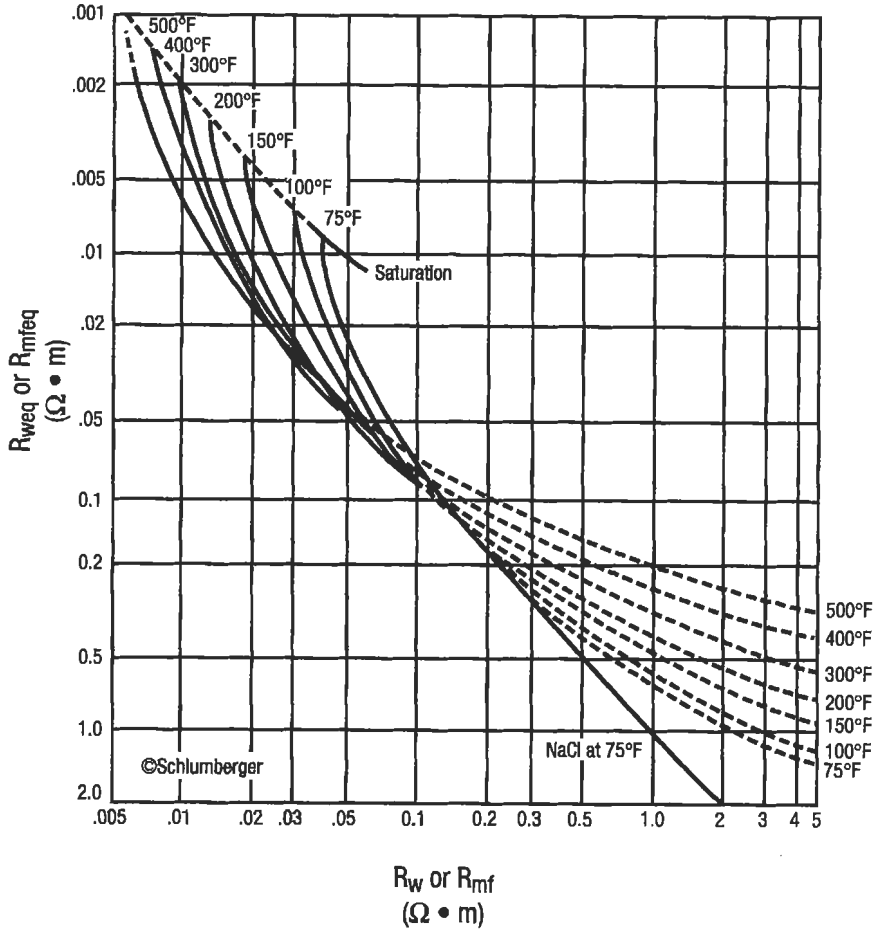


Figure 5-71. Chart for converting R_{mf} to R_{mfeq} and R_{weq} to R_w for SP- R_w calculations [199].

Interpretation of an SP log follows a few basic rules:

1. If the SP curve is concave to the shale line, the formation is permeable.
2. If the SP curve is convex to the shale line, the formation is impermeable.
3. Constant slope means high resistivity—usually impermeable.
4. High resistivity formations cause the bed boundaries to become rounded.
5. A thin permeable bed does not reach maximum deflection.
6. A thin shale streak does not reach the shale baseline.
7. Bed boundaries are picked at the inflection points in clean sands. Bed boundaries should be confirmed with some other log such as the gamma ray.

Resistivity Tools. The purpose of resistivity tools is to determine the electrical resistance of the formation (rock and fluid). Since most formation waters contain

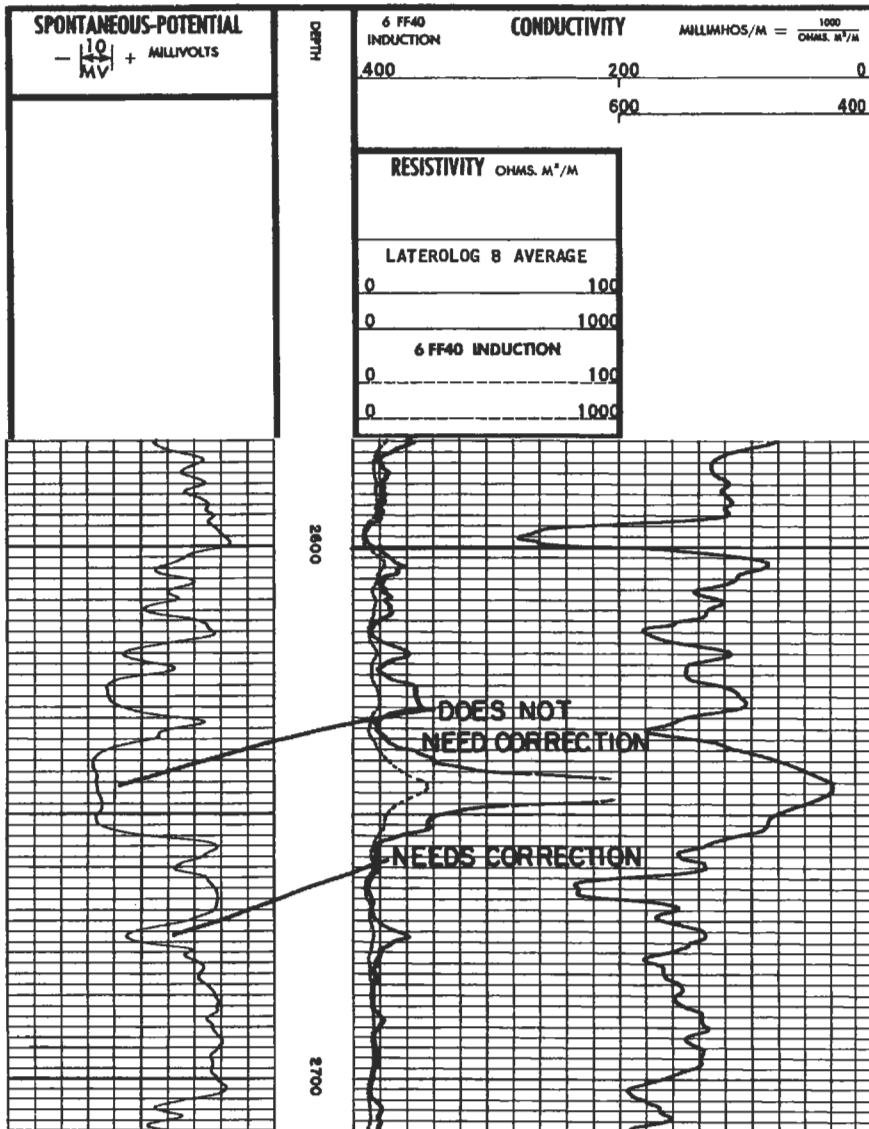


Figure 5-72. Example of an SP curve that requires correction and one that does not.

dissolved salts, they generally have low resistivities. Hydrocarbons do not conduct electricity, therefore rocks that contain oil and/or gas show high resistivity. This is the way hydrocarbon-bearing zones are differentiated from water zones.

Resistivity tools are divided into three types based on the way measurements are made: (1) non-focused (normal) tools, (2) induction tools, and (3) focused resistivity tools. Microresistivity tools will be treated under a separate heading.

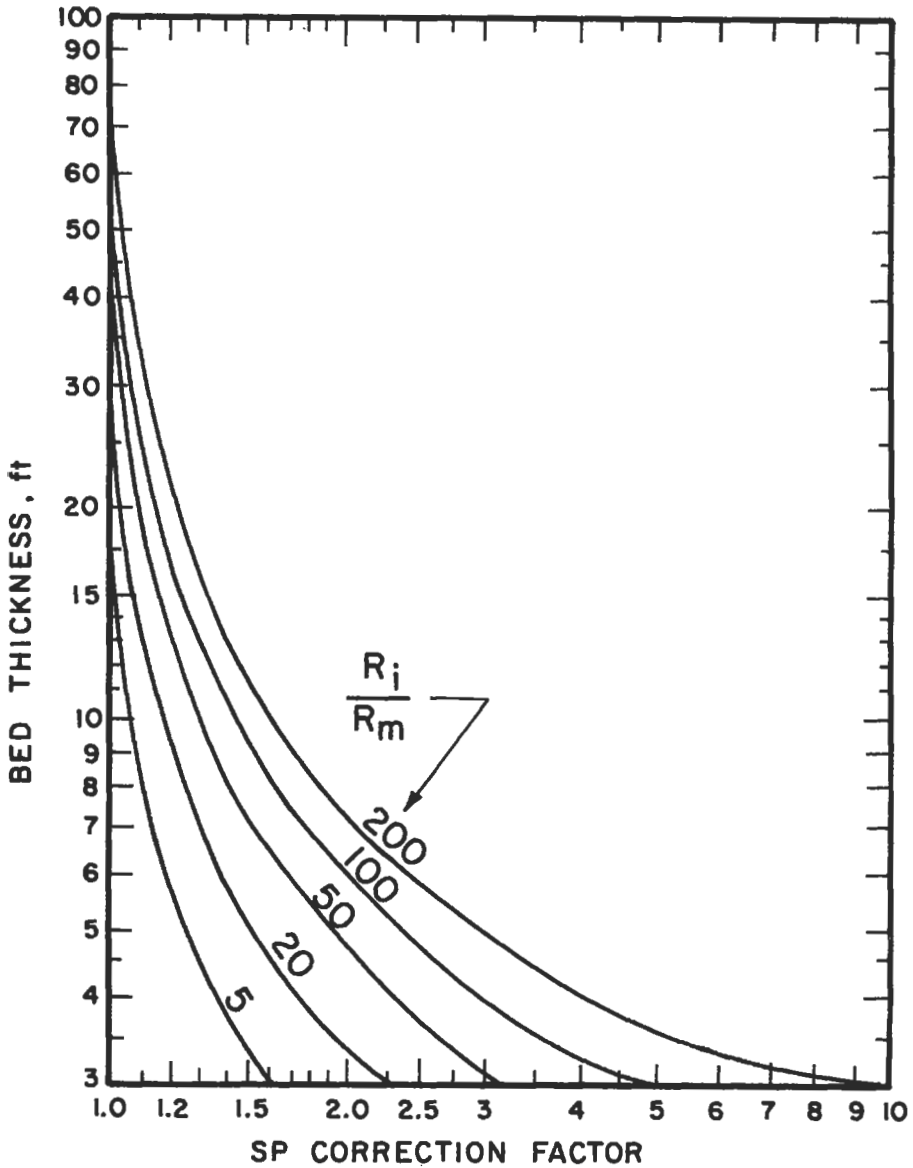
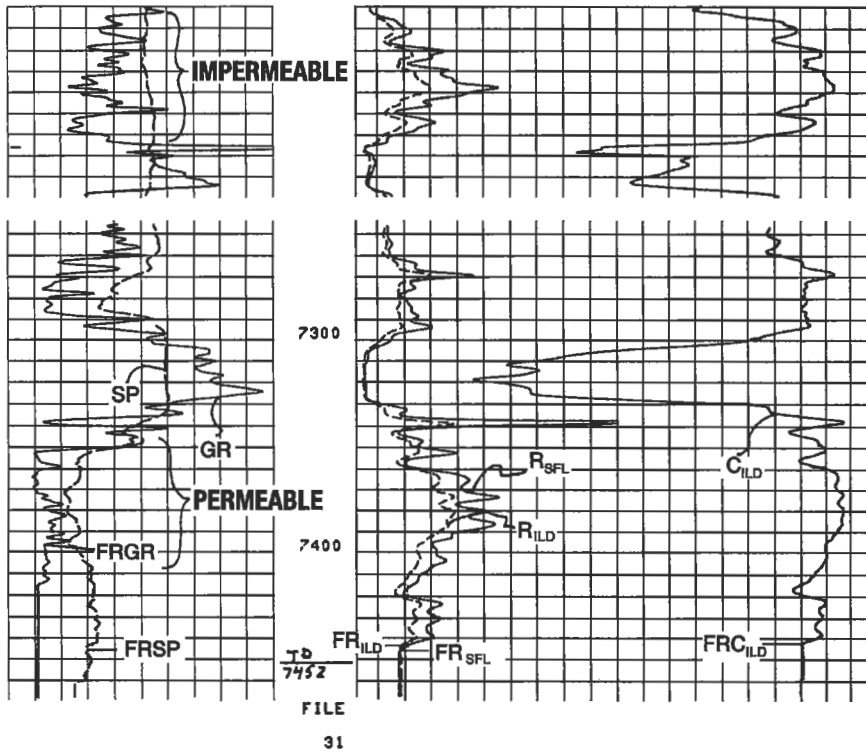


Figure 5-73. SP bed thickness correction chart for the SP [200,201].

Resistivity tools are further divided by depth of investigation. Tools may read the flushed zone (R_{xo}), the transition zone between the flushed and uninvaded zones (R_t), or the uninvaded zone (R_i). For purposes of this discussion, all tool names are for Schlumberger equipment. Comparable tools offered by other logging companies are summarized in Table 5-25.



		ILD (OHMM)	100.0
GR (GAPI)	200.0	SFLA (OHMM)	100.0
SP (MV)	-100.0 0.0	CILD (MM/M)	0.0
			400.0

Figure 5-74. Examples of an SP log through an impermeable and a permeable zone.

Theory Nonfocused (Normal Tools.) The first tools to be used were nonfocused tools [58]. The electrode arrangement is as shown in Figure 5-75a [58]. As shown earlier, resistivity, R, is found using Ohm's Law ($r = V/I$):

$$R = \frac{rA}{L} \tag{5-44}$$

- where V = voltage read from meter
- I = current read from meter
- A = surface area, m²
- L = length, m
- R = resistivity, ohm-m
- r = resistance, ohms

(text continued on page 134)

Table 5-25
Service Company Nomenclature

Schlumberger	Gearhart	Dresser Atlas	Welex
Electrical log (ES)	Electric log	Electrolog	Electric log
Induction electric log	Induction electrical log	Induction electrolog	Induction electric log
Induction spherically focused log			
Dual induction spherically focused log	Dual induction-laterolog	Dual induction focused log	Dual induction log
Laterolog-3	Laterolog-3	Focused log	Guard log
Dual laterolog	Dual laterolog	Dual laterolog	Dual guard log
Microlog	Micro-electrical log	Minilog	Contact log
Microlaterolog	Microlaterolog	Microlaterolog	F _o R _{xo} log
Proximity log		Proximity log	
Microspherically focused log			
Borehole compensated sonic log	Borehole compensated sonic	Borehole compensated acoustilog	Acoustic velocity log
Long spaced sonic log		Long spacing BHC acoustilog	
Cement bond/variable density log	Sonic cement bond system	Acoustic cement bond log	Microseismogram
Gamma ray neutron	Gamma ray neutron	Gamma ray neutron	Gamma ray neutron
Sidewall neutron porosity log	Sidewall neutron porosity log	Sidewall epithermal neutron log	Sidewall neutron log
Compensated neutron log	Compensated neutron log	Compensated neutron log	Dual spaced neutron
Thermal neutron decay time log		Neutron lifetime log	Thermal multigate decay
Dual spacing TDT		Dual detector neutron	
Formation density log	Compensated density log	Compensated densilog	Density log
Litho-density log			
High resolution dipmeter	Four-electrode dipmeter	Diplog	Diplog
Formation interval tester		Formation tester	Formation tester
Repeat formation tester	Selective formation tester	Formation multi tester	Multiset tester
Sidewall sampler	Sidewall core gun	Corgun	Sidewall coring
Electromagnetic propagation log			
Borehole geometry tool	X-Y caliper	Caliper log	Caliper Compensated
Ultra long spacing electric log			

**Table 5-25
(continued)**

Schlumberger	Gearhart	Dresser Atlas	Welex
Natural gamma ray spectrometry		Spectralog	Spectral natural gamma
Gamma ray spectroscopy tool log		Carbon/oxygen log	
Well seismic tool			
Fracture identification log	Fracture detection log		

From Reference 215.

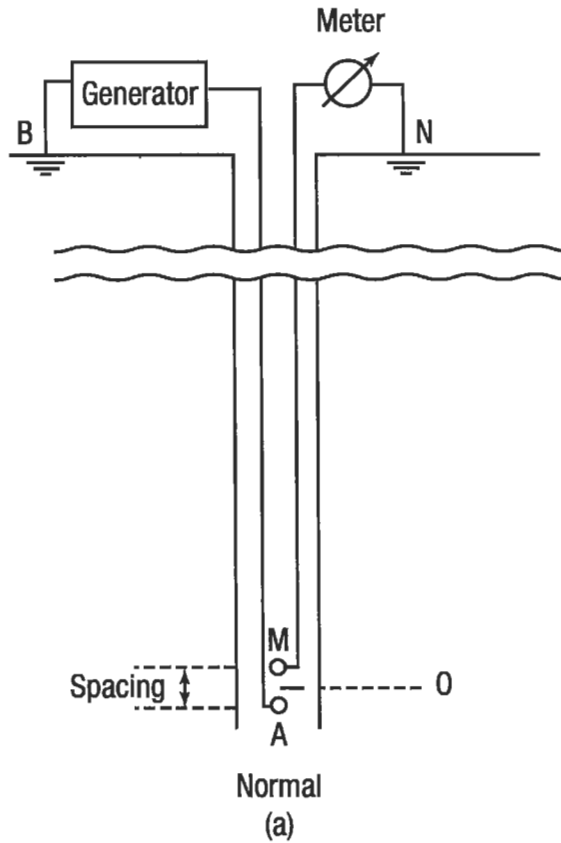
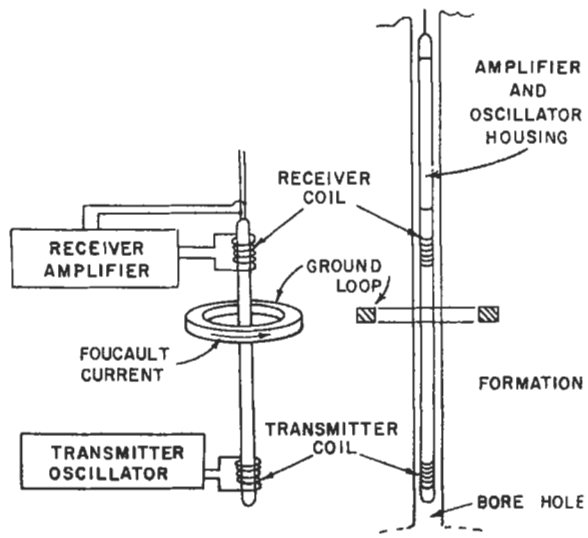
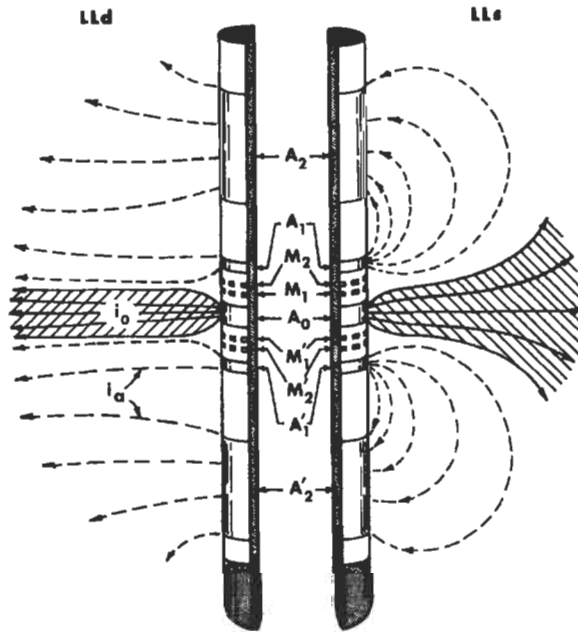


Figure 5-75. (a) Basic electrode arrangement of a normal device used in conventional electric logs. (b) Electrode arrangement for a basic, two coil induction log system. (c) Electrode arrangement and current flow paths for a dual laterolog sonde [58].



(b)



(c)

Figure 5-75. Continued.

(text continued from page 130)

The tools work well in low-resistivity formations with thick beds and in slightly conductive muds.

Induction Tools. Since a slightly conductive mud is necessary for the normal tools, they cannot be used in very fresh muds or in oil-base muds. The induction tool overcomes these problems by inducing a current into the formation instead of passing it through the mud-filled borehole. Figure 5-75b shows a simplified two-coil induction tool [58]. High-frequency alternating current is sent into the transmitter coil. The alternating magnetic field that is created induces secondary currents in the formation. These currents flow through a conductive formation in circular paths called ground loops. These currents in turn create a magnetic field which induces currents in the receiver coil. The signal received is proportional to the formation conductivity. Conductivity readings are then converted to resistivity. Additional coils are used to focus the tool so that conductive beds as thin as four feet can be detected. Induction tools work well in oil-base, foam, air, gas, and fresh mud. The induction tool is unreliable above 500 Ω -m and useless above 1,000 Ω -m or in salt muds. Readings are only considered reasonable below 100 Ω -m and are accurate between 1 and 20 Ω -m when mud is very fresh.

Phasor Induction Tools. Since the early 1960's, induction logging tools have become the principal logging device for fresh, slightly conductive to non-conductive (oil-base) muds. However, these devices are significantly affected by environmental (bore-hole size and mud composition) and geological (bed thickness and invasion) conditions. Also, high formation resistivities (> 50 to 100 Ω -m) dramatically increase the difference between apparent R_t and true R_t [58A, 199]. In 1986, Schlumberger introduced a new induction log to offset these problems [58A]. This device is known by the trade name Phasor Induction SFL and uses a standard dual induction tool array. The difference between the conventional and phasor devices is in signal processing made possible by miniaturization of computer components. Induction tools all produce two signals: the inphase (R-signal) induction measurement and the quadrature (X-signal) induction signal. The R-signal is what is presented on standard dual induction-SFL log presentations. The R-signal and X-signal measurements are combined during advanced processing in the logging tool itself to produce a log with real time corrections for environmental and geological conditions. Apparent R_t is nearly equal to true R_t in most situations. Vertical resolution of this device is about the same as conventional induction tools (about 6 feet), but enhanced and very enhanced resolution phasor tools are available that have vertical resolutions down to 2 feet [58A]. The primary advantages of this tool include much better R_t readings in high resistivity formations (i.e. > 100 Ω -m) and more accurate readings in salty muds than previously possible.

Focused Resistivity Tools (Laterologs). The Laterologs are the primary salt-mud resistivity tools. Salt mud presents a problem in that the path of least resistance is within the borehole. Therefore the current must be forced into the formation which has higher resistance. To do this, secondary electrodes (A_1 and A_2) are placed above and below the measuring current-emitting electrode (A_0). These secondary electrodes emit "focusing" or "guard" currents with the same polarity as the measuring currents. Small monitoring electrodes (M_1 , M_2 , M_1' and M_2') adjust the focusing currents so that they are at the same potential as A_1 and A_2 .

A sheet of current measuring one to two feet thick is then forced into the formation from A_0 . The potential is then measured between M_2 and M_1 and a surface ground. Since I_0 is a constant, any variation in M_1 and M_2 current is proportional to formation resistivity. Figure 5-75c shows the electrode arrangement [58].

Corrections. As previously mentioned, resistivity tools are affected by the borehole, bed thickness, and invaded (flushed) zone. If bed thickness and mud resistivity are known, these effects can be accounted for. Major service companies (Schlumberger, Atlas Wireline, Welex Halliburton) provide correction charts for their tools. Several charts for Schlumberger tools are included in this chapter (Figures 5-76 to 5-82) [199] and can be used with logs from other service companies. Complete chart books are available from most wireline service companies. Current chart books should be used and can be obtained by calling the appropriate service company or by asking the logging engineer. Correction and interpretation charts for older tools (normals and laterals) are no longer published by service companies, but can be found in a text by Hilchie [202]

(text continued on page 146)

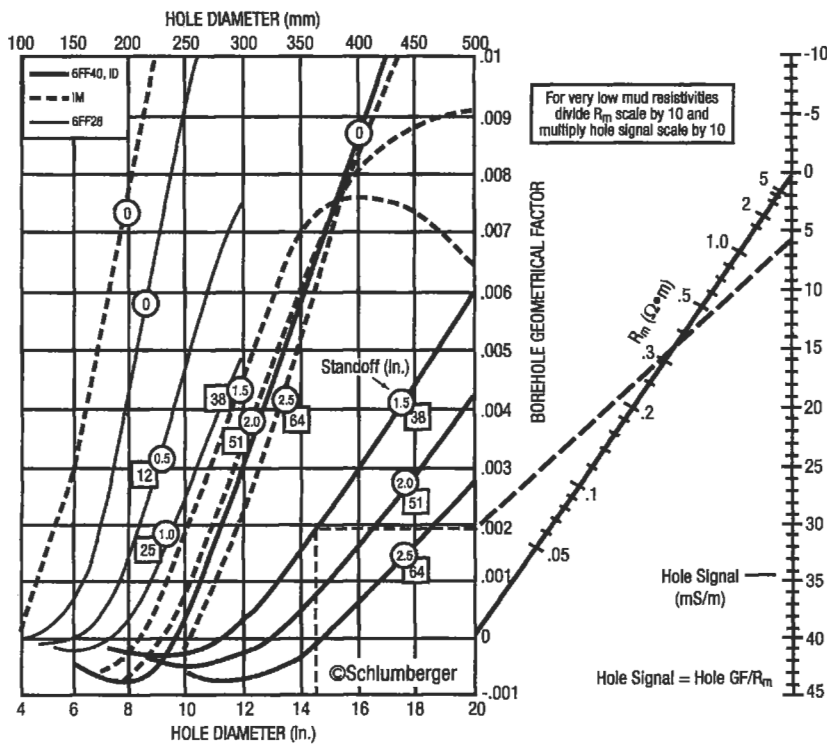


Figure 5-76. Borehole correction chart for induction log readings [199].

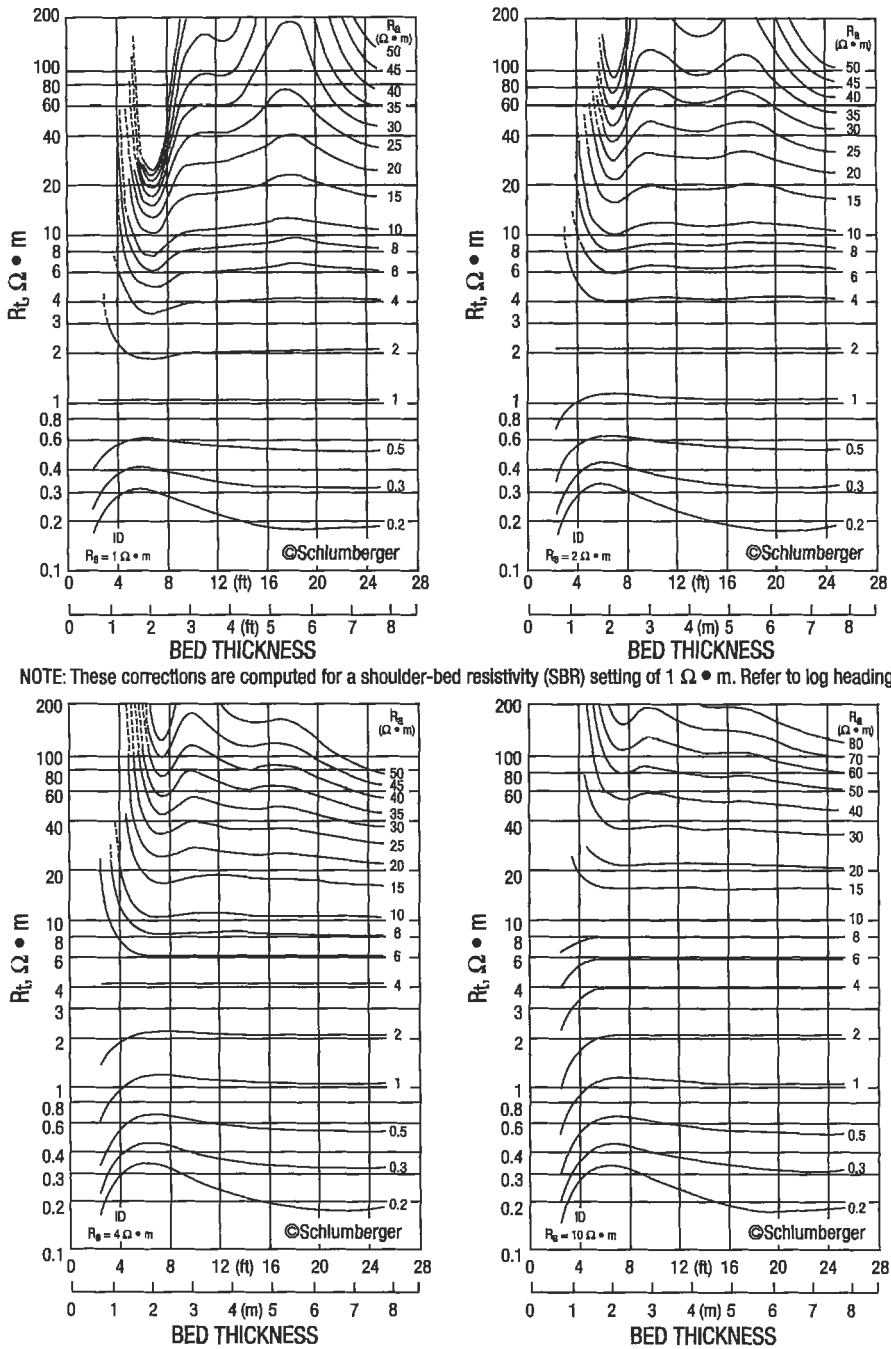


Figure 5-77. Bed thickness correction charts for the deep induction log [199].

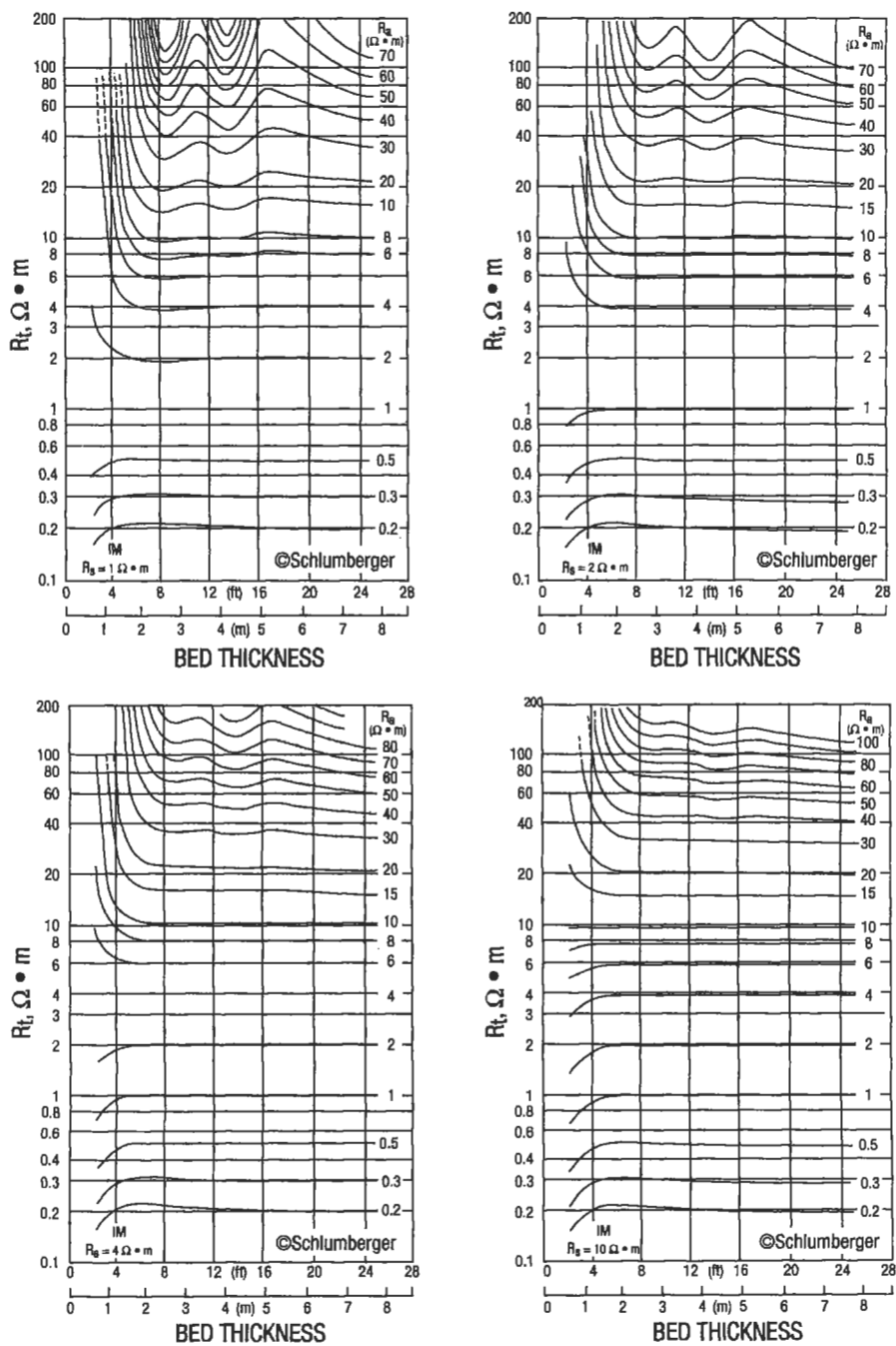


Figure 5-78. Bed thickness correction charts for the medium induction log [199].

Thick Beds, 8-in. (203-mm) Hole, Skin-Effect Corrected,
 $R_{xo}/R_m \approx 100$, DIS-DB or Equivalent

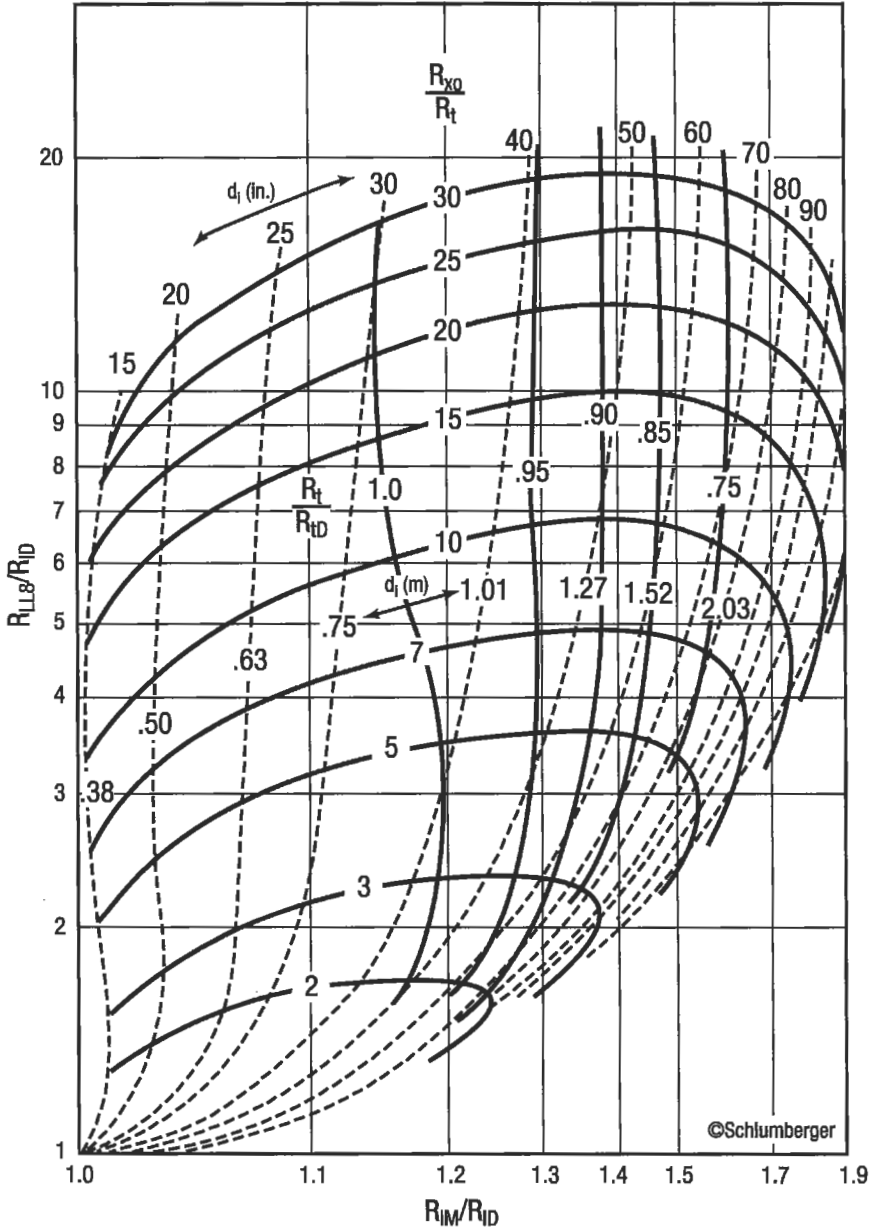
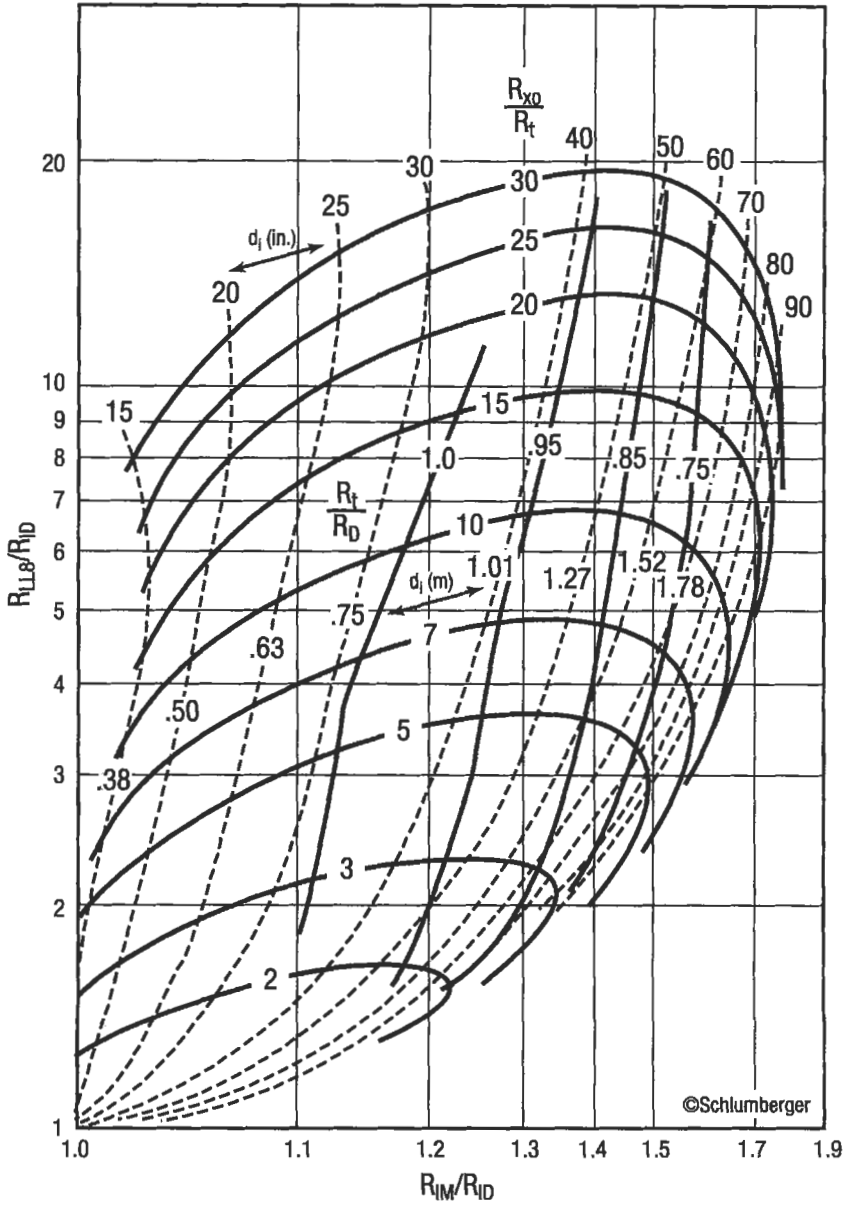


Figure 5-79a. Invasion correction charts for the dual induction-laterolog 8 combination [199].

Thick Beds, 8-in. (203-mm) Hole, Skin-Effect Corrected,
 $R_{xo}/R_m \approx 20$, DIS-DB or Equivalent



This chart may also be used with Dual Induction-Spherically Focused log.

Figure 5-79b.

Thick Beds, 8-in. (203-mm) Hole, Skin-Effect Corrected,
 $R_{xo}/R_m \approx 100$, DIS-EA or Equivalent

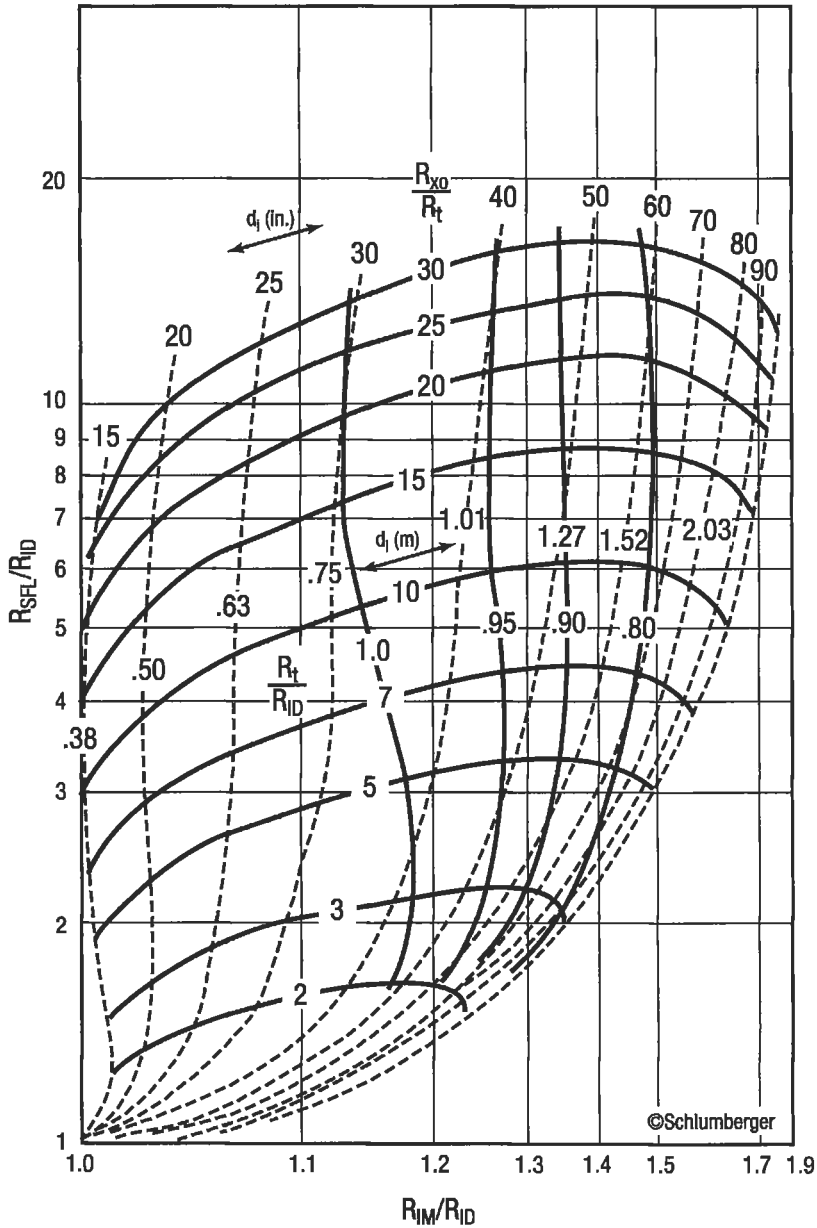
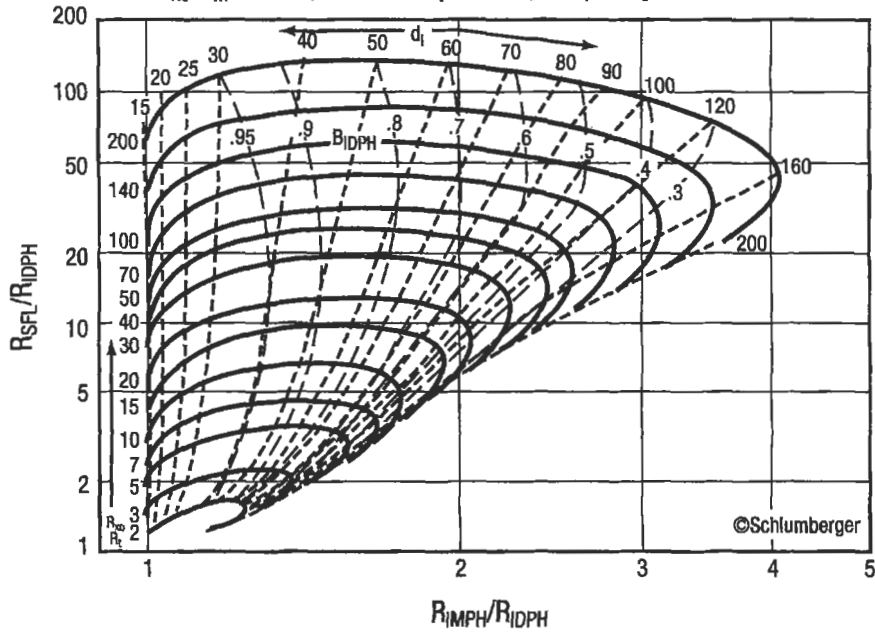


Figure 5-79c. Invasion correction chart for the dual induction-spherically focused log combination [199].

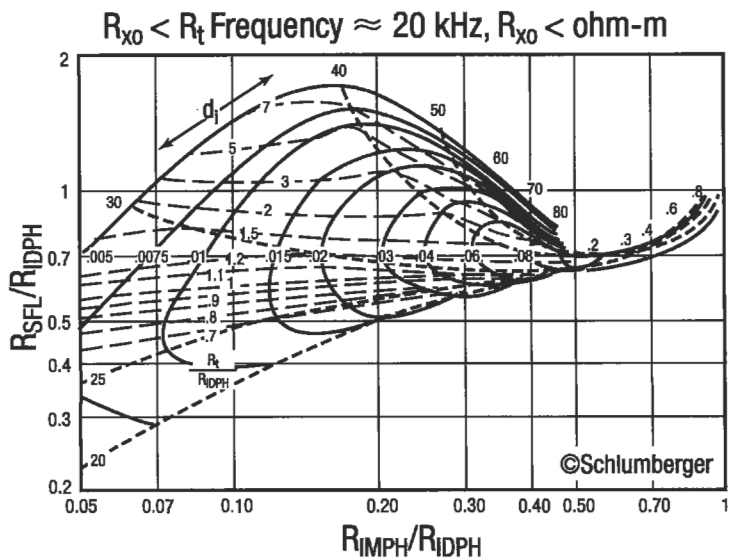
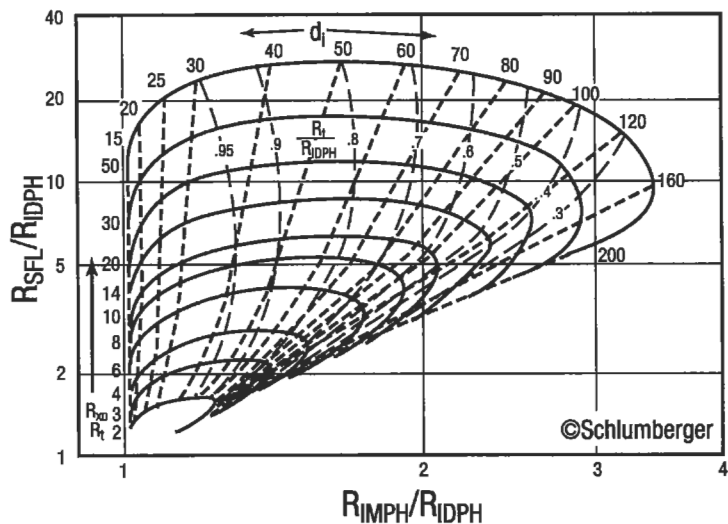
Thick Beds, 8-in. (203-mm) Hole, Skin-Effect and Borehole Corrected,
 $R_{xo}/R_m \approx 100$, DIT-E or Equivalent, Frequency = 20 kHz



These charts (Figures 5-79d and e) apply to the Phasor Induction tool when operated at a frequency of 20 kHz. Similar charts (not presented here) are available for tool operation at 10 kHz and 40 kHz. The 20 kHz charts do provide, however, reasonable approximations of R_{xo}/R_t and R_f/R_{IDPH} for tool operation at 10 kHz and 40 kHz when only moderately deep invasion exists (less than 100 inches).

Figure 5-79d. Invasion correction chart for the phasor dual induction-spherically focused log combination for $R_{xo}/R_m = 100$ [199].

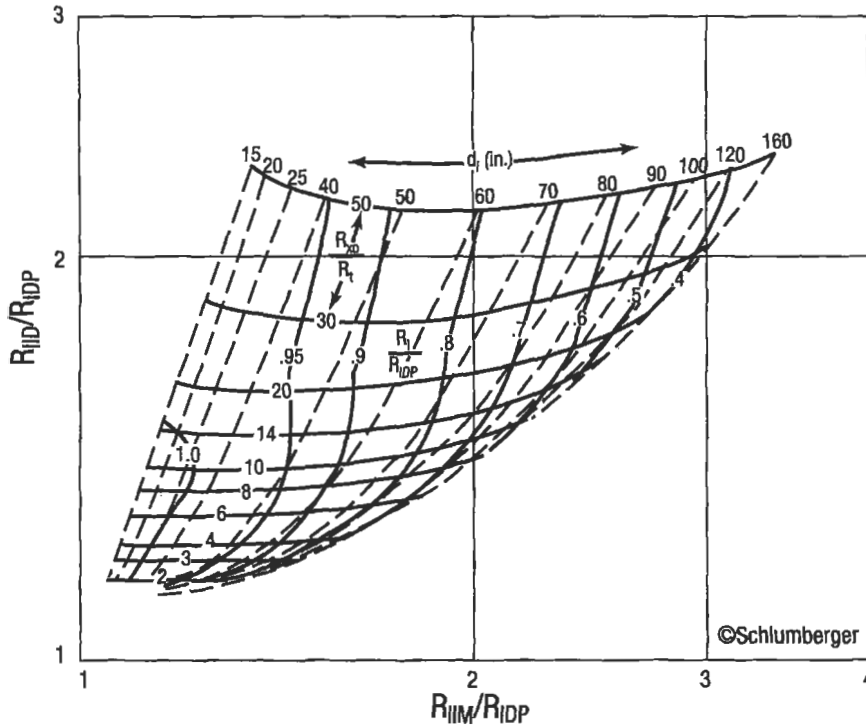
Thick Beds, 8-in. (203-mm) Hole, Skin-Effect and Borehole Corrected,
 $R_{xo}/R_m \approx 20$, DIT-E or Equivalent, Frequency = 20 kHz



Rint - 11b

Figure 5-79e. Invasion correction chart for the phasor dual induction-spherically focused log combination for $R_{xo}/R_m = 20$ [199].

Thick Beds, 8-in. (203-mm) Hole
 $R_{IDP} < 10 \Omega \cdot m$, DIT-E or Equivalent, Frequency = 20 kHz



This chart uses the raw, unboosted Induction signals and the ID-Phasor value to define the invasion profile in a rock drilled with oil-base mud. To use the chart, the ratio of the raw, unboosted medium induction signal (IIM) and the deep Phasor induction (IDP), is entered in abscissa. The ratio of the raw, unboosted deep induction signal (ID) and the deep Phasor Induction (IDP) is entered in ordinate. Their intersection defines d_i , R_{xo}/R_t , and R_t .

EXAMPLE: $R_{IDP} = 1.6 \Omega \cdot m$
 $R_{ID} = 2.4 \Omega \cdot m$
 $R_{IIM} = 2.4 \Omega \cdot m$
 Giving, $R_{ID}/R_{IDP} = 2.4/1.6 = 1.5$
 $R_{IIM}/R_{IDP} = 2.4/1.6 = 1.5$
 Therefore, $d_i = 50$ in.
 $R_{xo}/R_t = 15$
 $R_t/R_{IDP} = 0.94$
 $R_t = 0.94 (1.6)$
 $= 1.5 \Omega \cdot m$

Figure 5-79f. Invasion correction chart for the phasor dual induction log in oil-based mud [199].

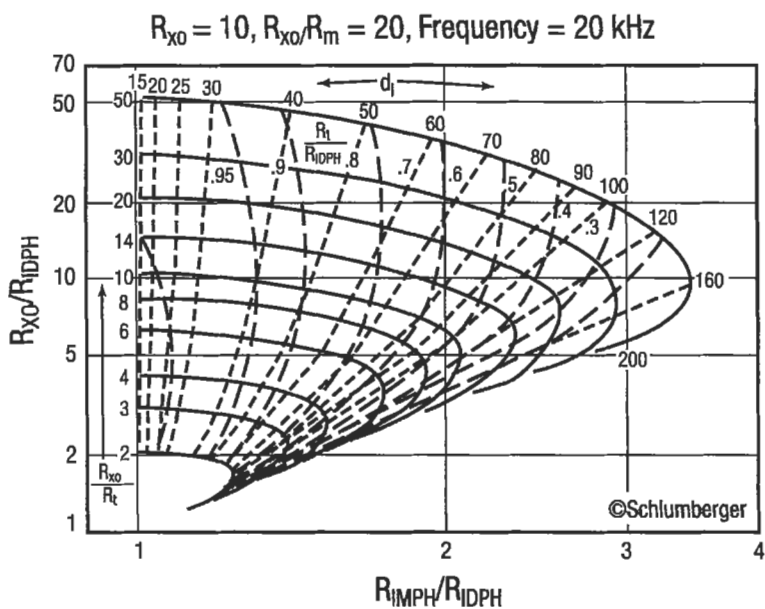


Figure 5-79g. Invasion correction chart for the phasor dual induction-Rxo log combination for $R_{XO} = 10, R_{XO}/R_m = 20$ [199].

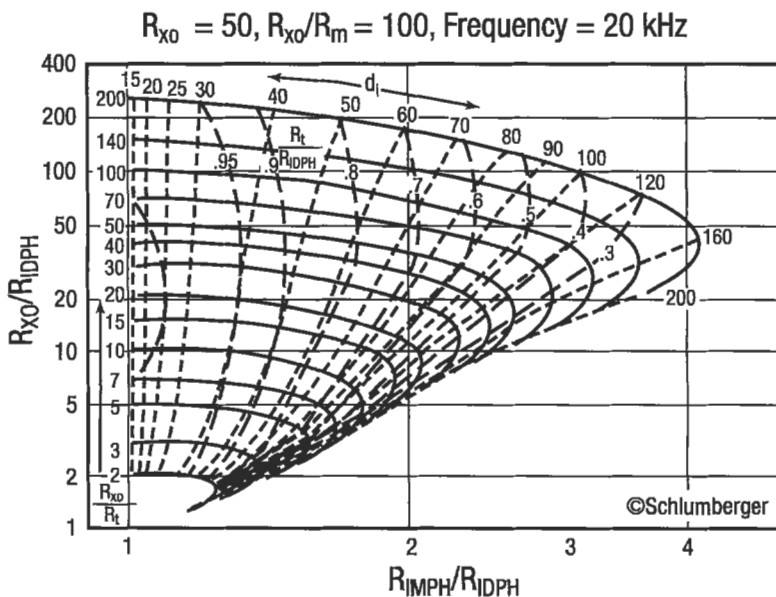


Figure 5-79h. Invasion correction chart for the phasor dual induction-Rxo log combination for $R_{XO} = 50, R_{XO}/R_m = 100$ [199].

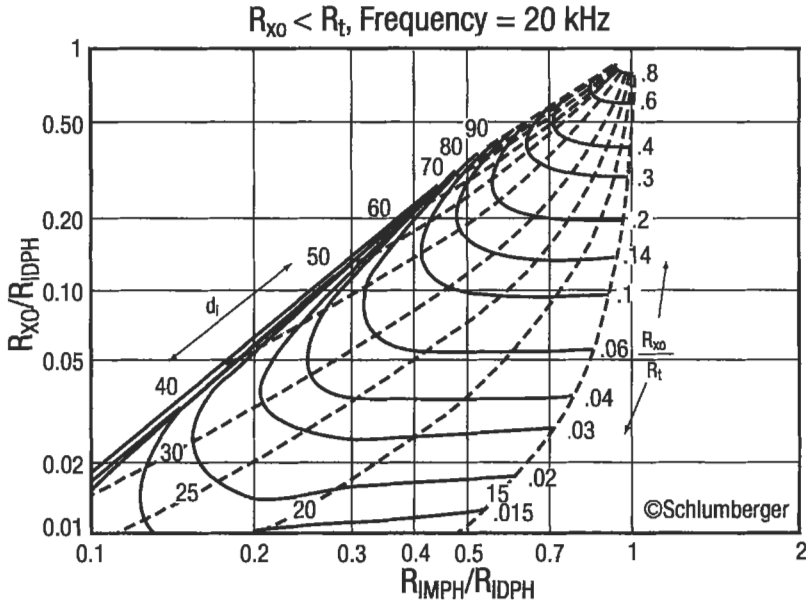


Figure 5-79i. Invasion correction chart for the phasor dual induction- R_{xo} log combination for $R_{xo} < R_t$ [199].

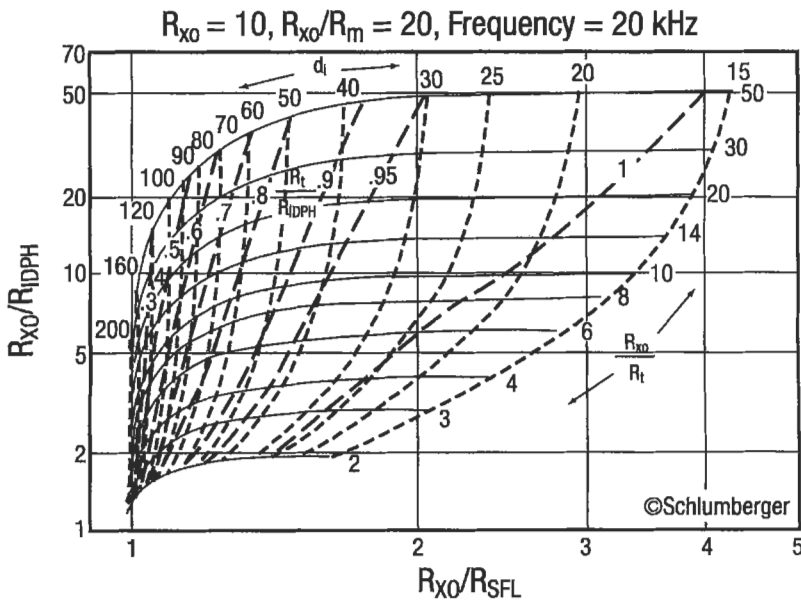


Figure 5-79j. Invasion correction chart for the phasor dual induction-spherically focused- R_{xo} log combination for $R_{xo} = 10, R_{xo}/R_m = 20$ [199].

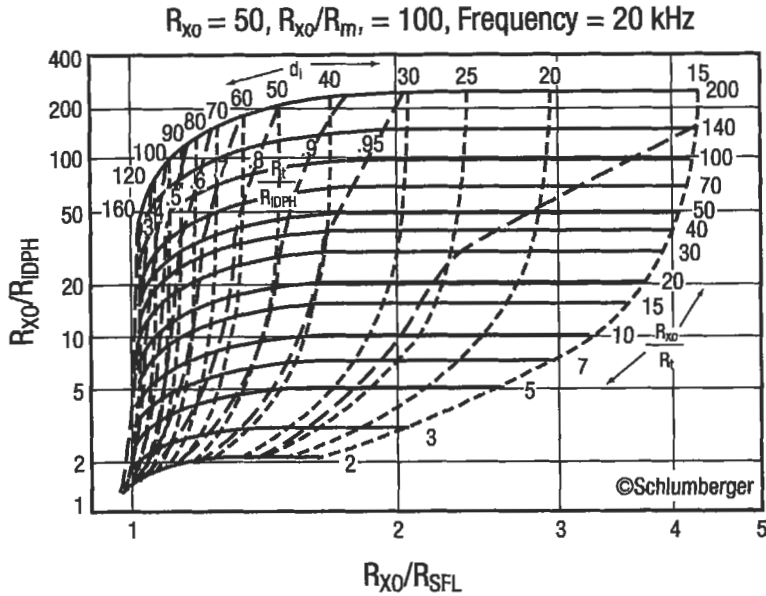


Figure 5-79k. Invasion correction chart for the phasor dual induction-spherically focused-Rxo log combination for $R_{xo} = 50, R_{xo}/R_m = 100$ [199].

(text continued from page 135)

and in a recent publication [203]. All log readings should be corrected with these charts to obtain accurate R_t and R_{xo} readings.

The dual induction logs should be corrected for borehole, bed thickness, and invasion effects if three curves are present. The induction-SFL, induction-LL-8, and induction-electric log combinations require an R_{xo} curve to make corrections. If no R_{xo} device is presented, the deep induction curve is assumed to read true R_t . The specific charts included in this text are Figure 5-76 for induction log borehole corrections, Figures 5-77 and 5-78 for induction log bed-thickness corrections, and Figure 5-79a to 5-79c for invasion corrections (check log to see if an SFL or a LL-8 log was used with the induction curves and select the appropriate Tornado chart) [199]. Phasor induction logs only require invasion correction. This is accomplished with the appropriate Tornado Charts (Figures 5-79d to 5-79k) [199]. An invasion correction Tornado Chart for phasor induction tools with other frequencies are also available [58a].

The dual laterolog- R_{xo} combination should be corrected for borehole effects; bed thickness corrections are not normally made. Figure 5-80 is used to make the borehole corrections of the deep and shallow laterologs, respectively [199]. Figure 5-81 is used to correct the micro-SFL logs for mud cake effects [199]. Invasion effects are corrected by using Figure 5-82 [199].

Interpretation. With Equation 5-70, water saturation can be found using corrected values of R_t derived from the Tornado charts. R_w can be found from an SP log or chemical analysis, and F_R from a porosity log and Table 5-7.

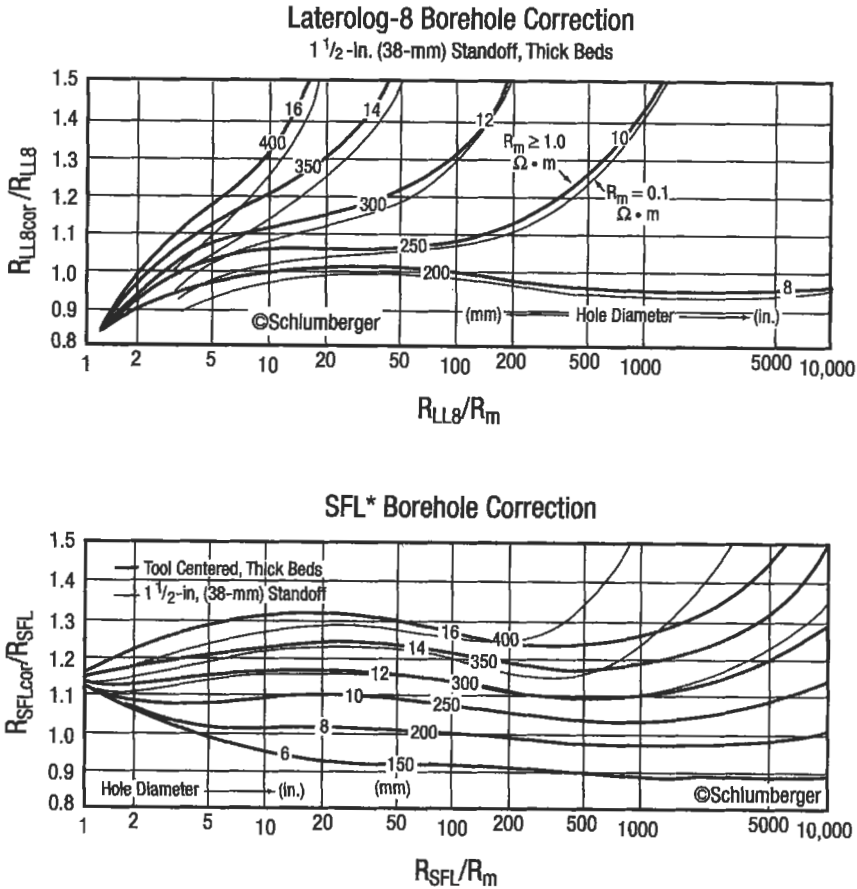


Figure 5-80a. Borehole correction charts for the laterolog and spherically focused logs [199].

If a porosity log is not available, F_R can be found using Equation 5-45. R_o is selected in a water-bearing zone from the deepest reading resistivity curve. Care should be taken to select R_o in a bed that is thick, permeable, and clean (shalefree). The zone should be as close to the zone of interest as possible. R_o can sometimes be selected from below the water/hydrocarbon contact within the zone of interest. Archie's equation (as described earlier) can then be used to calculate water saturation:

$$S_w = \left[\frac{F_R R_w}{R_t} \right]^{1/2} \tag{5-70}$$

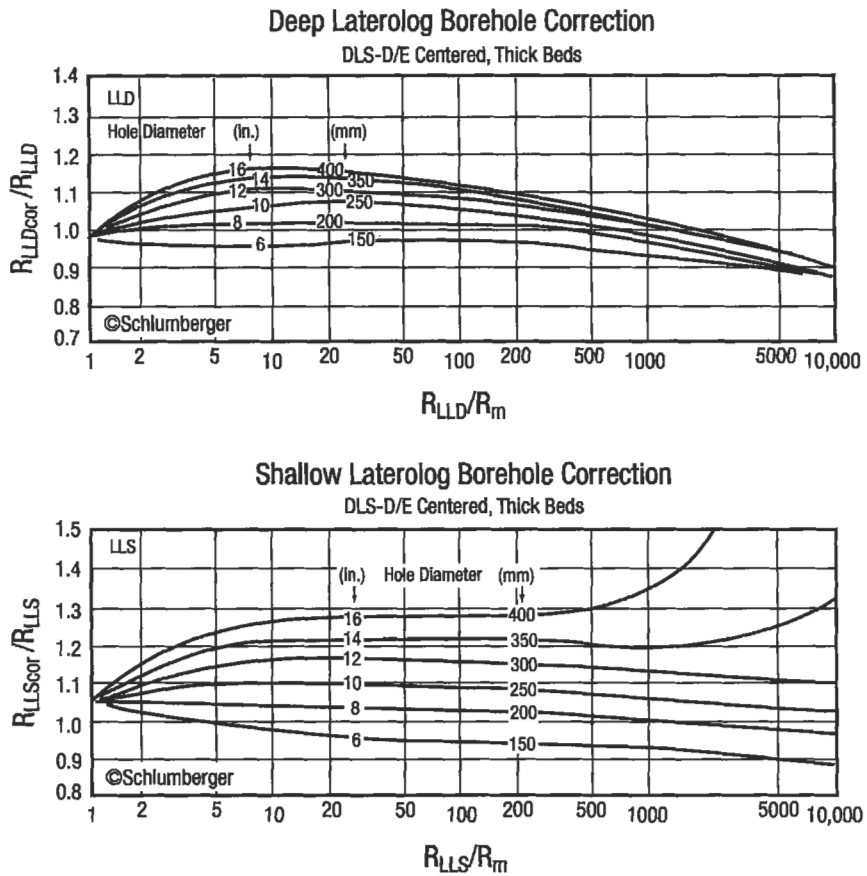


Figure 5-80b. Borehole correction charts for the dual laterolog [199].

If no porosity log or water zone is available, the ratio method can be used to find water saturation. The saturation of the flushed zone (S_{xo}) can be found by:

$$S_{xo} = \left[\frac{F R_{mf}}{R_{xo}} \right]^{1/2} \tag{5-98}$$

When Equation 5-70 is divided by Equation 5-98, the result is a ratio of water saturations:

$$\frac{S_w^2}{S_{xo}^2} = \frac{R_{xo} R_w}{R_t R_{mf}} \tag{5-99}$$

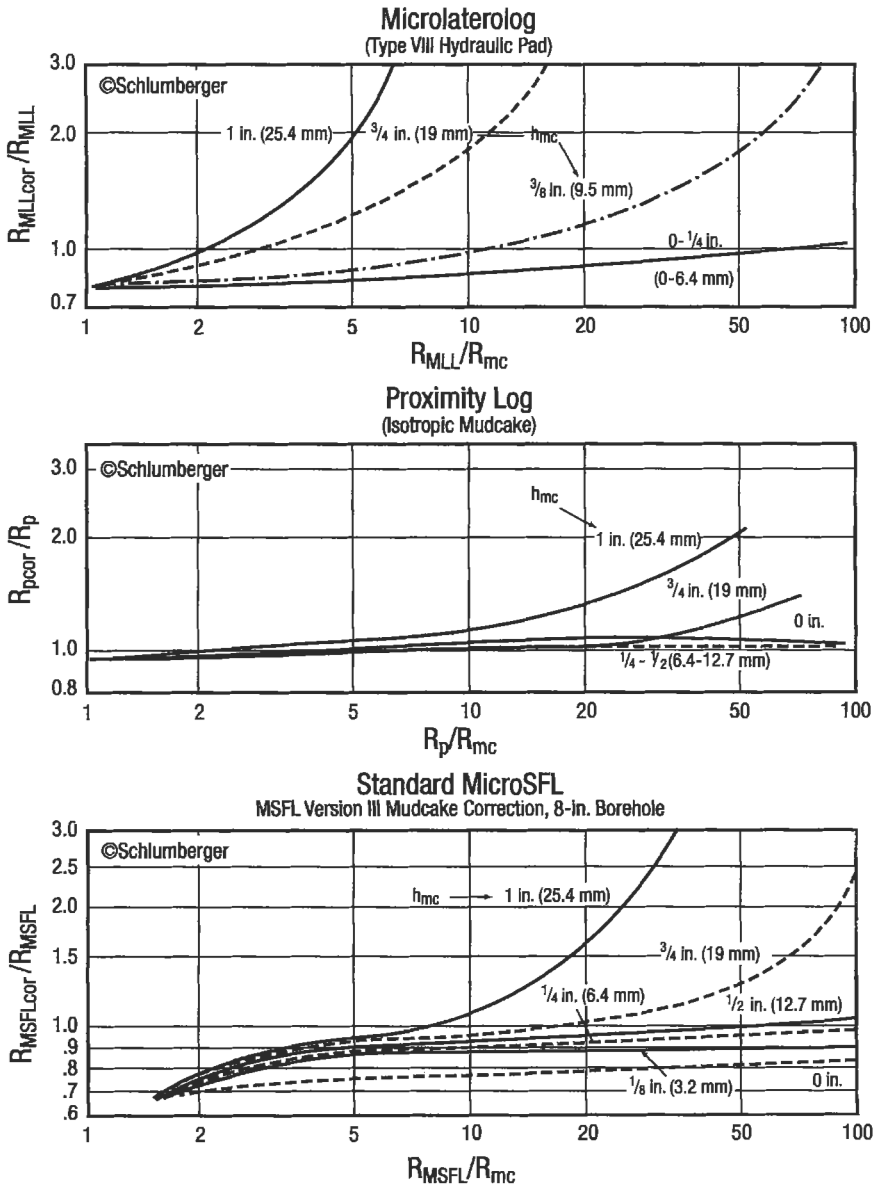


Figure 5-81. Mudcake correction for: (a) microlaterolog, (b) proximity log and (c) micro SFL log.

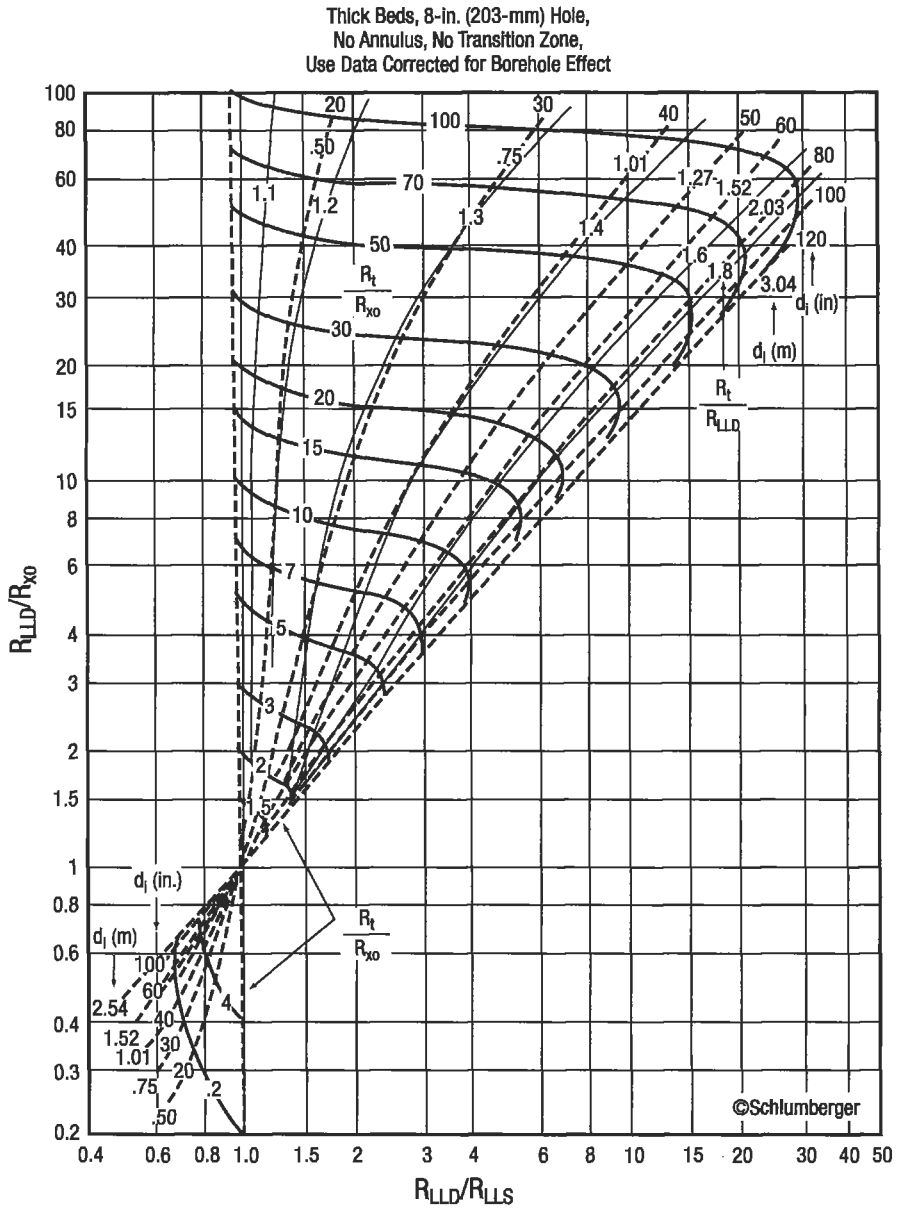


Figure 5-82. Invasion correction chart for the dual laterolog- R_{xo} log combination [199].

Poupon, Loy, and Tixier [204] found that for “average” residual oil saturations:

$$S_{xo} = S_w^{1/5} \quad (5-100)$$

Substituting Equation 5-100 into Equation 5-99 and rearranging terms:

$$S_w = \left[\frac{R_{xo}/R_i}{R_{mf}/R_w} \right]^{5/8} \quad (5-101)$$

With this equation, water saturation can be found without knowing ϕ . Note, however, that this interpretation method is based on the assumption that $S_{xo} = S_w^{1/5}$. This relation is for “average” granular rocks and may vary considerably in other rock types. Figure 5-83 is a chart [199] that solves Equation 5-101.

When two or more resistivity logs with different depths of investigation are combined, permeable zones can be identified. In a permeable zone, the area closest to the borehole will be flushed of its original fluids; mud filtrate fills the pores. If the mud filtrate has a different resistivity than the original formation fluids (connate water), the shallowest-reading resistivity tool will have a different value than the deepest-reading tool (Figure 5-84). Many times this difference is significant. The separation of the resistivity curves that result is diagnostic of permeable zones.

Care should be taken not to overlook zones in which curves do not separate. Curve separation may not occur if:

1. The mud filtrate and original formation fluids (i.e., connate water and hydrocarbons) have the same resistivity; both shallow and deep tools will read the same value. This is usually not a problem in oil or gas-saturated rocks.
2. Invasion of mud filtrate is very deep, both shallow and deep tools may read invaded-zone resistivity. This occurs when a long period of time elapses between drilling and logging or in a mud system with uncontrolled water loss.

Microresistivity Tools. Microresistivity tools are used to measure the resistivity of the flushed zone. This measurement is necessary to calculate flushed zone saturation and correct deep-reading resistivity tools for invasion. Microresistivity tools are pad devices on hydraulically operated arms. The microlog and proximity log are the two main fresh-mud microresistivity tools, while the micro SFL and microlaterolog are the two main salt-mud microresistivity tools.

Figure 5-85 [58,200,205] shows the electrode pads and current paths for the Microlog (5-85a), Micro SFL (5-85b), and proximity log (5-85c), and Micro-laterolog. Figure 5-85d shows the Micro SFL sonde.

Theory. The microlog makes two shallow nonfocused resistivity measurements, each at different depths. The two measurements are presented simultaneously on the log as the micronormal and microinverse curves. Positive separation (micronormal reading higher than the microinverse) indicates permeability. R_{xo} values can be found by using Figure 5-86 [199]. To enter Figure 5-86, R_{mc} must be corrected to formation temperature, and mudcake thickness (h_{mc}) must be found. To find h_{mc} subtract the caliper reading (presented in track 1) from the borehole size and divide by two. In washed out or enlarged boreholes, h_{mc} must

(text continued on page 155)

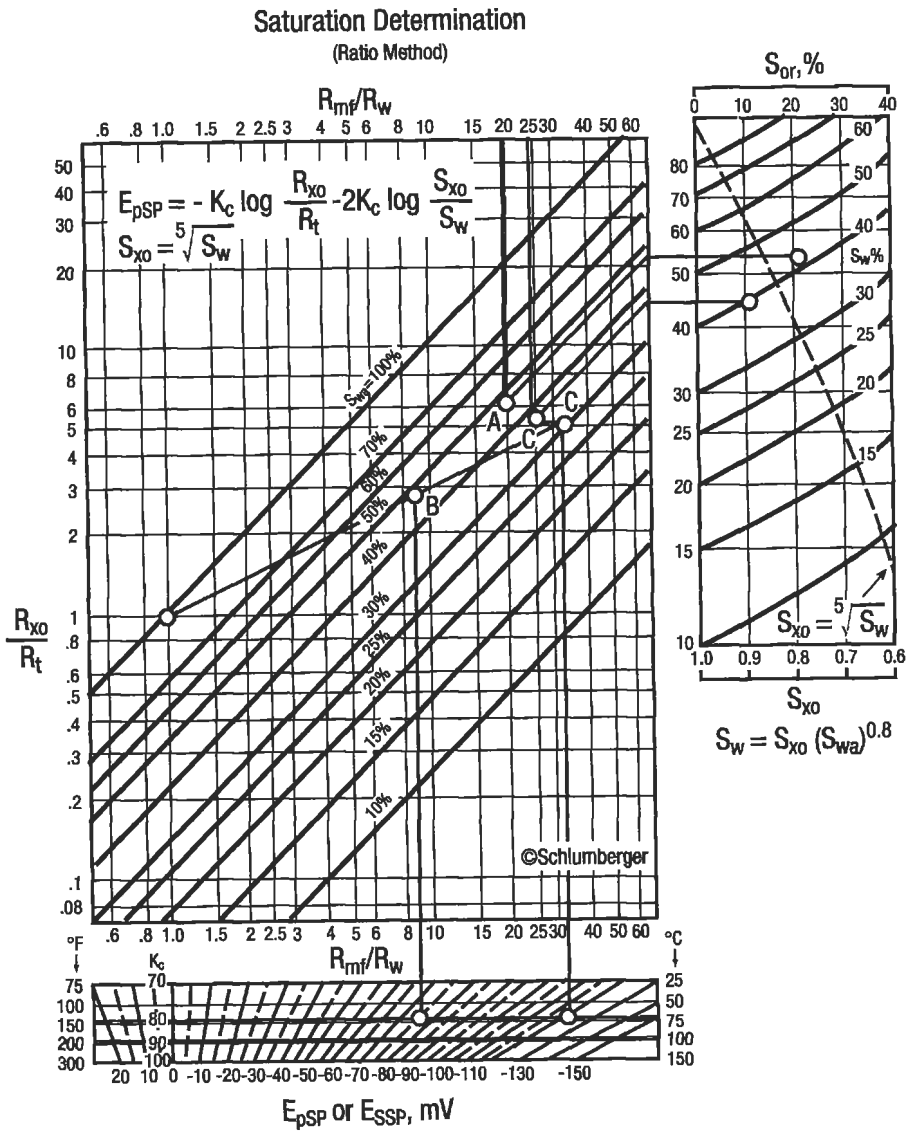


Figure 5-83. Chart for determining water saturation by the ratio method [199].

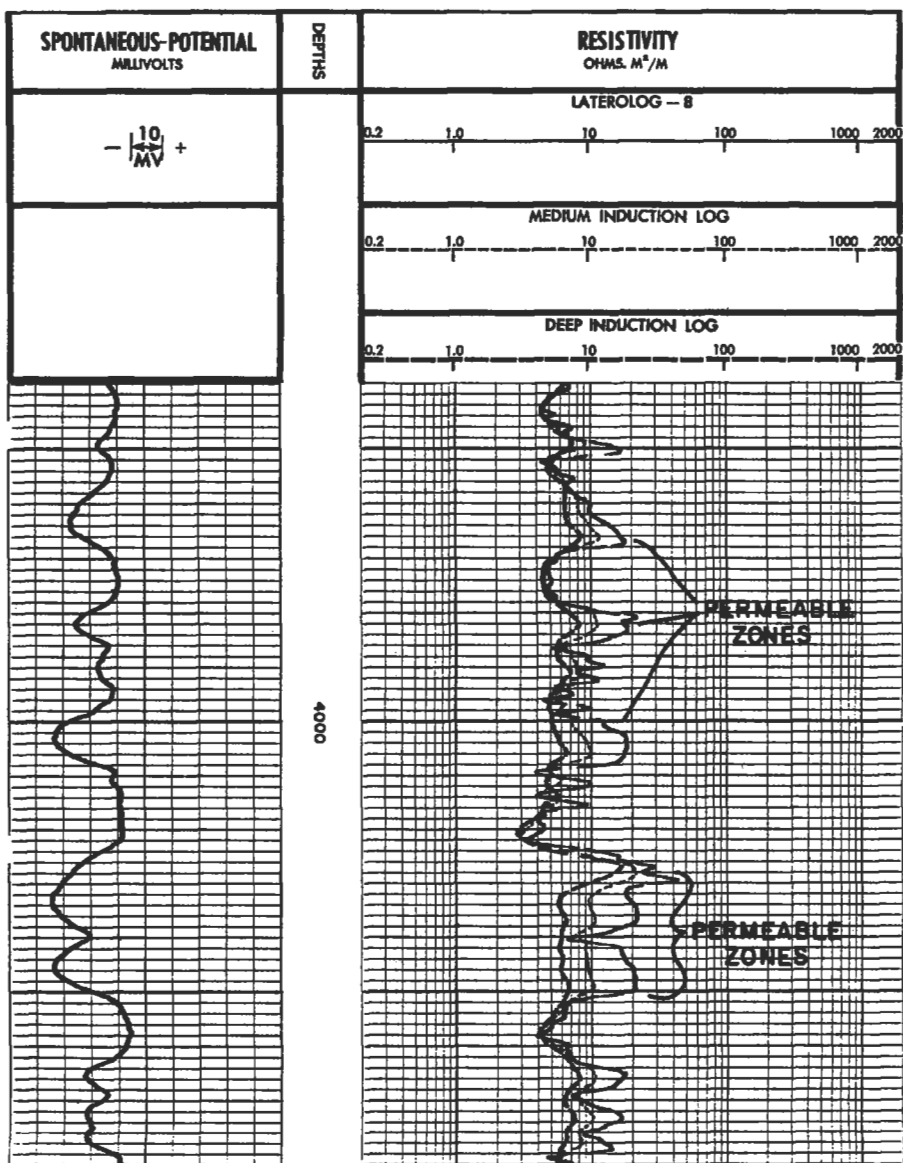


Figure 5-84. Example of resistivity log curve separation as an indication of permeability.

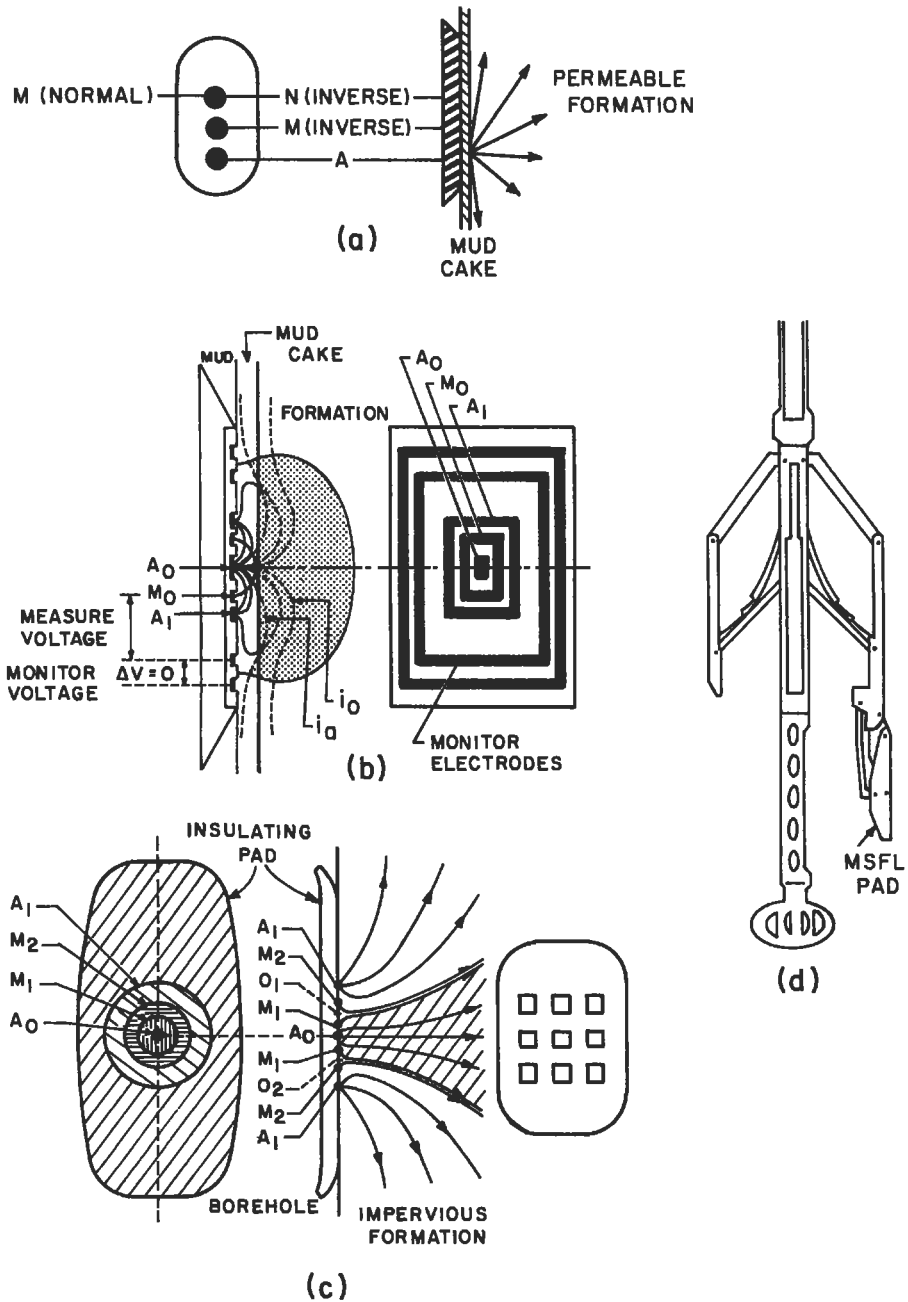


Figure 5-85. Electrode arrangements for various microresistivity devices:(a) microlog; (b) microspherically focused log; (c) microlaterolog; (d) location of the micro pad on the dual laterolog sonde [58,200,205].

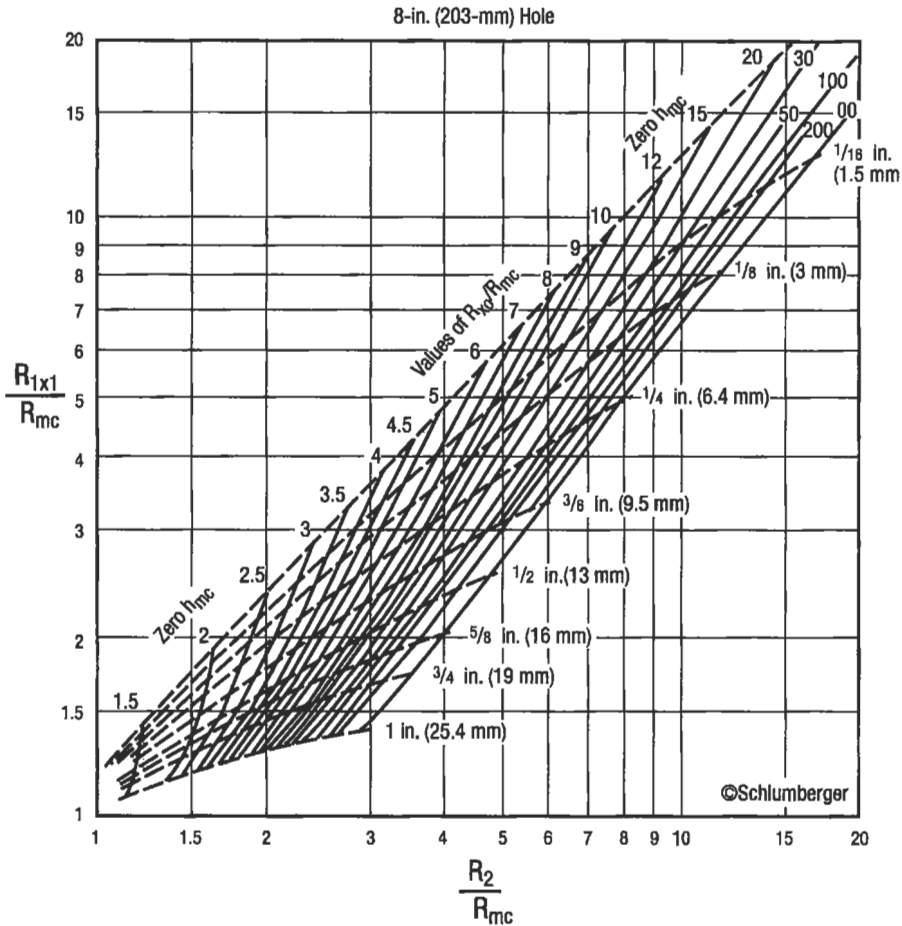


Figure 5-86. Chart for finding R_{xo} from microlog readings [199].

(text continued from page 151)

be estimated. The microlog gives a reasonable value of R_{xo} when mudcake thickness is known. The main disadvantage of this tool is that it cannot be combined with an R_t device, thus a separate logging run is required. The microlog is primarily a fresh mud device and does not work very well in salt-based muds [206]. Generally the mudcake is not thick enough in salt-based muds to give a positive separation opposite permeable zones. The backup arm on the microlog tool, which provides a caliper reading, is also equipped with either a proximity log or a Microlaterolog. The proximity log is designed for fresh muds where thick mudcakes develop opposite permeable formations. There is essentially no correction necessary for mudcakes less than $3/4$ in. If invasion is shallow, the R_{xo} measurement may be affected by R_t because the proximity log reads deeper into the formation than the other microresistivity logs. When the

microlog is run with a proximity log, it is presented in track 1 with a micro-caliper. The proximity log is presented in tracks 2 and 3 on a logarithmic scale (Figure 5-87).

Since its introduction, the microlog (Schlumberger) has become the standard tool for recognizing permeable zones. The theory behind it is similar to using multiple resistivity devices. The tool consists of three electrode buttons on a rubber pad which is pressed against the borehole wall.

In a permeable zone, mud filtrate will enter the formation leaving the clay particles behind on the borehole wall. These clay particles may form a mudcake up to an inch thick. The resistivity of the mudcake is less than the resistivity of the formation saturated with mud filtrate. Two resistivity readings, the micro-inverse and the micronormal, are taken simultaneously. The microinverse has a depth of investigation of only an inch; therefore, it reads mostly mudcake (if

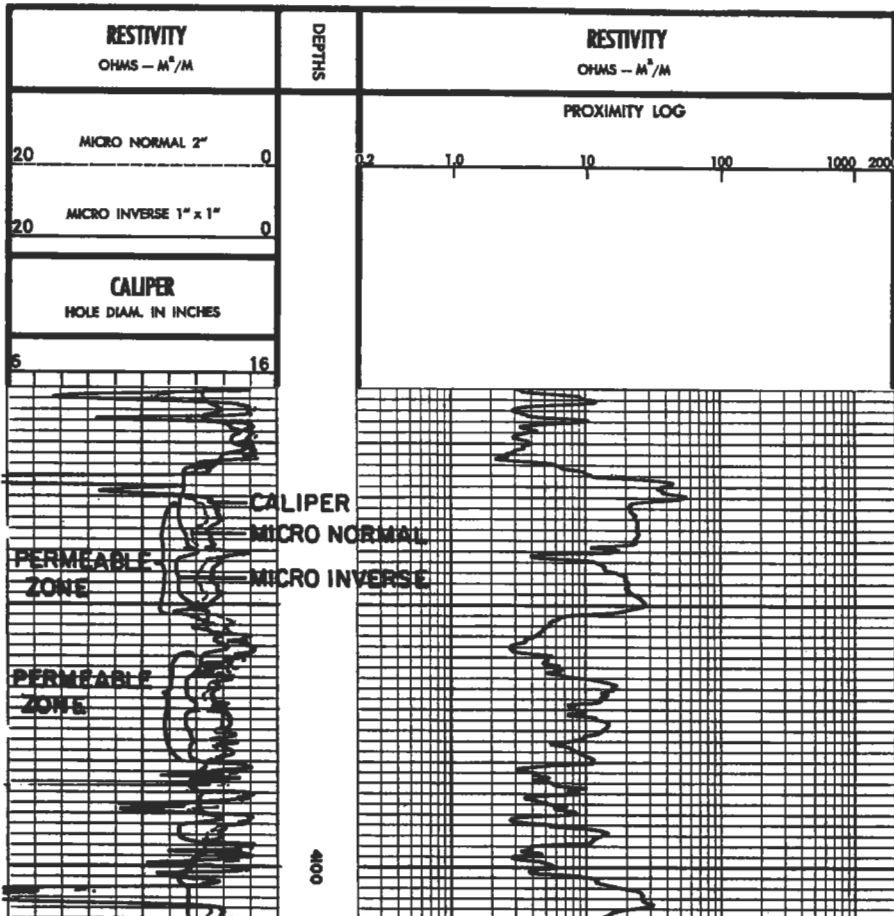


Figure 5-87. Example log showing positive separation of the microlog curves opposite a permeable formation at 4,030 to 4,050 feet.

present). The micronormal has a depth of investigation of 3 to 4 in. and is influenced primarily by fluids in the flushed zone. The difference in resistivity shows up on the log as a separation of the curves with the micronormal reading higher than the microinverse. This is referred to as "positive separation." In impermeable formations, both readings are very high and erratic, and negative separation may occur (micronormal less than microinverse). Shales commonly show negative separation with low resistivities (Figure 5-87).

In salt muds, the microlaterolog and micro spherically focused log (MSFL) are used for R_{xo} readings. The microlaterolog is a focused tool with a shallower depth of investigation than the proximity log. For this reason, the microlaterolog is very strongly affected by mudcakes thicker than $\frac{3}{8}$ in. It is presented in tracks 2 and 3 like the proximity log. The MSFL is the most common R_{xo} tool for salt muds. It is a focused resistivity device that can be combined with the dual laterolog, thus providing three simultaneous resistivity readings. Although the depth of investigation is only a few inches, the tool can tolerate reasonably thick mudcakes ($\frac{3}{4}$ in.). The tool is also available in a slim-hole version. The only disadvantage to this device is that the pad can be easily damaged in rough boreholes.

Interpretation. The saturation of the flushed zone can be found from Equation 5-99. R_{mf} must be at formation temperature. Moveable hydrocarbons can be found by comparing S_{xo} and S_w . If $S_w/S_{xo} < 0.7$ then the hydrocarbons in the formation are moveable (this is also related to fluid permeability). If $S_w/S_{xo} > 0.7$, either there are no hydrocarbons or the hydrocarbons present are not moveable.

Gamma Ray Logs. The gamma ray log came into commercial use in the late 1940s. It was designed to replace the SP in salt muds and in air-filled holes where the SP does not work. The gamma ray tool measures the amount of naturally occurring radioactivity in the formation. In general, shales tend to have high radioactivity while sandstone, limestone, dolomite, salt, and anhydrite have low radioactivity. There are exceptions. Recently, tools have been designed to separate gamma rays into their respective elemental sources, potassium (K), thorium (Th), and uranium (U).

Theory. Gamma rays are high-energy electromagnetic waves produced by the decay of radioactive isotopes such as $K40$, Th, and U. The rays pass from the formation and enter the borehole. A gamma ray detector (either scintillation detector or Geiger-Muller tube) registers incoming gamma rays as an electronic pulse. The pulses are sent to the uphole computer where they are counted and timed. The log, presented in track 1 in Figure 5-74, is in API units.

As previously mentioned, there are new gamma ray tools available that determine which elements are responsible for the radioactivity. The incoming gamma rays are separated by energy levels using special energy-sensitive detectors. The data are collected by the computer and analyzed statistically. The log presents total (combined) gamma ray in track 1 and potassium (in %), and uranium and thorium (in ppm) in tracks 2 and 3 (Figure 5-88). Combinations of two components are commonly presented in track 1. The depth of investigation of the natural gamma tools is 2-10 in. depending on mud weight, formation density, hole size, and gamma ray energies.

Interpretation. The interpretation of a total gamma ray curve is based on the assumption that shales have abundant potassium-40 in their composition. The open lattice structure and weak bonds in clays encourage incorporation of impurities. The most common of those impurities are heavy elements such as

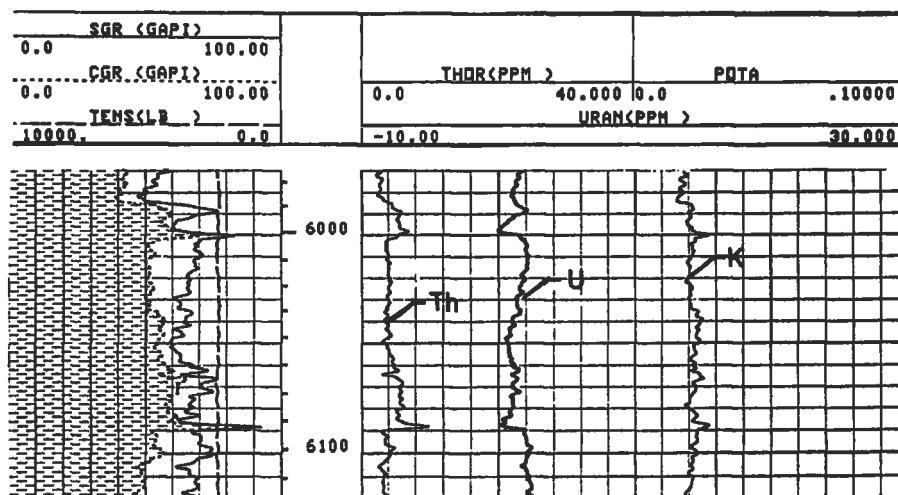


Figure 5-88. Example of a natural gamma spectroscopy log presentation.

uranium and thorium. Thus, shales typically have high radioactivity. Sandstones (quartzose), carbonates and evaporites have strong bonds and generally do not allow impurities. Limestones undergo rearrangement of crystal structure and addition of magnesium to become dolomites. Impurities like uranium (which is very soluble) may enter the crystal lattice during recrystallization. Feldspathic sandstones contain an abundance of potassium-40 and therefore show higher radioactivity than quartzose sandstone. Some evaporite minerals (such as KCl) contain high amounts of potassium-40 and may appear as shales on the log. Serra et al. [207] provide an excellent discussion of interpretation of the natural or spectral gamma-ray tool.

Sonic (Acoustic) Log. The sonic (acoustic or velocity) tool measures the time it takes for a compressional wave to travel through one vertical foot of formation. It can be used to determine porosity (if the lithology is known) and to determine seismic velocities for geophysical surveys when combined with a density log. The sonic log also has numerous cased hole applications.

Theory. A 20 khz sound wave is produced by the tool and travels through the mud into the formation. The wave travels vertically through the formation. The first arrival of the compressional wave is picked up by a receiver about one foot away from the transmitter. The wave continues through the formation and is picked up by the far receiver (normally 2-ft below the near receiver). The time difference between the near and far receivers is used to determine formation travel time (Δt). Fractures, vugs, unconsolidated formations, gas-cut mud, lost circulation materials, and rough boreholes can cause sharp increases in Δt , called cycle skips.

Interpretation. Table 5-26 shows the velocity and travel time for several commonly encountered oilfield materials. The t_{ma} value in the fourth column is at 0%

Table 5-26
Matrix Travel Times

Material	Velocity range ft/sec	Δt range μ sec/ft	Δt commonly used μ sec/ft	Δt at 10% porosity μ sec/ft
Sandstone	18,000–19,500	51.0–55.5	55.0 or 51.0	69.0 or 65.0
Limestone	21,000–23,000	43.5–47.6	47.5	61.8
Dolomite	23,000–24,000	41.0–43.5	43.5	58.0
Salt	15,000	66.7	66.7	—
Anhydrite	20,000	50.0	50.0	—
Shale	7,000–17,000	58.0–142	—	—
Water	5,300	176–200	189	—
Steel casing	17,500	57.0	57.0	—

From References 200 and 215.

porosity Porosity increases travel time. Wyllie and coworkers [208] developed an equation that relates sonic travel time to porosity:

$$\phi = \frac{\Delta t_{\log} - \Delta t_{ma}}{\Delta t_f - \Delta t_{ma}} \quad (5-102)$$

where Δt_{\log} = Δt value read from log, μ sec/ft
 Δt_{ma} = matrix velocity at 0% porosity, μ sec/ft
 Δt_f = 189–190 μ sec/ft (or by experiment)

The Wyllie equation works well in consolidated formations with regular intergranular porosity ranging from 5%–20% [209]. If the sand is not consolidated or compacted, the travel time will be too long, and a compaction correction factor (C_p) must be introduced [208]. The reciprocal of C_p is multiplied by the porosity from the Wyllie equation:

$$\phi = \left(\frac{\Delta t_{\log} - \Delta t_{ma}}{t_f - t_{ma}} \right) \left(\frac{1}{C_p} \right) \quad (5-103)$$

The compaction correction factor (C_p) can be found by dividing the sonic porosity by the true (known) porosity. It can also be found by dividing the travel time in an adjacent shale by 100:

$$C_p = \frac{\Delta t_{shale}}{100} C \quad (5-104)$$

where C is a correction factor, usually 1.0 [200]. In uncompacted sands, porosities may be too high even after correction if the pores are filled with oil or gas. Hilchie [200] suggests that if pores are oil-filled, multiply the corrected porosity by 0.9; if gas-filled, use 0.7 to find corrected porosity.

Raymer, Hunt, and Gardner [210] presented an improved travel-time to porosity transform that has been adopted by some logging companies. It is based

on field observations of porosity versus travel time:

$$\Delta t_{\log} = (1 - \phi)^2 \Delta t_{ma} + \phi \Delta t_f \tag{5-105}$$

This relationship is valid up to 37% porosity.

The heavy set of lines in Figure 5-89 [199] was derived using the Raymer et al. [210] transform, and the lighter set represents the Wyllie relationship.

The sonic porosity derived from the Wyllie equation (Equation 5-102) does not include secondary porosity (vugs and fractures), so it must be cautiously applied in carbonate rocks.

Density Log. The formation density tool measures the bulk electron density of the formation and relates it to porosity. It is a pad device with a caliper arm. The tool is usually run in combination with a neutron log, but it can be run alone.

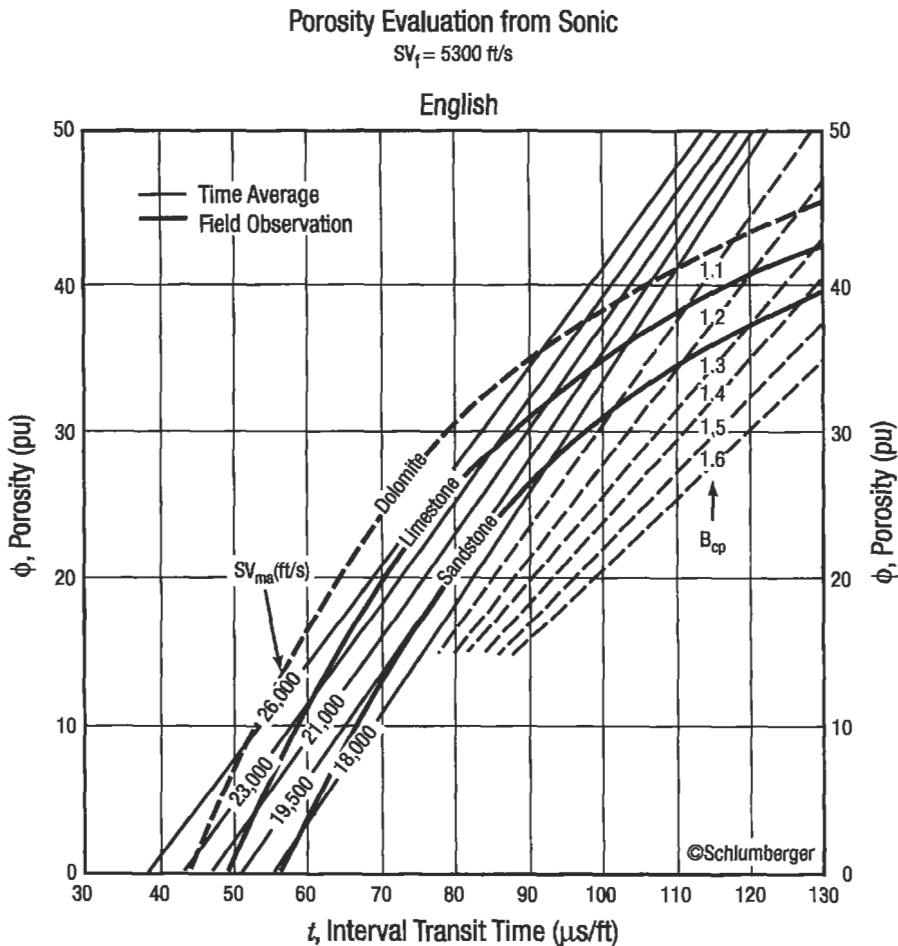


Figure 5-89. Chart for evaluating porosity with a sonic log [199].

Theory. The density tool emits medium energy gamma rays from a radioactive chemical source (usually Cs-137). The gamma rays penetrate the formation and collide with electron clouds in the minerals in the rock. With each collision the gamma ray loses some energy until it reaches a lower energy state. This phenomenon is called "Compton scattering." Some gamma rays are absorbed, and a high-energy electron is emitted from the atom. This phenomenon is called the "photoelectric absorption" effect, and is a function of the average atomic weight of each element. Both the Compton-scattered gamma ray and the photoelectrically produced electron return to the borehole where they are detected by scintillation tubes on the density tool. The main result is that a porous formation will have many returning gamma rays while a nonporous formation will have few returning gamma rays. Each tool has two detectors; one is near the source (short-spacing detector) and another is 1-1.5 ft (35-40 cm) away from the near detector (long-spacing detector).

The long-spacing detector provides the basic value of bulk electron density. The short-spacing detector is used to make a mudcake correction. This correction, made automatically by computer by most service companies, is based on the 'spine and ribs' plot (Figure 5-90) [211]. The "spine" is the heavy, nearly

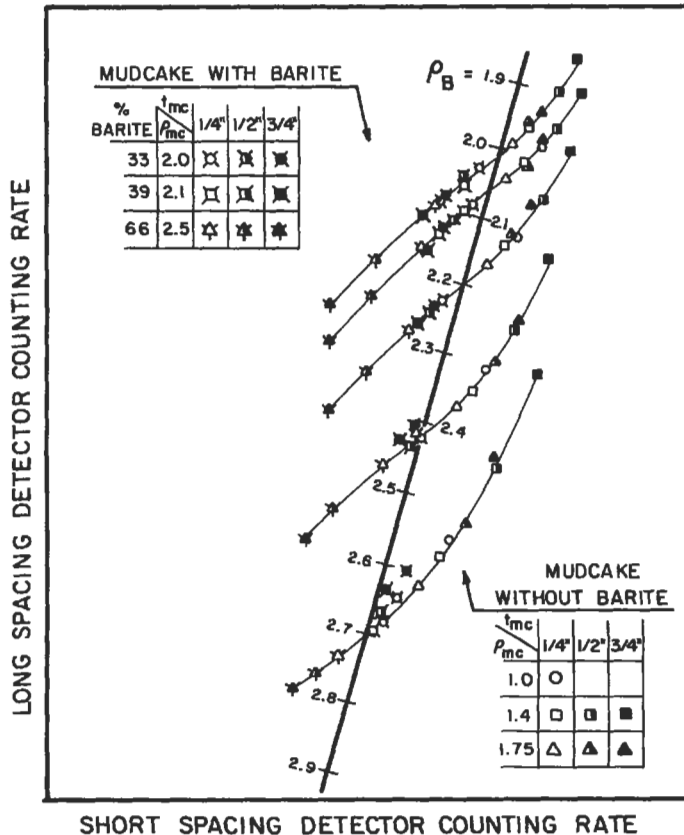


Figure 5-90. Spine and ribs plot used to correct bulk density readings for mudcake effects [58].

vertical line from 1.9 to 2.9 g/cc. The ribs are the lighter curved lines trending left to right. The experimental data for constructing the "ribs" are shown in the corners of the plot. Long-spacing count-rates are on the abscissa and short-spacing count-rates are on the ordinate axis. The computer receives data from the sonde and plots it on the chart. If the point falls off the "spine," it is brought back along one of the ribs. Bringing the point back along the "rib" will change the intersection point on the 'spine.' The correction that is produced is called $\Delta\rho$ and may be either positive or negative depending on the mud properties. Negative $\Delta\rho$ values occur in heavy (barite or iron), weighted muds. Positive values occur in light muds and when the density pad is not flush against the borehole wall (as occurs in rough or "rugose" boreholes. The $\Delta\rho$ curve is useful for evaluating the quality of the ρ_b reading. Excursions from 0 that are more than ± 0.20 gm/cc on the $\Delta\rho$ curve indicate a poor quality reading.

Interpretation. An equation similar to the Wyllie equation is used to calculate porosity values from bulk density.

$$\phi = \frac{\rho_{ma} - \rho_b}{\rho_{ma} - \rho_f} \quad (5-106)$$

where ρ_{ma} = bulk density of matrix at 0% porosity, g/cc
 ρ_b = bulk density from log, g/cc
 ρ_f = bulk density of fluid, g/cc

Table 5-27 lists commonly used values for ρ_{ma} and ρ_f and, along with Figure 5-91 shows how ρ_f changes with temperature and pressure [58]. As with the sonic tool, an incorrect choice of matrix composition may give negative porosity values.

If a zone is hydrocarbon saturated but not invaded by mud filtrates, the low density of the hydrocarbons will increase the porosity reading to a value that is too high. In this case, Hilchie [200] suggests using the following equation:

$$\phi = \frac{0.9 \left(\frac{R_w}{R_t} \right)^{1/2} (\rho_w - \rho_h) + \rho_{ma} - \rho_b}{\rho_{ma} - \rho_h} \quad (5-107)$$

where ρ_w = density of formation water, g/cc (estimated from Figure 5-91) [58]
 ρ_h = density of hydrocarbons, g/cc (from Figure 5-92) [199]

Neutron Log. Neutron tools measure the amount of hydrogen in the formation and relate it to porosity. High hydrogen content indicates water (H_2O) or liquid hydrocarbons (C_xH_y) in the pore space. Except for shale, sedimentary rocks do not contain hydrogen in their compositions.

Theory. Neutrons are electrically neutral particles with mass approximately equal to that of a hydrogen atom. High-energy neutrons are emitted from a chemical source (usually AmBe or PuBe). The neutrons collide with nuclei of the formation minerals in elastic-type collisions. Neutrons will lose the most energy when they hit something with equal mass, such as a hydrogen atom. A few microseconds after being released, the neutrons have lost significant energy and enter

Table 5-27
Bulk Densities Commonly Used for Evaluating
Porosity With a Density Log*

Material	ρ_{bulk}	ρ_{log} at 10% porosity (fresh water)
Unconsolidated sand	2.65 g/cc	2.48 g/cc
Silica cemented sand	2.65 g/cc	2.48 g/cc
Calcite cemented sand	2.68 g/cc	2.51 g/cc
Limestone	2.71 g/cc	2.54 g/cc
Dolomite	2.83–2.87 g/cc	2.64–2.68 g/cc
Salt	2.03 g/cc	—
Anhydrite	2.98 g/cc	—
Fresh water	1.0 g/cc	—
Salt water	1.1–1.2 g/cc	—

Fluid Densities for Water (Based on Salinity)**	
Salinity, ppm NaCl	ρ_f , g/cc
0–50,000	1.0
50,000–100,000	1.03
100,000–150,000	1.07
150,000–200,000	1.11
200,000–250,000	1.15
250,000–300,000	1.19

* From Reference 215.

** From Reference 200.

the thermal state. When in the thermal state, neutrons are captured by the nuclei of other atoms (Cl, H, B). The atom which captures the neutron becomes very excited and emits a gamma ray. The detectors on the tool may detect epithermal neutrons, thermal neutrons or high-energy gamma rays of capture. Compensated neutron tools (CNL) detect thermal neutrons and use a ratio of near-to-far detector counts to determine porosity. Sidewall neutron tools (SNP) detect epithermal neutrons and have less matrix effect (though they are affected by rough boreholes more than the CNL).

Interpretation. Neutron tools are seldom run alone. They are usually combined with a density-porosity tool. Older neutron logs are not presented as porosity but as count rates. Some logs do not specify a scale (Figure 5-93), but only which direction the count rate (or radiation) increases. An increase in radiation indicates lower porosity (less hydrogen). Newer logs present porosity (for a particular matrix, limestone, sandstone or dolomite) directly on the log. Most neutron logs are run on limestone matrix. Figure 5-94 corrects the porosity for matrix effect if the log is run on limestone matrix [199]. Neutron logs exhibit "excavation effect" in gas-filled formations. The apparent decrease in porosity is due to the spreading out of hydrogen in gas molecules; gases have less hydrogen *per unit volume* than liquids. Thus the neutron tool sees less hydrogen and assumes less porosity. The magnitude of the effect depends on gas saturation, gas density, and pressure. Care should be taken in using correction charts for neutron tools; each service company has a slightly different design, and the correct chart for the particular tool and service company should be used.

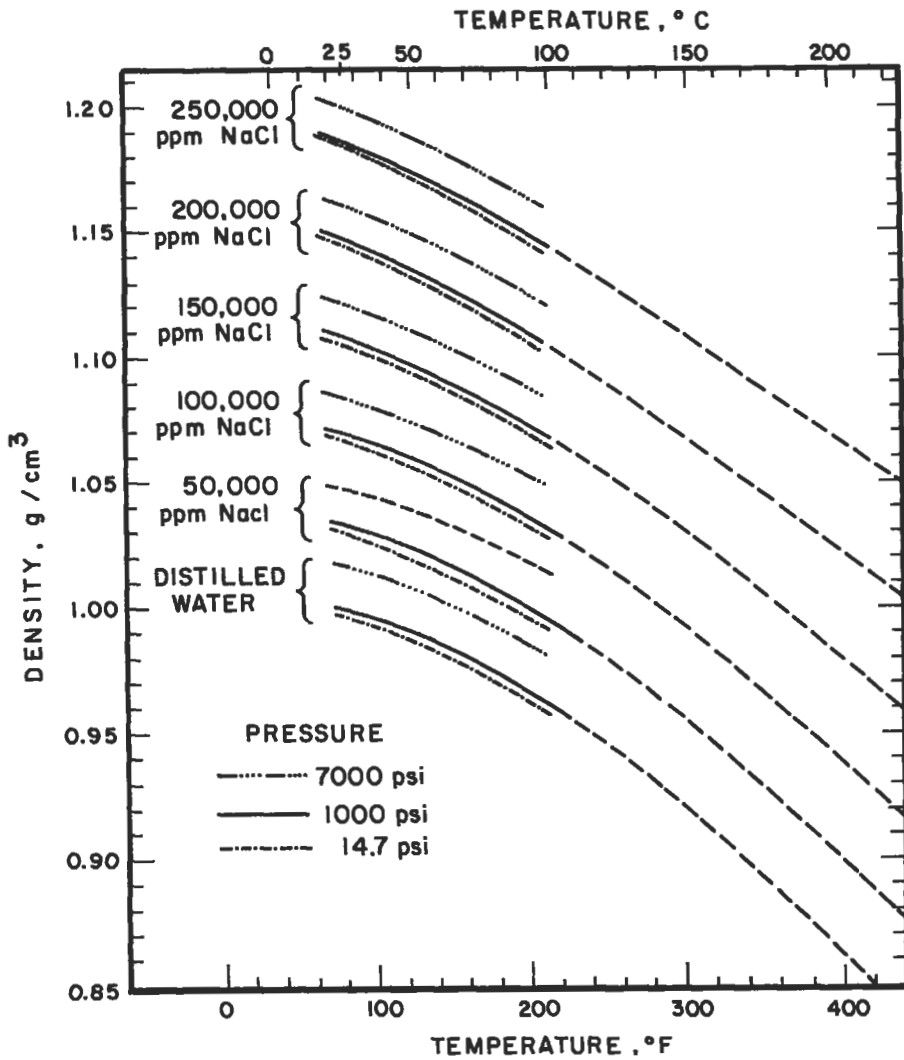


Figure 5-91. Chart showing relationship of water salinity to density and temperature [58].

Multiple-Porosity Log Interpretation. As mentioned earlier, the neutron, density, and sonic tools are lithology dependent. If the matrix is incorrectly selected, porosity may be off as much as 10 porosity units. If two lithology-dependent logs are run simultaneously on the same matrix and presented together, lithology and porosity can be determined. The most common and useful of combinations is the neutron and density. Figures 5-95 through 5-99 are crossplots of neutron, density, and sonic porosity [199]. The charts are entered with the appropriate values on the ordinate and abscissa. The point defines porosity and gives an indication of matrix. If a point falls between two

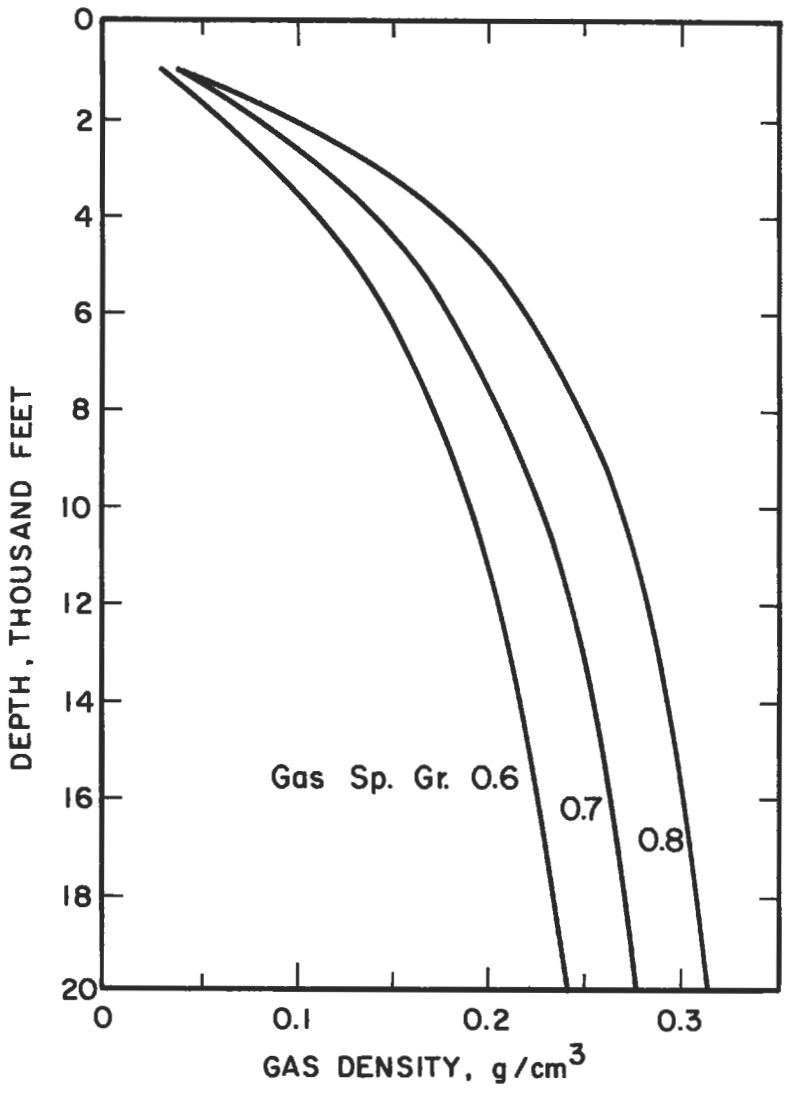


Figure 5-92. Chart for estimating density of gases from reservoir depth and gas specific gravity [200].

matrix lines, it is a combination of the two minerals or the neutron-density crossplots. Gas moves the points up and to the left. To correct for the gas effect, move parallel to the gas correction arrow to the assumed lithology. Note that a gassy limestone may look like a sandstone. Shales tend to bring points down and to the right depending on the shale composition. Typically, shaly sandstone will look like a limestone. The sonic-density crossplot is not very helpful in determining porosity or lithology but is extremely useful for determining evaporite mineralogy.

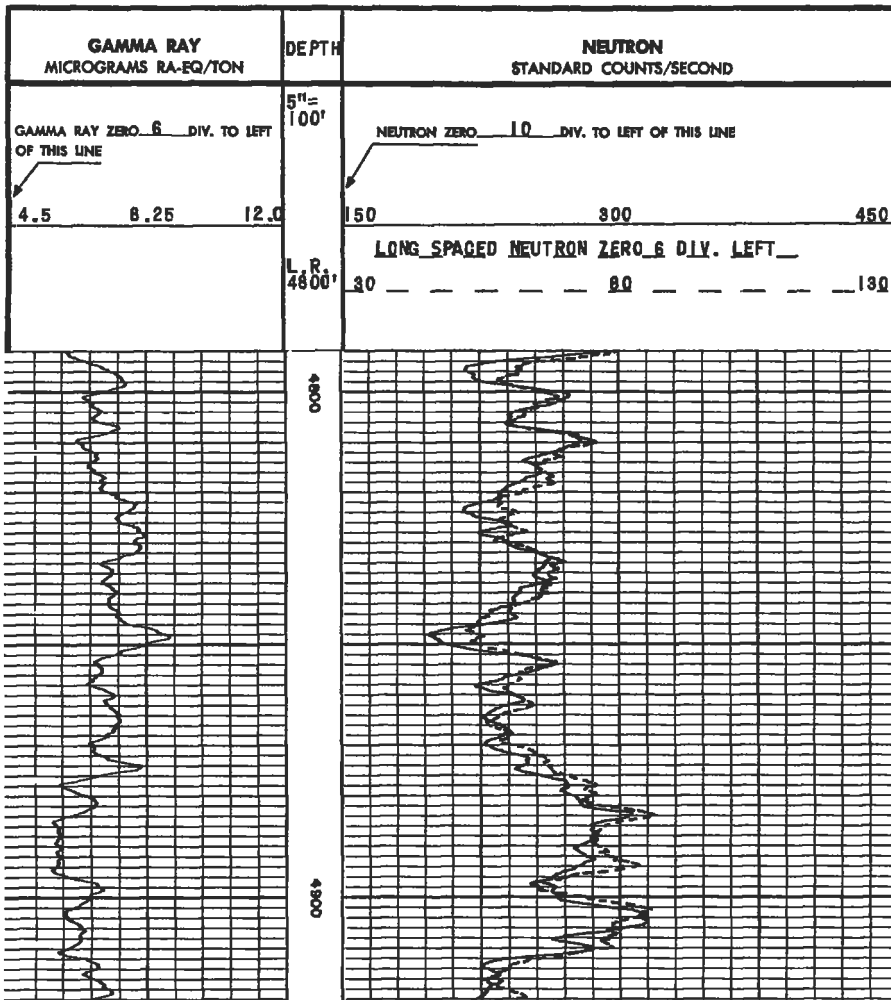


Figure 5-93. Old neutron log presentation.

In some areas, neutron and density tools are run on sandstone porosity and therefore cannot be entered in the charts directly. To use the neutron-density crossplots when the matrix is not limestone, another method must be applied. Remember that the vertical lines are constant neutron-porosity and the horizontal lines are constant density-porosity. Instead of entering the bottom or sides of the chart, select the appropriate lithology line in the interior of the chart. Draw a horizontal line through the density-porosity and a vertical line through the neutron-porosity. Lithology and porosity are determined at the intersection of these two lines.

Another device that provides good lithology and matrix control is the Litho-density tool (LDT). It combines a density tool with improved detectors and a P_{ef} curve (photoelectric effect). Combining the P_b and P_{ef} curve values, an

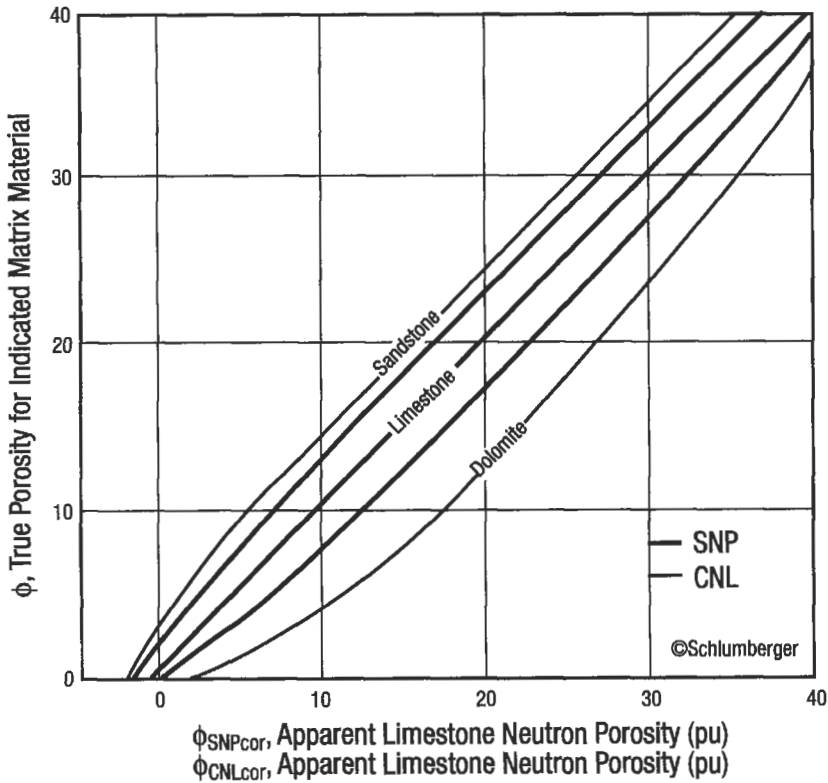


Figure 5-94. Matrix lithology correction chart for neutron porosity logs [199].

accurate 3- or 4-mineral composition can be determined from the charts in Figures 5-100 to 5-103 [199]. This also provides an excellent way to confirm neutron-density cross-plot interpretations.

Nuclear Magnetic Resonance (NMR). This log examines the nucleus of certain atoms in the formation. Of particular interest are hydrogen nuclei (protons) since these particles behave like magnets rotating around each other [212]. Hydrogen is examined because it occurs in both water and hydrocarbons.

The log measures fluid by applying a magnetic field, greater in intensity than the earth field, to the formation. Hydrogen protons align themselves with the induced field and when the field is suddenly removed, the protons precess about the earth's magnetic field much like a gyroscope. The nucleus of hydrogen has a characteristic precession rate called the Larmor frequency (~2,100 Hz), and can be identified by sensors on the tool [213]. The nuclei contributing to the total signal occur in the free fluid in the pores; fluid adsorbed on the grains makes no contribution. The signals are then processed in a computer and printed out onto a log.

Normally, proton precession decays along a time constant, T_2 . This is a result of each proton precession falling out of phase with other protons due to

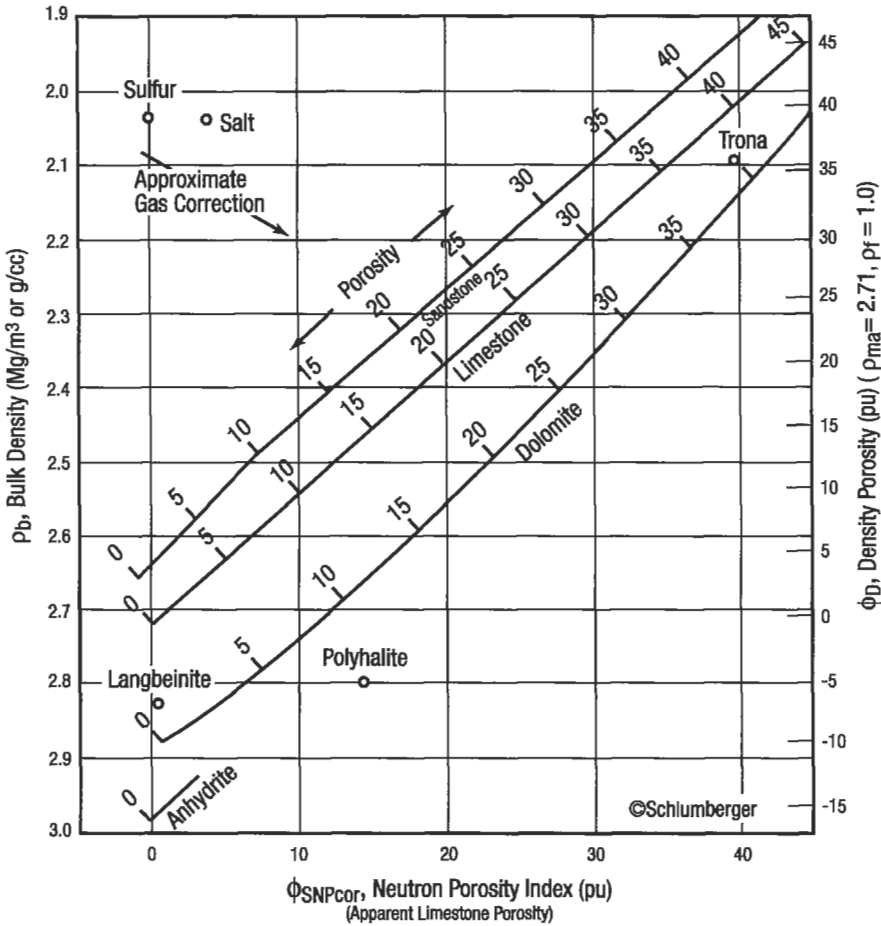


Figure 5-95. Chart for finding porosity and matrix composition from an FDC-SNP log combination in fresh water [199].

differences in the local magnetic fields. Moreover, each proton precesses at a slightly different frequency, depending on the kind of fluid it occurs in. This disharmonic relationship makes it possible to differentiate between free water and free oil in a reservoir [213].

Three log modes can be presented:

1. Normal mode—consists of the free fluid index (FFI) in percent obtained from a polarization time of two seconds, the Larmor proton frequency (LFRE), the decay-time constant (or longitudinal relaxation time) of the signal (T_2) and a signal-to-noise ratio (STNR).
2. Continuous mode—gives three free fluid index (FFI) readings taken at polarization times of 100, 200, and 400 ms, respectively, two longitudinal relaxation times (T_1 and T_2), and a signal-to-noise ratio (STNR).

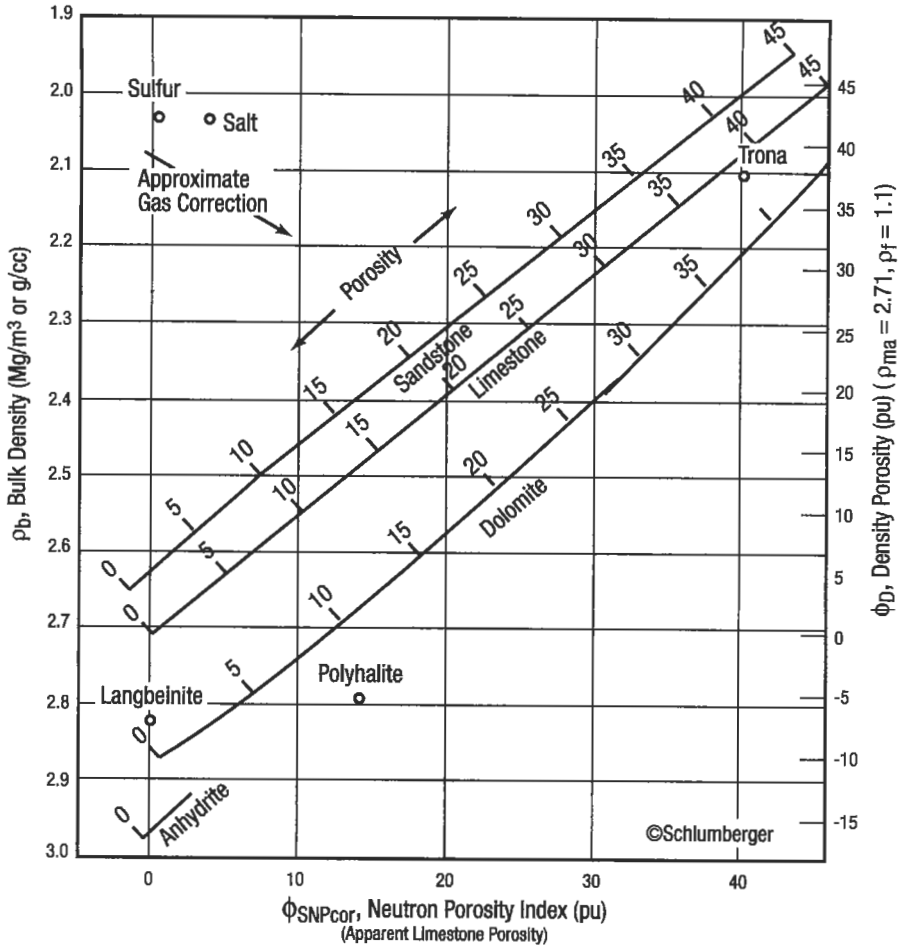


Figure 5-96. Chart for finding porosity and matrix composition from an FDC-SNP log combination in salt water [199].

3. Stationary display mode—a signal-stacking mode where eight signals are stacked from each of six polarization times to obtain precise T_1 , T_2 , and FFI values.

FFI readings yield porosity that is filled with moveable fluid and is related to irreducible water saturation (S_{iw}). Addition of paramagnetic ions to the mud filtrate will disrupt the water portion of the signal and residual oil saturation (S_{or}) can be determined.

Desbrandes [212] summarized the following uses for the NML:

1. Measuring free fluid volume in the pores (ϕ_f)
2. Evaluating permeability by comparing ϕ_f with ϕ_T (total porosity from a neutron-density log combination).

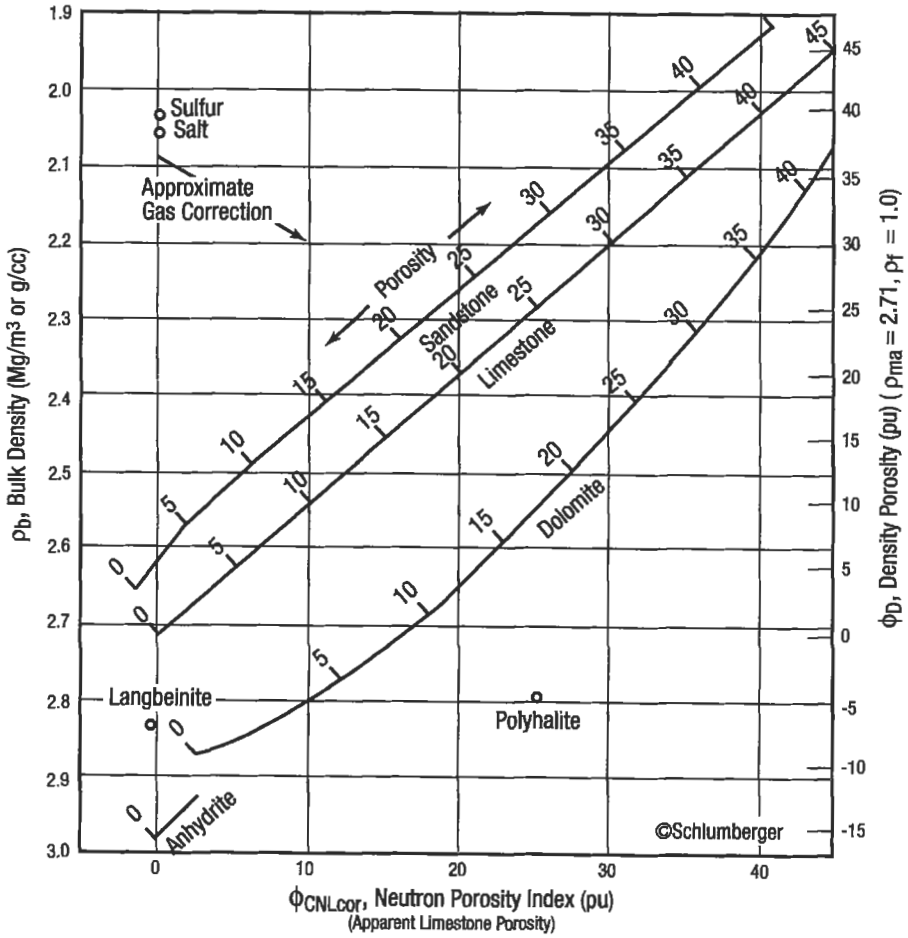


Figure 5-97. Chart for finding porosity and matrix composition from a FDC-CNL log combination in fresh water [199].

3. Locating intervals at irreducible water saturation by comparing ϕ_r with ϕ_T and R_v determined with other logs.
4. Determining residual oil saturation by adding paramagnetic ions to the mud filtrate to cancel the water signal and leave the oil signal.

Dielectric Measurement Tools. Dielectric measurement tools examine the formation with high frequency electromagnetic waves (microwaves) rather than high-frequency sound waves (as in the sonic or acoustic logging tools). The way the electromagnetic wave passes through a given formation depends on the dielectric constants (ϵ) of the minerals and fluids contained in the rock.

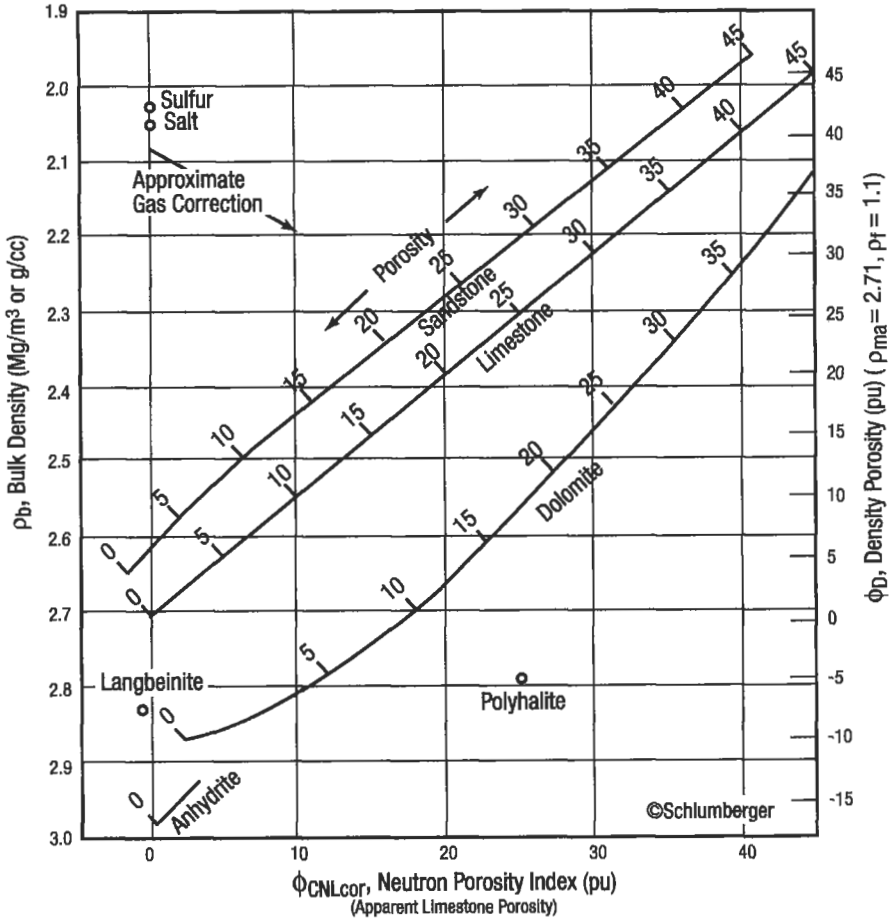


Figure 5-98. Chart for finding porosity and matrix composition from a FDC-CNL log combination in salt water [199].

Two types of tools are available [212]:

1. VHF sondes that have frequencies of 20–47 Mhz (found in the deep propagation tool [Schlumberger], and dielectric tools [Dresser-Atlas and Gearhart-Owen], and
2. UHF sondes that have a frequency of 1.1 GHz (found in the electromagnetic propagation tool [Schlumberger]).

The only tool that is currently available is Schlumberger’s electromagnetic propagation tool (EPT); the others are still experimental [212].

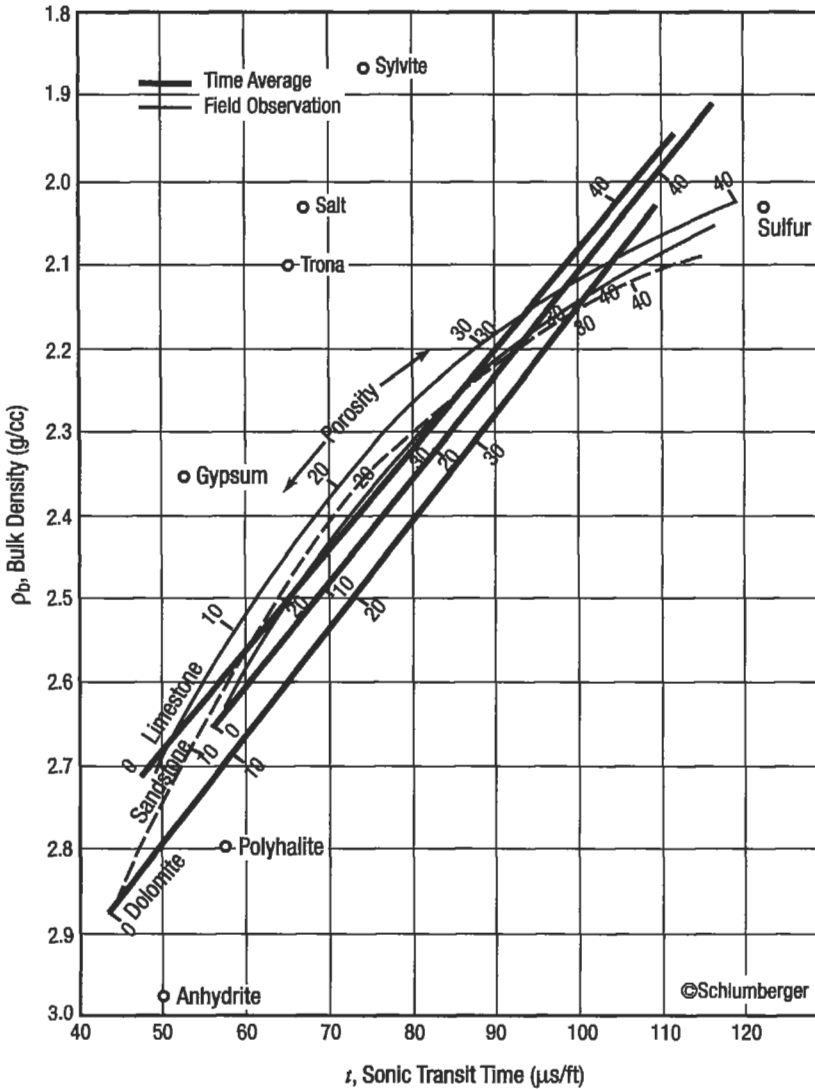


Figure 5-99. Lithology estimation chart for the FDC-sonic log combination in fresh water [199].

Theory. The EPT is a sidewall tool that measures the dielectric properties of a formation by passing spherically propagated microwaves into the rock. The tool consists of 2 transmitters (T_1 , and T_2) and 2 receivers (R_1 , and R_2) mounted in an antenna pad assembly. Its basic configuration is that of a borehole compensation array (much like the borehole compensated sonic (BHC) log). The transmitter fires a 1.1 GHz electromagnetic wave into the rock around the wellbore. As the wave passes through the rock and fluid there, it is attenuated, and

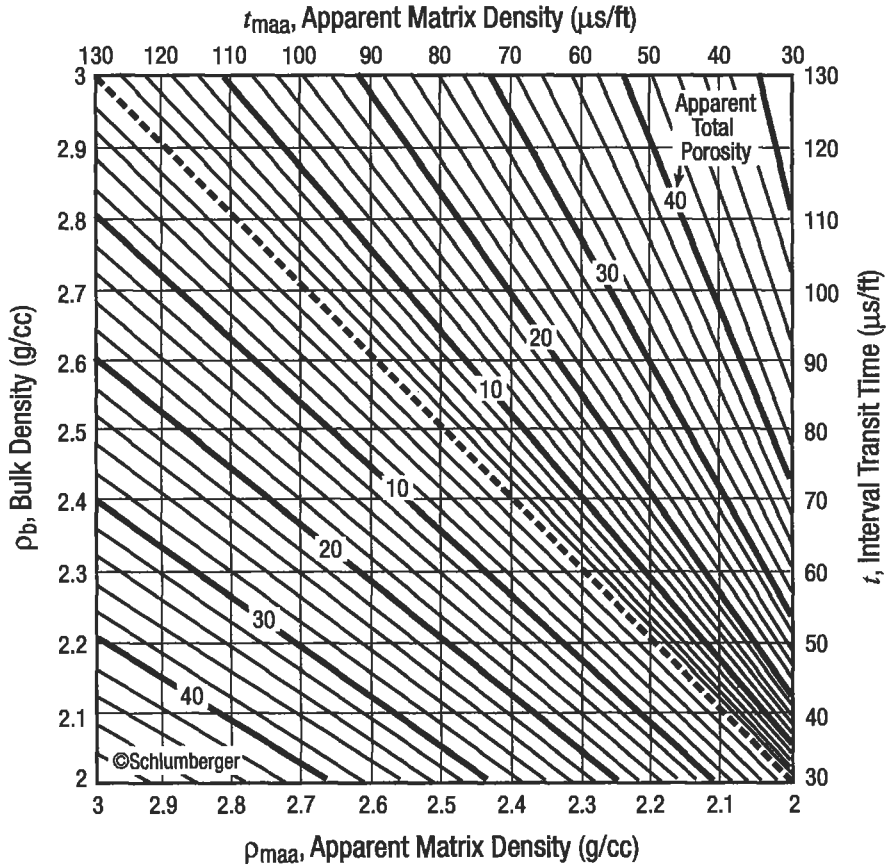


Figure 5-100. Chart for finding apparent matrix density or apparent matrix transit time from bulk density or interval transit time and apparent total porosity [199].

its propagation velocity is reduced. The wave then refracts to the borehole where it is sequentially detected by the two receivers. How much the wave is attenuated is a function of the dielectric permittivity of the formation. Rocks and oil have similar permittivities while water has a very different permittivity. Therefore, the wave responds to the water-filled porosity in the formation, and the response is a function of formation temperature.

Since the wave is attenuated by water (and is not too bothered by oil), the log response indicates either R_{wg} (in water-based mud systems) or bulk volume water (in oil-based mud systems).

In order to provide usable values, the velocity of the returning wave is measured and compared to the wave-propagation velocity in free space. The propagation velocity of the formation is then converted into propagation time (T_{pl}). A typical log presentation includes a T_{pl} curve (in nanoseconds/meter), an attenuation curve (EATT) in decibels/meter, and a small-arm caliper curve (which measures borehole rugosity) recorded in tracks 2 and 3. Figure 5-104

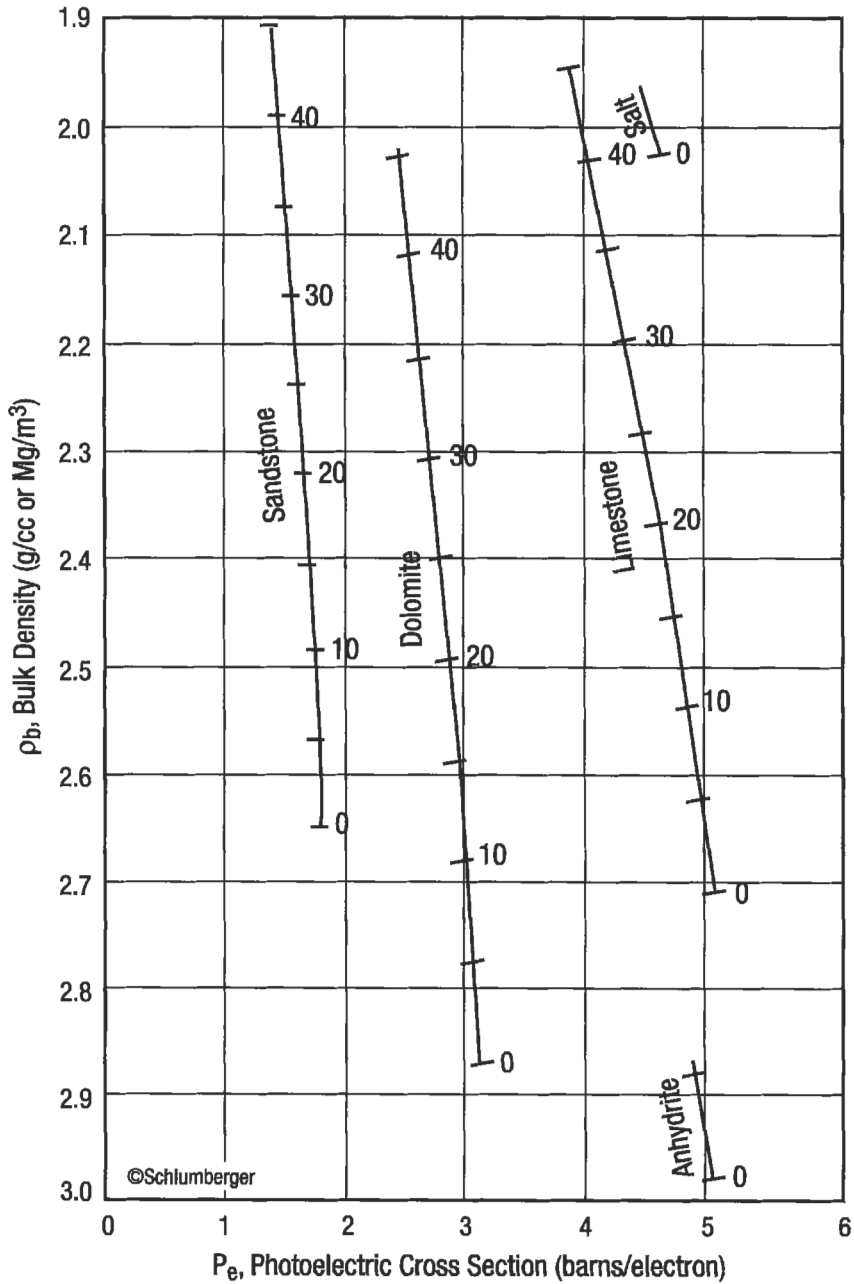


Figure 5-101. Chart for finding porosity and matrix composition from a litho-density log in fresh water [199].

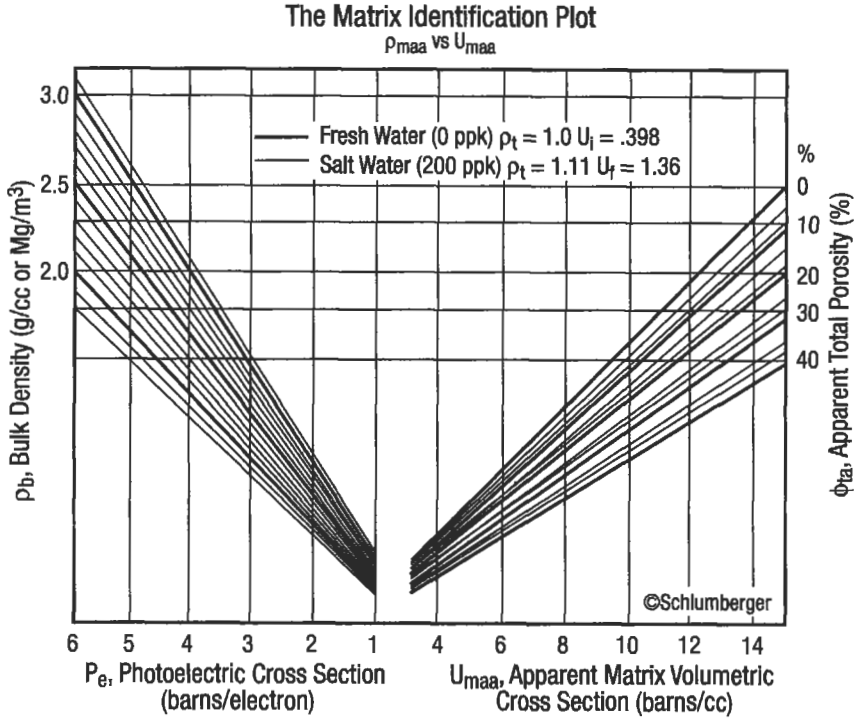


Figure 5-102. Chart for determining apparent matrix volumetric cross section from bulk density and photoelectric cross section [199].

shows the basic antenna configuration [214]. Figure 5-105 is an example of an EPT log presentation.

The depth of investigation of the tool varies between one and three inches and depends on formation conductivity; high conductivity reduces depth of investigation.

The tool is affected primarily by hole roughness (rugosity) and mud cakes > 3/8 in. thick. These effects reduce depth of investigation and in extreme situations (i.e., very rough holes and/or very thick mud cakes) keep the tool from reading the formation at all.

Interpretation. The most common way to interpret EPT logs is called the T_{po} method [214]. T_{po} in a clean formation is given by:

$$T_{po} = (\phi S_{xo} T_{pfo}) + \phi(1 - S_{xo}) T_{phyd} + (1 - \phi) T_{pma} \tag{5-108}$$

Rearranging terms and solving for S_{xo} :

$$S_{xo} = \frac{(T_{po} - T_{pma}) + \phi(T_{pma} - T_{phyd})}{\phi(T_{pfo} - T_{phyd})} \tag{5-109}$$

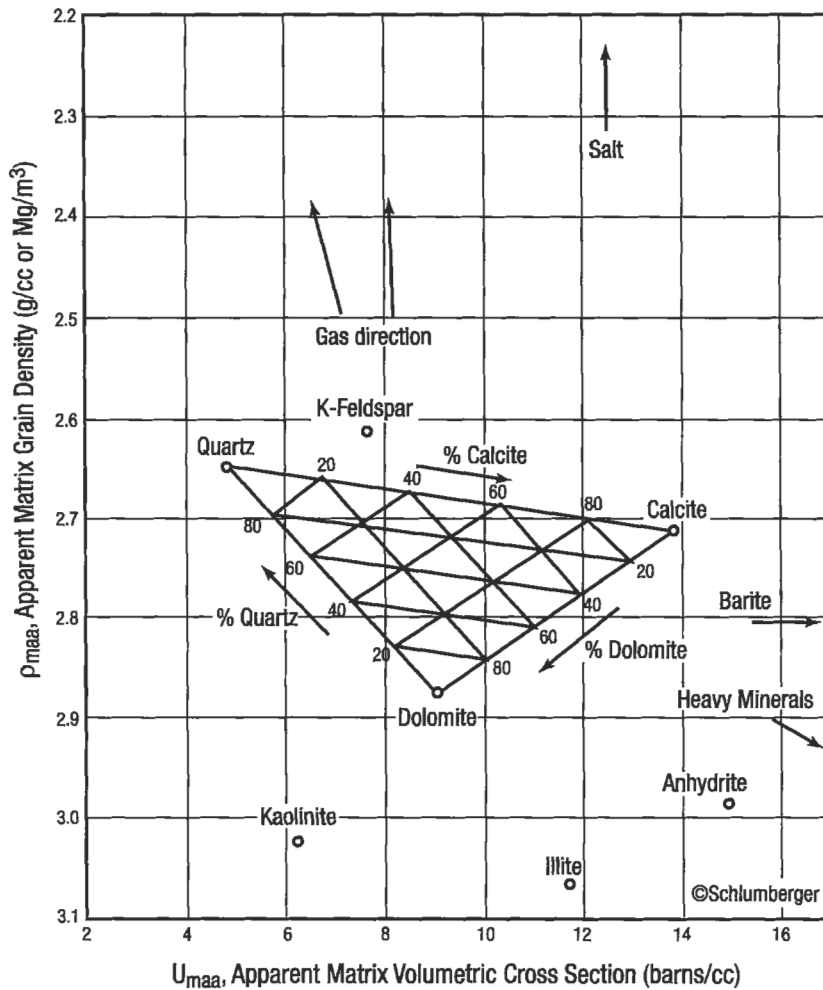


Figure 5-103. Matrix identification crossplot chart for finding matrix composition from apparent matrix density and apparent matrix volumetric cross section [199].

where $T_{po} = T_{pl}$ corrected for conductivity losses, nanosecs/m
 T_{pma} = the matrix propagation time, nanosecs/m
 T_{pbyd} = the hydrocarbon propagation time, nanosecs/m
 T_{pfo} = the fluid propagation time, nanosecs/m

T_{po} can be calculated by:

$$T_{po} = T_{pl}^2 - \left(\frac{A_c}{60.03} \right)^2 \quad (5-110)$$

Antenna configuration

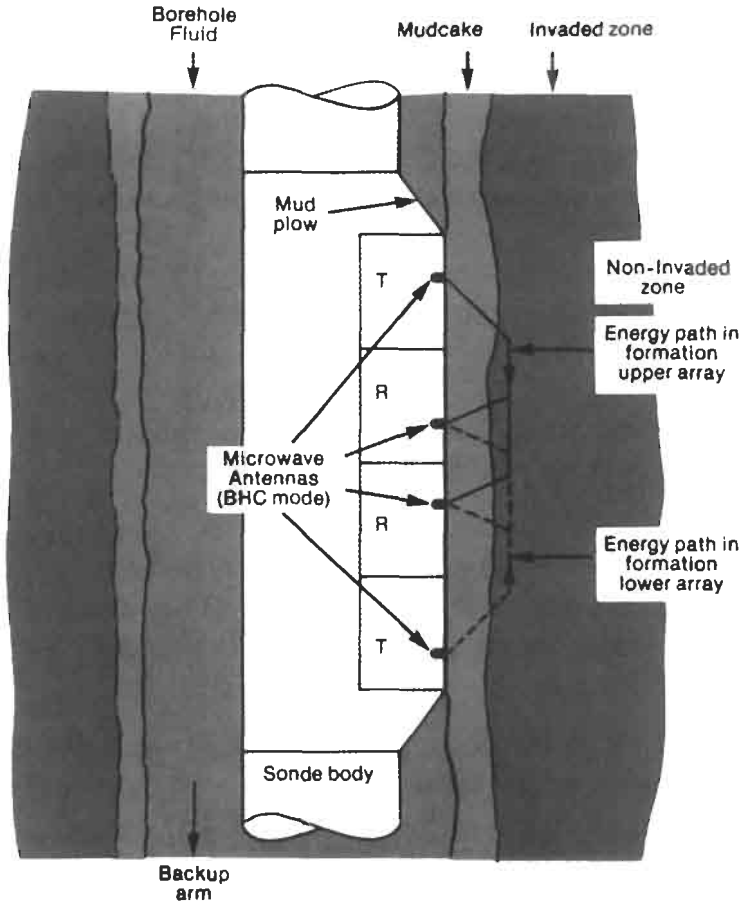


Figure 5-104. Diagram showing antenna-transmitter configuration for an EPT sonde and microwave ray paths through the mudcake and formation adjacent to the borehole [214].

$$\text{where } A_c = A_{\log} - 50 \tag{5-111}$$

(A_{\log} = EATT curve reading in dB/m)

T_{pfo} is a function of formation temperature (T) and can be found from:

$$T_{pfo} = \frac{20(710 - T/3)}{(440 - T/3)} \tag{5-112}$$

T_{pma} is taken from Table 5-28 and ϕ is taken from a neutron-density log (ϕ_{ND}). Equation 5-109 can be rearranged to find ϕ for a quick-look comparison with

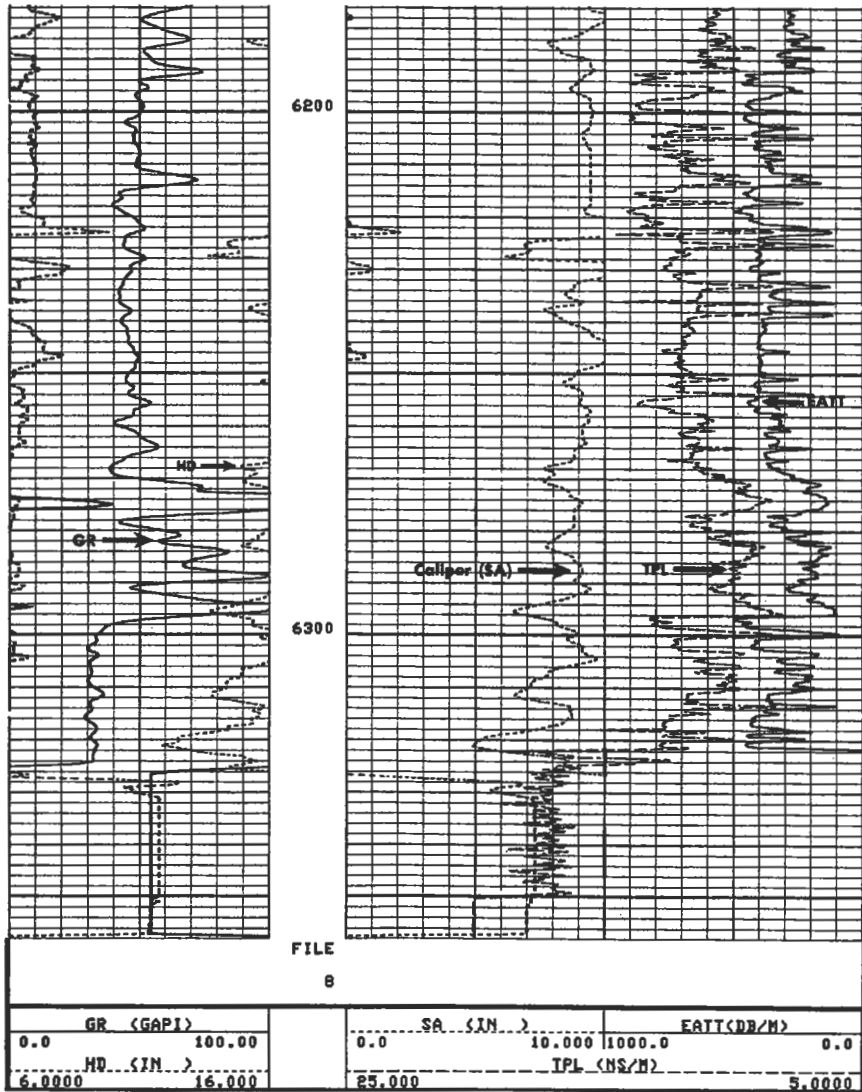


Figure 5-105. EPT log presentation.

other porosity devices (specifically the neutron-density log) [214]. By assuming $T_{\text{phyd}} \approx T_{\text{pfo}}$, T_{phyd} can be eliminated and:

$$S_{\text{so}} = \frac{1}{\phi} \frac{(T_{\text{po}} - T_{\text{pma}})}{(T_{\text{pfo}} - T_{\text{pma}})} \quad (5-113)$$

Since the EPT log measures water-filled porosity, by definition

Table 5-28
Matrix Propagation Times with the Electromagnetic
Propagation Tool for Various Minerals

Mineral	T _{pma} , nano sec/m
Sandstone	7.2
Dolomite	8.7
Limestone	9.1
Anhydrite	8.4
Dry colloids	8.0
K-feldspar	7.0-8.2
Muscovite	8.3-9.4
Biotite	7.3-8.2
Talc	7.1-8.2
Halite	7.9-8.4
Siderite	8.8-9.1
Gypsum	6.8
Sylvite (KCl)	7.2-7.3
Limonite	10.5- 11.0
Apatite	9.1-10.8
Sphalerite	9.3-9.6
Rutile	31.8-43.5
Petroleum	4.7-5.8
Shale	variable
Fresh water @ 250°C	29.0

From Reference 214.

$$\phi = \phi_{EPT} \frac{(T_{po} - T_{pma})}{(T_{pfo} - T_{pma})} \tag{5-114}$$

in a water zone ($R_t = R_o; S_w = 100\%$)
 So, in hydrocarbon zones:

$$S_{xo} = \frac{\phi_{EPT}}{\phi_{ND}} \tag{5-115}$$

Figure 5-106 is a quick look at ϕ_{EPT} response compared to FDC, CNL, and induction-log resistivity in gas, oil, fresh water-, and saltwater-bearing formations [214]. These responses also indicate moveable oil saturation ($1 - S_{xo}$) and, therefore permeability.

Special Openhole Logs and Services

Dipmeter. The dipmeter is a four-armed device with pads that read resistivity of thin zones. These four resistivity curves are analyzed by computer and correlated to determine formation dip and azimuth. The dips are presented on a computer-produced log. In addition to dip, hole deviation, borehole geometry, and fracture identification are also presented.

EPT Quicklook

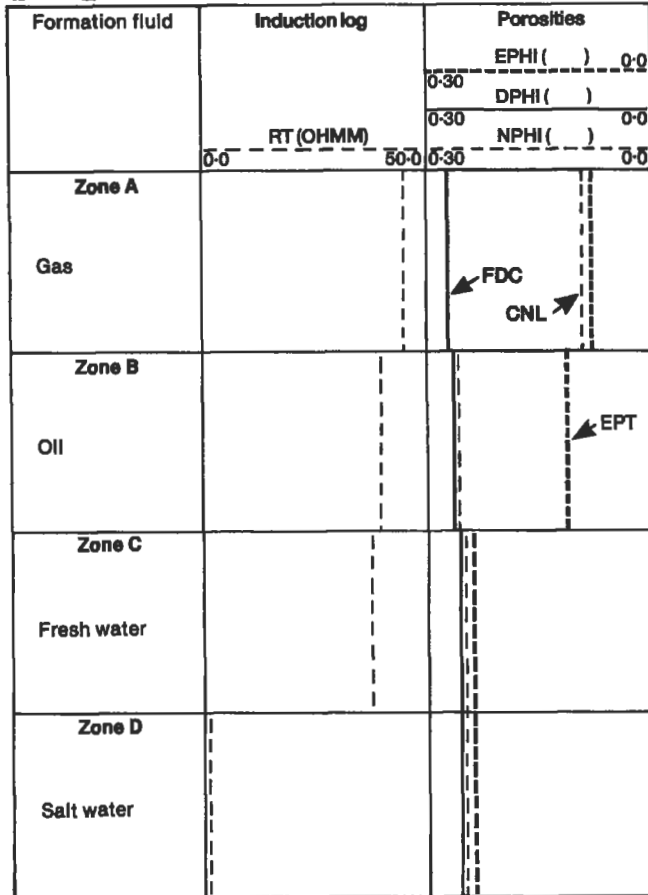


Figure 5-106. EPT quicklook chart comparing curve response of induction resistivity, neutron porosity, density porosity and EPT porosity in water bearing and hydrocarbon-bearing zones [214].

Repeat Formation Tester. The repeat formation tester measures downhole formation pressures. The tool is operated by an electrically driven hydraulic system so that several zones may be pressure tested on one trip into the hole. Once the drawdown pressure and the pressure buildup have been recorded, they can be processed by a computer at the well-site to provide Horner plots from which permeabilities are calculated. Permeabilities from the drawdown test often vary considerably from measured permeabilities and should be considered an order-of-magnitude estimate. This is usually due to a very shallow depth of investigation associated with drawdown tests [212]. The pressure buildup has a better depth of investigation than the drawdown pressure test. Accuracy depends on what type of pressure-wave propagation model is chosen [212,215,216] as well as the compressibility and viscosity of the formation fluids.

Sidewall Cores. After drilling, cores from the side of the borehole can be taken by wireline core guns or drills. Guns are less expensive but do not always recover usable cores. Sidewall drilling devices have become quite common in the last few years. Up to 20 cores may be cut and retrieved on one trip into the hole.

Cased Hole Logs. Cased hole logs are run to evaluate reservoir performance, casing/cement job quality, and to check flow rates from producing intervals. The reader is referred to Bateman's book [217] on cased hole logging which provides a more detailed discussion than is possible in this summary.

Cased hole logs can be broadly divided into two classes:

1. Logs that measure formation parameters through the casing.
2. Logs that measure the parameters within and immediately adjacent to the casing.

These logs are all combined to monitor fluids being produced, monitor reservoir performance, and monitor production-string deterioration with time. They differ from open-hole logs in that the majority of cased hole logs merely monitor fluid production rather than provide extensive data on formation characteristics.

Cased Hole Formation Evaluation. Two tools are currently being used to provide formation evaluation in cased holes:

1. Pulsed neutron logs.
2. Gamma spectroscopy tools (GST) logs.

Pulsed Neutron Logs. Pulsed neutron logs are used to monitor changes in fluid content and water saturation with respect to time. Current tools also provide a means of estimating porosity. They are particularly valuable for [217]:

1. Evaluating old wells when old open-hole logs are poor or nonexistent.
2. Monitoring reservoir performance over an extended period of time.
3. Monitoring the progress of secondary and tertiary recovery projects.
4. Formation evaluation through stuck drill pipe (generally a last resort).

Theory. A neutron generator that consists of an ion accelerator fires deuterium ions at tritium targets. This produces a burst of 14 keV neutrons which pass through the borehole fluid (must be fresh water), casing, and cement. The burst then forms a cloud of neutrons in the formation which are rapidly reduced to a thermal state by collisions with the atoms in fluids in the rock (made up primarily of hydrogen atoms). Once in a thermal state, they are most liable to be captured by chlorine (or boron). The capture process will produce a gamma ray of capture which is then detected by a scintillometer in the tool. The time it takes for the neutron cloud to die during the capture process is a function of the chlorine concentration in the formation fluid. This is then related to water saturation. Rapid disappearance of the thermal neutron cloud indicates high water saturation. Slower disappearance of the cloud indicates low water saturation (i.e., high hydrocarbon saturations). The rate of cloud decay is exponential and can be expressed by:

$$N = N_0 e^{(-\lambda t)} \quad (5-116)$$

where N = number of gamma rays observed at time t

N_0 = number of gamma rays observed at $t = 0$

t = elapsed time (microseconds)

τ = time constant of the decay process, microseconds

Of most interest is τ since it is strictly a function of the decay rate of the neutron cloud (or rather the slope of the exponential function). From τ the capture cross section, Σ , can be calculated:

$$\Sigma = 4,550/\tau \quad (5-117)$$

The tools that are available to measure τ include:

1. TDT-K (with 3 moveable gates or detectors)
2. DNLL (dual neutron lifetime log) (which uses 2 gates),
3. TDT-M (with 16 fixed gates), and
4. TMD (thermal multigate decay) (which uses 6 gates).

In general, these tools all perform the same function: they measure the decay rate of the neutron cloud in the formation. This is accomplished by using a series of windows to measure near and far-spacing counting rates, as well as background gamma ray rates. The first gates are not triggered until all neutrons in the cloud in the formation are thermalized. At this point neutron capture has started. By using certain gating times and gate combinations, the slope of the straight portion of the decay curve is measured and related to Σ . In addition, the ratio between the short-space-detector and long-space-detector counting rates is also calculated and is related to porosity. (It is similar in principle to the CNL porosity device used in openhole logging.)

Log Presentations. Figure 5-107 is an example of a DNLL log presentation. Most other TDT logs are presented in a similar way, except that the number of curves varies from company to company. The log shown in this figure consists of 5 curves:

1. Gamma ray curve (Track 1).
2. Gate 1 counting rate (CPM).
3. Gate 2 counting rate (CPM).
4. Ratio curve (\approx CNI. ratio).
5. Sigma curve (Σ).

In addition, the pips located on the left side of track 2 are the corrected casing collar locations.

Gate 1 and Gate 2 show the raw data from the detectors, the ratio curve shows relative hydrogen concentration (\approx water-filled porosity), and the σ curve shows the capture cross-section. Some logs also show a τ curve, but it is normally omitted [217].

Interpretation. Interpretation of pulsed neutron logs is very straightforward. It relies on knowledge of three parameters (four in hydrocarbon-bearing zones):

1. Σ_{log} (capture units).
2. Σ_{matrix}
3. Σ_{water}
4. $\Sigma_{\text{hydrocarbon}}$

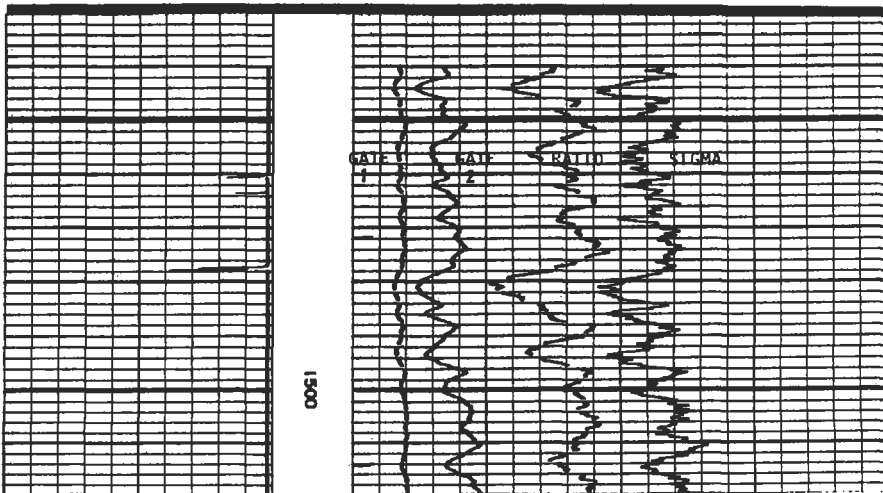
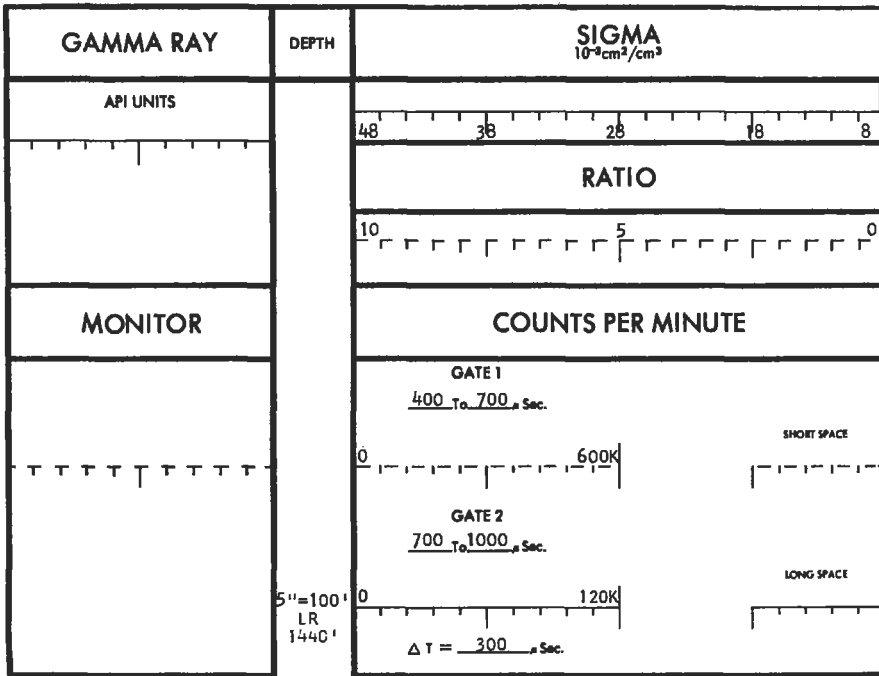


Figure 5-107. Dual neutron lifetime log (DNLL) presentation.

According to Schlumberger [220] the log response may be described as:

$$\Sigma_{log} = \Sigma_{ma}(1 - \phi) + \Sigma_w \phi S_w + \Sigma_{hy} \phi(1 - S_w) \tag{5-118}$$

Solving for S_w :

$$S_w = \frac{(\Sigma_{log} - \Sigma_{ma}) - \phi(\Sigma_{hy} - \Sigma_{ma})}{\phi(\Sigma_w - \Sigma_{hy})} \tag{5-119}$$

Porosity (ϕ) can be found either from an openhole porosity log or by combining the ratio curve and Σ_{log} . Figures 5-108 to 5-111 are charts to find porosity,

Sandstone, 5 1/2-in. Casing, 8-in. Borehole, Fresh Water Cement, Tool Eccentered

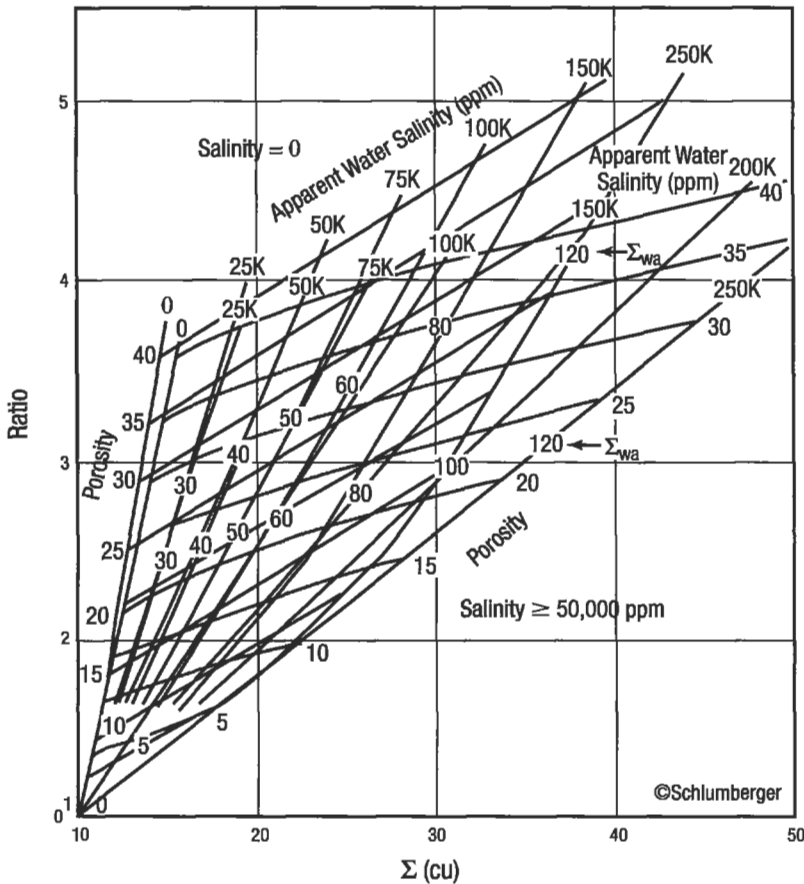
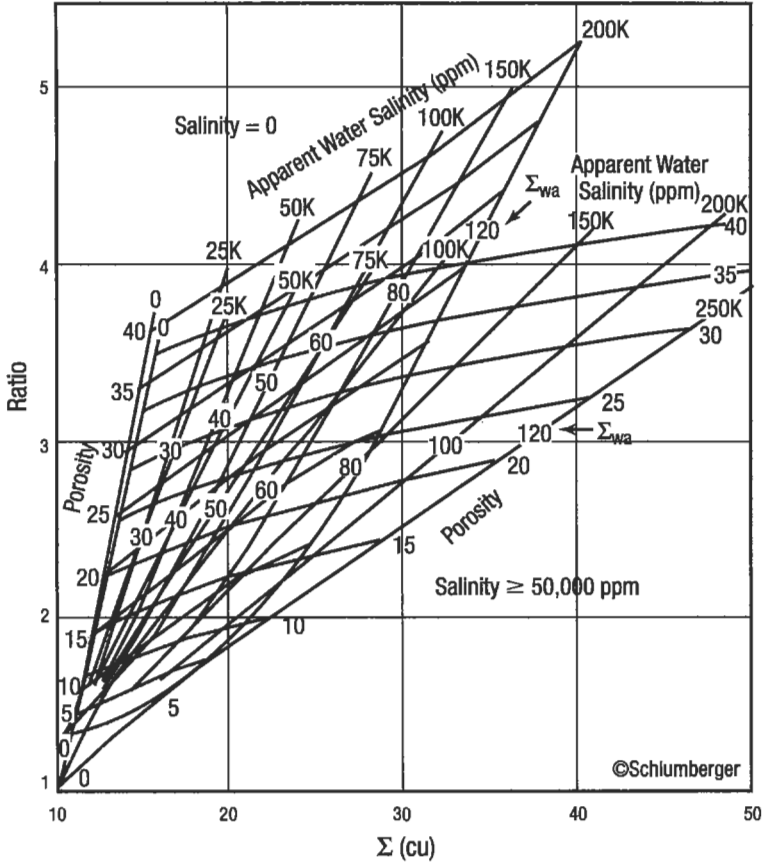


Figure 5-108. Chart for determining porosity and apparent water salinity from Σ_{log} and ratio curves in 5 1/2-in. casing and an 8-in. borehole [199].

Sandstone, 7-in. Casing, 10-in. Borehole, Fresh Water Cement, Tool Eccentered



Example: Ratio = 3.1
 $\Sigma_{LOG} = 20$ cu
 Borehole fluid salinity = 80,000 ppm
 5 1/2-in. casing cemented in 8 3/4-in. borehole

Thus, from Chart Tcor-3
 $\phi = 30\%$
 Apparent water salinity = 50,000 ppm
 $\Sigma_{wa} = 40$ cu

If this were a clean formation and connate water salinity was known to be 150,000 ppm, then

$$S_w = \frac{50,000}{150,000} = 33\%$$

Figure 5-109. Chart for determining porosity and apparent water salinity from Σ_{log} and ratio curves in 7-in. casing and a 9-in. borehole [199].

Sandstone, 7- to 9-in. Casing, 12-in. Borehole, Fresh Water Cement, Tool Eccentered

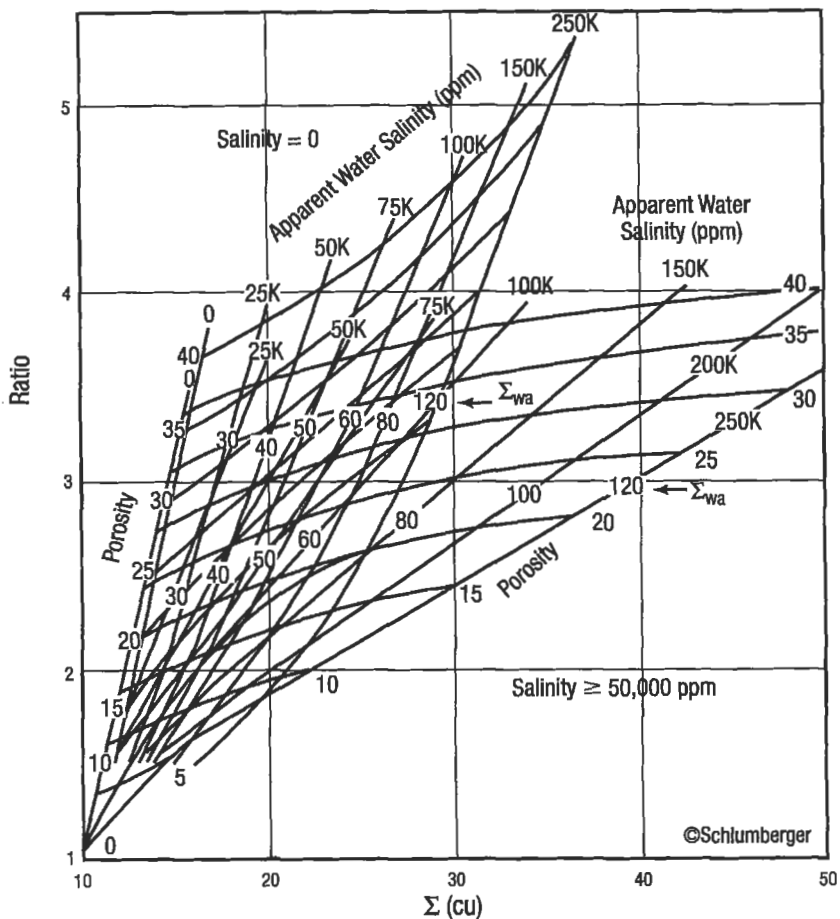


Figure 5-110. Chart for determining porosity and apparent water salinity from Σ and ratio curves in 7- to 9-in. casing and a 12-in. borehole [199].

apparent water salinity, and Σ_w , using this combination. By selecting the chart for the appropriate borehole and casing diameter, these values are easy to determine. Simply enter the proper axes with the log-derived values, and find porosity and Σ_w at the intersection of the two lines. If water salinity and formation temperature are known, use Figure 5-111 to find Σ_w .

Estimating Σ_{hy} is another matter. You must first know if the hydrocarbons are oil, methane, or heavier hydrocarbon gases (i.e., propane, butane, pentane). For oil, solution gas-oil ratio and oil gravity ($^{\circ}$ API) are needed. If the gas is methane, reservoir pressure and temperature are required. For gases other than methane, the specific gravity of the gas can be converted to equivalent methane using

Example: A reservoir section at 90°C temperature and 25 MPa pressure contains water of 175,000 ppm (NaCl) salinity: 30° API oil with a GOR of 2000 cu ft/bbl, and methane gas.

Thus, $\Sigma_w = 87$ cu ($\tau = 52 \mu s$)
 $\Sigma_o = 19$ cu ($\tau = 240 \mu s$)
 $\Sigma_g = 6.9$ cu ($\tau = 660 \mu s$)

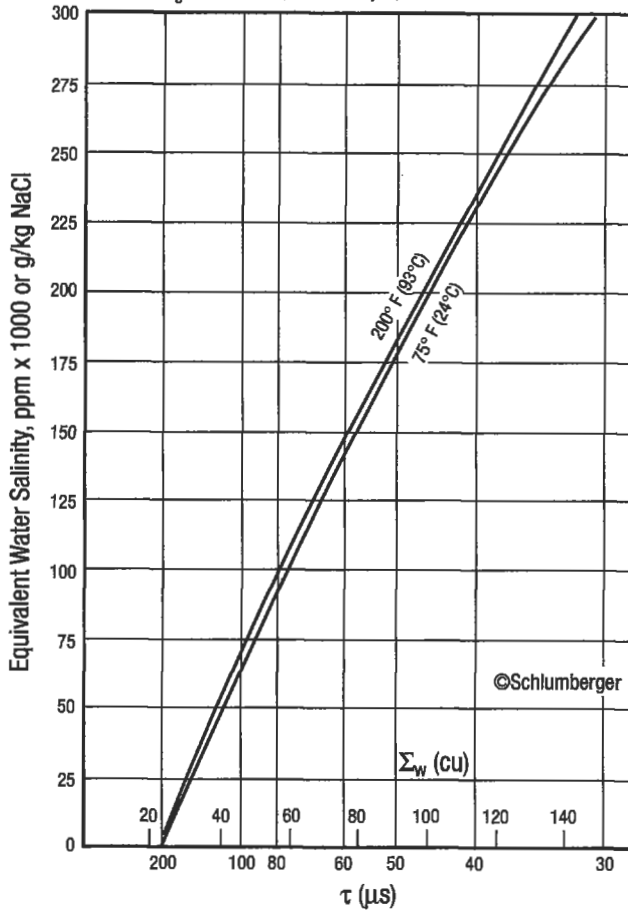


Figure 5-111. Chart for finding Σ_w from equivalent water salinity and formation temperature [199].

Figure 5-112, and then Figure 5-113 can be entered. Once all of the parameters have been found, Equation 5-119 is used to find S_w .

Applications. Pulsed neutron logs are most useful for monitoring changes in water saturation over time while a reservoir is produced. Initially, these logs are run prior to perforating a zone. Subsequent logs are run every few months (or years) depending on production rate and the amount of control desired. Water saturation is calculated for each run using Equation 5-119 and subtracted

(text continued on page 190)

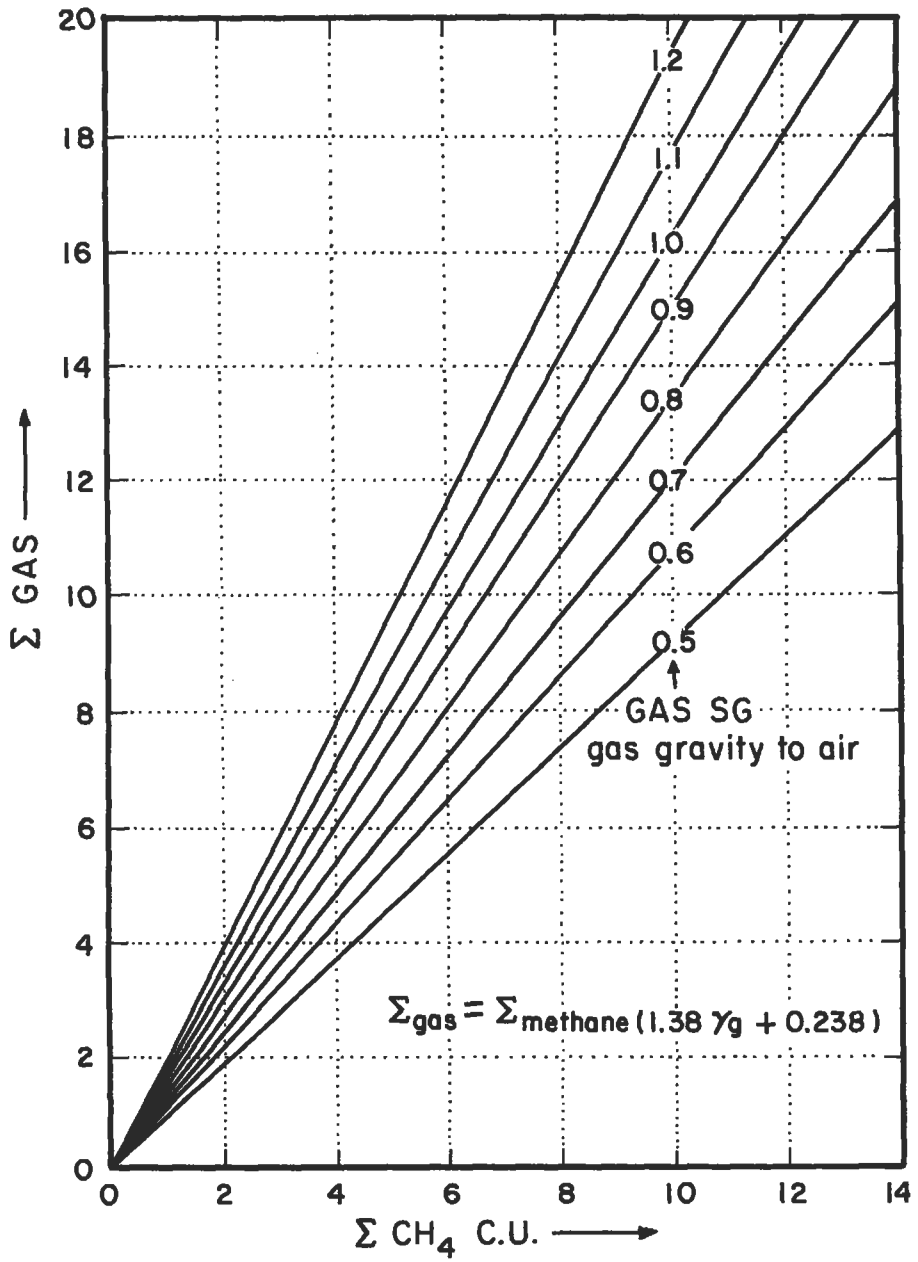


Figure 5-112. Chart for converting Σ_{gas} to Σ_{methane} [217].

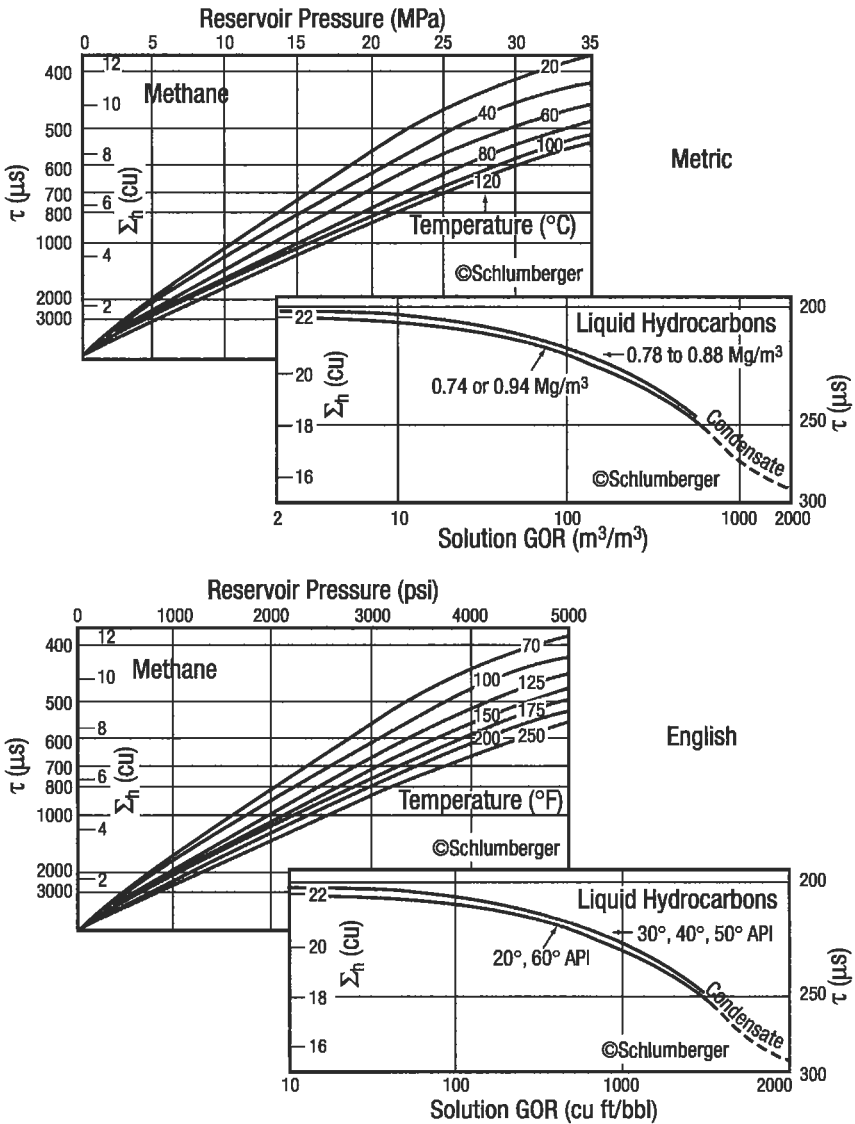


Figure 5-113. Charts for finding Σ_h (for methane and liquid hydrocarbons) from reservoir pressure and formation temperature (gas) or solution gas oil-ratio (GOR) and API gravity (liquid 7 hydrocarbons [199]).

(text continued from page 187)

from saturations determined from earlier runs. These values (ΔS_w) show the change in the position of the water table (hydrocarbon-water contact) versus time.

Another application is monitoring residual oil saturation in waterflood projects. The procedure outlined by Bateman [217] involves first running a base log (prior to injection). Next, salt water is injected and another log is run. Then fresh water is injected and another log run. If Σ_{brine} and Σ_{fresh} are known, Bateman [217] suggests using:

$$S_o = 1 - \frac{\Sigma_{\log(\text{brine})} - \Sigma_{\log(\text{fresh})}}{\phi(\Sigma_{\text{brine}} - \Sigma_{\text{fresh}})} \quad (5-120)$$

to find residual oil saturation (S_{or}). Additional details of estimating S_{or} are given later.

The main problem with using these logs is the presence of shale. Shale normally appears wet, and shale will make a reservoir look like it has higher S_w . Openhole logs and an NGS log are needed to confirm this interpretation although shaly sand corrections can easily be made [217].

Gamma Spectroscopy Tools (GST). Also known as the carbon-oxygen log, this device has recently been incorporated into pulsed neutron tools to aid in differentiating oil and gas from water. GST tools operate with the same neutron generator as the pulsed neutron devices, but gamma rays returning from the formation are measured.

Two types of gamma rays are produced when neutrons are fired into a formation:

1. Those that result from neutron capture by chlorine and boron.
2. Those that result from inelastic collisions with atoms.

The detector on this tool has energy windows set to receive certain returning gamma rays [218]. The detectors are protected from the fast neutron source by an iron shield, and from returning thermal neutrons by a boron shield.

The energy of the returning gamma rays depends on the atom involved in the collisions. The atoms of interest include carbon, oxygen, silicon, and calcium. Carbon-oxygen ratio is a carbon indicator and when combined with porosity, gives an estimate of water saturation if matrix lithology is known. Figure 5-114 is used for this determination. Silicon-calcium ratio is an indicator of matrix and is used to distinguish oil-bearing rock from calcareous rocks (such as limy sands and limestones) [218,219]. Figure 5-115 is an example of a carbon-oxygen log.

If capture gamma rays are also detected with separate energy windows, chlorine and hydrogen content can be determined and related to formation water salinity. Figures 5-116 and 5-117 are used for this purpose. All that is required to estimate salinity of formation waters is knowledge of borehole fluid salinity, Cl/H ratio, and response mode of the tool. These devices should *not* be confused with the natural gamma spectroscopy log which only measures naturally-occurring gamma rays.

The readings on the GST log are not affected by shale although carbonaceous shales can cause trouble because of the sensitivity to carbon. Usually, however, these effects can be calibrated for or taken into account when this log is interpreted. Much of the interpretation of this type of log is based in regional experience; the analyst should have a good idea of the types of rocks present

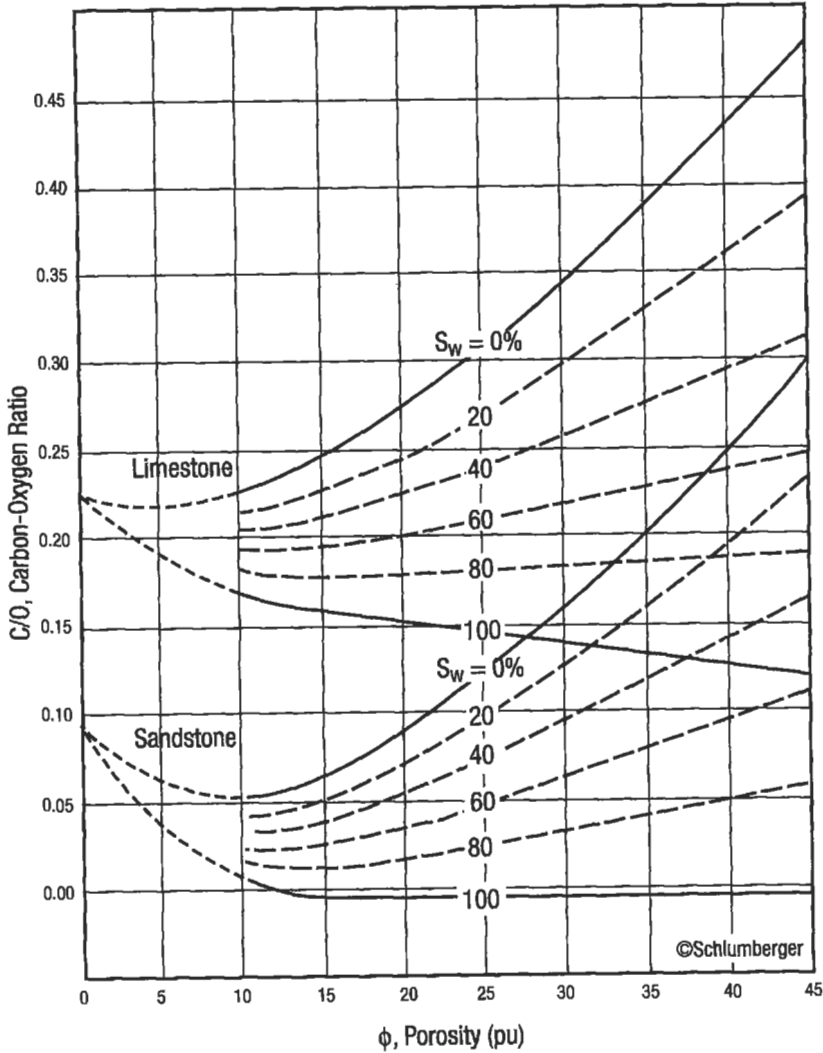


Figure 5-114. Chart for finding water saturation using the carbon-oxygen ratio curve and porosity if matrix lithology is known [199].

before trying to make an interpretation. No lithology crossplot charts are presently available to estimate lithology with these logs.

Natural Gamma Spectroscopy. This log operates in the same manner as its openhole counterpart. The main difference is that the log should be calibrated prior to being run in cased holes. No correction charts are currently available for cased hole applications with this device. Curve presentations are the same as for the open-hole version. Refer to the open-hole section for a discussion of this log.

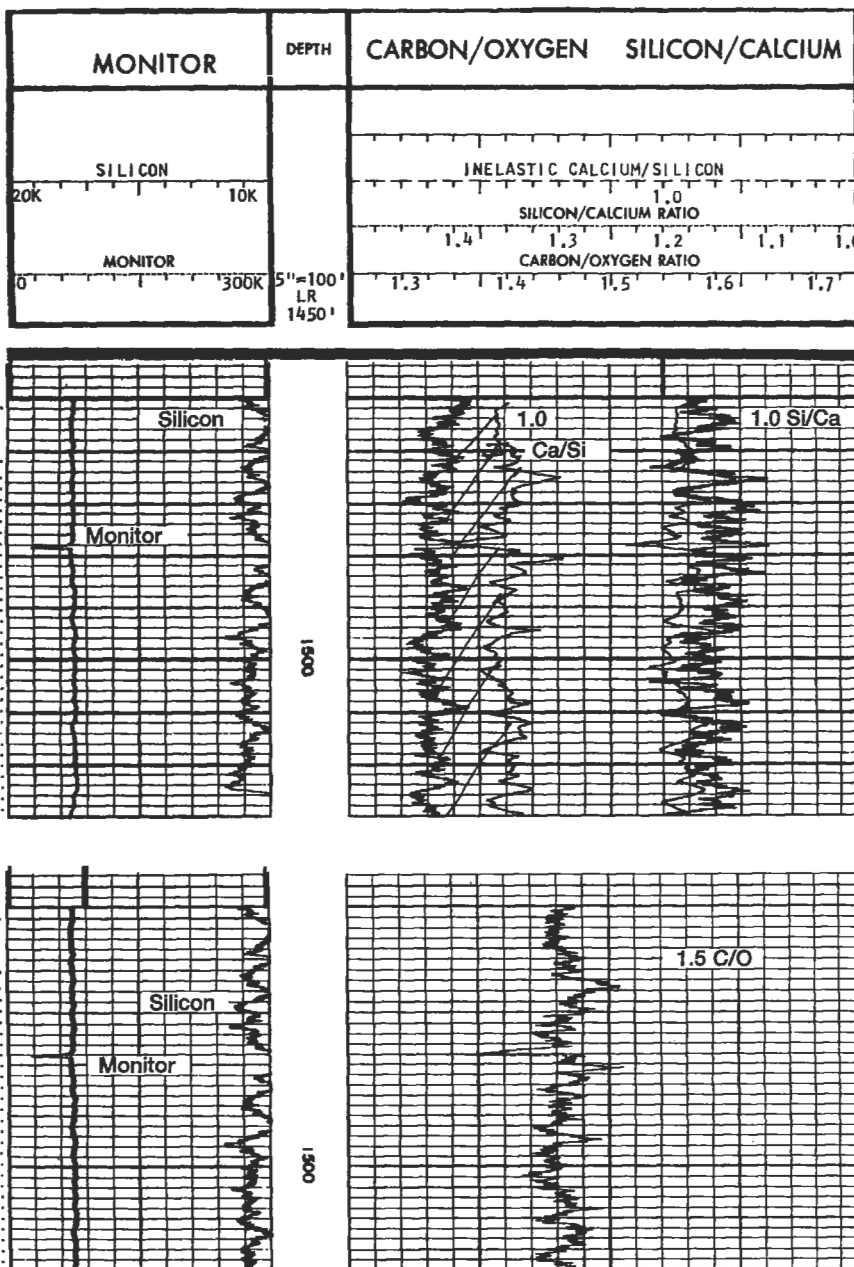


Figure 5-115. Carbon-oxygen and silicon-calcium ratio curves on a carbon-oxygen log.

Apparent Water Salinity Determination
from GST* Gamma Spectrometry Log—Inelastic Mode

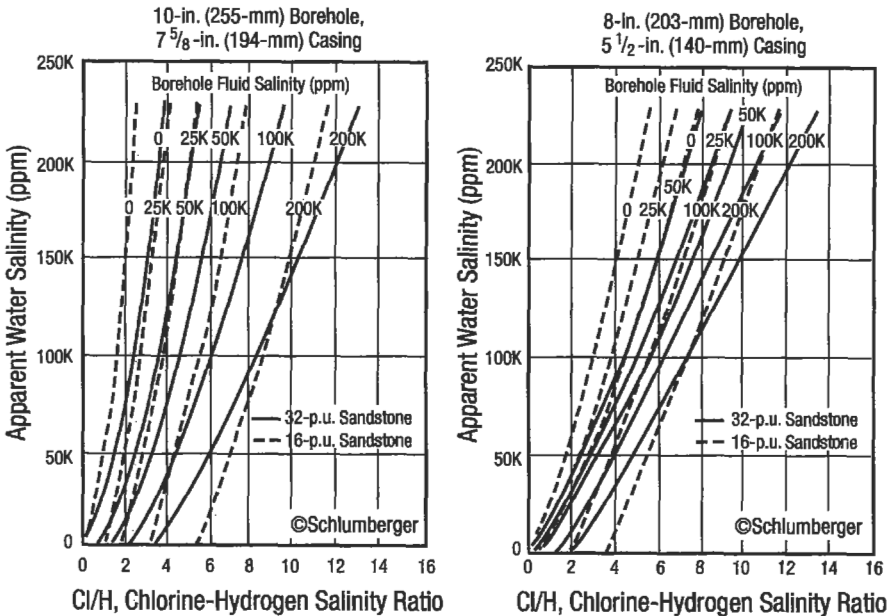


Figure 5-116. Chart for finding apparent water salinity from chlorine-hydrogen ratio and borehole fluid salinity from a GST log (in elastic mode) [199].

Cased-Hole Completion Tools. These tools examine cement bond and casing quality. They assure that no leakage or intercommunication will occur between producing horizons, or between water-bearing horizons and producing horizons. The most common completion tools include:

1. Cement bond logs (CBL).
2. Multifingered caliper logs.
3. Electromagnetic inspection logs.
4. Electrical potential logs.
5. Borehole televewers.

Cement bond logs (CBL-VDL). Cement bond logs are used to check cement bond quality behind the casing and to estimate compressive strength of the cement. It can also be used to locate pipe channeling in the cement or eccentric pipe and to check for microannulus.

Theory. The cement bond tool is the same as a conventional sonic tool except that the receiver spacings are much larger. It consists of a transmitter and two receivers. The near receiver is 3 ft below the transmitter and is used to find Δt for the casing. The far receiver is 5 ft below the transmitter and is used for the variable density log (VDL) sonic-wave-form output. The operation is the same as a conventional sonic except that the transmit time (one way) is measured. The transmitter is fired and a timer is triggered in both receivers. The wave

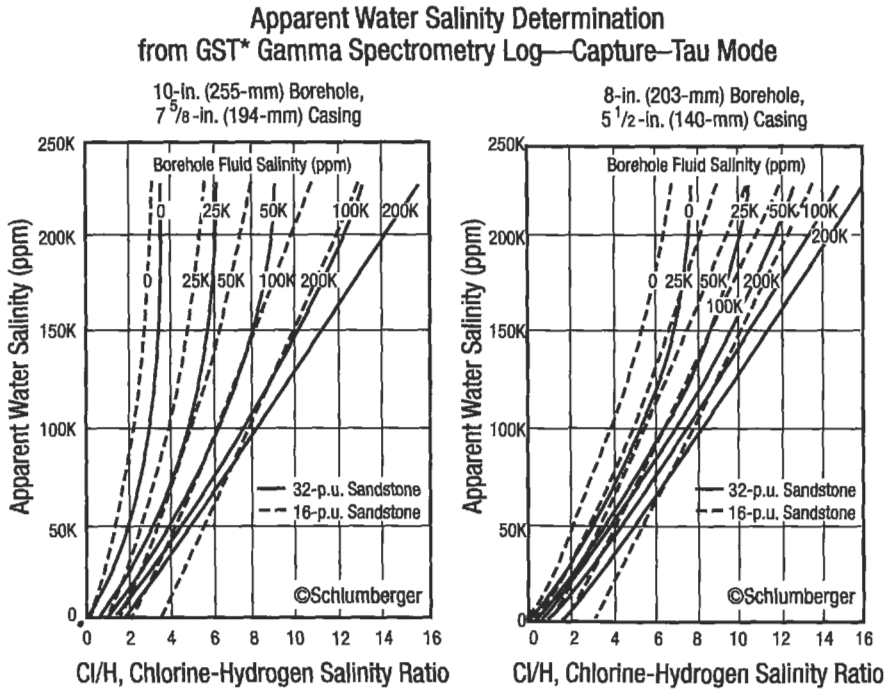


Figure 5-117. Chart for finding apparent water salinity from chlorine-hydrogen ratio and borehole fluid salinity derived from a GST log (Tau-capture mode) [199].

passes through the fluid in the casing, the casing, and the cement, and into the formation. The near receiver measures the first arrival of the compressional wave and the timer is shut off. This Δt is a function of whether the casing has cement behind it or not.

The sound wave is then picked up by the lower receiver which recognizes refracted compressional wave arrivals from the casing, cement, and formation, as well as Rayleigh, Stonely, and mud-wave arrivals. Figure 5-118 shows the basic tool configurations.

The most important parameter measured by this tool is compressive-wave attenuation-rate. This parameter is a function of the amount of cement present between the pipe and formation. Typically, cement must be at least 3/4 in. thick on the casing in order for attenuation to be constant [217]. Each part of the log reads different attenuations. The CBL registers attenuation of the compressional wave in the cement and casing which gives an indication of the cement-casing bond-quality. The VDL registers the attenuation of the compressional wave through casing, cement, and formation which gives an indication of acoustic coupling between casing, cement, and surrounding rock. This indicates not only the casing bond quality but also the cement-formation-bond quality

The basic parameter used to evaluate cement bonds is called the *bond index* and can be calculated by:

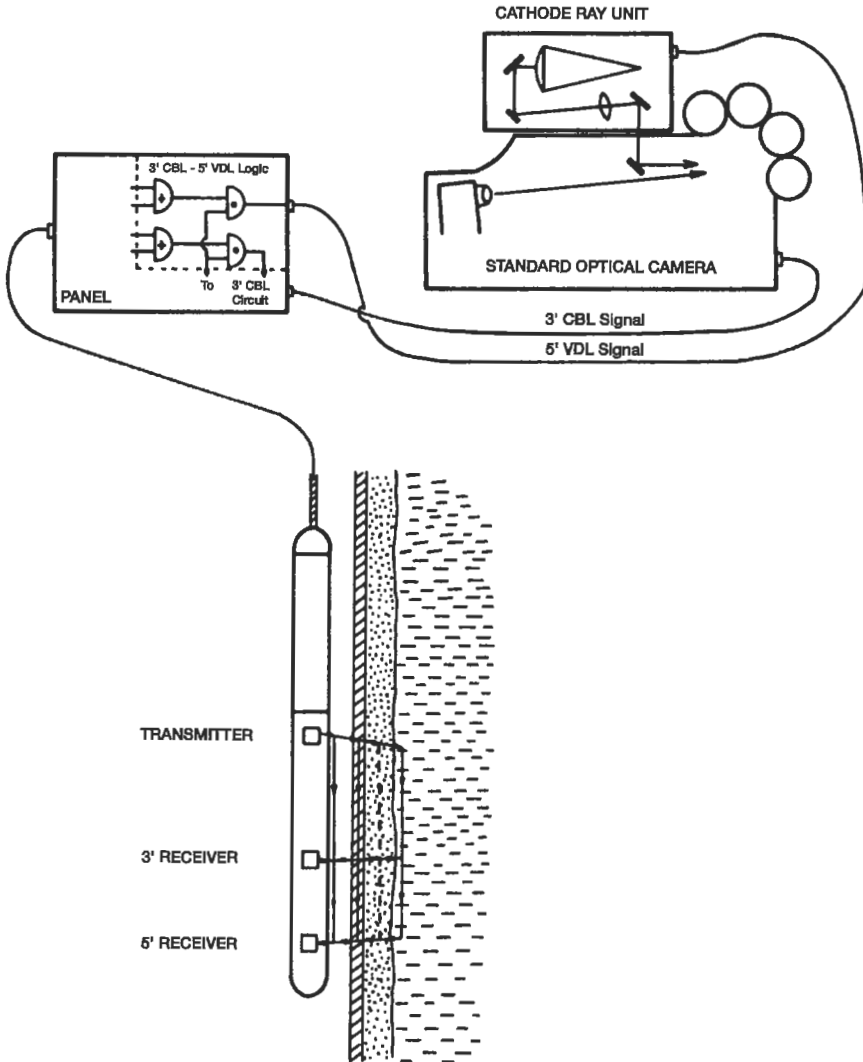


Figure 5-118. Transmitter-receiver arrangement and surface equipment for cement bond log-variable density log combination [220].

$$\text{bond index} = \frac{\text{attenuation in zone of interest (db/ft)}}{\text{attenuation in a well cemented section (db/ft)}} \quad (5-121)$$

Bond index gives a relative way to determine bond quality through any given section of pipe. The minimum value of bond index necessary for a good hydraulic seal varies from region to region, and depends on hole conditions

and type of cement used. Ideally, an index of 1.0 indicates excellent pipe-cement bonding; decreasing values show deteriorating conditions which may require squeezing to bring bonding up to acceptable standards. A bond index curve may be presented in track 2.

Log Presentations. Figure 5-119 shows a CBL-VDL log. Typically, three curves (and sometimes more, depending on the service company) are presented on the log. Track I contains total travel time and is a function of the casing size and tool centering. Other curves may be presented in this track, including gamma ray, neutron, and casing collar locator logs. Track 2 contains the cement bond logs amplitude curve. The log is scaled in millivolts and is proportional to the attenuation of the compressional-wave first-arrivals. High attenuation produces low-amplitude values; low attenuation produces high-amplitude values. The higher the amplitude, the poorer is the casing-to-cement bond. Direction of increasing amplitude is normally indicated by an arrow. Some presentations also include a bond index curve in track 2. Track 3 contains the variable density log (VDL) display. The most common presentation is dark- and light-colored bands that represent the peaks and valleys of the wave train. Figure 5-119 shows two possible types of arrivals:

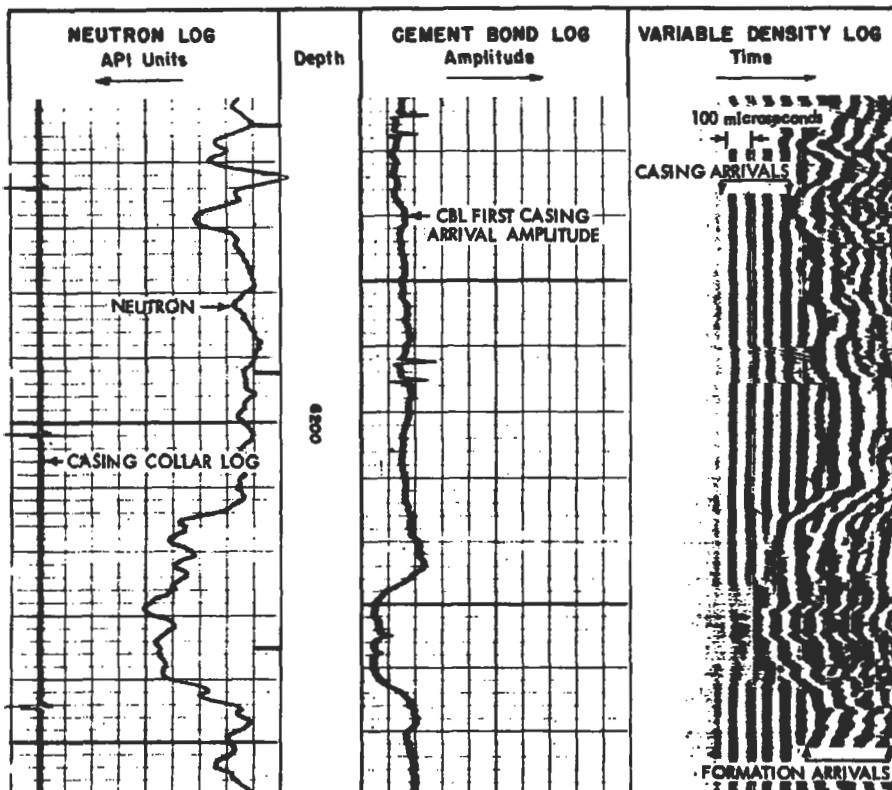


Figure 5-119. Basic CBL-VDL log presentation [220].

1. Those from the casing which appear as straight, parallel light and dark bands intermittently broken by small V-shaped spikes which indicate the position of casing collars.
2. Those from the formation which appear as wavy, irregular, and intermittent light and dark bands which represent curve attenuation in the rock surrounding the borehole.

Interpretation. Interpretation of CBL-VDL logs involves recognition of basic curve pattern for determining whether casing is properly bonded or not. These curve patterns are presented in Figures 5-120 to 5-123. Four basic types of patterns are apparent:

1. Those that show strong casing arrivals only.
2. Those that show strong casing and formation arrivals.
3. Those that show weak casing arrivals and strong formation arrivals.
4. Those that show both weak casing and weak formation arrivals.

Strong casing arrivals are shown in Figure 5-120 and are characterized by the pronounced casing arrival pattern (straight, alternating light and dark bands). No formation arrivals are present and cement-bond log-amplitude is moderate

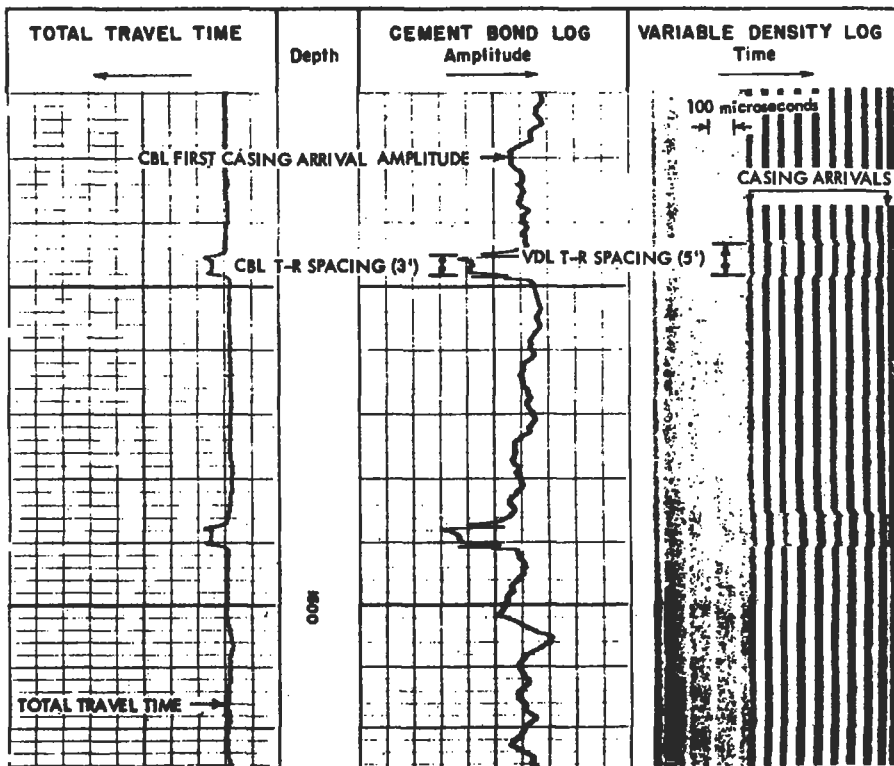


Figure 5-120. CBL-VDL log run in free pipe [220].

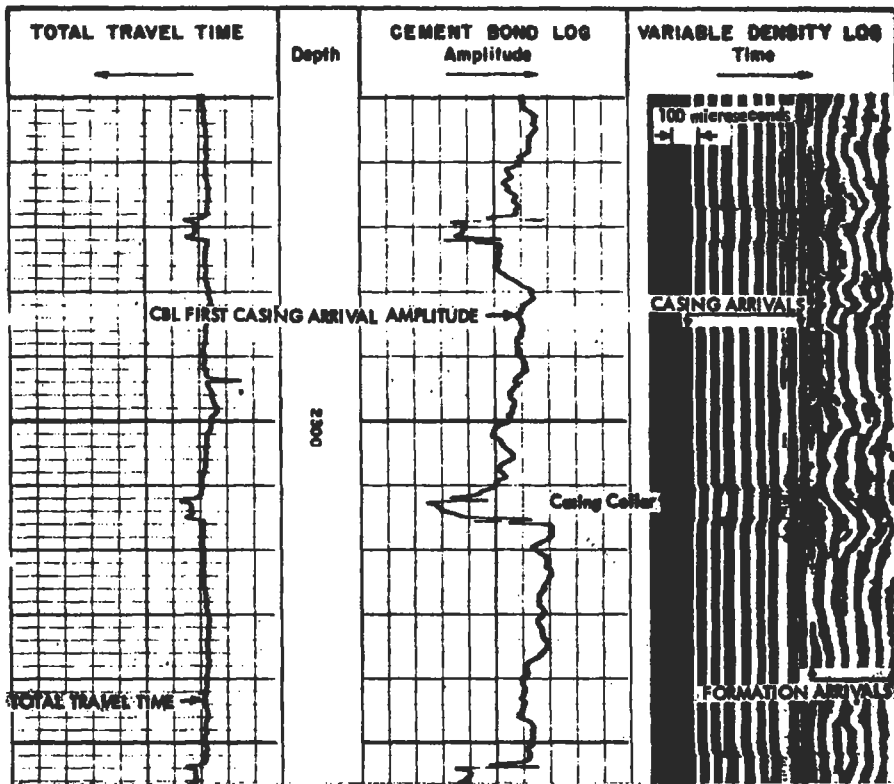


Figure 5-121. CBL-VDL log run in casing eccentric in borehole making contact with the formation [220].

to high. These indicate free pipe with no cement or cement-casing-formation coupling. A high amplitude curve reading indicates low attenuation, hence no cement in the annulus.

Strong casing and formation arrivals are shown in Figure 5-121. This pattern has both the clean, pronounced casing signature as well as a strong, wavy-formation signature. The lack of cement is indicated by the high cement bond log-amplitude (i.e., no cement attenuation). The combination of these signals is interpreted as eccentric casing in contact with the wall of the well-bore. In this situation, proper cementation may be impossible.

Weak-casing and strong-formation arrivals are shown in Figure 5-122. This pattern shows no apparent casing or very weak casing patterns and very strong formation-patterns nearly filling the VDL in track 3. This indicates good casing-cement-formation bonding, confirmed by the low cement bond log amplitude (high attenuation). Rayleigh and mud wave arrivals are also apparent along the right side of track 3.

Weak-casing and weak-formation arrivals are shown in Figure 5-123. This pattern shows what appears to be a slightly attenuated casing pattern but the cement bond log amplitude suggests otherwise. The curve indicates strong to

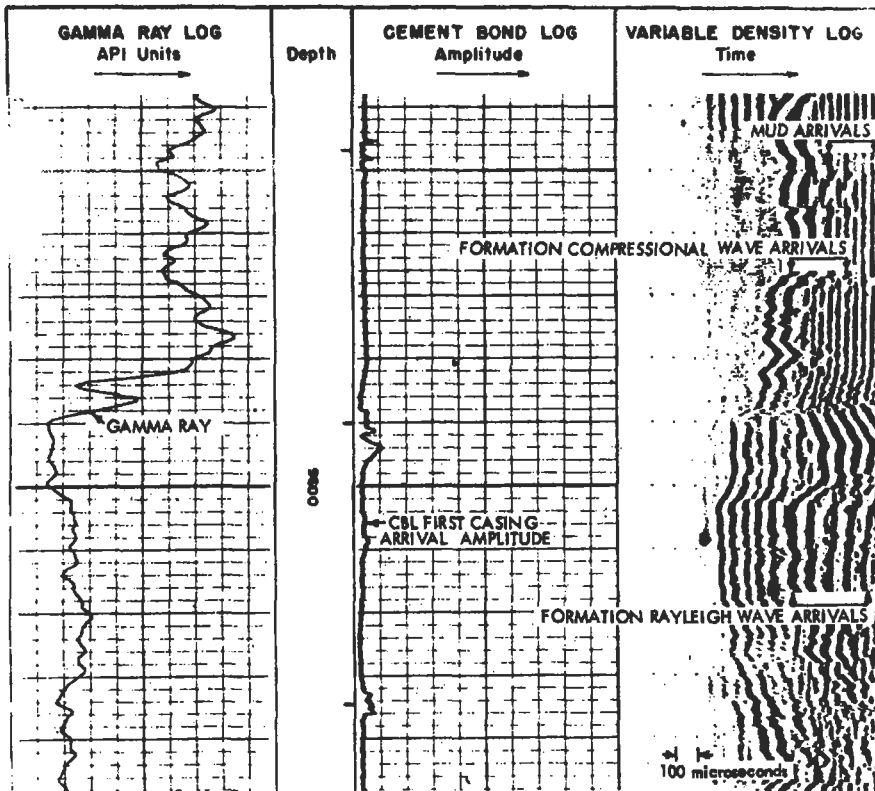


Figure 5-122. CBL-VDL log run in well-bonded casing [220].

very strong attenuation due to cement. Strongest attenuation occurs at "A" with a very weak formation pattern on the VDL. Comparison with the open-hole VDL (immediately to the right) shows no unusual attenuations of the formation signal. This also confirms poor acoustic coupling between cement and formation with good coupling between casing and cement.

Other possible interpretations for this type of pattern are possible.

1. Gas in the mud can be ruled out by examining long intervals of the log. Generally, this effect will occur over long rather than short sections in the well.
2. Eccentered tool in the casing, which causes destructive interference of compressive-wave first-arrivals, can be confirmed by checking for wiggly casing arrivals or a slight decrease in the casing-arrival time shown on the total-transit-time curve or VDL log [220].
3. Thin cement sheaths, caused by excessive mud cake thickness along a permeable formation, are a problem when cement sheaths are less than $\frac{3}{4}$ in. thick (which allows stronger casing arrivals). At times, the cement and formation have a slight acoustic coupling which gives the VDL a faint or weak formation signal.

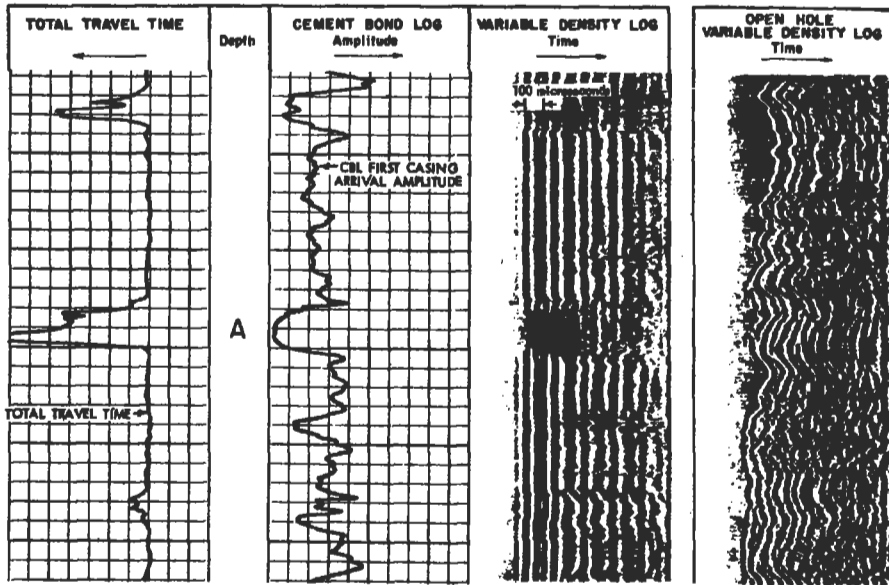


Figure 5-123. CBL-VDL log run in casing with a good cement-casing bond and a poor cement-formation bond [220].

Microannulus or Channeling in Cement. Microannulus occurs when the cement is emplaced and the casing is pressurized. When pressure is released after the cement has set, the casing “pops” away from the cement sheath. This generates a gap or microannulus between the casing and the cement. This can also occur if excessive pipe dope or varnish is present on the pipe. Microannulus due to pressurization primarily occurs opposite washed out portions of the borehole.

Channeling occurs when cement is in the annulus but does not completely surround, or is not bonded to, the pipe. This condition will not have proper fluid seal which allows oil, gas or water to pass up the hole outside the casing. Microannulus, on the other hand, may have a proper seal even though a small gap exists. It is very important to be able to distinguish between microannulus and channeling; squeezing may eliminate the channel altogether.

Figure 5-124 shows a case of microannulus. Figure 5-124a shows strong to weak casing-bond on the CBL amplitude and weak formation-arrivals on the VDL. This indicates poor acoustic coupling between casing, cement, and formation. The weaker the formation signal, the more pronounced the microannulus.

Microannulus can be easily differentiated from channeling by:

1. Pressurizing the pipe and rerunning the CBI-VDL. Microannulus conditions are confirmed by strengthened formation signals on the VDL and decreased CBL amplitude indicating better casing-cement acoustic coupling. Typically, channeling will produce little or no improvement in the signal when the casing is pressurized. Figure 5-124b shows a case of stronger formation arrivals indicating the presence of microannulus rather than channeling.

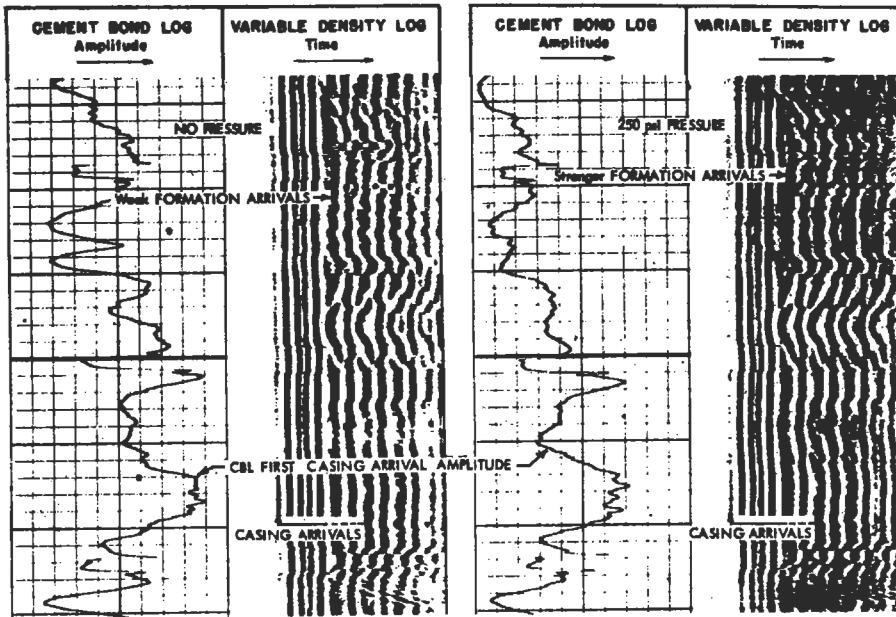


Figure 5-124. CBL-VDL log showing effects of microannulus and the change in signal strength on VDL in pressured and nonpressured pipe [220].

2. Microannulus tends to occur over long intervals of the log; channeling is a localized phenomena. This is a result of microannulus being directly related to pipe expansion during cementing operations.

Once the log has been interpreted, remedial measures can be applied as necessary.

Multifingered Calliper Logs. These logs incorporate up to 64 feelers or scratchers to examine pipe conditions inside the casing. Specifically, they can be combined with other logs to check:

1. Casing collar locations.
2. Corroded sections of pipe.
3. Casing wear.
4. Casing cracks or burstings.
5. Collapsed or crushed casing.
6. Perforations.
7. Miscellaneous breaks.

The number of feelers is a function of pipe diameter; smaller diameter pipe requires fewer feelers on the tool.

Electromagnetic Inspection Logs. This device induces a magnetic field into the casing and measures the returning magnetic flux. In general any disturbance in the flux from readings in normal pipe can be used to find:

1. Casing collars.
2. Areas of corroded pipe.
3. Perforations.
4. Breaks or cracks in the pipe.

This tool only records if corrosion has occurred on the pipe, not whether it is currently taking place. It does give an indication of casing quality and integrity without removing the pipe from the hole. The principle behind this tool is the same as the magna flux device used to detect flaws in metals in a machine shop.

Electrical Potential Logs. Similar in some respects to an SP log, this tool measures the potential gradient of a DC current circulating through a string of casing. This current is applied to provide the casing with cathodic protection thereby preventing casing corrosion; any deviation from a negative field suggests that the pipe is not receiving proper protection and is probably being corroded. Combined with an electromagnetic inspection log, areas currently undergoing corrosion as well as having a relative amount of damage can be determined with ease.

Borehole Televiewers. This tool incorporates an array of transmitters and receivers to scan the inside of the casing. The signals are sent to the surface where they are analyzed and recorded in a format that gives a picture of the inside of the casing. Any irregularities or cracks in the pipe are clearly visible on the log presentation. This allows engineers to fully scan older pipe and get an idea of the kind and extent of damage that might not otherwise be readable from multifinger caliper, electromagnetic inspection, or electrical potential logs. The main drawback to this device is that it must be run in a liquid-filled hole to be effective.

Production Logs. Production logs are those devices used to measure the nature and behavior of fluids in a well during production or injection. A Schlumberger manual [221] summarizes the potential benefits of this information:

1. Early evaluation of completion efficiency.
2. Early detection of disturbances which are not revealed by surface measurements (i.e., thief zones, channeled cement, plugged perforations, etc.).
3. Detailed information on which zones are producing or accepting fluid.
4. More positive monitoring of reservoir production.
5. Positive identification of encroachment, breakthrough, coring, and mechanical leaks.
6. Positive evaluation of injection efficiency.
7. Essential guidance for remedial workover and secondary or tertiary recovery projects.

The reader is referred to the Schlumberger volume [221] on production log interpretation for examples of various cased-hole-log situations. It is still free upon request .

The types of logs run include:

1. Temperature
2. Manometer and gradiomanometer
3. Flow meters
4. Radioactive tracers

Devices that measure water-holdup are also available. These logs can be run singly or in combination on a production combination tool so that a number of parameters may be recorded on the same log sheet.

Temperature Log. A thermometer is used to log temperature anomalies produced by the flow or fluid inside the casing or in the casing annulus. It is used to help determine flowrates and points of fluid entry or exit, and is, perhaps, most useful for finding fluid movement behind the casing.

Injection Wells. Figure 5-125 is the response of the temperature log when fluid is being injected into a reservoir. The sloping portion defines the geothermal gradient the vertical portion defines the zone taking the water and is a function of the geothermal gradient as well as the injection fluid temperature. Below the sloping position, the temperature/curve rapidly returns to normal formation temperature and the geothermal gradient. The vertical portion of the log clearly indicates where the fluid is leaving the casing.

Production Wells. Figure 5-126 is the response of the temperature log when fluid is flowing into a well from perforations in the casing. Three curves are presented. This figure shows that curve response depends on whether the fluid produced is hotter, the same as, or cooler than the geothermal gradient. If the fluid is hotter or cooler, then the entry point is obvious. If the fluid temperature is the same as the geothermal gradient, the change is so subtle that recognition of the entry point may be very difficult. In this case, a high resolution thermometer may be necessary to pinpoint the fluid entry location.

Flow Behind Casing (Annular Flow). Figure 5-127 is a typical response to annular flow down the outside of the casing in a shut-in well. The figure shows water entering the annulus at about 6,500 ft. Perforations are at ~8,500 ft.

In a producing well, the shape of the curve defines the top of the annular space and its relationship to the perforations.

Manometers and Gradiomanometers. Manometers are pressure-sensitive devices used to measure changes in pressure that result from:

1. Leaks in tubing or casing.
2. Fluid inflow through perforations.
3. Gradient measurements in a static mud column.

They are particularly useful for determining pressure opposite a gas-bearing horizon. This value is vital for calculating open-flow potentials in gas wells.

Gradiomanometers are used to check the difference in pressure over a 2-in. interval in a producing well. This is then related to water-holdup in polyphase fluid flow within the casing.

The pressure difference is converted to density and is used to interpret two-phase flow (usually consisting of water as the heavy component and oil as the lighter component). At any given level, the gradiomanometer measures the specific gravity (density) of any fluids entering the borehole. The log reading is related to water holdup and specific gravity by:

$$\rho_{\text{gradiomanometer}} = Y_w \rho_w + (1 - Y_w) \rho_o \quad (5-122)$$

where $\rho_{\text{gradiomanometer}}$ = specific gravity reading of the gradiomanometer, g/cc
 ρ_w = specific gravity of the formation water, g/cc
 ρ_o = specific gravity of the oil being produced with the water, g/cc
 Y_w = water holdup (or holdup of the heavy phase)

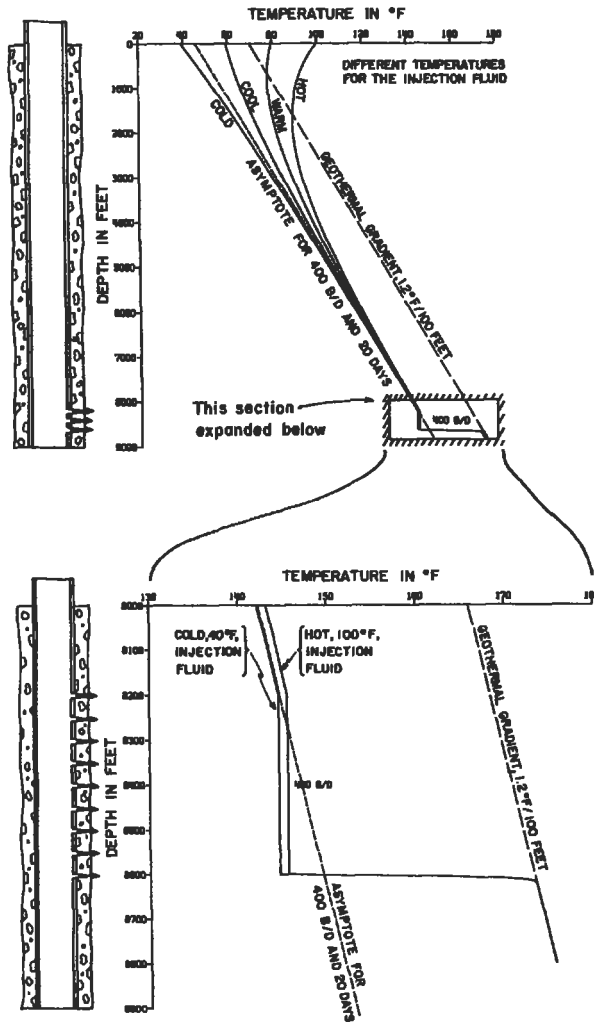


Figure 5-125. The effect of water injection on a temperature log for several injection water temperatures [221].

The specific gravity reading is not exclusively dependent on fluid density. Since the fluids are also flowing while measurements are being made, other terms must be added:

$$\rho_{\text{gradiomanometer}} = \rho_f(1.0 + K + F) \tag{5-123}$$

- where $\rho_{\text{gradiomanometer}}$ = specific gravity reading of the instrument, g/cc
- ρ_f = specific gravity of the fluid in the casing (oil + water + gas), g/cc
- k = a kinetic term
- F = a friction term from fluid flowing around the tool

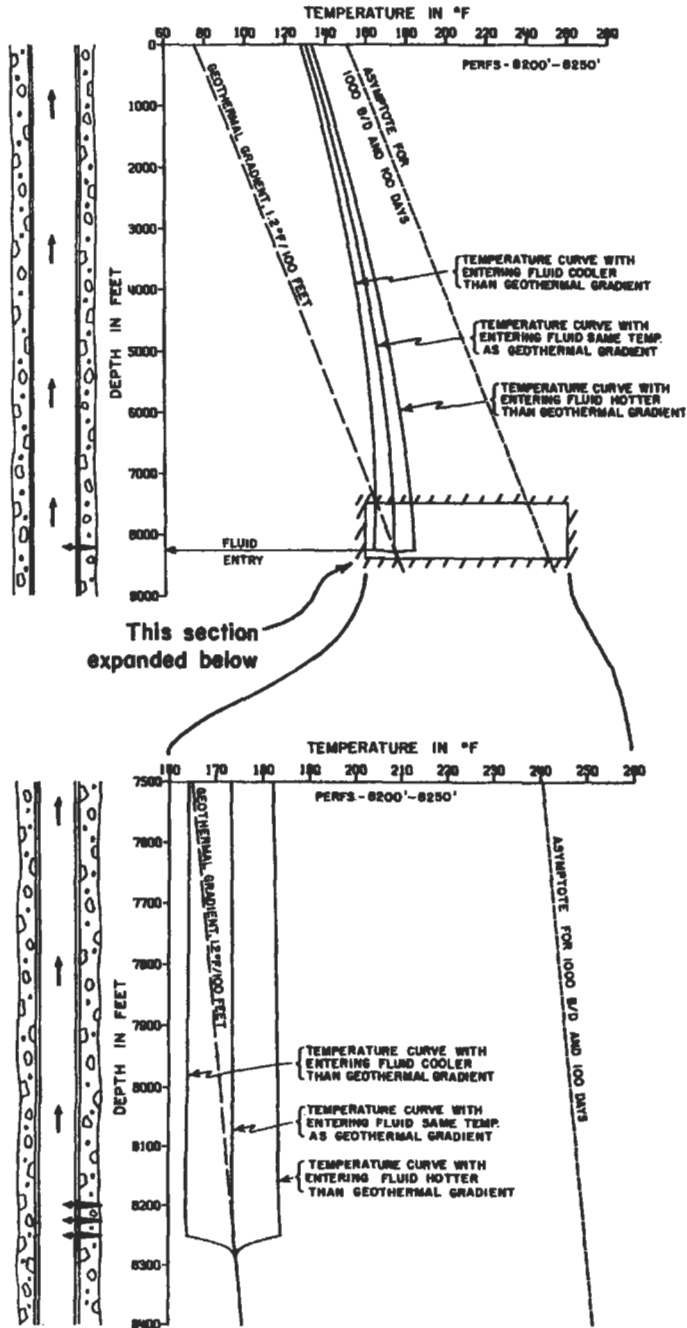


Figure 5-126. Temperature logs in a producing interval for formation fluids with different temperatures [221].

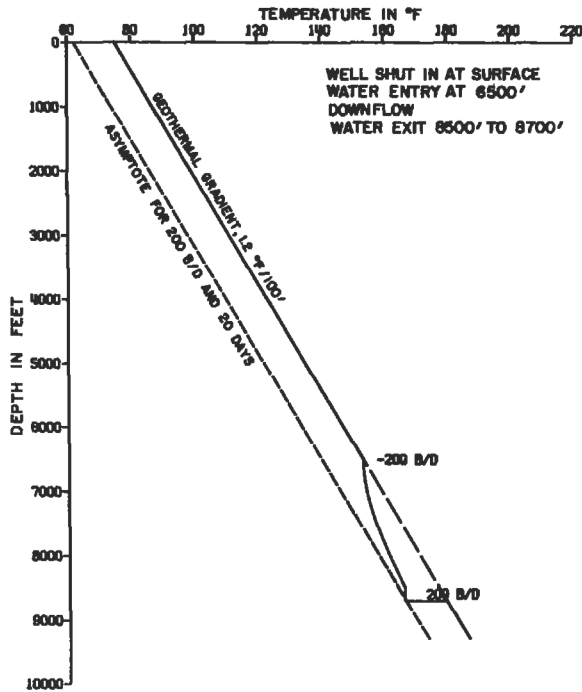


Figure 5-127. Temperature log showing water flow behind the casing. Water is flowing down to the producing interval [221].

At flow rates less than 2,000 bopd, F is negligible and $\rho_{\text{grad}} \approx \rho_f$ [221]. The kinetic term is important when logging from tubing into the casing. Fluid velocity changes become significant at the change in hole diameter. The change causes a sharp pressure increase on the log. The friction term is important at high flow rates in casing and when logging in small-diameter tubing or casing [221].

Another log similar to the gradiomanometer is the water-holdup meter. The main limitation is that it only reads water holdup and cannot be used if water is not present. It has the advantage over the gradiomanometer where sensitivity is required; small differences in density may not be seen by the gradiomanometer.

Flowmeters. Flowmeters are designed to measure fluid flow in the casing. This measurement is then related to volume of fluid being produced. Three types of flowmeters are available:

1. Fullbore-spinner flowmeter.
2. Continuous flowmeter.
3. Packer flowmeter.

Each is used in certain circumstances and is combinable with other devices so that improved flow rates can be obtained.

Fullbore-Spinner Flowmeter. This device measures velocities of fluid moving up the casing. These velocities are then related to volume of fluid moved with

charts available from the various service companies. In general, this tool can be used at flow rates as low as 20 barrels per day in monophasic flow situations (usually water). Polyphase flow raises this minimum to 300 barrels per day if gas is present (i.e., oil and water) in 5 1/2 in. casing. This tool is used in wells with hole diameters ranging from 5 1/2 to 9 5/8 in.

Continuous Flowmeter. This tool is similar to the fullbore-spinner flowmeter except that it can be applied to hole diameters between 3 1/2 in. and 6 3/8 in. It has a higher flow threshold (in barrels per day) and should be restricted to use in monophasic flow situations (i.e., waterfloods, high-flow-rate gas wells, and high-flow-rate oil wells) [221]. It can be combined with a spinner flowmeter for better flow measurements.

Packer Flowmeter. This is a small spinner-flowmeter with an inflatable packer that can be used in small-diameter tubing (1 11/16 to 2 1/8 in.). It has an operable flow range from 10 to 1,900 barrels per day and can be applied in low-flow wells as long as measurements are made in the tubing at a sufficient distance above the perforations. Flow measurements are related to volume of fluid flowing the same way found with the other spinner flowmeters.

Radioactive Tracers. Radioactive tracers are combined with cased hole gamma-ray logs to monitor:

1. Fluid velocities in monophasic fluid flow situations where flow velocity is at or near the threshold for spinner flowmeters.
2. Fluid movement behind the casing or to locate channeling in the cement.

Fluid velocity is measured by velocity-shot analysis. A shot of radioactive fluid is injected into the flow stream above two detectors located on a stationary gamma-ray tool. As the radioactive pulse moves down the hole, the amount of time required to move past the two detectors is measured. This travel time is then related to flow rate in the casing by:

$$q(\text{B/D}) = \frac{\text{spacing}(\text{in.}) \times \frac{1(\text{ft})}{12(\text{in.})} \times \frac{\pi}{4} (d_h - d_{\text{tool}})(\text{in.}^2) \times \frac{1(\text{ft.}^2)}{144(\text{in.}^2)} \times 256.5 \frac{\text{B/D}}{\text{ft}^3/\text{min}}}{\text{time}(\text{sec}) \times \frac{1(\text{min})}{60(\text{sec})}} \quad (5-124)$$

where q is flow rate in barrels per day, the spacing between detectors is in in., the time between detector responses is in seconds, d_h is the hole diameter in in., and d_{tool} is the tool diameter in in.

The main limitation is that slippage and water-holdup factors seriously affect the time reading so this technique cannot be applied in production wells. Moreover, the production of radioactive material is not desirable; therefore, use is mainly restricted to water- or gas-injection wells [221].

Fluid movement behind the casing can be measured with a timed-run radioactive survey. A slug of radioactive fluid is introduced at the bottom of the tubing, and movement is then monitored by successive gamma-ray log runs. Unwanted flow up any channels in the cement can be easily determined and remedial action taken. Again, this technique is mainly applied to water injection wells to monitor flood operations and injection-fluid losses. Figure 5-128 is an example of this type of application.

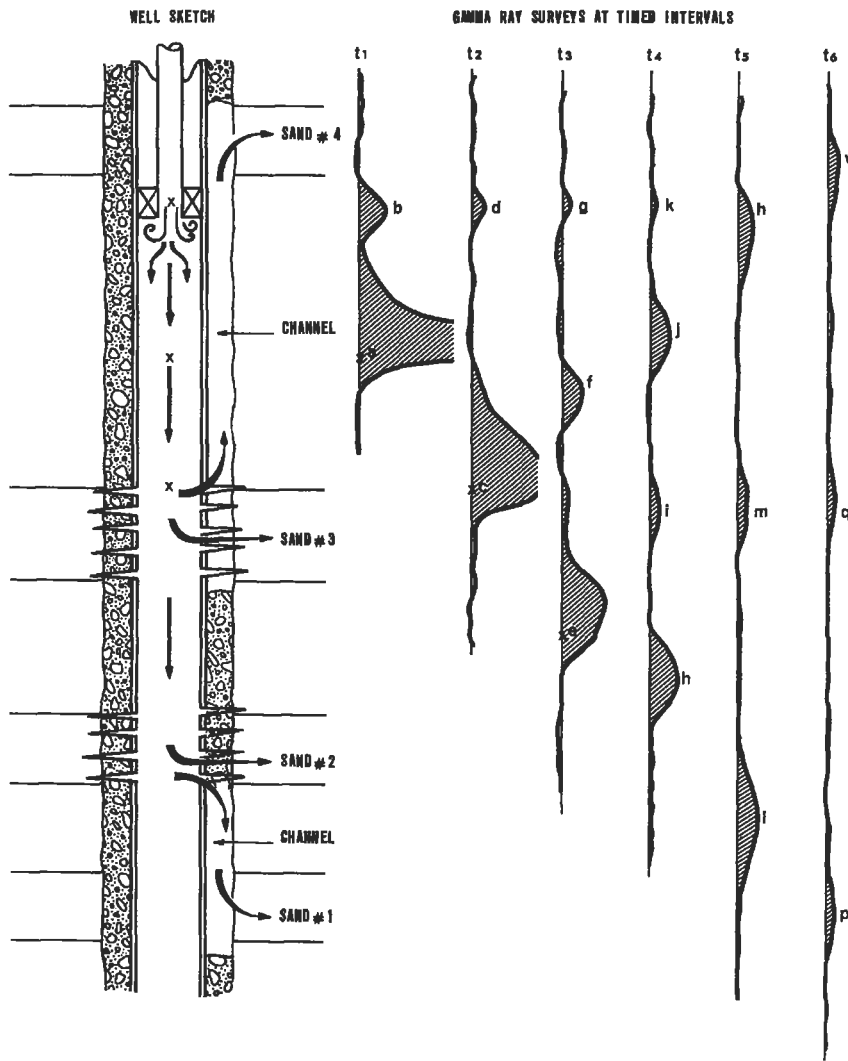


Figure 5-128. Radioactive tracer survey in an injection well where water is flowing behind the casing into another zone [221].

Determination of Initial Oil & Gas In Place

Initial Oil in Place

For undersaturated crude, the reservoir contains only connate water and oil with their respective solution gas contents. The initial or original oil in place can be estimated from the volumetric equation:

$$N = \frac{7,758 V_b \phi (S_{oi})}{B_{oi}} = \frac{7,758 A h \phi (1 - S_{wi})}{B_{oi}} \quad (5-125)$$

The constant 7,758 is the number of barrels in each acre-ft, V_b is bulk volume in acre-ft, ϕ is the porosity, (ϕV_b is pore volume), S_{oi} is the initial oil saturation, B_{oi} is the initial oil formation volume factor in reservoir barrels per stock tank barrel, A is area in ft², h is reservoir thickness in ft, and S_{wi} is the initial water saturation.

In addition to the uncertainty in determining the initial water saturation, the primary difficulty encountered in using the volumetric equation is assigning the appropriate porosity-feet, particularly in thick reservoirs with numerous non-productive intervals. One method is to prepare contour maps of porosity-feet that are then used to obtain areal extent. Another method is to prepare isopach maps of thickness and porosity from which average values of each can be obtained. Since recovery of the initial oil can only occur from permeable zones, a permeability cutoff is used to obtain the net reservoir thickness. Intervals with permeabilities lower than the cutoff value are assumed to be nonproductive. The absolute value of the cutoff will depend on the average or maximum permeability, and can depend on the relationship between permeability and water saturation. A correlation between porosity and permeability is often used to determine a porosity cutoff. In cases in which reservoir cores have been analyzed, the net pay can be obtained directly from the permeability data. When only logs are available, permeability will not be known; therefore a porosity cutoff is used to select net pay. These procedures can be acceptable when a definite relationship exists between porosity and permeability. However, in very heterogeneous reservoirs (such as some carbonates), estimates of initial oil in place can be in error. A technique [222] has been proposed in which actual pay was defined using all core samples above a specific permeability cutoff and apparent pay was defined using all core samples above a specific porosity cutoff; the relationship between these values was used to find a porosity cutoff.

Initial Gas In Place

For the foregoing case of an undersaturated oil (at the bubble point with no free gas), the gas in solution with the oil is:

$$G = \frac{7,758Ah\phi(1 - S_{wi})R_s}{B_{oi}} \quad (5-126)$$

where G is the initial gas in solution in standard cubic feet (scf), R_s is gas solubility in the oil or solution gas-oil ratio (dimensionless), and the other terms are as defined in Equation 5-125.

Free Gas In Place

Free gas within a reservoir or a gas cap when no residual oil is present can be estimated:

$$G = \frac{7,758V_g\phi(1 - S_{wi})}{B_{gi}} \quad (5-127)$$

where 7,758 is the number of barrels per acre-ft, V_g is the pore volume assigned to the gas-saturated portion of the reservoir in acre-ft, B_{gi} is the initial gas formation volume factor in RB/scf, and the other terms are as already defined. (Note: If the formation volume factor is expressed in ft³/scf, 7,758 should be replaced with 43,560 ft³/acre-ft.)

Productivity Index

The productivity index, J , is a measure of the ability of a well to produce hydrocarbon liquids:

$$J_o = \frac{q_o}{p_e - p_{wf}} \quad (5-128)$$

where q_o is the flow rate of oil in stock-tank barrels of oil per day, p_e is the external pressure in psi, p_{wf} is the flowing bottomhole pressure in psi, and the quantity $(p_e - p_{wf})$ is referred to as the pressure drawdown. Because the flow rate in this case is in STB/D, the oil productivity index (J_o) has units of STB/D/psi. Since only q and p_{wf} can be measured directly, p_e is commonly replaced with \bar{p} which can be determined from pressure transient testing.

After the well has been shut in for a period of time (usually at least 24 to 72 hours or longer depending on reservoir characteristics), the well is put on production at a low rate with a small choke. The rate of production is recorded as a function of flow time. When the production rate has stabilized, the flow rate is increased by increasing the choke, and flow rate is monitored with time. This process is repeated until a series of measurements has been recorded [19].

In order to attain a stabilized productivity index, a minimum time is required after each individual flow-rate change. This time can be approximated by two equations [66,197]:

$$t_s \cong \frac{380\phi\mu c_t A}{k} \quad (5-129)$$

$$t_s \cong \frac{0.04\phi\mu c_t r_e^2}{k} \quad (5-130)$$

where t_s is the stabilization time in hours, k is the permeability in md, ϕ is the porosity as a fraction, μ is viscosity in cp, c_t is total compressibility in psi^{-1} , A is area in ft^2 , and r_e is the external radius in feet which should be based on the distance to the farthest drainage boundary for the well. For large systems or reservoirs with low permeability, very long stabilization times may be required.

Equation 5-128 assumes that productivity index does not change with flow rate or time, and in some wells the flow rate will remain proportional to the pressure drawdown over a wide range of flow rates. However, in many wells, the direct relationship is not linear at high flow rates as shown in Figure 5-129. The causes for the deviation in the straight-line behavior can include insufficient producing times at each rate, an increase in gas saturation near the wellbore caused by the pressure drop in that region, a decrease in permeability of oil due to the presence of gas, a reduction in permeability due to changes in formation compressibility, an increase in oil viscosity with pressure drop below the bubble point, and possible turbulence at high rates of flow.

A plot of oil production rate versus bottomhole pressure, termed the inflow performance relationship (IPR), was proposed as a method of analysis of flowing and gas-lift wells [223]. Vogel [224] calculated dimensionless IPR curves for solution gas reservoirs that covered a wide range of oil PVT and relative permeability characteristics. From computer simulations, Vogel [224] showed that

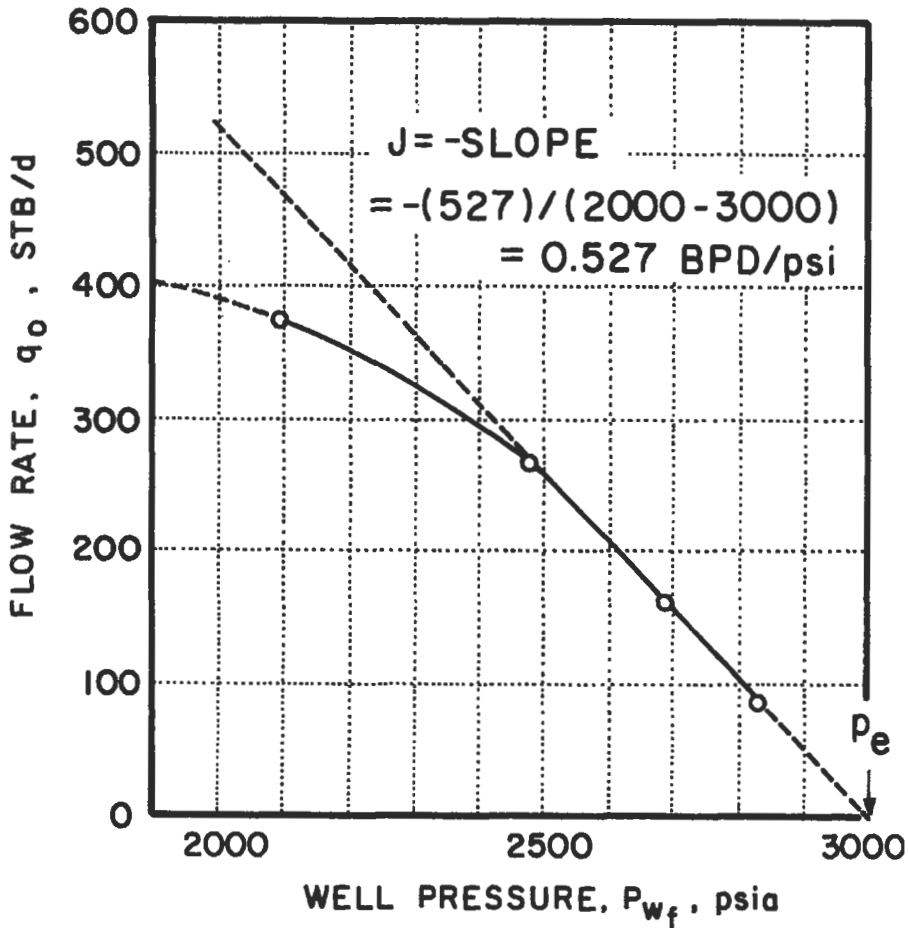


Figure 5-129. Productivity index [197].

any solution gas drive reservoir operating below the bubble point could be represented as shown by Figure 5-130 or by the following relationship:

$$\frac{q_o}{(q_o)_{\max}} = 1 - 0.2 \frac{P_{wf}}{\bar{p}} - 0.8 \left(\frac{P_{wf}}{\bar{p}} \right)^2 \tag{5-131}$$

where q_o is the oil flow rate in STB/D occurring at bottomhole pressure P_{wf} , $(q_o)_{\max}$ is the maximum oil flow rate in STB/D, P_{wf} is the flowing bottomhole pressure, and \bar{p} is the average reservoir pressure. From the well pressure and average reservoir pressure, the ratio of producing rate to maximum oil rate can be obtained; then from the measured production rate, the maximum oil production can be calculated.

Vogel's method handles the problem of a single well test when the permeability near a wellbore is the same as the permeability throughout the

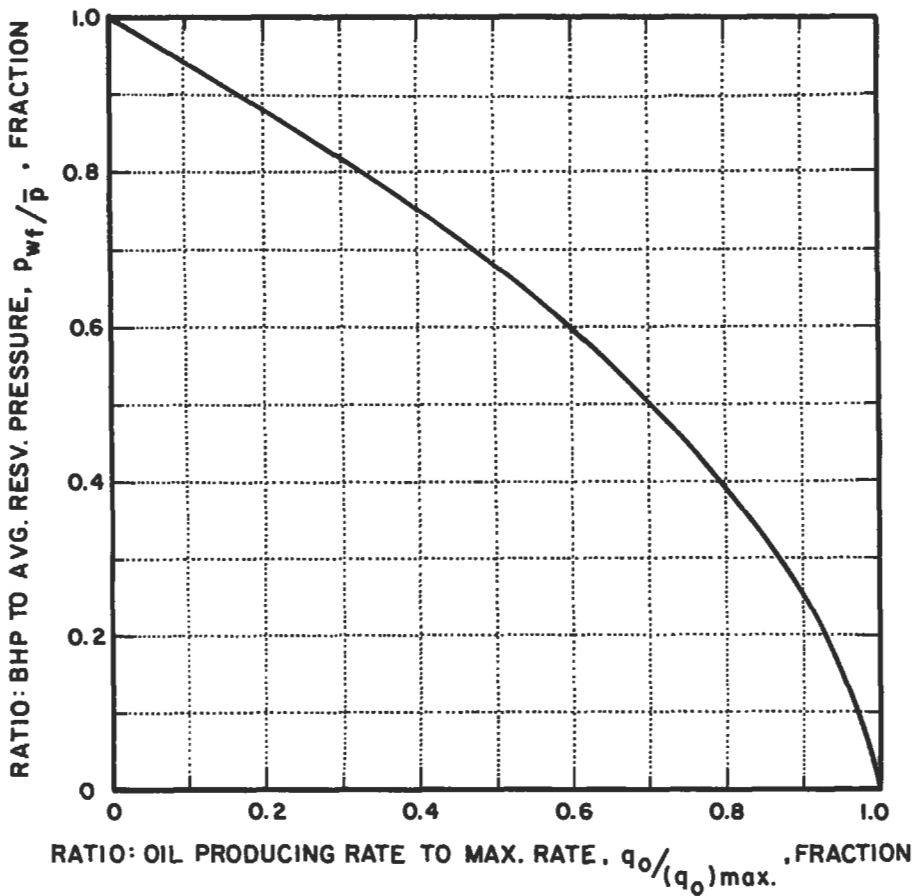


Figure 5-130. Vogel IPR curve [224].

reservoir. When a zone of altered permeability exists near the wellbore, the degree of damage (or improvement) is expressed in terms of a "skin effect" or "skin factor." (Skin effect will be discussed in more detail later.) A modification to Vogel's IPR curves has been proposed by Standing [225] for situations when a skin effect is present (see Figure 5-131). In this figure, Standing has provided a series of IPR curves for flow efficiencies between 0.5 and 1.5, where flow efficiency (FE) is defined as:

$$FE = \frac{\bar{p} - p_{wf} - \Delta p_s}{\bar{p} - p_{wf}} \quad (5-132)$$

where \bar{p} is the average reservoir pressure, p_{wf} is the flowing bottomhole pressure, and Δp_s is the pressure drop in the skin region. Thus, the Vogel curve is for a flow efficiency of 1.0.

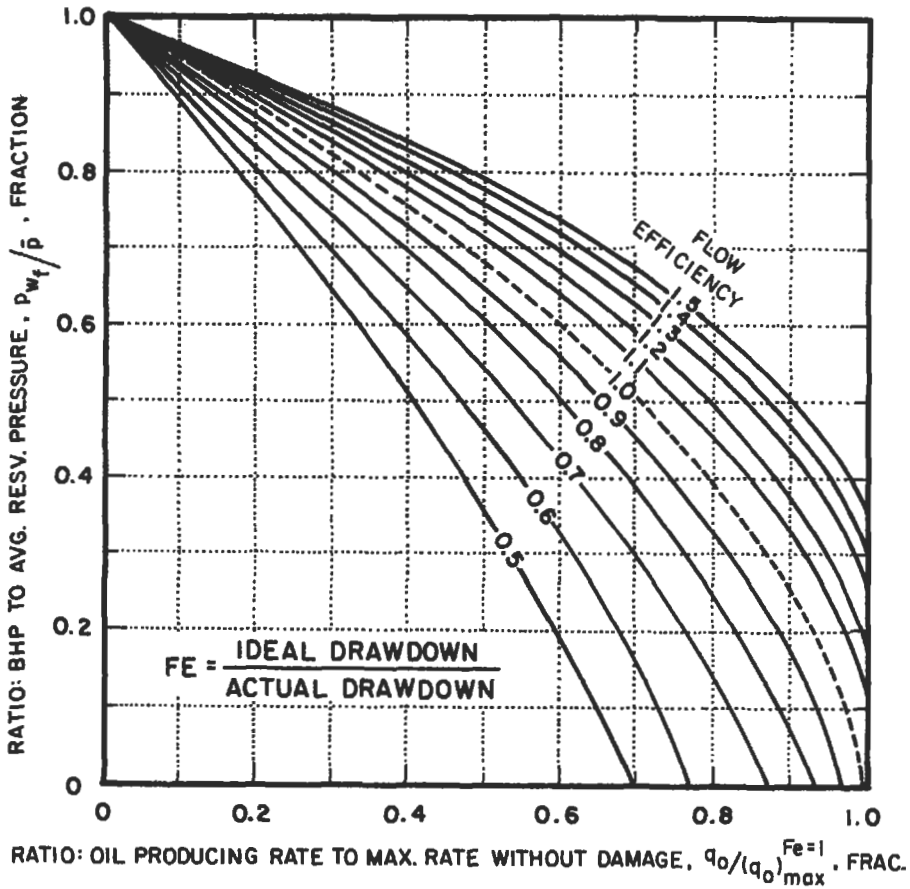


Figure 5-131. Standing's modification to IPR curves [225].

For reservoir systems operating below the bubble point when fluid properties and relative permeabilities vary with distance from the wellbore, Fetkovich [226] has proposed an empirical equation which combines single-phase and two-phase flow:

$$q_o = J'_o (p_b^2 - p_{wf}^2)^n + J_o (p_e - p_b) \tag{5-133}$$

where p_b is the bubble-point pressure in psia, \bar{p} may be substituted for p_e , J'_o is a form of productivity index and n is an exponent; both J'_o and n are determined from individual well multirate and pressure tests, or isochronal tests. For cases where the data required by the Fetkovich procedure are not available, a method for shifting the axes of the Vogel plot has been proposed [227]. In this latter method, only one set of production test data (rate and bottomhole flowing pressure) together with the shut-in bottomhole pressure (or average reservoir pressure) and bubble-point pressure are required to construct a reliable IPR.

PRESSURE TRANSIENT TESTING OF OIL AND GAS WELLS

Production rates depend on the effectiveness of the well completion (skin effect), the reservoir permeability, the reservoir pressure, and the drainage area. Pressure transient analysis is a powerful tool for determining the reservoir characteristics required to forecast production rates. Transient pressure data are generated by changing the producing rate and observing the change in pressure with time. The transient period should not exceed 10% of the previous flow or shut-in period. There are a number of methods to generate the transient data available to the reservoir engineer.

Single-well tests such as buildup, falloff, drawdown, injection, and variable-rate describe the isotropic reservoir adjacent to the test well while multiple well tests such as long term interference or short term pulse describe the characteristics between wells. Buildup and falloff tests are most popular because the zero flow rate is readily held constant. Drawdown and injection tests are run less frequently due to problems with maintaining a constant rate. Variable rate tests are useful when wellbore storage is a problem. Multiwell testing for characterizing anisotropic reservoirs has been popularized by the increased use of sophisticated simulation software.

Definitions and Concepts

Several excellent references on well test analyses are available [13,66,228], and a good discussion of difficulties in interpretation of data is available in a recent text [197]. From information in these references several definitions will be given, and the basic concepts of well test analysis will be summarized. More advanced concepts can be found in the foregoing references or in the extensive literature on this subject that has appeared in recent years.

Definitions

Transient Region. Flow regimes that occur at different flow times are shown in Figure 5-132 for a well flowing at a constant rate. The flowing bottomhole pressure is shown as a function of time on both linear and semilog plots. In the transient region, the reservoir is infinite-acting, and the flowing bottomhole pressure is a linear function of $\log \Delta t$. This region is amenable to analysis by transient methods, and occurs for radial flow at flow times up to approximately $t = \phi \mu c r_e^2 / 0.00264k$, where field units are used: t is time in hours, ϕ is porosity as a fraction, μ is viscosity in cp, c is compressibility in psi^{-1} , r_e is the external radius in ft, and k is permeability in md [13].

Late-Transient Region. At the end of the transient region and prior to the semisteady-state period, there is a transitional period called the late-transient region (see Figure 5-132). There are no simple equations that define this region, but the late-transient period may be very small or practically nonexistent.

Semisteady-State Region. If there is no flow across the drainage boundary and compressibility is small and constant, a semisteady- or pseudosteady-state region is observed in which the pressure declines linearly with time (see Figure 5-132). Pressures in the drainage area decrease by the same amount in a given time, and the difference between reservoir pressure and wellbore pressure remains constant during this period. For radial flow, semisteady-state flow conditions

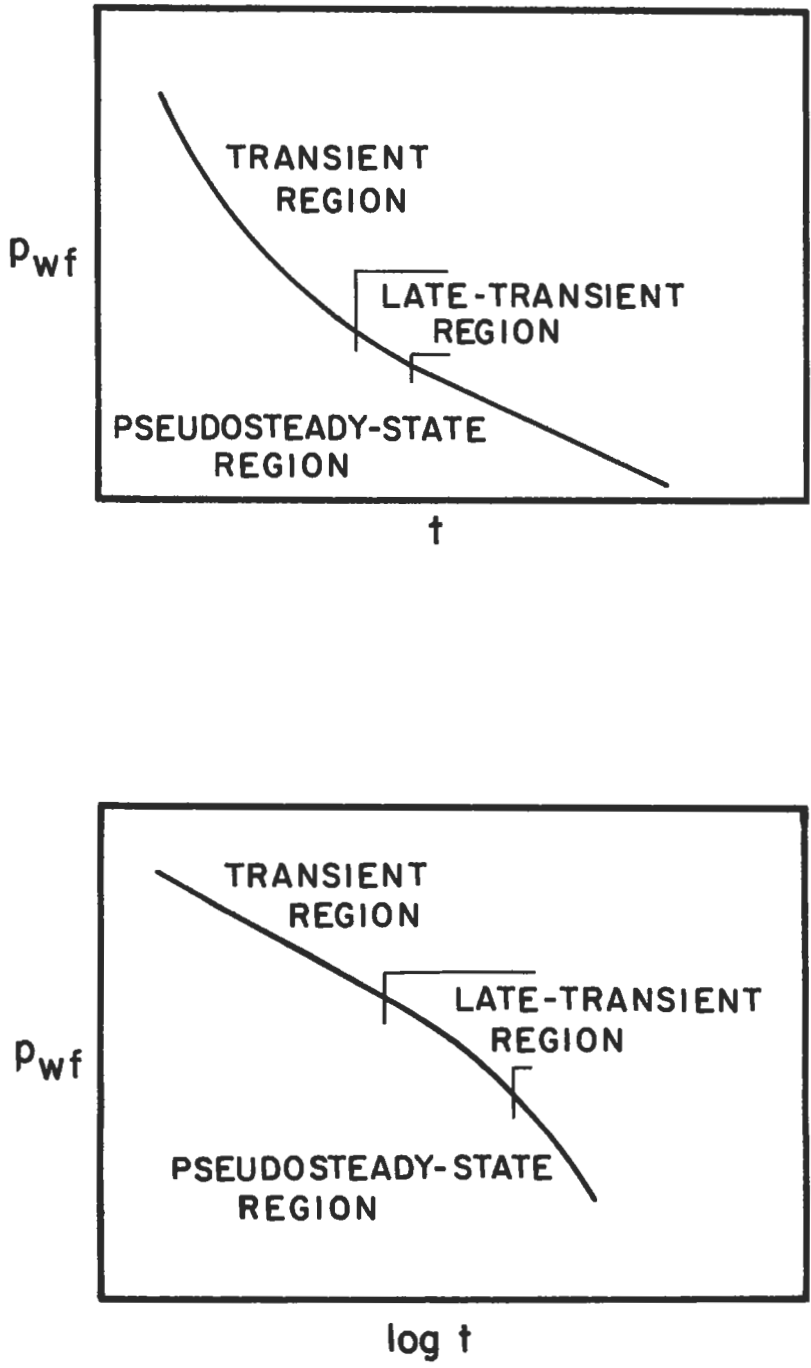


Figure 5-132. Flow regimes [13,228].

start at a flow time of about $t = \phi\mu cr_e^2/0.00088k$, in field units as already specified [13]. This region is suitable for reservoir limit tests in which reservoir size and distance to boundaries can be estimated. The most useful test to estimate reservoir limits is the drawdown test [197]; interpretation of reservoir limit tests can be difficult as discussed in the literature [197].

Steady-State Flow. At a constant flow rate for steady-state flow, the pressure at every point in the reservoir will remain constant with time. This condition is rarely encountered in most well test analyses; steady-state flow may be approached in reservoirs with strong water drives or in cases where reservoir pressure is maintained by gas injection or waterflooding.

Buildup Tests. Pressure buildup tests are conducted by: (1) producing an oil or gas well at a constant rate for sufficient time to establish a stabilized pressure distribution, (2) ceasing production by shutting in the well, and (3) recording the resulting increase in pressure. In most cases, the well is shut in at the surface and the pressure is recorded downhole. In pumping wells, buildup tests can be made by: (1) pulling the rods and running a pressure bomb in the tubing, (2) by measuring pressure in the annulus from sonic measurements obtained with an echo-device, or (3) occasionally by using surface-indicating gauges. The pressure buildup curve is analyzed for wellbore conditions such as damage or stimulation and for reservoir properties such as formation permeability, pressure in the drainage area, reservoir limits or boundaries, and reservoir heterogeneities.

Drawdown Tests. Pressure drawdown tests are conducted by: (1) having an oil or gas well shut in for sufficient time to establish a stabilized pressure distribution, (2) putting the well on production at a constant rate, and (3) recording the resulting decrease in bottomhole pressure. An ideal time to run a drawdown test is when the well is initially put on production because in addition to obtaining information on wellbore conditions and formation permeability, estimates of reservoir volume can be made also. A long, constant flow rate is required.

Falloff Tests. Pressure falloff tests are conducted in injection wells and are analogous to the pressure buildup tests in producers. A falloff test consists of: (1) injecting fluid at a constant rate, (2) shutting in the well, and (3) recording the decrease in pressure. As long as the mobility ratio between the injected fluid and in-situ fluids is near unity, the analysis of pressure transient tests in injection wells is relatively simple. The equations used in producing well tests are applicable with the exception that the flow is taken to be negative for injection whereas flow is positive for production.

Multiple-Rate Tests. The preceding tests apply to conditions in which the flow rate either has been or is constant. In some cases, maintaining a constant flow rate may not be possible or practical. In other cases, regulatory agencies may require that wells, especially gas wells, be tested at various flow rates. Multiple-rate tests may be conducted at variable flow rates or a series of constant rates, and are applicable to buildup or drawdown tests in producers or falloff tests in injectors. If accurate flow rate and pressure data are obtained, information on permeability, skin, and reservoir pressure can be deduced.

Interference Tests. In the prior tests, the pressure and flow rate applied to only one well at a time. With interference tests, two wells are involved. Inter-

ference tests are conducted by producing from or injecting into at least one well and observing the pressure response in at least one shut-in observation well. A change in rate (pressure) at the active producer or injector will cause a pressure interference at the observation well. A special form of multiple-rate testing is the pulse test in which the pressure caused by alternating periods of production (or injection) and shut-in periods is monitored at one or more observation wells. Multiple-rate tests are used to determine if wells are in communication with each other in the same reservoir as well as to provide estimates of formation permeability and the product of porosity and total compressibility.

Miller-Dyes-Hutchinson (MDH) Plot. One of the most useful methods of pressure test analysis is that of Miller, Dyes, and Hutchinson [229]. The MDH method is a plot of bottomhole pressure versus log time on semilog paper. A schematic of an MDH plot for a pressure buildup test is depicted in Figure 5-133; the region is identified where MDH and Horner plots are applicable.

Horner Plot. In the Horner plot [230] bottomhole pressure is plotted against $\log(t + \Delta t)/\Delta t$. The Horner method should be applied only to infinite-acting reservoirs; for radial flow, the Horner plot will be a straight line. Several

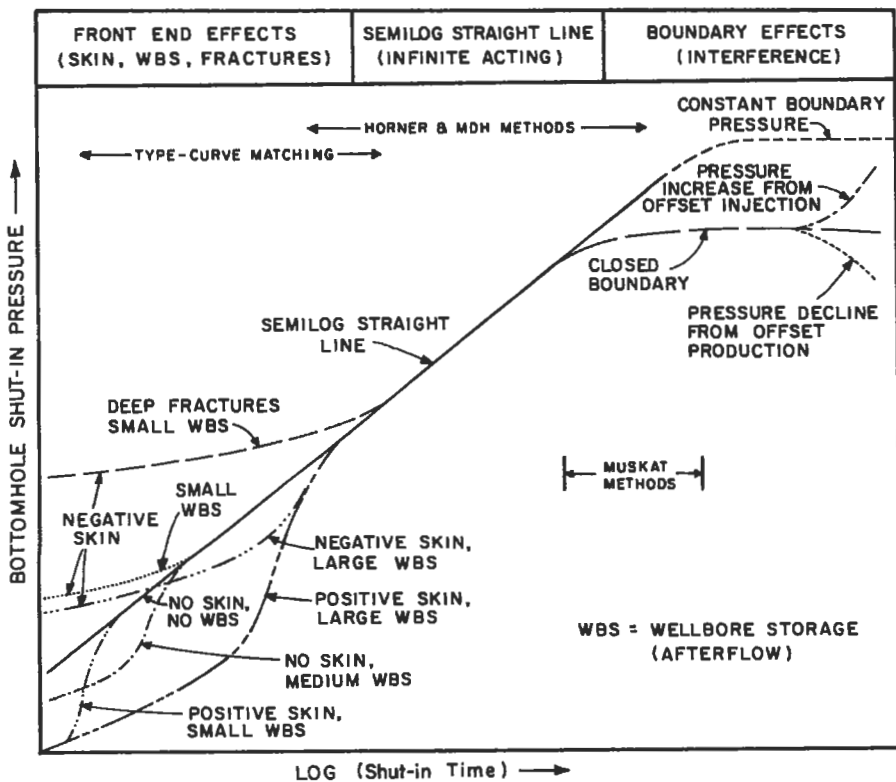


Figure 5-133. MDH plot [66].

conditions such as boundaries or changes in fluids or fluid properties, can cause the Horner plot to deviate from a straight line (see Figures 5-134 and 5-135).

Skin Factor. The skin effect refers to a zone of altered formation permeability near a wellbore as a result of drilling, completion, or stimulation [231,232]. The extent of altered permeability is expressed in terms of a skin factor, s , which is positive for damage and negative for improvement. Skin factor can range from about -5 for a hydraulically fractured well to a theoretical limit of infinity for

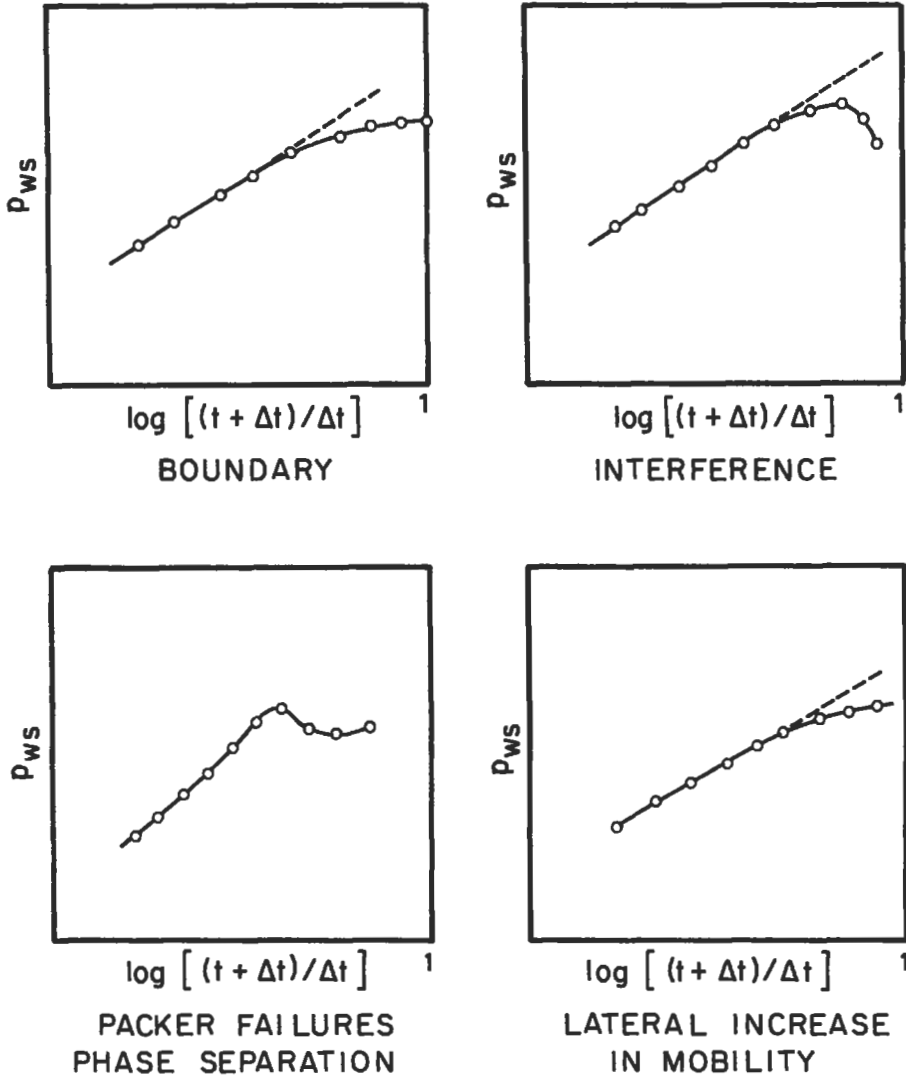


Figure 5-134. Downtrending Horner plots [13,180].

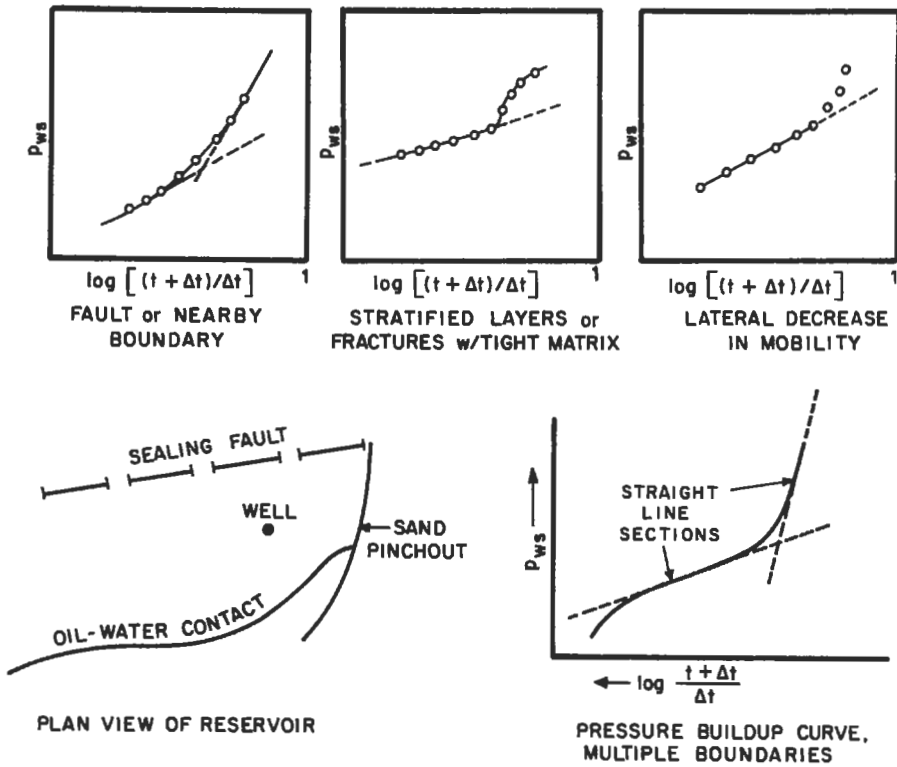


Figure 5-135. Uptrending Horner plots [13,180].

a severely damaged or plugged well. A schematic diagram of the pressure distribution near the wellbore of a damaged well is given in Figure 5-136. Effects of positive and negative skin are shown for the MDH plot in Figure 5-133.

Wellbore Storage. Wellbore storage, also referred to as afterflow, wellbore loading or unloading, afterproduction, and afterinjection, will affect short-time transient pressure behavior. This phenomenon has more of an effect on pressure buildup than drawdown tests, and can be especially important in low-permeability formations or in gas wells. During a buildup test, a well is closed in at the surface, but fluid may continue to flow into the wellbore for some time which causes a lag in the buildup at early times. Various levels of wellbore storage are shown in the MDH buildup plot in Figure 5-133. Storage can obscure the transient period thus negating the value of a semilog plot.

Concepts

Most techniques used in the analysis of transient tests assume a single well operating at a constant flow rate in an infinite reservoir. At early times, a well transient is like a single well in an infinite reservoir, but at late times, effects of other wells aquifers, or reservoir boundaries can cause the pressure behavior to deviate from the infinite-acting assumption. Other common assumptions

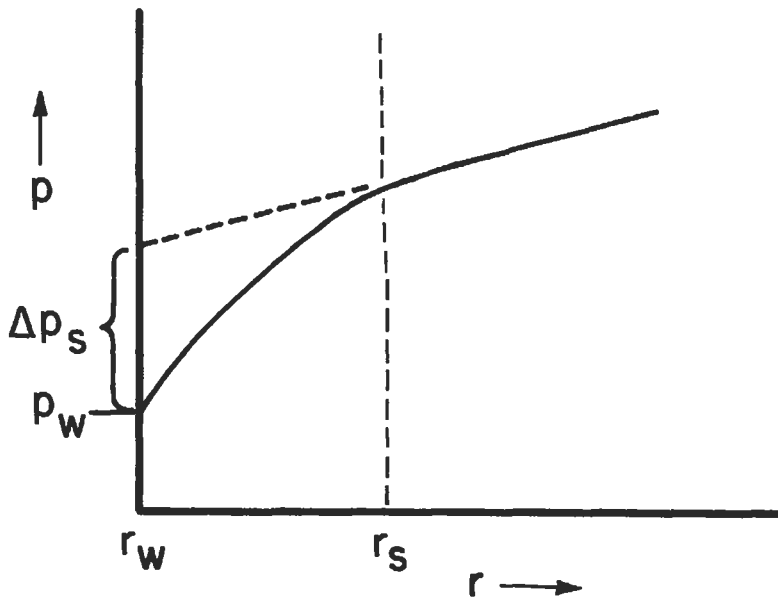


Figure 5-136. Skin region [228].

include: horizontal flow, negligible gravity effects, a single fluid of small and constant compressibility, a homogeneous and isotropic porous medium, the Darcy equation is obeyed, and several parameters (including porosity, permeability, viscosity, and compressibility) are independent of pressure.

Pressure transients arriving at the well following a rate change move through three regions on their way to the wellbore. Nearest the wellbore is the early-time region, ETR, where storage and skin effects dominate; next is the middle-time region, MTR, where the formation permeability is determined, and most distant is the late-time region, LTR, where drainage boundaries are sometimes observed (see Figure 5-137a for examples of a buildup test and Figure 5-137b for a drawdown test) [228]. As discussed earlier, the transient flow region (see Figure 5-132) is amenable to analysis by transient flow methods; this region consists of both the ETR and the MTR. The LTR can include the late-transient and the pseudosteady-state or semisteady-state regions. The crux of the analysis involves selecting the proper data to analyze.

Middle-time data will plot as a straight line on semilogarithmic paper. The slope and the intercept of the MTR straight line are used to calculate reservoir permeability, skin factor, and average reservoir pressure. Semilogarithmic straight lines can occur in the ETR and the use of their slopes and intercepts results in unrealistic reservoir characteristics. Typically, improper use of injection well ETR data indicates a tight, fractured reservoir while use of producing well ETR data indicates damaged permeable rock when that is not at all the case.

Flow conditions in the pseudosteady-state LTR occur when transients reach the no-flow drainage boundary during producing-well transient-tests. Flow conditions in the steady-state LTR occur when transients reach the constant pressure boundary in secondary recovery operations. The slope of a Cartesian

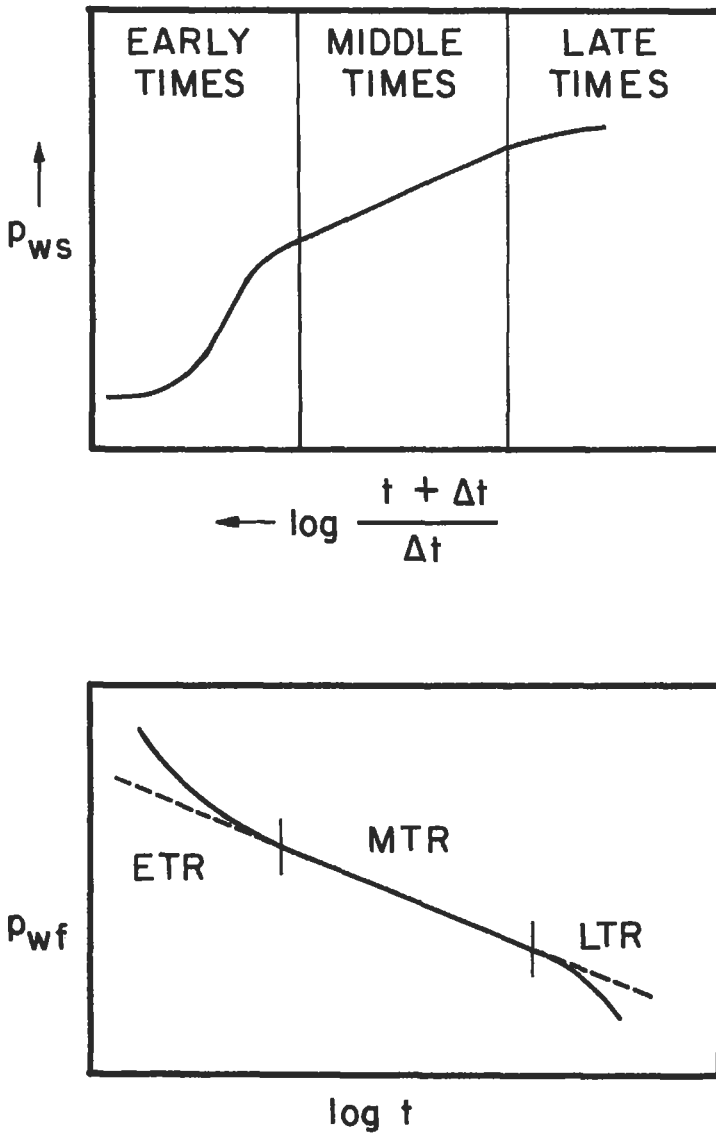


Figure 5-137. Early-, middle-, and late-time regions [228].

plot of an LTR drawdown can be useful in determining reservoir limits. Care should be taken to ensure that LTR data are not included in the MTR analysis.

The ETR region is dominated by skin and storage effects close to the wellbore. Storage effects occur when surface and sandface flow rates are unequal such as an injection well that goes on vacuum when shut in or a gas well where gas compresses in the tubing due to afterflow following surface shut in. Conventional pressure transient analysis is dependent on a constant sandface flow rate during

the test period and since zero is an easy constant flow rate to maintain, wellbore storage is a frequent problem. The length of the storage period is increased by skin damage since damage acts as an area of reduced permeability around the wellbore.

A logarithmic plot of the change in pressure, $p_i - p_{wf}$ versus the test time, dT , provides a practical means of determining the end of the ETR and the beginning of the MTR semilogarithmic straight line. A logarithmic plot with a unit-slope line (a line with 45° slope) indicates storage effects. The proper MTR semilogarithmic straight line begins at 50 times the end of the unit slope, that is, wellbore storage effects cease at about one and a half log cycles after the disappearance of the unit-slope line.

A logarithmic plot that exhibits a half-slope line (a line with a slope of 26.6°) indicates a fractured wellbore. The proper straight line begins at 10 times the end of the half-slope line if the fractures are unproped. Pressure drop at the start of the straight line is twice that at the end of the unit-slope line. Injection wells, acid jobs, or naturally fractured reservoirs are typical examples of the uniform flux, unproped fractures.

A well that has short, propped (infinite capacity) hydraulically induced fractures will exhibit the proper straight line at 100 times the end of the half-slope line. The pressure drop will be about 5 times that at the end of the half-slope line.

Hydraulically stimulated wells in tight formations (<0.01 md) with long (finite conductivity) fractures never exhibit the proper straight line during a conventional transient test time period. As a practical matter, all production from tight gas wells occurs during the ETR. Type curves or computer simulation are required to successfully analyze this type of ETR data. The ETR can range to hundreds of years in tight gas wells with finite-conductivity fractures.

Use of the logarithmic data plot to determine the start of the semilogarithmic straight line of course means that the ETR data must be recorded. Pressure changes need to be monitored by the minute and bottomhole pressure at the time of shut-in must be precisely determined. Occasionally a great deal of emphasis is placed on the accuracy of the pressure-measuring equipment when the emphasis should be on the clock.

A problem in determining the initial pressure frequently arises when pressure buildup data from pumping wells are analyzed. A Cartesian plot of the early-time bottomhole pressure versus shut-in time should result in a straight line with the proper initial pressure at the intercept.

Important Pressure Transient Analysis Equations

$$\text{permeability, } k = 162.6 \frac{q\mu B}{mh}, \text{ md} \quad (5-134)$$

$$\text{radius of investigation, } r_i = \left[\frac{kt}{948\phi\mu C_t} \right]^{1/2}, \text{ ft} \quad (5-135)$$

$$\text{skin factor (buildup), } s = 1.151 \left[\frac{p_{1hr} - p_{wf}}{m} - \log \left(\frac{k}{\phi\mu C_t r_w^2} \right) + 3.23 \right] \quad (5-136)$$

$$\text{skin factor (drawdown), } s = 1.151 \left[\frac{p_i - p_{1hr}}{m} - \log \left(\frac{k}{\phi \mu C_r r_w^2} \right) + 3.23 \right] \quad (5-137)$$

$$\text{pressure drop due to skin, } (\Delta p)_s = 0.869 ms \quad (5-138)$$

$$\text{average drainage area pressure, } \bar{p} = p_{wf} + \frac{141.2q\mu B \left(\ln \frac{r_e}{r_w} - \frac{3}{4} - s \right)}{kh} \quad (5-139)$$

$$\text{average pressure (steady - state), } \bar{p} = p_{wf} + \frac{141.2q\mu B \left(\ln \frac{r_e}{r_w} - \frac{1}{2} - s \right)}{kh} \quad (5-140)$$

$$\text{flow efficiency, } FE = \frac{\bar{p} - p_{wf} - \Delta p_s}{\bar{p} - p_{wf}} \quad (5-132)$$

For these equations, the following nomenclature is applicable:

rate	q, B/D
time	t, hr
formation volume factor	B, RB/STB
viscosity	μ , cp
thickness	h, ft
porosity	ϕ , fraction
total compressibility	c_t , psi ⁻¹
external drainage radius	r_e , ft
wellbore radius	r_w , ft
semilogarithmic MTR slope	m, psi/cycle
initial reservoir pressure	p_i , psi
flowing bottomhole pressure	p_{wf} , psi
shut-in bottomhole pressure	p_{ws} , psi
pressure drop across skin region	Δp_s , psi
MTR semilog intercept	p_{1hr} , psi

In the equation for skin factor during the pressure buildup, p_{ws} is measured just before shutting in the well, and p_{1hr} is obtained from the straight-line portion (extrapolated if necessary) of the buildup curve one hour after shut-in (see Figure 5-138a). Similarly, the straight-line portion of the drawdown data must be extrapolated to one hour if the data do not fall on the semilog straight-line (see Figure 5-138b).

Type-Curves

While at least one author [197] questions the uniqueness of pressure-transient type-curves and others [66,180] state that type-curves should only be used when conventional techniques cannot be used, curve-matching techniques have recently received more widespread use. In some cases where conventional analyses fail

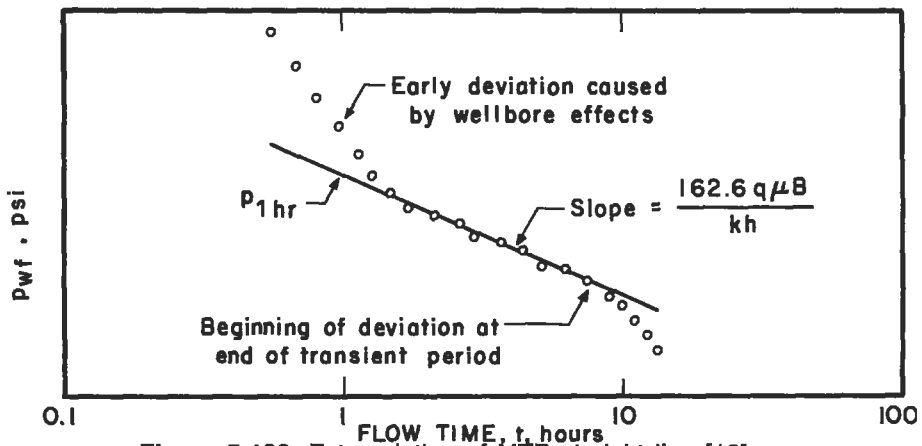
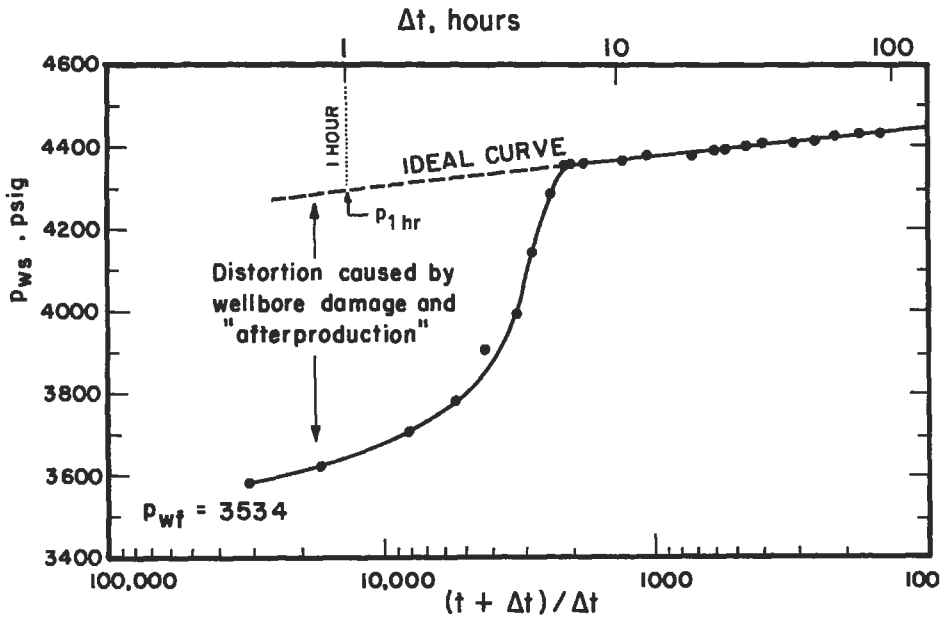


Figure 5-138. Extrapolation of MTR straight line [13].

such as when wellbore storage distorts most or all of the data, type-curves may be the only means of interpretation of the pressure data. Type-curves developed by Ramey et al. [233-235] and McKinley [236,237] for pressure buildup and constant-rate drawdown tests and by Gringarten [238] for vertically fractured wells are discussed in a recent monograph [228] Type-curves are used to estimate formation permeability, damage, and stimulation of the tested well as well as to identify the portion of the data that should be analyzed by conventional techniques. Families of type-curves for various conditions are available from the SPE book order department in Dallas.

MECHANISMS & RECOVERY OF HYDROCARBONS BY NATURAL MEANS

Petroleum Reservoir Definitions [17]

Accumulations of oil and gas occur in underground traps that are formed by structural and/or stratigraphic features. A reservoir is the portion of the trap that contains the oil and/or gas in a hydraulically connected system. Many reservoirs are hydraulically connected to water-bearing rocks or aquifers that provide a source of natural energy to aid in hydrocarbon recovery. Oil and gas may be recovered by: fluid expansion, fluid displacement, gravitational drainage, and/or capillary expulsion. In the case of a reservoir with no aquifer (which is referred to as a volumetric reservoir), hydrocarbon recovery occurs primarily by fluid expansion, which, in the case of oil, may be aided by gravity drainage. If there is water influx or encroachment from the aquifer, recovery occurs mainly by the fluid displacement mechanism which may be aided by gravity drainage or capillary expulsion. In many instances, recovery of hydrocarbon occurs by more than one mechanism.

At initial conditions, hydrocarbon fluids in a reservoir may exist as a single phase or as two phases. The single phase may be a gas phase or a liquid phase in which all of the gas present is dissolved in the oil. When there are hydrocarbons vaporized in the gas phase which are recoverable as liquids at the surface, the reservoir is called gas-condensate, and the produced liquids are referred to as condensates or distillates. For two-phase accumulations, the vapor phase is termed the gas cap and the underlying liquid phase is called the oil zone. In the two-phase case, recovery of hydrocarbons includes the free gas in the gas cap, gas evolving from the oil (dissolved gas), recoverable liquid from the gas cap, and crude oil from the oil zone. If an aquifer or region of high water saturation is present, a transition zone can exist in which the water saturation can vary as a function of vertical depth and formation permeability. Water that exists in the oil- or gas-bearing portion of the reservoir above the transition zone is called connate or interstitial water. All of these factors are important in the evaluation of the hydrocarbon reserves and recovery efficiency.

Natural Gas Reservoirs [17]

For reservoirs where the fluid at all pressures in the reservoir or on the surface is a single gaseous phase, estimates of reserves and recoveries are relatively simple. However, many gas reservoirs produce some hydrocarbon liquid or condensate. In the latter case, recovery calculations for the single-phase case can be modified to include the condensate if the reservoir fluid remains in a single phase at all pressures encountered. However, if the hydrocarbon liquid phase develops in the reservoir, additional methods are necessary to handle these retrograde, gas-condensate reservoirs.

Primary Recovery of Crude Oil

Initial crude oil production often takes place by the expansion of fluids which were trapped under pressure in the rock. The expanding fluids may be gas evolving from the oil, an expanding gas cap, a bottom- or edge-water drive, or a combination of these mechanisms. After the initial pressure in the reservoir falls to a low value, the oil no longer flows to the wellbore, and pumps are installed to lift the crude oil to the surface. This mode of oil production is referred to as primary production. Recovery of oil associated with natural

reservoir energy varies with producing mechanisms that are broadly classified as: solution-gas or depletion drive, gas cap drive, natural water drive, gravity drainage, and compaction drive. In some reservoirs, production can be attributed mainly to one of the mechanisms; in other cases, production may result from more than one mechanism, and this is referred to as a combination drive.

Statistical Analysis of Primary Oil Recovery

Most of the producing mechanisms are sensitive to the rate of oil production; only the solution gas drive mechanism is truly rate-insensitive [180]. Primary recoveries are usually reported [180] to be less than 25% of the original oil in place by solution gas drive, 30% to 50% of OOIP for water drive, and can exceed 75% of OOIP for gravity drainage in thick reservoirs with high vertical permeabilities. For water drive reservoirs, primary recovery efficiency can be low if the initial water saturation is more than 50%, if permeability is low, or if the reservoir is oil-wet [180]. From a recent statistical analysis [239], primary recovery from carbonate reservoirs tends to be lower than for sandstones (see Table 5-29 for recoveries by different drive mechanisms). Since primary recoveries tend to be lower for solution gas drive, these reservoirs are usually better candidates for waterflooding and will represent the bulk of the prospective candidates for enhanced oil recovery.

In the United States, much of the primary production involves solution gas reservoirs. Thus, this mechanism will be emphasized in this chapter, but non-U.S. production may involve other mechanisms. The differences in recovery mechanisms are important if an engineer is to avoid misapplication of methods; this subject has been addressed in Reference 197.

Table 5-29
Primary Recovery Efficiencies

Production mechanism	Lithology	State	Average primary recovery efficiency (% OOIP)
Solution gas drive	Sandstones	California	22
		Louisiana	27
		Oklahoma	19
		Texas 7C, 8, 10	15
		Texas 1-7B, 9	31
		West Virginia	21
		Wyoming	25
Solution gas drive	Carbonates	All	18
Natural water drive	Sandstones	California	36
		Louisiana	60
		Texas	54
		Wyoming	36
Natural water drive	Carbonates	All	44

From Reference 239.

Empirical Estimates of Primary Oil Recovery

Several attempts have been made to correlate primary oil recovery with reservoir parameters [239-242]. Based on field data [241] from water-drive reservoirs, a statistical study [242] yielded the following empirical relationship for primary oil recovery:

$$N_p = (0.2719 \log k + 0.25569S_w + 0.1355 \log \mu_o - 15,380\phi - 0.00035h + 0.11403) \left[7,758Ah\phi \frac{(1-S_w)}{B_{oi}} \right] \quad (5-141)$$

where N_p is oil production in STB, k is permeability in md, S_w is fractional water saturation, μ_o is oil viscosity in cp, ϕ is fractional porosity, h is pay thickness in ft, A is a real extent in ft², and B_{oi} is the initial formation volume factor of oil in reservoir barrels per STB. Based on the first API study [240], correlations were developed for recoverable oil. For solution gas drive reservoirs, the recoverable oil (RO) in stock tank barrels per net acre-ft was:

$$RO = 3,244 \left[\frac{\phi(1-S_w)}{B_{ob}} \right]^{1.1611} \left[\frac{k}{\mu_{ob}} \right]^{0.0979} [S_w]^{0.3722} \left[\frac{P_b}{P_a} \right]^{0.174} \quad (5-142)$$

For water drive reservoirs, the correlation was:

$$RO = 4,259 \left[\frac{\phi(1-S_w)}{B_{oi}} \right]^{1.0422} \left[\frac{k\mu_{wt}}{\mu_{oi}} \right]^{0.0770} [S_w]^{-0.1905} \left[\frac{P_i}{P_a} \right]^{-0.2159} \quad (5-143)$$

In the second API study [239], analysis of 116 solution gas drive reservoirs gave the following equation:

$$RO = 6,533 \left[\frac{\phi(1-S_w)}{B_{ob}} \right]^{1.312} \left[\frac{k}{\mu_{ob}} \right]^{0.0816} [S_w]^{0.465} \left[\frac{P_b - P_a}{P_b} \right]^{0.249} \quad (5-144)$$

However, the second study concluded that none of the equations developed in either study was statistically appropriate to provide a valid correlation. Furthermore, no statistically valid correlation was found between oil recovery and definable reservoir parameters. The second study found that when reservoirs were separated by lithology, geographical province, and producing mechanism, the only reasonable correlations that could be developed were between recoverable oil and original oil in place. Even then, the correlations were of poor quality as indicated by Figure 5-139 which presents the best correlation for Texas sandstone natural-water-drive reservoirs. The average primary recovery for various groups of reservoirs at the average value of OOIP for each group is listed by production mechanism in Table 5-29 [239,243].

In view of the lack of suitable correlations, primary oil recovery for an individual reservoir must be estimated by one of three methods: (1) material balance equations in conjunction with equations for gas-oil ratio and fluid

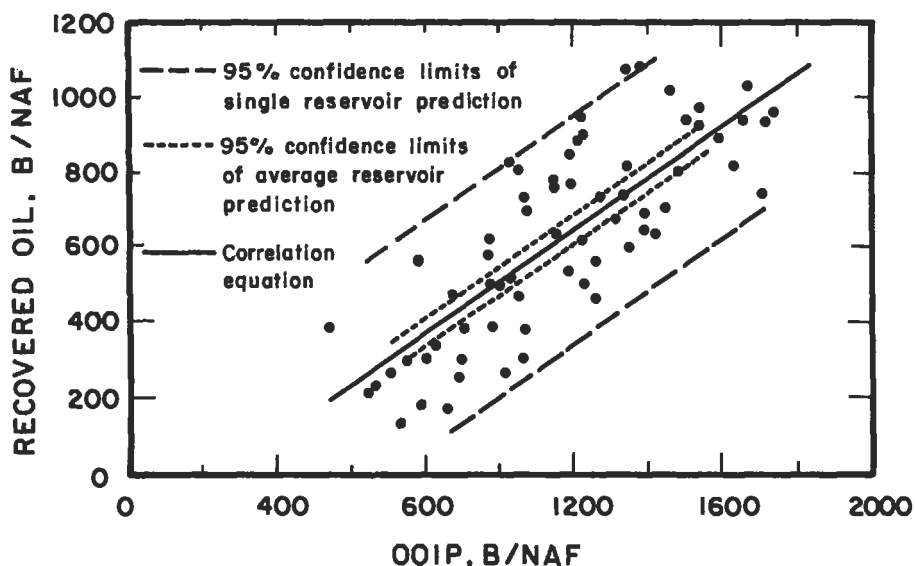


Figure 5-139. Correlation of primary oil recovery for water-drive reservoirs [239].

saturations, (2) volumetric equations if residual oil saturation and oil formation volume factor at abandonment are known or estimated, and (3) decline curve analysis, if production history is available. Each of these methods for estimating primary oil recovery and gas recovery, when appropriate, will be discussed in the following sections.

Primary Recovery Factors in Solution-Gas-Drive Reservoirs

Primary recovery from solution-gas-drive reservoirs depends on: type of geologic structure, reservoir pressure, gas solubility, fluid gravity, fluid viscosity, relative permeabilities, presence of connate water, rate of withdrawal, and pressure drawdown. From a statistical study [244,245] the primary recovery factors in Table 5-30 were obtained for different oil gravities and solution gas-oil ratios in sands sandstones, limestones, dolomite, and chert. Based on work of the same type in 135 reservoir systems, Wahl [246] presented a series of figures that can be used to estimate primary recovery. One of these figures, for a condition of a 2 cp reservoir oil and a 30% connate water saturation, is reproduced in Figure 5-140. To use these figures the following is required: oil viscosity at reservoir conditions, interstitial water saturation, bubble-point pressure, solution gas-oil ratio at the bubble-point pressure, and formation volume factor.

MATERIAL BALANCE AND VOLUMETRIC ANALYSIS

Methods of estimating hydrocarbons in place by volumetric methods were discussed. These estimates can be confirmed and future reservoir performance can be predicted with the use of material balance equations. In the most elementary form the material balance equation states that the initial volume in

Table 5-30
Primary Recovery In Percent of Oil In Place
for Depletion-Type Reservoirs

Oil solution GOR ft ³ /bbl	Oil gravity °API	Sand or sandstones			Limestone, Dolomite or Chert		
		maximum	average	minimum	maximum	average	minimum
60	15	12.8	8.6	2.6	28.0	4.0	0.6
	30	21.3	15.2	8.7	32.8	9.9	2.9
	50	34.2	24.8	16.9	39.0	18.6	8.0
200	15	13.3	8.8	3.3	27.5	4.5	0.9
	30	22.2	15.2	8.4	32.3	9.8	2.6
	50	37.4	26.4	17.6	39.8	19.3	7.4
600	15	18.0	11.3	6.0	26.6	6.9	1.9
	30	24.3	15.1	8.4	30.0	9.6	(2.5)
	50	35.6	23.0	13.8	36.1	15.1	(4.3)
1,000	15	—	—	—	—	—	—
	30	34.4	21.2	12.6	32.6	13.2	(4.0)
	50	33.7	20.2	11.6	31.8	12.0	(3.1)
2,000	15	—	—	—	—	—	—
	30	—	—	—	—	—	—
	50	40.7	24.8	15.6	32.8	(14.5)	(5.0)

From Reference 245.

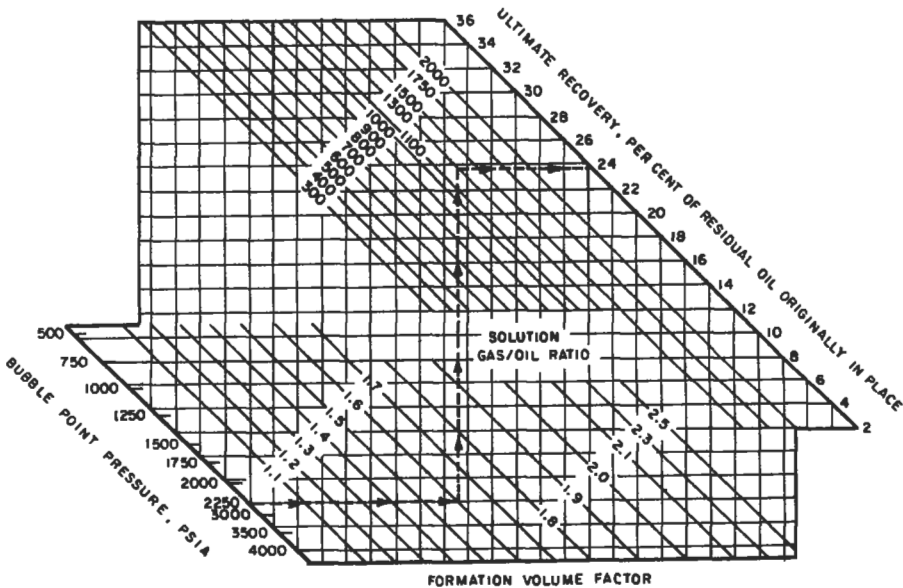


Figure 5-140. Estimates of primary recovery for a solution-gas-drive reservoir [246].

place equals the sum of the volume remaining and the volume produced [19]. Material balance equations [19] will be given for different reservoir situations. Nomenclature used in these equations is listed below [19,197,247].

- B_o = oil formation volume factor = volume at reservoir conditions per volume at stock-tank conditions, dimensionless (reservoir barrel per stock-tank barrel, RB/STB)
 B_g = gas formation volume factor = volume at reservoir conditions per volume at standard conditions, RB/scf (Note: if the gas formation volume factor is expressed in cu ft/scf, divide by 5.615 or multiply by 0.1781 to get RB/scf)
 B_w = water formation volume factor = volume at reservoir conditions per volume at standard conditions, dimensionless (RB/STB)
 $B_t = B_o + (R_{si} - R_i) B_g$ = composite oil or total oil formation volume factor = volume at reservoir conditions per volume at standard conditions
 c_f = formation (rock) compressibility = pore volume per pore volume per psi
 c_w = water compressibility = pore-volume per pore-volume per psi
 G = total initial gas in place in reservoir, scf
 G_e = cumulative gas influx (encroachment), scf
 ΔG_e = gas influx (encroachment) during an interval, scf
 G_i = cumulative gas injected, scf
 G_p = cumulative gas produced, scf
 k_{rg} = relative permeability to gas, dimensionless
 k_{ro} = relative permeability to oil, dimensionless
 $m = GB_{gi}/NB_{oi}$ = ratio of initial gas-cap/gas-reservoir volume to initial reservoir oil volume
 N = initial oil in place, STB
 N_p = cumulative oil produced, STB
 ΔN_p = oil produced during an interval, STB
 p = reservoir pressure, psia
 p_i = initial reservoir pressure, psia
 p_r = reduced pressure, dimensionless
 R_s = solution-gas-oil ratio (gas solubility in oil), scf/STB
 R_{si} = initial solution-gas-oil ratio, scf/STB
 R_{sw} = gas solubility in water, scf/bbl at standard conditions
 R_p = cumulative gas-oil ratio, scf/STB
 S_o = oil saturation, fraction of pore space
 S_g = gas saturation, fraction of pore space
 S_{iw} = irreducible or connate water saturation, fraction of pore space
 S_w = water saturation, fraction of pore space
 S_{wi} = initial water saturation, fraction of pore space
 W = initial water in place, reservoir bbl
 W_c = cumulative water influx, bbl at standard conditions
 W_p = cumulative water produced, bbl at standard conditions
 W_i = cumulative water injected, bbl at standard conditions
 μ_g = gas viscosity, cp
 μ_o = oil viscosity, cp
 z = gas deviation factor (compressibility factor), $z = pV/nRT$, dimensionless
 i = subscript, initial or original conditions
 1 = subscript for conditions at p_1
 2 = subscript for conditions at p_2

Material Balance for Gas Reservoirs

Material Balance Equations

Reservoirs that contain only free gas are called gas reservoirs. These reservoirs contain a mixture of gaseous hydrocarbons, which may be dry, wet, or condensate gas. Gas reservoirs may be volumetric with no water influx. For such reservoirs, the material balance is:

$$GB_{gi} = (G - G_p)B_g \tag{5-145}$$

where all terms have been defined earlier in the notation. In the case of a gas reservoir with water encroachment and water production, the material balance equation is:

$$GB_{gi} = (G - G_p)B_g + (W_e - W_p) \tag{5-146}$$

In either equation, the gas formation volume factor can be obtained, as a function of pressure and temperature, as outlined earlier. A schematic representation [197] of the material balance equations for dry-gas reservoirs is depicted in Figure 5-141.

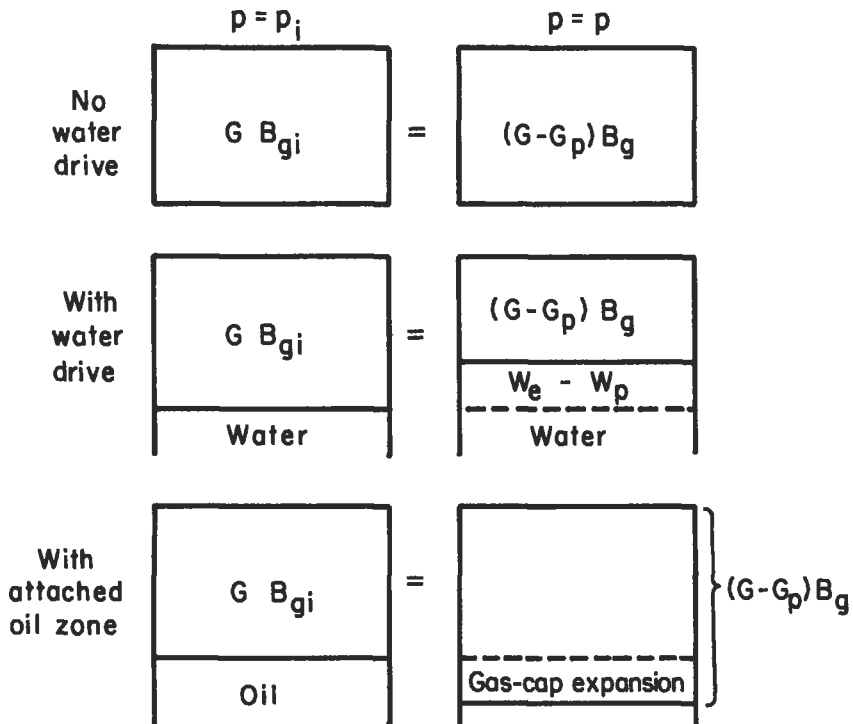


Figure 5-141. Schematic of material balance equations for a dry-gas reservoir [197].

Graphical Form of Material Balance (p/z Plots)

For volumetric gas reservoirs in which there is no water influx and negligible water production, the definition of gas formation volume factor (Equation 5-3) can be substituted into Equation 5-145, and the resulting equation can be rearranged to give [197]:

$$G_p = G - \frac{p}{z} \frac{Gz_i}{p_i} \quad (5-147)$$

where all terms are as defined previously and the subscript *i* refers to initial conditions. This equation indicates that for a volumetric gas reservoir a plot of cumulative gas production (G_p) in standard cubic feet versus the ratio p/z is a straight line. Within limits of error for average reservoir pressure and cumulative production, this plot is linear as shown in Figure 5-142. The straight line can be extrapolated to zero pressure to find the initial gas in place, or can be extrapolated to predict the cumulative production at any future average reservoir pressure. A plot of pressure versus cumulative production is not a straight line because the produced gas is not a perfect gas. Since the gas deviation factor, z , is a function of pressure, the ratio of p/z can be obtained conveniently from plots of p/z versus p , p_r/z versus z for different reduced temperatures, or from computer programs that have gas deviation factors in storage [197]. Other graphical interpretations have been suggested [248].

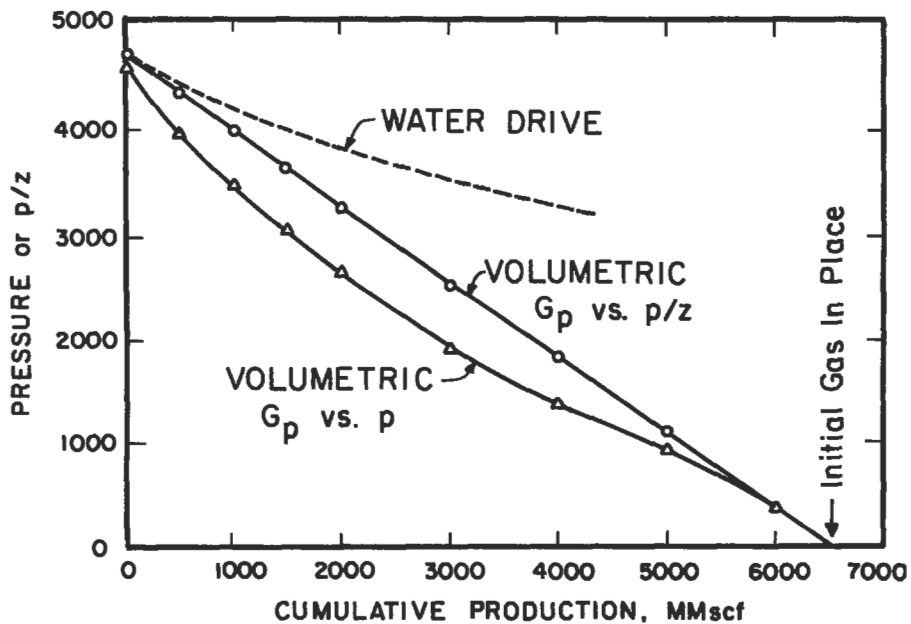


Figure 5-142. A p/z plot [17].

A plot of p/z versus G_p may not be a straight line for several reasons: an unexpected water drive may exist, average reservoir pressure may be inaccurate, or the reservoir pore volume may be changing unpredictably as a result of abnormally high reservoir pressures [197]. A water drive reduces relative permeability to gas and increases pressure at abandonment [180]. For reservoirs at moderate to high pressure in the absence of a water drive, the recovery efficiency under pressure depletion may range from about 80% to more than 90%; a water drive can reduce recovery to about 60%. To maximize efficiency, water-bearing zones should not be perforated if the water is movable, and production should be at a high rate since water entry is time dependent [180].

Material Balance Equations in Oil or Combination Reservoirs

When discovered, a reservoir may contain oil, gas, and water that can be intermingled or segregated into zones. As described earlier, recovery may be caused by solution gas drive, water drive, gas cap drive, or a combination of these mechanisms. A general material balance equation should be capable of handling any type of fluid distribution and any drive mechanism.

From the compressibilities given in the first section, water and formation compressibilities are less significant where there is appreciable gas saturation such as in gas reservoirs, gas cap reservoirs, and in undersaturated reservoirs below the bubble point. Because of this and because of the complications they would introduce in already complex equations, water and formation compressibilities are generally neglected, except in undersaturated reservoirs producing above the bubble point. Gas in solution in the formation is small and also generally neglected. One general material balance equation, the Schilthuis equation, is a volumetric balance stating that the sum of the volume changes in oil, gas, and water must be zero because the reservoir volume is constant.

$$\begin{aligned}
 & \text{oil zone} & \text{gas cap} & \text{water} & \text{cumulative oil} \\
 & [\text{expansion}] & + [\text{expansion}] & + [\text{influx}] & = [\text{zone production}] \\
 \\
 & N(B_t - B_d) + \frac{NmB_d(B_g - B_{gi})}{B_{gi}} + W_e = N_p B_t \\
 \\
 & + \left[\begin{array}{l} \text{cumulative gas cap} \\ \text{gas production} \end{array} \right] + \left[\begin{array}{l} \text{cumulative water} \\ \text{production} \end{array} \right] \\
 \\
 & + N_p(R_p - R_{si})B_g + B_w W_p \tag{5-148}
 \end{aligned}$$

All symbols have been defined earlier. Rearranging terms, Equation 5-148 can be written:

$$N \left[B_t - B_d + \frac{mB_d(B_g - B_{gi})}{B_{gi}} \right] = N_p [B_t + (R_p - R_{si})B_g] - W_e + B_w W_p \tag{5-149}$$

Material balance equations are often expressed in terms of the initial oil in place, N :

$$N = \frac{N_p [B_t + (R_p - R_{si})B_g] - (W_e - B_w W_p)}{B_t - B_{di} + \frac{mB_{di}}{B_{gi}}(B_g - B_{gi})} \quad (5-150)$$

This equation applies to a reservoir under any drive mechanism or to fields under the simultaneous influence of dissolved gas drive, water drive, or gas cap drive.

If there is no water drive, $W_e = 0$; therefore:

$$N = \frac{N_p [B_t + (R_p - R_{si})B_g] + B_w W_p}{B_t - B_{di} + \frac{mB_{di}}{B_{gi}}(B_g - B_{gi})} \quad (5-151)$$

When there is no original free gas, $m = 0$; therefore:

$$N = \frac{N_p [B_t + (R_p - R_{si})B_g] - (W_e - B_w W_p)}{B_t - B_{di}} \quad (5-152)$$

When there is neither an original gas cap nor any water drive, $m = 0$ and $W_p = 0$; therefore:

$$N = \frac{N_p [B_t + (R_p - R_{si})]B_g}{B_t - B_{di}} \quad (5-153)$$

Although connate water and formation compressibilities are quite small, relative to the compressibility of reservoir fluids above their bubble points they are significant and account for an appreciable fraction of the production above the bubble point. In cases when compressibilities can be important, Equation 5-150 can be written as:

$$N = \frac{N_p [B_t + (R_p - R_{si})B_g] - (W_e - B_w W_p)}{B_t - B_{di} + (c_f + c_w S_{iw}) \Delta p B_{di} / (1 - S_{iw}) + m B_{di} (B_g - B_{gi}) / B_{gi}} \quad (5-154)$$

Material balance equations for various drive mechanisms and different initial conditions are summarized in Table 5-31. Note that in this table B_g is expressed in ft^3/scf , and the conversion factor, 0.1781, is the reciprocal of 5.615 ft^3 per barrel.

Generalized Material Balance Equation

Many forms of the so-called general material balance equation have appeared in the literature. In the most general form, the material balance equation, expressed in terms of the initial oil in place, is:

$$N = \frac{N_p B_o + B_g (G_p - N_p R_s) - G (B_g - B_{gi}) - (W_e - W_p)}{B_o - B_{oi} + (R_{si} - R_s) B_g + (c_f + c_w S_{iw}) \Delta p B_{oi} / (1 - S_{iw})} \quad (5-155)$$

Table 5-31
Material Balance Equations

Gas reservoir with active water drive

$$G = \frac{G_p B_g - 5.615(W_o - W_p)}{B_g - B_{gl}}$$

Gas reservoir; no active water drive ($W_o = 0$)

$$G = \frac{G_p B_g + 5.615W_p}{B_g - B_{gl}}$$

Oil reservoir with gas cap and active water drive

$$N = \frac{N_p [B_t + 0.1781 B_g (R_p - R_{st})] - (W_o - W_p)}{mB_{oi} \left(\frac{B_t}{B_{gl}} - 1 \right) + (B_t - B_{oi})}$$

Oil reservoir with gas cap; no active water drive ($W_o = 0$)

$$N = \frac{N_p [B_t + 0.1781 B_g (R_p - R_{st})] + W_p}{mB_{oi} \left(\frac{B_t}{B_{gl}} - 1 \right) + (B_t - B_{oi})}$$

Initially undersaturated oil reservoir with active water drive ($m = 0$)

1. Above bubble point

$$N = \frac{\left[N_p (1 + \Delta p c_o) - \frac{W_o - W_p}{B_{oi}} \right] (1 - S_w)}{\Delta p [c_o + c_t - S_w (c_o - c_w)]}$$

2. Below bubble point

$$N = \frac{N_p [B_t + 0.1781 B_g (R_p - R_{st})] - (W_o - W_p)}{B_t - B_{oi}}$$

Initially undersaturated oil reservoir; no active water drive ($m = 0, W_o = 0$)

1. Above bubble point

$$N = \frac{\left[N_p (1 + \Delta p c_o) - \frac{W_p}{B_{oi}} \right] (1 - S_w)}{\Delta p [c_o + c_t - S_w (c_o - c_w)]}$$

2. Below bubble point

$$N = \frac{N_p [B_t + 0.1781 B_g (R_p - R_{st})] + W_p}{B_t - B_{oi}}$$

From Reference 180.

Note: In this table, B_g is expressed in ft³/SCF.

This equation can be obtained by substituting in Equation 5-154 the following terms:

$$B_1 = B_o + (R_{ci} - R_s) B_g; \quad B_{ui} = B_{oi}; \quad \text{and} \quad G_p = N_p R_p.$$

A schematic representation [19] of the possible changes in fluid distribution is presented in Figure 5-143. In order to not omit any of the significant reservoir

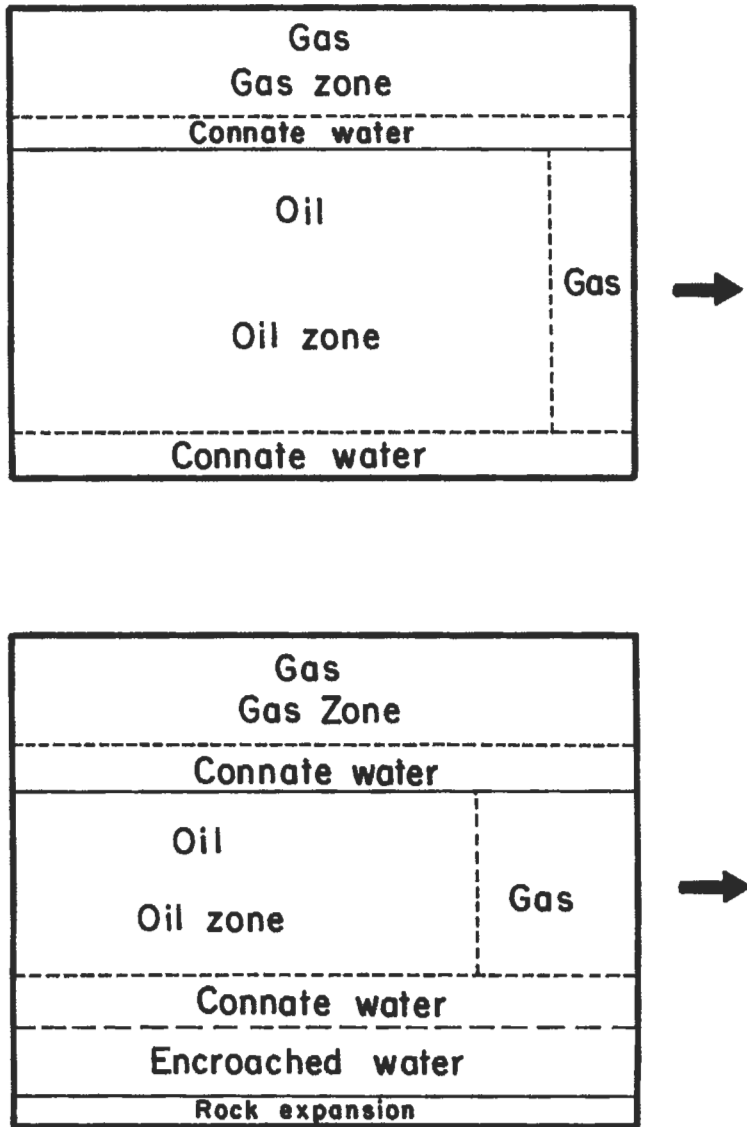


Figure 5-143. Schematic representation of fluid distributions [19].

energies, Slider [197] suggests beginning all material balance applications with Equation 5-155. With the use of Equation 5-155, it is not necessary to list separate equations for the various drive mechanisms and conditions since this one equation can be reduced to any of the individual cases. For reservoirs above the bubble point, some of the terms in Equation 5-155 become zero or else cancel out: $G = 0$ since there is no free gas, G_p , and $N_p R_s$ cancel out since the gas production term is equal to the total gas produced, $R_g - R_s$ is zero since the gas in solution at any pressure is equal to the gas originally in solution.

For a reservoir with no initial free gas saturation or no initial gas cap, $G = 0$. If there is no water encroachment, $W_e = 0$; however, the water production term should remain, even if there is no water drive, because connate water may be produced when the reservoir pressure declines.

When a reservoir contains free gas, the pore volume expansion or compressibilities of the formation and water are insignificant compared to the free gas terms. Since the gas compressibility is about 100 times the compressibility of the water and formation, a gas saturation of only 1% may provide as much energy as the water and formation compressibility terms. Thus, when the gas saturation is substantial the change in pore volume is insignificant.

Material Balance for Solution-Gas Drive Reservoirs

A schematic representation of material balance equations for solution-gas reservoirs, when the change in pore volume is negligible, is shown in Figure 5-144. When these reservoirs are producing above the bubble point or saturation pressure, no gas is liberated and production occurs by expansion of liquids in the reservoir. When reservoir pressure drops below the bubble point, gas is liberated in the reservoir and will be produced with the oil.

Liquid Expansion

For some very large reservoirs (often with limited permeability), production may occur for extended periods by expansion of liquids in the reservoir. If

	Oil		Oil									
For $p > p_s$	$N B_{oi}$ P_i	=	$(N - N_p) B_o$ $P_i > p > p_s$									
For $p < p_s$	$N B_{oi}$ P_i	=	<table style="width: 100%; border-collapse: collapse;"> <tr> <td style="width: 50%; text-align: center;">Oil</td> <td style="width: 50%; text-align: center;">Free Gas</td> </tr> <tr> <td style="border-right: 1px dashed black; padding: 5px; text-align: center;"> $(N - N_p) B_o$ </td> <td style="padding: 5px; text-align: center;"> $[NR_{si} - (N - N_p)R_s - G_p] B_g$ </td> </tr> <tr> <td style="border-right: 1px dashed black; text-align: center;">P_i</td> <td style="text-align: center;">$P < p_s$</td> </tr> </table>		Oil	Free Gas	$(N - N_p) B_o$	$[NR_{si} - (N - N_p)R_s - G_p] B_g$	P_i	$P < p_s$		
Oil	Free Gas											
$(N - N_p) B_o$	$[NR_{si} - (N - N_p)R_s - G_p] B_g$											
P_i	$P < p_s$											

Figure 5-144. Schematic of material balance equations for a solution-gas-drive reservoir [197].

production is caused only by liquid expansion, the material balance equation obtained from Figure 5-144 for pressures above the bubble point is:

$$N = \frac{(N - N_p)B_o}{B_{oi}} \quad (5-156)$$

Gas Liberation

When reservoir pressure declines below the bubble-point pressure, the original gas in solution has either been produced as G_p , is still in solution in the oil, $(N - N_p)R_s$, or exists as free gas. For this condition as shown in Figure 5-144, the material balance is:

$$N = \frac{N_p B_o + B_g (G_p - N_p R_s)}{B_o - B_{oi} + (R_{si} - R_s) B_g} \quad (5-157)$$

Predicting Primary Recovery In Solution-Gas Drive Reservoirs

Several methods for predicting performance of solution-gas behavior have appeared in the literature. These methods relate pressure decline to gas-oil ratio and oil recovery. Because neither water influx nor gravity segregation is considered, time is not a factor with solution-gas reservoirs, and time must be inferred from the oil in place and production rate [17]. The following assumptions are generally made: uniformity of the reservoir at all times regarding porosity, fluid saturations, and relative permeabilities; uniform pressure throughout the reservoir in both the gas and oil zones (which means the gas and oil volume factors, the gas and oil viscosities, and the solution gas will be the same throughout the reservoir); negligible gravity segregation forces; equilibrium at all times between the gas and the oil phases; a gas liberation mechanism which is the same as that used to determine the fluid properties, and no water encroachment and negligible water production.

The Schlithuis Method [249]

For solution-gas drive reservoirs where the reservoir pressure is about equal to the saturation pressure and for gas cap drive reservoirs, Equation 5-155 can be written [197]:

$$N = \frac{N_p B_o + (G_p - N_p R_s) B_g - G(B_g - B_{gi})}{B_o - B_{oi} + (R_{si} - R_s) B_g} \quad (5-158)$$

If this equation is rearranged and solved for cumulative oil produced:

$$N_p = \frac{N[B_o - B_{oi} + (R_{si} - R_s) B_g] + G(B_g - B_{gi}) - B_g G_p}{B_o - B_g R_s} \quad (5-159)$$

In order to predict the cumulative oil production at any stage of depletion, the original oil and gas in place and the initial reservoir pressure must be known.

The original pressure establishes values for B_{oi} , B_{gi} , and R_{si} , and the pressure at the given level of depletion establishes values of B_o , B_g , and R_s . Cumulative gas production can be obtained from:

$$G_p = \sum R_s \Delta N_p \quad (5-160)$$

A procedure for using this method is [197]:

1. At a set value of reservoir pressure, assume the cumulative amount of gas produced, G_p .
2. Calculate N_p by Equation 5-159.
3. Calculate S_o using Equation 5-175.
4. Determine the relative permeability ratio based on the liquid saturation from data such as that in Figure 5-55.
5. Calculate G_p using Equations 5-160 and 5-163.
6. Compare the calculated G_p with the assumed G_p from Step 1.
7. If the assumed and calculated values do not agree to a satisfactory degree, repeat the calculations from Step 1 for another value of G_p .
8. If the assumed and calculated G_p values agree, return to Step 1 and set a new pressure.

The Tarner Method

This [250] is a trial-and-error procedure based on the simultaneous solution of the material balance equation and the instantaneous gas-oil ratio equation. For a pressure drop from p_1 to p_2 , the procedure involves a stepwise calculation of cumulative oil produced $(N_p)_2$ and of cumulative gas produced $(G_p)_2$. Several variations in the procedure and equations are possible; the straightforward procedure outlined by Timmerman [180] is reproduced here.

1. During the pressure drop from p_1 to p_2 , assume that the cumulative oil production increases from $(N_p)_1$ to $(N_p)_2$. At the bubble point pressure, N_p should be set equal to zero.
2. By means of the material-balance equation for $W_p = 0$, compute the cumulative gas produced $(G_p)_2$ at pressure p_2 :

$$(G_p)_2 = (N_p)_2 (R_p)_2 = N \left[(R_{si} - R_s) - \frac{B_{oi} - B_o}{B_g} \right] - (N_p)_2 \left(\frac{B_o}{B_g} - R_s \right) \quad (5-161)$$

3. Compute the fractional total liquid saturation $(S_L)_2$ at pressure p_2 :

$$(S_L)_2 = S_w + (1 - S_w) \frac{B_o}{B_{oi}} \left[1 - \frac{(N_p)_2}{N} \right] \quad (5-162)$$

4. Determine the k_{rg}/k_{ro} ratio corresponding to the total liquid saturation $(S_L)_2$ and compute the instantaneous gas-oil ratio at p_2 :

$$R_2 = R_s + \frac{B_o}{B_g} \frac{\mu_o}{\mu_g} \frac{k_{rg}}{k_{ro}} \quad (5-163)$$

5. Compute the cumulative gas produced at pressure p_2 :

$$(G_p)_2 = (G_p)_1 + \frac{R_1 + R_2}{2} [(N_p)_2 - (N_p)_1] \quad (5-164)$$

where R_1 is the instantaneous gas-oil ratio computed at pressure p_1 .

Usually three judicious guesses are made for the value $(N_p)_2$ and the corresponding values of $(G_p)_2$ computed by both step 2 and step 5. When the values for $(G_p)_2$ are plotted against the assumed values for $(N_p)_2$, the intersection of the curve indicates the cumulative gas and oil production that will satisfy both equations. In actual application the method is usually simplified further by equating the incremental gas production $(G_p)_2 - (G_p)_1$ rather than $(G_p)_2$ itself. This equality signifies that at each pressure step the cumulative gas, as determined by the volumetric balance is the same as the quantity of gas produced from the reservoir, as controlled by the relative permeability ratio of the rock, which in turn depends on the total liquid saturation.

The Muskat Method

The Schilthuis and Tarner forms of material balance have been expressed in integral form. An approach presented by Muskat [251] expresses the material balance in terms of finite pressure differences in small increments. The changes in variables that affect production are evaluated at any stage of depletion or pressure. The assumption is made that values of the variables will hold for a small drop in pressure, and the incremental recovery can be calculated for the small pressure drop. The variables are recalculated at the lower pressure, and the process is continued to any desired abandonment pressure. If the PVT data and the gas-oil relative permeabilities are known at any liquid saturation, the unit recovery by pressure depletion can be computed from a differential form of the material balance equation:

$$\frac{dS_o}{dp} = \frac{\frac{S_o B_g}{B_o} \frac{dR_1}{dp} + \frac{S_o k_{rg} \mu_o}{B_o k_{ro} \mu_g} \frac{dB_o}{dp} + (1 - S_o - S_w) B_g \frac{d(1/B_g)}{dp}}{1 + \frac{k_{rg} \mu_o}{k_{ro} \mu_g}} \quad (5-165)$$

From the change in saturation at any pressure, the reservoir saturation at that time can be related to the change in oil production and the instantaneous gas-oil ratio. Calculations can be facilitated if the terms in the numerator that are functions of pressure only (B_g , B_o , R_1) are determined for various depletion pressures. Pressure increments of 10 psi or less may be necessary for acceptable accuracy [180].

Predicting Primary Recovery in Water-Drive Reservoirs

In the prediction of performance caused by water influx, predictions of water encroachment are made independent of material balance. The extent of water encroachment depends on the characteristics of the aquifer and is a function of the pressure history and time [252]. While several methods are available to predict water drive performance, some [197] feel that the theory of unsteady-

state compressible flow should be used, and that water encroachment generally follows the constant pressure solution to the radial diffusivity equation. Solutions to the radial diffusivity equation have been provided by van Everdingen and Hurst [253] in terms of dimensionless time, t_D , and a dimensionless fluid flow function, Q_{wD} , which is determined at t_D :

$$t_D = \frac{6.323 \times 10^{-3} kt}{\phi \mu c r^2} \quad (5-166)$$

where k is permeability in md, t is time in days, ϕ is the fractional porosity, c is the compressibility in psi^{-1} , and r is the reservoir radius in ft. Values of Q_{wD} are given in tabular form as a function of t_D in the paper by van Everdingen and Hurst [253] and have been reproduced in several texts [17,197]. Because of the length of the tables, they will not be reproduced in this section. The water encroachment, W_e in barrels, can be estimated from:

$$W_e = B \sum (dp)(Q_{wD}) \quad (5-167)$$

where dp is the pressure drop in psi, and the constant B is:

$$B = 1.12\phi h c r^2 \frac{\theta}{360} \quad (5-168)$$

where h is the reservoir thickness in ft, θ is the angle subtended by the reservoir circumference (θ is 360° for a circular reservoir and θ is 180° for a semicircular reservoir against a fault), and the other terms are as defined above [17]. From the slope of cumulative water influx at various times versus the summation term at those times, the aquifer constant, B , can be obtained, and the cumulative water influx for any pressure history can be estimated from Equation 5-167. Plots of Q_{wD} versus t_D for various dimensionless reservoir sizes are also available [17,253] and extensions of these data are available as well [197].

Volumetric Calculations for Recovery of Gas and Oil

The volumetric equations for original oil and gas in place were given earlier. In this section, volumetric equations will be given for the recovery of gas and oil reservoirs under several common instances.

Recovery of Gas

The volume of gas recovered, G_p in scf, from a dry-gas reservoir is:

$$G_p = 7,758 Ah \phi (1 - S_w) \left(\frac{1}{B_{gi}} - \frac{1}{B_g} \right) \quad (5-169)$$

where 7,758 is the number of barrels per acre-ft, A is the areal extent in acres, h is the reservoir thickness in ft, ϕ is the fractional porosity, S_w is the fractional water saturation, B_{gi} is the initial gas formation volume factor in reservoir barrels per scf, and B_g is the gas formation volume factor in RB/scf at the abandonment

pressure. (Note: if the formation volume factors are expressed in ft³/scf, 7,758 should be replaced with 43,560 ft³ per acre-ft.)

If Equation 5-145 is rearranged in terms of the initial gas in place:

$$G = \frac{G_p B_g}{(B_g - B_{gi})} \quad (5-170)$$

The recovery efficiency, E_R , which is the volume of gas recovered divided by the volume of gas initially in place, can be found from:

$$E_R = \frac{B_{gi} - B_g}{B_{gi}} \quad (5-171)$$

For volumetric gas reservoirs (which assumes no change in S_w) recoveries may range from 80% to 90% of the initial gas in place.

For gas reservoirs under water drive, recovery efficiency is:

$$E_R = \frac{(1 - S_{wi})B_{gi} - (S_{gr} B_g)}{(1 - S_{wi})B_{gi}} \quad (5-172)$$

where S_{gr} is the residual gas saturation and the other terms are as defined above.

Recovery of Oil

Solution-Gas or Depletion Drive. Oil recovery by depletion or solution-gas drive is:

$$N_p = 7,758 Ah\phi \left[\frac{(1 - S_w)}{B_{oi}} - \frac{(1 - S_w - S_{gr})}{B_o} \right] \quad (5-173)$$

where B_{oi} is the initial oil formation volume factor and B_o is the oil formation volume factor at abandonment, and the other terms are as previously defined. The ultimate free gas saturation is often estimated from the old data of Arps [245] and Craze and Buckley [241] in which the average S_g was 30% for a 2.2 cp oil with 400 ft³/bbl of solution gas. A general rule suggests that for each doubling of solution gas, S_g should be increased 3%; and for each doubling of oil viscosity, S_g should be decreased by 3% [14]. As a first approximation, S_{gr} can be taken to be about 0.25 [254]

For a volumetric, undersaturated reservoir,

$$N_p = \frac{N(B_o - B_{oi})}{B_o} \quad (5-174)$$

where N_p is the oil produced in stock tank barrels, N is the initial oil in place in STB and the other terms are as already given. In this case, the oil saturation after any stage of primary production, S_o , can be obtained from:

$$S_o = \frac{(N - N_p)B_o(1 - S_w)}{NB_{oi}} \quad (5-175)$$

If calculations are made at the abandonment of primary production, S_o will represent the oil saturation after primary. The gas saturation at any time, S_g , can be found from:

$$S_g = 1 - S_o - S_w \quad (5-176)$$

For a solution-gas drive reservoir with water encroachment [73]:

$$N_p = N \left[\frac{B_o - B_{oi}}{B_o} + \frac{W_e}{B_o} \right] \quad (5-177)$$

where W_e is the cumulative water influx in barrels and all other terms are consistent with the prior definitions.

Water-Drive Reservoir. Recovery from a water-drive reservoir (which assumes no appreciable decline in pressure) can be calculated from [14]:

$$N_p = 7,758(Ah\phi) \left[\frac{(1 - S_w)}{B_{oi}} - \frac{S_{or}}{B_o} \right] \quad (5-178)$$

where S_{or} is the residual oil saturation as a fraction of pore volume. Residual oil saturation can be obtained from cores taken with water base mud or from logs as described earlier. Methods of estimating residual oil saturation after water injection are discussed later. In the absence of data, residual oil saturations are sometimes obtained from the empirical data of Arps [245] and Craze and Buckley [241] which are given in Table 5-32. However, the caution given earlier is repeated here: from a more recent study [239] *no statistically valid correlation was found between oil recovery and definable reservoir parameters.*

The recovery efficiency in the case of water influx is given by:

$$E_R = \frac{(1 - S_w - S_{or})}{(1 - S_w)} \quad (5-179)$$

Gravity Drainage. For segregation drive reservoirs, Equation 5-178 can be used. Residual oil saturations for gravity drainage reservoirs tend to be low (possibly on the order of 0.10) [14].

Gas-Cap Drive. For a gas-cap drive reservoir with no water influx, the oil saturation can be estimated from [73]:

$$S_o = \left(\frac{N - N_p}{NB_{oi}} \right) (1 - S_w) \left[\frac{1}{1 - m(B_g - B_{gt})/B_{gt}} \right] \quad (5-180)$$

where m is the ratio of original gas zone to original oil zone in the reservoir and all other quantities have been defined.

Table 5-32
Approximation of Residual Oil Saturation

Reservoir oil viscosity, cp	Residual oil saturation, % PV
0.2	30
0.5	32
1.0	34.5
2.0	37
5.0	40.5
10.0	43.5
20.0	46.5

Average reservoir permeability, md	Deviation of residual oil saturation from viscosity trend, % PV
50	+12
100	+ 9
200	+ 6
500	+ 2
1,000	- 1
2,000	- 4.5
5,000	- 8.5

From Reference 245.

DECLINE CURVE ANALYSIS

The conventional analysis of production decline curves for oil or gas production consists of plotting the log of flow rate versus time on semilog paper. In cases for a decline in rate of production, the data are extrapolated into the future to provide an estimate of expected production and reserves.

The empirical relationships for the analysis of production decline curves were first proposed by Arps [255] in which a decline rate, a , was defined as the fractional change in the flow rate, q , with time, t :

$$a = \frac{-dq/dt}{q} \quad (5-181)$$

If time is in days, flow rate in this equation is expressed in terms of stock tank barrels per day in the case of oil and scf per day for gas. Other consistent units of flow rate and time can be used. As shown in Figure 5-145, three types of decline can occur: a constant percentage or exponential decline, a hyperbolic decline, and a harmonic decline [245]. For the semilog plot, the exponential decline is a straight line whereas the slopes of the hyperbolic and harmonic decline curves decrease with time. For the exponential decline, the drop in production per unit time is a constant fraction of the production rate. For a hyperbolic decline, the decrease in production per unit time as a fraction of the production rate is proportional to a fractional power (between 0 and 1) of

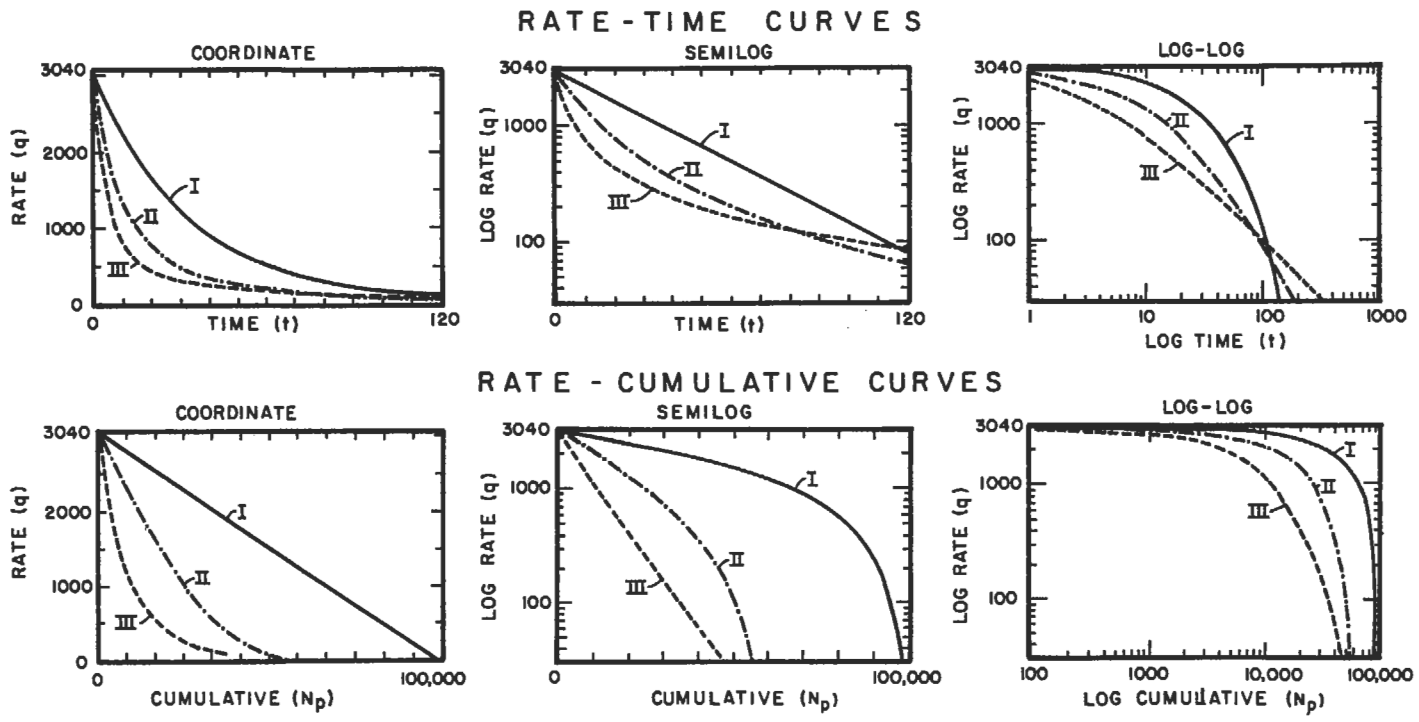


Figure 5-145. Decline curves [245].

the production rate. For a harmonic decline, the decrease in production per unit time as a fraction of the production rate is directly proportional to the rate. Slider [256] presented an equation for the hyperbolic decline that will reduce to the other types under certain circumstances:

$$\frac{a}{a_1} = \frac{q}{q_1}^n \quad (5-182)$$

where a is the decline rate when the production rate is q , and a_1 and q_1 are the decline rate and production at an initial time. As mentioned above, the exponent, n , is a number between, but not including zero and one for the hyperbolic decline. When n is zero, the decline rate is constant which is the exponential decline. When n is one, the decline rate is proportional to the rate which is the harmonic decline. Several early publications related to decline-curve analysis have appeared in the literature [257-262].

The exponential and hyperbolic types of decline curves are more common than the harmonic decline. The exponential or constant percentage decline is indicative of a homogeneous producing interval where the pressure response has been affected by the outermost reservoir limits [263-264]. The exponential decline may apply to pumping wells that are kept pumped off or gas wells and many oil wells that produce at a constant bottomhole pressure. The hyperbolic decline is indicative of either unsteady-state conditions or pressure response from a variable permeability reservoir [265]. Although frequently encountered, the harmonic decline may be observed with reservoirs that are dominated by gravity drainage [197]. Equations for each type of decline-curve are given in Table 5-33, and will be discussed for each case.

Exponential Decline

For the exponential or constant percentage decline, the nominal or instantaneous decline rate is:

$$a = \frac{\ln(q_1/q)}{t} \quad (5-183)$$

and as shown in Table 5-33, the rate-time relationship is:

$$q = q_1 e^{-at} \quad (5-184)$$

and the relationship between flow rate and cumulative production is:

$$N_p = \frac{q_1 - q}{a} \quad (5-185)$$

The annualized (effective) or continuous decline rate, d , is:

$$d = \frac{q_1 - q}{q} \quad (5-186)$$

from which the cumulative production, N_p , is:

$$N_p = \frac{q_1 - q}{-\ln(1-d)} \quad (5-187)$$

Table 5-33
Classification of Production Decline Curves

Decline type	I. Constant percentage decline	II. Hyperbolic decline	III. Harmonic decline
Basic characteristic	Decline is constant $n = 0$	Decline is proportional to a fractional power (n) of the production rate $0 < n < 1$	Decline is proportional to a production rate $n = 1$
Rate-time relationship	$q = q_i e^{-at}$	$q = \frac{q_i}{(1 + na_1 t)^{1/n}}$	$q = \frac{q_i}{1 + na_1 t}$
Rate-cumulative relationship	$N_p = \frac{(q_i - q)}{a}$	$N_p = \frac{q_i n}{a_1 (1 - n)} (q_i^{1-n} - q^{1-n})$ $q = \frac{q_i}{\left(1 + \frac{a_1 t}{h}\right)^h}$	$N_p = \frac{q_i}{a_1} \ln\left(\frac{q_i}{q}\right)$
$N_p = \left[\frac{h}{(h-1)}\right] \left[\frac{1}{a_1}\right] \left[q_i - q \left(1 + \frac{a_1 t}{h}\right) \right]$			

From Reference 255.

a = decline as a fraction of production rate
 t = time
 a_1 = initial decline
 N_p = cumulative oil production at time t

q_i = an initial production rate
 n = exponent
 q = production rate at time t
 $h = 1/n$

and the flow rate at time, t , is:

$$q = q_i + N_p f n (1 - d) \tag{5-188}$$

Hyperbolic Decline

As shown in Table 5-33, the time-rate relationship for the hyperbolic decline is:

$$q = \frac{q_i}{(1 + na_1 t)^{1/n}} \tag{5-189}$$

If h is substituted for $1/n$, the time-rate relationship is:

$$q = \frac{q_i}{\left(1 + \frac{a_1 t}{h}\right)^h} \tag{5-190}$$

where h is the hyperbolic decline constant.

For the hyperbolic decline, the rate-cumulative production relationship is:

$$N_p = \frac{q_i^n}{a_i(1-n)} (q_i^{1-n} - q^{1-n}) \quad (5-191)$$

and if h is substituted into this equation:

$$N_p = \left[\frac{h}{(h-1)} \right] \left[\frac{1}{a_i} \right] \left[q_i - q \left(1 + \frac{a_i t}{h} \right) \right] \quad (5-192)$$

Equation 5-190 can be rearranged to:

$$\frac{1}{a} = \frac{1}{a_i} + \frac{t}{h} \quad (5-193)$$

which represents a straight line. If the decline rate, $1/a$, is plotted on the y -axis versus the time interval on the x -axis, the intercept at $t = 0$ will yield $1/a_i$, and the slope will yield $1/h$. These values can be substituted into Equation 5-190 to give any future estimates of production rates [264].

Harmonic Decline

For a harmonic decline, the time-rate relationship is:

$$q = \frac{q_i}{(1 + na_i t)} \quad (5-194)$$

and the rate-cumulative production relationship as shown in Table 5-33 is:

$$N_p = \frac{q_i}{a_i} \ln \left(\frac{q_i}{q} \right) \quad (5-195)$$

Production Type-Curves

Semilog Plots

The complexity of the analysis of hyperbolic decline-curves led to the development of curve-matching techniques. One of the simpler techniques was proposed by Slider [256] with the development of an overlay method to analyze rate-time data. The actual decline-curve data are plotted on transparency paper and compared to a series of semilog plots that represent different combinations of a , and n . Tabular values needed to plot the hyperbolic type-curves are available [197] for values of n from 0.1 to 0.9, in increments of 0.1.

Gentry [266] prepared a series of plots of q_i/q versus $N_p/q_i t$ for different values of n from 0 to 1.0 in increments of 0.1. Using two rates, the cumulative production, and the intervening time, the value of n for a particular hyperbolic

decline-curve can be obtained. Gentry provided other curves to estimate a_i , or Equation 5-189 can be rearranged:

$$a_i = \frac{(q_i/q)^n - 1}{nt} \quad (5-196)$$

With the use of the semilog type-curves, caution must be exercised to ensure that the interval being analyzed is indeed a hyperbolic curve [197]. Another problem with the semilog plots is that an exact fit of the data may not be possible; however, the techniques are relatively rapid.

Log-log (Fetkovich) Type-Curves

Conventional decline-curve analysis should be used only when mechanical conditions and reservoir drainage remain constant and the well is producing at capacity [197]. An advanced approach for decline-curve analysis, which is applicable for changes in pressure or drainage, has been presented by Fetkovich [267,268]. This technique, which is similar to the approach used in pressure testing, involves log-log plots of q/q_i (or q_{Dd}) versus $a_i t$ (or t_{Dd}) for different values of n (see Figure 5-146). As shown in this figure, a log-log plot of the dimensionless rate and dimensionless time can identify transient data and/or depletion data, the Arps' equations given in Table 5-33 must only be applied to rate-time data that indicate depletion [268]. Use of transient data in the Arps' equations will result in incorrect forecasts that are overly optimistic.

The full-size Fetkovich type-curves can be ordered from the book order department of SPE. The field data are plotted on tracing paper that has the same log-log scale as the full-size type-curves. The log-log plot of flow rate and time can be in terms of barrels/day versus days, barrels/month versus months, or barrels/year versus years, depending on the time interval being studied. Using the best fit on the appropriate type-curve, a match point can be used to obtain q_i and a_i for the actual data. The appropriate equation can then be used to analyze the rate, time, and cumulative production behavior.

RESERVE ESTIMATES

Definition and Classification of Reserves

Definitions [269-271]

Crude Oil. This is defined technically as a mixture of hydrocarbons that existed in the liquid phase in natural underground reservoirs and remains liquid at atmospheric pressure after passing through surface facilities. For statistical purposes, volumes reported as crude oil include: (1) liquids technically defined as crude oil; (2) small amounts of hydrocarbons that existed in the gaseous phase in natural underground reservoirs but are liquid at atmospheric pressure after being recovered from oilwell (casinghead) gas in lease separators*; and (3) small amounts of nonhydrocarbons produced with the oil.

*From a technical standpoint, these liquids are termed "condensate"; however, they are commingled with the crude stream and it is impractical to measure and report their volumes separately. All other condensate is reported as either "lease condensate" or "plant condensate" and included in natural gas liquids.

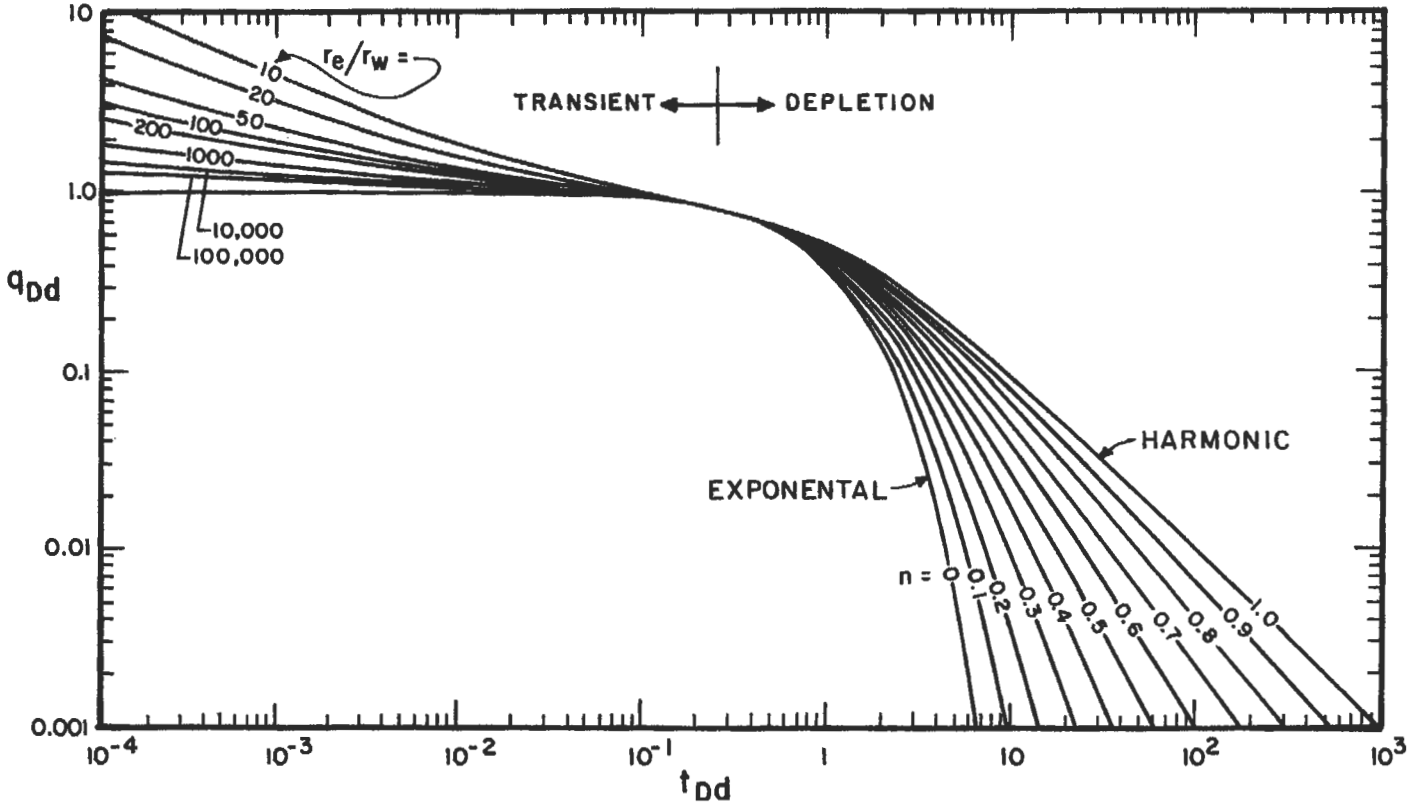


Figure 5-146. Log-log type curves [268].

Natural Gas. This is a mixture of hydrocarbons and varying quantities of nonhydrocarbons that exist either in the gaseous phase or in solution with crude oil in natural underground reservoirs. Natural gas may be subclassified as follows.

Associated gas is natural gas, commonly known as gas-cap gas, that overlies and is in contact with crude oil in the reservoir.**

Dissolved gas is natural gas that is in solution with crude oil in the reservoir.

Nonassociated gas is natural gas that is in reservoirs that do not contain significant quantities of crude oil.

Dissolved gas and associated gas may be produced concurrently from the same wellbore. In such situations, it is not feasible to measure the production of dissolved gas and associated gas separately; therefore, production is reported under the heading of associated-dissolved or casinghead gas. Reserves and productive capacity estimates for associated and dissolved gas also are reported as totals for associated-dissolved gas combined.

Natural Gas Liquids (NGLs). These are those portions of reservoir gas that are liquefied at the surface in lease separators, field facilities, or gas processing plants. Natural gas liquids include but are not limited to ethane, propane, butanes, pentanes, natural gasoline, and condensate.

Reservoir. A reservoir is a porous and permeable underground formation containing an individual and separate natural accumulation of producible hydrocarbons (oil and/or gas) which is confined by impermeable rock and/or water barriers and is characterized by a single natural pressure system. In most situations, reservoirs are classified as oil reservoirs or as gas reservoirs by a regulatory agency. In the absence of a regulatory authority, the classification is based on the natural occurrence of the hydrocarbon in the reservoir as determined by the operator.

Improved Recovery. This includes all methods for supplementing natural reservoir forces and energy, or otherwise increasing ultimate recovery from a reservoir. Such recovery techniques include (1) pressure maintenance, (2) cycling, and (3) secondary recovery in its original sense (i.e., fluid injection applied relatively late in the productive history of a reservoir for the purpose of stimulating production after recovery by primary methods of flow or artificial lift has approached an economic limit). Improved recovery also includes the enhanced recovery methods of thermal, chemical flooding, and the use of miscible and immiscible displacement fluids.

Reserves [271]. These are estimated volumes of crude oil, condensate, natural gas, natural gas liquids, and associated substances anticipated to be commercially recoverable and marketable from a given date forward, under existing economic conditions, by established operating practices, and under current government regulations. Reserves do not include volumes of crude oil, condensate, or natural gas liquids being held in inventory.

Reserve estimates are based on interpretation of geologic and/or engineering data available at the time of the estimate. Existing economic conditions are

** Where reservoir conditions are such that the production of associated gas does not substantially affect the recovery of crude oil in the reservoir, such gas may be classified as nonassociated gas by a regulatory agency. In this event, reserves and production are reported in accordance with the classification used by the regulatory agency.

prices, costs, and markets prevailing at the time of the estimate. Other assumed future economic conditions may lead to different estimates of recoverable volumes; these volumes are not considered reserves under existing economic conditions constraints, but may be identified as resources.

Marketable means that facilities to process and transport reserves to market are operational at the time of the estimate, or that there is a commitment to install such facilities in the near future, and there is a readily definable market or sales contract. Reserve estimates generally will be revised as reservoirs are produced, as additional geologic and/or engineering data become available, or as economic conditions change.

Natural gas reserves are those volumes which are expected to be produced and that may have been reduced by onsite usage, by removal of nonhydrocarbon gases, condensate or natural gas liquids.

Reserves may be attributed to either natural reservoir or improved recovery methods. Improved recovery includes all methods for supplementing natural reservoir energy to increase ultimate recovery from a reservoir. Such methods include (1) pressure maintenance, (2) cycling, (3) waterflooding, (4) thermal methods, (5) chemical flooding, and (6) the use of miscible and immiscible displacement fluids. Reserves attributed to improved recovery methods usually will be distinguished from those attributed to primary recovery.

All reserve estimates involve some degree of uncertainty, depending chiefly on the amount and reliability of geologic and engineering data available at the time of the estimate and the interpretation of these data. The relative degree of uncertainty may be conveyed by placing reserves in one of two classifications, either proved or unproved. Unproved reserves are less certain to be recovered than proved reserves and may be subclassified as probable or possible to denote progressively increasing uncertainty.

Classification of Reserves

Proved Reserves. Attributed to known reservoirs, proved reserves can be estimated with reasonable certainty. In general, reserves are considered proved if commercial producibility of the reservoir is supported by actual production or formation tests. The term proved refers to the estimated volume of reserves and not just to the productivity of the well or reservoir. In certain instances, proved reserves may be assigned on the basis of a combination of core analysis and/or electrical and other type logs that indicate the reservoirs are analogous to reservoirs in the same areas that are producing, or have demonstrated the ability to produce in a formation test. The area of a reservoir considered proved includes (1) the area delineated by drilling and defined by fluid contacts, if any, and (2) the undrilled areas that can be reasonably judged as commercially productive on the basis of available geological and engineering data. In the absence of data on fluid contacts, the lowest known structural occurrence of hydrocarbons controls the proved limit unless otherwise indicated by definitive engineering or performance data.

In general, proved undeveloped reserves are assigned to undrilled locations that satisfy the following conditions: (1) the locations are direct offsets to wells that have indicated commercial production in the objective formation, (2) it is reasonably certain that the locations are within the known proved productive limits of the objective formation, (3) the locations conform to existing well spacing regulation, if any, and (4) it is reasonably certain that the locations will be developed. Reserves for other undrilled locations are classified as proved undeveloped only in those cases where interpretation of data from wells indicates

that the objective formation is laterally continuous and contains commercially recoverable hydrocarbons at locations beyond direct offsets.

Reserves that can be produced through the application of established improved recovery methods are included in the proved classification when: (1) successful testing by a pilot project or favorable production or pressure response of an installed program in that reservoir, or one in the immediate area with similar rock and fluid properties, provides support for the engineering analysis on which the project or program is based and (2) it is reasonably certain the project will proceed.

Reserves to be recovered by improved recovery methods that have yet to be established through repeated commercially successful application are included in the proved category only after a favorable production response from the reservoir from either (1) a representative pilot or (2) an installed program that provides support for the engineering analysis on which the project or program is based.

Unproved Reserves. These are based on geologic and/or engineering data similar to that used in estimates of proved reserves, but technical, contractual, or regulatory uncertainties preclude such reserves being classified as proved. Estimates of unproved reserves may be made for internal planning of special evaluations, but are not routinely compiled.

Unproved reserves are not to be added to proved reserves because of different levels of uncertainty. Unproved reserves may be divided into two subclassifications: probable and possible.

Probable Reserves. These reserves are attributed to known accumulations and are less certain to be recovered than proved reserves. In general, probable reserves may include (1) reserves that appear to exist a reasonable distance beyond the proved limits of productive reservoirs, where fluid contacts have not been determined and proved limits are established by the lowest known structural occurrence of hydrocarbons, (2) reserves in formations that appear to be productive from core and/or log characteristics only, but that lack definitive tests or analogous producing reservoirs in the area, (3) reserves in a portion of a formation that has been proved productive in other areas in a field, but that is separated from the proved area by faults, (4) reserves obtainable by improved recovery methods and located where an improved recovery method (that has yet to be established through repeated commercially successful operation) is planned but not yet in operation, and where a successful pilot test has not been performed but reservoir and formation characteristics appear favorable for its success, (5) reserves in the same reservoir as proved reserves that would be recoverable if a more efficient primary recovery mechanism were to develop than that assumed in estimating proved reserves, (6) incremental reserves attributable to infill drilling where closer statutory spacing had not been approved at the time of the estimate, and (7) reserves that are dependent for recovery on a successful workover, treatment, retreatment, change of equipment, or other mechanical procedures, when such procedures have not been proved successful in wells exhibiting similar behavior in analogous formations.

Possible Reserves. These are associated with known accumulations and are less certain to be recovered than probable reserves. In general, possible reserves may include (1) reserves indicated by structural and/or stratigraphic extrapolation from developed areas, (2) reserves located where reasonably definitive geophysical interpretations indicate an accumulation larger than could be included

within the proved and probable limits, (3) reserves in formations that have favorable log characteristics but questionable productivity, (4) reserves in untested fault segments adjacent to proved reservoirs where a reasonable doubt exists as to whether such fault segment contains recoverable hydrocarbons, (5) incremental reserves attributable to infill drilling that are subject to technical or regulatory uncertainty, and (6) reserves from a planned improved recovery program that is not in operation and that is in a field in which formation, fluid, or reservoir characteristics are such that a reasonable doubt exists to its success.

Reserve Status Categories. These define the development and producing status of wells and/or reservoirs. They may be applied to proved or unproved (probable or possible) reserves.

Developed Reserves. These are expected to be recovered from existing wells (including reserves behind pipe). Improved recovery reserves are considered developed only after the necessary equipment has been installed, or when the costs to do so are relatively minor. Developed reserves may be subcategorized as producing or nonproducing.

Producing Reserves. These are expected to be recovered from completion intervals open at the time of the estimate and producing to market. Improved recovery reserves are considered to be producing only after an improved recovery project is in operation. Unproved (probable or possible) producing reserves are in addition to proved producing reserves, such as (1) reserves that may be recovered from portions of the reservoir downdip from proved reserves or (2) reserves that may be recovered if a higher recovery factor is realized than was used in the estimate of proved reserves.

Nonproducing Reserves. These include shut-in and behind-pipe reserves. Shut-in reserves are expected to be recovered from completion intervals open at the time of the estimate, but which have not started producing, or were shut in for market conditions of pipeline connection, or were not capable of production for mechanical reasons, and the time when sales will start is uncertain. Behind-pipe reserves are expected to be recovered from zones behind casing in existing wells, which will require additional completion work or a future recompletion prior to the start of production.

Undeveloped Reserves. These are expected to be recovered: (1) from new wells on undrilled acreage, (2) from deepening existing wells to a different reservoir, or (3) where a relatively large expenditure is required to (a) recomplete an existing well, or (b) install production or transportation facilities for primary or improved recovery projects. Undeveloped reserves usually will be distinguished from developed reserves. The ownership status of reserves may change due to the expiration of a production license or contract; when relevant to reserve assignment, such changes should be identified for each reserve classification.

Methods of Estimating Reserves

Methods of determining reserves progress from analogy, before a well is drilled, to history after it is plugged and abandoned. The accuracy with which reserves can be estimated progresses along the same path from speculation to history.

Analogy

The decision to drill a well is based upon the potential reserves that it will recover. This means that an engineer must be able to predict reserves before a well is drilled. The lack of information about the reservoir restricts the engineering methods available.

Analogy is the only method which can be used without specific well information such as porosity, reservoir thickness, and water saturation. Because analogy employs no specific information about a well, it is the least accurate method of determining reserves. Methods of analogous reserve determination depend on the proximity of similar reserves. The best analogy can be made by taking the median ultimate recovery of a number of wells that are closest and have the same formation and characteristics expected in the proposed well. When ultimate recovery data are not available, volumetric, decline curve or other methods of estimating ultimate recovery may be used.

Unless values of ultimate recovery figures for the group are relatively close, the median ultimate recovery should be calculated by making a normal probability plot. This plot is made by graphing estimated ultimate recovery against the cumulative percent of samples. A best-fit line is drawn through the points and the median is read where the line intersects fifty percent. A straight line indicates a normal distribution; if the line is not straight the distribution is skewed. If there are no similar wells in the area, data from those less similar may be used, but confidence goes down as similarity decreases.

Volumetric

If a well is drilled after reserves are determined by analogy, factual information becomes available and reserves can then be determined volumetrically. From log analysis the porosity, water saturation, and productive formation thickness are estimated. A reasonable drainage area is assigned and total hydrocarbons in place are then calculated. When enough wells have been drilled to delineate the field, a subsurface geological contour map showing the subsea sand top and bottom depth, oil-water contact, and gas-oil contact can be prepared. From this map the total areas in acre-feet of each contour are planimetered and graphed as the abscissa against the subsea depth as the ordinate. Lines are then drawn to connect the sand-top points and the sand-bottom-points, the area bounded by the oil-water-contact depth, the sand-top line, the sand-bottom line and the gas-oil-contact line. This area is the gross oil-bearing sand-volume in acre-feet. The area, if present, that is bounded by the gas-oil contact depth, the sand-top-line, the sand-bottom-line and the abscissa is the gross gas-bearing sand-volume in acre-feet. The engineer must determine from core data and/or electric logs the percentage of the gross sand volume that is productive and must then reduce the total acre-feet by that percentage. If there is no subsurface contour map available or if the reservoir is very heterogeneous, an isopach or an isovol map should be constructed. An isopach map is constructed by contouring net sand thickness. This kind of map works well when the reservoir is uniform and when porosity and water saturation are relatively constant. When the water saturation and porosity vary widely from well to well, an isovol map that indicates hydrocarbon thickness is useful. This map is constructed by contouring the value of net pay height multiplied by porosity and by one minus the water saturation. Care should be taken not to rely on the scale provided on the map especially when using xero-graphed copies, as this and other methods of reproduction can distort one or both axes as much as five percent. A known area such as a section

should be measured to calibrate the instrument. Once the contour areas have been planimetered, the net pay volume can be calculated in several ways. If the number of contour intervals is even, the volume can be calculated by Simpson's rule [272]:

$$V_R = 1/3h [(y_o + y_n) + 4(y_1 + y_3 + \dots + Y_{n-1}) + 2(y_2 + y_4 + \dots + y_{n-2})] \quad (5-197)$$

where V_R = reservoir volume, acre-ft
 h = contour interval, ft
 y_o = area on top of sand minus area on base of sand at the highest contour
 y_n = area on top of sand minus area on base of sand at the lowest contour

When the number of contours is uneven, the volume can be found using the slightly less accurate trapezoidal method:

$$V_R = h[1/2(y_o + y_n) + y_1 + y_2 + \dots + Y_{n-1}] \quad (5-198)$$

Once the reservoir volume is known, the oil in place, N , in stock tank barrels is calculated by an equation similar to that given earlier:

$$N = \frac{7,758V_o(1-S_w)}{B_o} \quad (5-199)$$

where N = reservoir oil initially in place, STB
 7,758 = number of barrels/ acre-ft
 V_o = net producing reservoir volume, acre-ft
 B_o = oil formation volume factor, RB/STB
 S_w = interstitial water saturation, fraction
 ϕ = formation porosity, fraction

Similarly gas-in-place, G , in thousands of standard cubic feet, is estimated by an expression similar to that given earlier:

$$G = \frac{43,560V_g\phi(1-S_w)pT_s}{zTp_s} \quad (5-200)$$

where G = gas in place, scf
 V_g = gas bearing volume of reservoir, acre-ft
 p_s = standard pressure, psia
 T = reservoir temperature, degrees absolute
 T_s = standard temperature base, degrees absolute
 z = gas deviation factor at reservoir conditions

Volumetric analysis yields the total hydrocarbon content of the reservoir; this figure must be adjusted by a recovery factor to reflect the ultimate recoverable reserves. Recovery factors are based upon empirical correlations, experience, or analogy.

Material Balance

If a field development program has been well planned and executed, enough information should be available to calculate reserves by the material balance equation. The material balance equation is derived on the assumption that the reservoir is a homogeneous vessel with uniform porosity, permeability, and fluid properties. The equation accounts for all quantities of materials that enter or leave the vessel. The simplest form of the equation is that initial volume is equal to the volume remaining plus the volume removed. As material is withdrawn from a constant-volume reservoir the pressure declines and remaining material expands to fill the reservoir. Laboratory PVT analysis of the reservoir fluid defines the change in volume per unit pressure drop. Knowing the amount of fluid withdrawn from the reservoir and the drop in pressure one can calculate the corresponding volume of fluid at the original reservoir pressure. The calculated reservoir size should remain constant as fluid is withdrawn and pressure drops. If the calculated reservoir size changes constantly in one direction as the field is produced the assumed production mechanism is probably wrong. Calculations should be repeated assuming different mechanisms until one is found that yields a constant reservoir size. Since Schilthuis [249] developed the original material balance equation in 1936 it has been rearranged to solve almost any unknown. The most frequently used forms of the equation are for these types of recovery mechanisms [272]:

1. Oil reservoir with gas cap and active water drive.
2. Oil reservoir with gas cap and no active water drive.
3. Initially undersaturated oil reservoir with active water drive: A. Above bubble point. B. Below bubble point.
4. Initially undersaturated oil reservoir with no active water drive: A. Above bubble point. B. Below bubble point.
5. Gas reservoir with active water drive.
6. Gas reservoir with no active water drive.

The material balance equation, when combined with reliable relative permeability data, can be used to predict future reservoir performance. Many times, reservoirs do not conform to the assumptions made in the material balance equation. Few reservoirs are homogeneous and no reservoirs respond instantaneously to changes in pressure. The precision with which reserves can be calculated or predicted with the material balance equation is affected by the quality of data available and the degree of agreement between the assumptions made in the equation and the actual reservoir conditions.

Model Studies

Predicting reservoir performance with the Turner [250] or the Muskat [251] method is a long and tedious process and, even with a programmable calculator, the process takes several hours. To resolve the problems caused by the assumptions inherent in the material balance equation, a reservoir would have to be broken up into parts small enough to be considered homogeneous. The material balance equation would then have to be calculated for each part and for each increment of production. This would entail thousands of calculations performed thousands of times and would drastically limit the number of reservoir simulations an engineer could run. Fortunately, computers have cut the required time to a few minutes. Numerical simulators divide the reservoir up into discreet

elements, each having the properties and spatial orientation of the associated blocks of a physical reservoir [273]. The simulator treats each block as a small reservoir, and keeps track of fluid entering or leaving the block. When a change in pressure due to injection or withdrawal of fluid occurs, the simulator solves the material balance equation for a number of time steps for each block until equilibrium is reached. Blocks are usually configured so that each well is in an individual block. Time steps are picked so that the required information is resolved without using excessive computer time. Since the simulator keeps track of fluid movement through the reservoir, the output can include a wide variety of parameters. Fluid fronts, saturation changes, pressure distribution, and oil-water contact movement are a few of the things that can be plotted. The three general classifications of simulators are gas, black oil, and compositional. Gas simulators model one or two phases (gas or gas and water). Black oil simulators are designed to model any proportion of gas, oil, and water, and they account for gas going into or out of solution. Compositional simulators are used when PVT data does not adequately describe reservoir behavior such as in condensate reservoirs. These simulators calculate the mass fraction of individual components in each phase and mass transfer between phases as each phase flows at different rates. Most models are run with limited information and must be tuned to properly predict actual reservoir performance. This is done by changing parameters such as relative permeability, porosity, and permeability data until the simulator matches the field history.

Production Decline Curves

The most widely used method of estimating reserves is the production rate decline-curve. This method involves extrapolation of the trend in performance. If a continuously changing continuous function is plotted as the dependent variable against an independent variable, a mathematical or graphical trend can be established. Extrapolation of that trend can then permit a prediction of future performance. For an oil reservoir, the plot of the logarithm of production rate against time is most useful. Although decline-curve analysis is empirical, if care is taken to ensure that production rates are not being affected by such things as the mechanical degradation of equipment or the plugging of the formation by fines or paraffin, the method is reasonably accurate. As discussed, there are three major types of decline curves: constant percentage or exponential, hyperbolic, and harmonic. Although analysis of a large number of actual production decline curves indicates that most wells exhibit a hyperbolic decline with an n value falling between 0 and 0.4, the constant-percentage exponential decline-curve is most widely used. The exponential decline curve is most popular because, when plotted on semilog paper the points make a straight line which is easiest to extrapolate to the economic limit. Now that programmable calculators and personal computers reside at most every engineer's desk, it is easy to punch in the production data and decide which decline curve is best.

Quality of Reserve Estimates

If reserve estimates contained no risk, no dry holes would be drilled. Unfortunately, risk is inversely proportional to knowledge and the least is known before a well is drilled. Hudson and Neuse [274] presented a graphical representation (reproduced in Figure 5-147) of reserve estimate quality throughout the life of a property. Section 1 shows the production history of the property. Section 2 indicates the probable risk factor associated with each stage of

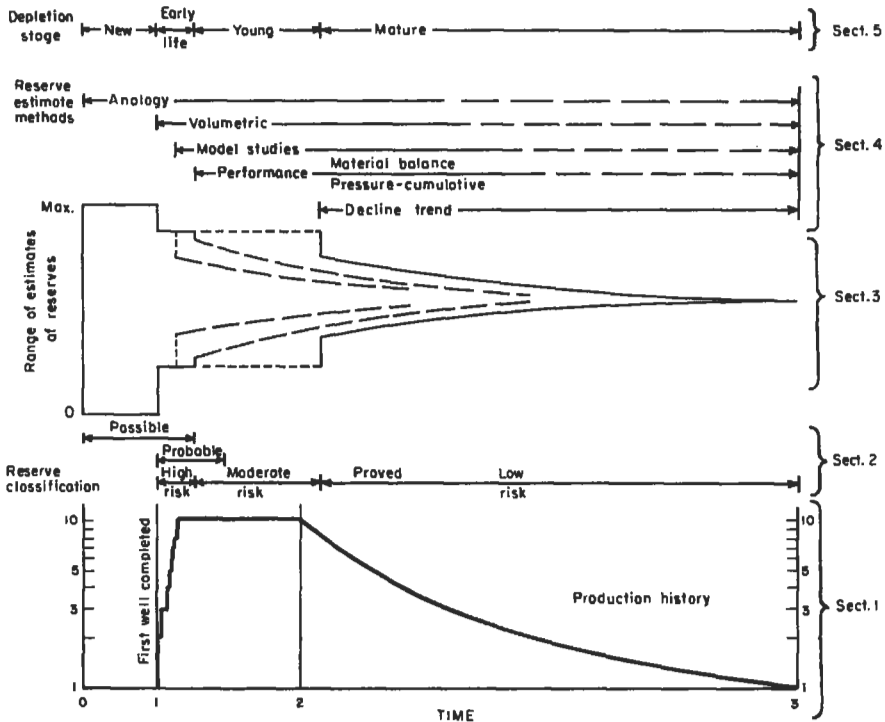


Figure 5-147. Quality of reserves [274].

production from completion to depletion. Section 3 shows the range of possible reserve estimates through the life of the property. Section 4 shows at what stage of the life of the property each method of reserve estimate method becomes available. The solid line indicates for what period each method is most applicable. Section 5 names the depletion stage of the reservoir.

The quality of reserve estimates throughout the industry should improve now that the SPE definitions for proved reserves are being accepted. When the definitions for probable and possible reserves are approved, uniform factors for risk analysis can be made [275].

SECONDARY RECOVERY

Definitions

Secondary and Tertiary Recovery

Primary recovery, as already discussed, refers to the recovery of oil and/or gas that is recovered by either natural flow or artificial lift through a single wellbore. Thus, primary recovery occurs as a result of the energy initially present in the reservoir at the time of discovery. When the initial energy has been depleted and the rate of oil recovery declines, oil production can be increased by the injection of secondary energy into the reservoir. Secondary recovery is the recovery of oil and/or gas that involves the introduction of artificial energy

into the reservoir via one wellbore and production of oil and/or gas from another wellbore. Conventional means of secondary recovery include the immiscible processes of waterflooding and gas injection. Currently in the United States, waterflooding is the dominant secondary recovery method in that about half of the oil production is recovered from waterflood projects. After secondary recovery, a substantial amount of oil may remain, and attempts to recover oil beyond primary and secondary recovery are referred to as tertiary recovery. Any method that recovers oil more effectively than plain waterflooding or gas injection is defined as enhanced recovery. The more sophisticated enhanced methods may be initiated as a tertiary process if they follow waterflooding or gas injection, or they may be a secondary process if they follow primary recovery directly. Many of the enhanced recovery projects are implemented after waterflooding. (Enhanced recovery methods are discussed later.)

Pressure Maintenance

Pressure maintenance is a secondary recovery process that is implemented early during the primary producing phase before reservoir energy has been depleted. Pressure maintenance projects, which can be accomplished by the injection of either gas or water, will almost always recover more oil reserves than are recoverable by primary producing mechanisms. For example, the return of gas to the formation early in the primary producing history of a field will permit higher rates of oil production.

Gas Injection

Historically, both natural gas and air have been used in gas injection projects, and in some cases nitrogen and flue gases have been injected. Many of the early gas injection projects used air to immiscibly displace crude oil from reservoirs. The injection of hydrocarbon gas may result in either a miscible or immiscible process depending on the composition of the injected gas and crude oil displaced, reservoir pressure, and reservoir temperature. Hydrocarbon miscible injection is considered as an enhanced recovery process and is discussed later.

Although the ultimate oil recovered from immiscible gas injection projects will normally be lower than for waterflooding, gas injection may be the only alternative for secondary recovery under certain circumstances. If permeability is very low, the rate of water injection may be so low that gas injection is preferred. In reservoirs with swelling clays, gas injection may be preferable. In steeply-dipping reservoirs, gas that is injected updip can very efficiently displace crude oil by a gravity drainage mechanism; this technique is very effective in low-permeability formations such as fractured shales. In thick formations with little dip, injected gas (because of its lower density) will tend to override and result in vertical segregation if the vertical permeability is more than about 200 md [254]. In thin formations especially if primary oil production has been by solution-gas drive, gas may be injected into a number of wells in the reservoir on a well pattern basis; this dispersed gas injection operation attempts to bank the oil in a frontal displacement mechanism. In addition to the external gas injection into reservoirs with dip as just described (which may be into a primary or secondary gas cap), a variation called attic oil recovery involves injection of gas into a lower structural position. If there is sufficient vertical permeability, the injected gas will migrate upward to create a secondary gas cap that can displace the oil downward where it is recovered in wells that are already drilled.

Volumetric calculations for gas injection are given in Table 5-34. The material balance equation for dispersed gas injection in a solution-gas-drive reservoir where there is no water influx, no water production, and no gas cap can be expressed in terms of the oil produced during an interval [254]:

$$\Delta N_p = \frac{(1 - N_{p1}) \left(\frac{dB_o}{dB_g} - dR_s \right) - d \left[\left(\frac{1}{B_g} \right) B_{ob} \right]}{\left(\frac{B_o}{B_g} - R_s \right)_2 + R_{avg}(1 - I)} \quad (5-201)$$

Table 5-34
Volumetric Calculations for Gas Injection

Gas drive field with gas cap

$$\frac{dS_o}{dp} = \frac{\frac{B_g S_o}{B_o} \frac{dR_s}{dp} + \frac{k_g \mu_o S_o}{k_o \mu_g B_o} \frac{dB_o}{dp} - \frac{(1 - S_o - S_w) + m(1 - S_w)}{B_g} \frac{dB_g}{dp}}{1 + \frac{k_g \mu_o}{k_o \mu_g}}$$

m = ratio of gas-cap pore volume to oil-zone pore volume, bbl/bbl or ft³/ft³. For each 1 bbl of oil zone there will be m bbls gas cap.

Reinjection of all produced gas-pressure maintenance

$$\frac{dS_o}{dp} = \frac{\frac{B_g S_o}{B_o} \frac{dR_s}{dp} - \frac{R_s B_g S_o}{B_o^2} \frac{dB_o}{dp} - \frac{(1 - S_o - S_w)}{B_g} \frac{dB_g}{dp}}{1 - \frac{R_s B_g}{B_o}}$$

Gas reinjection

$$\text{Producing GOR } R = \frac{k_g \mu_o B_o}{k_o \mu_g B_g} + R_s$$

$$\text{Net GOR } R = \left(\frac{k_g \mu_o B_o}{k_o \mu_g B_g} + R_s \right) (1 - I)$$

I = fraction of gas that is reinjected

$$\frac{dS_o}{dp} = \frac{\frac{B_g S_o}{B_o} \frac{dR_s}{dp} + \left[(1 - I) \frac{k_g \mu_o S_o}{k_o \mu_g B_o} - \frac{I R_s B_g S_o}{B_o^2} \right] \frac{dB_o}{dp} - \left[\frac{(1 - S_o - S_w) + m(1 - S_w)}{B_g} \frac{dB_g}{dp} \right]}{1 + (1 - I) \left(\frac{k_g \mu_o}{k_o \mu_g} \right) - \frac{I R_s B_g}{B_o}}$$

m = ratio of gas-cap volume to oil-zone volume

From References 14 and 254.

where I is the constant fraction of the produced gas which is reinjected into the oil reservoir, B_{ob} is the oil formation volume factor at bubble-point conditions, R is the producing gas-oil ratio, the subscripts 1 and 2 refer to the time increments at p_1 and p_2 , the other standard terms are as already defined, and R_{avg} is $(R_1 + R_2)/2$. As given in Table 5-34, the instantaneous gas-oil ratio, R , is:

$$R = R_s + \frac{B_o k_g \mu_o}{B_g k_o \mu_g} \quad (5-202)$$

where R_s is the solution gas-oil ratio, B is formation volume factor, k is permeability, μ is viscosity, and the subscripts o and g refer to oil and gas, respectively. The relative permeabilities are determined at the total liquid saturation, S_L :

$$S_L = S_w + S_o = S_w + (1 - S_w) \frac{(N - N_p) B_o}{N B_{ob}} \quad (5-203)$$

The simultaneous solution of these three equations will provide estimates of oil produced at any chosen conditions for a dispersed-gas-drive injection project. Additional details can be found in Reference 254.

Many of the flow equations and concepts for immiscible gas displacement are similar to those that will be presented later for waterflooding. Because of the importance of water injection processes in U.S. operations, waterflooding concepts will be emphasized.

Water Injection

Water injection processes may be designed to: (1) dispose of brine water, (2) conduct a pressure maintenance project to maintain reservoir pressure when expansion of an aquifer or gas cap is insufficient to maintain pressure, or (3) implement a water drive or waterflood of oil after primary recovery. As mentioned before, waterflooding is the dominant secondary recovery process which accounts for about 50% of the current oil production in U. S. operations. Because of the importance of waterflooding, fluid displacement in waterflooded reservoirs is covered as a separate discussion in a later section.

Spacing of Wells and Well Patterns

Spacing of Wells

One section (one sq mile or 5,280 ft by 5,280 ft) is 640 acres. If wells are drilled evenly such that each well is theoretically assigned to drain 40 acres, the 16 wells per section would be as spaced as in Figure 5-148. Each 40 acres ($1/4$ mile by $1/4$ mile or 1,320 ft by 1,320 ft) would contain $40 \times 43,560$ or 1,742,400 ft². The 10-acre region in Figure 5-148 would measure 660 ft by 660 ft and would contain 435,000 ft². Similarly, a 20-acre region would contain 871,200 ft² and would measure $[20 \times 871,200]^{1/2}$ or 933.4 ft by 933.4 ft.

In many parts of the United States, 40-acre spacing or less is common for oil wells, and 160-acre or 320-acre spacing is common for gas wells. Because drilling costs increase considerably with depth, deeper wells may be on larger spacing.

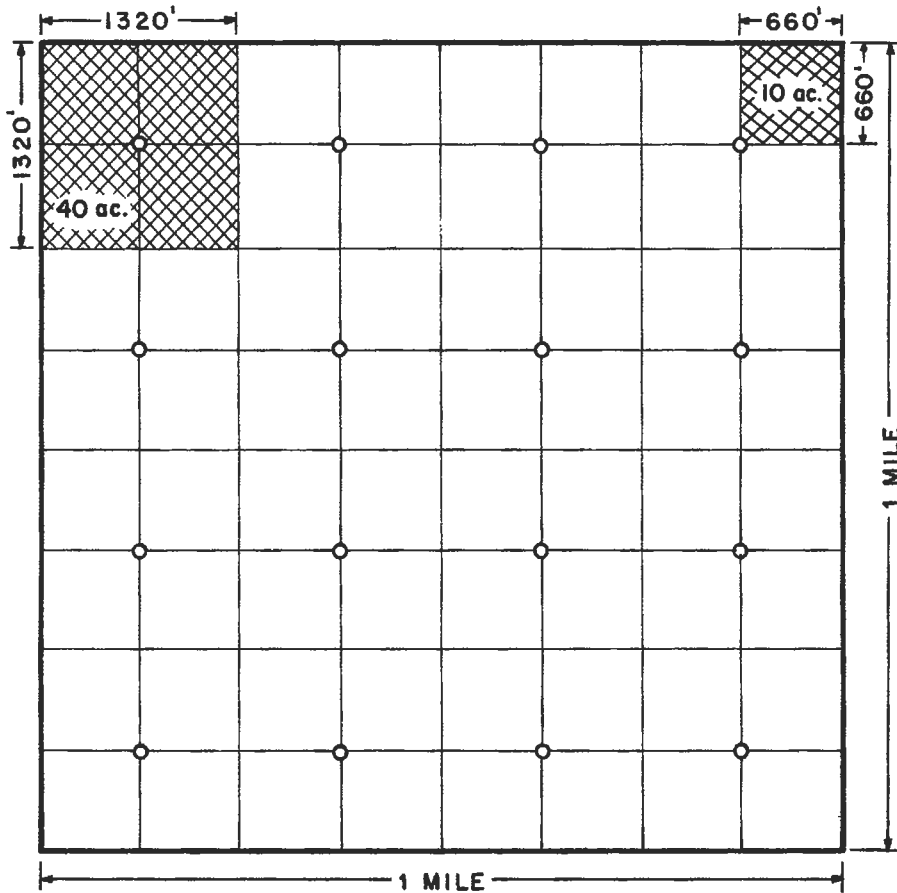


Figure 5-148. Well locations for 40-acre spacing.

Injection Well Placement

Wells may be spaced evenly or unevenly from each other based on surface topology, lease boundaries, regulations, or other factors. Many older fields were developed on irregular spacing. In more recent times, more uniform drilling patterns and well spacing have been used.

In most cases when an injection project is started, primary recovery has been implemented and producing wells will already be in place. For some projects, a number of existing wells will be converted from producers to injectors, and in other cases, new injection wells will be drilled. In either event, the injection well placement must be compatible with the existing wells and should [133]: (1) take advantage of known reservoir uniformities or nonuniformities (fractures, directional permeability, regional permeabilities, dip, etc.), (2) provide sufficient fluid injection rate to yield the desired production rate, (3) maximize recovery with a minimum of production of the injected fluid, and (4) in most cases, require a minimum of new wells. Two general types of well locations are

common: (1) peripheral or central flooding where the injectors are grouped together, and (2) pattern flooding where certain patterns are repeated throughout the field. The relative location of injectors and producers depends on the geology and type of reservoir, the volume of reservoir swept, and the time limitations that affect economics. When possible, the injection scheme should take advantage of gravity, i.e., dipping or inclined reservoirs, gas caps, or underlying aquifers.

Peripheral or Central Flooding

In peripheral flooding, the injectors are located around the periphery so that the flood progresses toward the center as shown in Figure 5-149. When the first row of producers flood out, they are converted to injection status. This type of flood can result in maximum oil recovery with a minimum of produced injectant, and less injectant is required for a given amount of production, but a peripheral flood usually takes longer than a pattern flood. In general, adequate permeability is required to permit movement of fluids at an acceptable rate with the available well spacing. Central flooding is the opposite case in which injectors are located in the center of the field, and the flood progresses outward (see Figure 5-149).

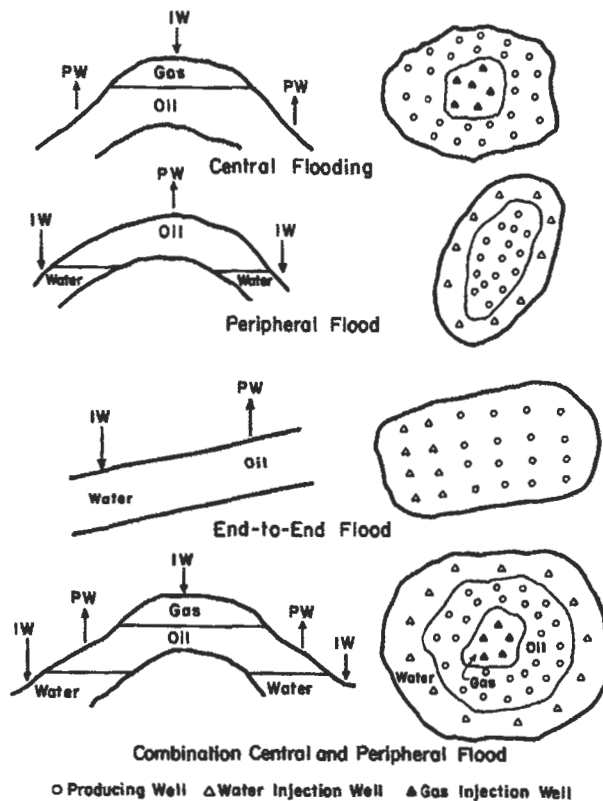


Figure 5-149. Peripheral and central flooding.

A form of peripheral flooding is an end-to-end flood such as that shown in Figure 5-149. This type of injection could include the injection of gas into a gas cap or the injection of water into an aquifer. The choice of peripheral or repeating pattern flood is usually made on the basis of: formation permeability, formation dip, area and dimensions of the reservoir, and the initial production response that is acceptable.

Pattern Flooding

In pattern flooding, the injectors are distributed among the producers in some repeating fashion. Examples of the common repeating patterns are shown in Figure 5-150. Pattern flooding is very common, and the selection of the type

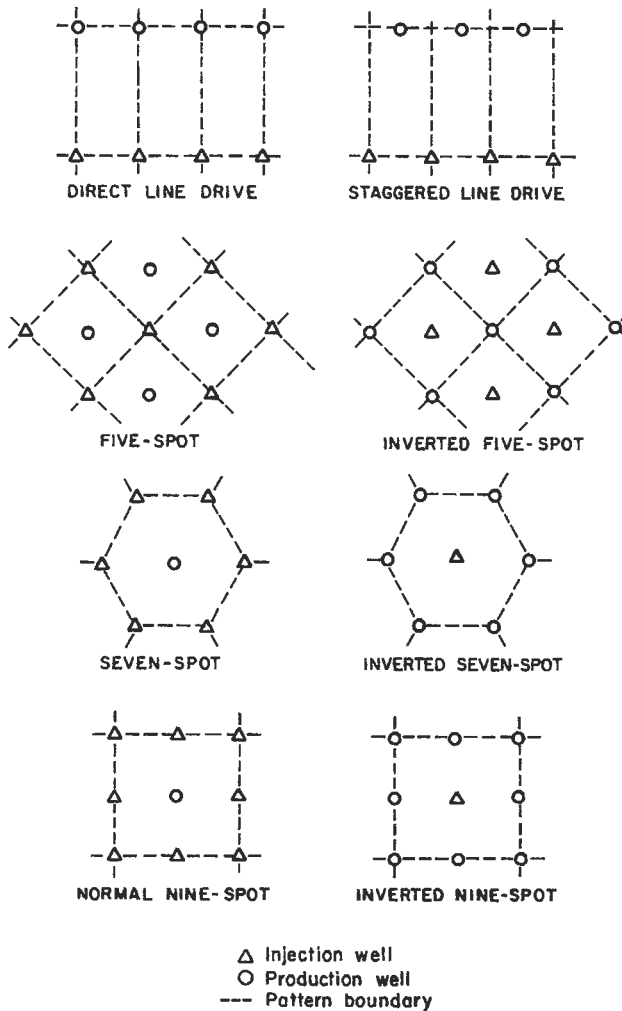


Figure 5-150. Well locations in pattern floods.

of pattern will depend on circumstances in a given field. If existing wells were drilled on square patterns, 5-spots and 9-spots are common, and both yield similar oil recovery and water-oil ratio performance. If the injected fluid is more mobile than the displacing fluid (which is often the case, especially when oil viscosity is high), a pattern having more producers than injectors may be desired to balance the injection and production rates. In cases where the injected fluid is less mobile or when the formation permeability is low, a pattern having more injectors than producers may be desired. From an inspection of Figure 5-150, the ratio of producers to injectors for the various patterns can be determined as given in Table 5-35. For either the normal (or regular) 5-spot or the inverted 5-spot (inverted means one injector per pattern), the ratio of producers to injectors is 1:1; in this case, the distinction between normal and inverted is only important if a few patterns are involved, such as for a small pilot flood. For the 7-spot and 9-spot patterns, the distinction between normal and inverted patterns is more important.

There is often confusion between well spacing (or density) and pattern size. As shown in Figure 5-151, the pattern area for a 5-spot is twice the well spacing or well density, and the pattern area for a 9-spot is four times the well spacing. When information is given concerning patterns of a given size, the reader is cautioned to find out if well spacing or pattern size is intended.

Dimensions of various distances for 5-spot patterns and 9-spot patterns with different well spacings are given in Table 5-36. For the 9-spot pattern, s refers to the shortest distance from a side injection well and the central producer (the opposite for an inverted pattern), and l refers to the longest or lateral distance from injector to producer. For the 5-spot pattern, l is the lateral or straight-line distance from injector to producer, a refers to the distance between wells that are alike, and d refers to the distance between the dissimilar wells. Distances of d and a for the line drive pattern and staggered line drive pattern are shown in Figure 5-152; the 5-spot pattern is a special case of the staggered line drive when d/a is 0.5.

Pattern selection is important because it can affect the area swept by the injected fluid. Areal or pattern sweep efficiency is discussed in the section under fluid movement in waterflooded reservoirs, but the principles apply to either water or gas injection.

Table 5-35
Well Patterns

Pattern	Ratio of producers to injectors	Drilling pattern
Direct line drive	1	Rectangle
Staggered line drive	1	Offset line of wells
5-spot	1	Square
Normal 7-spot	1/2	Equilateral triangle
Inverted 7-spot	2	Equilateral triangle
Normal 9-spot	1/3	Square
Inverted* 9-spot	3	Square

From Reference 133.

* Inverted: One injection well per pattern

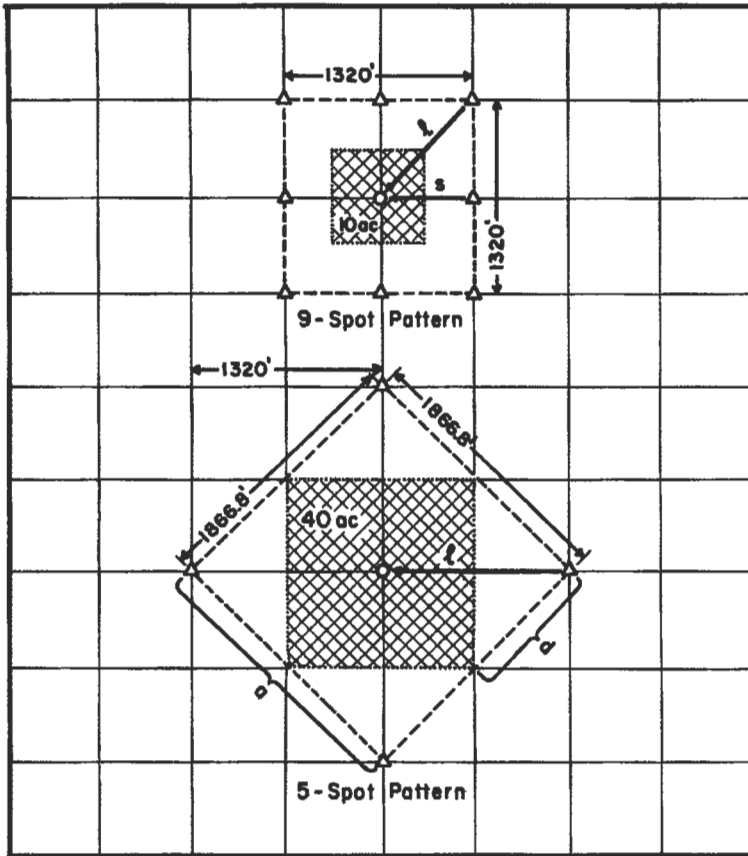
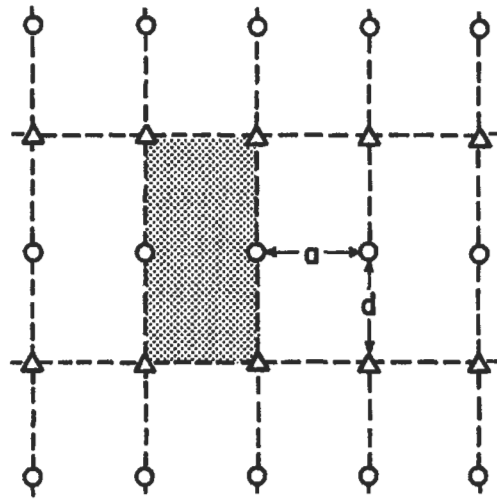


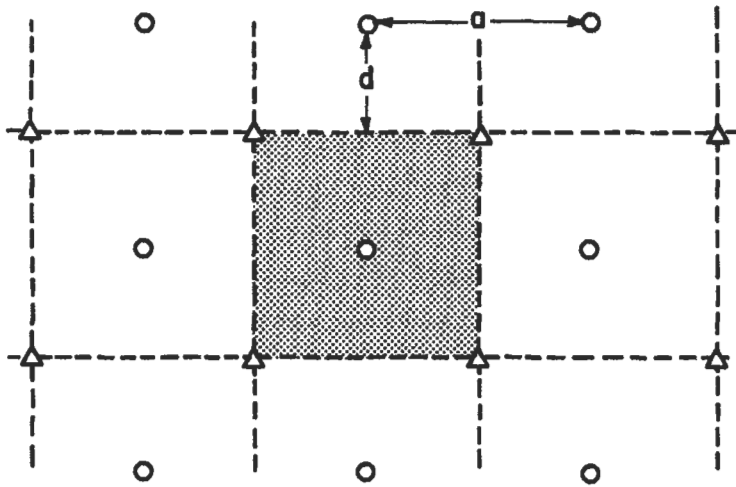
Figure 5-151. Pattern size for 9-spot and 5-spot patterns.

Table 5-36
Well Distances In 5-Spot and 9-Spot Patterns

		5-spot pattern		
Well spacing	Pattern size	a (ft)	d (ft)	l (ft)
5 acres	10 acres	660	330	467
10 acres	20 acres	933	467	660
20 acres	40 acres	1,320	660	933
40 acres	80 acres	1,867	933	1,320
		9-spot pattern		
Well spacing	Pattern size	s (ft)	l (ft)	
5 acres	20 acres	467	660	
10 acres	40 acres	660	933	
20 acres	80 acres	933	1,320	
40 acres	160 acres	1,320	1,867	



Direct Line Drive



Staggered Line Drive

○ Producing Well △ Injection Well --- Pattern Boundary

Figure 5-152. Distances in line drive patterns [25].

FLUID MOVEMENT IN WATERFLOODED RESERVOIRS

Many of the principles discussed in this section also apply to immiscible gas injection, primary recovery by gravity drainage, and natural bottom-water drive. However, because of the importance of waterflooding in the United States, the emphasis is placed on fluid movement in waterflooded reservoirs.

The importance of various factors that affect displacement of oil by water were discussed in the first section. In particular, the discussion on the effect of wettability on relative permeability characteristics is important in the understanding of oil displacement during waterflooding.

Several textbooks on waterflooding are available [133,254,276-278]. The source most often referred to in this section is the excellent SPE monograph by Craig [133]; many of the principles in this monograph are summarized in the Interstate Oil Compact Commission text [277] and in an SPE paper [279]. The text by Smith [254] contains many useful aspects of waterflooding, and the recent SPE text [278] contains a more thorough and mathematical treatment of the subject.

Displacement Mechanisms

Under ideal conditions, water would displace oil from pores in a rock in a piston-like manner or at least in a manner representing a leaky piston. However, because of various wetting conditions, relative permeabilities of water and oil are important in determining where flow of each fluid occurs, and the manner in which oil is displaced by water. In addition, the higher viscosity of crude oil in comparison to water will contribute to nonideal displacement behavior. Several concepts will be defined in order that an understanding of displacement efficiencies can be achieved.

Buckley-Leverett Frontal Advance. By combining the Darcy equations for the flow of oil and water with the expression for capillary pressure, Leverett [100] provided an equation for the fractional flow of water, f_w , at any point in the flow stream:

$$f_w = \frac{1 + \frac{k k_{ro}}{v_t \mu_o} \left(\frac{\partial P_c}{\partial L} - g \Delta \rho \sin \alpha_d \right)}{1 + \frac{\mu_w k_o}{\mu_o k_w}} \tag{5-204}$$

where f_w = fraction of water in the flowing stream passing any point in the rock (i.e., the water cut)

k = formation permeability

k_{ro} = relative permeability to oil

k_o = effective permeability to oil

k_w = effective permeability to water

μ_o = oil viscosity

μ_w = water viscosity

v_t = total fluid velocity (i.e., q_t/A)

P_c = capillary pressure = $p_o - p_w$ = pressure in oil phase minus pressure in water phase

L = distance along direction of movement

g = acceleration due to gravity
 $\Delta\rho$ = water-oil density differences = $\rho_w - \rho_o$
 α_d = angle of the formation dip to the horizontal.

This equation is derived in an appendix in the monograph by Craig [133]. Because relative permeabilities and capillary pressure are functions of only fluid saturation, the fractional flow of water is a function of water saturation alone. In field units, Equation 5-204 becomes [133]:

$$f_w = \frac{1 + 0.001127 \frac{k k_{ro}}{\mu_o} \frac{A}{q_t} \left(\frac{\partial P_c}{\partial L} - 0.433 \Delta\rho \sin \alpha_d \right)}{1 + \frac{\mu_w}{\mu_o} \frac{k_o}{k_w}} \quad (5-205)$$

where permeability is in md, viscosities are in cp, area is in sq ft, flow rate is in B/D, pressure is in psi, distance is in ft, and densities are in g/cc.

In practical usage, the capillary pressure term in Equation 5-204 is neglected [133]:

$$f_w = \frac{1 - \frac{k k_{ro}}{v \mu_o} (g \Delta\rho \sin \alpha_d)}{1 + \frac{\mu_w}{\mu_o} \frac{k_o}{k_w}} \quad (5-206)$$

and for a horizontal displacement of oil by water, the simplified form of this equation is [133]:

$$f_w = \frac{1}{1 + \frac{\mu_w}{\mu_o} \frac{k_{ro}}{k_{rw}}} \quad (5-207)$$

Examples of idealized fractional flow curves, f_w vs. S_w , are given in Figure 5-153 for strongly water-wet and strongly oil-wet conditions [133].

Based on the initial work of Leverett [100], Buckley and Leverett [152] presented equations to describe an immiscible displacement in one-dimensional flow. For incompressible displacement, the velocity of a plane of constant water saturation traveling through a linear system was given by:

$$v = \frac{q}{A\phi} \left(\frac{\partial f_w}{\partial S_w} \right) \quad (5-208)$$

where q is the flow rate in cc/sec (or ft³/D), A is the cross-sectional area in cm² (or ft²), ϕ is the fractional porosity, v is the velocity or rate of advance in cm/sec (or ft/D), and $(\partial f_w / \partial S_w)$ is the slope of the curve of f_w vs. S_w . This equation states that the rate of advance or velocity of a plane of constant water saturation is directly proportional to the derivative of the water cut at that water

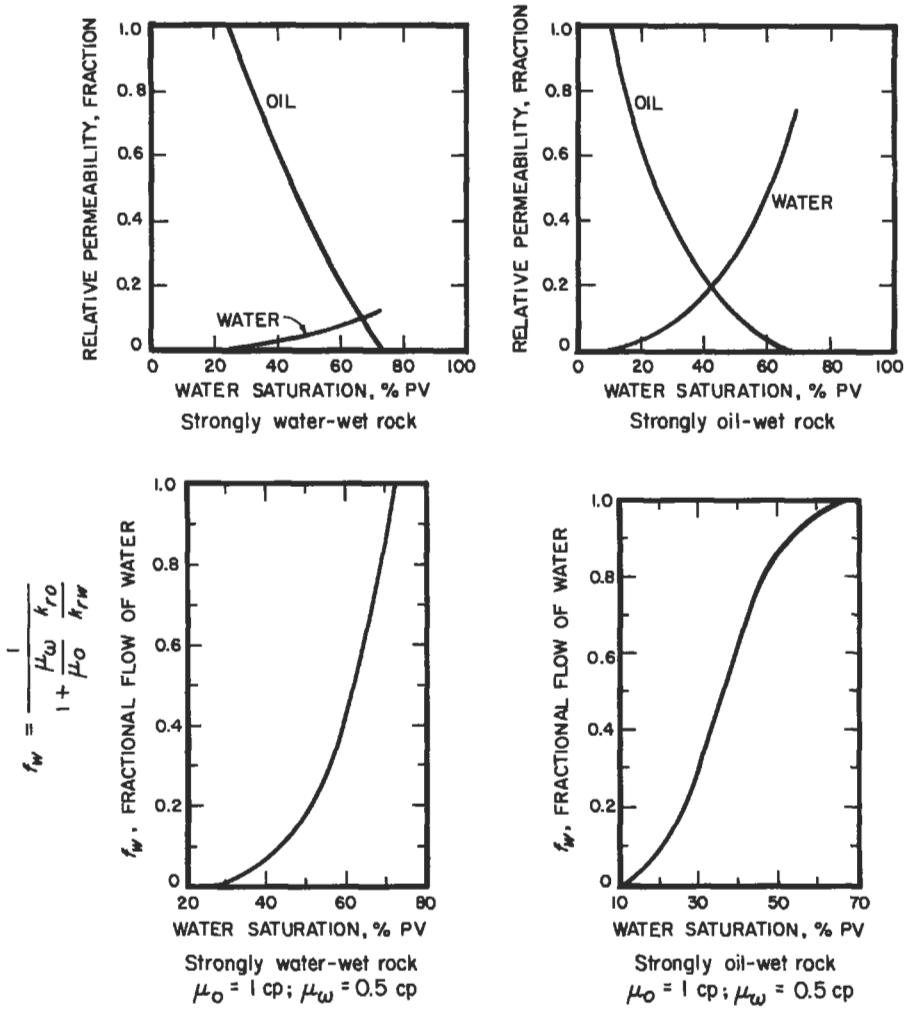


Figure 5-153. Effect of water saturation on relative permeabilities and fractional flow of water [133].

saturation. By integrating Equation 5-208 for the total time since the start of injection, the distance that the plane of given water saturation moves can be given by:

$$L = \frac{W_i}{A\phi} \left(\frac{\partial f_w}{\partial S_w} \right) \tag{5-209}$$

where W_i is the cumulative water injected and L is the distance that a plane of given saturation has moved.

If L is the distance from injector to producer, the time of water breakthrough, t_{bt} , is given by:

$$t_{bt} = \frac{L}{\frac{q_w}{A\phi} \left(\frac{\partial f_w}{\partial S_w} \right)} \quad (5-210)$$

Equation 5-209 can be used to calculate the saturation distribution in a linear waterflood as a function of time. According to Equation 5-209, the distance moved by a given saturation in a given time interval is proportional to the slope of the fractional flow curve at the saturation of interest. If the slope of the fractional flow curve is graphically obtained at a number of saturations, the saturation distribution in the reservoir can be calculated as a function of time. The saturation distribution can then be used to predict oil recovery and required water injection on a time basis. A typical plot of df_w/dS_w vs. S_w will have a maximum as shown in Figure 5-154. However, a problem is that equal values of the slope, df_w/dS_w , can occur at two different saturations which is not possible. To overcome this difficulty, Buckley and Leverett [152] suggested that a portion of the saturation distribution curve is imaginary, and that the real curve contains a saturation discontinuity at the front. Since the Buckley-Leverett procedure neglects capillary pressure, the flood front in a practical situation will not exist as a discontinuity, but will exist as a stabilized zone of finite length with a large saturation gradient.

Welge Graphical Technique. A more simplified graphical technique was proposed by Welge [153] which involves integrating the saturation distribution from the injection point to the front. The graphical interpretation of this equation is that a line drawn tangent to the fractional flow curve from the initial water saturation (S_{wi}) will have a point of tangency equal to water saturation at the front (S_{wf}). Additionally, if the tangent line is extrapolated to $f_w = 1$, the water saturation will correspond to the average water saturation in the water bank, \bar{S}_w . Construction of a Welge plot is shown in Figure 5-155. The tangent line should be drawn from the initial water saturation even if that saturation is greater than the irreducible water saturation.

Welge derived an equation that relates the average displacing fluid saturation to the saturation at the producing end of the system:

$$\bar{S}_w - S_{w2} = Q_i f_{o2} \quad (5-211)$$

where \bar{S}_w = average water saturation, fraction of PV

S_{w2} = water saturation at the producing end of the system, fraction of PV

Q_i = pore volumes of cumulative injected fluid, dimensionless

f_{o2} = fraction of oil flowing at the outflow end of the system

Equation 5-211 is important because it relates to three factors of prime importance in waterflooding [133]: (1) the average water saturation and thus the total oil recovery, (2) the cumulative injected water volume, and (3) the water cut and hence the oil cut.

Welge also related the cumulative water injected and the water saturation at the producing end:

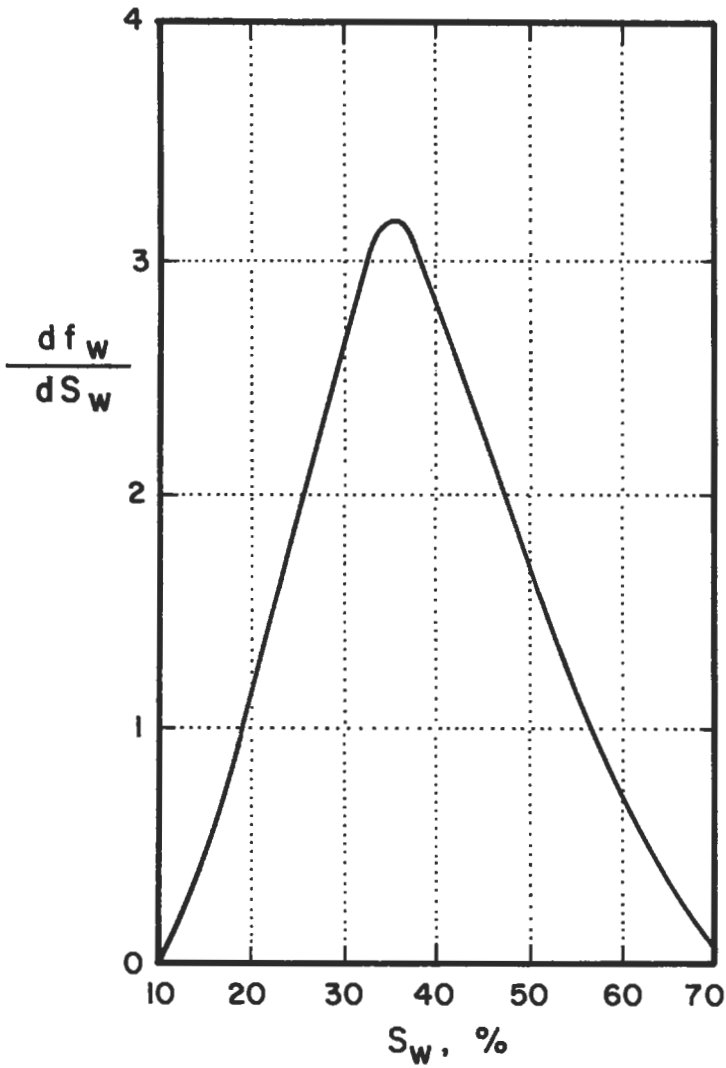


Figure 5-154. Change in fractional flow of water with change in water saturation [133].

$$Q_i = \frac{1}{\left(\frac{df_w}{dS_w}\right)_{S_{wt}}} \tag{5-212}$$

Thus, the reciprocal of the slope of the tangent line gives the cumulative water influx at the time of water breakthrough. When a value of Q_i and the injection rate are known, the time to reach that stage of the flood can be computed.

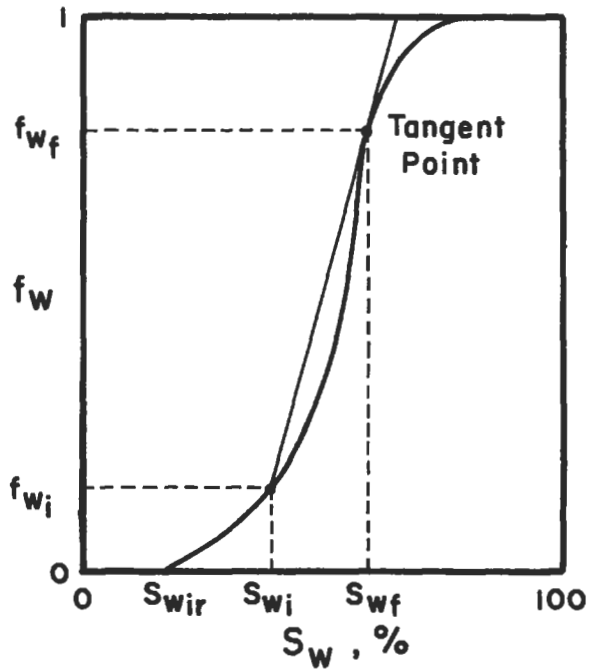
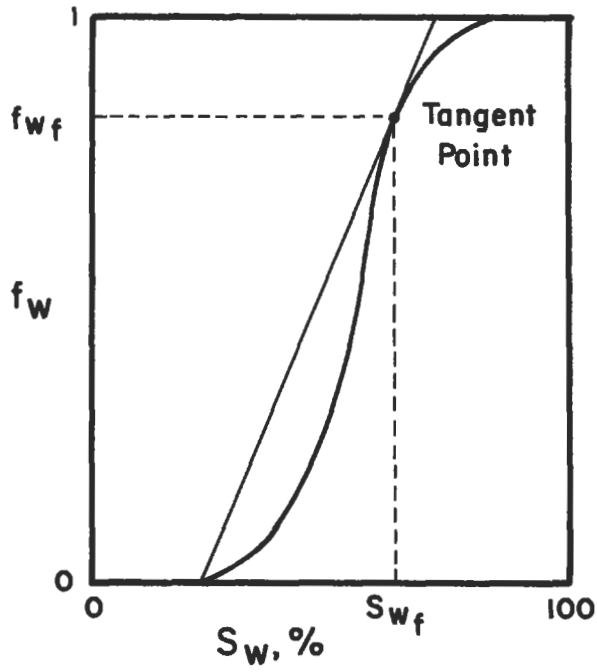


Figure 5-155. Welge graphical plot [153].

For a liquid-filled, linear system, the average water saturation at breakthrough, \bar{S}_{wbt} , is:

$$\bar{S}_{wbt} = S_{iw} + \frac{W_i}{A\phi L} \quad (5-213)$$

where S_{iw} is the irreducible or connate water saturation. If Equation 5-209 is substituted into Equation 5-213:

$$\bar{S}_{wbt} - S_{iw} = \frac{1}{\left(\frac{df_w}{dS_w}\right)} = \frac{S_{wf} - S_{iw}}{f_{wf}} \quad (5-214)$$

where S_{wf} is the water saturation at the flood front and f_{wf} is the water cut at the flood front. After breakthrough, water saturation is obtained from Equations 5-211 and 5-212 where, as mentioned earlier: (1) the tangent point, S_{w2} , represents the water saturation at the producing end of the system, (2) the value of f_w at the point of tangency is the producing water cut, (3) the saturation at which the tangent intersects $f_w = 1.0$ is the average water saturation, and (4) the inverse of the slope of the tangent line is equal to the cumulative injected fluid in pore volumes (Q_i). If connate water is mobile, appropriate corrections need to be made [133].

Oil production at breakthrough can be computed from [278]:

$$N_{pbt} = \frac{\phi AL}{B_o} (\bar{S}_{wbt} - S_{iw}) \quad (5-215)$$

After water breakthrough, a number of saturations greater than S_{wf} are selected; the slope of the tangent line and average water saturation are determined for each value of S_w chosen. Oil production after breakthrough is then determined by observing the change in water saturation [278]:

$$\Delta N_p = \frac{\phi AL}{B_o} (\bar{S}_w - \bar{S}_{wbt}) \quad (5-216)$$

The incremental oil production from Equation 5-216 can be added to the breakthrough production from Equation 5-215, and the resulting total production for the linear system can be listed as a function of S_w , time, or other parameters. If the pore volumes in these equations are in ft³, divide by 5.615 to get barrels.

Viscous Fingering

A problem often encountered in the displacement of oil by water is the viscosity contrast between the two fluids. The adverse mobility ratios that result promote fingering of water through the more viscous crude oil and can reduce the oil recovery efficiency. An example of viscous fingering is shown in Figure 5-156.

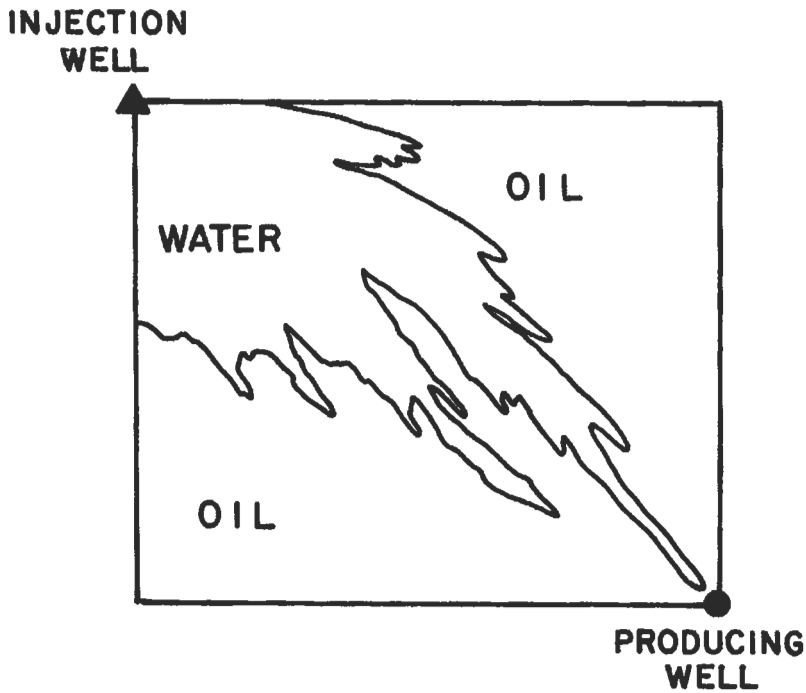


Figure 5-156. Viscous fingering.

Mobility and Mobility Ratio

Mobility of a fluid is defined as the ratio of the permeability of the formation to a fluid, divided by the fluid viscosity:

$$\lambda = \frac{k}{\mu} \tag{5-217}$$

where λ = mobility, md/cp

k = effective permeability of reservoir rock to a given fluid, md

μ = fluid viscosity, cp

When multiple fluids are flowing through the reservoir, relative permeabilities must be used along with viscosities of the fluids. By convention, the term mobility ratio is defined as the mobility of the displacing fluid divided by the mobility of the displaced fluid. For waterfloods, this is the ratio of water to oil mobilities. Thus the mobility ratio, M , for a waterflood is:

$$M = \frac{k_{rw}/\mu_w}{k_{ro}/\mu_o} = \frac{k_{rw}\mu_o}{k_{ro}\mu_w} \tag{5-218}$$

where k_{rw} and k_{ro} , are relative permeabilities to water and oil, respectively, μ_o is oil viscosity and μ_w is water viscosity. Prior to 1957, there was no accepted

definition, and many workers defined mobility ratio as oil to water mobility; in this case, the reciprocal of mobility ratio (as now accepted) must be used. The oil mobility used in Equation 5-213 refers to the location in the oil bank ahead of the flood front. For the water mobility, there are several possibilities regarding the location at which the relative permeability should be chosen: at the flood front, at residual oil saturation where only water is flowing (end point), or at some intermediate saturation. Craig [133] found a better correlation if the water mobility was determined at the average water saturation behind the flood front at water breakthrough. Thus for the mobility ratio expression, the relative permeability of water is found at the average water saturation at water breakthrough as determined by the Welge graphical approach. As Craig notes, the mobility ratio of a waterflood will remain constant before breakthrough, but it will increase after water breakthrough corresponding to the increase in water saturation and relative permeability to water in the water-contacted portion of the reservoir. Unless otherwise specified, the term mobility ratio is taken to be the value prior to water breakthrough. As will be discussed later in this section, mobility ratio is important in determining the volume of reservoir contacted by the waterflood.

Recovery Efficiency

Recovery efficiency is the fraction of oil in place that can be economically recovered with a given process. The efficiency of primary recovery mechanisms will vary widely from reservoir to reservoir, but the efficiencies are normally greatest with water drive, intermediate with gas cap drive, and least with solution gas drive. Results obtained with waterflooding have also varied. The waterflood recovery can range from less than the primary recovery to as much as 2.5 times the recovery obtained in some solution-gas drive reservoirs. A recent statistical analysis by the API [239] provided the average primary and secondary recovery efficiencies in Table 5-37. Generally, primary and ultimate recoveries from carbonate reservoirs tend to be lower than from sandstones. For pattern waterfloods, the average ratio of secondary to primary recovery ranges from 0.33 in California sandstones to greater than one in Texas carbonates. For edge water injection, the secondary-to primary ratio ranged from an average of 0.33 in Louisiana to 0.64 in Texas. By comparison, secondary recovery for gas injection into a gas cap averaged only 0.23 in Texas sandstones and 0.48 in California sandstones. Ultimate primary and secondary recovery performance for different drive mechanisms are given in Table 5-38. Solution-gas-drive reservoirs will generally have higher oil saturations after primary recovery, and are usually the better candidates for waterflooding.

Displacement of oil by waterflooding is controlled by fluid viscosities, oil-water relative permeabilities, nature of the reservoir rock, reservoir heterogeneity, distribution of pore sizes, fluid saturations (especially the amount of oil present), capillary pressure, and the location of the injection wells in relation to the production wells. These factors contribute to the overall process efficiency. Oil recovery efficiency (E_R) of a waterflood is the product of displacement efficiency (E_D) and volumetric efficiency (E_V), both of which can be correlated with fluid mobilities:

$$E_R = E_D E_V = E_D E_F E_I \quad (5-219)$$

where E_R = overall reservoir recovery or volume of hydrocarbons recovered divided by volume of hydrocarbons in place at start of project

Table 5-37
Ultimate Recovery (Primary Plus Secondary)

	Ultimate recovery at		Recovery efficiency			
	average OOIP B/NAF	Average OOIP B/NAF	Primary % OOIP	Secondary % OOIP	Ultimate % OOIP	Secondary to primary ratio
<i>Pattern waterfloods</i>						
California sandstones	1,311	463	26.5	8.8	35.3	0.33
Louisiana sandstones	1,194	611	36.5	14.7	51.2	0.40
Oklahoma sandstones	728	201	17.0	10.6	27.6	0.62
Texas sandstones	942	362	25.6	12.8	38.4	0.50
Wyoming sandstones	774	346	23.6	21.1	44.7	0.89
Texas carbonates	388	123	15.5	16.3	31.8	1.05
<i>Edge water injection</i>						
Louisiana sandstones	1,181	680	41.3	13.8	55.1	0.33
Texas sandstones	897	499	34.0	21.6	55.6	0.64
<i>Gas injection into cap</i>						
California sandstones	909	396	29.4	14.2	43.6	0.48
Texas sandstones	957	412	35.3	8.0	43.3	0.23

From References 239 and 243.

Recovery Efficiency: Average value of the recoverable oil divided by the average value of the original oil-in-place for the reservoirs in the classification.

OOIP: Original oil-in-place

B/NAF: Barrels per net acre-ft

Table 5-38
Secondary Recovery Efficiencies

Secondary recovery method	Lithology	State	Primary plus secondary recovery efficiency (% OOIP)	Ratio of secondary to primary recovery efficiency
Pattern waterflood	Sandstone	California	35	0.33
		Louisiana	51	0.40
		Oklahoma	28	0.62
		Texas	38	0.50
		Wyoming	45	0.89
Pattern waterflood	Carbonates	Texas	32	1.05
Edge water injection	Sandstone	Louisiana	55	0.33
		Texas	56	0.64
Gas cap injection	Sandstone	California	44	0.48
		Texas	43	0.23

From References 239 and 243.

- E_D = volume of hydrocarbons (oil or gas) displaced from individual pores or small groups of pores divided by the volume of hydrocarbons in the same pores just prior to displacement
- E_p = pattern sweep efficiency (developed from areal efficiency by proper weighting for variations in net pay thickness, porosity, and hydrocarbon saturation): hydrocarbon pore space enclosed behind the injected-fluid front divided by total hydrocarbon pore space of the reservoir or project
- E_I = hydrocarbon pore space invaded (affected, contacted) by the injection fluid or heat-front divided by the hydrocarbon pore space enclosed in all layers behind the injected fluid

Displacement Sweep Efficiency (E_p)

Factors affecting the displacement efficiency for any oil recovery process are pore geometry, wettability (water-wet, oil-wet, or intermediate), distribution of fluids in the reservoir, and the history of how the saturation occurred. Results are displayed in the relative permeability curves (Figure 5-153) from which the flowing water saturation (or conversely the oil saturation) can be obtained at any total fluid saturation. As shown in Figure 5-157, displacement efficiencies decrease as oil viscosities increase [133].

Volumetric Sweep Efficiency (E_v)

Whereas displacement efficiency considers a linear displacement in a unit segment (group of pores) of the reservoir, macroscopic or volumetric sweep takes

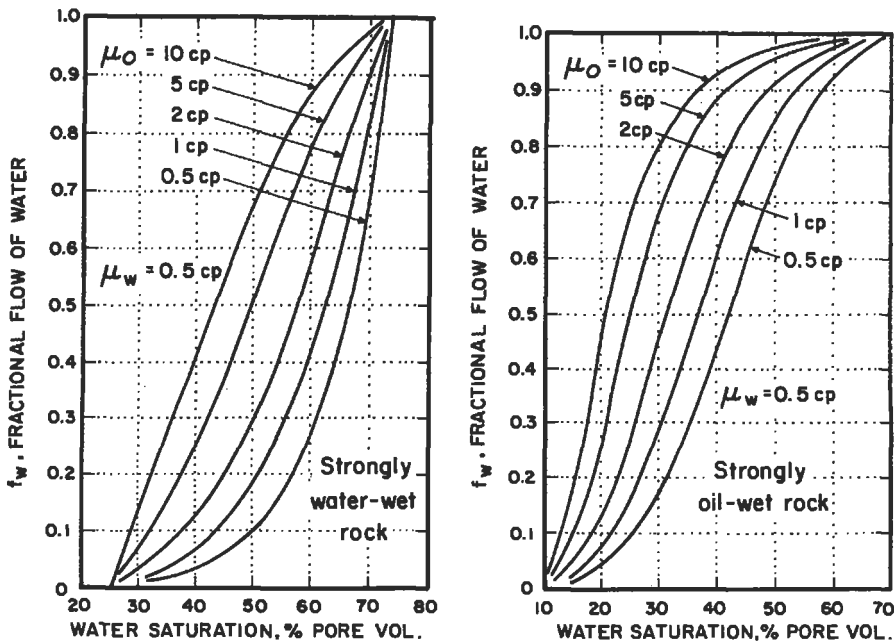


Figure 5-157. Effect of oil viscosity on fractional flow of water [133].

into account that fluid (i.e., water) is injected at one point in a reservoir and that other fluids (i.e., oil, water) are produced from another point (Figure 5-158). Volumetric sweep efficiency, the percentage of the total reservoir contacted by the injected fluid (often called fluid conformance), is composed of areal (or pattern) efficiency and vertical sweep.

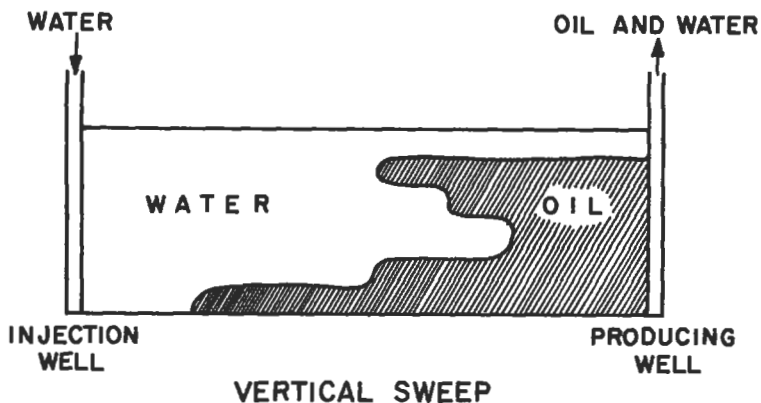
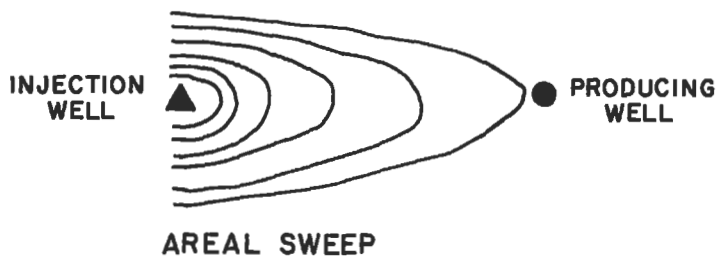
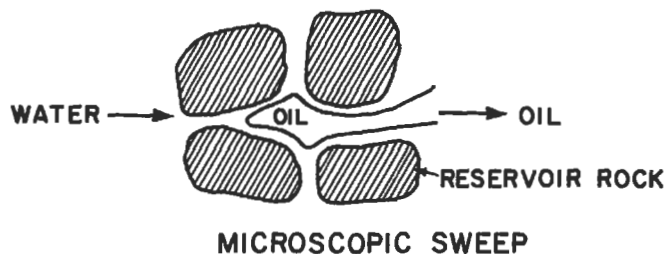


Figure 5-158. Sweep efficiencies.

Areal or Pattern Sweep Efficiency (E_p)

Areal sweep efficiency of an oil recovery process depends primarily on two factors: the flooding pattern and the mobilities of the fluids in the reservoir. In the early work on sweep efficiency and injectivity, Muskat and coworkers [25,280] presented analytical solutions for direct line drive, staggered line drive, 5-spot, 7-spot, and 9-spot patterns (patterns were discussed earlier; see Figure 5-150). Experimental studies on the effect of mobility ratio for different patterns were presented by Dyes, Caudle, and Erickson [281] (5-spot and line drives); Craig, Geffen, and Morse [282], Prats et al. [283], Caudle and Witte [284], and Haberman [285] (5-spot); and Kimbler, Caudle, and Cooper [286] (9-spot). The effect of sweepout beyond the pattern area was studied as well [287,288]. From a mathematical study the breakthrough sweep efficiency of the staggered line drive was presented by Prats [289]. A comparison of the areal sweep efficiency and the ratio d/a is shown in Figure 5-159 for direct and staggered line drives [25,289], and a review of the early work was provided by Crawford [290].

Areal sweep efficiency at breakthrough for a 5-spot pattern is shown in Figure 5-160, and the effect of mobility ratio on areal sweep is shown in Figure 5-161. These figures show that areal sweep efficiency is low when mobility ratio is high (note that the data in Figure 5-161 from Dyes, Caudle and Erickson are plotted in terms of the reciprocal of mobility ratio as currently defined). Areal sweep efficiencies at breakthrough, for different patterns and a mobility ratio of one, are summarized in Table 5-39 [133,277,279].

Areal sweep efficiency is more important for considering rate vs. time behavior of a waterflood rather than ultimate recovery because, at the economic limit, most of the interval flooded has either had enough water throughput to provide 100% areal sweep or the water bank has not yet reached the producing well so that no correction is needed for areal sweep [133].

When waterflooding calculations are performed, especially with computers or programmable calculators, the use of equations with adjustable coefficients

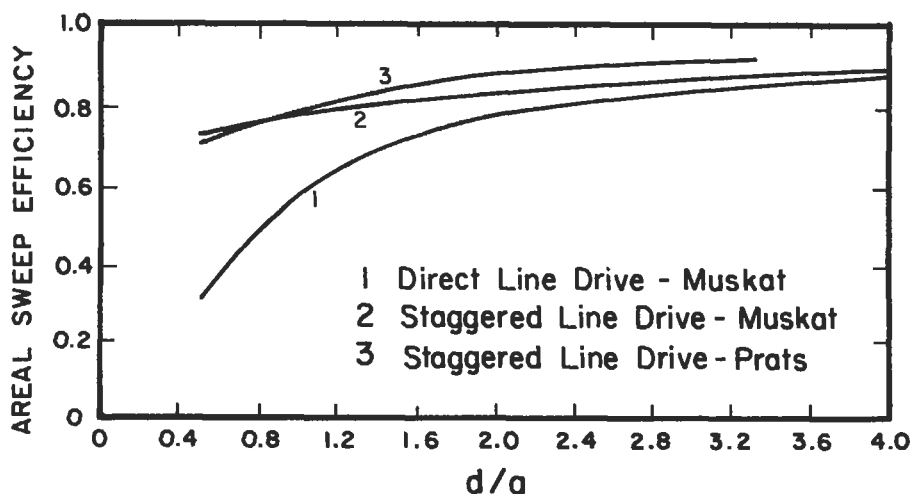


Figure 5-159. Areal sweep efficiencies for direct and staggered line drive patterns [25,289].

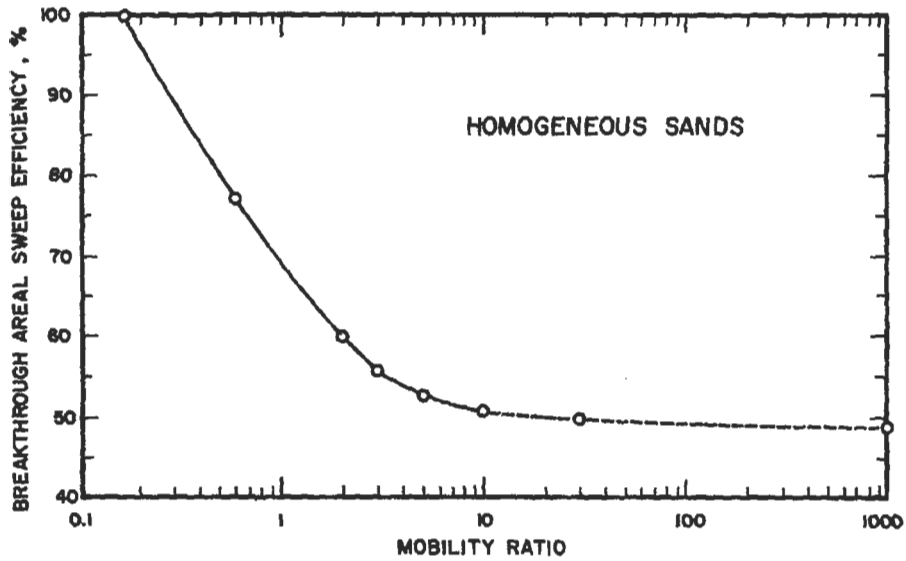


Figure 5-160. Effect of mobility ratio on areal sweep efficiency at breakthrough for a 5-spot pattern [133].

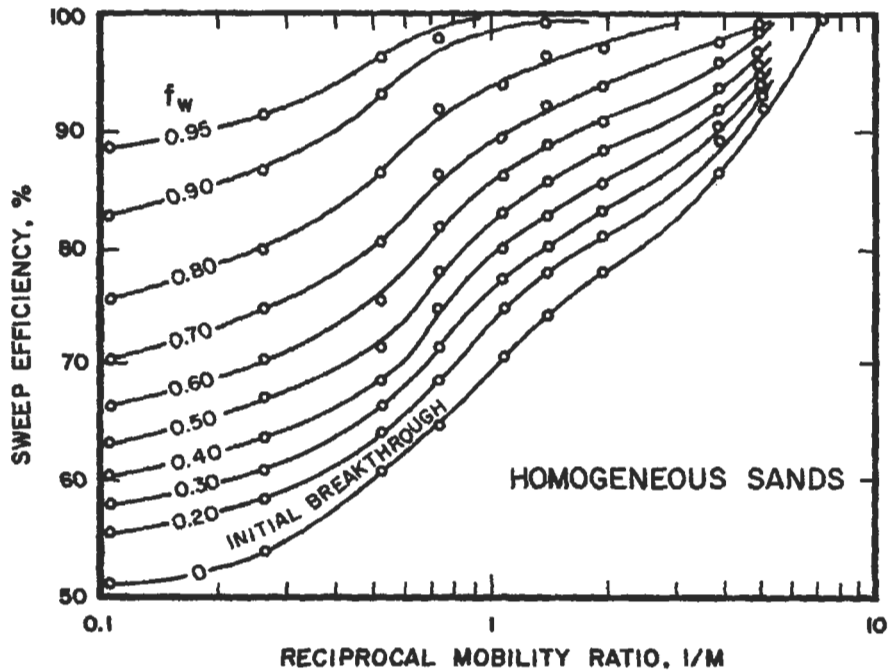


Figure 5-161. Effect of mobility ratio on areal sweep efficiency after breakthrough for a 5-spot pattern [281].

Table 5-39
Areal Sweep Efficiency at Breakthrough (M = 1)

Type of pattern	E_p , % [279]	E_p , % [277]*
Direct line drive (d/a = 1)	57.0	57
Direct line drive (d/a = 1.5)	70.6	—
Staggered line drive	80.0	75 (d/a = 1)
5-spot	72.3	68-72
7-spot	74.0	74-82
9-spot <i>diagonal/directional</i> rate		
0.5	—	49
1	—	54
5	—	69
10	—	78

From Reference 133.

* Based on summary of data presented by Craig.

are very useful. Recently, Fassihi [291] provided correlations for the calculation of areal and vertical sweep efficiencies. For these correlations of areal sweep, the data of Dyes, Caudle, and Erickson [281] were curve-fitted and the resulting equation was:

$$\frac{1 - E_p}{E_p} = [a_1 \ln(M + a_2) + a_3] f_w + a_4 \ln(M + a_5) + a_6 \quad (5-220)$$

where E_p is the areal sweep efficiency which is the fraction of the pattern area contacted by water, M is the mobility ratio, and the coefficients are as listed in Table 5-40 for the 5-spot, direct line drive, and staggered line drive. These coefficients are valid both before and after breakthrough, and apply to mobility ratios between zero and ten, which is within the range observed in many waterfloods. For the 5-spot pattern, these values of E_p are generally higher than in later experiments, and a correction has been suggested by Claridge [292] that should be multiplied by the E_p from the Dyes et al. data:

$$E_v = \frac{E_p/V_d}{\{M^{0.5} - [(M-1)(1 - E_p/V_d)]^{0.5}\}^2} \quad (5-221)$$

Table 5-40
Coefficients in Areal Sweep Efficiency Correlations

Coefficient	5-spot	Direct line drive	Staggered line drive
a_1	- 0.2062	- 0.3014	- 0.2077
a_2	- 0.0712	- 0.1568	- 0.1059
a_3	- 0.511	- 0.9402	- 0.3526
a_4	0.3048	0.3714	0.2608
a_5	0.123	- 0.0865	0.2444
a_6	0.4394	0.8805	0.3158

From Reference 291.

where E_v is the volumetric sweep efficiency in a linear displacement, V_d is the displaceable pore volumes injected, and the other terms are as already defined.

Vertical or Invasion Sweep Efficiency (E_v)

For well-ordered sandstone reservoirs, the permeability measured parallel to the bedding planes of stratified rocks is generally larger than the vertical permeability. For carbonate reservoirs, permeability (and porosity) may have developed after the deposition and consolidation of the formation; thus the concept of a stratified reservoir may not be valid. However, in stratified rocks, vertical sweep efficiency takes into account the inherent vertical permeability variations in the reservoir. Vertical sweep efficiency of a waterflood depends primarily upon the vertical distribution of permeabilities within the reservoir, on the mobility of fluids involved, and on the density differences between flowing fluids. As a result of nonuniformity of permeabilities in the vertical direction, fluid injected into an oil-bearing formation will seek the paths of least resistance and will move through the reservoir as an irregular front. Consequently, the injected fluid will travel more rapidly in the more permeable zones and will travel less rapidly in the tighter zones. With continued injection and displacement of some of the resident fluids, the saturation of the injected fluid will become greater in the more permeable areas than in the low-permeability strata. This can cause early breakthrough of injected fluid into the producing wells before the bulk of the reservoir has been contacted. In addition, as the saturation of the injected fluid increases in the highly permeable zones, the relative permeability to that fluid also increases. All of these effects can lead to channeling of the injected fluid, which is aggravated by the unfavorable viscosity ratio common in waterflooding. In many cases, permeability stratification has a dominant effect on behavior of the waterflood.

Permeability Variation

Two methods of quantitatively defining the variation in vertical permeabilities in reservoirs are commonly used. The extent of permeability stratification is sometimes described with the Lorenz coefficient [293] and is often described with the Dykstra-Parsons [294] coefficient of permeability variation.

Lorenz Coefficient. Schmalz and Rahme [293] suggested arranging the vertical distribution of permeabilities from highest to lowest, and plotting the fraction of total flow capacity (kh) versus the fraction of total volume ($h\phi$). To obtain the Lorenz coefficient (see Figure 5-162), the area ABCA is divided by the area ADCA. Values of the Lorenz coefficient can range from zero for a uniform reservoir to a theoretical maximum value of one. However, the Lorenz coefficient is not a unique measure of stratification, and several different permeability distributions can give the same Lorenz coefficient [133].

Dykstra-Parsons Coefficient of Permeability Variation. The coefficient of permeability variation described by Dykstra and Parsons [294] is also referred to as the permeability variation or permeability variance. This method assumes that vertical permeabilities in a reservoir will have a log-normal distribution. The procedure outlined by Dykstra and Parsons was to: (1) divide permeabilities (usually from core analysis) so that all samples are of equal thickness (often 1 ft), (2) arrange the permeabilities in descending order from highest to lowest, (3) calculate for each sample the percent of samples that have a higher permeability

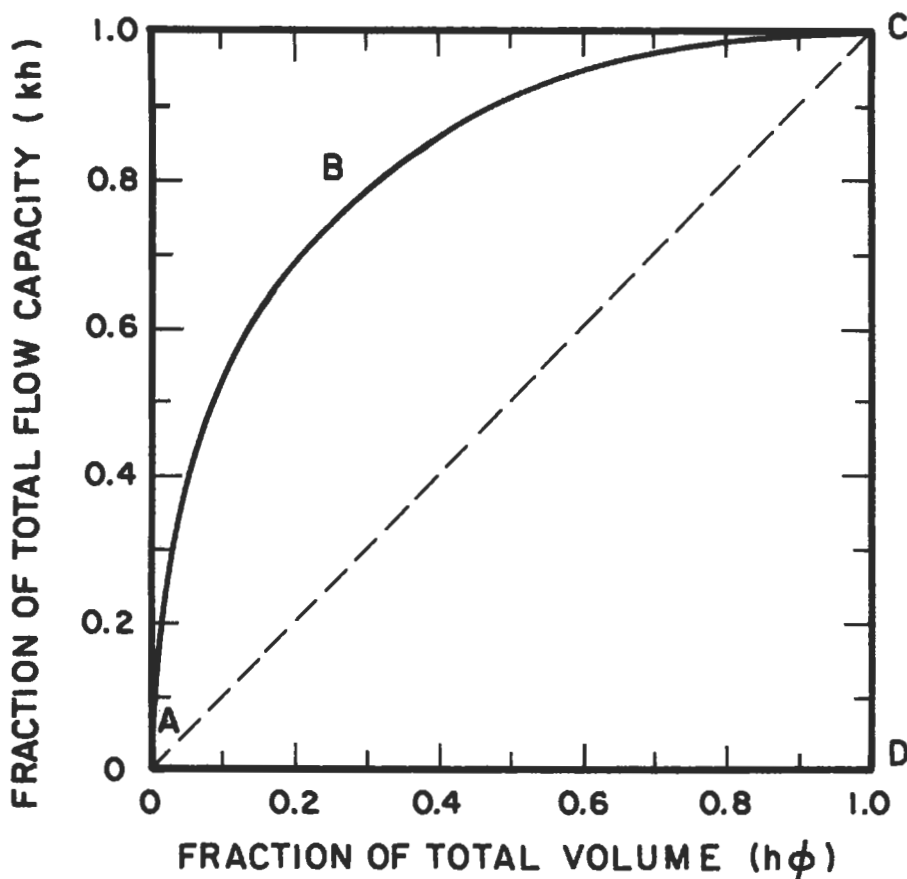


Figure 5-162. Lorenz coefficient plot [133].

(see example in Table 5-41), (4) plot the data from Step 3 on log-probability paper (see Figure 5-163) (5) draw the best straight line through data (with less emphasis on points at the extremities, if necessary), (6) determine the permeability at 84.1% probability ($k_{84.1}$) and the mean permeability at 50% probability (k_{50}), and (7) compute the permeability variation, V :

$$V = \frac{k_{50} - k_{84.1}}{k_{50}} \tag{5-222}$$

As with the Lorenz coefficient, the possible values of the Dykstra-Parsons permeability variation range from zero for a uniform reservoir to a maximum value of 1. In some cases, there may be a direct relation between the Lorenz and Dykstra-Parsons coefficients [295], but in many instances a direct relationship with field data will not be observed. Often, insufficient data are available to provide enough samples for adequate analysis, and in some cases, the data may not provide a log-normal distribution. In the remainder of this chapter,

Table 5-41
Data for Permeability Variation Plot

Permeability (md)	Percent of samples with greater than stated permeability
950	0
860	5
640	10
380	15
340	20
280	25
210	30
160	35
135	40
130	45
110	50
78	55
65	60
63	65
54	70
40	75
27	80
21	85
20	90
15	95

the term permeability variation will refer to the Dykstra-Parsons coefficient of permeability variation.

Increasing values of permeability variation indicate increasing degrees of vertical heterogeneity in a reservoir. Permeability variations often range from about 0.5 to 0.8; lower numbers may be observed for relatively uniform reservoirs, and higher numbers may be calculated for very nonuniform reservoirs. Using the data from Dykstra and Parsons, Johnson [296] provided a graphical technique to estimate recovery during an immiscible displacement. One of Johnson's plots is reproduced in Figure 5-164 for a producing water-oil ratio (WOR) of 100 which could represent the economic limit for many waterfloods. Lines of constant recovery are given as functions of permeability variation and mobility. Johnson also provided plots for WOR = 1, WOR = 5, and WOR = 25. At any WOR, an increase in vertical permeability variation yielded a lower recovery. As will be discussed later under prediction methods, the Dykstra-Parsons fractional recovery, R , as a percent of oil in place, must be multiplied by the areal sweep efficiency, E_p , to obtain an estimate of the oil recovered.

As mentioned earlier, correlations for calculating vertical and areal sweep efficiencies were recently provided by Fassihi [291]. The correlating parameter, Y , for vertical coverage, C , is:

$$Y = a_1 C^{a_2} (1 - C)^{a_3} \quad (5-223)$$

where $a_1 = 3.334088568$
 $a_2 = 0.7737348199$
 $a_3 = -1.225859406$

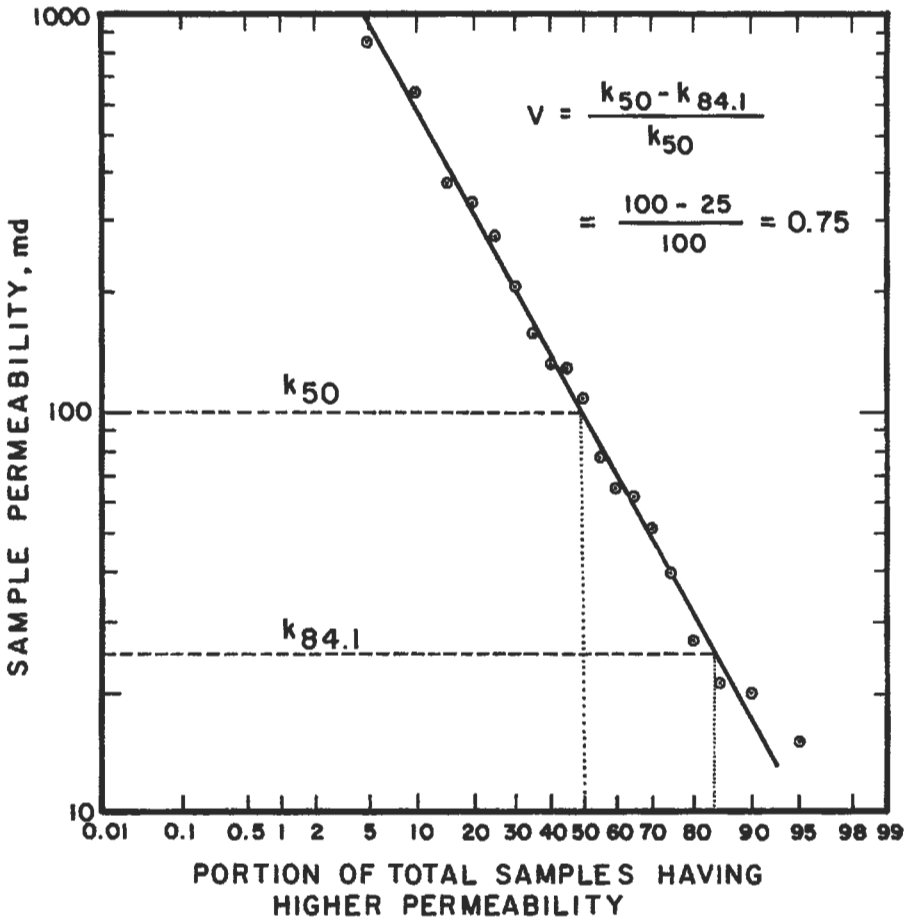


Figure 5-163. Dykstra-Parsons plot of permeability variation [133,294].

where the equation for Y was given by deSouza and Brigham [297] in terms of water-oil ratio (WOR), mobility ratio (M), and permeability variation (V):

$$Y = \frac{(WOR + 0.4)(18.948 - 2.499V)}{(M + 1.137 - 0.8094V)^{f(V)}} \tag{5-224}$$

where $f(V) = -0.6891 + 0.9735V + 1.6453V^2$

These equations are valid for mobility ratios ranging from 0 to 10 and for permeability variations ranging from 0.3 to 0.8.

Based on calculations of WOR vs. oil recovery for a 5-spot pattern, Craig [298] found that there was a minimum number of equal thickness layers required to obtain the same performance as with 100 layers. Table 5-42 shows the effect of permeability variation and mobility ratio on the minimum number of layers for WORs above 10. Craig [298] presented similar tables for lower WORs.

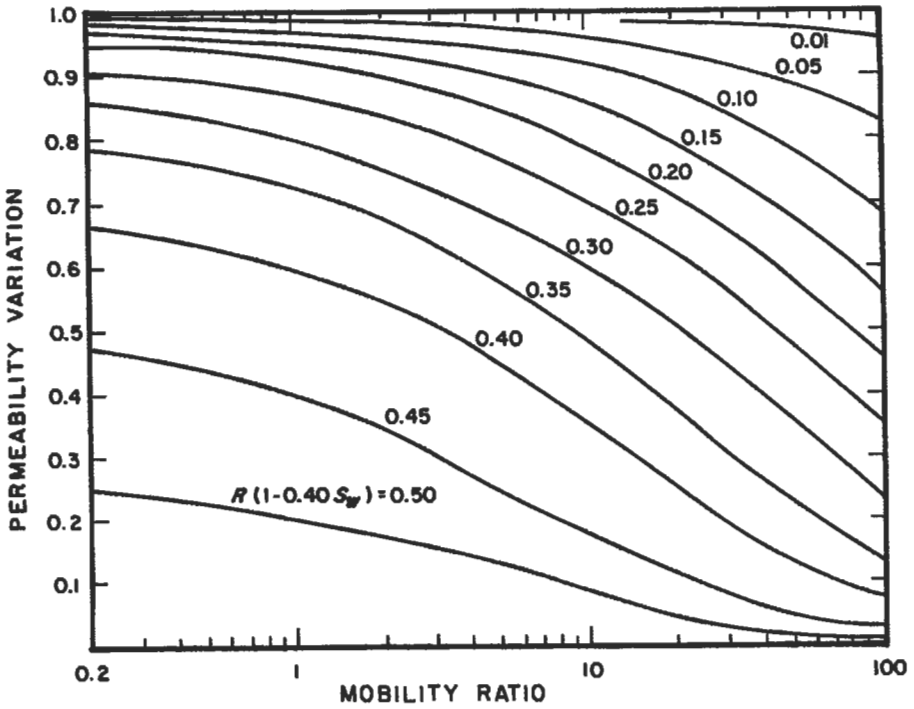


Figure 5-164. Effect of permeability variation and mobility ratio on vertical sweep efficiency at WOR = 100 [296].

Table 5-42
Minimum Number of Equal-Thickness Layers Required to Obtain Performance of a 100-Layer, 5-Spot Waterflood at Producing WOR's Above 10

Mobility Ratio	Permeability variation							
	0.1	0.2	0.3	0.4	0.5	0.6	0.7	0.8
0.05	1	1	1	2	4	5	10	20
0.1	1	1	1	2	5	5	10	20
0.2	1	1	2	3	5	5	10	20
0.5	1	1	2	3	5	5	10	20
1.0	1	1	2	3	5	10	10	50
2.0	1	2	3	4	10	10	20	100
5.0	1	3	4	5	10	100	100	100

From Reference 298.

A recent analytical extension [299] of the Dykstra-Parsons method allows calculations of total flow rates and flow rates in each layer for both a constant injection rate and for a constant pressure drop. The ability to calculate cumulative injection into a layer allows the incorporation of sweep efficiency of each layer as a function of mobility ratio and displaceable pore volumes injected for the pattern used in the waterflood.

Crossflow. In the usual cases where there is vertical communication between the different layers of varying permeabilities, the effect of vertical crossflow must be considered [300,301]. Goddin et al. [301] performed a numerical simulation in a 2-D, 2-layer, water-wet system. For mobility ratios ranging from 0.21 to 0.95, oil recovery with crossflow was between that computed for a uniform reservoir and that for a layered reservoir with no crossflow. Goddin et al. [301] defined a crossflow index, which is a measure of the extent the performance varies from that of a uniform permeability system:

$$\text{crossflow index} = \frac{N_{\text{pcf}} - N_{\text{pnfcf}}}{N_{\text{pu}} - N_{\text{pnfcf}}} \quad (5-225)$$

where N_{pu} = oil recovery from uniform system with the average permeability
 N_{pcf} = oil recovery from layered system with crossflow
 N_{pnfcf} = oil recovery from stratified system with no crossflow

Of the variables investigated, mobility ratio and the permeability ratio of the two layers had the largest effect on crossflow (see Figures 5-165 and 5-166, respectively). Crossflow was more pronounced at lower mobility ratios or at high ratios of layer permeabilities. The crossflow index of one means that the performance of the layered system with crossflow is identical to the performance of the system with uniform permeability.

Still at issue is the relative importance of mobility ratio and gravity in waterflooding stratified reservoirs [302-306]. For wetting conditions that are not strongly water-wet, additional complications will arise.

Estimates of Volumetric Sweep Efficiency. Volumetric sweep efficiency ranges from about 0.1 for very heterogeneous reservoirs to greater than 0.7 for homogeneous reservoirs with good flooding characteristics [278]. For a liquid-filled, 5-spot pattern, Craig [298] found that the volumetric sweep efficiency (E_v) at breakthrough decreases sharply as the permeability variation increases (see Figure 5-167). Similar trends were observed for initial gas saturations of 10% and 20%. These data indicated that the major effect of mobility ratio on E_v at breakthrough occurs for mobility ratios ranging from 0.1 to 10.

More recent simulations [307] of 5-spot patterns with a streamtube model yielded the volumetric sweep efficiencies shown in Figures 5-168 and 5-169 for WORs of 25 and 50, respectively. Mobility ratios of 0.1, 1, 10, 30, and 100 were used. The permeabilities in the 100-layer model were assumed to have a log-normal distribution, and pseudo-relative permeability expressions were used. In a companion paper [308] the streamtube model (no crossflow) was compared to the Dykstra-Parsons method (no crossflow) and with a model having the assumption of equal pressure gradient in each layer (with crossflow). The streamtube model was more closely described by the model with vertical communication for unfavorable (high) mobility ratios and by the Dykstra-Parsons model for favorable (low) mobility ratios.

(text continued on page 292)

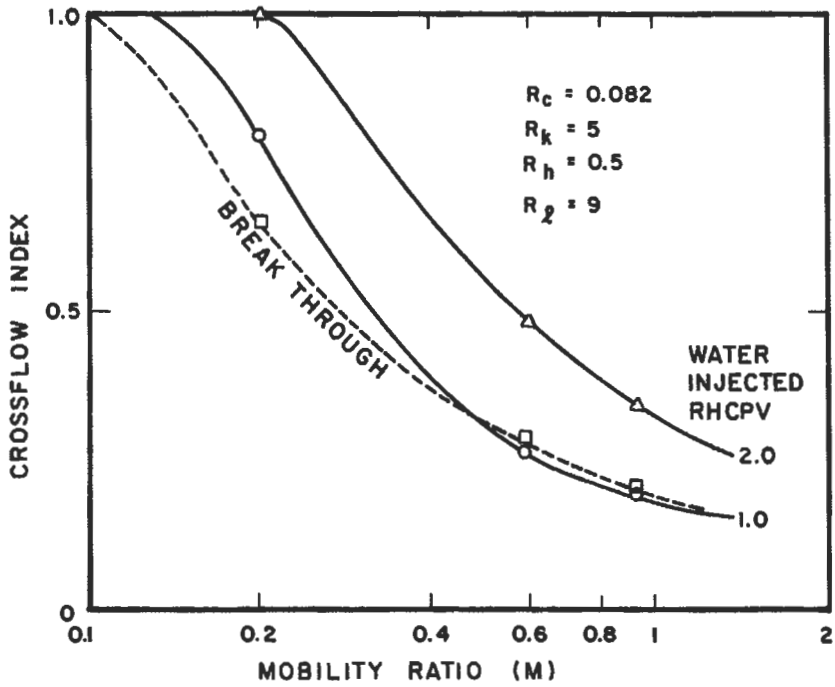


Figure 5-165. Influence of mobility ratio on vertical crossflow [301].

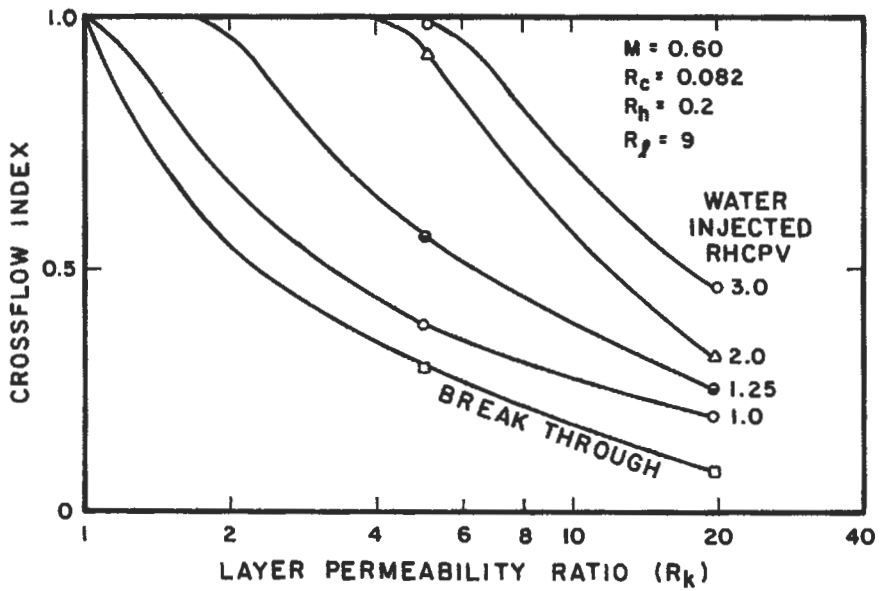


Figure 5-166. Effect of layer permeability ratio on crossflow [301].

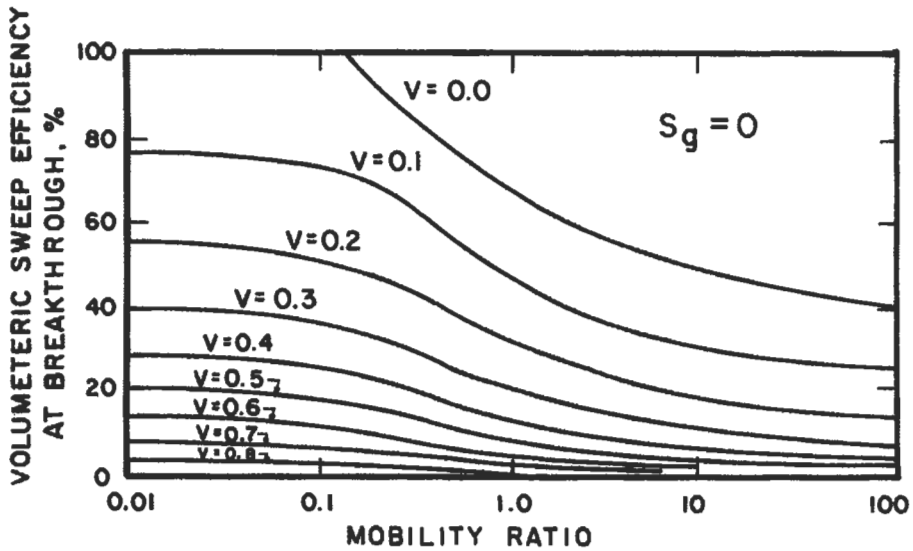


Figure 5-167. Effect of permeability variation and mobility ratio on volumetric sweep at breakthrough [298].

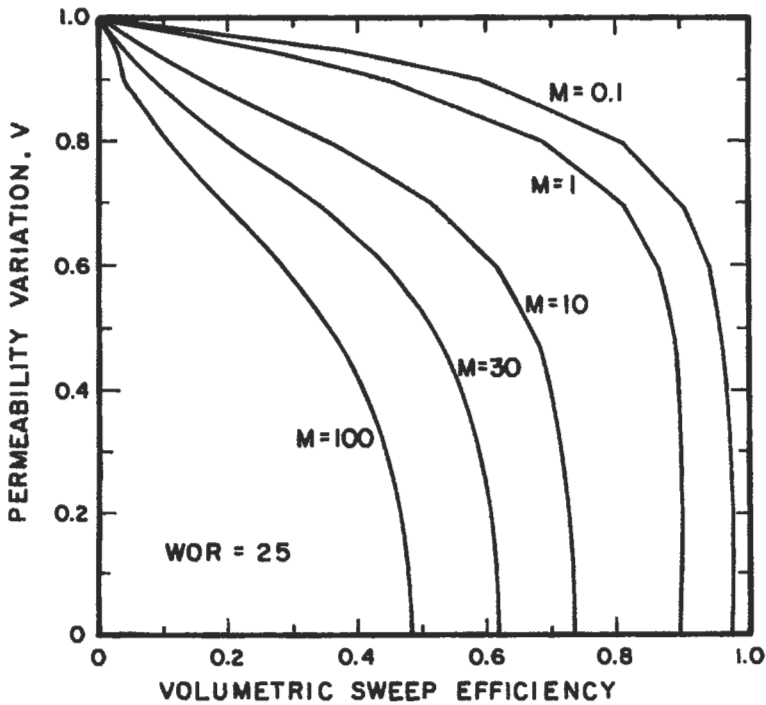


Figure 5-168. Effect of permeability variation and mobility ratio on volumetric sweep at breakthrough [307].

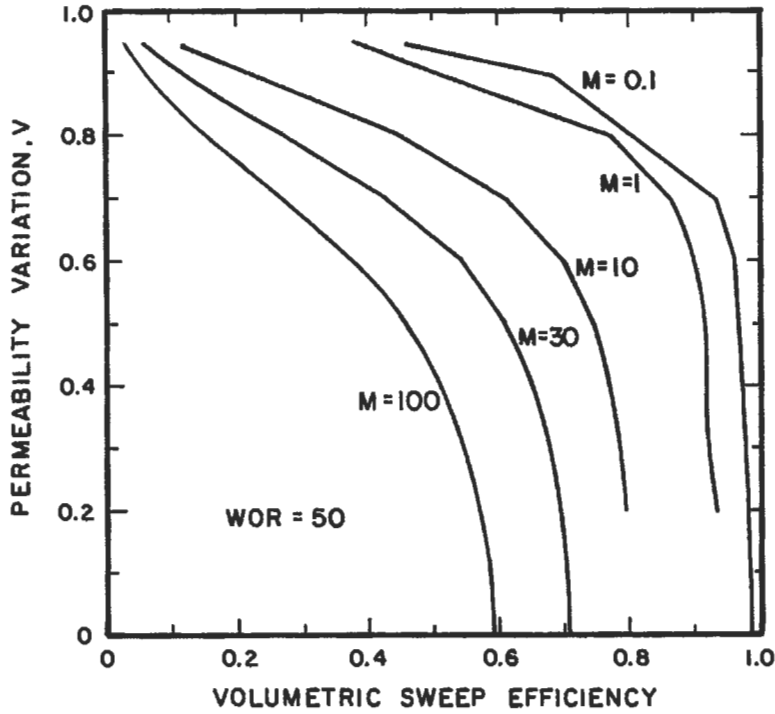


Figure 5-169. Effect of permeability variation and mobility ratio on volumetric sweep at WOR = 50 [307].

(text continued from page 289)

Estimation of Waterflood Recovery by Material Balance

Oil recovered by waterflooding, N_{pw} , in STB, can be estimated from [278]:

$$N_{pw} = \frac{7,758Ah\phi[S_{op} - E_v S_{or} - (1 - E_v)S_{oi}]}{B_o} \tag{5-226}$$

where 7,758 is the number of barrels per acre-ft, A is areal extent of the reservoir in acres, h is reservoir thickness in ft, ϕ is the fractional porosity, S_{op} is the oil saturation at the start of waterflooding, S_{or} is the waterflood residual oil saturation, S_{oi} is the initial oil saturation, B_o is the oil formation volume factor, and E_v is the volumetric sweep or fraction of the reservoir volume swept by the injected water when the economic limit has been reached. In terms of the original oil in place, the waterflood recovery is [278]:

$$N_{pw} = (N - N_p) - N \frac{B_{oi}}{B_o} \left[1 + E_v \left(\frac{S_{or}}{S_{oi}} - 1 \right) \right] \tag{5-227}$$

where N_{pw} = oil potentially recoverable by waterflooding, STB
 N = initial oil in place, STB
 N_p = oil produced during primary operations, STB
 B_{oi} = initial FVF

These equations can be altered to include a residual gas saturation, if present. The volumetric sweep efficiency can be estimated from one of the correlations given previously or can be obtained from an analogy from similar waterflood projects.

Prediction Methods

An extensive survey on prediction of waterflood performance was provided by Craig [133]. Of the methods reviewed, three appeared most promising: (1) the Higgins-Leighton streamtube model [309], (2) the Craig, Geffen, and Morse model [282], and (3) the Prats et al. method [283]. Discussion of the various prediction methods is beyond the scope of this text, and only two very simple methods will be presented for illustrative purposes. Both the Dykstra-Parsons [294] and Stiles [310] methods are very cursory and, if used, they are normally followed by more extensive evaluations, usually by computer simulation.

For either the Dykstra-Parsons or Stiles methods, the permeabilities are arranged in descending order. For the Dykstra-Parsons method, the permeability variation is determined as described earlier. Two options are then possible: a program [311] for hand-held calculators can be used, or the graphical technique presented by Johnson [296] can be used. The fractional recovery, R , (see Figure 5-164 for example) expressed as a fraction of the oil in place when the waterflood is started, must be multiplied by the areal sweep efficiency (for example from Figure 5-161) to obtain the waterflood recovery.

For the Stiles technique, a program [312] for hand-held calculators is available or the procedure summarized in Table 5-43 can be used. A straightforward presentation of the Stiles method is in the text by Craft and Hawkins [17]. The fractional recovery obtained with the Stiles method is a fraction of the recoverable oil ($S_{op} - S_{or}$) that has been recovered at a given reservoir water cut. Since a water-oil ratio (WOR) is measured at surface conditions, the fractional water cut at reservoir conditions, f_w , is obtained (assuming $B_w = 1.0$) from:

$$f_w = \frac{WOR}{WOR + B_o} \quad (5-228)$$

where B_o is the oil formation volume factor.

Performance Evaluation

Monitoring waterflood performance is crucial to the success of the flood. From a reservoir engineering standpoint, the primary concerns are water injectivity and oil productivity. A few important factors related to these concerns will be summarized.

Injectivity and Injectivity Index. Whereas productivity index was the ability of a well to produce hydrocarbons, injectivity index, I , in B/D/psi, is a measure of the ability of a well to accept fluids [17]:

Table 5-43
Stiles Method of Calculating Waterflood
Performance in Stratified Reservoirs

$$R = \frac{[k_j h_j + (c_t - c_j)]}{k_j h_j}$$

R = fraction of recoverable oil that has been produced
 c_t = total capacity of formation (md-ft)
 c_j = mid-ft which have been completely flooded with water
 h_t = total net thickness of formation (ft)
 h_j = total net thickness flooded (ft)
 k_j = permeability of layer just flooded out

Reservoir conditions at P.W.

Surface conditions

$$f_w = \frac{Mc_j}{[Mc_j + (c_t - c_j)]}$$

$$f'_w = \frac{Ac_j}{[Ac_j + (c_t - c_j)]}$$

f_w = fractional flow of water

$$A = \frac{k_{rw} \mu_o B_o}{k_{ro} \mu_w B_w}$$

$$M = \frac{k_{rw} \mu_o}{k_{ro} \mu_w}$$

B_o = oil formation volume factor

B_w = water formation volume factor

From Reference 17.

$$I = \frac{q_{sc}}{P_{wrf} - P_o} \quad (5-229)$$

where q_{sc} is the flow rate in B/D at surface conditions, P_{wrf} is the flowing bottomhole pressure in psi, and P_o is the external pressure in psi. Some engineers express injectivity in terms of q_{sc}/P_{wrf} so that when injectivity is given, the reader is cautioned to understand what base pressure was intended. By dividing I by reservoir thickness, a specific injectivity index (specific to one well) can be obtained in B/D/psi/ft. In addition to expressing injectivity in terms of fluid injection rate in B/D, injectivity also is given as B/D/ac-ft and B/D/net ft of producing interval. Values of injectivity depend on properties of the reservoir rock, well spacing, injection water quality, fluid-rock interactions, and pressure drop in the reservoir. Typical values of injectivity are in the range of 8-15 B/D/net ft or 0.75-1.0 B/D/net ac-ft. In waterflooding operations, water injection may begin into a reservoir produced by solution-gas-drive in which a mobile gas saturation exists, or injection may begin prior to the development of a mobile gas saturation. In the latter case, the system can be considered filled with liquid.

Injectivities for Various Flood Patterns. Analytical expressions for liquid-filled patterns were given by Muskat [25] and Deppe [313] for a mobility ratio of one (see Table 5-44). While these exact analytical solutions can be developed for steady-state pressure distributions, the equations in Table 5-44 cannot be used directly if the mobility is not one. However, the equations are useful in estimating injectivity in limiting conditions. For example, if k and μ are selected for

Table 5-44
Injection Rates in Fully Developed Patterns at Unit Mobility Ratio

Direct line drive $\frac{d}{a} \geq 1$	Staggered line drive
$i = \frac{0.003541 kh(\Delta p)}{\mu \left[\ln \left(\frac{a}{r_w} \right) + 1.571 \frac{d}{a} - 1.838 \right]}$ <p><i>Five-spot</i></p>	$i = \frac{0.003541 kh(\Delta p)}{\mu \left[\ln \left(\frac{a}{r_w} \right) + 1.571 \frac{d}{a} - 1.838 \right]}$ <p><i>Seven-spot</i></p>
$i = \frac{0.003541 kh(\Delta p)}{\mu \left[\ln \left(\frac{d}{r_w} \right) - 0.619 \right]}$ <p><i>Nine-spot</i></p>	$i = \frac{0.00472 kh(\Delta p)}{\mu \left[\ln \left(\frac{d}{r_w} \right) - 0.569 \right]}$ <p><i>Nine-spot</i></p>
$i = \frac{0.003541 kh(\Delta p)_{i,c}}{\left(\frac{1+R}{2+R} \right) \left[\ln \frac{d}{r_w} - 0.272 \right] \mu}$	$i = \frac{0.00782 kh(\Delta p)_{i,s}}{\left(\frac{3+R}{2+R} \right) \left[\ln \frac{d}{r_w} - 0.272 \right] - \frac{0.693}{2+R}} \mu$

R = ratio of producing rate of corner well to side well
 $(\Delta p)_{i,c}$ = pressure difference between injection well and corner well, and
 $(\Delta p)_{i,s}$ = pressure difference between injection well and side well.

From References 25 and 313.
 * Units in these equations are B/D, md, ft, psi, and cp.

oil at the connate water saturation, an estimate of initial injection rate can be obtained. Then if k and μ are selected for water at residual saturation, an estimate can be made of injectivity at 100% sweep. (These estimates can be useful when equipment is sized for a waterflood.) If data on skin factor are available, suitable corrections [197,254,278] can be inserted in the logarithm term in the denominator in these equations. For unit mobility ratio, the injection rate will remain constant during the flood. If the mobility ratio is more than one, the injection rate increases as more water is injected; if the mobility ratio is less than one, the injection rate decreases. Figure 5-170 shows for different mobility ratios, the change in relative injectivity as the water bank extends radially from the injector [298]. Figure 5-171 shows, for different mobility ratios, the change in relative injectivity as a 40-acre 5-spot is swept [298].

For water injection into a depletion drive reservoir, several stages can describe the progress of the flood [180]. The first stage is the period of radial flow from the start of injection until interference of oil banks from adjacent injectors occurs. The second stage is the period from interference until fill-up of the pre-existing gas space; after fill-up, production response begins. The third stage is the period from fill-up to water breakthrough into the producing wells; water production begins at breakthrough. The fourth and final stage is the period from water breakthrough until floodout. For a 5-spot pattern, the injection rate during fill-up and to the time of interference can be estimated by [278]:

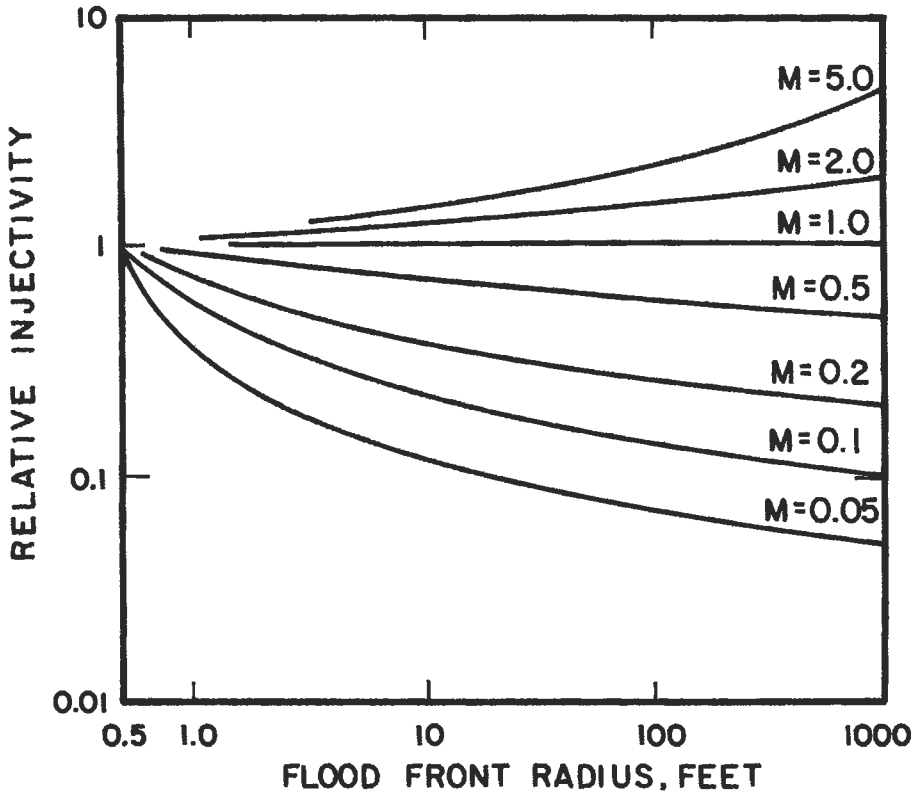


Figure 5-170. Change in injectivity at varying radial distances for different mobility ratios [298].

$$i = \frac{0.007082k_w \left(\frac{k_{ro}}{\mu_o} \right) h (p_{imf} - p_{wf})}{M \ln \frac{r_f}{r_w} + \ln \frac{r_{ob}}{r_f}} \tag{5-230}$$

where oilfield units of B/D, md, cp, ft, and psi are used, and

r_{ob} = radius of the oil bank, $r_w \leq r_{ob} \leq d/\sqrt{2}$
 r_f = radius of the flood-front saturation

Both r_{ob} and r_f can be obtained by a material balance on the injected water:

$$W_i = \pi(r_f^2 - r_w^2)(\bar{S}_w - S_{iw})h\phi \tag{5-231}$$

$$r_f = \sqrt{\frac{W_i}{\pi\phi h(\bar{S}_w - S_{iw})} + r_w^2} \tag{5-232}$$

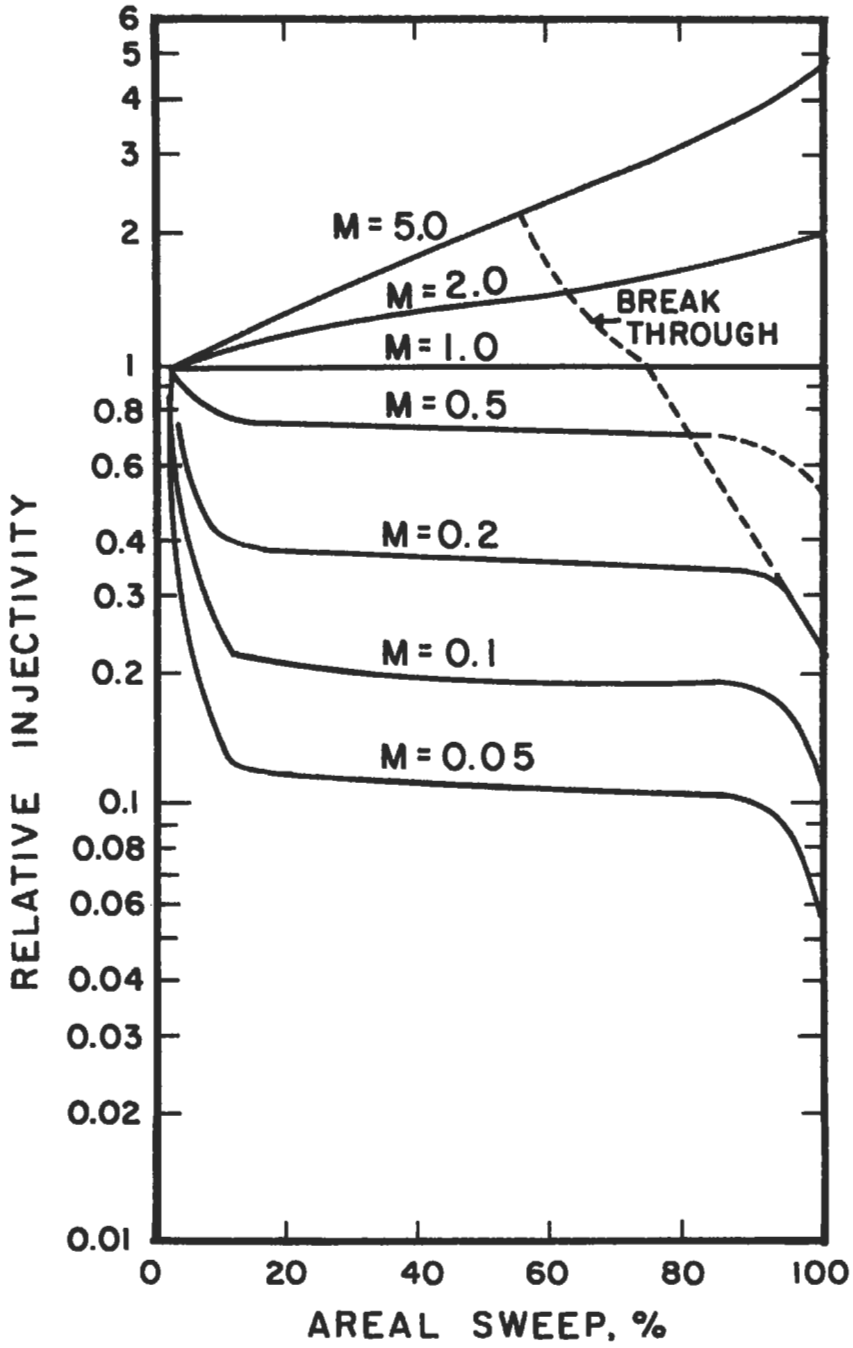


Figure 5-171. Change in injectivity as a function of area swept for different mobility ratios [298].

Since the volume of water injected to fill-up is equal to the volume of gas displaced by the oil bank as the initial gas saturation, S_{gi} , is reduced to the trapped-gas saturation, S_{gr} , a material balance for r_{ob} , is:

$$r_{ob} = \sqrt{\frac{W_i}{\pi\phi h(S_{gi} - S_{gr})}} + r_w^2 \quad (5-233)$$

At interference, $r_{ob} = d/\sqrt{2}$, and Equation 5-233 can be used to compute the volume of water required to reach interference. Usually, fill-up occurs in a relatively short time after interference, and the volume of water injected at fill-up is:

$$W_{if} = 2d^2\phi h S_{gi} \quad (5-234)$$

At fill-up, r_f is obtained by:

$$r_f = \sqrt{\frac{2d^2 S_{gi}}{\pi(\bar{S}_w - S_{iw})}} + r_w^2 \quad (5-235)$$

After interference, the equation in Table 5-44 for the 5-spot pattern can be used to estimate injectivity. Additional details of estimating injectivity can be found in several good texts on this subject [197,254,278].

Monitoring Injectivity. Injection well performance can be analyzed and monitored by several means. During and after a period of injection, the pressure transient methods discussed earlier can be used. Additionally, several bookkeeping methods of monitoring injection rates and pressures are quite useful.

Hearn [314] recently proposed a method to analyze injection well pressure and rate data. Permeability is obtained from the slope of a plot of $\Delta p/q_w$ versus the logarithm of cumulative water injected. However, the method can only be used during the initial injection period. After fill-up, $\Delta p/q_w$, the reciprocal of injectivity index, will cease to be a function of cumulative water injected unless the well experiences damage or is stimulated. In these cases, the plots suggested by Hall [315] are convenient for analysis of the data.

A Hall plot is a graph of cumulative pressure-time versus cumulative water injection. Such plots are useful in observing injection well plugging or any beneficial results of stimulation procedures. An improvement in injectivity is indicated if the slope decreases, whereas plugging is suspected if the slope steepens. Figure 5-172 shows an improvement in water injectivity that resulted from a surfactant treatment [316].

The reciprocal of the Hall plot slope is the injectivity index in bbl/D/psi. Effective pressures are obtained by subtracting the static reservoir pressure from the flowing bottomhole pressures [315]:

$$\text{effective pressure} = P_{twf} - \bar{p} = (p_{wh} + 0.45D - \Delta p_t) - \bar{p} \quad (5-236)$$

where p_{wh} is the wellhead pressure, 0.45 is the hydrostatic pressure gradient in psi/ft, D is the depth to the mid-point of the reservoir, and Δp_t is the pressure drop in the tubing. Although the Hall method assumes that only the wellhead pressure changes with cumulative water injected, the effective pressure drop

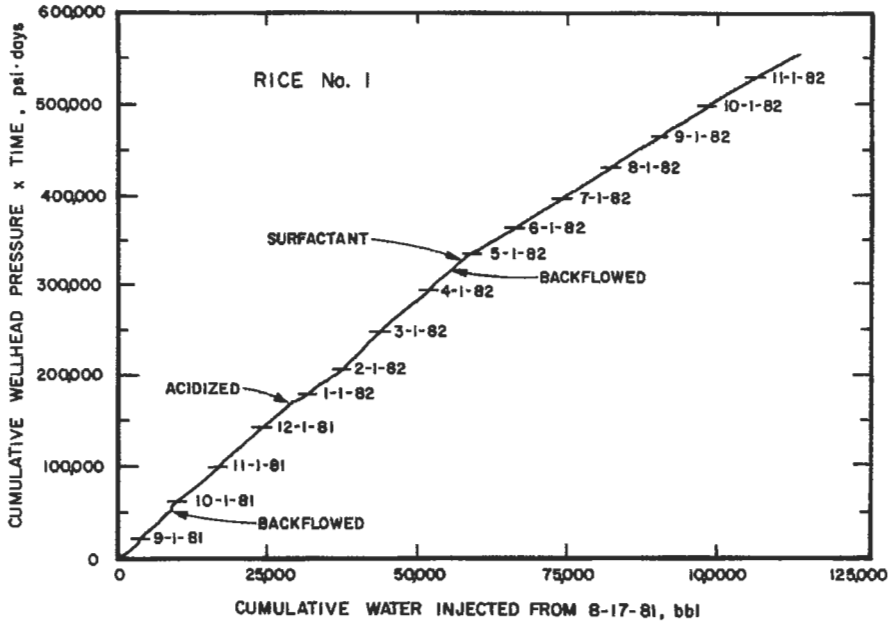


Figure 5-172. Hall plot [315].

should be used if permeability capacity, or transmissibility changes, are desired [315]. If the difference between reservoir pressure and the hydrostatic head is more than 15% of the wellhead pressure, serious quantitative errors can result when wellhead pressures are used in the construction of Hall plots; if the difference is less than 15%, only slight errors are caused [66].

Earlougher has presented a modified version of the Hall technique in which the slope, m' , is defined as [66]:

$$m' = \frac{141.2\mu}{kh} \left[\ln\left(\frac{r_c}{r_w}\right) + s \right] \tag{5-237}$$

The improvement in overall flow efficiency, E_f , can be obtained from [66]:

$$\frac{E_f \text{ after}}{E_f \text{ before}} = \frac{m' \text{ before}}{m' \text{ after}} = \frac{I \text{ after}}{I \text{ before}} \tag{5-238}$$

where the injectivity index, I , or Hall slopes are calculated using the pressure difference between the flowing bottomhole pressure and the formation pressure.

Production Curves. Plots of waterflood injection and production performance can be presented in a number of ways. For the history of the project, water injection rate, oil production rate, and water-oil ratio or water cut can be plotted vs. time (usually months). The actual water injection and oil production rates can be compared to the predicted rates on a time basis.

Future oil production and ultimate recovery are often extrapolated from graphical methods. One of the more popular methods is a plot of the WOR on a log scale vs. cumulative oil production on a linear scale or a linear plot of the fractional water cut (or percent water produced) vs. cumulative oil produced. Alternatively, the oil-water ratio can be plotted on a log scale vs. the cumulative production on a linear scale. One of the purposes of these plots is to predict the ultimate oil recovery by extrapolating the curve to some economic limit at which time it becomes no longer profitable to continue the flood. If the operating methods remain relatively unchanged, a method [317] has been proposed for a fully developed waterflood that permits an easy extrapolation of recovery to a given water cut. This latter method consists of a linear plot of E_{R} , fractional recovery of oil in place, vs. the term $- \{[(1/f_w) - 1] - (1/f_w)\}$. This method also provides an estimate of water-oil relative permeabilities.

Waterflood Parameters. Important parameters in waterflood operations are the water residual oil saturation, S_{or} , and the relative permeability to water, k_{rw} . A statistical study of these parameters, as well as peak oil rates, was provided by Felsenthal [318]. Data on S_{or} and k_{rw} from core data are listed in Table 5-45. Endpoint k_{rw} values were higher in carbonates than in sandstones; for a given lithology, k_{rw} decreased as the absolute permeability decreased.

Table 5-45
Waterflood Parameters

Waterflood residual oil saturations measured in core test samples			
	Sandstone	Carbonate Rock	
Mean average S_{or} , % pore space	27.7	26.2	
Median average S_{or} , % pore space	26.6	25.2	
Number of core samples tested	316	108	
Number of source reservoirs	75	20	
Standard deviation, % pore space	8.76	8.84	
Effect of lithology and K_a on the end points of oil/water relative permeability curves			
Permeability Group range of K_a , md	Low (1 to 10)	Medium (11 to 100)	High (101 to 2,000)
<i>Sandstone</i>			
Median k_{rw}^* at S_{or}	0.065	0.133	0.256
Median k_{rw}^{**} at S_{or}	0.033	0.095	0.210
Number of core samples tested	30	213	143
<i>Carbonate rock</i>			
Median k_{rw}^* at S_{or}	0.211	0.357	0.492
Median k_{rw}^{**} at S_{or}	0.179	0.303	0.428
Number of core samples tested	33	45	24

From Reference 318.

* Expressed as fraction of k_a at connate water saturation.

** Expressed as fraction of K_a .

ESTIMATION OF WATERFLOOD RESIDUAL OIL SATURATION

It is recognized throughout the industry that there is no single generally accepted method of measuring residual oil [319]. The available methods should be considered on their merits and some combination of methods should always be used as a cross-check. Each method provides somewhat different information about the amount and distribution of residual oil. This section discusses the various methods that are in current use, and recommendations are made as to how residual oil should be measured [320].

Material Balance

Material balance was one of the first and is the most widely used technique employed in estimating oil reserves and depletion. Overall estimates of the amount of in-place and recoverable oil are based mainly on material balance. These calculations are also used as a first screening point to determine if sufficient oil remains after waterflooding for application of tertiary recovery. The quantity of oil remaining in the reservoir, having pore volume V_p , in stock tank barrels, is given by the difference between the initial oil-in-place, N , and the amount of oil produced, N_p . The overall residual saturation $(S_{or})_{MB}$ is based on the volume of oil relative to the reservoir pore space [319].

$$(S_{or})_{MB} = \frac{(N - N_p)B_{or}}{V_p} \quad (5-239)$$

where B_{or} is the oil formation volume factor after waterflooding.

Many of the projects currently being evaluated as tertiary prospects were initially developed twenty to thirty years ago or longer. At that time, methods for estimating hydrocarbon content were not as accurate as methods presently available. In addition, adequate information relating to hydrocarbon volumes may be limited to only a few wells in a field and production data for the field may not always be reliable. In any event, even where material balance might yield a reasonable estimate of the amount of residual oil-in-place, it does not indicate the distribution of oil within the reservoir.

The value of $(S_{or})_{MB}$ will be dependent on both the microscopic displacement efficiency in swept zones and the vertical and horizontal sweep efficiency. It has been suggested that a high ratio of $(S_{or})_{MB}$ to S_{or} , determined by methods applying to the swept zone, indicates that the reservoir still contains an unusually high amount of oil in the unswept region. The reservoir should then receive special consideration as a candidate for obtaining additional oil recovery through infill drilling [319].

In application of tertiary recovery, the residual oil remaining in the swept zone is of most interest because this is the region that will most likely be contacted by a tertiary process. Thus, the material balance, even in more sophisticated forms than the foregoing simple volumetric balance, should only be used for rough screening in evaluating prospects for tertiary recovery. Furthermore, because of the many uncertainties in the measurements used to obtain a material balance, an enhanced recovery prospect should not be discounted on the basis of material balance alone.

When the volume of oil produced is known with reasonable precision, the accuracy of this method depends mainly on the reliability of the original oil-in-place estimate.

Well Test Analyses

In-situ oil saturations can be estimated by combining relative permeability data determined in the laboratory with field well test data such as:

Production data

Single well transient tests in producing wells

Pressure buildup

Pressure drawdown

Multiple-rate testing

Multiple-well transient tests

Interference tests

Pulse tests

Details of the methods for developing the well test data can be found in the literature [13,66,228], and were summarized earlier. If sufficient, good quality relative permeability data are available from laboratory tests that simulate downhole conditions, the techniques of correlating well test analyses can give some indication of the reservoir oil saturation. For these techniques to be applicable, numerous assumptions are made: the reservoir interval is homogeneous, horizontal, and isotropic with a small and constant compressibility; fluid properties and saturations are uniform in the formation; relative permeabilities are constant throughout the test area; there are no oil-water or gas-oil contacts; and the tested wells are not affected by other wells outside the test area [319]. The following discussion applies to waterflooded reservoirs with no free gas saturation, but could be extended to more complex systems.

Production Data

When the producing oil and water flow rates, formation volume factors, and viscosities are known, relative permeability ratios can be determined:

$$\frac{k_{rw}}{k_{ro}} = \frac{q_w B_w \mu_w}{q_o B_o \mu_o} \quad (5-240)$$

where k_r = relative permeability

q = flow rate

B = formation volume factor

μ = viscosity

and the subscripts w and o refer to water and oil, respectively. Thus, the relative permeability ratio between water and oil can be estimated from the producing water-oil ratio (WOR).

Relative permeabilities determined in the laboratory may be based on any one of the following measures of core permeability: air, water at 100% S_w , or oil at irreducible water saturations. Laboratory-derived permeability ratios can be used to find the water saturation at which the field-derived permeability ratio would occur. In the absence of gas saturation,

$$S_o = 1 - S_w \quad (5-241)$$

Provided core analysis data are available, this method is easy and rapid. However, no information is obtained regarding wellbore damage or specific permeabilities

to the flowing fluids. This important information can be obtained from the transient well tests.

Transient Tests

Whereas the producing well production data can only provide a relative permeability ratio, transient well testing can provide estimates of reservoir permeabilities to both oil and water (and free gas, if present):

$$k_o = \frac{162.6 q_o B_o \mu_o}{mh} \quad (5-242)$$

$$k_w = \frac{162.6 q_w B_w \mu_w}{mh} \quad (5-243)$$

where k , q , B , and μ are as previously defined and have units of millidarcies, barrels per day, reservoir barrels per stock tank barrel, and centipoise, respectively. The thickness of the interval, h , is in ft and m is the appropriate slope from the Miller-Dyes-Hutchinson (MDH) plot or the Horner plot.

Multiple well or single well tests can be used to estimate the effective permeability to oil by using type-curve matching:

$$k_o = \frac{141.2 q_o B_o \mu_o (p_D)_M}{h \Delta p_M} \quad (5-244)$$

where $(p_D)_M$ is the dimensionless pressure at the match point for type-curve matching, Δp_M is the pressure change from transient test data at the match point for type-curve matching, and the previously defined terms are in field units. Laboratory relative permeability curves are then used to find the saturations that correspond to the relative permeabilities obtained from the transient tests.

Multiple well testing can also be used to estimate oil saturation by using the total compressibility from the match point data and:

$$c_t = c_w S_w + c_o S_o + c_g S_g + c_f \quad (5-64)$$

where c_t is system total compressibility; C_f is the formation or pore volume compressibility; c_w , c_o , and c_g are compressibilities of water, oil and gas, all with units of psi^{-1} ; and S is the corresponding saturation [321]. Since the gas term is assumed to be zero for the waterflooded case and since $S_w = (1 - S_{or})$,

$$c_t = c_w(1 - S_o) + c_o S_o + c_f \quad (5-245)$$

By rearranging,

$$S_o = \frac{c_t - c_w - c_f}{(c_o - c_w)} \quad (5-246)$$

With a knowledge of oil, water, and formation pore volume compressibilities, and the total compressibility determined from the type-curve matching, reservoir oil saturation can be estimated [319]. Oil saturation based on compressibility

is generally less accurate than saturations determined from field relative permeability data and is normally regarded as an approximation.

Applicability

Because of the rigid requirements of the assumptions made, and the problems with interpreting the field data, oil saturations obtained from well test analyses are considered rough estimates. The saturation estimate is an overall average for the region of the reservoir influenced by the test. If permeability variations or other conditions cause a variation in the vertical saturation distribution, these techniques will not yield meaningful data. For these techniques to be considered for oil saturation determinations, good laboratory core analysis data are essential. However, because of the low costs and relative ease in conducting the tests, plus the additional important information obtained, well test analyses should be developed along with the other more direct methods of determining residual oil saturations.

Coring and Core Testing

Well Coring

Well coring is the process of obtaining representative samples of the productive formation. The choice of depth at which to begin coring can often be a problem. Cores from the regions of interest may not be obtained because of unexpected changes in stratigraphy. There is also the possibility that the region cored will be a nonproductive region which did not contain significant hydrocarbon content initially. However, analysis and testing of core samples continues to be an important method of determining residual oil [322,323].

Various techniques are used to obtain core samples: conventional diamond-bit coring, rubber-sleeve coring, pressure coring, sidewall coring, and recovery of cuttings generated from the drilling operation. The last two methods are not used for residual oil measurements. Conventional coring is normally done in competent formations to obtain full-diameter cores. In unconsolidated, or poorly consolidated formation, a core barrel containing a rubber sleeve is used. The core sample is held together by the sleeve and its properties during laboratory tests remain reasonably representative of conditions in the formation [322].

Two main problems in coring for determination of residual oil are that further flushing of oil to below-normal waterflood residuals can take place around the core bit, and that loss of oil occurs, due mainly to gas expansion, as the core is lifted to the surface.

Flushing During Coring. For a condition where the in-place oil saturation is at its waterflood residual value, no more oil can be produced at normal flow rates. During the coring operation, it is important to avoid extreme flushing conditions that could cause part of the residual oil to be mobilized [194]. Some of the variables that control the amount of residual oil flushed from a core by mud filtrate are: borehole-to-formation differential pressure (overbalance), interfacial tension, wettability (the following discussion applies principally to water-wet rocks), core permeability, coring penetration rate, core diameter, type of drill bit, drilling mud composition (including particle size distribution), depth of invasion of mud particles into the core, rate of filtrate production (both spurt loss and total fluid loss), permeability of the formation, and nature of the reservoir (uniformity, texture etc.) [324]. In one type of system investigated in

the laboratory, the amount of oil stripped from cores varied directly with the overbalance pressure, filtration production rate, and core permeability; it varied inversely with penetration rate and core diameter. The overbalance pressure is usually the critical variable [195].

Overbalance Pressure. Unintentional displacement of residual oil may occur in coring operations when large pressure gradients exist near the core bit. In this region when fluid velocities are high, the resulting viscous forces may become sufficient to overcome the capillary forces that hold the residual oil in place.

Results from an extensive laboratory coring program [195] showed a reduction in pre-test residual oil saturation of almost 20 percent to about 60 percent as the pressure gradients varied from about 350 to 1,700 psi/ft. In an evaluation of the same data, other authors [123] contend that when analyzing larger diameter cores (4-in. diameter) and considering radial flow, the estimated penetration would result in only a 10% change in residual oil. In addition, they contend that core samples used in retort analysis are usually taken from the center of the core where mud solid penetration into the core would be minimal. However, it is generally recognized that residual oil, which is immobile after normal waterflood operations, can become mobile and be stripped from the core, especially in the region adjacent to the core bit.

The ratio of viscous to capillary forces has been expressed as $\Delta P/L\sigma$, where $\Delta P/L$ is the pressure drop per unit length, and σ is the interfacial tension. In water-wet cores, at least, a critical value of $\Delta p/L\sigma$ must be exceeded before production of residual oil occurs [194]. In coring, the overbalance pressure must be kept low in order to minimize flushing. Furthermore, the drilling mud should not contain additives that cause significant reduction in interfacial tension that could mobilize residual oil. The use of dispersants, emulsifiers, lubricants, lost circulation materials, and oil should be avoided. If the overbalance pressure causes the critical displacement ratio to be exceeded, then there will be some displacement of residual oil. Linear displacement tests run in the laboratory show the critical displacement pressure to vary from about 1 (psi/ft)/(dyne/cm) for a 1,000 md sandstone to about 25 for a 100 md sandstone [194]. Thus, the permissible overbalance pressure will have significant dependence on the properties of the formation that is being cored (Figure 5-173).

Drilling Mud Properties. At bottomhole conditions, API filter loss for water-base muds is often in the range of 5 to 10 cc for 30 minutes, which is sufficient to drive most 3-in. to 4-in. diameter cores to the equivalent of the waterflood residual oil saturation if the region being cored is not already at this condition [123]. Higher mud water loss or smaller core diameters can lead to displacement of some of this residual oil. However, only general agreement has been found between API filter loss and the amount of oil stripped from cores. More consistent agreement has been observed between the amount of mobilized residual oil and spurt loss (the rapid fluid loss to the formation that occurs before an effective mud filter cake has built up). Spurt loss has been shown to correlate with solids content and particle size distribution which also influence filtration rates and amount of oil-stripping [195]. In general, when taking cores it is always preferable to use a bland water base drilling fluid which contains no oil or surface active materials [319].

Shrinkage and Bleeding. In reservoirs which have been depleted to low pressures and waterflooded to high water-oil ratios, changes in residual saturation in bringing the core to the surface should be fairly minimized. However, in most

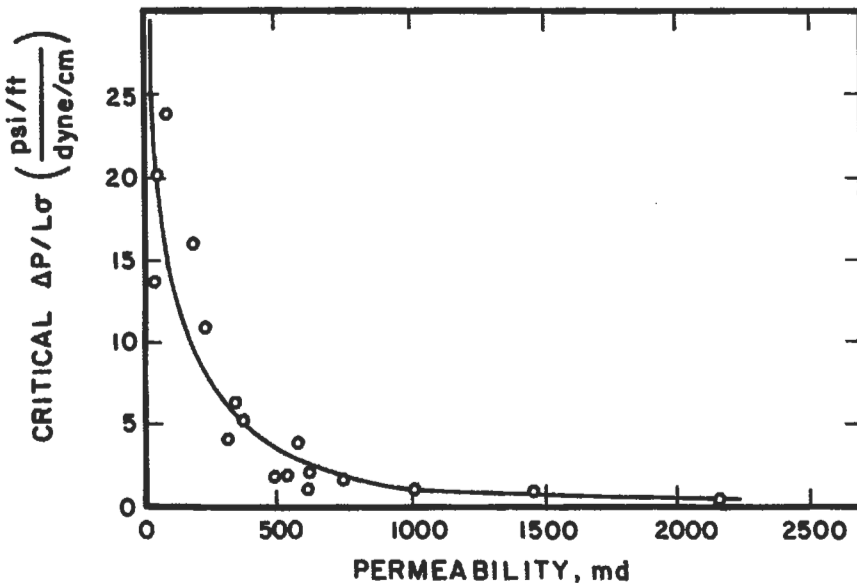


Figure 5-173. Critical capillary number as a function of permeability [194].

cases, as the core is raised, gases will come out of solution and can cause residual oil to bleed from the core. The loss of gas causes the oil to shrink.

Corrections for Shrinkage and Bleeding. Shrinkage of residual oil can be estimated from laboratory measurements of shrinkage when the pressure of bottom-hole oil samples is lowered. Reduction of temperature will also contribute to shrinkage. The following corrections have been proposed for the effects of shrinkage and bleeding [123].

$$(S_{or})_R = (S_{or})_c B_o E \quad (5-247)$$

where $(S_{or})_R$ = average post-waterflood residual oil saturation in the flooded region of the reservoir

$(S_{or})_c$ = average oil saturation from cores

B_o = oil formation volume factor at the time of coring

E = bleeding factor (in the absence of specific bleeding measurements, a value of 1.11 is assumed)

A modification to this calculation has been suggested [325] to compensate for waterflood displacement efficiency by dividing the reservoir residual oil saturation by the conformance factor. In the absence of a reservoir simulator that accounts for reservoir heterogeneity, capillary effects, mobility of oil, and mobility of water, it was suggested the conformance factor be estimated by $(1 - V^2)/M$

where M = mobility ratio or the ratio of the mobility of water at the average water saturation in the reservoir at breakthrough to the mobility of oil in the oil bank ahead of the displacing front

V = the Dykstra-Parsons permeability variation

Thus, the modified calculation would be

$$(S_{or})_R = (S_{or})_c B_o E \frac{M}{1 - V^2} \quad (5-248)$$

However, these corrections, particularly the one for bleeding factor, are only approximate at best and considerable attention has been given to recovering cores at reservoir pressure.

Pressure Core Barrel. Considerable development work has gone into developing a core barrel that will bring cores to the surface without major reduction in reservoir pressure, and thus prevent shrinkage and bleeding. The pressure core barrel is designed to cut the core and seal it within a cylinder before retrieval. Although the cores obtained are small in diameter ($\sim 2 \frac{1}{2}$ -in.), pressure coring has gained acceptance as one of the best methods of determining residual oil, particularly when information on the vertical profile of the oil saturation is wanting. Success in application of the core barrel depends to a great extent on the skill and experience of the personnel running the operation. The main criterion for success is retrieving cores at or close to formation pressure. Improvements over the years have led to the present success level of about 70% to 80% in consolidated formations [182,319,326-331].

Sponge Cores. A recent modification [332] to a conventional core barrel is the incorporation of a porous sponge to collect oil that bleeds from the core. The oil saturation measured by conventional techniques is corrected for the bleeding of oil as measured in the sponge. Oil saturations measured with this technique have approximated the values determined by pressure coring but at a cost that is closer to conventional coring.

Core Testing

Laboratory tests to estimate reservoir residual oil can be performed on cores that have been preserved at the wellsite or cores which are extracted with solvent and subsequently restored to reservoir conditions. Cores obtained with drilling muds that minimize wettability alteration, and that are protected at the wellsite to prevent evaporation or oxidation are called preserved cores. Cores that are cleaned with solvents and resaturated with reservoir fluids are called restored-state cores or extracted cores. The restoring process is often performed on non-preserved or weathered cores, but the same technique could apply to cores that had been preserved.

Core Handling. Conventional Cores. The precautions taken in handling cores once they have been recovered depends mainly on the measurements and tests that are to be performed on them. If the measurements are routine and can be run within a day or two, it is generally considered sufficient to wipe the cores, wrap them in plastic and protect them from exposure to the sun. However, it is better to keep the wrapped cores inside ice boxes to minimize evaporation, especially when longer transit times are anticipated. When maintenance of wettability conditions as they exist in the reservoir is attempted, the most widely preferred method of preservation is to wrap the core in thin sheets of plastic followed by aluminum foil and then isolate the wrapped core from the atmosphere by a coating of wax or plastic. An alternative method of preservation is to store the

cores in deoxygenated aqueous solution. This may be formation brine, synthetic brine or mud filtrate [319,333].

Pressure Cores. Special handling is needed for cores obtained using the pressure core barrel. This is normally carried out by the trained crew which assembled the barrel prior to testing. After retrieving the core barrel, drilling fluid is displaced at pressure by gelled kerosene. The complete barrel is then chilled in dry ice for several hours in order to freeze the water in the core sample. The pressure in the core barrel can then be released and an inner metal sleeve containing the core is removed. The core is cut into convenient lengths, of about three to four feet, and kept frozen by means of dry ice during transportation [319].

Measurement of Residual Oil in Recovered Cores. Various techniques are available for determining the oil content of cores. Examples that involve removal of the oil are vacuum distillation, a combination of distillation and solvent extraction (Dean Stark), and high temperature retorting. The Dean Stark method with toluene as solvent is normally used when displacement tests are to be carried out on the extracted cores. In this method, the oil saturation is determined by difference from the amount of water removed from the core [191,333,334].

In general, cores obtained with the pressure core barrel under conditions of minimal flushing are needed in order to obtain residual saturations that can be treated with reasonable confidence. Special analytical methods have evolved for treatment of pressure cores. The frozen cores are removed from the metal-containing sleeve and dressed while still frozen. The pressure cores are then allowed to thaw in an inert atmosphere, and volumes of evolved gases are recorded. Next, the free water is distilled from the core. Any remaining oil is removed by a toluene-CO₂ leaching. The amount of oil in the core is determined by adding the volume obtained by distillation to the volume removed during extraction and then making a correction for evolved gas. As a check on extent of penetration of mud filtrate into the core, a tracer can be added to the drilling mud which permits the radial depth of invasion to be estimated. However, filtrate invasion does not necessarily imply flushing of residual oil [319].

Residual Oil from Laboratory Core Floods. Most cores are subjected to cleaning before measurement of permeability and porosity. However, when the preservation of wetting properties is of main interest, displacement tests are run on the cores prior to cleaning.

Another approach to the problem of reservoir wettability is the restored state method. Cleaned cores are saturated with reservoir brine or brine of similar composition. The brine is displaced by reservoir crude to an equivalent connate water saturation. Recontacting the reservoir rock with the reservoir crude is believed to result in adsorption of those components from the crude oil which determined the in-situ wettability and hence restore the system to its original wetting condition.

Relatively little is known about the causes of reservoir wettability and its sensitivity to the numerous variables that may cause the wettability of recovered cores to be changed. It has been shown that wettability can have significant effect on residual oil [121,125]. This is the main reason why values of residual oil saturation determined by laboratory core flooding tests are treated with caution. Residual saturations determined by laboratory flooding tests are often used in estimating the amount of oil that will be recovered by waterflooding. However, when residual oil saturation is to be determined for evaluation of a tertiary

recovery prospect, laboratory flooding tests do not seem to be in favor. In a recent monograph on residual oil determination, results of such tests received a rating of only poor to fair [319]. Nevertheless, there seems to be consensus view in the industry that the problem of wettability as it relates to residual oil has been satisfactorily resolved. However, little attention appears to have been given to restoring cores to their in-situ residual oil saturation at wetting conditions which are representative of the reservoir even though this may be critical to proper laboratory testing of a tertiary process [335,336].

Even though laboratory flooding of reservoir cores may not be a generally acceptable method of determining residual oil, it is considered vital that tertiary processes be tested in the laboratory using these cores.

Tracer Tests for Determining Residual Oil

How Tracer Tests Work

The tracer test was conceived by applying principles of chromatographic separation to fluid movement in the reservoir. The outstanding advantage of the tracer test is its ability to investigate a relatively large volume of the formation. It was first suggested that the method could be applied to flow between two wells [337]. The method depends on the effect which the relative solubility of a tracer between oil and water has on the rate at which a pulse of low concentration tracer passes through the formation.

The condition where the reservoir has been flooded out and the oil is immobile is considered later, but the theory can also be applied where both oil and water are flowing, or where the water phase is immobile. If a formation containing residual oil is flooded with a bank of water containing a tracer which is mutually soluble in oil and water, part of the tracer will pass into the oil phase. If there is local equilibrium, the concentration of the tracer in the oil, C_{to} , is related to the concentration in the aqueous phase, C_{tw} , by the distribution coefficient, K_1 .

$$K_1 = \frac{C_{to}}{C_{tw}} \quad (5-249)$$

As a result of partitioning, part of the tracer temporarily resides in the immobile residual oil, and the overall velocity of the tracer is less than that of the flowing aqueous phase. The concentration of tracer in the oil together with the oil volume determines the fraction of tracer resident in the oil phase. Since oil volume is directly proportional to oil saturation, the rate at which a pulse of tracer concentration passes through the formation depends on the oil saturation in regions swept by the tracer.

Equilibration of the tracer between the residual oil and water following the tracer bank coupled with dispersion effects determines the shape of a peaked concentration distribution of tracer. Ahead of the peak there is net movement of tracer into the residual oil. Behind the peak there is net movement of tracer molecules from the residual oil back into the water.

From consideration of the way the tracer divides itself between the oil and water phases and the effect of the magnitude of the residual oil saturation on residence time of the tracer, the velocity of the tracer, v_p , is related to the velocity of the associated water, v_w , by

$$v_t = \frac{(1 - S_{or})v_w}{(1 - S_{or}) + K_1 S_{or}} \quad (5-250)$$

from which residual oil is given by

$$S_{or} = \frac{v_w - v_t}{v_w v_t + v_t K_1} \quad (5-251)$$

The long time needed for tracer to move between wells and the broad and uninterpretable residence time distribution that would arise because of streamline and heterogeneity effects for normal well spacings are cited as reasons why the well tracer test may be impractical as a between-well test, although there is still some interest in applying this method to small pilot areas [319].

Single-Well Tracer Technique

The single-well or backflow tracer technique to determine residual oil saturation is a recent innovation. Patents [337,338] assigned to Exxon Production Research Company in 1971 described the injection of tracers to measure in-situ oil saturation at distances of typically 10 to 30 ft away from the wellbore of a producing well. The single-well tracer test overcomes many of the difficulties that, in general, make the two-well test impractical.

Test Procedure. The method involves injection of a bank of water containing an alkyl ester as the tracer. The selection of the ester will depend on temperature of the reservoir. For example, ethyl acetate is used in higher temperature reservoirs and n-propyl formate is used at lower temperatures [339]. These tracers are suitable for reservoirs with bottomhole temperatures ranging from about 80°F to 200°F. The ester partially hydrolyzes within the formation to form an acetate and an alcohol, the latter serving as a secondary tracer. Methanol is also added as a material balance tracer to the injected bank and also to the water which is used to push the bank into the formation [339-342].

A desirable volume for the slug is 50-90 barrels per foot of formation. Injection and production rates may limit the size of test that can be conducted in a reasonable period of time. Primary tracer volumes have varied from 40-1,000 barrels while total water volumes have ranged from 175-2,000 barrels [339-342]. Primary tracer concentration has normally been between 0.5-1 volume percent. In an example given by Deans [338], 500 barrels of 1% ethyl acetate and 0.5% methanol in brine is followed by 1,500 barrels of brine containing 0.5 % methanol. These quantities are determined by simple volumetric balance based on the desired depth of invasion.

Depending on formation permeability, injection may normally require 1 to 3 days and shut-in time will be 3 to 12 days. After allowing a suitable time period for hydrolysis of about 10% of the ester (usually about 3-12 days), the well is put on production and tracer concentration in the produced water is monitored. Because the alcohol formed by hydrolysis is much more soluble in the aqueous phase than its parent ester, the alcohol is produced ahead of the ester. The greater this separation between the two tracers, the higher the residual oil saturation. The methanol tracer, which is soluble only in water, determines the drift rate in the reservoir and also indicates the fraction of chemical slug that is produced during the test [339-342].

Interpretation. Computer simulation is used to model the injection, reaction, partitioning, production of the tracers and to correct for overall drift of fluids past the wellbore [340]. Fluid drift is mainly caused by injection or production of fluids in the vicinity of the test well. A best fit is obtained for the injected and produced ester and methanol, and parameters given by this fit are used to model the alcohol production for a range of assigned values of residual saturation. The measured alcohol production curve is then compared with the simulated results in order to estimate the residual saturation in the formation. Reservoir heterogeneity and loss of tracer can present problems in interpretation.

Reservoir Heterogeneity. Although the tracer test samples a relatively large pore volume, results will be weighted towards the higher permeability zones. However, this may not be a disadvantage because these zones will normally be swept preferentially by tertiary processes.

The single-well tracer method is not recommended for fractured reservoirs. Fractures cause nonradial flow, which results in tracer profiles that are almost impossible to simulate [341]. Severe permeability variations are also difficult to interpret. Where gross permeability variations exist, it may be necessary to conduct frequent injection profile tests to determine the intervals that are experiencing high-rate fluid flow [342].

Loss of Tracer. When the chemical tracer is injected into zones that do not subsequently produce fluids, tracer will be lost to the reservoir. In one field test, loss of tracer was estimated at 15% of the injected amount [339]. Conversely, dilution of produced fluids by water from zones that did not receive tracer injection will also present interpretation problems. If high drift-rates cannot be controlled, the slug of water containing chemicals can move so far from the wellbore that tracer profiles may not be well defined. Drift-rate should be less than 1 ft/day [342].

In some cases, it may not be practical to perform tests in wells with large intervals open or in wells with large holdup volumes in the wellbore. In such instances, well workovers may be required [340].

With wells produced by gas lift, corrections are required to account for the loss of part of the more volatile tracers to the gas by stripping action in the wellbore. Tests conducted [341] with ethyl acetate in gas lift wells indicate a loss of about 30%. Appreciable gas accompanying crude oil lifted by other production methods may cause loss of tracer by stripping.

Accuracy. Success in application of the tracer test depends to a considerable extent on the skill and experience of those conducting the test. While there is no absolute measure of success, comparison of measurements with simulated results provides a useful guide as to the reliability and tolerance of the results. In about 10% of the early tests conducted, residual oil saturation could not be determined from results. Oil saturations of 10% to 20% pore volume have been measured with reported accuracies of $\pm 2\%$ to $\pm 4\%$. Although conventional methods of estimating residual oil cannot be considered an acceptable standard for determining absolute accuracy of the tracer technique, measurements obtained from tracer tests have generally agreed with values obtained from pressure core tests [319,339-342].

Field Application. Logistic considerations require adequate preplanning which means it may be difficult to schedule tests on quick notice [339]. As compared to well logging techniques, considerable time is required to obtain and interpret the data.

Geophysical Well Logging Techniques

Geophysical well logging has the advantage of being an in-situ measurement and is able to give a continuous estimate of residual oil saturation versus depth [343,344]. These features allow the calibration of the measurements in known water-saturated formations. A more detailed discussion of well logging is given earlier. An evaluation of logging techniques for measurement of S_{or} was provided by Fertl [344].

Logging Devices

Five measurements that have potential application are:

1. *Electrical resistivity.* Many devices of different depths of investigation are available [58, 345]. These devices cannot be used in cased holes unless one uses some nonconducting casing.
2. *Pulsed neutron capture.* This name (PNC) covers logs commercially available such as the Dresser Atlas Neutron Lifetime Log (NLL) and the Schlumberger Thermal Decay Time (TDT). The PNC has the virtue of being useful in cased holes.
3. *Carbon-oxygen.* This measurement has the virtues of being directly sensitive to carbon and of working in cased holes.
4. *Nuclear magnetism.* This service is not routinely used but has the unique virtue of being sensitive only to formation fluids.
5. *Dielectric constant.* This service is now routine but is limited to open holes. Its main advantage over resistivity measurements is that water salinity need not be known.

Electrical Resistivity. Resistivity measurements provide a great range of choice as to the volume of formation to be sampled, ranging from a few cubic inches to many cubic feet. Interpretation of the measurements for residual oil saturation requires a determination of the relation between water saturation and resistivity. If the true formation resistivity R_t and the water resistivity R_w are known, then for clean sandstones [42],

$$R_t = F_R R_w S_w^n \quad (5-252)$$

where F_R is the formation factor. If after measuring R_t , the fluid around the hole is replaced by water of resistivity R'_w (through chemical flushing followed by displacement with water of resistivity R'_w), then from Equation 5-252 it follows that

$$S_w = 1 - S_{or} = \left[\frac{R_t R'_w}{R'_t R_w} \right]^{1/n} \quad (5-253)$$

Clearly, n , the saturation exponent, must also be known. It is often taken to be $n = 2$. If cores or other logs are available, better estimates of n can be made.

Relations other than Equation 5-253 are required for carbonates and shaly sands [346,347].

Resistivity measurements cannot be made in cased holes. This may explain the limited documentation of such methods for residual oil determination in the literature.

Pulsed-Neutron-Capture. The device used for this measurement periodically emits brief bursts of high energy neutrons. Between bursts these neutrons are rapidly reduced in energy and then more slowly absorbed by formation nuclei. It is the rate of this relatively slow absorption that is measured.

Upon neutron absorption most formation nuclei are left in high energy states that decay to ground states through the emission of a characteristic set of gamma rays. That is, the gamma rays emitted have various energies and numbers at these energies that are unique to the capturing nucleus. However, carbon does not participate in this process.

The gamma rays emitted above a fixed energy (the fixed energy used in commercial tools varies from 50 kev to 200 kev) are detected and counted as a function of time. The analysis of this counting rate yields the apparent thermal decay time or equivalently the apparent capture cross-section of the formation. The apparent cross-section can be corrected to true formation cross-section through computation. Certain modes of operation [348] can yield results requiring little or no correction.

The formation capture cross-section Σ_t is related to the cross-sections of the constituents of the fluid-saturated rock (see Equation 5-118) by the formula [348,349]:

$$\Sigma_t = \Sigma_{ma} (1 - \phi) + \Sigma_w \phi S_w + \Sigma_h \phi (1 - S_w) \quad (5-254)$$

where Σ_{ma} is the capture cross-section of the rock (including clay or shale), ϕ is the porosity, Σ_w is the cross-section for the water, Σ_h is the cross-section of the hydrocarbons, and S_w is the water saturation. Thus $(1 - S_w)\phi$ is the oil volume per unit volume of formation.

Of course, the desire is to determine the residual oil saturation $(1 - S_w)$ or the residual oil per unit volume, $\phi(1 - S_w)$. Because many of the quantities on the right hand side of Equation 5-254 may be unknown, one employs the so-called log-inject-log technique [350-353].

If the porosity is known in addition to Σ_w , then the simplest form of the log-inject-log technique can be used. Here two successive logs are run. In the first, the normal formation water of cross-section Σ_w occupies the pores. The section of interest is then flushed (at low injection rate) with water of cross-section Σ'_w as different from Σ_w as possible. Σ_t and Σ'_t for these two conditions are measured. Then from Equation 5-254 it follows that $S_{or} = 1 - S_w$ is

$$S_{or} = 1 - \frac{\Sigma'_t - \Sigma_t}{\phi(\Sigma'_w - \Sigma_w)} \quad (5-255)$$

To obtain accurate values of Σ_t and Σ'_t one should use a very low logging speed, or stationary measurements, or repeat passes that can be averaged.

If porosity is not known, the water flush can be followed by a flush with chlorinated oil [352]. Here the chlorination is adjusted so that the oil has cross-section Σ'_w . Then from the viewpoint of the PNC response, it is just as if we had $S_w = 100\%$. Then Equation 5-254 yields

$$\phi = \frac{\Sigma_t'' - \Sigma_t}{\Sigma_w' - \Sigma_w} \quad (5-256)$$

where Σ_t'' is the measured value after the chlorinated oil flush.

The technique just outlined will suffer if Σ_w is small corresponding to low chloride concentration (below 30,000 parts per million). If Σ_w is unknown, it can be controlled by an initial water flush with water of known cross-section.

The most common practice has been to run a PNC log, inject fresh water, and run a second PNC log. Excellent results have been reported for initial water salinities in excess of 30,000 parts per million.

Carbon-Oxygen. The oil industry has long sought a logging method that directly measures oil saturation. The carbon-oxygen (C/O) log is the most recent method in this continuing effort. Since the method is sensitive to formation carbon and since oil is largely carbon, the ideal result would yield directly formation oil content [218,219,354-357].

The C/O log utilizes apparatus similar to that of the PNC log; namely, a pulsed neutron source and a gamma ray detector. The neutron bursts and the detector device are timed to emphasize gamma rays produced by high-energy neutrons scattering off of carbon and oxygen. The gamma rays are not simply counted but are also analyzed for their energy. The gamma rays produced during the neutron burst are primarily inelastic gamma rays, and it is in this time period that carbon contributes gamma rays to the detector. When the neutron source is off, capture gamma rays are detected and analyzed. Carbon does not contribute to the capture-gamma-ray spectrum. The capture gamma-ray spectrum is used to correct for interference in the carbon region of the inelastic spectrum due to calcium, silicon, and oxygen [355].

The device has serious limitations. These include problems with counting statistics, interfering gamma rays, carbonate rocks, and perturbations caused by casing and borehole. Best results are obtained when the tool is stationary for several minutes to overcome counting statistics, and when the formation porosity and oil saturation are high. The measurement may be improved using log-flush-log techniques, but only a few efforts have been documented at this time [344].

Nuclear Magnetism. This method has been thoroughly discussed in the literature [358-360]. The technique involves a polarization of the hydrogen magnetic moments via a large coil (3 ft long and 3 1/2 in. in diameter) carrying a large direct current. The idea is to align the hydrogen magnetic moments along the field created by the coil. This field ideally is at right angles to the earth's magnetic field. After a few seconds (up to about four), this coil-produced field is reduced to zero as quickly as possible. The polarized hydrogen moment then precesses about the earth's field at about 2,200 Hz. This induces a voltage into the coil which is detected and processed to yield a measure of the total number of hydrogen nuclei in the formation fluid. This number or concentration is called the free fluid index (FFI). Since oil and water have about the same concentration of hydrogen nuclei, FFI is a measure of porosity as given by the fluid contributing to the signal.

For the detection of residual oil saturation, one relies on the fact that the addition of paramagnetic ions to the formation water will cause the signal from the water to be annulled. The measurement thus utilizes the log-flush technique. A first measurement is made of FFI. The formation is then flushed with water

containing paramagnetic ions so that FFI is sensitive only to residual oil. The result is that S_{or} can be estimated from:

$$S_{or} = \frac{FFI'}{FFI} \quad (5-257)$$

This technique requires signal averaging over many repetitions of the basic measurement in order to compensate for the very poor signal to noise ratio.

The method cannot be used in cased holes and requires a fairly large (>7 in.) open hole. It has a very shallow penetration and highly viscous oils will not contribute to FFI. In this latter case, a separate measure of porosity will be needed. The service is still not widely available but in principle it is the most promising of all logging methods for the determination of S_{or} [361,362].

Dielectric Constant. The dielectric constants of rock and oil are distinctly different from that of water. The dielectric constant of bulk water is about 80 while those of oil and rock are 4 or less. In practice, however, due to polarization effects on heterogeneous media, this difference in dielectric properties is masked unless very high frequencies are employed in the measurement. One study shows that results of the expected order are obtained with use of very high frequencies and, furthermore, the measurements are unaffected by water salinity [363]. Several devices designed in accordance with these ideas have been designed and successfully field tested [364-374].

The use of this measurement for S_{or} determination could also benefit from the log-inject-log procedure. For example, after logging initially, one could displace the water with a fluid having about the same dielectric constant as oil. A further flush with a fluid removing all oil and of known dielectric constant could be made.

To interpret the measurements, one can use an equation similar to Equation 5-254:

$$\Delta t_t = \Delta t_{ma}(1 - \phi) + \Delta t_w \phi S_w + \Delta t_H(1 - \phi) S_H \quad (5-258)$$

where the Δt_t refers to travel time of the electromagnetic energy between the two receivers of the device. Δt_t is the measured parameter while the other Δt symbols refer to formation and fluid travel times. After the first flush, S_{or} is found from:

$$\phi S_{or} = \phi(1 - S_w) = \frac{\Delta t_t - \Delta t'_t}{(\Delta t_w - \Delta t'_w)} \quad (5-259)$$

After a second flush, ϕ could be determined from an equation similar to Equation 5-256. Equation 5-259 can be used to obtain the amount of oil per unit volume. If S_{or} is required, a porosity derived from a neutron-density log could be used.

Volume of Reservoir Sampled

It is important to know how large a volume of the reservoir is investigated by a given logging method. This is determined by the vertical resolution and depth of investigation, which have been estimated as follows:

Pulsed neutron capture	
Depth of investigation	~6 in.
Vertical resolution	~1½ ft
Resistivity	
Depth of investigation	~1 in. to 5 ft
Vertical resolution	~1 in. to 5 ft

This large range reflects the large number of resistivity devices available.

Carbon-oxygen	
Depth of investigation	~2 in.
Vertical resolution	~1½ ft
Nuclear magnetism	
Depth of investigation	~1 ½ in.
Vertical resolution	~3 ft
Dielectric constant	
Depth of investigation	~1 ½ in.
Vertical resolution	~1 ½ in.

These measurements are bulk measurements of the formation sampled. Thus, if there are heterogeneities due to fractures, permeability variations, etc., these will result in errors for elemental volumes. However, since for example, a low permeability zone may not contribute to a tertiary recovery process, this feature of the measurements may be an asset rather than a liability.

Accuracy of Logging Methods

The estimated uncertainty in residual oil saturations from electric logs is 5% to 10% under optimum conditions and could easily exceed 10% under less favorable conditions [349]. Accuracy of saturations derived from electric logs is generally in the range of ± 15 saturation percent [324], which is clearly inadequate for residual oil determinations.

From the laboratory measurements of the C/O ratio, it is known that the accuracy of this technique is poor when porosity is low [218]. Oil saturation probably cannot be reliably determined at porosities less than 15%. However, even in a 30% porosity sand, the accuracy of oil saturation measurements would only be $\pm 12.5\%$. While this uncertainty could be reduced by taking repeated measurements at the same depth, stability of resolution may still be a problem.

The accuracy requirement for the determination of residual oil is so great that the use of the log-inject-log technique is often required. Although this technique is applicable to various logging methods, practical application has been limited to the PNC and NML. The term log-inject-log (L-I-L) refers basically to the fact that the measurements are made with control over the properties of the fluid saturating the rock volume under study. Assumptions with this technique are that the formation is at residual oil saturation; no oil is displaced from the formation during injection the true total cross-section is measured; the formation water is completely displaced within the radius of investigation by the tool; and that shrinkage of oil due to gas stripping during injection is negligible.

With the pulsed-neutron-capture L-I-L technique, accuracy of $\pm 5\%$ oil saturation is obtainable [349,352]. For best results, the contrast in salinities of the two waters should be as great as possible. While this technique has been

successfully used, a test in a 100% water saturated formation yielded oil saturations of 40%–60% [353]. These obviously incorrect values may have resulted from incomplete displacement of formation water close to the wellbore by the injected low salinity water.

Accuracy of the nuclear magnetism log depends largely on the signal-to-noise ratio which can be improved by making repeated readings. Newer versions of the NML tool have improved signal-to-noise characteristics. As with other log-inject-log techniques, the possibility of fluid drift in the formation should be considered. Fluid drift should not be sufficient to move injected paramagnetic ions away from the wellbore which would cause erroneously high values of S_{or} [349].

Summary of Methods for Estimating Residual Oil

Economics of primary and secondary recovery processes are usually sufficiently attractive to permit considerable error in the estimation of recoverable reserves. However, for tertiary recovery the amount of oil remaining in a reservoir and its distribution must be known with reasonable confidence. Firstly, a reliable estimate of residual content is extremely important to technical evaluation of field tests. Secondly, the high front-end costs of tertiary processes are such that overestimates of residual oil saturation could have disastrous economic consequences. Thus, a well-planned effort to measure residual oil saturation is a necessity before any tertiary recovery application. Under favorable circumstances, accuracies of $\pm 2\%$ of reservoir pore space can be achieved. In general, accuracies will not be this good, but values within $\pm 5\%$ are considered necessary.

There is no absolute measure of residual oil saturation for a reservoir. When evaluating a tertiary prospect, a combination of methods should be used which provide information on both amount and distribution. Evaluation will normally begin with material balances using information that is already available. Frequently quoted nation-wide estimates of the amount of residual oil that is potentially available for tertiary recovery are based mainly on material balance. Comparisons of material balance with other methods of determining residual show unacceptable scatter, and on average, the material balance gives saturations which are too high by about 9% (by pore volume). This corresponds to about a 30%–50% overestimate in amount of residual oil. It has been suggested that a much higher ratio (say 2 to 1 or more) in residual oil determined by material balance to that given by other methods is an indication that the reservoir contains extensive regions of high oil saturation and may, therefore, be a good prospect for infill drilling.

In addition to material balance, other estimates of residual oil from resistivity logs and laboratory waterflood tests may also be available. However, in general, none of the conventional methods of determining residual oil saturation—analysis of conventional cores, laboratory displacement tests, conventional logging, material balance—are considered sufficiently reliable in themselves. They can provide useful guides as to whether a tertiary prospect should be investigated further.

Over the past 15–20 years there has been increased field testing of a number of more sophisticated techniques: pressure coring, tracer tests, and the various types of log-inject-log procedures. These methods vary in the conditions under which they can be applied and the type of information they provide.

Pressure coring and the sponge core technique provide information on the vertical distribution of residual oil and also have the advantage that the core analysis procedures directly demonstrate the presence of oil. Because of the possibility of flushing, results may tend to be conservatively low. For pressure

coring, the time taken to obtain results tends to be longer than other methods because of transportation and the specialized core analysis work that is needed.

After determining residual oil, the extracted cores are used to obtain needed information on reservoir properties, in particular vertical heterogeneity, and they also can be used in laboratory displacement tests. The reduced diameter (~2 1/2 in.) of pressure cores compared to those obtained by conventional coring is a disadvantage with respect to making laboratory displacement studies. The use of the sponge coring technique has increased because of the lower coring costs, reduced analysis costs, and, since larger diameter cores are obtained, core plugs can be obtained for subsequent conventional or specialized core testing.

The tracer test samples about a half million times more pore volume than the pressure core barrel. Results with the tracer test will be conservatively low because they are usually weighted towards the more permeable zones, where residual oil will tend to be lower. On balance this is probably an advantage because these zones will also tend to be swept more readily during a tertiary process. The tracer test can be used in old wells, but it is important that the well has not been fractured or stimulated severely.

Of the various log-inject-log procedures, the pulsed-neutron-capture method is the most widely tested. It has the advantage that it can be used in cased holes. Problems can arise with borehole rugosity effects and high values of residual oil if displacements are incomplete during the log-inject-log procedure. Results can be affected by flushing because of the small depth of investigation. The method can give accurate results under favorable circumstances. Stabilization of capture-cross-section values for the log-inject-log procedure can take unexpectedly long times and can present problems in interpretation. The nuclear magnetic log has been rated highly as to accuracy, but cannot be used in cased holes and it still has limited commercial availability. Log-inject-log resistivity measurements can give good results under favorable circumstances but are not applicable to cased holes.

Recommended Methods for Assessing Residual Oil

In determining residual oil saturation, at least two reliable methods should be compared. In most cases, a tracer test combined with injectivity profiles should be run in all situations unless there are clear reasons, such as excessive drift, why the tracer test would fail. The second method selected should provide information on vertical distribution of residual oil. The situations of old and new holes will be considered separately.

Existing Wells

Considerable cost can be saved if first measurements can be made on existing, preferably watered-out, producing wells. These wells will usually be cased. Old resistivity logs and core analysis data may be of value in estimating oil distribution and related heterogeneity. For more accurate determination of residual oil, the tracer test should be run together with the pulsed neutron capture log. However careful consideration must first be given to the past history of the well. There is no reliable method for determining residual oil if the well has been fractured or subjected to excessive stimulation. Inadvertent fracturing could have occurred during stimulation. Various forms of acidizing can have serious effects on near-borehole rock properties. The operator must also be sure that any injected chemicals which could affect results are absent from the test region, and that the well is clean and can be put on injection.

New Wells

When drilling new wells for residual oil determination, special attention should be given to using a bland drilling mud that contains no additives likely to alter interfacial tension or wetting properties. If full-diameter cores are obtained (which is desirable if economics permit), the sponge coring technique should be used with precautions being taken to ensure that flushing is minimal during coring. It is also recommended that the vertical distribution of residual oil be determined with a suite of open-hole logs that can include resistivity and dielectric constant. In cases where good data on capture cross-section are available, residual oil saturation can be obtained with a pulsed-neutron-capture log. If a log-inject-log scheme is used (for example, with PNC), this should not involve chemical flushing. The tracer test should be run after completion of logging measurements. All of these measurements can be backed up by laboratory displacement tests which should be carried out on preserved cores.

ENHANCED OIL RECOVERY METHODS

Definition

A general schematic of the enhanced oil recovery (EOR) process is depicted in Figure 5-174. The more common techniques that are currently being investigated include:

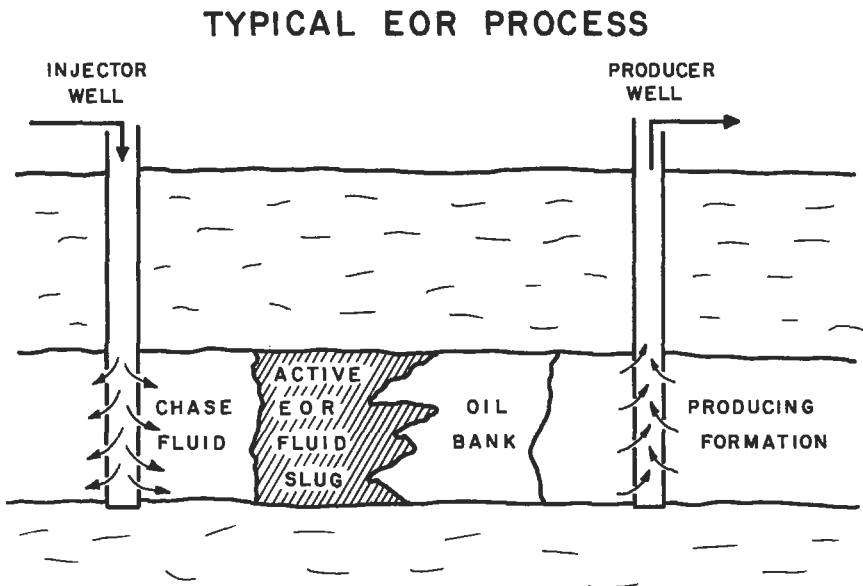


Figure 5-174. General schematic of enhanced oil recovery.

- Enhanced Oil Recovery*
- Chemical Oil Recovery or Chemical Flooding*
 - Polymer-augmented waterflooding
 - Alkaline or caustic flooding
 - Surfactant flooding
 - Low tension waterflooding
 - Micellar/polymer (microemulsion) flooding
- Hydrocarbon or Gas Injection*
 - Miscible solvent (LPG or propane)
 - Enriched gas drive
 - High-pressure gas drive
 - Carbon dioxide flooding
 - Flue gas
 - Inert gas (nitrogen)
- Thermal Recovery*
 - Steamflooding
 - In-situ combustion

These procedures are discussed in several texts on the subject [277,375-379]. Two studies by the National Petroleum Council [380,381] and several papers summarizing the later study are available [382-385]. The extensive literature on enhanced recovery will not be cited, and the reader is referred to Reference 386 which provides numerous citations and is the basis of the following discussion.

Chemical Flooding

Chemical oil recovery methods include polymer, surfactant/polymer (variations are called micellar-polymer, microemulsion, or low tension waterflooding), and alkaline (or caustic) flooding. All of these methods involve mixing chemicals (and sometimes other substances) in water prior to injection. Therefore, these methods require conditions that are very favorable for water injection: low-to-moderate oil viscosities, and moderate-to-high permeabilities. Hence, chemical flooding is used for oils that are more viscous than those oils recovered by gas injection methods but less viscous than oils that can be economically recovered by thermal methods. Reservoir permeabilities for chemical flood conditions need to be higher than for the gas injection methods, but not as high as for thermal methods. Since lower mobility fluids are usually injected in chemical floods, adequate injectivity is required. If previously waterflooded, the chemical flood candidate should have responded favorably by developing an oil bank. Generally, active water-drive reservoirs should be avoided because of the potential for low remaining oil saturations. Reservoirs with gas caps are ordinarily avoided since mobilized oil might resaturate the gas cap. Formations with high clay contents are undesirable since the clays increase adsorption of the injected chemicals. In most cases, reservoir brines of moderate salinity with low amounts of divalent ions are preferred since high concentrations interact unfavorably with the chemicals that are injected.

Polymer-Augmented Waterflooding

High mobility ratios cause poor displacement and sweep efficiencies, and result in early breakthrough of injected water. By reducing the mobility of water, water breakthrough can be delayed by improving the displacement, areal, and vertical sweep efficiencies; therefore more oil can be recovered at any given water

cut. Thus, the ultimate oil recovery at a given economic limit may be 4%–10% higher with a mobility-controlled flood than with plain water. Additionally, the displacement is more efficient in that less injection water is required to produce a given amount of oil.

The need to control or reduce the mobility of water led to the advent of polymer flooding or polymer-augmented waterflooding. Polymer flooding is viewed as an improved waterflooding technique since it does not ordinarily recover residual oil that has been trapped in pore spaces and isolated by water. However, polymer flooding can produce additional oil over that obtained from waterflooding by improving the displacement efficiency and increasing the volume of reservoir that is contacted. Dilute aqueous solutions of water-soluble polymers have the ability to reduce the mobility of water in a reservoir thereby improving the efficiency of the flood. Partially hydrolyzed polyacrylamides (HPAM) and xanthan gum (XG) polymers both reduce the mobility of water by increasing viscosity. In addition, HPAM can alter the flow path by reducing the permeability of the formation to water. The reduction in permeability to water that is achieved with HPAM solution can be fairly permanent while the permeability to oil can remain relatively unchanged. The resistance factor is a term that is commonly used to indicate the resistance to flow that is encountered by a polymer solution as compared to the flow of plain water. For example, if a resistance factor of 10 is observed, it is 10 times more difficult for the polymer solution to flow through the system, or the mobility of water is reduced 10-fold. Since water has a viscosity of about 1 cp, the polymer solution, in this case, would flow through the porous system as though it had an apparent or effective viscosity of 10 cp even though a viscosity measured in a viscometer could be considerably lower.

The improvement in areal sweep efficiency resulting from polymer treatment can be estimated from Figure 5-161. For example, if the mobility ratio for a waterflood with a 5-spot pattern is 5, the areal sweep efficiency is 52% at breakthrough. If the economic limit is a producing water-oil ratio of 100:1 ($f_w \cong 100/101 = 0.99$), the sweep efficiency at floodout is about 97%. If the polymer solution results in the mobility ratio being lowered to 2, sweep efficiencies are 60% at breakthrough and 100% at the same economic water-oil ratio.

A simplified approach to qualitatively observing the improvement with polymers in a stratified system is illustrated in Figure 5-164. For example, if the permeability variation is 0.7, the waterflood mobility ratio is 5, and the initial water saturation is 0.3, the fractional recovery of oil-in-place can be estimated. From the plot, $R(1 - 0.4 S_w) = 0.29$, and the fractional recovery, R , is $0.29/[1 - (0.4)(0.3)] = 0.33$. This R needs to be multiplied by the areal sweep efficiency of 0.97 to yield a recovery of 32% of the oil-in-place. If polymers again reduce the mobility ratio to 2 (and if no improvement in permeability variation occurs), a fractional recovery of 0.375 is obtained. Since the areal sweep with the polymer flood is 100%, a recovery of 37.5% of the oil-in-place is estimated. Thus the improvement with polymers is estimated at 0.375–0.32 or 5.5% of the oil-in-place. If the flow distribution with polymer solution lowered the permeability variation (which is not likely), the incremental production could be higher. These calculations are gross oversimplifications of actual conditions and only serve as a tool to show that reducing mobility ratio with polymers can improve the sweep efficiencies.

A properly sized polymer treatment may require the injection of 15%–25% of a reservoir pore volume; polymer concentrations may normally range from 250 to 2,000 mg/L. For very large field projects, millions of pounds of polymer may be injected over a 1–2 year period of time; the project then reverts to a

normal waterflood. The polymer flooding literature was reviewed in the late 1970s [387]. Recommendations on the design of polymer floods were recently made available [388].

Variations in the Use of Polymers

In-Situ Polymerization. A system is available in which acrylamide monomer is injected and polymerized in the reservoir. Both injection wells and producing wells have been treated.

Crosslinked or Gelled Polymers. Several methods are available for diverting the flow of water in reservoirs with high permeability zones or fracture systems. Some methods are only effective near the injection well while others claim the treatment can be effective at some depth into the reservoir. Both producing wells and injection wells can be treated.

One method is the aluminum citrate process which consists of the injection of a slug of HPAM polymer solution, aluminum ion chelated with citrate ion, and a second slug of polymer. Some of the polymer in the first slug adsorbs or is retained on the surfaces of the reservoir. The aluminum ion attaches to the adsorbed polymer and acts as a bridge to the second polymer layer. This sequence is repeated until the desired layering is achieved. The transport of aluminum ions through the reservoir may be a problem in certain cases, so the effects of the treatment may be limited to near the wellbore.

Another method is based on the reduction of chromium ions to permit the crosslinking of HPAM or XG polymer molecules. A polymer slug containing Cr^{+6} is injected followed by a slug of polymer containing a reducing agent. When the Cr^{+6} is reduced to Cr^{+3} , a gel is formed with the polymer. The amount of permeability reduction is controlled by the number of times each slug is injected, the size of each slug, or the concentrations used. An alternate treatment involves placing a plain water pad between the first and second polymer slugs.

In another variation of the above two methods for HPAM, a cationic polymer is injected first. Since reservoir surfaces are often negatively charged, the cationic polymer is highly adsorbed. When the foregoing sequential treatments are injected, there is a strong attraction between the adsorbed cationic polymer and the anionic polymers that follow.

Polymer concentrations used in these variations are normally low, on the order of 250 mg/L. With low molecular weight polymers or if a very stiff gel is desired, polymer concentrations of 1–1.5% are common. The type of polymers are similar to those used in conventional polymer flooding, but the products used for gelation command a higher price.

Methods developed recently, especially for fracture treatments, include Cr^{3+} (acetate)-polyacrylamide, colloidal silica, and resorcinol-formaldehyde.

Surfactant and Alkaline Flooding

Both alkaline flooding and surfactant flooding improve oil recovery by lowering the interfacial tension between crude oil and the displacing water. With alkaline flooding, the surfactants are generated in situ when the alkaline materials react with crude oil—this technique is normally only viable when the crude oil contains sufficient amount of organic acids to produce natural surfactants. Other possible mechanisms with the caustic materials include emulsification of the oil and alteration in the preferential wettability of the reservoir rock.

With surfactant flooding, surface-active agents are mixed with other compounds (such as alcohol and salt) in water and injected to mobilize the crude oil.

Polymer-thickened water is then injected to push the mobilized oil-water bank to the producing wells. Water-soluble polymers can be used in a similar fashion with alkaline flooding. For micellar/polymer flooding, the concentration of polymer used may be similar to the value given for polymer flooding, but the volume of polymer solution may be increased to 50% or more of a reservoir pore volume.

Alkaline Flooding. Alkaline or caustic flooding consists of injecting aqueous solutions of sodium hydroxide, sodium carbonate, sodium silicate or potassium hydroxide. The alkaline chemicals react with organic acids in certain crude oils to produce surfactants in situ that dramatically lower the interfacial tension between water and oil. The alkaline agents also react with the reservoir rock surfaces to alter wettability-either from oil-wet to water-wet, or vice versa. Other mechanisms include emulsification and entrainment of oil or emulsification and entrapment of oil to aid in mobility control. Since an early patent in the 1920s described the use of caustic for improved recovery of oil, much research and some field tests have been conducted. Slug size of the alkaline solution is often 10%–15% PV, concentrations of the alkaline chemical are normally 0.2% to 5%. Recent tests are using large amounts of relatively high concentrations. A preflush of fresh or softened water often precedes the alkaline slug, and a drive fluid (either water or polymer-thickened water) follows the alkaline slug.

Surfactant/Polymer Flooding. Surfactant use for oil recovery is not a recent development. Patents in the late 1920s and early 1930s proposed the use of low concentrations of detergents to reduce the interfacial tension between water and oil. To overcome the slow rate of advance of the detergent, Taber [389] proposed very high concentrations (~10%) of detergent in aqueous solution.

During the late 1950s and early 1960s, several different present-day methods of using surfactants for enhanced recovery were developed. A review of these methods is beyond the scope of this chapter and is available in the literature [390–393]. In some systems, a small slug (> about 5% PV) was proposed that included a high concentration of surfactant (normally 5%–10%). In many cases, the microemulsion includes surfactant, hydrocarbon, water, an electrolyte (salt), and a cosolvent (usually an alcohol). These methods ordinarily used a slug (30%–50% PV) of polymer-thickened water to provide mobility control in displacing the surfactant and oil-water bank to the producing wells. The polymers used are the same as those discussed in the previous section. In most cases, low-cost petroleum sulfonates or blends with other surfactants have been used. Intermediate surfactant concentrations and low concentration systems (low tension waterflooding) have also been proposed. The lower surfactant concentration systems may or may not contain polymer in the surfactant slug, but will utilize a larger slug (30%–100% PV) of polymer solution.

Alkaline/Surfactant/Polymer Flooding. A recent development uses a combination of chemicals to lower process costs by lowering injection cost and reducing surfactant adsorption. These mixtures, termed alkaline/surfactant/polymer (ASP), permit the injection of larger slugs of injectant because of the lower cost.

Gas Injection Methods

Hydrocarbon Miscible Flooding

Gas injection is certainly one of the oldest methods utilized by engineers to improve recovery, and its use has increased recently, although most of the new expansion has been coming from the nonhydrocarbon gases [394]. Because of

the increasing interest in CO₂ and nitrogen or flue gas methods, they are separated from the hydrocarbon miscible techniques.

Hydrocarbon miscible flooding can be subdivided further into three distinct methods, and field trials or extensive operations have been conducted in all of them. For LPG slug or solvent flooding, enriched (condensing) gas drive and high pressure (vaporizing) gas drive, a range of pressures (and therefore, depths) are needed to achieve miscibility in the systems.

Unless the reservoir characteristics were favorable, early breakthrough and bypassing of large quantities of oil have plagued many of the field projects. In addition, the hydrocarbons needed for the processes are valuable, and there is increasing reluctance to inject them back into the ground when there is some question about the percentage that will be recovered the second time around. Therefore, in the U.S. in recent years the emphasis has been shifting to less valuable nonhydrocarbon gases such as CO₂, nitrogen, and flue gases. Although nitrogen and flue gases do not recover oil as well as the hydrocarbon gases (or liquids), the overall economics may be somewhat more favorable.

Nitrogen and Flue Gas Flooding

As previously mentioned, nitrogen and flue gas (about 87% N₂ and 12% CO₂) are sometimes used in place of hydrocarbon gases because of economics. Nitrogen also competes with CO₂ in some situations for the same reason. The economic appeal of nitrogen stems not only from its lower cost on a standard Mcf basis, but also because its compressibility is much lower. Thus, for a given quantity at standard conditions, nitrogen will occupy much more space at reservoir pressures than CO₂ or even methane at the same conditions. However, both nitrogen or flue gas are inferior to hydrocarbon gases (and much inferior to CO₂) from an oil recovery point of view. Nitrogen has a lower viscosity and poor solubility in oil and requires a much higher pressure to generate or develop miscibility. The increase in the required pressure is significant compared to methane and very large (4–5 times) when compared to CO₂. Therefore, nitrogen will not reduce the displacement efficiency too much when used as a chase gas for methane, but it can cause a significant drop in the effectiveness of a CO₂ flood if the reservoir pressures are geared to the miscibility requirements for CO₂ displacements. Indeed, even methane counts as a desirable “light end” or “intermediate” in nitrogen flooding, but methane is quite deleterious to the achievement of miscibility in CO₂ flooding at modest pressures.

Carbon Dioxide Flooding

CO₂ is effective for recovery of oil for a number of reasons. In general, carbon dioxide is very soluble in crude oils at reservoir pressures; therefore, it swells the net volume of oil and reduces its viscosity even before miscibility is achieved by the vaporizing gas drive mechanism. As miscibility is approached, both the oil phase and the CO₂ phase (which contains many of the oil's intermediate components) can flow together because of the low interfacial tension and the relative increase in the total volumes of the combined CO₂ and oil phases compared to the water phase. However, the generation of miscibility between the oil and CO₂ is still the most important mechanism, and it will occur in CO₂-crude oil systems as long as the pressure is high enough. This so-called “minimum miscibility pressure” or MMP has been the target of several laboratory investigations and is no longer a mystery. The 1976 NPC report [380] showed that there is a rough correlation between the API gravity and the required MMP,

and that the MMP increased with temperature. Some workers have shown that a better correlation is obtained with the molecular weight of the C_6+ fraction of the oil than with the API gravity. In general the recent work shows that the required pressure must be high enough to achieve a minimum density in the CO_2 phase [395,396]. At this minimum density, which varies with the oil composition, the CO_2 becomes a good solvent for the oil, especially the intermediate hydrocarbons, and the required miscibility can be generated or developed to provide the efficient displacement normally observed with CO_2 . Therefore, at higher temperatures, the higher pressures are needed only to increase the CO_2 density to the same value as observed for the MMP at the lower temperature. Figure 5-175 shows the variation of minimum miscibility pressure with temperature and oil composition [397].

Although the mechanism for CO_2 flooding appears to be the same as that for hydrocarbon miscible floods, CO_2 floods may give better recoveries even if both systems are above their required miscibility pressures, especially in tertiary floods. Compared to hydrocarbons, CO_2 has a much higher solubility in water, and it has been observed in laboratory experiments to diffuse through the water phase to swell bypassed oil until the oil is mobile. Thus, not only are the oil and depth screening criteria easier to meet in CO_2 flooding, but the ultimate recovery may be better than with hydrocarbons when above the MMP. It must be noted, however that this conjecture has not been proved by rigorous and directly comparable experiments.

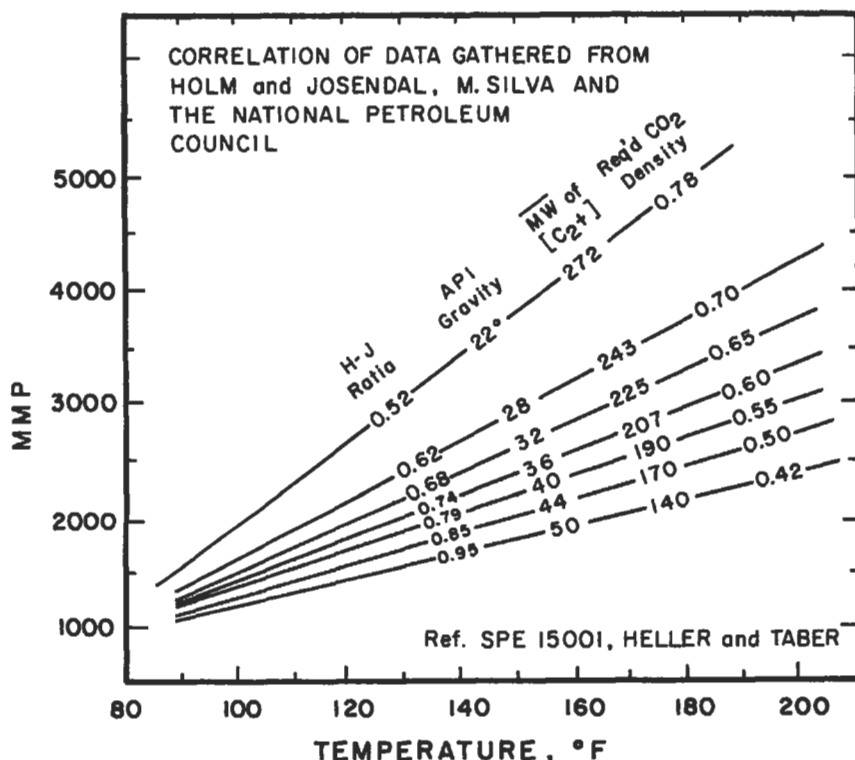


Figure 5-175. Correlations for CO_2 minimum miscibility pressure [397].

Thermal Recovery

In-Situ Combustion

The theory and practice of in-situ combustion or fireflooding is covered comprehensively in the recent SPE monograph on thermal recovery by Prats [378]. In addition, the continuing evolution of screening criteria for fireflooding [398,399] and steamflooding [400] have been reviewed and evaluated by Chu. A recent appraisal of in-situ combustion was provided by White [401] and the status of oxygen fireflooding was provided by Garon [402].

Part of the appeal of fireflooding comes from the fact that it uses the world's cheapest and most plentiful fluids for injection: air and water. However, significant amounts of fuel must be burned, both above the ground to compress the air, and below ground in the combustion process. Fortunately, the worst part of the crude oil is burned; the lighter ends are carried forward in advance of the burning zone to upgrade the crude oil.

Steam Flooding

Of all of the enhanced oil recovery processes currently available, only the steam drive (steamflooding) process is routinely used on a commercial basis. In the United States, a majority of the field testing with this process has occurred in California, where many of the shallow, high-oil-saturation reservoirs are good candidates for thermal recovery. These reservoirs contain high-viscosity crude oils that are difficult to mobilize by methods other than thermal recovery.

In the steam drive process, steam is continuously introduced into injection wells to reduce the viscosity of heavy oil and provide a driving force to move the more mobile oil towards the producing wells. In typical steam drive projects, the injected fluid at the surface may contain about 80% steam and 20% water (80% quality) [380]. When steam is injected into the reservoir, heat is transferred to the oil-bearing formation, the reservoir fluids, and some of the adjacent cap and base rock. As a result, some of the steam condenses to yield a mixture of steam and hot water flowing through the reservoir.

The steam drive may work by driving the water and oil to form an oil bank ahead of the steamed zone. Ideally this oil bank remains in front, increasing in size until it is produced by the wells offsetting the injector. However, in many cases, the steam flows over the oil and transfers heat to the oil by conduction. Oil at the interface is lowered in viscosity and dragged along with the steam to the producing wells. Recoverability is increased because the steam (heat) lowers the oil viscosity and improves oil mobility. As the more mobile oil is displaced the steam zone expands vertically, and the steam-oil interface is maintained. This process is energy-intensive since it requires the use of a significant fraction (25%–40%) of the energy in the produced petroleum for the generation of steam.

In steamflooding, the rate of steam injection is initially high to minimize heat losses to the cap and base rock. Because of reservoir heterogeneities and gravity segregation of the condensed water from the steam vapor, a highly permeable and relatively oil-free channel often develops between injector and producer. Many times this channel occurs near the top of the oil-bearing rock, and much of the injected heat is conducted to the caprock as heat loss rather than being conducted to oil-bearing sand where the heat is needed. In addition, the steam cannot displace oil efficiently since little oil is left in the channel. Consequently, neither the gas drive from the steam vapor nor the convective heat transfer

mechanisms work as efficiently as desired. As a result, injected steam will tend to break through prematurely into the offset producing wells without sweeping the entire heated interval.

Technical Screening Guides

In some instances, only one type of enhanced recovery technique is applicable for a specific field condition but, in many instances, more than one technique is possible. The selection of the most appropriate process is facilitated by matching reservoir and fluid properties to the requirements necessary for the individual EOR techniques. A summary of the technical screening guides for the more common EOR processes is given in Table 5-46. A distinction is made between the oil properties and reservoir characteristics that are required for each process. Generally, steamflooding is applicable for very viscous oils in relatively shallow formations. On the other extreme, CO₂ and hydrocarbon miscible flooding work best with very light oils at depths that are great enough for miscibility to be achieved. Both steamflooding and in-situ combustion require fairly high permeability reservoirs. Chemical flooding processes (polymer, alkaline, or surfactant) are applicable in low to medium viscosity oils; depth is not a major consideration except, at great depths, the higher temperature may present problems in the degradation or consumption of some of the chemicals.

Screening guides or criteria are among the first items considered when a petroleum engineer evaluates a candidate reservoir for enhanced oil recovery. A source often quoted for screening criteria is the 1976 National Petroleum Council (NPC) report on Enhanced Recovery [380], which was revised by the NPC in 1984 [381]. Both reports list criteria for six enhanced recovery methods.

Some reservoir considerations apply to all enhanced recovery methods. Because drilling costs increase markedly with depth, shallow reservoirs are preferred, as long as all necessary criteria are met. For the most part, reservoirs that have extensive fractures, gross heterogeneities, thief zones, or are highly faulted should be avoided. Ideally, relatively uniform reservoirs with reasonable oil saturations, minimum shale stringers, and good areal extent are desired.

Implementation of enhanced recovery projects is expensive, time-consuming, and people-intensive. Substantial costs are often involved in the assessment of reservoir quality, the amount of oil that is potentially recoverable, laboratory work associated with the EOR process, computer simulations to predict recovery, and the performance of the project. One of the first steps in deciding to consider EOR is, of course, to select reservoirs with sufficient recoverable oil and areal extent to make the venture profitable.

With any of the processes, the nature of the reservoir will play a dominant role in the success or failure of the process. Many of the failures with EOR have resulted because of unknown or unexpected reservoir problems. Thus, a thorough geological study is usually warranted.

The technique of using cursory screening guides is convenient for gaining a quick overview of all possible methods before selecting the best one for an economic analysis. Common sense and caution must be exercised since the technical guides are based on laboratory data and results of enhanced recovery field trials, and are not rigid guides for applying certain processes to specific reservoirs. Additionally, the technical merits of recent field projects are clouded by various incentive programs that make it difficult to discern true technical applications. Some projects may have been technical misapplications or failures, but economic successes. Certainly, there have been enough technical successes, but economic failures.

**Table 5-46
Summary of Screening Criteria for Enhanced Recovery Methods**

	Oil properties			Reservoir characteristics					
	Gravity °API	Viscosity cp	Composition	Oil Saturation	Formation Type	Net thickness ft	Average permeability md	Depth ft	Temperature °F
<i>Gas Injection methods</i>									
Hydrocarbon	> 35	< 10	High % of C2 – C7	> 30% PV	Sandstone or carbonate	Thin unless dipping	N.C.	> 2,000 (LPG) to > 5,000 (H.P. Gas)	N.C.
Nitrogen & flue gas	> 24	< 10	High % of C1 – C7	> 30% PV	Sandstone or carbonate	Thin unless dipping	N.C.	> 4,500	N.C.
Carbon dioxide	> 35 for N ₂	< 10	High % of C2 – C12	> 30% PV	Sandstone or carbonate	Thin unless dipping	N.C.	> 2,000	N.C.
<i>Chemical Flooding</i>									
Surfactant/polymer	> 25	< 30	Light intermediates desired	> 30% PV	Sandstone preferred	> 10	> 20	< 8,000	< 175
Polymer	> 25	< 150	N.C.	> 10% PV Mobile oil Above	Sandstone preferred; carbonate possible	N.C.	> 10 (normally)	< 9,000	< 200
Alkaline	13-35	< 200	Some organic acids	waterflood residual	Sandstone preferred	N.C.	> 20	< 9,000	< 200
<i>Thermal</i>									
Combustion	< 40 (10-25 normally)	< 1,000	Some asphaltic components	> 40-50% PV	Sand or sandstone with high porosity	> 10	> 100*	> 500	> 150 preferred
Steamflooding	< 25	> 20	N.C.	> 40-50% PV	Sand or sandstone with high porosity	> 20	> 200**	300-5,000	N.C.

From Reference 386.
N.C. = Not Critical

* Transmissibility > 20 md ft/cp
** Transmissibility > 100 md ft/cp

Nevertheless, some EOR processes can be rejected quickly because of unfavorable reservoir or oil properties, so the use of preferred criteria can be helpful in selecting methods that may be commercially attractive. If the criteria are too restrictive, some feasible method may be rejected from consideration. Therefore, the guidelines that are adopted should be sufficiently broad to encompass essentially all of the potential methods for a candidate reservoir.

For convenience, brief descriptions of the eight most common enhanced recovery methods are provided in the following sections. These descriptions list the salient features of each method along with the important screening guides. A few general comments are offered here on the relative importance of some individual screening guides to the overall success of the various methods. In addition, we will make some observations on the method itself and its relationship to other enhanced recovery choices that may be available.

Hydrocarbon Miscible Flooding [386]

Description. Hydrocarbon miscible flooding consists of injecting light hydrocarbons through the reservoir to form a miscible flood. Three different methods are used. One method uses about 5% PV slug of liquidified petroleum gas (LPG) such as propane, followed by natural gas or gas and water. A second method, called enriched (condensing) gas drive, consists of injecting a 10%–20% PV slug of natural gas that is enriched with ethane through hexane (C_2 to C_6), followed by lean gas (dry, mostly methane) and possibly water. The enriching components are transferred from the gas to the oil. The third method, called high pressure (vaporizing) gas drive, consists of injecting lean gas at high pressure to vaporize C_2 – C_6 components from the crude oil being displaced.

Mechanisms. Hydrocarbon miscible flooding recovers crude oil by:

- Generating miscibility (in the condensing and vaporizing gas drive)
- Increasing the oil volume (swelling)
- Decreasing the viscosity of the oil

Technical Screening Guides

Crude oil

Gravity	>35° API
Viscosity	<10 cp
Composition	High percentage of light hydrocarbons (C_2 – C_7)

Reservoir

Oil saturation	>30% PV
Type of formation	Sandstone or carbonate with a minimum of fractures and high permeability streaks
Net thickness	Relatively thin unless formation is steeply dipping
Average permeability	Not critical if uniform
Depth	>2,000 ft (LPG) to >5000 ft (high pressure gas)
Temperature	Not critical

Limitations.

- The minimum depth is set by the pressure needed to maintain the generated miscibility. The required pressure ranges from about 1,200 psi for the LPG process to 3,000–5,000 psi for the high pressure gas drive, depending on the oil.

- A steeply dipping formation is very desirable to permit some gravity stabilization of the displacement which normally has an unfavorable mobility ratio.

Problems.

- Viscous fingering results in poor vertical and horizontal sweep efficiency.
- Large quantities of expensive products are required.
- Solvent may be trapped and not recovered.

Nitrogen and Flue Gas Flooding [386]

Description. Nitrogen and flue gas flooding are oil recovery methods which use these inexpensive nonhydrocarbon gases to displace oil in systems which may be either miscible or immiscible depending on the pressure and oil composition. Because of their low cost, large volumes of these gases may be injected. Nitrogen or flue gas are also considered for use as chase gases in hydrocarbon-miscible and CO₂ floods.

Mechanisms. Nitrogen and flue gas flooding recover oil by:

- Vaporizing the lighter components of the crude oil and generating miscibility if the pressure is high enough.
- Providing a gas drive where a significant portion of the reservoir volume is filled with low-cost gases.

Technical Screening Guides

Crude oil

Gravity	>24° API (>35° for nitrogen)
Viscosity	<10 cp
Composition	High percentage of light hydrocarbons (C ₁ -C ₇)

Reservoir

Oil saturation	>30% PV
Type of formation	Sandstone or carbonate with few fractures and high permeability streaks
Net thickness	Relatively thin unless formation is dipping
Average permeability	Not critical
Depth	>4,500 ft
Temperature	Not critical

Limitations.

- Developed miscibility can only be achieved with light oils and at high pressures; therefore, deep reservoirs are needed.
- A steeply dipping formation is desired to permit gravity stabilization of the displacement which has a very unfavorable mobility ratio.

Problems.

- Viscous fingering results in poor vertical and horizontal sweep efficiency.
- Corrosion can cause problems in the flue gas method.
- The nonhydrocarbon gases must be separated from the saleable produced gas.

Carbon Dioxide Flooding [386]

Description. Carbon dioxide flooding is carried out by injecting large quantities of CO₂ (15% or more of the hydrocarbon PV) into the reservoir. Although CO₂ is not truly miscible with the crude oil, the CO₂ extracts the light-to-intermediate components from the oil, and, if the pressure is high enough, develops miscibility to displace the crude oil from the reservoir.

Mechanisms. CO₂ recovers crude oil by:

- Generation of miscibility
- Swelling the crude oil
- Lowering the viscosity of the oil
- Lowering the interfacial tension between the oil and the CO₂-oil phase in the near-miscible regions.

Technical Screening Guides

Crude oil

Gravity	>26° API (preferably >30°)
Viscosity	<15 cp (preferably <10 cp)
Composition	High percentage of intermediate hydrocarbons (C ₅ -C ₂₀), especially C ₅ -C ₁₂

Reservoir

Oil saturation	>30% PV
Type of formation	Sandstone or carbonate with a minimum of fractures and high permeability streaks
Net thickness	Relatively thin unless formation is steeply dipping.
Average permeability	Not critical if sufficient injection rates can be maintained.
Depth	Deep enough to allow high enough pressure (> about 2,000 ft), pressure required for optimum production (sometimes called minimum miscibility pressure) ranges from about 1,200 psi for a high gravity (>30° API) crude at low temperatures to over 4,500 psi for heavy crudes at higher temperatures.
Temperature	Not critical but pressure required increases with temperature.

Limitations.

- Very low viscosity of CO₂ results in poor mobility control.
- Availability of CO₂.

Problems.

- Early breakthrough of CO₂ causes several problems: corrosion in the producing wells; the necessity of separating CO₂ from saleable hydrocarbons; repressuring of CO₂ for recycling; and a high requirement of CO₂ per incremental barrel produced.

Surfactant/Polymer Flooding

Description. Surfactant/polymer flooding, also called micellar/polymer or microemulsion flooding, consists of injecting a slug that contains water, surfactant, electrolyte (salt), usually a cosolvent (alcohol), and possibly a hydrocarbon (oil). The size of the slug is often 5%–15% PV for a high surfactant concentration system and 15%–50% PV for low concentrations. The surfactant slug is followed by polymer-thickened water. Concentrations of the polymer often range from 500–2,000 mg/L; the volume of polymer solution injected may be 50% PV, more or less, depending on the process design.

Mechanisms. Surfactant/polymer flooding recovers crude oil by:

- Lowering the interfacial tension between oil and water
- Solubilization of oil
- Emulsification of oil and water
- Mobility enhancement

Technical Screening Guides

Crude oil

Gravity	>25° API
Viscosity	<30 cp
Composition	Light intermediates are desirable

Reservoir

Oil saturation	>30% PV
Type of formation	Sandstones preferred
Net thickness	>10 ft
Average permeability	>20 md
Depth	< about 8,000 ft (see temperature)
Temperature	<175°F

Limitations.

- An areal sweep of more than 50% on waterflood is desired.
- Relatively homogeneous formation is preferred.
- High amounts of anhydrite, gypsum, or clays are undesirable.
- Available systems provide optimum behavior over a very narrow set of conditions.
- With commercially available surfactants, formation water chlorides should be <20,000 ppm and divalent ions (Ca^{++} and Mg^{++}) <500 ppm.

Problems.

- Complex and expensive system.
- Possibility of chromatographic separation of chemicals.
- High adsorption of surfactant.
- Interactions between surfactant and polymer.
- Degradation of chemicals at high temperature.

Polymer Flooding [386]

Description. The objective of polymer flooding is to provide better displacement and volumetric sweep efficiencies during a waterflood. Polymer augmented

waterflooding consists of adding water soluble polymers to the water before it is injected into the reservoir. Low concentrations (often 250–2,000 mg/L) of certain synthetic or biopolymers are used; properly sized treatments may require 15%–25% reservoir PV.

Mechanisms. Polymers improve recovery by:

- Increasing the viscosity of water
- Decreasing the mobility of water
- Contacting a larger volume of the reservoir

Technical Screening Guides

Crude oil

Gravity	>25° API
Viscosity	<150 cp (preferably < 100)
Composition	Not critical

Reservoir

Oil saturation	>10% PV mobile oil
Type of formation	Sandstones preferred but can be used in carbonates
Net thickness	Not critical
Average permeability	>10 md (as low as 3 md in some cases)
Depth	< about 9,000 ft (see temperature)
Temperature	<200°F to minimize degradation

Limitations.

- If oil viscosities are high, a higher polymer concentration is needed to achieve the desired mobility control.
- Results are normally better if the polymer flood is started before the water-oil ratio becomes excessively high.
- Clays increase polymer adsorption.
- Some heterogeneities are acceptable, but for conventional polymer flooding, reservoirs with extensive fractures should be avoided. If fractures are present, the crosslinked or gelled polymer techniques may be applicable.

Problems.

- Lower injectivity than with water can adversely affect oil production rate in the early stages of the polymer flood.
- Acrylamide-type polymers lose viscosity due to shear degradation or increases in salinity and divalent ions.
- Xanthan gum polymers cost more, are subject to microbial degradation, and have a greater potential for wellbore plugging.

Alkaline Flooding [386]

Description. Alkaline or caustic flooding involves the injection of chemicals such as sodium hydroxide, sodium silicate or sodium carbonate. These chemicals react with organic petroleum acids in certain crudes to create surfactants in situ. They also react with reservoir rocks to change wettability. The concentration of the alkaline agent is normally 0.2 to 5%; slug size is often 10% to 50% PV, although one successful flood only used 2% PV, (but this project also included polymers

for mobility control). Polymers may be added to the alkaline mixture, and polymer-thickened water can be used following the caustic slug.

Mechanisms. Alkaline flooding recovers crude oil by:

- A reduction of interfacial tension resulting from the produced surfactants
- Changing wettability from oil-wet to water-wet
- Changing wettability from water-wet to oil-wet
- Emulsification and entrainment of oil
- Emulsification and entrapment of oil to aid in mobility control
- Solubilization of rigid oil films at oil-water interfaces (Not all mechanisms are operative in each reservoir.)

Technical Screening Guides

Crude oil

Gravity	13° to 35° API
Viscosity	<200 cp
Composition	Some organic acids required

Reservoir

Oil saturation	Above waterflood residual
Type of formation	Sandstones preferred
Net thickness	Not critical
Average permeability	>20 md
Depth	< about 9,000 ft (see temperature)
Temperature	<200°F preferred

Limitations.

- Best results are obtained if the alkaline material reacts with the crude oil; the oil should have an acid number of more than 0.2 mg KOH/g of oil.
- The interfacial tension between the alkaline solution and the crude oil should be less than 0.01 dyne/cm.
- At high temperatures and in some chemical environments, excessive amounts of alkaline chemicals may be consumed by reaction with clays, minerals, or silica in the sandstone reservoir.
- Carbonates are usually avoided because they often contain anhydrite or gypsum, which interact adversely with the caustic chemical.

Problems.

- Scaling and plugging in the producing wells.
- High caustic consumption.

In-Situ Combustion [386]

Description. In-situ combustion or fireflooding involves starting a fire in the reservoir and injecting air to sustain the burning of some of the crude oil. The most common technique is forward combustion in which the reservoir is ignited in an injection well, and air is injected to propagate the combustion front away from the well. One of the variations of this technique is a combination of forward combustion and waterflooding (COFCAW). A second technique is reverse combustion in which a fire is started in a well that will eventually become

a producing well, and air injection is then switched to adjacent wells; however, no successful field trials have been completed for reverse combustion.

Mechanisms. In-situ combustion recovers crude oil by:

- The application of heat which is transferred downstream by conduction and convection, thus lowering the viscosity of the crude.
- The products of steam distillation and thermal cracking which are carried forward to mix with and upgrade the crude.
- Burning coke that is produced from the heavy ends of the crude oil.
- The pressure supplied to the reservoir by the injected air.

Technical Screening Guides

Crude oil

Gravity	<40° API (normally 10–25°)
Viscosity	<1,000 cp
Composition	Some asphaltic components to aid coke deposition

Reservoir

Oil saturation	> 500 bbl/acre-ft (or >40–50% PV)
Type of formation	Sand or sandstone with high porosity
Net thickness	>10 ft
Average permeability	>100 md
Transmissibility	>20 md ft/cp
Depth	>500 ft
Temperature	>150°F preferred

Limitations.

- If sufficient coke is not deposited from the oil being burned, the combustion process will not be sustained.
- If excessive coke is deposited, the rate of advance of the combustion zone will be slow, and the quantity of air required to sustain combustion will be high.
- Oil saturation and porosity must be high to minimize heat loss to rock.
- Process tends to sweep through upper part of reservoir so that sweep efficiency is poor in thick formations.

Problems.

- Adverse mobility ratio.
- Complex process, requiring large capital investment, is difficult to control.
- Produced flue gases can present environmental problems.
- Operational problems such as severe corrosion caused by low pH hot water, serious oil-water emulsions, increased sand production, deposition of carbon or wax, and pipe failures in the producing wells as a result of the very high temperatures.

Steamflooding [386]

Description. The steam drive process or steamflooding involves the continuous injection of about 80% quality steam to displace crude oil towards producing wells. Normal practice is to precede and accompany the steam drive by a cyclic steam stimulation of the producing wells (called huff and puff).

Mechanisms. Steam recovers crude oil by:

- Heating the crude oil and reducing its viscosity
- Supplying pressure to drive oil to the producing well

Technical Screening Guides

Crude oil

Gravity	<25° API (normal range is 10°-25° API)
Viscosity	>20 cp (normal range is 100-5,000 cp)
Composition	Not critical but some light ends for steam distillation will help

Reservoir

Oil saturation	>500 bbl/acre-ft (or >40%-50% PV)
Type of formation	Sand or sandstone with high porosity and permeability preferred
Net thickness	>20 feet
Average permeability	>200 md (see transmissibility)
Transmissibility	>100 md ft/cp
Depth	300-5,000 ft
Temperature	Not critical

Limitations.

- Oil saturations must be quite high and the pay zone should be more than 20 feet thick to minimize heat losses to adjacent formations.
- Lighter, less viscous crude oils can be steamflooded but normally will not be if the reservoir will respond to an ordinary waterflood.
- Steamflooding is primarily applicable to viscous oils in massive, high permeability sandstones or unconsolidated sands.
- Because of excessive heat losses in the wellbore, steamflooded reservoirs should be as shallow as possible as long as pressure for sufficient injection rates can be maintained.
- Steamflooding is not normally used in carbonate reservoirs.
- Since about one-third of the additional oil recovered is consumed to generate the required steam, the cost per incremental barrel of oil is high.
- A low percentage of water-sensitive clays is desired for good injectivity.

Problems.

- Adverse mobility ratio and channeling of steam.

Criteria for Gas Injection

For LPG slug or solvent flooding, enriched (condensing) gas drive, and high pressure (vaporizing) gas drive, a range of pressures (and therefore, depths) are needed to achieve miscibility in the systems. Thus, there is a minimum depth requirement for each of the processes as shown earlier (see section on "Hydrocarbon Miscible Flooding"). The permeability is not critical if the structure is relatively uniform; permeabilities of the reservoirs for the current field projects range from less than 1 md to several darcies [403]. On the other hand, the crude oil characteristics are very important. A high-gravity, low-viscosity oil with a high percentage of the C₂-C₇ intermediates is essential if miscibility is to be achieved in the vaporizing gas drives.

As shown earlier under "Nitrogen and Flue Gas Flooding," the screening criteria for flooding with nitrogen or flue gas are similar to those for the high pressure gas drive. Pressure and depth requirements, as well as the need for a very light oil, are even greater if full miscibility is to be realized in the reservoir. The nitrogen and flue gas method is placed between hydrocarbon miscible and CO₂ flooding because the process can also recover oil in the immiscible mode. It can be economic because much of the reservoir space is filled with low cost gas.

Because of the minimum pressure requirement, depth is an important screening criteria, and CO₂ floods are normally carried out in reservoirs that are more than 2,000 ft deep. The oil composition is also important (see section on "Carbon Dioxide Flooding"), and the API gravity exceeds 30° for most of the active CO₂ floods [403]. A notable exception is the Lick Creek, Arkansas, CO₂/waterflood project which was conducted successfully, not as a miscible project, but as an immiscible displacement [404].

Criteria for Chemical Methods

For surfactant/polymer methods, oil viscosities of less than 30 cp are desired so that adequate mobility control can be achieved. Good mobility control is essential for this method to make maximum utilization of the expensive chemicals. Oil saturations remaining after a waterflood should be more than 30% PV to ensure that sufficient oil is available for recovery. Sandstones are preferred because carbonate reservoirs are heterogeneous, contain brines with high divalent ion contents, and cause high adsorption of commonly used surfactants. To ensure adequate injectivity, permeability should be greater than 20 md. Reservoir temperature should be less than 175°F to minimize degradation of the presently available surfactants. A number of other limitations and problems were mentioned earlier, including the general requirement for low salinity and hardness for most of the commercially available systems. Obviously, this method is very complex, expensive, and subject to a wide range of problems. Most importantly, the available systems provide optimum reduction in interfacial tension over a very narrow salinity range. Preflushes have been used to attempt to provide optimum conditions, but they have often been ineffective.

The screening guidelines and a description of polymer flooding are contained earlier in Section "Polymer Flooding." Since the objective of polymer flooding is to improve the mobility ratio without necessarily making the ratio favorable, the maximum oil viscosity for this method is 100 or possibly 150 cp. If oil viscosities are very high, higher polymer concentrations are needed to achieve the desired mobility control, and thermal methods may be more attractive. As discussed earlier, polymer flooding will not ordinarily mobilize oil that has been completely trapped by water; therefore, a mobile oil saturation of more than 10% is desired. In fact, a polymer flood is normally more effective when started at low producing water-oil ratios [405]. Although sandstone reservoirs are usually preferred, several large polymer floods have been conducted in carbonate reservoirs. Lower-molecular-weight polymers can be used in reservoirs with permeabilities as low as 10 md (and, in some carbonates, as low as 3 md). While it is possible to manufacture even lower-molecular-weight polymers to inject into lower permeability formations, the amount of viscosity generated per pound of polymer would not be enough to make such products of interest. With current polymers, reservoir temperature should be less than 200°F to minimize degradation; this requirement limits depths to about 9,000 ft. A potentially serious

problem with polymer flooding is the decrease in injectivity which must accompany any increase in injection fluid viscosity. If the decreased injectivity is prolonged, oil production rates and project costs can be adversely affected. Injection rates for polymer solutions may be only 40%–60% of those for water alone, and the reduced injectivity may add several million dollars to the total project costs. Other problems common to the commercial polymers are cited earlier.

Moderately low gravity oils (13°–35° API) are normally the target for alkaline flooding (see section on “Alkaline Flooding”). These oils are heavy enough to contain the organic acids, but light enough to permit some degree of mobility control. The upper viscosity limit (<200 cp) is slightly higher than for polymer flooding. Some mobile oil saturation is desired, the higher the better. The minimum average permeability is about the same as for surfactant/polymer (>20 md). Sandstone reservoirs are preferred since carbonate formations often contain anhydrite or gypsum which react and consume the alkaline chemicals. The alkaline materials also are consumed by clays, minerals, or silica; this consumption is high at elevated temperatures so the maximum desired temperature is 200°F. Caustic consumption in field projects has been higher than indicated by laboratory tests. Another potential problem in field applications is scale formation which can result in plugging in the producing wells.

Criteria for Thermal Methods

For screening purposes, steamflooding and fireflooding are often considered together. In general, combustion should be the choice when heat losses from steamflooding would be too great. In other words, combustion can be carried out in deeper reservoirs and thinner, tighter sand sections where heat losses for steamflooding are excessive. Screening guides for in-situ combustion are given earlier in Section “In-Situ Combustion.” The ability to inject at high pressures is usually important so 500 ft has been retained as the minimum depth, but a few projects have been done at depths of less than 500 ft. Since the fuel and air consumption decrease with higher gravity oils, there is a tendency to try combustion in lighter oils if the fire can be maintained, but no projects have been done in reservoirs with oil gravities greater than 32° API [403].

In summary, if all screening criteria are favorable, fireflooding appears to be an attractive method for reservoirs that cannot be produced by methods used for the lighter oils. However, the process is very complicated and beset with many practical problems such as corrosion, erosion and poorer mobility ratios than steamflooding. Therefore, when the economics are comparable, steam injection is preferred to a combustion drive [378].

Screening criteria for steamflooding are listed earlier in section “Steamflooding”. Although steamflooding is commonly used with oils ranging in gravity from 10°–25° API, some gravities have been lower, and there is recent interest in steamflooding light oil reservoirs. Oils with viscosities of less than 20 cp are usually not candidates for steamflooding because waterflooding is less expensive; the normal range is 100–5,000 cp. A high saturation of oil-in-place is required because of the intensive use of energy in the generation of steam. In order to minimize the amount of rock heated and maximize the amount of oil heated, formations with high porosity are desired; this means that sandstones or unconsolidated sands are the primary target, although a steam drive pilot has been conducted in a highly fractured carbonate reservoir in France. The product of oil saturation times porosity should be greater than about 0.08 [400]. The fraction of heat lost to the cap and base rocks varies inversely with reservoir thickness. Therefore, the greater the thickness of the reservoir, the greater

the thermal efficiency. Steamflooding is possible in thin formations if the permeability is high. High permeabilities (>200 md or preferably >500 md) are needed to permit adequate steam injectivity; transmissibility should be greater than 100 md ft/cp at reservoir conditions. Depths shallower than about 300 ft may not permit good injectivity because the pressures required may exceed fracture gradients. Heat losses become important at depths greater than about 2,500 ft. and steamflooding is not often considered at depths greater than 5,000 ft. Downhole steam generators may have potential in deeper formations if operational problems can be overcome.

Graphical Representation of Screening Guides

From the summary of screening guides in Table 5-46, the viscosity, depth, and permeability criteria are presented graphically in Figures 5-176 to 5-178. The figures have some features which permit the quick application of screening criteria but they cannot replace the table for detailed evaluations. In a sense, the figures present a truer picture than the table because there are few absolutes among the numbers presented as screening guides in the tables. Different authors and organizations may use different parameters for the same process, and most of the guidelines are subject to change as new laboratory and field information evolves. In field applications, there are exceptions to some of the accepted criteria, and the graphs accommodate these nicely. The "greater than" and "less than" designations of the tables can also be displayed better graphically.

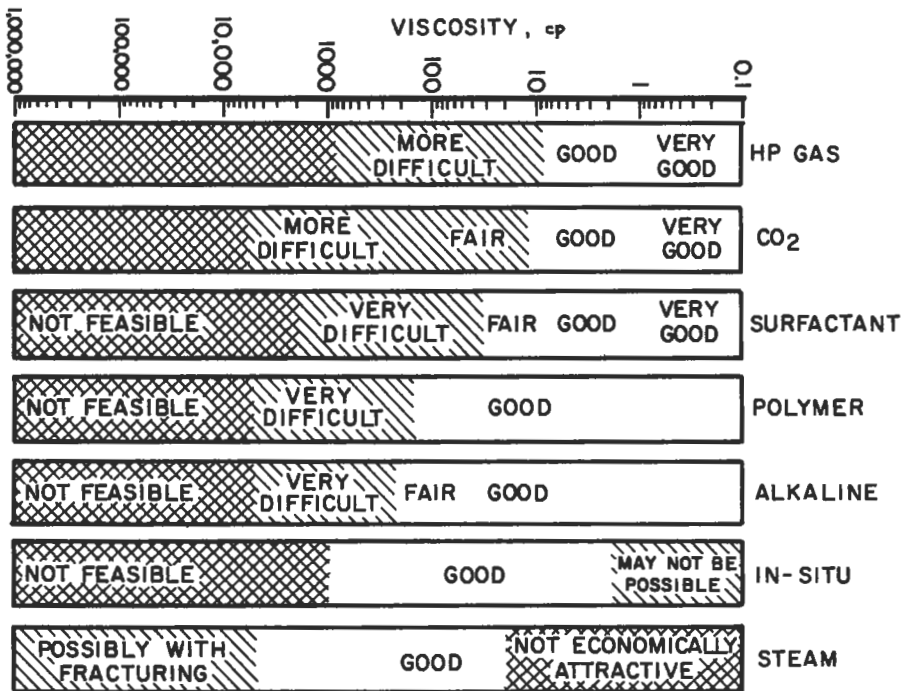


Figure 5-176. Viscosity ranges for EOR processes [386].

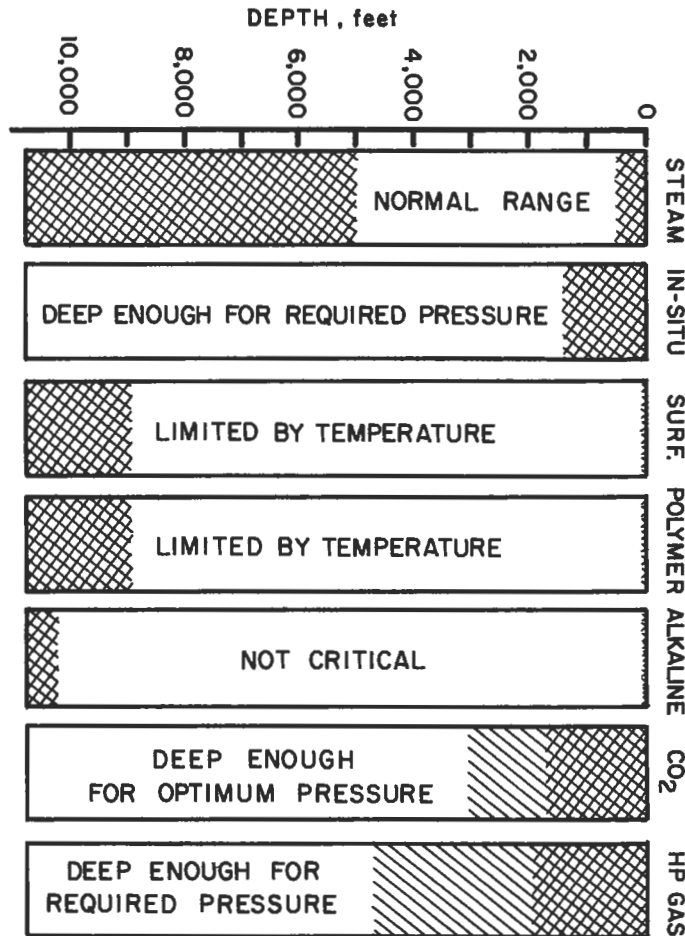


Figure 5-177. Depth requirements for EOR processes [386].

The range of values are indicated on the graphs by the open areas, and by cross-hatching along with general words such as "more difficult," "not feasible," etc. The "good" or "fair" ranges are those usually encompassed by the screening parameters in the table. However, the notation of "good" or "very good" does not mean that the indicated process is sure to work; it means simply that it is in the preferred range for that oil or reservoir characteristic.

The influence of viscosity on the technical feasibility of different enhanced recovery methods is illustrated in Figure 5-176. Note the steady progression, with increasing viscosity, from those processes that work well with very light oils (hydrocarbon miscible or nitrogen) to oils that are so viscous that no recovery is possible unless mining and extraction are employed.

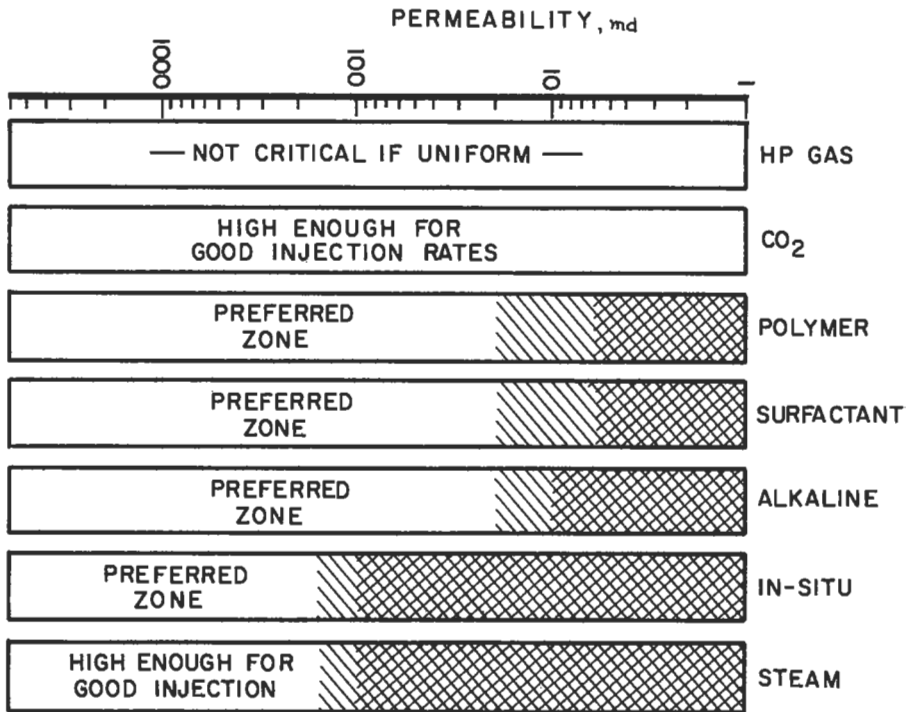


Figure 5-178. Permeability ranges for EOR methods [386].

For completeness, we have included the two “last resort” methods (special steamflooding techniques with shafts, fractures, drainholes, etc., and mining plus extraction) are listed in Figure 5-176. These methods are not included in Figures 5-177 and 5-178 because these unconventional techniques are not considered in most reservoir studies.

Figure 5-177 shows that those enhanced recovery processes that work well with light oils have rather specific depth requirements. As discussed, each gas injection method has a minimum miscibility pressure for any given oil, and the reservoir must be deep enough to accommodate the required pressure.

Figure 5-178 shows that the three methods that rely on gas injection are the only ones that are even technically feasible at extremely low permeabilities. The three methods that use backup waterflooding need a permeability of greater than 10 md in order to inject the chemicals or emulsions and to produce the released oil from the rock. Although most authors show a minimum permeability requirement of 20 md for polymers, we indicate a possible range down as low as 3 md for low molecular weight polymers, especially in some carbonate reservoirs.

The screening guides in the figures can perhaps be summarized by stating a fact well-known to petroleum engineers: oil recovery is easiest with light oil in very permeable reservoirs and at shallow or intermediate depths. Unfortunately, nature has not been kind in the distribution of hydrocarbons, and it is necessary to select the recovery method that best matches the oil and reservoir characteristics.

Laboratory Design for Enhanced Recovery

Preliminary Tests

Water Analysis. A complete water analysis is important to determine the effects of dissolved ions on the EOR processes (especially the chemical methods) or to ascertain any potential water problems such as scale or corrosion that may result when EOR processes are implemented. Water viscosity and density are also measured.

Oil Analysis. Oil viscosity and density are measured as well. A carbon number distribution of the crude may be obtained, especially if CO₂ flooding is being considered.

Core Testing. Routine core analyses, such as porosity, permeability, relative permeabilities, capillary pressure, and waterflood susceptibility tests are normally done by service companies that specialize in these types of tests. Specialized core tests, such as thin sections or scanning electron microscopy, are available to evaluate the relationship between pore structure and the process being considered. If required, stimulation or injectivity improvement measures can be recommended.

Polymer Testing

The desirability of adding polymers is determined by evaluating all available data to assess the performance of normal waterflooding. Any problems such as adverse viscosity ratios or large permeability variations should be identified. If the results of this study indicate that mobility control of the waterflood is warranted, the following laboratory tests are undertaken.

Viscosity Testing. Based on the permeability of the reservoir, relative permeability data, and the desired level of mobility control, polymers of certain molecular weights are selected for testing. Various concentrations of the polymers are dissolved in both the available injection water and in blends of the injection and formation waters. Polymer solutions may be non-Newtonian at certain shear rates, that is, the viscosity decreases at high shear rates (shear-thinning or pseudoplastic). This shear-thinning behavior is reversible and, if observed in the reservoir, is beneficial in that good injectivity can result from the lower viscosity observed at high shear rates near the injection well. At the lower shear rates encountered some distance from the injector, the polymer solution develops a higher viscosity. In this testing, it is important to consider not only the viscosity of the injected solution, but, more importantly, the in-situ viscosity that is achieved in the reservoir. Several things can happen that will reduce viscosity when the polymer solution is injected into the reservoir. Reduction in viscosity as a result of irreversible shear degradation is possible at the injection wellbore if the shear rates or shear stresses are large. Once in the reservoir, dilution with formation water or ion exchange with reservoir minerals can cause a reduction in viscosity, and the injected polymer concentration will need to be sufficiently high to compensate for all viscosity-reducing effects.

Polymer Retention. Retention of polymer in a reservoir can result from adsorption, entrapment, or, with improper application, physical plugging. Polymer retention tests are usually performed after a standard waterflood (at residual

oil saturation) or during a polymer flood oil recovery test. If polymer retention tests are conducted with only water initially present in the core, a higher level of retention will result from the increased surface area available to the polymer solution in the absence of oil. Effluent samples from the core are collected during both the polymer injection and a subsequent water flush. These samples are analyzed for polymer content. From a material balance, the amount of polymer retained in the core is calculated. Results are usually expressed in lbs per acre-ft. Excessive retention will increase the amount of polymer that must be added to achieve the desired mobility control. The level of polymer retained in a reservoir depends on a number of variables: permeability of the rock, surface area, nature of the reservoir rock (sandstone, carbonate, minerals, or clays), nature of the solvent for the polymer (salinity and hardness), molecular weight of the polymer, ionic charge on the polymer, and the volume of porosity that is not accessible to the flow of polymer solution. Polymer retention levels often range from less than 100 lb/acre-ft to several hundred lb/acre-ft.

Surfactant and Alkali Testing

Laboratory tests consist of measuring the interfacial tension (IFT) between the crude oil and the injected solution (alkaline or surfactant additive). This is usually done with a spinning drop interfacial tensiometer. With surfactants, the requirement for measuring tensions can be minimized by performing vial tests to determine solubilization parameters that can be correlated with IFT. Other tests include determining relative permeabilities, wettability, and total fluid mobilities. Once the optimum conditions are found, results of oil recovery tests with the chemical flood additives are conducted, usually at waterflood residual oil saturation.

CO₂ Flooding

For the gas injection projects, the trend in this country is toward the use of carbon dioxide although the full impact of CO₂ flooding will be felt in several years since construction of CO₂ pipelines into the west Texas area was completed in the 1980s. Carbon dioxide flooding is not a truly miscible process; that is, it does not dissolve in all proportions with crude oil. However, CO₂ can extract light to intermediate components out of the crude oil. This CO₂-rich mixture can develop miscibility and effectively displace additional crude oil. The main limitation involved is the very low viscosity of CO₂ that results in fingering of CO₂ through the more viscous crude oil. This causes premature breakthrough of the CO₂ and reduces the amount of oil recovered per unit volume of CO₂.

A prediction of the minimum pressure required to achieve miscibility can be made if the reservoir depth and basic properties of the crude oil are known. Laboratory tests often consist of some means of determining the minimum miscibility pressure, often by observing the oil displacement efficiency by CO₂ in a small-diameter tube (slim tube) packed with sand or glass beads. Carbon number distribution of the crude will be of value in determining if sufficient amounts of the C₅ to C₁₂ components are present.

Thermal Recovery

Viscosities of very viscous crude oils can be reduced by the use of thermal recovery methods. Fireflooding or in-situ combustion involves starting a fire in the reservoir and injecting air to sustain the burning of some of the crude oil.

Heat that is generated lowers the viscosity of the crude oil and results in improved recovery. With the steam drive or steamflooding process, steam is generated on the surface and injected into the injection wells. Some companies are now exploring the use of downhole steam generators in deeper wells where heat loss can be a serious problem. A primary problem with steam flooding is the channeling of steam through thin sections of the reservoir. To combat this problem, several organizations are studying the use of surfactants to create a foam in situ for improving sweep efficiency.

For steamflooding, the most important laboratory tests are, of course, viscosity of the crude oil and permeability of the reservoir core material. To be economically viable, steamfloods must be conducted in thick, very permeable, shallow reservoirs that contain very viscous crude.

REFERENCES

Basic Principles, Definitions, and Data

1. Standing, M. B., "A Pressure-Volume-Temperature Correlation for Mixtures of California Oils and Gases," *Drill. & Prod. Prac.*, API (1947), pp. 275-287.
2. Standing, M. B., *Volumetric and Phase Behavior of Oil Field Hydrocarbon Systems*, Reinhold Publishing Corp., New York (1952).
3. Katz, D. L., et al., *Handbook of Natural Gas Engineering*, McGraw-Hill Book Co., Inc., New York (1959).
4. Hocott, C. R., and Buckley, S. E., "Measurements of the Viscosities of Oils under Reservoir Conditions," *Trans.*, AIME, Vol. 142 (1941), pp. 131-136.
5. Beal, C., "The Viscosity of Air, Water, Natural Gas, Crude Oil and Its Associated Gases at Oil Field Temperature and Pressures," *Trans.*, AIME, Vol. 165 (1946), pp. 94-115.
6. Chew, J. N., and Connally, C. A., "A Viscosity Correlation for Gas-Saturated Crude Oils," *Trans.*, AIME, Vol. 216 (1959), pp. 23-25.
7. Beggs, H. D., and Robinson, J. R., "Estimating the Viscosity of Crude Oil Systems," *J. Pet. Tech.* (Sept. 1975), pp. 1140-1141.
8. Lohrenz, J., Bray, B. G., and Clark, C. R., "Calculating Viscosities of Reservoir Fluids from Their Compositions," *J. Pet. Tech.* (Oct. 1964), pp. 1171-1176; *Trans.*, AIME, Vol. 231.
9. Houpeurt, A. H., and Thelliez, M. B., "Predicting the Viscosity of Hydrocarbon Liquid Phases from Their Composition," paper SPE 5057 presented at the SPE 49th Annual Fall Meeting, Houston, Oct. 6-9, 1974.
10. Little, J. E., and Kennedy, H. T., "A Correlation of the Viscosity of Hydrocarbon Systems with Pressure, Temperature and Composition," *Soc. Pet. Eng. J.* (June 1968), pp. 157-162; *Trans.*, AIME, Vol. 243.
11. Swindells, J. F., Coe, J. R., and Godfrey, T. B., "Absolute Viscosity of Water at 20°C," Res. Paper 2279, *J. Res. Nat'l Bur. Stnds.*, Vol. 48 (1952), pp. 1-31.
12. *CRC Handbook of Chemistry and Physics*, 62nd edition, R. C. Weast (Ed.), CRC Press, Inc., Boca Raton, FL (1982).
13. Matthews, C. S., and Russell, D. G., *Pressure Buildup and Flow Tests in Wells*, Monograph Series, SPE, Dallas (1967), p. 1.
14. Pirson, S. J., *Oil Reservoir Engineering*, McGraw-Hill Book Co., Inc., New York (1958).
15. Kirkbride, C. G., *Chemical Engineering Fundamentals*, McGraw-Hill Book Co., Inc., New York (1947), p. 61.

16. Standing, M. B., and Katz, D. L., "Density of Natural Gases," *Trans.*, AIME, Vol. 146 (1942), pp. 140-149.
17. Craft, B. C., and Hawkins, M. F., *Applied Petroleum Reservoir Engineering*, Prentice-Hall, Inc., Englewood Cliffs (1959).
18. McCain, W. D., *The Properties of Petroleum Fluids*, Petroleum Publishing Co., Tulsa (1973).
19. Amyx, J. W., Bass, D. M., Jr., and Whiting, R. L., *Petroleum Reservoir Engineering*, McGraw-Hill Book Co., Inc., New York (1960).
20. Slider, H. C., *Practical Petroleum Engineering Methods*, Petroleum Publishing Co., Tulsa (1976).
21. Taylor, L. B., personal communication.
22. Dodson, C. R., and Standing, M. B., "Pressure-Volume-Temperature and Solubility Relations for Natural Gas-Water Mixtures," *Drill. & Prod. Prac.*, API (1944), pp. 173-179.
23. *Petroleum Production Handbook*, T. C. Frick (Ed.), Vol. II, Reservoir Engineering, SPE, Dallas (1962).
24. Burcik, E. J., *Properties of Petroleum Fluids*, Int'l. Human Resources Dev. Corp., Boston (1979).
25. Muskat, M., *Physical Principles of Oil Production*, McGraw-Hill Book Co., Inc., New York (1949).
26. Ramey, H. J., Jr., "Rapid Methods for Estimating Reservoir Compressibilities," *J. Pet. Tech.* (April 1964), pp. 447-454.
27. Trube, A. S., "Compressibility of Natural Gases," *Trans.*, AIME, Vol. 210 (1957), pp. 355-357.
28. Trube, A. S., "Compressibility of Undersaturated Hydrocarbon Reservoir Fluids," *Trans.*, AIME, Vol. 210 (1957), pp. 341-344.
29. "A Correlation for Water Viscosity," *Pet. Eng.* (July 1980), pp. 117-118.
30. Standing, M. B., *Volumetric and Phase Behavior of Oil Field Hydrocarbon Systems*, SPE, Dallas (1977).
31. Carr, N. L., Kobayashi, R., and Burrows, D. B. "Viscosity of Hydrocarbon Gases Under Pressure," *Trans.*, AIME, Vol. 201 (1954), pp. 264-272.
32. Hollo, R., and Fifadara, H., *TI-59 Reservoir Engineering Manual*, PennWell Books, Tulsa (1980).
33. Vazquez, M., and Beggs, H. D., "Correlations for Fluid Physical Property Prediction," *J. Pet. Tech.* (June 1980), pp. 968-970; paper SPE 6719 presented at the 52nd Annual Fall Tech. Conf. and Exhibition, Denver, Oct 9-12, 1977.
34. Meehan, D. N., "Improved Oil PVT Property Correlations," *Oil & Gas J.* (Oct. 27, 1980), pp. 64-71.
35. Meehan, D. N., "Crude Oil Viscosity Correlation," *Oil & Gas J.* (Nov. 10, 1980), pp. 214-216.
36. Meehan, D. N., and Vogel, E. L., *HP-41 Reservoir Engineering Manual*, Penn Well Books, Tulsa (1982).
37. Garb, F. A., *Waterflood Calculations for Hand-Held Computers*, Gulf Publishing Co., Houston (1982).
38. Hollo, R., Homes, M., and Pais, V., *HP-41CV Reservoir Economics and Engineering Manual*, Gulf Publishing Co., Houston (1983).
39. McCoy, R. L., *Microcomputer Programs for Petroleum Engineers, Vol. 1. Reservoir Engineering and Formation Evaluation*, Gulf Pub. Co., Houston (1983).
40. Sinha, M. K., and Padgett, L. R., *Reservoir Engineering Techniques Using Fortran*, Intl. Human Resources Dev. Corp., Boston (1985).
41. Smith, H. I., "Estimating Flow Efficiency From Afterflow-Distorted Pressure Buildup Data," *J. Pet. Tech.* (June 1974), pp. 696-697.

42. Archie, G. E., "The Electrical Resistivity Log as an Aid in Determining Some Reservoir Characteristics," *Trans.*, AIME (1942), pp. 54-61.
43. Wyllie, M. R. J., and Rose, W. D., "Some Theoretical Considerations Related to the Quantitative Evaluation of the Physical Characteristics of Reservoir Rock from Electrical Log Data," *Trans.*, AIME, Vol. 189 (1950), pp. 105-118.
44. Tixier, M. P., "Porosity Index in Limestone from Electrical Logs," *Oil & Gas J* (Nov. 15, 1951), pp. 140-173.
45. Winsauer, W. O., "Resistivity of Brine-Saturated Sands in Relation to Pore Geometry," *Bull.*, AAPG, Vol. 36, No. 2 (1952), pp. 253-277.
46. Wyllie, M. R. J., and Gregory, A. R., "Formation Factors of Unconsolidated Porous Media: Influence of Particle Shape and Effect of Cementation," *Trans.*, AIME, Vol. 198 (1953), pp. 103-109.
47. Cornell, D., and Katz, D. L., "Flow of Gases Through Consolidated Porous Media," *Ind. & Eng. Chem.*, Vol. 45 (Oct. 1953), pp. 2145-2152.
48. Owen, J. D., "Well Logging Study-Quinduno Field, Roberts County, Texas," Symp. on Formation Evaluation, AIME (Oct. 1955).
49. Hill, H. J., and Milburn, J. D., "Effect of Clay and Water Salinity on Electrochemical Behavior of Reservoir Rocks," *Trans.*, AIME, Vol. 207 (1956), pp. 65-72.
50. Wyllie, M. R. J., and Gardner, G. H. F., "The Generalized Kozeny-Carman Equation, Part 2-A Novel Approach to Problems of Fluid Flow," *World Oil* (April 1958), pp. 210-228.
51. Sweeney, S. A., and Jennings, H. Y., Jr., "Effect of Wettability on the Electrical Resistivity of Carbonate Rock from a Petroleum Reservoir," *J Phys. Chem.*, Vol. 64 (1960), pp. 551-553.
52. Carothers, J. E., "A Statistical Study of the Formation Factor Relation," *The Log Analyst* (Sept.-Oct. 1968), pp. 13-20.
53. Porter, C. R., and Carothers, J. E., "Formation Factor-Porosity Relation Derived from Well Log Data," *The Log Analyst* (Jan.-Feb. 1971), pp. 16-26.
54. Timur, A., Hemkins, W. B., and Worthington, A. W., "Porosity and Pressure Dependence of Formation Resistivity Factor for Sandstones," Proc. Cdn. Well Logging Soc., Fourth Formation Evaluation Symposium, Calgary, Alberta, May 9-12 (1972).
55. Perez-Rosales, C., "On the Relationship Between Formation Resistivity Factor and Porosity," *Soc. Pet. Eng. J.* (Aug. 1982), pp. 531-536.
56. Coates, G. R., and Dumanoir, J. L., "A New Approach to Log-Derived Permeability," *Trans.*, SPWLA 14th Annual Logging Symp. (May 6-9, 1973), pp. 1-28.
57. Amyx, J. W., and Bass, D. M., Jr., "Properties of Reservoir Rocks," Chap. 23 in *Pet. Prod. Handbook*, T. C. Frick and R. W. Taylor (Eds.), SPE, Dallas, 2 (1962) 23/1-23/40.
58. *Log Interpretation-Principles and Applications*, Schlumberger Educational Services, Houston (1972).
59. Patnode, H. W., and Wyllie, M. R. J., "The Presence of Conductive Solids in Reservoir Rocks as a Factor in Electric Log Interpretation," *Trans.*, AIME, Vol. 189 (1950), pp. 47-52.
60. Winn, R. H., "The Fundamentals of Quantitative Analysis of Electric Logs," *Proc.*, Symposium on Formation Evaluation (Oct. 1955), pp. 35-48.
61. Atkins, E. R., and Smith, G. H., "The Significance of Particle Shape in Formation Resistivity Factor-Porosity Relationships," *J. Pet. Tech.* (March 1961); *Trans.*, AIME, Vol. 222, pp. 285-291.
62. Koepf, E. H., "Core Handling-Core Analysis Methods," Chap. 3 in *Determination of Residual Oil Saturation*, Interstate Oil Compact Commission, Oklahoma City, Oklahoma (1978), pp. 36-71.

63. Sanyal, S. K., Marsden, S. S., Jr., and Ramey, H. J., Jr., "The Effect of Temperature on Electrical Resistivity of Porous Media," *The Log Analyst* (March-April 1973), pp. 10-24.
64. Hilchie, D. W., "The Effect of Pressure and Temperature on the Resistivity of Rocks," Ph.D. Dissertation, The University of Oklahoma (1964).
65. Ransom, R. C., "A Contribution Toward a Better Understanding of the Modified Archie Formation Resistivity Factor Relationship," *The Log Analyst* (March-April 1984), pp. 7-12.
66. Earlougher, R. C., Jr., *Advances in Well Test Analysis*, Monograph Series, SPE, Dallas (1977), Vol. 5.
67. Fatt, I., "Pore Volume Compressibilities of Sandstone Reservoir Rock," *J. Pet. Tech.* (March 1958), pp. 64-66.
68. Van der Knapp, W., "Nonlinear Behavior of Elastic Porous Media," *Trans.*, AIME, Vol. 216 (1959), pp. 179-187.
69. Hall, H. N., "Compressibility of Reservoir Rocks," *Trans.*, AIME, Vol. 198 (1953), pp. 309-311.
70. Carpenter, C. B., and Spencer, G. B., "Measurements of Compressibility of Consolidated Oil-Bearing Sandstones," RI 3540, USBM (Oct., 1940).
71. Newman, G. H., "Pore-Volume Compressibility of Consolidated, Friable, and Unconsolidated Reservoir Rocks Under Hydrostatic Loading," *J. Pet. Tech.* (Feb. 1973), pp. 129-134.
72. Martin, J. C., "Simplified Equations of Flow in Gas Drive Reservoirs and the Theoretical Foundation of Multiphase Pressure Buildup Analyses," *Trans.*, AIME, Vol. 216 (1959), pp. 309-311.
73. Calhoun, J. C., Jr., *Fundamentals of Reservoir Engineering*, U. of Oklahoma Press, Norman (1976).
74. Martin, M., Murray, G. H., and Gillingham, W. J., "Determination of the Potential Productivity of Oil-Bearing Formations by Resistivity Measurements," *Geophysics*, Vol. 3 (1938), pp. 258-272.
75. Jakosky, J. J., and Hopper, R. H., "The Effect of Moisture on the Direct Current Resistivities of Oil Sands and Rocks," *Geophysics*, Vol. 2 (1937), pp. 33-55.
76. Wyckoff, R. D., and Botset, H. G., "The Flow of Gas-Liquid Mixtures Through Unconsolidated Sands," *J. Applied Physics*, Vol. 7 (Sept. 1936), pp. 325-345.
77. Leverett, M. C., "Flow of Oil-Water Mixtures Through Unconsolidated Sands," *Trans.*, AIME (1938), pp. 149-171.
78. de Witte, L., "Relations Between Resistivities and Fluid Contents of Porous Rocks," *Oil & Gas J.* (Aug. 24, 1950), pp. 120-132.
79. de Witte, A. J., "Saturation and Porosity From Electric Logs in Shaly Sands," *Oil & Gas J.* (March 4, 1957), pp. 89-93.
80. Williams, M., "Estimation of Interstitial Water from the Electrical Log," *Trans.*, AIME, Vol. 189 (1950), pp. 295-308.
81. Rust, C. F., "Electrical Resistivity Measurements on Reservoir Rock Samples by the Two-Electrode and Four-Electrode Methods," *Trans.*, AIME, Vol. 192 (1952), pp. 217-224.
82. Wyllie, M. R. J., and Spangler, M. B., "Application of Electrical Resistivity Measurements to Problem of Fluid Flow in Porous Media," *Bull.*, AAPG, Vol. 36, No. 2 (1952), pp. 359-403.
83. Morse, R., Terwilliger, P. L., and Yuster, S. T., "Relative Permeability Measurements on Small Core Samples," *Oil & Gas J.* (Aug. 23, 1947), pp. 109-125.

84. Whiting, R. L., Guerrero, E. T., and Young, R. M., "Electrical Properties of Limestone Cores," *Oil & Gas J.* (July 27, 1953), pp. 309-313.
85. Dunlap, H. F., et al., "The Relation Between Electrical Resistivity and Brine Saturation in Reservoir Rocks," AIME, Vol. 186 (1949), pp. 259-264.
86. Dorfman, M. H., "Discussion of Reservoir Description Using Well Logs," *J. Pet. Tech.* (Dec. 1984), pp. 2195-2196.
87. Wilson, D. A., and Hensel, W. M., Jr., "The Cotton Valley Sandstones of East Texas: A Log-Core Study," *Trans.*, SPWLA, 23rd Annual Logging Symposium, Paper R (July 6-9, 1982), pp. 1-27.
88. Hilchie, D. W., "Author's Reply to Discussion of Reservoir Description Using Well Logs," *J. Pet. Tech.* (Dec. 1984), p. 2196.
89. Hocott, C. R., "Interfacial Tension Between Water and Oil Under Reservoir Conditions," *Pet. Tech.* (Nov. 1938), pp. 184-190.
90. Katz, D. L., Monroe, R. R., and Trainer, R. P., "Surface Tension of Crude Oils Containing Dissolved Gases," *Pet. Tech.* (Sept. 1943), pp. 1-10.
91. Swartz, C. A., "The Variation in the Surface Tension of Gas-Saturated Petroleum with Pressure of Saturation," *Physics*, Vol. 1 (1931), pp. 245-253.
92. Livingston, H. K., "Surface and Interfacial Tensions of Oil-Water Systems in Texas Oil Sands," *Pet. Tech.* (Nov. 1938), pp. 1-13.
93. Hjelmeland, O. S., and Larrondo, L. E., "Investigation of the Effects of Temperature, Pressure, and Crude Oil Composition on Interfacial Properties," *SPE Reservoir Engineering* (July 1986), pp. 321-328.
94. Defay, R., Prigogine, I., Bellemans, A., and Everett, D. H., *Surface Tension and Adsorption*, Longmans, London (1966).
95. Benner, F. C., Riches, W. W., and Bartell, F. E., "Nature and Importance of Surface Forces in Production of Petroleum," *Drill. & Prod. Prac.*, API (1938), pp. 442-448.
96. Benner, F. C., and Bartell, F. E., "The Effect of Polar Impurities Upon Capillary and Surface Phenomena in Petroleum Production," *Drill & Prod Prac.*, API (1942), pp. 341-348.
97. Benner, F. C., Dodd, C. G., and Bartell, F. E., "Evaluation of Effective Displacement Pressures for Petroleum Oil-Water Silica Systems," *Drill. & Prod. Prac.*, API (1942), pp. 169-177.
98. Nutting, P. G., "Some Physical and Chemical Properties of Reservoir Rocks Bearing on the Accumulation and Discharge of Oil," *Problems in Petroleum Geology*, AAPG (1934).
99. Schilthuis, R. J., "Connate Water in Oil and Gas Sands," *Trans.*, AIME (1938), pp. 199-214.
100. Leverett, M. C., "Capillary Behavior in Porous Solids," *Trans.*, AIME, Vol. 142 (1941), pp. 159-172.
101. Bartell, F. E., and Miller, F. L., "Degree of Wetting of Silica by Crude Petroleum Oils," *Ind. Eng. Chem.*, Vol. 20, No. 2 (1928), pp. 738-742.
102. Slobod, R. L., and Blum, H. A., "Method for Determining Wettability of Reservoir Rocks," *Trans.*, AIME, Vol. 195 (1952), pp. 1-4.
103. Taber, J. J., personal communication.
104. Wagner, O. R., and Leach, R. O., "Improving Oil Displacement Efficiency by Wettability Adjustment," *Trans.*, AIME, Vol. 216 (1959), pp. 65-72.
105. Denekas, M. O., Mattax, C. C., and Davis, G. T., "Effects of Crude Oil Components on Rock Wettability," *Trans.*, AIME, Vol. 216 (1959), pp. 330-333.
106. Moore, T. F., and Slobod, R. L., "The Effect of Viscosity and Capillarity on the Displacement of Oil by Water," *Prod. Monthly* (Aug. 1956), pp. 20-30.
107. Bobek, J. E., Mattax, C. C., and Denekas, M. O., "Reservoir Rock Wettability—Its Significance and Evaluation," *Trans.*, AIME, Vol. 213 (1958), pp. 155-160.

108. Amott, E., "Observations Relating to the Wettability of Porous Rock," *Trans., AIME*, Vol. 216 (1959), pp. 156-162.
109. Gatenby, W. A., and Marsden, S. S., "Some Wettability Characteristics of Synthetic Porous Media," *Prod. Monthly* (Nov. 1957), pp. 5-12.
110. Donaldson, E. C., Thomas, R. D., and Lorenz, P. B., "Wettability Determination and Its Effect on Recovery Efficiency," *Soc. Pet. Eng. J.* (March 1969), pp. 13-20.
111. Donaldson, E. C., et al., "Equipment and Procedures for Fluid Flow and Wettability Tests of Geological Materials," U.S. Dept. of Energy, Bartlesville, Report DOE/BETC/IC-79/5, May 1980.
112. Donaldson, E. C., "Oil-Water-Rock Wettability Measurement," *Proc.*, Symposium of Chemistry of Enhanced Oil Recovery, Div. Pet. Chem., Am. Chem. Soc., March 29-April 3, 1981, pp. 110-122.
113. Raza, S. H., Treiber, L. E., and Archer, D. L., "Wettability of Reservoir Rocks and Its Evaluation," *Prod. Monthly*, Vol. 33, No. 4 (April 1968), pp. 2-7.
114. Treiber, L. E., Archer, D. L., and Owens, W. W., "A Laboratory Evaluation of the Wettability of Fifty Oil-Producing Reservoirs," *Soc. Pet. Eng. J.* (Dec. 1972), pp. 531-540.
115. Morrow, N. R., "Capillary Pressure Correlation for Uniformly Wetted Porous Media," *J. Can. Pet. Tech.*, Vol. 15 (1976), pp. 49-69.
116. Chilingar, G. V., and Yen, T. F., "Some Notes on Wettability and Relative Permeabilities of Carbonate Reservoir Rocks, II," *Energy Sources*, Vol. 7, No. 1 (1983), pp. 67-75.
117. Brown, R. J. S., and Fatt, I., "Measurements of Fractional Wettability of Oil Field Rocks by the Nuclear Magnetic Relaxation Method," *Trans., AIME*, Vol. 207 (1956), pp. 262-264.
118. Fatt, I., and Klikoff, W. A., "Effect of Fractional Wettability on Multiphase Flow through Porous Media," *Trans., AIME*, Vol. 216 (1959), pp. 426-432.
119. Holbrook, O. C., and Bernard, G. C., "Determination of Wettability by Dye Adsorption," *Trans., AIME*, Vol. 213 (1958), pp. 261-264.
120. Iwankow, E. N., "A Correlation of Interstitial Water Saturation and Heterogeneous Wettability," *Prod. Monthly* (Oct. 1960), pp. 18-26.
121. Salathiel, R. A., "Oil Recovery by Surface Film Drainage in Mixed-Wettability Rocks," *Trans., AIME* (1973), pp. 1216-1224.
122. Morrow, N. R., Lim, H. T., and Ward, J. S., "Effect of Crude Oil Induced Wettability Changes on Oil Recovery," *SPE Formation Evaluation* (Feb. 1986), pp. 89-103.
123. Rathmell, J. J., Braun, P. H., and Perkins, T. K., "Reservoir Waterflood Residual Oil Saturation from Laboratory Tests," *J. Pet. Tech.* (Feb. 1973), pp. 175-185.
124. Sharma, M. M., and Wunderlich, R. W., "The Alteration of Rock Properties Due to Interactions With Drilling Fluid Components," paper SPE 14302 presented at the SPE 1985 Annual Technical Conference & Exhibition, Las Vegas, Sept. 22-25.
125. Richardson, J. G., Perkins, F. M., Jr., and Osoba, J. S., "Differences in Behavior of Fresh and Aged East Texas Woodbine Cores," *Trans., AIME*, Vol. 204 (1955), pp. 86-91.
126. Mungan, N., "Certain Wettability Effects in Laboratory Waterfloods," *J. Pet. Tech.* (Feb. 1966), pp. 247-252.
127. Rose, W. R., and Bruce, W. A., "Evaluation of Capillary Character in Petroleum Reservoir Rock," *Trans., AIME*, Vol. 186 (1949), pp. 127-133.
128. Klinkenberg, L. J., "The Permeability of Porous Media to Liquids and Gases," *Drill. & Prod. Prac.*, API (1941), pp. 200-213.

129. Jones, F. O., and Owens, W. W., "A Laboratory Study of Low-Permeability Gas Sands," *J. Pet. Tech.* (Sept. 1980), pp. 1631-1640.
130. Wei, K. K., Morrow, N. R., and Brower, K. R., "The Effect of Fluid, Confining Pressure, and Temperature on Absolute Permeabilities of Low-Permeability Sandstones," *SPE Formation Evaluation* (Aug. 1986), pp. 413-423.
131. Fatt, I., "The Effect of Overburden Pressure on Relative Permeability," *Trans.*, AIME (1953), pp. 325-326.
132. Bruce, W. A., and Welge, H. J., "The Restored-State Method for Determination of Oil in Place and Connate Water," *Drill. and Prod. Prac.*, API (1947), pp. 166-174.
133. Craig, F. F., Jr., "The Reservoir Engineering Aspects of Waterflooding," Monograph Series, SPE, Dallas, Vol. 3 (1971).
134. Muskat, M., et al., "Flow of Gas-Liquid Mixtures through Sands," *Trans.*, AIME (1937), pp. 69-96.
135. Hassler, G. L., Rice, R. R., and Leeman, E. H., "Investigations on the Recovery of Oil from Sandstones by Gas Drive," *Trans.*, AIME (1936), pp. 116-137.
136. Botset, H. G., "Flow of Gas-Liquid Mixtures through Consolidated Sand," *Trans.*, AIME, Vol. 136 (1940), pp. 91-105.
137. Leverett, M. C., and Lewis, W. B., "Steady Flow of Gas-Oil Water Mixtures through Unconsolidated Sands," *Trans.*, AIME, Vol. 142 (1941), pp. 107-116.
138. Krutter, H., and Day, R. J., "Air Drive Experiments on Long Horizontal Consolidated Cores," *Pet. Tech.*, T. P. 1627 (Nov. 1943).
139. Osoba, J. S., et al., "Laboratory Measurements of Relative Permeability," *Trans.*, AIME, Vol. 192 (1951), pp. 47-56.
140. Caudle, B. H., Slobod, R. L., and Brownscombe, E. R., "Further Developments in the Laboratory Determination of Relative Permeability," *Trans.*, AIME, Vol. 192 (1951), pp. 145-150.
141. Geffen, J. M., et al., "Experimental Investigation of Factors Affecting Laboratory Relative Permeability Measurements," *Trans.*, AIME, Vol. 192 (1951), pp. 99-110.
142. Richardson, J. G., et al., "Laboratory Determination of Relative Permeability," *Trans.*, AIME, Vol. 195 (1952), pp. 187-196.
143. Owens, W. W., Parrish, D. R., and Lamoreaux, W. E., "An Evaluation of a Gas-Drive Method for Determining Relative Permeability Relationships," *Trans.*, AIME, Vol. 207 (1956), pp. 275-280.
144. Hassler, G. L., "Method and Apparatus for Permeability Measurements," U.S. Patent No. 2,345,935.
145. Brownscombe, E. R., Slobod, R. L., and Caudle, B. H., "Relative Permeability of Cores Desaturated by Capillary Pressure Method," *Drill. & Prod. Prac.*, API (1949), pp. 302-315.
146. Gates, J. I., and Tempelaar-Lietz, W., "Relative Permeabilities of California Cores by the Capillary Pressure Method," *Drill. & Prod. Prac.*, API (1950), pp. 285-302.
147. Leas, W. J., Jenks, L. H., and Russell, C. D., "Relative Permeability to Gas," *Trans.*, AIME, Vol. 189 (1950), pp. 65-72.
148. Rapoport, L. A., and Leas, W. J., "Relative Permeability to Liquid in Liquid-Gas Systems," *Trans.*, AIME, Vol. 192 (1951), pp. 83-98.
149. Fatt, I., and Dykstra, H., "Relative Permeability Studies," *Trans.*, AIME, Vol. 192 (1951), pp. 249-256.
150. Corey, A. T., "The Interrelation Between Gas and Oil Relative Permeabilities," *Prod. Monthly*, Vol. 19 (Nov. 1954), pp. 38-41.
151. Loomis, A. G., and Crowell, D. C., "Relative Permeability Studies: Gas-Oil and Water-Oil Systems," Bull. 599, U.S. Bur. of Mines, Washington, 1962.

152. Buckley, S. E., and Leverett, M. C., "Mechanism of Fluid Displacement in Sands," *Trans.*, AIME, Vol. 146 (1942), pp. 107-116.
153. Welge, H. J., "A Simplified Method for Computing Oil Recovery by Gas or Water Drive," *Trans.*, AIME, Vol. 195 (1952), pp. 91-98.
154. Johnson, E. F., Bossler, D. P., and Naumann, V. O., "Calculation of Relative Permeability from Displacement Experiments," *Trans.*, AIME, Vol. 216 (1959), pp. 370-372.
155. Higgins, R. V., "Application of Buckley-Leverett Techniques in Oil-Reservoir Analysis," Bureau of Mines Report of Investigations 5568 (1960).
156. Guerrero, E. T., and Stewart, F. M., "How to Obtain a k_w/k_o Curve from Laboratory Unsteady-State Flow Measurements," *Oil & Gas J.* (Feb. 1, 1960), pp. 96-100.
157. Guerrero, E. T., and Stewart, F. M., "How to Obtain and Compare k_w/k_o Curves from Steady-State and Laboratory Unsteady-State Flow Measurements," *Oil & Gas J.* (Feb. 22, 1960), pp. 104-106.
158. Jones, S. C., and Rozelle, W. O., "Graphical Techniques for Determining Relative Permeability from Displacement Experiments," *Trans.*, AIME (1978), pp. 807-817.
159. Corey, A. T., et al., "Three-Phase Relative Permeability," *J. Pet. Tech.* (Nov. 1956), pp. 63-65.
160. Schneider, F. N., and Owens, W. W., "Sandstone and Carbonate Two- and Three-Phase Relative Permeability Characteristics," *Soc. Pet. Eng. J.* (March 1970), pp. 75-84.
161. Honarpour, M., Koederitz, L. F., and Harvey, A. H., "Empirical Equations for Estimating Two-Phase Relative Permeability in Consolidated Rock," *J. Pet. Tech.* (Dec. 1982), pp. 2905-2908.
162. Mungan, N., "Interfacial Effects in Immiscible Liquid-Liquid Displacement in Porous Media," *Soc. Pet. Eng. J.* (Sept. 1966), pp. 247-253.
163. Lefebvre du Prey, E. J., "Factors Affecting Liquid-Liquid Relative Permeabilities of a Consolidated Porous Medium," *Soc. Pet. Eng. J.* (Feb. 1973), pp. 39-47.
164. Miller, M. A., and Ramey, H. J., Jr., "Effect of Temperature on Oil/Water Relative Permeabilities of Unconsolidated and Consolidated Sands," *Soc. Pet. Eng. J.* (Dec. 1985), pp. 945-953.
165. Honarpour, M., DeGroat, C., and Manj Nath, A., "How Temperature Affects Relative Permeability Measurement," *World Oil* (May 1986), pp. 116-126.
166. Kinney, P. T., and Nielsen, R. F., "Wettability in Oil Recovery," *World Oil*, Vol. 132, No. 4 (March 1951), pp. 145-154.
167. Newcombe, J., McGhee, J., and Rzasa, M. J., "Wettability versus Displacement in Water Flooding in Unconsolidated Sand Columns," *Trans.*, AIME, Vol. 204 (1955), pp. 227-232.
168. Coley, F. N., Marsden, S. S., and Calhoun, J. C., Jr., "A Study of the Effect of Wettability on the Behavior of Fluids in Synthetic Porous Media," *Prod. Monthly*, Vol. 20, No. 8 (June 1956), pp. 29-45.
169. Jennings, H. Y., Jr., "Surface Properties of Natural and Synthetic Porous Media," *Prod. Monthly*, Vol. 21, No. 5 (March 1957), pp. 20-24.
170. Uren, L. D., and Fahmy, E. H., "Factors Influencing the Recovery of Petroleum from Unconsolidated Sands by Water-Flooding," *Trans.*, AIME, Vol. 77 (1927), pp. 318-335.
171. Kennedy, H. T., Burja, E. O., and Boykin, R. S., "An Investigation of the Effects of Wettability on the Recovery of Oil by Water Flooding," *J. Phys. Chem.*, Vol. 59 (1955), pp. 867-869.
172. Morrow, N. R., "Interplay of Capillary, Viscous and Buoyancy Forces in the Mobilization of Residual Oil," *J. Can. Pet. Tech.* (July-Sept. 1979), pp. 3546.

173. Melrose, J. C., and Brandner, C. F., "Role of Capillary Forces in Determining Microscopic Displacement Efficiency for Oil Recovery by Waterflooding," *J. Can. Pet. Tech.*, Vol. 13 (1974), pp. 54-62.
174. Owens, W. W., and Archer, D. L., "The Effect of Rock Wettability on Oil Water Relative Permeability Relationships," *J. Pet. Tech.* (July 1971), pp. 873-878.
175. McCaffery, F. G., and Bennion, D. W., "The Effect of Wettability on Two-Phase Relative Permeabilities," *J. Can. Pet. Tech.*, Vol. 13 (1974), pp. 42-53.
176. Killins, C. R., Nielsen, R. F., and Calhoun, J. C., Jr., "Capillary Desaturation and Imbibition in Rocks," *Prod. Monthly*, Vol. 18, No. 2 (Feb. 1953), pp. 30-39.
177. Rust, C. F., "A Laboratory Study of Wettability Effects on Basic Core Parameters," paper SPE 986G, presented at the SPE Venezuelan Second Annual Meeting, Caracas, Venezuela, Nov. 6-9, 1957.
178. Mungan, N., and Moore, E. J., "Certain Wettability Effects on Electrical Resistivity in Porous Media," *J. Can. Pet. Tech.* (Jan.-March 1968), pp. 20-25.
179. Morgan, W. B., and Pirson, S. J., "The Effect of Fractional Wettability on the Archie Saturation Exponent," *Trans.*, SPWLA, Fifth Annual Logging Symposium, Midland, Texas, May 13-15, 1964.

Formation Evaluation

180. Timmerman, E. H., *Practical Reservoir Engineering*, PennWell Books, Tulsa (1982)
181. Keelan, D., "Coring: Part 1—Why It's Done," *World Oil* (March 1985), pp. 83-90.
182. Park, A., "Coring: Part 2—Core Barrel Types and Uses," *World Oil* (April 1985), pp. 83-90.
183. Park, A., "Coring: Part 3—Planning the Job," *World Oil* (May 1985), pp. 79-86.
184. Park, A., "Coring: Part 4—Bit Considerations," *World Oil* (June 1985), pp. 149-154.
185. Park, A., "Coring: Part 5—Avoiding Potential Problems," *World Oil* (July 1985), pp. 93-98.
186. Toney, J. B., and Speights, J. L., "Coring: Part 6—Sidewall Operations," *World Oil* (Aug. 1, 1985), pp. 29-36.
187. Kraft, M., and Keelan, D., "Coring: Part 7—Analytical Aspects of Sidewall Coring," *World Oil* (Sept. 1985), pp. 77-90.
188. Keelan, D., "Coring: Part 8—Plug and Full Diameter Analysis," *World Oil* (Nov. 1985), pp. 103-112.
189. Kersey, D. G., "Coring: Part 9—Geological Aspects," *World Oil* (Jan. 1986), pp. 103-108.
190. Keelan, D. K., "Core Analysis for Aid in Reservoir Description" *J. Pet. Tech.* (Nov. 1982), pp. 2483-2491.
191. Anderson, G., *Coring and Core Analysis Handbook*, Pet. Pub. Co., Tulsa (1975).
192. "API Recommended Practice for Core-Analysis Procedure," API RP 40, API Prod. Dept., Dallas (Aug. 1960).
193. "Recommended Practice for Determining Permeability of Porous Media," API RP 27, third edition, API Prod. Dept., Dallas (Aug. 1956).
194. Stosur, J. J., and Taber, J. J., "Critical Displacement Ratio and Its Effect on Wellbore Measurement of Residual Oil Saturation," paper SPE 5509 presented at the SPE-AIME 50th Annual Fall Meeting, Dallas, Sept. 28-Oct. 1, 1975.

195. Jenks, L. H., et al., "Fluid Flow Within a Porous Medium Near a Diamond Core Bit," *J. Can Pet. Tech.*, Vol. 7 (1968), pp. 172-180.
196. Black, W. M., "A Review of Drill-Stem Testing Techniques and Analysis," *J. Pet. Tech.* (June 1956), pp. 21-30.
197. Slider, H. C., *Worldwide Practical Petroleum Reservoir Engineering Methods*, PenWell Pub. Co., Tulsa (1983).
198. Timur, A., "An Investigation of Permeability, Porosity, and Residual Water Saturation Relationships for Sandstone Reservoirs," *The Log Analyst* (July-Aug. 1968).
199. *Log Interpretation Charts*, Schlumberger Well Services (1991).
200. Hilchie, D. W., *Applied Openhole Log Interpretation*, second edition, Douglas W. Hilchie, Inc., Golden, CO (1982).
201. Doll, H. G., "The SP Log: Theoretical Analysis and Principles of Interpretation," *Trans.*, AIME, Vol. 179 (1948), pp. 146-185.
202. Hilchie, D. W., *Old Electrical Log Interpretation*, Douglas W. Hilchie, Inc., Golden, CO (1979).
203. Frank, R. W., *Prospecting with Old E-Logs*, Schlumberger, Houston (1986).
204. Poupon, A., Loy, M. E., and Tixier, M. P., "A Contribution to Electrical Log Interpretations in Shaly Sands," *J. Pet. Tech.* (June 1954); *Trans.*, AIME, pp. 27-34.
205. Suau, J., et al., "The Dual Laterolog-R_{xo} tool," paper SPE 4018 presented at the 47th Annual Meeting, San Antonio (1972).
206. Asquith, G., and Gibson, C., "Basic Well Log Analysis for Geologists," American Association of Petroleum Geologists, Methods in Exploration Series, Tulsa.
207. Serra, O., Baldwin, J., and Quirein, J., "Theory Interpretation and Practical Applications of Natural Gamma Spectroscopy," *Trans.*, SPWLA (1980).
208. Wyllie, M. R. J., Gregory, A. R., and Gardner, L. W., "Elastic Wave Velocities in Heterogeneous and Porous Media," *Geophysics*, Vol. 21, No. 1 (Jan. 1956), pp. 41-70.
209. Merkel, R. H., "Well Log Formation Evaluation," American Association of Petroleum Geologists, Continuing Education Course-Note Series #4.
210. Raymer, L. L., Hunt, E. R., and Gardner, J. S., "An Improved Sonic Transit Time-To-Porosity Transform," *Trans.*, SPWLA (1980).
211. Wahl, J. S., et al., "The Dual Spacing Formation Density Log," *J. Pet. Tech.* (Dec. 1964), pp. 1411-1416.
212. Desbrandes, R., *Encyclopedia of Well Logging*, Gulf Publishing Co., Houston (1985).
213. Tittman, J., "Geophysical Well Logging," *Methods of Experimental Physics*, Academic Press, Vol. 24 (1986).
214. *Electromagnetic Propagation Tool*, Schlumberger, Ltd., Houston (1984).
215. Bateman, R. M., "Open-Hole Log Analysis and Formation Evaluation," Intl. Human Resources Development Corp. (1985).
216. Bateman, R. M., "Log Quality Control," International Human Resources Development Corp. (1985).
217. Bateman, R. M., "Cased-Hole Log Analysis and Reservoir Performance Monitoring," Intl. Human Resources Development Corp. (1985).
218. Schultz, W. E., and Smith, H. D., Jr., "Laboratory and Field Evaluation of a Carbon/Oxygen (C/O) Well Logging System," *J. Pet. Tech.* (Oct. 1974), pp. 1103-1110.
219. Lock, G. A., and Hoyer, W. A., "Carbon-Oxygen (C/O) Log: Use and Interpretation," *J. Pet. Tech.* (Sept. 1974), pp. 1044-1054.
220. *Cased Hole Applications*, Schlumberger, Ltd., New York (1975).
221. *Production Log Interpretation*, Schlumberger, Ltd., New York (1973).

222. George, C. J., and Stiles, L. H., "Improved Techniques for Evaluating Carbonate Waterfloods in West Texas," *J. Pet. Tech.* (Nov. 1978), pp. 1547-1554.
223. Gilbert, W. E., "Flowing and Gas-lift Well Performance," *Drill. & Prod. Prac.*, API (1955), pp. 126-157.
224. Vogel, J. V., "Inflow Performance Relationships for Solution-Gas Drive Wells," *Trans.*, AIME (1968), pp. 83-92.
225. Standing, M. B., "Inflow Performance Relationships for Damaged Wells Producing by Solution-Gas Drive," *J. Pet. Tech.* (Nov. 1970), pp. 1399-1400.
226. Fetkovich, M. J., "The Isochronal Testing of Oil Wells," paper SPE 4529 presented at the SPE 48th Annual Fall Meeting, Las Vegas, Sept. 30-Oct. 3, 1973.
227. Patton, L. D., and Goland, M., "Generalized IPR Curves for Predicting Well Behavior," *Pet. Eng. International* (Sept. 1980), pp. 92-102.

Pressure Transient Testing of Oil and Gas Wells

228. Lee, J., *Well Testing*, SPE, Dallas (1982).
229. Miller, C. C., Dyes, A. B., and Hutchinson, C. A., Jr., "Estimation of Permeability and Reservoir Pressure From Bottom-Hole Pressure Build-Up Characteristics," *Trans.*, AIME, Vol. 189 (1950), pp. 91-104.
230. Horner, D. R., "Pressure Build-Up in Wells," *Proc.*, Third World Pet. Conf., The Hague (1951) Sec. II, pp. 503-523. Also *Reprint Series, No. 9-Pressure Analysis Methods*, SPE, Dallas (1967), pp. 25-43.
231. van Everdingen, A. F., "The Skin Effect and Its Influence on the Productive Capacity of a Well," *Trans.*, AIME, Vol. 198 (1953), pp. 171-176. Also *Reprint Series, No. 9-Pressure Analysis Methods*, SPE, Dallas (1967), pp. 45-50.
232. Hurst, W., "Establishment of the Skin Effect and Its Impediment to Fluid Flow Into a Well Bore," *Pet. Eng.* (Oct. 1953), B-6 through B-16.
233. Ramey, H. J., Jr., "Short-Time Well Test Data Interpretation in the Presence of Skin Effect and Wellbore Storage," *J. Pet. Tech.* (Jan. 1970), pp. 97-104; *Trans.*, AIME, Vol. 249.
234. Agarwal, R. G., Al-Hussainy, R., and Ramey, H. J., Jr., "An Investigation of Wellbore Storage and Skin Effect in Unsteady Liquid Flow: I. Analytical Treatment," *Soc. Pet. Eng. J.* (Sept. 1970), pp. 279-290; *Trans.*, AIME, Vol. 249.
235. Wattenbarger, R. A., and Ramey, H. J., Jr., "An Investigation of Wellbore Storage and Skin Effect in Unsteady Liquid Flow: II. Finite Difference Treatment," *Soc. Pet. Eng. J.* (Sept. 1970), pp. 291-297; *Trans.*, AIME, Vol. 249.
236. McKinley, R. M., "Wellbore Transmissibility From Afterflow-Dominated Pressure Buildup Data," *J. Pet. Tech.* (July 1971), pp. 863-872; *Trans.*, AIME, Vol. 251.
237. McKinley, R. M., "Estimating Flow Efficiency From Afterflow-Distorted Pressure Buildup Data," *J. Pet. Tech.* (June 1974), pp. 696-697.
238. Gringarten, A. C., Ramey, H. J., Jr., and Raghavan, R., "Unsteady-State Pressure Distributions Created by a Well With a Single Infinite-Conductivity Vertical Fracture," *Soc. Pet. Eng. J.* (Aug. 1974), pp. 347-360; *Trans.*, AIME, Vol. 257.

Mechanisms & Recovery of Hydrocarbons by Natural Means

239. "Statistical Analysis of Crude Oil Recovery and Recovery Efficiency," API BUL D14, second edition, API Prod. Dept., Dallas (Apr. 1984).
240. "A Statistical Study of Recovery Efficiency," API BUL D14, API Prod. Dept., Dallas (Oct. 1967).

241. Craze, R. C., and Buckley, S. E., "A Factual Analysis of the Effect of Well Spacing on Oil Recovery," *Drill. & Prod. Prac.*, API (1945), pp. 144-159.
242. Guthrie, R. K., and Greenberger, M. H., "The Use of Multiple-Correlation Analyses for Interpreting Petroleum-engineering Data," *Drill. & Prod. Prac.*, API (1955), pp. 130-137.
243. Doscher, T. M., "Statistical Analysis Shows Crude-Oil Recovery," *Oil & Gas J.* (Oct. 29, 1984), pp. 61-63.
244. Arps, J. J., and Roberts, T. G., "The Effect of the Relative Permeability Ratio, the Oil Gravity, and the Solution Gas-Oil Ratio on the Primary Recovery from a Depletion Type Reservoir," *Trans.*, AIME, Vol. 204 (1955), pp. 120-127.
245. Arps, J. J., "Estimation of Primary Oil Reserves," *Trans.*, AIME, Vol. 207 (1956), pp. 182-191.
246. Wahl, W. L., Mullins, L. D. , and Elfrink, E. B . , "Estimation of Ultimate Recovery from Solution Gas-Drive Reservoirs," *Trans.*, AIME, Vol. 213 (1958), pp. 132-138.

Material Balance and Volumetric Analysis

247. Mayer, E. H., et al., "SPE Symbols Standard," *J. Pet. Tech.* (Dec. 1984), pp. 2278-2332.
248. Ramey, H. J., Jr., "Graphical Interpretations for Gas Material Balance," *J. Pet. Tech.* (July 1970), pp. 837-838.
249. Schilthuis, R. J., "Active Oil and Reservoir Energy," *Trans.*, AIME (1936), pp. 33-52.
250. Tarner, J., "How Different Size Gas Caps and Pressure Maintenance Programs Affect Amount of Recoverable Oil," *Oil Weekly* (June 12, 1944), pp. 32-44.
251. Muskat, M., "The Production Histories of Oil Producing Gas-Drive Reservoirs," *Appl. Phys.*, Vol. 16 (March 1945), pp. 147-159.
252. Hurst, W., "Water Influx Into a Reservoir and Its Application to the Equation of Volumetric Balance," *Trans.*, AIME (1943), pp. 57-72.
253. van Everdingen, A. F., and Hurst, W., "The Application of the Laplace Transformation to Flow Problems in Reservoirs," *Trans.*, AIME (Dec. 1949), pp. 305-324.
254. Smith, C. R., *Mechanics of Secondary Oil Recovery*, Robert E . Krieger Publishing Co., New York (1975).

Decline Curve Analysis

255. Arps, J. J., "Analysis of Decline Curves," *Trans.*, AIME, Vol. 160 (1945), pp. 228-247.
256. Slider, H. C., "A Simplified Method of Hyperbolic Decline Curve Analysis," *J. Pet. Tech.* (March 1968), pp. 235-236.
257. Chatas, A. T., and Yankie, W. W., Jr., "Application of Statistics to the Analysis of Production Decline Data," *Trans.*, AIME, Vol. 213 (1958), pp. 399-401.
258. Gray, K. E., "Constant Per Cent Decline Curve," *Oil & Gas J.*, Vol. 58 (Aug. 29, 1960), pp. 67-74.
259. Gray, K. E., "How to Analyze Yearly Production Data for Constant Per Cent Decline," *Oil & Gas J.* (Jan. 1, 1962), pp. 76-79.
260. Brons, F., "On the Use and Misuse of Production Decline Curves," *Prod. Monthly*, Vol. 27, No. 9 (Sept. 1963), pp. 22-25.
261. Brons, F., and Silbergh, M., "The Relation of Earning Power to Other Profitability Criteria," *J. Pet. Tech.* (March 1964), pp. 269-275.

262. Ramsay, H. J., Jr., and Guerrero, E. T., "The Ability of Rate-Time Decline Curves to Predict Production Rates," *J. Pet. Tech.* (Feb. 1969), pp. 139-141.
263. Russell, D. G., and Prats, M., "Performance of Layered Reservoirs with Crossflow-Single-Compressible-Fluid Case," *Soc. Pet. Eng. J.* (March 1962), pp. 53-67.
264. Russell, D. G., and Prats, M., "The Practical Aspects of Interlayer Crossflow," *J. Pet. Tech.* (June 1962), pp. 589-594.
265. Poston, S. W., and Blasingame, T. A., "Microcomputer Applications to Decline Curve Analysis," *Geobyte* (Summer 1986), pp. 64-73.
266. Gentry, R. W., "Decline-Curve Analysis," *J. Pet. Tech.* (Jan. 1972), pp. 3841.
267. Fetkovich, M. J., "Decline Curve Analysis Using Type Curves" *J. Pet. Tech.* (June 1980), pp. 1065-1077.
268. Fetkovich, M. J., et al., "Decline Curve Analysis Using Type Curves: Case Histories," paper SPE 13169 presented at the SPE 1984 Annual Technical Conf. & Exhib., Houston, Sept. 16-19.

Reserve Estimates

269. "Society Adopts Proved Reserves Definitions," *J. Pet. Tech.* (Nov. 1981), pp. 2113-2114.
270. "Reserve Definitions Approved," *J. Pet. Tech.* (May 1987), pp. 576-578.
271. Guidelines for Application of the Definitions for Oil and Gas Reserves, Monograph 1, the Society of Petroleum Evaluation Engineers, Houston (1988).
272. Garb, F. A., "Oil and Gas Reserves, Classification, Estimation and Evaluation," *J. Pet. Tech.* (March 1985), pp. 373-390.
273. Crichlow, H. B., *Modern Reservoir Engineering—A Simulation Approach*, Prentice-Hall, Inc., New Jersey (1977).
274. Hudson, E. J., and Neuse, S. H., "Cutting Through the Mystery of Reserve Estimates," *Oil & Gas J.* (March 25, 1985), pp. 103-106.
275. Hudson, E. J., and Neuse, S. H., "Depletion Stage Determines Most Effective Methods for Reserve-Estimate Integrity," *Oil & Gas J.* (April 1, 1985), pp. 80-91.

Secondary Recovery

Fluid Movement In Waterflooded Reservoirs

276. Langnes, G. L., Robertson, J. O., Jr., and Chilingar, G. V., *Secondary Recovery and Carbonate Reservoirs*, American Elsevier Publishing Co., New York (1972).
277. *Improved Oil Recovery*, Interstate Oil Compact Commission, Oklahoma City (March 1983).
278. Willhite, G. P., *Waterflooding*, SPE, Richardson, TX (1986).
279. Singh, S. P., and Kiel, O. G., "Waterflood Design (Pattern, Rate, and Timing)," paper SPE 10024 presented at the SPE 1982 Intl. Pet. Exhibition & Tech. Symposium, Beijing, China, March 18-26.
280. Muskat, M., and Wyckoff, R. D., "A Theoretical Analysis of Waterflooding Networks," *Trans., AIME*, Vol. 107 (1934), pp. 62-76.
281. Dyes, A. B., Caudle, B. H., and Erickson, R. A., "Oil Production After Breakthrough—As Influenced by Mobility Ratio," *Trans., AIME*, Vol. 201 (1954), pp. 81-86.
282. Craig, F. F., Jr., Geffen, T. M., and Morse, R. A., "Oil Recovery Performance of Pattern Gas or Water Injection Operations from Model Tests," *J. Pet. Tech.* (Jan. 1955), pp. 7-15; *Trans., AIME*, Vol. 204.

283. Prats, M., et al., "Prediction of Injection Rate and Production History for Multifluid Five-Spot Floods," *J. Pet. Tech.* (May 1959), pp. 98-105; *Trans.*, AIME, Vol. 216.
284. Caudle, B. H., and Witte, M. D., "Production Potential Changes During Sweep-Out in a Five-Spot Pattern," *Trans.*, AIME, Vol. 216 (1959), pp. 446-448.
285. Habermann, B., "The Efficiency of Miscible Displacement As a Function of Mobility Ratio," *Trans.*, AIME, Vol. 219 (1960), pp. 264-272.
286. Kimbler, O. K., Caudle, B. H., and Cooper, H. E., Jr., "Areal Sweep-out Behavior in a Nine-Spot Injection Pattern," *J. Pet. Tech.* (Feb. 1964), pp. 199-202.
287. Caudle, B. H., Erickson, R. A., and Slobod, R. L., "The Encroachment of Injected Fluids Beyond the Normal Well Patterns," *Trans.*, AIME, Vol. 204 (1955), pp. 79-85.
288. Prats, M., Hazebroek, P., and Allen, E. E., "Effect of Off-Pattern Wells on the Performance of a Five-Spot Waterflood," *J. Pet. Tech.* (Feb. 1962), pp. 173-178.
289. Prats, M., "The Breakthrough Sweep Efficiency of the Staggered Line Drive," *Trans.*, AIME, Vol. 207 (1956), pp. 361-362.
290. Crawford, P. B., "Factors Affecting Waterflood Pattern Performance and Selection," *J. Pet. Tech.* (Dec. 1960), pp. 11-15.
291. Fasshi, M. R., "New Correlations for Calculation of Vertical Coverage and Areal Sweep Efficiency," *SPE Reservoir Engineering* (Nov. 1986), pp. 604-606.
292. Claridge, E. L., "Prediction of Recovery in Unstable Miscible Flooding," *Soc. Pet. Eng. J.* (April 1972), pp. 143-155.
293. Schmalz, J. P., and Rahme, H. D., "The Variation of Waterflood Performance With Variation in Permeability Profile," *Prod. Monthly*, Vol. 15, No. 9 (Sept. 1950), pp. 9-12.
294. Dykstra, H., and Parsons, R. L., "The Prediction of Oil Recovery by Waterflood," *Secondary Recovery of Oil in the United States*, API, Dallas (1950) second edition, pp. 160-174.
295. Warren, J. E., and Cosgrove, J. J., "Prediction of Waterflood Behavior in A Stratified System," *Soc. Pet. Eng. J.* (June 1964), pp. 149-157.
296. Johnson, C. E., Jr., "Prediction of Oil Recovery by Water Flood-A Simplified Graphical Treatment of the Dykstra-Parsons Method," *Trans.*, AIME, Vol. 207 (1956), pp. 345-346.
297. deSouza, A. O., and Bridham, W. E., "A Study on Dykstra-Parsons Curves," Tech. Report 29, Stanford University, Palo Alto (1981).
298. Craig, F. F., Jr., "Effect of Reservoir Description on Performance Predictions," *J. Pet. Tech.* (Oct. 1970), pp. 1239-1245.
299. Reznik, A. A., Emick, R. M., and Panvelker, S. B., "An Analytical Extension of the Dykstra-Parsons Vertical Stratification Discrete Solution to a Continuous, Real-Time Basis," *Soc. Pet. Eng. J.* (Dec. 1984), pp. 643-656.
300. Root, P. J., and Skiba, F. F., "Crossflow Effects During an Idealized Process in A Stratified Reservoir," *Soc. Pet. Eng. J.* (Sept. 1965), pp. 229-238.
301. Goddin, C. S., Jr., et al., "A Numerical Study of Waterflood Performance in a Stratified System With Crossflow," *J. Pet. Tech.* (June 1966), pp. 765-771.
302. El-Khatib, N., "The Effect of Crossflow on Waterflooding of Stratified Reservoirs," *Soc. Pet. Eng. J.* (April 1985), pp. 291-302.
303. Collins, H. N., and Wang, S. T., "Discussion of the Effect of Crossflow on Waterflooding of Stratified Reservoirs," *Soc. Pet. Eng. J.* (Aug. 1985), p. 614.
304. El-Khatib, N., "Author's Reply to Discussion of the Effect of Crossflow on Waterflooding of Stratified Reservoirs," *Soc. Pet. Eng. J.* (Aug. 1985), p. 614.

305. Collins, H. N., and Wang, S. T., "Further Discussion of the Effect of Crossflow on Waterflooding of Stratified Reservoirs," *SPE Reservoir Eng.* (Jan. 1986) p. 73.
306. El-Khatib, N., "Author's Reply to Further Discussion of the Effect of Crossflow on Waterflooding of Stratified Reservoirs," *SPE Reservoir Eng.* (Jan 1986), pp. 74-75
307. Hirasaki, G. J., Morra, F., and Willhite, G. P., "Estimation of Reservoir Heterogeneity from Waterflood Performance," SPE 13415, unsolicited paper.
308. Hirasaki, G. J., "Properties of Log-Normal Permeability Distribution for Stratified Reservoirs," SPE 13416, unsolicited paper.
309. Higgins, R. V., and Leighton, A. J., "A Computer Method to Calculate Two-Phase Flow in Any Irregularly Bounded Porous Medium," *J. Pet. Tech.* (June 1962), pp. 679-683; *Trans. AIME*, Vol. 225.
310. Stiles, W. E., "Use of Permeability Distribution in Water Flood Calculations," *Trans., AIME*, Vol. 186 (1949), pp. 9-13.
311. Garb, F. A., "Waterflood Calculations for Hand-held Computers. Part 8-Using Dykstra-Parsons Methods to Evaluate Stratified Reservoirs," *World Oil* (July 1980), pp. 155-160.
312. Garb, F. A., "Waterflood Calculations for Hand-held Computers. Part 7-Evaluating Flood Performance Using the Stiles Technique," *World Oil* (June 1980), pp. 205-210.
313. Deppe, J. C., "Injection Rates-The Effect of Mobility Ratio, Area Swept, and Pattern," *Soc. Pet. Eng. J.* (June 1961), pp. 81-91; *Trans., AIME*, Vol. 222.
314. Hearn, C. L., "Method Analyzes Injection Well Pressure and Rate Data," *Oil & Gas J.* (April 18, 1983), pp. 117-120.
315. Hall, H. N., "How to Analyze Waterflood Injection Well Performance," *World Oil* (Oct. 1963), pp. 128-130.
316. Martin, F. D., "Injectivity Improvement in the Grayburg Formation at a Waterflood in Lea County, NM," paper SPE 12599 presented at the 1984 Permian Basin Oil & Gas Recovery Conference, Midland, March 8-9.
317. Ershaghi, I., and Omoregie, O., "A Method for Extrapolation of Cut vs. Recovery Curves," *J. Pet. Tech.* (Feb. 1978), pp. 203-204.
318. Felsenthal, M., "A Statistical Study of Some Waterflood Parameters," *J. Pet. Tech.* (Oct. 1979), pp. 1303-1304.

Estimation of Waterflood Residual Oil Saturation

319. *Determination of Residual Oil Saturation*, Interstate Oil Compact Commission, Oklahoma City (June 1978).
320. Martin, F. D., Morrow, N. R., and Moran, J., "A Survey of Methods for Estimating Waterflood Residual Oil Saturations," PRRC Report 79-10, Petroleum Recovery Research Center, Socorro (May 1979).
321. Ramey, H. J., Jr., "Interference Analysis for Anisotropic Formations-A Case History," *J. Pet. Tech.* (October 1975), pp. 1290-1298.
322. Jennings, H. J., Jr., and Timur, A., "Significant Contributions in Formation Evaluation and Well Testing," *J. Pet. Tech.* (Dec. 1973), pp. 1432-1442.
323. Donaldson, E. C., and Crocker, M. E., *Review of Petroleum Oil Saturation and Its Determination*, U.S. Dept. of Energy, Bartlesville (1977).
324. Murphy, R., and Owens, W. W., "The Use of Special Coring and Logging Procedures for Defining Reservoir Residual Oil Saturations," *J. Pet. Tech.* (July 1973), pp. 841-850
325. Kazemi, H., "Determination of Waterflood Residual Oil Saturation from Routine Core Analysis," *J. Pet. Tech.* (Jan. 1977), pp. 31-32.

326. Hagedorn, A. R., and Blackwell, R. J., "Summary of Experience with Pressure Coring," paper SPE 3962 presented at the SPE 47th Annual Fall Meeting, San Antonio, Oct. 8-11, 1972.
327. Bilhartz, H. L., Jr., "Case History: A Pressure Core Hole," paper SPE 6389 presented at the 1977 Permian Basin Oil & Gas Recovery Conference, Midland, March 10-11.
328. Bilhartz, H. L., Jr., and Charlson, G. S., "Coring For In Situ Saturations in the Willard Unit CO₂ Flood Mini-Test," paper SPE 7050 presented at Improved Methods for Oil Recovery of SPE, Tulsa, Apr. 16-19, 1978.
329. Yell, L., "Pressure Coring Yields Valuable Reservoir Data," *Oil & Gas J.* (Oct. 30, 1978), pp. 95-99.
330. Sparks, R. L., "A Technique for Obtaining In Situ Saturations of Under-pressured Reservoirs," *J. Pt. Tech.* (Nov. 1982).
331. Hyland, C. R., "Pressure Coring—An Oilfield Tool," paper SPE 12093 presented at the 58th Annual Tech. Conf., San Francisco, Oct. 5-8, 1983.
332. Park, A., "Improved Oil Saturation Data Using Sponge Core Barrel," paper SPE 11550 presented at 1983 Production Operation Symp., Oklahoma City, Feb. 27-March 1.
333. *Fundamentals of Core Analysis, Mod II*, Core Laboratories, Inc.
334. Special Core Analysis and Industrial Water Technology, prepared by Special Core Analysis Studies Section, Core Laboratories, Inc., April 1972.
335. Grist, D. M., Langley, G. O., and Neustadter, E. L., "The Dependence of Water Permeability on Core Cleaning Methods in the Case of Some Sandstone Samples," *J. Can. Pet. Tech.* (April-June 1975), p. 48.
336. Cuiec, L., "Study of Problems Related to the Restoration of the Natural State of Core Samples," *J. Can. Pet. Tech.* (Oct.-Dec. 1977), pp. 68-80.
337. Cooke, C. E., Jr., "Method of Determining Residual Oil Saturation in Reservoirs," U.S. Patent 3,590,923 (July 6, 1971).
338. Deans, H. A., "Method of Determining Fluid Saturations in Reservoirs," U.S. Patent 3,623,842 (Nov. 30, 1971).
339. Sheely, C. Q., "Description of Field Tests to Determine Residual Oil Saturation by Single-Well Tracer Test," paper SPE 5840 presented at the Improved Oil Recovery Symposium, Tulsa, March 22-24, 1976.
340. Tomich, J. F., et al., "Single-Well Tracer Method to Measure Residual Oil Saturation," *J. Pet. Tech.* (Feb. 1973), pp. 211-218.
341. Bragg, J. R., Carlson, L. O., and Atterbury, J. H., "Recent Applications of the Single-Well Tracer Method for Measuring Residual Oil Saturation," paper SPE 5805 presented at the Improved Oil Recovery Symposium, Tulsa, March 22-24, 1976.
342. O'Brien, L. J., Cooke, R. S., and Willis, H. R., "Oil Saturation Measurements at Brown and East Voss Tannehil Fields," *J. Pet. Tech.* (January 1978), pp. 17-25.
343. Fertl, W. H., "Find ROS From Well Logs for Enhanced Recovery Projects," *Oil & Gas J.* (Feb. 12, 1979), pp. 120-127.
344. Fertl, W. H., "Well Logging and Its Applications in Cased Holes," *J. Pet. Tech.* (Feb. 1984), pp. 249-266.
345. *Log Interpretation Fundamentals*, Dresser Atlas Division, Dresser Industries (1975).
346. Waxman, M. H., and Thomas, E. C., "Electrical Conductivities in Oil-Bearing Shaly Sands," *Soc. Pet. Eng. J.* (June 1968), pp. 107-122.
347. Waxman, Mitt., and Smits, L. J. M., "Electrical Conductivities of Oil-Bearing Shaly Sands," *J. Pet. Tech.* (June 1965), pp. 107-122.
348. Richardson, J. E., et al. "Methods for Determining Residual Oil with Pulsed Neutron Capture Logs," *J. Pet. Tech.* (May 1973), pp. 593-606.

349. Wyman, R. E., "How Should We Measure Residual Oil Saturation?" *Bull. Cdn. Pet. Geol.*, Vol. 25, No. 2 (May 1977), pp. 233-270.
350. Murphy, R., and Owens, W. W., "Time-Lapse Logging, A Valuable Reservoir Evaluation Technique," *J. Pet. Tech.* (January 1964), pp. 15-19.
351. Murphy, R., Owens, W. W., and Dauben, D. L., "Well Logging Method," U.S. Patent 3,757,575 (Sept. 11, 1973).
352. Murphy, R., Foster, G. T., and Owens, W. W., "Evaluation of Waterflood Residual Oil Saturation Using Log-Inject-Log Procedures," *J. Pet. Tech.* (Feb. 1977), 178-186.
353. Bragg, J. R., et al., "A Comparison of Several Techniques for Measuring Residual Oil Saturation," paper SPE 7074 presented at the Fifth Symposium on Improved Oil Recovery, April 16-19, 1978.
354. Culver, R. B., Hopkinson, E. C., and Youmans, A. H., "Carbon-Oxygen (C/O) Logging Instrumentation," *Soc. Pet. Eng. J.* (Oct. 1974), pp. 463-470.
355. *Log Interpretation*, Volume II—Applications, Schlumberger Limited (1974).
356. Fertl, W. H., et al., "Evaluation and Monitoring of Enhanced Recovery Projects in California and Cased-Hole Exploration and Recompletions in West Texas Based on the Continuous Carbon/Oxygen Log," *J. Pet. Tech.* (Jan. 1983), pp. 143-157.
357. Westaway, P., Hertzog, R., and Plasek, R. E., "Neutron-Induced Gamma Ray Spectroscopy for Reservoir Analysis," *Soc. Pet. Eng. J.* (June 1983), pp. 553-564.
358. Robinson, J. D., et al., "Determining Residual Oil with the Nuclear Magnetism Log," *J. Pet. Tech.* (Feb. 1974), pp. 226-236.
359. Loren, J. D., and Robinson, J. D., "Relations Between Pore Size, Fluid and Matrix Properties, and NML Measurements," *Soc. Pet. Eng. J.* (Sept 1970), pp. 268-278.
360. Herrick, R. C., Couturie, S. H., and Best, D. L., "An Improved Nuclear Magnetism Logging System and its Application to Formation Evaluation," paper SPE 8361 presented at the 1979 SPE Annual Technical Conference and Exhibition, Las Vegas, Sept. 23-26.
361. Neuman, C. H., and Brown, R. J. S., "Application of Nuclear Magnetism Logging to Formation Evaluation," *J. Pet. Tech.* (Dec. 1982), pp. 2853-2862.
362. Neuman, C. H., "Logging Measurement of Residual Oil, Rangely Field, CO," *J. Pet. Tech.* (Sept. 1983), pp. 1735-1744.
363. Poley, J. Ph., Nootboom, J. J., and deWaal, P. J., "Use of V.H.F. Dielectric Measurements for Borehole Formation Analysis," *The Log Analyst* (May-June 1978), pp. 8-30.
364. Meador, R. A., and Cox, P. T., "Dielectric Constant Logging, A Salinity Independent Estimation of Formation Water Volume," paper SPE 5504 presented at Fall Meeting, Dallas, Sept. 30-Oct. 1, 1975.
365. Calvert, T. J., Rau, R. N., and Wells, L. E., "Electromagnetic Propagation—A New Dimension in Logging," paper SPE 6542 presented at the SPEAIME 52nd Annual Fall Technical Conference, Oct. 9-12, 1977.
366. Freedman, R., and Montaque, D. R., "Electromagnetic Propagation Tool (EPT): Comparison of Log Derived and in situ Oil Saturation in Shaly Fresh Water Sands," paper SPE 9266 presented at the 1980 SPE Meeting, Dallas, Sept. 21-24.
367. Wharton, R. P., et al., "Electromagnetic Propagation Logging: Advances in Technique and Interpretation," paper SPE 9267 presented at 55th Annual Fall Mtg., SPE, Dallas, Sept. 21-24, 1980.
368. Cox, P. T., and Warren, W. F., "Development and Testing of the Texaco Dielectric Log," SPWLA 24th Annual Logging Symp., June 27-30, 1983.

369. Eck, M. E., and Powell, D. E., "Application of Electromagnetic Propagation Logging in the Permian Basin of West Texas," paper SPE 12183 presented at 1983 SPE Annual Mtg., San Francisco, Oct. 5-8.
370. Geng, X., et al., "Dielectric Log-A Logging Method for Determining Oil Saturation," *J. Pet. Tech.* (Oct. 1983), pp. 1797-1805.
371. Dahlberg, K. E., and Ference, M. V., "A Quantitative Test of the Electromagnetic Propagation (EPT) Log for Residual Oil Determination," SPWLA 25th Annual Logging Symposium, New Orleans, June 10-13, 1984.
372. Shen, L. C., Manning, M. J., and Price, J. M., "Application of Electromagnetic Propagation Tool in Formation Evaluation," SPWLA 25th Annual Logging Symposium, New Orleans, June 10-13, 1984.
373. Iskander, M. F., Rattlingourd, S. O., and Oomrigar, J., "A New Electromagnetic Propagation Tool for Well Logging," paper SPE 13189 presented at the 59th Annual Conf., Houston, Sept. 16-19, 1984.
374. Shen, L. C., "Problems in Dielectric-Constant Logging and Possible Routes to Their Solution," *The Log Analyst* (Nov.-Dec. 1985), pp. 14-25.

Enhanced Oil Recovery Methods

375. van Poolen, H. K., and Associates, Inc., *Fundamentals of Enhanced Oil Recovery*, PenWell Publishing Co., Tulsa (1980).
376. Stalkup, F. I., Jr., *Miscible Displacement*, SPE Monograph Series, SPE, Dallas, Vol. 8 (1983).
377. Klins, M. A., *Carbon Dioxide Flooding*, International Human Resources Development Corp., Boston (1984).
378. Prats, M., *Thermal Recovery*, Monograph Series, SPE, Dallas, Vol. 7 (1982).
379. Latil, M., et al., *Enhanced Oil Recovery*, Gulf Publishing Co., Houston (1980).
380. Haynes, H. J., et al., *Enhanced Oil Recovery*, National Petroleum Council; Industry Advisory Council to the U.S. Department of the Interior (1976).
381. Bailey, R. E., et al., *Enhanced Oil Recovery*, Natl. Petroleum Council, Washington (June 1984).
382. Broome, J. H., Bohannon, J. M., and Stewart, W. C., "The 1984 Natl. Petroleum Council Study on EOR: An Overview," *J. Pet. Tech.* (Aug. 1986), pp. 869-874.
383. Doe, P. H., Carey, B. S., and Helmuth, E. S., "The Natl. Petroleum Council EOR Study: Chemical Processes," paper SPE 13240 presented at the 1984 Annual Tech. Conf. & Exhib., Sept. 16-19.
384. King, J. E., Blevins, T. R., and Britton, M. W., "The National Petroleum Council EOR Study: Thermal Processes," paper SPE 13242 presented at the 1984 SPE Annual Technical Conf. and Exhib., Houston, Sept. 16-19.
385. Robl, F. W., Emanuel, A. S., and Van Meter, O. E., Jr., "The 1984 Natl. Petroleum Council Estimate of Potential of EOR for Miscible Processes," *J. Pet. Tech.* (Aug. 1986), pp. 875-882.
386. Taber, J. J., and Martin, F. D., "Technical Screening Guides for the Enhanced Recovery of Oil," paper SPE 12069 presented at the SPE 1983 Annual Technical Conf. & Exhib., San Francisco, October 5-8.
387. Chang, H. L., "Polymer Flooding Technology—Yesterday, Today and Tomorrow," *J. Pet. Tech.* (Aug. 1978), pp. 1113-1128.
388. Martin, F. D., "Design and Implementation of a Polymer Flood," Southwestern Petroleum Short Course, *Proc.*, 33rd Annual Southwestern Petroleum Short Course, Lubbock, April 23-24, 1986.
389. Taber, J. J., "The Injection of Detergent Slugs in Water Floods," *Trans. AIME*, Vol. 213 (1958), pp. 186-192.

390. Gogarty, W. B., "Status of Surfactant or Micellar Methods," *J. Pet. Tech.* (Jan. 1976), pp. 93-102.
391. Gogarty, W. B., "Micellar/Polymer Flooding-An Overview," *J. Pet. Tech.* (Aug. 1978), pp. 1089-1101.
392. Gogarty, W. B., "Enhanced Oil Recovery Through the Use of Chemicals—Part 1," *J. Pet. Tech.* (Sept. 1983), pp. 1581-1590.
393. Gogarty, W. B., "Enhanced Oil Recovery Through the Use of Chemicals—Part 2," *J. Pet. Tech.* (Oct. 1983), pp. 1767-1775.
394. Taber, J. J., "Enhanced Recovery Methods for Heavy and Light Oils," *Proc., International Conference on Heavy Versus Light Oils: Technical Issues and Economic Considerations*, Colorado Springs, March 24-26, 1982.
395. Holm, L. W., and Josendal, V. A., "Effect of Oil Composition on Miscible Type Displacement by Carbon Dioxide," *Soc. Pet. Eng. J.* (Feb. 1982), pp. 87-98.
396. Orr, F. M., Jr., and Jensen, C. M., "Interpretation of Pressure-Composition Phase Diagrams for CO₂-Crude Oil Systems," paper SPE 11125 presented at SPE 57th Annual Fall Technical Conf. and Exhibition, New Orleans, Sept. 26-29, 1982.
397. Helier, J. P., and Taber, J. J., "Influence of Reservoir Depth on Enhanced Oil Recovery by CO₂ Flooding," paper SPE 15001 presented at the 1986 SPE Permian Basin Oil & Gas Recovery Conference, Midland, March 13-14.
398. Chu, C., "Current In-Situ Combustion Technology," *J. Pet. Tech.* (Aug. 1983), pp. 1412-1418.
399. Chu, C., "State-of-the-Art Review of Fireflood Field Projects," *J. Pet. Tech.* (Jan. 1982), pp. 19-36.
400. Chu, C., "State-of-the-Art Review of Steamflood Field Projects," *J. Pet. Tech.* (Oct. 1985), pp. 1887-1902.
401. White, P. D., "In-Situ Combustion Appraisal and Status," *J. Pet. Tech.* (Nov. 1985), pp. 1943-1949.
402. Garon, A. M., Kumar, M., and Cala, G. C., "The State of the Art Oxygen Fireflooding," *In Situ*, Vol. 10, No. 1 (1986), pp. 1-26.
403. Leonard, J., "Increased Rate of EOR Brightens Outlook," *Oil & Gas J.* (April 14, 1986), pp. 71-101.
404. Reid, R. B., and Robinson, J. J., "Lick Creek Meakin Sand Unit Immiscible CO₂/Waterflood Project," *J. Pet. Tech.* (Sept. 1981), pp. 1723-1729.
405. Agnew, H. J., "Here's How 56 Polymer Oil-Recovery Projects Shape Up," *Oil & Gas J.* (May 1972), pp. 109-112.

Production Engineering

Michael Economides, Ph.D.

Texas A&M University
College Station, Texas

Kazimierz Glowacki, Ph.D.

Consultant
Energy and Environmental Engineering
Krakow, Poland

Reza G. Kashmiri

International Lubrication and Fuel, Inc.
Rio Rancho, New Mexico

Joseph V. LaBlanc

Consultant, Petroleum Engineering
Conroe, Texas

Julius P. Langlinais, Ph.D.

Louisiana State University
Baton Rouge, Louisiana

Charles Nathan, Ph.D., P.E.

Consultant
Corrosion Engineering
Houston, Texas

Floyd Preston, Ph.D.

University of Kansas
Lawrence, Kansas

Chris S. Russell, P.E.

Consultant
Environmental Engineering
Las Cruces, New Mexico

Oleg Salzberg

Consultant
Corrosion Engineering
Houston, Texas

Ardeshir K. Shahraki, Ph.D.

Dwight's Energy Data, Inc.
Richardson, Texas

Pudji Permadi, Ph.D.

Institut Teknologi Bandung
Bandung, Indonesia

Properties of Hydrocarbon Mixtures	365
Compressibility Factor and Phase Behavior 365. Classification of Hydrocarbon Fluids 372.	
Reservoir Conditions Phase Behavior 374. Sampling Process and Laboratory Measurements 380.	
Vapor-Liquid Equilibrium by Equation of State 413.	
Flow of Fluids	426
Basic Parameters of Multiphase Flow 432. Stratified Flow Regime 449. Annular Flow Regime 471.	
Slug Flow Regime 478. Bubbly Flow Regime 481. Correction for Acceleration Effects 483.	
Limitation 484. Semi-empirical Methods 488.	
Natural Flow Performance	533
Oil Flow Performances 534. Gas Flow Performances 544. Two-Phase Flow Performance 561.	
Artificial Lift Methods	594
Sucker Rod Pumping 594. Gas Lift 642. Oil Well Jet Pumps 658. Electrical Submersible Pumps 662.	
Stimulation and Remedial Operations	664
Fracturing 665. Matrix Stimulation 696.	
Surface Oil Production Systems	702
Nomenclature of Separating Vessels 702. Storage Classification 705. Phase Separation 705.	
Separator Design and Construction 709. Gas-Oil-Water Separation 722. Two-Stage Separation Systems 731. Crude Oil Treating Systems 733.	
Gas Production Engineering	754
Gas-Water Systems and Dehydration Methods 754. Gas Flow Measurement 799. Compressor Stations 847. Gas Piping System 868. Gas Cooling 871.	

364 Production Engineering

Corrosion and Scaling **889**
Production Operations 889. Hydrogen Sulfide Corrosion 891. Carbon Dioxide Corrosion 892.
Recommended Procedures for Corrosion Control 923. Transportation and Storage Equipment 924.

Environmental Considerations **939**
Hydrocarbon Contamination 939. Production Site Remediation 948. Produced Water 954.
Class II Injection Wells 961.

Offshore Operations **964**
Primary Considerations 965. Environmental Considerations 966. Geographical Considerations 966.
Operational and Design Considerations 967. Safety Shut-Down Systems 968. Flare and Emergency
Relief Systems 968. Ventilation 969. Transportation 969. Pollution Prevention 969. Regulatory
Agencies 970.

References **971**

6

Production Engineering

PROPERTIES OF HYDROCARBON MIXTURES

This section contains correlation and procedures for the prediction of physical properties of natural gas and oil. Physical constants of single components are given in Table 6-1.

Compressibility Factor and Phase Behavior

The compressibility factor Z is a dimensionless factor independent of the quantity of gas and determined by the character of the gas, the temperature, and pressure.

$$Z = \frac{PV}{nRT} = \frac{MPV}{mRT} \quad (6-1)$$

	Field Units	SI Units
P = absolute pressure	psia	kPa
V = volume	ft ³	m ³
n = moles	m/M	m/M
m = mass	lb	kg
M = molecular mass	lb/lb mole	kg/kmole
T = absolute temperature	°R	K
R = universal gas constant	10.73 [psia • ft ³ /°R • lb mole mole]	8.3145 [kPa m ³ /kmol • K]
ρ = density	slug/ft ³	kg/m ³

A knowledge of the compressibility factor means that the density ρ is also known from the relationship

$$\rho = \frac{PM}{ZRT} \quad (6-2)$$

Compressibility Factor Using the Principle of Corresponding States (CSP)

The following terms are used, P_r , T_r and V_r , such that

$$P_r = \frac{P}{P_c}, \quad T_r = \frac{T}{T_c}, \quad V_r = \frac{V}{V_c} \quad (6-3)$$

where P_r , T_r and V_r = reduced parameters of pressure, temperature and volume
 P_c , T_c and V_c = critical parameters of P , T and V from Table 6-1

(text continued on page 368)

Table 6-1
Physical Constants of Hydrocarbons

PHYSICAL CONSTANTS OF HYDROCARBONS									
No.	Compound	Formula	1.	2.	3.	Critical constants			
						Molecular mass	Boiling point, °C (101.325 kPa)	Vapor pressure, kPa (atm) 40°C	Freezing point, °C (101.325 kPa)
1	Methane	CH ₄	16.043	-161.5(228)	936 000.	-182.47 ^a	4 604	190.55	0.008 17
2	Ethane	C ₂ H ₆	30.070	-88.56	(9 000.)	-182.60 ^a	4 850.	306.49	0.004 92
3	Propane	C ₃ H ₈	44.097	-42.07	1 341.	-187.98 ^a	4 248.	399.82	0.004 80
4	n-Butane	C ₄ H ₁₀	58.124	-0.49	377.	-138.36	3 797.	425.18	0.004 59
5	Isobutane	C ₄ H ₁₀	58.124	-11.81	535.	-129.80	3 645.	426.13	0.004 52
6	n-Pentane	C ₅ H ₁₂	72.151	36.06	116.69	-128.73	3 395.	459.6	0.004 21
7	Isopentane	C ₅ H ₁₂	72.151	27.84	161.3	-129.60	3 381.	460.29	0.004 24
8	Neopentane	C ₅ H ₁₂	72.151	9.50	288.	-128.55	3 198.	433.76	0.004 20
9	n-Hexane	C ₆ H ₁₄	86.178	68.74	37.29	-95.32	3 012.	507.4	0.004 29
10	2-Methylpentane	C ₆ H ₁₄	86.178	60.23	50.58	-103.99	3 010.	497.45	0.004 26
11	3-Methylpentane	C ₆ H ₁₄	86.178	63.27	48.73	-104.24	3 194.	504.4	0.004 26
12	Neohexane	C ₆ H ₁₄	86.178	48.73	73.41	-99.870	3 081.	488.73	0.004 17
13	2,2-Dimethylbutane	C ₆ H ₁₄	86.178	67.99	55.34	-128.64	3 127.	489.93	0.004 15
14	n-Heptane	C ₇ H ₁₆	100.205	98.42	12.34	-60.682	2 736.	540.2	0.004 31
15	2-Methylhexane	C ₇ H ₁₆	100.205	90.05	17.22	-118.27	2 734.	530.31	0.004 20
16	3-Methylhexane	C ₇ H ₁₆	100.205	91.24	16.16	-119.60	2 814.	535.19	0.004 05
17	3-Ethylpentane	C ₇ H ₁₆	100.205	93.48	15.27	-119.60	2 691.	540.57	0.004 15
18	2,2-Dimethylpentane	C ₇ H ₁₆	100.205	79.19	26.32	-123.81	2 773.	520.44	0.004 17
19	2,4-Dimethylpentane	C ₇ H ₁₆	100.205	80.48	24.84	-119.24	2 737.	518.73	0.004 16
20	3,5-Dimethylpentane	C ₇ H ₁₆	100.205	85.08	20.98	-134.46	2 844.	538.34	0.004 19
21	Triptane	C ₇ H ₁₆	100.205	80.88	25.40	-24.81	2 954.	531.11	0.003 97
22	n-Octane	C ₈ H ₁₈	114.232	125.67	4.148	-58.76	2 486.	595.76	0.004 31
23	Diisobutyl	C ₈ H ₁₈	114.232	109.11	8.417	-61.200	2 486.	548.98	0.004 22
24	Isooctane	C ₈ H ₁₈	114.232	99.24	12.90	-107.36	2 665.	543.89	0.004 10
25	n-Nonane	C ₉ H ₂₀	128.259	160.62	1.40	-33.49	2 235.	634.59	0.004 27
26	n-Decane	C ₁₀ H ₂₂	142.286	174.16	0.4732	-29.84	2 099.	617.4	0.004 24
27	Cyclopentane	C ₅ H ₁₀	70.135	48.25	73.97	-63.868	4 602.	611.0	0.003 71
28	Methylcyclopentane	C ₆ H ₁₂	84.162	71.91	33.25	-142.48	3 785.	632.73	0.003 79
29	Cyclohexane	C ₆ H ₁₂	84.162	60.73	24.93	-93.54	4 074.	633.5	0.003 65
30	Methylcyclohexane	C ₇ H ₁₄	98.189	100.93	12.213	-128.59	3 472.	572.12	0.003 75
31	Ethane (Ethylene)	C ₂ H ₄	28.054	-103.77(29)	—	-169.15 ^a	5 041.	282.26	0.004 67
32	Propane (Propylene)	C ₃ H ₆	42.061	-47.72	1 696.	-185.85 ^a	4 800.	364.85	0.004 30
33	1-Butene (Butylene)	C ₄ H ₈	56.106	-6.32	451.9	-185.39 ^a	4 025.	419.63	0.004 28
34	cis-2-Butene	C ₄ H ₈	56.106	3.72	357.8	-139.81	4 233.	453.65	0.004 17
35	trans-2-Butene	C ₄ H ₈	56.106	0.58	365.8	-108.59	4 047.	428.83	0.004 24
36	Isobutene	C ₄ H ₈	56.106	-6.91	452.3	-140.36	3 698.	417.80	0.004 26
37	1-Pentene	C ₅ H ₁₀	70.138	26.96	141.85	-160.22	3 629.	484.78	0.004 22
38	1,2-Butadiene	C ₄ H ₆	54.092	10.55	225.	-125.19	(4 200.)	(444.)	(0.004 05)
39	1,3-Butadiene	C ₄ H ₆	54.092	-4.41	434.	-108.81	6 350.	425.	0.004 09
40	Isoprene	C ₅ H ₈	68.119	34.07	123.77	-146.95	(3 850.)	(484.)	(0.004 06)
41	Acetylene	C ₂ H ₂	26.038	-84.69 ^a	—	-80.9 ^a	6 139.	308.33	0.004 84
42	Benzene	C ₆ H ₆	78.114	80.09	24.38	5.933	4 896.	562.16	0.003 28
43	Toluene	C ₇ H ₈	92.141	110.63	7.265	-94.991	4 105.	591.90	0.003 45
44	Ethylbenzene	C ₈ H ₁₀	106.168	136.20	2.87	-94.975	3 609.	617.20	0.003 83
45	o-Xylene	C ₈ H ₁₀	106.168	144.43	2.08	-25.18	3 734.	580.33	0.003 49
46	m-Xylene	C ₈ H ₁₀	106.168	136.12	2.83	-47.67	3 535.	617.05	0.003 64
47	p-Xylene	C ₈ H ₁₀	106.168	136.26	2.85	13.26	3 511.	616.53	0.003 66
48	Styrene	C ₈ H ₈	104.122	145.14	1.85	-30.61	3 925.	647.9	0.003 38
49	Isopropylbenzene	C ₉ H ₁₂	120.195	152.41	1.47	-96.035	3 209.	631.1	0.003 57
50	Methyl alcohol	CH ₃ O	32.042	64.54	38.43	-97.06	8 069.	612.64	0.003 66
51	Ethyl alcohol	C ₂ H ₅ O	46.069	78.29	17.70	-114.1	6 383.	613.92	0.003 62
52	Carbon monoxide	CO	28.010	-191.49	—	-252.0 ^a	5 499.(30)	(32.62(33))	(0.003 39(33))
53	Carbon dioxide	CO ₂	44.010	-78.51 ^a	—	-88.67 ^a	7 382.(28)	(304.19(33))	(0.002 14(33))
54	Hydrogen sulfide	H ₂ S	34.076	-60.31	2 961.	-88.58 ^a	9 005.	373.5	0.002 87
55	Sulfur dioxide	SO ₂	64.069	-10.02	630.8	-76.48 ^a	7 804.	430.9	0.001 90
56	Ammonia	NH ₃	17.031	-33.33(30)	1 613.	-77.74 ^a	11 290.	406.6	0.004 25
57	Air	N ₂ + O ₂	28.964	-181.2(2)	—	—	8 777.(2)	132.4(2)	0.003 29(3)
58	Hydrogen	H ₂	2.016	-252.87 ^a	—	-252.9 ^a	1 267.	33.	0.003 24
59	Oxygen	O ₂	31.999	-182.962 ^a	—	-218.9 ^a	5 061.	154.7(33)	0.002 29
60	Nitrogen	N ₂	28.013	-169.80(31)	—	-210.0 ^a	3 399.	128.1	0.003 22
61	Chlorine	Cl ₂	70.908	-34.03	1 134.	-101.0 ^a	7 711.	417.	0.001 76
62	Water	H ₂ O	18.015	100.00 ^a	—	—	22 118.	647.3	0.003 10
63	Helium	He	4.003	-268.93(32)	—	—	227.5(32)	5.2(32)	0.014 36(32)
64	Hydrogen chloride	HCl	36.461	-85.00	6 304.	-114.19 ^a	8 309.	324.7	0.002 22

NOTES

- a Air saturated liquid.
- b Absolute values from weights in vacuum.
- c The apparent values from weight in air are shown for users' convenience and compliance with ASTM-IP Petroleum Measurement Tables. In the United States and Great Britain, all commercial weights are required by law to be weights in air. All other mass data are on an absolute mass (weight in vacuum) basis.
- d At saturation pressure (triple point).
- e Sublimation point.
- f The + sign and number following signify the ASTM octane number corresponding to that of 2,2,4-trimethylpentane with the indicated number of cm³ of TEL added per gal.
- g Determined at 100°C.
- h Saturation pressure and 15°C.
- i Apparent value at 15°C.
- l Average value from octane numbers of more than one sample.
- k Relative density (specific gravity), 48.3°C/15°C (sublimation point; solid C₂H₂/liquid H₂O).

- m Densities of liquid at the boiling point.
- n Heat of sublimation.
- p See Note 10.
- s Extrapolated to room temperature from higher temperature.
- t Gross calorific values shown for ideal gas volumes are not direct conversions of each other using only the gas volume per liquid volume value shown herein. The values differ by the heat of vaporization to ideal gas at 288.15 K.
- v Fixed points on the 1968 International Practical Temperature Scale (IPTS-68).
- w Value for normal hydrogen (25% para, 75% ortho). The value for equilibrium mixtures of para and ortho is -0.218; however, in most correlations, 0 is used.
- x Densities at the boiling point in kg/m³ for: Ethane, 548.4; propane, 581.0; propene, 608.8; hydrogen sulfide, 960.; sulfur dioxide, 1482.; ammonia, 681.8; hydrogen chloride, 1192.
- * Calculated values.
- () Estimated values.
- † Values are estimated using 2nd virial coefficients.

Table 6-1
(continued)

PHYSICAL CONSTANTS OF HYDROCARBONS																
4.					5.		6.		7.		8.			9.		No.
Density of liquid 101.3250 kPa (aba), 15°C					Temperature coefficient of density, 1/°C	Phase transition factor, α	Compressibility factor at liquid sat. Z _l 101.3250 kPa (aba), 15°C	Ideal gas* 101.3250 kPa (aba), 15°C			Specific heat capacity 101.3250 kPa (aba), 15°C					
Relative density 15°C/15°C	kg/m ³ (lbm/ft ³)	kg/m ³ (lbm/ft ³)	kg/m ³ (lbm/ft ³)	kg/m ³ (lbm/ft ³)				Relative density at 15°C	Specific volume m ³ /kg	Volume ratio gas/liquid at liquid sat. (v/v)	Ideal gas C _p , kJ/(kg·°C)	Liquid C _p , kJ/(kg·°C)				
0.37	500.7	500.7	0.005	—	0.0126	0.6961	0.6539	1.474	0.6539	2.204	—	1				
0.551 ³	357.8 ³	356.6 ³	0.004 04 ³	—	0.0876	0.8615	1.0362	0.7893	281.3 ³	1.705	3.907	2				
0.5083 ³	507.5 ³	508.7 ³	0.008 84 ³	—	0.1541	0.9610	1.6225	0.5362	272.3 ³	1.626	2.478	3				
0.5947 ³	564.2 ³	563.1 ³	0.009 43 ³	0.002 11 ³	0.2015	1.0441	2.0068	0.4368	227.7 ³	1.822	2.968(41)	4				
0.5537 ³	653.2 ³	652.1 ³	0.103 23 ³	0.002 14 ³	0.1540	0.9665	2.0068	0.4368	225.1 ³	1.816	2.968(41)	5				
0.5316	631.0	629.8	0.114 8	0.001 67	0.2524	0.9427	2.4911	0.3277	206.8	1.822	2.922(41)	6				
0.6250	624.4	623.3	0.115 6	0.001 82	0.2286	0.9461	2.4911	0.3277	204.8	1.800	2.237	7				
0.5972 ²	608.7 ²	606.6 ²	0.120 6 ²	0.001 87 ²	0.1987	0.8536	2.4911	0.3277	186.3 ²	1.624	2.137	8				
0.6844	693.5	692.7	0.129 0	0.001 35	0.2586	0.8101	2.9763	0.2744	182.1	1.613	2.231	9				
0.6583	657.7	656.9	0.131 0	0.001 40	0.2734	—	2.9763	0.2744	160.5	1.632	2.205	10				
0.6894	698.6	697.7	0.128 9	0.001 35	0.2741	—	2.9763	0.2744	163.5	1.673	2.170	11				
0.6845	693.9	692.6	0.131 8	0.001 40	0.2933	—	2.9763	0.2744	179.4	1.593	2.146	12				
0.6868	696.2	695.1	0.129 4	0.001 35	0.2476	—	2.9763	0.2744	182.8	1.596	2.145	13				
0.6886	696.0	695.6	0.145 6	0.001 24	0.3404	0.6021	3.4906	0.2390	162.4	1.608	2.206	14				
0.6835	692.8	691.7	0.148 6	0.001 22	0.3629	—	3.4906	0.2390	161.1	1.586	2.193	15				
0.6821	691.6	690.4	0.144 6	0.001 24	0.3299	—	3.4906	0.2390	163.2	1.584	2.137	16				
0.7032	702.8	701.5	0.142 8	0.001 28	0.3107	—	3.4906	0.2390	165.8	1.613	2.150	17				
0.6767 ²	678.0	676.9	0.147 6	0.001 30	0.2876	—	3.4906	0.2390	160.0	1.613	2.181	18				
0.7177	677.1	676.0	0.148 0	0.001 30	0.3291	—	3.4906	0.2390	159.8	1.651	2.193	19				
0.6650	667.4	666.3	0.143 7	0.001 17	0.2681	—	3.4906	0.2390	164.8	1.603	2.098	20				
0.6860	684.4	683.3	0.144 3	0.001 24	0.2509	—	3.4906	0.2390	163.0	1.578	2.086	21				
0.7073	708.7	706.6	0.161 8	0.001 12	0.3691	0.7037	3.9439	0.2070	146.5	1.601	2.191	22				
0.6864	687.7	686.6	0.163 7	0.001 17	0.3354	—	3.9439	0.2070	144.4	1.573	2.136	23				
0.6866	686.0	684.9	0.164 1	0.001 17	0.3241	—	3.9439	0.2070	144.1	1.599	2.049	24				
0.7224	721.7	720.6	0.177 7	0.001 18	0.4462	—	4.4282	0.1843	133.0	1.586	2.184	25				
0.7346	733.9	732.6	0.169 9	0.000 96	0.4904	—	4.9125	0.1882	122.0	1.589	2.179	26				
0.7506	746.1	745.1	0.083 4 ⁴	0.001 23	0.1946	0.8491	2.4216	0.3371	252.9	1.133	1.763	27				
0.7547	753.4	752.3	0.111 7	0.001 39	0.2938	—	2.4216	0.3371	211.7	1.286	1.843	28				
0.7838	783.1	782.0	0.107 8	0.001 22	0.2098	—	2.9057	0.2808	220.0	1.211	1.911	29				
0.7744	773.7	772.6	0.120 9	0.001 13	0.2984	—	3.3000	0.2406	186.3	1.324	1.839	30				
0.8231	822.5 ²	821.4 ²	0.090 8 ²	0.003 40 ²	0.1443	0.9699	0.9696	0.6423	—	1.614	—	31				
0.6016 ³	601.4 ³	600.3 ³	0.083 3 ³	0.002 09 ³	0.1949	0.9703	1.4529	0.5919	293.9 ³	1.480	2.443	32				
0.6277 ³	627.1 ³	626.0 ³	0.096 4 ³	0.001 76 ³	0.2033	0.9600	1.8372	0.4214	263.4 ³	1.483	2.237	33				
0.6106 ³	610.2 ³	609.1 ³	0.091 9 ³	0.001 62 ³	0.2129	0.9661	1.8372	0.4214	297.1 ³	1.629	2.236	35				
0.6017 ³	602.9 ³	601.8 ³	0.093 4 ³	0.001 69 ³	0.2028	0.9698	1.8372	0.4214	263.1 ³	1.547	2.296	36				
0.6462	845.5	844.4	0.108 6	0.001 80	0.2334	0.9487	2.4316	0.3371	217.7	1.619	2.241(43)	37				
0.6679 ²	857.4	856.3	0.082 3 ²	0.001 76 ²	0.2840	0.8489	1.8676	0.4371	397.5 ²	1.446	2.262	38				
0.6280 ³	627.4 ³	626.3 ³	0.098 1 ³	0.002 09 ³	0.1971	0.9665	1.8676	0.4371	274.2 ³	1.420	2.134	39				
0.6886	688.0	686.9	0.099 30	0.001 56	0.1567	0.9491	2.3519	0.3471	236.1	1.492	2.171	40				
0.811 ²	—	—	—	—	0.1583	0.9425	0.2990	0.9081	—	1.699	—	41				
0.8650	864.2	863.1	0.088 34	0.001 19	0.2095	0.9297	2.9669	0.3037	267.8	1.014	1.715	42				
0.8723	871.6	870.6	0.106 7	0.001 06	0.2633	0.9031	3.1812	0.2568	223.7	1.086	1.877	43				
0.8721	871.3	870.3	0.121 9	0.000 97	0.3631	—	3.9965	0.2327	194.0	1.189	1.721	44				
0.8660	864.2	863.1	0.120 1	0.000 96	0.3113	—	3.9965	0.2327	189.8	1.216	1.741	45				
0.8661	868.3	867.2	0.122 3	0.000 97	0.3257	—	3.9655	0.2327	193.4	1.193	1.996	46				
0.8661	865.3	864.2	0.122 7	0.000 97	0.3214	—	3.9655	0.2327	192.7	1.167	1.708	47				
0.8116	910.6	909.5	0.114 4	0.001 03	0.1987	—	3.9969	0.2320	206.7	1.193	1.734	48				
0.8667	868.0	866.9	0.109 0	0.000 97	0.3230	—	4.1468	0.1967	170.4	1.219	1.732	49				
0.7967	796.0	794.9	0.040 26	0.001 17	0.2648	—	1.1093	0.7379	567.4	1.322	2.484	50				
0.7922	791.5	790.4	0.066 20	0.001 07	0.6908	—	1.6906	0.6132	408.2	1.369	2.548	51				
0.7893 ²	788.6 ² (34)	—	0.058 52	—	0.0442	0.9695	0.9671	0.8441	—	1.040	—	52				
0.8229 ²	821.9 ² (36)	820.8 ²	0.053 9 ²	—	0.2867	0.8643	1.6196	0.5373	444.7 ²	0.8390	—	53				
0.7927 ²	793.0 ² (36)	791.9 ²	0.043 1 ²	—	0.0620	0.8603	1.1795	0.6939	547.5 ²	0.9660	2.08(26)	54				
1.267 ²	1398.2 ² (36)	1396.7 ²	0.046 8 ²	—	0.2648	0.8601 ¹	2.2117	0.3691	515.3 ²	0.6062	1.369(26)	55				
0.6163 ³	617.7 ³ (30)	616.6 ³	0.027 87 ³	—	0.2676	0.8699(30)	0.6900	1.368	857.4	0.709	4.069(30)	56				
0.8269 ³ (36)	898.7 ³	—	0.033 3 ³	—	—	0.9696	1.0000	0.8163	—	1.005	—	57				
0.0719 ³	71.0 ³ (37)	—	0.023 39 ³	—	-0.210 ³	1.0008	0.0096	11.73	—	14.24	—	58				
1.1422 ² (23)	1141.1 ² (38)	—	0.028 04 ²	—	0.0200	0.9698(38)	1.1048	0.7389	—	0.9166	—	59				
0.8069 ² (26)	808.9 ² (31)	—	0.034 64 ²	—	0.0372	0.8997	0.9872	0.8441	—	1.040	—	60				
1.429	1424.5	1423.5	0.049 78	—	0.0737	0.9879 ² (38)	2.4481	0.3399	473.0	0.4760	—	61				
1.000	999.1	998.0	0.016 03	0.000 14	0.3494	—	0.3220	1.312	1511.	1.669	4.191	62				
0.1261 ²	126.0 ² (32)	—	0.032 02 ²	—	0	1.000 5(40)	0.1382	0.507	—	0.192	—	63				
0.8536	853.6 ²	851.9	0.042 74	0.006 03	0.1282	—	1.2598	0.6486	663.2	0.7961	—	64				

- Molecular mass (M) is based on the following atomic weights: C = 12.011; H = 1.008; O = 15.9995; N = 14.0067; S = 32.06; Cl = 35.453.
- Boiling point—the temperature at equilibrium between the liquid and vapor phases at 101.3250 kPa (aba).
- Freezing point—the temperature at equilibrium between the crystalline phase and the air saturated liquid at 101.3250 kPa (aba).
- All values for the density and molar volume of liquids refer to the air saturated liquid at 101.3250 kPa (aba), except when the boiling

volume—cubic meter, m³
 pressure—Pascal, Pa (1 Pa = N/m²)
 Physical constants for molar volume = 22.41383 ± 0.00031
 gas constant, R = 8.31441 J/(K ° mol)
 8.31441 × 10⁻⁸ m³ ° KPa/(K ° mol)
 1.98719 cal/(K ° mol)
 1.98599 Btu(IT)²/R ° lb-mol

Conversion factors
 1 m³ = 35.31487 ft³ = 264.1720 gal
 1 kg = 2.204823 lb
 1 kg/m³ = 0.08242795 lb/ft³ = 0.001 g/cm³
 1 kPa = 0.01 bar = 9.869233 × 10⁻⁸ atm
 = 0.1450377 lb/in²
 1 atm = 101.3250 kPa = 14.69595 lb/in²
 = 760 Torr
 1 kJ = 0.2390057 kcal(thermochemical)
 = 0.2388459 kcal(IT)
 = 0.9478171 Btu(IT)

COMMENTS
 Units—all dimensional values are reported in SI units, which are derived from the following basic units:
 mass—kilogram, kg
 length—meter, m
 temperature—International Practical Temperature Scale of 1988 (IPTS-88), where 0°C = 273.15 K
 Other derived units are:

see Rosini, F. D. "Fundamental Measures and Constants for Science and Technology"; CRC Press: Cleveland, Ohio, 1974.

(text continued from page 365)

Compressibility factors of many components are available as a function of pressure in most handbooks [1,2]. In application of CSP to a mixture of gases, pseudocritical temperature (T_{pc}) and pressure (P_{pc}) are defined for use in place of the true T_c and P_c to determine the compressibility factor for a mixture.

$$P_{pc} = \sum y_i P_{ci}, \quad T_{pc} = \sum y_i T_{ci} \tag{6-4}$$

$$P_{pr} = P/P_{pc}, \quad T_{pr} = T/T_{pc} \tag{6-5}$$

where subscript i = component in the gas mixture

y_i = mole fraction of component "i" in the gas mixture

For given values of P_{pr} and T_{pr} , compressibility factor Z can be determined from Figure 6-1. If a gas mixture contains significant concentrations of carbon dioxide and hydrogen sulfide, then corrected pseudocritical constants (T'_{pc} , P'_{pc}) are defined as follows:

$$T'_{pc} = T_{pc} - e \tag{6-6}$$

$$P'_{pc} = \frac{P_{pc} T'_{pc}}{T_{pc} + y_{H_2S}(1 - y_{H_2S})e} \tag{6-7}$$

where

$$e = 120[(y_{CO_2} + y_{H_2S})^{0.9} - (y_{CO_2} + y_{H_2S})^{1.6}] + 15(y_{H_2S}^{0.5} - y_{H_2S}^{4.0}) \tag{6-8}$$

where y_{CO_2} , y_{H_2S} = mole fraction of CO_2 and H_2S in mixture

Direct Calculation of Z Factors

The Hall-Yarborough equation is one of the best:

$$Z = \frac{0.06125P_{pr} t \exp[-1.2(1-t)^2]}{y} \tag{6-9}$$

where: P_{pr} = the pseudoreduced pressure

t = the reciprocal, pseudoreduced temperature T_{pc}/T

y = the reduced density which can be obtained as the solution of the equation

$$\begin{aligned} & -0.06125P_{pr} t \exp[-1.2(1-t)^2] + \frac{y + y^2 + y^3 - y^4}{(1-y)^3} \\ & - (14.76t - 9.76t^2 + 4.58t^3)y^2 \\ & + (90.7t - 24.2t^2 + 42.4t^3)y^{(2.18+2.82t)} = 0 \end{aligned} \tag{6-10}$$

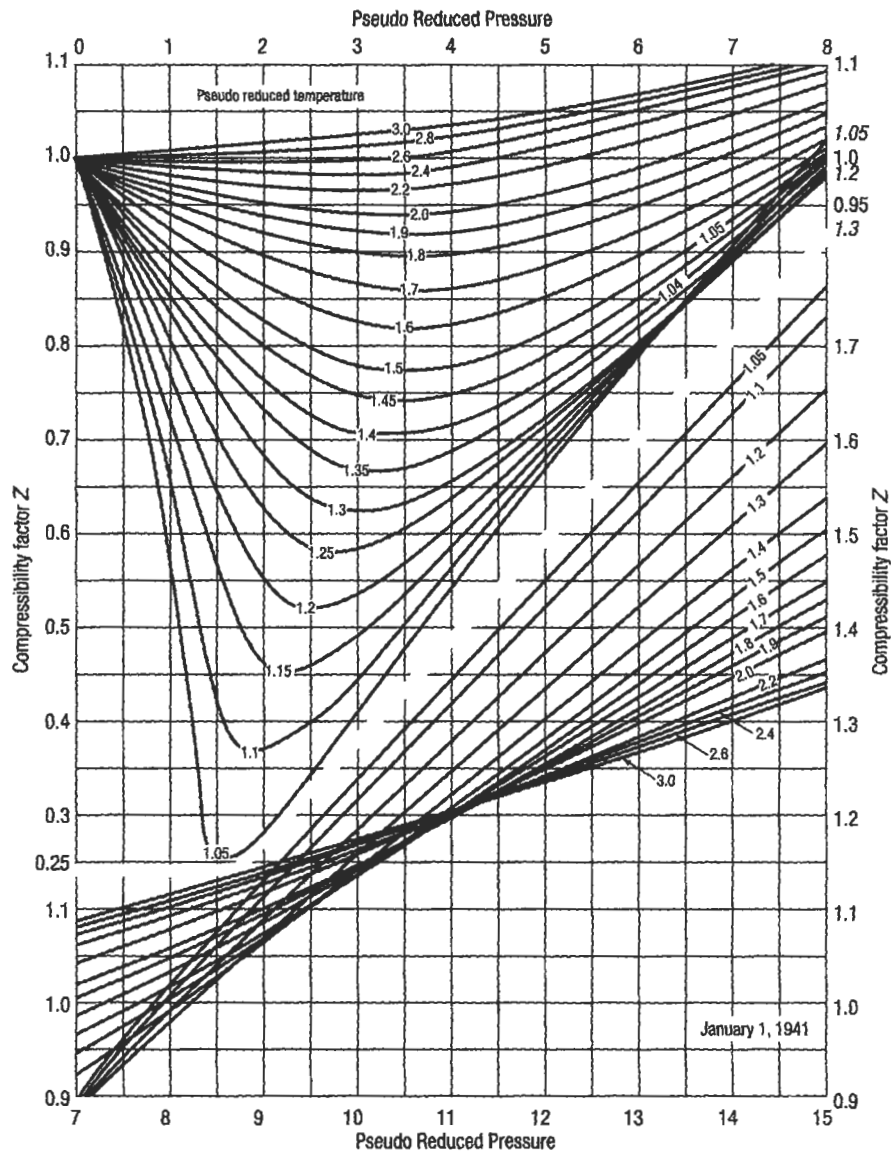


Figure 6-1. Compressibility factor for natural gases [1].

This nonlinear equation can be conveniently solved for y using the simple Newton-Raphson iterative technique.

Good results give cubic equation of state and its modifications. Most significant of the modifications are those of Soave and Peng and Robinson.

The Soave equation (SRK) is

$$P = \frac{RT}{V - b} - \frac{a}{V(V + b)} \tag{6-11}$$

$$Z^3 = Z^2 + (A - B - B^2)Z - AB = 0 \quad (6-12)$$

where $b = \sum x_i b_i$ for a mixture

$$b_i = 0.08664RT_{ci}/P_{ci} \text{ for a single component}$$

$$a = \sum_i \sum_j x_i x_j (a_i a_j)^{0.5} (1 - k_{ij}) \text{ for a mixture}$$

$$a_i = a_{ci} \alpha_i \text{ for a single component}$$

$$a_{ci} = 0.42748(RT_{ci})^2/P_{ci}$$

$$\alpha_i^{0.5} = 1 + m_i(1 - T_{ci}^{0.5})$$

$$m_i = 0.48 + 1.574\omega_i - 0.176\omega_i^2$$

$$A = aP/(RT)^2, \quad B = bP/RT$$

The Peng-Robinson equation (PR) is

$$P = \frac{RT}{V - b} - \frac{a}{V(V + b) + b(V - b)} \quad (6-13)$$

$$Z^3 - (1 - B)Z^2 + (A - 2B - 3B^2)Z - (AB - B^2 - B^3) = 0 \quad (6-14)$$

where $b = \sum x_i b_i$

$$b_i = 0.077796RT_{ci}/P_{ci}$$

$$a = \sum_i \sum_j x_i x_j (a_i a_j)^{0.5} (1 - k_{ij})$$

$$a_i = a_{ci} \alpha_i$$

$$a_{ci} = 0.457237(RT_{ci})^2/P_{ci}$$

$$\alpha_i^{0.5} = 1 + m_i(1 - T_{ci}^{0.5})$$

$$m_i = 0.37646 + 1.54226\omega_i - 0.26992\omega_i^2$$

$$A, B \text{ as in SRK equation}$$

where P = pressure (absolute units)

T = temperature ($^{\circ}R$ or K)

R = universal gas constant

Z = compressibility factor

ω = acentric Pitzer factor (see Table 6-1)

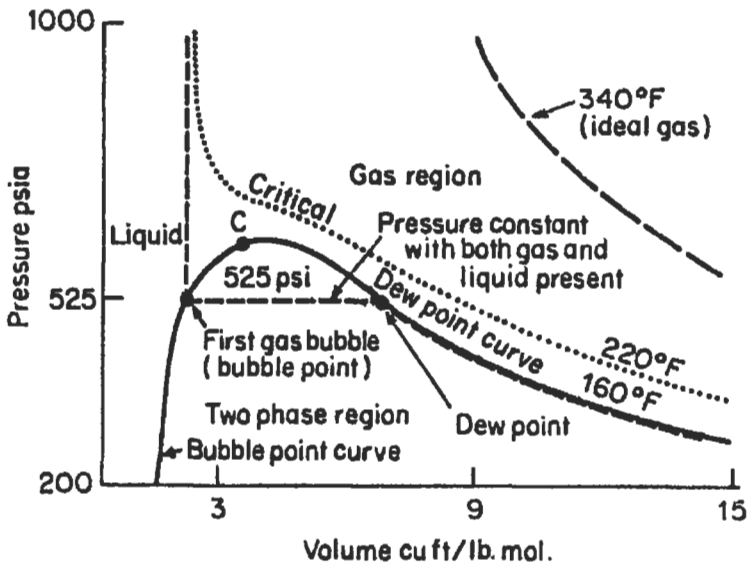
T_{ci} , P_{ci} = critical parameters (see Table 6-1)

k_{ij} = interaction coefficient (= 0 for gas phase mixture)

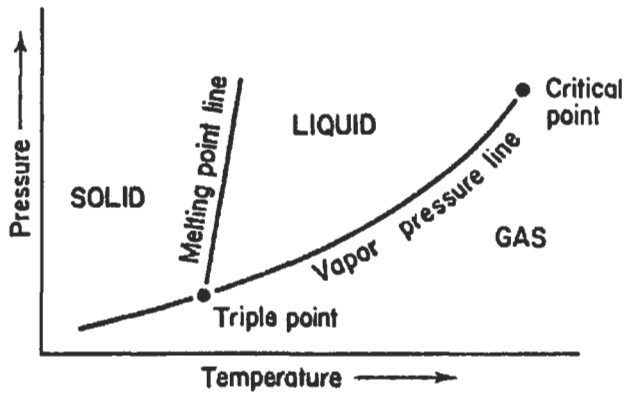
Both SRK and PR equations are used to predict equilibrium constant K value. See derivation of vapor-liquid equilibrium by equation of state at end of this subsection.

Full description of gas, oil and water properties are given in Chapter 5, "Reservoir Engineering." Reservoir hydrocarbon fluids are a mixture of hydrocarbons with compositions related to source, history and present reservoir conditions. Consider the pressure-specific volume relationship for a single-component fluid at constant temperature, below its critical temperature initially hold in the liquid phase at an elevated pressure. This situation is illustrated in Figure 6-2. Bubble point and dew point curves in Figure 6-2a correspond to the vapor pressure line in Figure 6-2b. A locus of bubble points and a locus of dew points that meet at a point C (the critical point) indicate that the properties of liquid and vapor become indistinguishable.

Multicomponent systems have different phase behavior than pure component. In the P - T diagram instead of the vapor-pressure line we have an area limited by saturation line (bubble point + dew point), see Figure 6-3. The diagram's shape is more or less the same for two or three-component systems as for multicomponent



(a)



(b)

Figure 6-2. Phase diagram for a single component.

systems. For isothermal production in the reservoir, position A indicates reservoir fluid found as an undersaturated oil, position B indicates reservoir fluid found as a gas condensate and position C indicates reservoir fluid found as a dry gas. Expansion in the liquid phase to the bubble point at constant temperature is similar to a pure component system. Expansion through the two-phase region does not occur at constant pressure, but is accompanied by a decrease in pressure as the composition of liquid and vapor changes.

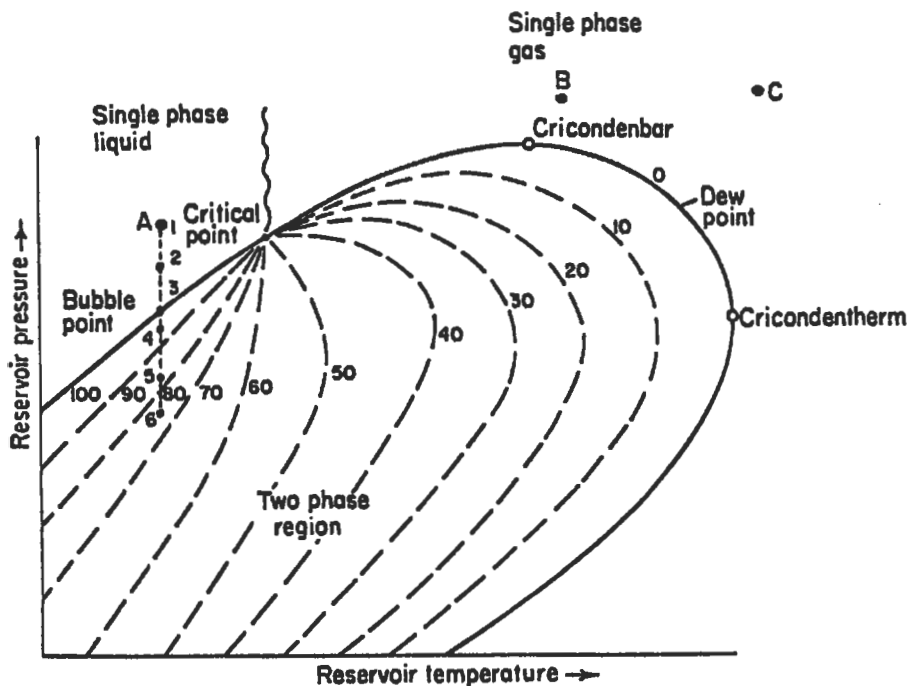


Figure 6-3. Pressure-temperature diagram for reservoir fluids.

Classification of Hydrocarbon Fluids

Hydrocarbon fluids usually are classified as to the phase behavior exhibited by the mixture. Figure 6-4 shows the pressure-temperature phase diagram of the four general classifications of fluids: dry gas, gas condensate, volatile oil and black oil. As it can be seen, the source temperature also plays a role in the determination of fluid type. According to MacDonald each type of fluid has composition as given in Table 6-2. Sometimes hydrocarbon mixtures are classified as follows: dry gas, wet gas, gas condensate and black oil (see Figure 6-4).

In the case of dry gas, a light hydrocarbon mixture existing entirely in gas phase at reservoir conditions and a decline in reservoir pressure will not result in the formation of any reservoir liquid phase; it is a rather theoretical case. Usually gas reservoirs fall into the next group—wet gas.

Gas condensate or retrograde gas system is the case when the critical temperature of system is such that reservoir temperature is between critical and cricodentherm as shown in Figure 6-4c. If the pressure is reduced to the cricodenbar pressure, the liquid phase is increasing, but the liquid phase may reevaporate later on. This phenomena—the condensation of liquid upon decrease in pressure—is termed isothermal retrograde condensation. The liquid phase recovered from a condensate system is recovered from a phase that is vapor at reservoir conditions. This is also partly true of volatile oil systems where the vapor phase in equilibrium with the reservoir liquid phase is particularly rich in liquefiable constituents (C_3 to C_8), and a substantial proportion of stock tank liquid may derive from a reservoir vapor phase. We normally do not expect to

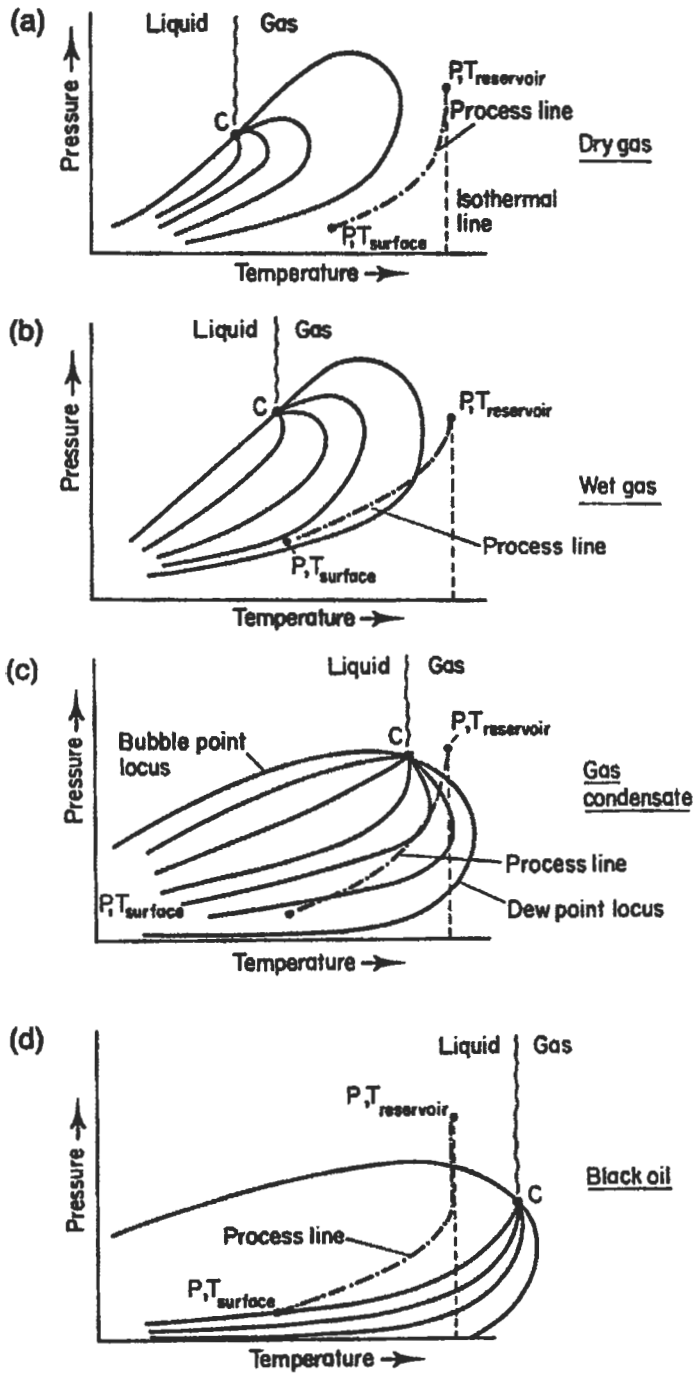


Figure 6-4. Hydrocarbon mixture classification.

Table 6-2
Typical Compositions of Hydrocarbons Fluids [7]

	Dry Gas	Wet Gas	Retrograde Condensate	Volatile Oil or Near Critical Oils	Black Oil	Heavy Oil
C_1 (mole %)	90		70	55		30
C_2-C_8 (mole %)	9		22	30		35
C_{7+} (mole %)	1		8	15		35
GOR[ft ³ /bbl]	∞	150000	3000-150000 (10000+)*	2000-3000 (3000-6000)*		< 2000
[m ³ /m ³]	∞	> 27000	540-27000	360-540		< 360
API Liquid Gravity	-		40-60	45-70	30-45	< 20
Liquid Specific Gravity	-		0.83-0.74	0.8-0.7	0.88-0.8	>.94

see retrograde behavior at reservoir pressures below about 2,500 psi (17.2 MPa). Volatile oil systems are those within the two-phase region under reservoir conditions, the vapor phase corresponding to condensate compositions and conditions. Volatile oil is not an apt description because virtually all reservoir fluids are volatile. What is really meant is that the reservoir fluid exhibits the properties of an oil existing in the reservoir at a temperature near its critical temperature. These properties include a high shrinkage immediately below the bubble point. In extreme cases, this shrinkage can be as much as 45% of the hydrocarbon pore space within 10 psi (0.7 bar) below the bubble point. Near-critical oils have formation factor B_0 of 2 or higher; the compositions are usually characterized by 12.5 to 20 mole % heptanes or more.

Ordinary oils are characterized by GOR from 0 to approximately 200 ft³/bbl (360 m³/m³) and B_0 less than 2. Oils with high viscosity (about 10 cp), high oil density and negligible gas/oil ratio are called heavy oils. At surface conditions may form tar sands. Oils with smaller than 10 cp viscosity are known as a black oil or a dissolved gas oil system; no anomalies are in phase behavior. There is no sharp dividing line between each group of reservoir hydrocarbon fluid; however, liquid volume percent versus pressure diagram (Figure 6-5) is very useful to understand the subject.

The significant point to be made is that when an oil system exists in intimate contact with an associated gas cap, the bubble point pressure of the oil will be equal to the dew point pressure of the gas cap and both of those values will be equal to the static reservoir pressure at the gas-oil contact (Figure 6-6).

Reservoir Conditions Phase Behavior

There is one phase flow in reservoir conditions if well flowing pressure P_{wf} is higher than bubble point pressure P_b or dew point pressure P_d and two-phase flow occurs by a wellbore. Reservoir depletion and production consist of two separate processes: flash liberation (vaporization) and differential liberation. A schematic representation of flash vaporization is shown in Figure 6-7. At stage 1 reservoir fluid is under reservoir pressure and temperature at known volumes V_r . The pressure in the cell is covered by increasing the space available in the cell for the fluid V_{c2} . This procedure is repeated until a large change in the

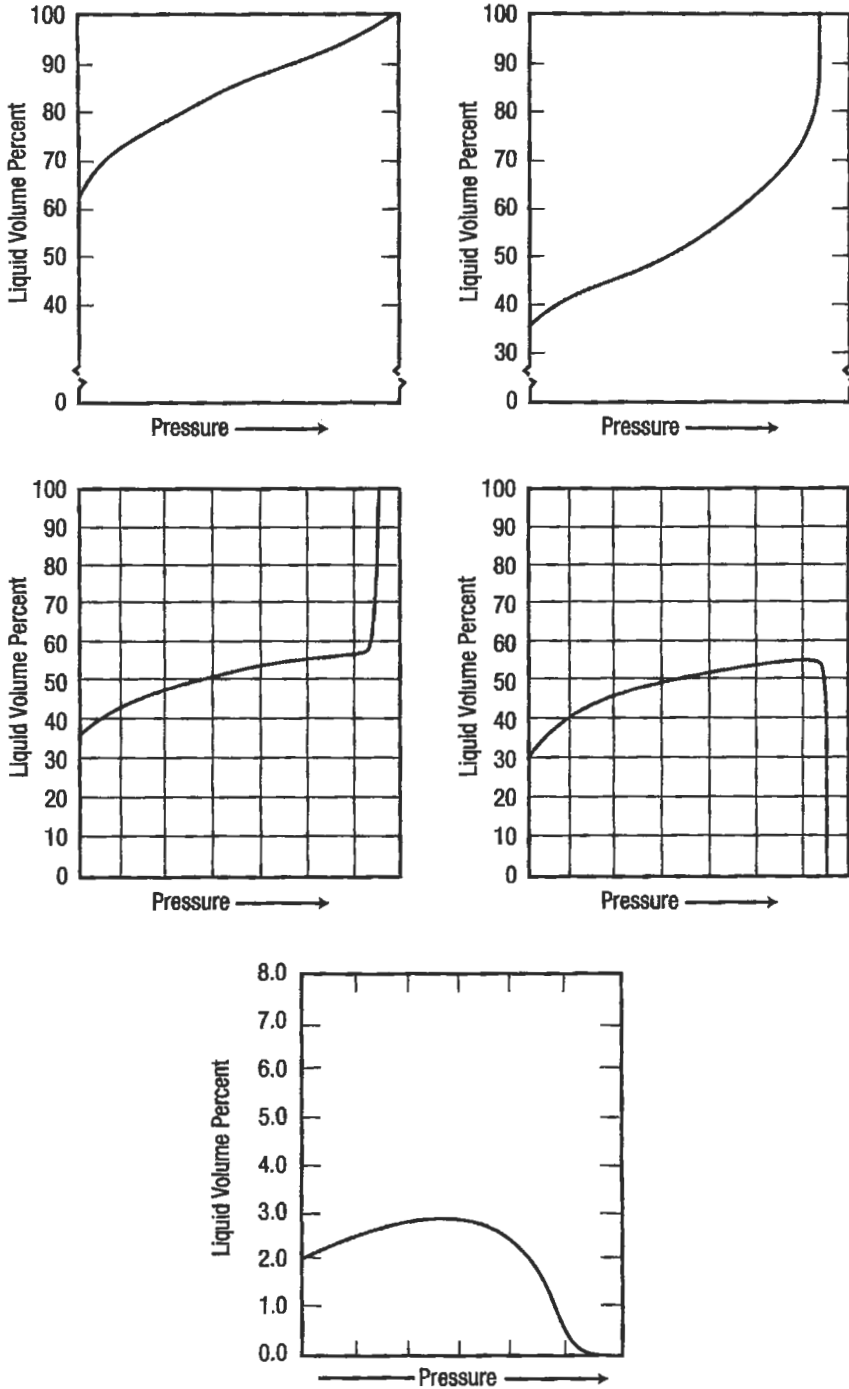


Figure 6-5a-e. Liquid volume percent—pressure diagram for reservoir fluid [6].

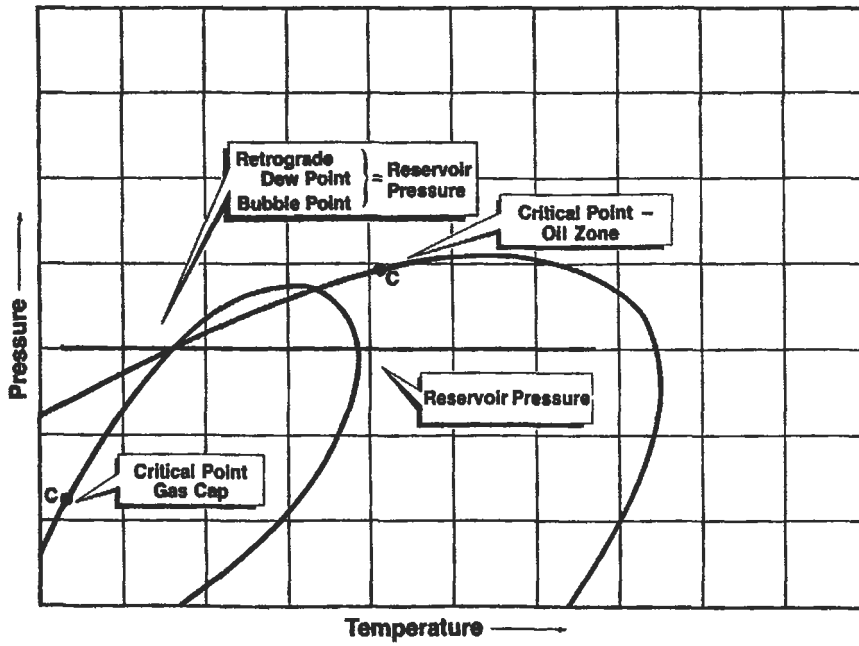


Figure 6-6. Pressure-temperature diagram for gas cap and associated oil [6].

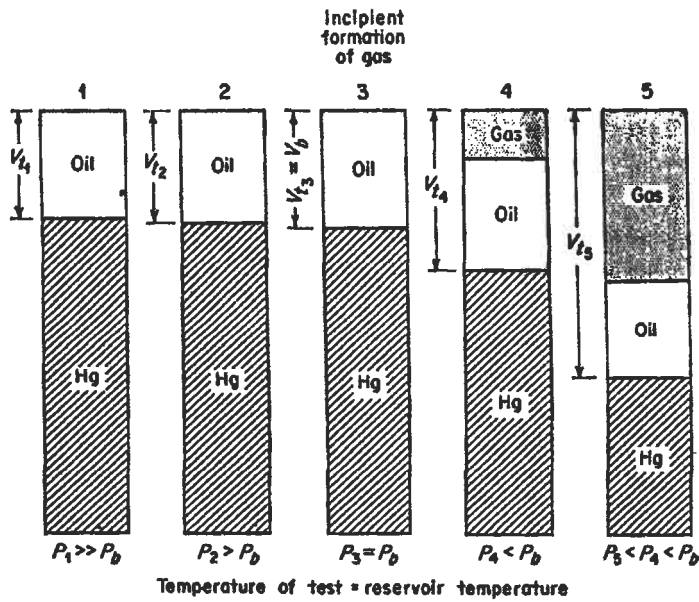


Figure 6-7. Schematic representation of laboratory P-V equilibrium (flash vaporization) [10].

pressure-volume slope is indicated. The above procedure indicates that flash vaporization is a phase-changing process due to change pressure and temperature if the mass of reservoir fluid or total composition system remains constant and can be expressed as follows:

$$zF = xL + yV \tag{6-15}$$

- where z = mole fraction of component in a reservoir fluid mixture
- F = number of moles of sample at initial reservoir pressure and temperature
- x = mole fraction of component in liquid (e.g., P_2)
- L = number of moles of equilibrium liquid
- y = mole fraction component in gas mixture
- V = number of moles of equilibrium gas phase

Equilibrium or flash liberation calculations may be made for reservoir fluid that divides into two phases at any temperature and pressure.

Schematic representation of differential liberation in laboratory conditions is shown in Figure 6-8. It begins in the same manner as flash vaporization. The sample is placed in a pressure higher than bubble point pressure. The pressure is lowered until such time that free gas is liberated in the cell. Then for pre-determined pressure or volume increments, mercury is withdrawn from the cell, gas is released from solution and the cell is agitated until the liberated gas is in the equilibrium with the oil. All the free gas is ejected from the cell at a

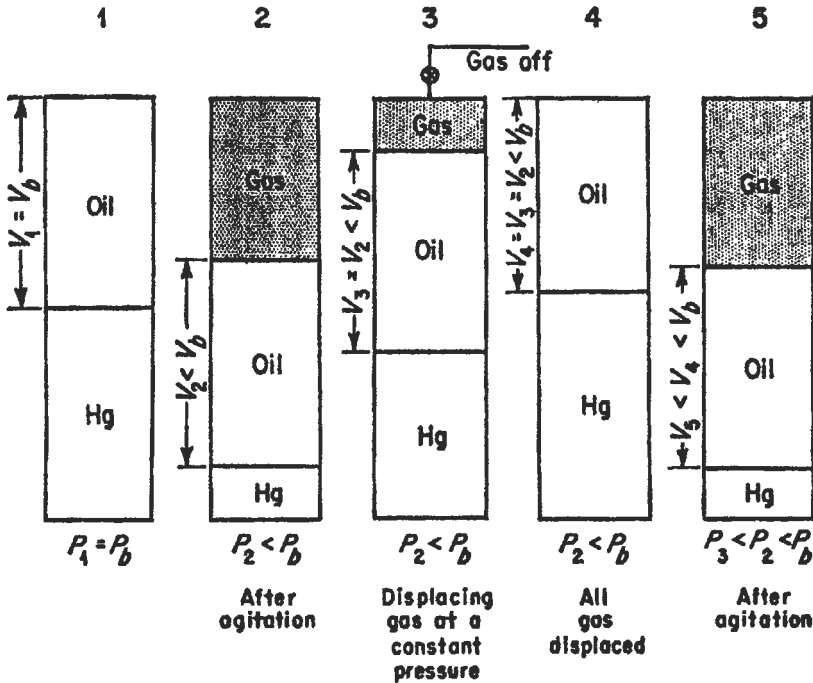


Figure 6-8. Schematic representation of laboratory differential vaporization [10].

constant pressure by injection mercury. The volume of the free gas is displaced and the oil remaining in the cells are thus measured at cell conditions. This procedure is repeated for all the pressure increments until only oil remains in the cell at reservoir temperature and atmospheric pressure.

In contrast to flash vaporization, differential vaporization is undertaken with the decreasing mass participating in the process. Equation 6-15 cannot be applied because F is not constant anymore at the given set pressure and temperature.

The question arises: Which process occurs in reservoir conditions? Some specialists, e.g., Moses [8], assume that the reservoir process is a combination of differential and flash. Such statements are incorrect. They produce misunderstanding and confusion. The following is meant to classify and straighten out this problem:

1. In reservoir conditions, differential process always occurs.
2. In production tubing and surface pipeline flow and in the separators the flash process takes place (subject to some limiting assumption).

Flash process refers to the conditions where the mass of the considered system does not vary with changes in pressure and temperature. Flash process in two-phase regions (vaporization or condensation) can be defined in terms of total system composition. The total system composition (z_i) can be measured at any point outside of saturation line, e.g., points A, B and C (Figure 6-3). As a substitution the following treatment can be used; the total system composition in two-phase region flash process remains constant. The flash process may ensue for a composition z_1 that separates into two phases for the values of pressures and temperatures inside the saturation curve area. After the temperature and pressure are chosen, all the gas is in equilibrium with all the oil. In other words, a change of pressure or temperature, or both, in a flash process can change the equilibrium conditions according to the Gibbs phase rule. This rule provides the number of independent variables that, in turn, define intensive properties. Flash vaporization may be a batch or a continuous process. Treating two-phase flow in tubing as a steady state, neglecting the gas storage effect, and gas slippage result in a flash process. In a horizontal flow, and in separators, a similar flash process comes about.

The same kind of equilibrium, but with its fluid mass decreasing differentially, is called a differential process (liberation or condensation).

In reservoir conditions the hydrocarbon pore volume (HCPV) remains constant if the expansion of interstitial water and rock compressibility are neglected. For such constant HCPV it must be made clear that differential process occurs always as differential vaporization or differential condensation. Differential vaporization takes place when the reservoir temperature is less than critical temperature of solution ($T_{res} < T_c$), and also it takes place during retrograde gas reservoir depletion, but only in the region pressure and temperature where the retrograde liquid is vaporized.

In differential condensation, the oil reservoir pressure is maintained constant or almost constant—for example, by gas injection. Differential condensation can also occur just below the dew point in a gas-condensate reservoir.

Above the bubble point and the dew point curves, the virtual (apparent) value of vaporization and/or condensation is zero, but because the mass of the fluid in a depleted reservoir is changing as a result of decreasing pressure, the process could be assumed to be differential. One important statement has to be added: there is no qualitative difference between the reservoir fluid in either differential or flash process, if pressure and temperature fall into the area outside of the

saturation curve (Figure 6-3). A schematic representation of differential vaporization of oil in reservoir conditions is shown in Figure 6-9. As indicated in Figure 6-9, six hypothetical cases are distinguished. Study Figure 6-9 simultaneously with Figures 6-3 and 6-10.

Consider a first sample where there is a fixed mass of oil at given temperature, pressure and HCPV. When the pressure P_1 drops to P_2 , the volume of oil increases but the HCPV does not change, so the difference in oil-removed volume equals the total oil production when the pressure changes from P_A to P_2 (sample 2).

The third sample is considered at the bubble point; the oil volume change between P_2 and P_b resembles that between P_1 and P_2 . Beginning at P_b the first gas bubbles are released. Pressure P_4 corresponds to the lowest value of GOR (Figure 6-10) and coincides with the highest pressure in a two-phase region, in which only one phase (oil) still flows. Pressure P_4 could be called a *gas flow saturation pressure*. Between P_b and P_4 compositions x , y , and z are changed. HC mass in pore volume is decreasing, so it is the differential process that is contrary to Moses' belief that this is a flash process.

At point 5, HCPV remains constant as in steps 1 to 4, the oil volume has changed and the system is into a two-phase region. An amount of released gas exceeds the gas flow saturation pressure P_4 ; gas begins to run and is partially removed from the HCPV. This is how a two-phase flow is generated. Sample 6 characterizes the same process very close to the bottomhole area. The reservoir fluid mass difference in steps 1 and 6 equals the total production from an HCPV.

In conclusion, it has been shown that the flash process occurs whenever we are dealing with a closed system or a steady-state flow, e.g. a two-phase flow in vertical tubing, in horizontal pipe flow and in separators. For any open system, such as a reservoir formation, or for an unsteady-state flow, the differential process is properly describing the quasiequilibrium conditions.

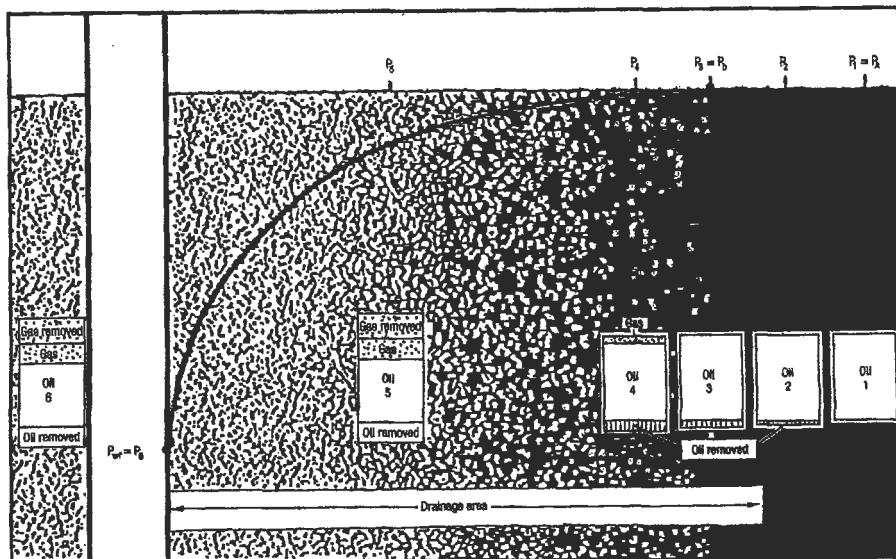
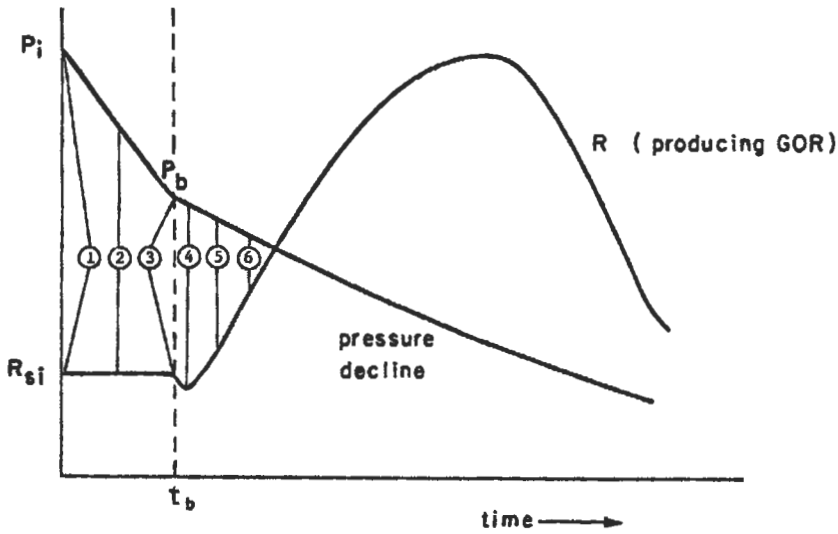


Figure 6-9. Schematic representation of differential vaporization in reservoir conditions.



Sample #	1	2	3	4	5	6
Reservoir parameters						
HCPV (V)	$V_1 - V$	$V_2 - V$	$V_3 - V$	$V_4 - V$	$V_5 - V$	$V_6 - V$
HC Mass in Pore Volume (m)	$m_1 - m$	$m_2 < m_1$	$m_3 < m_2$	$m_4 < m_3$	$m_5 < m_4$	$m_6 < m_5$
Pressure (P)	$P_1 = P_A$	$P_2 < P_1$	$P_b < P_2$	$P_4 < P_b$	$P_5 < P_4$	$P_6 < P_5$
Temperature (T)	assumed constant reservoir temperature					
Total Reservoir Composition z_i	$z_{i1} - z_{iA}$	$z_{i2} - z_{i1}$	$z_{i3} - z_{i1}$	$z_{i4} - z_{i1}$	$z_{i5} - z_{i1}$	$z_{i6} - z_{i1}$
Gas Composition y_i	$y_{i1} - y_{iA} = 0$	$y_{i2} - y_{iA} = 0$	$y_{i3} - y_{iA} = 0$	$y_{i4} - y_{i1}$	$y_{i5} - y_{i1}$	$y_{i6} - y_{i1}$
Oil Composition x_i	$x_{i1} - x_{iA} - z_{i1}$	$x_{i2} - x_{i1} - z_{i1}$	$x_{i3} - x_{i1} - z_{i1}$	$x_{i4} - x_{i1} - z_{i1}$	$x_{i5} - x_{i1} - z_{i1}$	$x_{i6} - x_{i1} - z_{i1}$

Figure 6-10. Schematic representation reservoir pressure (P) and GOR vs. time and mass and composition in reservoir differential vaporization process.

Sampling Process and Laboratory Measurements

The overall quality of the reservoir fluid study and the subsequent engineering calculations based upon that study can be no better than the quality of the fluid samples originally collected during the field sampling process.

Samples representative of the original reservoir can be obtained only when the reservoir pressure is equal to or higher than the original bubble point or dew point.

The pressure drawdown associated with normal production rates will cause two-phase flow near the wellbore if the fluid in the formation was initially saturated or only slightly undersaturated. Relative permeability effects may then cause the material entering the wellbore to be different from the original overall (total) composition fluid existing at the boundary of drainage area. The problem

of drawdown in a saturated reservoir cannot be eliminated; therefore, it is necessary to reduce the pressure drawdown by reducing the flowrate to the lowest possible stable rate while sampling.

There are two basic methods of sample collection: subsurface (bottomhole) and surface (separator). The fluid sampling method to be used dictates the remainder of the conditioning process. If the bottomhole samples are to be collected, the period of reduced flowrate will generally last from one to four days, depending on the formation and fluid characteristics and the drainage area affected. After this reduced flowrate period, the well would be shut in and allowed to reach static pressure. The shut-in period would last about one day or up to a week or more depending on formation characteristics. For the case of the saturated reservoir, the shut-in period has the resultant effect of forcing gas into solution in the oil, thus raising the saturation pressure. In some cases, the desired value of P_b is obtained; however, in most cases this value is only approached and the final difference is a function of well productivity, production rate and fluid properties. At the conclusion of the shut-in period, the well would be properly conditioned and ready for bottomhole sampling. Subsurface sampling is generally not recommended for gas-condensate reservoirs; the same is true for oil reservoirs producing substantial quantities of water. If separator gas and liquid samples are to be collected, the gas and liquid rates must be monitored continually during the period of stable flow at reduced flowrates. A minimum test of 24 hr is recommended, but more time may be needed if the pressure drawdown at the formation has been high. Surface sampling, called *separator sampling*, has wider applications than subsurface sampling, and is the only recommended way of sampling a gas-condensate reservoir, but often can be used with good success for oil reservoirs as well. There are three requirements to successful separator sampling:

1. stable production at a low flowrate
2. accurate measurement of gas and liquid flowrates
3. collection of representative samples of first-stage gas and first-stage liquid

The above procedure is described in detail in API Standard 811-08800 [9].

The reservoir process is stimulated in the laboratory by flash differential vaporization (Figures 6-7 and 6-8). Based on both figures, it is possible to prepare the reservoir fluid data for engineering calculations.

In the laboratory, the differential liberation consists of a series—usually 10 to 15—of flash liberations. An infinite series of flash liberations is the equivalent of a true differential liberation. At each pressure level, gas is evolved and measured. The volume of oil remaining is also measured at each depletion pressure. This process is continued to atmospheric pressure. The oil remaining at atmospheric pressure is measured and converted to a volume at 60°F (15.6°C). This final volume is referred to as the residual oil. The volume of oil at each of the higher pressures is divided by the volume of residual oil at 60°F (15.6°C).

Example 1 [11]

Surface separator samples were collected from a well on completion of a 2-hr test on June 8, 1984. The gas/liquid ratio measured on this test was 4,565 ft³ of separator gas per barrel of separator liquid and was used as the basis for this recombination. The resultant reservoir fluid exhibited a dew point of 4,420 psia at $T_{res} = 285^\circ\text{F}$. The reservoir fluid exists as a gas (an undersaturated gas) at $P_{res} = 12,920$ psia.

A constant volume depletion study is also performed on the reservoir fluid. The produced compositions and volumes from the depletion study are used in conjunction with equilibrium constants to calculate cumulative STO and separator gas recoveries resulting from conventional field separation. Gas plant products in both the primary separator gas and the full well stresses should also be reported.

Sampling Conditions

Date sampled (on 20/64 choke)	06-08-84 for 1,330 hr
Tubing pressure, flowing	9,960 psig
Primary separator temperature	95°F
Primary separator pressure	900 psig
Primary separator gas rate (Table 6-3)	2,229.7 MCF/day
Liquid rate (2nd stage @ 50 psig)	396 bbl/day
Gas/liquid ratio (GOR)	5,631 SCF 1st stg. gas/bbl 50 lb liq.
Shrinkage factor (vol. 50 lb liq./vol. sep. liq.)	0.8108
Gas/liquid ratio (GOR)	4,565 SCF 1st stg. gas/bbl 900 lb liq.
Shrinkage factor (vol. S.T. liq./vol. sep. liq.) through 50-lb 2nd stage	0.7445
Pressure base	15.025 psia @ 60°F

Table 6-3
Calculation of Gas Rate [11]

$\sqrt{Hw Pf}$ = 165.6804	Hw = 30.0 "H ₂ O,	Pf = 915.00 psia
Fb = 455.0300	D = 5.761 " ,	d = 1.50 "
Fpb = 0.9804	15.025 psia	
Fr = 1.0002	b = 0.0367	
Y ₂ = 1.0002	Hw/Pf = 0.033 ,	d/D = 0.260
Fg = 1.1953	Gravity = 0.6999 ,	Fg = $\sqrt{1/0.6999}$
Ftf = 0.9680	Temp. = 95 degrees F,	Ftf = $\sqrt{520/555}$
Fpv = 1.0859	pTr' = 1.441 ,	pPr' = 1.372
	Z = 0.8480 ,	Fpv = $\sqrt{1/Z}$
Acid Gas Correction Factor	Epsilon = 3.57	
$Q = \sqrt{Hw Pf} \times Fb \times Fpb \times Fr \times Y2 \times Fg \times Ftf \times Fpv \times 24$		
Q = 2229.7 MCF/day @ 15.025 PSIA @ 60 Degrees F		

The samples of separator gas and separator liquid were analyzed and the results are reported in Table 6-4, sharing both composition of each sample and the computed analysis of the well stream based on the GOR in the primary separator. The separator liquid (oil) production was calculated from the measured second-stage production by applying the determined shrinkage factor.

**Table 6-4
Hydrocarbon Analysis of Separator Products
and Calculated Wellstream [11]**

Component	Separator Liquid		Separator Gas		Well Stream	
	Mol %	Liq. Vol. %	Mol %	GPM @ 15.025 PSIA	Mol %	GPM @ 15.025 PSIA
Carbon Dioxide	0.41	0.19	2.18		1.84	
Nitrogen	0.00	0.00	0.16		0.13	
Methane	22.36	10.16	82.91		71.30	
Ethane	8.54	6.12	8.22	2.243	8.28	2.259
Propane	10.28	7.58	3.82	1.073	5.06	1.421
Iso-Butane	5.69	4.99	1.11	0.372	1.99	0.664
N-Butane	5.11	4.32	0.80	0.256	1.63	0.523
Iso-Pentane	4.84	4.75	0.30	0.113	1.17	0.437
N-Pentane	2.01	1.95	0.17	0.064	0.52	0.193
Hexanes	8.16	8.75	0.22	0.091	1.74	0.731
Heptanes Plus	32.60	51.19	0.11	0.053	6.34	3.907
Total	100.00	100.00	100.00	4.265	100.00	10.135

Calculated Specific Gravity (Air = 1.00) = 0.6999 Separator Gas 1.0853 Well Stream

Sep. Gas Heat of Combustion (BTU/Cu.Ft. @ 15.025 PSIA & 60 Degrees F) Dry = 1206.8 Real

Sep. Gas Heat of Combustion (BTU/Cu.Ft. @ 15.025 PSIA & 60 Degrees F) Wet = 1185.7 Water Sat.

Sep. Gas Compressibility (@ 1 ATM. & 60 Degrees F) Z = 0.9968

Properties of Heptanes Plus:

Specific Gravity = 0.7976
Molecular Weight = 152
Cu.Ft./Gal. = 16.24

Properties of Separator Liquid:

0.6562 @ 60/60 Degrees F
78.7
25.81 @ 15.025 PSIA & 60 Degrees F

Properties of Stock Tank Liquid:

Gravity = 56.8 Degrees API @ 60°F

Basis of Recombination:

Separator Liquid Per MMSCF Separator Gas = 219.05 BBLs.

Equilibrium Cell Determinations. Following the compositional analyses, portions of the primary separator liquid and gas were physically recombined in their produced ratio in a variable volume, glass-windowed equilibrium cell. Determinations on this mixture were divided into the following two main categories.

1. Dew point pressure determination and pressure-volume relations on a constant weight of reservoir fluid at the reservoir temperature: the procedure consisted of establishing equilibrium between gas and liquid phases at a low pressure and measuring volumes of liquid and gas in equilibrium at that pressure. The pressure was raised by the injection of mercury into the cell and phase equilibrium established again at the higher pressure. This procedure was repeated until all of the liquid phase had vaporized, at which point the saturation pressure was observed. The cell pressure was then raised above the dew point pressure in order to determine the supercompressibility characteristics of the single-phase vapor. As a check on all readings and, particularly, to verify the dew point, the cell pressure was incrementally reduced, equilibrium established and volumetric readings made. Reported in Table 6-5 are the relative volume relations (Figure 6-11) and specific volumes of the reservoir fluid over a wide range of pressures as well as compressibility factors (Figure 6-12), the single-phase vapor above the dew point. Reported in Table 6-6 are the dew point pressures (Figure 6-13) resulting from recombinations at gas/liquid ratios above and below the ratio measured at the time of sampling.
2. Compositions of the produced wellstream and the amount of retrograde condensation resulting from a stepwise differential depletion: This procedure consisted of a series of constant composition expansions and constant pressure displacements with each displacement being terminated

Table 6-5
Pressure-Volume Relation of Reservoir Fluid at 285°F [11]

Pressure (PSIA)	Relative Volume (V/V _{sat})	Specific Volume (Cu.Ft./Lb.)	Retrograde BPMMCF*	Liquid Vol. %**	Deviation Factor (Z)	Calculated Viscosity (Centipoise)
***12920 Res.	0.6713	0.03635			1.8485	0.0793
10000	0.7201	0.03898			1.5346	0.0674
8000	0.7741	0.04191			1.3197	0.0579
6000	0.8639	0.04677			1.1047	0.0471
5000	0.9373	0.05075			0.9988	0.0412
4420 D.P.	1.0000	0.05414	0.00	0.00	0.9420	0.0374
					(Two Phase)	
4000	1.0677	0.05781	10.58	1.30	0.9102	
3500	1.1764	0.06369	69.83	8.55	0.8775	
3000	1.3412	0.07261	94.17	11.53	0.8575	
2500	1.5879	0.08597	107.92	13.21	0.8460	
2000	1.9831	0.10737	114.27	13.99	0.8453	
1500	2.6605	0.14404	114.27	13.99	0.8505	
1000	4.0454	0.21902	107.92	13.21	0.8621	

*BBLs. per MMSCF of Dew Point Fluid.

**Percent of Hydrocarbon Pore Space at Dew Point.

***Extrapolated.

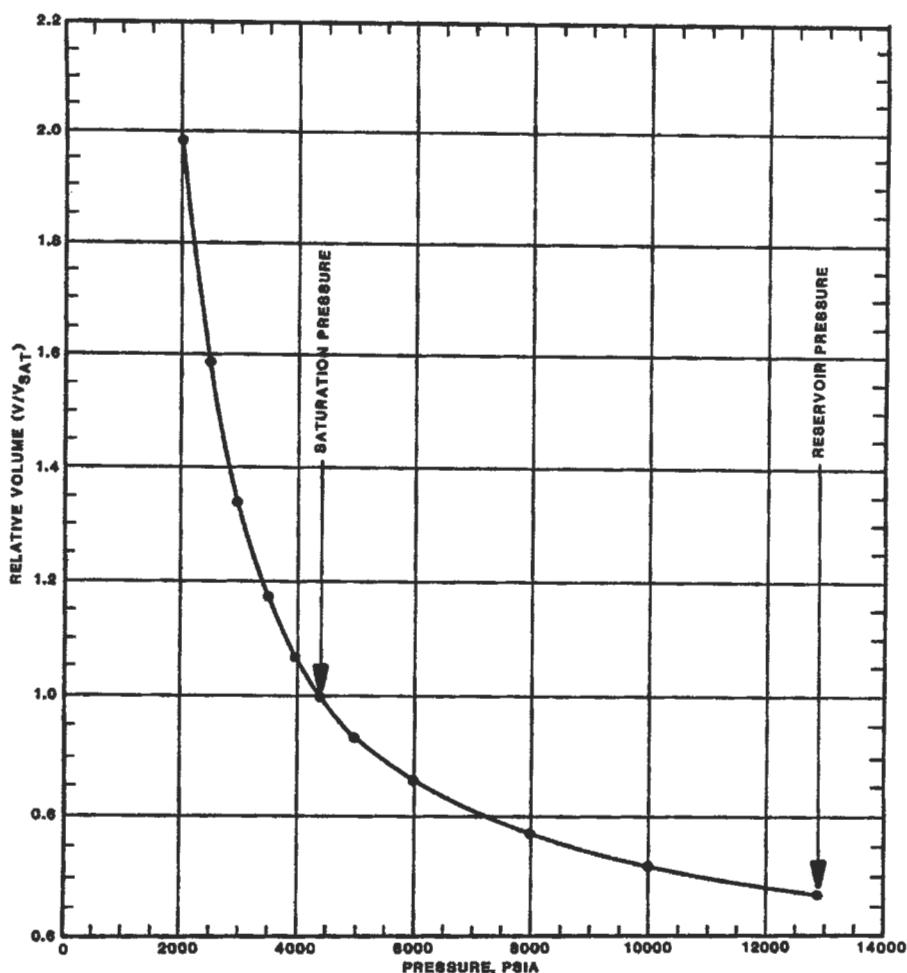


Figure 6-11. Pressure-volume relation of reservoir fluid at 285°F (constant mass expansion) [11].

at the original cell volume. The gas removed during the constant pressure displacement was analyzed. The determined compositions (Figure 6-14), computed GPM content (Figure 6-15), respective compressibility (deviation) factors and volume of wellstream produced during depletion (Figure 6-16) are presented in Table 6-7. The volume of retrograde liquid resulting from the gas depletion is shown in Table 6-8 (and Figure 6-17), both in terms of barrels of reservoir liquid and percent of hydrocarbon pore space. Shown in Table 6-7 are the compositions of the gas and liquid remaining in the reservoir after depletion to abandonment pressure.

Equilibrium Flash Calculations. The produced compositions and volumes from a depletion study were used in conjunction with equilibrium constants K (derived from a Wilson modified R-K equation of state) to calculate cumulative stock

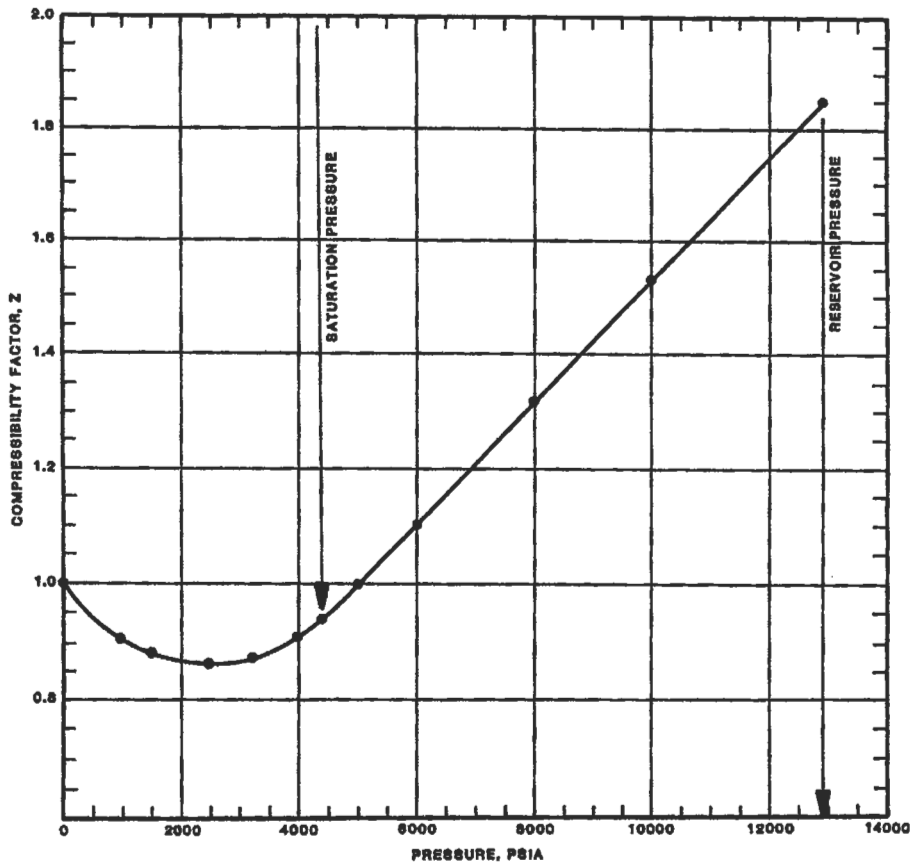


Figure 6-12. Compressibility factor "Z" of wellstream during depletion at 285°F [11].

Table 6-6
Observed Saturation Pressures From Stepwise
Recombination at 285°F

Gas-Liquid Ratio (SCF 1st Stg. Gas)	Saturation Pressure (Psia)
(BBL. 1st Stg. Lq.)	
9000	6000 Dew Point
4565 (Produced)	4420 Dew Point
2500	3830 Dew Point

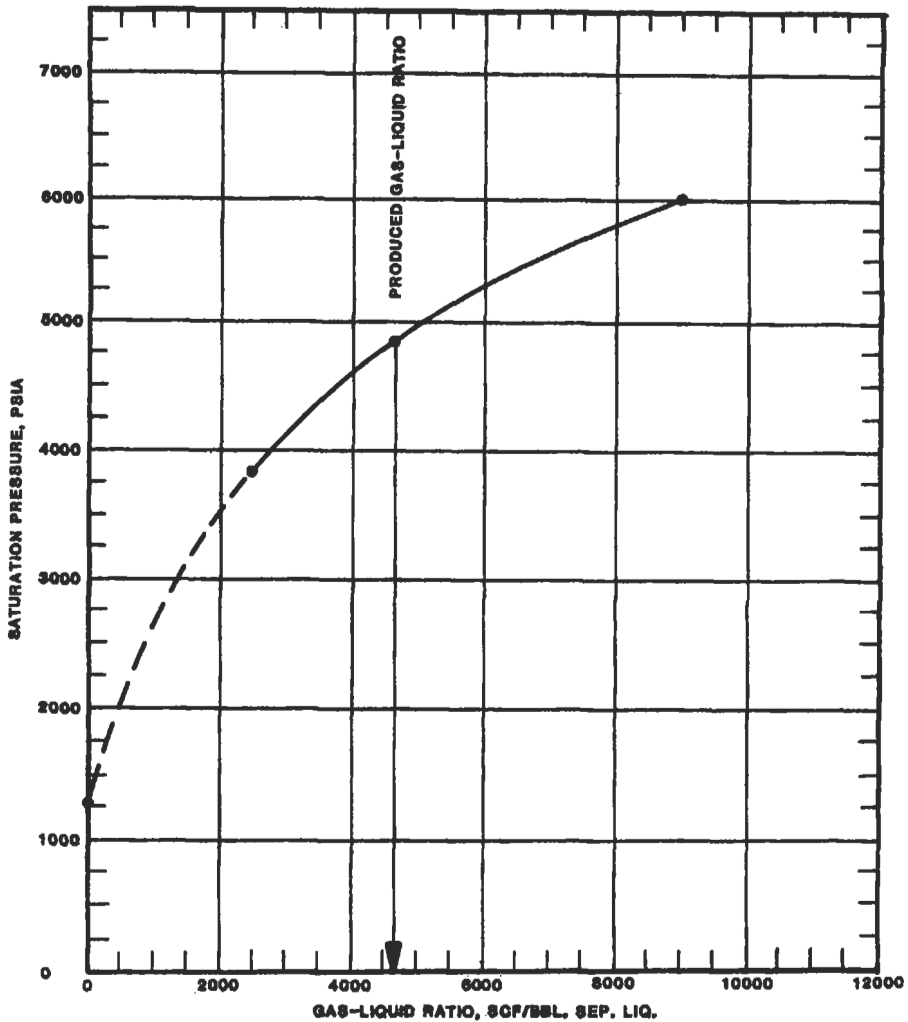


Figure 6-13. Effect of gas/liquid ratio upon saturation pressure at 285°F [11].

tank liquid and separator gas recoveries resulting from conventional separation. These data are reported in Table 6-9 and Figure 6-18. Also, gas plant products in both the primary separator gas and the full wellstream are attached.

Example 2 [8]

This is a black oil problem. From differential vaporization (Table 6-11) and separator test data (Table 6-12) discuss the B_o and R_s calculation method.

Figures 6-19 and 6-20 illustrate laboratory data. These data are reported in a convention other than in Example 6.1. The residual oil in the reservoir is never at 60°F (15.6°C), but always at T_{res} . Reporting these data relative to the residual

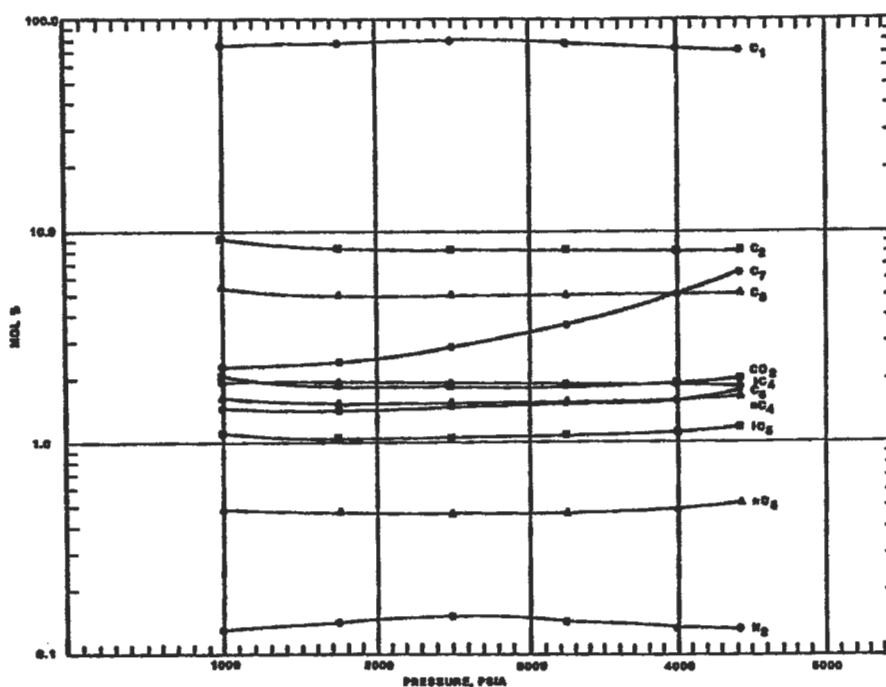


Figure 6-14. Hydrocarbon composite of wellstreams produced during pressure depletion [11].

oil at 60°F (15.6°C) gives the relative-oil-volume curve the appearance of an FVF curve, leading to its misuse in reservoir calculations. A better method of reporting these data is in the form of a shrinkage curve. We may convert the relative-oil-volume data in Figure 6-19 and Table 6-11 to a shrinkage curve by dividing each relative oil volume factor B_{od} by the relative oil volume factor at the bubblepoint, B_{odb} .

The shrinkage curve now has a value of 1 at the bubblepoint and a value of less than 1 at subsequent pressures below the bubblepoint, as in Figure 6-21. As pressure is reduced and gas is liberated, the oil shrinks. The shrinkage curve describes the volume of this original barrel of oil in the reservoir as pressure declines. It does not relate to a stock-tank barrel or surface barrel.

We now know the behavior of the oil in the reservoir as pressure declines. We must have a way of bringing this oil to the surface through separators and into a stock tank. This process is a flash process. Most reservoir fluid studies include one or more separator tests to stimulate this flash process. Table 6-12 is a typical example of a set of separator tests. During this test, the FVF is measured. The FVF is the volume of oil and dissolved gas entering a wellbore at reservoir pressure and temperature divided by the resulting stock-tank oil volume after it passes through a separator.

The FVF is B_o ; because separators result in a flash separation, we showed a subscript, B_{or} . In most fluid studies, these separator tests are measured only on the original oil at the bubble point. The FVF at the bubble point is B_{ob} . To make solution-gas-drive or other material-balance calculations, we need values

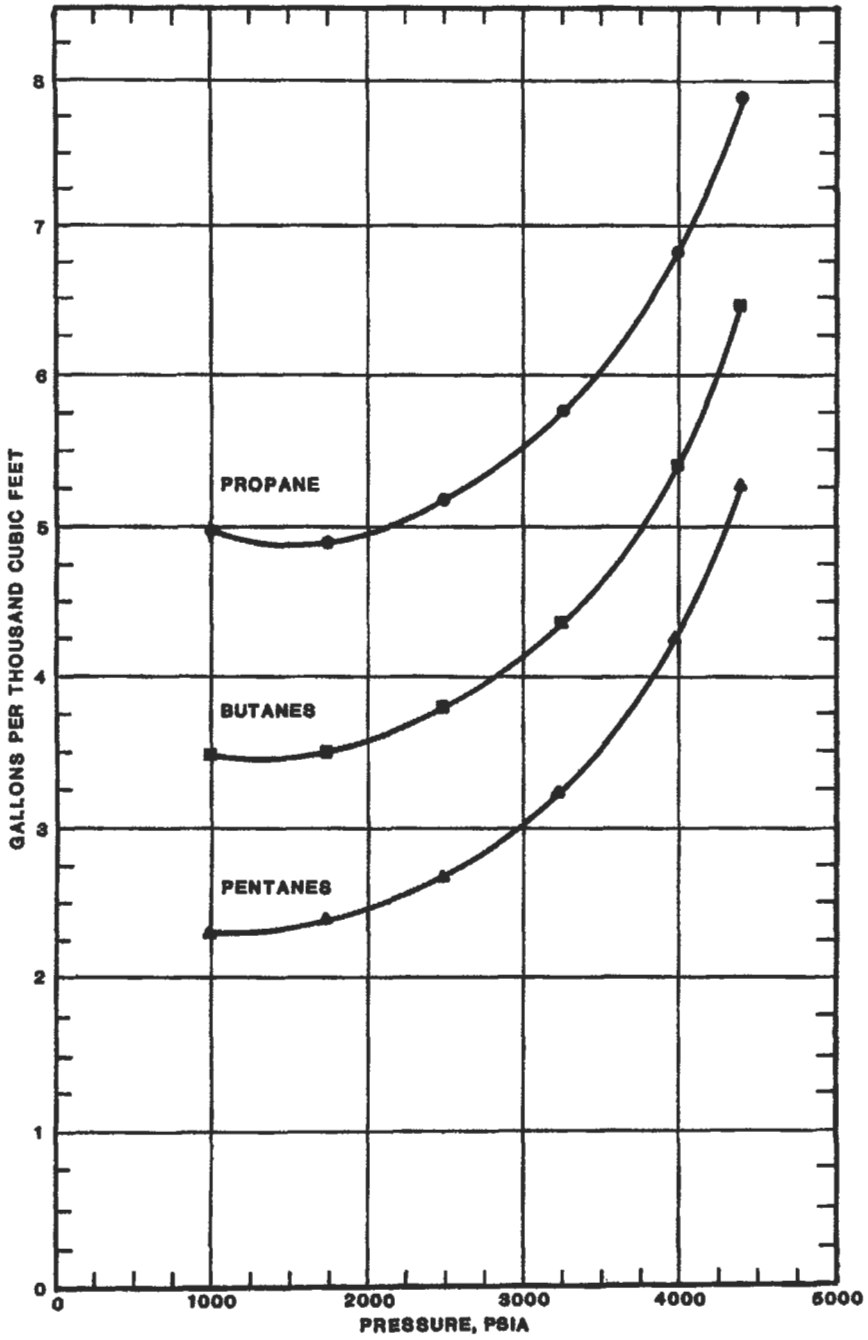


Figure 6-15. GPM content of hydrocarbons produced during depletion at 285°F [11].

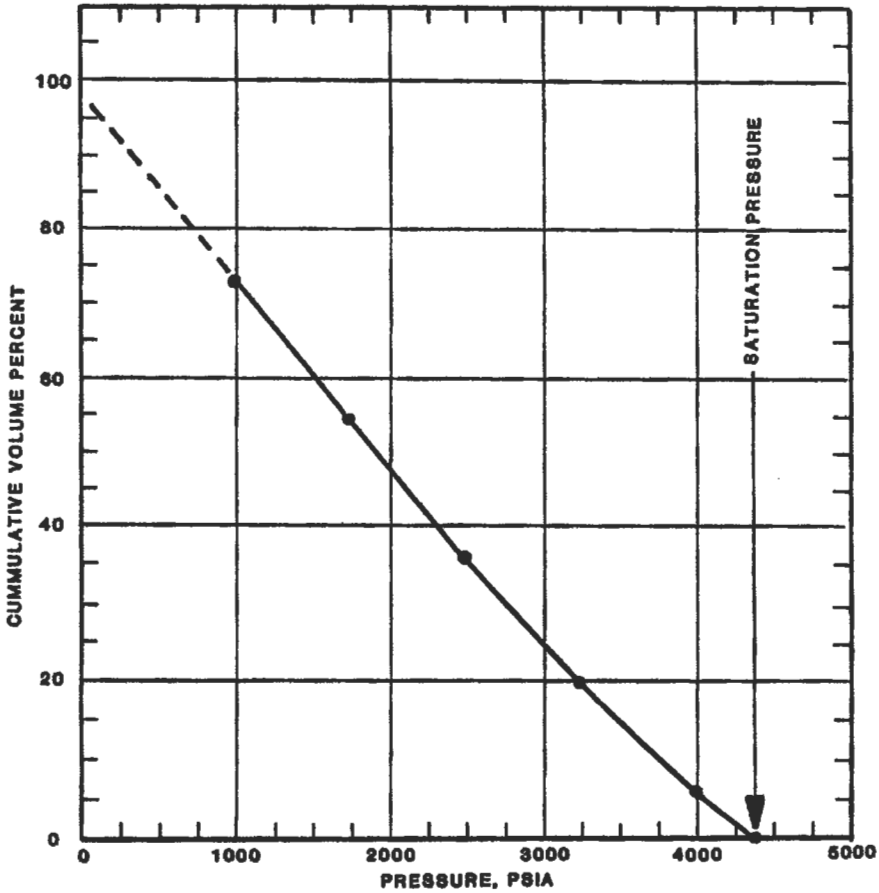


Figure 6-16. Volume of wellstream produced during depletion [11].

of B_{of} at lower reservoir pressures. From a technical standpoint, the ideal method for obtaining these data is to place a large sample of reservoir oil in a cell, heat it to reservoir temperature and pressure-deplete it with a differential process to stimulate reservoir depletion. At some pressure a few hundred psi below the bubble point, a portion of the oil is removed from the cell and pumped through a separator to obtain the flash FVF, B_{of} at the lower reservoir pressure. This should be repeated at several progressively lower reservoir pressures until a complete curve of B_{of} versus reservoir pressure has been obtained. The process is time consuming and consequently adds to the cost of a study. Most studies include only values of B_{ob} , the FVF at the bubble point. The values of B_{of} at lower pressures must be obtained by other means.

The method calls for multiplying the flash FVF at the bubble point B_{ob} by the shrinkage factors at various reservoir pressures obtained earlier. The shrinkage factor was calculated by dividing the relative oil volume factors B_{od}

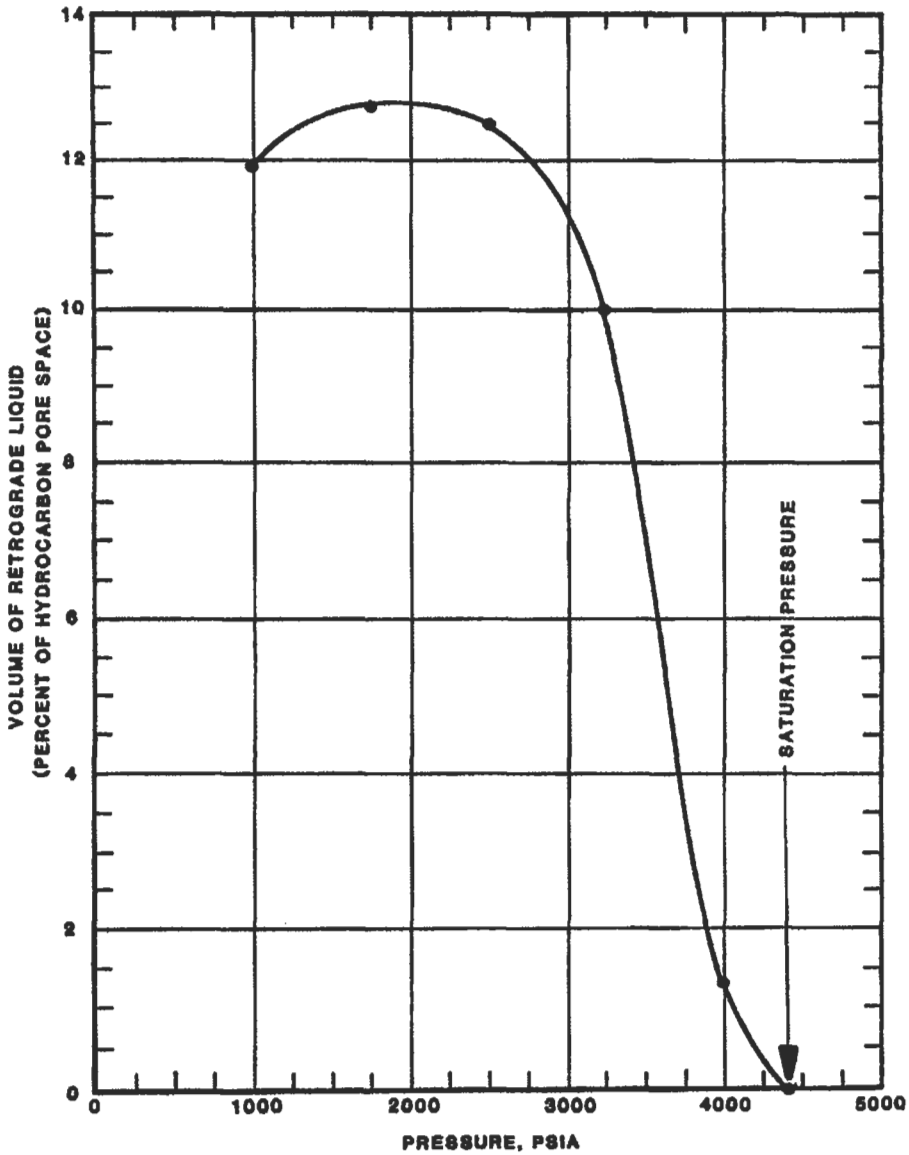


Figure 6-17. Retrograde condensation during depletion at 285°F [11].

by the relative oil volume factor at the bubble point B_{ob} . If we combine both calculations, we can start with the differential-relative-volume curve and adjust it to separator or flash conditions by

$$B_o = B_{od} \frac{B_{ofb}}{B_{ob}} \tag{6-16}$$

(text continued on page 394)

Table 6-7
Depletion Study at 285°F [11]

Component	Reservoir Pressure—PSIA						Aband. Liquid 1000
	Dew Point Fluid 4420	4000	3250	2500	1750	1000	
Nitrogen	0.13	0.13	0.14	0.15	0.14	0.13	0.04
Carbon Dioxide	1.84	1.87	1.90	1.92	1.94	1.93	0.67
Methane	71.30	73.09	74.76	75.69	76.09	74.71	16.61
Ethane	8.28	8.18	8.14	8.12	8.15	9.05	4.76
Propane	5.06	5.01	4.97	4.94	4.93	5.29	4.60
Iso-Butane	1.99	1.93	1.89	1.87	1.89	2.02	2.66
N-Butane	1.63	1.59	1.56	1.55	1.54	1.61	2.37
Iso-Pentane	1.17	1.12	1.09	1.06	1.06	1.10	2.37
N-Pentane	0.52	0.48	0.47	0.46	0.47	0.48	1.17
Hexanes	1.74	1.59	1.51	1.45	1.40	1.43	5.96
Heptanes Plus	6.34	5.01	3.57	2.79	2.39	2.25	58.77
Totals	100.00	100.00	100.00	100.00	100.00	100.00	100.00
Well Stream Gravity (Air = 1)	1.0853	1.0043	0.9251	0.8823	0.8595	0.8606	

Properties of Heptanes Plus

Specific Gravity	0.7976	0.7900	0.7776	0.7652	0.7523	0.7381	0.8181
Molecular Weight	152	145	136	128	120	112	171

GPM Content of Produced Well Stream (Gal/MSCF)

Propane	1.421	1.407	1.396	1.387	1.384	1.485
Iso-Butane	0.664	0.644	0.631	0.624	0.631	0.674
N-Butane	0.524	0.511	0.502	0.498	0.495	0.518
Iso-Pentane	0.437	0.418	0.407	0.396	0.396	0.411
N-Pentane	0.192	0.177	0.174	0.170	0.177	0.177
Hexanes	0.730	0.667	0.633	0.608	0.587	0.600
Heptanes Plus	3.904	2.992	2.018	1.508	1.232	1.103
Totals	7.872	6.816	5.761	5.191	4.902	4.968

Deviation Factor "Z" of Well Stream Produced	0.942	0.910	0.876	0.867	0.882	0.911
--	-------	-------	-------	-------	-------	-------

Calculated Viscosity of Well Stream Produced (CP)	0.0374	0.0317	0.0251	0.0206	0.0174	0.0152
---	--------	--------	--------	--------	--------	--------

Well Stream Produced Cumulated Percent	0.00	5.98	20.01	36.71	54.73	72.95
--	------	------	-------	-------	-------	-------

Table 6-8
Retrograde Condensation During Gas
Depletion at 285°F [11]

Pressure (PSIA)	Reservoir Liquid	
	(BBL/MMSCF of Dew Point Fluid)	(Volume* Percent)
4420 D.P. @ 285°F	0.00	0.00
4000	10.58	1.30
3250	81.47	9.98
2500	101.57	12.46
1750	103.69	12.70
1000	97.34	11.92

*Percent of Reservoir Hydrocarbon Pore Space @ Dew Point.

(text continued from page 391)

This calculation is illustrated in Figure 6-22.

To perform material-balance calculations, we must also have the separator and stock-tank gas in solution as a function of reservoir pressure. These values are expressed as standard cubic feet per barrel and usually are designated R_{st} . The separator test gives us this value at the bubble point, R_{sb} . As pressure declines in the reservoir, gas is evolved from solution. The amount of gas remaining in solution in the oil is then somewhat less. The differential vaporization tells us how much gas was evolved from the oil in the reservoir: $(R_{adb} - R_{sd})$, where R_{adb} is the amount of gas in solution at the bubble point as measured by differential vaporization at the reservoir temperature and R_{sd} is the gas in solution at subsequent pressures.

The units of R_{adb} and R_{sd} are standard cubic feet per barrel of residual oil. Because we must have the gas in solution in terms of standard cubic feet per barrel of stock-tank oil, this term must be converted to a stock-tank basis. If we divide $(R_{adb} - R_{sd})$ by B_{odb} , we have the gas evolved in terms of standard cubic feet per barrel of bubble point oil. If we then multiply by B_{ofb} , we will have the gas evolved in terms of standard cubic feet per barrel of stock-tank oil. This expression now is $(R_{adb} - R_{sd})(B_{ofb}/B_{odb})$. The gas remaining in solution then is $R_s = R_{stb} - (R_{adb} - R_{sd})(B_{ofb}/B_{odb})$ standard cubic feet per stock-tank barrel. For every pressure studied during the differential liberation, R_s may be calculated from this equation. This calculation is illustrated in Figure 6-23.

It is a fairly common practice to use differential vaporization data for material-balance calculations. Values of B_{od} and R_{sd} are almost always higher than the corresponding values from separator tests; consequently, calculations of OIP and recoverable oil will usually be lower than is correct. The differential vaporization data should be converted to separator flash conditions before use in calculations.

Vapor-Liquid Equilibrium Calculations

The basic equilibrium calculations are the bubble point, dew point and flash (or two-phase equilibrium). In the general flash calculation, the temperature and pressure are usually fixed and L/f is the dependent variable. All equilibrium calculations are based on the definition of the K value, such that

(text continued on page 400)

**Table 6-9
Calculated Cumulative Recovery During Depletion [11]**

Cumulative Recovery Per MMSCF of Original Fluid	Reservoir Pressure—PSIA						
	Initial in Place	Dew Point Pressure 4420	4000	3250	2500	1750	1000
<i>Well Stream—MSCF</i>	1000.00	0.	59.80	200.10	367.10	547.30	729.50
<i>Normal Temperature Separation*</i>							
<i>Stock Tank Liquid—Barrels</i>							
Cumulative Produced.	0.	0.	7.06	19.79	30.80	41.53	50.84
Remaining in Vapor in Res.	131.31	131.31	97.16	55.34	34.07	20.89	11.77
Remaining in Liquid in Res.	0.	0.	27.10	56.18	66.44	68.90	68.70
Primary Sep. Gas—MSCF	794.65	0.	48.49	166.85	312.88	473.15	635.04
Second Stage Gas—MSCF	82.58	0.	4.59	13.72	22.59	31.22	40.51
Stock Tank Gas—MSCF	14.75	0.	0.83	2.56	4.31	6.06	7.95
<i>Total "Plant Products" in Primary Separator Gas—Gallons**</i>							
Propane Plus	1822.09	0.	111.98	392.31	754.17	1161.68	1587.72
Butanes Plus	811.70	0.	50.35	179.85	353.88	554.50	764.40
Pentanes Plus	250.79	0.	15.72	57.75	117.78	189.38	265.12
<i>Total "Plant Products" in Well Stream—Gallons</i>							
Propane Plus	7872.05	0.	439.19	1321.39	2235.80	3144.93	4043.82
Butanes Plus	6451.15	0.	354.64	1040.24	1722.29	2381.70	3019.14
Pentanes Plus	5263.11	0.	284.57	809.73	1303.52	1760.39	2186.72

*Primary Separator at 915 PSIA and 95 Degrees F., Second Stage Separator @ 65 PSIA and 70 Degrees F, Stock Tank at 15 PSIA and 75 Degrees F.

**Recover Assumes 100 Percent Plant Efficiency.

All Gas Volumes Calculated at 15.025 PSIA and 60 Degrees F and Stock Tank Liquid Measured at 60 Degrees F.

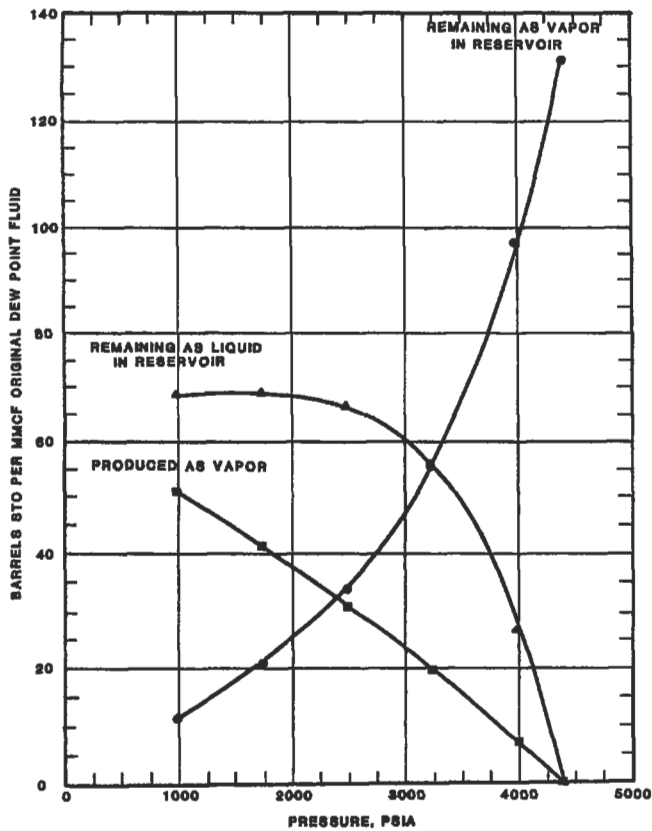


Figure 6-18. Stock-tank liquid production and retrograde condensation during constant volume production at 285°F [11].

Table 6-10
Calculated Wellstream Yields* [11]

Pressure, PSIA	4420 D.P.	4000	3250	2500	1750	1000
Gas—Liq. Ratio**						
SCF 1st. Stg. Gas						
BBL. S.T. Liq.	6,052	7,899	11,194	14,617	16,842	17,951
BBLs. S.T. Liq.						
MMSCF 1st Stg. Gas	165.23	126.60	89.33	68.41	59.38	55.71
BBLs. S.T. Liq.						
MMSCF Well Stream Fld.	131.31	104.70	76.86	61.50	52.86	49.40

*Primary Separator at 915 PSIA and 95 Degrees F., Second Stage Separator at 65 PSIA and 70 Degrees F, Stock Tank at 15 PSIA and 70 Degrees F.

**All Gas Volumes Calculated at 15.205 PSIA and 60 Degrees F and Stock Tank Liquid Measured at 60 Degrees F.

Table 6-11
Differential Vaporization at 220°F [66]

Pressure PSiG	Solution Gas/Oil Ratio(1)	Relative Oil Volume(2)	Relative Total Volume(3)	Oil Density gm/cc	Deviation Factor Z	Gas Formation Volume Factor(4)	Incremental Gas Gravity
	R_{od}	B_{od}					
2620	854	1.600	1.600	0.6562			
2350	763	1.554	1.665	0.6655	0.846	0.00685	0.825
2100	684	1.515	1.748	0.6731	0.851	0.00771	0.818
1850	612	1.479	1.859	0.6808	0.859	0.00882	0.797
1600	544	1.445	2.016	0.6889	0.872	0.01034	0.791
1350	479	1.412	2.244	0.6969	0.887	0.01245	0.794
1100	416	1.382	2.593	0.7044	0.903	0.01552	0.809
850	354	1.351	3.169	0.7121	0.922	0.02042	0.831
600	292	1.320	4.254	0.7198	0.941	0.02931	0.881
350	223	1.283	6.975	0.7291	0.965	0.05065	0.988
159	157	1.244	14.693	0.7382	0.984	0.10834	1.213
0	0	1.075		0.7892			2.039

② 60°F. = 1.000

Gravity of residual oil = 35.1°API @ 60°F.

- (1) Cubic feet of gas at 14.65 psia and 60°F. per barrel of residual oil at 60°F.
 (2) Barrels of oil at indicated pressure and temperature per barrel of residual oil at 60°F.
 (3) Barrels of oil plus liberated gas at indicated pressure and temperature per barrel of residual oil at 60°F.
 (4) Cubic feet of gas at indicated pressure and temperature per cubic foot at 14.65 psia and 60°F.

Table 6-12
Separator Test [8]

Separator Pressure (psig)	Temperature (°F)	GOR, R_{sb} *	Stock-Tank Oil Gravity (°API at 60°F)	FVF, B_{ofb} **
50	75	737	40.5	1.481
to 0	75	41		
		778		
100	75	676	40.7	1.474
to 0	75	92		
		768		
200	75	602	40.4	1.483
to 0	75	178		
		780		
300	75	549	40.1	1.495
to 0	75	246		
		795		

*GOR in cubic feet of gas at 14.65 psia and 60°F per barrel of stock-tank oil at 60°F.

**FVF is barrels of saturated oil at 2,620 psig and 220°F per barrel of stock-tank oil at 60°F.

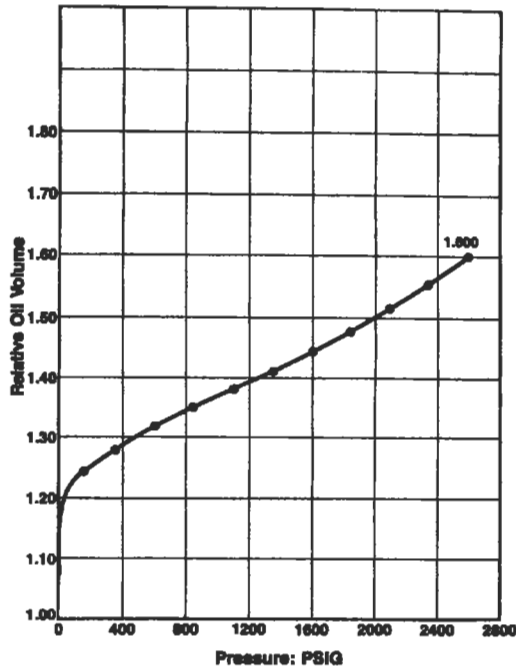


Figure 6-19. Adjustment of oil relative volume curve to separator conditions [6].

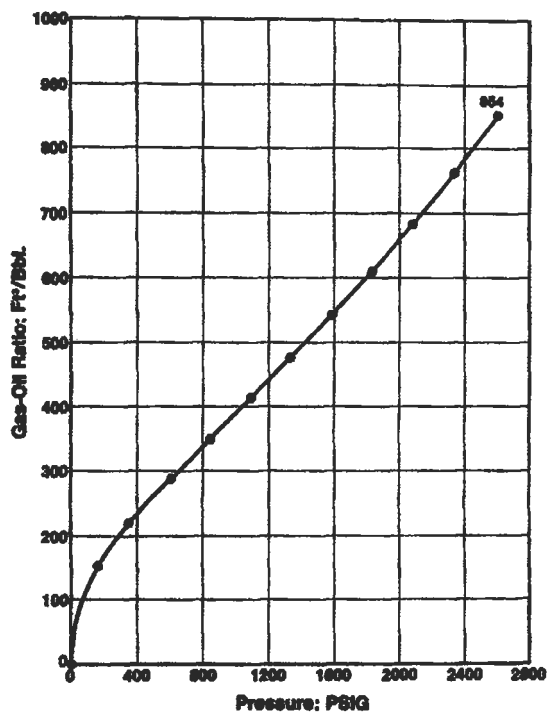


Figure 6-20. Adjustment of gas in solution curve to separator conditions [6].

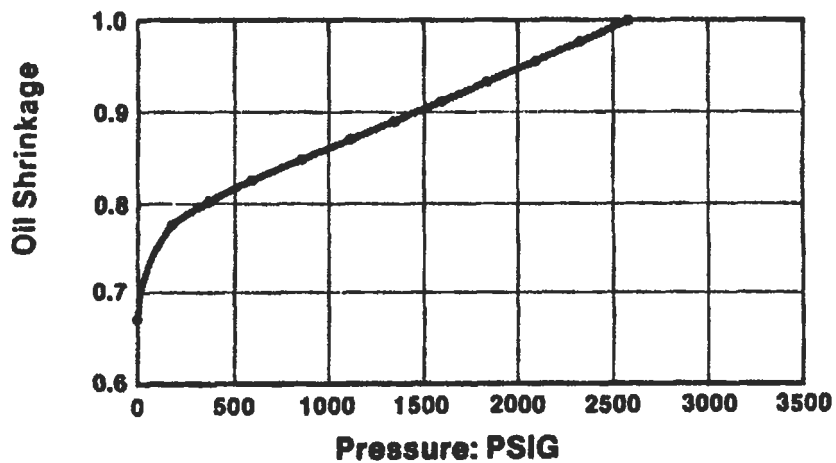


Figure 6-21. Oil-shrinkage curve [8].

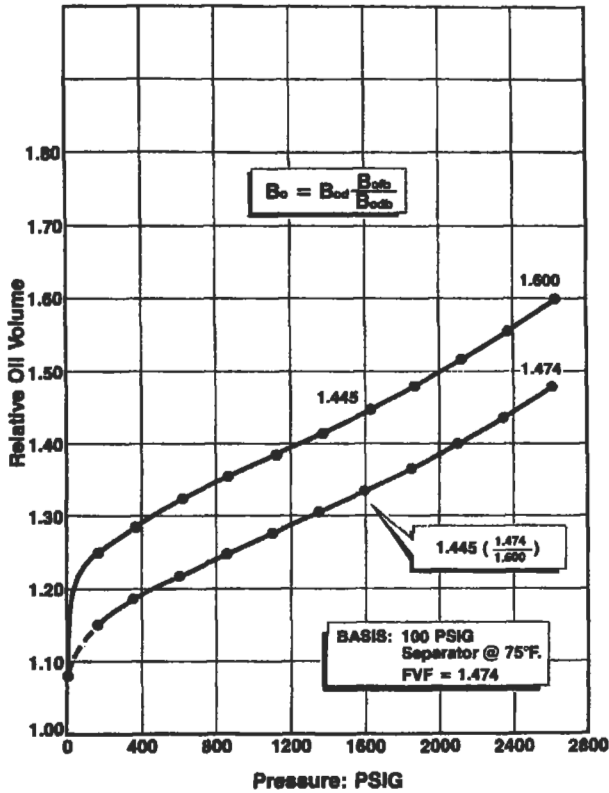


Figure 6-22. Adjustment of oil relative volume curve to separator conditions [6].

(text continued from page 394)

$$K_i = \frac{y_i}{x_i} = \frac{\text{concentration of "i" component in vapor phase}}{\text{concentration of "i" component in liquid phase}} \quad (6-16)$$

In bubble point calculations, x_i is known and either T or P is fixed. The vapor phase composition (y_i) and P or T of the system are unknown.

$$y_i = K_i x_i \quad (6-17)$$

Several different values of the dependent variable are assumed. The correct value is the one that yields

$$\sum_{i=1}^n K_i x_i = \sum_{i=1}^n y_i = 1.0 \quad (6-18)$$

An additional requirement when using composition dependent K values is

$$|y_i^{m+1} - y_i^m| \leq \epsilon, \quad i = 1 \text{ to } n \quad (6-19)$$

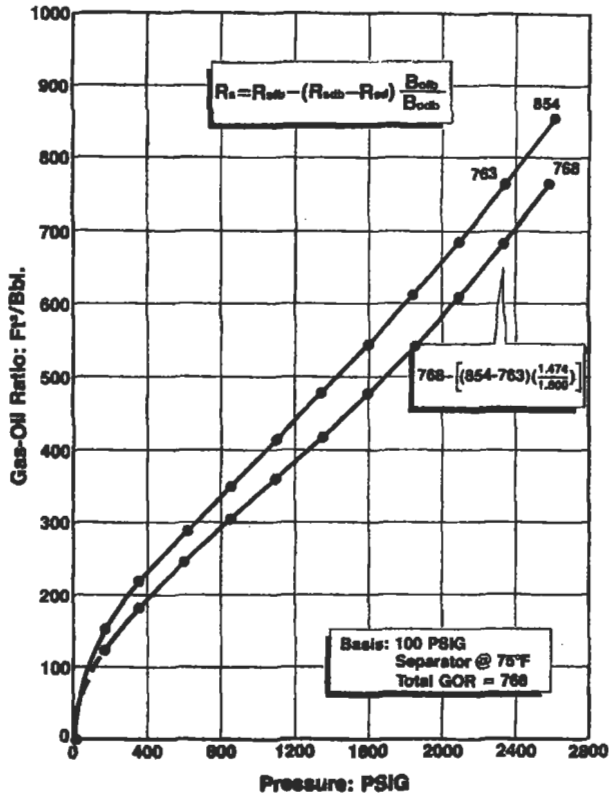


Figure 6-23. Adjustment of gas in solutions curve to separator conditions [6].

where the value of ϵ is arbitrarily small (10^{-4} to 10^{-6}), This requirement is a consequence of using composition dependent K values. If the composition y_i is not correct, the predicted K_i values will not be correct. As a result, the composition of the vapor phase must be stabilized even though the correct value of the dependent variable has been determined. Iterations through the bubble point calculation must be continued until both Equations 6-18 and 6-19 are satisfied. A logical diagram illustrating the basic bubble point calculation is shown in Figure 6-24.

How can we assume initial vapor phase composition? One approach that has been successful is to assume that the mole fraction of the lowest boiling component in the systems is equal to unity with the remaining component mole fractions set to 10^{-6} . Another approach is to get the K value from GPSA [2]. The vapor composition is adjusted after each interaction.

Dew point calculations are the opposite of bubble point calculations: y_i is known and x_i and T or P are to be calculated. The specific equation used in the dew point calculations is

$$x_i = \frac{y_i}{K_i} \tag{6-20}$$

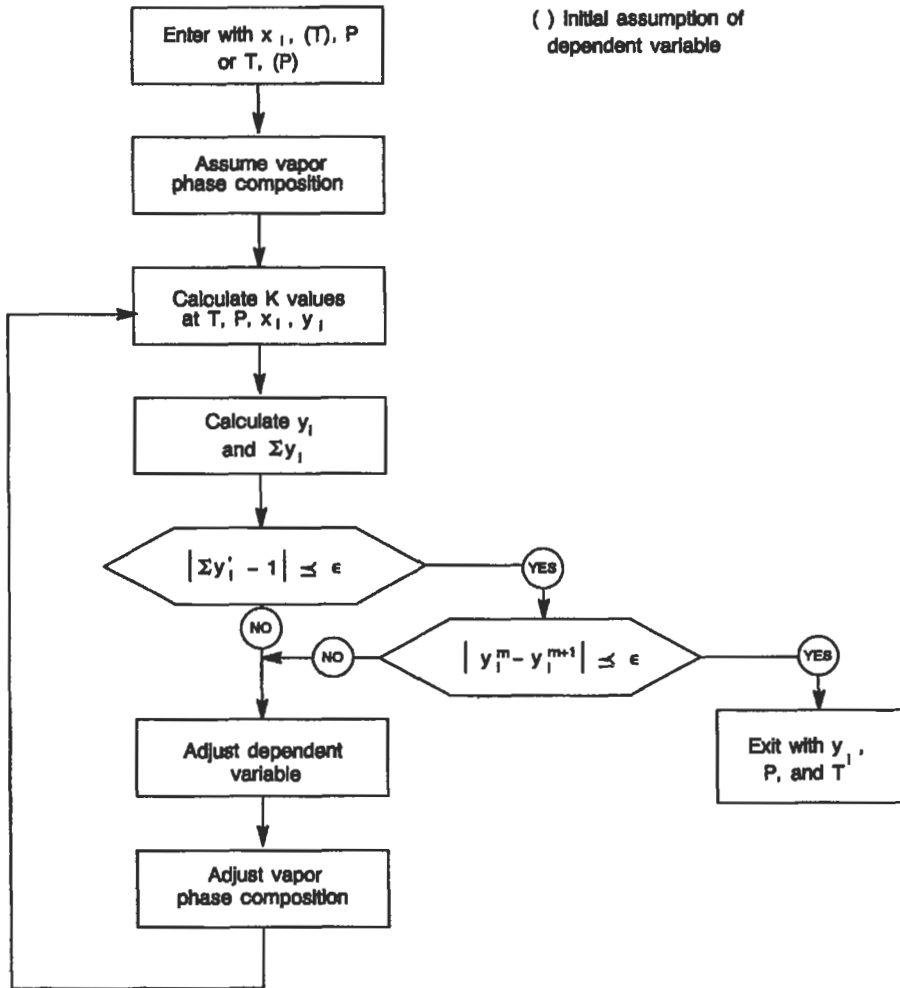


Figure 6-24. Block diagram for bubble point calculations.

As in the bubble point calculation, several different values of the dependent variable are assumed:

$$\sum_{i=1}^n \frac{y_i}{K_i} = \sum_{i=1}^n x_i = 1.0 \tag{6-21}$$

subject to the condition that

$$|x_i^{m+1} - x_i^m| \leq \epsilon, \quad i = 1 \text{ to } n \tag{6-22}$$

A logical diagram for dew point calculation sequence is shown in Figure 6-25. In this case x_i is initially unknown and must be assumed. A procedure is to

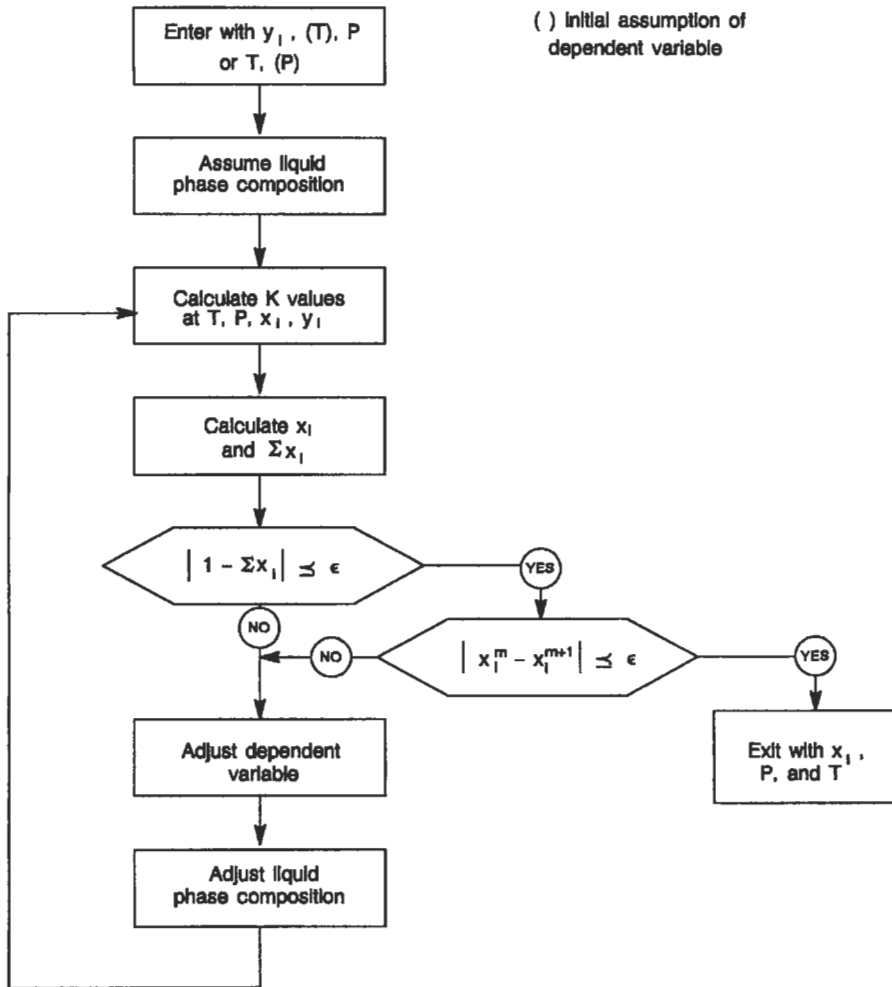


Figure 6-25. Block diagram for dew point calculations.

assume that the mole fraction of the highest boiling component in the system is equal to unity. The remaining component mole fractions are set to 10^{-6} . Liquid phase compositions are adjusted by linear combinations of the assumed and calculated value during each iteration. The convergence algorithms for (T) and (P) dependent calculations are given in Figures 6-26 and 6-27.

The purpose of flash calculations is to predict the composition and amount of the coexisting vapor and liquid phases at a fixed temperature and pressure. According to Equations 6-15 and 6-16

$$\phi \left(\frac{L}{P} \right)^m = \sum_{i=1}^n \frac{z_i (1 - K_i)}{L/F(1 - K_i) + K_i} = 0.0 \quad (6-23a)$$

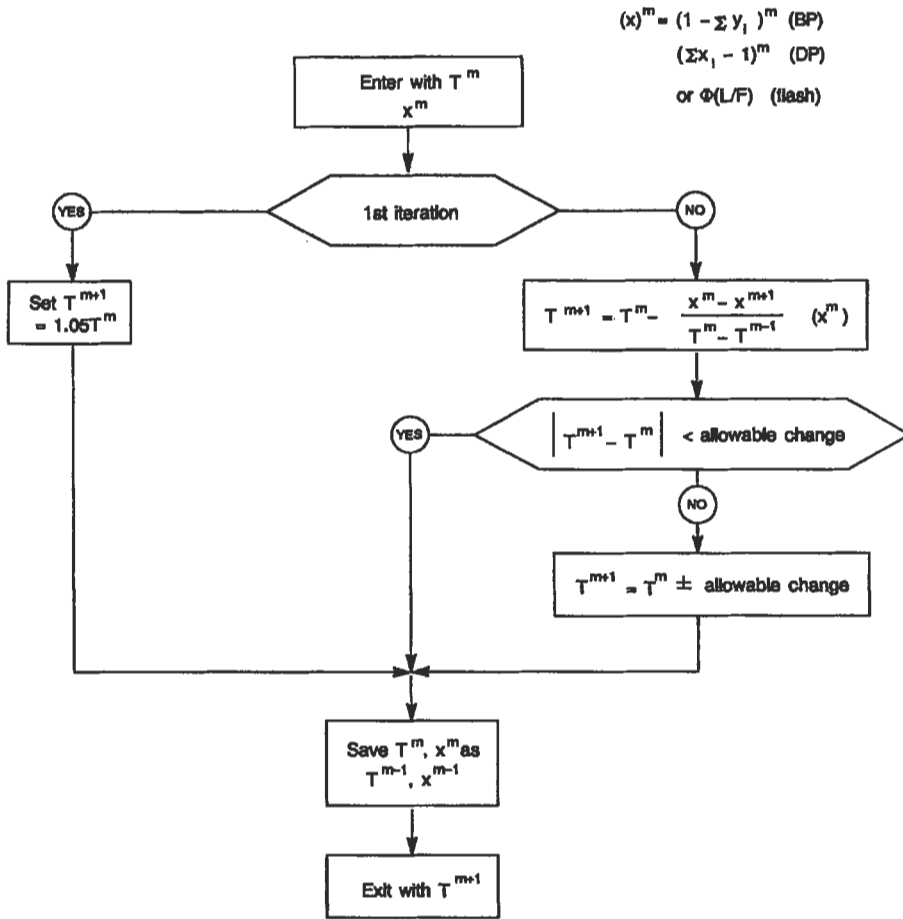


Figure 6-26. Temperature adjustment diagram for equilibrium calculations.

or

$$\phi\left(\frac{L}{P}\right)^m = 1.0 \tag{6-23b}$$

This equation is applicable to a wide of L/F conditions.

In the basic flash calculation, T, P and the overall composition (z_i) are fixed. The unknown variables are x_i , y_i and L/F. A convergence algorithm that can be used with Equation 6-23 is

$$\left(\frac{L}{F}\right)^{m+1} = \left(\frac{L}{F}\right)^m - \frac{\phi\left(\frac{L}{F}\right)^m}{\phi\left(\frac{L}{F}\right)^{m-1}} \tag{6-24a}$$

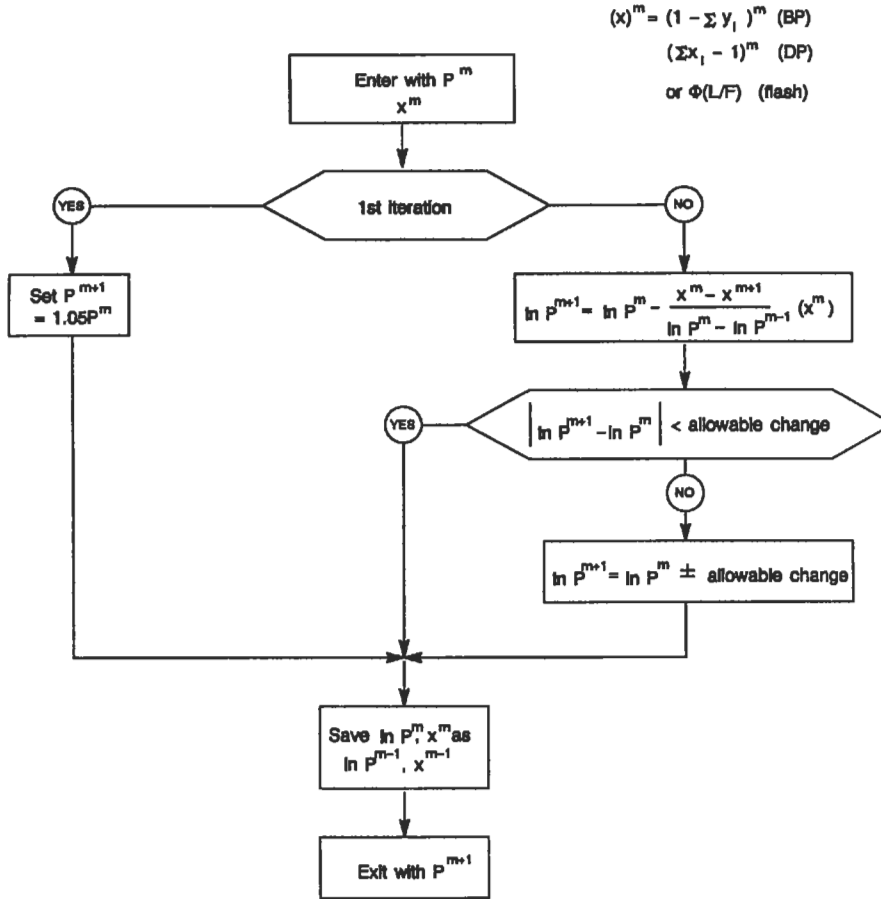


Figure 6-27. Pressure adjustment diagram for equilibrium calculations.

where

$$\Phi\left(\frac{L}{P}\right)^m = -\sum_{i=1}^n \frac{z_i(1 - K_i)^2}{L/F(1 - K_i) + K_i^2} \tag{6-24b}$$

This convergence algorithm is very reliable provided the values of $(L/F)^{m+1}$ are constrained to be valid by material balance considerations:

$$0.0 < (L/F)^{m+1} \leq 1.0 \tag{6-25}$$

The classical bubble point/dew point checks

$$\sum K_i z_i > 1.0 \text{ and } \sum z_i / K_i > 1.0 \tag{6-26}$$

(to assure that the mixture is in two-phase region) cannot be conveniently used in most computer equation-of-state-based flash calculations because the K values for a given system are not known until the final solution has been reached. Consequently, the flash calculation (and its convergence algorithm) must be capable of performing "flash calculation" on single phase systems (subcooled liquids, superheated vapors and dense gas systems) as well as reliably predicting the amount of vapor and liquid present in a two-phase system. When the above flash equation/convergence algorithm is used on single phase systems, the final predicted value of L/F will usually be outside the interval described by Equation 6-25 unless the material balance constraint is enforced. Should a value of $(L/F)^{m+1}$ outside the limits defined by Equation 6-25 be detected in an iteration, we recommend that the value of L/F predicted by Equation 6-24a be replaced by the appropriate value described by the following equations:

$$\text{if } (L/F)_{m+1} < 0.0, \quad (1/F)^{m+1} = (1/F)^m/2.0$$

or

$$\text{if } (L/F)^{m+1} > 1.0, \quad (L/F)^{m+1} = [1 + (L/F)^m]/2.0$$

This procedure eliminates most of the problems associated with flash calculations in single-phase regions and yields excellent results in relatively few iterations inside the two-phase region. Some problems still occur when attempting flash calculations in the dense gas regions.

Initial estimates of the phase composition must be made to initiate the flash calculation. Several procedures are available. It was found that a combination of the bubble point/dew point initial phase estimation procedures works quite well [12]. Set the vapor phase mole fraction of the highest component in the system to 1.0 and the liquid phase mole fraction of the heaviest component in the system at 1.0. All other mole fractions are set to 10^{-6} . This procedure is believed to be superior to the technique of basing the initial assumption of the phase composition on some noncomposition dependent K value estimation procedure, particularly when a wide range of temperatures, pressures, component types, composition ranges, etc., is to be considered.

The estimated vapor and liquid phase compositions must be compared with the calculated phase compositions. Equations 6-19 and 6-23 describe this checking procedure. If the restraints described by these equations for any component (in either phase) are not satisfied, the calculations must be repeated even though an acceptable value for L/F has been determined. Some feel that this detailed checking procedure is unnecessary. It probably is unnecessary for most problems involving moderate temperature-pressure-composition conditions. However, at extreme conditions of temperature, pressure and composition (low-temperatures, high-pressure, high-acid-gas compositions) failure to perform these composition checks will lead to results that are completely incorrect (poor estimates of the phase compositions and incorrect L/F ratios). Unfortunately, the boundary changes in temperature, pressure or composition can completely alter the difficulty of a given problem. Consequently, careful application of these checks in all calculations is strongly recommended since one can never be sure that a particular problem will not fall into the area of extreme conditions.

A logic diagram illustrating the basic flash calculation is shown in Figure 6-28. All the necessary features described earlier are embodied in this diagram.

Flash calculations at fixed L/F and temperature or pressure are frequently necessary. In these calculations, the dependent variable becomes pressure or

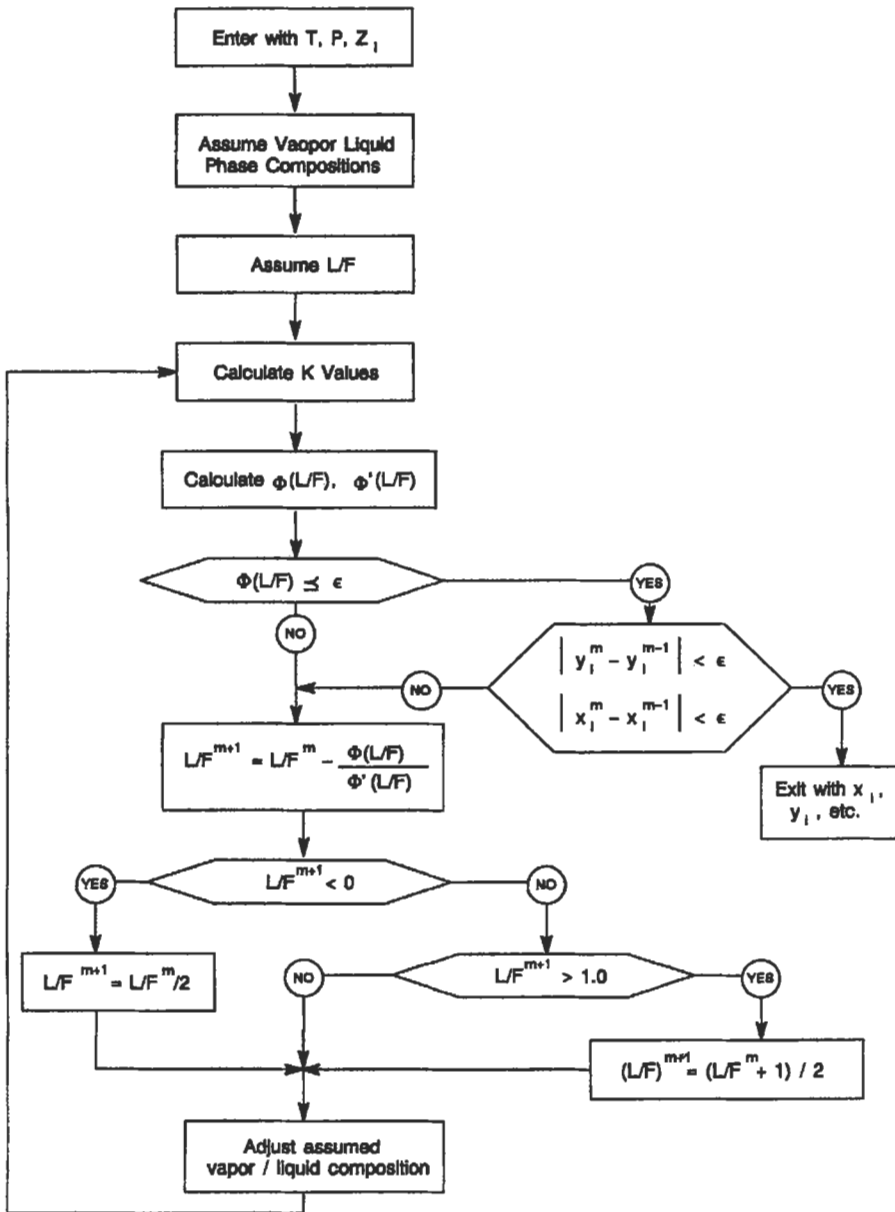


Figure 6-28. Block diagram for two-phase equilibrium calculations.

temperature and the flash calculation becomes similar in principle to a bubble point or dew point calculation. The flash calculation equation described earlier, Equation 6-23, can be coupled with the temperature or pressure adjusting algorithms described for bubble point/dew point calculations to perform these calculations. Initial estimates of the vapor or liquid phase compositions must

be made and the approach described in the flash at fixed temperature–pressure conditions can be used quite effectively. The logic diagram for this type of calculation can be deduced from earlier diagrams.

Predicting the Properties of Hexane Plus (C_{6+}) Fractions

Physical properties light hydrocarbons are given in Table 6-1. In naturally occurring gas and oil C_{6+} is unknown and makes a problem. Since the C_{6+} is a combination of paraffins (P), naphthenes (N) and aromatics (A) of varying molecular mass (M), these fractions must be defined or characterized in some way. Changing the characterization of C_{6+} fractions present in even small amounts (at 1.0% mole level) can have a significant effect on the predicted phase behavior of a hydrocarbon system. The dew point of the gas is heavily dependent upon the heaviest components in the mixture.

The SRK (Equation 9-11) and PR (Equation 9-13) require the smallest number of parameters of any of the equations of state. They require the critical temperature, the critical pressure and the acentric factor. There are many different approaches that can be utilized to predict these parameters for C_{6+} fractions or other mixtures of undefined components.

Some minimum of information must be available on the C_{6+} fraction, usually it is specific gravity (S) average boiling point (T_b) and molecular mass (M) of the fraction.

The following equation is used [14] to estimate the molecular mass (M) of petroleum fractions

$$M = 2.0438 \times 10^2 \exp(0.00218T) \exp(-3.07S) T^{0.118} S^{1.88} \quad (6-27)$$

where T = mean average boiling point of petroleum fraction, °R (from ASTM D86 test, see Figure 6-29)

S = specific gravity, 60°F/60°F

The following equation is to be used to calculate the initial temperature (T_c) of pure hydrocarbons; it is applicable for all families of hydrocarbons:

$$\log T_c = A + B \log S + C \log T_b \quad (6-28)$$

T_c (°R); T_b and S given; A, B and C as below:

Type Compound	A	B	C
Paraffin	1.47115	0.43684	0.56224
Napthene	0.70612	-0.07165	0.81196
Olefin	1.18325	0.27749	0.65563
Acetylene	0.79782	0.30381	0.79987
Diolefin	0.14890	-0.39618	0.99481
Aromatic	1.14144	0.22732	0.66929

For petroleum fractions, physical properties can be predicted more accurately if the fraction of paraffins (P), naphthenes (N) and aromatics (A) are known. If θ is a physical property to be predicted and the molecular type fractions are known, a pseudocompound, i.e., a compound having the same boiling point and specific gravity as the fraction, for each molecular type can be defined. These properties can be combined by

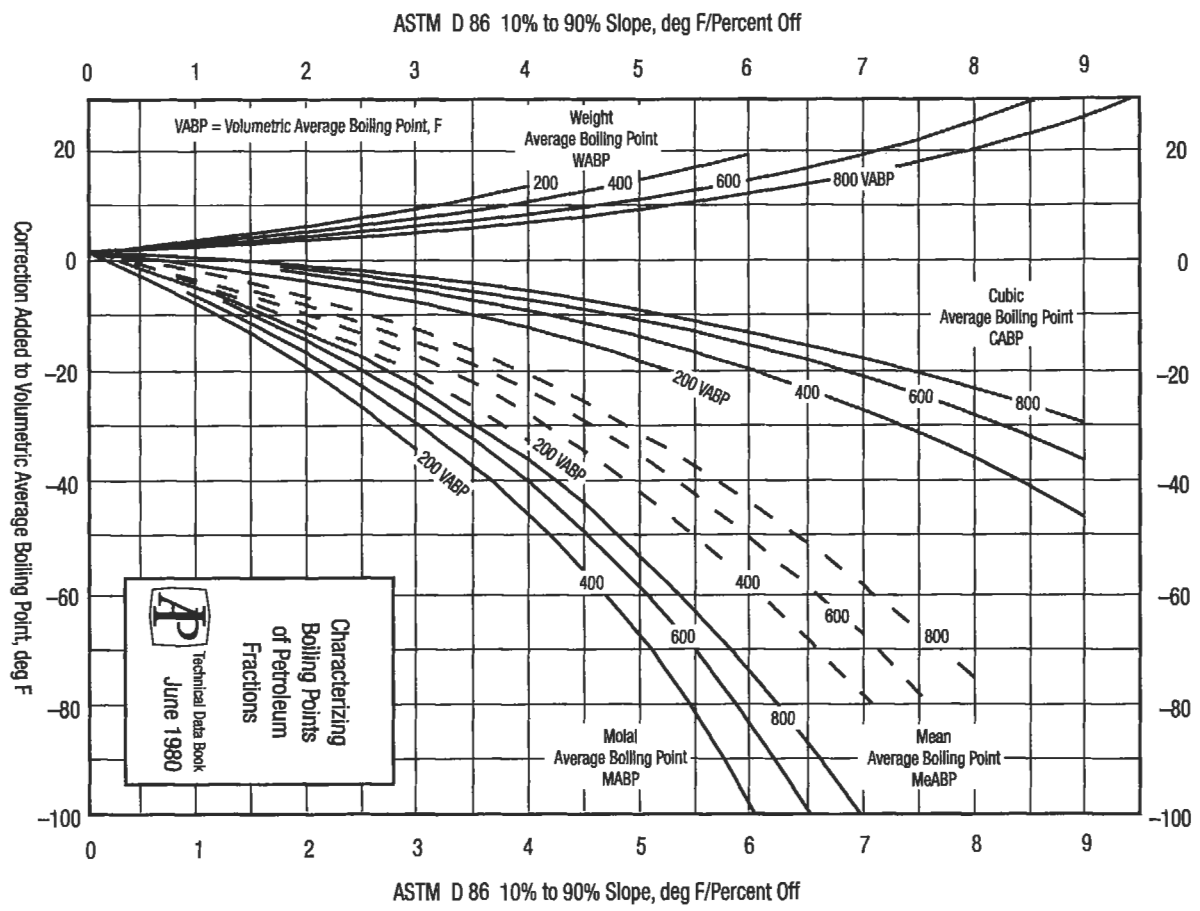


Figure 6-29. Characterizing boiling points of petroleum fractions.

$$\theta = P\theta_p + N\theta_N + A\theta_A \tag{6-29}$$

where P + N + A = 1.0, are the sum of paraffins, naphthenes and aromatics present in the fraction.

The basic equation for any value of property θ is [15]

$$\theta = aT_b^{bSc} \tag{6-30}$$

Correlation constants are given in Table 6-13.

Next, correlation of critical properties and acentric factor (ω) of hydrocarbons and derivatives is developed in terms of M , T_b and S . Since molecular mass is readily determined by experiments, it is introduced as a correlating variable to obtain more general results. The specific gravity is the ratio of the density of the liquid at 20°C to that of water at 4°C.

The critical properties and acentric factor of C_1 to C_{20} n-alkanes are correlated with M by the following equation:

$$\theta_A = C_1 + C_2M + C_3M^2 + C_4M^3 + C_5/M \quad (6-31)$$

where θ_A represents T_c , L_nP_c , V_c or ωT_c of a n-alkane. The coefficients C_1 to C_5 are reported in Table 6-14 for each property. It was additionally correlated S and T_b of the n-alkanes by Equation 6-31 and the coefficients are included in Table 6-14. The correlated S_A and T_{bA} of the n-alkanes will be required in the perturbation equations to follow as independent variables.

The average absolute deviations (AAD) of the correlations from the American Petroleum Institute project 44 table values are 0.15% for T_c , 1.0% for p_c (excluding methane), 0.8% for V_c , 1.2% for ω , 0.11% for T_b and 0.07% for S . The specific gravity correlation applies only to C_5 - C_{16} , which are the only n-alkanes that are liquids at 20°C.

Properties of the general hydrocarbons and derivatives are correlated as perturbations of those of n-alkanes according to the equation

$$\begin{aligned} \theta = \theta_A + A_1\Delta S + A_2\Delta T_b + A_3(\Delta S)^2 + A_4(\Delta S)(\Delta T_b) + A_5(\Delta T_b)^2 \\ + A_6(\Delta S)^3 + A_7(\Delta S)^2(\Delta T_b) + A_8(\Delta S)(\Delta T_b)^2 + A_9(\Delta T_b)^3 \end{aligned} \quad (6-32a)$$

with

$$\Delta S = S - S_A \quad (6-32b)$$

$$\Delta T_b = T_b - T_{bA} \quad (6-32c)$$

Table 6-13
Correlation Constants for Equation 6-30

θ	a	b	c
M (Molecular mass)	4.5673×10^{-5}	2.1962	-1.0164
T_c (Critical Temperature °R)	24.2787	0.58848	0.3596
P_c (Critical Pressure, psia)	3.12281×10^9	-2.3125	2.3201
V_c^m (Molar critical volume ft ³ /lb mole)	7.0434×10^{-7}	2.3829	-1.683
V_c (Critical Volume ft ³ /lb)	7.5214×10^{-3}	0.2896	-0.7666
V (Liquid molar volume at 20°C and 1 atm (cm ³ /g mole)	7.6211×10^{-5}	2.1262	-1.8688
ρ (Liquid density g/cc)	0.982554	0.002016	1.0055

Table 6-14
Coefficients for θ_A in Equation 6-31

θ_A	C_1	C_2	C_3	C_4	C_5
T_c	2.72697×10^2	3.91999	-1.17706×10^{-2}	1.48679×10^{-5}	-2.27789×10^3
$\ln P_c$	1.77645	-1.01820×10^{-2}	2.51106×10^{-5}	-3.73775×10^{-5}	3.50737
V_o	1.54465×10	4.04941	1.73999×10^{-4}	1.05086×10^{-6}	2.99391×10^2
ωT_c	-1.56752×10	1.22751	9.96848×10^{-3}	-2.04742×10^{-5}	-6.90883×10
S	6.64050×10^{-1}	1.48130×10^{-3}	-5.07021×10^{-5}	6.21414×10^{-9}	-8.45218
T_b	1.33832×10^2	3.11349	-7.08978×10^{-3}	7.69085×10^{-5}	-1.12731×10^3

T_c and T_b are in K, P_c in MPa, V_o in cm^3/mol .

where S_A and T_{bA} are the gravity and boiling point of the hypothetical n-alkane of the M of the substance of interest and are given by Equation 6-31.

The coefficients A_i in Equation 6-32a are given by

$$A_i = a_i + b_i M$$

Table 6-15 presents the coefficients a_i and b_i that have been determined by fitting Equation 6-32d to the properties of a large number of hydrocarbons and derivatives.

State-of-the-art Equation 6-32 gives the best results.

The five general categories of experimental data availability for C_{6+} fractions are:

1. *The specific or API gravity of the C_{6+} fraction.* The molecular mass may have been determined experimentally or estimated from some correlation of specific gravity and molecular mass.
2. *Chromatographic analysis.* The C_{6+} fraction has been analyzed by gas-liquid chromatography. These results may be reported as a series of equivalent n-paraffins up to as high as nC_{30} or as a true boiling point analysis. The specific gravity and/or molecular mass of the fraction may or may not be reported.
3. *ASTM (D158 or equivalent) analysis.* This analysis is equivalent to a non-refluxed single-stage batch distillation. Usually the boiling point temperature at seven different points (START, 10%, 30%, 50%, 70%, 90%, END) will be recorded. The points correspond to the volume fraction of the C_{6+} distilled into the receiver vessel. The specific gravity and molecular mass of the total C_{6+} fraction are normally also measured.

Table 6-15
Coefficients for Equation 6-32d

θ				
	T_c	$\ln P_c$	V_c	ωT_c
a_1	1.58025×10^3	9.71572	-1.18812×10^3	-1.16044×10^3
a_2	-5.68509	-3.32004×10^{-2}	-1.18745	3.48210
a_3	-1.21659×10^4	-8.60375×10	7.36085×10^3	2.78317×10^4
a_4	7.50653×10	5.50118×10^{-1}	6.83380×10	-2.05257×10^2
a_5	-9.66385×10^{-2}	-9.00036×10^{-4}	-2.12107×10^{-1}	4.55767×10^{-1}
a_6	2.17112×10^4	1.85927×10^2	-4.84696×10^3	-7.13722×10^4
a_7	-1.57999×10^2	-1.51115	-4.12064×10^2	5.08888×10^2
a_8	3.60522×10^{-1}	4.32808×10^{-3}	2.02114	-8.10273×10^{-1}
a_9	-2.75762×10^{-4}	-3.81526×10^{-6}	-2.48529×10^{-3}	-1.68712×10^{-3}
b_1	-1.18432×10	-7.50370×10^{-2}	1.17177×10	1.89761
b_2	5.77384×10^{-2}	3.15717×10^{-4}	-3.48927×10^{-2}	2.41662×10^{-2}
b_3	1.10697×10^2	8.42854×10^{-1}	-1.34146×10^2	-2.67462×10^2
b_4	-6.58450×10^{-1}	-5.21464×10^{-3}	5.63667×10^{-2}	2.06071
b_5	7.82310×10^{-4}	7.87325×10^{-6}	9.52631×10^{-4}	-5.22105×10^{-3}
b_6	-2.04245×10^2	-1.85430	1.80586×10^2	7.66070×10^2
b_7	1.32064	1.36051×10^{-2}	2.56478	-5.75141
b_8	-2.27593×10^{-3}	-3.23929×10^{-6}	-1.74431×10^{-2}	8.66667×10^{-3}
b_9	8.74295×10^{-7}	2.18899×10^{-8}	2.50717×10^{-5}	1.75189×10^{-5}

4. *A partial TBP analysis.* A true boiling point (TBP) distillation has been performed on the C_{6+} fraction. The TBP distillation is a batch distillation similar to an ASTM distillation but the distillation apparatus contains several trays (usually 10 or more or the equivalent amount of packing) and a high reflux ratio is used. The TBP gives a sharper separation between the subfractions than an ASTM distillation. Normally, at least five temperatures are reported as a function of liquid volume percent distilled over. Frequently, more than 20 temperatures will be reported. The specific gravity and molecular mass of the total fraction are usually reported.
5. *A complete TBP analysis.* A true boiling point distillation has been performed on the total C_{6+} fraction. The specific gravity and molecular mass have been measured for each of the reported distillate subfractions. Between five and fifty temperatures and subfraction properties will be reported.

Table 6-15 shows typical information as it may be reported for each of the five categories of C_{6+} characterization. The complete TBP analysis is believed to be the best form of C_{6+} analysis to be used with today's thermodynamic property prediction procedures. Consequently, it is recommended that all noncomplete TBP analyses be converted to this form. This section deals with these conversion techniques. These techniques are based on empirical correlations and, in some cases, experience and judgment. There is also one basic constraint that must be used in these conversion techniques—that is, maintenance of volume-mass-molar relationships in the C_{6+} fraction along with consistency in the composition of the total stream. One cannot capriciously change the molecular mass or specific gravity of the total C_{6+} fraction without simultaneously adjusting the reported composition. All of the procedures reported here strive to maintain consistency of the specific gravity, molecular mass and, when possible, the boiling point(s) of the total C_{6+} fraction.

The various procedures for converting noncomplete TBP analyses to complete TBP analyses are illustrated in the following section. A common sample problem is used to illustrate the basic conversion procedure. In addition, the results of several equilibrium calculations are reported for each type of characterization. The gas composition, true boiling point data, gravity and molecular weight measurements for the C_{7+} fraction are shown in Table 6-16. Though the particular system chosen shows C_{7+} as a basis for the heavy and characterization C_{6+} will be used. There are several isomers of hexane, as well as other materials, that can appear in the C_{6+} subfraction. The molecular mass tabulated for the fractions in Table 6-16 makes them appear to be normal paraffins. This, however, is not true and a complete TBP analysis was made on the C_{7+} fraction.

Calculations made based on the different C_{7+} characterizations are compared with experimental values, Table 6-17 and Figure 6-30. The complete TBP characterization provides the best predictions of the phase behavior and the liquid formation, though there is only a little difference between the full TBP and the partial TBP results. The lumped specific gravity-molecular mass characterization and the lumped n-paraffin characterization give the poorest predictions. All of the characterizations in Table 6-18 are in better agreement with experimental values than one would normally expect.

Vapor-Liquid Equilibrium by Equation of State

Prediction of a vapor-liquid mixture is more complicated than prediction of pure component VLE.

(text continued on page 416)

Table 6-16
Sample Analysis for Five Categories of C₆₊ Analysis [12]

Categories											
1		2*		3		4		5			
Specific Gravity		Molar Chromatographic		ASTM		Partial TBP		Complete TBP			
Information	Values Reported	Information Reported	Values mol %	Information Reported LV%	Values Reported T, °F	Information Reported LV%	Values Reported T, °F	Information Reported LV%	Values Reported T, °F	sp gr	mol wt
specific gravity (°API)	0.7268 (63.2)	C ₆	.335								
		C ₇	.327	ST	258	ST	155	ST	155		
		C ₈	.341	10	247	S	190	17.52	238	0.745	100
		C ₉	.268	30	283	10	212	33.12	280	0.753	114
molecular mass	104	C ₁₀	.166	50	331	20	246
				70	403	30	270
				90	500	40	304
		C ₃₃	.004	GP	596	50	348
		C ₃₄	.004			60	380
		C ₃₅₊	.006	specific gravity API	.7867	70	431
		specific gravity	?		48.37	80	481
						90	538
						95	583	99.73	.	.	.
		molecular mass	?	molecular mass	141.26	EP	700	EP	698	0.878	310
						specific gravity	.7867				
						molecular mass	141.26				

*Chromatographic TBP will be similar to ASTM or partial TBP

Table 6-17
Experimental Data for Illustrative Calculations [12]

<u>Component</u>	<u>mol %</u>	<u>BPT °F</u>	<u>sp gr</u>	<u>mol wt</u>
C ₁	91.35			
C ₂	4.03			
C ₃	1.53			
iC ₄	0.39			
nC ₄	0.43			
iC ₅	0.15			
nC ₅	0.19			
C ₆	0.39			
Fraction 7	0.361	209	0.745	100
8	0.285	258	0.753	114
9	0.222	303	0.773	128
10	0.158	345	0.779	142
11	0.121	384	0.793	156
12	0.097	421	0.804	170
13	0.083	456	0.816	184
14	0.069	488	0.836	198
15	0.050	519	0.840	212
16	0.034	548	0.839	226
17	0.023	576	0.835	240
18	0.015	603	0.850	254
19	0.010	628	0.865	268
20	0.006	653	0.873	282
21	0.004	676	0.876	296
22	0.002	698	0.878	310

mol % C₇₊ = 1.540
 mol wt C₇₊ = 141.26
 sp gr C₇₊ = 0.7867 (48.35 °API)

Phase Behavior Data

dew point at 201°F - 3837 psia

Liquid Formation at 201°F

<u>Pressure psia</u>	<u>Bbl/MMSCF</u>	<u>Specific Gravity Liquid</u>
2915	9.07	0.6565
2515	12.44	0.6536
2015	15.56	0.6538
1515	16.98	0.6753
1015	16.94	0.7160
515	15.08	0.7209

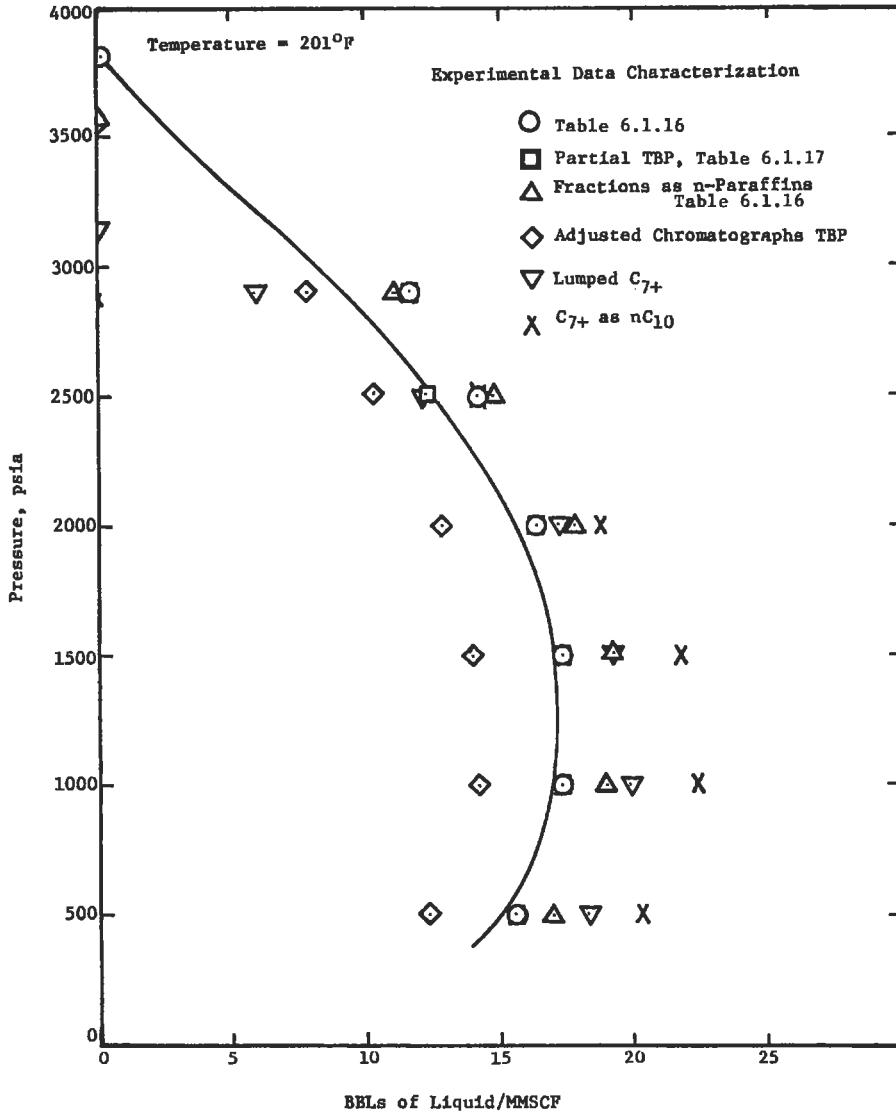


Figure 6-30. Effect of C₆₊ characterization on predicted liquid formation [12].

(text continued from page 413)

The following condition equations for mixture VLE can be derived from classical thermodynamics:

$$T^V = T^L \tag{6-33}$$

$$P^V = P^L \tag{6-34}$$

$$f_i^V = f_i^L \tag{6-35}$$

Table 6-18
Effect of C₇₊ Characterization on Predicted Sample Problem Phase Behavior [12]

	Experiment Values	C ₇₊ from Table 6.1.16	Partial TBP	C ₇₊ Predicted Values for Characterization Chromatographic			
				Fractions as n-paraffins	Fractions from ASTM dest. curve	Lumped C ₇₊	C ₇₊ as nC ₁₀
Dew Point at 201° F, psig	3822	3824	3800	3583	3553	3150	2877
Amount of liquid at BBL/MMSCF							
2900 psig	9.07	11.57	11.50	11.07	7.37	5.95	0.0
2500 psig	12.44	14.26	14.22	14.89	10.21	12.40	14.09
2000 psig	15.56	16.43	16.44	17.77	12.66	17.09	18.77
1500 psig	16.98	17.48	17.49	19.08	14.00	19.35	21.74
1000 psig	16.94	17.38	17.39	18.99	14.15	19.91	22.25
500 psig	15.08	15.56	15.59	16.98	12.46	18.11	20.32

*Based on 10 equal LV% fractions

What does “ f_i ” mean?

The equilibrium constants, or K values, are defined as the ratio of vapor and liquid compositions:

$$K_i = \frac{y_i}{x_i} \quad (6-36)$$

The Gibbs free energy is a property of particular importance because it can be related to the equilibrium state and at the same time can be expressed as a function of T and P:

$$dG_i = -SdT + VdP \quad (6-37)$$

If Equation 6-37 is applied to an ideal gas it becomes

$$dG_i = RT d(\ln P) \quad (6-38)$$

If we now define a property such that Equation 6-38 will apply for all gases under all conditions of temperature and pressure

$$dG_i = RT d(\ln f_i) \quad (6-39)$$

f_i is called the fugacity of component “i” and has a units of pressure. If Equation 6-39 is integrated for an ideal gas:

$$f_i = cP \quad (6-40)$$

“c” is constant and for an ideal gas is equal to 1.0. For real gases the only condition under which the gas will behave ideally is at zero pressure. This can be expressed as

$$\lim_{P \rightarrow 0} \frac{f_i}{P} = 1.0 \quad (6-41)$$

The fugacity of a single component in a mixture is defined in a manner similar to Equation 6-36:

$$dG = RTd(\ln f_i) \quad (6-42)$$

and by analogy to Equation 6-39

$$\lim_{P \rightarrow 0} \frac{f_i}{x_i P} = 1.0 \quad (6-43)$$

The fugacity is sometimes referred to as a *corrected pressure*. A more valuable parameter for use in correlative procedures would be a variable with characteristics similar to fugacity, but which ranged over a much smaller range of numbers. It is the fugacity coefficient ϕ_i .

For a pure component

$$\phi_i = \frac{f_i}{P} \quad (6-44)$$

For a component in a mixture

$$\phi_i = \frac{f_i}{x_i P} \quad (6-45)$$

The fugacity coefficients are readily calculated from P-V-T data for both, pure component and mixture.

P-V-T of a fixed composition system can be developed in pressure explicit forms, i.e.,

$$P = \phi(V, T) \quad (6-46)$$

The basic equation of state may be transformed to a compressibility factor Z , but the basic expression given by Equation 6-44 still applies. Equilibrium K values are predicted from fugacity, which is related to Gibbs free energy. One of the basic definitions of fugacity gased K values is

$$K = \frac{y_i}{x_i} = \frac{\phi_i^L}{\phi_i^V} = \frac{f_i^L / (P x_i)}{f_i^V / (P y_i)} \quad (6-47)$$

The fugacity coefficient ϕ_i is related to the pressure, volume and temperature by

$$\ln \phi_i = -\frac{1}{RT} \int_V^{\infty} \left[\left(\frac{\partial P}{\partial n_i} \right)_{T, V, n_j} - \frac{RT}{V} \right] dV - \ln Z \quad (6-48)$$

Applying the SRK equation,

$$\ln \phi_i = -\ln \left(Z - \frac{Pb}{RT} \right) + (Z-1)B'_i - \frac{a}{bRT} (A'_i - B'_i) \ln \left(1 + \frac{b}{V} \right) \quad (6-49)$$

or

$$\ln \phi_i = -\ln(Z - B) + (Z-1)B'_i - \frac{A}{B} (A'_i - B'_i) \ln \left(1 + \frac{B}{Z} \right) \quad (6-50)$$

where

$$B_i = \frac{b_i}{b} \quad (6-51)$$

$$A'_i = \frac{1}{a} \left[2a_i^{0.5} \sum_j^N x_j a_j^{0.5} (1 - k_{ij}) \right] \quad (6-52)$$

Notations are as for Equations 6-11 and 6-12. For values k_{ij} see Tables 6-19 and 6-20. The data in Table 6-19 was prepared for the Peng-Robinson equation,

(text continued on page 422)

Table 6-19
 Values of Interaction Parameters k_{ij} for Use in the Peng-Robinson Equation

($k_{ij} = 100$)

Methane	Ethane	Propane	i-Butane	n-Butane	i-Pentane	n-Pentane	n-Hexane	n-Heptane	n-Octane	n-Nonane	n-Decane	Nitrogen	Carbon Dioxide	Hydrogen Sulfide	Toluene	Benzene	Cyclohexane	Water	
0.0	0.0	0.0	0.0	0.0	0.0	0.0	0.0	0.0	0.0	0.0	0.0	3.6	10.0	8.5	4.0	4.0	3.5	50.0	Methane
	0.0	0.0	0.0	0.0	0.0	0.0	0.0	0.0	0.0	0.0	0.0	5.0	13.0	8.4	2.0	2.0	2.0	48.0	Ethane
		0.0	0.0	0.0	0.0	0.0	0.0	0.0	0.0	0.0	0.0	8.0	13.5	7.5	2.0	2.0	2.0	48.0	Propane
			0.0	0.0	0.0	0.0	0.0	0.0	0.0	0.0	0.0	9.5	13.0	5.0	0.0	0.0	0.0	48.0	i-Butane
				0.0	0.0	0.0	0.0	0.0	0.0	0.0	0.0	9.0	13.0	6.0	0.0	0.0	0.0	48.0	n-Butane
					0.0	0.0	0.0	0.0	0.0	0.0	0.0	9.5	5.0	6.0	0.0	0.0	0.0	48.0	i-Pentane
						0.0	0.0	0.0	0.0	0.0	0.0	10.0	5.0	6.5	0.0	0.0	0.0	48.0	n-Pentane
							0.0	0.0	0.0	0.0	0.0	10.0	5.0	6.0	0.0	0.0	0.0	48.0	n-Hexane
								0.0	0.0	0.0	0.0	10.0	5.0	6.0	0.0	0.0	0.0	48.0	n-Heptane
									0.0	0.0	0.0	10.0	11.5	5.5	0.0	0.0	0.0	48.0	n-Octane
										0.0	0.0	10.0	11.0	5.0	0.0	0.0	0.0	48.0	n-Nonane
											0.0	10.0	11.0	4.5	1.0	1.0	1.0	0.0	n-Decane
												0.0	2.0	18.0	18.0	16.0	10.0	0.0	Nitrogen
													0.0	10.0	9.0	7.5	10.0	0.0	Carbon Dioxide
														0.0	0.0	0.0	0.0	0.0	Hydrogen Sulfide
															0.0	0.0	0.0	0.0	Toluene
																0.0	0.0	0.0	Benzene
																	0.0	0.0	Cyclohexane
																		0.0	Water

Table 6-20
Values of Interaction Parameters k_{ij} Proposed by Starling

Methane	Ethylene	Ethane	Propylene	Propane	i-Butane	n-Butane	i-Pentane	n-Pentane	Hexane	Heptane	Octane	Nonane	Decane	Undecane	Nitrogen	Carbon dioxide	Hydrogen Sulfide	
0.0	1.0	1.0	2.1	2.3	2.75	3.1	3.6	4.1	5.0	6.0	7.0	8.1	9.2	10.1	2.5	5.0	5.0	Methane
	0.0	0.0	0.3	0.31	0.4	0.45	0.5	0.6	0.7	0.85	1.0	1.2	1.3	1.5	7.0	4.8	4.5	Ethylene
		0.0	0.3	0.31	0.4	0.45	0.5	0.6	0.7	0.85	1.0	1.2	1.3	1.5	7.0	4.8	4.5	Ethane
			0.0	0.0	0.3	0.35	0.4	0.45	0.5	0.65	0.8	1.0	1.1	1.3	10.0	4.5	4.0	Propylene
				0.0	0.3	0.35	0.4	0.45	0.5	0.65	0.8	1.0	1.1	1.3	10.0	4.5	4.0	Propane
					0.0	0.0	0.08	0.1	0.15	0.18	0.2	0.25	0.3	0.3	11.0	5.0	3.6	i-Butane
						0.0	0.08	0.1	0.15	0.18	0.2	0.25	0.3	0.3	12.0	5.0	3.4	n-Butane
							0.0	0.0	0.0	0.0	0.0	0.0	0.0	0.0	13.4	5.0	2.8	i-Pentane
								0.0	0.0	0.0	0.0	0.0	0.0	0.0	14.8	5.0	2.0	n-Pentane
									0.0	0.0	0.0	0.0	0.0	0.0	17.2	5.0	0.0	Hexane
										0.0	0.0	0.0	0.0	0.0	20.0	5.0	0.0	Heptane
											0.0	0.0	0.0	0.0	22.8	5.0	0.0	Octane
												0.0	0.0	0.0	26.4	5.0	0.0	Nonane
													0.0	0.0	29.4	5.0	0.0	Decane
														0.0	32.2	5.0	0.0	Undecane
															0.0	0.0	0.0	Nitrogen
																0.0	0.0	Carbon dioxide
																	0.0	Hydrogen sulfide

(text continued from page 419)

while the data from Table 6-20 was used for the Benedict-Webb-Rubin equation modified by Starling [16].

Applying Peng-Robinson equation

$$\ln \phi_i = -\ln\left(Z - \frac{Pb}{RT}\right) + (Z-1)B'_i - \frac{a}{2^{1.5}bRT}(A'_i - B'_i) \ln\left[\frac{V + (2^{0.5} + 1)b}{V - (2^{0.5} - 1)b}\right] \quad (6-53a)$$

or

$$\ln \phi_i = -\ln(Z - B) + (Z-1)B'_i - \frac{A}{2^{1.5}B}(A'_i - B'_i) \ln\left[\frac{Z + (2^{0.5} + 1)B}{Z - (2^{0.5} - 1)B}\right] \quad (6-53b)$$

where

$$B_i = \frac{b_i}{b} \quad (6-54)$$

$$A'_i = \frac{1}{a} \left[2a_i^{0.5} \sum_j x_j a_j^{0.5} (1 - k_{ij}) \right] \quad (6-55)$$

Notations are as in Equations 6-13 and 6-14.

The objectives of any equation-of-state solution method are the reliable and accurate prediction of the volumetric properties of the fluid mixture under consideration. The overall solution procedure is as follows:

- fix the total composition, temperature and pressure
- calculate constants for the equation of state
- solve equation for the volumetric property (specific volume, density or compressibility factor)

When pressure and temperature fall to a two-phase region, the equation must be solved twice, separately for vapor and liquid. The composition of each phase will be different so the equation of state constants will have to be evaluated for both the liquid and the vapor phases. Both SRK and PR are cubic equations, so the solution always gives three roots, as is shown in Figure 6-31 [17]. However, the P_r - V_r relationship at a given T_r is discontinuous at $V_r = b'_1$, $V_r = b'_2$, and $V_r = b'_3$. We are interested in only $V_r > b'_1$, which in case the SRK equation is equal 0.08664 and 0.077796 for the PR equation. For $V_r > b'_1$ and $T_r > 1.0$, there is only one value of the compressibility factor that will satisfy the equation of state. For $V_r > b'_1$ and $T_r < 1.0$ we will get three values of Z . The largest Z of the vapor Z^v is chosen for the vapor and the smallest amount the liquid Z^l is chosen for the liquid. However, in an earlier stage of the iterative VLE calculations, it is not uncommon to encounter a single root, mainly because of incorrect compositions [17].

A logic diagram for a trial-and-error solution procedure for cubic equations of state is given in Figure 6-32. This diagram shows a traditional Newton-Raphson approach with an interval halving limiting procedure superimposed on

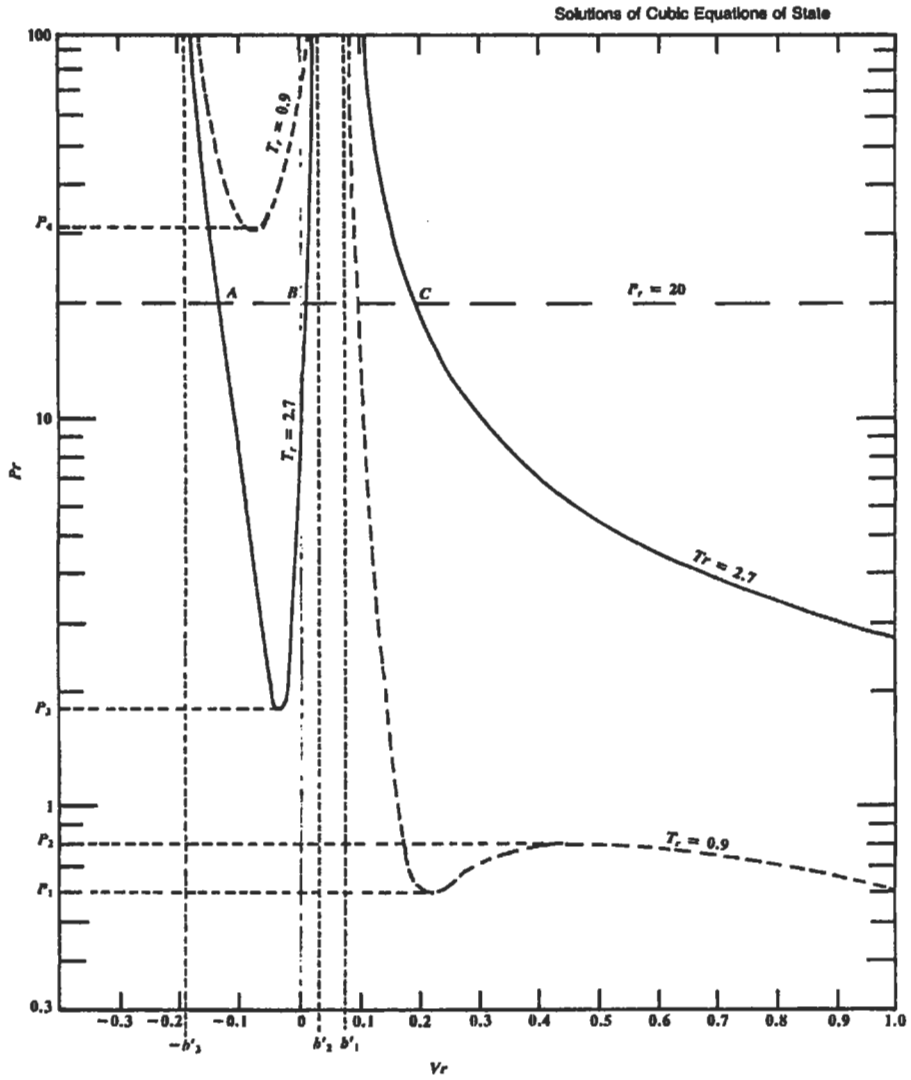


Figure 6-31. P_r vs. V_r plot for Peng-Robinson equation [17].

it [18]. For purposes of the procedure for locating the boundaries of the liquid and vapor phase compressibility factors in the two-phase region discussion, assume that the equation of state is given in the form

$$Z^3 + \alpha Z^2 + \beta Z + \gamma = 0 \tag{6-56}$$

where γ , β are arbitrary constants.

From Figure 6-33a-d in the two phase region the equation of state will have a maximum and a minimum or two points at which the slope of the equation

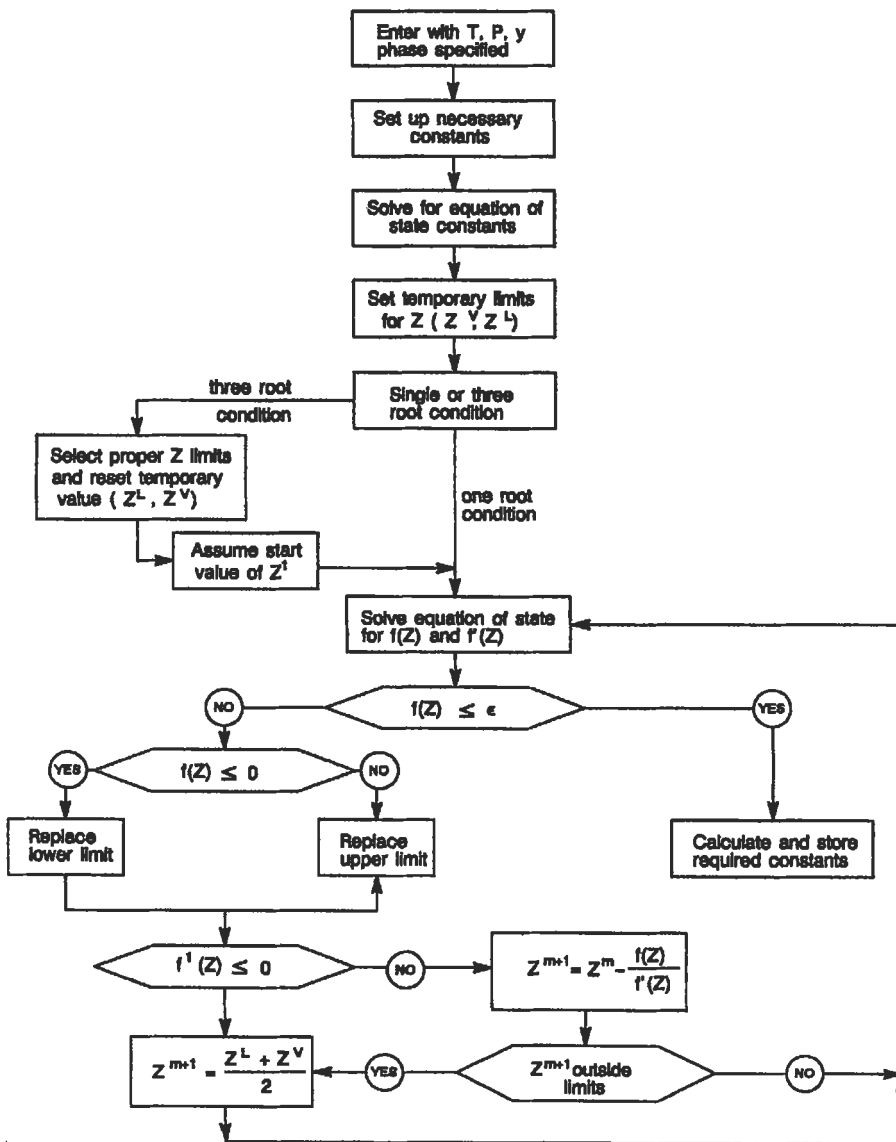


Figure 6-32. Logic diagram for equation-of-state solution.

is zero. The value of the compressibility factor at the maximum defines the largest possible value for the liquid phase compressibility factor. If Equation 6-56 is differentiated and set equal to zero the following equation results:

$$Z^2 + \frac{2\alpha Z}{3} + \frac{\beta}{3} = 0 \tag{6-57}$$

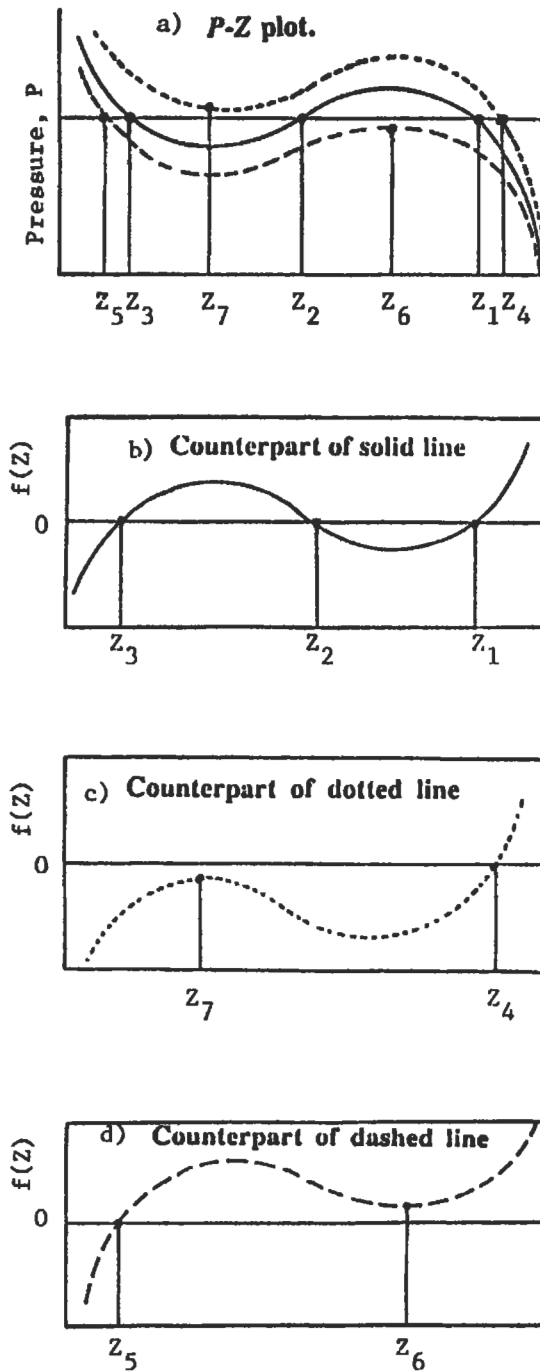


Figure 6-33a-d. Typical behavior of cubic equation of state [17].

Solving the above equation for the values of Z at the maximum and minimum gives

$$Z_{1,2} = \frac{-2\frac{\alpha}{3} \pm 4\frac{\alpha^2}{9} - 4\frac{\beta}{3}}{2} \quad (6-58)$$

If the algebraic expression under the square root sign is negative or zero, only one real value of the compressibility factor will satisfy the equation of state (Figure 6-33c or d). If, however, the value of the expression under the radical is positive, three real roots exist and limits for the vapor and liquid phase compressibility factors can be determined from Equation 6-58. The solutions of Equation 6-58 represent the value of Z at the maximum and minimum points of Figure 6-33b. The value of the maximum will represent the largest possible value for the liquid compressibility factor and the value at the minimum represents the smallest possible value of the vapor compressibility factor. These limits can then be used with arbitrary values for the other limit to assure that the root obtained is the valid one. The limits thus set up are adjusted at the end of each iteration to narrow the interval of search.

FLOW OF FLUIDS

Fluid is defined as a single phase of gas or liquid or both. Each sort of flow results in a pressure drop. Three categories of fluid flow: vertical, inclined and horizontal are shown in Figure 6-34. The engineer involved in petroleum production operations has one principal objective to move the fluid from some location in an underground reservoir to a pipeline that may be used to transport it or storage. Possible pressure losses in complete production system and production pressure profile are shown in Figures 6-35 and 6-36, respectively. On the way from reservoir to pipeline or storage tank, fluid is changing its temperature, pressure and, consequently, composition of each phase. In case of dry gas reservoir a change in pressure and temperature does not create two-phase flow; also in case of black oil with very small GOR, it could be assumed that two-phase flow does not occur.

Based on the law of conservation of energy, the total energy of a fluid at any particular point above datum plane is the sum of the deviation head, the pressure head and velocity head as follows:

$$H = Z_{el} + \frac{144p}{\gamma} + \frac{v^2}{2g} \quad (6-59)$$

In reality, whenever fluid is moving there is friction loss (h_L). This loss describes the difference in total energy at two points in the system. Expressing the energy levels at point 1 versus point 2 then becomes

$$Z_{e1} + \frac{144p_1}{\gamma_1} + \frac{v_1^2}{2g} = Z_{e2} + \frac{144p_2}{\gamma_2} + \frac{v_2^2}{2g} + h_L \quad (6-60)$$

All practical formulas for fluid flow are derived from the above, where H = total energy of fluid; Z_{el} = pipeline vertical elevation rise (ft); p_1 , p_2 = inlet and outlet

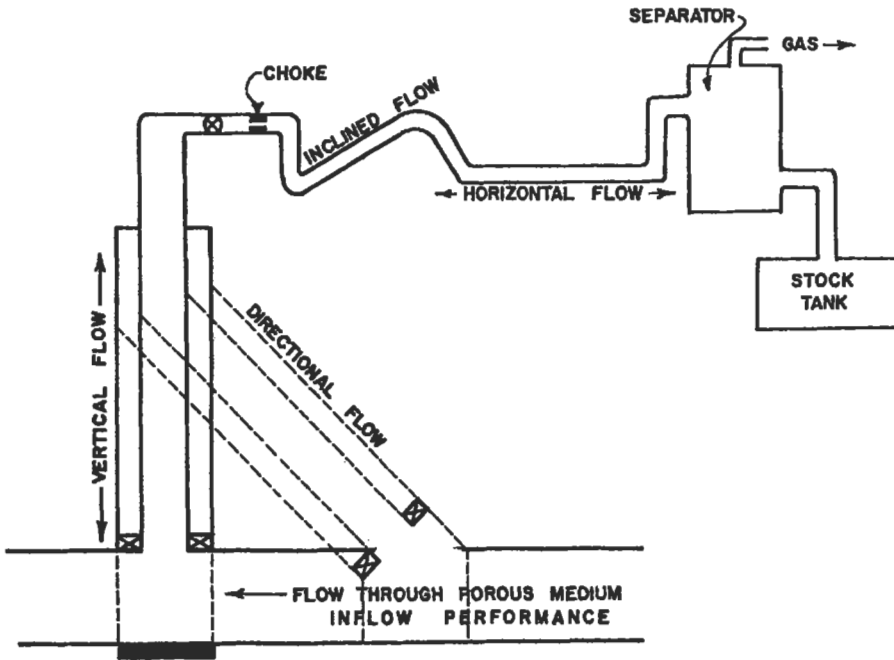


Figure 6-34. Overall production system [19].

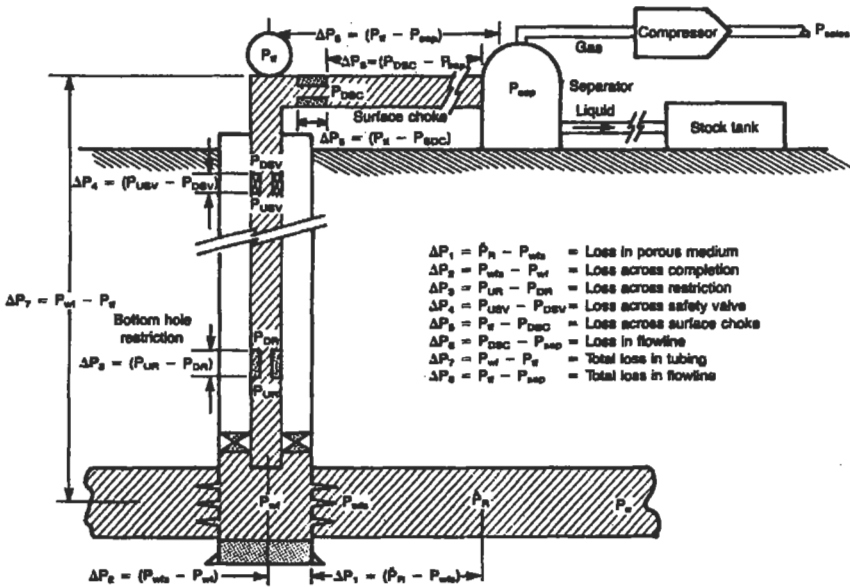


Figure 6-35. Possible pressure losses in complete system [19].

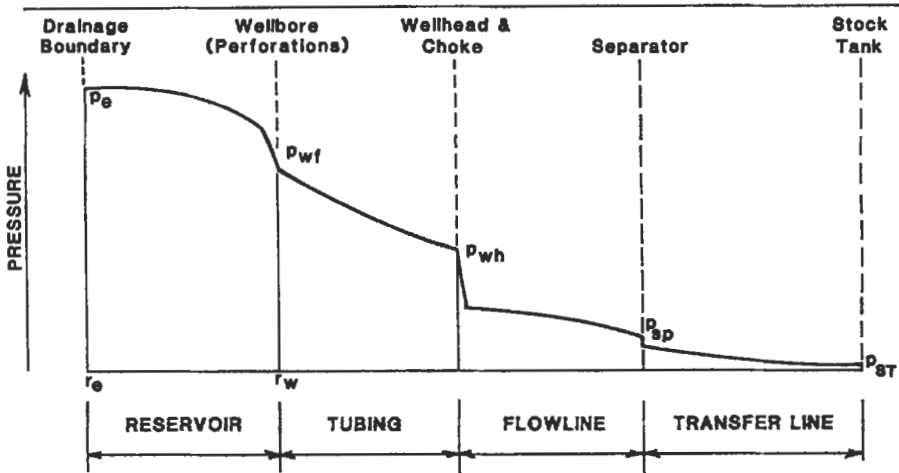


Figure 6-36. Production pressure profile [20].

pressures (psia); $\gamma_1\gamma_2$ = inlet and outlet fluid specific weight; v_1, v_2 = inlet and outlet fluid velocity; g = acceleration; h_L = loss of static pressure head due to fluid flow. Equation 6-60 can be written in differential form as

$$\frac{dp}{\gamma} + \frac{v dv}{g} + dL \sin \theta + dL_w = 0 \quad (6-61)$$

where $dL \sin \theta = dZ$ and dL_w refers to friction multiplying the equation by γ/dL to give

$$\frac{dp}{dL} = \frac{\gamma v dv}{gdL} + \gamma \sin \theta + \gamma \left(\frac{dL_w}{dL} \right)_f = 0 \quad (6-62)$$

Solving this equation for pressure gradient, and if we consider a pressure drop as being positive in the direction of flow,

$$\frac{dp}{dL} = \gamma \sin \theta + \frac{\gamma v dv}{gdL} + \left(\frac{dp}{dL} \right)_f \quad (6-63)$$

where

$$\left(\frac{dp}{dL} \right)_f = \frac{\gamma dL_w}{dL}$$

Equation 6-62 contains three terms that contribute to the total pressure gradient, i.e.:

1. pressure gradient due to elevation

$$\gamma \sin \theta = \left(\frac{dp}{dL} \right)_{el}$$

2. pressure gradient due to acceleration

$$\frac{\gamma v dv}{gdL} = \left(\frac{dp}{dL} \right)_{acc}$$

3. pressure gradient due to viscous forces (friction)

$$\frac{\gamma dL_w}{dL} = \left(\frac{dp}{dL} \right)_f$$

$$\frac{dp}{dL} = \left(\frac{dp}{dL} \right)_{el} + \left(\frac{dp}{dL} \right)_{acc} + \left(\frac{dp}{dL} \right)_f \quad (6-64)$$

The acceleration element is the smallest one and sometimes is neglected.

The total pressure at the bottom of the tubing is a function of flowrate and constituting three pressure elements:

1. wellhead pressure—back pressure exerted at the surface from choke and wellhead assembly
2. hydrostatic pressure—due to gravity and the elevation change between wellhead and the intake to the tubing
3. friction losses, which include irreversible pressure losses due to viscous drag and slippage

Figure 6-37 illustrates this situation for each single-phase and two-phase flow. Possible pressure losses in a complete system are shown in Figure 6-35. For a given flowrate, wellhead pressure and tubing size there is a particular pressure distribution along the tubing. The pressure-depth profile is called a pressure traverse and is shown in Figure 6-38. Gas liberation, gas expansion and oil shrinkage along the production tubing can be treated as a series of successive incremental states where saturated oil and gas coexist in equilibrium (flash process). This model is shown in Figure 6-39. At (a) the single-phase oil enters the wellbore; (b) marks the first evolution of gas, at the mixture's bubble point; and both (c) and (d) show the traverse into the two-phase region. Note that the gas and oil P-T diagrams describing equilibrium phases at points (c) and (d) are not the same. This means that the composition of equilibrium gas and oil phases changes continuously in the two-phase region. As the two-phase region is entered and gas is liberated, oil and gas phases change in volume and composition, but they are always in a saturated state, the gas at its dew point and the oil at its bubble point. In Figure 6-40 the separation process is shown in forms of the resulting gas and oil.

Engineering analysis of two-phase fluid flow in pipes has focused primarily on the problem of predictive pressure drop, or pressure gradient from Equation 6-64.

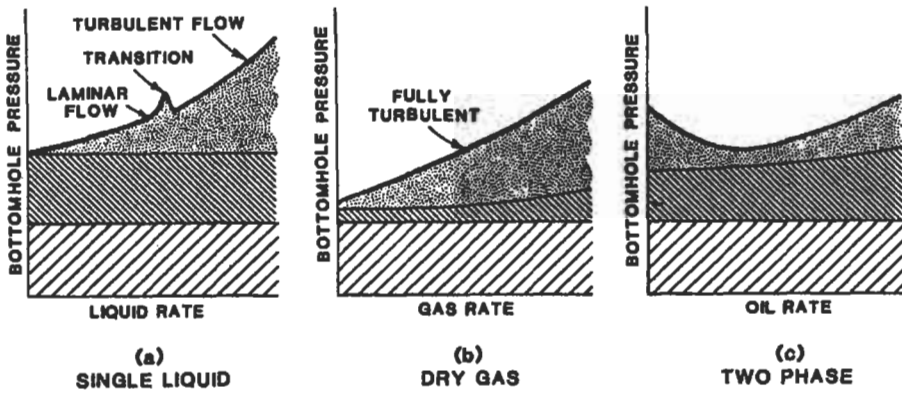


Figure 6-37. Components of pressure losses in tubing [20].

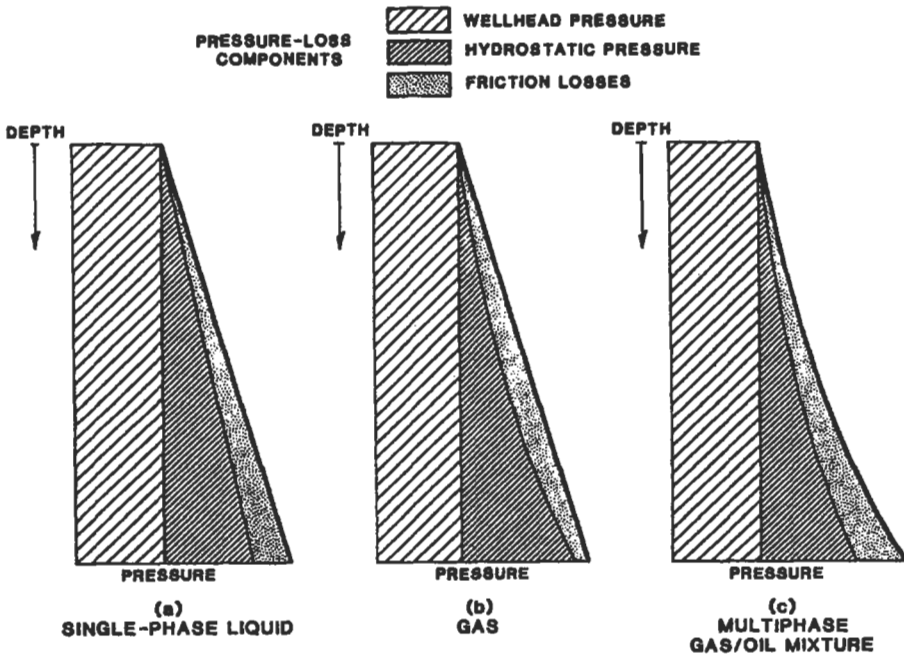


Figure 6-38. Pressure traverse for single-phase liquid, gas and multiphase gas-oil mixture [20].

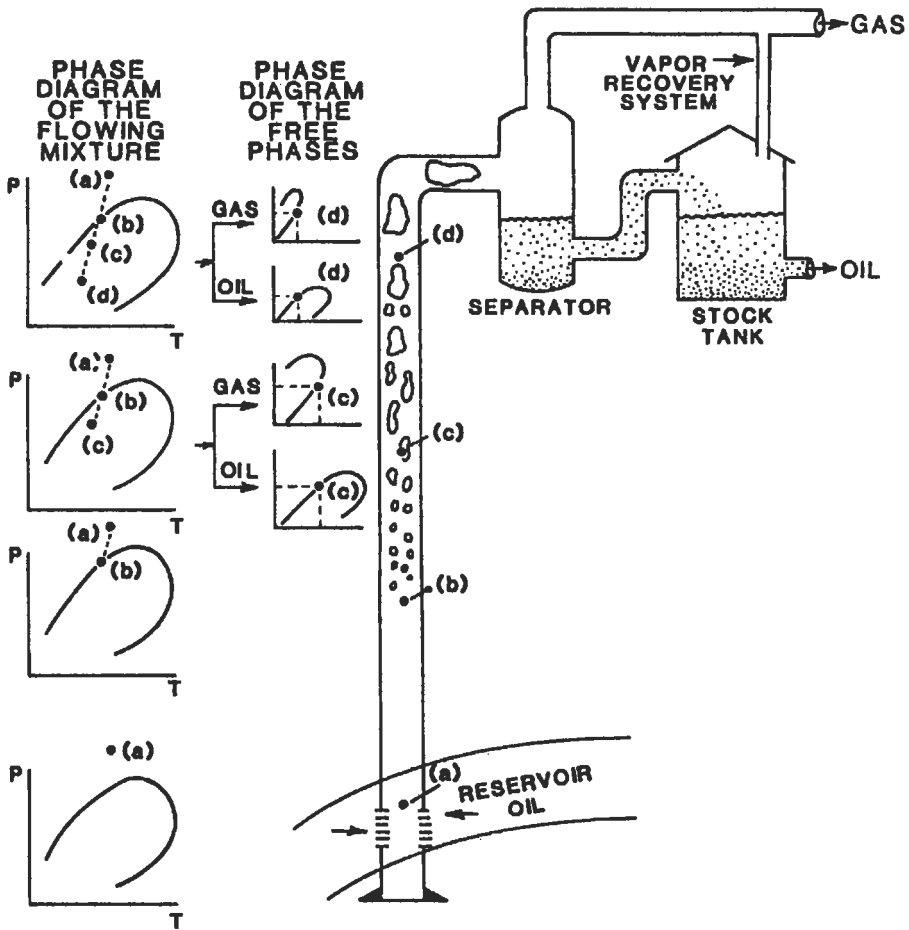


Figure 6-39. Changes in phase behavior in the production tubing [20].

In many cases, it has become possible to treat two-phase pipeline problems with empirical numerical techniques that yield reasonably accurate pressure drops. Most of two-phase pipeline simulation currently is performed using "black oil" simulators. A black oil model's validity rests on the assumption that the hydrocarbon mixture is composed of two phases, denoted oil and gas, each with fixed composition. A black-oil model usually treats P-V-T properties (solution gas, densities and viscosities) as single-value function of pressure. More sophisticated models include the temperature effect on fluid properties as well. The multicomponent or compositional approach is designed for gas condensate and volatile oil systems. These fluids are represented as N-component hydrocarbon mixtures, where N might be equal to components C_1 , C_2 , C_3 , $i-C_4$, $n-C_4$, $i-C_5$, $n-C_5$, C_6 and C_{7+} . Equations of state (SRK, PR, SBWR) are used to determine physical properties. The term "compositional" implies that the overall or *in situ*

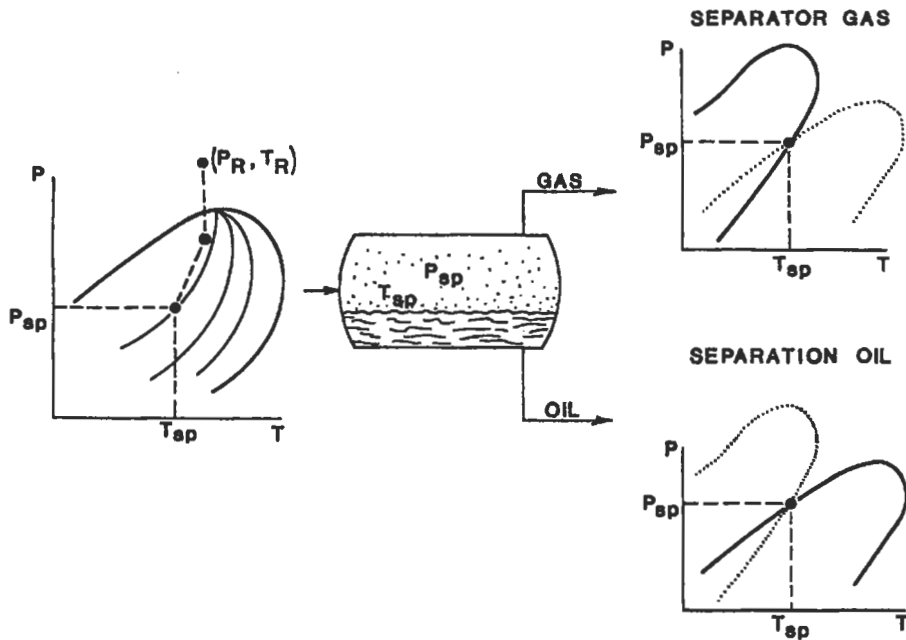


Figure 6-40. Pressure–temperature phase diagram used to describe surface separation [20].

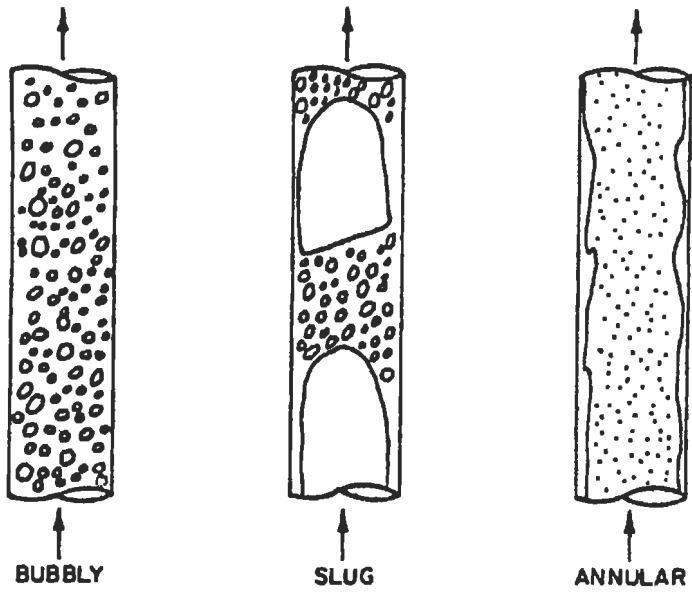
fluid composition varies point by point with distance as is shown in Figure 6-39. When a multicomponent gas–liquid mixture flows through a pipe, the composition, pressure, temperature and liquid holdup distributions are related.

Basic Parameters of Multiphase Flow [19]

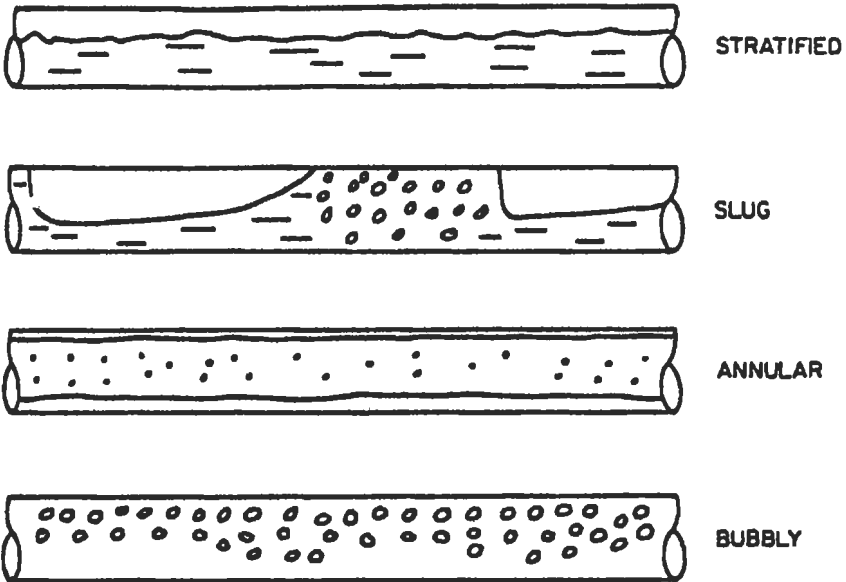
Knowledge of the flow regime determines the selection of the appropriate model for pressure gradient and liquid holdup. The flow regime, pressure gradient, and liquid holdup are calculated for each segment of the pipeline. The information needed to make the calculations includes:

1. pipeline inlet and outlet boundary conditions (liquid and gas flowrates, temperature and pressure)
2. pipeline geometry, with segments specifications (any riser or well, down-comer, inclined section)
3. fluid properties (assume constant properties, compositional analysis, black oil approaches); this includes gas, oil and water density, viscosity and surface tension

It is assumed by flow regime that the distribution of each phase in the pipe is relative to one another. Prediction of flow patterns for horizontal flow is a more difficult task than for vertical flow. Possible flow regimes are shown in Figure 6-41. An example of the complexity of two-phase flows in Figure 6-42 shows a schematic sequence of flow patterns in vertical pipe. Numerous authors [19,20,21,22] have



A) VERTICAL FLOW



B) HORIZONTAL FLOW

Figure 6-41. Gas-liquid flow regimes.

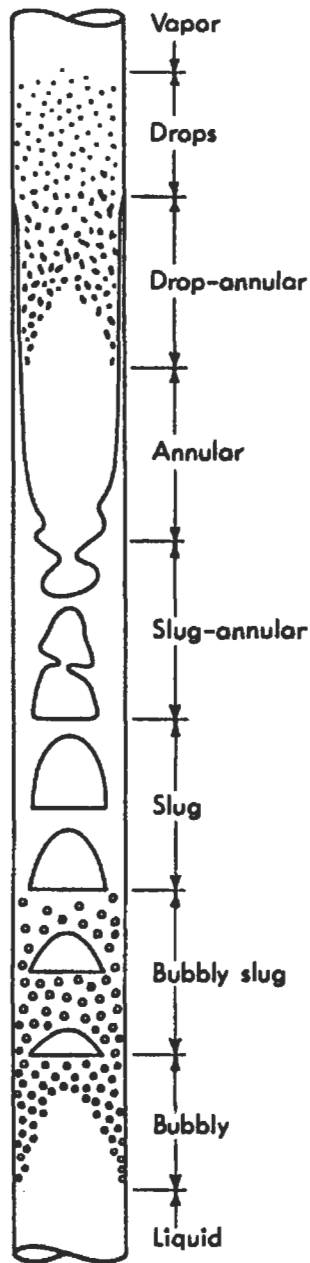


Figure 6-42. Possible sequence of flow patterns in a vertical tube [21].

presented flow-pattern and flow-regime maps in which various areas are indicated on a graph for which there are two independent coordinates. Maps are also dependent on ranges of pipe inclination from vertical upward to vertical downward [19]. Selection of the appropriate flow regime map is based solely on the pipe segment inclination θ from the horizontal, as shown below:

Range of Inclination from the Horizontal	Regime Maps
$\theta = 90^\circ$ to 15°	Upward inclined
$\theta = 15^\circ$ to -10°	Near horizontal
$\theta = -10^\circ$ to -90°	Downward inclined

Flow Regimes

The steps in the determination of the flow regime are as follows:

1. Calculate dimensionless parameters.
2. Refer to flow regime maps laid out in coordinates of these parameters.
3. Determine the flow regime by locating the operating point on the flow regime map.

The discussions in the following sections treat the flow regime maps for vertical upward ($\theta = 90^\circ$); slightly inclined ($\theta = 15^\circ$ to -10°) and vertical downward inclinations.

To proceed with the calculations of the flow regime, it is necessary to calculate the superficial velocities for each flow phase. The superficial velocities for the gas, oil and water are

$$v_{sg} = q_g/A_p \quad (6-65a)$$

$$v_{so} = q_o/A_p \quad (6-65b)$$

$$v_{sw} = q_w/A_p \quad (6-65c)$$

where A_p = pipe flow area in ft^2
 q = volumetric flowrate at flow conditions in ft^3/s

The superficial velocities of liquid phase (oil and water) are calculated as

$$v_{sL} = v_{so} + v_{sw} \quad (6-65d)$$

The mixture velocity that will be used in some of the calculations is the sum of the superficial velocities of the gas and the liquid phases:

$$v_m = v_{sL} + v_{sg} \quad (6-65e)$$

The average velocity of each phase is related to the superficial velocity through the liquid holdup:

$$U_L = v_L = v_{sL}/H_L \quad (6-65f)$$

$$U_g = v_g = v_{vg}/(1-H_L) \tag{6-65g}$$

For a homogeneous model both phases are assumed to have equal velocities and each is equal to a two-phase (or mixture) velocity:

$$v_L = v_g = v_m \tag{6-65h}$$

H_L in Equations 6-65f and 6-65g refers to liquid holdup.

Liquid holdup is defined as the ratio of the volume of a pipe segment occupied by liquid to the volume of the pipe segment:

$$H_L = \frac{\text{volume of liquid in a pipe segment}}{\text{volume of pipe segment}} \tag{6-66a}$$

In some cases, e.g., for stratified horizontal flow regime, liquid holdup can be calculated as follows:

$$H_L = \frac{A_L}{A_L + A_g} \tag{6-66b}$$

where A_L = cross-sectional area occupied by liquid (oil and water)
 A_g = cross-sectional area occupied by gas

Slightly Inclined Pipes ($-10^\circ < \theta < 15^\circ$)

As can be seen from Figure 6-41, there are four flow regimes of interest: stratified, slug, annular and bubbly; and three flow regime transition zones.

Step 1. Dimensionless Parameters

1. Martinelli parameter—this is the ratio of the liquid and gas phases as if each flowed alone in the pipe:

$$X = \left[\frac{(dp/dL)_{ls}}{(dp/dL)_{gs}} \right]^{0.5} = \left(\frac{2f_{hl} \gamma_L v_d^2 / D}{2f_{wg} \gamma_g v_{vg}^2 / D} \right) \tag{6-67a}$$

According to standard fluid mechanics book

$$f(*) = \begin{cases} 0.046/Re^{0.2} & \text{if } Re = \gamma Dv/\mu > 1,500 \\ 16/Re & \text{if } Re < 1,500 \end{cases} \tag{6-67b}$$

2. Gas Froude number (dimensionless gas flowrate):

$$F_g = v_{vg} \left(\frac{\gamma_g}{(\gamma_L - \gamma_g)gD} \right)^{0.5} \tag{6-68}$$

(*) Calculated separately for "ls" and "gs."

3. Turbulence level

$$T = \left[\frac{(dp/dL)_{Ls}}{g(\gamma_L - \gamma_g) \cos \theta} \right] = \left[\frac{2f_{wL} \gamma_L v_{sL}^2 / D}{g(\gamma_L - \gamma_g) \cos \theta} \right] \quad (6-69)$$

4. Dimensionless inclination (slope parameter)

$$Y = \left[\frac{g(\gamma_L - \gamma_g) \sin \theta}{(dp/dL)_{gs}} \right] = \left[\frac{g(\gamma_L - \gamma_g) \sin \theta}{2f_{wg} \gamma_g v_{sg}^2 / D} \right] \quad (6-70)$$

Step 2. Flow Regime Map

The parameter Y is used to select the flow regime map to be used from Figure 6-43. This figure presents nine flow regime maps (a to i) for a wide range of dimensionless inclinations Y in the range of interest.

Step 3. Flow Regime Selection

The flow regime maps are prepared in Froude number–Martinelli parameter–turbulence level (F_g - X - T). Four flow regimes are noted on the maps, doing with the three transition boundaries. Regimes are: stratified, slug, annular and bubbly. The flow conditions for the current pipe segment are located using the X, F_g coordinates. If the located point is in the region labeled “stratified,” then the flow regime is indeed stratified. If the located point is outside of the stratified region, then determine whether the point is to the left or right of the vertical line representing the transition between annular and slug flow regimes. If the point X, F_g is on the right side of the vertical line, X, T coordinates are necessary to use.

Risers and Wells ($\theta = 90^\circ$)

There are three possible flow regimes, including annular, slug and bubbly, and two regime transitions.

Step 1. Dimensionless Parameters

For this regime map, three dimensionless parameters are calculated. The parameters include dimensionless groups, which represent a balance between buoyancy, inertial and surface tension forces. These are called Kutateladze numbers.

$$K_g = \frac{\gamma_g^{0.5} v_{sg}}{[g\sigma_{gs}(\gamma_L - \gamma_g)]^{0.25}} \quad (6-71)$$

$$K_L = \frac{\gamma_L^{0.5} v_{sL}}{[g\sigma_{gs}(\gamma_L - \gamma_g)]^{0.25}} \quad (6-72)$$

(text continued on page 447)

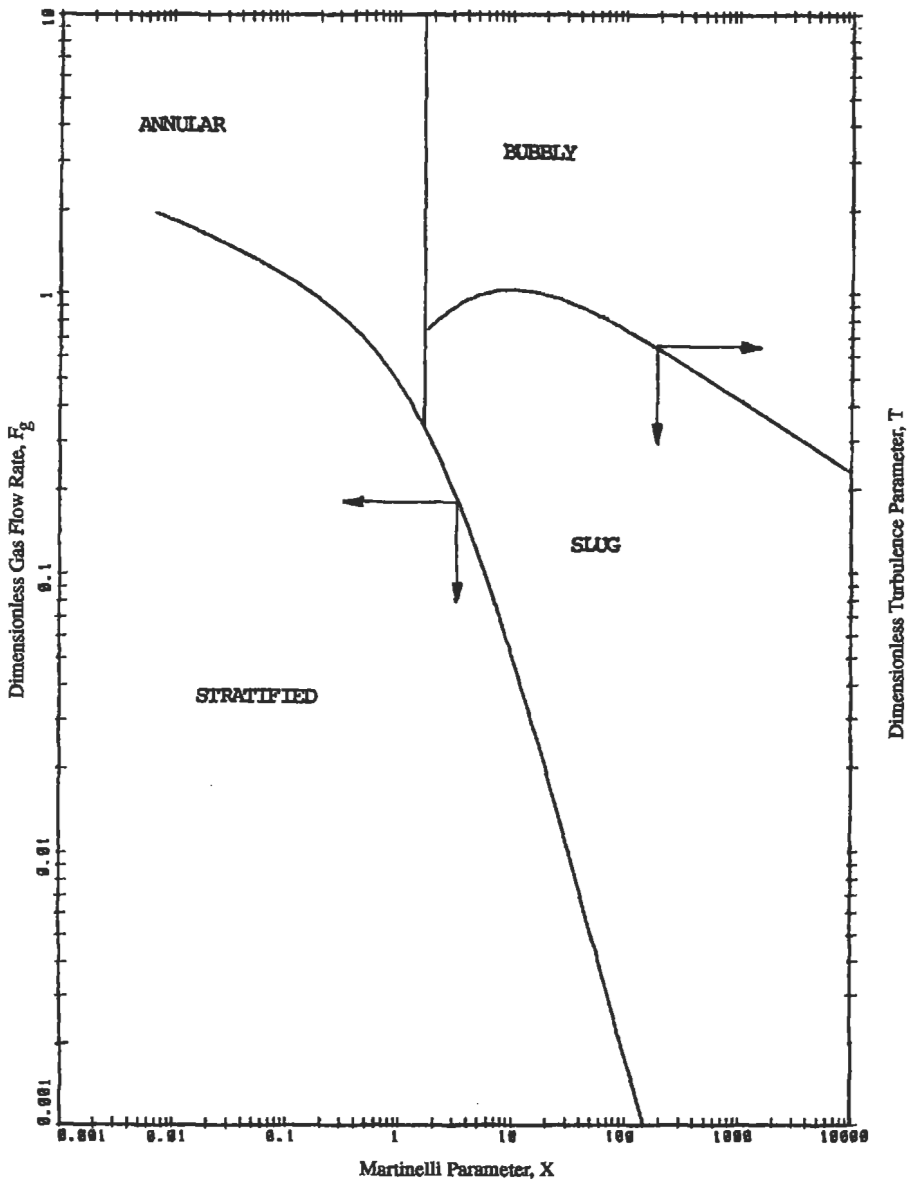


Figure 6-43a. Flow regime map for slightly inclined pipes (horizontal) [22].

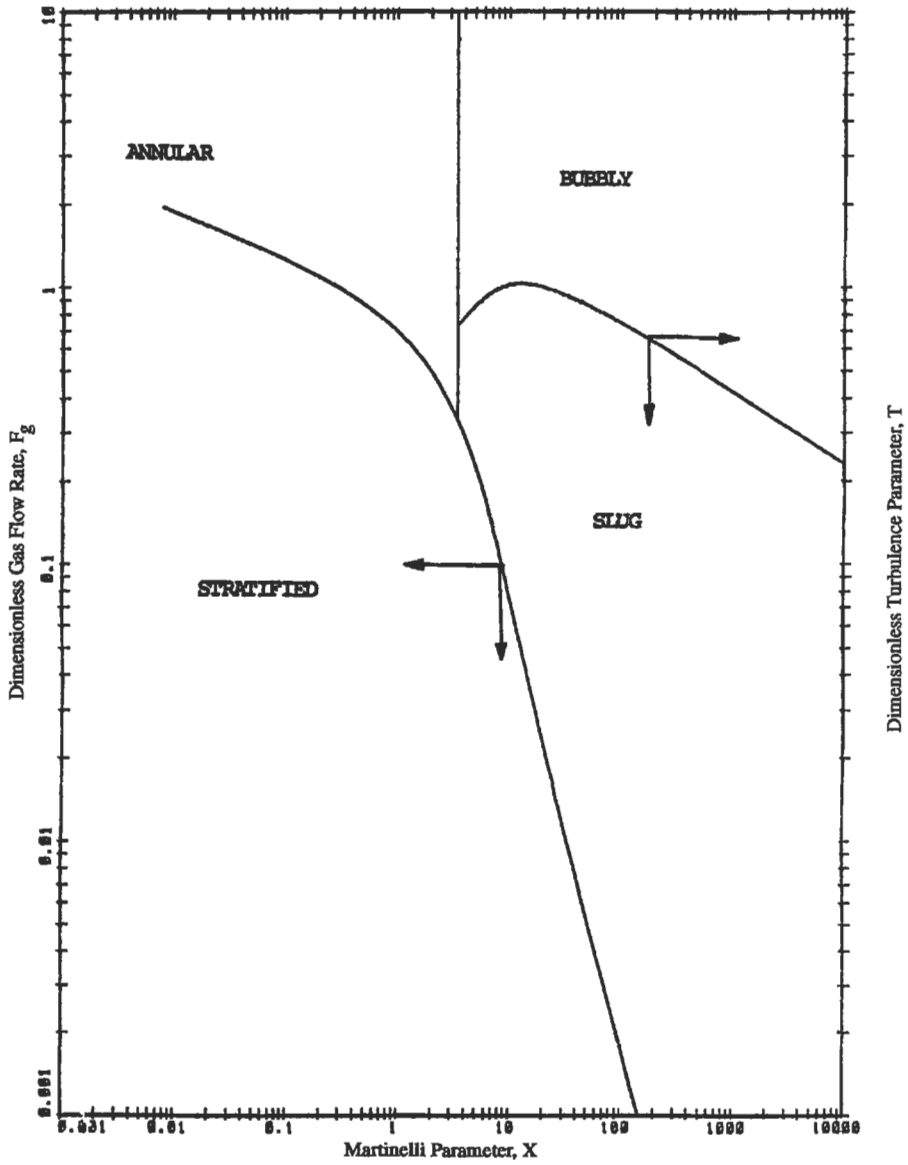


Figure 6-43b. Flow regime map for slightly inclined pipes ($Y = -100$) [22].

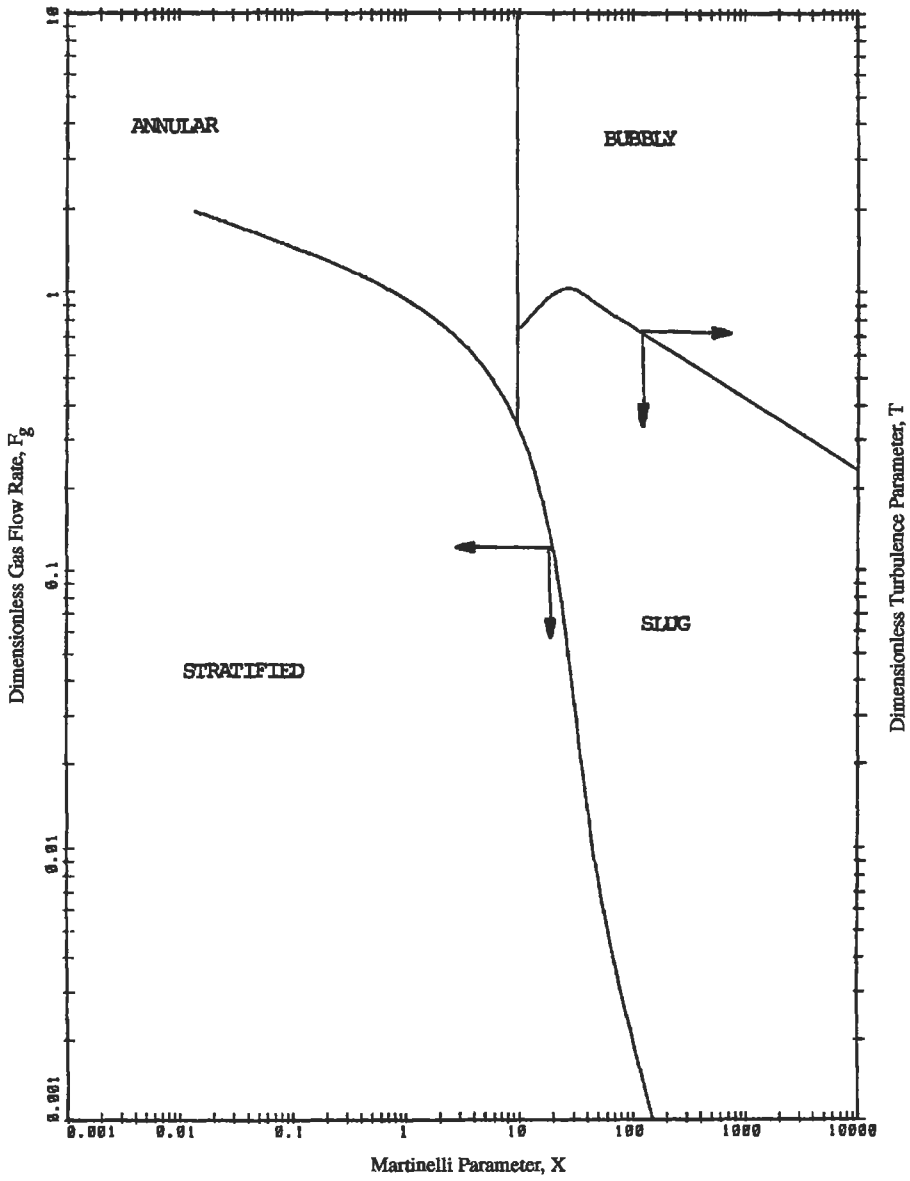


Figure 6-43c. Flow regime map for slightly inclined pipes ($Y = -1000$) [22].

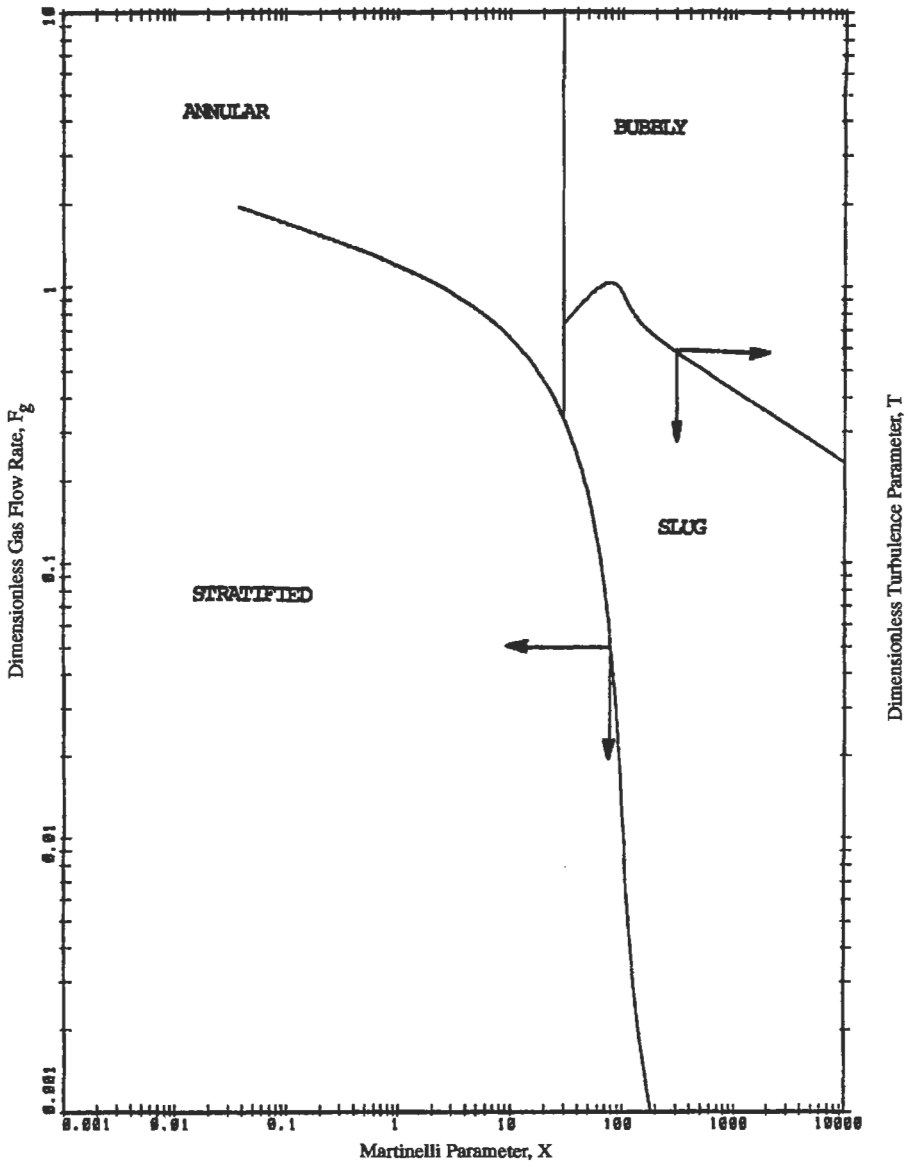


Figure 6-43d. Flow regime map for slightly inclined pipes ($Y = -10,000$) [22].

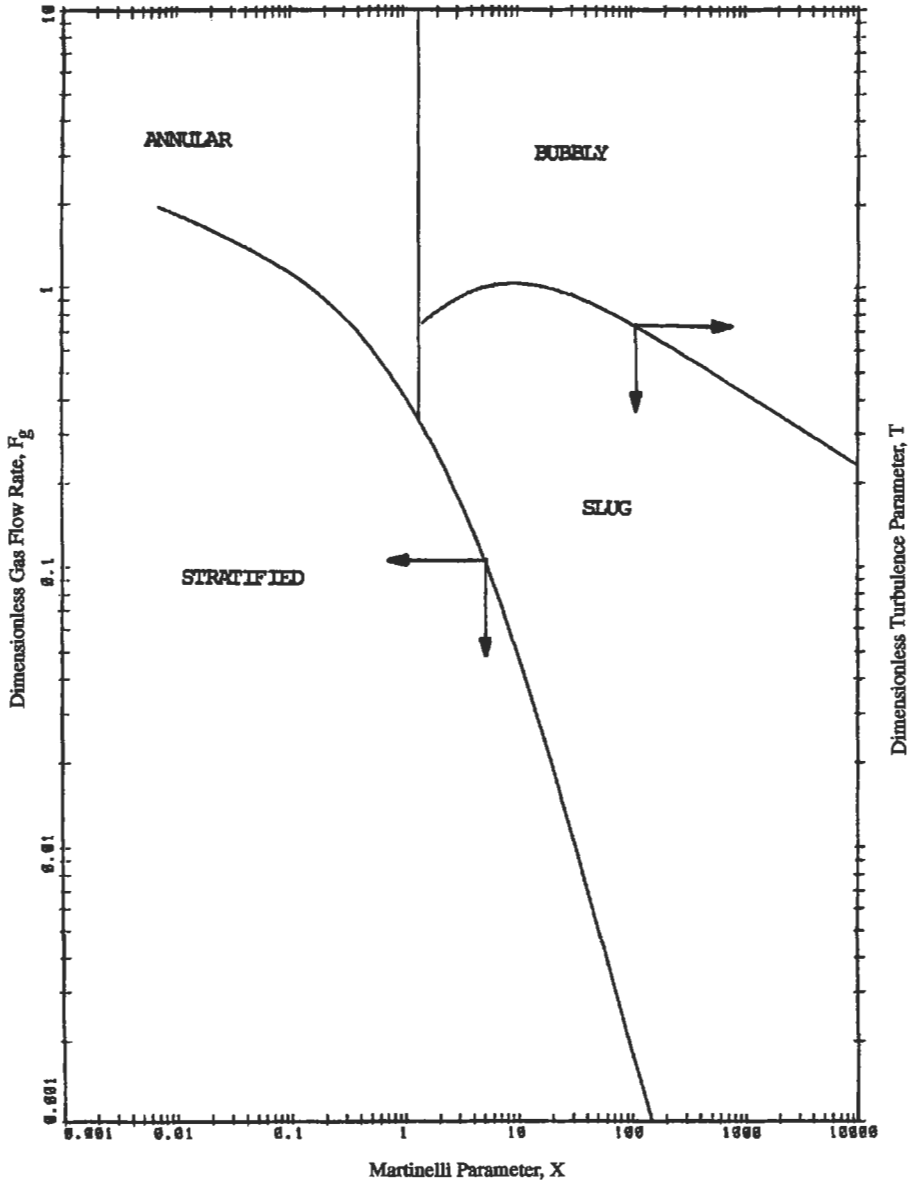


Figure 6-43e. Flow regime map for slightly inclined pipes ($Y = 10$) [22].

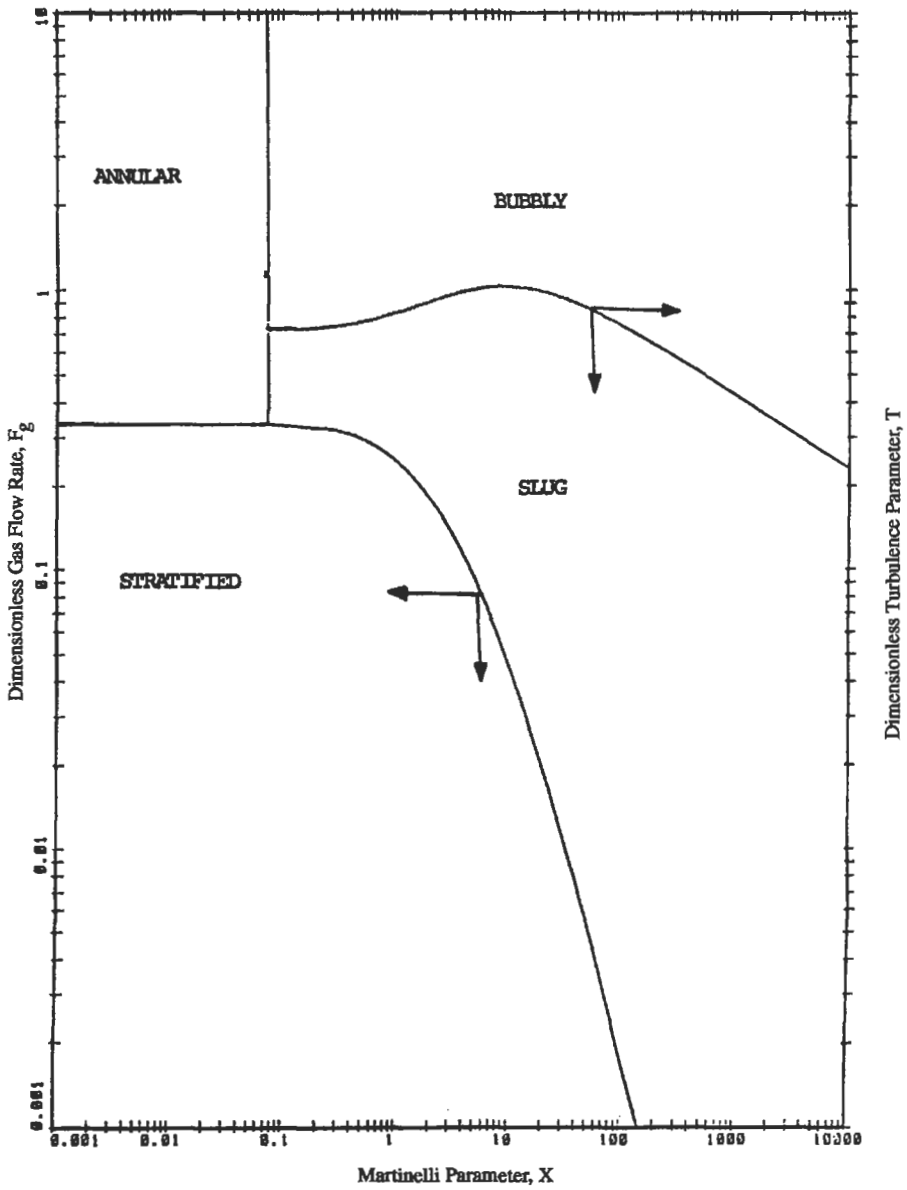


Figure 6-43f. Flow regime map for slightly inclined pipes ($Y = 30$) [22].

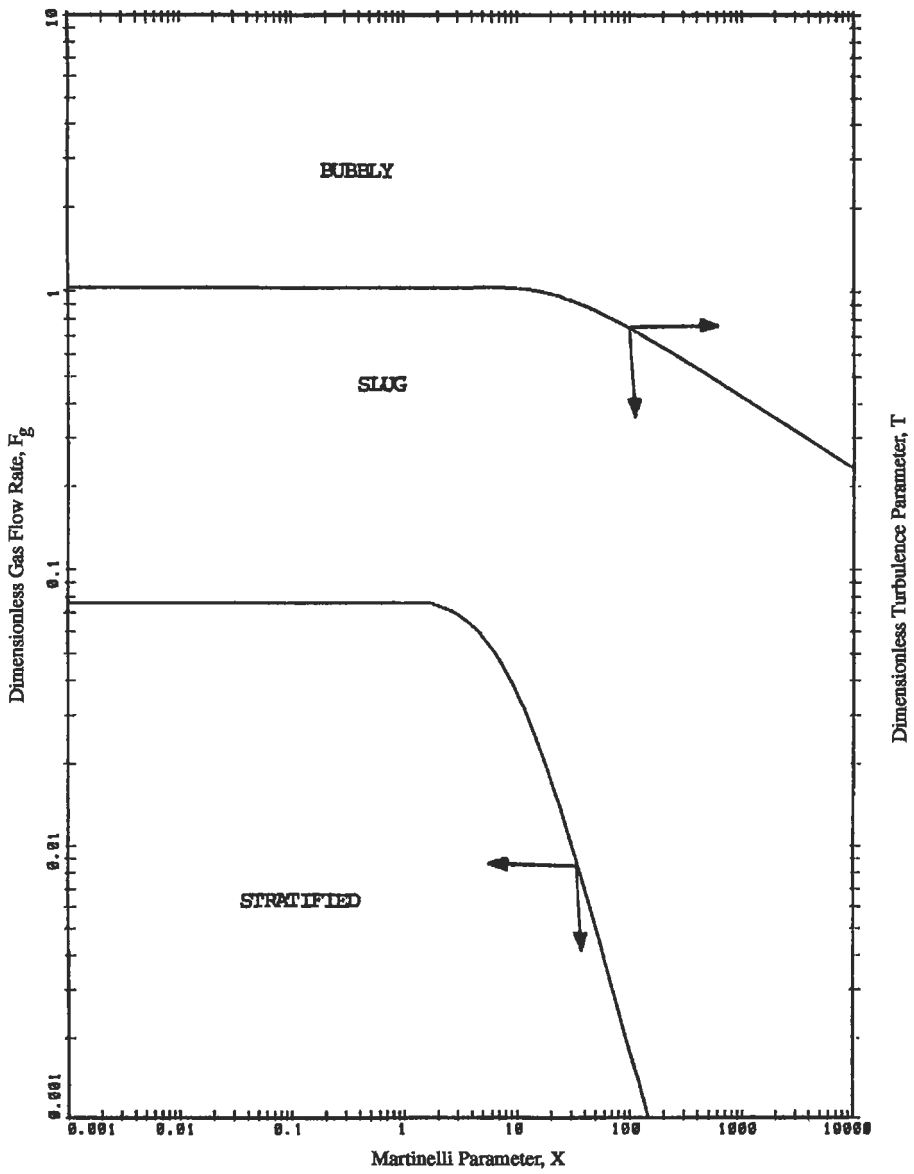


Figure 6-43g. Flow regime map for slightly inclined pipes ($Y = 100$) [22].

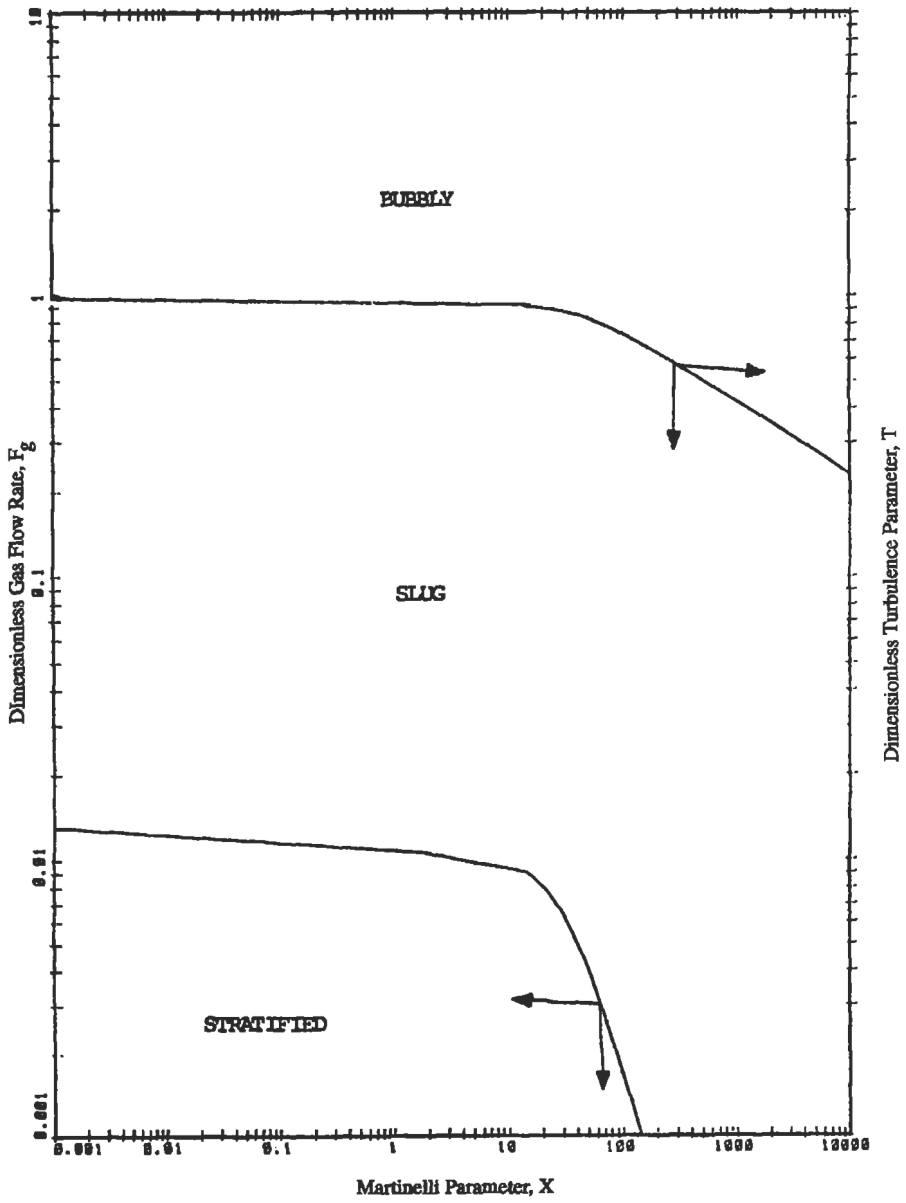


Figure 6-43h. Flow regime map for slightly inclined pipes ($\gamma = 1000$) [22].

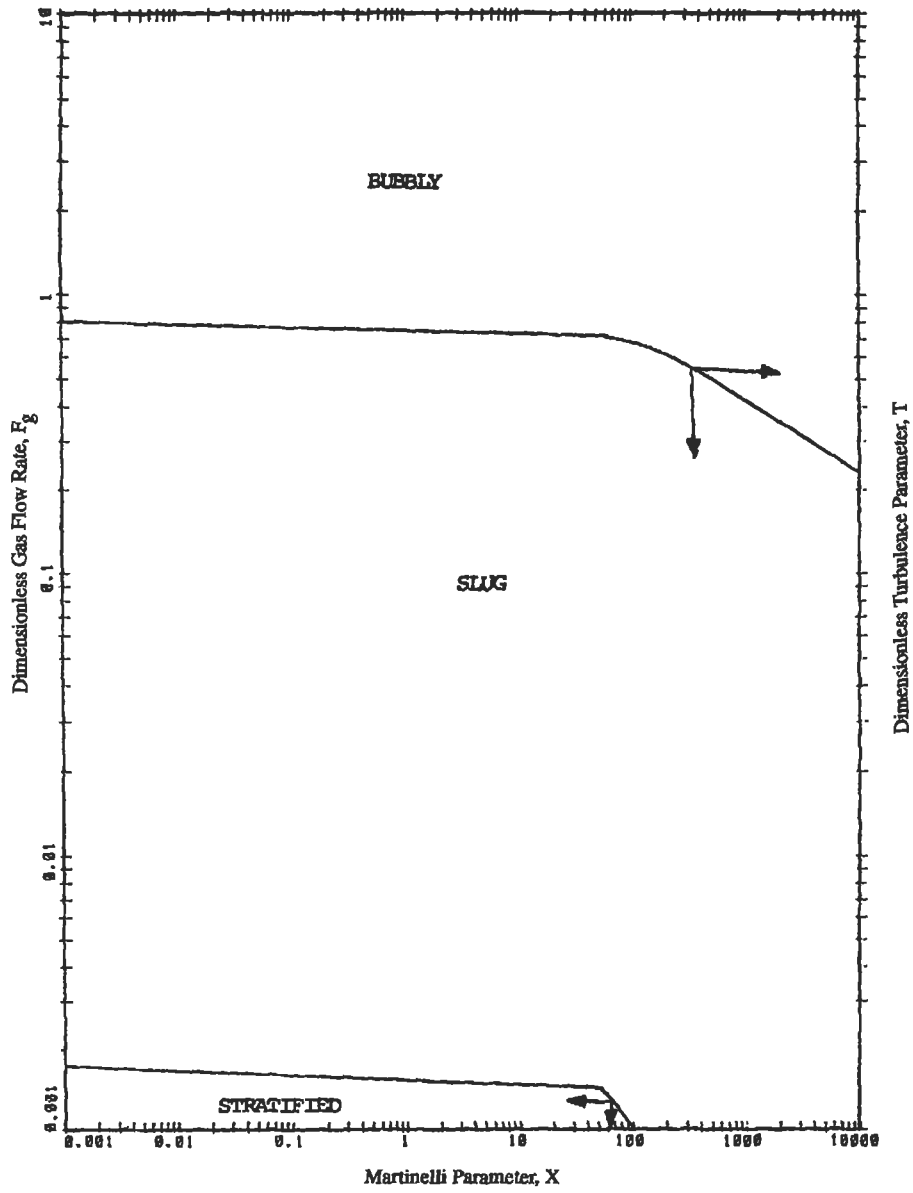


Figure 6-43i. Flow regime map for slightly inclined pipes ($Y = 10,000$) [22].

(text continued from page 437)

$$\rho^* = \left(\frac{\rho_L}{\rho_g} \right) \tag{6-73}$$

where K_g, K_L = dimensionless gas and liquid flowrates
 ρ_g, ρ_L = density of gas and liquid phases in lb_m/ft^3
 v_{sg}, v_{sL} = superficial gas and liquid velocities in ft/s
 σ_{go} = surface tension between gas-oil phases in lb_f/ft
 ρ^* = dimensionless density ration
 g = acceleration of gravity in ft/s^2

Step 2. Flow Regime Map

Once these dimensionless parameters are calculated, then the point with the coordinates (K_g, K_L) is located on the flow regime map in Figure 6-44.

Step 3. Flow Regime Selection

The boundary for the appropriate density ratio is located for the transition boundary between the slug and bubbly flow regimes. Once the appropriate boundary line is found, then the flow regime is simply bubbly, slug or annular depending upon the region in which the point falls. This slug to annular transition applies only if the pipe size D is larger than a critical diameter D_{crit} given by

$$D_{crit} = 1.9 \left[\frac{\sigma_{go} (\gamma_L - \gamma_g)}{g \gamma_L} \right]^{0.25} N_L^{(-0.4)} \tag{6-74a}$$

where

$$N_L = \frac{\mu_L}{(\gamma_L \sigma_{go})^{0.5} [\sigma_{go}/g (\gamma_L - \gamma_g)]^{0.25}} \tag{6-74b}$$

μ_L = liquid phase viscosity in $\text{lb}_m/(\text{ft}\cdot\text{s})$

Usually, the critical pipe size is about 2 in. for conditions of gas and oil pipelines so that Figure 6-44 can be used often. The criterion should be checked each time, however. If $D < D_{crit}$, another method has to be used; see Reference 22, Vol. 3.

Downcomers ($\theta = -90^\circ$)

There are also three possible flow regimes: annular, slug and bubbly. There are two flow regime transitions to be calculated. Two different maps will be used, one for transition between annular and slug flow regimes and a second for the transition between the slug and bubbly flow regimes.

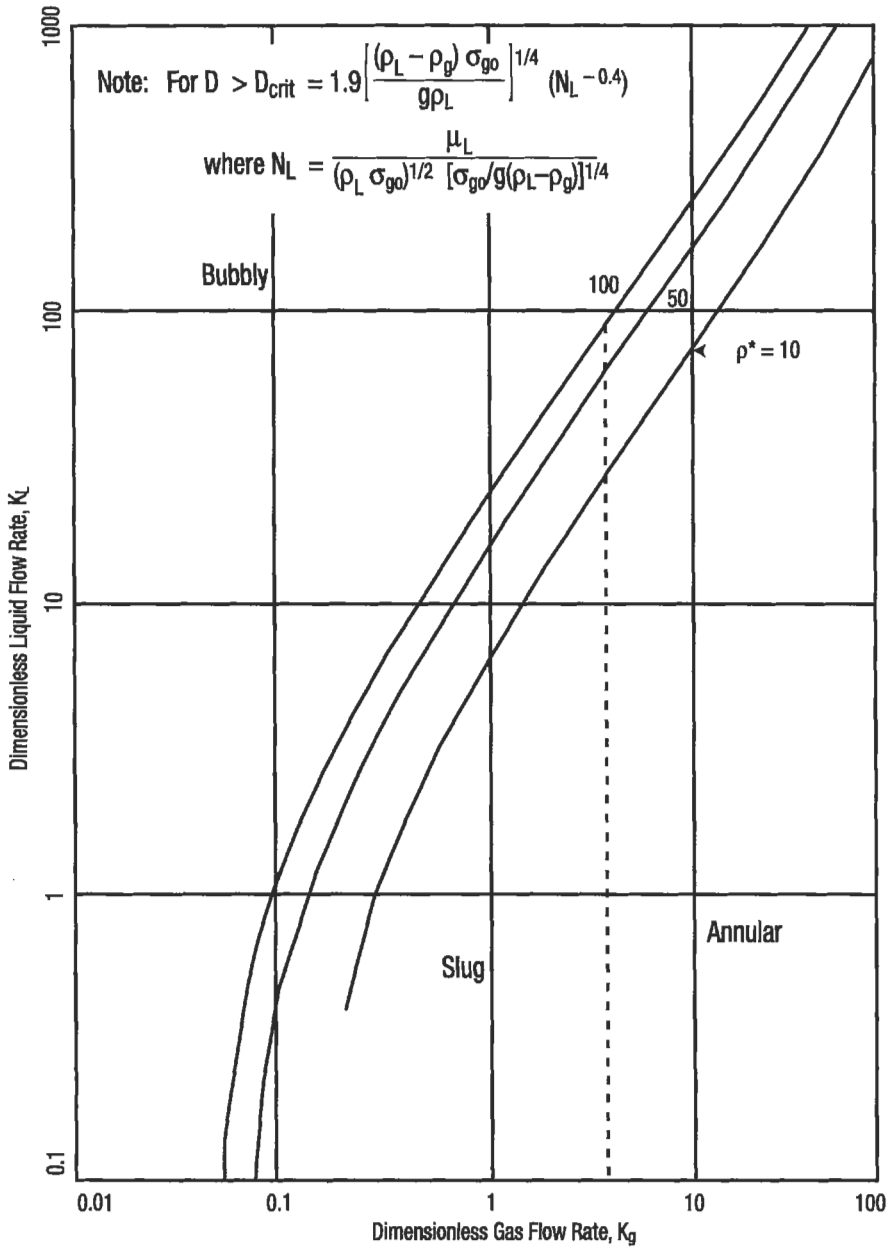


Figure 6-44. Flow regime map for vertical upward inclinations ($\theta = 90^\circ$) [22].

Annular-Slug Transition

1. Dimensionless parameters X and $|Y|$ from Equation 6-67a and 6-70, respectively.
2. Flow regime map, see Figure 6-45.
3. Flow regime selection. Locate the point with $(X, |Y|)$ coordinates; if the point falls in the region "annular," then the flow regime is annular. If the point falls in region "slug" or "bubbly," then the map from Figure 6-47 must be used.

Slug-Bubbly Transition

1. Calculate dimensionless parameters K_g , K_L and ρ^* ; use Equations 6-72 and 6-73, respectively.
2. The appropriate regime boundary for the specific weight ratio γ^* is selected on the regime map with K_g , K_L coordinates.
3. Flow regime selection. Depending upon which region of the map the data point falls into, flow regime is slug or bubbly.

Similarly as for ($\theta = 90^\circ$) Figure 6-46 applies for pipes greater than a certain critical diameter.

$$D > D_{crit} = 19 \left[\frac{(\gamma_L - \gamma_g) \sigma_{go}}{g \gamma_L^2} \right]^{0.5} \quad (6-75)$$

The above procedure is valid for $D > 2$ in.

For each flow regime there is a separate pressure gradient and holdup calculation method.

Stratified Flow Regime

First, the *liquid holdup* H_L and f_i/f_{wg} (friction factor ratio) are calculated. The liquid holdup as a function of X (Equation 6-67a), Y (Equation 6-70) and (f_i/f_{wg}) is read from Figure 6-47a-d. $f_i/f_{wg} = 10$ is recommended to be used as a preliminary estimate. For better accuracy f_i/f_{wg} can be calculated. H_L should be first estimated by the method described above and

$$\frac{f_i}{f_{wg}} = 1.0 \quad \text{if Equation 6-76b} < 1.0 \quad (6-76a)$$

$$\frac{f_i}{f_{wg}} = \left[2 + \frac{0.000025 Re_{Ls}}{D / 3.281} \right] (1 - H_L)^{5/2} (1 + 75 H_L) \quad (6-76b)$$

$$\text{if Equation 6-76b} > (1 + 75 H_L) \quad (6-76c)$$

(D is in in.).

Figure 6-48a-h shows Equation 6-76 for pipe diameters ranging from 4 to 36 in. The friction factor ratio (f_i/f_{wg}) can be estimated from the plots in Figure 6-48 or as a result of calculation.

(text continued on page 464)

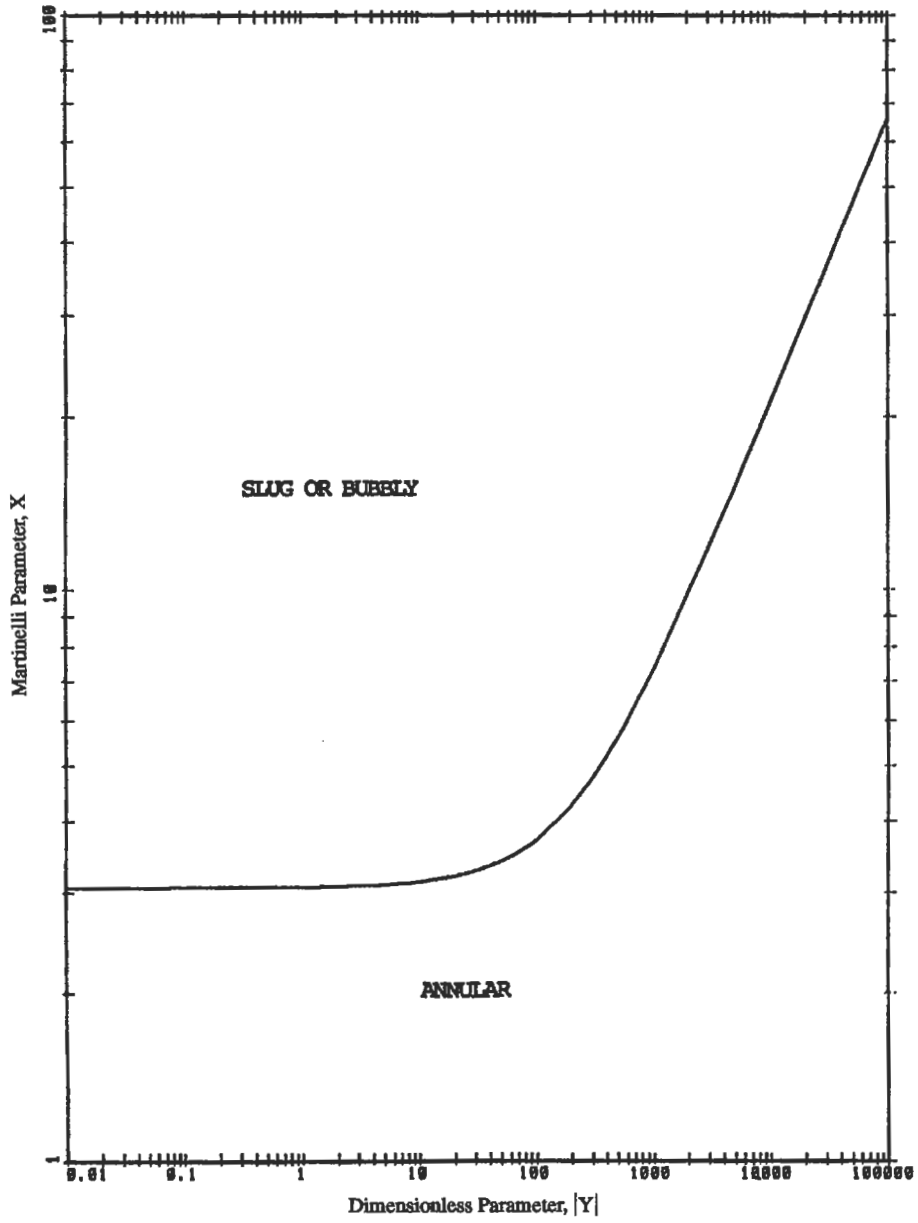


Figure 6-45. Flow regime map for slug-annular transition for vertical downward inclination ($\theta = -90^\circ$) [22].

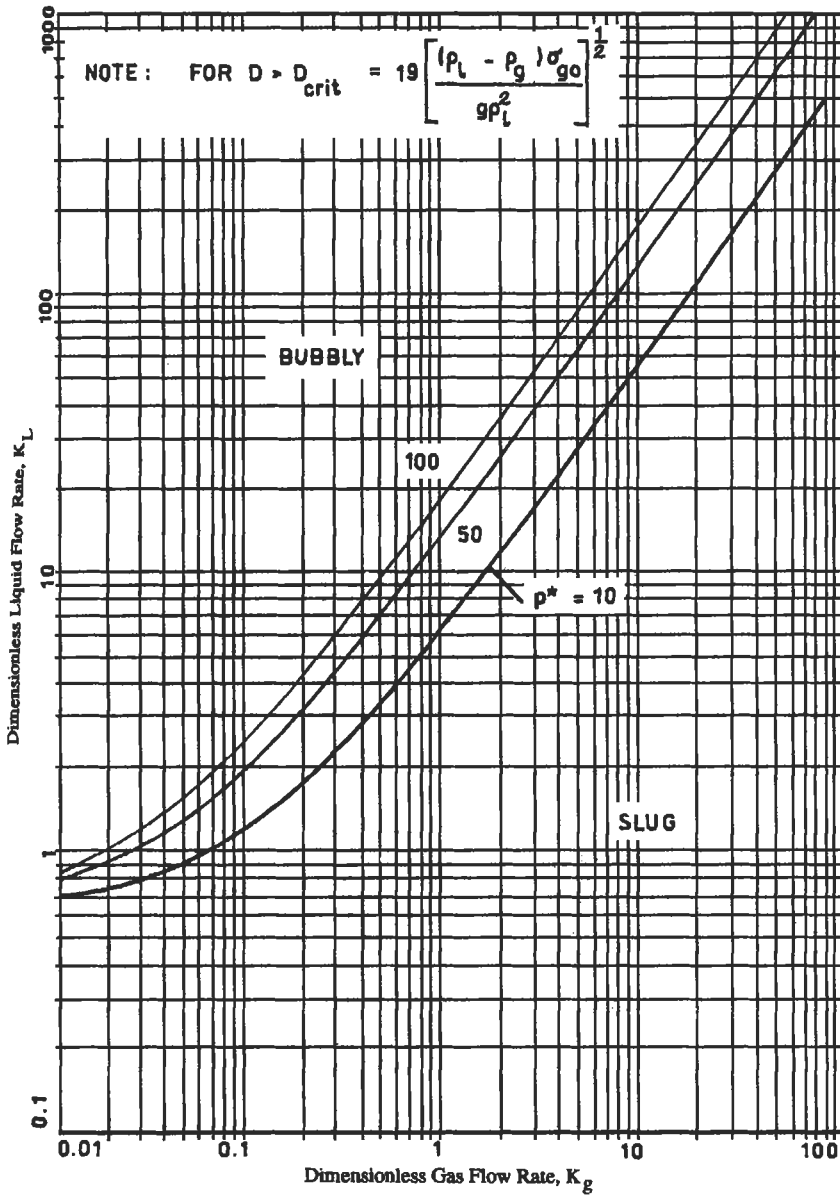


Figure 6-46. Flow regime map for bubble-slug transition for vertical downward inclination ($\theta = -90^\circ$) [22].

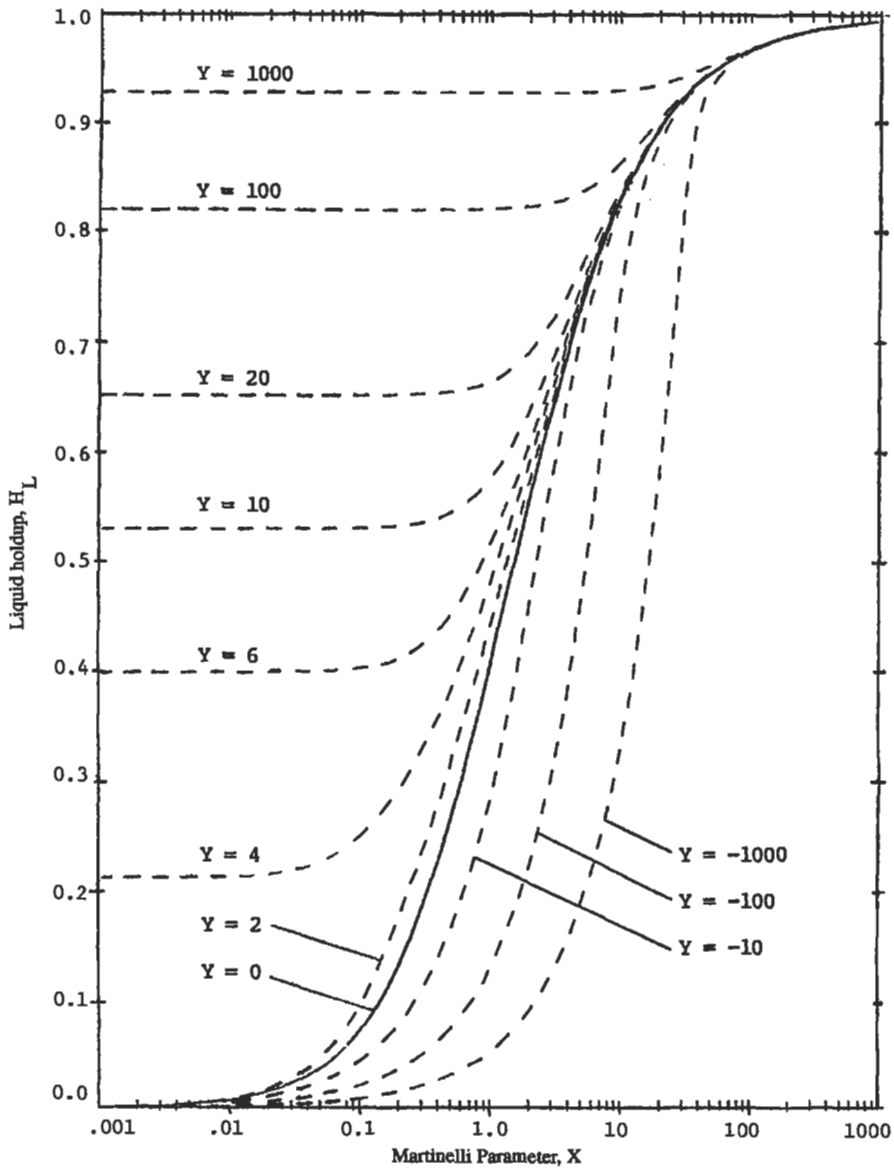


Figure 6-47a. Liquid holdup in stratified flow regime ($f_r/f_{wg} = 1$) [22].

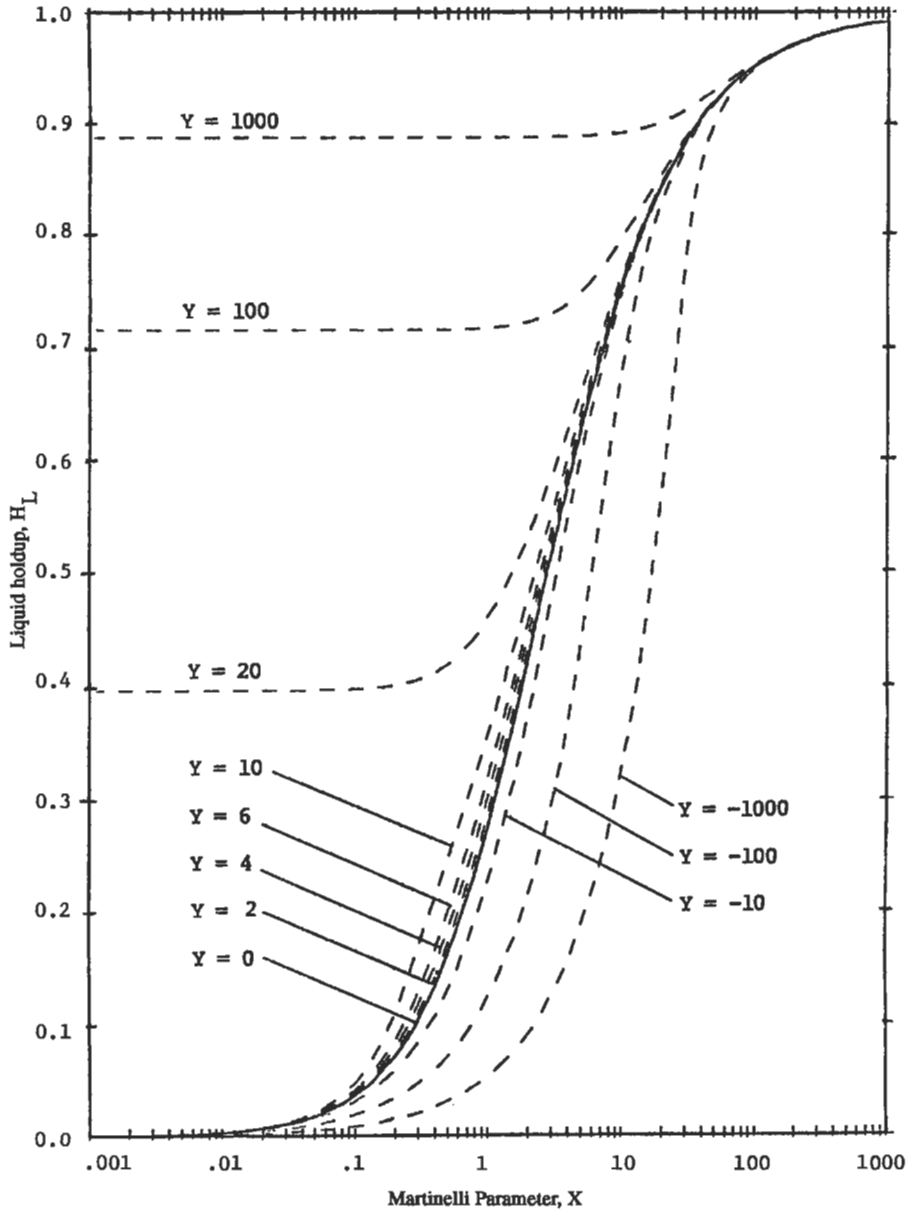


Figure 6-47b. Liquid holdup in stratified flow regime ($t/t_{w0} = 5$) [22].

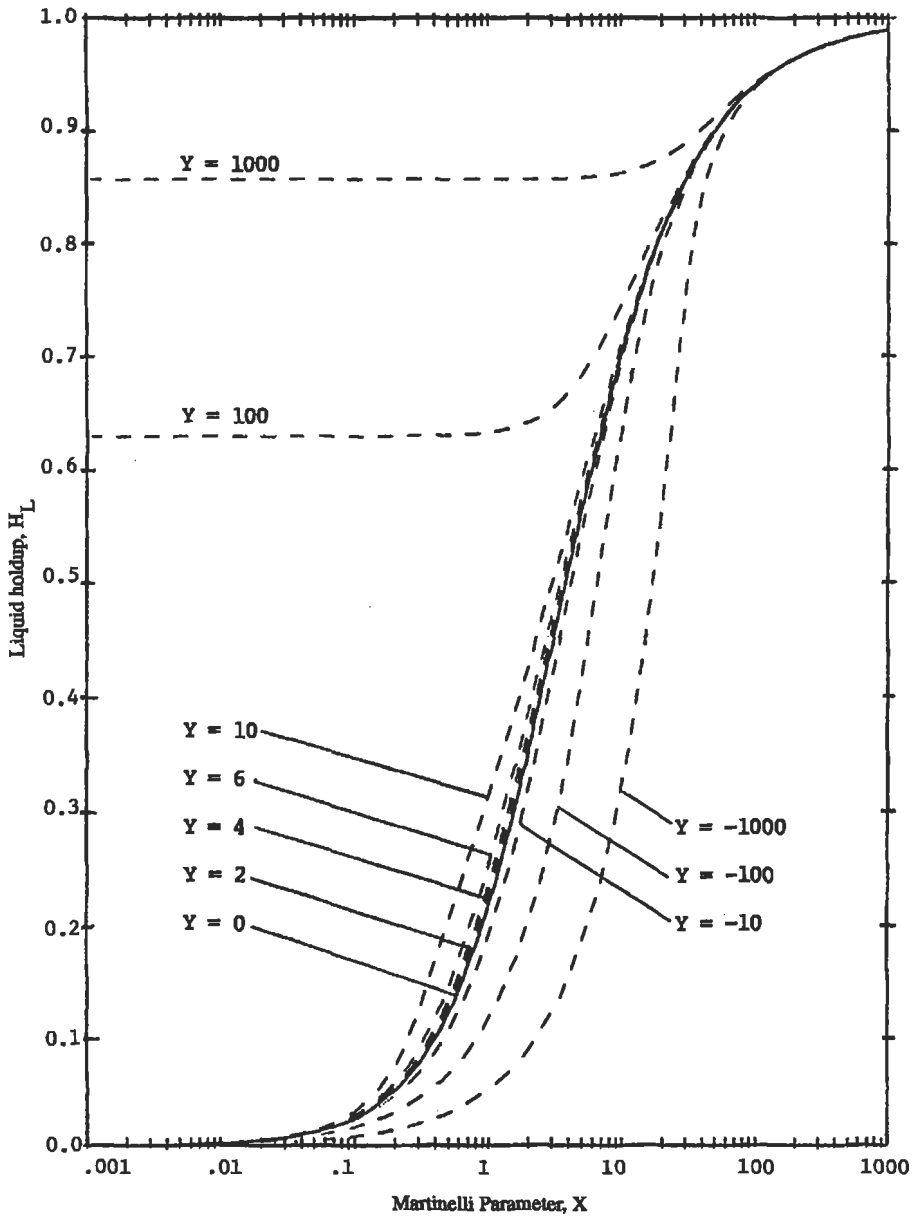


Figure 6-47c. Liquid holdup in stratified flow regime ($t/t_{wg} = 10$) [22].

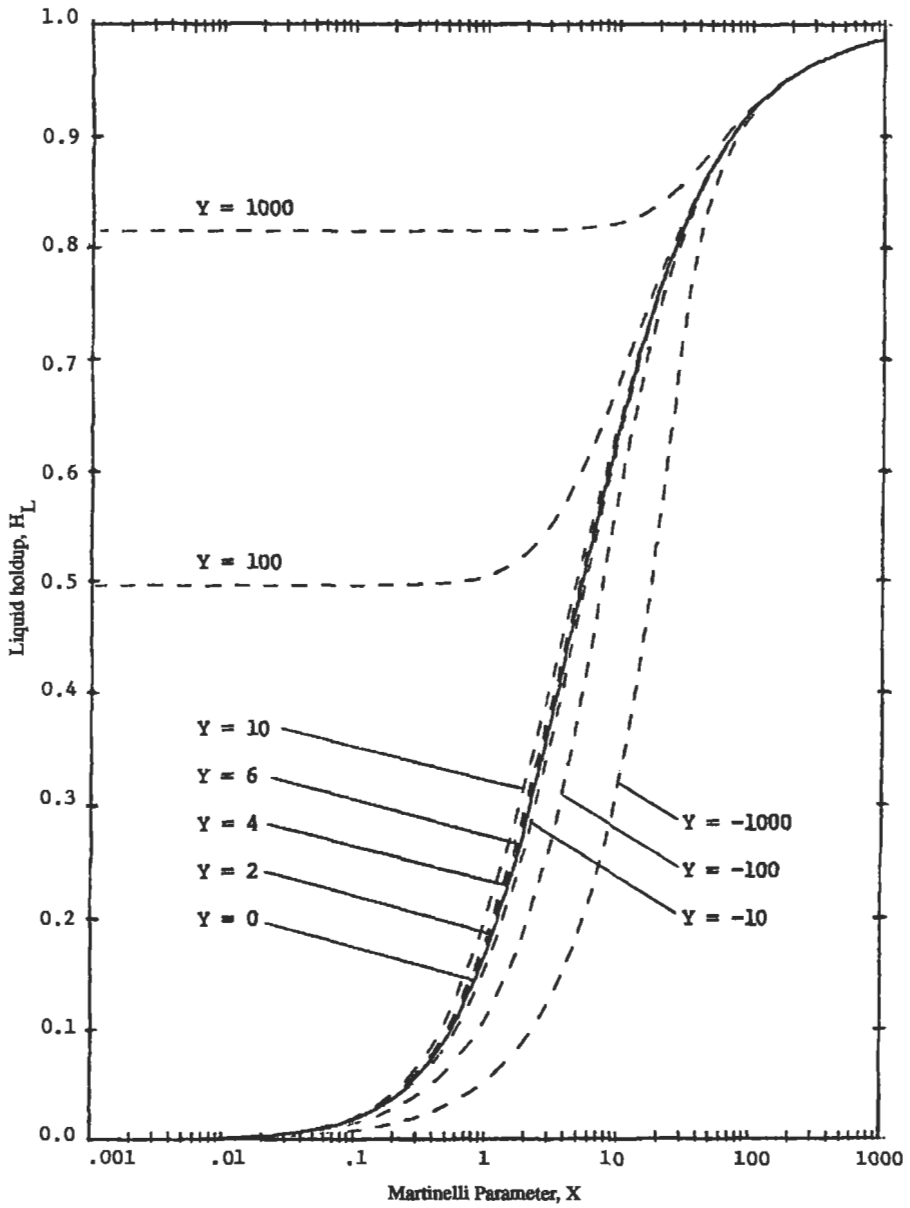


Figure 6-47d. Liquid holdup in stratified flow regime ($f_f/t_{w0} = 20$) [22].

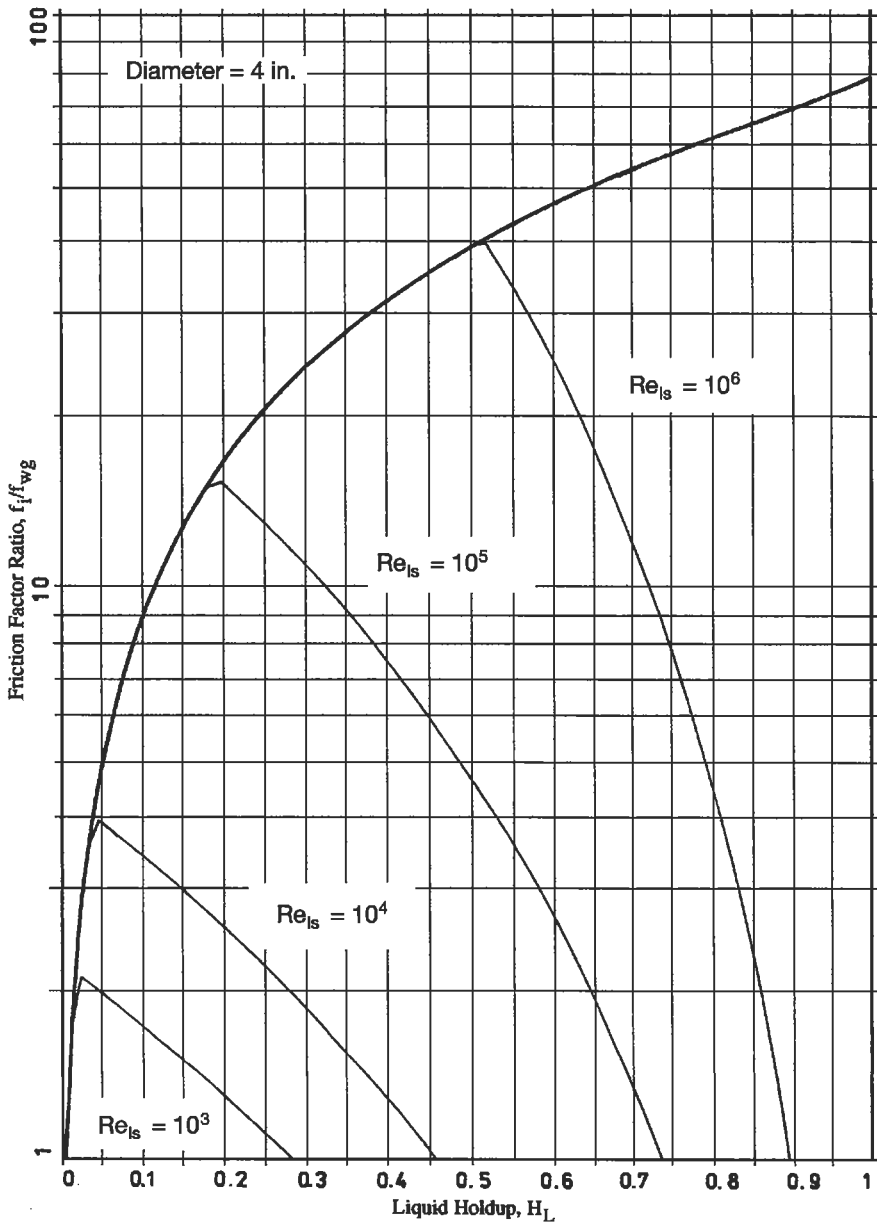


Figure 6-48a. Interfacial friction factor ratio for stratified flow regime (D = 4 inches) [22].

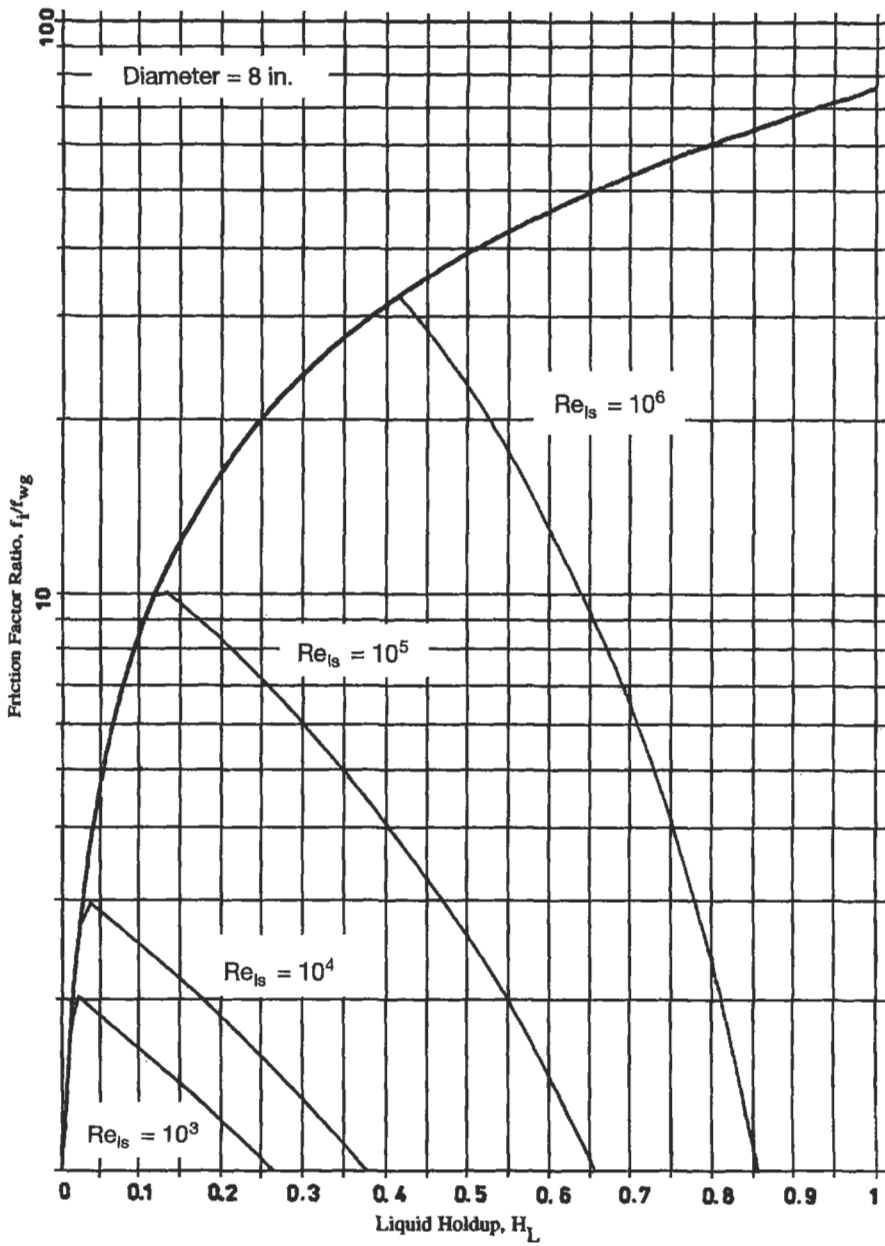


Figure 6-48b. Interfacial friction factor ratio for stratified flow regime ($D = 8$ inches) [22].

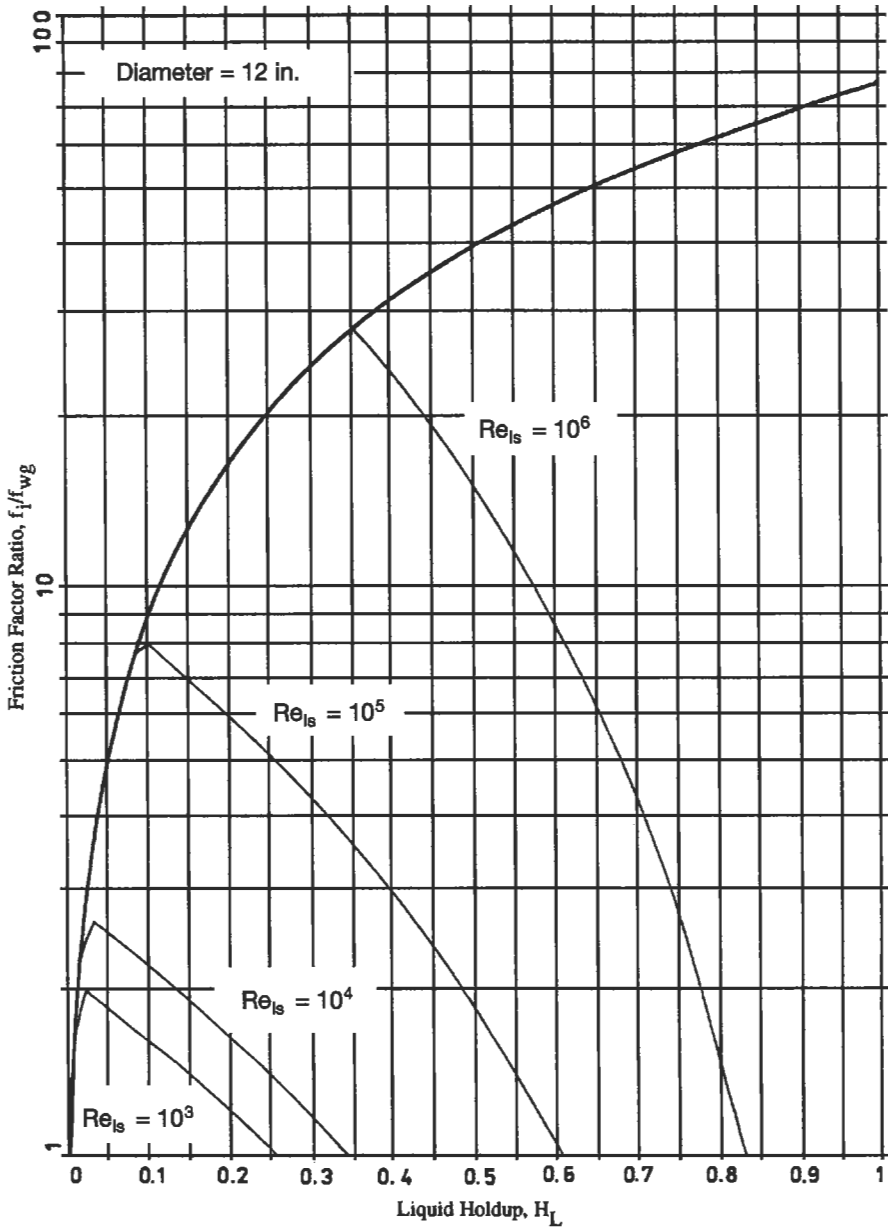


Figure 6-48c. Interfacial friction factor ratio for stratified flow regime (D = 12 inches) [22].

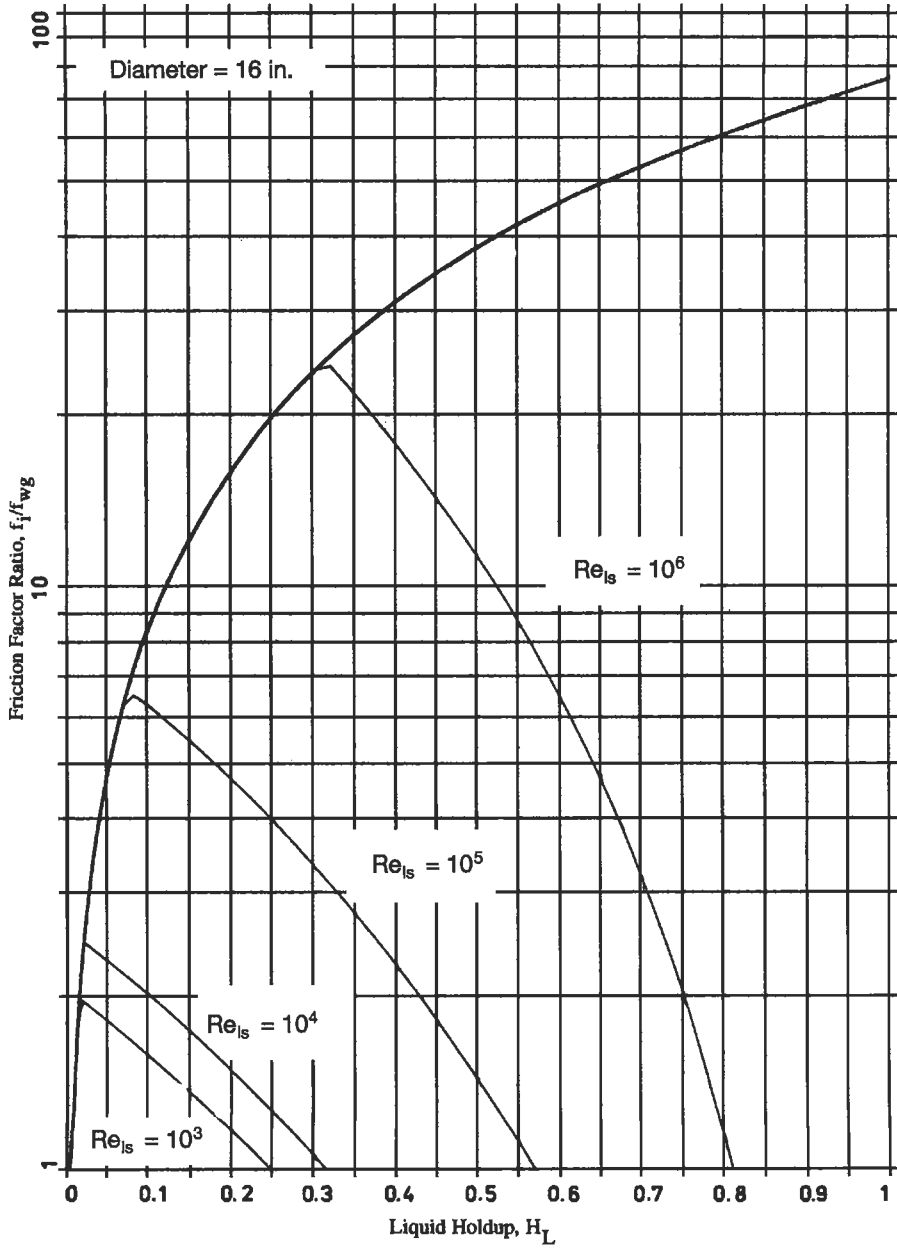


Figure 6-48d. Interfacial friction factor ratio for stratified flow regime (D = 16 inches) [22].

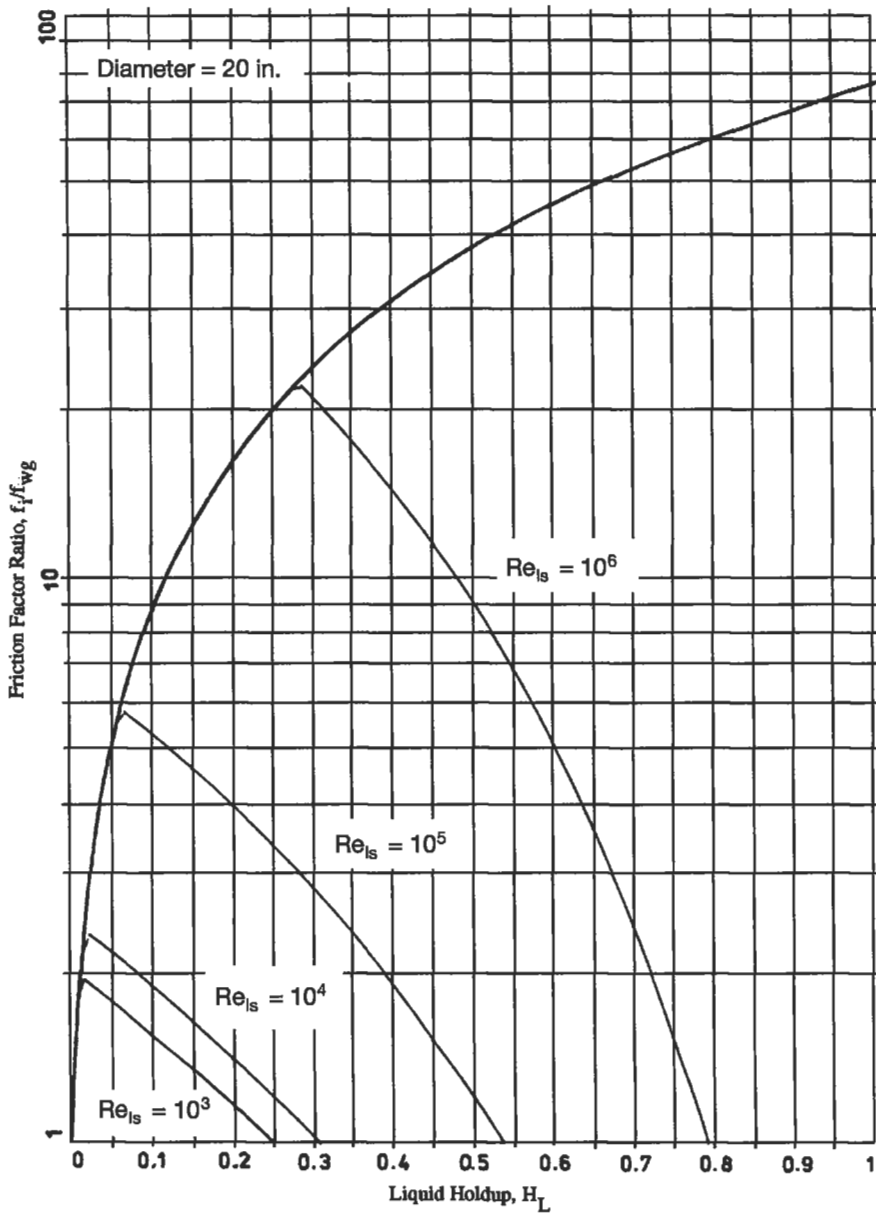


Figure 6-48e. Interfacial friction factor ratio for stratified flow regime (D = 20 inches) [22].

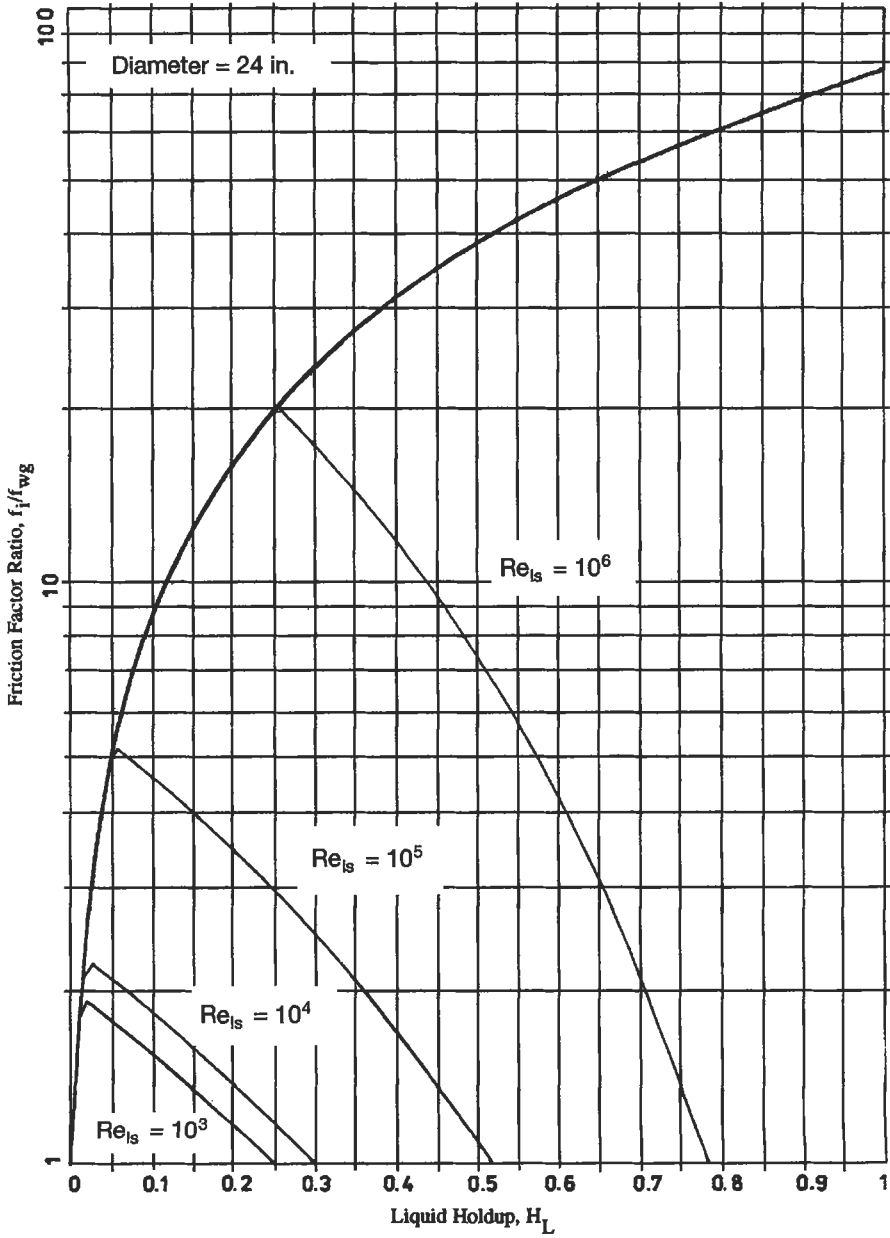


Figure 6-48f. Interfacial friction factor ratio for stratified flow regime (D = 24 inches) [22].

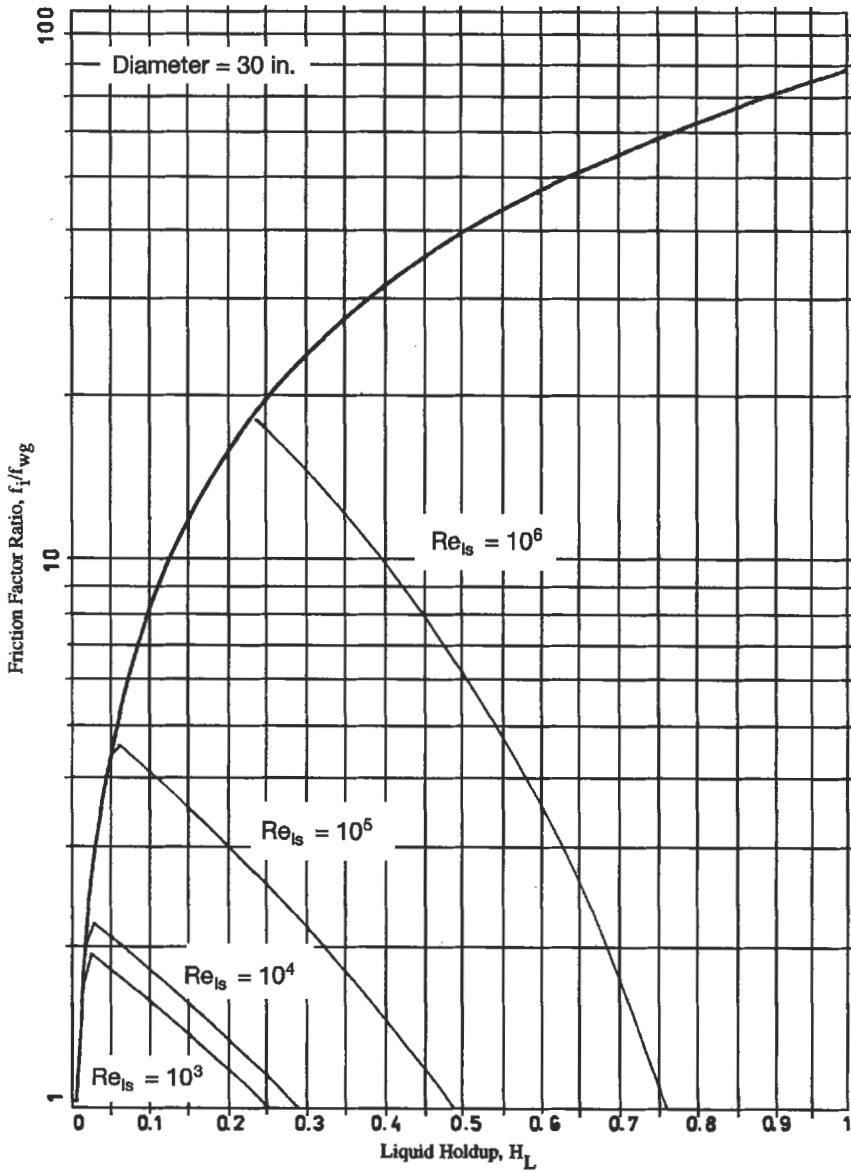


Figure 6-48g. Interfacial friction factor ratio for stratified flow regime ($D = 30$ inches) [22].

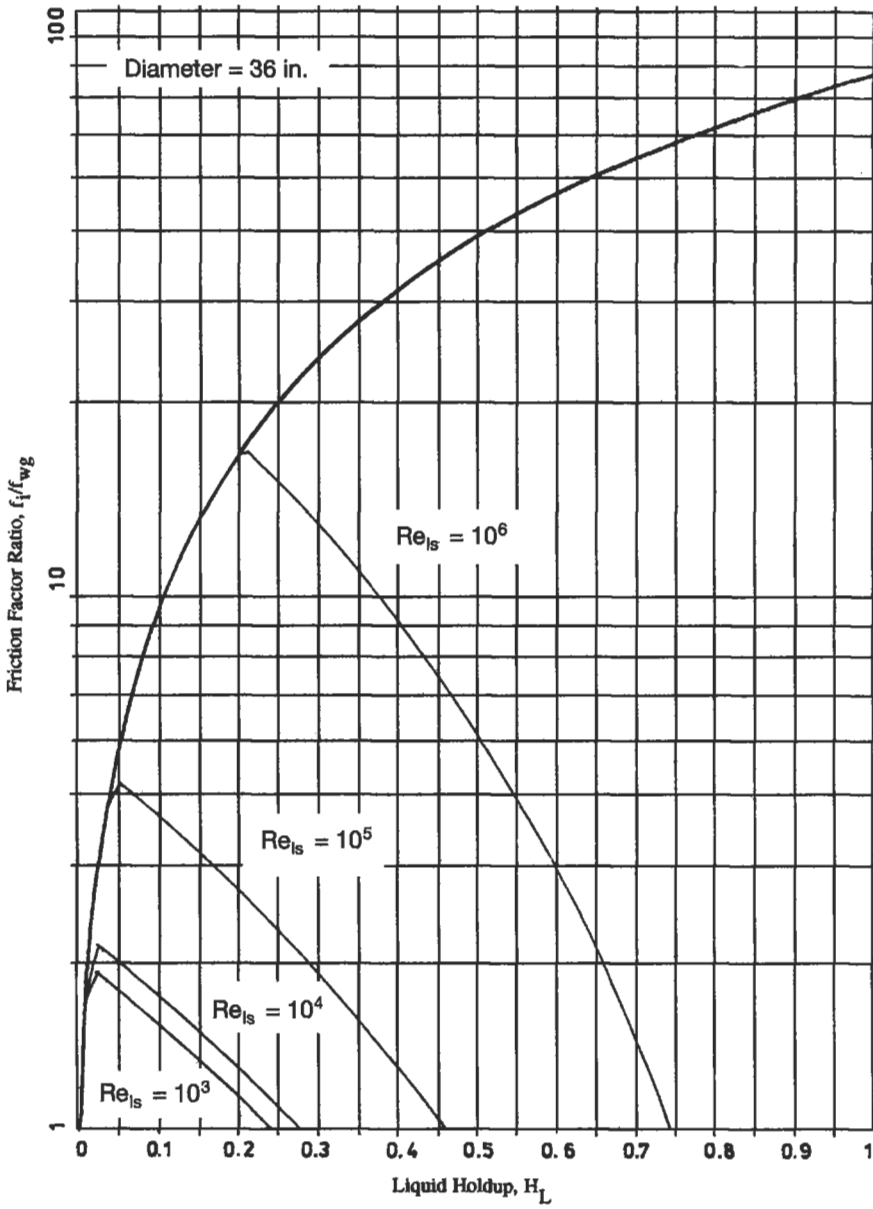


Figure 6-48h. Interfacial friction factor ratio for stratified flow regime (D = 36 inches) [22].

(text continued from page 449)

When the friction factor is determined correctly, Figure 6-47 should again be used to estimate a new value of the liquid holdup. If the new value of the liquid holdup obtained is different from determined previously, this new value should be used in Equation 6-76 or Figure 6-48 to refine the estimate for f_l/f_{wg} . This is simply an iteration process.

Pressure Gradient

Knowing the liquid holdup H_L , calculations for the pressure gradients due to friction and gravitational effects are straightforward. First, some geometric parameters are calculated:

1. Dimensionless cross-sectional area occupied by gas (A_G) and by liquid (A_L)

$$A_G = 0.25[\cos^{-1}(2h^*-1) - (2h^* - 1)[1 - (2h^* - 1)^2]^{0.5}] \quad (6-77a)$$

$$A_L = 0.25[\pi - \cos^{-1}(2h^* - 1) + (2h^* - 1)[1 - (2h^* - 1)^2]^{0.5}] \quad (6-77b)$$

2. Dimensionless wetted perimeter for gas phase (S_G) and for liquid phase (S_L)

$$S_G = \cos^{-1}(2h^* - 1) \quad (6-78a)$$

$$S_L = [\pi - \cos^{-1}(2h^* - 1)] \quad (6-78b)$$

3. Dimensionless interfacial length between gas and liquid phases (S_i)

$$S_i = [1 - (2h^* - 1)]^{0.5} \quad (6-79)$$

4. Dimensionless hydraulic diameter for gas phase (D_G) and liquid phase (D_L)

$$D_G = 4A_G/(S_L + S_i) \quad (6-80a)$$

$$D_L = 4A_L/S_L \quad (6-80b)$$

where h = dimensionless liquid height in pipe ($= H_L/D$)

Dimensionless liquid level h can be expressed in terms of H_L as shown in Figures 6-49 to 6-52, but in terms of h that approach is much easier for the circular pipe cross-section.

Since the liquid holdup is

$$H_L = 4A_L/\pi \quad (6-81)$$

It is necessary to find h first, using the expression in Equations 6-77 to 6-80. The value of h must be found numerically, or alternatively, it can be estimated from Figure 6-53. After geometric parameters are calculated (Equations 6-77 to 6-80) the friction factors for the gas and liquid phase has to be calculated:

(text continued on page 470)

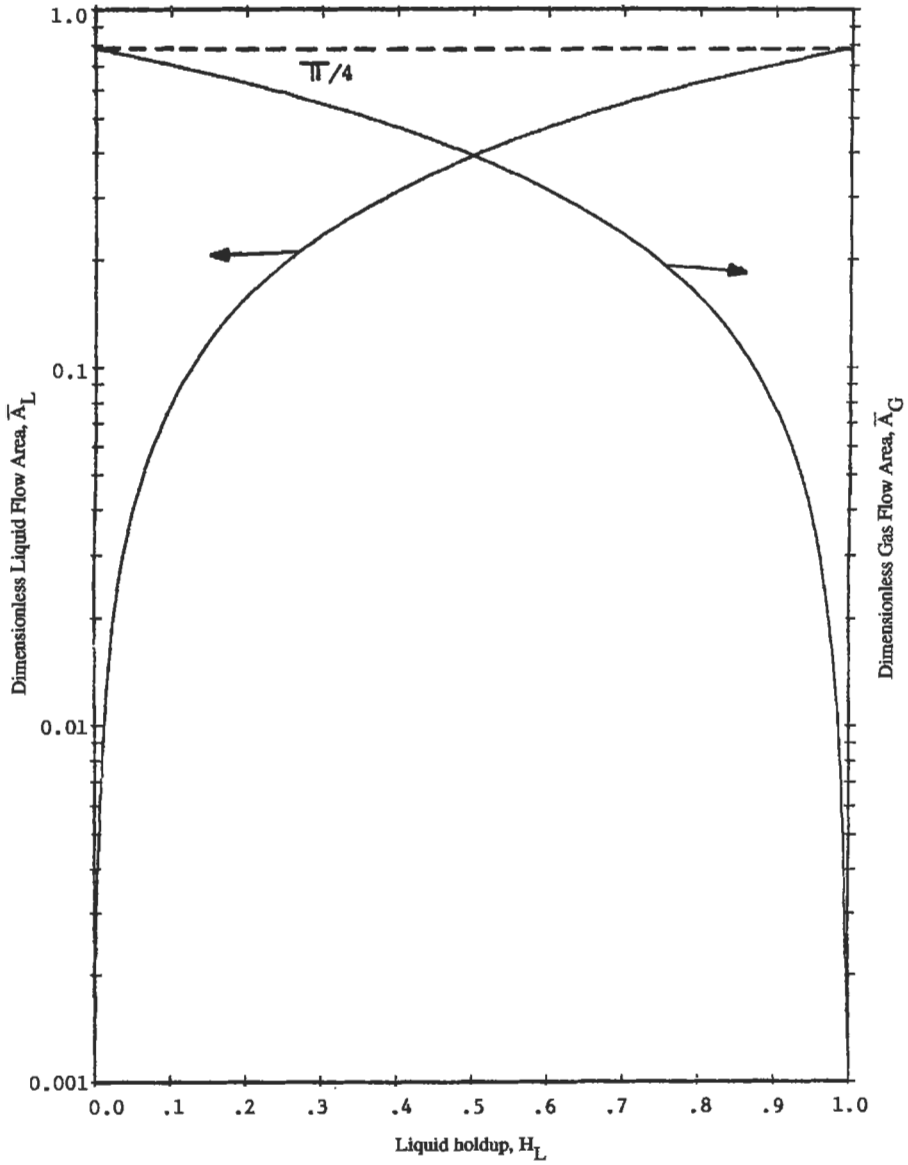


Figure 6-49. Dimensionless cross-sectional areas in stratified flow regimes [22].

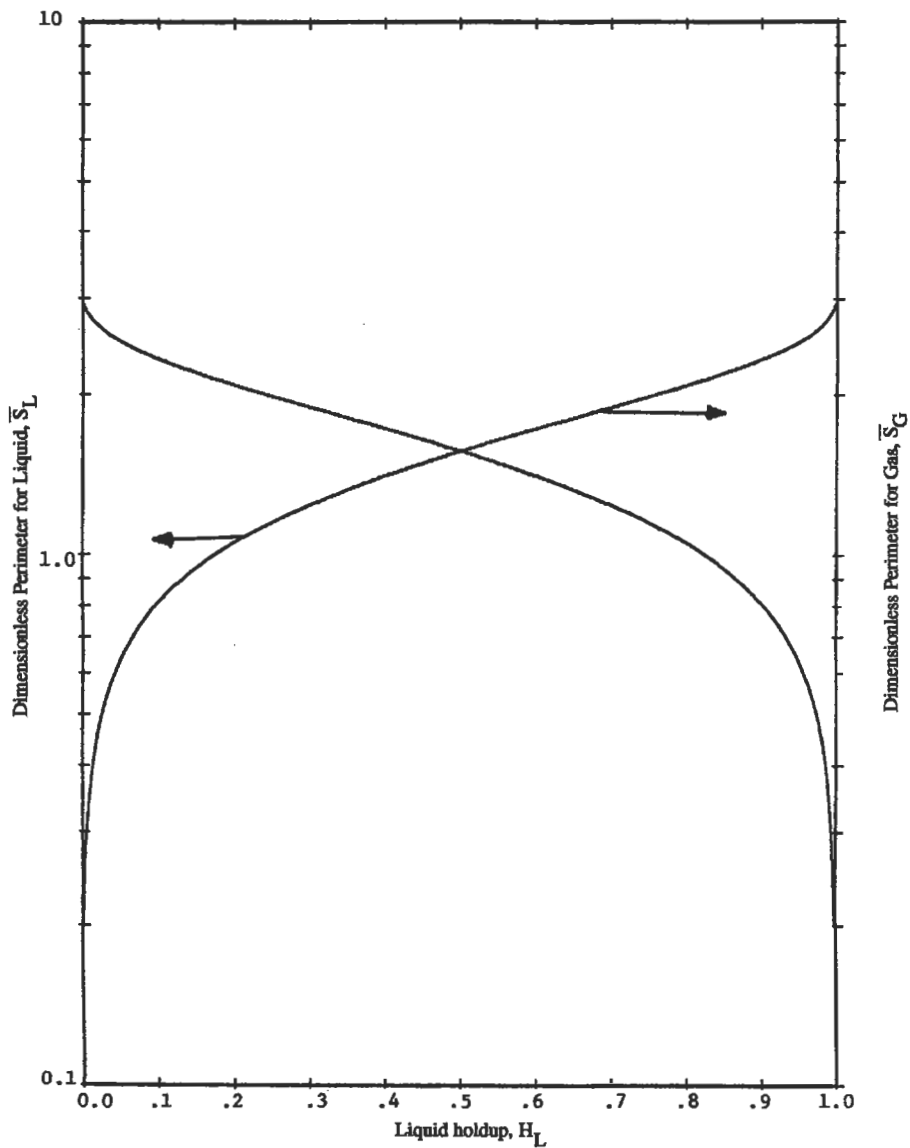


Figure 6-50. Dimensionless wetted perimeters in stratified flow regimes [22].

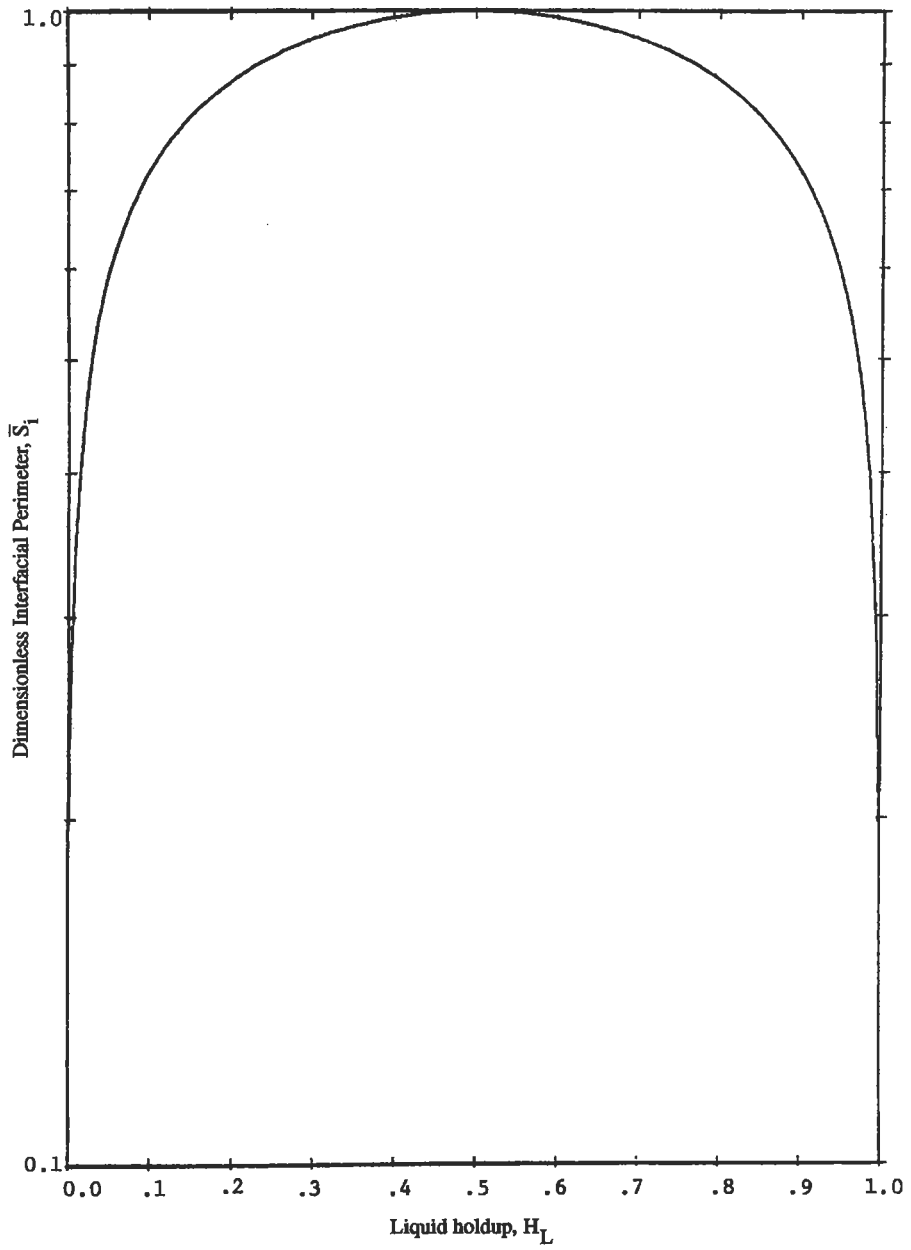


Figure 6-51. Dimensionless interfacial perimeters in stratified flow regimes [22].

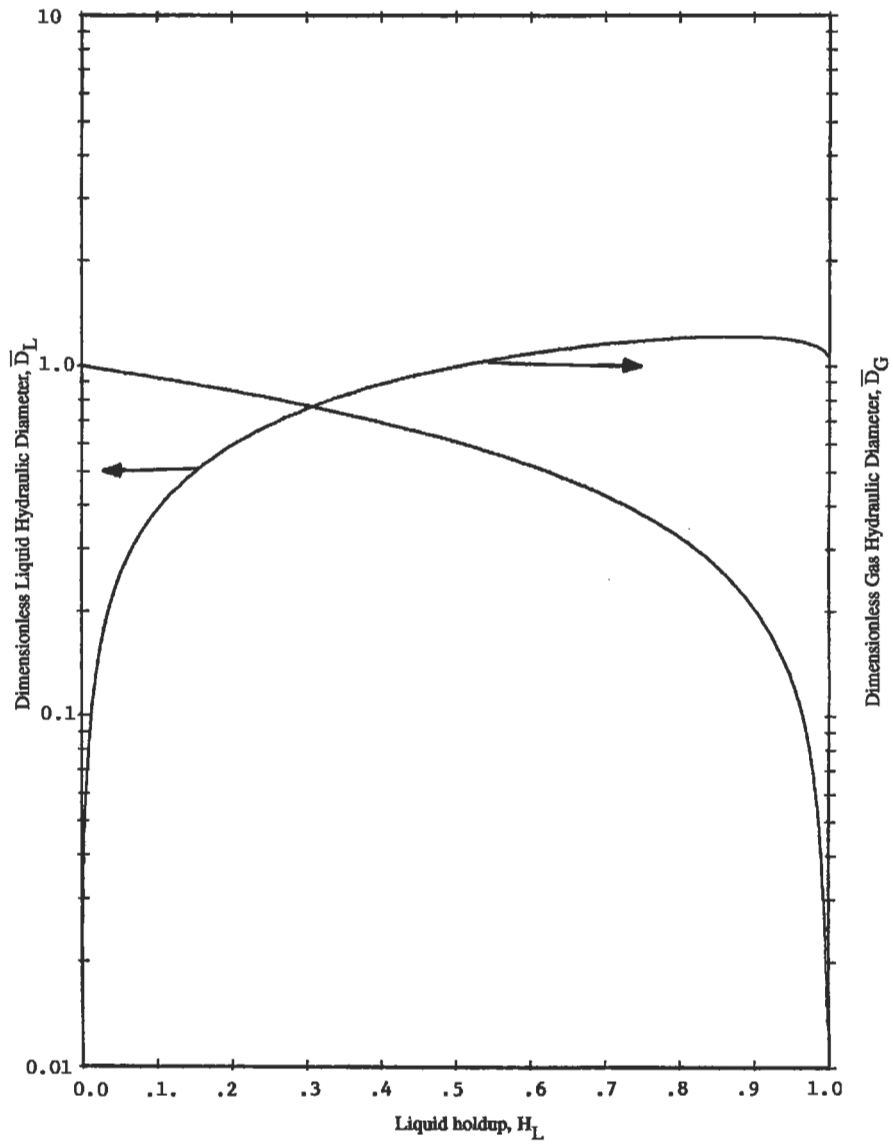


Figure 6-52. Dimensionless hydraulic diameters in stratified flow regimes [22].

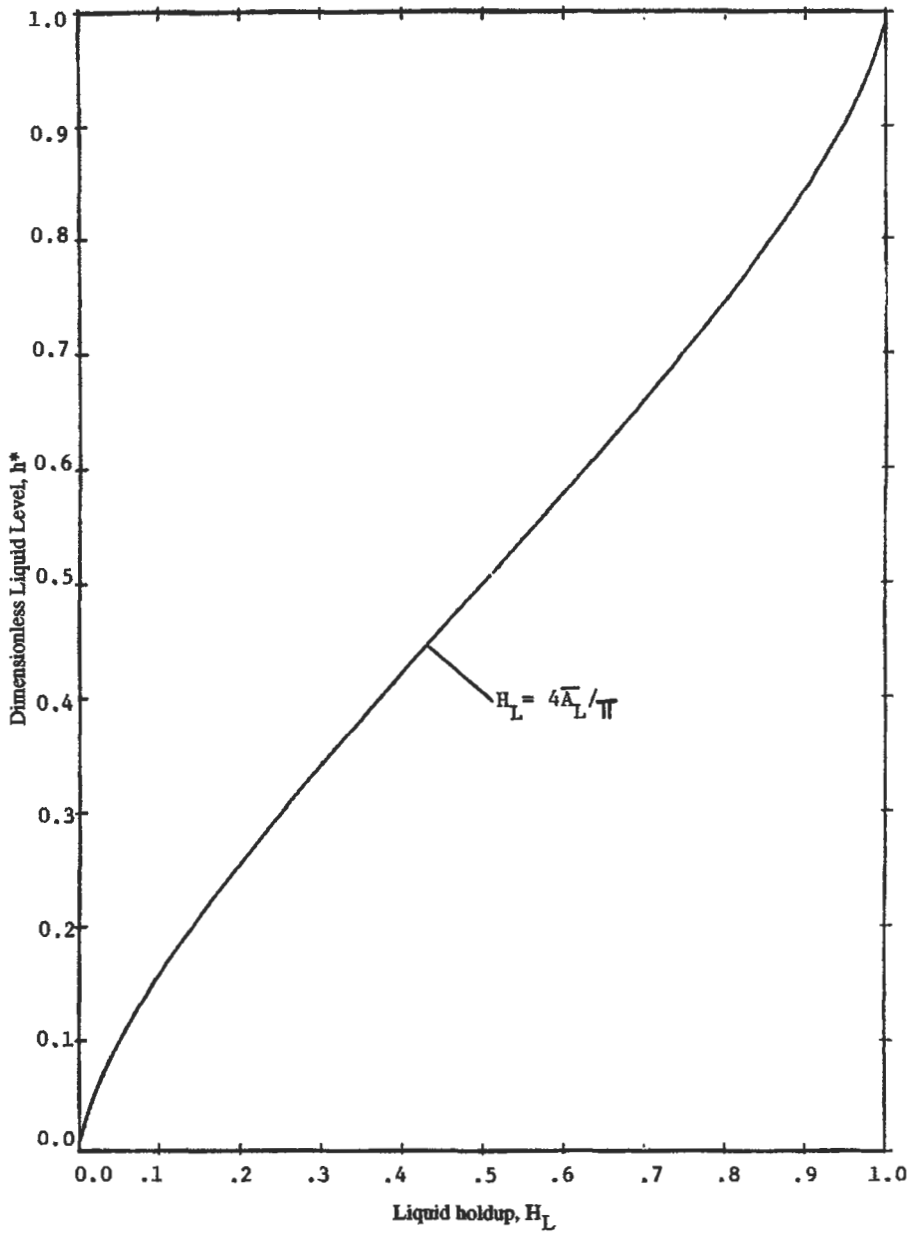


Figure 6-53. Dimensionless liquid level stratified flow regimes [22].

(text continued from page 464)

$$f_{wg} = \begin{cases} 0.046/\text{Re}_g^{0.2} & \text{if } \text{Re}_g = \left(\frac{\gamma_g D_G Dv_{wg}}{\mu_g (1 - h_L)} \right) \geq 1,500 \\ 16/\text{Re}_g & \text{if } \text{Re}_g < 1,500 \end{cases} \quad (6-82a)$$

$$f_{wL} = \begin{cases} 0.046/\text{Re}_L^{0.2} & \text{if } \text{Re}_L = \left(\frac{\gamma_L D_L Dv_{wL}}{\mu_L H_L} \right) \geq 1,500 \\ 16/\text{Re}_L & \text{if } \text{Re}_L < 1,500 \end{cases} \quad (6-82b)$$

Then the frictional and gravitational pressure gradients given by expression 6-64 are

$$\left(\frac{dp}{dL} \right)_f = - \left[2f_{wL} \left(\frac{\gamma_L v_{wL}^2}{\pi D} \right) \left(\frac{1}{H_L} \right)^2 (S_L) \right] - \left[2f_{wg} \left(\frac{\gamma_g v_{wg}^2}{\pi D} \right) \left(\frac{1}{1 - H_L} \right) (S_C) \right] \quad (6-83a)$$

$$\left(\frac{dp}{dL} \right)_d = \left(\frac{dp}{dZ} \right) \sin \theta = -g [H_L \gamma_L + (1 - H_L) \gamma_g] \sin \theta \quad (6-83b)$$

where L = distance in ft

z = vertical coordinate in ft

S = pipeline inclination from the horizontal in degree

Special Cases for Low and High Liquid Holdup

As $H_L \approx 1.0$ or 0.0 , it becomes difficult to determine the liquid holdup accurately. Small errors in the estimation lead to large errors in the frictional portion of the pressure gradient by Equation 6-83a; therefore, in such cases as above, it is recommended that the pressure gradient be calculated by the following methods. If the liquid holdup $H_L > 0.99$, then

$$\begin{aligned} \left(\frac{dp}{dL} \right)_f &= - \left[f_{wL} \left(\frac{\gamma_L v_{wL}}{2D} \right)^2 \left(\frac{1}{H_L} \right)^2 \left(\frac{S_L}{A_L} \right) \right] \\ &+ \left[\left(\frac{f_i}{f_{wg}} \right) f_{wg} \left(\frac{\gamma_g v_{wg}}{2D} \right) \left(\frac{1}{1 - H_L} \right)^2 \left(\frac{S_i}{A_L} \right) \right] - g \gamma_L \sin \theta \end{aligned} \quad (6-84a)$$

If the liquid holdup $H_L < 0.01$, then

$$\left(\frac{dp}{dL} \right)_f = - \left\{ f_{wg} \frac{\gamma_g v_{wg}^2}{2D} \left(\frac{1}{1 - H_L} \right)^2 \left[\left(\frac{S_G}{A_C} \right) + \left(\frac{f_i}{f_{wg}} \right) \left(\frac{S_i}{A_C} \right) \right] \right\} - g \gamma_g \sin \theta \quad (6-84b)$$

where the gravitational pressure gradient is still the same as in Equation 6-83b and the frictional pressure gradient can be determined by subtraction from Equation 6-84a or 6-84b.

Annular Flow Regime

In the annular flow regime, the extent of liquid entrainment must first be estimated, then the liquid holdup and the pressure gradient can be calculated.

Liquid Entrainment E_d

Calculation methods in this area have not been validated and may be poor. First, calculation v_c (critical gas velocity on set of entrainment) is made as follows:

$$v_c = 0.00025 \left(\frac{\gamma_L}{\gamma_g} \right)^{0.5} \left(\frac{\sigma_{gp}}{\mu_g} \right) \quad (6-85)$$

If the value of the $v_{sg} < v_c$, then there is no entrainment $E_d = 0$. If $v_{sg} > v_c$, then the entrainment fraction should be estimated by

$$E_d = 1 - \exp \left[0.23 \left(\frac{v_c - v_{sg}}{v_c} \right) \right] \quad (6-86)$$

where E_d = mass fraction or volume fraction of the total liquid flow that is in the form of entrained droplets

Equation 6-86 is an empirical correlation without experimental basis. Figure 6-54 graphically shows the liquid entrainment fraction for various values of the critical entrainment velocity, v_c .

Liquid Holdup H_L

After E_d fraction is calculated, the liquid holdup can be estimated. To determine H_L , dimensionless specific weight ratio γ_c^* has to be known:

$$\gamma_c^* = \frac{\gamma_c}{\gamma_g} = \left[E_d \left(\frac{\gamma_L}{\gamma_g} \right) \left(\frac{v_{sl}}{v_{sg}} \right) + 1 \right] \quad (6-87)$$

$$\gamma_c^* = \frac{\text{density of a gas-droplet mixture in the core of the annular flow}}{\text{density of the gas phase}}$$

with this density ratio, other dimensionless parameters could be defined:

$$X_a = \frac{X}{(\gamma_c^*)^{0.5}} \quad (6-88a)$$

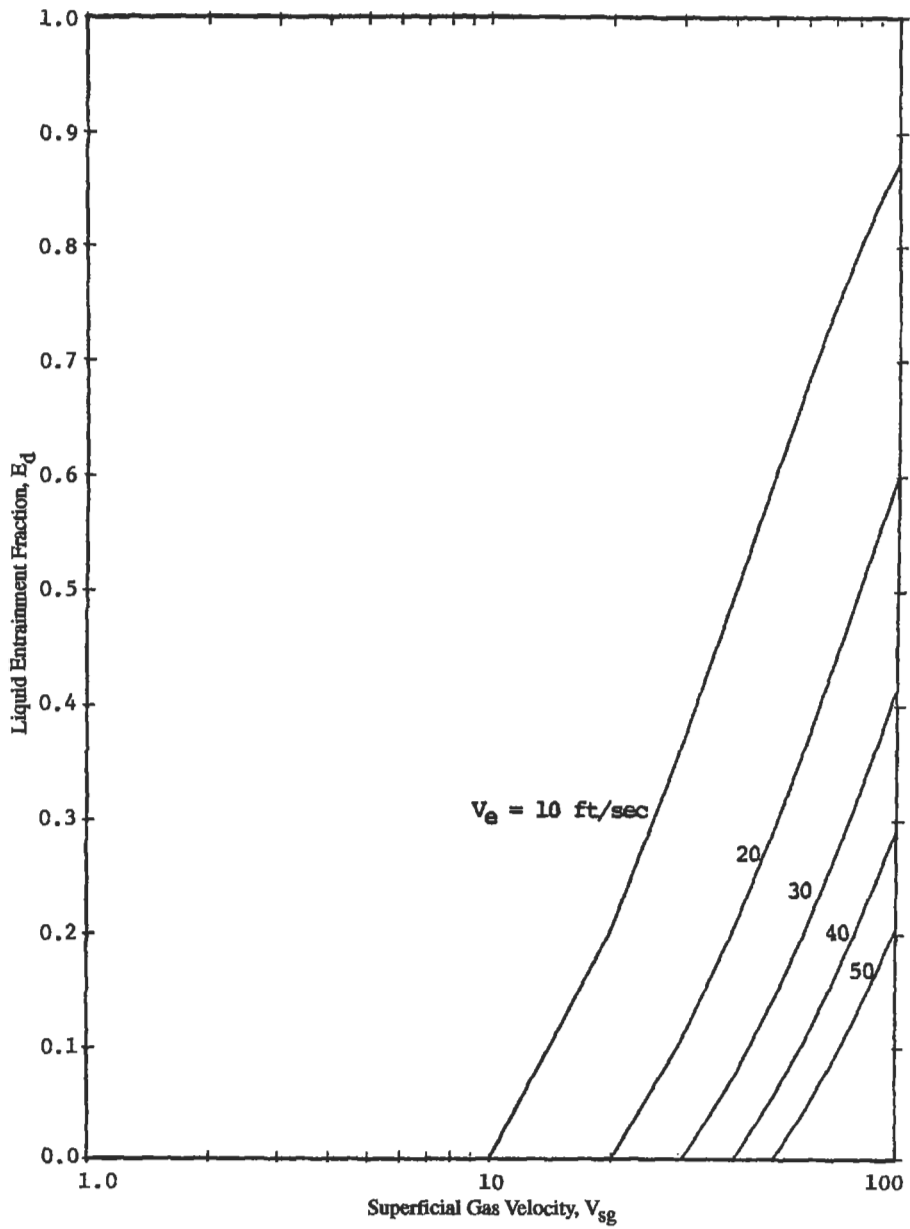


Figure 6-54. Liquid entrainment fraction in annular flow regime [22].

$$Y_s = \left(\frac{Y}{\gamma_c} \right) \left(\frac{\gamma^* - \gamma_c}{\gamma^* - 1} \right) \quad (6-88b)$$

where X and Y are the same as the values for the stratified flow regime.

With these parameters, Figure 6-55a-d can be used to estimate the liquid holdup in the liquid film H_{Lr} for the annular flow regime.

The total liquid holdup in the annular flow regime is calculated as follows:

$$H_L = H_{Lr} + \left(\frac{E_d v_{dL}}{E_d v_{dL} + v_{sg}} \right) \quad (6-89)$$

Pressure Gradient

The friction factor for the liquid phase needs to be calculated first.

$$f_{wL} = \begin{cases} 0.046/Re_L^{0.2} & \text{if } Re_L = \left[\frac{\gamma_L D v_{dL} (1 - E_d)}{\mu_L} \right] \geq 1,500 \\ 16/Re_L & \text{if } Re_L < 1,500 \end{cases} \quad (6-90)$$

The fractional and gravitational pressure gradients are

$$\left(\frac{dp}{dL} \right)_f = - \left[2f_{wL} \left(\frac{\gamma_L v_{dL}^2}{D} \right) \left(\frac{1 - E_d}{H_{Lr}} \right)^2 \right] \quad (6-91a)$$

and

$$\left(\frac{dp}{dL} \right)_g = g [\gamma_L H_{Lr} + (1 - H_{Lr}) \gamma_c] \sin \theta \quad (6-91b)$$

Special Case for Low Liquid Holdup

For low values of the liquid holdup, the approach described below is recommended. If $H_{Lr} < 0.002$, then

$$f_{wg} = \begin{cases} 0.046/Re_g^{0.2} & \text{if } Re_g = \left[\frac{\gamma_g D v_{sg}}{\mu_g (1 - H_{Lr})} \right] \geq 1,500 \\ 16/Re_g & \text{if } Re_g < 1,500 \end{cases} \quad (6-92a)$$

(text continued on page 478)

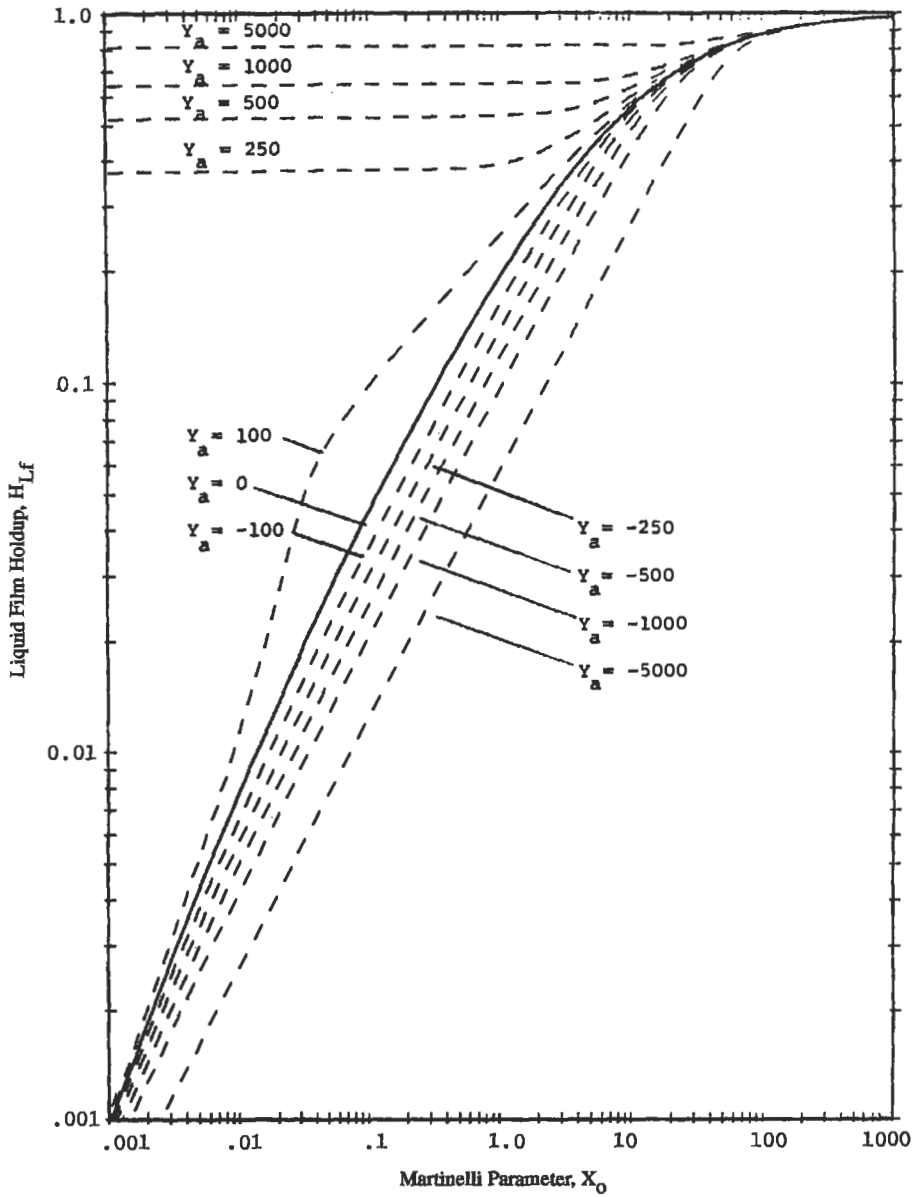


Figure 6-55a. Liquid holdup in annular flow regime ($E_d = 0$), (Expanded Y scale) [22].

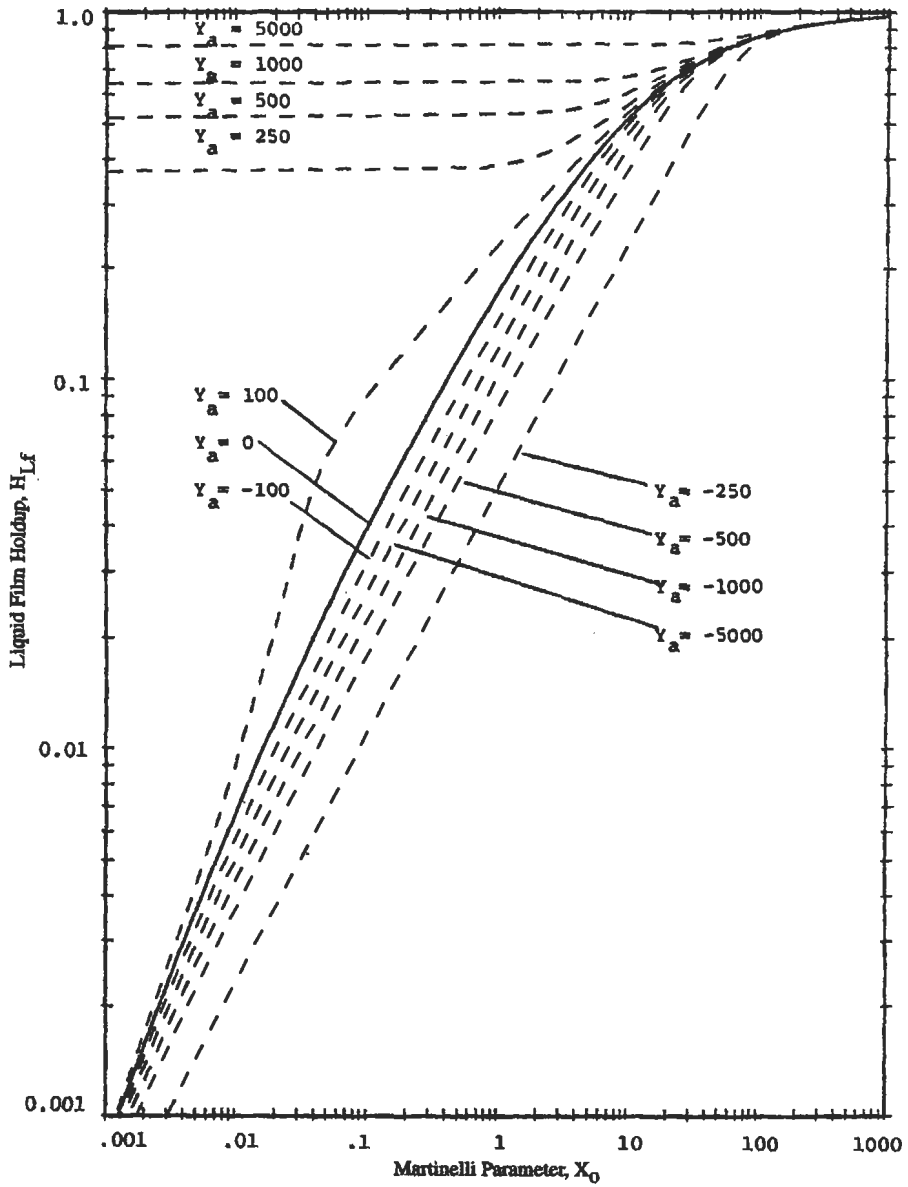


Figure 6-55b. Liquid holdup in annular flow regime ($E_d = 0.2$), (Expanded Y scale) [22].

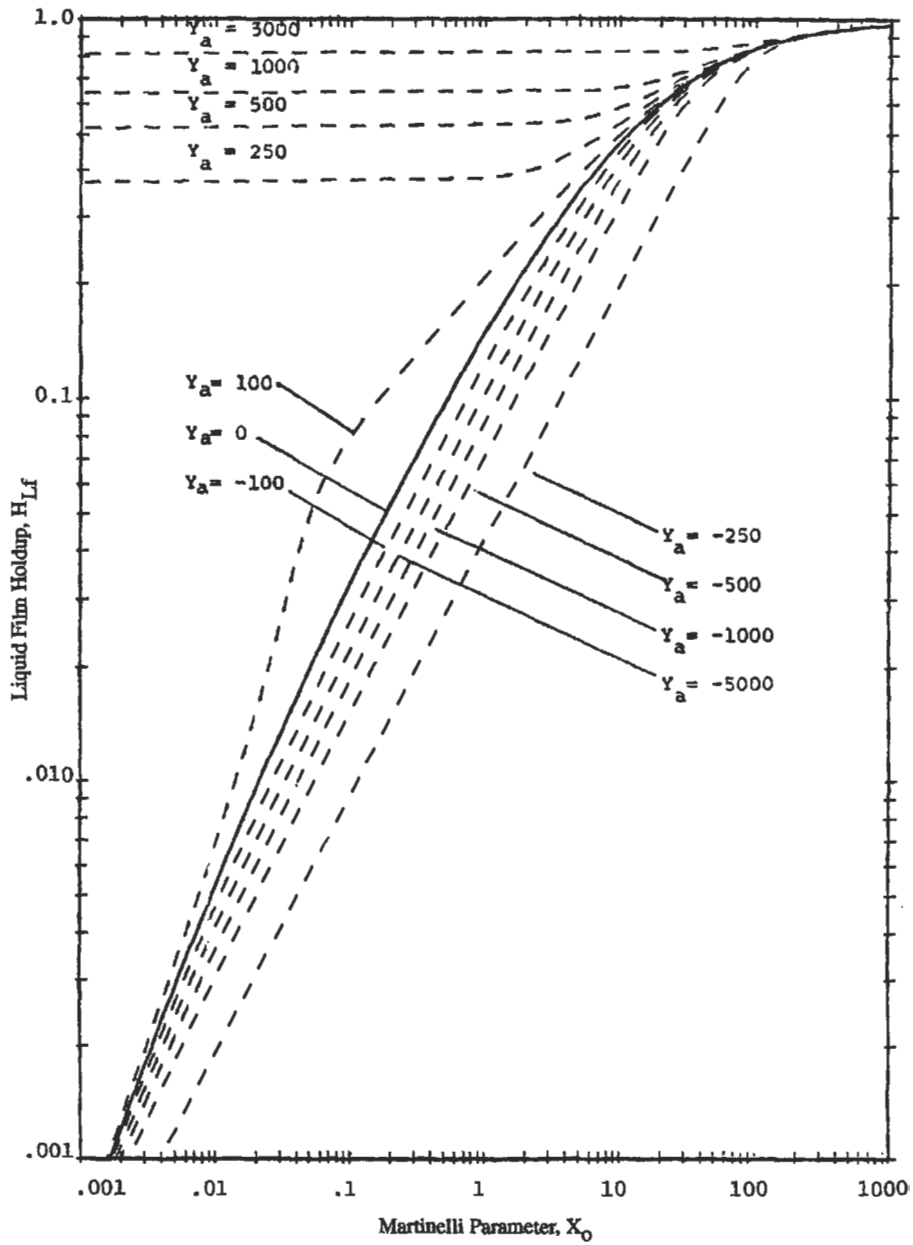


Figure 6-55c. Liquid holdup in annular flow regime ($E_d = 0.4$), (Expanded Y scale) [22].

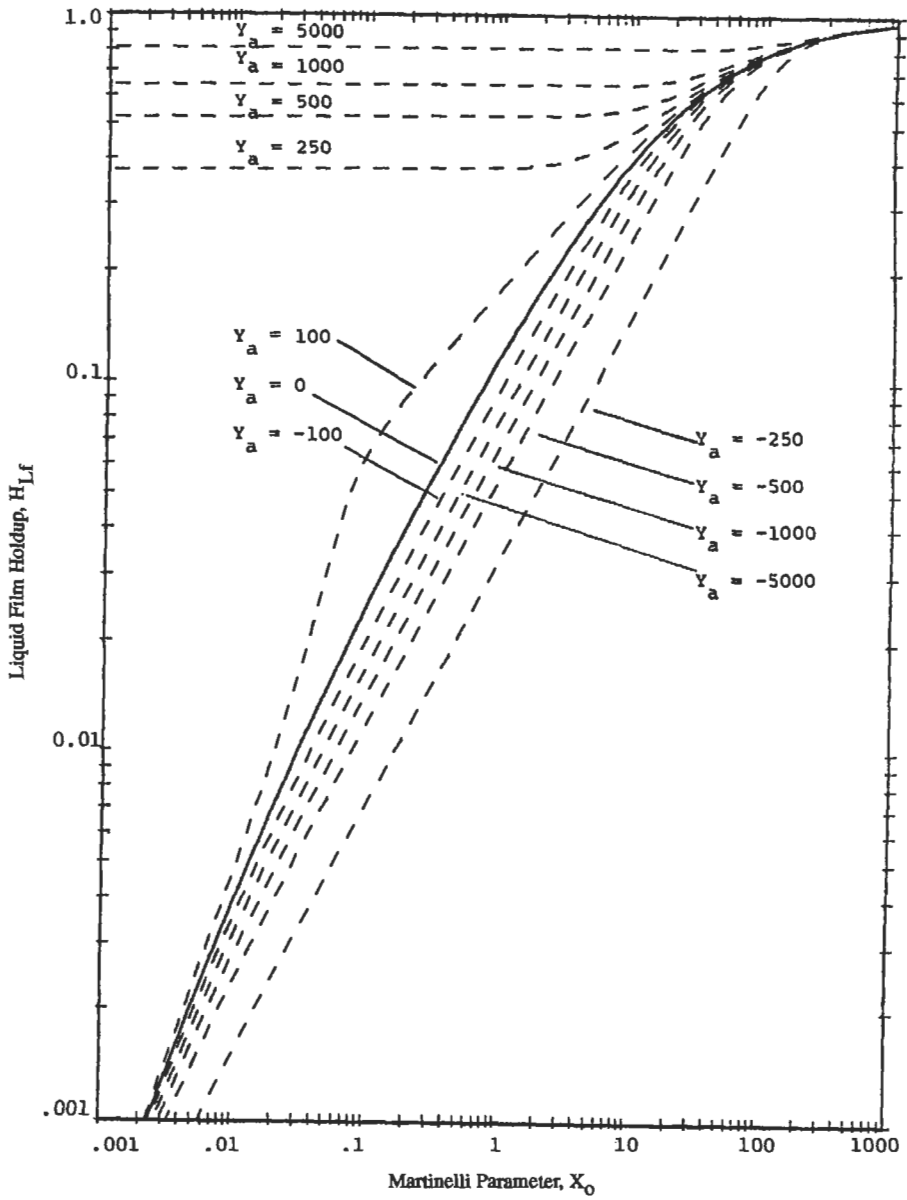


Figure 6-55d. Liquid holdup in annular flow regime ($E_d = 0.6$), (Expanded Y scale) [22].

(text continued from page 473)

Then the total pressure gradient is

$$\left(\frac{dp}{dL}\right)_{\text{total}} = -2(1 + 75H_{Lr})(f_{wg})\left(\frac{\gamma_c v_{wg}^2}{D}\right)\left(\frac{1}{1 - H_{Lr}}\right)^{5/2} - g\gamma_c \sin \theta \quad (6-92b)$$

$(dp/dL)_g$ from Equation 6-91b could be calculated.

Slug Flow Regime

In slug flow, the liquid slugs tend to contain some gas. The fraction of liquid in the liquid slugs can be estimated by

$$E_{Ls} = \frac{1}{1 + \left(\frac{v_m}{28.4}\right)^{1.59}} \quad (6-93)$$

Figure 6-56 shows the liquid holdup versus the mixture velocity v_m by this correlation.

Slug Velocity

The velocity of the liquid slugs or gas bubbles is determined by

$$v_s = C_0 v_m + k \left[\frac{gD(\gamma_L - \gamma_g)}{\gamma_L} \right]^{0.5} \quad (6-94)$$

For C_0 and k see Table 6-21.

Liquid Holdup

The overall liquid holdup is obtained by

$$H_L = 1 - \frac{v_{sg} + (1 - E_{Ls})(v_s - v_m)}{v_s} \quad (6-95)$$

Pressure Gradient

Two cases will be considered, slightly inclined flow and vertical flow. Pressure for slightly inclined flow is a function of an average liquid velocity v_L , a friction factor f_L and an average slug density ρ_{Ls} .

$$v_L = v_{sl}/H_L \quad (6-96a)$$

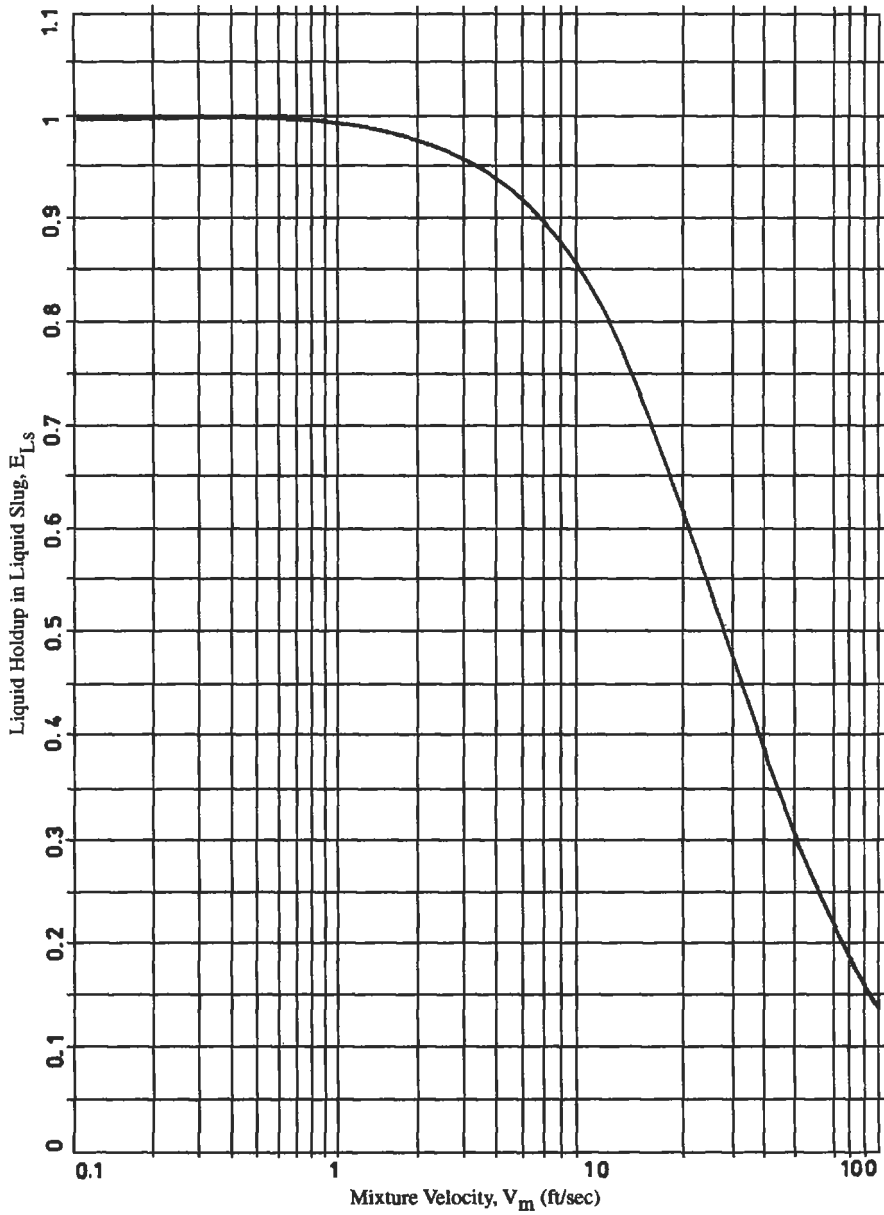


Figure 6-56. Liquid holdup in liquid slug [22].

Table 6-21
Drift-Flux Parameters for Slug Flow Regime

Pipe Inclination	C_o	k
$80^\circ < \theta \leq 90^\circ$	1.2	0.35
$0^\circ < \theta \leq 80^\circ$	1.3	0.50
$\theta = 0$	1.3	0
$-80^\circ \leq \theta < 0^\circ$	1.3	-0.5*
$-90^\circ < \theta < -80^\circ$	0.9	-0.6*

**if the slug velocity becomes small as a result of having the mixture superficial velocity, V_m , very small, then the slug velocity, V_s , should be limited to the mixture velocity.*

$$f_L = \begin{cases} 0.046/Re_L^{0.2} & \text{if } Re_L = \left(\frac{\gamma_L D v_L}{\mu_L} \right) \geq 1,500 \\ 16/Re_L & \text{if } Re_L < 1,500 \end{cases} \quad (6-96b)$$

$$\gamma_{sl} = [E_L \gamma_L + (1 - E_L) \gamma_g] \quad (6-96c)$$

The frictional pressure gradient is then calculated by

$$\left(\frac{dp}{dL} \right)_f = - \left(\frac{2f_L \gamma_L v_L^2}{D} \right) \quad (6-97a)$$

and the gravitational pressure gradient is

$$\left(\frac{dp}{dL} \right)_g = -g [H_L \gamma_L + (1 - H_L) \gamma_g] \sin \theta \quad (6-97b)$$

For vertical flow, the fractional pressure gradient is calculated by

$$\left(\frac{dp}{dL} \right)_f = - \left[2f_m \left(\frac{\gamma_L v_m^2}{D} \right) H_L \right] \quad (6-98)$$

where γ_L , from Equation 6-96c, with $E_L = 0.75$

$$H_L = \frac{v_{sl}}{v_L} = \frac{\text{liquid superficial velocity}}{\text{avg. liquid velocity in slug flow}}$$

and f_m , from Equation 6-96b, using the mixture velocity v_m (replacing v_L) in the Reynolds number.

Optional Correction

The approximation to the pressure gradient above neglects the liquid holdup in the liquid film around the gas bubble. This holdup may be significant for long gas bubbles that occur in wells of gas and oil pipelines. Thus Equations 6-98 and 6-97b will overpredict the pressure gradient. If greater accuracy is desired, a closer estimate (which may tend to underpredict the pressure gradient) is possible.

The thickness δ^* (dimensionless thickness of liquid film in slug bubble) of the liquid film is estimated and the result used to modify the liquid holdup. To get the liquid film thickness, two dimensionless parameters are first calculated; dimensionless velocity ratio for slug flow in risers N_r and dimensionless velocity ratio for slug flow in risers v^* :

$$N_r = [D^3 g(\gamma_1 - \gamma_g) \gamma_L]^{0.5} / \mu_L \tag{6-99a}$$

$$v^* = v_m \gamma_L^{0.5} / k [gD(\gamma_L - \gamma_g)]^{0.5} \tag{6-99b}$$

In Figure 6-57, the line of constant v^* is found first, then the line of constant N_r is located. The "turbulent film" line is a limiting case for large values of N_r . The intersection of these two lines determines the film thickness δ^* . The liquid holdup calculated by Equation 6-95 is then modified by

$$H'_L = 1 - (1 - H_L) / (1 - 2\delta^*)^2 \tag{6-100}$$

This modified value of the liquid holdup is used in Equation 6-98 and 6-97b) to determine the pressure gradient, where the other parameters are calculated as before.

Bubbly Flow Regime

The *liquid holdup* is found by a drift-flux model

$$H_L = 1 - \left(\frac{v_{sg}}{C_0 v_m + kv_\infty} \right) \tag{6-101a}$$

where the velocity v_∞ is

$$v_\infty = \left[\frac{g \sigma_{gp} (\gamma_L - \gamma_g)}{\gamma_L^2} \right]^{0.25} \tag{6-101b}$$

and the parameters C_0 and k are determined as below:

Pipe Inclination	C_0	k
$>0^\circ$	$1.2 - 0.2(\gamma_g/\gamma_L)^{0.5}$	1.4
0°	$1.2 - 0.2(\gamma_g/\gamma_L)^{0.5}$	0
$<0^\circ$	0.9	0

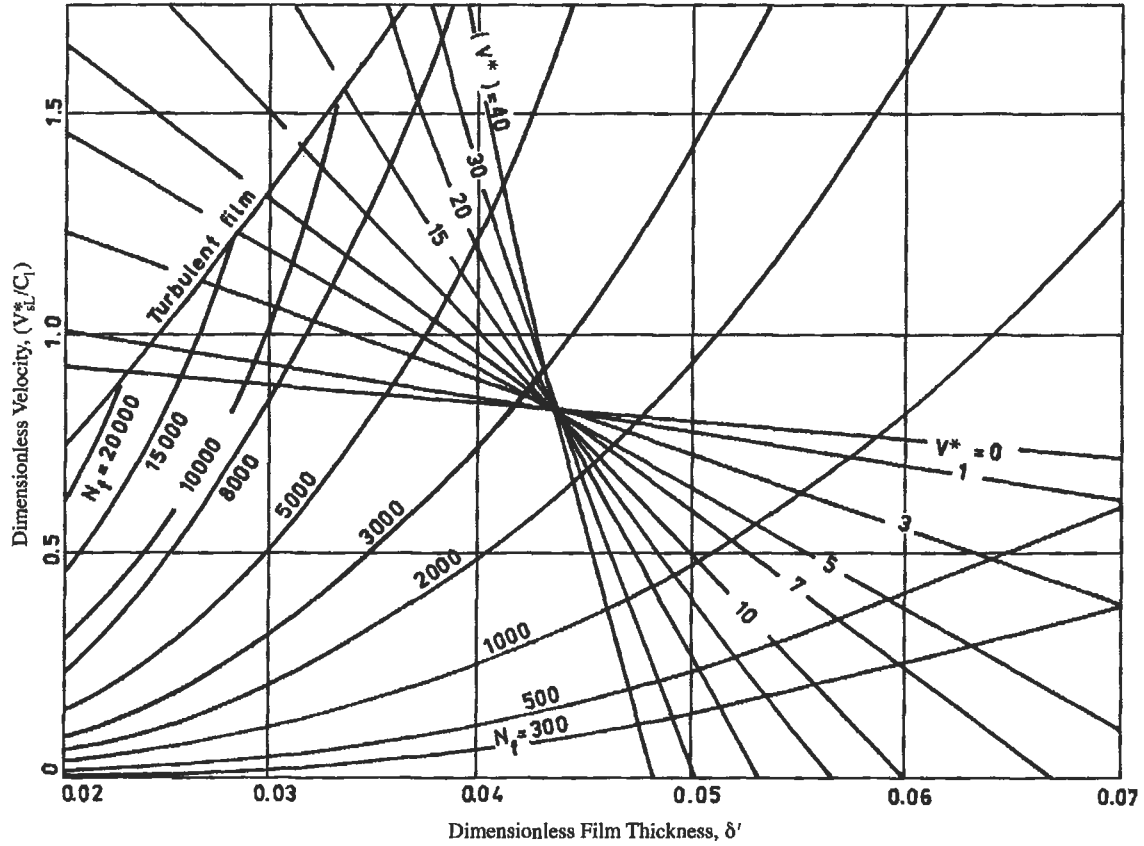


Figure 6-57. Dimensionless film thickness for well in slug flow [22].

Pressure Gradient

The friction factor for the liquid is first calculated by

$$f_{wLm} = \begin{cases} 0.046/Re_{Lm}^{0.2} & \text{if } Re_{Lm} = \left(\frac{\gamma_L D v_m}{\mu_g} \right) \geq 1,500 \\ 16/Re_{Lm} & \text{if } Re_{Lm} < 1,500 \end{cases} \quad (6-102a)$$

The pressure gradient due to friction in the bubbly flow regime is evaluated from

$$\left(\frac{dp}{dL} \right)_f = \frac{2f_{wLm} v_m (\gamma_g v_{vg} + \gamma_L v_{sL})}{D} \quad (6-102b)$$

and the gravitational pressure gradient

$$\left(\frac{dp}{dL} \right)_g = -g [H_L \gamma_L + (1 - H_L) \gamma_g] \sin \theta \quad (6-102c)$$

Correction for Acceleration Effects

The methods used in this section so far neglected the contribution of acceleration effects to the pressure gradient.

The acceleration pressure gradient in pipeline flow is due to the changes in the fluid properties through the pipe segment. These changes include expansion of the gas phase, expansion of the liquid phase and the changes in quality (due to phase behavior).

To account for acceleration effects, the total pressure gradient should be calculated by:

$$\left(\frac{dp}{dL} \right)_t = \frac{\left(\frac{dp}{dL} \right)_f + \left(\frac{dp}{dL} \right)_g}{1 + A} \quad (6-103a)$$

where the parameter A is calculated by the method appropriate for each flow regime as follows:

$$A \begin{cases} = 0 & \text{to neglect acceleration effects} \\ = (\gamma_g v_{vg} + \gamma_L v_{sL})^2 \left[X \left(\frac{dV_g}{dp} \right) + (1 - X) \left(\frac{dV_L}{dp} \right) \right] & \text{for bubbly or slug flow regime} \\ = (\gamma_g v_{vg} + \gamma_L v_{sL})^2 \left[\frac{X^2}{(1 - H_L)} \left(\frac{dV_g}{dp} \right) + \frac{(1 - X)^2}{H_L} \left(\frac{dV_L}{dp} \right) \right] & \text{for stratified or annular flow regime} \end{cases} \quad (6-103b)$$

d_g/d_p and d_L/d_p represent the change in specific volume for each phase with a change in pressure as evaluated from the fluid properties. The acceleration portion of the pressure gradient is calculated by

$$(dp/dL)_a = -A(dp/dL)_t \quad (6-103c)$$

Limitation

The described-above methods can be applied under the following conditions:

1. flow mass in pipe in constant (steady-state flow)
2. only the gas-liquid phase flow is considered; the liquid phase is treated as an oil
3. the temperature is constant and equal to the average temperature

The above procedure presents the multiphase methods in a simplified form to permit quick prediction to be made. The same problems can be solved based on computer methods that are presented in Volumes 2 and 3 of the AGA Project [19].

Example 1

Calculate the pressure gradient for a horizontal pipeline using the flow regime maps. The following data are given:

$$q_g = 40 \text{ MMscf/d}$$

$$q_o = 40,000 \text{ stb/d}$$

$$\text{ID} = 9 \text{ in.}$$

$$\text{API (gravity)} = 33^\circ$$

$$P_{\text{avg}} = 2,000 \text{ psia}$$

$$T_{\text{avg}} = 80^\circ\text{F}$$

$$\text{S.G.} = 0.75 \text{ at } 14.7 \text{ psia and } T = 60^\circ\text{F}$$

$$R_p = 990 \text{ scf/bbl}$$

Also calculate missing fluid properties using proper correlations.

$$dp/dL = ?$$

1. Stock-tank oil specific weight γ_{sto}

$$\begin{aligned} \gamma_{\text{sto}} &= 62.37 [141.5 / (131.5 + ^\circ\text{API})] \\ &= 62.37 [141.5 / (131.5 + 33)] \\ &= 53.65 \text{ lb/ft}^3 \end{aligned}$$

2. Gas specific weight at std conditions γ_{gsc}

$$\begin{aligned}\gamma_{gsc} &= 0.0763\gamma_g = 0.0763(0.75) \\ &= 0.05723 \text{ lb/ft}^3\end{aligned}$$

3. Pipe flow area

$$A_p = (\pi/4)D^2 = \pi/4(9/12)^2 = 0.4418 \text{ ft}^2$$

4. Calculate Z , μ_g , μ_o and GOR at P_{avg} and T_{avg} . From Gas P-V-T Program (see Chapter 5) at $p = 2,000$ psia

$$T = 80^\circ\text{F}$$

$$Z = 0.685$$

$$\mu_g = 0.0185 \text{ cp}$$

From Oil P-V-T program at $p = 2,000$ psia

$$T = 80^\circ\text{F}$$

$$R_p = 990 \text{ scf/bbl}$$

$$\mu_o = 2.96 \text{ cp}$$

5. Calculate γ_g at P_{avg} , T_{avg} and Z_{avg}

$$\gamma_g = \frac{28.97(\gamma)P_{avg}}{Z_{avg}RT_{avg}} = \frac{28.97(0.75)(2,000)}{10.685(10.73)(80 + 460)} = 10.95 \text{ lb/ft}^3$$

6. Calculate vapor superficial velocity, v_{vg} from Equation 6-65

$$v_{vg} = \frac{q_g \rho_{gsc}}{A_p \rho_g (24) 3,600} = \frac{(40 \times 10^6) 0.05724}{0.4418 \times 10.95 \times 24 \times 3,600} = 5.48 \text{ ft/s}$$

7. Calculate liquid superficial velocity v_{sl}

$$v_{sl} = \frac{q_L}{A_p} = \frac{40,000(42)}{(7.481)24(3,600)0.4418} = 5.88$$

8. Reynolds number and friction factor based on the superficial velocity, from Equation 6-67b

a) Liquid

$$R_{cl} = \frac{\gamma_L D v_{sl}}{\mu_{lg}} = \frac{(53.56)(9/12)(5.88)}{(2.86)2.0886 \times 10^{-5}(32.2)} = 118,851.7 > 1,500$$

$$f_{wL} = \frac{0.046}{R_{eL}^{0.2}} = \frac{0.046}{(118,851.7)^{0.2}} = 4.44 \times 10^{-5}$$

where 2.0886×10^{-5} is a unit conversion factor

b) Gas

$$R_{eG} = \frac{\gamma_g D v_{sg}}{\mu_g g} = \frac{(10.95)(9/12)(5.48)}{(0.0187)(2.0886 \times 10^{-5})(32.2)} = 3,623,080 > 1,500$$

$$f_{wG} = \frac{0.046}{R_{eG}^{0.2}} = \frac{0.046}{(3,623,080)^{0.2}} = 2.24 \times 10^{-3}$$

9. Martinelli parameter X from Equation 6-67a

$$X = \left(\frac{2f_{wL} \gamma_L v_{sL}^2 / D}{2f_{wG} \gamma_g v_{sG}^2 / D} \right)^{0.5} = \left[\frac{4.44 \times 10^{-5} (53.65)(5.88)^2}{2.24 \times 10^{-3} (10.95)(5.48)^2} \right]^{0.5} = 3.3$$

10. Dimensionless inclination Y from Equation 6-70

$$Y = \frac{g(\gamma_L - \gamma_g) \sin \theta}{2f_{wG} \gamma_g v_{sG}^2 / D}$$

since $\sin \theta = 0$ (horizontal pipe)

$$Y = 0$$

11. Calculate gas Froude number

$$F_g = v_{sg} \left[\frac{\gamma_g}{(\gamma_L - \gamma_g) g D} \right]^{0.5} = 5.48 \left[\frac{10.95}{(53.65 - 10.95) 32.2 (9/12)} \right]^{0.5} = 0.56$$

12. Select flow regime for X = 3.3 and Y = 0. Figure 6-43a indicates slug flow.

13. Liquid holdup in the liquid slug, E_{sL} , from Equation 6-65e

$$v_m = v_{sL} + v_{sg} = 5.88 + 5.48 = 11.36 \text{ ft/s}$$

from Equation 6-93

$$E_{sL} = \frac{1}{1 + \left(\frac{v_m}{28.4} \right)^{1.99}} = \frac{1}{1 + \left(\frac{11.36}{28.4} \right)^{1.99}} = 0.781$$

14. Slug velocity v_s from Equation 6-94

$$v_s = c_0 v_m + K \left[\frac{gD(\gamma_L - \gamma_g)}{\gamma_L} \right]^{0.5}$$

where $C_0 = 1.3$ and $K = 0$ for $\theta = 0^\circ$

$$v_s = 1.3(11.36) + 0 = 14.768 \text{ ft/s}$$

15. Liquid holdup H_L , Equation 6-95,

$$\begin{aligned} H_L &= 1 - \frac{v_{sg} + (1 - E_{Ls})(v_s - v_m)}{v_s} \\ &= 1 - \frac{5.48 + (1 - 0.781)(14.768 - 11.36)}{14.768} = 0.578 \end{aligned}$$

16. For $\theta = 0^\circ$, calculate average liquid velocity, v_L ,

$$v_L = \frac{v_{dL}}{H_L} = \frac{5.88}{0.578} = 10.17 \text{ ft/s}$$

17. Calculate R_{eL} and f_{wL} from Equation 6-97b

$$R_{eL} = \frac{\gamma_L D v_L}{\mu_{LG}} = \frac{53.65(9/12)(10.17)}{12.96(32.2)(2.0886 \times 10^{-5})} = 205,565 > 1,500$$

$$f_{wL} = \frac{0.046}{R_{eL}^{0.2}} = \frac{0.046}{(205,564)^{0.2}} = 3.983 \times 10^{-3}$$

18. Average slug density γ_{Ls} from Equation 6-97c

$$\begin{aligned} \gamma_{Ls} &= E_{Ls} \gamma_L + (1 - E_{Ls}) \gamma_g \\ &= 0.781(53.65) + (1 - 0.7)(10.95) \\ &= 44.3 \text{ lb/ft}^3 \end{aligned}$$

19. The fractional pressure gradient from Equation 6-97a

$$\begin{aligned} \left(\frac{dp}{dL} \right)_f &= - \left(\frac{2f_L \gamma_{Ls} v_L^2}{Dg} \right) = - \frac{2(3.983 \times 10^{-3})(44.3)(10.17)^2}{(9/12)(32.2)} \\ &= -1.51132 \text{ lb/ft}^3 \end{aligned}$$

20. The total pressure gradient, since $\theta = 0^\circ$

$$\left(\frac{dp}{dL}\right)_{\text{gravitational}} = 0$$

and

$$\left(\frac{dp}{dL}\right)_{\text{total}} = \left(\frac{dp}{dL}\right)_f = 1.51132 \text{ lb/ft}^3$$

or

$$\left(\frac{dp}{dL}\right)_{\text{total}} = -1.0495 \times 10^{-2} \text{ psi/ft}$$

Semiempirical Methods

Many empirical correlations have been developed for predicting two-phase flowing pressure gradients which differ in the manner used to calculate three components of the total pressure gradient (see Equation 6-64). Some of them are described below.

The Duns-Ros Method [20,21]

To better understand the initial concept of the Duns-Ros method, Figure 6-58 shows a generalized flow diagram. This work was designed to cover ranges of low pressure, low rate, high gas/oil ratios and viscous oils. Figure 6-59 shows that pressure gradient and holdup also depend significantly on superficial gas velocity.

At low gas flowrates, the pipe essentially is full of liquid since the gas bubbles are small. Holdup is approximately equal to unity. At liquid rates less than 1.3 ft/s (0.4 m/s) increased gas rate causes the number and size of the bubbles to increase. Ultimately, they combine into plugs that become unstable and collapse at still higher gas concentrations to form slugs. At gas rates greater than 49 ft/s (15 m/s), with the same liquid rate, mist flow is initiated, and gas is the continuous phase with liquid drops dispersed in it. When the liquid velocity is over 5.3 ft/s (16 m/s) the flow patterns are not as observable. As gas flow increases, no plug flow is observed; flow is turbulent and frothy until some degree of segregation takes place at higher rates. For this degree of liquid loading, mist flow does not occur until gas velocity reaches at least 164 ft/s (50 m/s).

Figure 6-60 graphically outlines the flow regime areas. Duns and Ros mathematically defined these areas as functions of the following dimensionless numbers:

$$N_{vg} = v_{sg} A (\gamma_L / \sigma)^{0.25} \quad \text{gas velocity number} \quad (6-104)$$

$$N_{vL} = v_{sL} A (\gamma_L / \sigma)^{0.25} \quad \text{liquid velocity number} \quad (6-105)$$

$$N_d = dB (\gamma_L / \sigma)^{0.5} \quad \text{diameter number} \quad (6-106)$$

$$N_{L\mu} = N_L = \mu_L C (1 / \gamma_L \sigma^3)^{0.25} \quad \text{liquid velocity number} \quad (6-107)$$

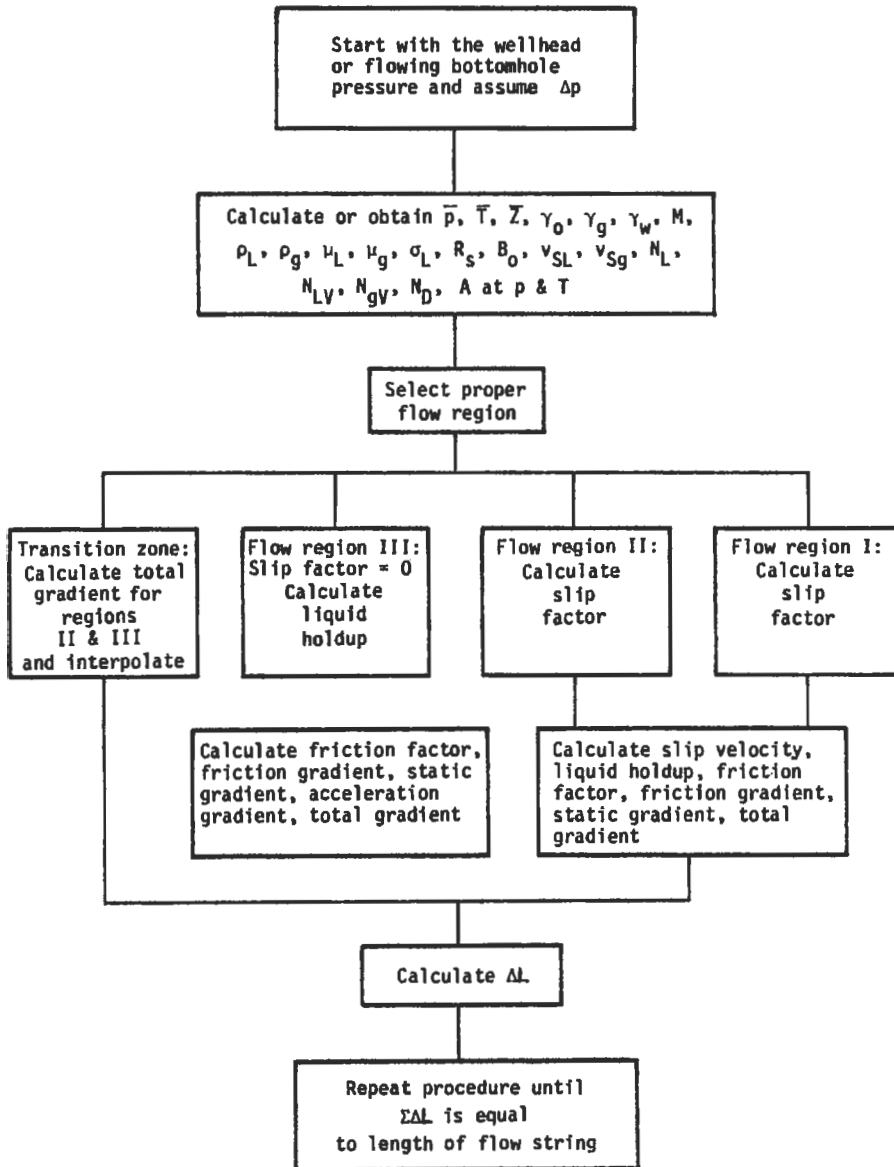


Figure 6-58. Flow diagram for the Duns-Ros method [19].

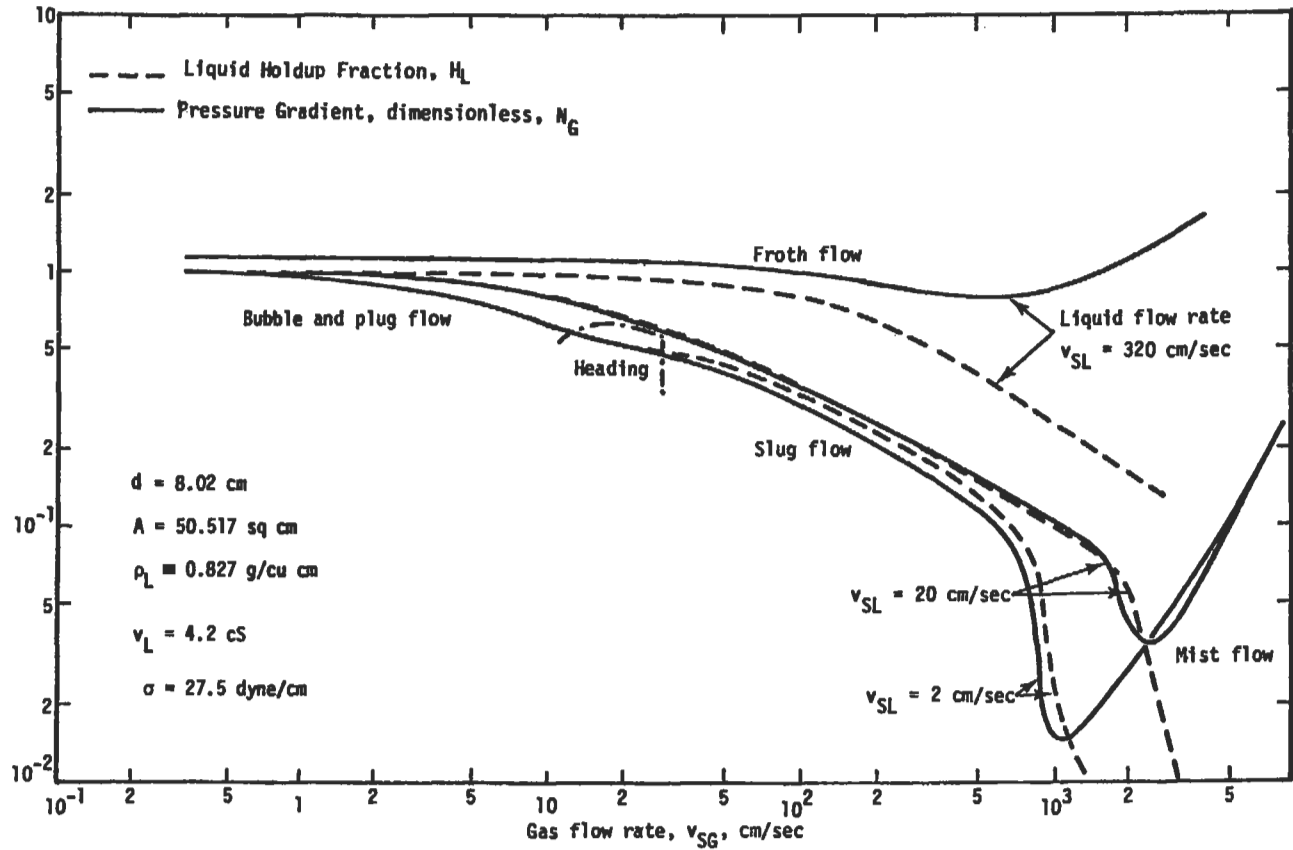


Figure 6-59. Example of two-phase flow in vertical pipe [23].

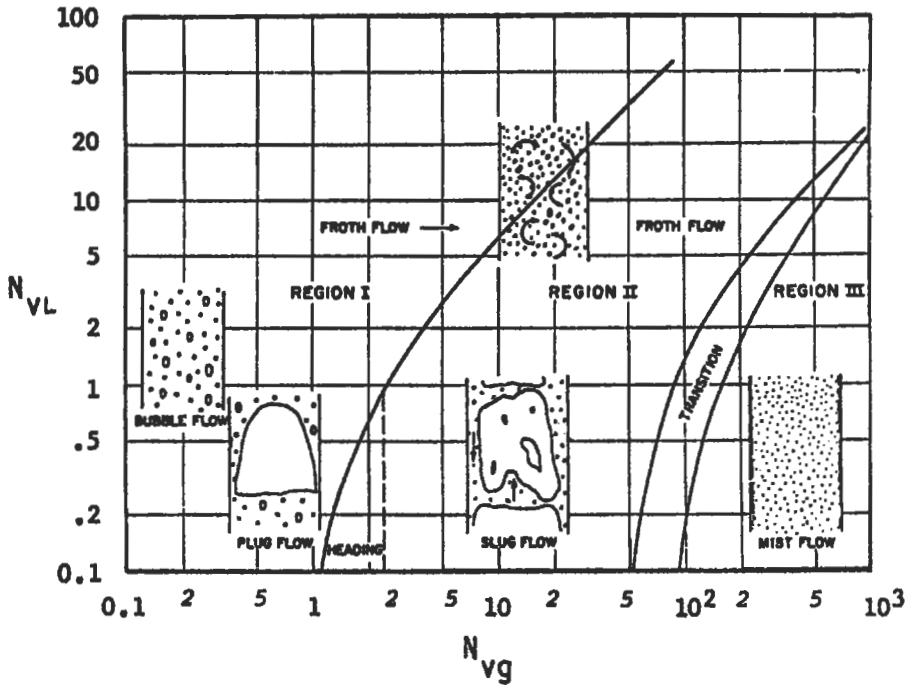


Figure 6-60. Region of occurrence of different flow regimes [23].

Any consistent units system may be used, e.g.,

	English	Metric
ρ_L (liquid density)	slugs/ft ³	kg/m ³
d (diameter of pipe)	ft	m
σ (liquid surface tension)	dyn/cm	dyn/cm
μ_L (liquid viscosity)	cp	cp

Equations contain a "g" term that was included into the mist conversion factors A, B and C.

	English	Metric
A	1.938	3.193
B	120.9	99.03
C	0.1573	0.3146

At high liquid rates the pressure gradient varied significantly with the gas rate. The various flow regions were divided into three main regions depending on the amount of gas present.

Region I. The liquid phase is continuous and bubble flow, plug flow and part of the froth-flow regime exists.

Region II. In this region the phases of liquid and gas alternate. The region thus covers slug flow and the remainder of the froth flow regime.

Region III. The gas is in a continuous phase and the mist-flow regime exists.

The different nature of these three main regions necessitates separate correlations for friction and holdup for each region; therefore, in principle, six different correlations are to be expected. The identification of flow region is a function of N_{Lv} , N_{gv} , L_1 , L_2 and N_d . The regions of validity of the correlations are plotted and presented in Figure 6-61 as a function of the liquid velocity number N_{Lv} and gas-velocity number N_{gv} . Because N_{Lv} and N_{gv} are directly related to liquid flowrate and gas flowrate, respectively, it can be seen from Figure 6-61 that a change in one or both of these rates affects the region of flow.

Duns and Ros suggested the following limits for various flow regions:

- Region I: $0 \leq N_{gv} \leq (L_1 + L_2 N_{Lv})$
- Region II: $(L_1 + L_2 N_{Lv}) < N_{gv} < (50 + 36 N_{Lv})$
- Region III: $N_{gv} > (75 + 84 N_{Lv}^{0.75})$

L_1 and L_2 are functions of N_d , and their relationships are presented in Figure 6-62. It was also found that the liquid holdup is related to the slip velocity, v_s , as follows:

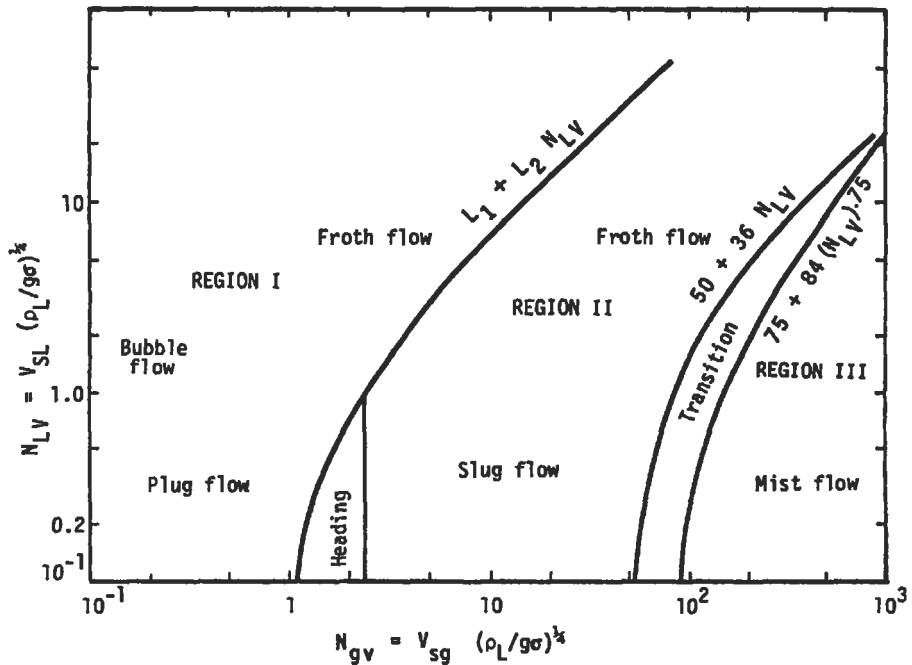


Figure 6-61. Region of validity of Duns-Ros correlation [23].

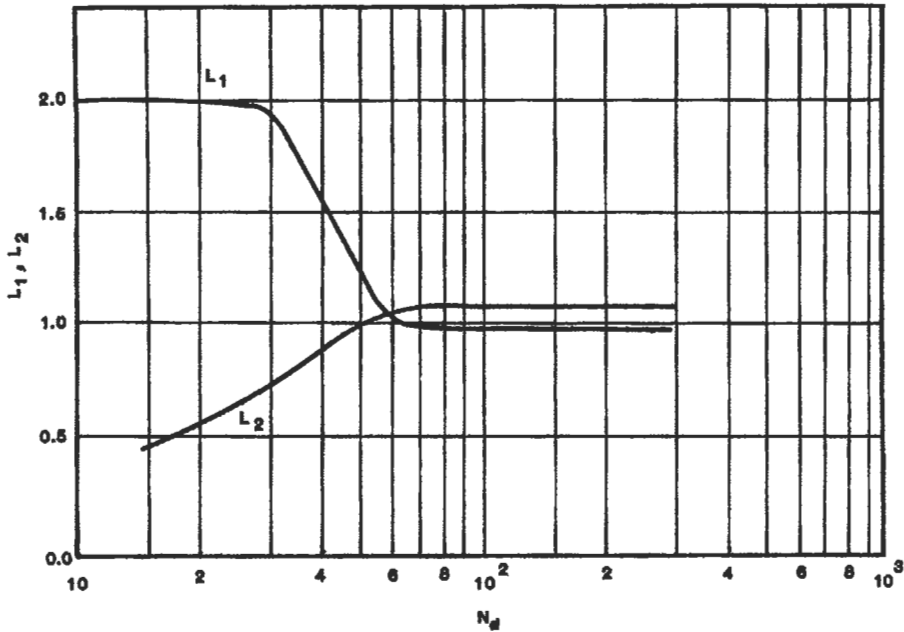


Figure 6-62. L factors vs. diameter number, N_d [23].

$$v_s = v_{sg}/(1 - H_L) - v_{sl}/H_L \tag{6-108}$$

where v_{sg} , v_{sl} are average gas and average liquid superficial velocities, respectively. The slip velocity was expressed in dimensionless form as

$$S = v_s (\gamma_L/g\sigma)^{0.25}$$

As soon as S has been determined, v_s , H_L and, finally, $(dp/dL)_u$ can be determined.

Different formulas are used for calculating S in each of the three flow regions. These formulas, which are functions of the four dimensionless numbers, N_{Lv} , N_{gv} , N_d , N_L , are found in the example below and make use of Figures 6-63 and 6-64.

Example 2

Show stepwise procedure for calculation of the pressure traverse by the Duns-Ros method. Apply this procedure to solve the following problem.

Determine the distance ΔL between two pressure points starting surface conditions if $\Delta p = 500$ psig.

Given that tubing size $d = 2$ in. = 1.995 in. ID

wellhead pressure 1,455 psig = p_1

$p_L = p_1 + 500 = 1,955$ psig

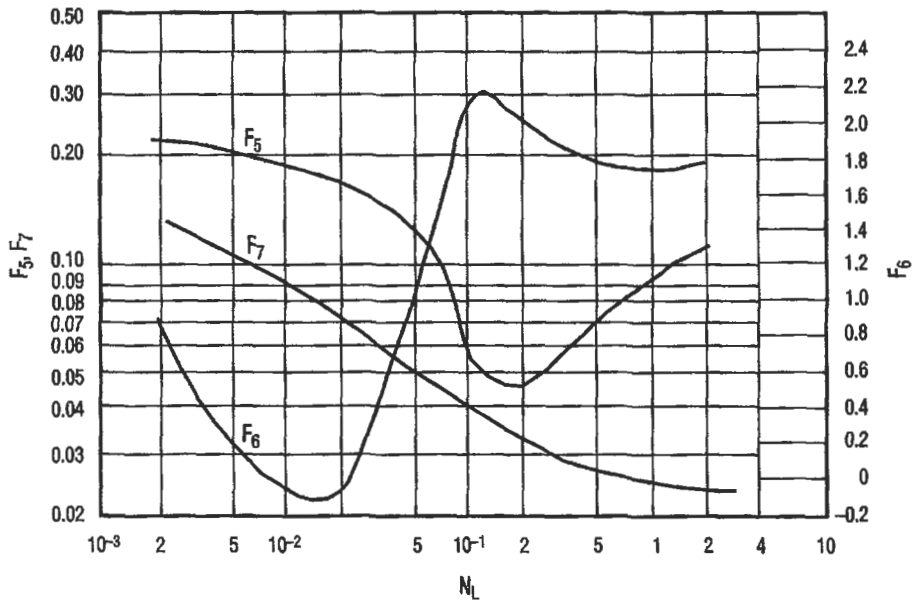


Figure 6-63. F_5 , F_6 , F_7 against viscosity number, N_L [23].

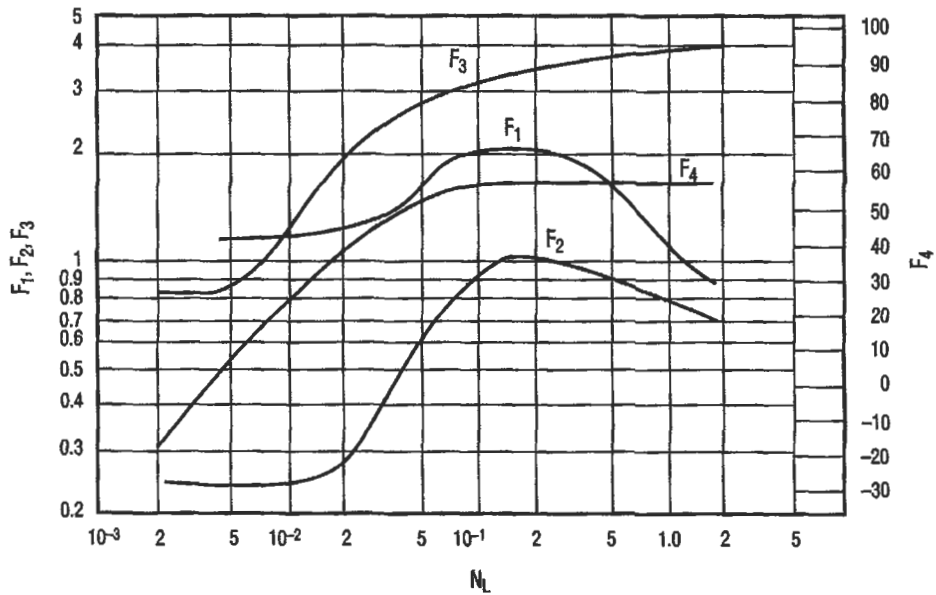


Figure 6-64. F_1 , F_2 , F_3 and F_4 vs. viscosity number, N_L [23].

$$p_{\text{bar}} = 14.7 \text{ psia}$$

$$T_1 = 75^\circ\text{F}$$

$$T_2 = 105^\circ\text{F}$$

$$\text{S.G.}_g = 0.752$$

$$\text{S.G.}_o = 54^\circ\text{API}$$

$$q_{\text{oil}} = 480 \text{ bpd (std)} \quad q_{\text{water}} = 0 \text{ bpd (std)}$$

$$q_L = q_w + q_o$$

$$\mu_g = 0.020 \text{ cp (constant value)}$$

$$\sigma_o = 28 \text{ dyn/cm}$$

$$\text{GLR} = \text{GOR} = 3393 \text{ scf/bbl}$$

Choose a commercial steel pipe.

Solutions

1. Determine the specific gravity of the oil:

$$\text{SG}_o = \frac{141.5}{131.5 + ^\circ\text{API}} = \frac{141.5}{131.5 + 54} = 0.763$$

2. Find the weight associated with 1 bbl of stock-tank liquid:

$$\begin{aligned} m &= \text{SG}_o(350)\left(\frac{1}{1+\text{WOR}}\right) + \text{SG}_w(350)\left(\frac{\text{WOR}}{1+\text{WOR}}\right) + (0.0764)(\text{GLR})(\text{SG}_g) \\ &= 0.763(350)\left(\frac{1}{1+0}\right) + 0.763(350)\left(\frac{1}{1+0}\right) + 0.0764(3393)(0.752) \\ &= 462 \text{ lb/stb of oil} \end{aligned}$$

3. Determine the specific weight of the liquid phase:

$$\begin{aligned} \gamma_L &= 62.4 \left[\text{SG}_o \left(\frac{1}{1+\text{WOR}} \right) + \text{SG}_w \left(\frac{\text{WOR}}{1+\text{WOR}} \right) \right] \\ &= 62.4 \left[0.763 \left(\frac{1}{1+0} \right) + \text{SG}_w \left(\frac{1}{1+0} \right) \right] \\ &= 47.6 \text{ lb/ft}^3 \end{aligned}$$

4. Find the average pressure:

$$p_{\text{avg}} = \frac{p_1 + p_2}{2} + p_{\text{bar}} = \frac{1,455 + 1,955}{2} + 14.7 = 1,719.7 \text{ psia}$$

5. Find the average temperature:

$$T_{\text{avg}} = \frac{T_1 + T_2}{2} = \frac{75 + 105}{2} = 90^\circ \text{ F} = 550^\circ \text{ R}$$

6. Find Z_{avg} for gas phase

$$\begin{aligned} Z_{\text{avg}} &= f(T_r, p_r) \\ &= 0.72 \end{aligned}$$

$$T_r = T/T_{\text{pc}} = 550/394 = 1.4$$

$$p_r = 1,719.7/660 = 26$$

7. Find the average specific weight of the gas phase:

$$\begin{aligned} \gamma_g &= SG_g (0.0764) \left(\frac{p}{14.7} \right) \left(\frac{520}{5} \right) \left(\frac{1}{Z} \right) = SG_g (0.0764) 1/B_g \\ &= 0.752 (0.0764) \frac{1,719.7}{14.7} \frac{520}{550} \frac{1}{0.72} = 8,823 \text{ lb/ft}^3 \end{aligned}$$

8. Find R_s at T_{avg} and p_{avg} (see Chapter 5)

$$R_s = SG_g \left(\frac{p}{18} \times \frac{10^{0.0125(\text{API})}}{10^{0.00091(T)}} \right)^{1.2048}$$

$$T_{\text{avg}} = 90^\circ \text{ F}, \quad p_{\text{avg}} = 1,719.7 \text{ psia}$$

$$R_s = 0.752 \left(\frac{1,719.7}{28} \times \frac{10^{0.0125(54)}}{10^{0.00091(90)}} \right)^{1.2048} = 947.3 \text{ scf/stb}$$

9. Calculate the average viscosity of the oil from correlations (see Chapter 5)

$$\mu_{\text{od}} = 10^x - 1.0$$

$$X = T^{-1.163} \exp(6.9824 - 0.04658 \text{ } ^\circ\text{API})$$

$$X = 90^{-1.163} \exp(6.9824 - 0.04658 \times 54) = 0.4646$$

$$\mu_{od} = 1.915 \text{ cP}$$

$$\mu_o = A\mu_{od}^B$$

$$A = 10.715(R_s + 100)^{-0.515} = 10.715(947.3 + 100)^{-0.515}$$

$$A = 0.2983$$

$$B = 5.44(R_s + 150)^{-0.388} = 5.44(947.3 + 150)^{-0.388}$$

$$B = 0.5105$$

$$\mu_{os} = 0.2983 \times 1.915^{0.5105} = 0.416 \text{ cp}$$

10. Determine the average water viscosity. No water is in the example.
 11. Calculate the liquid mixture viscosity:

$$\mu_L = \mu_o \left(\frac{1}{1 + \text{WOR}} \right) + \mu_w \left(\frac{\text{WOR}}{1 + \text{WOR}} \right) = \mu_o = 0.416 \text{ cp}$$

12. Find the liquid mixture surface tension:

$$\sigma_L = \sigma_o \left(\frac{1}{1 + \text{WOR}} \right) + \mu_w \left(\frac{\text{WOR}}{1 + \text{WOR}} \right) = \sigma_o = 28 \text{ dyn/cm}$$

13. Find B_o at p_{avg} and T_{avg} .

$$B_o = 0.972 + 0.00147F^{1.175}$$

$$F = R_s \left(\frac{\gamma_g}{\gamma_o} \right)^{0.5} + 1.25\% [T(^{\circ}\text{F})] = 947.3 \left(\frac{0.752}{0.763} \right)^{0.5} + 1.25(90) = 1052.9$$

$$B_o = 1.495 \text{ bbl/stb}$$

14. Find the turbine flow area A_p :

$$A_p = \frac{\pi d^2}{4} = \frac{\pi}{4} + \left(\frac{1.995}{12} \right)^2 = 0.0217 \text{ ft}^2$$

15. Find the liquid viscosity number:

$$N_L = 0.1573 \times (0.5) \left(\frac{1}{(28)^3 47.6} \right)^{0.25} = 2.05 \times 10^{-3}$$

16. Find v_{Ll} (assume $B_w = 1.0$):

$$\begin{aligned}
 v_{dL} &= \frac{5.61q_L}{86400A_p} \left[B_o \left(\frac{1}{1+WOR} \right) + B_w \left(\frac{WOR}{1+WOR} \right) \right] \\
 &= \frac{5.61(480)}{86400(0.0217)} \left[1.495(1.0) + 1.0 \left(\frac{0}{1+0} \right) \right] = 2.147 \text{ ft/s}
 \end{aligned}$$

17. Find the liquid velocity number:

$$N_{Lv} = 1.938 v_{dL} \left(\frac{\gamma_L}{\sigma_L} \right)^{1/4} = 1.938(2.147) \left(\frac{47.6}{28} \right)^{1/4} = 4.75$$

18. Find the superficial gas velocity:

$$\begin{aligned}
 v_{sg} &= \frac{q_L \left[GLR - R_s \left(\frac{1}{1+WOR} \right) \right]}{86,400A_p} \left(\frac{14.7}{p_{avg}} \right) \left(\frac{T_{avg}}{520} \right) \left(\frac{Z_{avg}}{1} \right) \\
 &= \frac{q_L \left[GLR - R_s \left(\frac{1}{1+WOR} \right) \right] B_g}{86,400A_p} \\
 &= \frac{480 \left[3,393 - 947.3 \left(\frac{1}{1+0} \right) \right] 14.7 \times 550(0.72)}{86,400(0.0217) 1719.5 \times 520} = 4.08 \text{ ft/s}
 \end{aligned}$$

19. Find the gas velocity number:

$$N_{gv} = 1.938 v_{sg} \left(\frac{\gamma_L}{\sigma_L} \right)^{1/4} = 1.938 \times 4.08 \left(\frac{47.6}{28} \right)^{1/4} = 9.03$$

20. Find the pipe diameter number:

$$N_d = 120.9d \left(\frac{\gamma_L}{\sigma_L} \right)^{0.5} = 120.9 \left(\frac{1.995}{12} \right) \left(\frac{47.6}{28} \right)^{0.5} = 26.2$$

21. Select the proper flow regime from Figure 6-61:

$$N_{gv} = 9.03$$

$$N_{Lv} = 4.75$$

These numbers fall in Region II; see Figure 6-61.

22. Determine the proper slip factor depending upon the region found in step 21.

a) For Region I: determine the slip factor determination. The slip factor is found by the following formula:

$$S = F_1 + F_2 N_{Lv} + F_3' \left(\frac{N_{gv}}{1 + N_{Lv}} \right)^2$$

F_1 and F_2 are found in Figure 6-64.

$F_3' = F_3 - F_4/N_d$ where F_3 and F_4 are found in Figure 6-64. For annular flow N_d is based on the wetted perimeter; thus, $d = (d_c + d_i)$. Region I extends from zero N_{Lv} and N_{gv} up to $N_{gv} = L_1 + L_2 N_{Lv}$, where L_1 and L_2 can be found in Figure 6-62.

b) For Region II:

$$S = (1 + F_5) \frac{(N_{gv})^{0.982} + F_6'}{(1 + F_7 N_{Lv})^2}$$

F_5 , F_6 and F_7 can be found in Figure 6-63 where $F_6 = 0.029N_d + F_6'$. Region II extends from the upper limit of Region I to the transition zone to mist flow given by $N_{gv} = 50 + 36N_{Lv}$.

c) For Region III (mist flow):

$$S = 0$$

$$\text{Therefore, } H_L = \frac{1}{1 + v_{sg}/v_{sl}}$$

This is valid for $N_{Lv} > 75 + 84 N_{Lv}^{0.75}$. Calculations for Region II from Figure 6-63 if $N_L = 2.05 \times 10^{-3}$, then

$$F_5 = 0.218, F_6 = 0.58, F_7 = 0.12$$

$$F_6' = 0.029N_d + 0.58 = 0.029 \times (2.62) + 0.58 = 1.34$$

$$S = (1 + 0.20) \frac{9.03^{0.982} + 1.34}{[1 + (0.12 \times 4.751)]^2} = 4.88$$

23. Determine the slip velocity if in Region I or II:

$$v_s = \frac{S}{1.938(\gamma_L/\sigma_L)^{0.5}}$$

It is Region II; hence

$$v_s = \frac{4.88}{1.938(47.61/28)^{0.5}} = 1.933$$

24. Determine the liquid holdup:

$$\begin{aligned}
 H_L &= \frac{v_s - v_{sg} - v_{sl} + [(v_s - v_{sg} - v_{sl})^2 + 4v_s v_{sl}]^{0.5}}{2v_s} \\
 &= \frac{1.933 - 4.08 - 2.147 + [(1.933 - 4.08 - 2.147)^2 + 4(1.933)(2.147)]^{0.5}}{2 \times 1.933} \\
 &= 0.4204 = 0.42
 \end{aligned}$$

This value can be checked

$$v_s = \frac{v_{sg}}{1 - H_L} - \frac{v_{sl}}{H_L} = \frac{4.08}{1 - 0.42} - \frac{2.147}{0.42} = 1.923$$

25. Determine the liquid Reynolds number:

$$\begin{aligned}
 N_{Re} &= \frac{1,488\gamma_L v_{sl} d}{\mu_L} \\
 (N_{Re})_L &= \frac{1,488 \times 47.6 \times 2.147 \times 0.16625}{0.416} = 60,773
 \end{aligned}$$

26. Determine the friction gradient according to the flow region.

a) For Region I and II

$$G_{fr} = 2f_w \frac{N_{Lv}(N_{Lv} + N_{gV})}{N_d}$$

$$\text{where } f_w = (f_1) \frac{f_2}{f_3}$$

f_1 is found in Figure 6-65 and f_2 is found in Figure 6-66.

The abscissa must be determined in Figure 6-66 and is $f_1 R N_d^{2/3}$

$$\text{where } R = \frac{v_{sg}}{v_{sl}}$$

$$f_3 = 1 + f_1(R/50)^{0.5}$$

The friction factor f_w is valid in Regions I and II and covers heading also. It is good from zero N_{Lv} and N_{gV} up to the limit given by $N_{gV} = 50 + 36 N_{Lv}$.

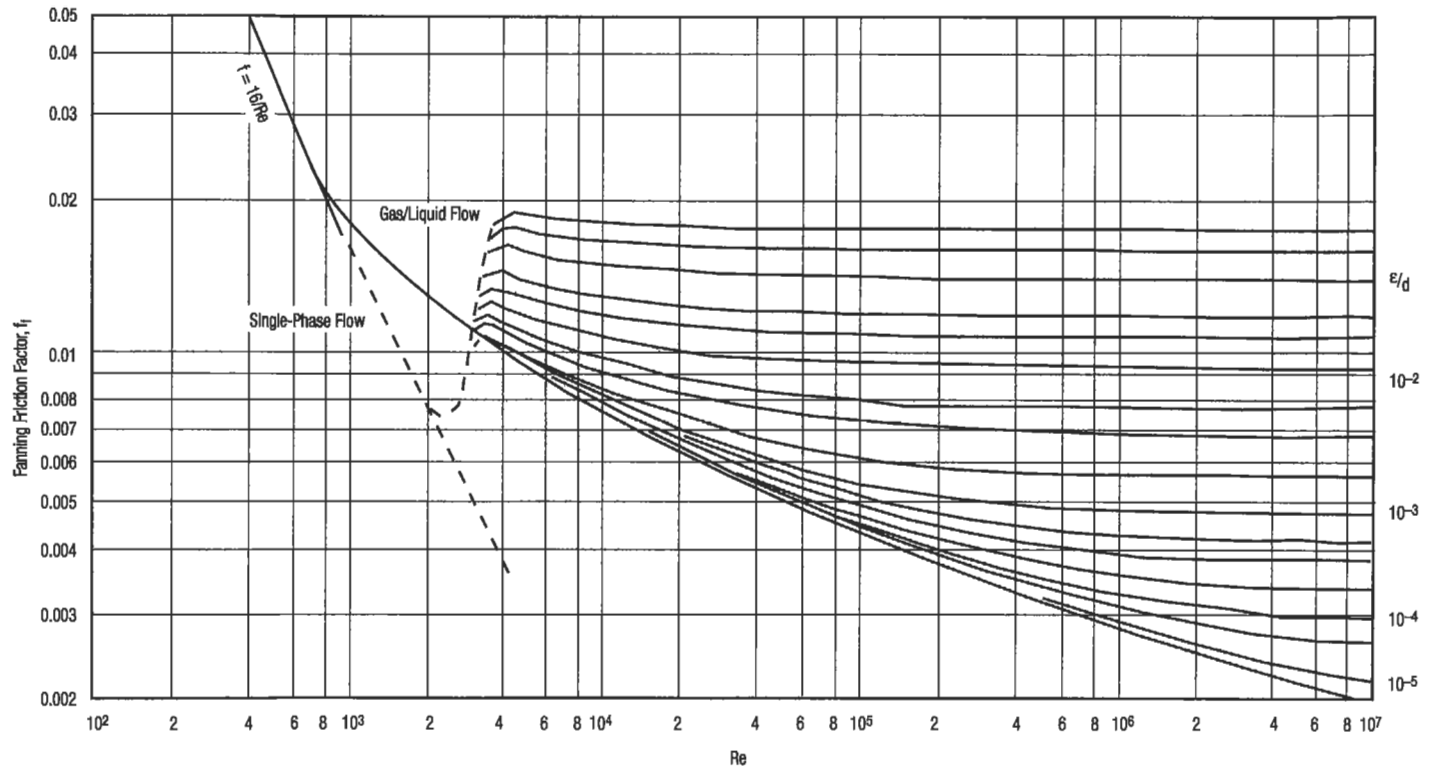


Figure 6-65. Fanning friction factor f_f vs. Reynolds number [23].

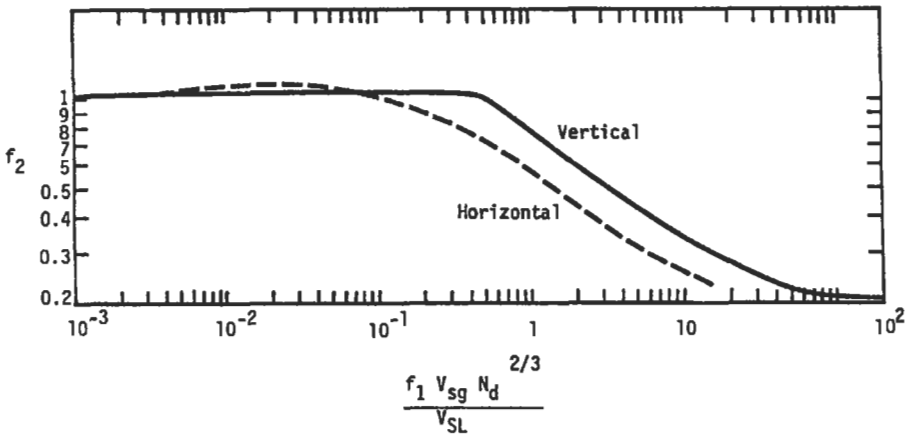


Figure 6-66. Bubble friction correction [23].

b) For Region III:

In mist flow where $N_{gv} > 75 + 84N_{Lv}^{0.75}$

$$G_{\epsilon} = 2f_w N_p \frac{(N_{gv})^2}{N_d}$$

where $N_p = \rho_g / \rho_L$

In Region III f_w is taken as f_1 and may be taken from Figure 6-65. For $\epsilon > 0.05d$ the value of f_1 is calculated by

$$f_1 = \frac{1}{[4 \log_{10}(0.027\epsilon/d)]^2} + 0.067(\epsilon/d)^{1.75}$$

For $\epsilon > 0.05d$, the value of $d - \epsilon$ should be substituted for d throughout the friction gradient calculation, and also this substitution should be made:

$$v_{sg} = \frac{v_{sg} d^2}{(d - \epsilon)^2}$$

It is Region II; hence, calculate f_1 , f_2 and f_3 such that

$$f_w = (f_1) \frac{f_2}{f_3}$$

From Figure 6-65 read f_1 , but first determine a value for ϵ/d . If the value for ϵ is not known, a good value to use is 0.00015 ft, which is an average value given for commercial sted.

$$\frac{\epsilon}{d} = \frac{0.00015(12)}{1.995} = 9.02 \times 10^{-4}$$

For given Reynolds number (60,773) and ϵ/d

$$f_1 = 0.005$$

From Figure 6-66

$$\text{where } f_1 \left(\frac{v_{sg}}{v_{sl}} \right) N_d^{2/3} = 0.005 \left(\frac{4.08}{2.147} \right) 26.2^{2/3} = 0.0839$$

$$f_2 = 1.01$$

$$f_3 = 1 + f_1 \left(\frac{4.08}{2.147 \times 50} \right)^{0.5} = 1 + 0.005(0.038)^{0.5} = 1.001$$

$$f_w = 0.005 \left(\frac{1.01}{1.001} \right) = 0.00505$$

calculate friction gradient G_f :

$$G_f = 2(0.00505) \frac{4.75(4.75 + 9.03)}{26.2} = 0.0252$$

27. Determine the static gradient:

$$\begin{aligned} G_{st} &= H_L + (1 - H_L) \frac{\gamma_g}{\gamma_L} \\ &= 0.42 + (1 - 0.42) \frac{8.823}{47.6} = 0.5275 \text{ (dimensionless)} \end{aligned}$$

28. Determine the total pressure gradient.

a) For Regions I and II:

$$G = G_{st} + G_f$$

b) For Region III (accounting for accelerations):

$$\begin{aligned} G &= \frac{G_{st} + G_f}{1 - (\gamma_L v_{sl} + \gamma_g v_{sg})(v_{sg}/\gamma)} \\ &= G_{st} + G_f = 0.5275 + 0.0252 = 0.5527 \end{aligned}$$

29. Convert to gradient in psi/ft:

$$\frac{dp}{dL_u} = \frac{G_p \gamma_L}{144}, \quad \frac{dp}{dL_{(fr)}} = \frac{G_p \gamma_L}{144}, \quad \text{or} \quad \frac{dp}{dL_{total}} = \frac{G \gamma_L}{144}$$

$$\frac{dp}{dL} = \frac{0.5527(47.6)}{144} = 0.1827 \text{ psi/ft}$$

30. Determine distance ΔL:

$$\Delta L = \frac{(1,955 - 1,455) \text{psi}}{0.1827 \text{ psi/ft}} = 2,737 \text{ ft}$$

If water flows together with oil, it is recommended that the calculations be made using the average oil-water mixture properties.

The Orkiszewski Method [24,25]

This method is recognized for four types of flow pattern and separate correlations are prepared to establish the slippage velocity and friction for each. The four types of flow curve are bubble, slug, transition and mist. The correlation is applicable to high-velocity flow range and gas condensate wells in addition to oil wells and has proven accuracy. To make calculations, a computer is preferable. Figure 6-67 shows a generalized flow diagram of this method. After assuming a pressure difference and calculating the various required properties, a flow region is selected. Depending on the flow region, the pressure loss calculations—which, in general, include friction and holdup—are made. The vertical length corresponding to the pressure difference is then determined.

The flow regime is found by testing the following limits:

Regime	Limits of Boundary Lines, L
Bubble	$q_g/(q_g + q_l) < L_b$ or $v_{sg}/v_m < L_b$
Slug	$q_g/(q_g + q_l) > L_b$, $N_{vg} < L_s$
Transition	$L_m > N_{vg} > L_s$
Mist	$N_{vg} > L_m$

The foregoing new variables are defined as follows:

Bubble:

$$L_b = 1.071 - (0.2218v_{m}^2/d) \text{ but } \geq 0.13 \tag{6-109}$$

Slug:

$$L_s = 50 + 36N_{vg} q_{l1}/q_g \text{ (or } 36N_{vg} v_{sl}/v_{sg}) \tag{6-110}$$

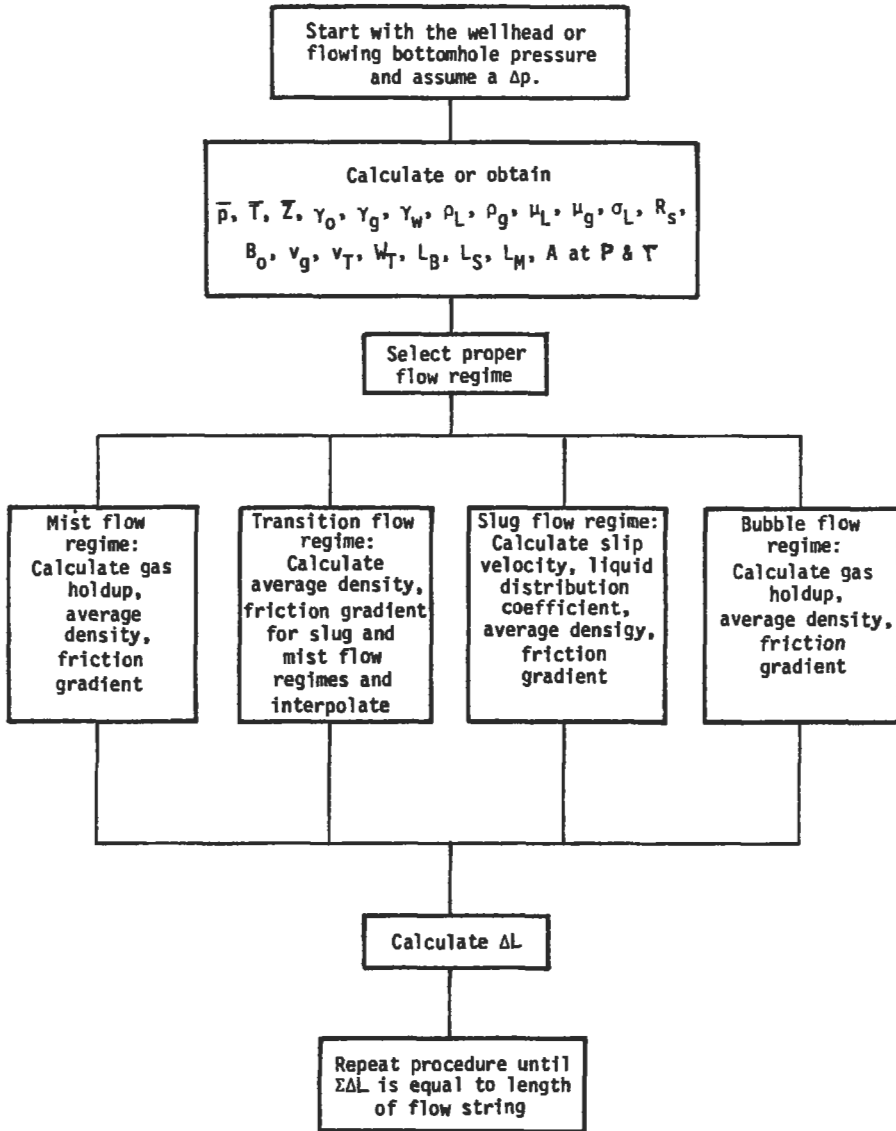


Figure 6-67. Flow diagram for the Orkiszewski method [19,24].

Mist:

$$L_m = 75 + 84(N_{vg}q_l/q_g)^{0.75} \text{ [or } 84(N_{vg}v_{sl}/v_{sg})^{0.75}]$$

where v_t = total fluid velocity ($v_{sl} + v_{sg} = v_m$)

q_t = volumetric total flow ($q_L + q_g$)

N_{vg} = dimensionless velocity influence number

$$= v_{sg}(\gamma_l/g\sigma)^{0.25}$$

Bubble Flow

The γ_m required knowledge of the holdup H_L , such that

$$\gamma_m = \gamma_L H_L + \gamma_g (1 - H_L)$$

In this the H_L is calculated as follows:

$$H_L = 1 - 0.5[1 + v_m/v_s - (1 + v_m/v_s)^2 - 4v_{sg}/v_s]^{0.5} \quad (6-111)$$

where v_s = slip velocity = 0.8 ft/s (0.244 m/s)

Therefore, the friction gradient is

$$dp/dL = 2f\gamma_L v_L^2 / (H_L g_c d) \quad (6-112)$$

where f = Fanning friction factor obtained from Figure 6-65

$$R_e = dv_{sL}\gamma_L/\mu_L \quad (6-113)$$

The elevation gradient is

$$dp/dL = \gamma_m F_e \quad (6-114)$$

and the acceleration gradient is negligible. However, Orkiszewski's equation for all these effects is

$$\frac{dp}{dL} = \frac{\gamma_m F_e + 2f\gamma_L v_{sL}^2 / (H_L g_c d)}{1 - m_1 q_g / (A_p^2 P_{avg} g_c)} \quad (6-115)$$

which is essentially the same as adding the three gradients.

Slug Flow

Slug flow specific weight γ_s is difficult to know and difficult to assume. An attempt was made such that

$$\gamma_s = \frac{m_1 + \gamma_L v_s A_p}{q_1 + v_s A_p} + \delta \gamma_L \quad (6-116a)$$

in a slightly different term arrangement using velocities, or

$$\gamma_s = \frac{\gamma_L (v_{sL} + v_s) + \gamma_g v_{sg}}{v_m + v_s} + \delta \gamma_L \quad (6-116b)$$

where m_1 = total mass/s

A_p = area of pipe

v_s = correlation factor, $C_1 C_2 (gd)^{0.5}$, slip velocity

δ = liquid distribution coefficient

(6-117)

C_1 and C_2 are functions of a Reynolds number as follows:

$$C_1 \propto (f)dv_s\gamma_L/\mu_L, \text{ or } Re_b \text{ (Figure 6-68)}$$

and

$$C_2 \propto (f)Re_b \text{ and } Re_n = dv_s\gamma_L/\mu_L \text{ (Figure 6-69)}$$

Since v_s is a dependent variable, it must be found by iteration. A value of v_s is assumed, Re_b is calculated and C_1 and C_2 are determined. If the calculated value of v_s does not agree with the assumed value, try again. [A good initial try, $v_s = 0.5(gd)^{0.5}$.] For details see Example 3. Now determine δ as follows:

(a) If $v_m < 10$ (continuous phase is water)

$$\delta = [(0.013 \log \mu_L/d^{1.38}) - 0.681 + 0.232 \log v_m - 0.428 \log d] \quad (6-118a)$$

(b) If $v_m < 10$ (continuous phase is oil)

$$\delta = [0.0127 \log (\mu_L + 1)/d^{1.415}] - 0.284 + 0.167 \log v_m + 0.113 \log d \quad (6-118b)$$

(c) If $v_m > 10$ (continuous phase is water)

$$\delta = [(0.045 \log \mu_L)/d^{0.799}] - 0.709 - 0.162 \log v_m - 0.888 \log d \quad (6-118c)$$

(d) If $v_m > 10$ (continuous phase is oil) (μ_L in cp)

$$\delta = [0.0274 \log (\mu_L + 1)/d^{1.371}] + 0.161 + 0.569 \log d + x \quad (6-118d)$$

where

$$x = - \log v_m [(0.01 \log(\mu_L + 1)/d^{1.571}) + 0.397 + 0.63 \log d]$$

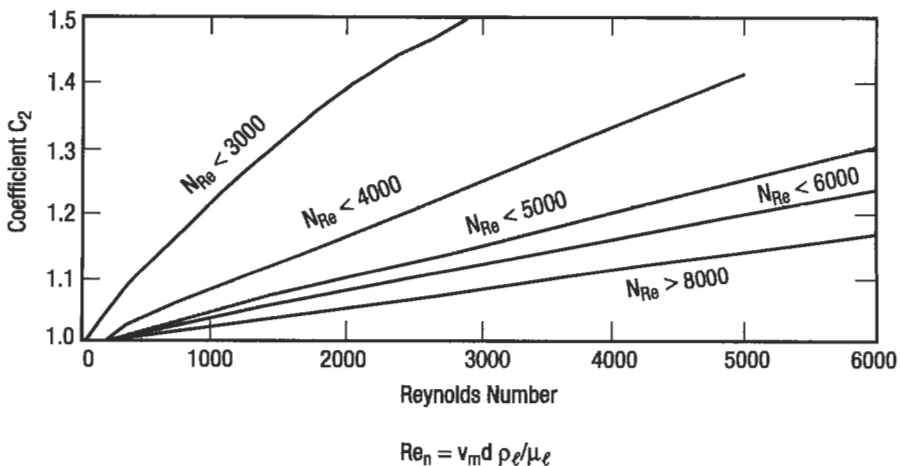


Figure 6-68. C_2 constant vs. bubble Reynolds number [26].

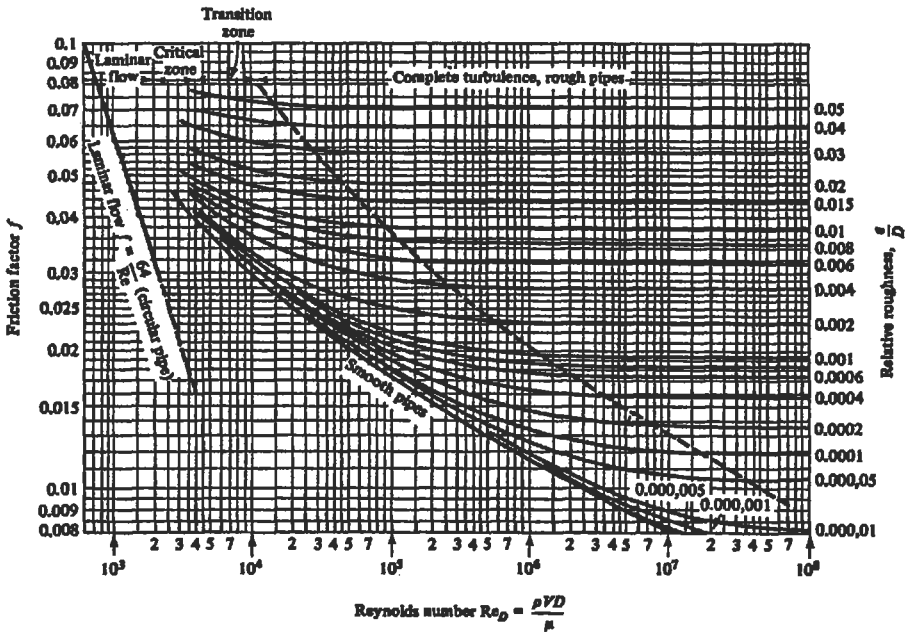


Figure 6-69. Friction factor [27].

These constraints apply to δ :

$$\text{If } v_m < 10, \delta \geq -0.065 v_m$$

$$\text{If } v_m > 10, \delta \geq (-v_x)(1 - \gamma_v/\gamma_L)/(v_m + v_x)$$

Finally, the friction gradient term is

$$\left(\frac{dp}{dL}\right)_f = \frac{2f_f \gamma_L v_m^2}{gd} \left(\frac{v_{sl} + v_s}{v_m + v_s} + \delta\right) \tag{6-119}$$

where f_f is obtained from Figure 6-65 using the following:

$$Re = dv_m \gamma_L / \mu_L \tag{6-120}$$

Again, the total pressure gradient includes the evaluation (static), friction and acceleration (negligible) components.

Transition Flow

Orkiszewski used linear interpolation between slug and mist.

Mist Flow

The Duns-Ros method is used.

Example 3

Apply Orkiszewski method to solve Example 2 with the pipe diameter $d = 2$ in.

1. Select the starting point as the 1,455 psig pressure.
2. The temperature at each point of pressure is given as 75°F at 1,455 psig and 105°F at 1,955 psig.
3. Δp is equal to 500 psig.
4. It is not necessary to assume depth increment since the temperature at 1,955 psia is known.
5. The average temperature of the increment is $(105 + 75)/2 = 90^\circ\text{F}$
6. The following calculations are made in order to complete step 7 to determine flow regime.
 - a) The average flow conditions are

$$\Delta p = (1,455 + 1,955)/2 + 14.7 = 1,719.5$$

$$T = 90^\circ\text{F} = 550^\circ\text{R}$$

$$Z = 0.72$$

$$R_s = 947.3 \text{ scf/stb}$$

$$B_0 = 1.495 \text{ bbl/stb}$$

- b) The corrected volumetric flowrates are

$$\begin{aligned} q_L &= 480 \text{ bpd} = 6.4984 \times 10^{-5} \times 480 \text{ scf/s} \\ &= 6.4984 \times 10^{-5} (q_0 B_0 + q_w B_w) = 6.4984 \times 10^{-5} \times 480 \times 1.495 \\ &= 0.0466 \text{ ft}^3/\text{s} \end{aligned}$$

$$\begin{aligned} q_g &= 3.27 \times 10^{-7} \times (\text{GLR} - R_s) q_L (T + 460)/p \\ &= 3.27 \times 10^{-7} (0.72) (3,397 - 947.3) 480 (550)/1,719.5 \\ &= 0.08855 \text{ ft}^3/\text{s} \end{aligned}$$

$$q_t = q_g + q_L = 0.08855 + 0.0466 = 0.1352 \text{ ft}^3/\text{s}$$

- c) The corrected weight flowrates are

$$\begin{aligned} \dot{w}_L &= 4.05(10^{-3})(q_0 SG_0 + q_w SG_w) + 8.85 \times (10^{-7}) q_L SG_g (R_s) \\ &= 4.05(10^{-3})(480 \times 0.763 + 0) + 8.85(10^{-7}) 480(0.752) 947.3 \\ &= 1.483 + 0.303 = 1.7856 \text{ lb/s} \end{aligned}$$

$$\begin{aligned} \dot{w}_g &= 8.85(10^{-7}) q_L g_g (\text{GLR} - R_s) \\ &= 8.85(10^{-7}) 480(0.752)(3393 - 947.3) = 0.7813 \text{ lb/s} \end{aligned}$$

510 Production

$$\dot{w}_t = \dot{w}_L + \dot{w}_g = 1.7856 + 0.7813 = 2.567 \text{ lb/s}$$

d) The corrected specific weights are

$$\gamma_L = \dot{w}_L/q_L = 1.7856/0.0466 = 38.32 \text{ lb/ft}^3$$

$$\gamma_g = \dot{w}_g/q_g = 0.7813/0.08855 = 8.82 \text{ lb/ft}^3$$

7. Determine the type of flow regime:

a) Test variables

$$A_p = 0.0217 \text{ ft}^2$$

$$v_m = v_t = \frac{q_t}{A_p} = \frac{0.1352}{0.0217} = 6.23 \text{ ft/s}$$

$$\frac{q_g}{q_t} = \frac{0.08855}{0.1352} = 0.655$$

$$N_{vg} = 1.938 v_{sg} \left(\frac{\gamma_L}{\sigma_L} \right)^{0.25}$$

$$v_{sg} = \frac{q_g}{A_p} = \frac{0.08855}{0.0217} = 4.081$$

$$N_{vg} = 1.938(4.081) \left(\frac{38.32}{28} \right)^{0.25} = 8.55$$

b) Boundary limits

$$d = 2/12 = 0.1662 \text{ ft}$$

$$\begin{aligned} \text{From Equation 6-109 } L_b &= 1.071 - (0.2218v_m^2/d) \\ &= 1.071 - (0.2218 \times 6.23^2/0.1662) \\ &= -50.7 \end{aligned}$$

Because L_b has such a low value, we must use $L_b = 0.13$ from Equation 6-111 $L_s = 50 + 36N_{vg}q_L/q_g$.

$$L_s = 50 + 36(8.55)0.0466/0.09955 = 212$$

These two values, L_b and L_s , indicate that the regime is slug flow.

8. Determine the average density and the friction loss gradient

a) Slip velocity, v_s

$$\begin{aligned} Re_n &= dv_m \gamma_L / \mu_L = (0.1662)(6.23)(38.32)/(0.5 \times 0.000672) \\ &= 118,080 \end{aligned}$$

Since this value exceeds limits of the graph (Figure 6-69) v_s must be calculated using the extrapolation equation.

$$v_s = 0.5(gd)^{0.5} = 0.5(32.2 \times 0.1662)^{0.5}$$

$$= 1.155 \text{ (first try)}$$

$$Re_b = (1.155)(38.32)(0.1662)/(0.5 \times 0.000672) = 21,892$$

C_1 cannot be read from graph (Figure 6-70). To solve this problem, Orkiszewski proposed the following equations:

if $Re_b \leq 3,000$

$$v_s = (0.546 + 8.74 \times 10^{-6} \times Re_n)(g_c d)^{0.5}$$

if $Re_b \geq 8,000$

$$v_s = (0.35 + 8.74 \times 10^{-6} Re_n)(g_c d)^{0.5}$$

if $3,000 < Re_b < 8,000$

$$v_s = 0.5F + [F^2 + 13.59\mu_L/(\gamma_L d^{0.5})]$$

where $F = (0.251 + 8.74 \times 10^{-6} Re_n)(g_c d)^{0.5}$

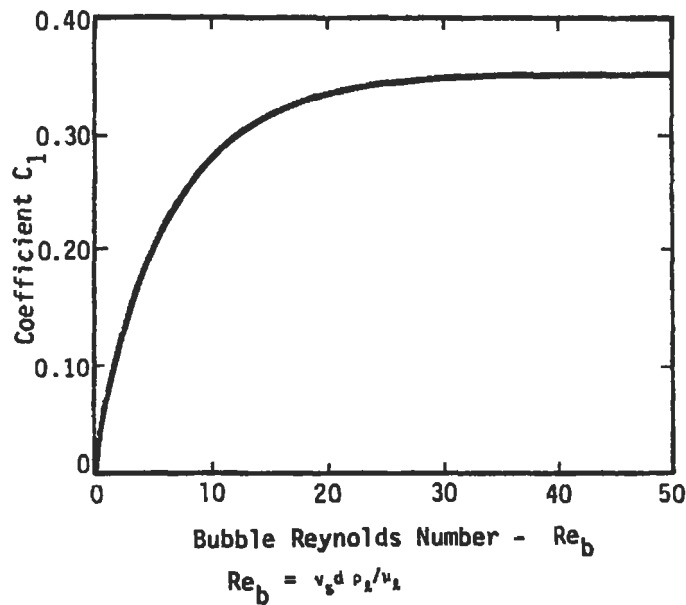


Figure 6-70. C_1 constant vs. bubble Reynolds number [26].

512 Production

$$\begin{aligned} \text{In this example } v_s &= 0.35 + 8.74 \times 10^{-6} \times 118,080 \times (32.2 \times 0.1662)^{0.5} \\ &= 3.19 \text{ ft/s} \end{aligned}$$

- b) Liquid distribution coefficient δ and friction factor f Equation 6-118b is used to evaluate δ since $v_s < 10$ and there is no water.

$$\begin{aligned} \delta &= 0.0127 \log(0.5 + 1)/0.1662^{1.415} - 0.284 + 0.167 \log 6.23 \\ &\quad + 0.113 \log(0.1662) \\ &= -0.211 \end{aligned}$$

Checking this value

$$-0.211 \geq -0.065 \text{ (6.23)}$$

$$-0.211 \geq -0.405$$

Therefore, δ is okay

$$\epsilon/d = 0.00015/0.166 = 0.00009$$

and $Re_p = 21892$

$$f_f = 0.0065 \text{ (Fanning factor from Figure 6-65)}$$

or $f = 0.025$ (friction factor from Figure 6-70)

because $f = 4f_f$, so results are consistent.

- c) Evaluation of average flowing specific weight from Equation 6-116

$$\begin{aligned} \gamma_s &= \frac{\dot{w}_t + \gamma_L v_s A_p}{q_t + v_s A_p} + \delta \gamma_L \\ &= \frac{2.57 + 38.32 \times 3.19 \times 0.0217}{0.1352 + (3.19)(0.0217)} + (-0.211)(38.32) = 17.45 \text{ lb}_m/\text{ft}^3 \end{aligned}$$

- d) Wall friction loss from Equation 6-119

$$\left(\frac{dp}{dL} \right)_f = \frac{2f_f \gamma_L v_m^2}{gd} \left(\frac{v_{sl} + v_s}{v_m + v_s} + \delta \right)$$

$$v_{sl} = 2.147 \text{ (see Example 2)}$$

$$\left(\frac{dp}{dL} \right)_f = \frac{2(0.0065)(38.32)(6.23)^2}{(32.2)(0.1662)}$$

$$\left[\frac{2.174 + 3.19}{6.23 + 3.19} + (-0.211) \right]$$

$$\left(\frac{dp}{dL} \right)_f = 1.255 \frac{\text{lb}}{\text{ft}^3} = 0.0087 \text{ psi/ft}$$

$$\left(\frac{dp}{dL} \right)_{\text{total}} = \left(\frac{dp}{dL} \right)_d + \left(\frac{dp}{dL} \right)_f + \left(\frac{dp}{dL} \right)_{\text{acc}}$$

↓

neglected

$$\begin{aligned} \left(\frac{dp}{dL} \right)_d &= \gamma_s \left(\frac{g}{g_c} \right) = 17.45 \frac{32.2}{32.2} \left(\frac{\text{lb}_m \text{ ft}}{\text{ft}^3 \text{ s}^2} \frac{\text{lb}_f \text{ s}^2}{\text{lb}_m \text{ ft}} \right) \\ &= 17.45 \frac{\text{lb}}{\text{ft}^3} = 17.45 \left(\frac{\text{lb}_f}{144 \text{ in.}} \right) \frac{1}{\text{ft}} \end{aligned}$$

$$\left(\frac{dp}{dL} \right)_d = 0.1212 \text{ psi/ft}$$

$$\left(\frac{dp}{dL} \right)_{\text{total}} = 0.1212 + 0.0087 = \underline{\underline{0.1299 \text{ psi/ft}}}$$

if $\Delta p = 500$ psi since $\Delta L = 500/0.1299 = 3,849$ ft

The Hagedorn-Brown Method [25]

This correlation obtained from field data for pipe size ranging 1 to 4 in. nominal parameter. The equation for calculating pressure gradient is proposed as the following:

The equation for calculating pressure gradient is proposed as

$$\frac{\Delta p}{\Delta L} = \gamma_{\text{hb}} (F_c) + \frac{f_f q_L^2 m_o^2}{A d^5 \gamma_m} + \frac{(\gamma_{\text{hb}} \Delta [v_m^2 / 2g])}{\Delta L} \quad (6-121)$$

We have one consistent set of units, where:

	English	Metric
p = pressure	lb/ft ²	kPa
L = length (height)	ft	m
f _f = Fanning friction factor	—	—
q _L = total liquid flowrate	bbl/day	m ³ /s
m ₀ = total mass flowing/vol. liquid	slug/bbl	kg/m ³
d = pipe ID	ft	m
v _m = avg. velocity = v _{sl} + v _{sg}	ft/sec	m/s
g = conversion factor, force from mass	32.2ft/sec ²	9.81 m/sec ²
A = unit conversion constant	7.41 (10 ¹⁰)	8.63 (10 ⁴)
γ _{H_B} = Hagedorn-Brown specific weight = γ _L H _L + γ _g (1 - H _L)		
based on pseudoholdup	lb/ft ³	kg/m ³
γ _m = avg. two-phase specific weight	lb/ft ³	kg/m ³
v _{sl} = superficial liquid velocity	ft/s	m/s
v _{sg} = superficial gas velocity	ft/s	m/s
γ _L = liquid specific weight	lb/ft ³	kg/m ³
γ _g = gas specific weight	lb/ft ³	kg/m ³
H _L = liquid holdup, a fraction		
F _e = force equivalent	1.0	9.81

The friction factor used in Equation 6-121 is found from Figure 6-65. Figure 6-71 provides a relative roughness number. For this method, the Reynolds number for use with Figure 6-65 is

$$R_e = \frac{2.2(10^{-2})q_L m_0}{d \mu_m} \quad (6-122)$$

where:

	English	Metric
q = volumetric flowrate total all fluids	ft ³ /s	m ³ /s
μ _m = averaged viscosity, using an equation of the form of Arrhenius:		

$$\mu_m = \mu_L^H \mu_g^{(1-H)}$$

and

$$q_L \times \dot{m}_0 = \dot{w}_t$$

The equation would be solved over finite segments of pipe. Δv_m² is the changed velocity at points 1 and 2, the inlet to and outlet from that section. γ_m is the specific weight at the average p and T in the section.

Figure 6-72 also contains two empirical correction factors C and ψ. A plot of the data showed that holdup versus viscosity was a series of essentially straight lines. Water was chosen arbitrarily as a base curve (C = 1.0). C then is used for

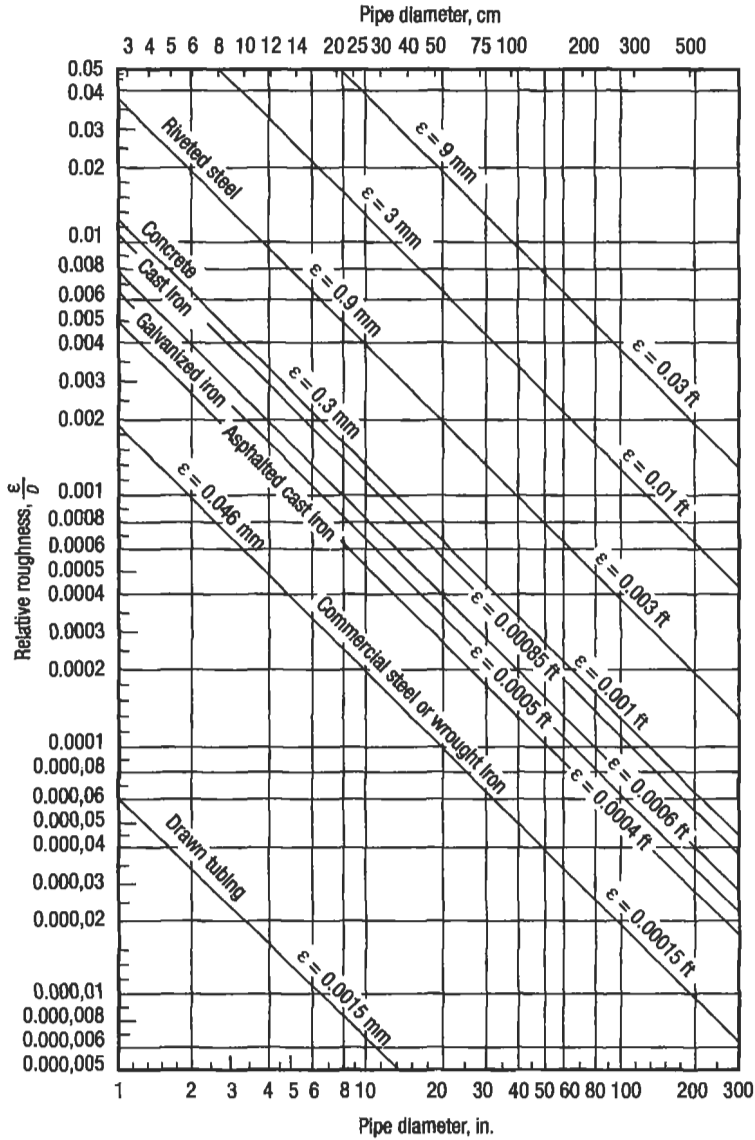


Figure 6-71. Relative roughness for various kinds of pipe [27].

other viscosity fluids to make the parallel curves coincident. The viscosity correction curve obtained is shown in Figure 6-73.

The factor ψ was included to fit some of the data where it was postulated that a transition would occur before mist flow begins, with gas velocity as the major variable. As gas velocity approached that required for mist flow, it breaks through the liquid phase and the turbulence produces a liquid “ring,” which increases slippage. As velocity increases even further, the shear forces on this

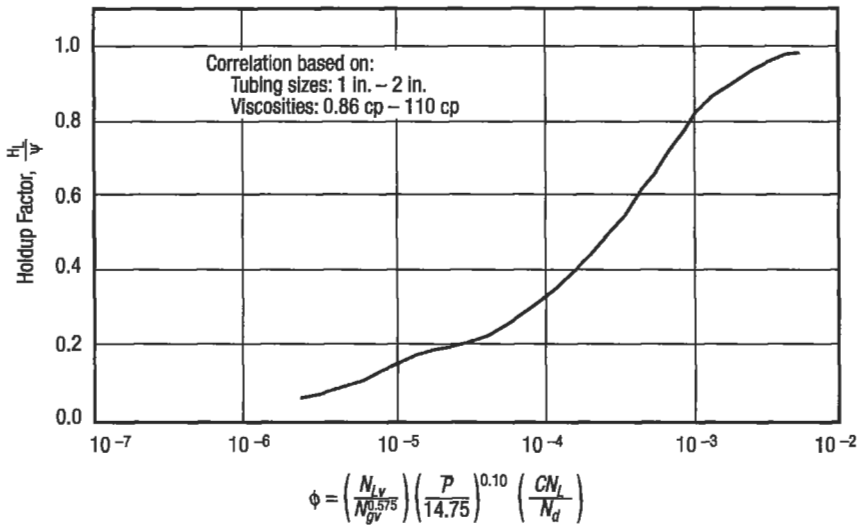


Figure 6-72. Holdup factor correlation [28].

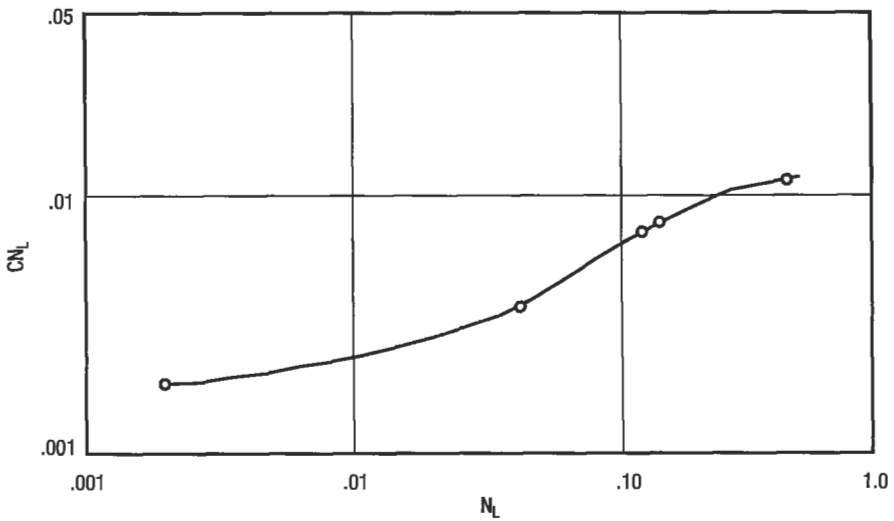


Figure 6-73. Correlation for viscosity number coefficient [29].

ring dissipate it until the primary mechanism is mist flow. Figure 6-74 shows the correlation for ψ . In most cases ψ will be equal to 1.0.

The basic correlating equation, 6-122, can be converted to a form similar to that for either single flow by allowing $H_L \rightarrow 0$ for gas or $H_L \rightarrow 1.0$ for liquids. As gas rate or liquid rate approaches zero the pressure gradient obtained likewise approaches that for the other single phase. One, therefore, has a

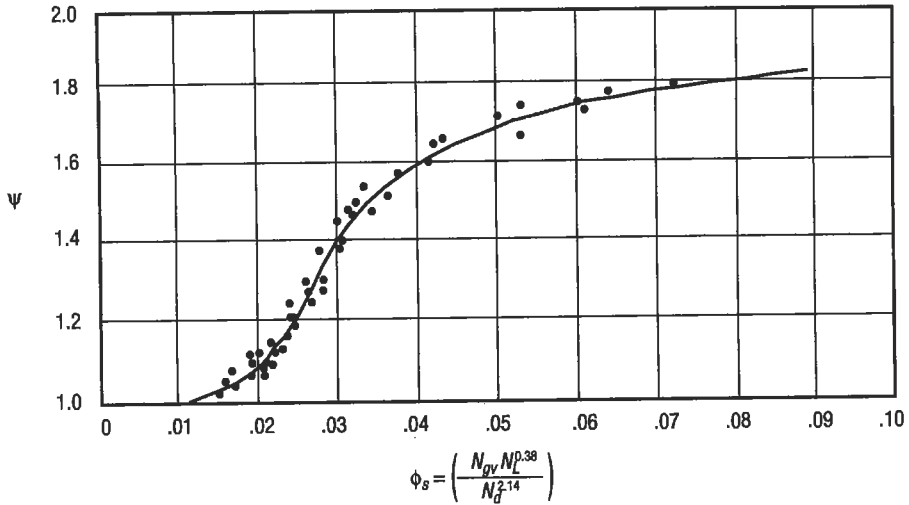


Figure 6-74. Correlation for secondary factor correction [29].

continuous gradient from liquid to two-phase to gas, an important aspect of the model.

Reviewing the foregoing calculation summary, it is necessary to make the calculation for a given diameter pipe and a given flowrate to avoid a trial-and-error solution. One can find R_c and all of the velocity associated numbers to solve Equation 6-122. This would have to be repeated for various pipe size holdup calculations based primarily on data from 1.25-in. (0.031-m) tubing, the correlation in Figure 6-72 resulted. Some of the forms in this figure are the output from characterizing numbers and secondary correlations. Four dimensionless characterizing numbers were first proposed by Ros and adapted by others. They are given by Equations 6-103 to 6-107.

When the liquid stream contains both oil and water, calculate the properties as follows:

the liquid specific weight γ_L :

$$\gamma_L = \left[\frac{SG_o(62.4) + R_w SG_g(0.0764) / 5.614}{B_o} \right] \left(\frac{1}{1 + WOR} \right) + \left[SG_w(62.4) \left(\frac{WOR}{1 + WOR} \right) \right] \tag{6-123}$$

the total weight associated with one bbl of stock tank liquid, w:

$$w = SG_o(350) \left(\frac{1}{1 + WOR} \right) + SG_w(350) \left(\frac{WOR}{1 + WOR} \right) + (0.0764)(GLR)SG_g \tag{6-124}$$

518 Production

the weight flowrate \dot{w}_t :

$$\dot{w}_t = \dot{w}(q_w + q_o) \quad (6-125)$$

the liquid mixture viscosity μ_L :

$$\mu_L = \mu_o \left(\frac{1}{1 + \text{WOR}} \right) + \mu_w \left(\frac{\text{WOR}}{1 + \text{WOR}} \right) \quad (6-126)$$

the liquid mixture surface tension σ :

$$\sigma_L = \sigma_o \left(\frac{1}{1 + \text{WOR}} \right) + \sigma_w \left(\frac{\text{WOR}}{1 + \text{WOR}} \right) \quad (6-127)$$

the superficial liquid velocity v_{sL} in ft/s (assuming $B_w = 1.0$):

$$v_{sL} = \frac{5.61q_L}{86,400A_p} \left[B_o \left(\frac{1}{1 + \text{WOR}} \right) + B_w \left(\frac{\text{WOR}}{1 + \text{WOR}} \right) \right] \quad (6-128)$$

the superficial gas velocity v_{sg} :

$$v_{sg} = \frac{q_L \left[\text{GLR} - R_s \left(\frac{1}{1 + \text{WOR}} \right) \right]}{86,400A_p} \left(\frac{14.7}{p} \right) \left(\frac{T}{520} \right) \left(\frac{Z}{1} \right) \quad (6-129)$$

Mixture specific weight is calculated by both using the Hagedorn-Brown holdup correlation and assuming no slippage. The higher value is then used.

If bubble flow is the dominant regime, the pressure gradient is used in the same way as in the Orkiszewski approach (step 7).

Example 4

Solve the problems in Example 2 using the Hagedorn-Brown method:

$$p_1 = 1,455 \text{ psig}$$

$$p_2 = 1,955 \text{ psig}$$

$$d = 1.995 \text{ in ID } (A_p = 0.0217)$$

$$p_{\text{bar}} = 14.7 \text{ psia}$$

$$T_1 = 75^\circ\text{F}$$

$$T_2 = 105^\circ\text{F}$$

$$\text{SG}_g = 0.752$$

$$SG_0 = 54^\circ \text{API}$$

$$q_b = 480 \text{ bpd}$$

$$q_w = 0$$

$$\mu_s = 0.020 \text{ cp}$$

$$\sigma_0 = 28 \text{ dyn/cm}$$

$$\text{GLR} = 3,393 \text{ scf/bbl}$$

Solution

1. $p = (1,455 + 1,955)/2 + 14.7 = 1,179.7$
2. $T = (75 + 105)/2 = 90^\circ \text{ F}$
3. $SG_0 = 0.763$ from Example 2
4. Total mass flowing from volume liquid- $m_o = 462 \text{ lb/stb}$ of oil from Example 2
5. Solution gas/oil ratio R_s and oil formation volume factor B_o

$$R_s = 947.3 \text{ scf/stb}$$

$$B_o = 1.495 \text{ bbl/stb}$$

6. Liquid specific weight γ_L and gas specific weight γ_g from Equation 6-123

$$\gamma_L = \frac{(0.763)62.4 + 947.3(0.752)(0.0764)}{(1.495)(5.614)} = 38.33 \text{ lb/ft}^3$$

$$\gamma_g = 8.823 \text{ lb/ft}^3$$

7. Oil viscosity, μ_{os} and oil surface tension, σ_o

$$\mu_{os} = 0.5 \text{ cp}$$

$$\sigma_o = \sigma_L = 28 \text{ dyn/cm}$$

8. $N_{Lv} = 0.1573(0.5)(1/(38.33 \times 28^3))^{0.25} = 2.6 \times 10^{-3}$ from Equation 6-107
9. $CN_L = 0.0022$ (from Figure 6-73)
10. $v_{sl} = (5.61 \times 480)/(86,400 \times 0.0217)1.495 = 2.147 \text{ ft/s}$ from Equation 6-128
11. $N_{vL} = 1.938(2.147)(38.33/28)^{0.25} = 4.5$ from Equation 6-123
12. $v_g = 4.08 \text{ ft/s}$ from Equation 6-129
13. $N_{gv} = 1.938 \times 4.08(38.33/28)^{0.25} = 8.55$ from Equation 6-104
14. Check the flow regime; calculate A and B:

$$A = L_B = 1.071 - [0.2218(4.08 + 2.147)^2]/0.1662$$

$$= -50.68 \text{ from Equation 6-109}$$

The minimum limit for L_B is 0.13. To assume 0.13

$$B = v_{sg}/(v_{sL} + v_{sg}) = 4.08/(4.08 + 2.147) = 0.655$$

Since $B - A = 0.616 - 0.13 = 0.486$, the difference is positive; so continue the Hagedorn-Brown procedure. In case $B-A$ is negative, use the Orkiszewski method to find flow regime.

15. $N_d = 120.9(0.1662)(38.33/28)^{0.5} = 23.5$
 16. Calculate holdup correlating function ϕ

$$\phi = \frac{N_{Lv}}{N_{gv}^{0.575}} \left(\frac{p}{14.7} \right)^{0.1} \left(\frac{CN_L}{N_d} \right) = \frac{4.5}{8.55^{0.575}} \left(\frac{1719.7}{14.7} \right)^{0.1} \left(\frac{0.0022}{23.5} \right) = 0.000197$$

17. Now from Figure 6-72 $H_L/\psi = 0.42$
 18. Calculate secondary correlation factor ϕ_s

$$\phi_s = \frac{N_{gv} N_L^{0.38}}{N_d^{2.14}} = \frac{8.55 \times (2.6 \times 10^{-3})^{0.38}}{(23.5)^{2.14}} = 0.001036$$

19. From Figure 6-74 $\psi = 1.0$
 20. Liquid holdup $H_L = (H_L/\psi)(\psi) = 0.42 \times 1.0 = 0.42$
 21. The two-phase Reynolds number $(Re)_{tp}$ is

$$Re_{tp} = \frac{2.2 \times 10^{-2} \times 221,760}{(0.1662)0.5^{0.42}0.02^{0.58}} = 379,760$$

22. Relative roughness $\epsilon/d = 0.00015/0.1662 = 0.0009$
 23. Fanning friction factor from Figure 6-65,

$$f_r = 0.00510$$

24. Calculate the average two-phase specific weight γ_m using two methods:

a) $\gamma_m = \gamma_{HB} = \gamma_L H_L + \gamma_g (1 - H_L) = 38.33(0.42) + 8.823(0.58) = 21.22 \text{ lb/ft}^3$

b)
$$\gamma_m = \frac{\dot{w}}{v_m} = \frac{350SG_0 + 0.0764SG_g(\text{GOR}) + 350SG_w(\text{WOR})}{5.61B_o + 5.61(\text{WOR}) + (\text{GOR} - R_s)B_g}$$

$$= \frac{350 \times 0.763 + 0.0764(0.752)3393 + 0}{5.61(1.495) + (3393 - 947.3)(14.7/1719.7)(550/520)(0.72)}$$

$$= 19.006 \text{ lb/ft}^3$$

Use 21.22 lb/ft³ as a proper value.

25. Calculate
 a) Z_1 , B_{01} , R_{s1} , v_{s12} and v_{g1} at T_1 , p_1
 (repeat steps 6, 7, 9, 16, 18)

$$T_1 = 75^\circ; p_1 = 1,455 \text{ psig}$$

$$\left. \begin{aligned} T_r &= (75 + 460)/394 = 1.358 \\ p_r &= 1,455/660 = 2.2 \end{aligned} \right\} Z_1 = 0.71$$

$$R_{01} = 0.752[(1455/18) \times 10^{0.0125(54)}/10^{0.00091(75)}]1.2048$$

$$= 804.4 \text{ scf/stb}$$

$$B_{01} = 0.972 + 0.000147F^{1.175} = 1.403 \text{ bbl/stb}$$

$$\text{where } F = 804.4(0.752/0.763)^{0.5} + 1.25(75) = 892.3$$

$$v_{sL1} = \left(\frac{5.61 \times 480}{86,400 \times 0.0217} \right) (1.403) = 2.02 \text{ ft/s}$$

$$v_{sg1} = \frac{[480(3,393 - 804.4)14.7 \times 535 \times 0.71]}{86,400 \times 0.0217 \times 1,455 \times 520} = 4.89 \text{ ft/s}$$

b) Z_2 , B_{02} , R_{02} , v_{sL2} , and v_{sg2} at T_2 , p_2

$$T_2 = 105^\circ\text{F}, \quad p_2 = 1,955$$

$$\left. \begin{aligned} T_r &= (105 + 460)/394 = 1.434 \\ p_r &= 1,955/660 = 2.962 \end{aligned} \right\} Z_2 = 0.73$$

$$R_{02} = 0.752 [(1955/18) \times 10^{0.0125(54)}/10^{0.00091(105)}]1.2048$$

$$= 1064.5 \text{ scf/stb}$$

26. Calculate the two-phase velocity at both P_q and P_2 :

$$V_{m1} = V_{sL1} + V_{sg1} = 2.02 + 4.89 = 6.91$$

$$V_{m2} = V_{sL2} + V_{sg2} = 2.262 + 3.368 = 5.63$$

27. Determine value $\Delta(V_m^2)$

$$\Delta(V_m^2) = (6.91^2 - 5.63^2) = 16.05$$

28. From Equation 6-122

$$\Delta L = \frac{\Delta p - \gamma_{HB} \Delta \left(\frac{V_m^2}{2g_c} \right)}{\gamma_{HB}(F_c) + (f_r Q^2 m^2 / A d^5 \gamma_m)}$$

$$\Delta p = 500 \text{ psi} = 500 \times 144 \text{ lb/ft}^2$$

$$\gamma_{HB} = \gamma_m = 21.22, \quad A = 7.41 \times 10^{10}$$

$$\Delta L = \frac{500(144) - 21.22 \frac{16.05^2}{2 \times 32.2}}{21.22(1) + \frac{[0.0051(480)^2(462)^2]}{[7.41 \times 10^{10}(0.1662)^2 21.22]}}$$

$$= (72,000 - 84.88)/(21.22 + 0.005774) = \underline{\underline{3,388 \text{ ft}}}$$

or

$$\frac{\Delta p}{\Delta L} = \frac{500}{3,388} = 0.1476 \text{ psi/ft}$$

The Beggs-Brill Method [20,25]

The parameters studied in this method and their range of variation were as follows:

gas flowrate 0 to 300 Mscfd
 liquid flowrate 0 to 30 gal/min
 average system pressure 35 to 95 psia
 pipe diameter 1 and 1.5 in.
 liquid holdup 0 to 0.870
 pressure gradient 0 to 0.8 psi/ft
 inclination angle -90° to $+90^\circ$ also horizontal flow patterns

A flow diagram for calculating a pressure traverse in a vertical well is shown in Figure 6-75. The depth increment equation for ΔL is

$$\Delta L = \frac{\Delta p \left(1 - \frac{\gamma_t v_t v_{sg}}{gP} \right)}{\gamma_t \sin \theta + \frac{f_t G_t v_t}{2gd}} \quad (6-130)$$

where γ_t = two-phase specific weight in lb/ft³
 v_t = two-phase superficial velocity ($v_t = v_{sl} + v_{sg}$) in ft/s
 f_t = two-phase friction factor
 G_t = two-phase weight flux rate (lb/s • ft²)

A detailed procedure for the calculation of a pressure traverse is following:

1. Calculate the average pressure and average depth between the two points:

$$p = (p_1 + p_2)/2 + 14.7$$

2. Determine the average temperature T at the average depth. This value must be known from a temperature versus depth survey.
3. From P-V-T analysis or appropriate correlations, calculate R_p , B_o , B_w , μ_o , μ_w , μ_h , σ_o , σ_w and Z at T and p .

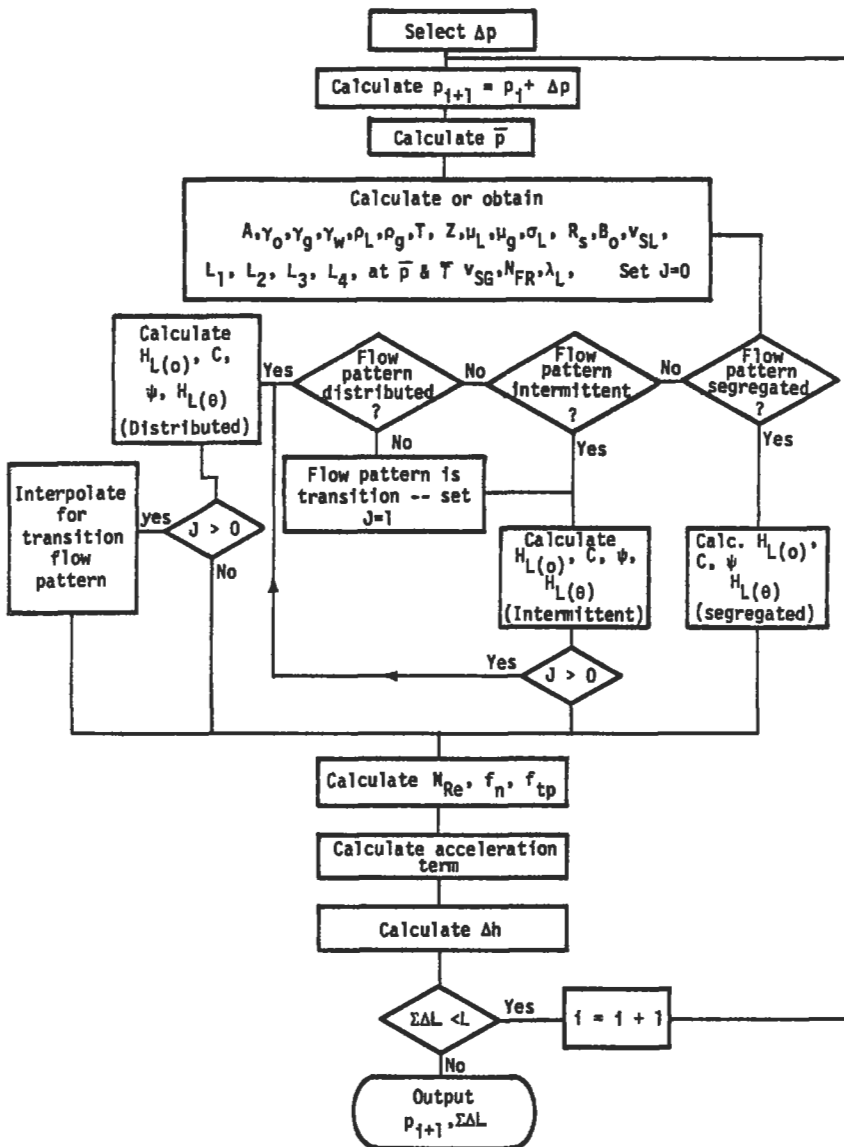


Figure 6-75. Flow diagram for the Beggs-Brill method [19].

4. Calculate the specific gravity of the oil SG_o :

$$SG_o = \frac{141.5}{131.5 + API}$$

5. Calculate the liquid and gas densities at the average conditions of pressure and temperatures:

$$\gamma_L = \gamma_o \left(\frac{1}{1 + \text{WOR}} \right) + \gamma_w \left(\frac{1}{1 + \text{WOR}} \right) = \gamma_o f_o + \gamma_w f_w$$

$$\gamma_o = \frac{350SG_o + 0.0764R_s SG_g}{5.615}$$

$$\gamma_w = \frac{350SG_w}{5.615B_w}$$

$$\gamma_g = \frac{0.0764SG_{gp}(520)}{(14.7)(T + 460)Z}$$

6. Calculate the *in situ* gas and liquid flowrates.

$$q_g = \frac{3.27 \times 10^{-7} Z q_o (R - R_s)(T + 460)}{P}$$

$$q_L = 6.49 \times 10^{-5} (q_o B_o + q_w B_w)$$

7. Calculate the *in situ* superficial gas, liquid and mixture velocities:

$$v_{sL} = q_L / A_p$$

$$v_{sg} = q_g / A_p$$

$$v_t = v_{sL} + v_{sg}$$

8. Calculate the liquid, gas and total weight flux rates:

$$G_L = \gamma_L v_{sL}$$

$$G_t = G_L + G_g$$

$$G_g = \gamma_g v_{sg}$$

9. Calculate the input liquid content (no-slip holdup):

$$\lambda = \frac{q_L}{q_L + q_g}$$

10. Calculate the Froude number N_{FR} , the liquid viscosity, μ_L , the mixture viscosity μ_m and the liquid surface tension σ_L :

$$N_{FR} = \frac{v_t^2}{gd}$$

$$\mu_L = \mu_o f_o + \mu_w f_w$$

$$\mu_t = \mu_L \lambda + \mu_g (1 - \lambda) (6.72 \times 10^{-4})$$

$$\sigma_L = \sigma_0 f_0 + \sigma_w f_w$$

11. Calculate the no-slip Reynolds number and the liquid velocity number:

$$(N_{Re})_{ns} = \frac{G_t d}{\mu_t}$$

$$N_{LV} = 1.938 v_{sl} \left(\frac{\gamma_L}{\sigma_L} \right)^{0.25}$$

12. To determine the flow pattern that would exist if flow were horizontal, calculate the correlating parameters,

L_1 , L_2 , L_3 and L_4 :

$$L_1 = 316 \lambda^{0.0302}$$

$$L_3 = 0.10 \lambda^{-1.4516}$$

$$L_2 = 0.0009252 \lambda^{-2.4684}$$

$$L_4 = 0.5 \lambda^{-6.738}$$

13. Determine flow pattern using the following limits:

Segregated:

$$\lambda < 0.01 \text{ and } N_{FR} < L_1$$

or

$$\lambda \geq 0.01 \text{ and } N_{FR} < L_2$$

Transition:

$$\lambda \geq 0.01 \text{ and } L_2 < N_{FR} < L_3$$

Intermittent:

$$0.01 \leq \lambda < 0.4 \text{ and } L_3 < N_{FR} < L_1$$

or

$$\lambda \geq 0.4 \text{ and } L_3 < N_{FR} \leq L_4$$

Distributed:

$$\lambda < 0.4 \text{ and } N_{FR} \geq L_1$$

or

$$\lambda \geq 0.4 \text{ and } N_{FR} > L_4$$

14. Calculate the horizontal holdup $H_L(O)$:

$$H_L(O) \frac{a\lambda^b}{N_{FR}^c}$$

where a, b and c are determined for each flow pattern from the following table:

Flow pattern	a	b	c
Segregated	0.98	0.4846	0.0868
Intermittent	0.845	0.5351	0.0173
Distributed	1.065	0.5824	0.0609

15. Calculate the inclination correction factor coefficient:

$$C = (1 - \lambda) \ln(d\lambda^e N_{LV}^f N_{FR}^g)$$

where d, e, f, and g are determined for each flow condition from the following table:

Flow Pattern	d	e	f	g
Segregated uphill	0.011	-3.768	3.539	-1.614
Intermittent uphill	2.96	0.305	-0.4473	0.0978
Distributed uphill	No correction		C = 0	
All flow patterns downhill	4.70	-0.3692	0.1244	-0.5056

16. Calculate the liquid holdup inclination correction factor:

$$\psi = 1 + C[\sin(1.8\theta) - 0.333 \sin^3(1.8\theta)] = 1 + 0.3C$$

for vertical well

17. Calculate the liquid holdup and the two-phase density:

$$H_L(\theta) = H_L(0)\psi$$

$$\rho_t = \rho_L H_L + \rho_g (1 - H_L)$$

18. Calculate the friction factor ratio:

$$f_t/f_m = e_s$$

$$\text{where } S = [\ln(y)] / \{-0.0523 + 3.182 \ln(y) - 0.8725 [\ln(y)]^2 + 0.01853 [\ln(y)]^4\}$$

$$y = \lambda/[H_L(\theta)]^2$$

S becomes unbounded at a point in the interval $1 < y < 1.2$; and for y in this interval, the function S is calculated from

$$S = \ln(2.2y - 1.2)$$

19. Calculate the no-slip friction factor:

$$f_{ns} = 1/[2 \log [N_{Re_{ns}}/(4.5223 \log N_{Re_{ns}} - 3.8215)]]^2$$

or

$$f_{ns} = 0.0056 + 0.5/(N_{Re_{ns}})^{0.32}$$

20. Calculate the two-phase friction factor:

$$f_t = f_{ns}/(f_t/f_{ns})$$

21. Calculate ΔL . If the estimated and calculated values for ΔL are not sufficiently close, the calculated value is taken as the new estimated value and the procedure is repeated until the values agree. A new pressure increment is then chosen and the process is continued until the sum of the ΔL 's is equal to the well depth.

Example 5

Solve the problem in Example 2 using the Beggs-Brill method.

Solution

1. $p = 1,719.7$ psia
2. $T = 90^\circ\text{F}$
3. $R_s = 947.3$ scf/stb $B_0 = 1.495$ bbl/stb
 $\mu_{os} = 0.5$ cp, $\sigma_0 = 28$ dyn/cm, $Z = 0.72$
4. $SG_0 = 0.736$, $\gamma_g = 8.823$ lb/ft³
5. $\gamma_0 = 38.32$ lb/ft³ (from Example 3)
6. $q_g = 0.08855$ ft³/s
 $q_L = 0.0466$ ft³/s
7. $A_p = 0.0217$ ft²
 $v_{sL} = q_L/A_p = 2.147$ ft/s, $v_{sg} = 4.081$ ft/s
8. Calculate the liquid, gas and total weight flux rates:

$$G_L = \gamma_L v_{sL}, \quad G_g = \gamma_g v_{sg}$$

$$\begin{aligned} G_t &= G_L + G_g = 38.32 \times 2.147 + (8.823) \times 4.081 \\ &= 118.3 \text{ lb}/(\text{s} \cdot \text{ft}^2) \end{aligned}$$

9. Calculate the input liquid (no-slip holdup):

$$\lambda = \frac{q_L}{q_L + q_g} = \frac{0.0466}{0.0466 + 0.08855} = 0.3448 = 0.345$$

10. The Froude number, viscosity and surface tension

$$N_{FR} = \frac{v_t^2}{gd} = \frac{6.23^2}{32.174 \times 0.1662} = 7.26$$

$$\mu_L = \mu_o f_o + \mu_w f_w = 0.5(1.0) + \mu_w(0.0) = 0.5$$

$$\begin{aligned} \mu_t &= (6.72 \times 10^{-4})[0.5 \times 0.345 + 0.02(1 - 0.345)] = 1.164 \times 10^{-4} \\ &= 0.0001164 \text{ lb}_m/(\text{ft}/\text{s}) \end{aligned}$$

$$\sigma_L = \sigma_o f_o + \sigma_w f_w = 28 \times 1.0 = 28 \text{ dyn/cm}$$

11. Calculate the no-slip Reynolds number and the liquid velocity number:

$$(N_{Re})_{ns} = \frac{G_t d}{\mu_t} = \frac{118.3(0.1662)}{0.000464} = 168,884$$

$$N_{LV} = 1.938 \times 2.147(38.32/28)^{0.25} = 4.5$$

12. Determine the flow pattern that would exist if flow were horizontal:

$$L_1 = 316\lambda^{0.302} = 316 \times (0.345)^{0.302} = 229.14$$

$$L_2 = 0.0009252(0.345)^{-2.4684} = 1.2796 \times 10^{-2}$$

$$L_3 = 0.10\lambda^{-1.4516} = 0.10(0.345)^{-1.4516} = 0.4687$$

$$L_4 = 0.5\lambda^{-6.738} = 0.5(0.345)^{-6.738} = 650.3$$

13. Determine flow pattern:

$$0.4 > \lambda > 0.01 \text{ and } L_2 < N_{FR} < L$$

The flow pattern is intermittent.

14. Calculate the horizontal holdup:

$$H_L(O) = 0.845(0.345)^{0.5951}/7.26^{0.0173} = 0.462$$

15. Calculate the inclination correction factor coefficient:

$$\begin{aligned} C &= (1 - 0.345) \ln(2.96 \times 0.345^{0.305} 4.5^{-0.4473} 7.26^{0.0978}) \\ &= 0.18452 \end{aligned}$$

16. Calculate the liquid holdup inclination correction factor:

$$\begin{aligned} \psi &= 1 + C[\sin(1.8 \times 90) - 0.333 \sin^3(1.9 \times 90)] \\ &= 1 + C(0.309 - 0.009826) = 1 + 0.3C \\ &= 1 + 0.3(0.18452) = 1.055 \end{aligned}$$

17. Calculate the liquid holdup and the two-phase density:

$$H_L(90) = H_L(O)\psi = 0.462 \times 1.055 = 0.4876$$

$$\begin{aligned}\gamma_t &= \gamma_L H_L + \gamma_g (1 - H_L) = 38.32(0.4876) + 8.823 (1 - 0.4876) \\ &= 23.2 \text{ lb/ft}^3\end{aligned}$$

18. Calculate the friction factor ratio:

$$y = [0.345/(0.4876)^2] = 1.451, \ln 1.451 = 0.3723$$

$$\begin{aligned}f_t/f_{ns} &= \exp[0.3723/(-0.0523 + 3.182 \times 0.3723) - 0.8725 \times 0.3723^2 \\ &\quad + 0.1853 \times 0.3723^4] \\ &= \exp(0.3723/1.0118) = 3^{0.36796} = 1.4447\end{aligned}$$

19. Calculate the no-slip friction factor:

$$\begin{aligned}f_{ns} &= 1/[2 \log[N_{Re_{ns}}/(4.5223 \log N_{Re_{ns}} - 3.8215)]]^2 \\ &= 1/36.84 = 0.0271\end{aligned}$$

20. Calculate the two-phase friction factor:

$$f_t = f_{ns}(f_t/f_{ns}) = 0.0271(1.4447) = 0.0391$$

21. Determine the distance ΔL for $\Delta p = 500$ psi from Equation 6-130

$$\Delta L = \frac{500 \left[1 - \frac{23.2(6.23)4.081}{32.174 \times 1,719.7} \right]^{1.44}}{23.2(1.0) + \frac{0.0391(118.3)6.23}{2(32.174)0.1662}} = \frac{72,000(0.9893)}{25.894} = 2,750 \text{ ft}$$

and

$$\frac{\Delta p}{\Delta L} = \frac{500}{2,750} = 0.18 \text{ psi/ft}$$

Example 6

Solve example 1 using the Beggs-Brill method:

$$q_g = 40 \text{ MMscf/d, } p_{\text{avg}} = 2,000 \text{ psia}$$

$$q_o = 40,000 \text{ stb/d, } T_{\text{avg}} = 80^\circ\text{F}$$

$$\text{ID} = 9 \text{ in. } \quad \text{SG}_g = 0.75 \text{ at } p = 14.7 \text{ psia in } T = 60^\circ\text{F}$$

$$R_p = 990 \text{ scf/bbl}$$

Solution

1. $SG_0 = 141.5/131.5 + API = 0.86$
2. Calculate R_s , B_0 , μ_0 , μ_g , Z_g at p_{avg} and T_{avg} :

$$Z_g = 0.685$$

$$\mu_g = 0.0184 \text{ cp}$$

$$R_s = 477 \text{ scf/stb}$$

$$B_0 = 1.233 \text{ rb/stb}$$

$$\mu_0 = 2.96 \text{ cp}$$

3. Calculate γ_0 and γ_g at average parameters:

$$\gamma_0 = \frac{350(0.86) + 0.0764(477)(0.75)}{5.614(1.233)} = 47.42 \text{ lb/ft}^3$$

$$\gamma_g = \frac{0.0764\gamma_{gp}(520)}{(14.7)(T + 460)Z_g} = \frac{0.0764(0.73)(2,000)(520)}{(14.7)(80 + 460)(0.685)} = 10.96 \text{ lb/ft}^3$$

4. Calculate the *in situ* gas and liquid flowrates,

$$\begin{aligned} q_g &= \frac{3.27 \times 10^{-7} Z_g q_0 (R - R_s)(T + 460)}{p} \\ &= \frac{3.27 \times 10^{-7} (0.685)(40,000)(990 - 477)(80 + 460)}{2,000} \\ &= 1.241 \text{ ft}^3/\text{s} \end{aligned}$$

$$\begin{aligned} q_L &= 6.49 \times 10^{-5} (q_0 B_0 + q_w B_w) \\ &= 6.49 \times 10^{-5} [40,000(1.233) + 0] \\ &= 3.201 \text{ ft}^3/\text{s} \end{aligned}$$

5. Calculate A_p :

$$A_p = \frac{\pi}{4} D^2 = \frac{\pi}{4} \left(\frac{9}{12} \right)^2 = 0.4418 \text{ ft}^2$$

6. Calculate the *in situ* superficial gas, liquid and mixture velocities:

$$v_{Ls} = q_L/A_p = 3.201/0.4418 = 7.25 \text{ ft/s}$$

$$v_{\text{sg}} = q_{\text{g}}/A_{\text{p}} = 1.241/0.4418 = 2.81 \text{ ft/s}$$

$$v_{\text{m}} = v_{\text{sl}} + v_{\text{sg}} = 7.25 + 2.81 = 10.06 \text{ ft/s}$$

7. Calculate the liquid, gas and total mass flux rates:

$$G_{\text{L}} = \rho_{\text{L}} v_{\text{sl}} = (47.42)(7.25) = 343.6 \text{ lb/(s} \cdot \text{ft)}$$

$$G_{\text{g}} = \rho_{\text{g}} v_{\text{sg}} = (10.96)(2.81) = 30.79 \text{ lb/(s} \cdot \text{ft)}$$

$$G_{\text{m}} = G_{\text{L}} + G_{\text{g}} = 343.6 + 30.8 = 374.4 \text{ lb/(s} \cdot \text{ft)}$$

8. Calculate the no-slip holdup:

$$\lambda = \frac{q_{\text{L}}}{q_{\text{L}} + q_{\text{g}}} = \frac{3.201}{32 + 1.241} = 0.72$$

9. Calculate the Froude number N_{FR} , the mixture viscosity μ_{m} and surface tension σ_{L} :

$$N_{\text{FR}} = \frac{v_{\text{m}}^2}{gd} = \frac{(10.06)^2}{(32.2 \times 9)} = 4.186$$

$$\begin{aligned} \mu_{\text{m}} &= 6.27 \times 10^{-4} [\mu_{\text{L}}\lambda + \mu_{\text{g}}(1 - \lambda)] \\ &= 6.27 \times 10^{-4} [2.96(0.72) + 0.0184(0.28)] \\ &= 1.44 \times 10^{-3} \text{ lb/(ft} \cdot \text{s)} \end{aligned}$$

$$\sigma_{\text{L}} = 37.5 - 0.257(\text{API}) = 37.5 - 0.257(33) = 29.0 \text{ dyn/cm}$$

10. Calculate the non-slip Reynolds number and the liquid velocity number:

$$\text{Re}_{\text{NS}} = \frac{G_{\text{m}}d}{\mu_{\text{m}}} = \frac{(374.4)(9)}{(1.44 \times 10^{-3})12} = 195,000$$

$$N_{\text{LV}} = 1.938 v_{\text{sl}} \left(\frac{\gamma_{\text{L}}}{\sigma_{\text{L}}} \right)^{0.25} = 1.938(7.25)(47.42/29)^{0.25} = 15.88$$

11. Calculate L_1 , L_2 , L_3 and L_4 :

$$L_1 = 316\lambda^{0.302} = 316(0.721)^{0.302} = 286$$

$$L_2 = 0.000952\lambda^{-2.4684} = 0.0009252(0.721)^{-2.4684} = 0.0021$$

$$L_3 = 0.10\lambda^{-1.4516} = 0.10(0.721)^{-1.4516} = 0.161$$

$$L_4 = 0.5\lambda^{-6.758} = 0.5(0.721)^{-6.758} = 4.53$$

12. Determine flow pattern:

$$\text{Since } 0.721 \geq 0.4 \text{ and } L_3 < N_{FR} \leq L_4$$

Flow is intermittent.

13. Calculate the horizontal holdup $H_L(O)$:

$$H_L(O) = a\lambda^b/N_{FR}^c = 0.845 \times 0.721^{0.5551}/7.186^{0.0173} = 0.692$$

14. Calculate ψ and $H_L(O)$ and two-phase specific weight:

$$\text{Since } \theta = 0^\circ, \lambda = 1 + 0 = 1$$

$$H_L(0^\circ) = H_L(0)\lambda = 0.692$$

$$\begin{aligned} \gamma_t &= \gamma_L H_L + \gamma_g(1 - H_L) = 47.42(0.692) + 10.96(1 - 0.692) \\ &= 36.19 \text{ lb/ft}^3 \end{aligned}$$

15. Calculate the friction factor ratio:

$$y = \frac{\lambda}{H_L^2} = \frac{0.721}{(0.692)^2} = 1.506$$

$$\ln(y) = 0.4092$$

$$\begin{aligned} S &= \ln(y)/[-0.0523 + 3,182 \ln y - 0.8725(\ln y)^2 + 0.01853(\ln y)^4] \\ &= 0.3706 \end{aligned}$$

$$f_t/f_{ns} = e^S = e^{0.3706} = 1.449$$

16. Calculate the non-slip friction factor f_{ns} :

$$\begin{aligned} f_{ns} &= 1/[2 \log\{\text{Re}_{ns}/(4.5223 \log \text{Re}_{ns} - 3,8215)\}]^2 \\ &= 1/[2 \log\{195,000/(4.5223 \log 195,000 - 3,8215)\}]^2 \\ &= 0.01573 \end{aligned}$$

17. Calculate the two-phase friction factor:

$$f_t = f_{ns}(f_t/f_{ns}) = 0.01573(1.449) = 0.0227$$

18. Calculate the pressure gradient:

$$\begin{aligned} \frac{\Delta L}{\Delta p(144)} &= \frac{1 - \frac{\gamma_t v_m v_{sg}}{gP}}{\gamma_g \sin \theta + \frac{f_t G_m v_m}{2gd}} = \frac{1 - \frac{(36.19)(10.06)(2.81)}{(32.2)2,000(144)}}{36.19(1)(0) + \frac{0.0227(374.4)(10.06)}{2(32.2)(9/12)}} \\ &= 0.5646 \end{aligned}$$

$$\frac{\Delta L}{p} = 81.3 \quad \text{or} \quad \frac{\Delta p}{\Delta L} = 1.23 \times 10^{-2} \text{ psi/ft}$$

because pressure is decreasing in flow direction to proper value of $\Delta p/\Delta L = -1.23 \times 10^{-2}$ psi/ft.

Summary

In this work attention was paid only to five methods. These are flow regime maps, the Duns-Ros method, the Orkiszewski method, the Hagedorn-Brown method and the Beggs-Brill method. They are the most often used. However, it is necessary to point out that in literature [19,20,25,26,27] it is possible to find a lot of other methods. Large numbers of correlations indicate that this problem has not been properly solved so far. Pressure loss in pipe is a function of a few parameters. The most important are sort of fluid mixture, working temperature and pressure, pipe diameters and inclination. In practice the best way to evaluate methods is to make measurement of pressure drop distribution in wells or pipes, and, next, adjust a proper correlation. It means that for various oil-gas fields different methods could satisfy the above requirements.

For production purposes pressure gradient is often evaluated based on Gilbert's type curves. This method is not accurate, but still is used.

NATURAL FLOW PERFORMANCE

The most important parameters that are used to evaluate performance or behavior of petroleum fluids flowing from an upstream point (in reservoir) to a downstream point (at surface) are pressure and flowrate. According to basic fluid flow through reservoir, production rate is a function of flowing pressure at the bottomhole of the well for a specified reservoir pressure and the fluid and reservoir properties. The flowing bottomhole pressure required to lift the fluids up to the surface may be influenced by size of the tubing string, choke installed at downhole or surface and pressure loss along the pipeline.

In oil and gas fields, the flowing systems may be divided into at least four components, as follow:

1. reservoir
2. wellbore
3. chokes and valves
4. surface flowline

Each individual component, through which reservoir fluids flow, has its own performance and, of course, affects each other. A good understanding of the flow performances is very important in production engineering. The combined performances are often used as a tool for optimizing well production and sizing equipment. Furthermore, engineering and economic judgments can depend on good information on the well and reasonable prediction of the future performances.

As has been discussed in previous sections, hydrocarbon fluids produced can be either single phase (oil or gas) or two phases. Natural flow performance of oil, gas and the mixture will therefore be discussed separately. Some illustrative examples are given at the end of each subsection.

Oil Flow Performances

Inflow Performance

Inflow performance represents behavior of a reservoir in producing the oil through the well. For a heterogeneous reservoir, the inflow performance might differ from one well to another. The performance is commonly defined in term of a plot of surface production rate (stb/d) versus flowing bottomhole pressure (P_{wf} in psi) on cartesian coordinate. This plot is defined as inflow performance relationship (IPR) curve and is very useful in estimating well capacity, designing tubing string and scheduling an artificial lift method.

For single-phase liquid flow, radial flow equation can be written as (for oil)

1. semi-steady-state condition

$$q_0 = 0.00708k_0h \frac{(P_r - P_{wf})}{\bar{\mu}_0 \bar{B}_0 \left(\ln \frac{r_e}{r_w} - \frac{3}{4} + s \right)} \quad (6-131a)$$

2. steady-state condition

$$q_0 = 0.00708k_0h \frac{(P_r - P_{wf})}{\bar{\mu}_0 \bar{B}_0 \left(\ln \frac{r_e}{r_w} - \frac{1}{2} + s \right)} \quad (6-131b)$$

where q_0 = surface measured oil rate in stb/d

k_0 = permeability to oil in md

h = effective formation thickness in ft

P_r = average reservoir pressure in psia

P_{wf} = flowing bottomhole pressure in psia

$\bar{\mu}_0$ = oil viscosity evaluated at $\frac{(P_r + P_{wf})}{2}$ in cp

\bar{B}_0 = oil formation volume factor evaluated at $\frac{(P_r + P_{wf})}{2}$ in bbl/stb

r_e = drainage radius in ft

r_w = wellbore radius in ft

s = skin factor, dimensionless

Assuming all parameters but P_{wf} are constants in the equations above, it is also clear that flowrate q_0 is linearly proportional to flowing pressure P_{wf} . Therefore, for laminar flow the plot q_0 versus P_{wf} on a cartesian coordinate must be linear. This is illustrated in Figure 6-76. Strictly speaking, it shows the behavior of single-phase liquid flowing over the range of P_{wf} . In actual cases, however, straight line IPR may be shown by reservoirs producing at P_r and P_{wf} above the bubble point pressure P_b , and by strong water-drive reservoirs.

Productivity index, usually denoted by the symbol J , is commonly expressed in practice for well performance. It is mathematically defined as

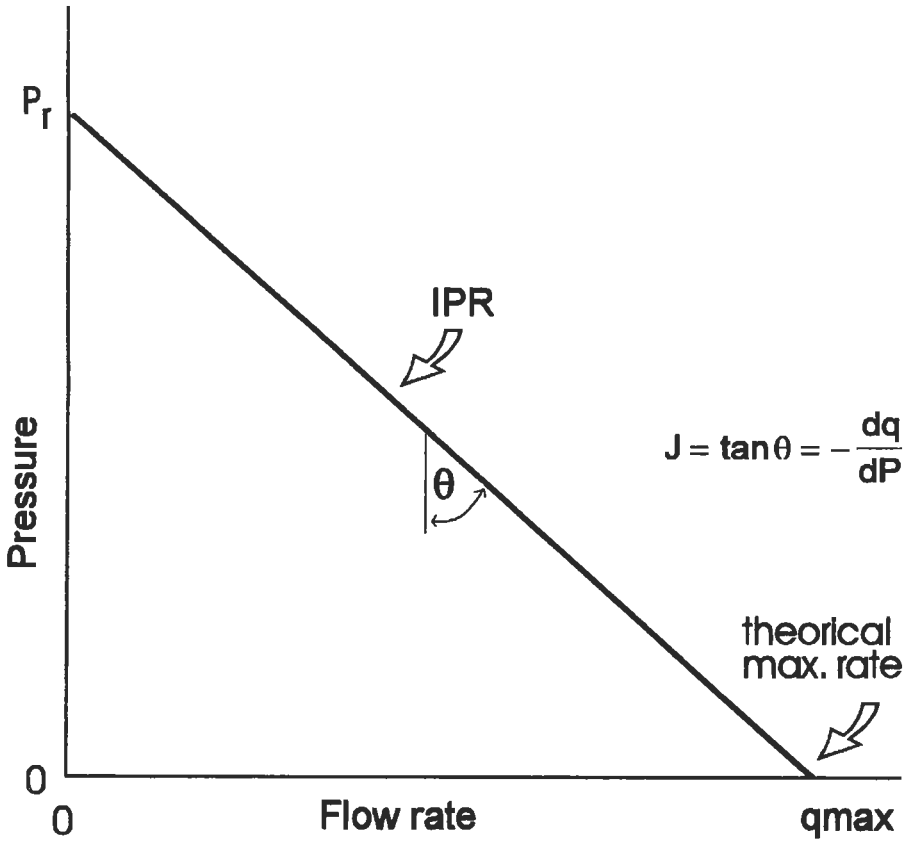


Figure 6-76. Inflow performance relationship of single-phase oil reservoirs.

$$J = \frac{q_o}{P_r - P_{wf}} \tag{6-132}$$

where J is in stb/d/psi . The term $(P_r - P_{wf})$ is called *pressure drawdown*. Equation (6-131a) or (6-131b) can be rearranged to be used in estimating well productivity index.

By knowing reservoir pressure P_r , it is possible to construct an oil IPR curve from a single flow test on a well. Or, due to the linearity of liquid IPR curves, by conducting a two-point flow test (two different flowrates while measuring the flowing bottomhole pressure) on a well, the static reservoir pressure can be determined.

The equations discussed above are derived from the laminar Darcy's law. In a case where turbulent flow occurs, a modified equation should be used. The occurrence of turbulence at the bottomhole may indicate too few open perforations or too narrow fracture in fractured well or other incorrect completion method applied. All these bring about inefficient production operation because

the high drawdown encountered results in insufficient flowrate. The symptom may be analyzed using the correlation of Jones et al. [30]:

$$\frac{\Delta P}{q_0} = C + Dq_0 \quad (6-133)$$

where

$$C = \frac{\mu_0 \bar{B}_0}{0.00708k_o h} \left(\ln \frac{r_e}{r_w} - \frac{3}{4} + s \right) \quad (6-134)$$

is called the laminar flow coefficient, and

$$D = \frac{9.08 \times 10^{-13} \beta \bar{B}_0^2 \gamma_0}{4\pi^2 h^2 r_w} \quad (6-135)$$

is the turbulence coefficient, with β = the turbulence factor in ft^{-1}
 γ_0 = oil specific weight in lb/ft^3

and other terms are the same as in the previous equations. The magnitude of the turbulent factor is in the order of 10^{-5} to 10^{-8} and is usually negligible when compared with the laminar flow coefficient in most oil wells. But if this is not the case, plot $(\Delta P/q)$ versus q on a cartesian coordinate paper. If the flow is fully laminar, then the plot has a slope of zero. But when turbulence is measurable, the plot has nonzero positive slope, which also means that the productivity decreases as flowrate increases.

Predicting Future Oil Well IPR. Pertaining to our problem here dealing with single-phase oil flow in reservoirs, we always assume that gas does not develop over the whole range of flowing pressure at downhole. The consequence is that the following equations are valid for wells that produce only oil (and water).

Recalling the radial flow equation for oil (Equation 6-131 for instance), we obtain

$$q_{0_{\max}} = \frac{0.00708k_o h P_r}{\bar{\mu}_0 \bar{B}_0 \left(\ln \frac{r_e}{r_w} - \frac{3}{4} + s \right)} \quad (6-136)$$

where $q_{0_{\max}}$ is a theoretical possible maximum flowrate when $P_{wf} \approx 0$.

Assuming no changes in producing interval, skin factor and drainage radius occur during a period of time from present to the future, and also $\bar{\mu}_0$ and \bar{B}_0 are nearly constant over the whole range of pressure, the future possible maximum flowrate is

$$(q_{0_{\max}})_f = (q_{0_{\max}})_p \times \frac{(k_{ro} \times P_r)_f}{(k_{ro} \times P_r)_p} \quad (6-137)$$

Because no gas develops in the reservoir, the relative permeability to oil can be a function of water saturation. Figure 6-77 suggests the possibility of changes in oil inflow performance curves with time ($t_2 > t_1$).

Tubing Performance

A tubing performance may be defined as the behavior of a well in giving up the reservoir fluids to the surface. The performance is commonly showed as a plot of flowrate versus flowing pressure. This plot is called the tubing performance relationship (TPR). For a specified wellhead pressure, the TPR curves vary with diameter of the tubing. Also, for a given tubing size, the curves vary with wellhead pressure. Figure 6-78 shows the effect of tubing size and wellhead pressure [31].

For single-phase liquid flow, pressure loss in tubing can be determined using a simple fluid flow equation for vertical pipe, or using some graphical pressure loss correlations where available with GLR = 0.

Tubing performance curves are used to determine the producing capacity of a well. By plotting IPR and TPR on the same graph paper, a stabilized maximum production rate of the well can be estimated. Figure 6-78 shows the combined plots for determining the flowrate. The larger the diameter of tubing, the higher the flowrate that can be obtained. But there is a critical diameter limiting the rate, even lowering the well capacity. For a specified tubing size, the lower the wellhead pressure, the higher the production rate.

Choke Performance

A choke can be installed at the wellhead or downhole to control natural flow or pressure. Chokes are widely used in oil fields. Several reasons in installing chokes are to regulate production rate, to protect surface equipments from slugging, to avoid sand problem due to high drawdown or to control flowrate in order to avoid water or gas coning.

There are two types of wellhead choke that are commonly used, positive chokes and adjustable chokes. A positive choke has a fixed size in diameter so that it must be replaced to regulate production rate. An adjustable choke permits gradual changes in the size of the opening.

Placing a choke at the wellhead can mean fixing the wellhead pressure and thus flowing bottomhole pressure and production rate. For a given wellhead pressure, by calculating pressure loss in the tubing the flowing bottomhole pressure can be determined. If reservoir pressure and productivity index of the well are known, the flowrate can then be determined using Equation 6-132.

The rate of oil flowing through a choke (orifice or nozzle) depends upon pressure drop in the choke, the inside diameters of pipe and choke and density of the oil. For incompressible fluids, the Equation 6-138 may be used to estimate the flowrate of oil:

$$q_o = 10,285CA \sqrt{\frac{\Delta P}{\gamma_o}} \quad (6-138)$$

where q_o = oil rate in bbl/day

C = flow coefficient as function of diameter ratio and Reynolds number
(see Figure 6-79)

(text continued on page 541)

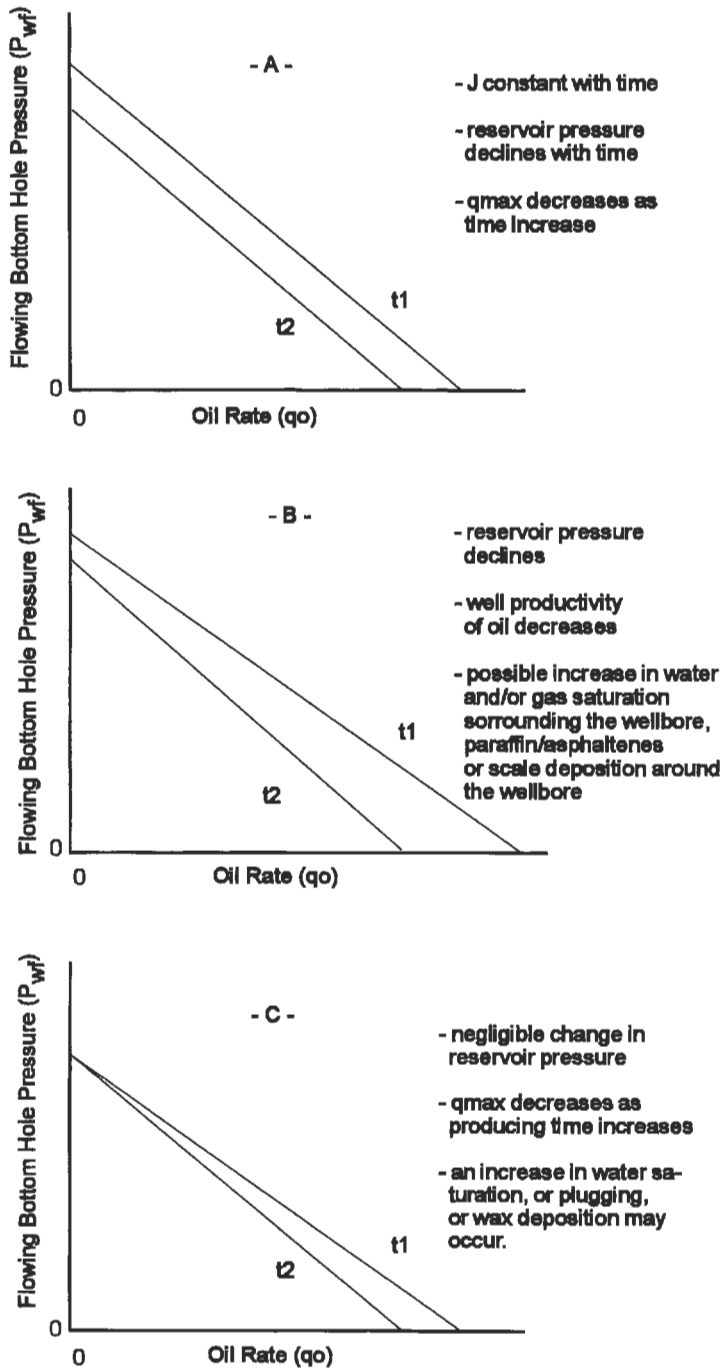


Figure 6-77. Possibility of changes in wells productivity.

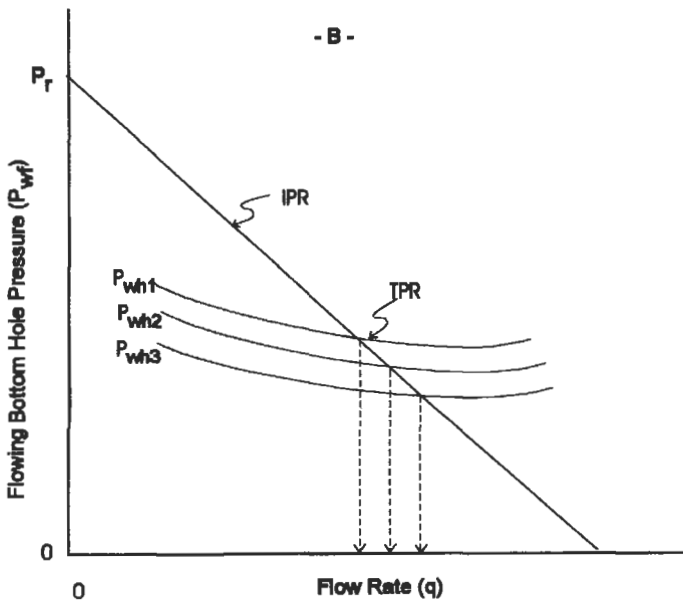
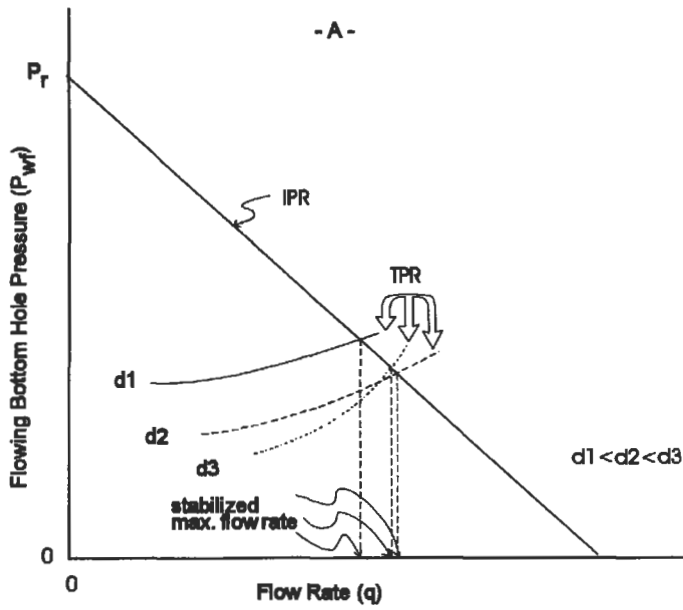
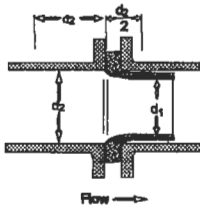
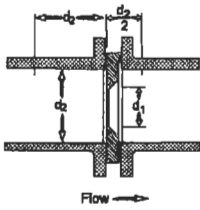
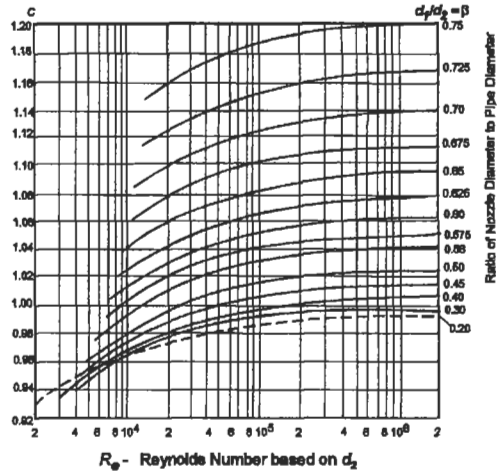


Figure 6-78. Effects of tubing size and tubing head pressure on a well productivity.



$$C = \frac{C_d}{\sqrt{1-\beta^4}}$$

Example : The flow coefficient C for a diameter ratio β of 0.60 at a Reynolds number of 20,000 (2×10^4) equal 1.03



$$C = \frac{C_d}{\sqrt{1-\beta^4}}$$

$$K_{orifice} \approx \frac{1-\beta^2}{C^2\beta^4}$$

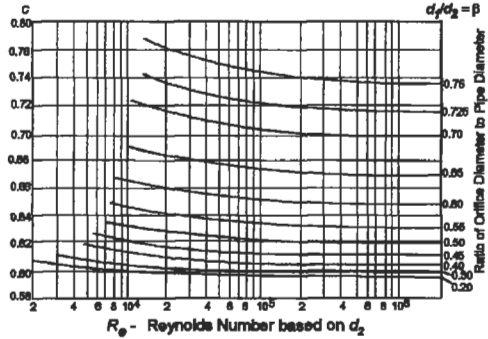
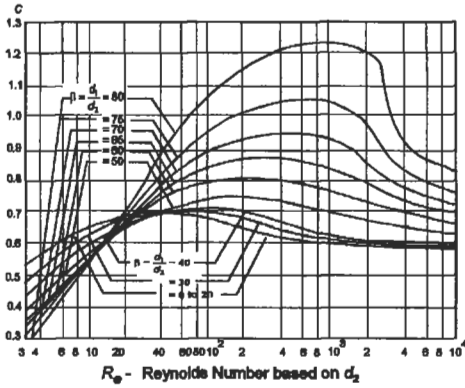


Figure 6-79. Flow coefficient versus diameter ratio and Reynolds number [31].

(text continued from page 537)

- A = cross-sectional area of choke in in.²
- ΔP = pressure drop across the choke in psi
- γ_o = oil specific weight in lb/ft³

In installing a choke, the downstream pressure of the choke is usually 0.55 of the upstream pressure, or even less to ensure no change in flowrate or upstream pressure. This condition is called a sonic flow. A subsonic flow occurs when the upstream pressure or flowrate is affected by a change in downstream pressure.

Flowline Performance

After passing through a choke installed at the wellhead, the oil flows through flowline to a separator. If the separator is far from the wellhead and the pressure loss in the flowline cannot be neglected, pressure-flowrate relationship for flowline can be generated similar to tubing performance curves. Usually the separator pressure is specified. Then by using pressure gradient curves available for horizontal pipes or using a simple horizontal fluid flow equation, the wellhead pressure or downstream pressure of the choke or intake pressure of the flowline can be determined as function of flowrate. This pressure-flowrate plot is useful in sizing the flowline. Figure 6-80 illustrates the relationship between the wellhead pressure and flowrate for some different flowline diameters. This plot is called *flowline performance curve*.

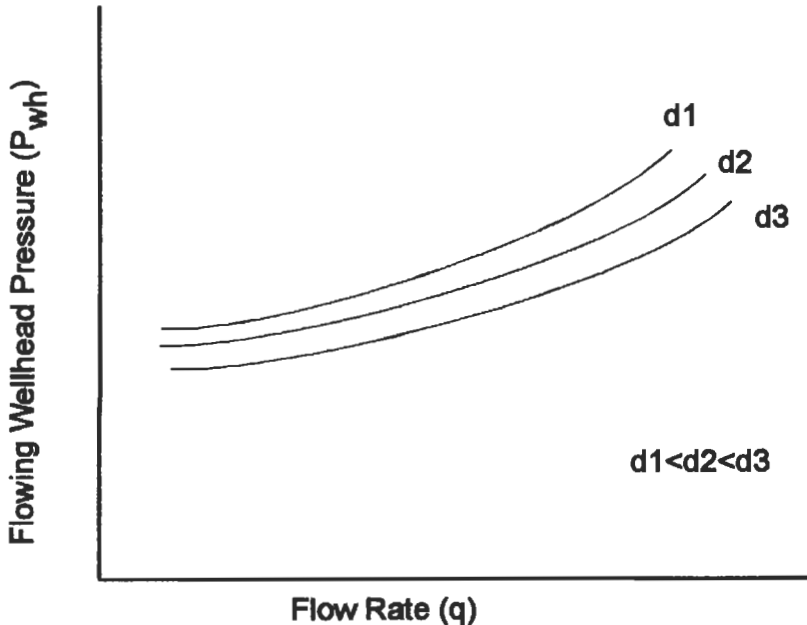


Figure 6-80. Flowline performance curves for different flowline diameters.

By plotting TPR in term of wellhead pressure for various tubing sizes and flowline performance curves on the same graph (see Figure 6-81), selecting tubing string-flowline combination for a well can be established based on the pipe's availability, production scheme planned and economic consideration.

Example A

Determination of oil inflow performance.

Suppose two flowrates are conducted on an oil well. The results are as follows:

	Test 1	Test 2
q_o , stb/d	200	400
P_{wh} , psi	2400	1800

Gas/oil ratios are very small. Estimate the reservoir pressure and productivity index of the well, and also determine the maximum flowrate.

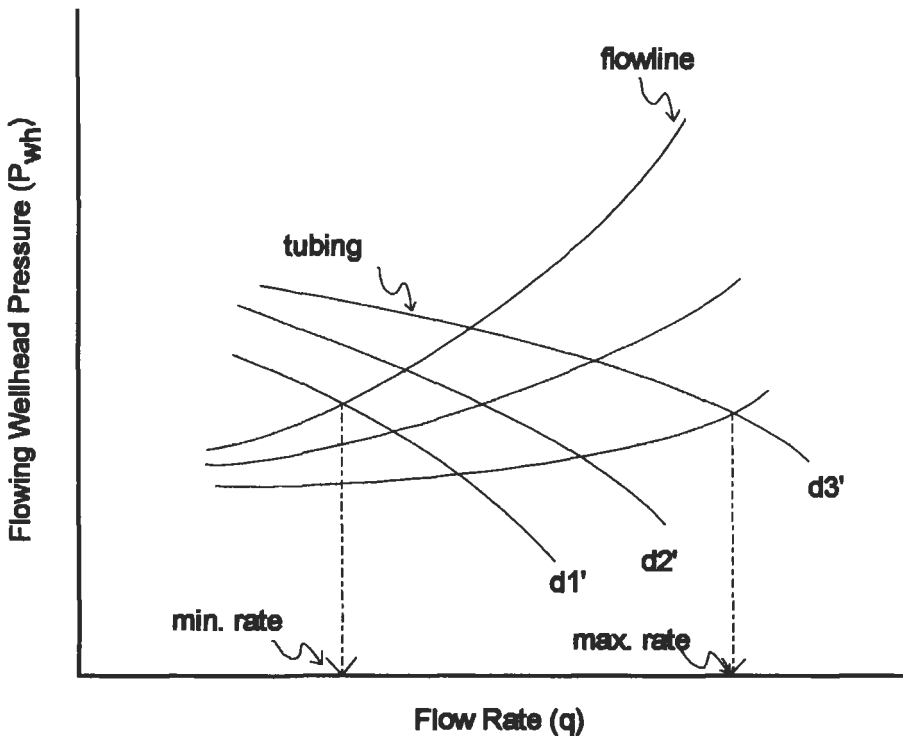


Figure 6-81. Combined tubing-flowline performance curves.

Solution

1. Plot the two data points on a cartesian coordinate graph paper (q_o versus P_{wf}), see Figure 6-82. Draw a straight line through these two points, the intersection with ordinate is the estimated reservoir pressure which is about 3,000 psi.
2. The productivity index is

$$J = \frac{200}{3,000 - 2,400} = 0.333 \text{ stb/d/psi}$$

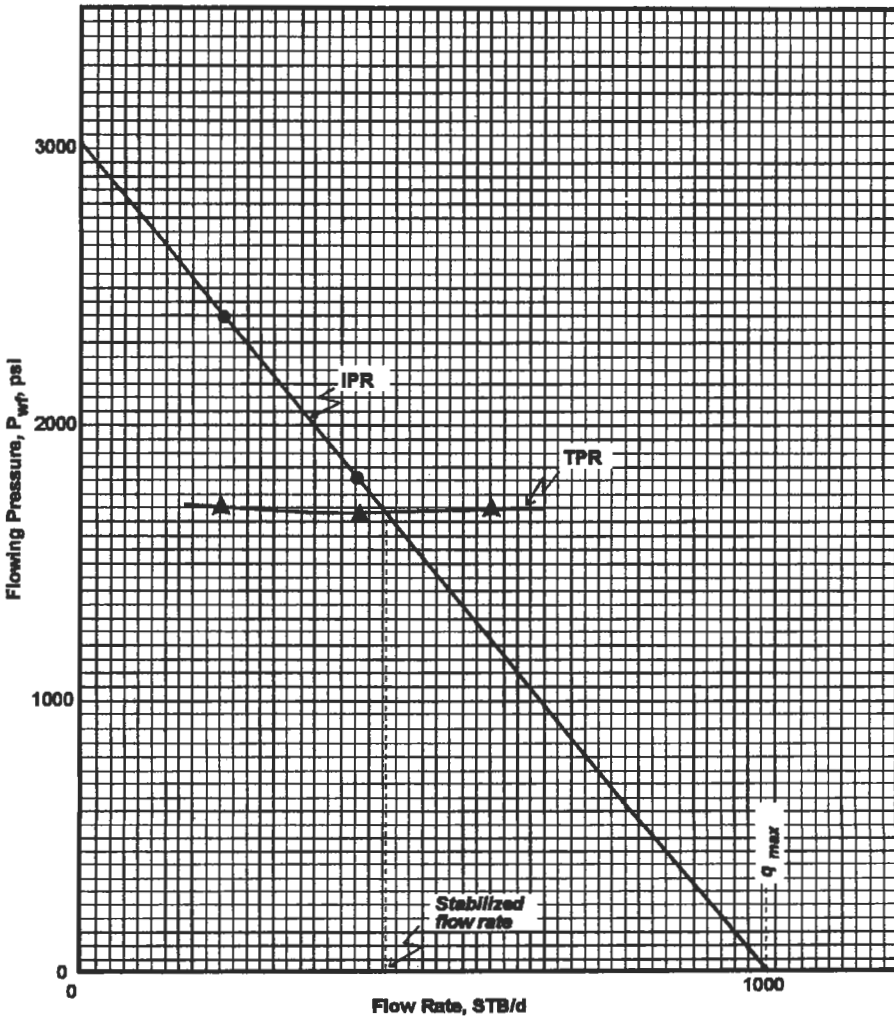


Figure 6-82. Pressure-rate relationship for Examples A and B on pages 542 to 544.

3. The theoretical maximum flowrate is:

$$q_{\max} = 0.333(3,000 - 0) = 1,000 \text{ stb/d}$$

Example B

The well illustrated in Example A has vertical depth of 4,100 ft. Tubing string of $2\frac{3}{8}$ in. has been installed. The flowing pressure at wellhead is 210 psi. What is the stabilized oil rate achieved?

Solution

Using Gilbert's correlation we obtain:

q, stb/d	P _{wf} , psi
200	1,700
400	1,695
600	1,690

Plot these values of q and P_{wf} on the same graph paper used for solving problem Example A above (see Figure 6-82). What we get is the TPR curve intersecting the IPR curve. This intersection represents the stabilized rate achieved, which is 435 stb/d.

Example C

The oil well of Example A is producing 25°API oil. If a positive choke with diameter of $\frac{1}{64}$ in. is installed at the wellhead, determine the pressure at the downstream of the choke.

Solution

$$\gamma_o = \frac{141.5}{131.5 + 25} \times 62.4 = 56.42 \text{ lb/ft}^3$$

Rearranging Equation 6-138 and assuming that C ≈ 1.0

$$\Delta P = 56.42 \times \left(\frac{435}{10,285(1.0)(0.03758)} \right)^2 = 72 \text{ psi}$$

$$P_{\text{downstream}} = (210 - 72) \text{ psi} = 138 \text{ psi}$$

Gas Flow Performances

As for oil wells, performance curves characterizing a gas production system are very useful tools used to visualize and graphically predict the effects of declining reservoir pressure, changes in tubular size, increasing water production or installing gas compressors.

Gas Inflow Performance

A mathematical expression commonly used to relate gas flowrate and flowing bottomhole pressure is

$$q = C(P_r^2 - P_{wf}^2)^n \tag{6-139}$$

where q = gas flowrate in Mscf/d

P_r = shut-in reservoir pressure in psia

P_{wf} = flowing bottomhole pressure in psia

C = stabilized performance coefficient, constant

n = numerical exponent, constant

Equation 6-139 was firstly introduced by Rawlins and Schellhardt [32] in 1935 and is known as a back-pressure equation. From gas well test data, plotting q versus $(P_r^2 - P_{wf}^2)$ on a log-log graph will give a straight line passing through the data points, see Figure 6-83. This plot was made based on a stabilized four-point test. The information that can be obtained from this plot is the absolute

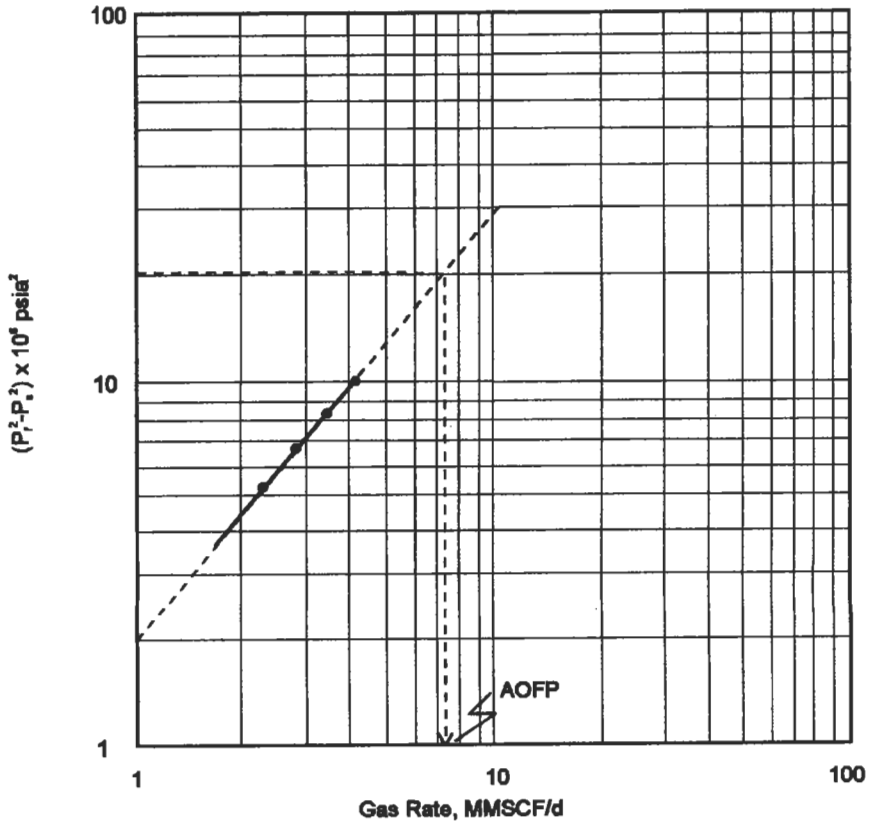


Figure 6-83. Stabilized four-point test and open flow potential of a gas well.

open flow potential (AOFP) of the well. This is defined as the theoretical maximum flowrate when flowing pressure at the sand face is zero.

Determination of the exponent n and the coefficient C is given here using Figure 6-83 as follows.

1. Choose two values of q arbitrarily but separated one cycle each other.
2. Read corresponding values of $(P_r^2 - P_{wf}^2)$.
3. Calculate

$$n = 1/\text{slope} = \frac{\log q_2 - \log q_1}{\log(P_r^2 - P_{wf}^2)_2 - \log(P_r^2 - P_{wf}^2)_1}$$

Choosing $q_1 = 1$ gives $(P_r^2 - P_{wf}^2)_1 = 1.5$ and $q_2 = 10$ gives $(P_r^2 - P_{wf}^2)_2 = 20\%$. Then

$$n = \frac{\log 10 - \log 1}{\log 20.7 - \log 1.5} = 0.877$$

4. Rearranging Equation 6-139 we obtain

$$C = \frac{q}{(P_r^2 - P_{wf}^2)^n} = \frac{10,000}{(20.7 \times 10^6)^{0.877}} = 3.84 \times 10^{-3} \text{ Mscf/d/psia}^{2n}$$

The AOFP of the well can then be calculated as

$$\begin{aligned} \text{AOFP} = q_{\max} &= 3.84 \times 10^{-3}(3887^2 - 0^2)^{0.877} = 7,585 \text{ Mscf/d} \\ &= 7.585 \text{ MMscf/d} \end{aligned}$$

From the graph, the AOFP = 7.6 MMscf/d

The inflow performance relationship curve can be constructed by using the deliverability equation above. By taking some values of P_{wf} arbitrarily, the corresponding q 's can be calculated. The IPR curve for the example here is shown in Figure 6-84.

For situations where multipoint tests cannot be run due to economic or other reasons, single-point test data can be used to generate the inflow performance curve provided that a shutin bottomhole pressure is known. Mishra and Caudle [33] proposed a simple method for generating a gas IPR curve from just a single-point test data. Employing the basic gas flow in term of pseudo-pressure function, they developed a dimensionless IPR curve to be used as a reference curve. As an alternative, the dimensionless IPR equation to the best-fit curve is introduced

$$\frac{q}{q_{\max}} = \frac{5}{4} \left(1 - 5 \frac{m(P_{wf}) - 1}{m(P_r)} \right) \quad (6-140)$$

where q_{\max} = AOFP in Mscf/d

$m(P_{wf})$ = pseudo-pressure function for real gas and defined as

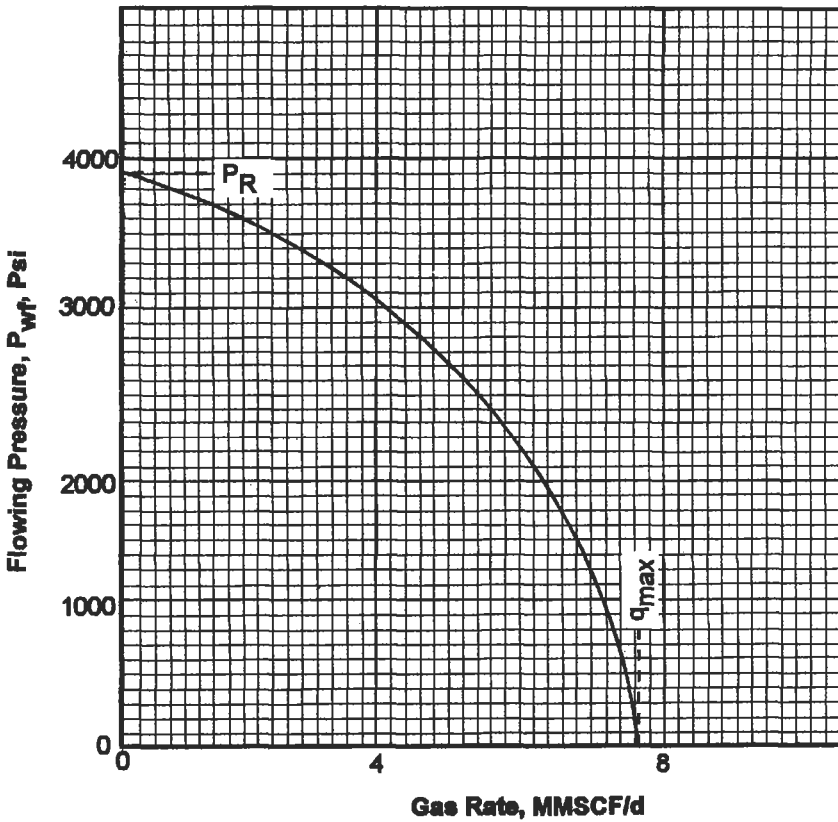


Figure 6-84. Inflow performance relationship for a gas reservoir.

$$m(P_{wf}) = 2 \int_{P_b}^{P_{wf}} \left(\frac{P}{\mu Z} \right) dP$$

$$m(P_r) = 2 \int_{P_b}^{P_r} \left(\frac{P}{\mu Z} \right) dP \tag{6-141}$$

where μ = gas viscosity (function of P at isothermal condition) in cp
 Z = gas compressibility factor, dimensionless

The use of pseudopressure function is quite complex. A numerical integration technique, however, can be applied to this problem. A detail example in applying this numerical technique can be found in a reservoir engineering textbook [34].

More recently, Chase and Anthony [35] offered a simpler method that is a modification to the Mishra-Caudle method. The method proposed involves substitution of real pressure P or P² for the real gas pseudopressure function m(P). The squared pressure P² is used for pressures less than approximately 2,100 psia, and the relevant equation is

$$\frac{q}{q_{\max}} = \frac{5}{4} \left(1 - 5 \left(\frac{P_{wf}}{P_r} - 1 \right) \right) \quad (6-142)$$

The real pressure P is suggested for pressures greater than approximately 2,900 psia. By having the average reservoir pressure P_r , and a single-point test data P_{wf} and q , it is possible to determine the AOF P and to generate the inflow performance curve:

$$\frac{q}{q_{\max}} = \frac{5}{4} \left(1 - 5 \left(\frac{P_{wf}}{P} - 1 \right) \right) \quad (6-143)$$

For pressures ranging from 2,100 to 2,900 psia, the original Mishra-Caudle's technique is recommended.

Low-Permeability Well Tests. The requirement of the back-pressure method of testing is that the data be obtained under stabilized conditions. That means that the coefficient C of Equation 6-139 is constant with time. This coefficient depends on reservoir characteristics, extent of drainage radius and produced fluid characteristics.

Wells completed in highly permeable formations stabilize quickly. As demand for gas increased over the years, wells were completed in less permeable formations. In wells of this type the stabilization period may be very long. Therefore, methods were needed that would permit testing of this type of well without undue waste of time.

In 1955 M. H. Cullender described the isochronal method for determining flow characteristics [36]. The method is based on the assumption that the slope of performance curves of gas wells, exponent n of Equation 6-139, is independent of the drainage area. It is established almost immediately after the well is opened. However, the performance coefficient C decreases with time as the radius of drainage recedes from the well. When the radius reaches the boundary of the reservoir or the area of interference of another well, C becomes a constant and the flow is stabilized.

Under the method the well is opened, the flow and pressure data are obtained at specific time intervals without changing the rate of flow. The well is then closed in until the shut-in pressure is reached, approximately the same as at the beginning of the first test. The well is then opened, produced at a different rate, and the pressure and flow data are collected. This procedure is repeated as many times as desired.

Plotting of these data on log-log paper results in a series of parallel lines, the slope of which gives the coefficient n . This is illustrated in Figure 6-85. Relationship of coefficient C and time for a gas well is illustrated in Figure 6-86.

From these test and theoretical considerations different procedures have been developed that permit prediction of the coefficients of performance of gas wells produced from low-permeability formations.

Predicting Future IPR. Predicting the wells' deliverability is important to be able to plan some changes required to maintain the production capacity. Here simple but reliable methods are introduced to forecasting future inflow performance gas wells.

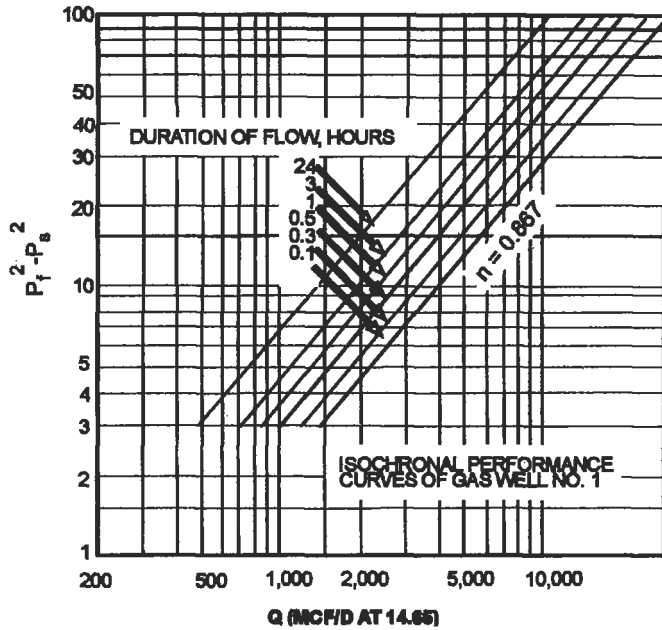


Figure 6-85. Isochronal performance curves of gas well no. 1.

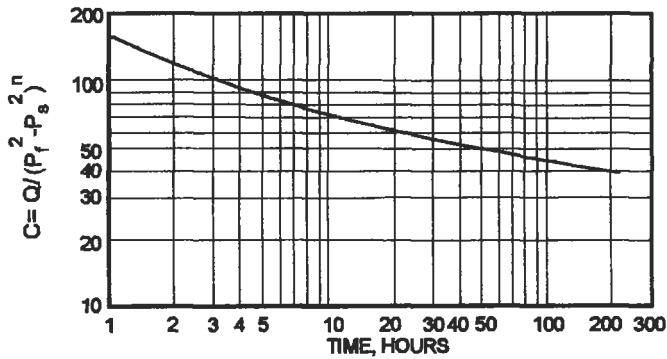


Figure 6-86. Relationship of coefficient of performance and time of gas well no. 3.

Accompanying Equation 6-140, Mishra and Caudle presented an empirical equation for predicting gas wells productivity [33]. The equation is

$$\frac{(q_{max})_f}{(q_{max})_p} = \frac{5}{3} \left(1 - 0.4 \frac{m(R)_f}{m(R)_p} \right) \tag{6-144}$$

where subscripts f and p refer to future and present time, respectively. Later, Chase and Anthony [35] also proposed the simplified form of Equation 6-144 by substituting real pressure for pseudo-pressure function.

To estimate the AOF of a gas well, one does not have to run well tests as discussed above. An alternative method is to calculate bottomhole pressure, static and flowing, without running a pressure gage down into the well, by knowing pressures at the wellhead. The calculation of flowing bottomhole pressures will be discussed later. Below, the equations for calculating static bottomhole pressure are given.

One of the most common methods in estimating static bottomhole pressure of a gas well is that of Cullender and Smith, which treats the gas compressibility factor as a function of depth [37]. If we divide the well by equal length, one can calculate the static bottomhole pressure as follows:

1. Having a knowledge of static wellhead pressure, pressure at midpoint of the well is calculated by trial and error:

$$0.0375G_g \frac{H}{2} = (P_{ms} - P_{ws})(I_{ms} - I_{ws}) \quad (6-145)$$

where G_g = gas gravity (air = 1.0)
 H = well depth in ft

$$I_{ms} = (T_{ms} \times Z_{ms})/P_{ms} \quad (6-146)$$

T_{ms} = absolute temperature at midpoint in °R
 P_{ms} = pressure at midpoint (assumed to calculate Z_{ms}) in psia
 Z_{ms} = gas compressibility factor evaluated at T_{ms} and P_{ms}
 P_{ws} = static wellhead pressure in psia

$$I_{ws} = \frac{T_{ws} Z_{ws}}{P_{ws}} \quad (6-147)$$

T_{ws} = absolute temperature at wellhead in °R
 Z_{ws} = gas compressibility factor evaluated at T_{ws} and P_{ws}

The problem here is to calculate P_{ms} . If calculated $P_{ms} \approx P_{ms}$ assumed to determine Z_{ms} , then calculation of bottomhole pressure is the next step. If not, use calculated P_{ms} to determine new Z_{ms} and again use Equations 6-146 and 6-147 to calculate a new P_{ms} . Repeat this procedure until calculated P_{ms} is close to assumed P_{ms} .

2. The same procedure is used, and the equation for static bottomhole pressure P_{bs} is

$$0.0375G_g \frac{H}{2} = (P_{bs} - P_{ms})(I_{bs} + I_{ms}) \quad (6-148)$$

3. The very last step is to apply Simpson's rule to calculate P_{bs} :

$$0.0375G_g H = \frac{P_{bs} - P_{ws}}{3} (I_{ws} + 4I_{ms} + I_{bs}) \quad (6-149)$$

For wells producing some liquids, the gas gravity G_g in Equations 6-145 and 6-148 must be replaced by γ_{mix} :

$$G_{mix} = \frac{G_g + 4584G_o/R}{1 + 132800G_o/RM_o} \tag{6-150}$$

where G_{mix} = specific gravity of mixture (air = 1.00)
 G_g = dry gas gravity
 G_o = oil gravity
 R = surface producing gas-oil ratio in scf/stb
 M_o = molecular weight of oil in lbm/lb-mole

The G_{mix} is then used to determine the pseudocritical properties for calculation of the compressibility factor.

If water production is quite significant, the following equation may be used [38]:

$$G_{mix} = \frac{G_g + 4,584 \left(\frac{G_o}{R} + \frac{1}{R_w} \right)}{1 + 132,800 \left(\frac{G_o}{RM_o} + \frac{1}{18R_w} \right)} \tag{6-151}$$

where R_w = producing gas/water ratio in scf/stb

Tubing Performance

In a gas well, tubing performance can be defined as the behavior of the well in producing the reservoir gas through the tubing installed. At a specified surface pressure, the flowing bottomhole pressure can be calculated by using an equation for vertical flow of gas. Katz presented the equation that is simple but valid only for dry gas [39]:

$$q_g = 200,000 \left(\frac{sD^5 (P_{wf}^2 - e^f P_{wh}^2)}{G_g \bar{T} Z H f (e^f - 1)} \right)^{0.5} \tag{6-152}$$

where q_g = gas flowrate in scf/d
 D = diameter of tubing in in.
 P_{wf} = bottomhole flowing pressure in psia
 P_{wh} = wellhead flowing pressure in psia
 G_g = gas gravity (air = 1.0)
 \bar{T} = average temperature in °R
 Z = average gas compressibility factor
 H = vertical depth in ft
 f = friction factor = $\{2\log[3.71/(\epsilon/D)]\}^{-2}$
 ϵ = absolute pipe roughness, $\cong 0.0006$ in.

$$s = 0.0375G_g H/\bar{T}Z \tag{6-153}$$

The average temperature used in the Equation 6-152 is simply the arithmetic average between wellhead temperature and bottomhole temperature. The gas compressibility factor \bar{Z} is evaluated at the average temperature and the arithmetic average between the flowing wellhead and bottomhole pressures. This method is a trial-and-error technique, but one or two iterations is usually sufficiently accurate.

By knowing all parameters in Equation 6-152 but q_g and P_{wf} , the tubing performance curve (TPR) can then be constructed. The use of TPR here is the same as discussed previously for oil wells. Figure 6-87 shows an idea of the effect of wellhead pressure on a well deliverability. A decrease in P_{wh} , thus an increase in flowrate, can be done by changing a choke/bean diameter to a bigger one.

For a specified wellhead pressure, the flowing bottomhole pressure can be estimated as a function of flowrate and tubing diameter. Equation 6-152 can be used to do this.

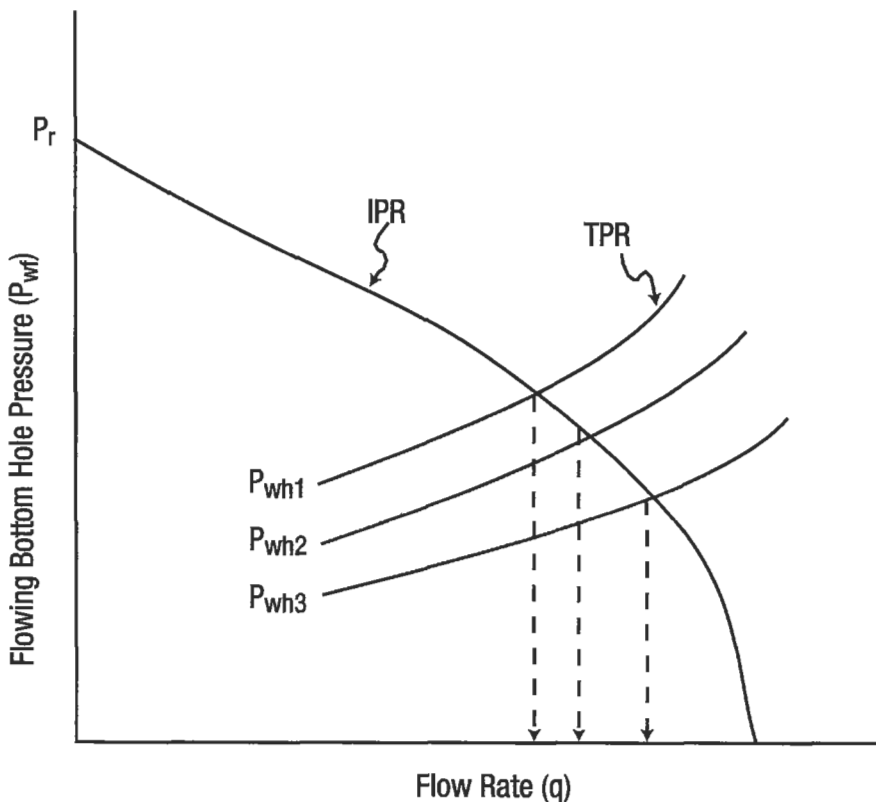


Figure 6-87. Effect of well head pressure on gas well deliverability.

In many cases gas wells produce some liquids along with the gas itself. The equations for dry gas should be modified to account for liquid content. One of the modifications presented in the literature was made by Peffer, Miller and Hill [38]. For steady-state flow and assuming that the effects of kinetic energy are negligible, the energy balance can be arranged and written as:

$$\frac{G_g H}{53.34} = \int_{P_{wh}}^{P_{wf}} \frac{\left(\frac{P}{TZ}\right)}{F^2 + \left(\frac{P}{TZ}\right)^2} dP \tag{6-154}$$

where P_{wf} = flowing bottomhole pressure in psia
 P_{wh} = flowing wellhead pressure in psia

$$F^2 = \frac{2666.5fQ^2}{d^5} \tag{6-155}$$

d = inside diameter of tubing in in.
 f = friction factor, dimensionless
 Q = flowrate, MMscf/d

Evaluation of friction factor f depends on the stream fluids in the well. For single-phase (dry gas) and fully developed turbulent flow with an absolute roughness of 0.0006 in., Cullender and Smith [37] suggested the use of

$$F = \frac{0.10797Q}{d^{2.612}} \quad \text{for } d < 4.277 \text{ in.} \tag{6-156}$$

and

$$F = \frac{0.10337Q}{d^{2.582}} \quad \text{for } d > 4.277 \text{ in.} \tag{6-157}$$

When some liquids are present in the flowing stream Peffer *et al.* suggested the use an apparent roughness of 0.0018 instead of using an absolute roughness of 0.0006. Also, adjustment in specific gravity of the fluids should be made by using Equations 6-150 or 6-151. Applying these adjustments, the method of Cullender and Smith may be used for a wide range of gas-condensate well condition.

However, whenever the Reynold's number for a specific condition can be calculated and pipe specifications are available, the friction factor can then be easily determined to be used for pressure loss calculations. Equations 6-158 and 6-159 can be used to calculate the Reynold's number and friction factor, respectively:

$$R_e = \frac{20011G_g Q}{\mu_g d} \tag{6-158}$$

$$\frac{1}{\sqrt{f}} = 2.28 - 4 \log \left(\frac{\epsilon}{d} + \frac{21.28}{R_e^{0.9}} \right) \tag{6-159}$$

where R_c = Reynolds number
 G_g = gas gravity (air = 1.00)
 Q_g = gas flowrate in MMscf/d
 μ_g = gas viscosity in cp
 d = inside diameter of pipe in in.
 ϵ = absolute roughness in in.
 f = friction factor, dimensionless

For a well divided in equal lengths the upper half of the well has a relation

$$37.5 G_g \frac{H}{2} = (P_{MF} - P_{WH})(I_{MF} + I_{WH}) \quad (6-160)$$

where P_{MF} = flowing pressure at midpoint in psia
 P_{WH} = flowing wellhead pressure in psia
 $I = (P/TZ)/[F^2 + (P/TZ)^2]$
 F = shown in Equation 6-146
 H = well depth in ft

and the lower half of the well has the relation

$$37.5 G_g \frac{H}{2} = (P_{WF} - P_{MF})(I_{WF} + I_{MF}) \quad (6-161)$$

where P_{WF} = flowing bottomhole pressure in psia
 After trial and error as previously discussed, Simpson's rule applies:

$$37.5 G_g H = \frac{P_{WF} - P_{WH}}{3} (I_{WH} + 4I_{MF} + I_{WF}) \quad (6-162)$$

Choke Performance

Chokes or beans are frequently installed in gas wells. These restrictions can be at the surface or at the subsurface. A surface choke is usually installed for:

1. regulating production rate
2. maintaining sufficient back pressure to avoid sand production
3. protecting surface equipment from pressure surge
4. preventing water coning
5. obeying regulatory bodies

Subsurface restrictions can be a tubing safety valve, a bottomhole choke or a check valve. A tubing safety valve functions to stop flowstream whenever the surface control equipment is damaged or completely removed. A bottomhole choke is installed if low wellhead pressure is required or freezing of surface control equipment and lines are expected. A check valve is installed to prevent backflow of an injection well. Basically there are two types of flow conditions: subsonic or subcritical flow and sonic flow. The criteria to distinguish subsonic from sonic flow has been discussed previously in the section titled "Choke Performance."

For subsonic flow, the following equation given by Nind can be used to calculate gas flowrate [40].

$$Q = 1248CAP_u \left\{ \frac{k}{(k-1)G_g T_u} \left[\left(\frac{P_d}{P_u} \right)^{2/k} - \left(\frac{P_d}{P_u} \right)^{\frac{k+1}{k}} \right] \right\}^{0.5} \quad (6-163)$$

where Q = gas flowrate in Mcf/d
 C = discharge coefficient, ≈ 0.86
 A = cross-sectional area of choke or restriction in in.²
 P_u = upstream pressure in psia
 P_d = downstream pressure in psia
 G_g = gas gravity (air = 1.00)
 T_u^g = upstream temperature in °R
 k = specific heat ratio, C_p/C_v

Equation 6-163 shows that subsonic flow is affected by upstream and downstream pressure.

In critical or sonic flow, gas flowrate depends only on upstream pressure as shown as

$$Q = 879CAP_u \left[\frac{k}{G_g T_u} \left(\frac{2}{k+1} \right)^{\frac{k+1}{k-1}} \right]^{0.5} \quad (6-164)$$

where Q = flowrate in Mcf/d
 C = discharge coefficient
 A = choke area in in.²
 P_u = upstream pressure in psia
 T_u^g = upstream temperature in °R
 G_g = gas gravity (air = 1.00)
 k = specific heat ratio

The discharge coefficient C can be determined using Figure 6-79 by having a knowledge of diameter ratio β and Reynold's number. Reynolds number may be calculated using the following equation:

$$R_e = \frac{20.011QG_g}{\mu_g d} \quad (6-165)$$

where Q = gas flowrate in Mcf/d
 G_g = gas gravity (air = 1.00)
 μ_g = gas viscosity, evaluated at upstream pressure and temperature in cp
 d = internal diameter of pipe (not choke) in in.

Gas flow through restriction (orifice) may also be estimated using Figure 6-88. For conditions that differ from chart basis, correction factors are required. A gas throughput read from the chart must be multiplied by the proper correction factor,

$$Q = \text{Gas throughput} \times 0.0544 \sqrt{G_g T}, \text{ Mcf/d} \quad (6-166)$$

where T is the absolute operating temperature in °R.

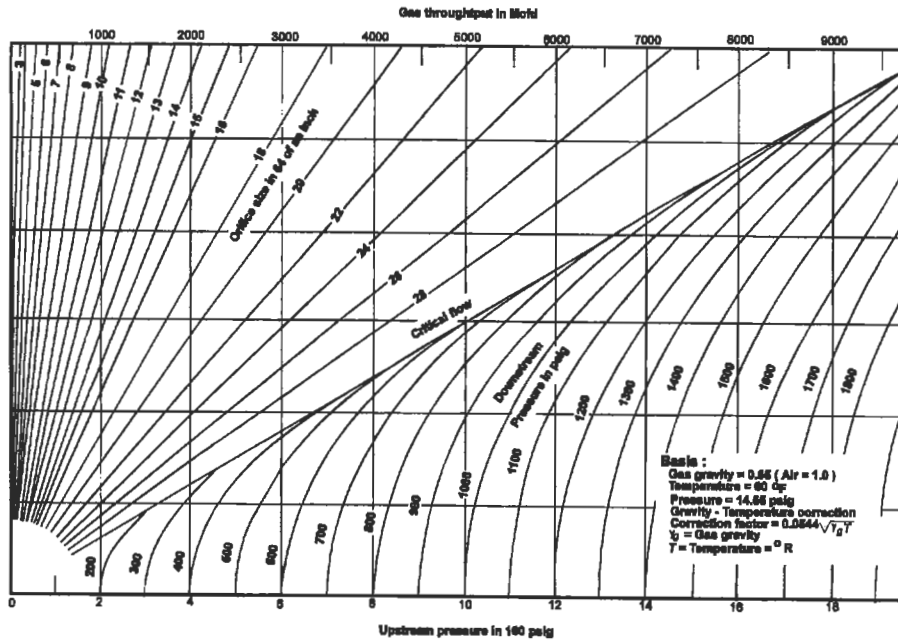


Figure 6-88. A correlation for gas flow through orifice [41].

Flowline Performance

For a single-phase gas flow, pressure-rate relation may be obtained from a known Weymouth equation,

$$Q = 433.49 \frac{T_b}{P_b} \left(\frac{(P_u^2 - P_d^2) d^{16/3}}{G_g \bar{T} Z L} \right)^{0.5} E \tag{6-167}$$

- where Q = gas flowrate in scf/d
- T_b = base temperature in °R
- P_b = base pressure in psia
- P_u = upstream pressure in psia
- P_d = downstream pressure in psia
- d = inside diameter of pipe in in.
- G_g = gas gravity (air = 1.00)
- \bar{T} = average flow line temperature in °R
- \bar{Z} = average gas compressibility factor
- L = pipe length in mi
- E = pipe line efficiency, fraction

or the modified Panhandle (Panhandle B) equation (for long lines),

$$Q = 737 \left(\frac{T_b}{P_b} \right)^{1.02} \left(\frac{P_u^2 - P_d^2}{\bar{T} Z L G_g^{0.961}} \right)^{0.510} d^{2.530} E \tag{6-168}$$

with terms and units the same as in the Weymouth equation.

The pipeline efficiency E depends on flowstream and pipeline conditions. A gas stream may contain some liquids; the higher the liquid content, the lower the line efficiency. The pipeline may be scaled, or condensate-water may accumulate in low spots in the line. Ikoku presents the information about line efficiency as shown below [41].

Type of line	Liquid Content	E (gal/MMcf)
Dry-gas field	0.1	0.92
Casing-head gas	7.2	0.77
Gas and condensate	800	0.60

This gives an idea in estimating E for a particular condition.

Example A [33]

A gas well was flowed at a rate of 7.20 MMscf/d. The stabilized sandface pressure at the end of the flow test was 1,155 psia, and the current average reservoir pressure was estimated to be 1,930 psia. Determine the following parameters using modified Mishra-Caudle’s method:

- (a) AOFPP at current conditions ($P_r = 1,930$ psia)
- (b) deliverability at $P_{wf} = 1,000$ psia
- (c) AOFPP at a future average pressure $P_{ri} = 1,600$ psia
- (d) deliverability at a future $P_{wf_i} = 1,155$ psia

Solution

The readers may refer to the original paper. Here the modified one is given.

(a) For a pressure less than 2,100 psia, Equation 6-142 is used.

$$\frac{q}{q_{max}} = \frac{5}{4} \left[1 - 5 \left(\frac{P_w^2}{P_r^2} - 1 \right) \right]$$

$$AOFPP = q_{max} = \frac{7.2 \text{ MMscf/d}}{\frac{5}{4} \left[1 - 5 \left(\frac{1155^2}{1930^2} - 1 \right) \right]} = 8.94 \text{ MMscf/d}$$

$$\begin{aligned} \text{(b) } q &= 8.94 \times 10^6 \times \frac{5}{4} \left[1 - 5 \left(\frac{1000^2}{1930^2} - 1 \right) \right] \\ &= 7.73 \text{ MMscf/d} \end{aligned}$$

$$(c) \frac{(\text{AOF})_f}{(\text{AOF})_p} = \frac{5}{3} \left[1 - 0.4 \frac{P_{wf}^2}{P_p^2} \right]$$

$$\begin{aligned} (\text{AOF})_f &= 8.94 \times 10^6 \times \frac{5}{3} \left(1 - 0.4 \frac{1600^2}{1990^2} \right) \\ &= 6.96 \text{ MMscf/d} \end{aligned}$$

(d) Again use Equation 6-142:

$$\begin{aligned} q_f &= (\text{AOF}) \times \frac{5}{4} \left[1 - 5 \left(\frac{P_{wf}^2}{P_p^2} \right)^{-1} \right] \\ &= 6.96 \times 10^6 \times \frac{5}{4} \left[1 - 5 \left(\frac{1155}{1600} \right)^{-1} \right] \\ &= 4.675 \text{ MMscf/d} \end{aligned}$$

Example B

The following data are obtained from a producing gas well.

Gas gravity = 0.65
 Well depth (vertical) = 6,000 ft
 Wellhead temperature = 570°R
 Formation temperature = 630°R
 Flowing wellhead pressure = 1,165 psia
 Flowrate = 10.0 MMscf/d
 Tubing ID = 2.441 in.
 Pseudocritical temperature = 374°R
 Pseudocritical pressure = 669 psia
 Absolute roughness = 0.00065

Calculate the following bottomhole pressure using Equation 6-152

Solution

Rearranging Equation 6-152 we obtain

$$P_{wf} = \left(e^s P_{wh}^2 + \frac{q_g^2}{4 \times 10^{10}} \times \frac{G_g \overline{TZ} H_f (e^s - 1)}{SD^5} \right)^{0.5}$$

Assume $P_{wf} = 2,000$ psia:

$$\bar{P} = \frac{2,000 + 1,165}{2} = 1,582.5 \text{ psia}$$

$$T = \frac{570 + 630}{2} = 600^\circ \text{R}$$

$$\left. \begin{aligned} pP_r &= \frac{1,582.5}{669} = 2.365 \\ pT_r &= \frac{600}{374} = 1.064 \end{aligned} \right\} \rightarrow \bar{Z} = 0.848$$

$$S = 0.0375(0.65)(6,000)/(600)(0.848) = 0.287$$

$$f = \left\{ 2 \log \left[371 / \left(\frac{0.00065}{2.441} \right) \right] \right\}^{-2}$$

$$\begin{aligned} P_{wf} &= \left\{ e^{0.287(1,165)^2} + \frac{(10 \times 10^6)^2}{4 \times 10^{10}} \times \frac{(0.65)(600)(0.848)(6,000)}{(0.287)(2.441)^5} \times [0.0146(e^{0.287} - 1)] \right\}^{0.5} \\ &= 1,666 \text{ psia } (<< 2,000 \text{ psia assumed}) \end{aligned}$$

Assume 2nd $P_{wf} = 1,666$ psia:

$$\bar{P} = \frac{1,666 + 1,165}{2} = 141.5 \text{ psia}$$

$$\left. \begin{aligned} pP_r &= \frac{141.5}{669} = 2.116 \\ pT_r &= 1.604 \end{aligned} \right\} \rightarrow \bar{Z} = 0.857$$

$$S = 0.0375(0.65)(6,000)/(600)(0.857)$$

$$P_{wf} = 1,666.7 \text{ psia } (\cong 1,666 \text{ psia assumed})$$

To construct the tubing performance curve for a specific P_{wh} , some other values of q_g can be chosen and calculate for P_{wf} using the same procedure. To simplify, \bar{Z} could be kept constant so that no more trial and error.

Example C

Suppose the gas well in the example B is produced through a flowline of 2.5 in. in diameter and 1,250 ft long. The average operating temperature is 100°F. Additional data given are specific heat ratio, $k = 1.3$ and the estimated gas viscosity at the operating condition, $\mu_g = 0.0131$ cp.

Find the positive choke size required for critical condition, and the pressure at downstream of the flowline.

Solution

(1) For a critical flow, Equation 6-164 can be used.

$$\begin{aligned}
 Q &= 879 \times C \times A \times P_u \left[\frac{k}{G_g T_u} \left(\frac{2}{k+1} \right)^{\frac{k+1}{k-1}} \right]^{0.5} \\
 &= 879 \times C \times \frac{\pi}{4} d_{ch}^2 \times 1165 \left[\frac{1.3}{0.65 \times 570} \left(\frac{2}{1.3+1} \right)^{\frac{1.3+1}{1.3-1}} \right]^{0.5} = 27,881 C d_{ch}^2 \text{ (Mscf/d)}
 \end{aligned}$$

$$R_e = \frac{20 \times 10,100 \times 0.65}{0.013 \times 2.5} = 4.01 \times 10^6$$

Assume a diameter choke, such that $d_{ch} = 0.7$ in. Use Figure 6-79 to find coefficient C:

$$\beta = \frac{d_{ch}}{d_{pipe}} = \frac{0.7}{2.5} = 0.28$$

For $R_e = 4.01 \times 10^6$ and $\beta = 0.28$, $C = 0.998$, so

$$Q = 27,881 \times 0.998 \times (0.7)^2 = 13.63 \text{ MMscf/d.}$$

If we assume another choke size, let $d_{ch} = 0.6$ in.:

$$\beta = \frac{0.6}{2.5} = 0.24 \rightarrow C = 0.997$$

$$Q = 27,881 \times 0.997 \times (0.6)^2 = 10.0 \text{ MMscf/d}$$

(2) For a critical flow, we may assume $(P_{d/choke}) = 0.5(P_{u/choke})$. Let's take $T_b = 530^\circ\text{R}$ and $P_b = 15$ psia. Then using Equation 6-167 with $E = 0.92$,

$$\begin{aligned}
 P_d^2 &= P_u^2 - \left(\frac{Q/E}{433.4 T_b/P_b} \right)^2 \times \frac{G_g \bar{T} Z L}{d^{1.93}} \\
 &= \left(\frac{1165}{2} \right)^2 - \left(\frac{10^7/0.92}{15,317} \right)^2 \times \frac{(0.65)(560)(\bar{Z}) \left(\frac{1250}{5280} \right)}{(2.5)^{1.93}} = 339,306 - 327,422 \bar{Z}
 \end{aligned}$$

Assume that $P_d = 200$ psia to find \bar{Z} such that

$$\bar{P} = \frac{200 + (0.5 \times 1165)}{2} = 391.2 \text{ psia}$$

$$\left. \begin{aligned} pP_r &= \frac{391.25}{669} = 0.585 \\ pT_r &= \frac{560}{374} = 1.497 \end{aligned} \right\} \rightarrow \bar{Z} = 0.939$$

$$P_d^2 = 339,306 - 327,422 \times 0.939$$

$$P_d = 178.5 \text{ psi} (\neq P_{d_{\text{assumed}}} = 200 \text{ psia})$$

Assume now that $P_d = 178.5$ psia such that

$$\bar{P} = \frac{178.5 + (0.5 \times 1165)}{2} = 380.5 \text{ psia}$$

$$\left. \begin{aligned} pP_r &= \frac{380.5}{669} = 0.569 \\ pT_r &= 1.497 \end{aligned} \right\} \rightarrow \sim \bar{Z} = 0.940$$

$$P_d^2 = 339,306 - 327,422 \times 0.940$$

$$P_d = 177.5 \text{ psia} (\cong P_{d_{\text{assumed}}} = 178.5 \text{ psia})$$

Two-Phase Flow Performance

Two-Phase Inflow Performance

When a reservoir pressure is below the bubble point pressure, the simple equation of inflow performance (e.g., the productivity index is constant) is no longer valid, because at this condition the oil flowrate will decline much faster at increasing drawdown than would be predicted by Equation 6-131 or 6-132. An illustrative comparison of the two types of IPR is shown in Figure 6-89.

Vogel's Method. The well-known inflow performance equation for two-phase flow has been proposed by Vogel [42]. The equation is

$$\frac{q_o}{q_{\max}} = 1 - 0.2 \frac{P_{wf}}{P_r} - 0.8 \left(\frac{P_{wf}}{P_r} \right)^2 \quad (6-169)$$

which fits a general dimensionless IPR shown in Figure 6-90. The reference curve and Equation 6-169 is valid for solution gas drive reservoir with reservoir pressures below the bubble point. The formation skin effect is not taken into account. The method is originally developed with flowing efficiency $FE = 1.0$. However, for a given well with any FE known, Equation 6-169 or the reference curve may be used to generate the IPR curve.

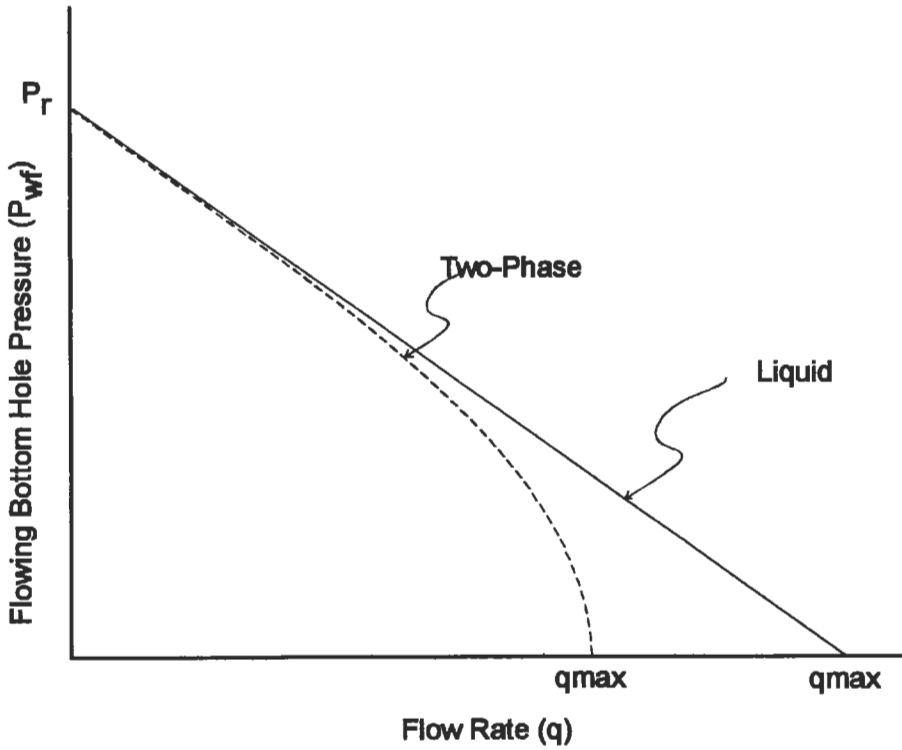


Figure 6-89. Illustrative comparison of liquid and two-phase IPR curves.

For reservoir pressures above the bubble point but with flowing pressures below the bubble point, the constant J equation and Vogel's equation can be combined to estimate the IPR curves. The equation is

$$q_o = q_b + (q_{max} - q_b) \left[1 - 0.2 \frac{P_{wf}}{P_r} - 0.8 \left(\frac{P_{wf}}{P_r} \right)^2 \right] \tag{6-170}$$

The maximum flowrate q_{max} is calculated using the following equation:

- where q_o = oil flowrate in stb/d
- q_{max} = the theoretical maximum flowrate when $P_{wf} = 0$ in stb/d
- q_b = oil flowrate at $P_{wf} = P_b$ in stb/d
- P_b = bubble point pressure in psia
- P_{wf} = flowing bottomhole pressure in psia
- P_r = average reservoir pressure in psia

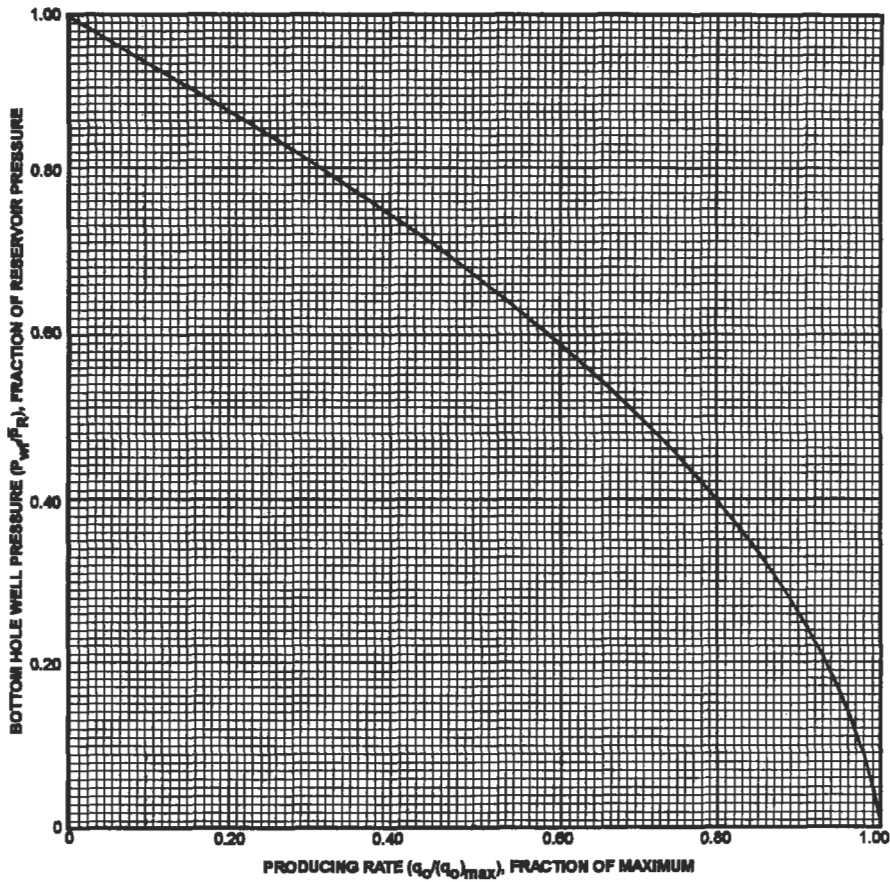


Figure 6-90. A general dimensionless IPR for solution gas drive reservoirs [42].

$$q_{max} = q_b + \frac{J \times P_b}{1.8} \tag{6-171}$$

The productivity index J is determined based on the flowing bottomhole pressure of the test:

1. For $(P_{wf})_{test} > P_b$, then
$$J = \frac{(q_o)_{test}}{P_r - (P_{wf})_{test}} \tag{6-172}$$

2. For $(P_{wf})_{test} < P_b$, then
$$J = \frac{(q_o)_{test}}{P_r - P_b + (P_b \times M/1.8)} \tag{6-173}$$

where $M = 1 - 0.2(P_{wf}/P_b) - 0.8(P_{wf}/P_r)^2$
 $P_{wf} = (P_{wf})_{test}$

The q_b is calculated using Equation 6-132 with $P_{wf} = P_b$

Fetkovich Method. Analyzing isochronal and flow-afterflow multipoint back-pressure tests conducted on oil wells, Fetkovich found that back-pressure curves for oil wells followed the same form as for gas wells [43]; that is

$$q_0 = J'_0(P_r^2 - P_{wf}^2)^n \quad (6-174)$$

where J'_0 = back-pressure curve coefficient, stb/d/(psia)²ⁿ
 n = back-pressure curve exponent or exponent of inflow performance curve

The plot of q_0 versus $(P_r^2 - P_{wf}^2)$ on log-log paper is considered as good as was obtained from gas well back-pressure tests. Conducting a multipoint back pressure test on a well, Equation 6-174 can be used to predict the IPR curve for the well.

Figure 6-91 shows a comparison of IPR's for liquid, gas and two-phase (gas and liquid). Fetkovich reported that Vogel's equation yields $n = 1.24$ (see Figure 6-92).

For reservoir pressures above bubble point pressures, the inflow performance curves can be constructed using the following equation:

$$q_0 = J'_0(P_b^2 - P_{wf}^2)^n + J(P_r - P_b) \quad (6-175)$$

The maximum flowrate of a well can be determined using the following equation:

$$q_{max} = q_0 \left[1 - \left(\frac{P_{wf}}{P_r} \right)^2 \right]^n \quad (6-176)$$

Modified Standing's Method. Vogel's reference curve is originally derived for undamaged or unformulated wells. In other words, the curve is only valid for wells with skin factor $s = 0$. Later, Standing presented a set of companion curves that can be used to predict IPR curves for damaged or stimulated wells [44]. His method is based on the definition of single-phase flow efficiency. In fact, solution-gas drive reservoirs producing oil at $P_{wf} < P_b$ and/or $P_r < P_b$ have inflow performance of two-phase flow. The IPR of this type of reservoirs have been shown to have quadratic forms as suggested by Vogel and Fetkovich.

Camacho and Raghavan found that Standing's definition of flow efficiency is incorrect to be used in two-phase flow behavior [45]. It is suggested that the definition of flow efficiency must also reflect the quadratic form of the inflow performance equation. This is expressed by

$$FE = \frac{(1 + VP'_{wf}/P_r)(1 - P'_{wf}/P_r)}{(1 + VP_{wf}/P_r)(1 - P_{wf}/P_r)} \quad (6-177)$$

where FE = flowing efficiency

V = quadratic curve factor ($V = 0.8$ for Vogel and $V = 1.0$ for Fetkovich)

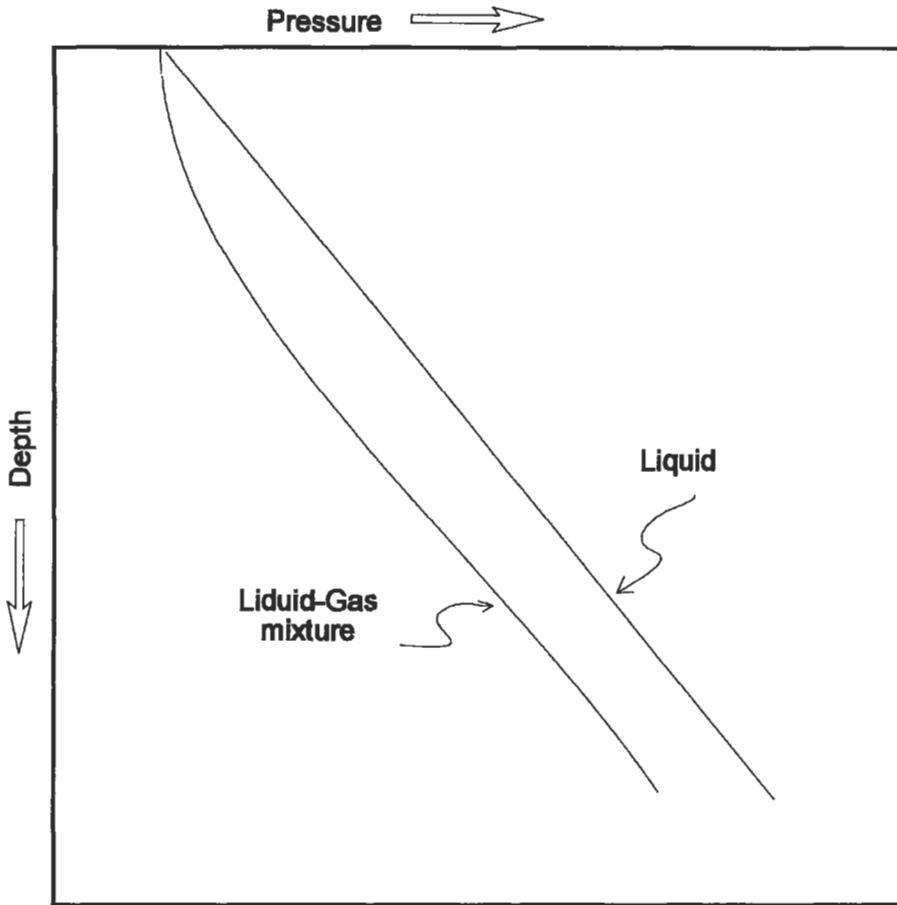


Figure 6-91. Pressure gradients of flowing liquid and liquid-gas mixture.

P'_{wf} = ideal flowing bottom hole pressure (e.g., when skin factor $s = 0$) in psia

P_{wf} = actual flowing bottomhole pressure in psia

P_r = average reservoir pressure in psia

The flowrate when $FE \neq 1.0$ can be calculated using

$$\frac{q_0}{q_{max}^{FE=1.0}} = FE \left[1 + V \left(\frac{P_{wf}}{P_r} \right) \right] \left[1 - \left(\frac{P_{wf}}{P_r} \right) \right] \tag{6-178}$$

where $q_{max}^{FE=1.0}$ = maximum flow rate for undamaged/unstimulated well or when $FE = 1.0$

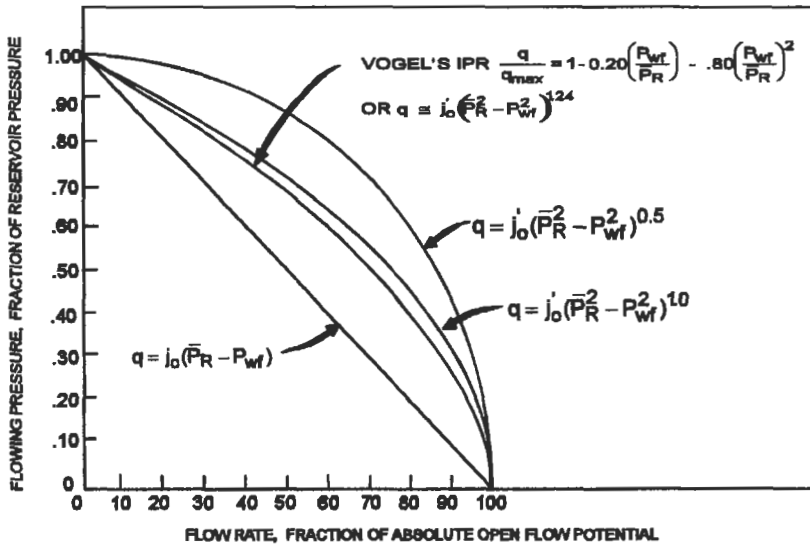


Figure 6-92. Inflow performance relationship for various flow equations [43].

Predicting Future IPR. Predicting future well deliverability is frequently needed in most oil fields. Some of the many reasons are

- to estimate when the choke should be changed or adjusted to maintain the production rate
- to predict well capability and evaluate if the tubing has to be changed
- to do planning for selecting future artificial lift methods
- to do planning reservoir pressure maintenance or secondary recovery project

Some prediction methods available in the literature are discussed.

Standing's Method [46]. The method has been developed based on Vogel's equation, the definition of productivity index and the assumption that the fluid saturation is to be the same everywhere in the reservoir. Three basic equations presented are

$$J_p^* = \frac{1.8(q_{max})_p}{(P_r)_p} \tag{6-179}$$

$$J_f^* = J_p^* \left\{ \frac{[K_{ro}/(\mu_o B_o)]_f}{[k_{ro}/(\mu_o B_o)]_p} \right\} \tag{6-180}$$

$$(q_{max})_f = (J_f^* \cdot P_{rf})/1.8 \tag{6-181}$$

where J^* = productivity index at zero drawdown in stb/d/psi
 k_{ro} = relative permeability to oil, fraction

μ_o = oil viscosity in cp
 B_o = oil formation volume factor in bbl/stb

and subscript p and f refer to present and future conditions, respectively. The relative permeability to oil is at corresponding oil saturation in the reservoir. A method for determining oil saturation and k_{ro} may be found in the reservoir engineering chapter. In the example presented by Standing, Tarner's method was used and k_{ro} was evaluated using Corey-type relationship:

$$K_{ro} = \left(\frac{S_o - S_{or}}{1 - S_{wc} - S_{or}} \right)^4 \tag{6-182}$$

where S_{or} = residual oil saturation, fraction
 S_{wc} = connate water saturation, fraction

Combined Fetkovich-Vogel Method. Fetkovich suggested that a future well deliverability may be estimated by the relation $J'_f/J'_p = (P_r)_f/(P_r)_p$. Recalling Equation 6-174 and taking $n = 1$ we can write

$$\frac{(q_{max})_f}{(q_{max})_p} = \left[\frac{(P_r)_f}{(P_r)_p} \right]^3 \tag{6-183a}$$

or

$$(q_{max})_f = (q_{max})_p \times \frac{(P_r)_f^3}{(P_r)_p^3} \tag{6-183b}$$

After calculating the maximum flowrate using Equation 6-183b, the inflow performance curve into future can be constructed using Vogel's equation. This method is valid only for undamaged wells.

Unified Method. Recently Kelkar and Cox proposed a new method for predicting future IPR [47]. This method is a result of unification of some methods discussed previously. The relationship suggested can be applied to any of the referenced methods. Two sets of data points (each at different average reservoir pressure) are required to predict the future inflow performance curve. The procedure is as follows:

1. Calculate the maximum flowrate (q_{max} or Q_{max}) for both tests conducted using the reference method (Vogel, Fetkovich or Modified Standing).
2. Calculate J^* :

$$J_1^* = \frac{(q_{max})_1}{(P_r)_1} \quad \text{and} \quad J_2^* = \frac{(q_{max})_2}{(P_r)_2} \tag{6-184}$$

3. Determine constants A' and B' as

$$A' = \frac{J_1^* - J_2^*}{(P_r)_1^2 - (P_r)_2^2} \tag{6-185}$$

$$B' = \frac{\frac{J_1^*}{(P_r^2)_1} - \frac{J_2^*}{(P_r^2)_2}}{\frac{1}{(P_r^2)_1} - \frac{1}{(P_r^2)_2}} \quad (6-186)$$

4. Calculate the maximum flowrate of the corresponding future pressure $(P_r)_f$:

$$(q_{\max})_f = A'(P_r^2)_f + B'(P_r)_f \quad (6-187)$$

5. Construct the future inflow performance curve using the reference inflow performance equation used in Step 1 above for reservoir pressure $(P_r)_f$ and the maximum flowrate calculated in Step 4.

Tubing Performance

The problem of simultaneous flow of oil, gas and water through the vertical tubing of an oil well is complex. The fluid is a compressible mixture, its density increasing with depth. The gradient line has a distinct curvature (see Figure 6-91). Along the gradient line of a given well different flow regimes occur, which may range from a mist flow in the region of low pressures to a single-phase flow at the pressures when all gas is in the solution.

The knowledge of tubing performance of flowing wells is important for efficient operations. Present and future performance of the wells may be evaluated. This may suggest changes in operating practices and equipment to prolong the flowing life of a well. Figures 6-93 and 6-94 show the idea of the effects of tubing size and a change in IPR on a well performance, respectively.

For a given wellhead pressure, flowing bottomhole pressure varies with production rate. Plotting these two flowing parameters on a cartesian coordinate will give a curve called *tubing performance relationship* (TPR). By plotting TPR and IPR of an oil well on a graph paper, the stabilized production capacity of the well is represented by the intersection of the two curves (see Figure 6-93).

To construct a TPR curve for a given well, the fluids and well geometry data should be available. The section titled "Flow of Fluids" provides some good multiphase flow correlations that can be used. In cases where these data and accessibility to computer are limited, a graphical flowing gradients correlation is needed. In fact, many improved graphical correlations covering a broad range of field conditions are available in the literature. The readers may refer to Reference 48 to get a complete set of flowing gradient curves. Sometimes a different company has a different set of curves. Although the best correlation is available, a particular field condition might have specific well characteristics such as salt or asphaltene deposition in the tubing or severe emulsification that may bring about a higher pressure drop than would be estimated from existing graphical correlations. The discrepancy might be used for analyzing the wells. So, it is recommended that a good multiphase flow equation be used instead of a graphical correlation.

For convenience, however, a set of working curves developed by Gilbert [49] is presented for illustrating their use in solving well performance problems. The curves are shown in Figures 6-95 through 6-106, and available only for small flowrate (50–600 stb/d) and tubing sizes of 1.66, 1.90, 2.375, 2.875 and 3.50 in.

The procedure how to use these flowing gradient curves in production engineering problems is given in the example later.

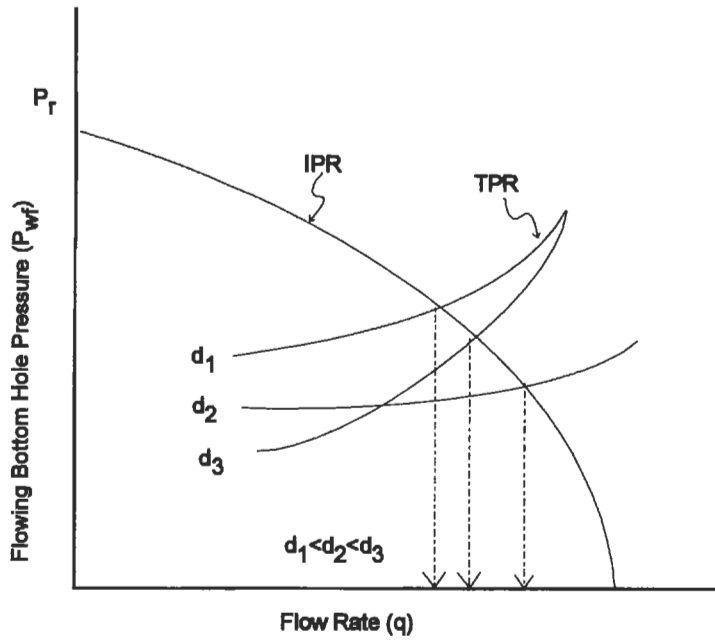


Figure 6-93. Effect of tubing size on oil well deliverability.

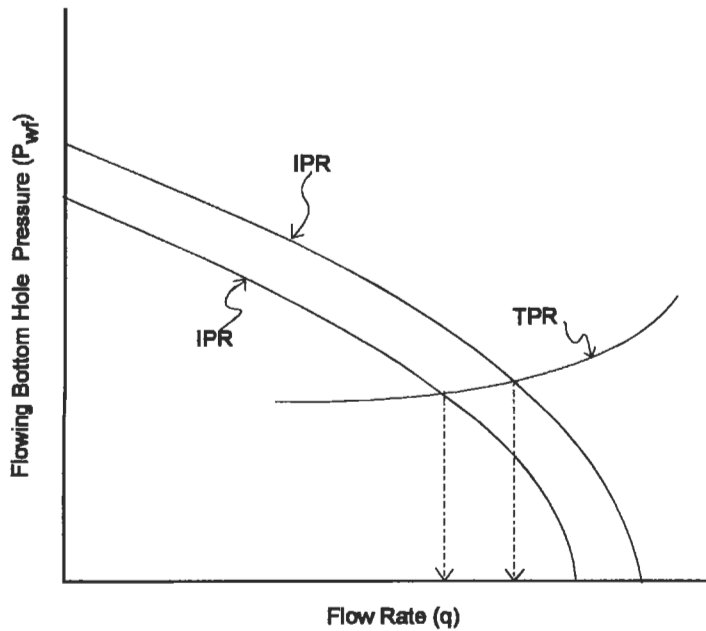


Figure 6-94. Effect of changes in inflow performance on oil well productivity.

Use of Vertical Pressure Gradients. In the preceding section of single-phase flow performances, the functions of vertical flow performance curves have been discussed. The following is a more detailed discussion on the applications of pressure gradients in analyses of flowing well performance. Accurate well test data, obtained under stabilized flow conditions, are needed for such analyses.

Subsurface Data. With flowing tubing known and well test data available, the flowing bottomhole pressure for a given rate of production can be determined by calculating the flowing pressure gradient to the bottom of the well.

If the static bottomhole pressure is known, the productivity index of the well can be determined from one production rate by determining the flowing bottomhole pressure for the rate of production.

If only surface data are available, the productivity index of the well may be estimated by determining the flowing bottomhole pressures for two or more rates of production.

Tubing Size. As stated, the size of the tubing is one of the important parameters affecting the pressure gradients. For low velocity the slippage of gas by the liquid contributes to the pressure losses. For high velocities friction becomes the controlling factor. Between these two extremes there is a range of velocities giving the optimum gradient at the inlet of tubing in the bottom of the well.

If the future range of expected rates and gas/oil ratios can be estimated, selection of the tubing size can be made, which would assure operation within the efficient range of the gradients, with the resulting increase in the flowing life of the well. Such selection can be made by calculating gradients for different tubing sizes for a given set of conditions.

Water Content. As the gas/oil ratio decreases, the flowing gradients, of course, increase, other conditions being equal. This is clearly illustrated in Figure 6-95, for example. As the water content of the produced fluid increases, the overall gas/liquid ratio decreases. If the future behavior of the water content increase can be estimated, future behavior of the well can be evaluated.

Wellhead Pressure. To a degree, the wellhead pressure is controllable because it depends, among other things, on the size, length and geometry of flow lines and on the separator pressure. At the same time the wellhead pressure has a marked effect on the slope characteristics of the gradient because of the question of density which is involved. For a given reduction of the wellhead pressure the reduction of the bottomhole flowing pressure may be substantially higher. This is particularly true in case of high-density flow.

The reduction of the bottomhole flowing pressure should result in increase of production. It can be seen from the above that the degree of this increase cannot be estimated from the surface data alone. It can be estimated if information is available also on the flowing gradient and the productivity index of the well.

Predicting the Flowing Life. The natural flow of an oil well continues as long as there exists a proper balance between two conflicting pressure requirements at the bottom of the well. First, this pressure must be sufficiently high to sustain the vertical lift. Second, it must be sufficiently low to create a pressure differential that permits the reservoir fluids to enter the well.

This balance may be destroyed by either one or a combination of two sets of conditions: (1) increase in flowing pressure gradients, for any of the reasons

mentioned above, increases the lift pressure requirements above the point needed for maintaining the pressure differential with the available reservoir energy, or (2) the declining reservoir energy is not able to maintain this differential for the required vertical lift pressure. In either case the natural flow of the well either declines to an uneconomical rate or ceases completely.

The uses of the flowing pressure gradients discussed above may be applied to estimating the length of the flowing life of a well. Additional information needed are the estimate of the static bottom hole pressure of water encroachment, and of gas/oil ratio behavior at different future stages of the cumulative production of the well. Graphic methods have been developed for making such estimates.

Choke Performance

The reasons involved in installing chokes in oil and gas fields have been mentioned before. The graphical correlations and empirical or semiempirical equations used for single-phase oil or gas are not valid for two-phase conditions.

The correlations for multiphase flow through chokes have been published but not one of them gives satisfactory results for all ranges of operating conditions (flow parameters). Theoretically, the correlations are developed with the assumption that the simultaneous flow of liquid and gas is under critical flow conditions so that when an oil well choke is installed fluctuations in line pressure is gradually increased, there will be no change in either the flowrate or the upstream pressure until the critical-subcritical flow boundary ($P_{\text{downstream}} \cong 0.5-0.55P_{\text{upstream}}$) is reached.

In more oil fields, the most popular correlations are of Gilbert [49] and Poetmann and Beck [50]. Ashford [51] also developed a correlation for multiphase flow through chokes.

Gilbert's Correlation. The equation developed to estimate a parameter of fluid flow through the orifice is

$$P_{\text{wh}} = \frac{435R^{0.546}q}{d^{1.89}} \quad (6-188)$$

where P_{wh} = wellhead pressure in psig
 R = gas/liquid ratio in Mscf/stb
 q = gross liquid rate in stb/d
 d = choke (bean) size in $\frac{1}{64}$ in.

This equation is derived using regularly reported daily individual well production data from Ten Section Field in California. Gilbert noted that an error of $\frac{1}{128}$ in. in bean size can give an error of 5 to 20% in pressure estimates. In the type of formula used, it is assumed that actual mixture velocities through the bean exceed the speed of sound, for which condition the downstream, or flowline, pressure has no effect upon the tubing pressure. Thus, the equation applies for tubing head pressure of at least 70% greater than the flowline pressure.

Poetmann-Beck's Correlation. F. H. Poetman and R. L. Beck developed charts for estimating flow of oil and gas through chokes [50]. The charts, shown in Figures 6-105 through 6-107, relate the variables of gas/oil ratio, oil production

(text continued on page 585)

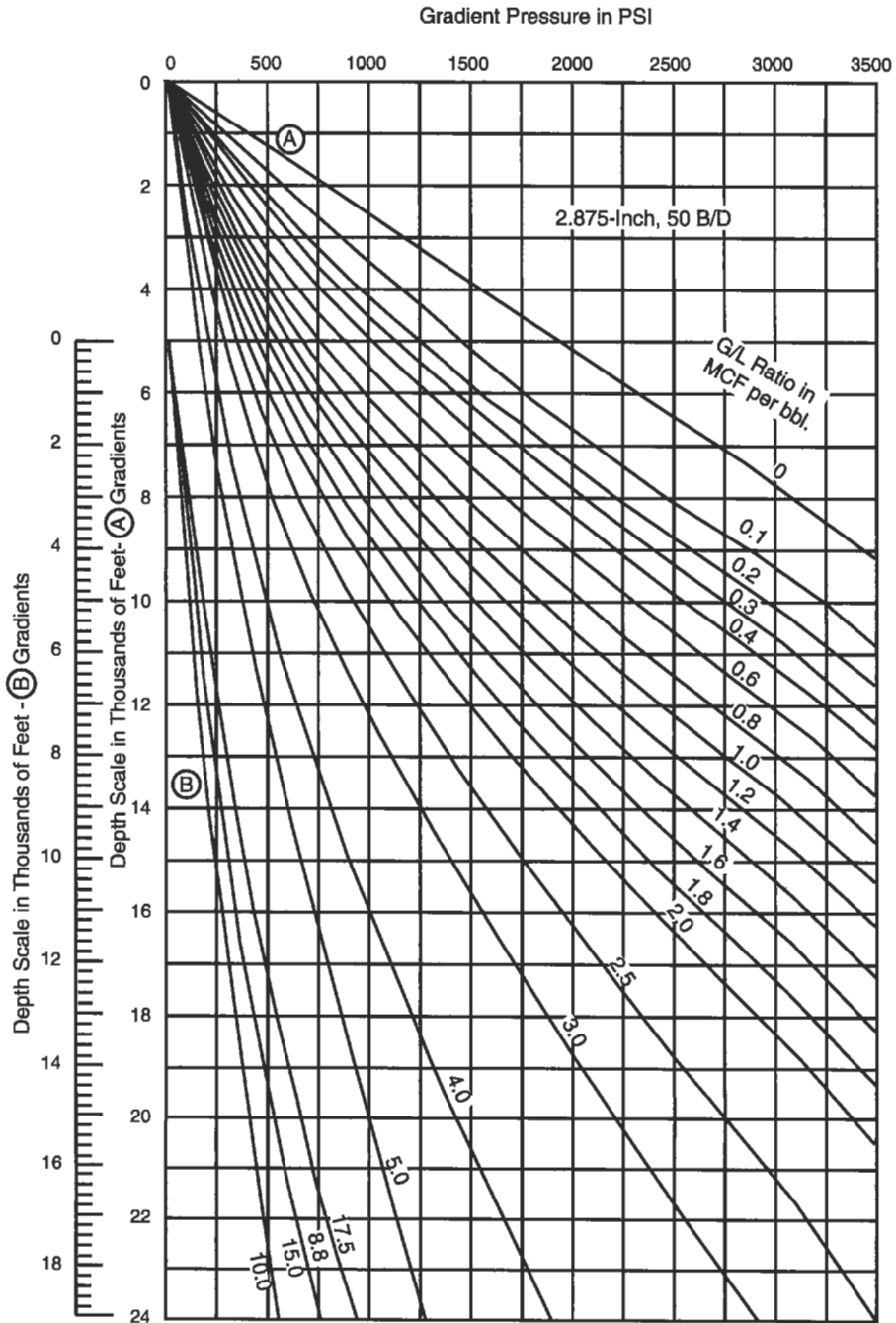


Figure 6-95. Flowing pressure gradients for 2.875-in. tubing with rate of 50 bpd.

Gradient Pressure in PSI

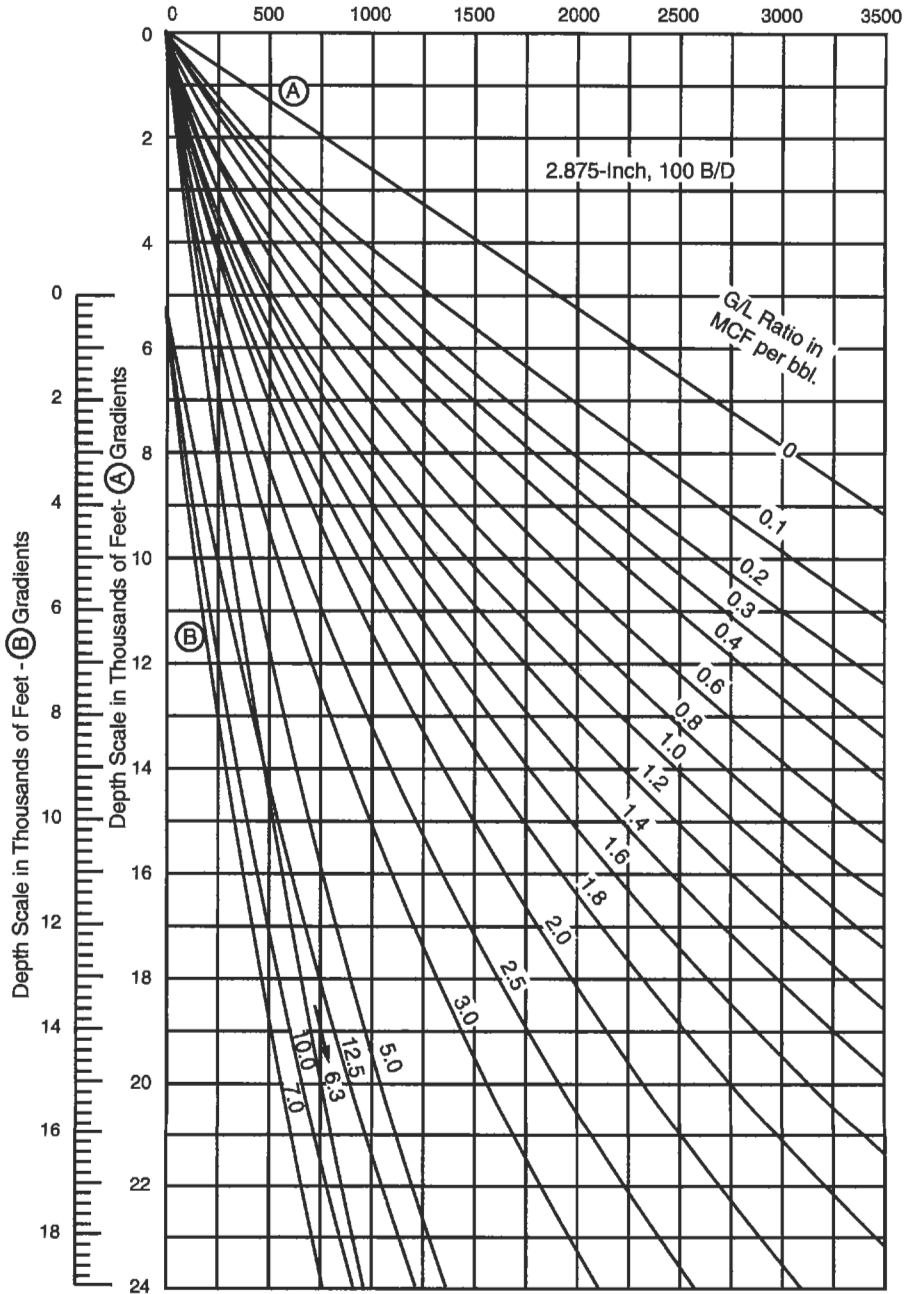


Figure 6-96. Flowing pressure gradients for 2.875-in. tubing with rate of 100 bpd.

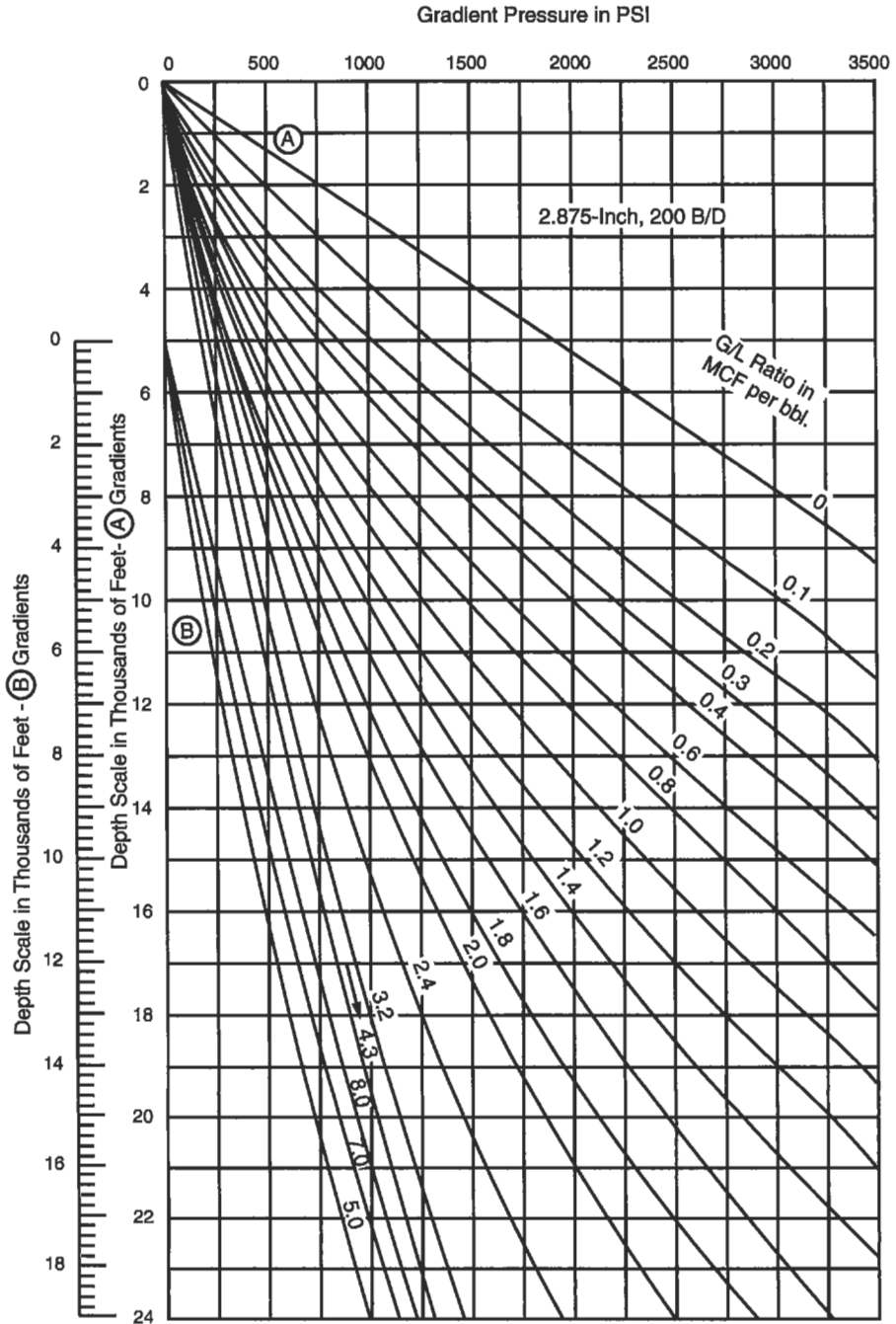


Figure 6-97. Flowing pressure gradients for 2.875-in. tubing with rate of 200 bpd.

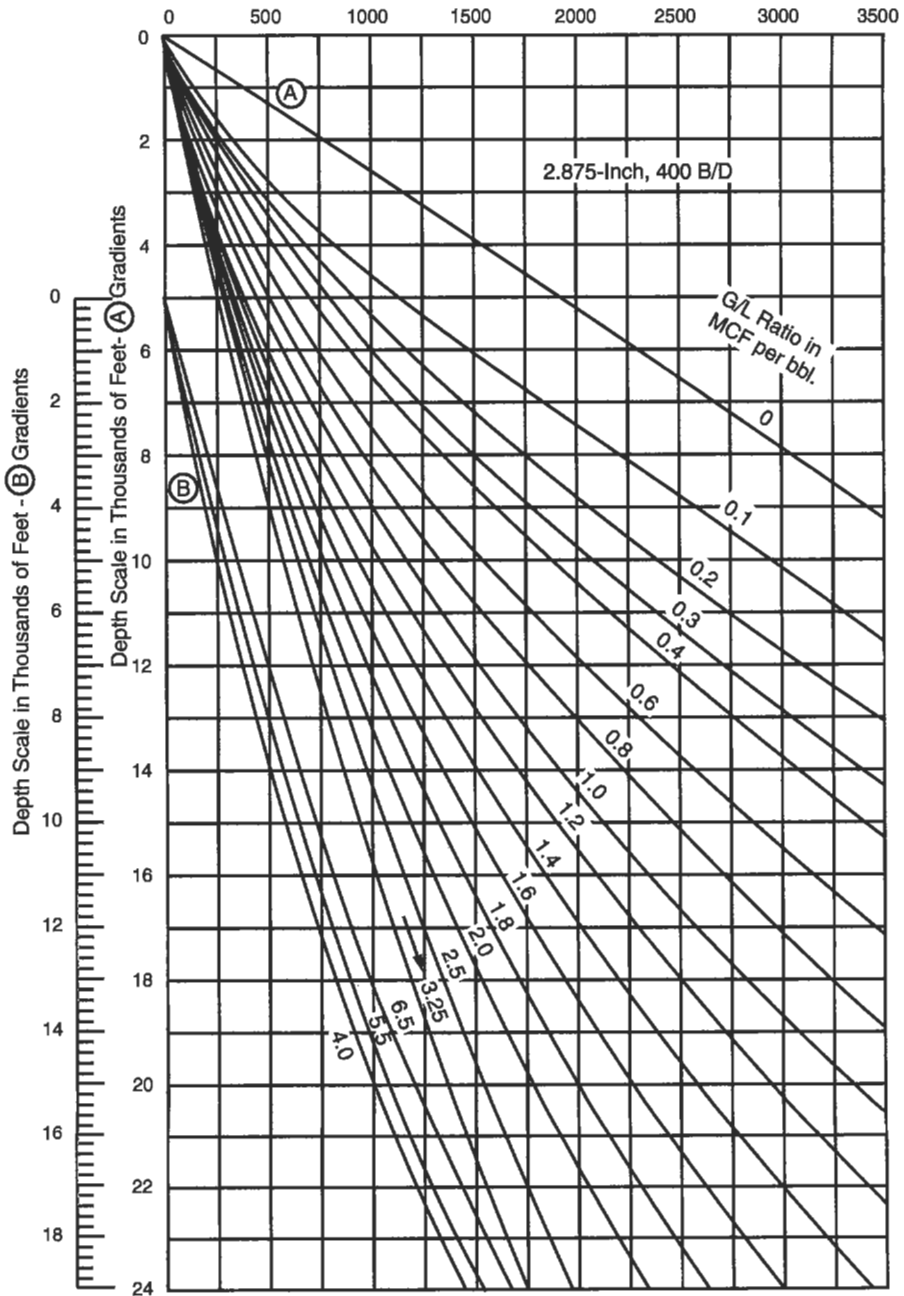


Figure 6-98. Flowing pressure gradients for 2.875-in. tubing with rate of 400 bpd.

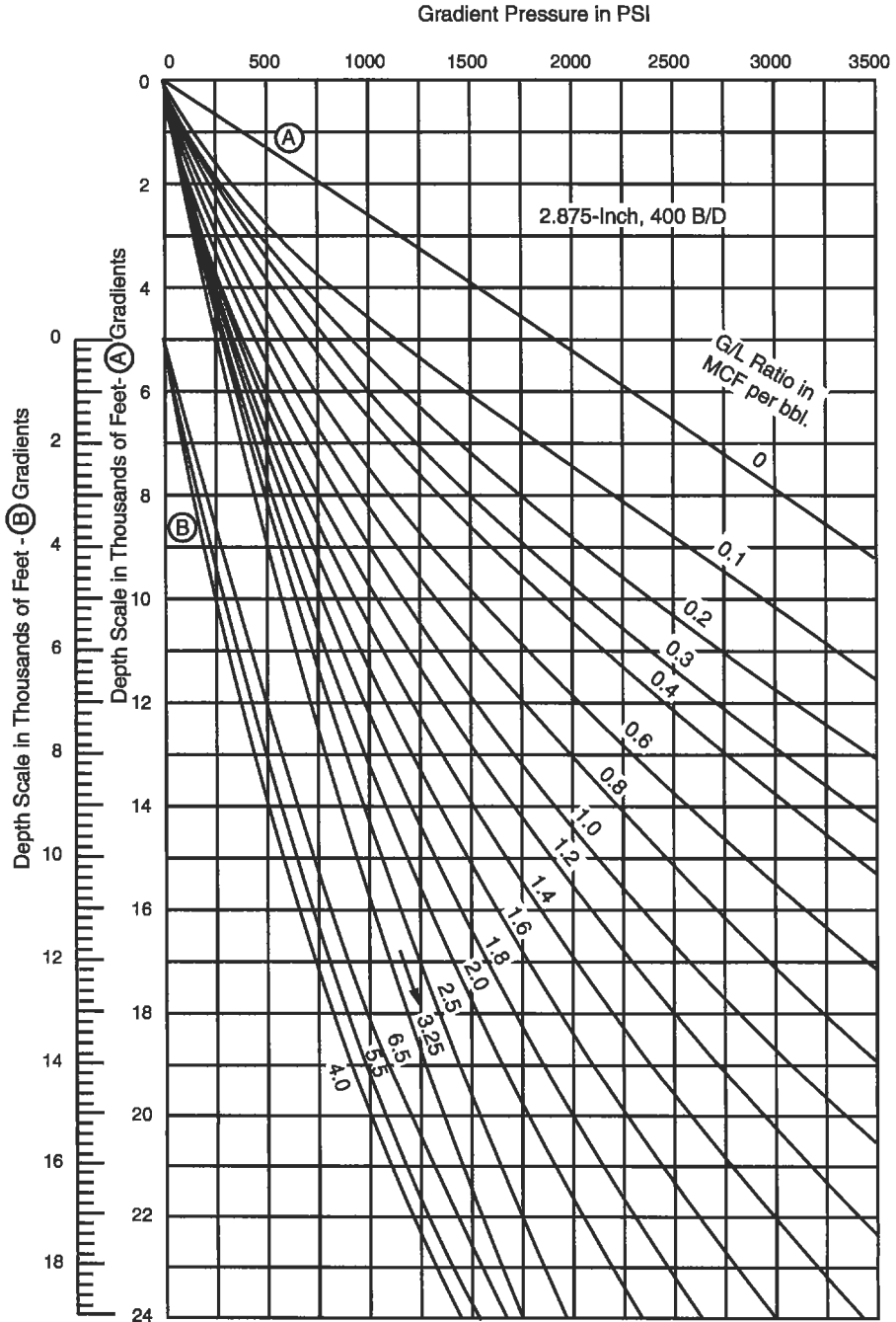


Figure 6-99. Flowing pressure gradients for 2.875-in. tubing with rate of 600 bpd.

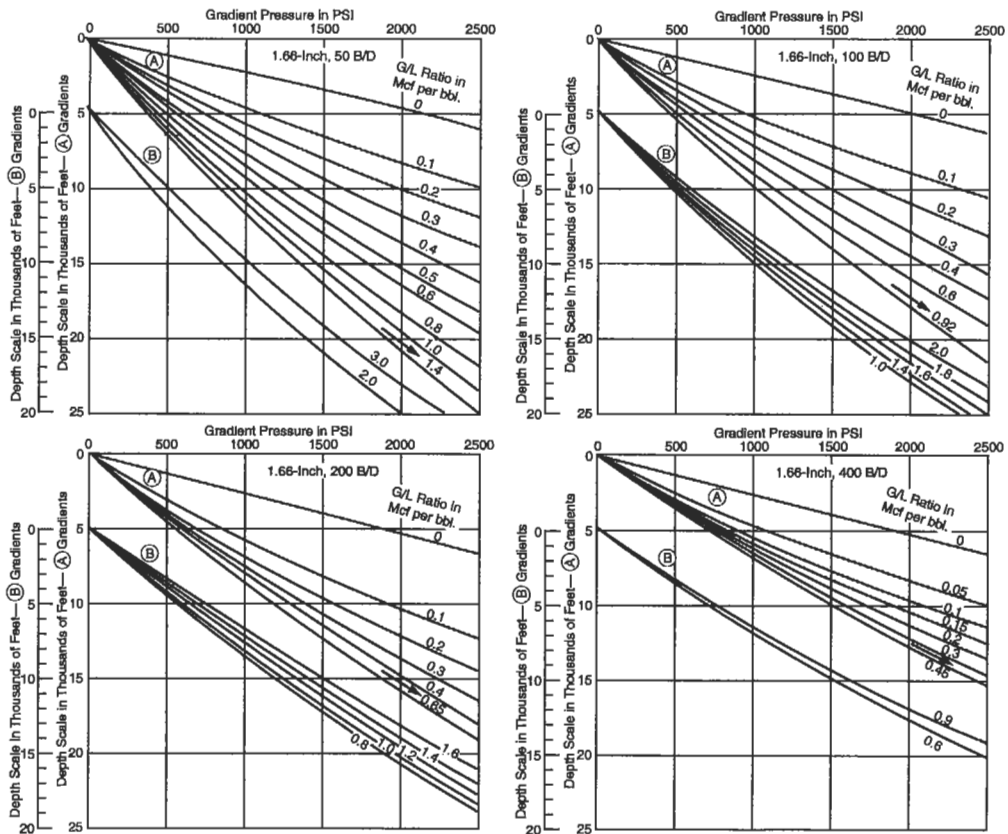


Figure 6-100. Flowing pressure gradients for 1.66-in. tubing with rate of 50–400 bpd.

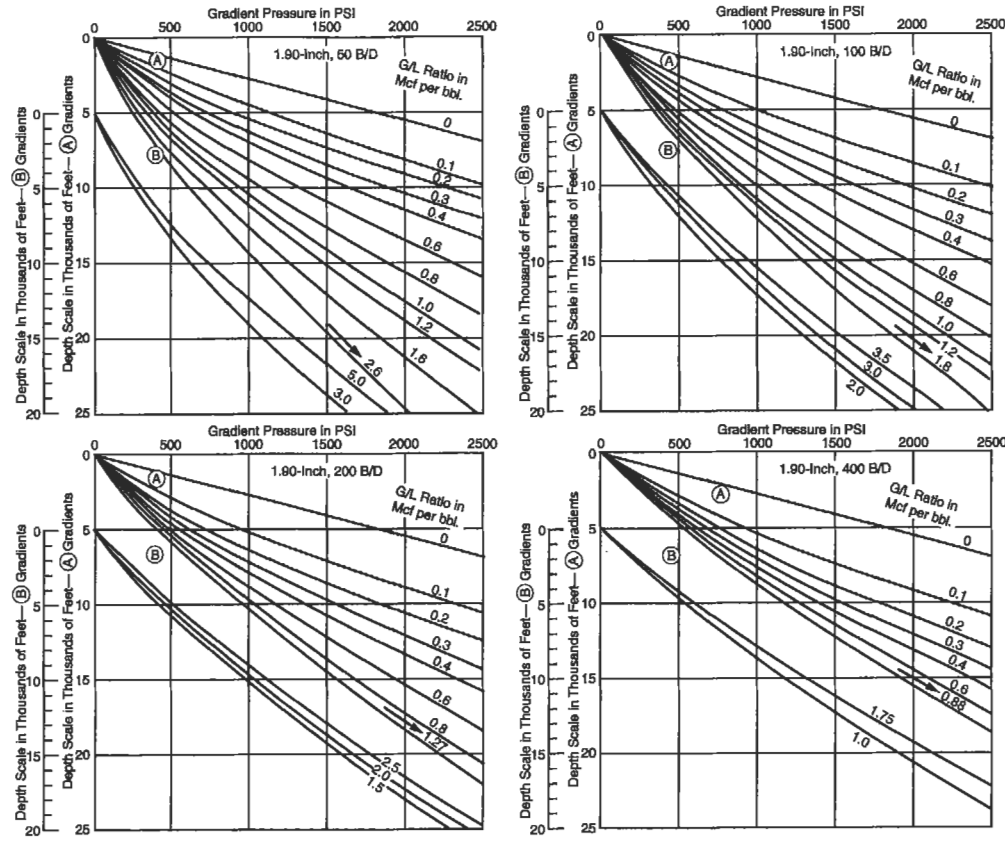


Figure 6-101. Flowing pressure gradients for 1.90-in. tubing with rate of 50–400 bpd.

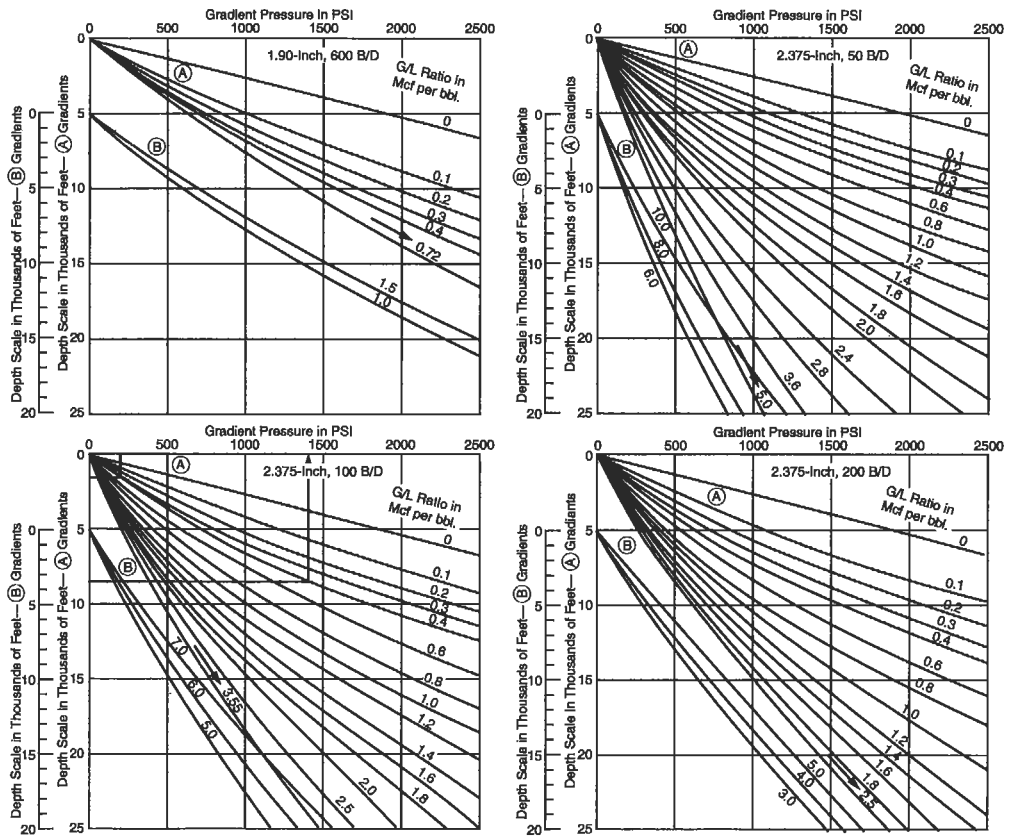


Figure 6-102. Flowing pressure gradients for 1.90-in. tubing with rate of 600 bpd and 2.375-in. tubing with rate of 50–200 bpd.

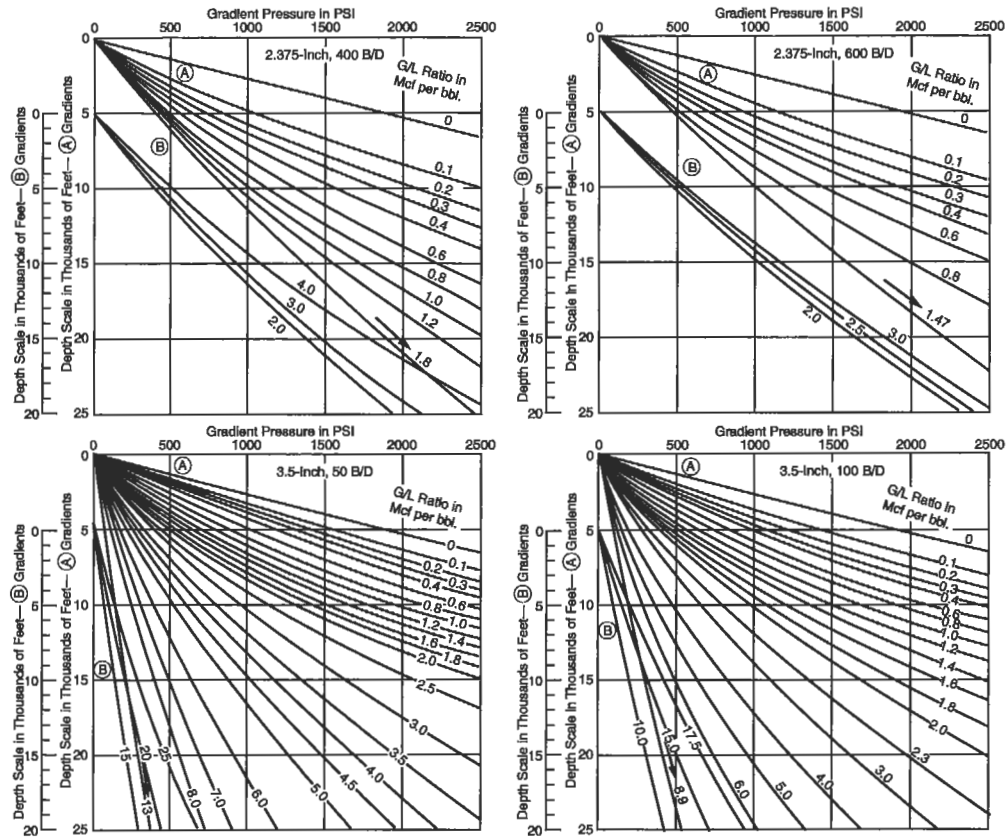


Figure 6-103. Flowing pressure gradients for 2.375-in. tubing with rate of 400–600 bpd and 3.5-in. tubing with rate of 50–100 bpd.

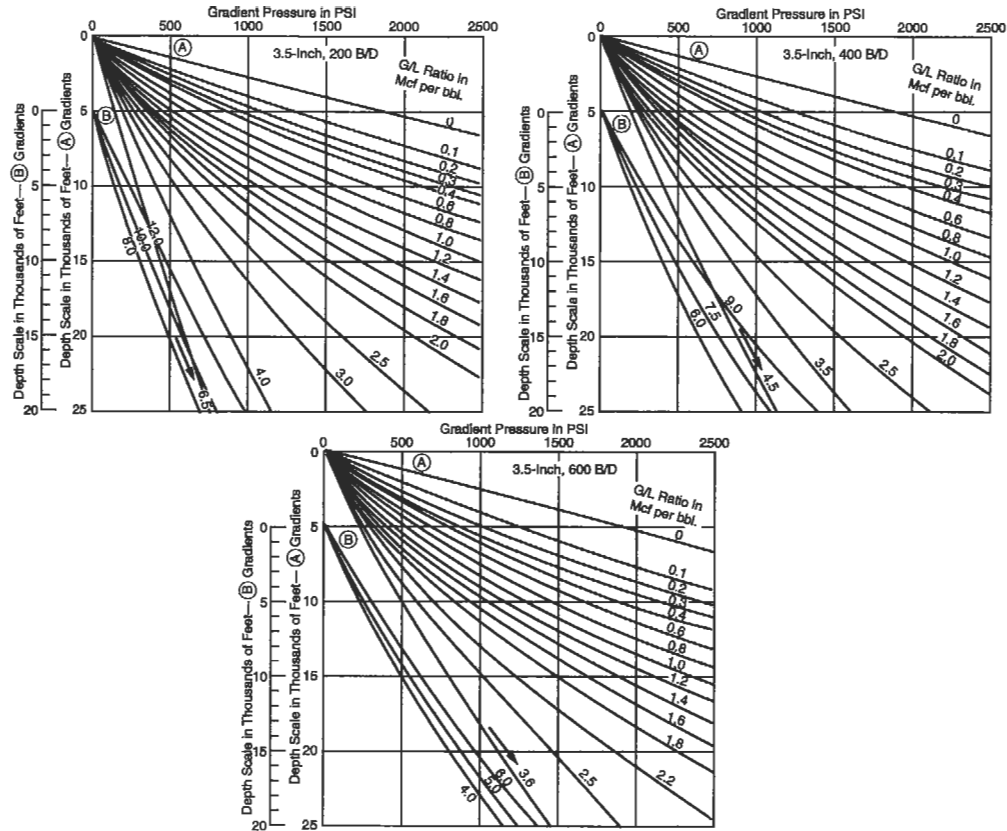


Figure 6-104. Flowing pressure gradients for 3.5-in. tubing with rate of 200–600 bpd.

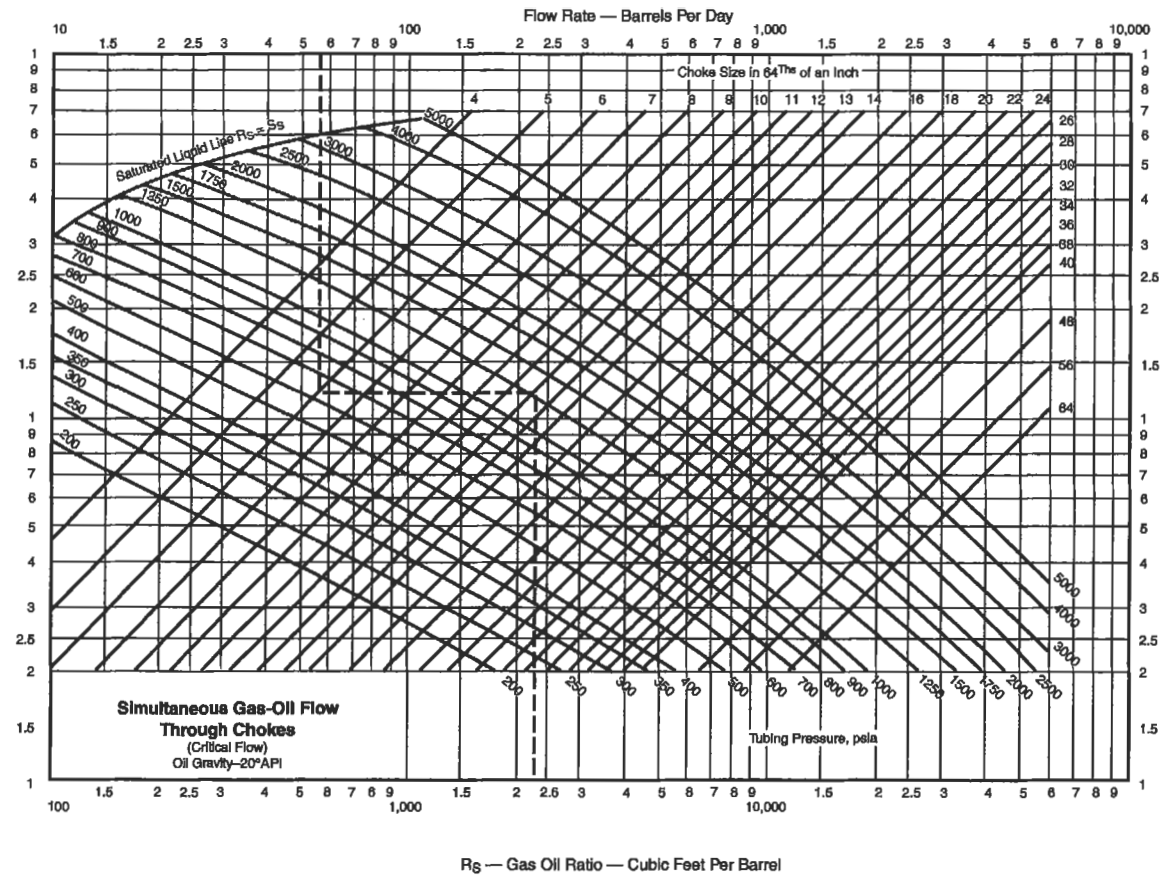


Figure 6-105. A correlation for two-phase flow through chokes with oil gravity of 20°API.

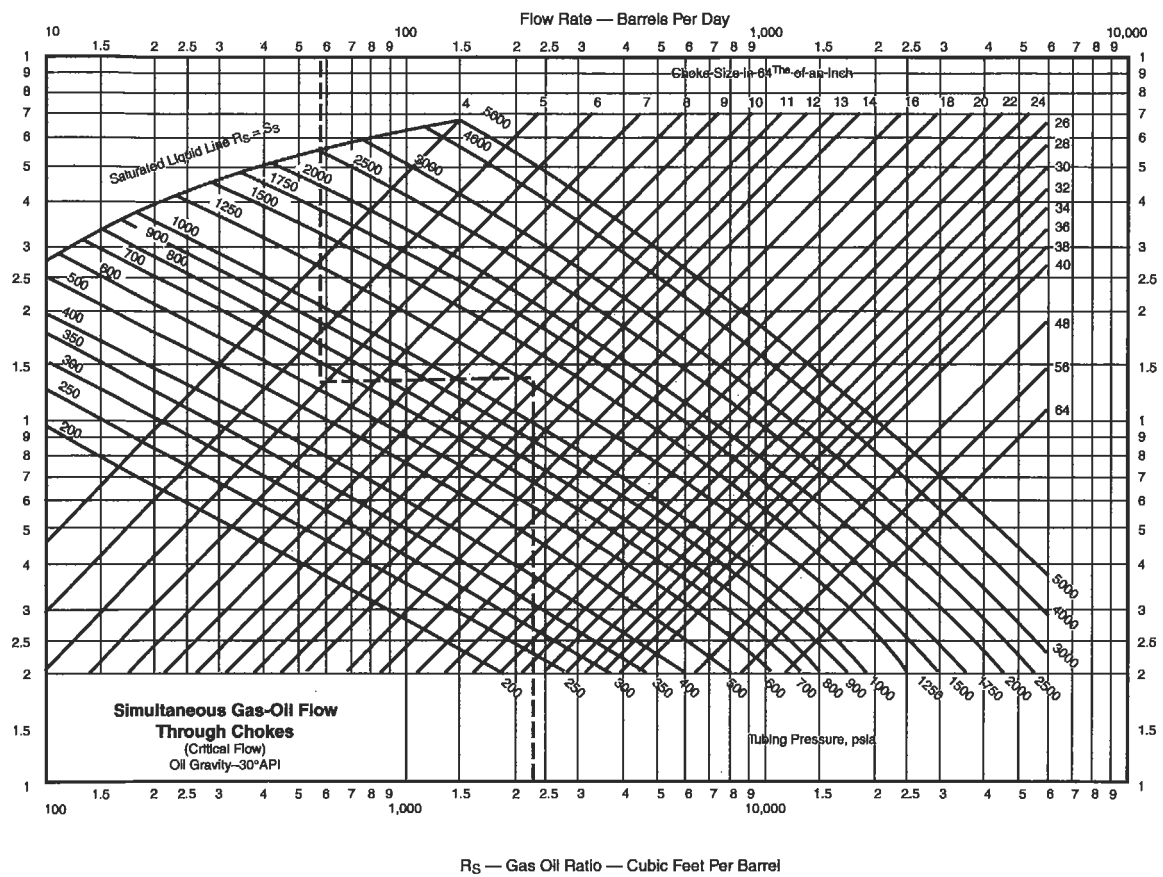


Figure 6-106. A correlation for two-phase flow through chokes with oil gravity of 30°API.

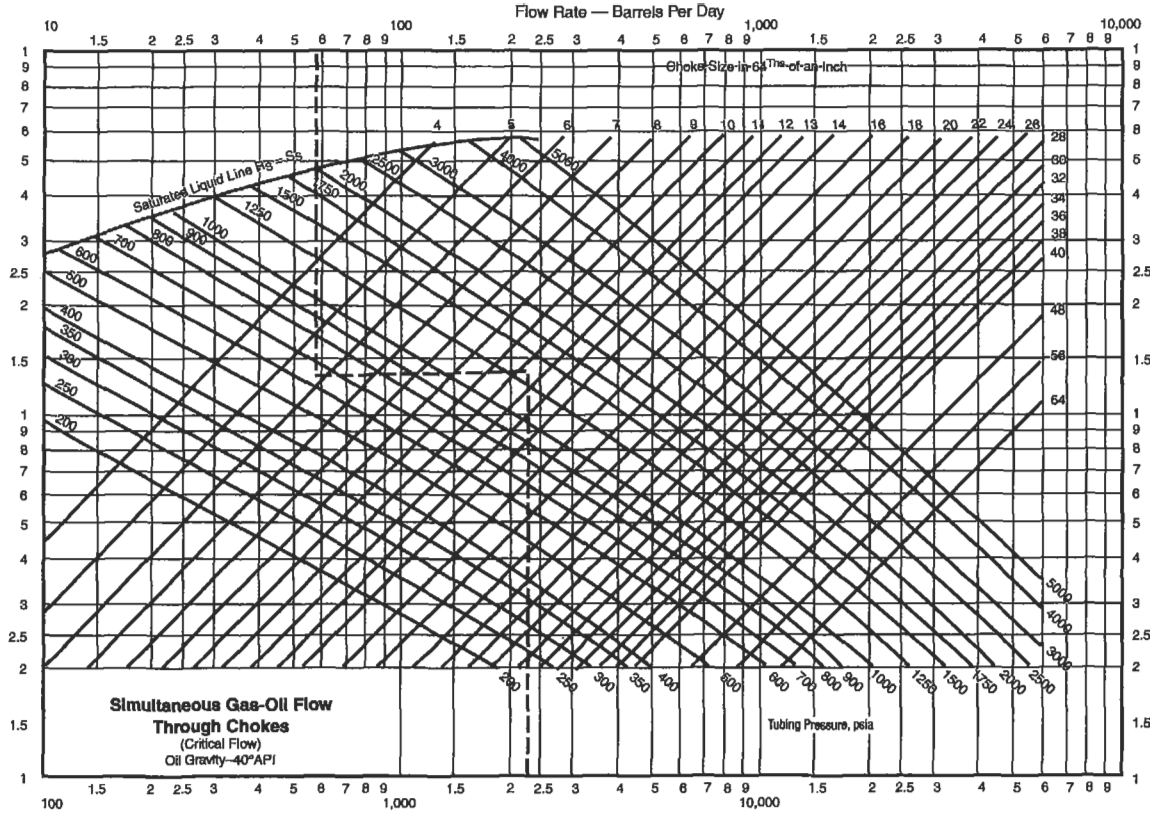


Figure 6-107. A correlation for two-phase flow through chokes with oil gravity of 40°API.

(text continued from page 571)

rate, tubing pressure and choke size. With three of the variables known, the fourth can be determined. The charts are valid only under following conditions:

1. The flow is a simultaneous, two-phase flow of oil and gas. The charts are not valid if water is present.
2. The flow through the choke is at the critical flow conditions; that is, at acoustic velocity. This occurs when the downstream (flowline) pressure is 0.55 or less of the upstream (tubing) pressure. Under such conditions the rate of flow is not affected by downstream pressure.

Actually, this last limitation is of small practical significance since chokes are usually selected to operate at critical flow conditions so that well's rate of flow is not affected by changes in flowline pressure.

The manner of use of charts is as follows:

1. The 20°, 30°, and 40°API gravity charts can be used for gravity ranges of 15° to 24°, 25° to 34° and 35° and up, respectively.
2. When the starting point is the bottom scale, a vertical line is drawn to intersection with tubing pressure curve, then horizontal line to intersection with the choke size, then vertical line to the upper scale. Reverse procedure is used when the upper scale is the point of beginning.
3. Performance of a given size choke for a given gas/oil ratio can be plotted. Such plot would show relationship between different rates and corresponding tubing pressures for a given choke.
4. Free gas in tubing can be estimated by use of charts. For instance, in case of Figure 6-107 for 2,250 ft³/bbl gas/oil ratio, 1,265 psi tubing pressure and $\frac{5}{8}$ in. choke, the rate was found to be 60 bbl/day. For 1,265-psi tubing pressure the solution gas is 310 ft³/bbl. Therefore, the free gas is 2,250 - 310 = 1,940 ft³/bbl.

The results obtained by use of these charts compared very favorably with observed data obtained on 108 wells covering wide ranges of conditions.

Ashford's Correlations. Ashford developed a model for multiphase flow through choke by applying the polytropic expansion theory [51]. The final form of his equation is

$$q_o = 1.53 \frac{Cd^2 P_u}{(B_o + WOR)^{1/2}} \times \frac{[(T_u Z_u (R - R_s) + 151P_u)]^{1/2}}{T_u Z_u (R - R_s) + 111P_1} \times \frac{[G_o + 0.000217G_g R_s + (WOR)G_w]^{1/2}}{G_o + 0.000217G_g R + (WOR)G_w} \tag{6-189}$$

where q_o = oil flowrate in stb/d
 C = orifice discharge coefficient
 d = choke diameter in $\frac{1}{8}$ in.
 P_u = upstream choke pressure in psia
 B_o = oil formation volume factor in bbl/stb

- WOR = water/oil ratio
 R = producing gas-oil ratio at standard condition in scf/stb
 R_s = solution gas-oil ratio at choke condition, scf/stb
 T_u = upstream choke temperature in °R
 Z_u = gas compressibility factor evaluated at upstream conditions
 G_g = gas gravity (air = 1.00)
 G_o = oil gravity (water = 1.00)
 G_w = formation water gravity (water = 1.00)

Ashford stated that once C (discharge coefficient) has been fairly well defined for a given production province or operation the Equation 6-189 may be used in a conventional manner to evaluate (1) flowrates arising from changes in choke sizes, (2) wellhead pressures arising from changes in choke sizes and (3) choke sizes necessary to achieve a given wellhead pressure for a known liquid rate. If C is unknown, a value of 1.0 may be used to obtain a reasonable estimate of choke performance. Later, based on an extensive study, Sachdeva *et al.* recommended that $C = 0.75$ be used for a choke configuration involving an elbow upstream from the choke, and $C = 0.85$ be used for a choke free of upstream disturbances [52].

Flowline Performance

Understanding the behavior of multiphase fluids flow in horizontal or inclined pipe is important too because the efficiency of a producing system is accomplished by analyzing all components through which the fluids flow. In the analysis a flowline may be considered as a restriction because higher pressure loss resulted. For instance, for a given set of fluids data 2.5-in. line causes higher pressure loss when compared with 3 and 4-in. line so one tends to take the larger size to produce more oil. The diameter, however, should not be oversized because additional slugging and heading may occur. Some operators just add a parallel line instead of replacing the current line with a larger size. It should be remembered that production capacity, pipes availability, separator pressure and other constraints may be involved in judging a final design of producing system.

The knowledge of pressure-flowrate relationship is very useful in designing an efficient flowing system. The procedure used to generate a flowline performance for a given set of fluids data and a given diameter of the pipe is similar with the one for single phase. No pressure loss correlations for horizontal or inclined pipes are given. The reader can, however, find some good correlations in the section titled "Flow of Fluids."

Example A

Consider an oil reservoir producing at an average reservoir pressure below $P_r = 2,400$ psi, which is the bubble point pressure. A single-point flow test conducted on a well at stabilized condition resulted in $q = 500$ stb/d and $P_{wf} = 250$ psi. Measured GOR is 400 scf/stb. The well of total depth of 7,000 ft is produced through 2 $\frac{3}{8}$ -in. tubing. Find (1) the maximum rate possible assuming $P_{wh} = 200$ psi, and (2) the productivity index for the condition corresponding to the maximum possible flowrate.

Solution (assume FE = 1.0)

(1)

- Using Vogel's equation, calculate q_{max}

$$\frac{500}{q_{max}} = 1 - 0.2 \left(\frac{250}{2,400} \right) - 0.8 \left(\frac{250}{2,400} \right)^2$$

$$q_{max} = 515 \text{ stb/d (= oil AOF)}$$

- Choose some values of P_{wf} and determine corresponding q 's using Vogel's equation

$$q = 515 \left[1 - 0.2 \left(\frac{P_{wf}}{2,400} \right) - 0.8 \left(\frac{P_{wf}}{2,400} \right)^2 \right]$$

P_{wf} , psi	q , stb/d
500	476
800	435
1200	361
1500	290
2000	143
2400	0

Plot P_{wf} versus q to get the IPR curve (see Figure 6-108).

- Let's select Gilbert's working curves shown in Figures 6-101 and 6-102 for 2 $\frac{3}{8}$ -in. tubing and choose the curves with rate of 100, 200 and 400 stb/d.
- Determine the equivalent length depth of $P_{wf} = 200$ psi. This is done by tracing down a vertical line through pressure point of 200 psi at zero depth until the line of GLR = 400 scf/stb is found and read the depth. This is the equivalent depth. Add this equivalent depth to the actual well depth. Then find the pressure at this total equivalent depth for rate and GLR given. For all three rates chosen, we can obtain

q , stb/d	P_{wf} , psi
100	1,410
200	1,370
400	1,310
(600)	(1,400)

- Plot these values on the same graph made in Step 2 above.
- Read the coordinate points (q , P_{wf}) of the intersection between the two curves (IPR and TPR), see Figure 6-108. It is obtained that the maximum possible rate is 332 stb/d.

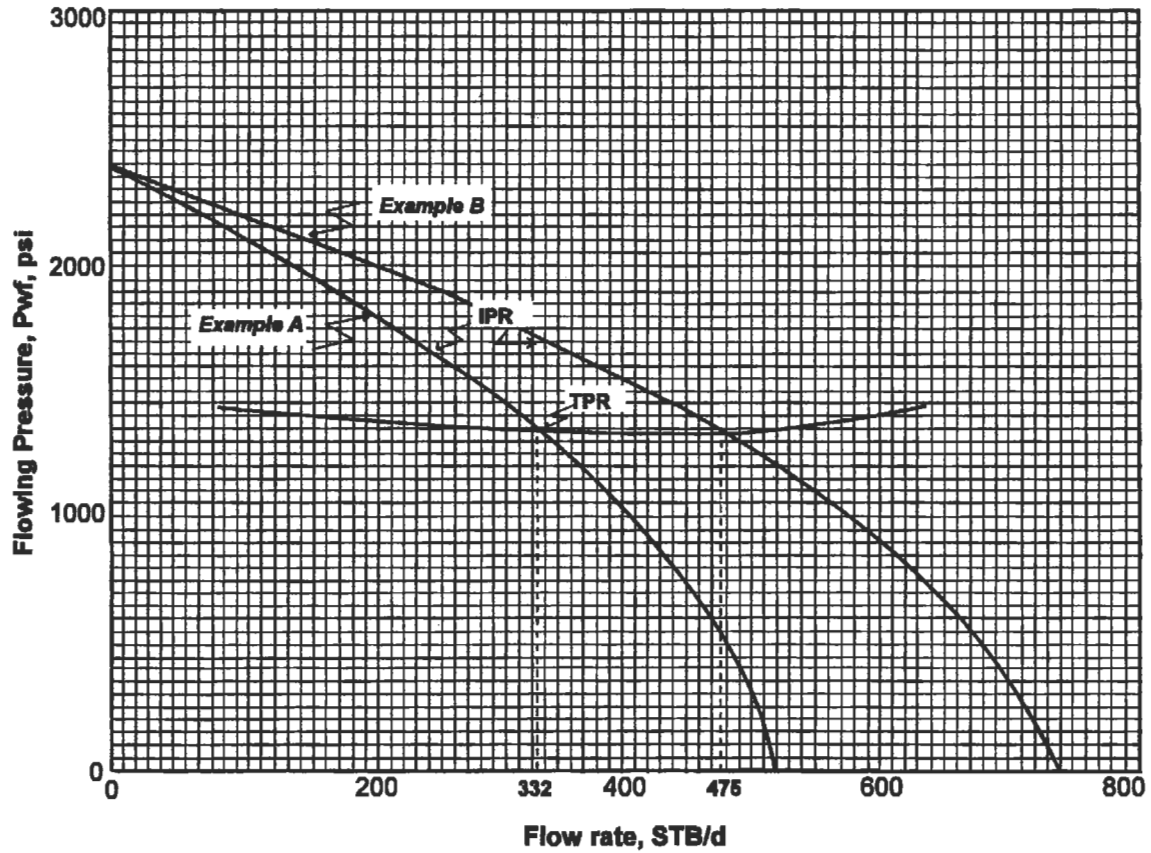


Figure 6-108. Pressure-rate relationship for Example A on page 586.

(2) The productivity index J of two-phase fluids may be defined as

$$J = -dq/dP_{wf} = -\left[-0.2 \frac{q_{max}}{P_r} - 1.6 \frac{q_{max}}{P_r} (P_{wf})\right]$$

$$= 0.2 \times \frac{515}{2,400} + 1.6 \times \frac{515}{(2,400)^2} (1,325) = 0.232 \text{ stb/d/psi}$$

Example B

Suppose we have more test data for Example A. The additional data given are $FE = 0.7$. (1) What is the AOF when the skin effect is removed ($FE = 1.0$)? (2) What is the actual maximum potential (AOF) of the well? (3) Determine the maximum possible rate. (4) Determine the maximum possible rate if no damage occurred.

Solution:

1. Using Equation 6-178, for $V = 0.8$,

$$\frac{500}{q_{max}^{FE=1}} = 0.7 \left[1 + 0.8 \left(\frac{250}{2,400} \right) \right] \left[1 - \left(\frac{250}{2,400} \right) \right]$$

$$q_{max}^{FE=1} = 736 \text{ stb/d}$$

2. The maximum potential will occur when $P_{wf} = 0$,

$$q_{max}^{FE=0.7} = q_{max}^{FE=1} \times 0.7 \left[1 + 0.8 \left(\frac{0}{2,400} \right) \right] \left(1 - \frac{0}{2,400} \right) = 515.2 \text{ stb/d}$$

3. The maximum rate possible is 332 stb/d (already determined in Example A).
 4. Construct an IPR with $FE = 1.0$. Vogel's equation is valid now,

$$q_0 = 736 \left[1 - 0.2 \left(\frac{P_{wf}}{2,400} \right) - 0.8 \left(\frac{P_{wf}}{2,400} \right)^2 \right]$$

P_{wf} , psi	q , stb/d
500	680.0
800	621.5
1,200	515.2
1,500	414.0
2,000	204.4

Plotting P_{wf} versus q , we can determine that $q = 477 \text{ stb/d}$ (Figure 6-108).

Example C

An oil well is produced at $P_{wf} > P_b$. Data given are

$$H = 5,000 \text{ ft}$$

$$d = 2.375 \text{ in}$$

$$P_r = 1,500 \text{ psi}$$

$$J = 0.4 \text{ stb/d/psi}$$

$$\text{GLR} = 0.8 \text{ Mscf/stb}$$

Find the production rate of liquid and gas if (a) the bean size is $\frac{22}{64}$ in. or (b) the bean size is $\frac{30}{64}$ in. Assume critical flow conditions and use Gilbert's equation.

Solution

Since the well is operated above the reservoir bubble point, we can treat the inflow performance as a linear one:

$$P_{wf} = P_r - \frac{q}{J} = 1,500 - \frac{q}{0.4}$$

Choose some values of q (e.g., 100, 200 and 400 stb/d) and use the gradient curves for 2.375-in. tubing. Gilbert's curves are used here for convenience. For a given P_{wf} , P_{wh} is found with a procedure opposite to that for determining P_{wf} for a known P_{wh} (solution to Example A, (1), Step 4). Doing so, we can get the following:

q , stb/d	P_{wf} , psi	P_{wh} , psi
100	1250	540
200	1000	400
400	500	40

Plot q versus P_{wh} (shown in Figure 6-109). Generate other q versus P_{wh} for the two choke sizes using

$$P_{wh} = 435R^{0.546}q/S^{1.89}$$

where (a) $q = (22^{1.89} \times P_{wh}) / (435 \times 0.8^{0.546})$ or (b) $q = (30^{1.89} \times P_{wh}) / (435 \times 0.8^{0.546})$

These are straight line equations through the origin. Draw the choke performance curves (see Figure 6-109). From this figure we can determine that

- installing a $\frac{22}{64}$ -in. choke:

$$q_{\text{liquid}} = 264 \text{ stb/d}$$

$$q_{\text{gas}} = 264 \times 0.8M = 0.211 \text{ MMscf/d}$$

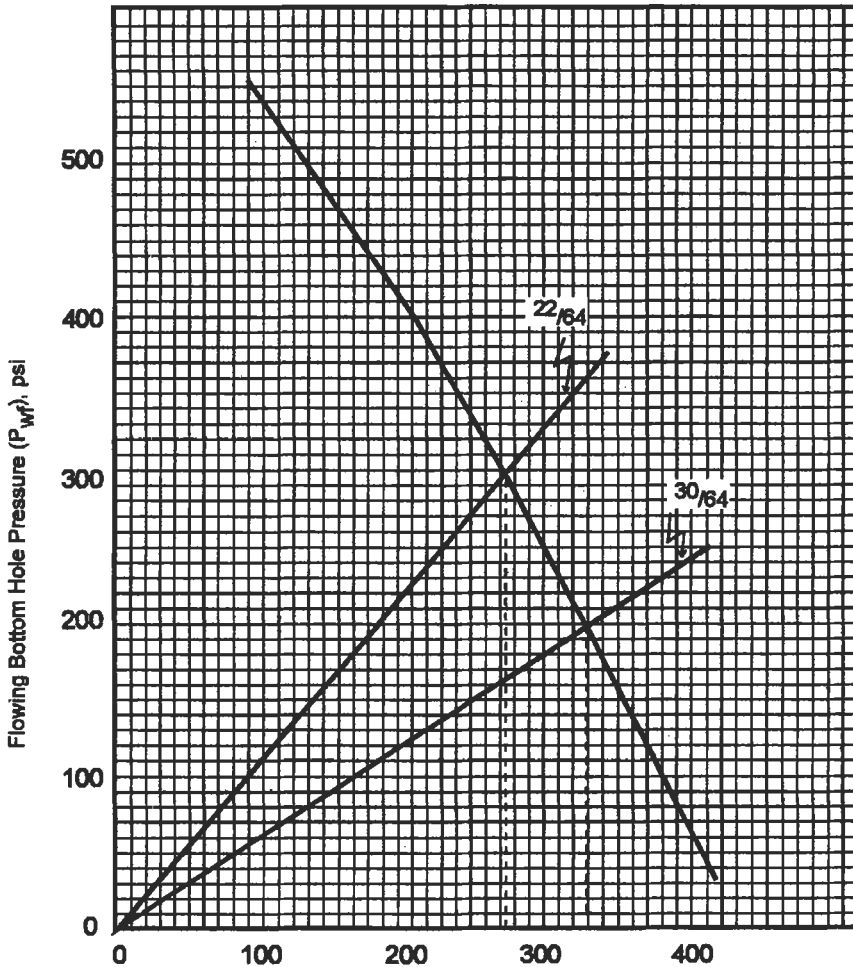


Figure 6-109. Pressure-rate relationship for Example C on page 590.

2. installing a $\frac{30}{64}$ -in. choke:

$$q_{\text{liquid}} = 319 \text{ stb/d}$$

$$q_{\text{gas}} = 0.255 \text{ MMscf/d}$$

Example D

Constructing an IPR curve of an oil well is sometimes difficult in terms of data available. The present reservoir pressure is not available or measured. Some oil companies do not want to lose their production caused by closing the well to measure the static reservoir pressure. A practical means of overcoming this problem is to test the well at two different rates while measuring the flowing bottomhole pressure.

This technique does not require expensive, time-consuming tests. The pressure measurements can be very accurate, using a subsurface gage on flowing wells; they can be obtained with surface-recording downhole gage; or they can simply be obtained with casing pressure and fluid level shots, depending on the well condition.

A typical two-point test datum is taken from a well in the Judy Creek Beaverhill Lake 'A' Pool producing under a solution gas drive [53].

	Test 1	Test 2
q, stb/d	690.6	470
P _{wh} , psi	1152.0	1970
P _b , psi	2290.0	2290

The task is to estimate the static reservoir pressure and to construct IPR for this well.

Solution

$$\left(\frac{q}{q_{\max}}\right)_1 = 1 - 0.2\left(\frac{1,152}{2,290}\right) - 0.8\left(\frac{1,152}{2,290}\right)^2 = 0.697$$

$$\left(\frac{q}{q_{\max}}\right)_2 = 1 - 0.2\left(\frac{1,970}{2,290}\right) - 0.8\left(\frac{1,970}{2,290}\right)^2 = 0.236$$

$$q_c = (470 - 690.6)/(0.236 - 0.697) = 478.5 \text{ stb/d} = (q_{\max} - q_b)$$

Flowrate at bubble point,

$$q_b = 470 - (0.236)(478.5) = 357 \text{ stb/d}$$

$$J_b = 1.8 \times (478.5/2,290) = 0.376$$

$$P_r = 2,290 + (357/0.376) = 3,239 \text{ psia}$$

The calculated reservoir pressure from the two-point test was 3,239 psia, which is consistent with static pressures measured in this area of the 'A' Pool.

Figure 6-110 is the constructed IPR. A third run was run to verify this curve, with a rate of 589 stb/d at 1,568 psia. This point fell essentially on the curve generated by the original two-test points.

Example E

A reservoir with a back-pressure curve slope $(1/n) = 1.12$ has the following two flow tests:

	\bar{P} , psia	q _c , stb/d	P _{wh} , psia
Test 1	2355.9	335.1	1300
Test 2	2254.9	245.8	13

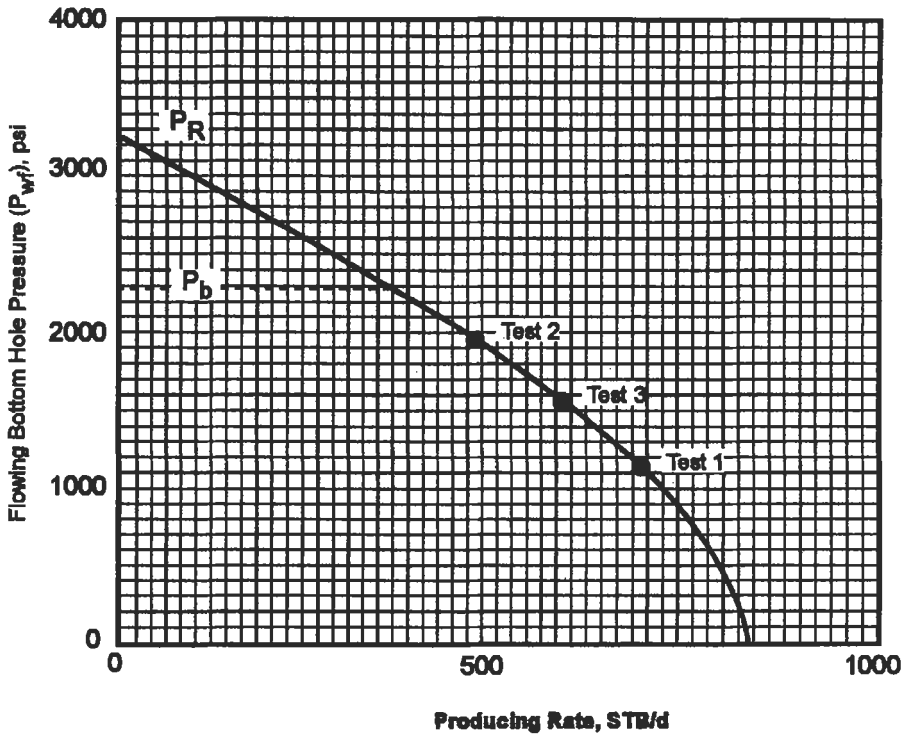


Figure 6-110. Pressure-rate relationship for Example D on page 591.

Calculation of future IPR:

- Using Fetkovich's method:

$$q_{max} = \frac{q_0}{\left[1 - \left(\frac{P_{wf}}{P}\right)^2\right]^n}$$

$$q_{max1} = \frac{335.1}{\left[1 - \left(\frac{1300}{2355.4}\right)^2\right]^{0.893}} = 463.5 \text{ stb/d}$$

$$q_{max2} = \frac{254.8}{\left[1 - \left(\frac{1300}{2254.9}\right)^2\right]^{0.893}} = 365.5 \text{ stb/d}$$

- Calculate J^* :

$$J_1^* = \frac{463.5}{2355.4} = 0.197 \text{ stb/d/psi}$$

$$J_2^* = \frac{365.5}{2254.9} = 0.162 \text{ stb/d/psi}$$

- Calculate A' and B' :

$$A' = \frac{0.197 - 0.162}{(2,355.4)^2 - (2,254.9)^2} = 7.554 \times 10^{-8}$$

$$B' = \frac{\frac{0.197}{(2355.4)^2} - \frac{0.162}{(2254.9)^2}}{\frac{1}{(2355.4)^2} - \frac{1}{(2254.9)^2}} = -0.222$$

- Calculate maximum future rate (for instance, a future reservoir pressure of 1,995 psia):

$$q_{\max} = 7.554 \times 10^{-8}(1995)^3 + (-0.222)(1,995) = 157 \text{ stb/d}$$

- The future IPR curve can then be predicted using the equation

$$q_o = 157 \left[1 - \left(\frac{P_{wf}}{1,995} \right)^2 \right]^{0.895}$$

ARTIFICIAL LIFT METHODS

Sucker Rod Pumping

Pumping Units

Components of Pumping System. The walking beam sucker rod system for producing fluids from wells is of ancient origin, and widely used. Over 90% of artificially lifted wells use beam-type pumps [54].

The system consists of surface and downhole components. Surface components are shown in Figure 6-111. The key components of the downhole pumping assembly are shown in Figure 6-112 for the two principal types of downhole sucker rod pumps.

Pumping Unit Operation. As the prime mover in Figure 6-111 drives the gear reducer, the walking beam oscillates about the saddle bearing and imparts a reciprocating motion to the sucker rods. As the sucker rods start the upstroke, they lift the plunger and traveling valve, creating a reduced pressure below it inside the working barrel. During this part of the cycle, the traveling valve is

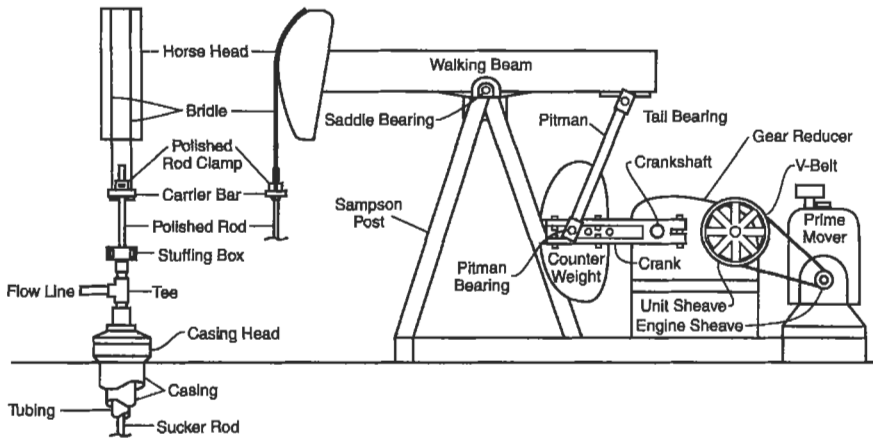


Figure 6-111. Surface equipment of a sucker rod pumping installation [60].

closed and the standing valve is open. This reduced pressure within the working barrel allows fluid to flow from the formation and the casing-tubing annulus (formation and casing-tubing annulus are not shown in Figure 6-112) through the mud anchor, dip tube, and standing valve and into the working barrel. On the downstroke, the traveling valve opens and the standing valve closes, allowing fluid in the barrel to move up into the tubing above the traveling valve. This fluid is in the annulus between the rods and the inside of the tubing. With each complete stroke, more fluid fills this annulus, and within a short time production appears at the surface. Because of compression of the fluid and elasticity in the system, production at the surface may appear continuous, but in reality production only occurs on the upstroke of the pump.

Pumping Unit Types and Specifications. Four types of beam pumping units are recognized. The classification is based on where the fulcrum is placed (Class I or Class III) and how they are counterbalanced (air, crank or beam). Three types are shown in Figure 6-113. In a Class I lever system (also called a *conventional pumping unit*), the fulcrum is near the center of the walking beam and the pitman applies lifting force by pulling downward at the rear of the walking beam. In a Class III lever system, the lifting force of the pitman is applied upward near the center of the beam. These Class III units are also referred to as units with *front mounted geometry*. The Lufkin Mark II is one such unit. A variation on the Class III system that normally has a crank-type counterbalance has, instead, a piston and cylinder filled with compressed air as the counterbalance.

Conventional pumping units in smaller sizes can have the counterbalance weights mounted at the rear of the walking beam (beam balanced units) or mounted on the crank arm (crank balanced units). Larger conventional units are all crank balanced.

In selecting a pumping unit, three principal specifications should be given:

1. torque rating of the pumping unit gear reducer in in.-lb
2. structural capacity of the unit; i.e., the load bearing capacity, in lb
3. maximum stroke length in in.

(text continued on page 598)

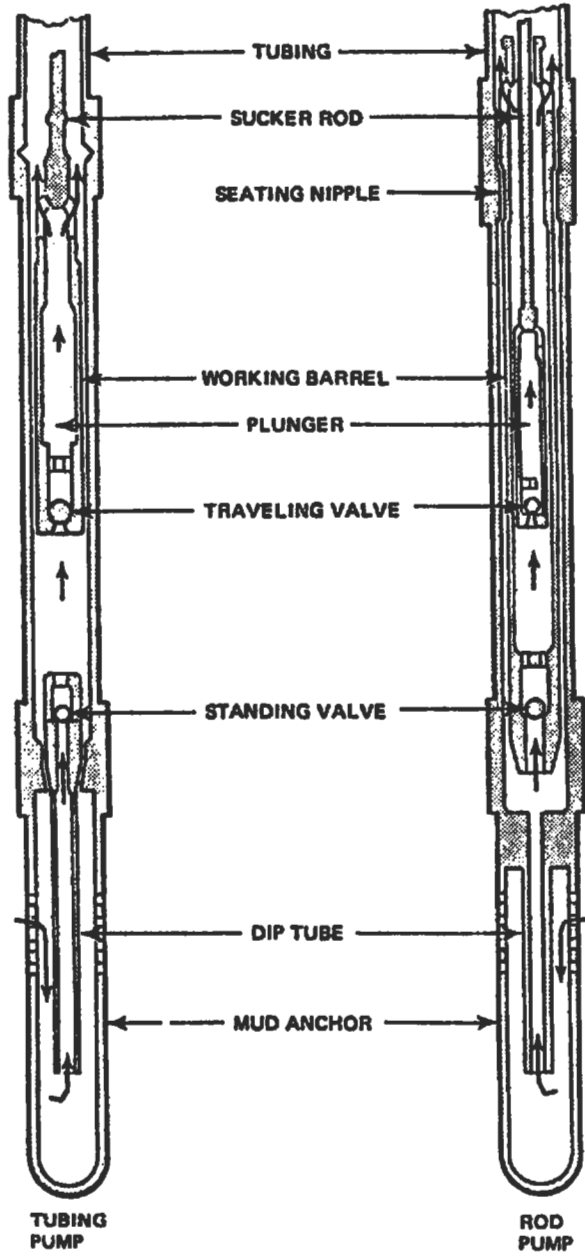
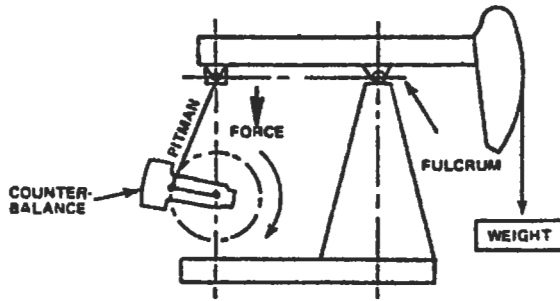
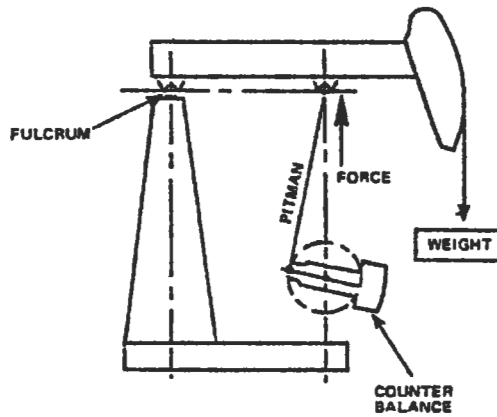


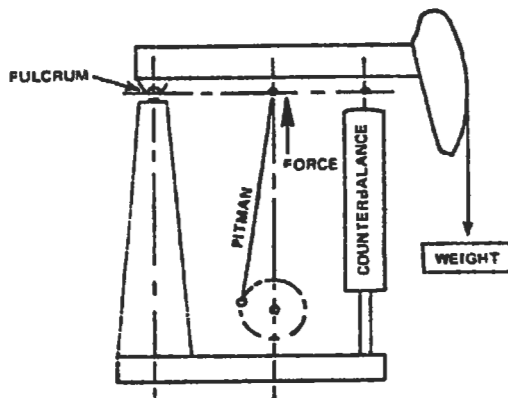
Figure 6-112. Downhole components for a tubing pump and rod pump [61].



CLASS I LEVER SYSTEM - CONVENTIONAL UNIT.



CLASS III LEVER SYSTEM - LUFKIN MARK II.



CLASS III LEVER SYSTEM - AIR BALANCED SYSTEM.

Figure 6-113. Simplified lever diagrams of Class I and Class III pumping units [61].

(text continued from page 595)

Table 6-22 lists these specifications for API standard units. Some manufacturers have additional intermediate sizes not shown in Table 6-22. Not all manufacturers make all sizes. The specification is a three-part code. A unit rating of 160-173-64 identifies a pumping unit having a gear reducer rating of 160,000 in./lb of torque, a structural load-bearing capacity as measured at the polished rod of 17,300 lb force and a maximum stroke length of 64 in.

Each pumping unit size generally has two to four stroke lengths at which it can operate, the largest stroke length of the two to four being the one given in the unit rating. One should refer to manufacturers' catalogues to find which smaller stroke lengths are available with each size of unit.

Table 6-22
Pumping Unit Size Ratings [62]

1	2	3	4	1	2	3	4
Pumping Unit Size	Reducer Rating, in.-lb	Structure Capacity, lb	Max. Stroke Length, in.	Pumping Unit Size	Reducer Rating, in.-lb	Structure Capacity, lb	Max. Stroke Length, in.
6.4-32-16	6,400	3,200	16	920-213-86	920,000	21,300	86
6.4-21-24	6,400	2,100	24	920-256-100	920,000	25,600	100
10-32-24	10,000	3,200	24	920-305-100	920,000	30,500	100
10-40-20	10,000	4,000	20	920-213-120	920,000	21,300	120
16-27-30	16,000	2,700	30	920-256-120	920,000	25,600	120
16-53-80	16,000	5,300	80	920-256-144	920,000	25,600	144
25-53-80	25,000	5,300	80	456-256-120	456,000	25,600	120
25-56-36	25,000	5,600	36	456-305-120	456,000	30,500	120
25-67-36	25,000	6,700	36	456-365-120	456,000	36,500	120
40-89-36	40,000	8,900	36	456-256-144	456,000	25,600	144
40-76-42	40,000	7,600	42	456-305-144	456,000	30,500	144
40-89-42	40,000	8,900	42	456-305-168	456,000	30,500	168
40-76-48	40,000	7,600	48	456-305-188	456,000	30,500	188
57-76-42	57,000	7,600	42	640-305-120	640,000	30,500	120
57-89-42	57,000	8,900	42	640-256-144	640,000	25,600	144
57-95-48	57,000	9,500	48	640-305-144	640,000	30,500	144
57-109-48	57,000	10,900	48	640-365-144	640,000	36,500	144
57-76-54	57,000	7,600	54	640-305-168	640,000	30,500	168
80-109-48	80,000	10,900	48	640-305-192	640,000	30,500	192
80-135-48	80,000	13,500	48	912-427-144	912,000	42,700	144
80-119-54	80,000	11,900	54	912-305-168	912,000	30,500	168
80-135-54	80,000	13,500	54	912-365-168	912,000	36,500	168
80-119-64	80,000	11,900	64	912-305-192	912,000	30,500	192
114-135-54	114,000	13,500	54	912-427-192	912,000	42,700	192
114-143-64	114,000	14,300	64	912-470-240	912,000	47,000	240
114-173-64	114,000	17,300	64	912-427-216	912,000	42,700	216
114-143-74	114,000	14,300	74	1280-427-168	1,280,000	42,700	168
114-119-86	114,000	11,900	86	1280-427-192	1,280,000	42,700	192
160-173-64	160,000	17,300	64	1280-427-216	1,280,000	42,700	216
160-143-74	160,000	14,300	74	1280-470-240	1,280,000	47,000	240
160-173-74	160,000	17,300	74	1280-470-300	1,280,000	47,000	300
160-200-74	160,000	20,000	74	1824-427-192	1,824,000	42,700	192
160-173-86	160,000	17,300	86	1824-427-216	1,824,000	42,700	216
228-173-74	228,000	17,300	74	1824-470-240	1,824,000	47,000	240
228-200-74	228,000	20,000	74	1824-470-300	1,824,000	47,000	300
228-213-86	228,000	21,300	86	2560-470-240	2,560,000	47,000	240
228-246-86	228,000	24,600	86	2560-470-300	2,560,000	47,000	300
228-173-100	228,000	17,300	100	3648-470-240	3,648,000	47,000	240
228-213-120	228,000	21,300	120	3648-470-300	3,648,000	47,000	300

Sucker Rods

Types, Sizes and Grades. For steel sucker rods, Table 6-23 gives data useful in calculations of sucker rod pumping problems. A companion table, Table 6-24, gives useful design data on the common sizes of tubing used. See the section titled "Natural Flow Performance" for full data on tubing. General dimensions

Table 6-23
Sucker Rod Data [57]

1	2	3	4
Rod Size	Metal Area, Sq in.	Rod Weight in air, lb per ft W_r	Elastic Constant, in. per lb ft E_r
½	0.196	0.72	1.990×10^{-6}
¾	0.307	1.13	1.270×10^{-6}
1	0.442	1.63	0.883×10^{-6}
1½	0.601	2.22	0.649×10^{-6}
2	0.785	2.90	0.497×10^{-6}
2½	0.994	3.67	0.393×10^{-6}

Table 6-24
Tubing Data Useful for Pumping System Design [57]

1	2	3	4	5
Tubing Size	Outside Diameter, in.	Inside Diameter, in.	Metal Area, sq. in.	Elastic Constant, in. per lb ft E_t
1.900	1.900	1.610	0.800	0.500×10^{-6}
2¾	2.375	1.995	1.304	0.307×10^{-6}
2¾	2.875	2.441	1.812	0.221×10^{-6}
3¾	3.500	2.992	2.590	0.154×10^{-6}
4	4.000	3.476	3.077	0.130×10^{-6}
4½	4.500	3.958	3.601	0.111×10^{-6}

and tolerances for steel sucker rods are given in Figure 6-114. Specifications for full size and slimhole couplings appear in Tables 6-25 and 6-26, respectively, and are diagrammed in Figure 6-115. The recently published API specifications for reinforced plastic sucker rods are given in Figure 6-116.

From the point of view of the materials used in their manufacture, all commercial available rods are divided into two classes, steel and reinforced plastic sucker rods. The steel rods are available in three API grades: K, C and D. Composition and tensile strength of these rods are shown in Table 6-27. Commonly available recommended sucker rod endurance limits are shown in Table 6-28. The range of tensile strength available is accomplished by altering the chemical content of the steel and by the treatment process used in rod manufacturing such as tempering, normalizing, quenching, and case hardening.

In general, the maximum allowable stress on rods should not exceed 30,000 psi to 40,000 psi. In any case, the maximum stress and range at stress should be checked against the Goodman diagram maximum allowable stress discussed in the section titled "Allowable Rod Stress and Stress Range." An exception is the "Electra" rods of the Oilwell Division of United States Steel that have ratings of 40,000 psi and 50,000 psi. The Goodman diagram analysis procedure is not applicable to these rods.

Selection of API Steel Sucker Rods. The principal considerations in selection of API steel sucker rods are the range of stress, the level of stress that the rods will experience and the degree of corrosiveness of the environment in which they will operate. Rods should be selected to be able to withstand not only the maximum stress that they will experience but also the range of stress. This requires the use of the modified Goodman diagram described in the section titled "Allowable Rod Stress and Stress Range."

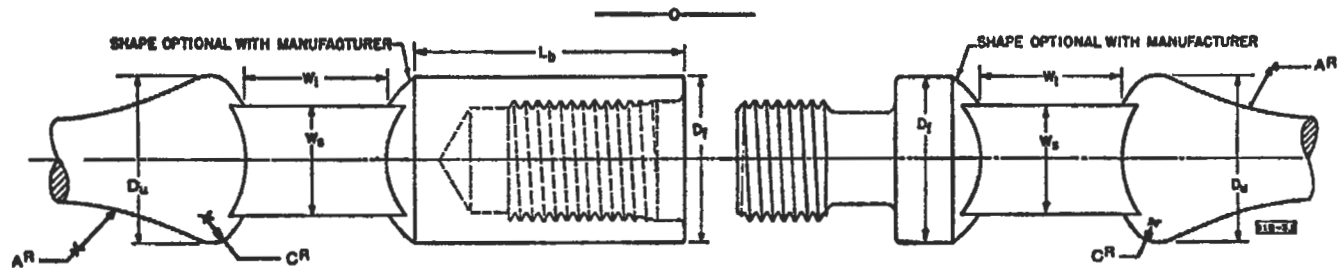
Chemical inhibition programs can be effective in overcoming corrosion. Refer to Chapter 7 for a discussion of corrosion mitigation procedures. No existing grade of rods will withstand all possible corrosion conditions and some treatment may be needed even for mild corrosion environments.

For nonsour (so-called sweet crudes) one should select the lowest grade rod which meets the stress and stress range conditions.

Where sulfide stress cracking exists, one should use a rod with a Rockwell hardness less than 23. Grade C rods meet this requirement. The stress and stress range must be checked to see if the C rods also meet this stress criterion. D grade rods are not recommended for sour crude environments unless an effective corrosion inhibition program is applied.

Grade K rods are available when other grades have not performed satisfactorily.

Allowable Rod Stress and Stress Range. A string of sucker rods when in normal operation is subject to alternating high and low stress because of the nature of the pumping cycle. On the upstroke, the rods bear a load that includes their own weight, the weight of the fluid they are lifting, friction and effects of acceleration. On the downstroke, the rods carry some friction load and the load of their own weight diminished by effects of deceleration. The ratio of upstroke to downstroke load and hence ratio of upstroke to downstroke stress can be 2 to 1 or often 3 to 1 or more. This cycle of alternating high and low stress occurs at a frequency at least equal to the pumping speed. A unit pumping at 20 strokes per minute goes from high stress to low stress every 3 s or 10,500,000 cycles per year. This process repeated on the rods over months and years can easily lead to metal fatigue.



**GENERAL DIMENSIONS FOR SUCKER-ROD
BOX AND PIN ENDS**

Figure 6-114. General dimensions and tolerances for sucker rods and pony rods [63].

Table 6-25
Dimensions of Fullsize Couplings and Subcouplings [63]

1	2	3	4	5	6
Nominal Coupling Size*	Outside Diameter	Length	Length of Wrench Flat	Dist. Between Wrench Flats	Used With
	+0.005 -0.010	Min.	Wrench Flat	0-3/16 (0-.8mm)	Min. O.D.
	<i>W</i>	<i>N_L</i>	<i>W_L**</i>	<i>W_j</i>	Tubing Size
3/8 (15.9)	1 1/2 (38.1)	4 (101.6)	1 1/2 (31.8)	1 1/2 (34.9)	2 1/2 (52.4)
1/2 (19.1)	1 3/4 (41.3)	4 (101.6)	1 1/2 (31.8)	1 1/2 (38.1)	2 3/4 (60.4)
5/8 (22.2)	1 7/8 (46.0)	4 (101.6)	1 1/2 (31.8)	1 1/2 (41.3)	2 7/8 (73.0)
1 (25.4)	2 (55.6)	4 (101.6)	1 1/2 (38.1)	1 1/2 (47.6)	3 (88.9)
1 1/8 (28.6)	2 1/8 (60.3)	4 1/2 (114.3)	1 1/2 (41.3)	2 1/2 (53.9)	3 1/2 (88.9)

*Also size of rod with which coupling is to be used.

**Minimum length exclusive of fillers.

Table 6-26
Dimensions of Slimhole Couplings and Subcouplings [63]

1	2	3	4
Nominal Coupling Size*	Outside Diameter	Length	Used With
	.005-.010 in.	Min.	Min.
	(.13-.25 mm)	<i>N_L</i>	Tubing Size O.D.
3/8 (12.7)	1 (25.4)	2 1/2 (69.9)	1.660 (42.2)
1/2 (15.9)	1 1/4 (31.8)	4 (101.6)	1.990 (50.6)
5/8 (19.1)	1 1/2 (38.1)	4 (101.6)	2 1/16 (52.4)
3/4 (22.2)	1 3/4 (41.3)	4 (101.6)	2 1/8 (60.4)
1 (25.4)	2 (50.8)	4 (101.6)	2 1/4 (73.0)

*Also size of rod with which coupling is to be used.

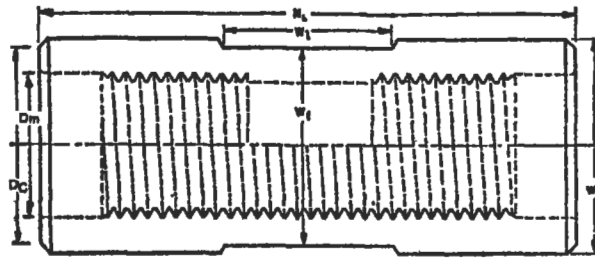
In designing API steel sucker rod strings, it is recommended that the modified Goodman diagram shown in Figure 6-117 be used as the basis for stress analysis. This method of analysis compensates for the deleterious effects of cyclic stress and helps to prevent premature metal fatigue caused by cyclic stress. The key applicable terms for the diagram and the associated equation are given in the diagram. However, more explanation is given below for the terms of greatest interest. The diagram can be reduced to an equation as follows:

$$S_A = (T/4 + 0.5625 \times S_{min}) \times SF \quad (6-190)$$

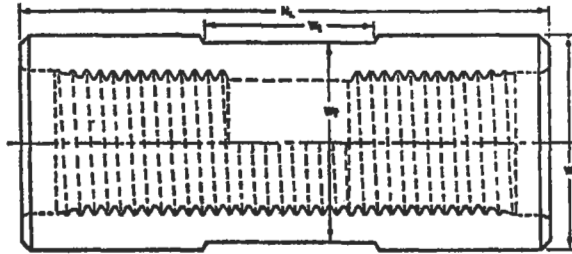
The equation in the form above can be used in either English or metric units. An example is given below. The terms in the equation have the following significance:

S_A = Maximum allowable stress in the rods for a given value of minimum stress, S_{min} and service factor (see definitions below).

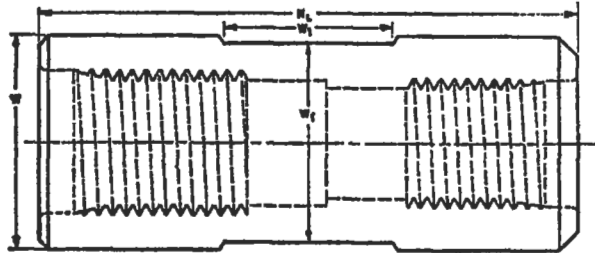
T = Minimum tensile stress for rods of a given API rating. Refer to Table 6-27 for these minimum tensile strength values. (Example: for C rods, T = 90,000 psi.)



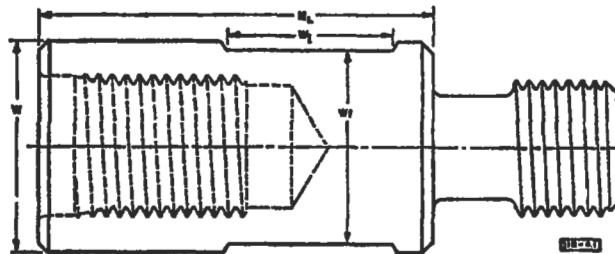
**SUCKER-ROD COUPLING
(DO NOT USE ON POLISHED RODS)**



POLISHED-ROD COUPLING



**BOX AND BOX SUBCOUPLING
(TYPE I)**



**BOX AND PIN SUBCOUPLING
(TYPE II)**

Figure 6-115. Dimensions of sucker rod couplings, polished rod couplings and subcouplings [63].

1	2	3	4	5	6	7	8	9	10	11
Nominal Size of Rod Body ±0.015	Rod Pin Size	Nominal Diameter of Pin P	Outside Diameter of Pin Shoulder +0.005 -0.010 D _f	Width of Wrench Square ±1/32 W _s	Length of Wrench Square (1) W ₁	Maximum Diameter of End Fitting D _e	Maximum Length of End Fitting L	Maximum Diameter of Extension (2) X	Length of Pin-and-Pin Sucker Rod ±0.5 in. (3)	Length of Pin-and-Pin Pony Rod ±0.5 in. (8)
.625	1/4	3/8	1.000	3/8	1 1/4		Not to Exceed		25,30,37.5	3,6,9,18
.750	3/8	1/2	1.250	1	1 1/4	Not to Exceed	10 Inches Exclusive of Extension If Used	See Note (2)	25,30,37.5	3,6,9,18
.875	1/2	5/8	1.500	1 1/8	1 1/4	Not to Exceed	10 Inches Exclusive of Extension If Used	See Note (2)	25,30,37.5	3,6,9,18
1.000	3/4	3/4	1.625	1 1/8	1 1/4	Not to Exceed	10 Inches Exclusive of Extension If Used	See Note (2)	25,30,37.5	3,6,9,18
1.250	1	1 1/4	2.000	1 1/2	1 1/4	Not to Exceed	10 Inches Exclusive of Extension If Used	See Note (2)	25,30,37.5	3,6,9,18

(1) Minimum length exclusive of fillet.

(2) The extension is that portion of the rod body or that portion of the end fitting which is immediately adjacent to the smaller end of the elevator taper. If this section of the end fitting is longer than .25", the maximum outside diameter shall not be more than .200" larger than the diameter of the rod body. If this section of the end fitting is .25" or less in length, the outside diameter shall not be more than .25" larger than the diameter of the rod body.

(3) The length of pin-and-pin rods shall be measured from contact face of pin shoulder to contact face on the field end of the coupling.

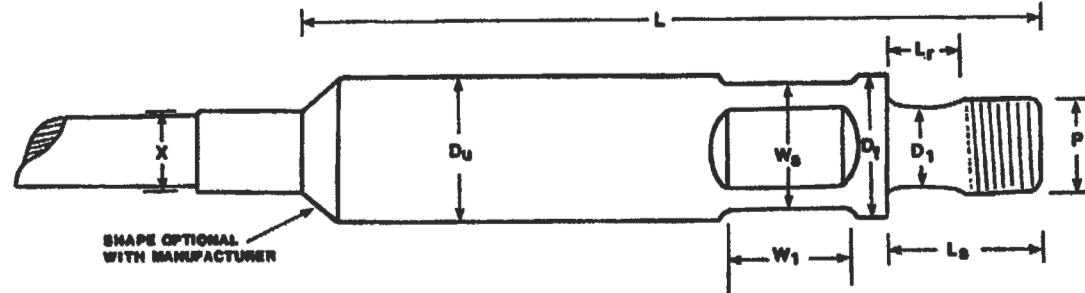


Figure 6-116. General dimensions and tolerances for reinforced plastic sucker rods and pony rods [64].

Table 6-27
Chemical and Mechanical Properties of Steel Sucker Rods [63]

1	2	3	4
Grade	Chemical Composition	Tensile Strength, psi	
		Min. (PSI)	Max. (PSI)
		(MPA)	(MPA)
K	AISI 46XX	85,000 (586)	115,000 (793)
C	AISI 1536 ⁽¹⁾	90,000 (620)	115,000 (793)
D	Carbon or Alloy ⁽²⁾	115,000 (793)	140,000 (965)

⁽¹⁾Generally manufactured from, but not restricted to, AISI 1536.

⁽²⁾Any composition which can be effectively heat treated to the minimum ultimate tensile strength.

S_{\min} = Minimum stress to be experienced by the rods in the pump cycle.

SF = Service factor. This is a factor that adjusts, usually downward, the estimated allowable maximum stress to account for corrosive conditions. See Table 6-29 for suggested service factors for API Grade C and D rods.

Equation 6-190 can be written in forms applicable to specific API rod grades as follows:

Grade C rods:

$$S_A = (22,500 + 0.5625 \times S_{\min}) \times SF \quad (6-191)$$

Grade D rods:

$$S_A = (28,750 + 0.5625 \times S_{\min}) \times SF \quad (6-192)$$

$$S_A, S_{\min} = \text{lb/in.}^2 \text{ or psi}$$

SF is dimensionless.

Example Calculation

Given: A 77 Grade D rod string operating in a saltwater-crude oil environment has a minimum polished rod load measured with a dynamometer of 15,000 lbf.

Desired: Maximum allowable stress and load for this rod string.

Solution

Step 1: A 77-rod string has a cross-section area of 0.601 in.² (See Table 6-23). Use this area to compute rod stress from rod load.

Table 6-28
Recommended Endurance Limits of Sucker Rods

Rod type	AISI-ASAE steel grade	Endurance limit in corrosive fluid ^a , psi	
		With H ₂ S	Without H ₂ S
Carbon Steel	C1033		
	C1035		
	C1036		
	C1038		
	C1039		
	C1040		
	C1042		
	C1043		
Alloy Steel	Mn 1335		
	Ni-Cr 3310		
	Ni-Cr (Mayar)	22,000	30,000
	Ni-Mo 4620	22,000	30,000
	Ni-Mo 4621	22,000	30,000
	Ni-Mo 4800 series	22,000	

^a Corrosive fluids effectively treated with a chemical inhibitor may be considered noncorrosive.

$$S_{\min} = \frac{\text{Min. load}}{\text{Rod area}} = \frac{15,000 \text{ lbf}}{0.601 \text{ in.}^2} = 24,960 \text{ psi}$$

Step 2: Determine the service factor. From Table 6.29, for a Grade D rod, the service factor for saltwater (brine) service is recommended to be 0.90.

Step 3: Use the Goodman diagram equation to compute S_A . Use Equation 6-192 for Grade D rods.

$$\begin{aligned} S_A &= (28,750 + 0.5625 \times S_{\min}) \times SF \\ &= (28,750 + 0.5625 \times 24,960) \times 0.90 = 38,510 \text{ psi} \end{aligned}$$

**Table 6-28
(continued)**

Rod type	Endurance limit in non-corrosive fluid for stress range ^b , psi		
	<60%	>60%	<30%
Carbon Steel	30,000		
	30,000		
	30,000		
	30,000		
	30,000		
	30,000		
	30,000		
	30,000		
Alloy Steel		30,000	40,000
			40,000
		30,000	40,000
		30,000	40,000
		30,000	40,000

^b Stress range is given as per cent of maximum operating stress.
(Courtesy Bethlehem Steel Corp.)

Step 4: Compute maximum allowable loads by multiplying S_A by rod area.

$$\text{Max allowable load} = S_A \times \text{rod area}$$

$$38,510 \text{ psi} \times 0.601 \text{ in}^2 = 23,140 \text{ lbf}$$

Service factors should be considered as guidelines and not as highly precise universal parameters. Experience from a given area should be used to determine proper service factors for given types of corrosive environments.

Sucker Rod Pumps

Pump Designations. The API presents a standardized notation for designating subsurface sucker rod pumps. This notation is shown in Figure 6-118.

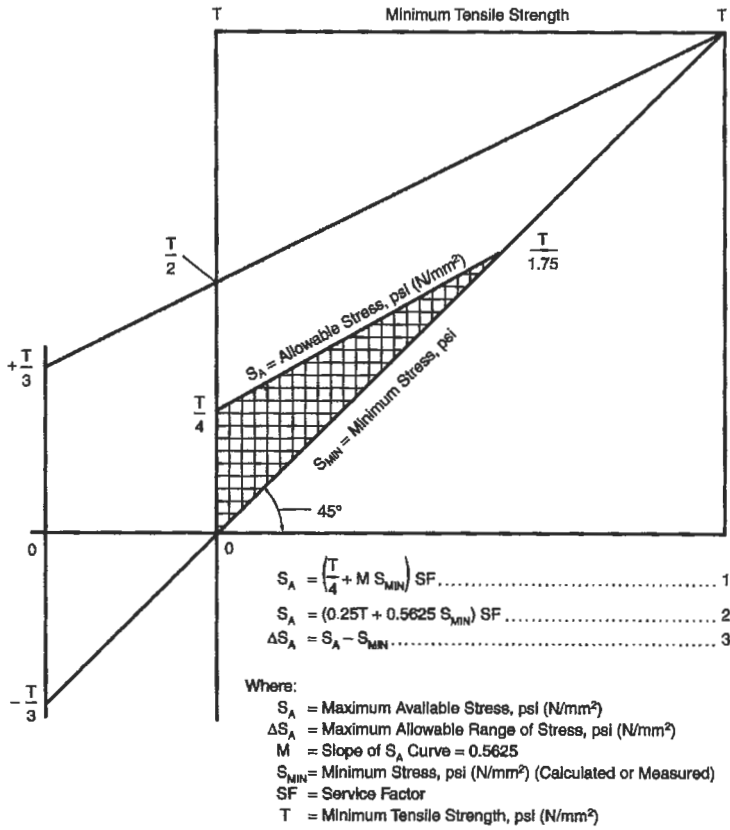


Figure 6-117. Modified Goodman diagram for allowable stress and range of stress in noncorrosive service [66].

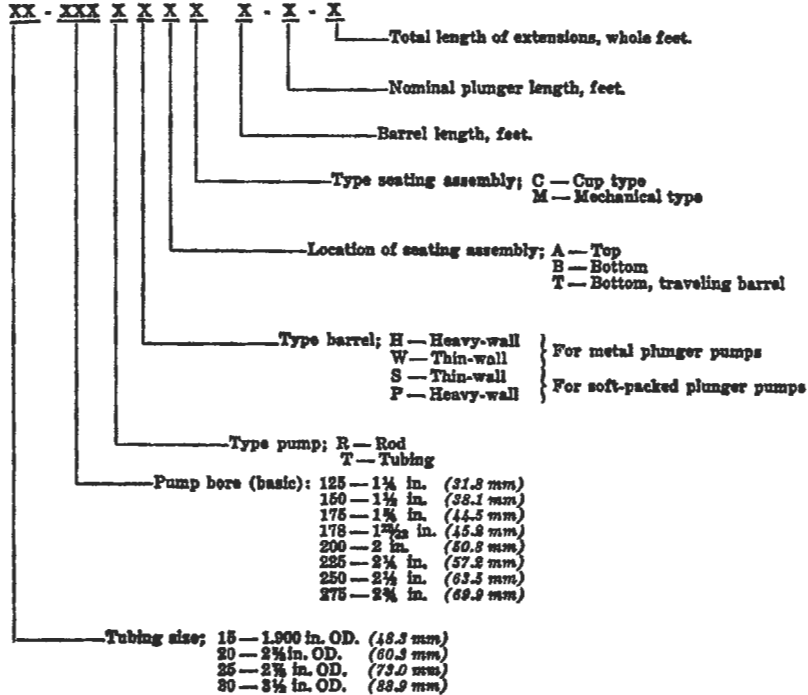
Table 6-29
Suggested Service Factors for API Grade C
and Grade D Rods in Corrosive Conditions [61]

Service	API C	API D
Non-corrosive	1.00	1.00
Salt water	0.90	0.65
Hydrogen sulfide	0.70	0.50

The basic types of pumps and letter designation covered by this specification are as follows:

Type of Pump	Letter Designation			
	Metal Plunger Pumps		Soft-packed Plunger Pumps	
	Heavy-Wall Barrel	Thin-Wall Barrel	Heavy-Wall Barrel	Thin-Wall Barrel
Rod Pumps				
Stationary Barrel, Top Anchor	RHA	RWA	RSA
Stationary Barrel, Bottom Anchor	RHB	RWB	RSB
Traveling Barrel, Bottom Anchor	RHT	RWT	RST
Tubing Pumps	TH	TP

2.2 Complete pump designations include: (1) nominal tubing size, (2) basic bore diameter, (3) type of pump, including type of barrel and location and type of seating assembly, (4) barrel length, (5) plunger length, and (6) total length of extensions when used, as follows:



Example: A 1 1/4 in. (31.8 mm) bore rod type pump with a 10 ft. (3.048 m) heavy wall barrel and 2 ft. (0.610 m) of extensions, a 4 ft. (1.219 m) plunger, and a bottom cup type seating assembly for operation in 2 in. (50.8 mm) tubing, would be designated as follows:

20-125 RHBC 10-4-2

- 2.3 In addition to the pump designation described in Par. 2.2, it is necessary for the purchaser to provide the following additional information:

- Barrel material
- Plunger material
- Plunger clearance (ft)
- Valve material
- Length of each extension

NOTE: Metallic Materials for Subsurface Sucker Rod Pumps for Hydrogen Sulfide Environments are listed in NACE Std MR-01-76.

Figure 6-118. API pump designation [54].

As indicated in Figure 6-112, two types of pumps are available, tubing pumps and rod pumps. Both have metal barrels and plungers. The running seals may be either metallic or nonmetallic.

Tubing Pumps. The barrel of the tubing pump is attached directly to the tubing at or near the lower end of the tubing. A seating nipple placed below the pump barrel is used to hold the standing valve. After the pump barrel is in place, the plunger and traveling valve assembly is run into the well. The lower end of the

plunger assembly has a standing valve puller to which is attached the standing valve. During the pump installation process, when the standing valve reaches the seating nipple, the standing valve is locked in place. The rods are then rotated counterclockwise to disconnect the standing valve puller from the standing valve. The plunger is then raised sufficiently to allow minimum clearance on the downstroke. At least 1 ft of clearance is recommended to compensate for overtravel of the pump plunger during pumping. Final spacing of the pump is done by proper placement of the polished rod clamp.

Rod Pumps. A rod pump has the same component parts as a tubing pump, namely standing valve, seating nipple, pump barrel, plunger and traveling valve, but they are connected in such a way that the plunger, traveling valve, standing valve and pump barrel can be pulled from the tubing using the rod string. In a tubing pump, the tubing as well as the rods must be pulled to remove the pump barrel. Rod and tubing pumps are spaced in the same way. Clearance at the bottom of the pump stroke must be kept to a minimum in gassy wells to maximize pump fillage on the upstroke.

The choice between a tubing pump and a rod pump for a given installation is an important one. A comparison of rod and tubing pumps and of top and bottom anchors for the pumps is given in Table 6-30. Additional information is available in Reference [54].

Obtaining Optimum Performance

Pump Submergence. The energy to fill the pump should be supplied by the formation rather than by a high fluid head in the casing tubing annulus if maximum production is desired. Where feasible, pump intake should be below the perforations or as close above them as possible.

Gas Separation. Gas evolution within the pump barrel or below the standing valve can cause significant reduction in pump volumetric efficiency. Where gas evolution is a problem, some type of downhole gas separator (commonly called a *gas anchor*) should be used.

Sand Control. Where sand production exists, some method of sand control, such as gravel packs, screens, or formation bonding agents, should be used to maximize pump life.

Common Pump Problems and Solutions. Several frequently occurring operating problems and their solutions are discussed in Reference [54] and are summarized here.

Corrosion. The principal corroding agents in pumping wells are carbon dioxide, hydrogen sulfide, oxygen and brine, either singly or in combination. The failure mechanisms that these agents can create are sulfide stress cracking, corrosion fatigue, erosion corrosion, stress corrosion, galvanic corrosion, pitting and wear abrasion.

When corrosive conditions exist, the metallurgy of the pump and downhole accessories should be chosen to resist the corrosion. Chemical inhibitors can be helpful but will not prevent corrosion in all cases. Such inhibitors protect casing, tubing, and rods better than the pump parts. Thus, corrosion resistance here is best obtained through proper selection of pump materials for construction. Refer to Chapter 7 for more details on corrosion mitigation.

Table 6-30
Comparison of Pump Types and Anchor Types

Tubing Pumps	
Advantages	Disadvantages
<ul style="list-style-type: none"> • Largest displacement • Strongest 	<ul style="list-style-type: none"> • Must pull tubing to remove pump • Poor for gassy wells • Large rod load
Rod Pumps	
Traveling Barrel, Bottom Anchor	
Advantages	Disadvantages
<ul style="list-style-type: none"> • Sand kept in motion near barrel • Good for intermittent pumps • Strong plunger-rod connection • Open cages allow low pressure drop • Low pressure drop across barrel 	<ul style="list-style-type: none"> • Less desirable for low static level wells • Long pull tubes can become bowed
Stationary Barrel, Bottom Anchor	
Advantages	Disadvantages
<ul style="list-style-type: none"> • Generally suited for deep wells • Useful for low static level wells • Useful for gassy wells 	<ul style="list-style-type: none"> • Hazardous to use in sandy wells • Not recommended for intermittently produced wells
Stationary Barrel, Top Anchor	
Advantages	Disadvantages
<ul style="list-style-type: none"> • Useful for sandy wells • Useful for some low fluid level gassy wells 	<ul style="list-style-type: none"> • Thin wall pump barrels can burst in deep wells

Fluid Pound. A fluid pound condition exists when insufficient liquid enters the pump barrel on the pump upstroke. Above the liquid, a gas space is created between the traveling valve and the standing valve. During the next downstroke, the traveling valve does not open until the plunger hits the liquid. This impact sends a strong shock wave up the rods to the surface. In some instances the shock can be carried to the gear reducer of the beam pumping unit. When this pounding or shock is repeated with each pump cycle and for significant periods

of time, major structural damage can occur in the downhole and surface equipment. This damage can include:

- a. gear tooth failure in pumping units
- b. damage to the pumping unit base structure
- c. rod fatigue and failure
- d. accelerated wear on traveling valve cages, balls and seats
- e. accelerated wear on tubing threaded connections

Fluid pound can be caused by one of two conditions: (1) a "pumped-off" condition of the well in which the well cannot produce as much fluid as the pump can lift to the surface, and (2) restricted intake to the pump because of mechanical blockage at the pump.

The pumped-off condition can be prevented by slowing down the pump, using a smaller size pump or shorter stroke length, or putting the pump on a percentage timer if the prime mover is electric. Various pump-off controllers are available to sense when a well is nearing a pumped-off condition. The controllers then shut off the pump for a predetermined period.

If the fluid pound is caused by restricted fluid entry, none of the above alternative remedies are appropriate. Only proper pump servicing will remove the restriction.

Gas Pound. Gas pound has a behavior and observed effect somewhat similar to that of fluid pound but has a different cause. It occurs when no "pumped-off" condition exists. There may or may not be an intake flow restriction. The cause of gas pound is occurrence of excessive gas in the pump barrel on the pump upstroke. It can be caused by inadequate downhole gas separation or gas breakout due to oil flow through flow restrictions in the standing valve or dip tube. A gassy crude can evolve significant gas if it is forced at high velocity through a flow restriction. If the gas pound is caused by excessive free gas and there is ample flow area in the standing valve port and cages, then a better gas anchor is needed. If flow restrictions exist, then more open cages and large-diameter dip tubes should be tried.

Sand Accumulation. Although proper choice of metallurgy for downhole pump barrels, plungers, valves and cages will help in alleviating a sand accumulation problem, sand control methods should be evaluated also.

Scale Formation. Chemical scale deposits can occur in some producing wells, and in extreme cases be so severe as to seriously restrict flow of oil through the pump and tubing. Chemical scale inhibition agents are available that will either eliminate or significantly reduce the effect of scale deposition. Because scale deposition is a cumulative effect, treatment must follow a fixed and uninterrupted treatment regime. Refer to Chapter 7 for a complete discussion of the causes and control procedures for scale deposition.

Primer Movers

Both internal combustion engines and electric motors have been used as prime movers for pumping units. Internal combustion engines operating on gas are preferred in areas where ample lease gas is available and wells can be pumped continuously. Where intermittent operation is required or gas must be purchased

and electricity is available, electric motors have become widely used. Electric motors are more easily adaptable to remote monitoring and control for lease automation.

Electric-Motor Types. Four classes of electric motors within the National Electrical Manufacturers Association (NEMA) classification are in common use for pumping unit prime movers.

1. NEMA C normal slip (less than 5%): low initial cost, moderately high starting torque
2. NEMA D medium slip (5 to 8%): higher starting torque and slip than class C
3. NEMA D high slip (8 to 13%): widely used now as having an attractive price performance ratio.
4. Ultrahigh slip motors (slip up to 30%): relatively new; motor is more fully loaded during the entire pump cycle; designed specifically for beam pumping units

Slip is the difference in motor speed between its synchronous (unloaded) and loaded condition divided by the unloaded speed. An induction motor that has a synchronous speed of 1,200 rpm and a loaded speed of 1,050 rpm has a slip of

$$\frac{1,200 - 1,050}{1,200} \times 100 = 12.5\% \text{ slip}$$

Most oilfield pumping unit electric prime movers are three-phase induction motors. Single-phase motors are restricted to shallow low-volume pumping units.

Internal Combustion Engines. Internal combustion engines designed to run on natural gas or propane and serve as pumping unit prime movers can be classified based on their speed, strokes per cycle and the number of cylinders. Slow-speed engines are those having a crankshaft rpm of 750 rpm or less. High-speed engines have speeds up to 2,000 rpm; these are multicylinder engines. Some engine designs employ two strokes per cycle and others use four strokes per cycle. The two-stroke engines have been widely used since the early days of the oil industry. The two-strokes-per-cycle engine (often called a *two-cycle engine*) are mostly slow-speed engines in single or multiple cylinders and having horse-power rating from 15 to 325 hp.

The four strokes per cycle engine (often called a *four-cycle engine*) is usually a multicylinder engine. These can run on natural gas, LPG or gasoline.

Selecting Prime Mover Size. Several empirical equations are in use for scaling theoretical or hydraulic horsepower rating such as obtained from beam pumping system design procedures (see the section titled "Selection of Beam Pumping Unit Installation") to brake or prime mover horsepower. These have been discussed by Brown [55] and by Curtis and Showalter [56]. These empirical equations are all essentially of the form

$$HP_{pm} = \frac{q \times D}{PMF} \quad (6-193)$$

where HP_{pm} = primer mover in hp
 q = oil and water daily production in bbls/d

d = net lift of liquid in ft
 PMF = prime mover factor

This prime mover factor PMF consists of two components: a units conversion factor that accepts the other terms of Equation 6-193 in the given units and converts the numerator product to horsepower; and a component that increases the horsepower to account for energy losses such as friction, and needed engine derating because of the cyclic nature of the engine load. The influence of these extra effects is not easily estimated. Thus an empirical adjustment is made based on experience.

If the lifted fluid has a specific gravity of 1.0 and is lifted with 100% efficiency, the PMF would be 135,735. The computed horsepower would be the theoretical or hydraulic horsepower. Because of the need for a prime mover rating considerably above the theoretical, various manufacturers use PMFs from 1.8 to 3.0 times smaller than 135,735. Curtis and Showalter indicate that for high slip NEMA D motors or slow-speed internal combustion engines, the recommended prime mover horsepower can be obtained from the following equation:

$$HP_{pm} = \frac{q \times D}{56,000} \quad (6-194)$$

For high-speed internal combustion engines or normal slip NEMA C motors, the prime mover horsepower suggested is

$$HP_{pm} = \frac{q \times D}{45,000} \quad (6-195)$$

Example Problem

Determine the prime mover horsepower for lifting 100 bpd of oil and water production having a composite specific gravity of 1.0. The net lift is 10,000 ft. Assume a slow-speed internal combustion engine or a high slip NEMA D motor will be selected.

Solution

Use Equation 6-194, such that

$$HP_{pm} = \frac{\frac{100 \text{ bbl}}{d} (10,000 \text{ ft})}{54,000} = 17.9 \text{ hp}$$

The actual engine or motor would be selected, with the nearest larger name-plate rating at 20 hp.

Selection of Beam Pumping Unit Installation

Computation Procedures. Selection of the proper equipment for a new well follows an orderly sequence based on computation of pumping unit performance. The

method suggested here is that recommended by API [57]. Various commercially available computer programs make complete calculations for a wider variety of pumping unit types, rod types, depth and inclination of the hole. Some of these programs base their design on dynamic analysis of the elastic behavior of the rods and tubing and can include inertial effects of the surface equipment. With correct input as to well conditions and equipment characteristics, these latter programs can make a very precise estimate of loads and stresses in the pumping system and lead to an optimal design. Simpler microcomputer programs are now available quite inexpensively to perform the calculations described here for manual use. This API RP11L calculation procedure is intended for design of conventional geometry (Class I) units pumping in nondeviated wells at depths of less than 12,000 feet. The method is based on use of API grade steel sucker rods.

Required information. Before the API RP11L calculation procedure can be started, the following information must be available for the well.

- a. expected oil and water production, in bbl/d, and their specific gravities
- b. casing and tubing sizes
- c. anchoring depth (if any) for tubing
- d. pump setting depth
- e. fluid level during production (when pumping)

The design considerations in proper selection of each of these items are discussed separately in the following sections.

Expected Fluid Production. Expected production depends upon how much the pump in the well can lift and on how much oil the formation can produce. The volume of oil that can theoretically be displaced or moved by the pump is called the *pump displacement* PD and is given by the following equation:

$$PD = A_p \times S_p \times N \times \text{Con} \quad (6-196)$$

The volume of oil actually produced at the surface is given by

$$Q = E_v \times PD \quad (6-197)$$

where PD = theoretical displacement of the pump in bpd

A_p = cross section area of plunger in in.²

S_p = effective stroke length of the plunger in in.

N = pumping speed in strokes/min

Con = a units conversion constant, 0.1484

Q = rate of oil and/or water produced at the surface in bpd

E_v = volumetric efficiency of pump displacement process (a fraction)

To simplify the calculations, the terms A_p and Con are frequently lumped together to give a pump constant, K. Pump displacement is then computed from

$$PD = K \times S_p \times N \quad (6-198)$$

Table 6-31 gives pump constants K for various sizes of plungers and can be used to compute pump displacement.

Table 6-31
Pump Factors or Constants [57]

Plunger diam in.	Area of plunger sq. in. (A_p)	Pump Constant (K)
$\frac{5}{8}$	0.307	0.046
$\frac{3}{4}$	0.442	0.066
$\frac{15}{16}$	0.690	0.102
*1	0.785	0.117
* $1\frac{1}{16}$	0.886	0.132
$1\frac{1}{8}$	0.994	0.148
* $1\frac{1}{4}$	1.227	0.182
* $1\frac{1}{2}$	1.767	0.262
* $1\frac{3}{4}$	2.405	0.357
* $1\frac{25}{32}$	2.488	0.370
*2	3.142	0.466
* $2\frac{1}{4}$	3.976	0.590
* $2\frac{1}{2}$	4.909	0.728
* $2\frac{3}{4}$	5.940	0.881
* $3\frac{3}{4}$	11.045	1.640
* $4\frac{3}{4}$	17.721	2.630

*API sizes

Example Problem

Given: A $1\frac{1}{2}$ -in. plunger is being used to pump oil at 16 strokes per minute and an effective downhole stroke of 51.5 in. The pump volumetric efficiency is estimated to be 70%.

Desired: Daily surface production of oil, bpd

Solution

Step 1. Using data from Table 6-31 and Equation 6-196 we obtain pump displacement:

$$\begin{aligned} PD &= A_p \times S_p \times N \times Con \\ &= (1.767 \text{ in.}^2) \times (51.5 \text{ in.}) \times (16 \text{ spm}) \times 0.1484 \\ &= 216 \text{ bpd} \end{aligned}$$

Step 2. Determine surface production from Equation 6-197.

$$\begin{aligned} Q &= E_v \times PD \\ &= 0.70 \times 216 \text{ bpd} = 151 \text{ bpd} \end{aligned}$$

An alternate solution using pump constants is

$$\begin{aligned} PD &= K \times Sp \times N \\ &= (0.262)(51.5)(16) = 216 \text{ bpd} \end{aligned}$$

Volumetric efficiency E_v is normally between 70 and 100%. In unusual circumstances where a well is partially flowing while pumping, the E_v can be above 100% (flumping wells). Several factors contribute to decrease E_v below 100%. These include slippage past the plunger on the upstroke and gas evolution from the oil as the oil enters the pump barrel and as gas evolves from the oil as it rises up the tubing. This latter effect is accounted for by the oil formation volume factor. An oil with a formation volume factor of 1.15 requires 1.15 barrels of oil at reservoir condition to yield 1.0 barrels at the surface. This factor, alone, without any pump slippage would give an E_v of $(1/1.15) \times 100 = 87\%$.

The pump can displace the computed pump displacement PD only if the formation can produce this much oil. Optimal performance is obtained when the pump production at the surface matches the ability of the formation to produce, or when the pump produces at the statutory limit on production or the limit determined by prudent reservoir operation.

The estimate of the formation's ability to produce should be based on one or more well tests whenever possible. A productivity index or inflow performance relation should be used to determine the volume of fluid which the formation can produce under various conditions of flowing bottom hole pressure. A method widely used for solution gas drive fields producing oil, gas, and only a small amount of water, or none is based on Vogel's curve [58]. The curve is reproduced here as Figure 6-119. This method needs only a single point production test, wherein reservoir shut in pressure is measured and total liquid production (oil and water) and flowing bottomhole pressure are measured. The equation for this curve is given below as

$$\frac{q_0}{(q_0)_{\max}} = 1 - 0.2 \frac{(P_{wf})}{(Pr)} - 0.8 \frac{(P_{wf})^2}{(Pr)^2} \quad (6-199)$$

where q_0 = total liquid production per unit of time at flowing bottomhole pressure P_{wf}

$(q_0)_{\max}$ = maximum possible flow per unit of time when $P_{wf} = 0$

P_{wf} = flowing bottomhole pressure

Pr = average reservoir pressure

The equation is used to compute the expected flowrate q_0 at any given flowing bottomhole pressure P_{wf} . Values of Pr and $(q_0)_{\max}$ are constants that must be determined from a flow test. Pr is measured during the flow test and $(q_0)_{\max}$ is computed using Equation 6-199 and the flowrate data.

An example calculation is given below:

Given: A reservoir flow test indicated that the well flowed 100 bpd when the flowing bottomhole pressure was 1,500 psia and the reservoir average pressure was 2,000 psi.

Desired: Determine the flowrate in bp/d when the flowing bottomhole pressure is 250 psia.

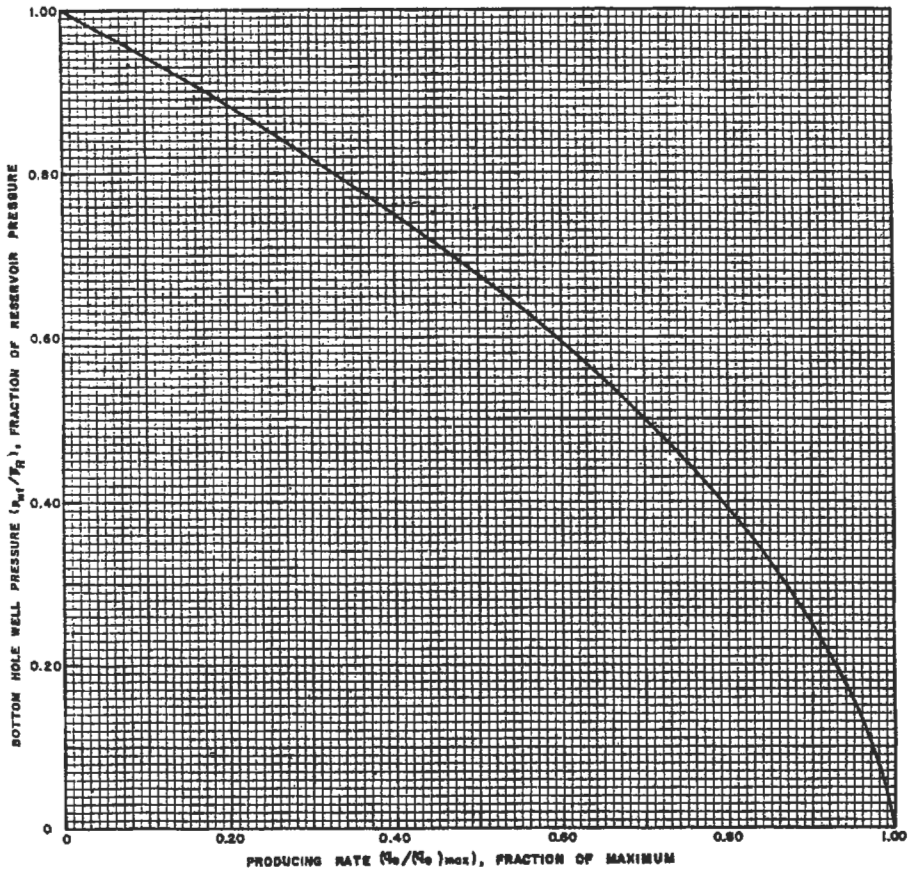


Figure 6-119. Inflow performance relationships for solution gas drive reservoirs [58].

Solution

Step 1: Compute $(q_0)_{max}$ using Equation 6-199, such that

$$\frac{(q_0)}{(q_0)_{max}} = 1 - 0.2 \frac{(P_{wf})}{(P_r)} - 0.8 \frac{(P_{wf})^2}{(P_r)^2}$$

$$\frac{100}{(q_0)_{max}} = 1 - 0.2 \frac{(1,500)}{(2,000)} - 0.8 \frac{(1,500)^2}{(2,000)^2}$$

$$(q_0)_{max} = 250 \text{ bbl/d}$$

Step 2. Use P_r and $(q_0)_{max}$ with desired P_{wf} in Equation 6-199 to compute q_0 , such that

$$\frac{q_0}{250} = 1 - 0.2 \frac{(250)}{(2,000)} - 0.8 \frac{(250)^2}{(2,000)^2}$$

$$q_0 = 241 \text{ bpd}$$

Estimation of water production should be done in company with determination of the oil production.

Where the size of the selected pumping unit is critical or where little data are available, it may be desirable to use a test pumping unit to determine not only flow capacity but also working fluid levels.

Casing and Tubing Size and Tubing Anchor. Casing size is usually determined long before the decision is made to install a beam pumping unit. Frequently, tubing is also already in place. However, its diameter and weight and weight per foot should be known. If tubing is already in place, it is not cost effective to change out the tubing for a large size as a means of installing a larger pump. Where a pump is needed that is larger than possible with the existing tubing, a casing pump should be investigated.

Tubing anchors have the advantage of keeping the tubing from buckling and oscillating during the pump cycle. Not only does this reduce wear on the tubing, but, as will be seen in the API RP11L calculations, anchors increase the net effective bottomhole stroke over that for unanchored tubing. Anchors can create problems in wells with severe scale, sand, or corrosion conditions as these conditions may so damage the anchor that it cannot be released to allow tubing removal.

Pump Setting Depth. Whenever possible, the pump should be set at a depth in the well where pump intake pressure is above the bubble point of the oil as it is produced. This would suggest locating the pump one to three tubing joints below the perforations. Sometimes this is not possible because of total well depth, nor desirable because of sand production. Alternatively, the pump should be placed out of and above the turbulence zone near the perforations (three to six joints above the perforations). In any case, the pump should have significant submergence, 50 to 100 ft of fluid, to assist in rapid fluid fillage of the pump barrel. For low productivity wells, this amount of submergence may not be either possible or economically feasible but the consequence will be that wells with lower submergence may experience pump-off and some type of pump-off controller would be needed.

Expected Pump Fluid Level. This is one of the needed parameters about which there will be much uncertainty in a new installation. If a well test and an inflow performance relationship is available for the well, one can possibly convert flowing bottomhole pressure to flowing liquid height. Such a calculation would be fairly accurate for nearly dead oils or for wells producing mostly water. An alternative, conservative design approach is to assume that the flowing liquid level is at the pump depth. Once a unit is in operation, one of the commercially available acoustical well sounders can be used to measure the working fluid level. This value would be useful in any comparison of the well's current performance with that predicted by the API RP11L procedure.

Preliminary Design Data. In addition to selecting the data listed in the section titled "Required Information" which items are generally constant for a given

pumping installation, the user of the API RP11L calculation procedure must select initial or tentative values for each of the following four parameters:

- a. plunger diameter
- b. pumping speed
- c. stroke length
- d. sucker rod string design

The following paragraphs give guidelines for proper selection of these parameters.

Plunger Diameter. For a given size tubing there is a maximum pump size for each type of pump. Refer to Table 6-32. An additional guide to plunger size selection for a given fluid volume and pumping depth is found in Table 6-33.

Pumping Speed. For any given selection of stroke length there is a maximum recommended pumping speed. If this speed is exceeded, the rods are likely to "float" or go into compression on the downstroke. Rods are normally under tension on the downstroke as well as the upstroke. If they are put into compression, they will buckle, causing wear on rods and tubing. The range of stress will be large, thus reducing the Goodman diagram maximum allowable stress. The alternating tension and compression will cause severe stress on rod threads and coupling and accelerate rod parting from fatigue and accelerated effects of corrosion. Dynamometer tests (to be discussed later) can detect floating rods. The maximum pumping speed for given stroke lengths is given in Figures 6-120, 6-121, and 6-122. These figures are for three widely used types of pumping units.

Table 6-32
Maximum Pump Size and Type [61]

Pump type	Tubing size, in.			
	1.900	2%	2%	3%
Tubing one-piece, thin-wall barrel (TW)	1½	1¾	2¼	2¾
Tubing one-piece, heavy-wall barrel (TH)	1½	1¾	2¼	2¾
Tubing liner barrel (TL)	—	1¾	2¼	2¾
Rod one-piece, thin- wall barrel (RW)	1½	1¾	2	2½
Rod one-piece, heavy wall barrel (RH)	1⅞	1¾	1¾	2¾
Rod liner barrel (RL)	—	1¾	1¾	2¾

Table 6-33
Pump Plunger Sizes Recommended for Optimum Conditions [67]

Net lift of fluid ft	Fluid production—Barrels per day—80 pct efficiency									
	100	200	300	400	500	600	700	800	900	1000
2000	1½	1¾	2	2¼	2½	2¾				
	1¼	1½	1¾	2	2¼	2½	2¾	2¾	2¾	2¾
3000	1½	1¾	2	2¼	2½	2½	2¾	2¾	2¾	2¾
	1¼	1½	1¾	2	2¼	2¼	2½			
4000	1¼	1¾	2	2¼	2¼	2¼	2¼	2¼		
		1½	1¾	2	2					
5000	1¼	1¾	2	2	2¼	2¼				
		1½	1¾	1¾	2					
6000	1¼	1½	1¾	1¾						
		1¼	1½							
7000	1¼	1½								
	1½	1¾								
8000	1¼									
	1½									

In this tabulation surface pumping strokes up to 74 in. only are considered.

Stroke Length. Stroke length is a primary variable in determining pumping unit size. Because of the small number of stroke lengths (usually 2 to 4) available for any pumping unit, it is wise to select an available stroke length, then use this length in Equation 6-196 to determine an appropriate first estimate of strokes per minute. The selected stroke and speed combination should be checked to see that the rods do not float. Use Figure 6-120, 6-121, or 6-122, whichever is appropriate.

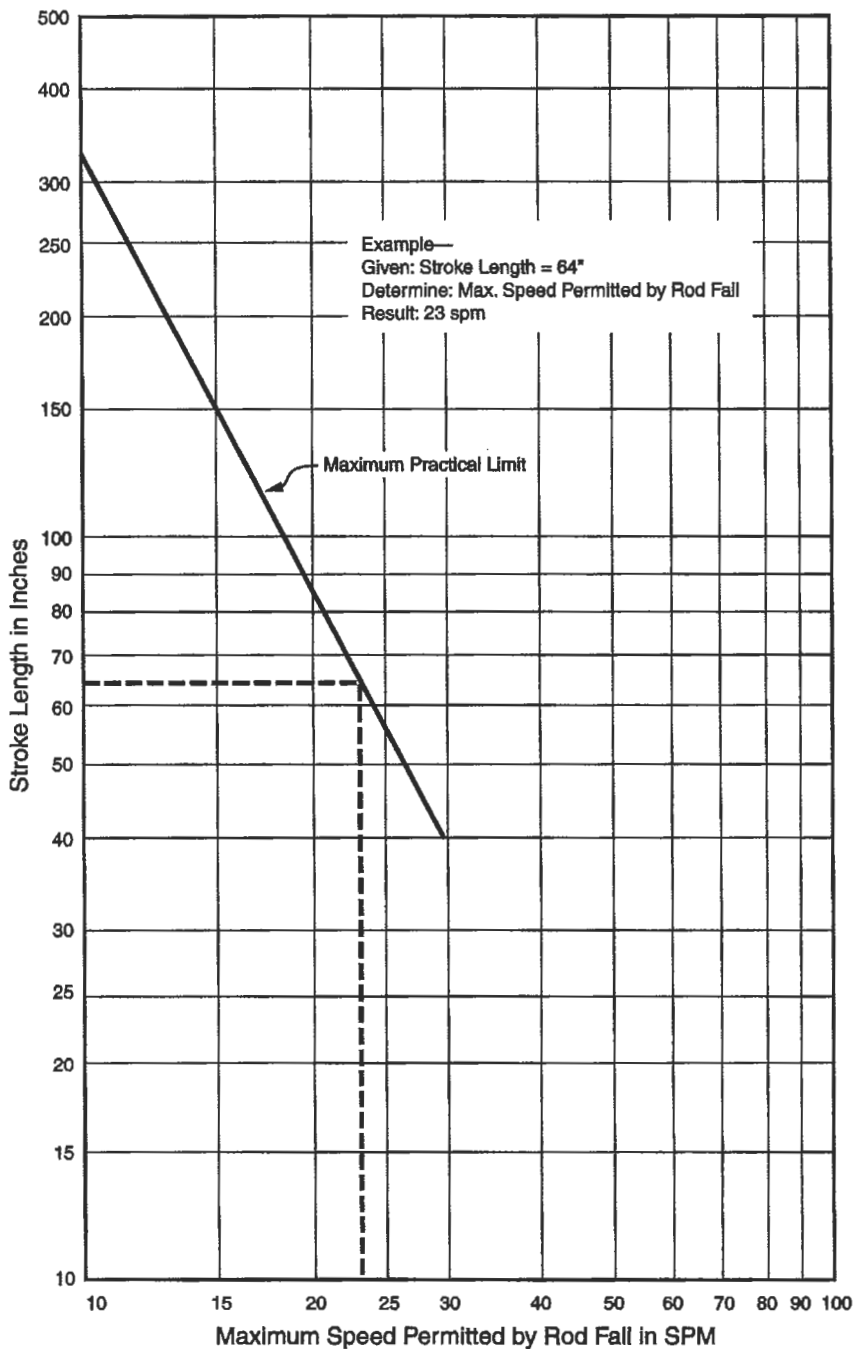


Figure 6-120. Maximum practical pumping speed, conventional unit [61].

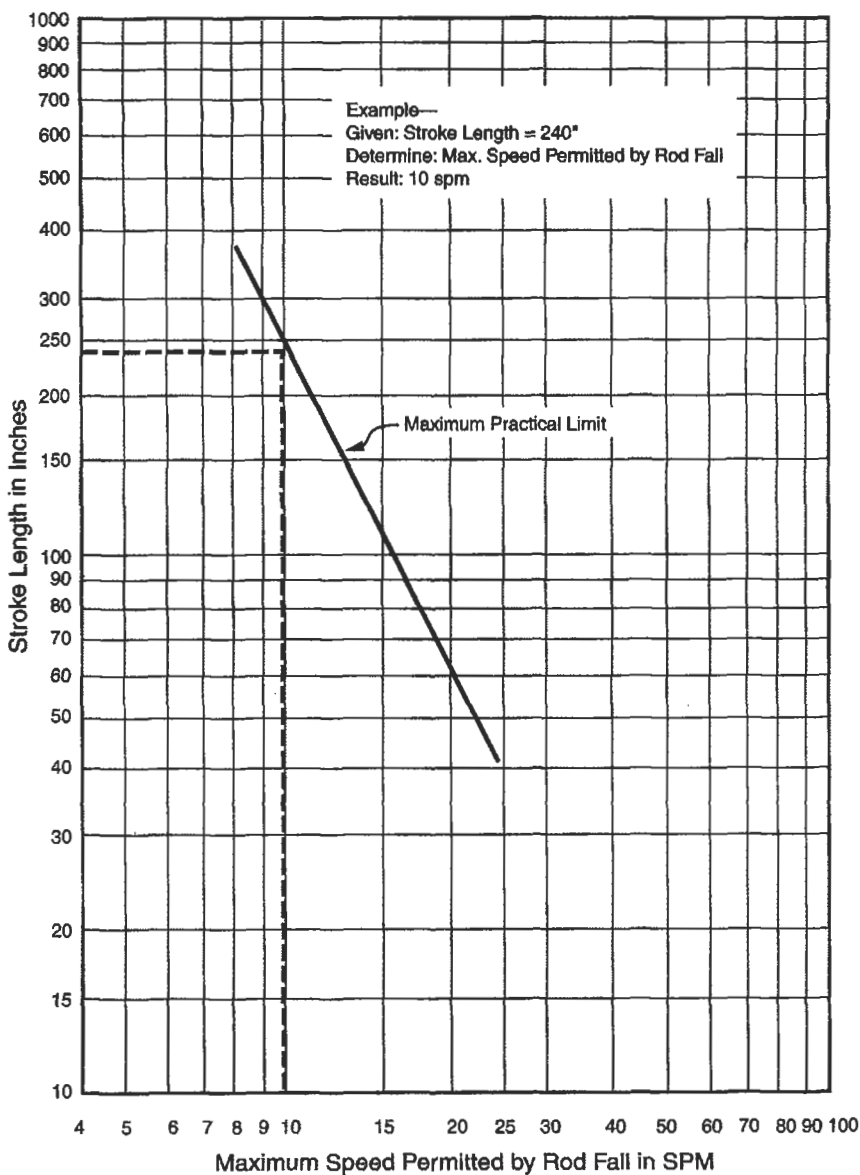


Figure 6-121. Maximum practical pumping speed, air balanced unit [61].

Sucker Rod String Selection. For shallow wells, less than 2,000 ft most pumping installations will use sucker rods of the same diameter from the top of the well to the pump. Since the load on the rods is at its greatest at the top of the rod string on the upstroke, for single size rod strings one needs only to check the stress at this point using the Goodman diagram to see if the rods

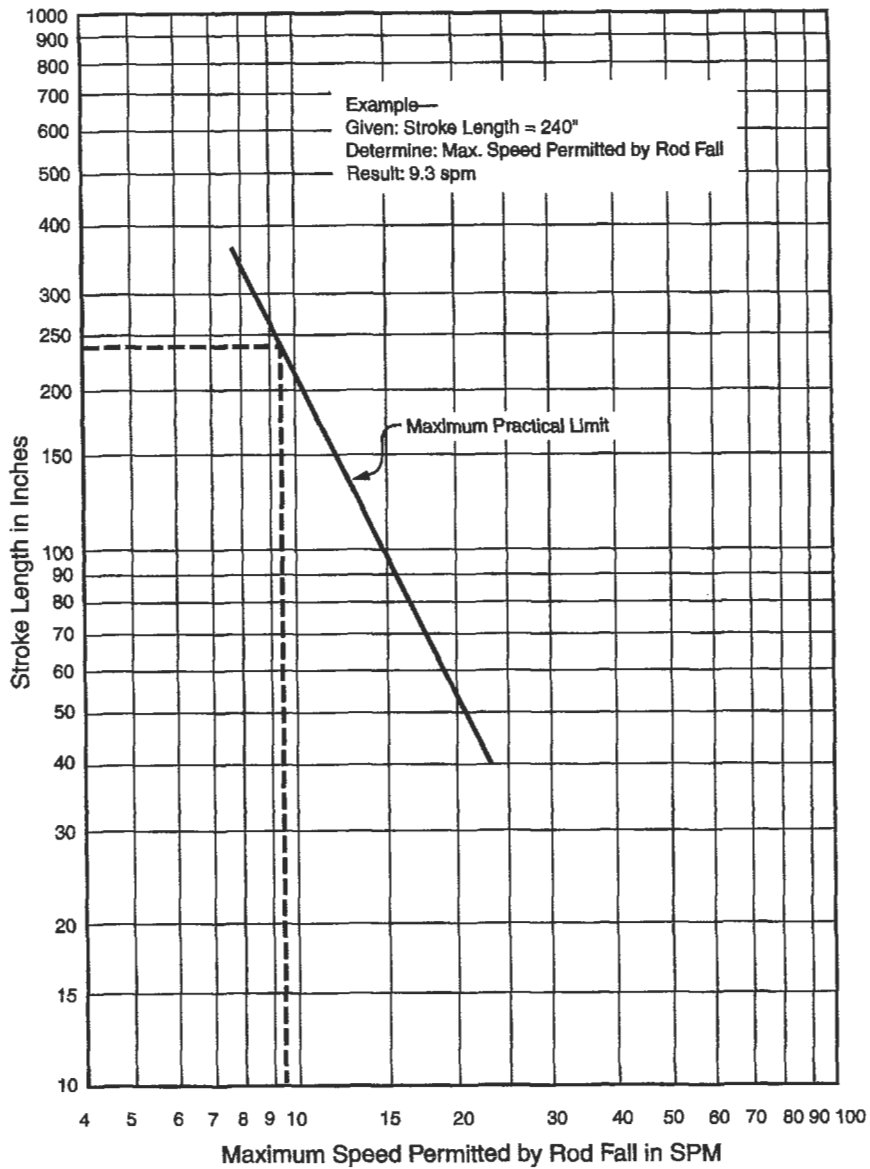


Figure 6-122. Maximum practical pumping speed, Mark II unit [61].

are satisfactory. For deeper wells, one usually uses a larger-diameter rod near the surface and smaller-diameter rods further down the well. Such multiple-size rod strings are called *tapered rods*. A coding system for designating the sizes has been adopted. A 76-rod string consists of $\frac{7}{8}$ -in. rods near the top and $\frac{6}{8}$ - (or $\frac{3}{4}$ -) in. rods near the bottom. An 88-rod string has 1-in. (i.e., eight $\frac{1}{8}$ -s) rods

throughout its length. A 75-rod string has $\frac{7}{8}$ -in. rods near the top, $\frac{6}{8}$ - (or $\frac{3}{4}$ -) in. rods near the middle and $\frac{5}{8}$ -in. rods near the plunger. This is called a three-way tapered rod string. Four-way tapers are also possible. This coding scheme does not specify what percent of each rod size is used in the string.

Two approaches have been used in determining the percent of each rod size. In the first, one starts at the plunger depth and adds rods of the smallest size (for example $\frac{5}{8}$ -in. rods in a 75-rod string design). These are added until the stress at the top of these rods is the maximum allowable according to some criterion such as the Goodman diagram. At that point, one changes to the next large size ($\frac{3}{4}$ -in. rods in the current 75-rod string example). One then continues to add rods until the stress at the top of these rods meets the same maximum stress criterion. At this point, one then changes to the largest size and adds rods until either the top of the hole is reached (a successful design) or until the maximum stress criterion is met but the top of the hole has not been reached. In this latter case, one does not have an acceptable design. One would need either to change to a larger-diameter string such as an 86-rod design or go to a four-way taper (85-rod string in the present instance), adding 1-in. rods to the top of the string.

The above maximum stress method leads to the lightest rod string. It is not as conservative as the next or balanced stress method. In the balanced stress method, the percentages of each size rod in the 75 rod combination, for example, are adjusted until the same stress exists at the top of each size of rods. Usually this stress is less than the maximum allowable stress. The rod string selected by this method is somewhat heavier than that selected by the first method and is generally to be preferred.

The API, using this latter approach, has given rod size and percent length of rods for available rod combinations and plunger diameter. These percentages appear in columns 6 through 11 of Table 6-34. For example, a 76-rod string using a 1.50-in. plunger would have 33.8% $\frac{7}{8}$ -in. rods and 66.2% $\frac{3}{4}$ -in. rods. An 85-rod string with 1.75-in. plunger would have 29.6%, 30.4%, 29.5% and 10.5% of 1-in., $\frac{7}{8}$ -in., $\frac{3}{4}$ -in. and $\frac{5}{8}$ -in. rods, respectively.

API RP11L Calculations. The calculation sequence to design a pumping unit installation is best explained through an example calculation. Assume that the following data are available for a pumping well.

1. desired surface production, 150 bpd
2. estimated pumping volumetric efficiency, 85%
3. pump setting depth, 5,000 ft
4. fluid level during pumping, 4,500 ft
5. tubing is 2 in. nominal, not anchored
6. pumping speed, 16 spm
7. stroke length at surface, 54 in.
8. plunger diameter, 1.50 in.
9. fluid specific gravity, 0.90
10. sucker rod design (API)

Desired calculated results are:

1. effective downhole stroke, in.
2. pump displacement, bpd
3. peak polished rod load, lbf

(text continued on page 628)

Table 6-34
Rod and Pump Data [57]

1 Rod* no.	2 Pinger diam., inches	3 Rod weight lb per ft	4 Elastic constant, in. per lb ft E_r	5 Frequency Factor, F_p	6-11 Rod string, % of each size					
					6 1/8	7 1	8 3/4	9 3/8	10 3/2	11 3/4
44	All	0.726	1.990×10^{-6}	1.000	—	—	—	—	—	100.0
54	1.06	0.906	1.668×10^{-6}	1.138	—	—	—	—	44.6	55.4
54	1.25	0.929	1.633×10^{-6}	1.140	—	—	—	—	49.5	50.5
54	1.50	0.957	1.584×10^{-6}	1.137	—	—	—	—	56.4	43.6
54	1.75	0.990	1.525×10^{-6}	1.122	—	—	—	—	64.6	35.4
54	2.00	1.027	1.460×10^{-6}	1.095	—	—	—	—	73.7	26.3
54	2.25	1.067	1.391×10^{-6}	1.061	—	—	—	—	83.4	16.6
54	2.50	1.108	1.318×10^{-6}	1.023	—	—	—	—	93.5	6.5
55	All	1.135	1.270×10^{-6}	1.000	—	—	—	—	100.0	—
64	1.06	1.164	1.362×10^{-6}	1.229	—	—	—	33.3	33.1	33.5
64	1.25	1.211	1.319×10^{-6}	1.215	—	—	—	37.2	35.9	26.9
64	1.50	1.275	1.232×10^{-6}	1.184	—	—	—	42.3	40.4	17.3
64	1.75	1.341	1.141×10^{-6}	1.145	—	—	—	47.4	45.2	7.4
65	1.06	1.307	1.138×10^{-6}	1.098	—	—	—	34.4	65.6	—
65	1.25	1.321	1.127×10^{-6}	1.104	—	—	—	37.3	62.7	—
65	1.30	1.343	1.110×10^{-6}	1.110	—	—	—	41.8	58.2	—
65	1.75	1.369	1.090×10^{-6}	1.114	—	—	—	46.9	53.1	—
65	2.00	1.394	1.070×10^{-6}	1.114	—	—	—	52.0	48.0	—
65	2.25	1.426	1.045×10^{-6}	1.110	—	—	—	58.4	41.6	—
65	2.50	1.460	1.018×10^{-6}	1.099	—	—	—	65.2	34.8	—
65	2.75	1.497	0.990×10^{-6}	1.082	—	—	—	72.5	27.5	—
65	3.25	1.574	0.930×10^{-6}	1.037	—	—	—	88.1	11.9	—
66	All	1.634	0.883×10^{-6}	1.000	—	—	—	100.0	—	—
75	1.06	1.566	0.997×10^{-6}	1.191	—	—	27.0	27.4	45.6	—
75	1.25	1.604	0.973×10^{-6}	1.193	—	—	29.4	29.8	40.8	—
75	1.50	1.664	0.935×10^{-6}	1.189	—	—	33.3	33.3	33.3	—
75	1.75	1.732	0.892×10^{-6}	1.174	—	—	37.8	37.0	25.1	—
75	2.00	1.803	0.847×10^{-6}	1.151	—	—	42.4	41.3	16.3	—
75	2.25	1.875	0.801×10^{-6}	1.121	—	—	46.9	45.8	7.2	—
76	1.06	1.802	0.816×10^{-6}	1.072	—	—	28.5	71.5	—	—
76	1.25	1.814	0.812×10^{-6}	1.077	—	—	30.6	69.4	—	—
76	1.50	1.833	0.804×10^{-6}	1.082	—	—	33.8	66.2	—	—
76	1.75	1.855	0.795×10^{-6}	1.088	—	—	37.5	62.5	—	—
76	2.00	1.880	0.785×10^{-6}	1.093	—	—	41.7	58.3	—	—
76	2.25	1.908	0.774×10^{-6}	1.096	—	—	46.5	53.5	—	—
76	2.50	1.934	0.764×10^{-6}	1.097	—	—	50.8	49.2	—	—
76	2.75	1.967	0.751×10^{-6}	1.094	—	—	56.5	43.5	—	—
76	3.75	2.039	0.722×10^{-6}	1.078	—	—	68.7	31.3	—	—
76	3.75	2.119	0.690×10^{-6}	1.047	—	—	82.3	17.7	—	—
77	All	2.224	0.649×10^{-6}	1.000	—	—	100.0	—	—	—
85	1.06	1.883	0.873×10^{-6}	1.261	—	22.2	22.4	22.4	33.0	—
85	1.25	1.943	0.841×10^{-6}	1.253	—	23.9	24.2	24.3	27.6	—
85	1.50	2.039	0.791×10^{-6}	1.232	—	26.7	27.4	26.8	19.2	—
85	1.75	2.138	0.738×10^{-6}	1.201	—	29.6	30.4	29.5	10.5	—
86	1.06	2.058	0.742×10^{-6}	1.151	—	22.6	23.0	34.3	—	—
86	1.25	2.087	0.732×10^{-6}	1.156	—	24.3	24.5	51.2	—	—
86	1.50	2.133	0.717×10^{-6}	1.162	—	26.8	27.0	46.3	—	—
86	1.75	2.185	0.699×10^{-6}	1.164	—	29.4	30.0	40.6	—	—
86	2.00	2.247	0.679×10^{-6}	1.161	—	32.8	33.2	33.9	—	—
86	2.25	2.315	0.656×10^{-6}	1.153	—	36.9	36.0	27.1	—	—
86	2.50	2.385	0.633×10^{-6}	1.138	—	40.6	39.7	19.7	—	—
86	2.75	2.455	0.610×10^{-6}	1.119	—	44.5	43.3	12.2	—	—

Table 6-34
(continued)

1 Rod* no.	2 Plunger diam., inches	3 Rod weight lb per ft	4 Elastic constant, in. per lb ft E_r	5 Frequency Factor, F_r	6-11 Rod string, % of each size					
					1 1/4	1	3/4	1/2	1/4	1/8
87	1.06	2.390	0.612×10^{-6}	1.055	—	24.3	75.7	—	—	—
87	1.25	2.399	0.610×10^{-6}	1.058	—	25.7	74.3	—	—	—
87	1.50	2.413	0.607×10^{-6}	1.062	—	27.7	72.3	—	—	—
87	1.75	2.430	0.603×10^{-6}	1.068	—	30.3	69.7	—	—	—
87	2.00	2.450	0.598×10^{-6}	1.071	—	33.2	66.8	—	—	—
87	2.25	2.472	0.594×10^{-6}	1.075	—	36.4	63.6	—	—	—
87	2.50	2.496	0.588×10^{-6}	1.079	—	39.9	60.1	—	—	—
87	2.75	2.523	0.582×10^{-6}	1.082	—	43.9	56.1	—	—	—
87	3.25	2.575	0.570×10^{-6}	1.084	—	51.6	48.4	—	—	—
87	3.75	2.641	0.556×10^{-6}	1.078	—	61.2	38.8	—	—	—
87	4.75	2.793	0.522×10^{-6}	1.038	—	83.6	16.4	—	—	—
88	All	2.904	0.497×10^{-6}	1.000	—	100.0	—	—	—	—
96	1.06	2.382	0.670×10^{-6}	1.222	19.1	19.2	19.5	42.3	—	—
96	1.25	2.435	0.655×10^{-6}	1.224	20.5	20.5	20.7	38.3	—	—
96	1.50	2.511	0.633×10^{-6}	1.223	22.4	22.5	22.8	32.3	—	—
96	1.75	2.607	0.606×10^{-6}	1.213	24.8	25.1	25.1	25.1	—	—
96	2.00	2.703	0.578×10^{-6}	1.196	27.1	27.9	27.4	17.6	—	—
96	2.25	2.806	0.549×10^{-6}	1.172	29.6	30.7	29.8	9.8	—	—
97	1.06	2.645	0.568×10^{-6}	1.120	19.6	20.0	60.3	—	—	—
97	1.25	2.670	0.563×10^{-6}	1.124	20.8	21.2	58.0	—	—	—
97	1.50	2.707	0.556×10^{-6}	1.131	22.5	23.0	54.5	—	—	—
97	1.75	2.751	0.548×10^{-6}	1.137	24.5	25.0	50.4	—	—	—
97	2.00	2.801	0.538×10^{-6}	1.141	26.8	27.4	45.7	—	—	—
97	2.25	2.856	0.528×10^{-6}	1.143	29.4	30.2	40.4	—	—	—
97	2.50	2.921	0.515×10^{-6}	1.141	32.5	33.1	34.4	—	—	—
97	2.75	2.989	0.503×10^{-6}	1.135	36.1	35.3	28.6	—	—	—
97	3.25	3.132	0.475×10^{-6}	1.111	42.9	41.9	15.2	—	—	—
98	1.06	3.068	0.475×10^{-6}	1.043	21.2	78.8	—	—	—	—
98	1.25	3.076	0.474×10^{-6}	1.045	22.2	77.8	—	—	—	—
98	1.50	3.089	0.472×10^{-6}	1.048	23.8	76.2	—	—	—	—
98	1.75	3.103	0.470×10^{-6}	1.051	25.7	74.3	—	—	—	—
98	2.00	3.118	0.468×10^{-6}	1.055	27.7	72.3	—	—	—	—
98	2.25	3.137	0.465×10^{-6}	1.058	30.1	69.9	—	—	—	—
98	2.50	3.157	0.463×10^{-6}	1.062	32.7	67.3	—	—	—	—
98	2.75	3.180	0.460×10^{-6}	1.066	35.6	64.4	—	—	—	—
98	3.25	3.291	0.453×10^{-6}	1.071	42.2	57.8	—	—	—	—
98	3.75	3.289	0.445×10^{-6}	1.074	49.7	50.3	—	—	—	—
98	4.75	3.412	0.428×10^{-6}	1.064	65.7	34.3	—	—	—	—
99	All	3.676	0.393×10^{-6}	1.000	100.0	—	—	—	—	—
107	1.06	2.977	0.524×10^{-6}	1.184	16.9	16.8	17.1	49.1	—	—
107	1.25	3.019	0.517×10^{-6}	1.189	17.9	17.8	18.0	46.3	—	—
107	1.50	3.085	0.506×10^{-6}	1.195	19.4	19.2	19.5	41.9	—	—
107	1.75	3.158	0.494×10^{-6}	1.197	21.0	21.0	21.2	36.9	—	—
107	2.00	3.238	0.480×10^{-6}	1.195	22.7	22.8	23.1	31.4	—	—
107	2.25	3.336	0.464×10^{-6}	1.187	25.0	25.0	25.0	25.0	—	—
107	2.50	3.435	0.447×10^{-6}	1.174	26.9	27.7	27.1	18.2	—	—
107	2.75	3.537	0.430×10^{-6}	1.156	29.1	30.2	29.3	11.3	—	—
108	1.06	3.325	0.447×10^{-6}	1.097	17.3	17.8	64.9	—	—	—
108	1.25	3.345	0.445×10^{-6}	1.101	18.1	18.6	63.2	—	—	—
108	1.50	3.376	0.441×10^{-6}	1.106	19.4	19.9	60.7	—	—	—
108	1.75	3.411	0.437×10^{-6}	1.111	20.9	21.4	57.7	—	—	—
108	2.00	3.452	0.432×10^{-6}	1.117	22.6	23.0	54.3	—	—	—
108	2.25	3.498	0.427×10^{-6}	1.121	24.5	25.0	50.5	—	—	—
108	2.50	3.548	0.421×10^{-6}	1.124	26.5	27.2	46.3	—	—	—
108	2.75	3.603	0.415×10^{-6}	1.126	28.7	29.6	41.6	—	—	—
108	3.25	3.731	0.400×10^{-6}	1.123	34.6	33.9	31.6	—	—	—
108	3.75	3.873	0.383×10^{-6}	1.108	40.6	39.5	19.9	—	—	—

Table 6-34
(continued)

1 Rod* no.	2 Punger diam., inches	3 Rod weight lb per ft	4 Elastic constant, in. per lb ft E_r	5 Frequency Factor, F_r	6-11 Rod string, % of each size					
					6 1½	7 1¼	8 1	9 ¾	10 ½	11 ¼
109	1.06	3.839	0.378×10^{-6}	1.035	18.9	81.1	—	—	—	—
109	1.25	3.845	0.378×10^{-6}	1.036	19.6	80.4	—	—	—	—
109	1.50	3.855	0.377×10^{-6}	1.038	20.7	79.3	—	—	—	—
109	1.75	3.867	0.376×10^{-6}	1.040	22.1	77.9	—	—	—	—
109	2.00	3.880	0.375×10^{-6}	1.043	23.7	76.3	—	—	—	—
109	2.25	3.896	0.374×10^{-6}	1.046	25.4	74.6	—	—	—	—
109	2.50	3.911	0.372×10^{-6}	1.048	27.2	72.8	—	—	—	—
109	2.75	3.930	0.371×10^{-6}	1.051	29.4	70.6	—	—	—	—
109	3.25	3.971	0.367×10^{-6}	1.057	34.2	65.8	—	—	—	—
109	3.75	4.020	0.363×10^{-6}	1.063	39.9	60.1	—	—	—	—
109	4.75	4.120	0.354×10^{-6}	1.066	51.5	48.5	—	—	—	—

*Rod No. shown in first column refers to the largest and smallest rod size in eighths of an inch. For example, Rod No. 76 is a two-way taper of ¾ and ½ rods. Rod No. 85 is a four-way taper of ¾, ½, ¼, and ⅜ rods. Rod No. 109 is a two-way taper of 1½ and 1¼ rods. Rod No. 77 is a straight string of ¾ rods, etc.

(text continued from page 625)

4. minimum polished rod load, lbf
5. peak torque, lbf-in
6. polished rod horsepower, hp
7. counterbalance effect, lbf measured at polished rod

The calculation sequence is shown in Figure 6-123. Blank calculation sheets similar to Figure 6-123 can be obtained from API. The stepwise sequence for performing the calculations is described below.

- Step 1. Record on the calculation sheet the factors W_r , E_r , F_r , from Table 6-34 and E_s from Table 6-34 for the selected rod design (calculation lines 1-4).
- Step 2. Using the data recorded in Step 1 and the given data, compute the nondimensional parameters F_0/Sk_r , N/N_0 , N/N_0 and the term $1/k_r$ (calculation lines 5-11).
- Step 3. Compute the effective stroke length S_p and the pump displacement PD (calculation lines 12-14). For line 12, one needs to get S_p/S from Figure 6-124 using the previously computed values for F_0/Sk_r and N/N_0 .
- Step 4. Compare the computed pump displacement with that desired. The calculated value of PD is 175 bbl/d. Use Equation 6-197 to compute Q and compare it to the desired Q:

$$Q = EV \times PD$$

$$= (0.85) \times 175 \text{ bpd} = 149 \text{ bpd}$$

This is close enough to the desired production to proceed to the next step of the calculations.

Calculation line 14 is a crucial intermediate checkpoint. If the production is close to the desired production, then one should proceed with calculation lines 15 through 27. However, if production is considerably different from that desired, one should make different selections for some of the eight parameters that are listed on the calculation sheet as known or assumed data. Parameters

Known or Assumed Data:

Fluid Level, H = 4,500 ft. Pumping Speed, N = 16 SPM Plunger Diameter, D = 1.50 in.
 Pump Depth, L = 5,000 ft. Length of Stroke, S = 54 in. Spec. Grav. of Fluid, G = 0.9
 Tubing Size 2 in. Is it anchored? Yes, (No) Sucker Rods 33.8% - 7" 6 66.2% - 7"

Record Factors:

- 1. $W_r = \frac{1.833}{}$
- 2. $E_r = \frac{809 \times 10^{-6}}{}$
- 3. $F_o = \frac{1.082}{}$
- 4. $E_o = \frac{307 \times 10^{-6}}{}$

Calculate Non-Dimensional Variables:

- 5. $F_o = .340 \times G \times D^2 \times H = .340 \times 0.9 \times 2.25 \times 4,500 = 3,098$ lbs.
- 6. $1/k_r = E_r \times L = \frac{809 \times 10^{-6} \times 5,000}{} = 4.020 \times 10^{-3}$ in/lb.
- 7. $Sk_r = S + 1/k_r = 54 + \frac{4.020 \times 10^{-3}}{} = 13,433$ lbs.
- 8. $F_o/Sk_r = \frac{3,098}{13,433} = .231$
- 9. $N/N_o = NL + 245,000 = 16 \times 5,000 + 245,000 = 326$
- 10. $N/N_o' = N/N_o + F_o = \frac{326}{} + \frac{1.082}{} = .301$
- 11. $1/k = E_r \times L = \frac{809 \times 10^{-6} \times 5,000}{} = 4.020 \times 10^{-3}$ in/lb.

Solve for S_p and PD:

- 12. $S_p/S = .86$
- 13. $S_p = [(S_p/S) \times S] - [F_o \times 1/k_r] = [.86 \times 54] - [3,098 \times 1.535 \times 10^{-3}] = 41.7$ in.
- 14. $PD = 0.1166 \times S_p \times N \times D^2 = 0.1166 \times 41.7 \times 16 \times 2.25 = 175$ barrels per day

If the calculated pump displacement fails to satisfy known or anticipated requirements, appropriate adjustments must be made in the assumed data and steps 1 through 14 repeated. When the calculated pump displacement is acceptable, proceed with the Design Calculation.

Determine Non-Dimensional Parameters:

- 15. $W = W_r \times L = 1.833 \times 5,000 = 9,165$ lbs.
- 16. $W_{r1} = W[1 - (.128G)] = 9,165 [1 - (.128 \times .9)] = 8,110$ lbs.
- 17. $W_o/Sk_r = \frac{8,110}{13,433} = .604$

Record Non-Dimensional Factors:

- 18. $F_1/Sk_r = .465$
- 19. $F_2/Sk_r = .213$
- 20. $2T/S^2k_r = .37$
- 21. $F_3/Sk_r = .29$
- 22. $T_s = .997$

Solve for Operating Characteristics:

- 23. $PFRL = W_{r1} + [(F_1/Sk_r) \times Sk_r] = 8,110 + [.465 \times 13,433] = 14,356$ lbs.
- 24. $MPRL = W_{r1} - [(F_2/Sk_r) \times Sk_r] = 8,110 - [.22 \times 13,433] = 5,249$ lbs.
- 25. $PT = (2T/S^2k_r) \times Sk_r \times S/2 \times T_s = .37 \times 13,433 \times 2.7 \times .997 = 133,793$ lb inches
- 26. $FRFP = (F_3/Sk_r) \times Sk_r \times S \times N \times 2.53 \times 10^{-4} = .29 \times 13,433 \times 54 \times 16 \times 2.53 \times 10^{-4} = 8.5$
- 27. $CBE = 1.06(W_{r1} + 1/2 F_o) = 1.06 \times (8,110 + 1/2 \times 3,098) = 10,239$ lbs.

Figure 6-123. Example design calculations—conventional sucker rod pumping system [57].

that allow greatest change in pump displacement are stroke length and plunger diameter. Stroke lengths should be selected that are available from the manufacturers' catalogues, stroke and speed combination should not allow rods to float, and the plunger diameter should be one possible for the given tubing size. When relatively small adjustments are needed, one usually changes pumping speed first, then changes stroke length if necessary.

In making calculations for lines 5 through 11, one should try to select input data that will keep F_o/Sk_r less than about 0.35 and N/N_o less than about 0.5 for optimal pumping performance.

Step 5. Compute nondimensional terms for calculation lines 15 through 17.
 Step 6. Using the previously computed values for F_o/Sk_r , N/N_o' , and N/N_o record from Figures 6-125 through 6-128 the values needed in lines 18 through 22.

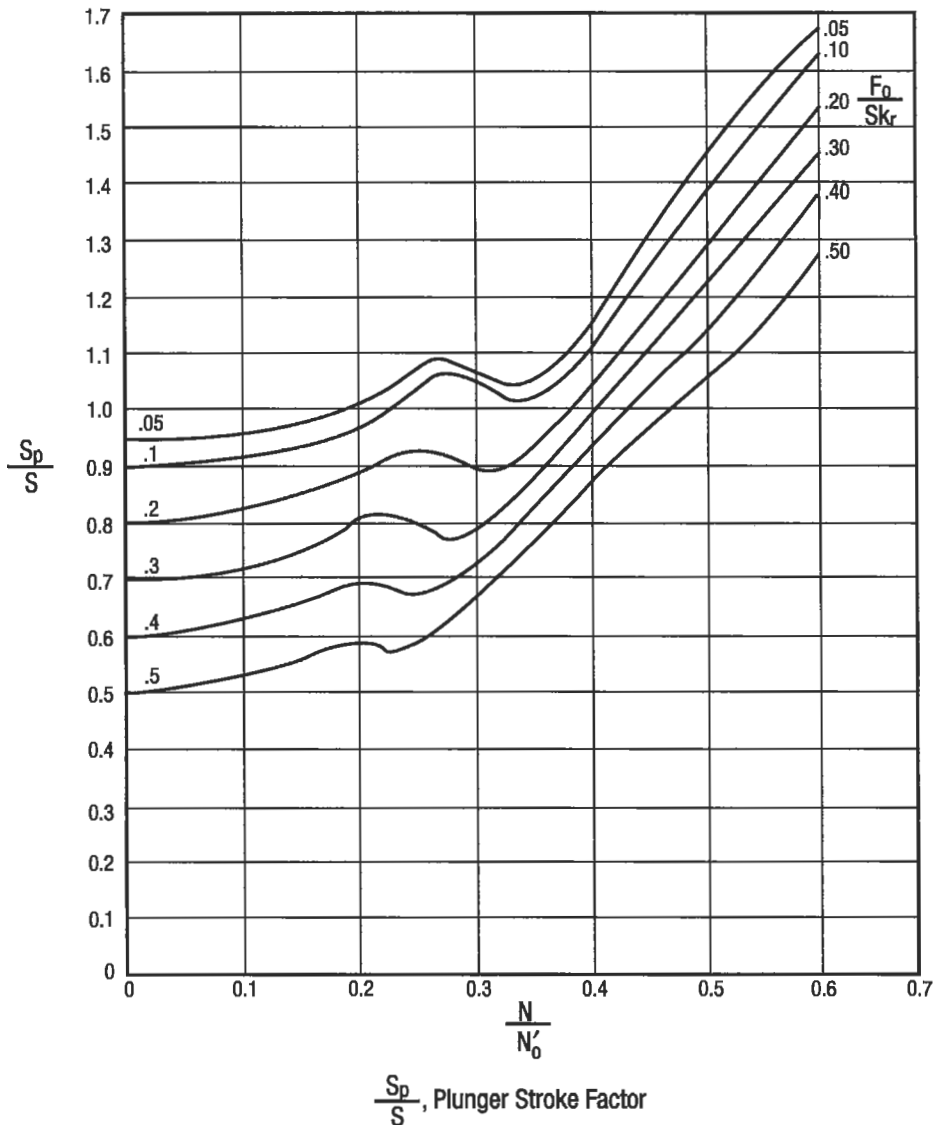


Figure 6-124. Plunger stroke factor [57].

Note the special correction procedure needed for T_a from Figure 6-129 when Wrf/Sk_r is different from 0.30.

Step 7. Compute the five operating characteristics of the pumping unit. This step is the final one in the calculation sequence if the operating characteristics are acceptable. However, because the overall task is to design not just a feasible pumping unit but rather to seek an optimal design, it may be necessary to select other alternate values for the assumed data and then repeat

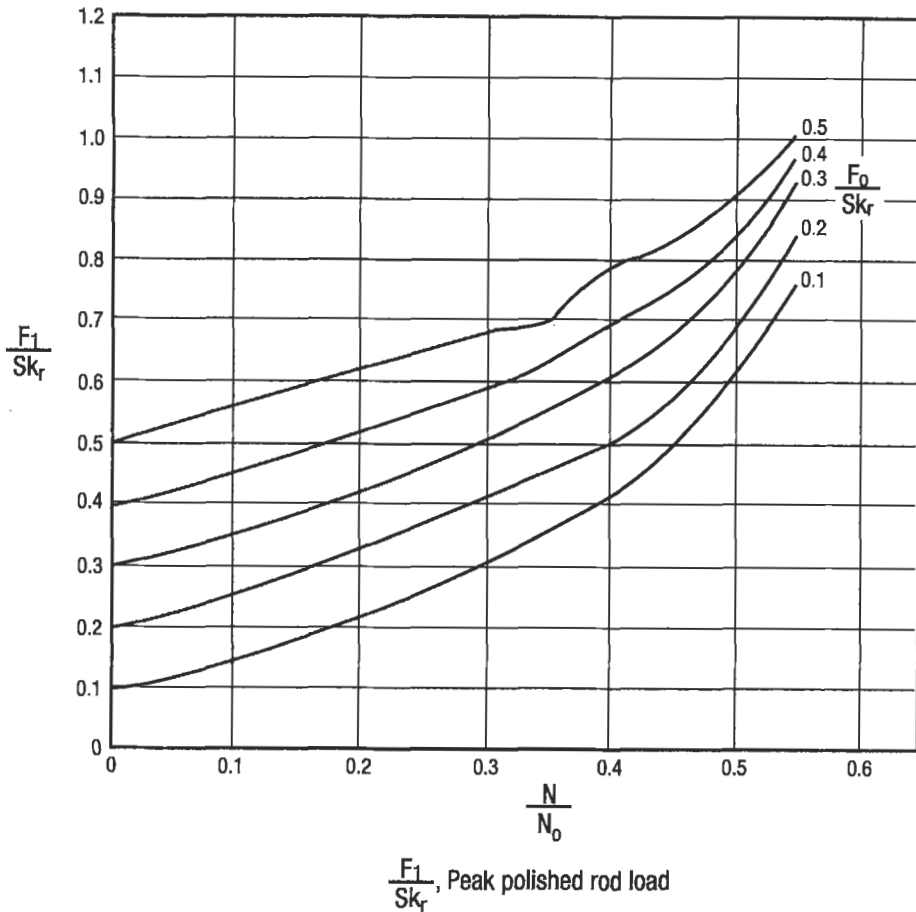


Figure 6-125. Peak polished rod load factor [57].

the calculation. It is the repetitive nature of the calculation that makes it attractive for a computer solution.

Testing the Design. The five operating characteristics of the pumping unit (lines 23 through 27) are used to specify more completely the selected unit. The operating characteristics will allow one to:

- a. determine whether the rods are overstressed
- b. specify feasible specifications for pumping unit such as:
 1. Peak torque
 2. Structural capacity
 3. Stroke length
 4. Prime mover horsepower

(text continued on page 634)

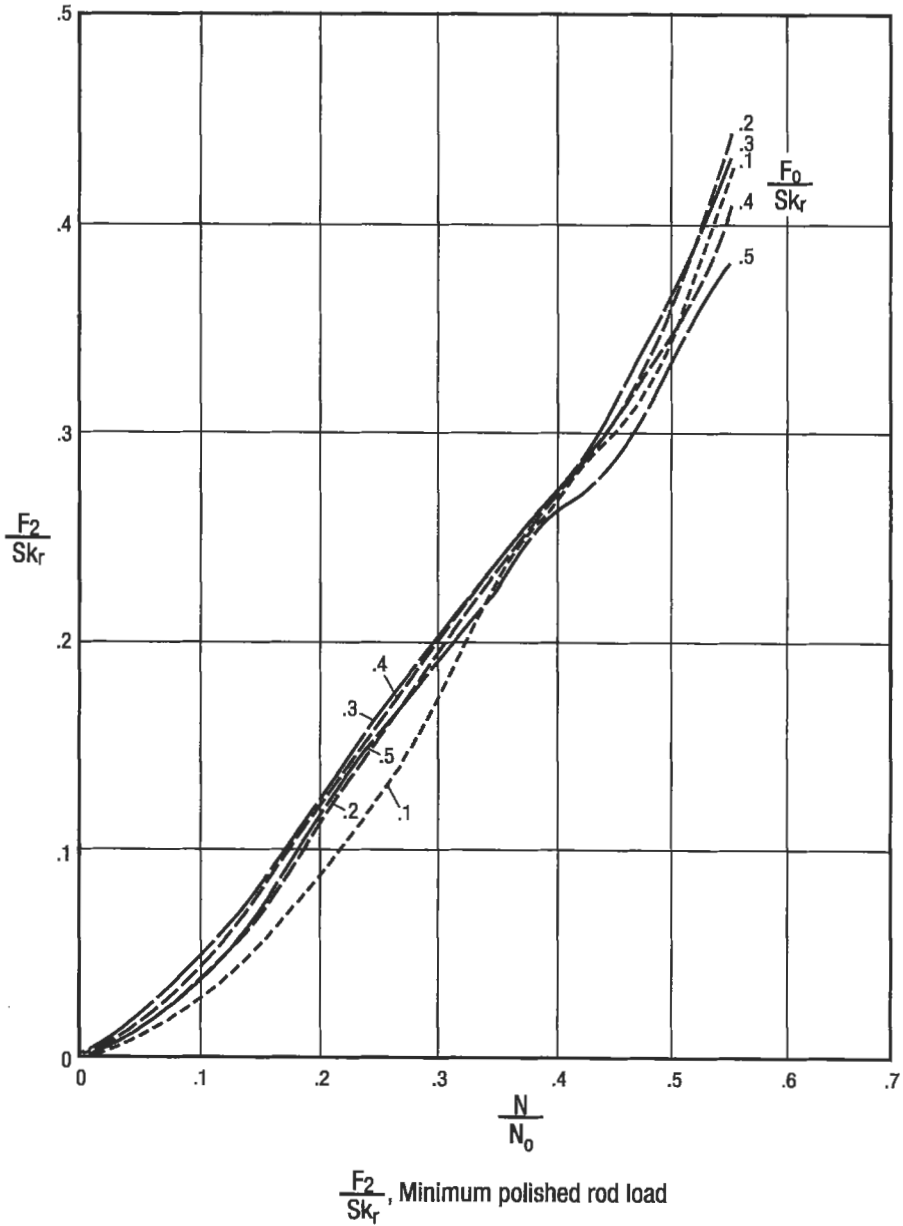


Figure 6-126. Minimum polished rod load factor [57].

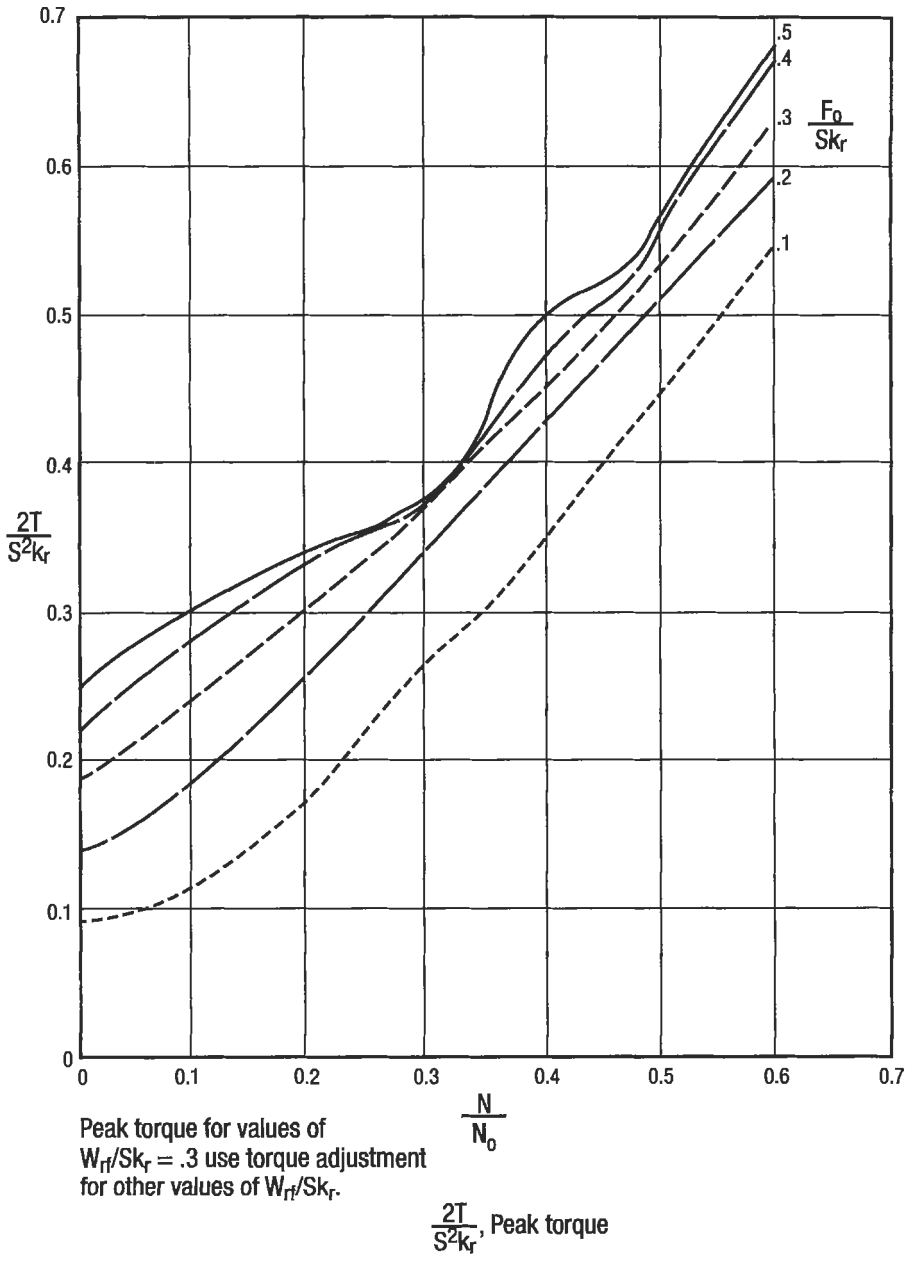


Figure 6-127. Peak torque factor [57].

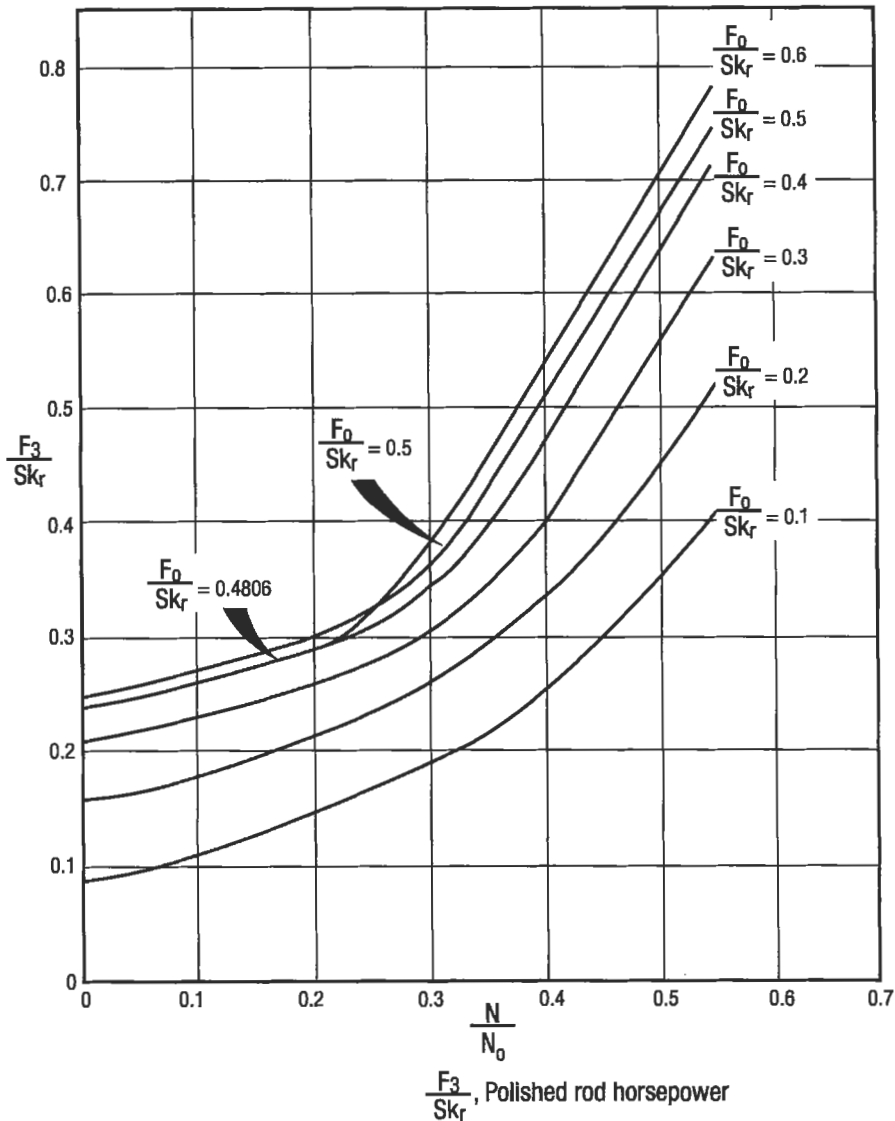
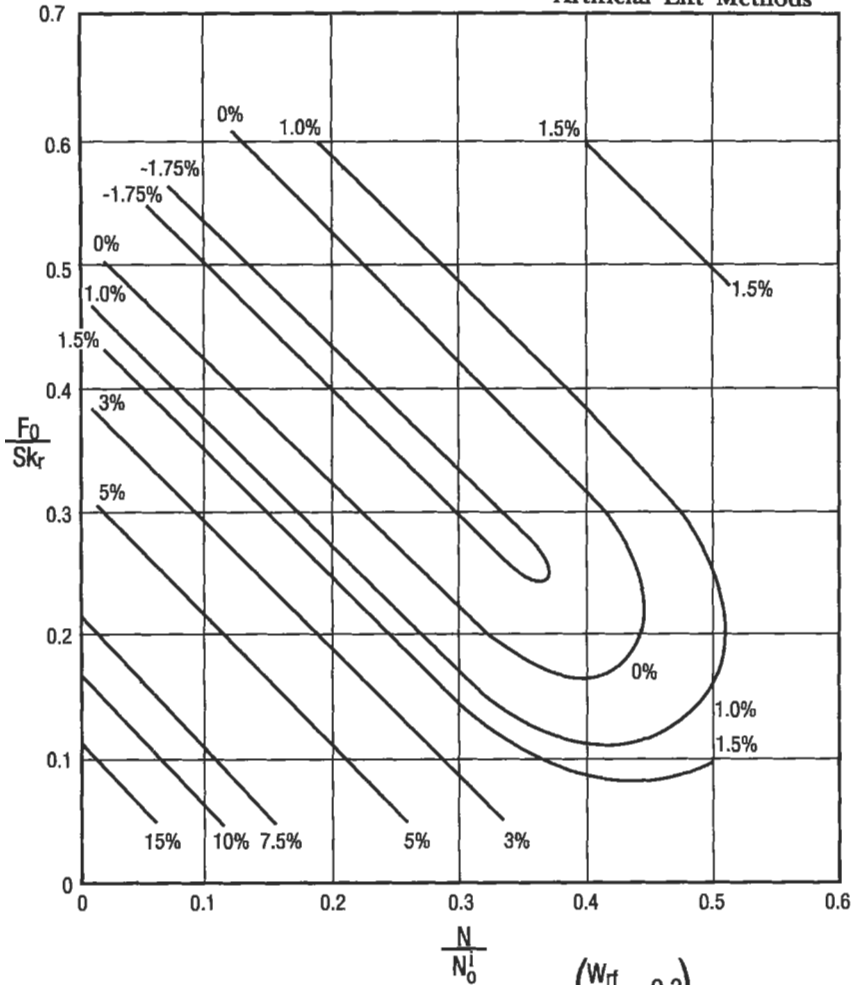


Figure 6-128. Polished rod horse power factor [57].

(text continued from page 631)

An explanation and definition of each of these five operating characteristics of calculation lines 23 through 27 is given below. This is followed by a description of how to use these operating characteristics to choose feasible specifications for the pumping unit operating characteristics. The operating characteristics of lines 23 through 27 have the following significance.



To use: Multiply % indicated on curve by $\frac{(W_{rf} / Sk_r - 0.3)}{0.1}$

For example: $\frac{W_{rf}}{Sk_r} = 0.600$

$\frac{N}{N_0} = 0.200$ $\frac{F_0}{Sk_r} = 0.188$

Adjustment = 3% for each 0.1 increase in $\frac{W_{rf}}{Sk_r}$ above 0.3

Total adjustment = 3 x 3% = 9%

$T_a = 1.00 + 0.09 = 1.09$

Note: if $\frac{W_{rf}}{Sk_r}$ is less than 0.3 adjustment becomes negative

T_a Adjustment for Peak Torque For Values of $\frac{W_{rf}}{Sk_r}$ Other Than 0.3

Figure 6-129. Adjustment for peak torque factor [57].

PPRL = peak polished rod load in pounds. This is the maximum load on the polished rod during the upstroke.

MPRL = minimum polished rod load in pounds. This is the minimum load on the polished rod during the downstroke.

PT = peak torque in inch-pounds. This is the maximum torque generated on the gear reducer during the pumping cycle.

PRHP = theoretical horsepower needed by the pumping unit.

CBE = Counterbalance effect. This is the pounds of counterbalance effect measured at the polished rod needed to properly counterbalance the unit. It is *not* equal to the pounds of counterbalance weights needed. See discussion below.

Rod Stress. One should use the PPRL and MPRL in a stress analysis of the rod string to determine whether the rods are overstressed. For this, the Goodman diagram is used. The procedure is explained using the above calculation example.

Step 1. Convert the rod loads (PPRL and MPRL) to stress by dividing by the rod cross section area.

Since PPRL and MPRL are computed at the polished rod, one uses the cross-section area of the largest rod ($\frac{7}{8}$ -in. diameter in this case). The cross-section areas of the rods are listed in Table 6-23. For $\frac{7}{8}$ -in. rods, the cross-section area is 0.601 in.². The stress's are

$$\frac{\text{PPRL}}{\text{Rod area}} = \frac{14,356 \text{ lb}}{0.601 \text{ in.}^2} = 23,887 \text{ lb/in.}^2$$

$$\frac{\text{MPRL}}{\text{Rod area}} = \frac{5,249 \text{ lb}}{0.601 \text{ in.}^2} = 8,734 \text{ lb/in.}^2$$

Step 2. Select the rod grade and tensile strength. Refer to Table 6-27. Let us assume that the rods are Grade C. These have a minimum tensile strength of 90,000 lbf/in.². Minimum rather than maximum tensile strength is used to give a more conservative design and to reduce the possibility of rod failure.

Step 3. Apply the modified Goodman diagram equation. Refer to the section titled "Allowable Rod Stress and Stress Range" for a discussion of this equation. Thus

$$S_A = (T/4 + 0.5625 \times S_{\min}) \times SF$$

where T = minimum tensile strength in psi

S_{\min} = minimum tensile stress experience by the rod

S_f = service factor

S_A = allowable maximum stress in rod in psi

Here T = 90,000 psi for a Grade C rod

S_{\min} = 8734 psi from Step 2.

Let us assume a service factor of 1.0, i.e., normal noncorrosive conditions (no H₂S, CO₂ or brine)

Step 4. Compute S_A :

$$S_A = (T/4 + 0.5625 \times S_{\min}) \times SF$$

$$= (90,000/4 + 0.5625 \times 8734) \times 1.0 = 27,412 \text{ psi}$$

Step 5. Compare allowable maximum stress S_A with the design maximum.

The API RP11L design gives a maximum stress of 23,887 psi. The modified Goodman diagram allowable stress is 27,412 psi. Thus this rod string will not be overstressed. The design stress is $(23,887/27,412) \times 100 = 87\%$ of the maximum stress. The actual design stress should not be more than 95% of the Goodman diagram allowable stress. If this percent value is much less than 50%, a lighter rod string could be used. The comparison of actual to allowable stress in this step is critically dependent upon the value chosen for the service factor. In this example, a service factor of 0.80 would mean that the allowable stress was

$$S_A = (90,000/4 + 0.5625) \times 0.80 = 21923 \text{ psi}$$

which gives a percentage of the allowable stress of

$$\frac{23,887 \text{ psi}}{21,923 \text{ psi}} \times 100 = 109\%$$

and so the rods would be overstressed.

Peak Torque. The calculated peak torque for this example design is 133,793 lb-in. The unit selected must have a gear reducer torque rating larger than this computed value. Refer to Table 6-22 for available ratings. Any unit having a rating of 160,000 lb-in. or larger would serve. Normally one would choose a 160,000-lb-in. unit rather than a 228,000 or 320,000-lb-in. unit. Normal notation is to refer to a 160,000-lb-in. unit as a 160 unit.

Structural Capacity. Structural capacity is based on the peak polished rod load (PPRL). In each torque rating class, several structural capacities are available. One chooses a structural capacity rating larger than the PPRL. A 17,300-lb structural capacity unit would be selected here.

Stroke Length. Although a stroke length of 54 in. was initially chosen, one now needs to see if the selected pumping unit with 160,000 lb-in. of torque and 17,300 lbf structural capacity is available in a 54-in. stroke. The API unit closest to that desired is 160-173-64. The 64 refers to the *largest* stroke available in this size. One would need to check manufacturers' catalogues to see what smaller strokes are possible for a 160-173-64 unit. If, for instance, a 53-in. stroke were available as a second stroke length setting, one would need to increase the pumping speed slightly to overcome the reduction in stroke length.

Prime Mover Horsepower. The computed polished rod horsepower rating PRHP is a theoretical horsepower value and is less than the rated capacity of any prime mover that should be selected. The value also does not indicate whether one should use an electrical motor or an internal combustion engine. Refer to the section titled "Selecting Prime Mover Site" for a discussion of prime mover selection criteria. If a slow-speed internal combustion engine or a high slip NEMA D electric motor were selected, the prime mover horsepower would be computed by Equation 6-194

$$\begin{aligned} \text{HP}_{\text{pm}} &= \frac{q \times D}{\text{PMF}} \\ &= \frac{(150 \text{ bpd}) \times (4,500 \text{ ft})}{56,000} = 12.0 \end{aligned}$$

Note that the actual lifting depth, 4500 ft, and the surface flow rate 150 bpd were used. The efficiency given as 85% is incorporated into the value selected for PMF. One would choose the next size larger available nameplate rating for the engine or motor to serve as prime mover.

Analyzing Existing Pumping Units

Several different procedures are available to test an existing pumping installation. Because causes of malfunction are many and because the observed consequences of many malfunctions can be the same, the process of identifying one or more problems that can exist can be complex. In most instances, the most rapid and accurate analysis will occur where the largest amount of precise data are available. The benefit of the extra data comes in less work over expense and less lost production due to downtime.

Dynamometers. An extremely valuable tool for analysis of well performance is the well dynamometer. Several manufacturers provide these devices that measure polished rod load versus polished rod position. The new electronic dynamometers also allow rod position and rod load to be recorded versus time. If an electric prime mover is used, some new dynamometer systems also provide a graph of motor current versus rod position and versus time. This latter graph is a simple and rapid way to determine proper counterbalance. The load measuring part of the dynamometer is attached to the polished rod so that the load can be sensed and sent to a recorder. A companion part of the dynamometer attached to the walking beam senses the polished rod position and sends it to the same recorder. The graph produced is called a *dynagraph* or more commonly a *dynamometer* or *dynagraph card*. A typical card is shown in Figure 6-130.

Force \times distance equals work. The dynamometer measures force on the polished rod and distance the polished rod moves. The dynamometer thus

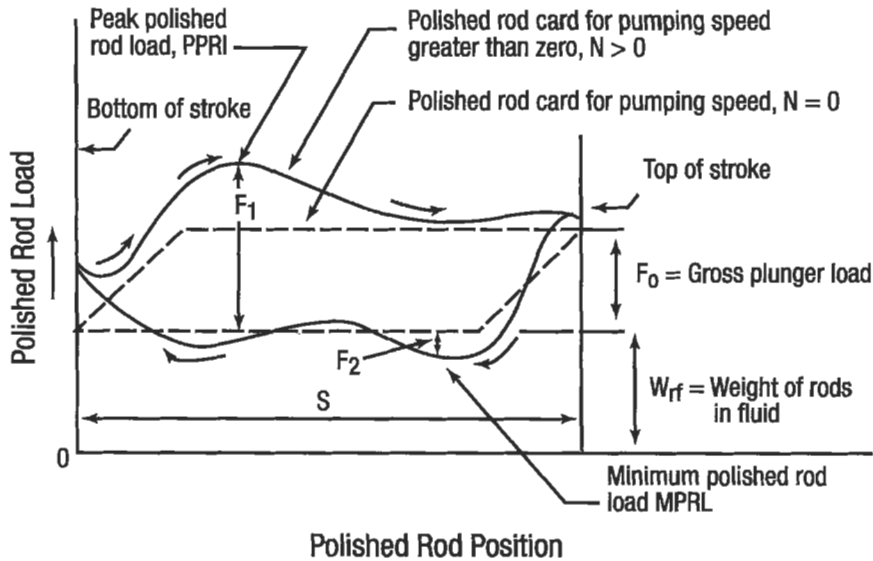


Figure 6-130. Dynamometer card [57].

records work done during one pump cycle. Because power is the rate of doing work, and because the time to create one pumping cycle, creating one dynamograph card is known, the rate of doing work, namely the horsepower at the polished rod can be estimated from the dynamometer card.

The rods, fluid and tubing (if unanchored) constitute an elastic system whose motion under the action of the reciprocating pump can be very complex. The dynamometer records the changing load versus position at one point in the system, i.e., the polished rod. To understand the behavior of the system at points other than at the point of measurement is very difficult in many installations. Older references to the pumping system as following simple harmonic motion represent a gross oversimplification for moderate to deep wells. For such wells, the only reasonably precise estimation of downhole behavior based on dynamometer cards can be obtained through computer programs based on solutions to the wave equation such as described by Gibbs [59]. However, for troubleshooting of wells, several types of problems can easily be identified through qualitative analysis of the appearance of the dynamometer card. Other problems can be identified through simple computations using dynamometer card data. In any program of troubleshooting of wells with a dynamometer, it is always helpful to have a dynamometer card for the well when it is operating normally. The card when taken during a troubleshooting test should be run under identical conditions of pumping speed, stroke length and dynamometer constant settings as when the well was running normally. In the following paragraphs, some of the more common and easily identified problems will be described where these problems can be identified through card shape.

Fluid Pound. Refer to the section titled "Fluid Pound" for a discussion of the causes and cure for fluid pound. Its presence is indicated by a relatively steep drop in the load somewhere along the downstroke portion of the dynamograph. The farther that this drop occurs to the left, the farther the plunger has moved down the pump barrel before it hits liquid. A typical example of fluid pound appears in Figure 6-131. A more severe example of fluid pound is given in Figure 6-132.

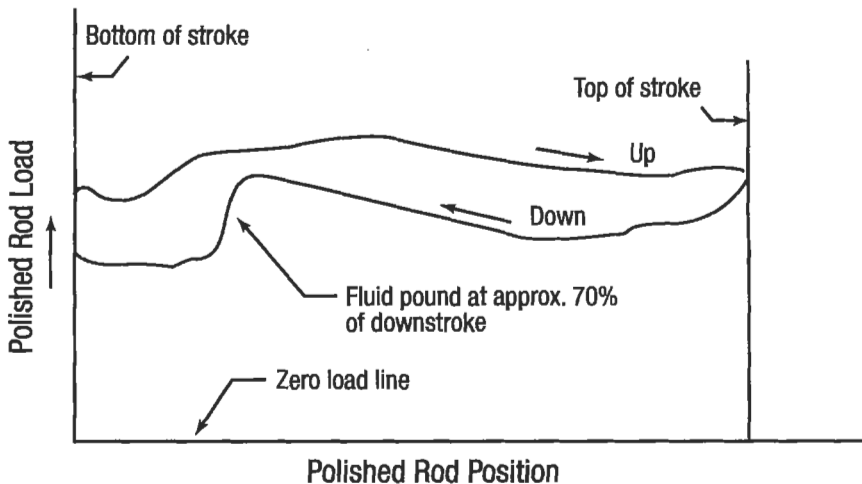


Figure 6-131. Example of fluid pound [68].



Figure 6-132. Severe case of fluid pound [61].

Gas Pound. This effect is similar to that of fluid pound and cannot always be positively distinguished from fluid pound based solely on card shape. Gas pound shows a more gradual load decrease on the downstroke relative to fluid pound. An example of gas pound is shown in Figure 6-133.

Well Pumping Off. Under normal conditions, exactly the same dynamograph is traced on each pump cycle. However, when a condition of fluid pound exists and the drop off of load occurs later and later in the downstroke cycle, then a well pump off condition exists. The well cannot produce as much as the pump is attempting to lift to the surface so the pump barrel fills less with each successive cycle. This condition is shown in Figure 6-134.

Additional Qualitative Dynamometer Tests. Analysis of problem wells is enhanced if a few extra simple tests are made while the dynamometer is in place. These tests include (1) traveling valve check, (2) standing valve check and (3) counterbalance effect measurement. Each is described below and typical diagnostic examples are shown.

For the traveling valve check, leave the dynamometer in place recording a stable card. Stop the pumping unit about half way through the upstroke and pull the polished rod position indicator cord sharply four or five times at 1-s intervals. A nonleaking traveling valve will show a single horizontal line on the card. A leaking valve will appear as in Figure 6-135. The constant line across the middle of the diagram labeled "Traveling Valve" is the line that would appear for a nonleaking valve. However, when the valve leaks, fluid above the valve

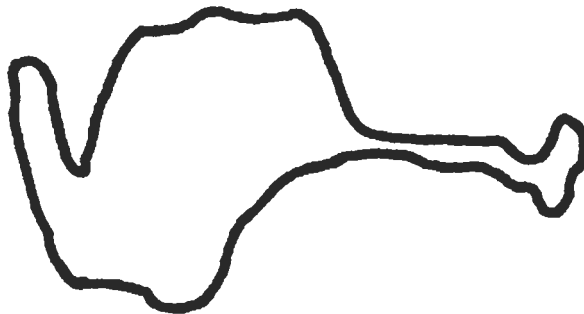


Figure 6-133. Example of gas pound [61].



Figure 6-134. Example of well pumping off [61].

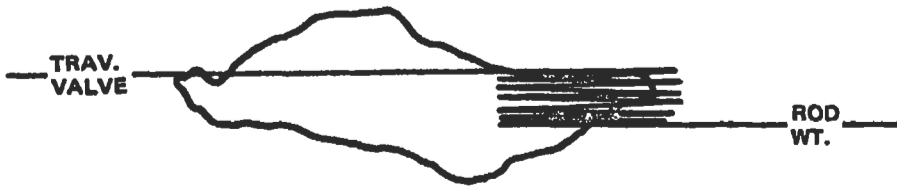


Figure 6-135. Traveling valve with severe leak [61].

moves downward through the leak and exerts a pressure on the standing valve and reduces the load on the traveling valve and plunger. In the case of a severe leak, the entire fluid load will bear on the standing valve and the dynamometer will indicate only the buoyant weight of the rods.

The standing valve check is done in a manner similar to that for the traveling valve but on the downstroke rather than the upstroke. At approximately half way through the downstroke, stop the unit and pull the polished rod position indicator cord sharply four or five times at 1-s intervals. If the traveling valve holds and the standing valve leaks, the dynamometer card will appear as in Figure 6-136. When the standing valve leaks, the fluid in the barrel, instead of going up through the traveling valve, will go downward through the leaky standing valve. This fluid motion will cause fluid to move downward through the traveling valve causing it to close. The dynamometer will then sense an increase in load on the rods. This is the cause for the rise shown on the example card in Figure 6-136.

The counterbalance effect measurement will indicate whether a pumping unit is properly counterbalanced. Proper counterbalancing is important to reduce power consumption and to ensure long life to the prime mover and pumping unit gear reducer. To measure the effect in pounds that the counterweights have at the polished rod, install the dynamometer as when preparing a dynagraph, then when a stable card has been obtained, stop the unit where the maximum counterbalance is operative, i.e., where the weights are acting vertically downward on the upstroke. Install a polished rod clamp above the stuffing box, then chain the clamp to the casing head so that the polished rod will not move upward when the brake is released. Now release the brake and pull the polished rod position indicator cord. The line created on the dynagraph occurs at a load equal to the counterbalance effect (CBE). An example of a card for a properly balanced well is shown in Figure 6-137. On this figure the normal, nonleaking standing valve (SV) and traveling valve (TV) check lines are also shown to indicate that effectively counterbalanced units have the CBE line approximately half way between the TV and SV lines.

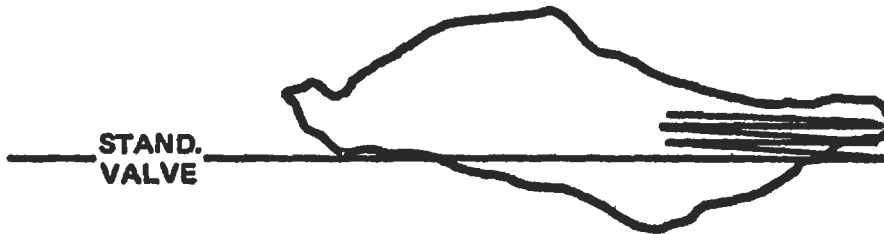


Figure 6-136. Standing valve with severe leak [61].

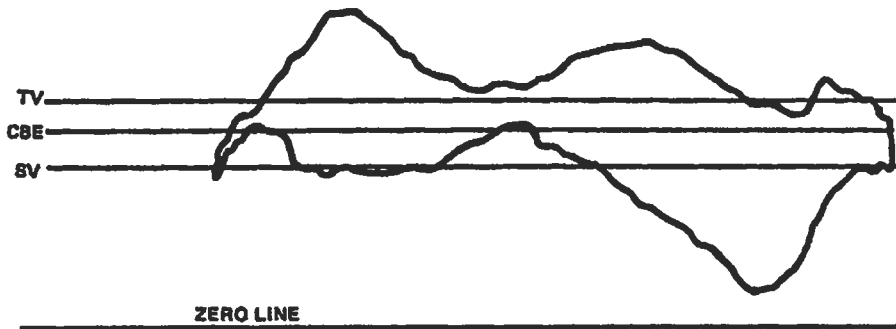


Figure 6-137. Effective counterbalance [61].

Gas Lift

The technique of gas lift is a very important one, particularly in those cases where downhole pumps cannot be used, such as wells on offshore platforms and deviated holes. Gas lift utilizes the energy of compression in the gas to decrease the hydrostatic gradient in a liquid column and thus cause the column to reach the surface. This is accomplished with the use of gas lift valves (pressure and flowrate regulating valves) located between the tubing and casing annulus. Gas is compressed and fed into the casing annulus and passed into the tubing at a regulated rate by a gas lift valve. Then, the combination of gas and well fluid is carried to the surface. Here the fluids are separated and the low-pressure gas is either recompressed for reuse as gas lift gas or compressed for the sales line if excessive gas is produced. At the heart of this artificial lift technique is the gas lift valve, which acts as a pressure regulator, attempting to maintain either a constant casing pressure or a constant tubing pressure, depending on the construction of the valve.

Gas lift is utilized in one of two ways: (1) by continuous gas injection into the tubing causing a continuous flow of reservoir fluid or (2) by rapid injection of very large quantities into the tubing, causing a slug of fluid in the tubing to be carried to the surface. The valve then closes, awaiting another column of fluid to build in the tubing. The first method is called *continuous lift* and is used in wells with production capacity such that it will flow continuously. The second method refers to intermittent lifting of wells where the reservoir is of very limited productivity. Quite obviously, the intermittent lift method is

inefficient and requires specialized surface equipment to handle the large rates involved whenever a slug of production reaches the surface. Due to the limited use of intermittent gas lift, this treatment will be confined to continuous gas lift. Continuous lift can be accomplished with casing-operated valves, tubing-operated valves, or valves that have characteristics of both. These will be described later.

The next sections will describe concepts necessary for gas lift design and then will give example designs. First, some knowledge of the productivity of the reservoir is necessary to determine the required drawdown on the perforations. If there is too little drawdown, the well underproduces. If there is too large, a drawdown and the perforations (gravel packs, etc.) could be damaged. Consequently, an engineering knowledge of the production capabilities of similar wells is required.

Another tool needed by the designer is a generator of (computer program) or a comprehensive set of gradient curves for multiphase flow of oil, water and gas in vertical pipes. These will be described in a later section. Also, an engineer designing gas lift installations needs a working concept of valve mechanics. This topic is covered in the third section. An important function of gas lift valves is to unload the well, that is, remove the casing annulus fluid such that gas can be injected into the tubing at the desired depth. This topic is also covered in a later section.

After a working knowledge of these topics is covered, an example design of both tubing-operated and casing-operated valves will be presented. These are offered as simple examples under certain assumptions. They can be elaborated upon and changed under certain conditions. In other words, there are many sound engineering variations leading to working designs. A trained representative of a reputable gas lift service company should be consulted for further design techniques.

Inflow Performance

Inflow performances of a reservoir can be defined as the functional relationship between the flowing bottomhole pressure and the resulting flowrate. Several models are available, such as straight line (productivity index, or PI), Vogel's method, the Fetkovich method, and others [48].

First, the straight line, or PI, is given as the ratio of the total barrels of fluid produced to the pressure drawdown across the reservoir (drawdown is defined as the average reservoir pressure minus flowing bottomhole pressure), or

$$PI = \frac{q(\text{bpd})}{\delta P(\text{psi})}$$

This value can be obtained by direct measurement on a particular well by physically measuring the flowing and shut-in bottomhole pressure while also noting the surface flowrate. This number is valid only while the oil/water ratio for the well remains fairly constant. The effect of changing oil/water ratios can be seen below. If measured values are not available, one can estimate the PI with the approximate relationship obtained from the Darcy equation. This is done by utilizing a typical relative permeability relationship and correlations for viscosity and formation volume factors:

$$PI = HK_a \left(\frac{K_{r0}}{\mu_o B_o} + \frac{K_{rw}}{\mu_w B_w} \right)$$

where K_a = absolute permeability of the rock in darcies

K_{ro} = relative permeability to oil

K_{rw} = relative permeability to water

B = formation volume factor

μ = viscosity

H = reservoir thickness in ft

A second method is that developed by Vogel, originally obtained for volumetric reservoirs at bubble point pressure where resulting gas saturations around the vicinity of the wellbore cause a decrease in the relative permeability. The relationship derived is given as

$$\frac{q}{q_0} = 1 - 0.2 \left(\frac{P_w}{P_b} \right) - 0.8 \left(\frac{P_w}{P_b} \right)^2$$

where q = flowrate in bpd

q_0 = flowrate at maximum drawdown in bpd

P_w = flowing bottomhole pressure of interest in psig

P_b = bubble point and reservoir pressure in psig

With this method, a measured value of flowing bottomhole pressure, average reservoir pressure and the associated flowrate is required to define q_0 . Once the equation is thus normalized, it can then be used to predict the well's performance at any drawdown.

A third method occasionally used is that of Fetkovich, where flowrate is given by

$$q = C(P_r - P_w)^n$$

where C and n are constants and must be determined by conducting two separate flow tests. The parameter P_r is the average reservoir pressure.

Example

A well flowing 50% water (viscosity = 0.5 cp and FVF = 1) and 50% oil (viscosity = 4 cp and FVF = 1.5) from a 20-ft-thick reservoir. Core analysis indicates the absolute permeability to be 300 md. Estimate the PI of this well.

Answer

Assuming typical relative permeability relationships, we estimate the relative permeability of the reservoir to oil to be 0.25 and to water of 0.25. This yields a $PI = 3.25$ bfpd/psi. Note that when this well produced all oil, the PI would be estimated at 1 bopd/psi.

If this well is tested at a flowrate of 200 bopd and 200 bwpd, with a shut-in bottomhole pressure of 4,500 psig, and a flowing bottomhole pressure of 4,350 psig, what is the calculated PI? What is the expected production rate for a drawdown of 1,000 psi by the PI method?

Answer

$PI = 2.67$ bfpd/psi, implying a rate of 2,670 bfpd for a 1,000-psi drawdown.

If a well is tested at 400 bopd for a drawdown of 150 psi, what does the Vogel method predict for a 1,000-psi drawdown? The reservoir pressure (also the bubble point pressure) is 4,500 psi.

Answer

$q_0 = 6,767$ bopd, and yields a flowrate of 2,439 bopd for a 1000 psi-drawdown.

A second test on this well shows a production rate of 1,000 bopd for a 500-psi drawdown. What flowrate does the Fetkovich method predict for the 1,000-psi drawdown?

Answer

$C = 0.006$ and $n = 0.79$; flowrate = 1,704 bfpd at the 1,000-psi drawdown.

Neither of these calculation techniques can be considered preferable; each depends on the engineer's experience and the actual reservoir conditions.

Gradient Curves

The first concept needed in gas lift design is that of gradient curves. For the case of single fluid flow in pipes one can calculate the total pressure difference between two points with well-defined mathematical equations, requiring only a friction factor empirical relationship for the case of turbulent flow. Even in the case of non-Newtonian fluids, appropriate assumptions have been made enabling the calculation of pressure difference with a single equation for pipe or annular flow. In the case of multiphase flow involving gas-liquid mixtures, a single equation is not possible. Pressure variation along the length of the pipe causes gas volume changes. In the case of oil-gas flow, the oil may liberate solution gas into the flow stream. Consequently, a change of the *in situ* gas-liquid fraction implies a constantly changing hydrostatic component of pressure, a constantly changing friction factor and, possibly, an acceleration component of pressure change.

The only method of calculating pressure differences for multiphase flow is to resort to computer numerical evaluation utilizing incrementing type algorithms. Starting conditions in the first increment are used to estimate conditions in the next increment and so on until the total pressure difference is calculated. Calculation techniques are available in the literature such as Poettmann and Carpenter, Hagedorn and Brown, Orkiszewski, Beggs and Brill, Duns and Ros, and many others [69]. The reader is encouraged to use appropriate computer programs with which to obtain gradient curves for design work. The appropriate choice of calculation technique is dependent on such factors as the geographical area the wells are located, etc. The author will refer to the gradient curves given by K. Brown in *The Technology of Artificial Lift Methods* [48].

Gradient curves for multiphase flow in vertical pipes are used in one of three ways: (1) to predict the pressure at the bottom of a measured interval if the pressure at the top of the interval, the gas/liquid ratio, and the liquid flowrate are known; (2) to predict the pressure at the top of a measured interval if the pressure at the bottom of the interval, the gas/liquid ratio, and the liquid flowrate are known; or (3) to predict the gas/liquid ratio required if the pressures at both ends of a measured interval and the liquid flowrate are known.

First, one must realize that the vertical axis on typical gradient curves (see Figure 6-138) does not represent absolute depth but rather a relative vertical length. The user must determine the appropriate section of a gradient curve

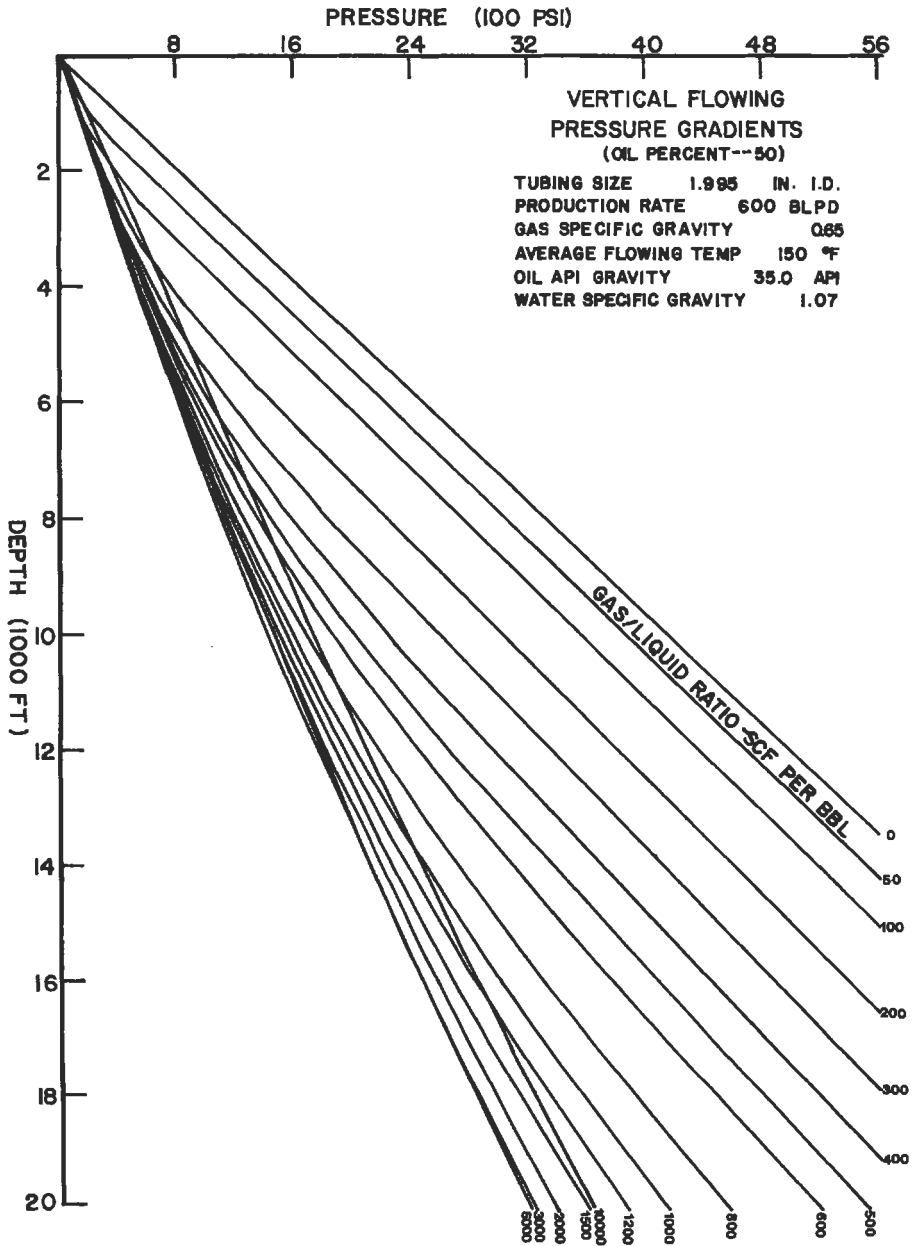


Figure 6-138. Example vertical flowing pressure gradient for multiphase flow.

to use for his or her particular problem. For (1) above, one first identifies the appropriate gradient curve and then locates the pressure of interest at the top of the interval, noting the vertical ordinate for that point. The interval length of interest is then added to this vertical ordinate. This identifies the appropriate interval of interest. The pressure at the interval bottom is the predicted pressure. In the case of (2) above, this process is reversed. For (3) above, we imagine two vertical lines drawn at the end pressures. These lines intersect the entire family of gradient curves, but only one curve (perhaps an interpolated one) has the prescribed vertical interval. This process is a trial-and-error one until the correct curve is identified. Of course, a computer program with which to calculate gradient curves would be somewhat easier to use.

Example Problem

Three example problems will be worked below for a well with 2-in. tubing (1.995" ID) flowing all oil at a rate of 600 bpd and a GLR of 400 scf/bbl. It is assumed that the gas and oil properties given by Brown [48; 3a, page 194] are appropriate (see Figure 6-138).

1. If the well is flowing with a surface pressure of 400 psig, what is the pressure at a depth of 5,000 ft? At 10,000 ft? The answers are 1,520 psig; 3,280 psig.
2. If the same well is flowing with a bottomhole pressure of 4,000 psig at a depth of 8,000 ft, what is the pressure at the surface? At 4,000 ft? The answers are 1,240 psig; 2,520 psig.
3. The same well is flowing with an unknown gas/liquid ratio. The surface pressure is 600 psig and a known pressure of 1,600 psig at a depth of 5,000 ft. What is the flowing gas/liquid ratio? The answer is a pressure difference of 1,000 psi over the 5,000-ft interval implies approximately 600 scf/bbl.

Valve Mechanics

Gas lift valves, by necessity, are constructed as shown in Figure 6-139, where all components must be built into a small cylindrical-shaped tube. The diameter and length will vary according to size restrictions imposed by tubing size, mandrel size, etc. A typical valve must have a closing force (provided by a spring, gas pressured chamber, or both of these), an opening force (provided by a metal bellows upon which either tubing or casing pressure acts) and a flow-regulating orifice.

If tubing pressure is exerted against the bellows causing gas flow regulation, this valve is referred to as a tubing-operated or fluid-operated valve. If casing pressure is applied on the bellows, causing gas flow regulation, then we have a casing-operated or pressure-operated valve.

Gas lift valves operate similarly to pressure regulators. Note that a casing-operated valve acts to maintain a set casing pressure. If casing pressure increases, the valve opens further, attempting to relieve the additional pressure. Conversely, a pressure decrease causes the valve to pinch down in an attempt to decrease gas flow and thereby maintain casing pressure.

On the other hand, a tubing-operated valve attempts to maintain a set tubing pressure. An increase in tubing pressure opens the valve to allow additional gas into the tubing in an attempt to lighten the fluid column above. If tubing pressure decreases, then the valve pinches down in an attempt to increase the tubing fluid gradient by reducing the gas flow into the tubing. There are several

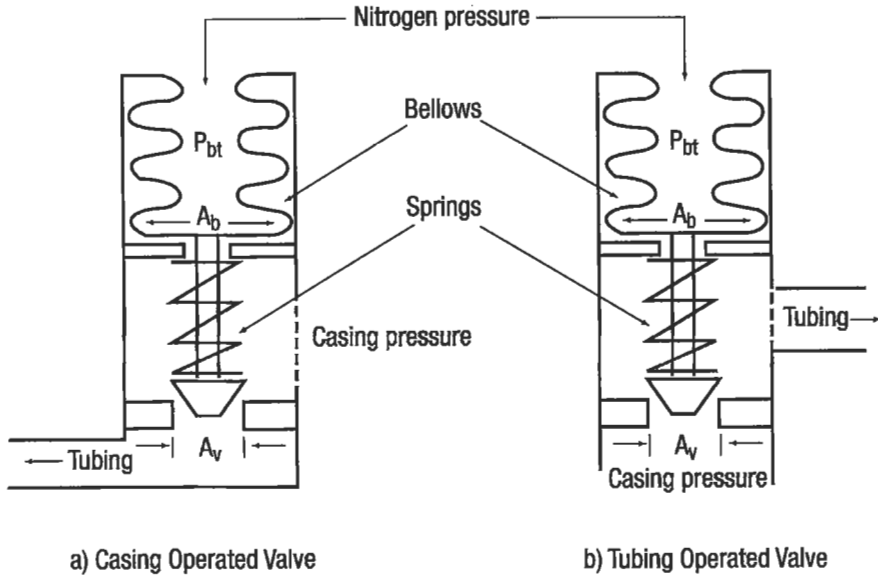


Figure 6-139. Casing and tubing operated valves.

variations on this arrangement such as balanced valves, etc., but these will not be covered here.

The force balance equations (see Craft, Holden, and Graves [60]) give the following relationships for a casing-operated valve that is open and on the verge of closing:

$$P_{vc} = P_{bT} + S_t(1 - A_v/A_b)$$

where A_v = area of the valve port

A_b = effective area of the bellows

S_t = spring constant in psig

P_{bT} = bellows pressure temperature T in psig

P_{vc} = casing pressure opposite the valve at closing in psig

In the case of a valve fully closed and on the verge of opening, we have the equation

$$P_{v0} = \frac{P_{bT}}{(1 - A_v/A_b)} + S_t - \left[\frac{A_v/A_b}{(1 - A_v/A_b)} \right] P_t$$

where P_t = tubing pressure opposite the valve in psig

P_{v0} = casing pressure opposite the valve at opening in psig

Note that P_{v0} and P_{vc} are not equal due to the fact that the casing pressure is applied to the valve stem during flow and tubing pressure is applied to the valve stem during closed conditions. This difference is called the *valve spread* and is utilized in the gas lift unloading process to ensure that valves above the lifting valve are closed. Hence, a casing-operated valve will have a gas passage somewhat

as shown below in Figure 6-140. For exact valve characteristics, one would have to consult the valve manufacturer.

In the case of a tubing-operated valve, the situation is somewhat different in that a valve spread is meaningless. One would calculate a valve tubing closing pressure at a tubing pressure greater than the valve tubing opening pressure. This is impossible; thus the actual closing pressure for a tubing operated valve is determined experimentally in a test rack at the shop; however, the valve closing equation above for a casing operated valve is very close if we substitute tubing pressure for P_{vc} .

Since the bellows volume can be considered constant, the bellows pressure at any temperature is related to that at shop conditions of 60°F by the equation

$$\frac{P_{bT}}{Z_T(460 + T)} = \frac{P_{b60}}{Z_{60}(460 + 60)}$$

The gas deviation factor for nitrogen is given by Sage and Lacy [70] or Craft, Holden and Graves [60; Figure 6.13]. However, Z factors for nitrogen are very close to 1.0 and only deviate from that value by up to 5%.

Example

A casing-operated valve is to be run at a depth of 2,000 ft, where the operating temperature is expected to be 95°F. The valve has an A_v/A_b ratio of 0.1, and a spring effect of 200 psig. What nitrogen pressure at depth is required in the bellows if the closing pressure desired at depth is 900 psig? What nitrogen pressure must be placed in the valve at 60°F?

Answer

$P_{bT} = 720$ psig; $P_{b60} = 683$ psig using a Z factor of 1.006 for nitrogen at 95°F. One must also calculate the pressure increase for static gas columns due to its own density. A good approximation for methane is

$$\delta P = 0.25 (P_{wb}/100) (D/100)$$

For example, if the available casing surface pressure P_{wh} is 1,000 psig, then the casing pressure will increase 25 psi/1,000 ft of depth. This can be rewritten as

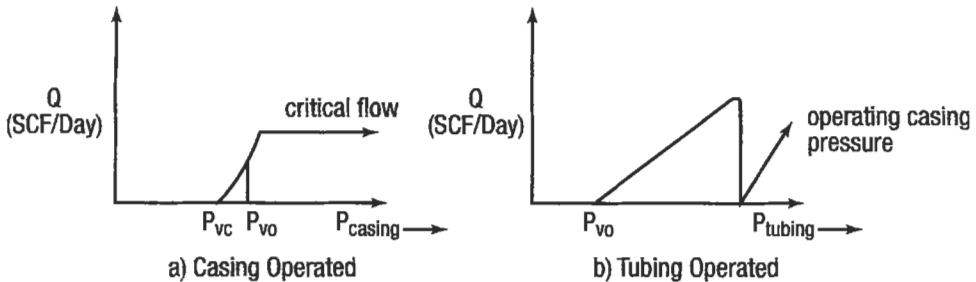


Figure 6-140. Gas passage characteristics for casing and tubing operated valves.

$$P_b = P_{wh}(1 + D/4.0 \times 10^4)$$

where P_b is the pressure at the bottom of an interval D in feet, and P_{wh} is the surface pressure, in psia. Typical gas lift situations have a large annular casing cross-section and the gas flow to the valve can be thought of as a static column. For greater accuracy, we have

$$P_b = P_{wh} \exp(0.01875\sigma D/Z_{avg} T_{avg})$$

where σ = gas specific gravity (air = 1.0)

Z_{avg} = average Z factor over the interval

T_{avg} = average temperature of the gas column in °R

For gas flow in small pipes, frictional pressure losses may be critical. Butthod and Whitely [71] have developed the following equation

$$P_b^2 = B(P_{wh}^2 - A) + A$$

where $B = \exp(0.0376\sigma D/Z_{avg} T_{avg})$

$$A = 1.51 \times 10^{-5} (q T_{avg} Z_{avg})^2 / d^{5.25}$$

d = equivalent flow channel diameter in in.

q = gas flow rate in Mcf/d

For example, 300 Mcf/d of gas flow down a 1-in. ID tubing ($\sigma = 0.65$, $T_{avg} = 560$ °R, and $Z_{avg} = 1$), with a surface pressure of 1,000 psig, will have a pressure at a 2,000-ft depth of 1,025 psig as compared to the expected 1,050 psig for a static gas column.

Unloading the Well

A phenomena one must address in gas lift design is that of unloading the casing annulus. Unloading simply means removing all the casing (packer) fluid left in the well between the tubing and casing at the time of completion and replacing it with gas down to the point of injection. First, if drilling mud or other abrasive fluid is in the casing annulus, it must be replaced with clean water by using a circulating pump. In the case of tubing retrievable valves, this task is easily accomplished at the time the pulling rig is on location. For wireline retrievable valves, a mandrel below the expected point of gas injection should be opened, and clean water circulated until the packer fluid is completely replaced.

It is very likely that the desired point of gas injection will be deeper than can be unloaded with a single valve. Imagine a U-tube that is filled with liquid on both sides and has a gas pressure applied to one side. The fluid will move from one side to the other, spilling over at the top, and continuing until the pressure at the bottom on both sides become equal. If the U-tube is too long, this process will stop whenever the pressures equalize. For example, if the desired depth of injection is at 5,000 ft and the casing fluid is formation water of density given by 0.465 psi/ft, a gas pressure at the valve of 2,325 psig would be required to unload the well with a single valve. Since this gas pressure is excessive, the conclusion is that one simply cannot unload the well with a single valve.

By this logic, several valves will be needed. The depth to the first valve can be determined by the equation

$$P_{ts} + \sigma_w D_1 = P_{CS} + \sigma_g D_1$$

- where P_{ts} = surface tubing pressure in psig
- P_{CS} = surface casing pressure in psig
- σ_w = water density in psi/ft
- σ_g = average gas density in psi/ft
- D_1^g = depth to first valve in ft

This equation can be solved either algebraically or graphically (see Figure 6-141) by plotting the left and right sides independently, finding the intersection. This is done by plotting pressure on the X axis and depth on the negative Y axis (standard plot for gas lift design). For example, if the well is being unloaded to a separator whose pressure is 50 psi, with a packer fluid of 0.5 psi/ft, and the available casing pressure is 1,000 psig, then the first valve can be run as deep as 2,000 ft. Of course, a more shallow depth would ensure successful unloading to the first valve, but would cause the deepest possible point of lift.

Once this first valve has been uncovered, it can be used to reduce the hydrostatic pressure in the tubing above that point by gas injection. Reduction of the hydrostatic pressure simply means that a second valve can be run below and the casing gas pressure will push the packer fluid down, through the second valve so it can be lifted to the surface by the first valve. Again, the depth to the second valve is determined by a pressure balance condition given by

$$P_{ts} + \sigma_{min} D_1 + \sigma_w (D_2 - D_1) = P_{CS} + \sigma_g D_2$$

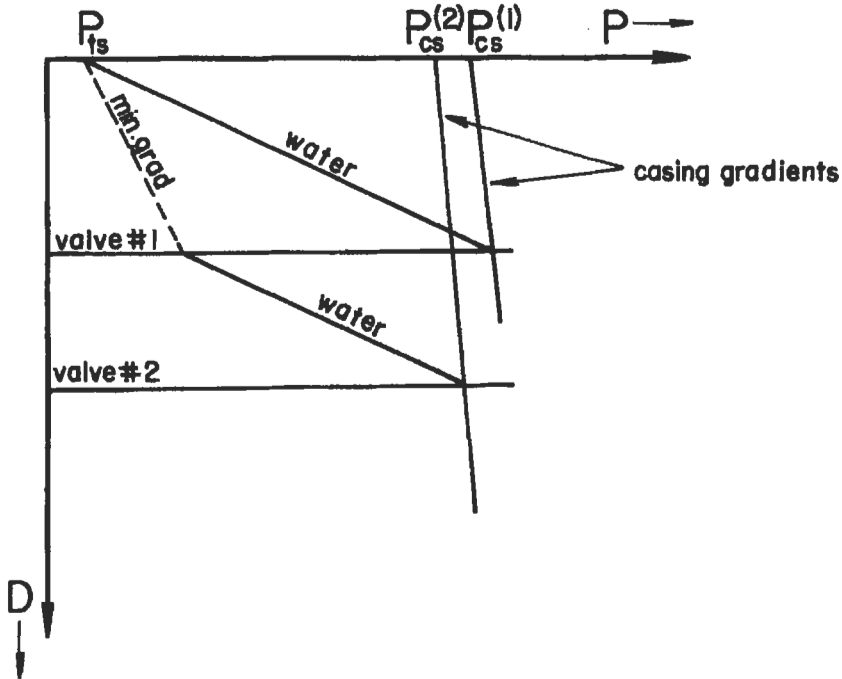


Figure 6-141. Locating the unloading valve depths.

where σ_{\min} = the average minimum two-phase gradient that can be developed by the first valve in psi/ft.

The value of P_{cs} to be used here may differ from that used to locate the first valve. For example, a design for casing-operated valves will require that the casing pressure be reduced. Therefore, the value to be used is the surface casing pressure available for that valve. In the example above for the first valve, assume the average minimum gradient to be 0.15 psi/ft and the surface casing pressure available for the second valve is 975 psig. The deepest depth to which the second valve can be run is therefore 3,421 ft.

This process would continue to locate subsequent valve depths until the casing pressure (right side of the equation) can no longer produce the minimum gradient. Note that the distance between valves is decreasing. Typically, whenever a minimum incremental distance (on the order of 400 ft or less) or the expected lift depth is reached, several valves will be positioned, if possible, at this distance apart. This accounts for any errors made in the design and increases the probability that one of these valves will be the optimum lift depth.

At this point, another definition is needed, that of the deepest point of injection. This depth is defined by the equation

$$\text{FBHP} - \sigma_{\text{ave}}(D_T - D_{\text{iv}}) = P_{\text{ca lift}} + D_{\text{iv}}\sigma_g$$

where FBHP = flowing bottomhole pressure in psig

σ_{ave} = average flowing gradient in the tubing from the perforations to the lift valve in psi/ft

D_T = total depth of the well to the perforations in ft

D_{iv} = depth to the injection valve in ft

$P_{\text{ca lift}}$ = surface casing pressure operating the lift valve in psig

The average flowing gradient in the tubing can be estimated to be the average density of the flowing liquids. This assumes that essentially no gas is liberated from solution until the liquid is above the lift valve. If, on the other hand, gas is liberated, then a straight line approximation is no longer valid, and a gradient curve should be used to approximate the second term on the left side of the equation above. Graphically, we can solve the above expression as shown in Figure 6-142.

Now, the logic of the unloading process must be explained. First, the casing operated valve design will be examined. An adjustable gas flow valve at the surface at the entrance to the casing annulus is required to have the valves function properly. Note that once lift is achieved, opening the surface casing valve will cause an increase in the casing pressure and will thereby cause the lift valve to open (allowing more gas into the tubing) since a casing-operated valve attempts to maintain a preset value of pressure. Conversely, pinching down on the surface valve causes the lift valve to reduce the gas passage. This is true unless the valve is fully opened and flow through the orifice is critical.

In the unloading process, gas pressure is applied to the casing annulus, causing water to be pushed through the valves until the first valve is uncovered and begins passing gas. To maintain a constant casing pressure, the surface valve is set to a gas flowrate that is essentially equal to the gas passage rate of the first valve that is now uncovered. Remember, packer fluid is being pushed through lower valves into the tubing and is being lifted to the surface by the first valve. Once the second valve is uncovered, gas is passed into the tubing by both valves. However, since the surface valve is set to a rate equal to one

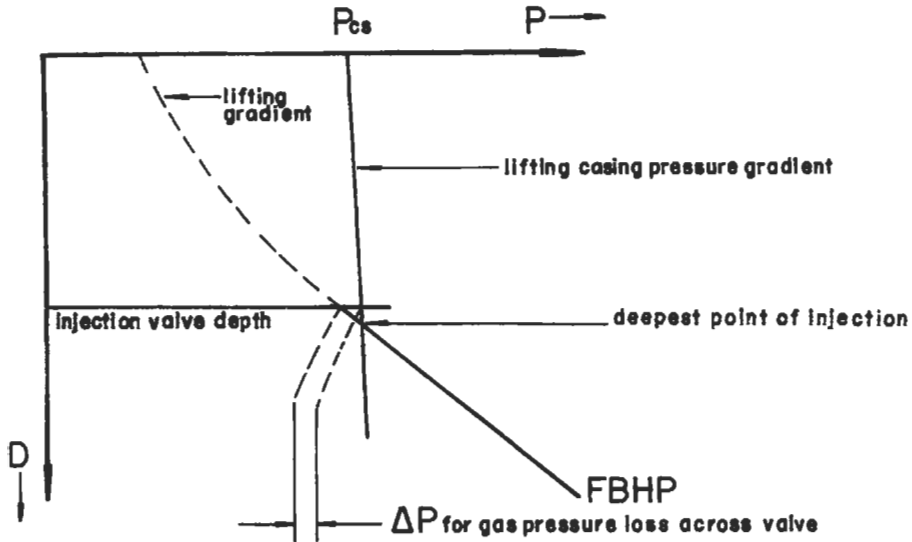


Figure 6-142. Locating the injection valve depth.

valve, the casing pressure will drop. The second valve closes when the casing pressure drops to the set closing pressure of the first valve. The casing pressure will then remain at this new, lower valve as long as the surface valve has a flowrate equal to that of the second valve. By manipulating the surface valve, a pumper must at this time ensure that the casing pressure remains at this new value, below the opening pressure of the first valve.

This process is repeated when the third valve is uncovered, and the casing pressure is again lowered, consequently closing the second valve. This continues until all the unloading valves have been closed and the lifting valve is the only valve injecting gas into the tubing. Note that if the well supplies formation fluid at such a rate that the next lower valve cannot be uncovered, the well is flowing, which is the desired result. If conditions become favorable in the future, the next valve may be uncovered and the well will begin lifting from the lower valve.

The use of casing-operated valves implies that one has temporarily available gas at a higher than lift pressure for the unloading process, or the well will be lifted with less than available casing pressure, thereby lowering efficiency. However, due to the operating characteristics of casing valves, the pumper, by manipulating the surface valve, has some surface control of the lifting valve. This design could not be used in the case of a dual lift, that is, when there are two tubing strings in a single wellbore.

Tubing-operated valves are sometimes referred to as automatic valves since the unloading process proceeds without pumper assistance. These valves respond primarily to tubing pressure and one causes the valves to respond to tubing pressure only by maintaining a constant casing pressure. The design process is done graphically, and requires first that the injection valve depth be identified, and then that the expected lifting gradient be determined. Since the flowing gradient-injection valve intersection determines a pressure and depth, and the flowing surface tubing pressure is known, the lifting gradient can be obtained from a family of gradient curves as described above in the *gradient curve* section or by a computer program.

The depth to the first valve is obtained as described above. The valve closing pressure is now dictated to be a value as close to, yet greater than, the lifting gradient; that is, to the right of the lifting gradient on a graphical design. This condition is required such that when this lifting gradient is achieved by the lifting valve, all valves above will be closed. The process starts with gas pressure applied to the casing annulus, causing the water to be pushed through the valves and up the tubing to the surface. When the first valve is uncovered, it will lighten the fluid column above because a temporary lifting gradient from the first valve is created when water enters the tubing from lower valves. This temporary gradient will become lighter and approach the final lifting gradient but not reach it due to the valve closing tubing pressure. Consequently, the depth to the second valve is found by the condition where

$$P_{ts} + P_{TG} + P_{safety} + \sigma_w(D_2 - D_1) = P_{CS} + \sigma_g D_2$$

where P_{TG} = total pressure difference of temporary gradient in psi
 P_{safety} = small margin to ensure flow through valve in psi

Once the depth to the second valve is determined, its valve closing pressure is also chosen at a tubing pressure that is larger than the lifting gradient at that depth. Again, a temporary gradient is found from the surface unloading pressure to the second valve, and the above process is repeated for the next valve depth. This process continues until a transfer can be made to the injection valve found earlier.

Tubing-operated valves are typically used whenever minimal pumper surveillance is desired. Also, in the case of dual completions, tubing-operated valves are the only choice. Tubing-operated valves allow maximum utilization of the available casing pressure, thereby increasing efficiency. However, a string of tubing-operated valves usually require more unloading valves than a string of casing operated valves.

Tubing Operated Valves Example

Now that all the tools have been developed, a comprehensive example using tubing operated valves (see Figure 6-143) will be presented. The well is 10,000 ft deep (2 $\frac{7}{8}$ -in. tubing) with a shut-in bottomhole pressure of 4,000 psig and a measured PI of 1.33 bfpd/psi. The well flows 20% oil (30° API) and 80% water (specific gravity of 1.07). The surface pressure during lift is expected to be 50 psig, and the available gas pressure is 1,000 psi (approximately 0.025 psi/ft increase due to density). The bottomhole temperature is 200 °F and the expected flowing temperature is 100°F. The design flowrate is 800 bfpd.

The flowing bottomhole pressure is 3,400 psi. The expected gradient below the injection valve is 0.45 psi/ft. This information indicates the lowest possible point of gas injection to be at 4,950 ft, where casing pressure is equal to the flowing tubing gradient. Consequently, the design point of injection is chosen at approximately 4,700 ft where a differential of 100 psi is available between the tubing gradient and casing pressure. This differential allows for the pressure loss for gas flow through the valve and a safety margin for design error.

The packer fluid is assumed to be 0.5 psi/ft density. An actual value can be used if it is known. However, since lease water is typically used, a high estimate is used as a design factor. This implies that the first valve can be run as deep as 2,000 ft. In the case of mandrels already run in the well, any depth above 2,000 ft would work. The second valve depth is determined by first finding the

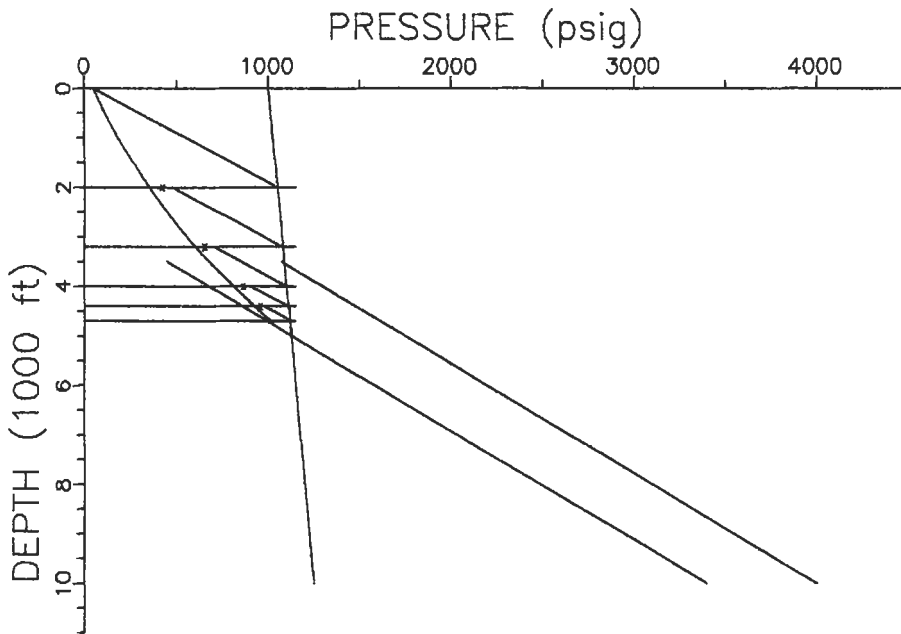


Figure 6-143. Example design using tubing-operated valves.

design GLR curve from the lowest valve. By trial and error, the GLR curve connecting the surface tubing pressure of 50 psi and the design point of injection-flowing gradient intersection of 1,020 psi at 4,700 ft is found to be approximately 210 scf/bfpd. This GLR curve indicates a pressure of 350 psi at 2,000 ft. Consequently, the closing pressure of the first valve must be greater than 350 psi. The actual number is dependent on engineering judgment and the manufacturer of the valve used. In this example, we choose 425 psig, or 75 psi greater than the GLR curve.

A column of water will exist between the first and second valve, and a temporary GLR curve will exist between the first valve and the surface. The temporary gradient must be at least as heavy as 425 psig at the first valve since this is the closing pressure of the first valve. For a design factor, we will choose 475 psi, which we will call the transfer point. Adding a water column of 0.5 psi/ft to this 475 psi, we see that this tubing pressure is equal to the casing pressure at a depth of 3,200 ft. Note that once the second valve begins admitting gas into the tubing, the gradient will become lighter and begin closing the first valve. During the time when the gradient from valve two is somewhat heavy, the first valve will be open and assist in reducing the gradient. Also, if no fluid is in the casing, such as with a well shut-in after it has been unloaded, the deepest valve that can open and allow gas into the tubing will do so. This would then start a process similar to unloading in that the opened valve lightens the gradient, allowing a deeper valve to begin passing gas and thus close the valve above. By definition, this condition must exist somewhere in the well; we simply cannot gas lift the well if the liquid column is below or unable to open the lowest valve.

The lifting gradient has a pressure of 600 psig at the second valve at 3,200 ft. A typical closing pressure of 650 psi is chosen for the second valve, and the liquid column transfer point from the third valve is chosen at 700 psi. This gives a depth of 4,000 ft for the third valve. The gradient pressure at the third valve is 815 psig, giving a closing pressure of 860 psig and a transfer point of 900 psig. The fourth valve is therefore located at 4,400 ft with a gradient pressure of 860 psig. The valve closing pressure is taken as 950 psig and the transfer point as 985 psig.

This unloading process continues uncovering the next lowest valve and closing the valve above until a reservoir drawdown is achieved and formation fluid is lifted. In the example, formation fluid will be lifted by the third valve during the unloading process, but will be in small volumes since it will be on the order of perhaps 400 bfpd according to our PI information. If the PI used is correct and the lower valves are sized to input the correct gas flowrate, the well will continue to increase the drawdown until the last valve is lifting the well. If we can expect the well to produce 50 Mcfpd from the formation, then an injection rate of approximately 118 Mcfpd is required to bring the GLR up to 210 scf/bf. The valve chosen must be capable of varying gas flowrates from the 118 Mcfpd to 168 Mcfpd by throttling to accommodate those situations where the formation gas does not materialize, such as in the case of heading, etc. Its closing pressure will be less than 1,000 psi, the value of the final lifting gradient at the valve depth.

Note that if our PI information were incorrect, a GLR gradient would indeed establish itself. For example, if the actual PI is higher, then the well will lift from a more shallow valve, perhaps the third or fourth. This would be a heavier gradient than the 210 GLR designed, but would establish itself at a greater liquid flowrate determined by the available gas and GLR actually established. If, on the other hand, the actual PI is less than expected, the well will unload to the deepest valve and establish a flowrate of less liquid with the available gas passage rate at a steeper lifting gradient. The designer must be aware of both of these possibilities since a greater than expected liquid flowrate can be damaging to the formation (gravel pack, etc.) as can a greater than expected drawdown across the formation.

A malfunctioning gas lift design would require testing to determine the difficulty. For example, a casing fluid level determination as used in pumping wells can be useful in cases when the unloading process is not successful. Also, a flowing pressure survey (pressures taken while the well is lifting at various points in the tubing) can determine the actual point of gas injection. Pressure charts on the tubing and casing can sometimes pinpoint lift problems. Furthermore, a temporary increase, if available, of the casing pressure will help ensure a successful unloading of the well. After unloading, the casing pressure can be reduced to the designed value.

Casing Operated Valves Example

The same well described in the tubing-operated valves example will now be designed for gas lift with casing-operated valves. Several design techniques are available for casing-operated valves and one of these will be presented here. Further, an important assumption must be made concerning the casing pressure available. In this example, it is assumed that the 1,000-psi lift gas is the maximum available pressure, that is, casing pressure cannot be increased, even temporarily. This assumption implies that the available casing pressure must be able to open all valves, even when there is no packer fluid in the casing annulus. This is the

case whenever the well is shut-in (no packer fluid in the casing annulus) and the unloading valves are used to again start the well flow.

Some repetitive calculations are required since the actual operating casing pressure is not known until later in the design procedure. This is due to the fact that the casing pressure is reduced in order to close the upper valves. First, casing pressure traverses are drawn on the pressure versus depth (see Figure 6-144). Lines spaced 50 psi apart are drawn for reference. The static tubing pressure and flowing tubing pressure lines from the perforations are also placed on the graph.

The depth to the first valve is found in the same way as the tubing operated valves at 2,000 ft. Because of the condition mentioned above, the opening pressure of the first valve is chosen to be 1,050 psig, or the casing pressure at depth. If the valves chosen have an A_v/A_b of 0.067, the closing pressure of the valve at depth is 980 psig. This is an observed surface casing pressure of approximately 930 psig. Also, if the valve has a 200-psi spring effect, the required bellows pressure at depth is 793 psig, or a test rack pressure of 702 psig nitrogen pressure must be loaded into the bellows at 60°F. This surface casing pressure of 930 psig becomes the operating pressure of the second valve.

The depth to the second valve is chosen as that depth at which the U-tube pressures are equal: that of the casing (corresponding to a surface casing pressure of 930 psig) and the tubing. The tubing pressure is again a water gradient between the first and second valves and a GLR gradient from the first valve to the surface. A convenient gradient to use is the design lifting gradient from the deepest valve. Since this depth is not known at this point, it must be decided. By knowing the valves below the first are to be closed by a decrease of 30 psi surface casing pressure, we determine that four valves are needed. This

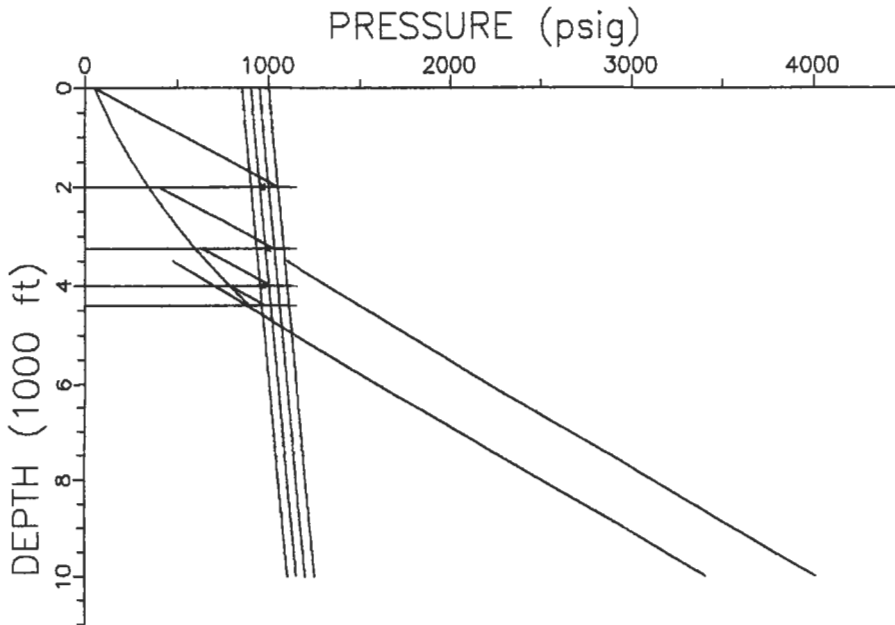


Figure 6-144. Example design using casing-operated valves.

implies that the final surface casing lifting pressure is 870 psig and the design depth of injection is approximately 4,400 ft. Using the Hagedorn-Brown correlation, the design GLR curve is found to be approximately 230 scf/bbl.

The logic of using this GLR curve as the gradient above the valves is that during unloading, the valves can certainly achieve this condition since this is the design lift condition. Consequently, using a transfer point of 400 psig and a 0.5 psi/ft water density, the second valve should be run at 3,250 ft where the casing pressure at depth is 1,025 psig. The closing pressure of the second valve, therefore, is taken to be 995 psig (surface casing pressure of 920). This casing pressure becomes the operating pressure for the third valve, which has a value of 1,010 psi at the third valve at a depth of 4,000 ft. This valve depth is found by using a transfer point of 635 psig at the second valve. The closing pressure of the third valve is therefore 980 psig (a surface casing pressure of 870 psig). Since this is the last valve to close, the operating pressure for the lift valve is a surface casing pressure of 870 psig.

The closing pressure of the valve at 4,400 ft must be chosen such that the gas rate through the valve achieves the design GLR curve of 230 scf/bbl. If the formation can furnish 50 Mcfpd, then the valve must supply an additional 134 Mcfpd. This setting would depend on the type of valve and manufacturer used.

With an expected surface flowing temperature of 100°F and a Bht of 200°F, the design temperatures at the valves are 120, 132.5, 140 and 144°F. The bellows pressures needed in the second and third valves are therefore 808 and 793 psig. The surface rack nitrogen pressure needed for proper operation is 700 and 678 psig. By the choke equation [60], the orifice required in the lifting valve should be taken as $\frac{3}{8}$ -in., ensuring that excessive flowrates are prevented since this represents a maximum flowrate of 150 Mcf/d.

Oil Well Jet Pumps

An oil well jet pump is a venturi-type device where high-pressure fluid is caused to accelerate to a high velocity and thereby create a low-pressure area into which reservoir fluids will flow. The pump has no moving parts. A typical downhole jet pump is shown in Figure 6-145. A closer look at the effective mechanism is shown in Figure 6-146. These pumps require a high-pressure fluid pump on the surface, and this fluid is circulated down the well, typically the tubing. The fluid flows through the jet causing a low-pressure region, and the power fluid-produced fluid mixture is brought to the surface by a second conduit, typically the casing annulus. Once installed, the pump jet can be changed by simply reversing circulation and circulating the pump up the tubing to the surface for repair. A replacement is pumped into place.

Jet pumps can produce high volumes and can handle free gas very well. However, they are not as efficient as positive displacement pumps, thus leading to higher surface horsepower requirements. A thorough coverage of the application of jet pumps is given by Petrie et al. [72]. This type of pump is very useful in certain situations, for example, where high production rates are desired. Also, locations where beam pumping units, for whatever reasons, cannot be used, such as populated areas, offshore platforms, where gas lift is not available, etc., are all possible installations for this pump. Deviated wells are candidates as well if gas lift is not possible.

Since fluid density, gas and viscosity effects are variables needed in the calculations to simulate a jet pump performance, the calculations are complex and require iterative solutions. Here, the computer enters the picture. Any service company in the jet pump business can furnish characteristic plots of the

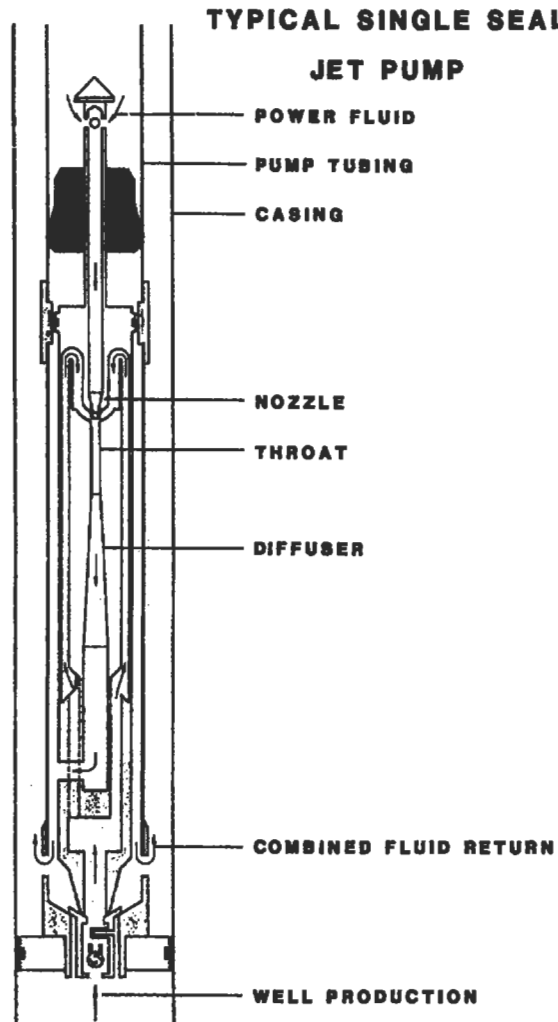


Figure 6-145.

form shown in Figure 6-147. This plot is for a particular pump size and well since the PI of that well is needed as well as tubing length and diameter, fluid type, and fluid properties. However, once this plot has been generated, an engineer can predict the power fluid and surface pressure requirements for a desired production rate. Since the pump size is known, the intake pressure generated is predicted as well. Since PI must be known to design any lifting mechanism, the well's performance will follow the PI line overlaid on the graph. Note that the cavitation zone is also shown, above which the pump cannot operate. That is, if one attempts to pump a very high rate of power fluid at a high surface pressure, the pump will cease pumping reservoir fluid due to cavitation.

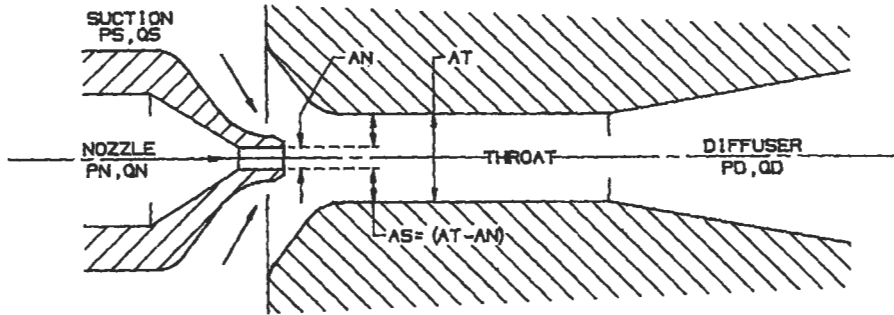


Figure 6-146.

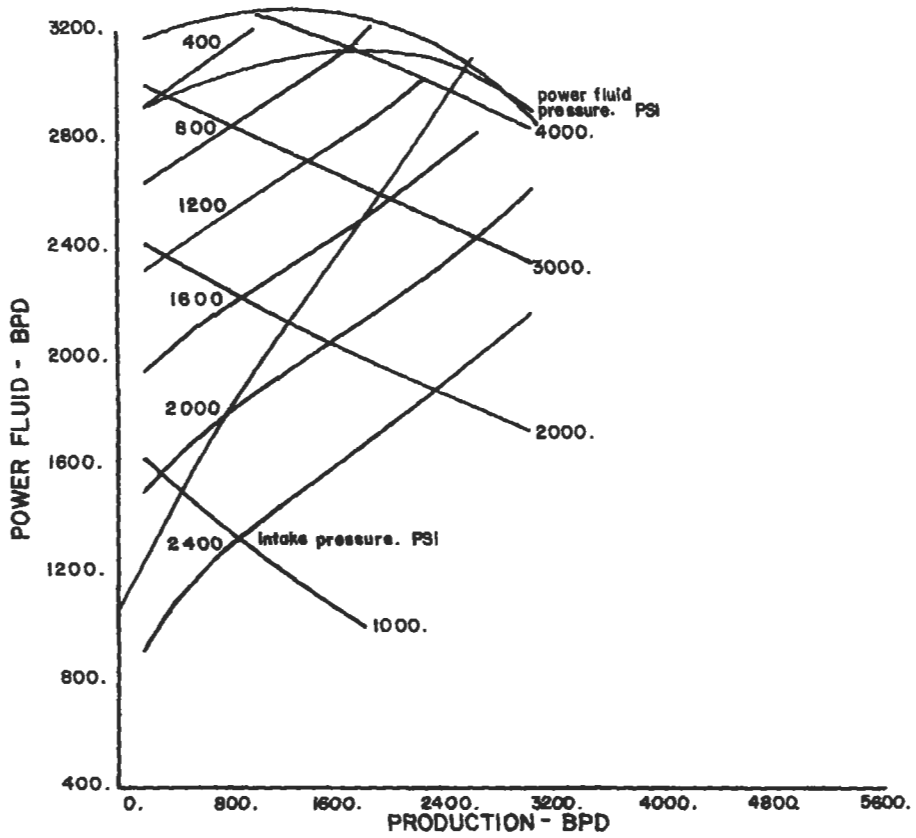


Figure 6-147.

The first step in the design process is to determine the pump minimum annular area needed to avoid cavitation. This is done with the equation

$$ASM = (AT - AN)$$

or

$$ASM = \frac{QS}{691} \sqrt{\frac{GS}{PS}} + \frac{QS(1 - WC)GOR}{24650PS}$$

where AT = flow area of the throat in in.²

AN = flow area of the nozzle in in.²

GS = gradient of the produced fluid in psi/ft

PS = producing bottom hole pressure in psia

QS = production flow rate from formation in bpd

GOR = producing gas oil ratio in scf/bbl

A nozzle and throat combination which has an annular area greater than ASM would then be chosen from a list of standard nozzle and throat sizes such as the partial list below:

Nozzle		Throat	
No.	Area	No.	Area
DD	0.0016	000	0.0044
CC	0.0028	00	0.0071
BB	0.0038	0	0.0104
A	0.0055	1	0.0143
B	0.0095	2	0.0189
C	0.0123	3	0.0241
etc.		etc.	

The next step becomes one of trial and error. The curves such as Figure 9 must be developed, assuming several surface-operating pressures and conducting the iterative calculations for each. The iterative nature is due to the fact that flowrates in the tubing and casing annulus (or another tubing string, depending on the actual configuration of the well) are required to calculate frictional pressure losses, but are not known until final pressures are known. The power fluid rate is determined by the nozzle equation

$$QN = 832 AN \sqrt{\frac{PN - PS}{GN}}$$

where PN = pressure at the nozzle entrance in psia

PS = producing bottomhole pressure in psia

GN = gradient of the power fluid through in psi/ft

QN = power fluid flowrate through nozzle in bpd

The produced fluid is the sum of the power fluid and reservoir production. This combination may require the use of two-phase flowing gradients such as described in the section on gas lift to predict the flowing gradient. As one can see, this procedure becomes very complex and is not efficient for each operating engineer to attempt, especially since computer programs are already available

with which to make these calculations. Any of the major vendors (National, Guiberson, or Kobe) can furnish this service.

For example, a particular well has a PI = 2.65 bfpd/psi, and is expected to flow approximately 2,000 bfpd (98% water of sp. gr. = 1.03). The well is 7,000 ft deep with 2 $\frac{3}{4}$ -in. tubing in 7-in. casing. The well produces with a GOR of 1250 scf/bbl. The shut-in bottomhole pressure is 2,250 psig, therefore implying that the flowing bottomhole pressure is 1,500 psig. (Figure 6-147 illustrates the solution to this problem). This graphical solution indicates the pump will require 2,700 bbl of power fluid per day at a surface pressure of approximately 3,300 psi. Note that reducing the power fluid pumped to 2,150 bpd at a surface pressure of 2,000 psig will result in just over 1,200 bbl of produced fluid.

Electrical Submersible Pumps

The electrical submersible pump (ESP) is a relatively efficient system of artificial lift, and under certain conditions even more efficient than a beam pump, with lower lifting costs and a broader range of production rates and depths [73]. The system is divided into the surface components and subsurface components. Belowground components are the pump, motor, seal, electric cable and perhaps a gas separator. The aboveground components are the motor controller or variable speed controller, transformers and surface cables. The system operates like any electric pump commonly used in other industrial applications. Electrical energy is transported to the downhole motor via the electric cables, typically run alongside the tubing, where the motor drives the pump. The pump imparts energy to the fluid in the form of hydraulic power, lifting fluid to the surface.

The ESP operates over a wide range of depths and volumes, to depths of 12,000 ft and flowrates of 1,300 gpm. However, environmental variables such as free gas, temperature, viscosity, depth, sand and paraffin can severely limit the pump's performance. Excessive free gas results in motor load fluctuations and cavitation leading to reduced run life and reliability. Temperature may limit application because of limitations of the thrust bearing, epoxy encapsulations, insulation, and elastomers. Viscosity increases cause a reduction in the head the pump system can generate, leading to an increased number of pump stages and motor horsepower. Depth limitations are due to the burst pressure ratings of the components such as the pump housing and the thrust bearing. Sand and paraffin problems lead to component wear and choking conditions inside the pump.

The pump consists of several pump stages, each consisting of an impeller connected to the drive shaft and a diffuser that directs the flow of fluid from one stage to the next. The number of stages required is determined by the lift and volume of fluid. Sizes vary from less than 3 $\frac{1}{2}$ to over 10 in. in diameter, and from 40 to 344 in. in length. The motor is a three-phase, squirrel cage induction motor varying from 10 to 750 hp at 60 Hz, ranging from 3 $\frac{1}{4}$ to 7 $\frac{1}{4}$ in. in diameter. Voltage requirements vary from 420 to 4200 V at 60 Hz.

The seal section serves to separate the well fluids present in the pump from the motor oil in the motor. Well fluids must be kept from entering the motor, regardless of differential pressure. Also, this seal must accommodate expansion of the motor oil due to heating. The electric cable supplies electric energy to the downhole motor, and must therefore be capable of operating in fluids at high temperatures and pressures, and deliver maximum electric currents efficiently.

The motor controller serves to energize the submersible motor, sense such conditions as motor overload, well pump-off, etc., as well as shutdown or startup in response to pressure switches, tank levels or remote commands. They are available in conventional electromechanical and solid-state devices. Conventional controllers give a fixed-speed, fixed-rate pump. This limitation can be overcome with a variable-

speed controller where the frequency of the electric current is varied, thereby changing the rpm of the motor and the resulting produced volumes. This device allows changes to be made whenever a well changes volume, pressure, GOR, or water cut, as well as in wells where PI is not accurately known. The transformer simply changes the voltage of the distribution system to a voltage required by the ESP system.

To design an downhole pump and motor, one must first have a knowledge of the productivity index (PI) for the well. The desired operating conditions will determine the depth at which the pump is run to ensure submergence below the pumping fluid level as well as the size of the pump and motor. The desired flowrate and tubing size will determine the total dynamic head (TDH) requirements on the pump. The TDH is defined as the pressure above the pump in the tubing, converted to feet of head, and is given by the sum of the fluid column measured from the pumping fluid level to the surface, frictional pressure loss in the tubing and the surface discharge pressure, all converted to feet of head.

For example, a well has a pumping fluid level at a depth of 4,000 ft (the actual depth of the pump below 4,000 ft does not contribute), flows into a separator with a pressure of 50 psi and has a frictional pressure loss of 100 psi (as determined by flowrate and the length of tubing from the pump to the surface). The fluid being pumped has a specific gravity of 0.85 (0.37 psi/ft). This generates a head requirement by the pump of 3,418 ft plus (150 psi) \times (2.31), or 3,762 ft of head, water equivalent. Now, if the desired production rate for this installation were 37 gpm and the casing were 5½-in., Table A below would

Table A
Typical Example of Available Tables to Aid Pump Selection
This Table is for 4-in. Pumps, in 5½-in. or Larger Casing

Pump Capacity, GPM	11	16	27	34	48	61	69	80	100
Peak efficiency 60 Hz b/d	360	600	380	1,200	1,600	1,900	2,150	2,700	3,350
m ³ /d	57	95	140	191	254	302	342	429	533
50 Hz b/d	300	500	733	1,000	1,333	1,583	1,792	2,250	2,792
m ³ /d	48	79	117	159	212	252	285	358	444
Optimum range 60 Hz b/d	182 to 492	440 to 730	660 to 1,080	840 to 1,400	1,125 to 2,050	1,250 to 2,350	1,500 to 2,650	1,750 to 3,500	2,200 to 4,350
m ³ /d	30 to 78	70 to 116	105 to 172	134 to 223	178 to 326	199 to 374	238 to 421	278 to 556	350 to 692
60 Hz b/d	152 to 410	373 to 608	550 to 900	770 to 1,187	937 to 1,708	1,042 to 1,958	1,250 to 2,205	1,458 to 2,917	1,833 to 3,625
m ³ /d	25 to 65	59 to 97	87 to 143	111 to 185	149 to 272	185 to 312	199 to 351	232 to 464	291 to 578

Table B
Motor Specifications for 5½-in., 20-lb/ft and Larger Casing Sizes

Size, hp		Volts/amps		Length		Weight	
60Hz	50Hz	60Hz	50Hz	in.	m	lb	kg
60	50	735/51	612/51	202	5.13	840	381
60	50	840/44	700/44	202	5.13	840	381
60	50	945/40	787/40	202	5.13	840	381
60	50	1270/30	1058/30	202	5.13	840	381

indicate that a 34 gpm pump would be the appropriate choice since it has the highest efficiency for the desired production rate.

This choice then sends us to a typical performance chart such as Figure 6-148. The recommended operating range for this pump is shown as the shaded region. At 1,268 bpd (37 gal/min) the chart indicates this particular pump has a head capacity of 18.5 ft of head per stage, 0.26 brake horsepower per stage, and a pump efficiency of 68%. This indicates that 203 stages are needed in the 34 gal/min pump. The horsepower requirements are then given by the product of the horsepower per stage and the number of stages. In this example, 52.8 hp would be required. Next, a look at Table B indicates a 60-hp, 1,270-V, 30-A motor will accomplish the task.

STIMULATION AND REMEDIAL OPERATIONS

Reservoir stimulation deals with well productivity, and a successful stimulation treatment requires the accurate identification of the parameters controlling the well production. As a result, causes of impaired production must be identified. Furthermore, it must be determined whether or not a particular treatment can improve production. This is the very first step of the stimulation job design.

Darcy's law in its simplest form is adequate to study the issue. For oil, a familiar expression (for steady-state and in a radial reservoir) is written as

$$q = \frac{kh(p_e - p_{wf})}{141.2 B\mu(\ln r_e/r_w + s)} \tag{6-200}$$

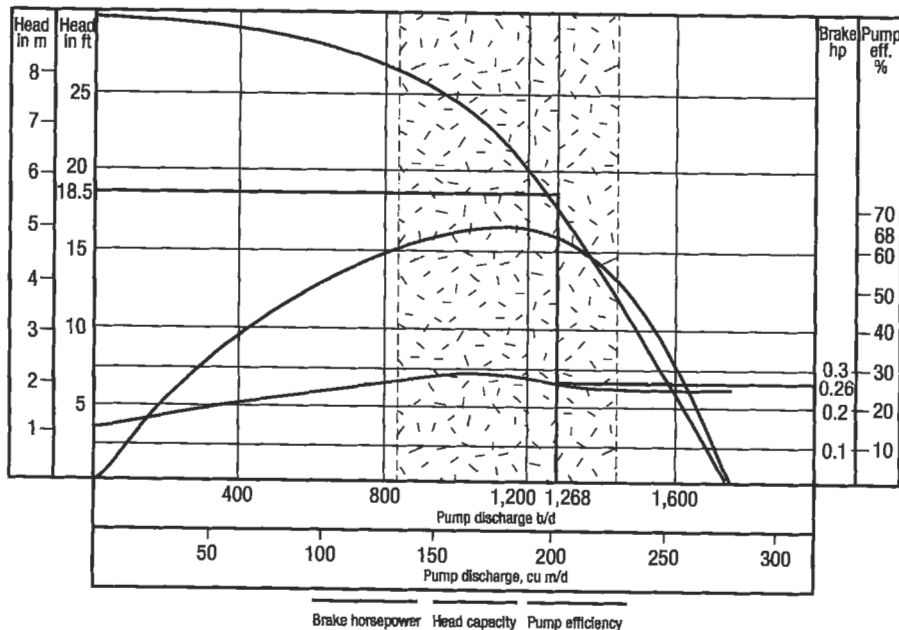


Figure 6-148. Typical performance curves for a 34-gpm, 4-in. pump in 5 1/2-in. casing, lifting water at 3,475 rpm. (From "ESP, the Electrical Submersible Pump" article, Part 4.)

where q = well flowrate (STB/d)
 k = reservoir permeability in md
 h = reservoir thickness in ft
 p_e = outer boundary reservoir pressure in psi
 p_{wf} = flowing bottomhole pressure in psi
 B = formation volume factor in resbbl/STB
 μ = fluid viscosity in cp
 r_e = equivalent drainage radius in ft
 r_w = well radius in ft
 s = skin effect

Each of the variables on the right-hand side of Equation 6-200 affects well productivity and certain actions may favorably change its impact. Of particular interest to the stimulation engineer are the permeability and the skin effect. Both of these variables may be obtained from a pretreatment pressure transient test. Ignorance of these two variables would result in an inappropriate or less than optimum stimulation treatment; in addition, a posttreatment analysis and job evaluation would be impossible.

As can be easily seen from Equation 6-200, a low value of the permeability (tight reservoir) or a high value of the skin effect (damaged or badly completed well) would result in low well productivity. There is virtually nothing practical that can be done to the permeability, although certain investigators have erroneously suggested that hydraulic fracturing increases the effective reservoir permeability. A hydraulic fracture is a superimposed structure on a reservoir which remains largely undisturbed outside of the fracture. The fracture, however, can greatly improve the well productivity by creating a large contact surface between the well and the reservoir. The production improvement results from effectively increasing the wellbore radius.

Matrix stimulation is generally intended to reduce a large skin effect resulting from permeability damage around the wellbore during completion or production. Often, there is confusion in distinguishing matrix acidizing (a form of matrix stimulation) from acid fracturing. The latter requires that the treatment is done at formation fracturing pressure and it relies on a residual *etched* width of the created fracture. The two methods of stimulation are applicable to entirely different types of formations: matrix acidizing is applied to high-permeability reservoirs whereas acid fracturing is appropriate for low-permeability, acid-soluble, reservoirs such as carbonates.

All stimulation practices adjust the skin effect, either by improving a negative component (fracturing) or by reducing a positive value caused by damage (matrix stimulation) [74].

Fracturing

Hydraulic fracturing of petroleum reservoirs is a reasonably new activity, spanning 40 years. The understanding of fracture propagation, its geometry, and direction is even newer, and additions to the body of knowledge of fracturing as a reservoir stimulation treatment is a very active process.

A classic concept introduced in 1957 [75] concluded that fractures are "approximately perpendicular to the axis of least stress." The stress field can be decomposed into three principal axes: a vertical and two horizontal which are unequal. For most reservoirs the minimum stress is horizontal, resulting in vertical hydraulic fractures.

Stress Distribution

In a sedimentary environment, the vertical stress σ_v is equal to the weight of the overburden and can be calculated from

$$\sigma_v = \frac{1}{144} \int_0^H \rho \, dH \quad (6-201)$$

where ρ = density of each layer in lb/ft³
 H = thickness of overburden in ft

Equation 6-201 can be evaluated using a density log. In its absence, a value of 1.1 psi/ft can be used as a reasonable approximation.

A porous medium, containing fluid, is subjected to an *effective* stress, rather than the absolute stress given by Equation 6-201. The effective stress σ' is related to the pore pressure p by

$$\sigma' = \sigma - \alpha p \quad (6-202)$$

where α is Biot's "poroelastic" constant and it varies from 0 to 1. For most petroleum reservoirs it is equal to 0.7. It is important that the concept of the effective stress is understood. An implication is that in a propped hydraulic fracture, the effective stress on the proppant is greatest during production ($p = p_{wf}$) and must be considered in the proppant selection.

While the absolute and effective overburden stress can be computed via Equations 6-202 and 6-203, the two principal horizontal stresses are more complicated and their determination requires either field or laboratory measurements.

In a tectonically inactive formation the elastic properties of the rock (Poisson ratio) may be used to relate the effective vertical stress with the effective minimum horizontal stress

$$\sigma'_{H,\min} = \frac{\nu}{1 - \nu} \sigma'_v \quad (6-203)$$

where ν = Poisson ratio.

For sandstone formations, the Poisson ratio is approximately equal to 0.25, leading to a value of $\sigma'_{H,\min}$ approximately equal to $\frac{1}{3}\sigma'_v$. For most shales the Poisson ratio is larger leading to abrupt changes in the horizontal stress profile. This variation, which can envelope a sandstone reservoir because of overlying and underlying shales, is the single most important reason for fracture height containment.

Vertical versus Horizontal Fractures

Consider Figure 6-149. Graphed are the three principal stresses, σ_v , $\sigma_{H,\min}$, $\sigma_{H,\max}$. The first is given by Equation 6-201, whereas $\sigma_{H,\min}$ can be extracted from Equation 6-203. The maximum horizontal stress $\sigma_{H,\max}$ can be considered as equal to $\sigma_{H,\min}$ plus some tectonic component σ_{tec} . If the original ground surface remains in place, then $\sigma_{H,\min}$ is less than σ_v , leading always to a vertical fracture which would be perpendicular to $\sigma_{H,\min}$. However, if the present ground surface

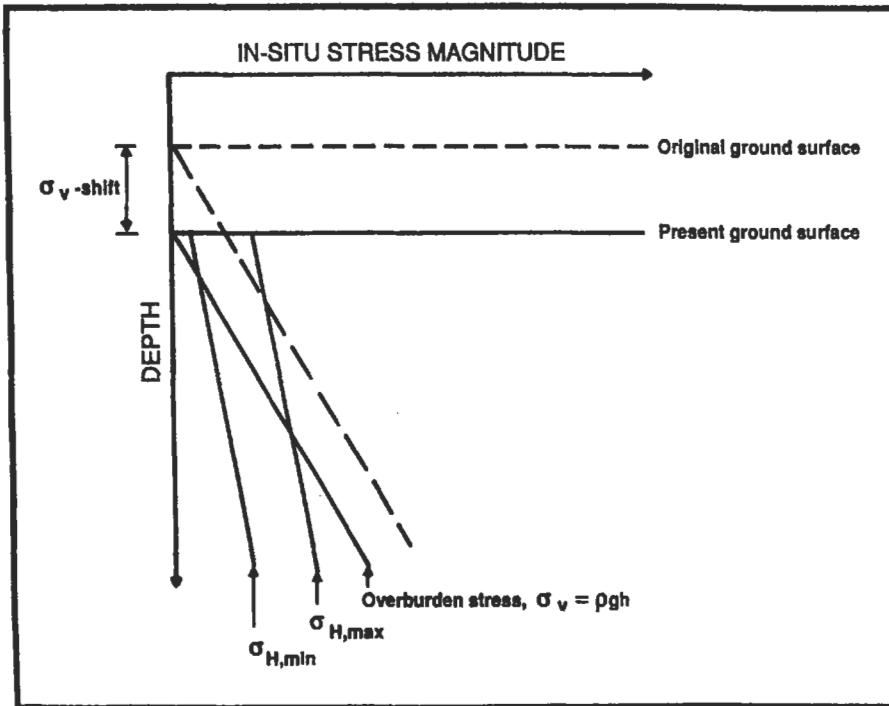


Figure 6-149. Stress profiles (vertical and two horizontal stresses). Glaciation and erosion reduced the overburden, enabling a critical depth above which horizontal fractures may be generated. Below, only vertical fractures, normal to the minimum horizontal stress, are generated.

has been the result of massive glaciation and erosion, as depicted in Figure 6-149, the overburden is reduced. Since the horizontal stresses are “locked” in place, there exists a critical depth, shallower of which the minimum horizontal stress is no longer the minimum stress. In such a case, a horizontal fracture will be created in the reservoir. This has been observed in a number of shallow reservoirs.

The definition of *principal* stress direction implies that all shear stresses vanish. Thus, when a vertical well is drilled, usually it coincides with a principal stress direction. This is not the case when a deviated or horizontal well is drilled (unless, in the latter case, the well is drilled in the direction of one of the principal horizontal stresses). However, for the mass of deviated wells that are drilled from platforms or drilling pads, their direction implies a nonvanishing shear stress [76]. The implications for fracturing are substantial. A deviated well requires a higher fracture initiation pressure. Furthermore, the production performance of a fractured deviated well is impaired. This point will be addressed in a later subsection.

Breakdown Pressure (Fracture Initiation Pressure)

The fracture initiation pressure is estimated via Terzaghi’s criterion [77] giving an upper bound for the value of the breakdown pressure p_b , such that

$$P_b = 3\sigma_{H,\min} - \sigma_{H,\max} + T_0 - p \quad (6-204)$$

where T_0 = tensile strength of the formation (psi)

Hence, hydraulic fracturing describes the tensile failure of the rock and Equation 6-204 can be used during a fracture calibration treatment to calculate the horizontal stress components.

Determination of Closure Pressure

Closure pressure is defined as the pressure when the fracture width becomes zero. In a homogeneous reservoir and where $\sigma_{H,\min}$ is the smallest stress, the closure pressure is approximately equal to this value. Nolte [78,79] pioneered the analysis of the pressure response during fracture calibration treatments and the calculation of important fracture variables.

The pressurization/repressurization cycles shown in Figure 6-150 can be refined and used in accordance with Nolte's analysis to calculate the closure pressure and, as will be shown in the next subsection, the leakoff coefficient and fracturing fluid efficiency. The closure pressure is not exactly the minimum horizontal stress. With very little fluid leakoff (i.e., not upsetting the pore pressure in Equation 6-202) and with a contained fracture height, the closure pressure is very near the minimum horizontal stress. Otherwise, the closure pressure is a bulk variable taking into account fluid leakoff and especially horizontal stress heterogeneities along the fracture area. If the injected fluid is minimized, then with both leakoff and fracture height migration also minimized, the closure pressure is approximately equal to the effective minimum horizontal stress.

The pump-in/flowback test, which can be done as the first peak in Figure 6-150 has been devised to allow for the estimation of the closure pressure. The test,

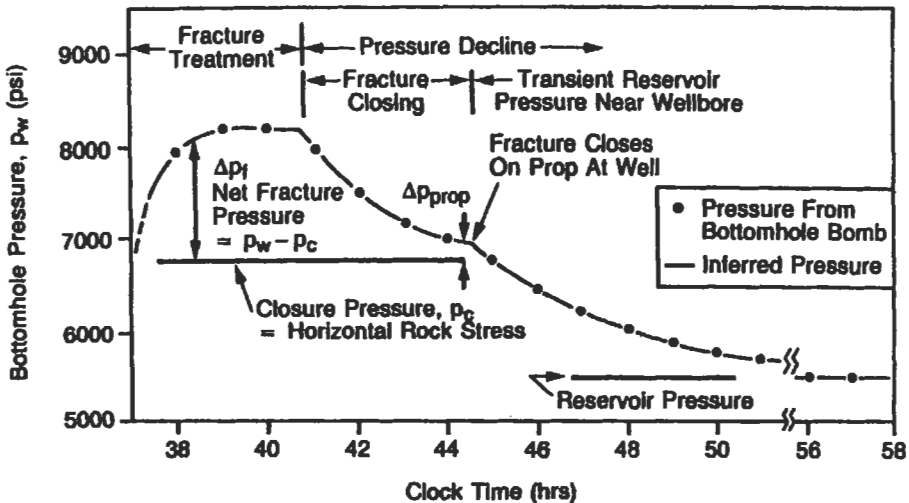


Figure 6-150. Expected pressure response during a hydraulic fracture treatment [79].

involves injecting fluid, normally treated water, at rates (e.g., 5 to 10 bpm) and volumes (e.g., 30 to 50 bbl) sufficient to create a fracture.

Of particular importance is the flowback period. This must be done at rates between $\frac{1}{3}$ and $\frac{1}{4}$ of the injection rate. The flowback rate must be held constant via a regulating valve exactly to prevent any flowrate transients to mask the pressure response. During this flowback period the interpretation is qualitative, and is based on a deduction of the ongoing closure process and should have two distinctly different periods:

- while the fracture is closing
- after the fracture is closed

The pressure profile would then have two regions reflecting the two different phenomena. These two regions would be separated by a clear change in slope, and the pressure corresponding to this inflection point is the fracture closure pressure.

Fracturing Pressure Decline Analysis

Castillo [80] extended Nolte's techniques for pressure decline analysis. He introduced a time function $G(\Delta t_D)$ which, graphed against pressure during the closing period of the fracture calibration treatment, forms a straight line.

Figure 6-151 is a graphical depiction after Castillo [80]. First, the necessity of an independent determination of the closure pressure (e.g., through a pump-in/flowback test) becomes obvious. The closure pressure would mark the *end* of the straight line, an important point of concern when dealing with real field data. Castillo's time function is given by

$$G(\Delta t_D) = \frac{16}{3\pi} [(1 + \Delta t_D)^{3/2} - \Delta t_D^{3/2} - 1] \quad (\text{upper bound}) \quad (6-205)$$

A second expression, for lower bound, is given in Reference 80. The dimensionless time Δt_D is simply the ratio of the closing time Δt and the injection time t_p .

The slope of the straight line in Figure 6-151 m_p , is

$$m_p = \frac{\pi C_L r_p \sqrt{t_p}}{2c_f} \quad (6-206)$$

where C_L = leakoff coefficient in ft/min^{1/2}

r_p = ratio of the leakoff height (h_p) to the fracture height (h_f)

t_p = pumping time in min

c_f = fracture compliance in ft/psi

The fracture compliance is model-dependent. For the Perkins and Kern (PKN) model is given by

$$c_f = \frac{\pi \beta h_f}{2E'} \quad (6-207)$$

where

$$\beta = \frac{2n' + 2}{2n' + 3 + a} \quad (6-208)$$

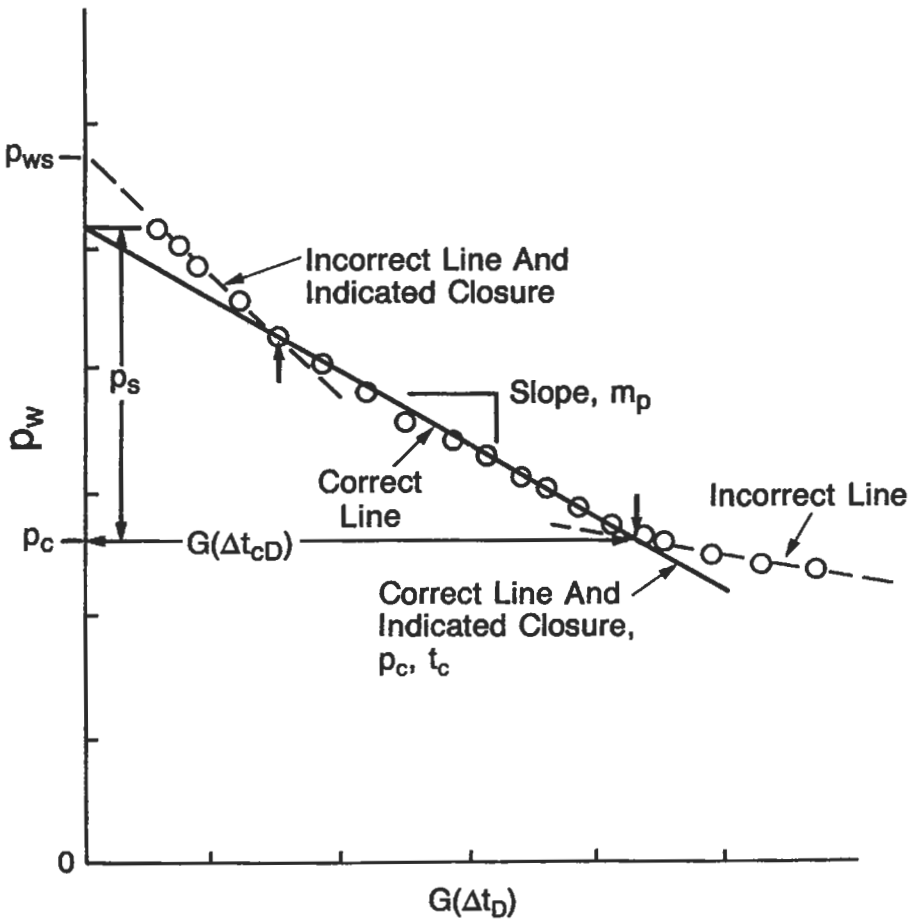


Figure 6-151. Pressure decline analysis [80].

and

$$E' = \frac{E}{1 - \nu^2} \tag{6-209}$$

(Fracturing models will be described later.)

In Equations 6-208 and 6-209,

n' = fluid power law exponent

a = viscosity degradation coefficient (0: linear degradation, 1: zero viscosity at the tip)

E = Young's modulus in psi

ν = Poisson ratio

Reference 79 contains all pertinent equations for fracturing pressure decline analysis.

Another important variable that can be extracted from pressure decline analysis is the fluid efficiency. The independently determined closure pressure not only identifies the end of the straight line in Figure 6-151 but also the fracture closure time, corresponding to Δt_{cD} . This dimensionless closure time can then be used with Figure 6-152 to estimate the fluid efficiency. This is a particularly important variable and allows the determination of the total fluid requirements and the ratio of "pad" volume to the proppant carrying fluid.

Recently Mayerhofer, Economides and Nolte [81,82] investigated the stress sensitivity of crosslinked polymer filtercakes in an effort to decouple the components of fracturing pressure decline. Fracturing fluid leakoff can be regarded as a linear flow from the fracture into the reservoir. Therefore, a new approach to analyze the pressure decline of a fracturing treatment is visualized.

The concept of individual pressure drops in series, constituting the overall pressure drop between the fracture and the reservoir, can be used and is given by

$$\Delta p_{total} = \Delta p_{cake} + \Delta p_{fz} + \Delta p_{res} \tag{6-210}$$

where Δp_{cake} = pressure drop across the filtercake
 Δp_{fz} = pressure drop within the polymer invaded zone
 Δp_{res} = pressure drop in the reservoir

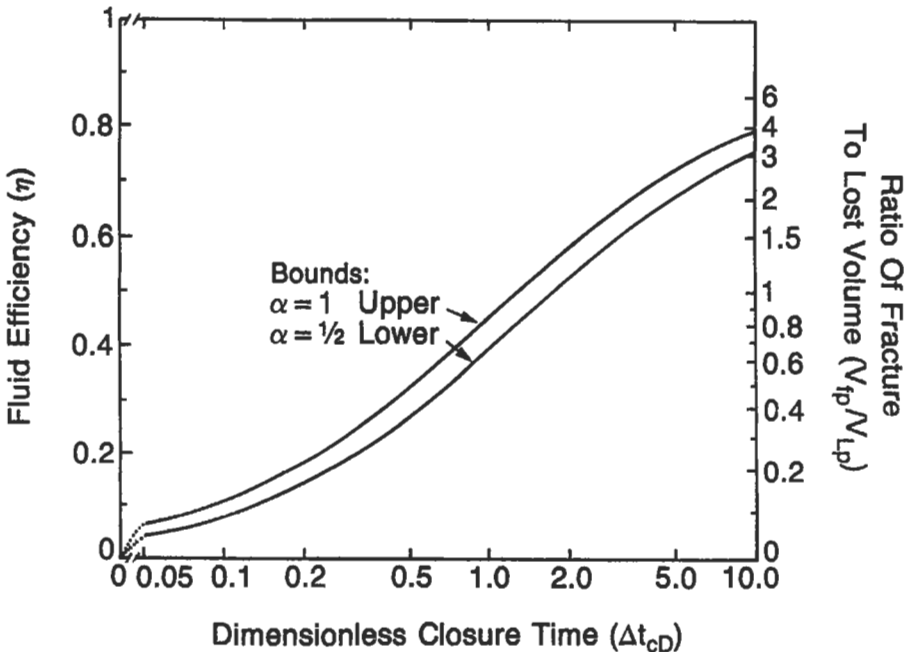


Figure 6-152. Fracturing fluid efficiency correlation. The dimensionless closure time Δt_{cD} is the ratio of the closure time to the pumping time [79].

Figure 6-153 is a conceptual diagram of the individual zones and the corresponding pressure drops.

The effects of stress-sensitive filtercake leakoff were described by the hydraulic filtercake resistance, which is defined (with Darcy's law) as [81-83]

$$R = \frac{l_c}{k_c} = \frac{\Delta p_{\text{cake}} A}{\mu q} \quad (6-211)$$

The dimensionless resistance was also introduced:

$$R_D = \frac{\Delta p q_{\text{ref}}}{q \Delta p_{\text{ref}}} \quad (6-212)$$

which is a rate-normalized pressure at any time with respect to a reference value.

It was found [81,82] that polymer filtercakes behave as viscoelastic bodies. The Kelvin or Voight model, which is a mechanical analog commonly used in linear viscoelastic theory, was found to be an appropriate model for analyzing the relation between differential pressure across the filtercake and the dimensionless resistance:

$$R_D(t) = \frac{1}{\mu} \int_0^t \sigma(t - \tau) e^{-\tau/\lambda} d\tau \quad (6-213)$$

where $\sigma(t - \tau)$ = change of the differential pressure
 λ = retardation time
 μ = viscosity

The viscoelastic filtercake relaxation, which was described by Equation 6-213, and the additional cake increase are the essential features during closure [81,82].

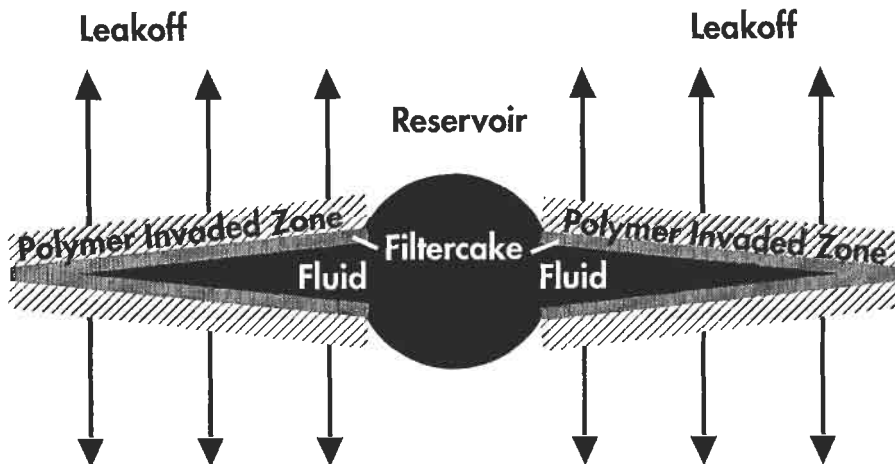


Figure 6-153. Hydraulic fracture with filtercake and invaded zone.

Figure 6-154 shows in a plot of R_D vs. Δp the dominance of the stress-sensitive relaxation of the filtercake deposited and compressed during pumping over the additional cake increase.

The stress-sensitive filtercake resistance is equivalent to a skin-effect and can therefore be incorporated as a component of the linear flow from the fracture into the reservoir.

Properties of Fracturing Fluids

The expected functions of the fracturing fluid are to initiate and propagate the fracture and to transport the proppant with minimum leakoff and minimum treating pressure.

Fluid viscosity is thus critical. An ideal fracturing fluid should have very low viscosity in the tubing (to avoid unnecessary friction pressure losses), and high viscosity within the fracture where a large value can provide bigger fracture width and transport the proppant more efficiently. However, what a high viscosity fracturing fluid does, inadvertently, is to plug the formation creating a highly unfavorable mobility. A mechanism to reduce the viscosity after the job to a very low value is then necessary. How are these, apparently contradictory, demands accomplished?

A typical, water-base, fracturing fluid consists of water and a thickening polymer such as hydroxypropyl guar (HPG). The polymer concentrations could vary from 20 to 80 lb/1,000 gal depending on the required viscosity.

Such polymer solutions produce viscous fluids at ambient temperatures. At reservoir conditions these solutions thin substantially. Hence, organometallic

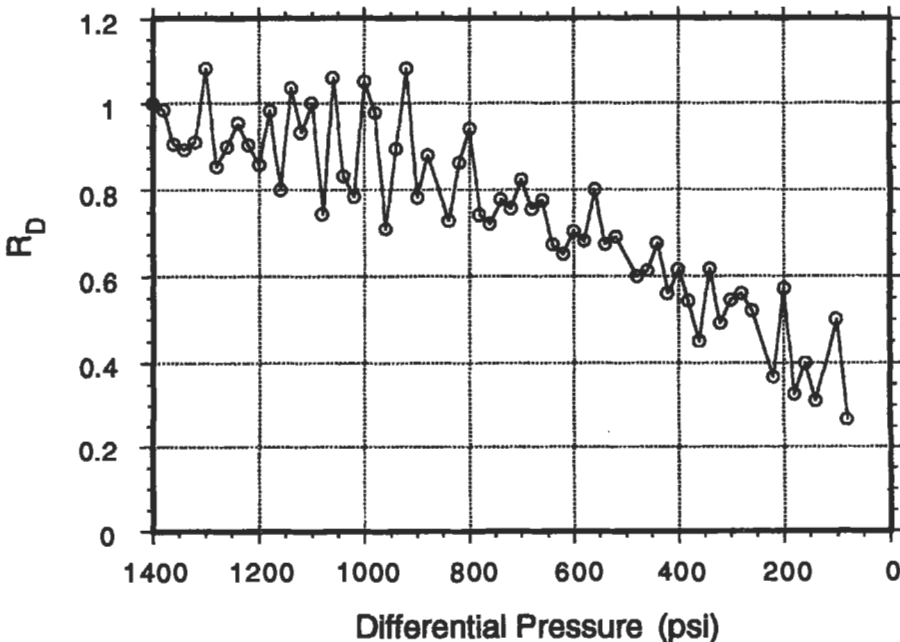


Figure 6-154. Stress-sensitive dimensionless resistance [81].

crosslinkers (some of them "delayed" to reduce tubing friction pressure) have been used resulting in substantial viscosity increases. For low to moderate temperature applications (<250°F) borates have been found effective. For higher temperatures (up to 350°F) titanate- and zirconate-delayed-crosslinked complexes have produced excellent fracturing fluids.

In addition to water-base fluids, there are other types of fracturing fluids. Oil-base fluids were the first fluids to be used. They can be thickened via an "associative" mechanism using an aluminium-phosphate ester polymer chain. However, oil-base fluids are expensive to use and dangerous to handle. Hence, they are applied to formations that are particularly water sensitive. Multiphase fluids such as emulsions (oil and water) and foams (gas and water) have been used widely.

The most common emulsion is composed of 67% hydrocarbon (internal) phase and 33% water (external) viscosified phase. Emulsions are very viscous fluids, providing good proppant transport, but result in high friction pressures and high fluid costs. They also thin significantly and thus they cannot be used in hot wells.

Foams (gas, water and a surfactant to stabilize the mixture) are particularly popular as fracturing fluids because the contained gas provides a very rapid "cleanup" following the treatment. However, fracture face damage and speed of cleanup must be balanced with the expected fracture performance which is affected to a much greater degree by the quality of the proppant pack.

Figure 6-155 from Reference 84 is a recommended fracturing fluid selection guide, representing several thousand treatments, done during the past few years. This guide covers most ranges of temperature, pressure and rock sensitivity in both gas and oil wells.

For all fracturing fluids, the injected polymer chains need to be broken after the treatment. Breakers, such as oxidative compounds (e.g., peroxydisulfates) or enzymes (e.g., hemicellulose) are used to reduce the length of the polymer chains and their molecular weight. The viscosity of the fluid is reduced and cleanup is accomplished.

Unfortunately, as can be expected, not all chains are broken or cleaned up. Certain polymers are more resistant than others, leading to only partial decomposition and bridging of polymer residue within the proppant pack. This phenomenon, if uncontrolled, can lead to a substantial proppant pack permeability damage with devastating effects on the fractured well performance.

The effects of the type of breaker, its quantity and the mode of application are shown in Figure 6-156. Encapsulated, effective, breakers are desirable because they become active when the fracturing treatment is over. Early action is detrimental since it degrades the needed viscosity. No action is particularly problematic because it may lead to permanent proppant-pack permeability impairment. Thus, appropriate amounts of encapsulated breakers is the most desirable method for fracturing applications [85].

Proppants

During the execution of the fracture treatment, the imposed hydraulic pressure holds the fracture open. However, when the pumping stops, it is up to the injected particulates to hold the fracture propped. The propped fracture width and, thus, the amount of proppant required will be addressed in the design subsection. However, two other variables are important in the determination of the proppant pack permeability: the proppant strength and the grain size. For a given stress under which the proppant pack will be subjected, the maximum value of the fracture permeability can be estimated. Bauxite, a high strength

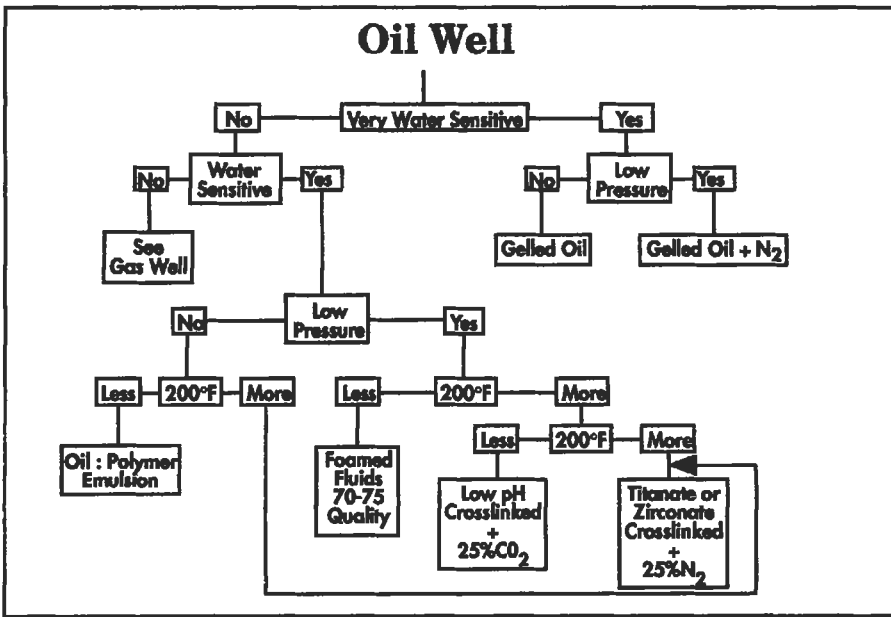
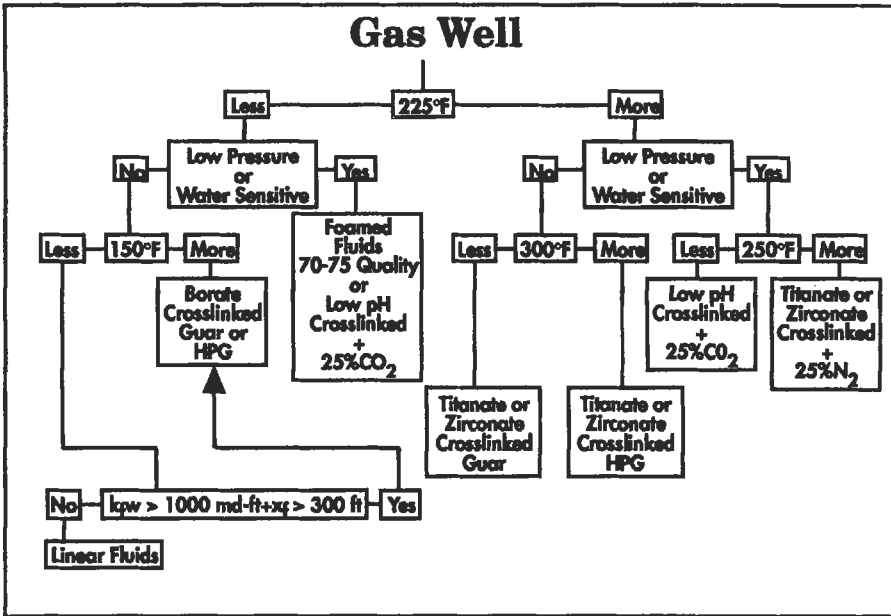


Figure 6-155. Fracturing fluid selection guide [84].

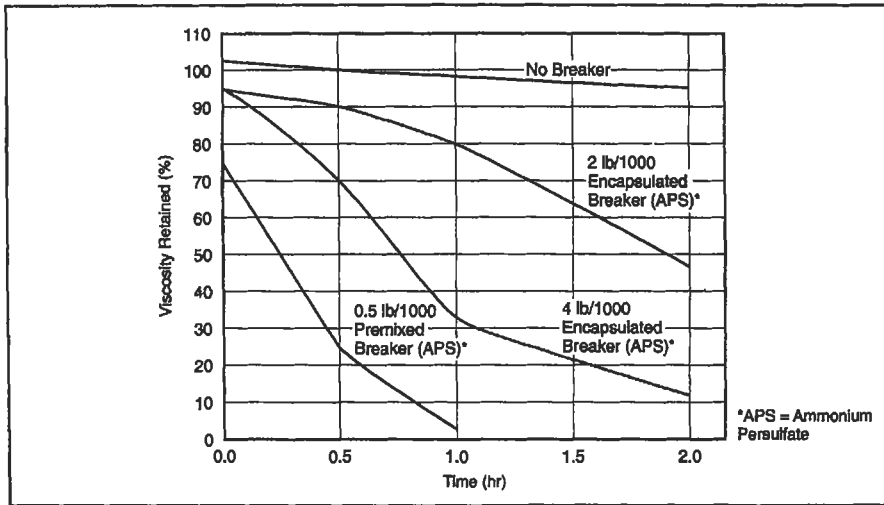


Figure 6-156. Viscosity degradation of fracturing fluids with and without encapsulated breakers [85].

proppant, and ISP (Intermediate Strength Proppant, a synthetic material) maintain a large portion of their permeability at high stresses. Sand, however, experiences more than an order of magnitude permeability reduction when the stress increases from 4,000 to 8,000 psi. This is important in the selection of a proppant because, while sands are less costly, they crumple readily and therefore higher-strength, but more costly, proppants are indicated at higher stresses.

Proppant size is also important. Larger grain sizes result in larger fracture permeability. However, larger sizes are more susceptible to crumpling as stresses increase and the relative reduction in the pack permeability is much larger in the larger-size proppants. Reference 86 contains a number of correlations for size and size distribution effects on proppant pack permeability.

These permeabilities are maximum values. As mentioned earlier, fracture permeability damage is caused by unbroken polymer residue which is by far the biggest culprit. Thus, while proppant strength and size selection can be done using formation strength criteria, damage due to fracturing fluid residue must be controlled. Otherwise, additional damage factors, as high as 80 to 90%, can be experienced after the stress-induced permeability impairment is accounted for.

Propped Fracture Design

The previous information was intended to serve as background information for propped fracture design. Meng and Brown [87] and Balen *et al.* [88] presented the concept and applications of the net present value (NPV) as a systematic approach to fracture design. Others have also outlined similar schemes. The complexity of the various design components and their interrelationships invariably require an economic criterion for meaningful comparisons of design options and fracture sizes.

Figure 6-157 contains the steps and components for optimizing fracture design. First, a fracture half-length x_f is selected. This is done incrementally, with each new fracture half-length longer than the previous, e.g., by 100 ft.

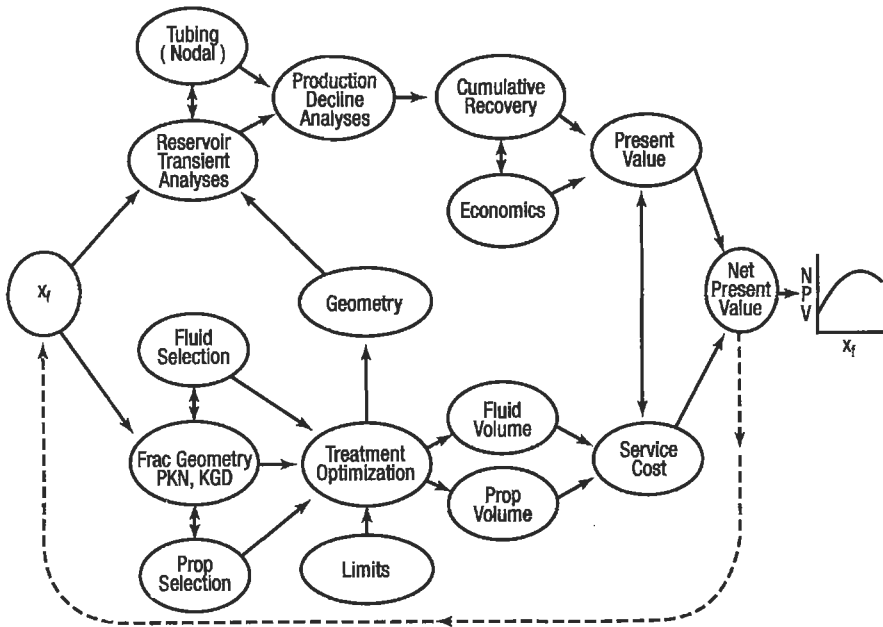


Figure 6-157. The components of the fracture net present value (NPV) calculation [87].

At first, let's follow the lower branch on Figure 6-157. For a given formation, the lithology, temperature and reservoir fluids would dictate the choice of the fracturing fluid while the state of stress and the desired fractured performance would point towards the proppant selection. A fracture propagation simulator may then describe the fracture geometry. There are several types of simulators including fully 3-D, planar 3-D, pseudo-3-D (coupled 3-D fracture and 2-D fluid flow) and the classic, analytical 2-D models. The latter include the PKN model (Perkins and Kern [89]; Nordgren, [90]) and the KGD model (Khristianovich and Zheltov [91]; Geertsma and de Klerk [92]).

The higher the complexity of the simulation the higher the demand for appropriate data and the longer the simulation time. For the purpose of this exercise, the elegant, analytical PKN and KGD models will be used. A depiction of the PKN geometry is given in Figure 6-158. For this simulation two limits are necessary: the fracture height, h_p and the maximum allowable or available treating pressure.

Thus the fracture geometry can be determined and, with the imposed limits, a treatment optimization may be done. The average width of a fracture of half-length x_f can be obtained from

$$\bar{w} = 0.3 \left[\frac{q_i \mu (1 - \nu) x_f}{G} \right]^{1/4} \left(\frac{\pi}{4} \gamma \right) \tag{6-214}$$

- where q_i = injection rate in bpm
- μ = fracturing fluid viscosity in cp
- G = elastic shear modulus in psi
- γ = geometric factor = 0.75

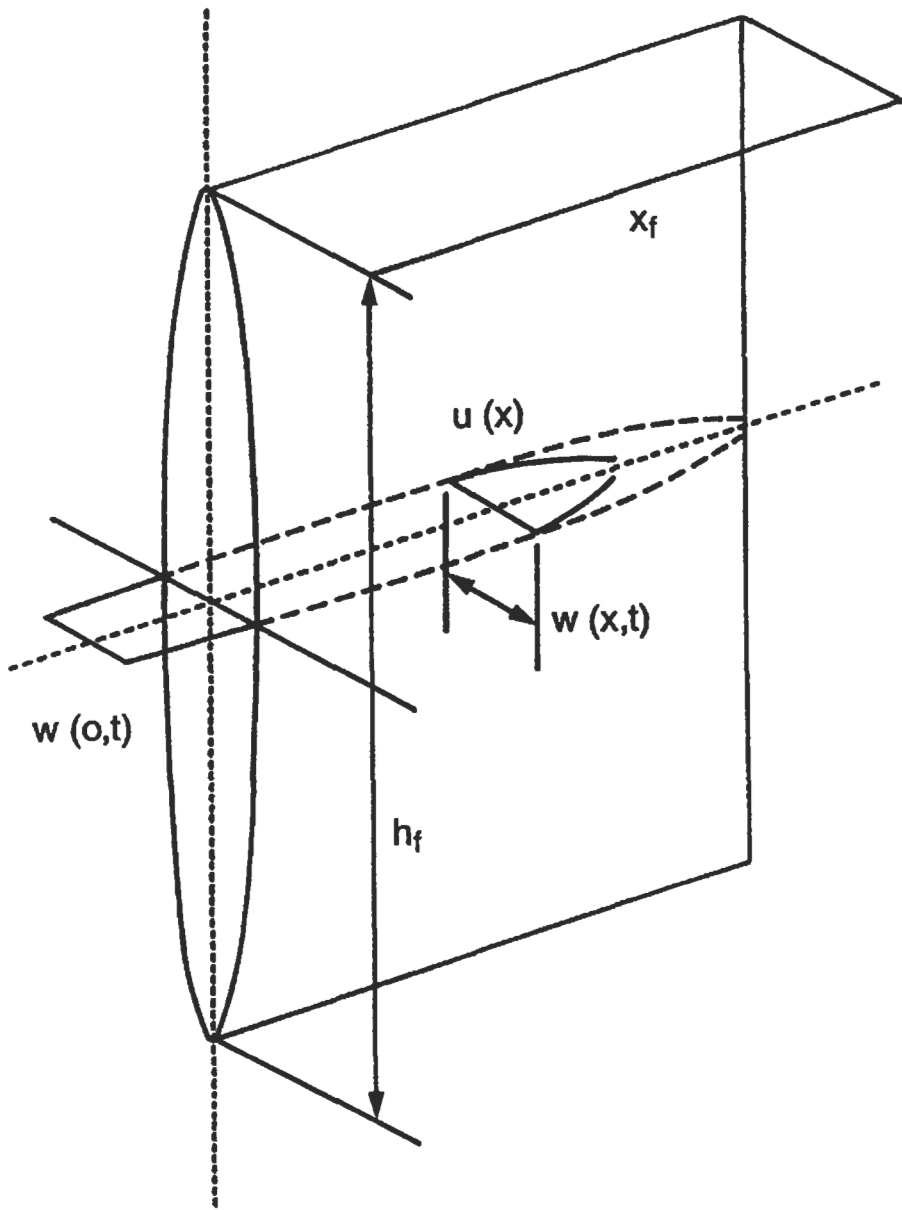


Figure 6-158. The geometry of the Perkins and Kern [89] and Nordgren [90] model (PKN).

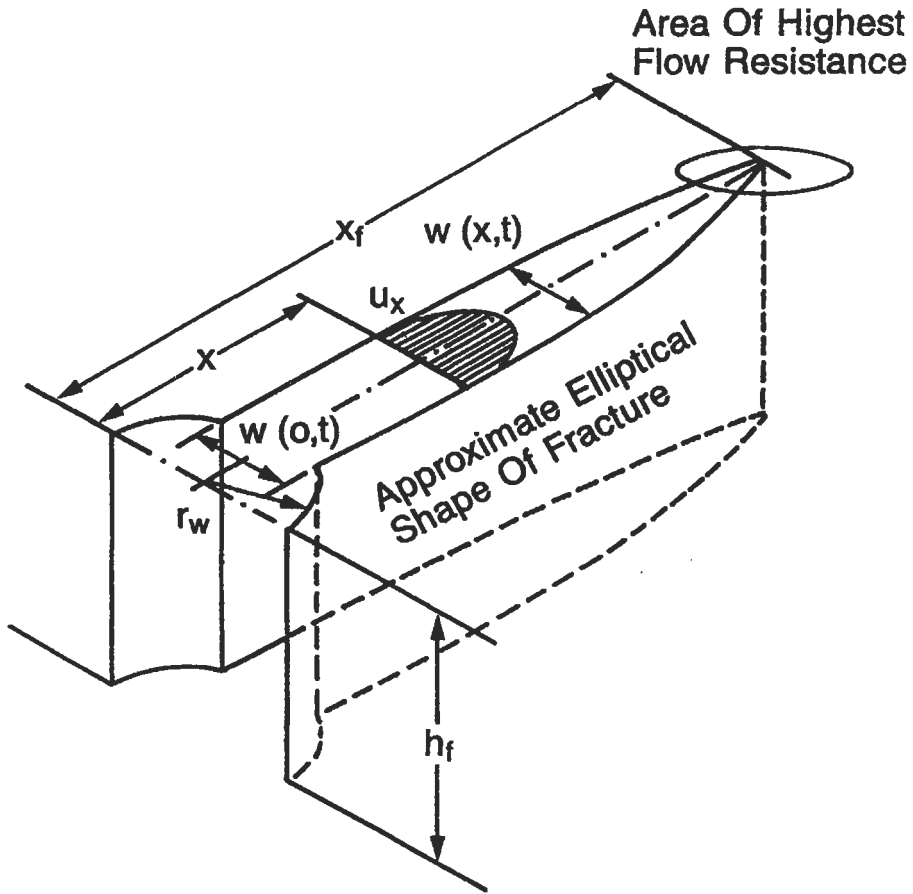


Figure 6-159. The geometry of the Khristianovich and Zheltov [91] and Geertsma and de Klerk [92] model (KGD).

The bracketed expression on the right hand side of Equation 6-215 gives the maximum width value (at the wellbore), whereas the multiplier in the parentheses provides a geometrically averaged width.

For the KGD model, depicted in Figure 6-159, the analogous expression is

$$\bar{w} = 0.29 \left[\frac{q_i \mu (1 - \nu) x_f^2}{G h_r} \right]^{1/4} \left(\frac{\pi}{4} \right) \quad (6-215)$$

In both Equations 6-215 and 6-216, the relationship between viscosity or injection rate and the fracture width is quarter root, indicating that to double the width a 16-fold increase in either of these two variables is needed.

The calculation of fracture width, the assumed fracture height and half-length and the fluid leakoff lead towards a simple material balance.

$$q_1 t_i = \frac{\bar{w} A_f}{2} + \frac{(K_L C_L A_f r_p) \sqrt{t_i}}{2} \quad (6-216)$$

where the left-hand side is equal to the fluid volume injected, the first term on the right-hand side is the volume of the fracture created and the second term represents the fluid leakoff. The latter is a square root of time relationship.

The area A_f is total fracture area and is equal to $4x_f h_f$. All other variables in Equation 6-216 have been described earlier except K_L , which is a multiplier to the leakoff coefficient and is applicable during pumping. Nolte [78] has shown that

$$K_L = \frac{8}{3} \eta + \pi(1 - \eta) \quad (6-217)$$

where η = fluid efficiency

is a good approximation.

Equation 6-216 is a quadratic relationship for the square root of the injection time t_i , and can be solved readily. Thus the product $q_1 t_i$ can be calculated, representing the total amount of fluid V_i required to generate a fracture of the calculated geometric and leakoff features.

The pad volume has been related to the total volume injected, V_p , in Reference 79, such that

$$\text{Pad volume} = V_i \frac{(1 - \eta)}{(1 - \eta)} \quad (6-218)$$

The next item is to calculate the proppant volume and its injection schedule. The latter is given by

$$c_p(t) = c_f \left(\frac{t - t_{\text{pad}}}{t_i - t_{\text{pad}}} \right) \quad (6-219)$$

where $c_p(t)$ = slurry concentration (lb/gal added) as a function of time
 c_f = desired slurry concentration at the end of the job (lb/gal absolute)
 t_{pad} = time for pad injection

The continuous proppant addition described by Equation 6-219 (and shown schematically in Figure 6-160, opposed to the classic "stairstep" proppant addition) from t_{pad} to t_i can provide the total amount of proppant injected. This amount, divided by the fracture area, can provide the proppant concentration within the fracture C_p given in lb/ft³. The propped width may then be calculated from

$$w = \frac{12C_p}{(1 - \phi_p) \rho_p} \quad (6-220)$$

where ϕ_p = proppant pack porosity in fraction
 ρ_p = proppant density in lb/ft³

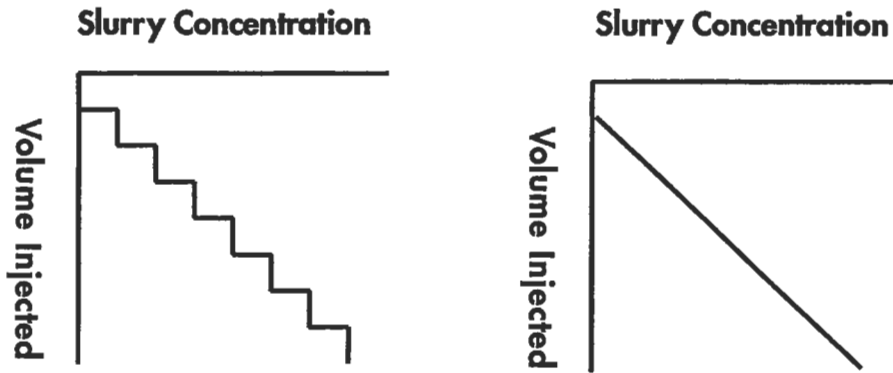


Figure 6-160. Continuous vs. "stairstep" proppant addition. The continuous pressure addition is superior and is described by Equation 6-219.

Finally, the net fracturing pressure to generate a half length equal to x_f may be calculated for the PKN model and (for a Newtonian fluid)

$$\Delta p_f = 0.0254 \left[\frac{G^3 q_i \mu x_f}{(1 - \nu)^3 h_f^4} \right]^{1/4} \quad (6-221)$$

and for the KGD model

$$\Delta p_f = 0.050 \left[\frac{G^3 q_i \mu}{(1 - \nu)^3 h_f x_f^2} \right]^{1/4} \quad (6-222)$$

The treatment pressure is then simply

$$p_f = \sigma_{H,\min} + \Delta p_f \quad (6-223)$$

Equations 6-221 and 6-222 show the classic pressure patterns which may reveal during execution the type of fracture that is generated. For the PKN model and for a constant fracture height (Equation 6-221) there is an increasing pressure profile for increasing fracture length, whereas for the KGD model (Equation 6-222) there is a decreasing pressure profile for a propagating fracture.

Assuming also that the treating pressure must be kept below a certain level to avoid migration, then a PKN-type fracture can be propagated at constant net pressure. This can be accomplished by decreasing the fluid viscosity or the injection rate as can be concluded from Equation 6-221. Given the choice, treatment optimization has shown that reduction in viscosity is more desirable than a reduction in injection rate.

The calculation of the fluid volume (Equation 6-215) and proppant mass requirements (Equation 6-219) injection rates and treatment pressures (Equation 6-223) lead to the calculation of the cost to create the fracture.

The second branch in Figure 6-157 may now be addressed. The calculated propped fracture width w (Equation 6-220), the fracture half-length x_f , the

proppant pack permeability (stress- and damage-adjusted proppant) k_f , and the known reservoir permeability lead to the dimensionless fracture conductivity

$$F_{CD} = \frac{k_f w}{k x_f} \quad (6-224)$$

Cinco-Ley *et al.* [93] presented the solution for the performance of finite-conductivity fractures. Their type curves are in the standard form of a log-log graph of dimensionless pressure p_D against dimensionless time t_{Drf} for a range F_{CD} s. Hence, any real time corresponds to a dimensionless time, and the dimensionless pressure value is related to the real flowrate and real pressure drop. Thus, the expected performance can be calculated. No-flow boundary conditions for various reservoir geometries have been given in Reference 87. The flowrate decline curve can then be coupled with the tubing performance resulting in wellhead rates.

It is a very easy step to integrate these rates into the cumulative production. The incremental cumulative production (above the one the unstimulated well could deliver) multiplied by the unit price of the hydrocarbons (oil or gas) and discounted to time zero is the present value of the incremental revenue.

If the cost to perform the job, calculated from the first branch in Figure 6-157, is subtracted from the present value of the incremental revenue, it results in the net present value NPV.

A plot of the construction is given in Figure 6-161. The fracture half-length is graphed against the NPV. Optimum fracture design corresponds to the maximum NPV. Two case studies are graphed: Case A, which provides a positive

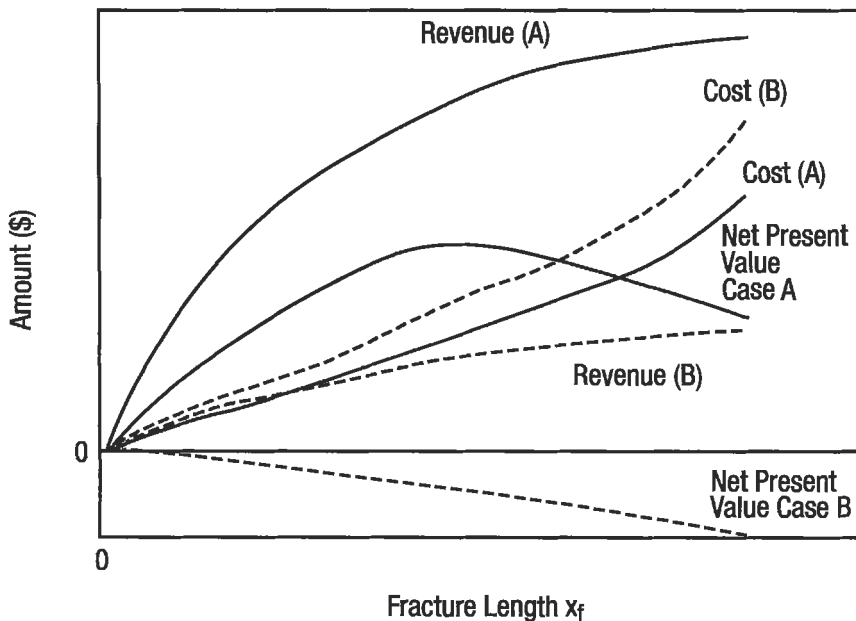


Figure 6-161. Case studies of the NPV design procedure. Case A is positive, Case B is negative.

NPV, and Case B, in which the incremental revenue does not recover the stimulation cost. In this case hydraulic fracturing should not be done.

Potentially, one of the most powerful applications of the NPV approach is to perform parametric studies. If a variable (e.g., permeability or slurry concentration) is not known or determined, then a sensitivity analysis can be done to assess the impact of its variation on the optimum design. Large spread in the maximum NPV could be considered as the "cost of ignorance". In that case, measurement of the unknown variable via some type of testing is warranted. An example parametric study with the reservoir permeability is shown in Figure 6-162.

Fracture Propagation Modeling

Common to all descriptions of fracture propagation are (a) a material balance equation relating volume change to flow across the boundaries, (b) an elasticity relationship between fracture aperture and net pressure, (c) a fluid-flow equation relating the flowrate with the pressure gradient in the fracture and (d) a tip propagation criterion.

Width Equations. The theory of linear elasticity provides solutions to idealized problems. One of them, the pressurized crack problem, deals with a crack (a straight line) of length $2b$ which is in an infinite plain. The stress σ , acting far from the crack and normal to its direction is compressive, trying to close it. On the other hand a pressure p is acting against the stress, trying to open the crack from the inside. If the net pressure, $\Delta p = p - \sigma$, is positive, the crack will be open and its shape will be elliptic. The maximum width is given by

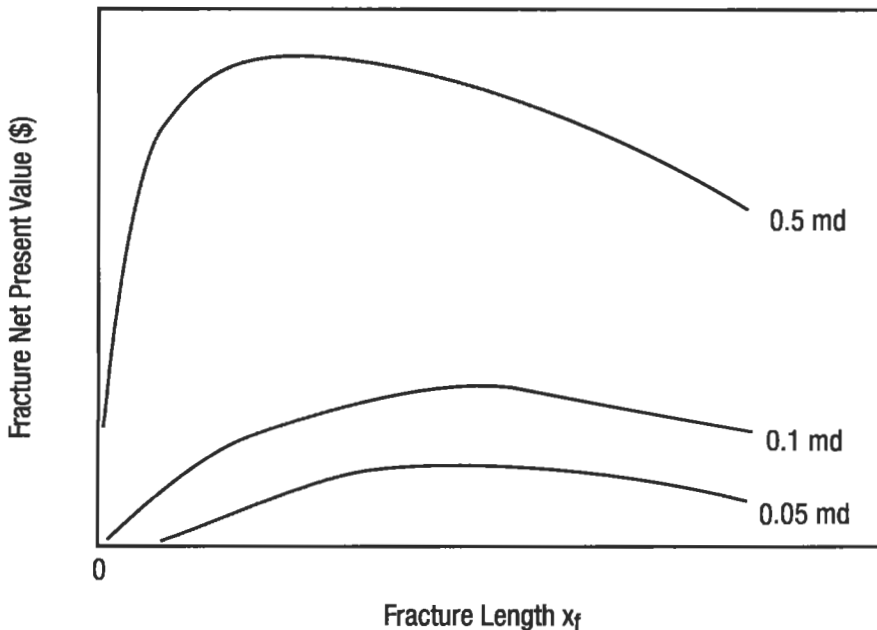


Figure 6-162. NPV fracture design parametric study of reservoir permeability.

$$w_{\max} = \frac{(1-\nu)}{G} (2b)\Delta p \quad (6-225)$$

(The equations, unless otherwise stated, are written in a coherent system of units in this section.) Several models, originating from Perkins and Kern [89] figure the hydraulically induced fracture as a constant height channel obeying Equation 6-225 in every vertical cross-section, with $2b$ replaced by h_f . In such a channel of elliptical shape (with a width significantly less than the height) a Newtonian fluid having constant flowrate q is driven by the pressure drop

$$\frac{dp}{dx} = -\frac{64\mu q}{\pi w^3 h_f} \quad (6-226)$$

The elasticity relation (6-225) and the fluid-flow equation (6-226) are combined to establish a relation between width at the wellbore and fracture length. To obtain a closed form solution, the fluid leakoff is neglected at this stage of the model development. In addition, zero width (zero net pressure) is assumed at the tip. With these assumptions the created width profiles are similar and, hence, a constant multiplier can be used to transform the wellbore width into the average width.

Historically, the KGD model [91,92] preceded the PKN model. It is also based on the pressurized crack solution but applied in the horizontal direction. There are additional differences, e.g., the pressure drop equation is written for a channel with rectangular cross section and the existence of a nonwetted (non-pressurized) zone is assumed near the tip.

The two widely used width equations were presented earlier as Equations 6-214 and 6-215. The PKN equation has been considered as a suitable approximation for long fractures (compared to height), whereas the KGD has been suggested as more appropriate for fractures with significant height compared to length.

A width equation such as Equation 6-214 or 6-215 leaves only one degree of freedom for the geometry of the fracture. If we give (directly or indirectly) the fracture volume, the shape is determined. The additional information on the fracture volume is provided through the material balance.

Material Balance. Material balance suggests that the injected fluid either generates fracture volume or leaks off. In describing leakoff Carter [94] applied two important assumptions. In his formulation the following was presented:

$$\frac{V_L}{A_L} = 2C_L \sqrt{t} + S_p \quad (6-227)$$

where V_L = volume of the fluid leaked off
 A_L = area available for leakoff
 C_L = leakoff coefficient
 S_p = spurt loss coefficient

The first term represents decreasing intensity of the fluid leakoff with time elapsed, and the second term is an additional volume which is lost at the very moment of opening (the spurt loss). In addition, Carter assumed that *from the*

point of view of the material balance the fracture geometry can be well approximated by a constant rectangular cross-section, with the only dimension changing with time being the length. He wrote the material balance for a unit time interval in the form

$$q_i = 4 \int_0^t \frac{C_L}{\sqrt{t-\tau}} h_f \frac{dx_f}{d\tau} d\tau + 2h_f w \frac{dx_f}{d\tau} \quad (6-228)$$

where q_i = opening time

The solution of the above integral equation is

$$x_f(t) = \frac{q_i w}{8\pi h_f C_L^2} \left[\exp(\alpha^2) \operatorname{erf} c(\alpha) + \frac{2\alpha}{\sqrt{\pi}} - 1 \right] \quad (6-229)$$

where

$$\alpha = \frac{2C_L \sqrt{\pi t}}{w} \quad (6-230)$$

(Note that x_f is the length of one wing and q_i is the injection rate for two wings.) The complementary error function $\operatorname{erf} c(x)$ is available in the form of tables or computer algorithms.

If we want to apply the above equation, we have to decide how to estimate the constant width in this relation. It is the sum of the average width and the spurt width,

$$w = \bar{w} + 2S_p \quad (6-231)$$

where, strictly speaking, the averaging should be done not only in space but also in time.

The combination of Equation 6-229 with one of the width equations results in a system which is completely determined if either the length or the injection time is given. For the solution simple iterative methods can be applied.

The use of Equation 6-229 is somewhat complicated. The material balance would take a simple form if the volume leaked off could be determined. Unfortunately, it depends on the opening time *distribution* which, in turn, reflects the history of the fracture growth process. A simple version of the material balance is derived assuming some plausible bounds on the distribution of the opening time. Then the fluid lost during pumping (in the two wings,) $2V_L$ is bounded by [78]

$$\pi > \frac{2V_L}{2C_L x_f h_f \sqrt{t}} > \frac{8}{3} \quad (6-232)$$

The upper bound corresponds to low fluid efficiency and the lower bound to high fluid efficiency. At any medium efficiency we can use a linear interpolation between these two bounds. Therefore Equation 6-229 can be replaced by

$$x_f = \frac{(1 - \eta)q_i t}{\left[\frac{8}{3} \eta + \pi(1 - \eta) \right] 2h_f C_L \sqrt{t}} \quad (6-233)$$

where the fluid efficiency is computed from

$$\eta = \frac{2x_f h_f \bar{w}}{q_i t} \quad (6-234)$$

The combination of Equation 6-233 with one of the width equations is another short-cut two-dimensional model. Essentially the same concept was used in the design section (see Equations 6-216 and 6-217).

Detailed Models. Clearly, the short-cut two-dimensional models are based on several approximations, some of those being contradictory. For example, the geometric picture behind the Carter equation (and behind the upper and lower bounds) would require a fracture propagating with a constant width. The PKN or KGD width equations, on the other hand, give width changing in time as well.

Nordgren [90] presented a constant-height model in the form of a partial differential equation which contains coherent assumptions on the geometry. Kemp [95] showed the correct tip boundary condition for Nordgren's equation. Interestingly, the numerical solution does not differ much from the one of the short-cut PKN models. The main reason is that in both the detailed Nordgren model and in the short-cut PKN versions the fracture tip propagation rate is controlled by the linear velocity of the fluid at the tip. In other words, in these models there is no mechanism to hamper the opening of the fracture faces once the fluid arrives there. This later statement is valid also for the different KGD variations.

Appearance of irregular pressure profiles and posttreatment observation of fracture height growth initiated a departure from the ideal geometry assumptions. This generated additional-dimension models and prompted the introduction of improved calculation procedures. The two most important concepts are the vertical distribution of the (minimum-horizontal) stress and the fracture toughness.

Most of the researchers agree that stress distribution is the major factor controlling the height growth of hydraulically induced fractures (see Reference 96). Building this concept into a three-dimensional (3-D) or pseudo-three-dimensional (P-3-D) model, a more realistic fracture shape can be computed. The fracture is contained in the pay layer if the minimum principal stress is significantly higher in the neighboring layers. On the other hand, if the stress in the neighboring layers is only moderately higher than in the pay layer, then a limited height growth is predicted. The 3-D and P-3-D models differ in how detailed the computation of the height is and to what degree it is coupled with the fluid flow equation (see Reference 97). While the significance of the vertical distribution of the stress is well understood, the usefulness of this concept is somewhat limited by the fact that the necessary data are often lacking. (In fact, even the value of the minimum horizontal stress in the pay layer might be uncertain within a range of several hundred psi.)

There is less consensus in the usefulness of the concept of fracture toughness. This material property is defined as the critical value of the stress intensity factor necessary to initiate the rupture. The stress intensity factor is a quantity having the dimension pressure (i.e., stress) multiplied by the square root of

length. Its value increases with both the net pressure and the size of the fracture. Several investigators have arrived at the conclusion that within the physically realistic range of the fracture toughness its influence on fracture propagation is not significant.

In certain cases net treating pressures observed during hydraulic fracturing are several times greater than predicted by simple two-dimensional propagation models [98]. The attempts to explain these “abnormally high pressures” based on (artificially increased) fracture toughness were not convincing. Other investigations have suggested different modifications of the fracture geometry, essentially stating that the elasticity relation can be disregarded at least in some part of the fracture. A more promising approach to understand and describe the phenomena is based on a fracture propagation criterion derived from *continuum damage mechanics* (CDM). According to CDM, under stress the material structure may begin to disintegrate. Small cracks may form and such deterioration weakens the material and lowers its load carrying capacity. The deterioration is characterized by the quantifiable damage variable. The time needed for damage evolution is incorporated into the so-called Kachanov law of damage growth. Starting from the rupture criterion of continuum damage mechanics and applying some simplifying assumptions on the stress distribution ahead of a moving crack, the following equation has been derived [99]:

$$u = \frac{C_K \bar{l}^2}{\sigma_{H,\min}} \frac{x_f \Delta p_L^2}{(\bar{l} + x_f)^2} \tag{6-235}$$

- where u = tip propagation rate
- C_K = Kachanov parameter
- \bar{l} = scale parameter (or “average distance of microcracks”)
- $\sigma_{H,\min}$ = minimum horizontal principal stress
- x_f = fracture length
- Δp_L = net pressure at tip

Note that the net pressure (and hence, the width) at the tip is not zero in this model. There are two parameters in the above expression, C_K and \bar{l} . A small value of the Kachanov parameter and/or the average distance of the microcracks leads to retarded fracture propagation with treating pressures several times larger than usual. Applying the above equation as a boundary condition, a modified version of the Nordgren equation can be introduced. The solution of the resulting CDM-PKN model [99] is presented using dimensionless variables:

$$x_f = c_1 x_{fD}, \quad t = c_2 t_D, \quad w_0 = c_3 w_{0D}, \quad \Delta p = c_4 w_D \tag{6-236}$$

- where x_f = length in ft
- t = injection time in min
- w_0 = maximum width at wellbore in in.
- Δp = net treating pressure in psi

The constants c_1 to c_4 are given by

$$\frac{c_1}{\text{ft}} = 1.178 \times 10^{-2} \left[\frac{(1 - \nu)\mu(q_i/2)^5}{C_L^2 G h_f} \right]^{1/3}$$

$$\frac{c_2}{\text{min}} = 1.758 \times 10^{-5} \left[\frac{(1-\nu)\mu(q_i/2)^2}{C_L^2 h_f G} \right]^{2/3}$$

$$\frac{c_3}{\text{in.}} = 0.1282 \left[\frac{(1-\nu)\mu(q_i/2)^2}{C_L^2 G h_f} \right]^{1/3}$$

$$\frac{c_4}{\text{psi}} = 1.068 \times 10^{-2} \left[\frac{G^2 \mu (q_i/2)^2}{C_L^2 (1-\nu)^2 h_f^4} \right]^{1/3} \quad (6-237)$$

where the variables and dimensions were defined in Equation 6-214. When designing a fracture treatment we can assume that $l_D \ll x_{TD}$. Then the combined parameter $C_{KD} \bar{l}_D^2$ is sufficient to describe the retardation effect. It can be calculated from the formula

$$C_{KD} \bar{l}_D^2 = 60 \frac{c_2 c_4^2}{c_1^2 \sigma_{H,\text{min}}} C_K \bar{l}^2 \quad (6-238)$$

where the units are the same as in Equation 6-237. In a study [100] of published case studies it was found that if damage dominates the combined parameter, then $C_K \bar{l}^2$ is in the range 0.003 to 0.05 ft²/psi•s. The smaller the combined parameter, the larger the deviations in both net pressure and fracture geometry compared to the corresponding PKN values. As a result of the slowdown of the tip propagation where the length is smaller, the width, net pressure and the fluid efficiency are larger than the corresponding values computed from the traditional models at the same amount of injected fluid. Figures 6-163 to 6-165 show the dimensionless fracture length, fluid efficiency and dimensionless width (or net pressure) at the wellbore as a function of dimensionless time. When the combined parameter is known, these figures can be used to obtain the main characteristics (length, fluid efficiency, net pressure) for any injection time.

Evaluation of Fracture Design

Successful stimulation is when the optimum design treatment is performed and the posttreatment flowrate coincides with the one forecasted. Figure 6-166 shows a posttreatment well performance showing a good agreement with the predicted flowrate from the designed fracture length. If the two deviate and especially if posttreatment performance is far below expectations, then an evaluation procedure should be implemented.

Primarily, two items should be examined:

- Fracture height migration. This can be done via a posttreatment temperature or radioactive log.
- Fracture permeability reduction—which could be the result of proppant pack damage or a choke (overdisplacement or other reasons that reduce the contact between well and fracture). Assessment of the geometric and conductivity characteristics of the fracture can be done via a posttreatment pressure transient test using the model outlined in Reference 93.

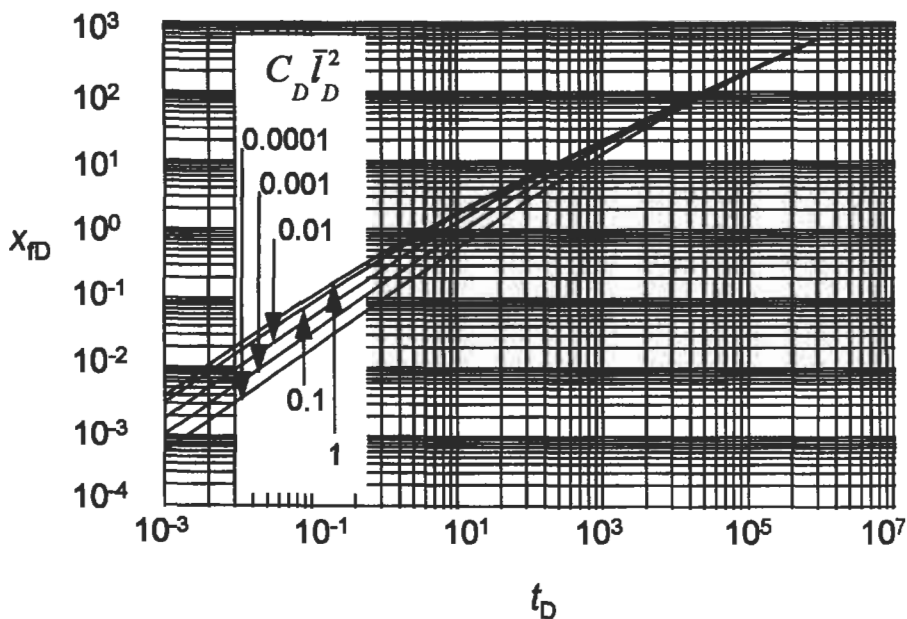


Figure 6-163. Dimensionless length versus time, $\bar{l}_D \ll x_{rD}$ [99].

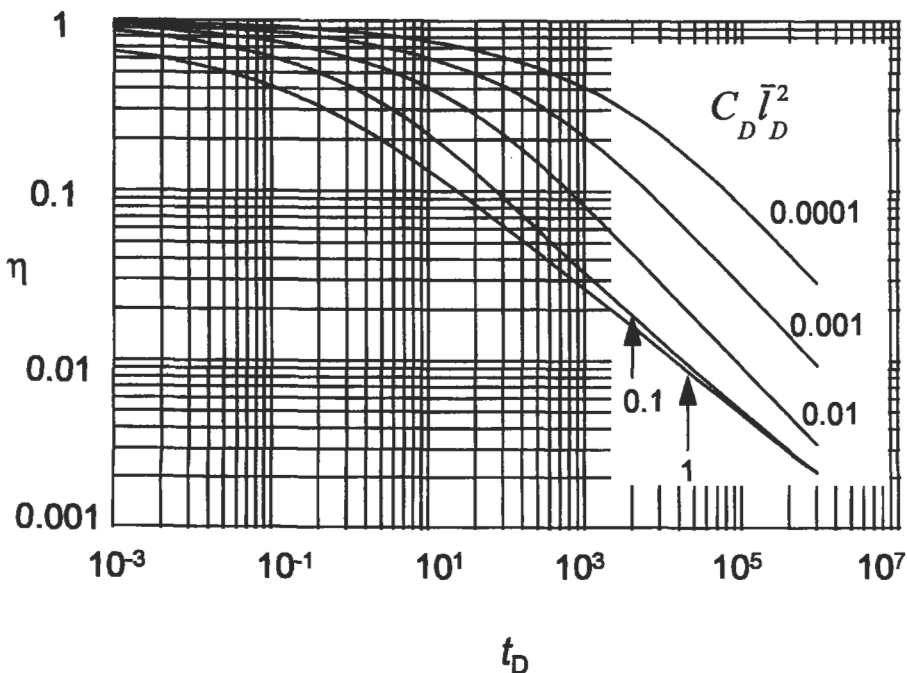


Figure 6-164. Fluid efficiency, $\bar{l}_D \ll x_{rD}$ [99].

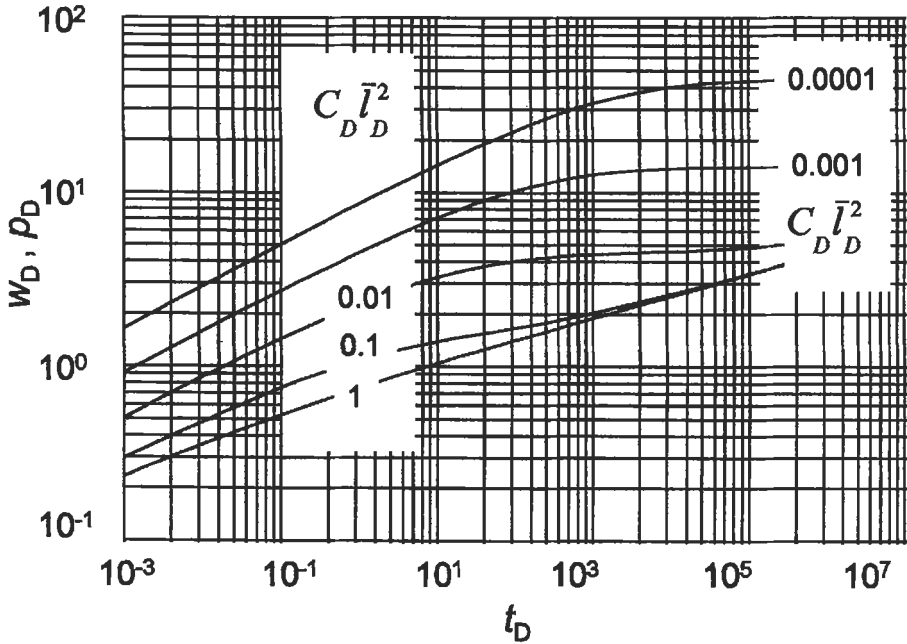


Figure 6-165. Dimensionless width (or net pressure) at wellbore versus time, $l_D \ll x_{fD}$ [99].

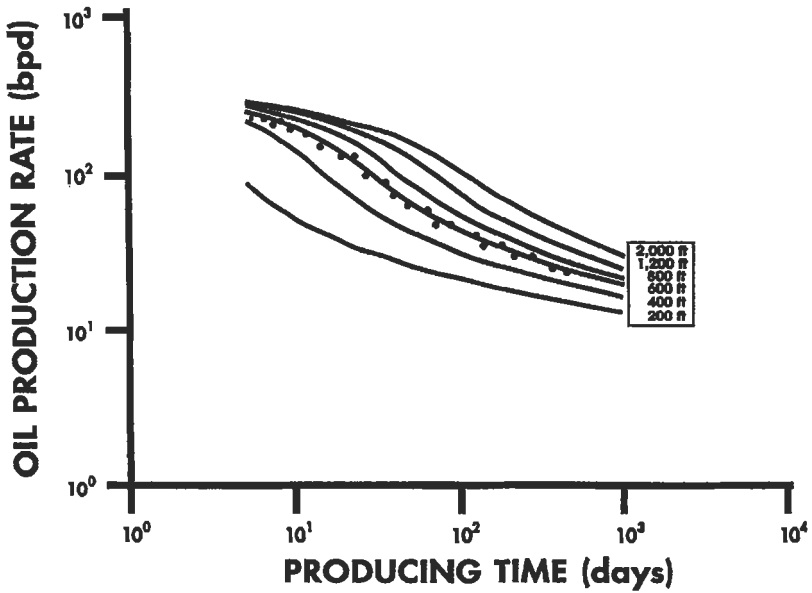


Figure 6-166. Posttreatment fractured well performance and comparison with predicted flowrate.

Acid Fracturing

Formations such as limestones (CaCO_3), dolomites (CaCO_3 , MgCO_3) and chalks (soft, high-porosity CaCO_3) react with acids to form water-soluble salts, water and carbon dioxide. The reaction converts a water-insoluble rock into a highly soluble salt and it has been used in the development of acid fracturing as a stimulation technique. Acid is injected at fracturing pressures, parts the formation and etches the walls of the induced fracture. When pumping stops, the pressure falls off to its original level. Because of uneven etching a residual width remains which provides the fracture conductivity.

There are certain comparative advantages and disadvantages of acid fractures (versus propped fractures) in carbonate reservoirs.

- Acid fractures have placement advantages in highly fissured reservoirs because of the problem of proppant screenouts.
- Fracture length decidedly favors propped fractures because it can be controlled readily. In acid fracturing, acid reacts with the walls of the created fracture, becomes "spent" laterally and thus it results in very short fracture half-lengths on the order of 100 ft [101].
- Operationally, acid fracturing has an advantage over propped fracturing because no proppant cleanout problems or proppant production problems are encountered.

The maximum fracture conductivity $k_{f,w}$ for an acid fracture is given by

$$k_{f,w}(\text{md/in.}) = 9.39 \times 10^{15} \left(\frac{w^3}{12} \right) \quad (6-239)$$

However, this value is affected by two variables: the effective stress σ' and the rock embedment strength S_{rock} . Nierode and Kruk [102] proposed fracture conductivity correlations based on experimental data.

$$k_{f,w} = C_1 e^{-C_2 \sigma'} \quad (6-240)$$

where

$$C_1 = 1.77 \times 10^8 w^{2.47} \quad (6-241)$$

and

$$C_2 = (13.9 - 1.3 \ln S_{\text{rock}}) \times 10^{-3} \quad (6-242)$$

for

$$S_{\text{rock}} < 20,000 \text{ psi} \quad (6-243)$$

and

$$C_2 = (3.8 - 0.28 \ln S_{\text{rock}}) \times 10^{-3} \quad (6-244)$$

for

$$S_{\text{rock}} > 20,000 \text{ psi} \quad (6-245)$$

(Note: In the original publication Equation 6-242 had a typographical error. Instead of the correct 13.9 it was written as 19.9.)

Ben-Naceur and Economides [103] have presented acid fracture performance type curves for a range of effective stresses (3,000 to 9,000) and rock embedment strengths (30,000 to 200,000).

Fracturing of Deviated and Horizontal Wells

Horizontal wells are rapidly emerging as a major type of well completions. There are three meaningful comparisons of performance between a vertical and a horizontal well in the same reservoir.

- Open-hole or fully perforated completions (i.e., no well configuration skin effects) in the vertical and horizontal cases.
- A vertical well with a vertical hydraulic fracture and a fully completed horizontal well.
- A vertical well with a vertical hydraulic fracture and a horizontal well with one or more vertical hydraulic fractures.

Only the second and third comparisons are of interest to the fracturing engineer.

For a reservoir with permeability isotropy in the horizontal plane ($k_x = k_y$), but accounting for permeability anisotropy in the vertical plane, the relationship for equal productivity indexes is [104]

$$r'_{\text{wD}} x_f = \frac{2r_{\text{ev}}/L}{\left(a + \sqrt{a^2 - (L/2)^2}\right) \left(\frac{\beta h}{(\beta + 1)r_w}\right)^{\beta h/L}} \quad (6-246)$$

where β is the vertical-to-horizontal permeability anisotropy ratio and is defined as

$$\beta = \sqrt{k_H/k_v} = \sqrt{(k_x k_y)^{0.5}/k_v} \quad (6-247)$$

Also, the large axis of the drainage ellipse a is given by

$$a = \frac{L}{2} \left\{ 0.5 + \left[0.25 + \left(\frac{r_{\text{eff}}}{L/2} \right)^4 \right]^{0.5} \right\}^{0.5} \quad (6-248)$$

Equation 6-241 is for a fully producing along its length, undamaged, horizontal well. It is also valid for reservoirs where the horizontal permeability is the same in all directions. However, in highly anisotropic formations, while the direction of the fracture is likely to be normal to the smallest permeability [105], the horizontal well can be drilled normal to the maximum permeability. In such a case the situation will be considerably different from the one for a horizontally isotropic reservoir.

Equation 6-241 can be used for a comparison of the performance of an unfractured horizontal well of length L with a fractured vertical well with a fracture half-length x_f .

Figure 6-167 is such a comparison for five permeabilities and $\beta h = 150$ ft. The optimum fracture lengths are also marked. This graph shows the required

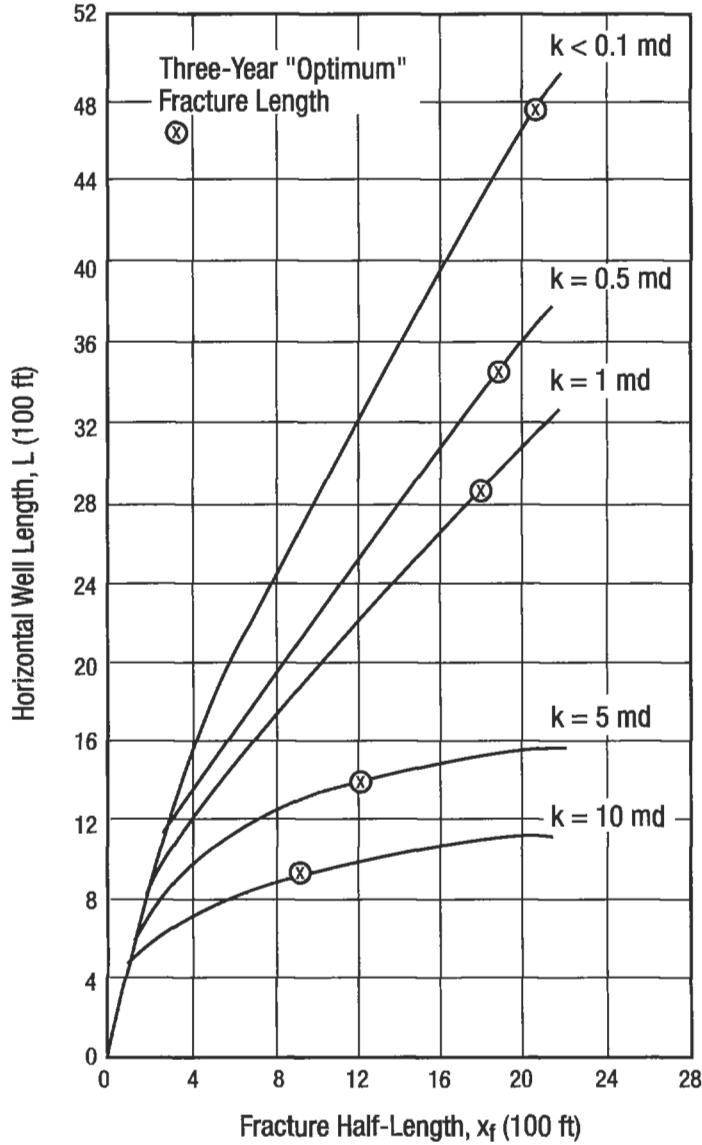


Figure 6-167. Fracture half-length in vertical well and required horizontal well length for equal productivity index ($\beta h = 150$ ft).

horizontal well lengths to deliver the same productivity index. Clearly, while detailed economic calculations on the costs versus benefits of all options may be undertaken, it is evident that in reservoirs where vertical wells are usually fractured ($k < 1$ md), horizontal wells without fractures are not viable alternatives. The required horizontal well lengths would be far more expensive from the indicated optimum fracture half-lengths. For higher permeability reservoirs, the required horizontal well lengths are more attractive. However, in all cases, these horizontal wells must be fully stimulated to remove damage and allow flow contributions from the entire well length. Production logging often indicates that less than one-half of the wellbore length contributes to production. A well with this type of producing interval would require the horizontal well lengths to be more than doubled from those reported above.

However, reservoirs with $\beta h = 25$ ft are normally naturally fractured. While the theoretically optimum fracture half-lengths may require certain equivalent horizontal well lengths, actual fracture executions may not deliver the desired fracture lengths. Screenouts because of excessive leakoff or the opening of fissures normal to the hydraulic fracture trajectory may prevent the creation of these lengths. Thus, horizontal wells may be good alternatives to the fracture lengths that *can* be created.

Finally, *horizontal* permeability anisotropy is exceptionally important. In moderately to highly anisotropic formations, horizontal wells can be good substitutes for fractured vertical wells.

Of particular importance is the third comparison which allows the possibility to drill the horizontal well either in the direction that would result in transverse fractures or in the direction that would result in largely longitudinal (parallel) fractures. A comprehensive review of the issue has been presented by McLennan *et al.* [106].

The drilling of a highly deviated or horizontal well (that does not coincide with a principal stress axis) results in a nonvanishing shear stress component. This was addressed in an earlier subsection and it frequently implies additional pressure requirements for fracture initiation. The fracturing pressure of horizontal wells is affected by the stress concentrations near the well given by [107]

$$\begin{array}{l} \sigma_{xx} \\ \sigma_{yy} \\ \sigma_{zz} \\ \tau_{yz} \\ \tau_{zx} \\ \tau_{xy} \end{array} = \begin{array}{l} \left| \begin{array}{ccc} 1 & 0 & 0 \\ 0 & \sin^2 a & \sin^2 a \\ 0 & \cos^2 a & \cos^2 a \end{array} \right. \\ \left| \begin{array}{ccc} 0 & -\sin a \cos a & -\sin a \cos a \\ 0 & 0 & 0 \\ 0 & 0 & 0 \end{array} \right. \end{array} \begin{array}{l} \sigma_v \\ \sigma_{H,\min} \\ \sigma_{H,\min} \end{array} \quad (6-249)$$

and at the borehole wall by

$$\sigma_{rr} = p_w \quad (6-250)$$

$$\sigma_{\theta\theta} = (\sigma_{xx} + \sigma_{yy} - p_w) - 2(\sigma_{xx} - \sigma_{yy}) \cos(2\theta) - 4\tau_{xy} \sin(2\theta) \quad (6-251)$$

$$\sigma_{zz} = \sigma_{zz} - 2\nu(\sigma_{xx} - \sigma_{yy}) \cos(2\theta) - 4\nu\tau_{xy} \sin(2\theta) \quad (6-252)$$

$$\tau_{r\theta} = \tau_{rz} = 0 \quad (6-253)$$

$$\tau_{\theta z} = 2(-\tau_{xz} \sin \theta + \tau_{yz} \cos \theta) \quad (6-254)$$

Figure 6-168 presents the theoretical fracturing pressure of horizontal wells at different deviation angles from the fracture direction in a reservoir. Also, six actual wells, with multiple (in certain cases more than ten) fracturing treatments are indicated. The agreement between predicted and observed values is excellent.

Since in highly deviated wells the direction of fracture initiation is likely to differ from the ultimate direction of propagation, this turning of the fracture direction can have major implications during fracture execution (screenouts as a result of inadequate width "around a bend") and a choked fracture for the production after the treatment.

A most attractive element is the option to drill a horizontal well in the direction of minimum horizontal stress (i.e., transverse fractures will be initiated) or in the direction of maximum horizontal stress (i.e., a longitudinal fracture will be initiated). In Reference 106 guidelines are given to decide on either of these two options.

The base case is a vertical well with a vertical fracture. If $F_{CD} > 10$, then a horizontal well with transverse orthogonal fractures is indicated. If $F_{CD} < 2$, a horizontal well with a colinear, longitudinal, fracture is indicated. For F_{CD} values between 2 and 10 a more detailed calculation is needed. This is again outlined in Reference 106.

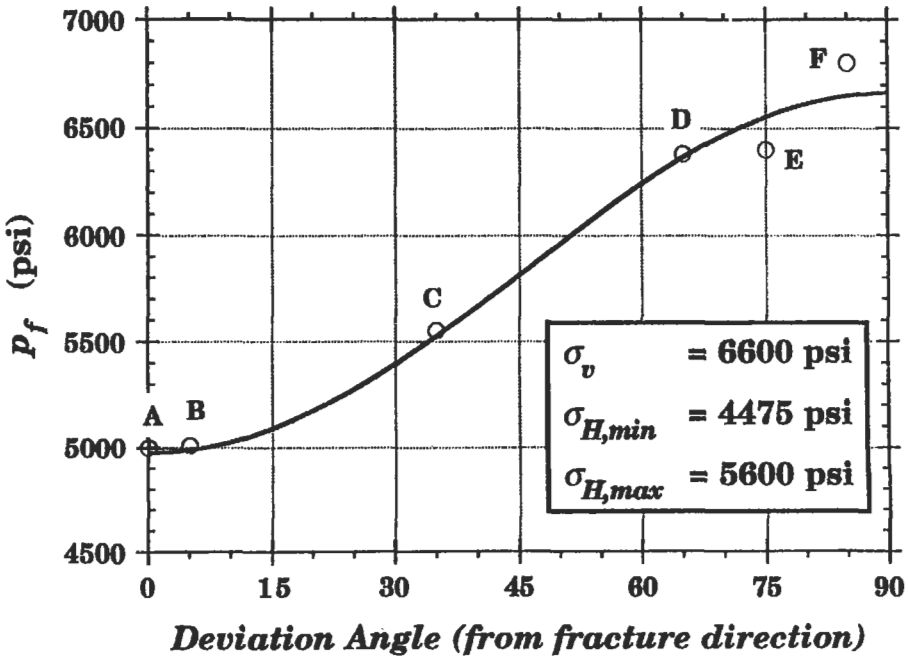


Figure 6-168. Fracturing pressure of six arbitrarily oriented horizontal wells [107].

In all cases the decision to drill a horizontal well instead of a vertical well must be done on the basis of NPV calculations. The incremental performance, if any, must cover the incremental cost of drilling the horizontal well.

For transverse fractures, each individual fracture is penalized by a skin effect describing the inefficient contact between well and fracture [104]. Then the sum of the individual NPVs is optimized. Each fracture is assessed a share of the drainage area and a portion of the incremental drilling costs.

Matrix Stimulation

Damage around the wellbore may severely reduce the production or injection rate of the well. This damage, which may have a variety of origins, may also be of different type and nature.

Flow impairment around the wellbore has been described by a positive skin effect as has been introduced in Equation 6-200. A common representation of the skin effect due to damage is given by Hawkins' formula:

$$s = \left(\frac{k}{k_s} - 1 \right) \ln \frac{r_s}{r_w} \quad (6-255)$$

where k_s = permeability of damage zone in md
 r_s = extent of damage zone in ft.

The skin effect, influencing the well performance (and the one obtained from a pressure transient test), is a multicomponent variable including mechanical effects, phase and rate-dependent effects, along with the near-wellbore damage. Thus the total skin effect s_t is

$$s_t = s_d + s_{c+g} + s_p + \sum ps \quad (6-256)$$

where s_d = skin due to damage

s_{c+g} = skin effect due to partial penetration and slant [108]

s_p = skin effect due to perforations [109]

$\sum ps$ = rate and phase-dependent pseudoskin factors.

The s_{c+g} and s_p can be calculated as outlined in References 108 and 109, respectively, while $\sum ps$ can be usually quantified by variations (and correlation) of the producing pressure and rate. This exercise is necessary for every well in order to isolate the damage-induced skin effect, which is the only one that can be removed via matrix treatments. The other components of the skin effect can be large, and their quantification is necessary in the design and evaluation of matrix stimulation treatments. To remove damage, fluids are injected at "matrix" rates in order to prevent unintentional fracturing of the formation. This is critical for the success of these treatments.

Because not all damage is acid-removable, an identification of the different types of damage and their treatments are shown in Figure 6-169 from Reference 110. Only damage caused by silts and clays (under heading number 7) can be removed by acid.

Sandstone acidizing and the appropriate fluid selection depends on mineralogy, temperature and nature of damage. Figure 6-170 from Reference 111 outlines a treatment selection guide for damage removal in sandstone reservoirs. The "mud acid" referred to in Figure 6-170 is a mixture of HF (0.5 to 3%) and HCl (3 to 13.5%).

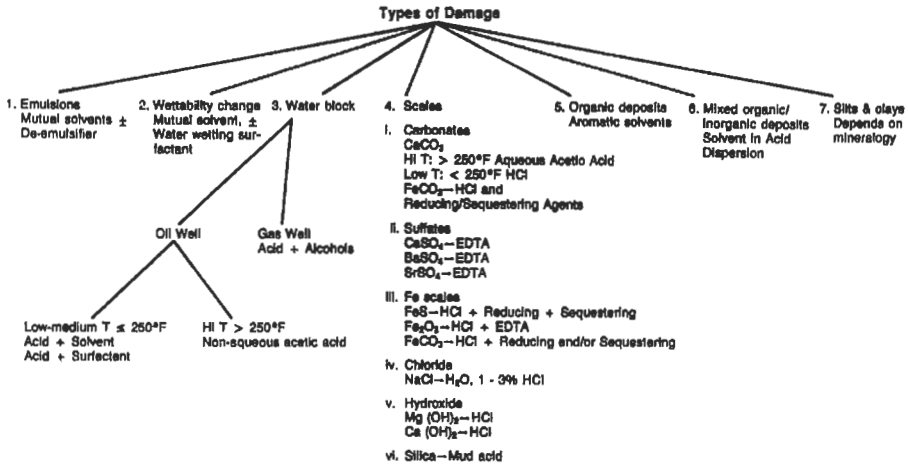


Figure 6-169. Types of damage and suggested matrix treatments [110].

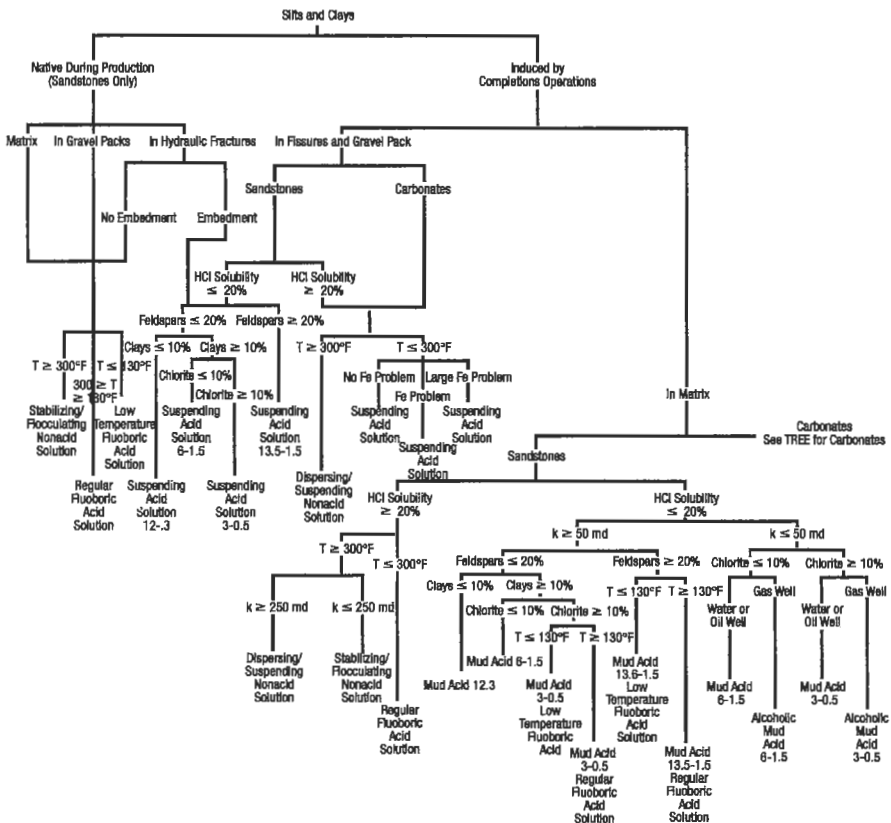


Figure 6-170. Fluid selection for sandstone matrix acidizing [111].

Matrix Acidizing Design

Reference 112 lists the major steps necessary for a matrix acidizing design:

1. Ensure that the well is damaged and that a high skin effect is not mechanically induced.
2. Establish the nature of damage.
3. Determine the appropriate fluid for the treatment (see Figure 6-169 for general fluid selection and Figure 6-170 for acidizing treatments).
4. Calculate maximum rate and pressure to avoid unintentional formation fracturing.
5. Determine volume requirements for treatment.
6. If the formation is multilayered or if it presents a substantial vertical permeability anisotropy, determine a placement technique (diversion).
7. Evaluate treatment for its success (or failure) and consider these findings in future, similar, treatments.

Of the above, items 5, 6 and 7 will be outlined.

Fluid Volume Requirements

For sandstones, a matrix acidizing treatment usually consists of a preflush, an acid and an overflush volume. The preflush provides a separation between conate water and HF to help prevent the formation of damaging sodium and potassium fluosilicates and reacts with carbonate minerals to prevent their reaction with HF (and thus its spending). Usual preflush is 5 to 15% HCl. The acid volume is generally 12 to 3% mixture of HCl and HF. The optimum design, based on experience, is 125 to 200 gal/ft of formation [105].

The overflush volume, ranging from 50 gal/ft to 1 to 5 times the volume of the acid formulation, is usually either 3 to 10% HCl, NH_4Cl or a light hydrocarbon, such as diesel. For a gas well, nitrogen may be used.

For carbonate reservoirs, the flow and reaction of acid within the formation is significantly more complicated. Viscous fingering, but particularly special instabilities called *wormholes*, are generated. The quantification of the wormholing phenomenon as it pertains to the skin effect reduction was presented by Daccord *et al.* [113]:

$$s = -\frac{1}{d} \ln \left(1 + \text{Ac} N_{\text{Pe}}^{-1/d} \frac{bV}{\pi h \phi_w^d} \right) \quad (6-257)$$

where d = fractal dimension (≈ 1.6 for mass-transfer-limited kinetics and ≈ 2 for surface-reaction kinetics)

Ac = acid capacity number [113]

N_{Pe} = Peclet number

V = volume of acid injected.

Diversion in Matrix Acidizing

When fluids are injected in a multilayered reservoir, the natural trend is to follow the path of least resistance, i.e., the higher permeability and/or least-damage zone. However, in order to stimulate the formation effectively, all damage must be removed and thus an injection profile modification is necessary.

In the past, mechanical diverting techniques were used. These included inflatable packers, “frac baffles” and ball sealers. Recently, chemical diverters such as water-soluble benzoic acid (for water injection wells) and hydrocarbon resins (for oil producers) have been employed. These diverters, injected preferably just prior to the acid injection or with the acid itself, are deposited on the sandface, creating a diverter cake of a resistance R_{cake} and thus a temporary skin factor s_{cake} [83]:

$$s_{\text{cake}} = \frac{2\pi kh}{A} R_{\text{cake}} \tag{6-258}$$

where A is the area of flow and R_{cake} is experimentally determined. The amount of diverter deposited on the sandface increases as long as the layer takes a disproportionate amount of fluid. Cake deposition ends when the flowrate is distributed only as a function of the layer height. Figure 6-171 is a depiction of matrix stimulation injection without and with a diverter.

Currently, work is done to use foams as diverting agents. They appear to work both in the manner described above for chemical diverters, but also as “inadvertent” diverters: they decompose in the oil zone (thus allowing acid penetration) and they are stable in water zones (thus plugging acid flow).

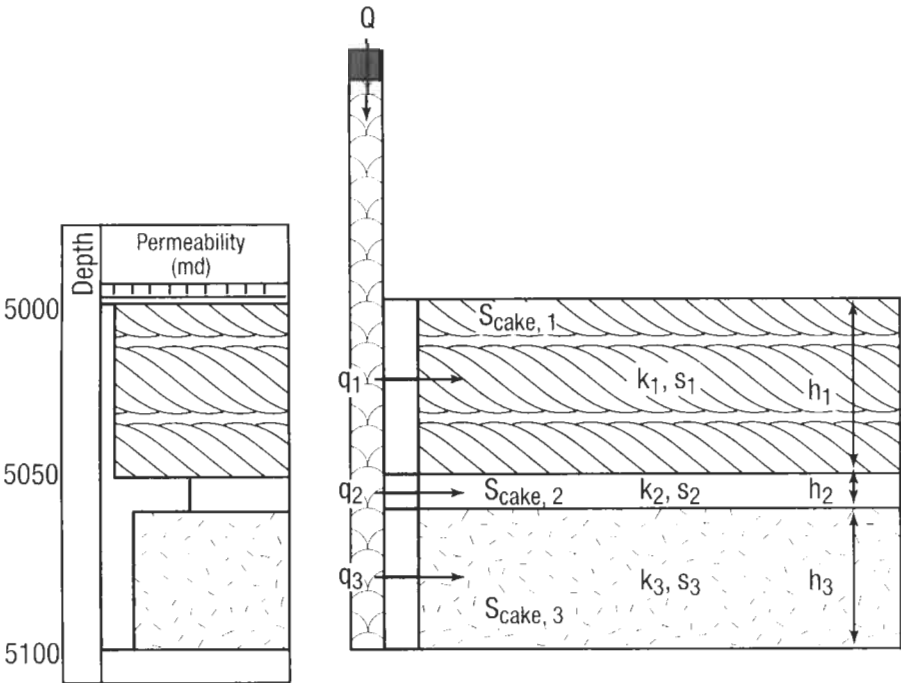


Figure 6-171. Fluid distribution for matrix stimulation injection in a multi-layered reservoir. On the left, without diverters; on the right, with diverters.

Matrix Stimulation in Horizontal Wells

To evaluate a proper matrix stimulation treatment in horizontal wells, a description of the damage profile along and normal to the horizontal well trajectory is necessary. Frick and Economides [114] have shown that the distribution of formation damage surrounding a horizontal well is neither radial nor is it evenly distributed along the wellbore.

During drilling and well completion, mud filtrate and completion fluids penetrate the pay zone. Since the exposure time of the formation to drilling and completion fluids is longer at the horizontal section nearer the vertical section, the shape of damage distribution along the wellbore will be a truncated cone, with the larger base near the vertical section of the well. This profile of damage is evident also during production, because the pressure gradient normal to the well nearer the vertical section is (usually) the largest.

Permeability anisotropy, represented by β , generates an elliptical shape of damage distribution normal to the well. The geometrical shape of a truncated elliptical cone results in an expression for the skin effect around a horizontal well [114]:

$$s'_{\text{eq}} = \left(\frac{k}{k_s} - 1 \right) \ln \left[\frac{1}{(\beta) + 1} \sqrt{\frac{4}{3} \left(\frac{a_{H,\text{max}}^2}{r_w^2} + \frac{a_{H,\text{max}}}{r_w} + 1 \right)} \right] \quad (6-259)$$

where $a_{H,\text{max}}$ is the horizontal half-axis of the larger base of the elliptical cone of damage, as shown in Figure 6-172 along with cross-sections of damage for various β . This expression is analogous to Hawkins' formulation for vertical wells and can be used in the usual manner, implying a steady-state pressure drop.

Stimulation Considerations. Horizontal wells have such long exposed intervals that stimulation fluid volumes per unit length, used in vertical wells, are not practical. While pumping as much as 150 gal/ft is routine in vertical wells, such a coverage implies 300,000 gal of acid in a 2,000-ft horizontal well. Pumping at 1 bpm, these volumes would require 120 h of pumping.

A further constraint is proper placing of acid (diversion): acid has a tendency to extend existing flow paths. Thus, acid thief zones are either natural or created, and there is therefore a need for substantial optimization of matrix stimulation in terms of technical and economic considerations.

When planning for a partial removal of the damage, the distribution of the stimulation fluid is a crucial issue. A simple calculation of posttreatment skin effect determines that the distribution of the stimulation fluid should mimic the shape of damage. Deliberate blanking of horizontal well segments and complete damage removal in the perforated sections offer another potential for significant optimization of the stimulation treatment.

The previous considerations require a methodology of acid placement. Bull-heading the fluids into the horizontal portion is not recommended. Such treatments stimulate only a minor portion of the horizontal well near the vertical section. Coiled tubing is a proper tool for the distribution of stimulation fluids. The rate of coiled tubing withdrawal can be calculated and depends on the injection rate and volumetric coverage.

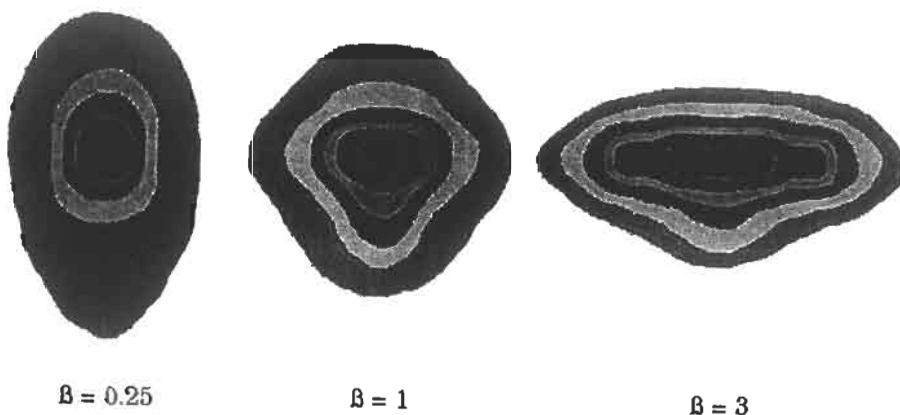
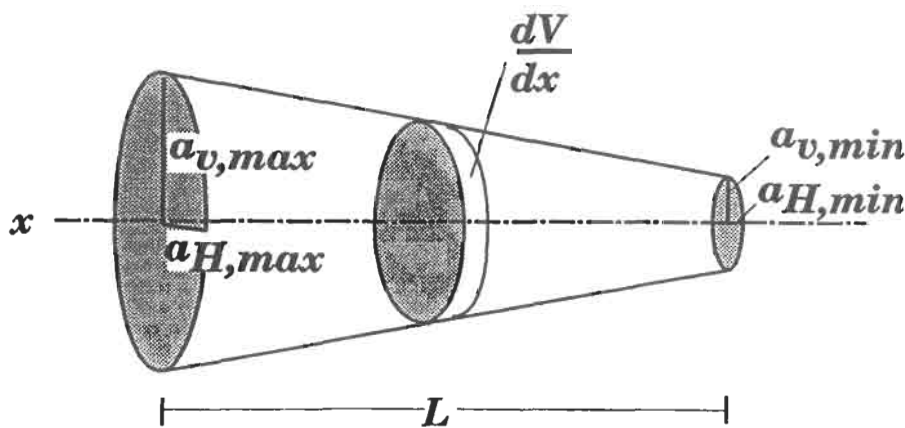


Figure 6-172. Shape of damage along and normal to a horizontal well [114].

Evaluation of Matrix Acidizing Treatments

Paccaloni [115] was the first to use instantaneous pressure and rate values to compute the changing skin effect at any time during the treatment and thus evaluate the progress of the job. He used a steady-state pressure response and defined a "damage ratio," DR:

$$DR = \frac{\ln(r_e/r_w) + s}{\ln(r_e/r_w)} \tag{6-260}$$

The method allows the estimation of both the original (damage) skin effect as well as its evolution.

A new technique, which does not use a steady-state assumption, was introduced by Prouvost and Economides [116]. The method uses reservoir transients during

acid injection to simulate pressure response and compares it with measured values. The difference between these values is attributed to the changing skin effect, i.e.,

$$\Delta s = \frac{kh\Delta p_{\text{departure}}}{141.2qB\mu} \quad (6-261)$$

where $\Delta p_{\text{departure}}$ = difference between simulated pressure (with a constant non-removable skin effect) and the measured value. The technique is illustrated on Figure 6-173.

The simulated pressure requires a knowledge of reservoir and well parameters, namely the permeability k , and the skin effect that cannot be removed by acid. If the latter is not known, then zero can be used. The two pressure curves would then be apart at the end of the job by a constant value, proportional to the nonremovable skin effect.

A graph of the evolving skin can then be drawn as shown in Figure 6-174.

SURFACE OIL PRODUCTION SYSTEMS

The purpose of the surface production facility is:

- to separate the wellstream into three phases: gases, liquids and some solid impurities
- to remove water from the liquid phase
- crude oil treating
- gas conditioning (see Figure 6-175)

This chapter is a discussion of the design, use, functions, operation and maintenance of all facility types. Classification of production facilities by type is rather difficult because they differ in production rates, fluid properties, location and disposal requirements.

From a technical point of view producing equipments can be divided into two groups:

- separating pressure vessels
- storage tanks

Nomenclature of Separating Vessels

Separating vessels in oilfield terminology designate pressure vessels used for separating well fluids produced from oil and gas wells into gaseous and liquid components. The following are examples of separating vessels.

Scrubber or Knockout: A vessel designed to handle streams with high gas/liquid ratios. The liquid is generally entrained as mist in the gas or is free, flowing along the pipe wall. These vessels usually have a small liquid collection section. The terms scrubber and knockout are often used interchangeably.

Separator: A vessel used to separate a mixed-phase stream into gas and liquid phases that are "relatively" free of each other. Other terms used are scrubbers, knockouts, line drips and decanters.

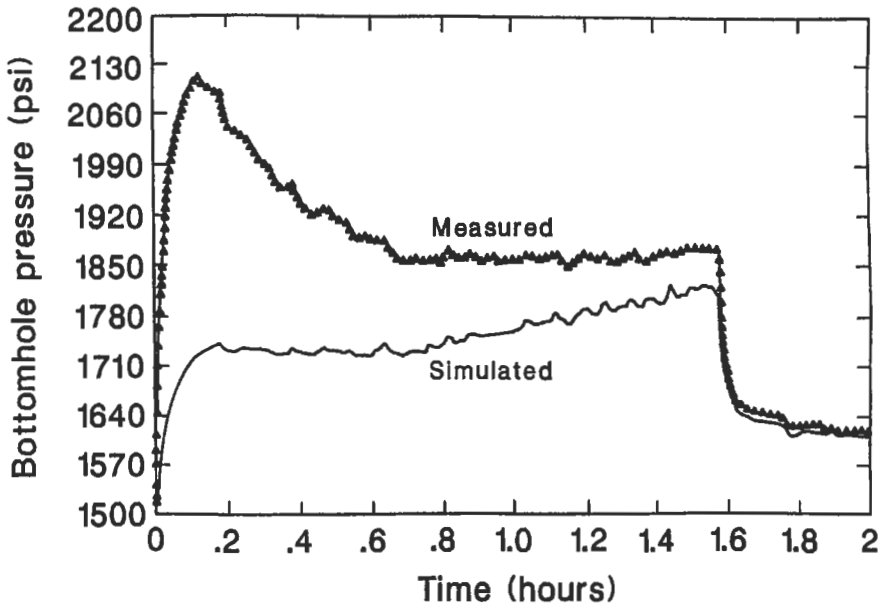


Figure 6-173. Simulated and measured pressure response during a matrix acidizing treatment [116].

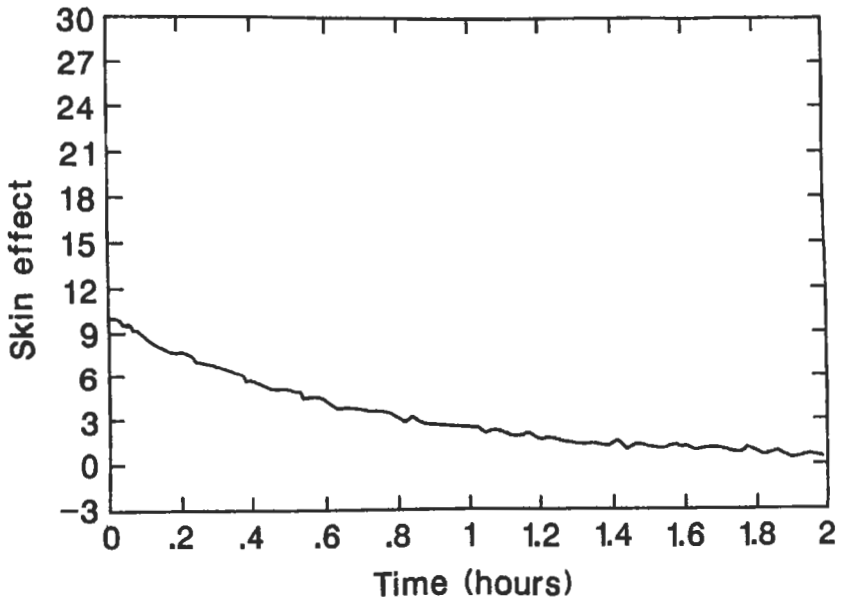


Figure 6-174. Evolution of skin effect [116].

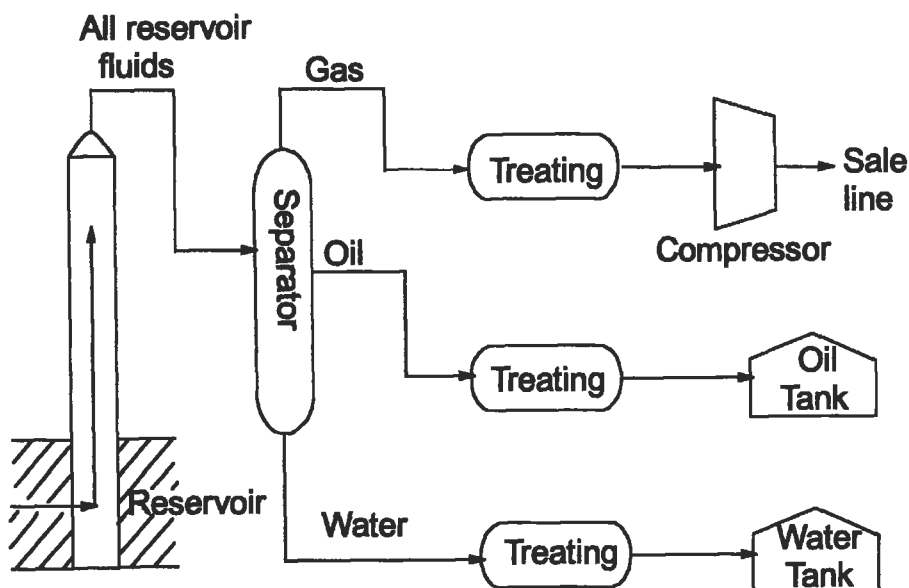


Figure 6-175. Schematic view of a surface production system.

Three-Phase Separator: A vessel used to separate gas and two immiscible liquids of different densities (e.g., gas, water and oil).

Liquid-Liquid Separators: Two immiscible liquid phases can be separated using the same principles as for gas and liquid separators. Liquid-liquid separators are fundamentally the same as gas-liquid separators except that they must be designed for much lower velocities. Because the difference in density between two liquids is less than between gas and liquid, separation is more difficult.

Filter Separators: A filter separator usually has two compartments. The first compartment contains filter-coalescing elements. As the gas flows through the elements, the liquid particles coalesce into larger droplets, and when the droplets reach sufficient size, the gas flow causes them to flow out of the filter elements into the center core. The particles are then carried into the second compartment of the vessel (containing a vane-type or knitted wire mesh mist extractor) where the larger droplets are removed. A lower barrel or boot may be used for surge or storage of the removed liquid.

Line Drip: Typically used in pipelines with very high gas/liquid ratios to remove only free liquid from a gas stream, and not necessarily all the liquid from a gas stream. Line drips provide a place for free liquids to separate and accumulate.

Slug Catcher: A particular separator design able to absorb sustained in-flow of large liquid volumes at irregular intervals. Usually found on gas-gathering systems or other two-phase pipeline systems. A slug catcher may be a single large vessel or a manifolded system of pipes.

Flash Tank (Chamber, Trap or Vessel): Conventional oil and gas separator operated at low pressure, with the liquid from a higher-pressure separator being

“flashed” into it. This flash chamber is quite often the second or third stage of separation, with the liquid being discharged from the flash chamber to storage. *Expansion Vessel:* First-stage separator on a low-temperature or cold-separation unit. This vessel may be equipped with a heating core to melt hydrates or a hydrate-preventive liquid (such as glycol) may be injected into the well fluid just before expansion into this vessel.

Storage Classification [117]

Atmospheric

Atmospheric pressure tanks are designed and equipped for storage of contents at atmospheric pressure. This category usually employs tanks of vertical cylindrical configuration that range in size from small shop welded to large field erected tanks. Bolted tanks, and occasionally rectangular welded tanks, are also used for atmospheric storage service.

Low Pressure (0 to 17 kPa or 0 to 2.5 psig)

Low-pressure tanks are normally used in applications for storage of intermediates and products that require an internal gas pressure from close to atmospheric up to a gas pressure of 2.5 psig. The shape is generally cylindrical with flat or dished bottoms and sloped or domed roofs. Low-pressure storage tanks are usually of welded design. However, bolted tanks are often used for operating pressures near atmospheric. Many refrigerated storage tanks operate at approximately 0.5 psig.

Medium Pressure (17 to 103 kPa or 2.5 to 15 psig)

Medium-pressure tanks are normally used for the storage of higher volatility intermediates and products that cannot be stored in low-pressure tanks. The shape may be cylindrical with flat or dished bottoms and sloped or domed roofs. Medium-pressure tanks are usually of welded design. Welded spheres may also be used, particularly for pressures at or near 15 psig.

High Pressure (Above 103 kPa or 15 psig)

High pressure tanks are generally used for storage of refined products or fractionated components at pressure above 15 psig. Tanks are of welded design and may be of cylindrical or spherical configuration. All above tanks are aboveground storage.

Gas-processing industry liquids may be stored underground, conventionally mined or solution mined caverns. No known standard procedures are available for this storage type; however, there are many publications and books covering the subject. For more details about storage classification, see Table 6-35.

Phase Separation [117–120]

Practical separation techniques for liquid particles in gases are discussed. The principles used to achieve physical separation of gas and liquids or solids are momentum, gravity settling and coalescing. Any separator may employ one or more of those principles, but the fluid phases must be immiscible and have different densities for separation to occur.

Table 6-35
Storage Classification [117]

	Storage				
	Atmospheric Pressure†‡	0 to 2.5 psig†‡	2.5 to 15 psig†‡	Above 15 psig‡	Underground
Crude Oils	X	X	X	-	X
Condensate	X	X	X	X	X
Oils	X	X	-	-	X
Natural Gasoline	X	X	X	-	X
Butanes	-	Xo	Xo	X	X
Propane	-	Xo	Xo	X	X
Raw NGLs	-	Xo	Xo	X	X
Ethane	-	Xo	Xo	X	X
Petrochemicals	-	Xo	Xo	X	X
Natural Gas	-	-	-	X	X
LNG	-	Xo	Xo	X	-
Treating Agents	X	X	-	-	-
Dehydration Fluids	X	X	-	-	-
Specialty Chemicals	X	X	X	-	-
Solid Materials	X	-	-	-	-
Water	X	-	-	-	-

* Some Materials may require a slight positive pressure to exclude air, oxygen, and/or water, and conserve valuable/toxic vapors. API specifications 12D and 12F may also apply.

† API Standard 650 governs

‡ API Standard 620 governs

§ ASME Unfired Pressure Vessel Code, Section VIII governs

o Refrigerated only

Note: Vacuum conditions may exist and must be considered in tank design. Examples: low ambient temperatures or evacuating without relieving.

Momentum

Fluid phases with different densities will have different momentum. If a two-phase stream changes direction sharply, greater momentum will not allow the particles of the heavier phase to turn as rapidly as the lighter fluid, so separation occurs. Momentum is usually employed for bulk separation of the two phases in a stream.

Gravity Settling

Liquid droplets will settle out of a gas phase if the gravitational force acting on the droplet is greater than the drag force of the gas flowing around the droplet (see Figure 6-177). These forces can be described mathematically. Drag force (F) on a liquid droplet in a gas stream is determined from

$$F = C_D A_p \gamma_g \frac{V_t^2}{2g} \quad (6-262)$$

Hence,

$$V_t = \left(\frac{2Fg}{C_D A_p \gamma_g} \right)^{0.5}$$

and from Newton's second law

$$F = \frac{w}{g} g \quad \text{and} \quad \text{if} \quad w = \frac{\gamma_L - \gamma_g}{\gamma_L} W_p$$

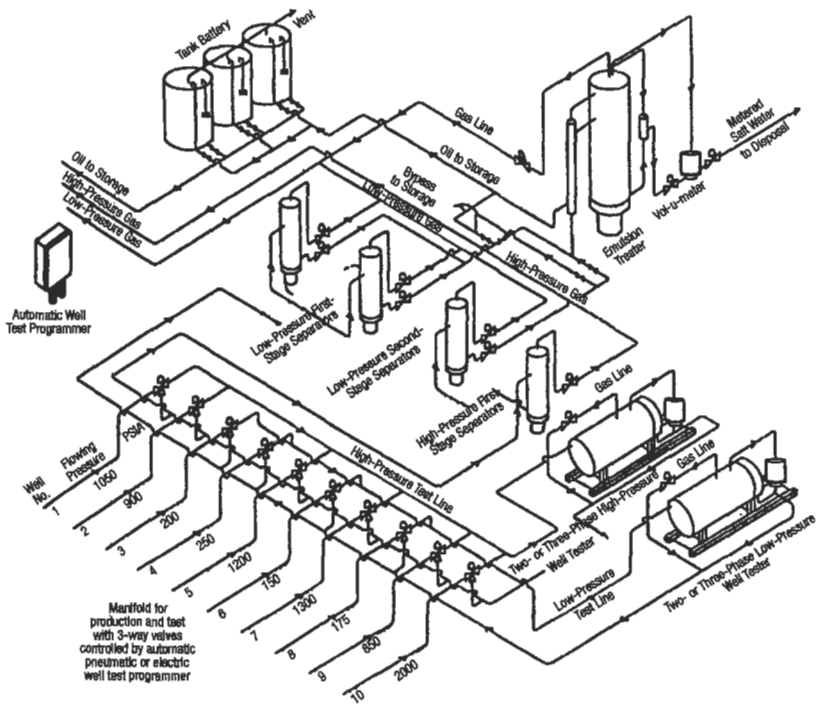


Figure 6-176. Typical surface production equipment.

Forces on Liquid Droplet in Gas Stream

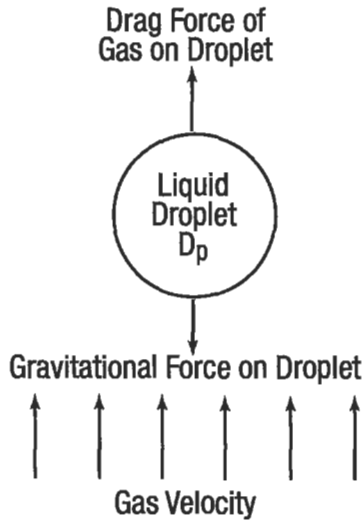


Figure 6-177. Forces on liquid input in gas system [117].

$$V_t = \left[\frac{2gW_p(\gamma_l - \gamma_g)}{\gamma_l \gamma_g A_p C_D} \right]^{0.5} = \left[\frac{4gD_p(\gamma_l - \gamma_g)}{3\gamma_g C_D} \right]^{0.5} \quad (6-263)$$

where F = drag force in lb

V_t = terminal velocity in ft/s

g = acceleration due to gravity in ft/s²

W_p = weight of particle in lb

$\gamma_{l,g}$ = liquid and gas-phase specific weights in lb/ft³

A_p = particle cross-sectional area in ft²

D_p = droplet diameter in ft

C_D = drag coefficient of particle (dimensionless)

The drag coefficient has been found to be a function of the shape of the particle and the Reynolds number of the flowing gas. For the purpose of this equation, particle shape is considered to be a solid, rigid sphere.

Reynolds number is defined as

$$Re = \frac{1,488D_p V_t \gamma_g}{\mu} \quad (6-264)$$

where μ = viscosity (cp)

In this form, a trial-and-error solution is required since both particle size D_p and terminal velocity V_t are involved. To avoid trial and error, values of the drag coefficient are presented in Figure 6-178 as a function of the product of drag coefficient C_D times the Reynolds number squared; this technique eliminates velocity from the expression. The abscissa of Figure 6-178 is represented by

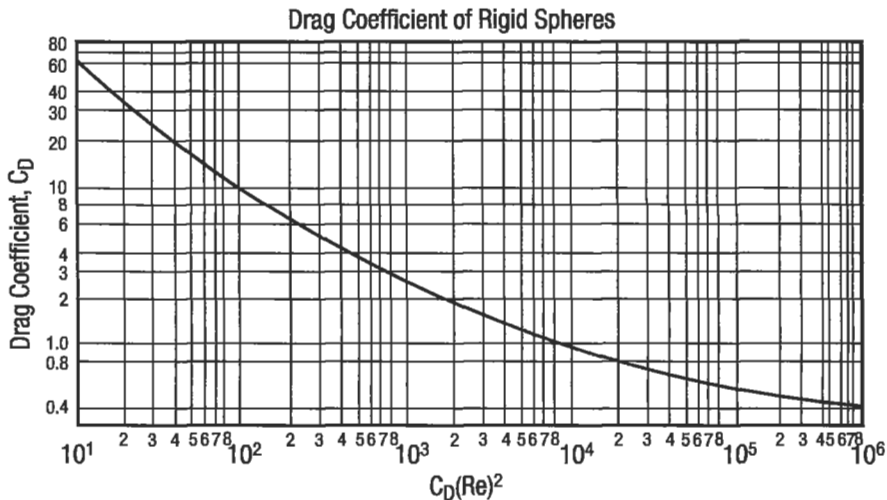


Figure 6-178. Drag coefficient of rigid sphere [117].

$$C_D(\text{Re})^2 = \frac{(0.95)(10^8)\gamma_g D_p^3 (\gamma_l - \gamma_g)}{\mu^2} \quad (6-265)$$

For production facility design (turbulent flow), the following formula for drag coefficient is proper:

$$C_D = \frac{24}{\text{Re}} + \frac{3}{(\text{Re})^{0.5}} + 0.34 \quad (6-266)$$

and if D_p is expressed in micrometers $\rightarrow d_m$

$$V_t = 0.0119 \left[\left(\frac{\gamma_l - \gamma_g}{\gamma_g} \right) \frac{d_m}{C_D} \right]^{0.5} \quad (6-267)$$

Equations 6-266 and 6-267 can be solved by an iterative solution as follows

1. Write the equation for laminar flows ($C_D = 0.34$)

$$V_t = 0.0204 \left[\frac{(\gamma_l - \gamma_g)}{\gamma_g} d_m \right]^{-0.5}$$

2. Calculate $\text{Re} = 0.0049(\gamma_g d_m V_t / \mu)$
3. From Equation 6-266 calculate C_D .
4. Recalculate V_t using Equation 6-267.
5. Go to Step 2.

The above technique is proper assuming that known diameter drops are removed (e.g., 100 μm).

Separator Design and Construction

There are three types of separators: vertical, horizontal (single and double tube) and sometimes spherical (Figure 6-179).

Vertical separators are usually selected when the gas/liquid ratio is high or total gas volumes are low. In this sort of vessel, the fluids enter the vessel striking a diverting plate which initiates primary separation.

Liquid removed by the inlet diverter falls to the bottom of the vessel. The gas moves upward, usually passing through a mist extractor to remove suspended mist, and then flows out. Liquid removed by the mist extraction is coalesced into larger droplets that fall down to the liquid reservoir in the bottom. Mist extractors can significantly reduce the required diameter of vertical separators.

Horizontal separators are most efficient for large volumes of total fluids and when large amounts of dissolved gas are present with the liquid. The greater liquid surface area provides optimum conditions for releasing gas from liquid.

According to API Standards [121,122], Tables 6-36 through 6-38 are for nominal industry standards.

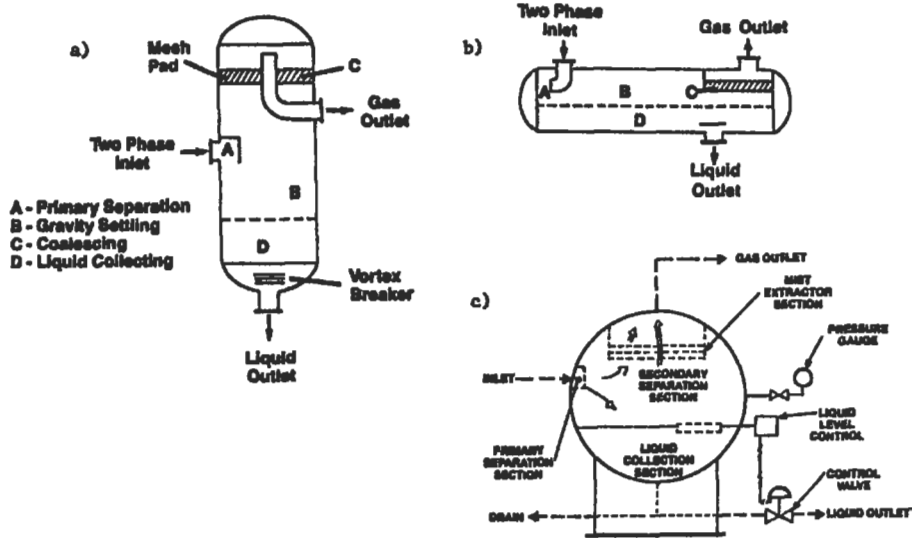


Figure 6-179. Gas liquid separators: (a) vertical, (b) horizontal, (c) spherical [117].

Vertical Separators

The following calculations are presented as a guide to the design and sizing of two-phase separators. Sizing should be based on the maximum expected instantaneous rate.

For practical purposes, for vertical separator, Equation 6-263 is written as

$$V_t = K \left(\frac{\gamma_L - \gamma_g}{\gamma_g} \right)^{0.5} \quad (6-268)$$

where V_t = terminal velocity of liquid droplets or maximum allowable superficial velocity of gas in ft/s

K = a constant depending on design and separating conditions in ft/s; see Table 6-39

Example 1

A vertical gravity separator is required to handle 10 MMssfd of 0.6 specific gravity gas at an operating pressure of 1,000 psia and a temperature of 60°F. Liquid flow = 2,000 bpd of 40°API oil, $\mu_g = 0.014$ cp.

Solution

1. Find K from Table 6-39 where $K = 0.26$ ft/s.
2. Calculate minimum diameter, such that if

Table 6-36
Vertical Separators. Size and Working Pressure Ratings [121]

Nominal Diameter, Inches	Maximum Allowable Working Pressure, PSIG @ 100°F.						
	230	600	1000	1200	1440	2000	
16	...	230	600	1000	1200	1440	2000
20	125	230	600	1000	1200	1440	2000
24	125	230	600	1000	1200	1440	2000
30	125	230	600	1000	1200	1440	2000
36	125	230	600	1000	1200	1440	2000
42	125	230	600	1000	1200	1440	2000
48	125	230	600	1000	1200	1440	2000
54	125	230	600	1000	1200	1440	2000
60	125	230	600	1000	1200	1440	2000

Notes: a. Shell length is generally expanded in 2½ foot increments measured from head seam to head seam and is typically 5 feet, 7½ feet, or 10 feet. A minimum length-to-diameter ratio of 2.0 is normally used.

b. Vessel diameter is generally expanded in 6 inch increments, measured either as outside diameter (OD) or inside diameter (ID). OD separators are normally furnished up to 24 inch diameter. Separators above this size may be either OD or ID vessels.

Table 6-37
Horizontal Separators. Size and Working Pressure Ratings [121]

Nominal Diameter, Inches	Maximum Allowable Working Pressure, PSIG @ 100°F.						
	230	600	1000	1200	1440	2000	
12½	...	230	600	1000	1200	1440	2000
16	...	230	600	1000	1200	1440	2000
20	125	230	600	1000	1200	1440	2000
24	125	230	600	1000	1200	1440	2000
30	125	230	600	1000	1200	1440	2000
36	125	230	600	1000	1200	1440	2000
42	125	230	600	1000	1200	1440	2000
48	125	230	600	1000	1200	1440	2000
54	125	230	600	1000	1200	1440	2000
60	125	230	600	1000	1200	1440	2000

Notes: a. Shell length is generally expanded in 2½ foot increments measured from head seam to head seam and is typically 5 feet, 7½ feet, or 10 feet. A minimum length-to-diameter ratio of 2.0 is normally used.

b. Vessel diameter is generally expanded in 6 inch increments, measured either as outside diameter (OD) or inside diameter (ID). OD separators are normally furnished up to 24 inch diameter. Separators above this size may be either OD or ID vessels.

Table 6-38
Spherical Separators. Size and Working Pressure Ratings [121]

Nominal Outside Diameter, Inches	Maximum Allowable Working Pressure, PSIG @ 100°F.						
	230	600	1000	1200	1440	2000	
24	...	230	600	1000	1200	1440	2000
30	...	230	600	1000	1200	1440	2000
36	...	230	600	1000	1200	1440	2000
41	125	230	600	1000	1200	1440	2000
42	125	230	600	1000	1200	1440	2000
48	125	230	600	1000	1200	1440	2000
54	125	230	600	1000	1200	1440	2000
60	125	230	600	1000	1200	1440	2000

Table 6-39
Typical K Factor Values in Equation 6-268 [117]

Separator Type	K Factor (ft/sec)
Horizontal (w/vert. pad)	0.40 to 0.50
Spherical	0.20 to 0.35
Vrt. or Horz. (w/horiz. pad)	0.18 to 0.35
@ Atm. Pressure	0.35
@ 300 psig	0.33
@ 600 psig	0.30
@ 900 psig	0.27
@ 1500 psig	0.21
Wet Steam	0.25
Most vapors under vacuum	0.20
Salt & Caustic Evaporators	0.15

Note: (1) $K = 0.35$ @ 100 psig—Subtract 0.01 for every 100 psi above 100 psig.

(2) For glycol and amine solutions, multiply K by 0.6–0.8.

(3) Typically use one-half of the above K values for approximate sizing of vertical separators without woven wire demisters.

(4) For compressor suction scrubbers and expander inlet separators multiply K by 0.7–0.8.

$$V_t = K \left(\frac{\gamma_L - \gamma_g}{\gamma_g} \right)^{0.5}$$

then

$$V_g = \frac{Q_A \text{ ft}^3/\text{s}}{A_g \text{ ft}^2}$$

$$A_g = \frac{\pi}{4} D^2$$

Gas specific weight is $\gamma_g = (PM/ZRT)$

$$M = 0.6 \times 29 = 17.4$$

$$P = 1,000 \text{ psia}$$

$$T = 520^\circ\text{R}$$

$$R = 10.73 \text{ ft}^3 \cdot \text{psia} \cdot \text{lb}^{-1}_{\text{mol}}, \text{ R}^{-1} \quad Z = 0.84 \text{ (for given P, T, M)}$$

$$\gamma_g = \frac{1000 \times 17.4}{0.84 \times 10.73 \times 520} = 3.713 \text{ lb/ft}^3$$

Liquid specific weight is

$$\gamma_L = 62.4 \times SG_o = 62.4 \frac{141.5}{131.5 + 40} = 51.48 \text{ lb/ft}^3$$

Weight rate of flow \dot{w} , (lb/s) is

$$\dot{w} = \frac{Q(\text{scf})17.4(\text{lb}_m/\text{lb mol})}{379.4(\text{scf}/\text{lb mol}) \times (24 \times 3,600)\text{s}} = \frac{10 \times 10^6 \times 17.4}{379.4 \times 86,400} = 5.3 \text{ lb/s}$$

$$Q_A = \frac{w}{\gamma_g} = \frac{5.3 \text{ lb}_m/\text{s}}{3,713 \text{ lb}_m/\text{ft}^3} = 1.43 \text{ ft}^3/\text{s}$$

$$V_g = \frac{Q_A}{A_g} = \frac{143 \times 4}{\pi D^2} = \frac{1.82}{D^2}$$

$$V_t = V_g$$

$$\frac{1.82}{D^2} = 0.26 \left(\frac{51.48 - 3.713}{3.713} \right)^{0.5} = 0.99 \text{ ft/s}$$

$$D = 1.39 \text{ ft} = 16.76 \text{ in.}$$

Minimum diameter is 20 in. (See Table 6-36). If

$$V_t = \left[\frac{4gD_p(\gamma_L - \gamma_g)}{3\gamma_g C_D} \right]^{0.5}$$

D_p is usually 100–150 μm .
Assume

$$\begin{aligned} D_p &= 150 \mu\text{m} \approx 150 \times 0.00003937/12 \\ &= 4.92 \times 10^{-6} \text{ ft} \end{aligned}$$

From Equation 6-265

$$C_D(\text{Re})^2 = \frac{0.95 \times 10^9 \times 3.713(0.000492)^3(51.48 - 3.713)}{(0.014)^2} = 10,238$$

From Figure 6-178

$$C_D = 0.99$$

$$V_t = \left(\frac{4 \times 32.174 \times 0.000492(51.48 - 3.713)}{3 \times 3.713 \times 0.99} \right)^{0.5} = 0.52 \text{ ft/s}$$

$$V_g = \frac{1.82}{D^2} = 0.52 \text{ ft/s}$$

714 Production

$$D = 1.87 \text{ ft} = 22.5 \text{ in.}$$

and from Table minimum diameter is 24 in. Assume

$$\begin{aligned} D_p &= 100 \text{ } \mu\text{m} = 100 \times 0.00003937/12 \\ &= 0.000328 \text{ ft} \end{aligned}$$

$$C_D(\text{Re})^2 = \frac{0.95 \times 10^8 \times 3.713(0.000328)^3(51.48 - 3.713)}{(0.014)^2} = 2,592$$

From Figure 6-178

$$C_D = 1.75$$

$$V_t = \frac{(4 \times 32.174 \times 0.000328 \times 48.307)}{3 \times 3.713 \times 1.75} = 0.1046 \text{ ft/s}$$

$$V_s = \frac{1.82}{D^2} = 0.1046$$

$$D = 4.17 \text{ ft} = 50 \text{ in.}$$

The maximum allowable superficial velocity calculated from the factors in Table 6-39 is for separators normally having a wire mesh mist extractor (see Figure 6-180). This rate should allow all liquid droplets larger than 10 μm to settle out of the gas. The maximum allowable superficial velocity should be considered for other types of mist extractors.

Further calculations refer to $D = 20$ in. (separator with a mist extractor). Diameters $D = 24$ in. and $D = 50$ in. refer to separator without mist extractor.

3. Calculate liquid level h . A certain liquid storage is required to ensure that the liquid and gas reach equilibrium at separator pressure. This is defined as "retention time" where liquid is retained in the vessel assuming plug flow. The retention time is thus the volume of the liquid storage in the vessel divided by the liquid flowrate. Basic design criteria for liquid retention time in two-phase separators are generally as follows [121]:

Oil Gravities	Minutes (Typical)
Above 35°API	1
20–30°API	1 to 2
10–20°API	2 to 4

$$t = \frac{\text{Vol. ft}^3}{Q \text{ ft}^3/\text{s}}$$

$$\text{Vol.} = \frac{\pi D^2 h}{4 \cdot 12} = \frac{\pi d^2 h}{4(144)12} = 4.545 \times 10^{-4} d^2 h$$

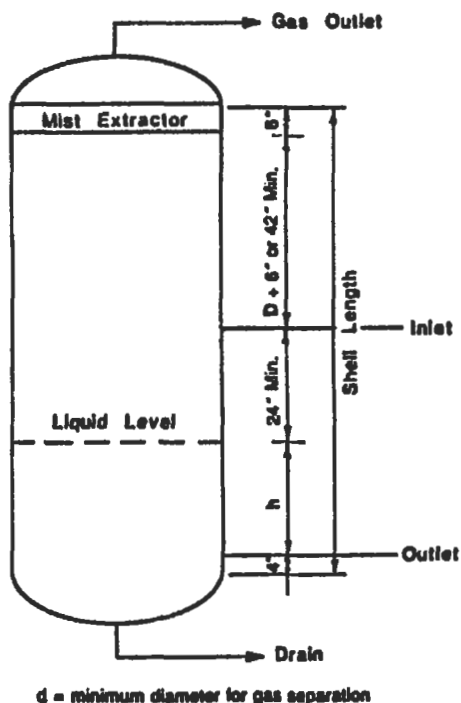


Figure 6-180. The geometry of a vertical separator [119].

$$D = 20 \text{ in.}$$

$$\text{Vol.} = 0.1818h$$

$$Q_L = \text{bpd}$$

$$Q = Q_L \times 5.615 \frac{\text{ft}^3}{\text{barrel}} \times \frac{\text{day}}{24 \text{ hr}} \times \frac{\text{hr}}{3,600\text{s}} = 0.000065Q_L$$

$$t = \frac{0.1818h}{0.000065Q_L} = 2,797 \frac{h}{Q_L}$$

Assume $t_r = 1 \text{ min}$ (API = 40°)

So,

$$h = \frac{t_r Q_L}{2,797} = \frac{2,000}{2,797} = 0.715 \text{ ft} = 8.6 \text{ in.}$$

4. Calculate seam-to-seam length (L_{ss}). The seam-to-seam length of the vessel should be determined from the geometry of the vessel once a diameter and weight of liquid volume are known.

$$L_{ss} = \frac{h + 76}{12} \text{ (in.)} \quad \text{or} \quad L_{ss} = \frac{h + D + 40}{12}$$

$$= \frac{8.6 + 76}{12} = 7.05 \text{ ft}$$

5. Compute slenderness ratio (L_{ss}/D), which is usually in the range 3 to 4, such that

$$\frac{L_{ss}}{D} = \frac{7.05 \times 12}{20} = 4.23$$

6. Choosing the diameter, because (L_{ss}/D) > 4 lets assume higher diameter $D = 24$ (next higher diameter from Table 6-36).

$$\text{Vol} = 0.2618h$$

$$t = \frac{0.2618h}{0.000065Q_L} = 4,028 \frac{h}{Q_L}$$

If

$$t = 1 \text{ min}$$

then

$$h = \frac{2,000}{4,028} = 0.5 \text{ ft} = 6 \text{ in.}$$

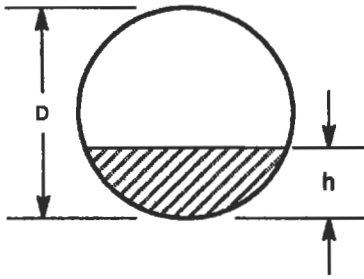
$$L_{ss} = \frac{6 + 76}{12} = 6.83 \text{ ft} = 82 \text{ in.}$$

$$\frac{L_{ss}}{D} = \frac{82}{24} = 3.4$$

Proper size of separator is 24 in. \times 7 ft.

Horizontal Separators

In the case of horizontal separators, the gas drag force does not directly oppose the gravitational settling force. The true droplet velocity is assumed to be the vector sum of the vertical terminal velocity and the horizontal gas velocity. The minimum length of the vessel is calculated by assuming the time for the gas to flow from the inlet to outlet is the same as the time for the droplet to fall from the top of the vessel to the surface of the liquid. In calculating the gas capacity of horizontal separators, the cross-sectional area of that portion of the vessel occupied by liquid (at maximum level) is subtracted from the total vessel cross-sectional area, as shown in Figure 6-181.



h/D	F	h/D	F
0	1.0	0.30	0.748
0.05	0.981	0.35	0.688
0.10	0.948	0.40	0.628
0.15	0.906	0.45	0.564
0.20	0.858	0.50	0.500
0.25	0.804	0.55	0.436

Figure 6-181. The fraction of the total area available for gas flow in horizontal separator.

Separators can be any length, but the ratio L_{ss} to D of vessel is usually in the range 2:1 to 4:1, so that

$$V_t = K \left(\frac{\gamma_L - \gamma_g}{\gamma_g} \right) \left(\frac{L}{10} \right)^{0.56} \quad (\text{ft/s}) \quad (6-269)$$

Sometimes separators without mist extractors are sized using Equation 6-268 with a constant K of typically one-half of that used for vessels with mist extractors.

Example 2

Solve Example 1 in case of horizontal separator with mix extractor if $F = 0.564$ and 0.436 .

1. Find K value from Table 6-39 where $K = 0.3$.
2. The gas capacity constraint is determined from

$$V_g = \frac{Q}{A_g}$$

$$A_g = 0.564 \times \frac{\pi}{4} D^2 = 0.443 D^2$$

$$Q = Q_g \times \frac{10^6 \text{ scf}}{\text{MMscf}} \times \frac{\text{day}}{24 \text{ hr}} \times \frac{\text{hr}}{3,600 \text{ s}} \times \frac{14.7}{P} \times \frac{TZ}{520} = 0.327 \frac{TZ}{P} Q_g$$

$$V_g = \frac{0.327 T Z Q_g}{0.443 D^2 P} = 0.74 \frac{T Z Q_g}{D^2 P}$$

The residence time of the gas (t_g) has to be equal to the time required for the droplet to fall to the gas-liquid interface t_f :

$$t_g = \frac{L_{\text{eff}}}{V_g} = \frac{\text{Effective length for separator}}{\text{Gas velocity}} = \frac{L_{\text{eff}} D^2 P}{0.74 T Z Q_g}$$

$$t_d = \frac{D - h}{V_t}$$

If $F = 0.564$, then $h/D = 0.45$, where $h = 0.45D$ and $t_d = 0.55D/V_t$.
If $L_{ss} = L_{eff} + D$ for gas capacity, the

$$V_t = K \left(\frac{\gamma_L - \gamma_g}{\gamma_g} \right)^{0.5} \left(\frac{L_{eff} + D}{10} \right)^{0.56}$$

and

$$t_d = \frac{0.55D}{0.3 \left(\frac{\gamma_L - \gamma_g}{\gamma_g} \right)^{0.5} \left(\frac{L_{eff} + D}{10} \right)^{0.56}}$$

where $t_g = t_d$ and

$$\frac{L_{eff} D^2 P}{0.74 T Z Q_g} = \frac{0.55 D}{0.3 \left(\frac{\gamma_L - \gamma_g}{\gamma_g} \right)^{0.5} \left(\frac{L_{eff} + D}{10} \right)^{0.56}}$$

$$D^2 L_{eff} = \frac{6D}{(L_{eff} + D)^{0.56}}$$

From the above constraint for given D , L_{eff} could be calculated, but gas capacity does not govern.

3. Liquid capacity constraint is calculated from

$$t_r = \frac{\text{Vol.}}{Q}$$

$$\begin{aligned} \text{where Vol.} &= (\pi D^2/4)(1 - F)L_{eff} = 0.343 D^2 L_{eff} \\ Q &= Q_L \times 5.615 (\text{ft}^3/\text{barrel}) \times (\text{day}/24 \text{ hr}) \times (\text{hr}/3,600 \text{ s}) = 0.000065 Q_L \\ t_r &= 0.343 D^2 L_{eff} / 0.000065 Q_L \\ D^2 L_{eff} &= (t_r \times 0.000065 Q_L) / 0.343 \end{aligned}$$

If t_r is in minutes, then an $D^2 L_{eff} = 0.01137 t_r Q_L$.

4. Assume retention time $t_r = 1$ min. Compute combination D (see Table 6-37) and L_{eff} , such that

$$D = 2 \text{ ft} \quad L_{eff} = 5.7 \text{ ft} \quad L_{ss} = \frac{4}{3} L_{eff} = 7.6 \text{ ft}$$

$$D = 2.5 \text{ ft} \quad L_{eff} = 3.6 \text{ ft} \quad L_{ss} = \frac{4}{3} L_{eff} = 4.9 \text{ ft}$$

5. Compute slenderness $(L_{ss}/D) = 3.8$ and 1.96 , respectively. $D = 2$ ft is a proper size.

A second case is where $F = 0.436$. The gas capacity constant is determined from

$$V_g = \frac{Q}{A_g} \quad \text{where} \quad Q = 0.327 \frac{TZQ_g}{P}$$

$$A_g = 0.436 \times \frac{\pi}{4} D^2 = 0.342D^2$$

$$V_g = \frac{0.327TZQ_g}{0.342D^2P} = 0.96 \frac{TZQ_g}{D^2P}$$

$$t_g = \frac{L_{\text{eff}}}{V_g} = \frac{L_{\text{eff}}D^2P}{0.96TZQ_g}$$

$$t_d = \frac{D-h}{V_t} \quad \text{if} \quad F = 0.436, \quad \frac{h}{D} = 0.55, \quad h = 0.55D$$

$$t_d = \frac{0.45D}{V_t} \quad \text{if} \quad V_t = K \times 3.587 \left(\frac{L_{\text{ss}}}{10} \right)^{0.56}$$

$L_{\text{ss}} = L_{\text{eff}} + D$ for gas capacity, such that

$$V_t = 0.988K(L_{\text{eff}} + D)^{0.56} \quad \text{where} \quad K = 0.3$$

$$t_d = \frac{1.52D}{(L_{\text{eff}} + D)^{0.56}}$$

$$t_g = t_d$$

$$\frac{L_{\text{eff}}D^2P}{0.96TZQ_g} = \frac{1.52D}{(L_{\text{eff}} + D)^{0.56}}$$

Substituting Q_g , P , T , Z gives

$$L_{\text{eff}}D^2 = \frac{6.4D}{(L_{\text{eff}} + D)^{0.56}}$$

Liquid capacity constraint is determined from

$$t_r = \frac{\text{Vol.}}{Q}$$

where $\text{Vol.} = (\pi D^2/4)(1 - F)L_{\text{eff}} = 0.443D^2L_{\text{eff}}$

$$\begin{aligned}
 Q &= 0.000065Q_L \\
 t_r &= 0.443D^2L_{\text{eff}}/0.000065Q_L \quad \text{if } t_r \text{ is in min} \\
 D^2L_{\text{eff}} &= 0.0088 t_r Q_L
 \end{aligned}$$

Assume retention time $t_r = 1$ min and $D = 2$ ft

$$L_{\text{eff}} = \frac{0.0088 \times 1 \times 2,000}{4} = 4.4 \text{ ft}$$

$$L_{\text{ss}} = \frac{4}{3} \times 4.4 = 5.9 \text{ ft}$$

$$D = 2.5$$

$$L_{\text{eff}} = \frac{0.0088 \times 1 \times 2,000}{2.5 \times 2.5} = 2.8 \text{ ft}$$

$$L_{\text{ss}} = \frac{4}{3} \times 2.8 = 3.8 \text{ ft}$$

As you can see, the liquid level has significant meaning for separator length. Usually, the fraction of the total area F available for gas flow is equal to 0.5. The liquid level control placement of a horizontal separator is more critical than in a vertical separator and the surge space is somewhat limited.

For the above two-phase, oil-gas separation calculation, a FORTRAN program is available [123].

Vessel Internals [124]

The proper selection of internals can enhance significantly the operation of separators. Proprietary internals often are helpful in reducing liquid carryover at design conditions. But they cannot overcome a basically improper design or operation at off-design conditions.

Production equipment involving the separation of oil and gas often uses impingement-type mist-extraction elements. This element is usually of the vane type or of knitted wire.

The vane type consists of a labyrinth formed with parallel metal sheets with suitable liquid collection "pockets." The gas, in passing between plates, is agitated and has to change direction a number of times. Obviously, some degree of centrifugation is introduced, for as the gas changes direction the heavier particles tend to be thrown to the outside and are caught in the pockets provided.

Coalescence of small particles into those large enough to settle by gravity is provided by two mechanisms: agitation and surface. The surface of the element is usually wet, and small particles striking it are absorbed. Inasmuch as the pockets are perpendicular to the gas flow, the liquid thus formed does not have to flow against the gas. Consequently, small compact units have a large capacity.

As the plates are placed closer together and more pockets are provided, greater agitation, centrifugal force and collection surface are provided, but the pressure drop is increased correspondingly. Thus, for a given flowrate, the collection efficiency is normally some function of the pressure drop.

In the average application this pressure drop varies from 1.2 to 10 in. (3 to 25 cm) of water. Because of this pressure drop and to prevent gas bypassing the extractor, a liquid-collection pan incorporating a liquid seal is necessary for the liquid to drain properly.

Increased use has been made of mist extractors composed of a knitted wire mesh supported on a lightweight support. This material has given generally favorable results and has a low installed cost.

The element consists of wire knitted into a pad having a number of unaligned, asymmetrical openings. Although similar in appearance to filter media, its action is somewhat different. The latter are rather dense and have small openings. This knitted wire, on the other hand, has about 97 to 98% free voids and collects the particles primarily by impingement.

The material is available in single wound units of varying thickness in diameters up to 35 in. (90 cm) or in laminated strips for insertion through manholes in large process vessels.

The principle of separation is similar to that of the vane-type unit. The gas flowing through the pad is forced to change direction a number of times, although centrifugal action is not so pronounced. Impingement is the primary mechanism.

A liquid particle striking the metal surface, which it does not "wet," flows downward where adjacent wires provide some capillary space. At these points, liquid collects and continues to flow downward. Surface tension tends to hold these drops on the lower face of the pad until they are large enough for the downward force of gravity to exceed that of the upward gas velocity and surface tension.

Efficiency is a function of the number of targets presented. This may be accomplished by increasing the pad thickness, changing wire diameter, or the closeness of the weave.

The wire mesh normally used falls within the following range

Wire diameter—0.003–0.011 in. (0.0076–0.028 cm)
 Void volume—92 to 99.4%
 Specific weight—3–33 lb/ft³ (48–529 kg/m³)
 Surface area—50–600 ft²/ft³ (164–1970 m²/m³)

The most commonly used wire has a void volume of 97 to 98%, a bulk specific weight of approximately 12 lb/ft³ (192 kg/m³), a surface area of 100 to 125 ft²/ft³ (328–410 m²/m³), with a wire diameter of 0.011 in. (0.028 cm). A pad thickness of 4–6 in. (10–15 cm) is sufficient for most separator applications, although thicknesses up to 3 ft (0.9 m) have been reported. In separator service, 4–6 in. (10–15 cm) will normally suffice.

Any common metal may be used in these units, including carbon steel, stainless steel, aluminum, monel, etc. The pressure drop is a function of the entrainment load, the pad design, and gas velocity, but will not exceed 3 cm of water in the average installation. Because of this small pressure drop, the elements do not have to be "held down" and are normally only wired to the support grid to prevent shifting unless surging flow is anticipated.

Experience has shown that the support grid should contain at least 90% free area in order to eliminate any restrictions to liquid drainage. The pads are light in weight so that a light angle-iron support is adequate.

When both liquid and solids are present, a portion of the latter obviously will be scrubbed out. When only dry solids are present, the efficiency is substantially less. At the present time, though, this type unit is considered primarily for liquid removal.

Many vessel carryover problems are encountered. Foaming is a major culprit and requires more than simply better mist extraction. Most such problems develop by default. The vendor automatically uses his or her standard sizing curves and equipment, and the buyer assumes this will be good enough.

With glycols, amines and similar materials, which tend to foam, I would normally specify a dual mist extractor—the lower one being of the vane type and the upper one being a wire mesh. A space of 6–12 in. (15–30 cm) would be left between them. The vane type will handle large volumes of liquid but is relatively inefficient on small droplets. It, therefore, serves as a bulk removal device (and helps coalesce foam). The wire mesh, which has limited liquid capacity, may therefore operate more effectively.

When using the vane-type mist extractor one must be careful that the pressure drop across it does not exceed its height above the liquid level if a downcomer pipe is used. Otherwise, liquid will be “sucked out” overhead. The downcomer pipe can become partially plugged to accentuate the problem. Two wire mesh pads may be used in like fashion, with the first being used as a coalescer. As a rule of thumb, the coalescer pad should have about half the free space area of the second pad. Any wire mesh pad should be installed so that the flow is perpendicular to the pad face (pad is horizontal in a vertical vessel).

With materials like glycol and amine, which wet metal very well, Teflon-coated mesh may prove desirable. Remember, the liquid must be nonwetting in order to stay as droplets that can run down the wires and coalesce into bigger droplets. A wetting fluid will tend to “run up” the wires.

It has been noted that centrifugal force is an integral part of separation processes. The standard oil and gas separator may have an inlet that utilizes centrifugal force to separate the larger droplets.

The same principle is used in some mist-extractor elements except that higher velocities are needed to separate the smaller droplets. The velocity needed for separation is a function of the particle diameter, particle and gas specific weight and the gas viscosity.

With a given system, the size of particle collected is inversely proportional to the square root of the velocity. Consequently, the success of a cyclonic mist extractor is dependent on the velocity attained. Furthermore, the velocity needed to separate a given size of particle must increase as the density of the particle becomes less. In addition to producing the necessary velocity, the mist extractor must provide an efficient means of collecting and removing the particles collected in order to prevent reentrainment.

One common type of equipment is often called a *steam separator* since it has been widely used to separate condensate and pipe scale in steam systems. It is normally a relatively small vessel that imparts a high velocity to the incoming gas and then makes the gas change direction radically to prevent reentrainment. In general, it will separate particles 40 and larger very efficiently.

Another type uses the same principle but, in addition, forces the gas to pass through a labyrinth that introduces impingement effects and forces the gas to change direction a number of times. This is, in reality, a combination type and is relatively efficient. The general performance characteristics are the same as efficient mist extractors of other types. Some, however, are complex and relatively expensive.

Gas–Oil–Water Separation

Two liquids and gas or water–oil–gas separation can be easily accomplished in any type of separator by installing either special internal baffling to construct

a water lap or crater siphon arrangement or by use of an interface liquid level control. A three-phase feature is difficult to install in a spherical due to the limited internal space available. With three-phase separation two liquid level controls and two liquid damp valves are required. Figures 6-182 to 6-184 illustrate schematic three-phase separators. The basic design aspects of three-phase

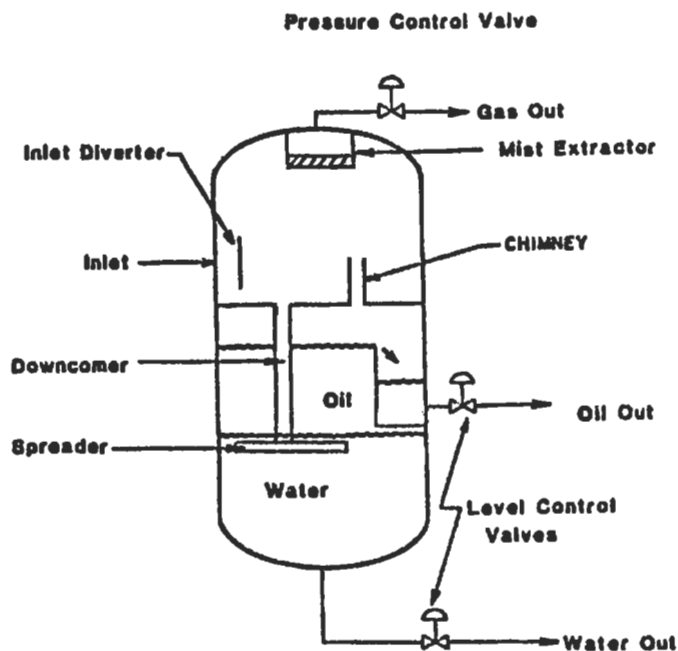


Figure 6-182. Water-oil-gas vertical separator [119].

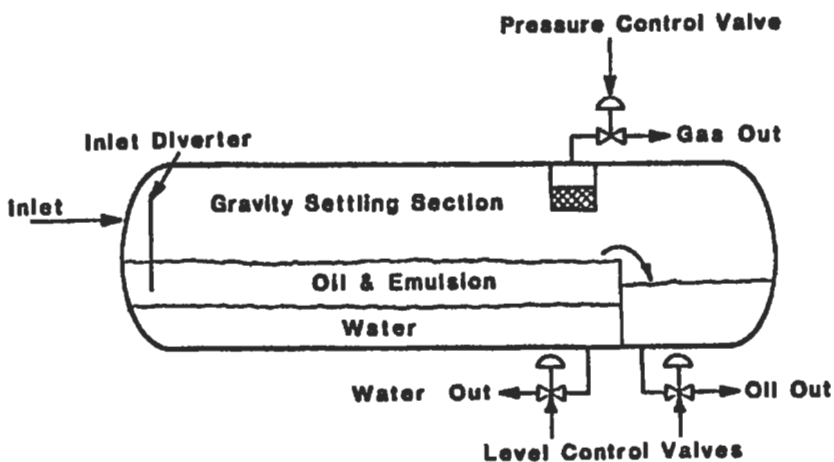


Figure 6-183. Three-phase horizontal separator [119].

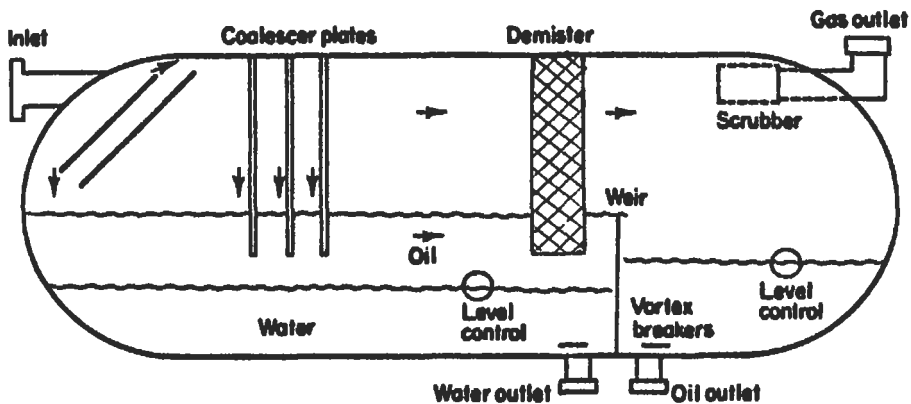


Figure 6-184. Three-phase horizontal separator with coalescer plates.

separation have been covered under “Sizing of Two-Phase Oil-Gas Separators.” Regardless of shape, all three-phase vessels must meet the following requirements:

- Liquid must be separated from gas in a primary separating section.
- Gas velocity must be lowered to allow liquids to drop out.
- Gas must be scrubbed through an efficient mist extractor.
- Water and oil must be diverted to a turbulence-free section of the vessel.
- Liquids must be retained in the vessel long enough to allow separation.
- The water-oil interface must be maintained.
- Water and oil must be removed from the vessel at their respective outlets.

Sizing a three-phase separator for water removal is mainly a function of retention time. Required retention time is related to the volume of the vessel, the amount of liquid to be handled and the relative specific gravities of the water and oil. The effective retention volume in a vessel is that portion of the vessel in which the oil and water remain in contact with one another. As far as oil-water separation is concerned, once either substance leaves the primary liquid section, although it may remain in the vessel in a separate compartment, it cannot be considered as a part of the retention volume. There are two primary considerations in specifying retention time:

- oil settling time to allow adequate water removal from oil
- water settling time to allow adequate oil removal from water

Basic design criteria for liquid retention time in three-phase separators are given in the Table 6-40 [117].

Example 3

Determine the size of a vertical separator to separate: 6,300 bpd of oil from its associated gas, water 500 bpd ($SG = 0.75$) at a pressure of 300 psig and a temperature with $SG_g = 1.03$, 100°F . The oil has a density of 49.7 lb/ft^3 and solution gas/oil ratio^o of 580 scf/STB at 60°F and 14.7 psia.

- The gas capacity constraint $V_g = V_v$, such that

Table 6-40
Typical Retention Time for Liquid-Liquid Separation [117]

<u>Type of Separation</u>	<u>Retention Time</u>
Hydrocarbon/Water Separators	
Above 35° API Hydrocarbon	3 to 5 min.
Below 35° API Hydrocarbon	
100 °F and above	5 to 10 min.
80 °F	10 to 20 min.
60 °F	20 to 30 min.
Ethylene Glycol/Hydrocarbon Separators (Cold Separators)	20 to 60 min.
Amine/Hydrocarbon Separators	20 to 30 min.
Coalescers, Hydrocarbon/Water Separators	
100 °F and above	5 to 10 min.
80 °F	10 to 20 min.
60° F	20 to 30 min.
Caustic/Propane	30 to 45 min.
Caustic/Heavy Gasoline	30 to 90 min.

$$V_g = \frac{Q}{A_g} \quad Q = \frac{R_s \times Q_o}{86,400} \times \frac{14.7}{P} \times \frac{TZ}{520}$$

$$P = 300 \quad T = 560 \quad Z = 0.94 \text{ (from chart)}$$

$$Q = 2.1 \text{ ft}^3/\text{s}$$

$$A_g = \frac{\pi D^2}{4} = 0.785D^2$$

$$V_t = K \left(\frac{\gamma_o - \gamma_g}{\gamma_g} \right)^{0.5} \quad K = 0.33 \text{ (from Table 6.39)}$$

$$\gamma_o = 49.7 \text{ lb/ft}^3$$

$$\gamma_g = \frac{PM}{ZRT} = \frac{300 \times 29 \times 0.75}{0.94 \times 10.73 \times 560} = 1.155 \text{ lb/ft}^3$$

$$\left(\frac{\gamma_o - \gamma_g}{\gamma_g} \right)^{0.5} = \left(\frac{49.7 - 1.155}{1.155} \right)^{0.5} = 6.48$$

$$V_t = 2.14 \text{ ft/s}$$

$$\frac{2.1 \text{ ft}^3}{S \times 0.785D^2} = 2.14 \text{ ft/s}$$

$$D = 1.117 \text{ ft} = 13.4 \text{ in.}$$

2. Calculate minimum diameter from requirement for water droplets to fall through oil layer. Use 500- μm droplets if no other information is available. For μ_0 assume 3.0 cp.

$$V_t = V_0$$

According to Stokes law

$$V_t = 2,660 \frac{(\gamma_w - \gamma_o)}{\mu} D_p^2$$

$$V_t(\text{ft/s}); \gamma_w, \gamma_o(\text{lb/ft}^3); D_p(\text{ft}); \mu(\text{cp})$$

$$V_0 = \frac{Q}{A} \quad Q(\text{ft}^3/\text{s}); A(\text{ft}^2); Q_0(\text{bpd})$$

$$Q = 6.49 \times 10^{-5} Q_0$$

$$A = \frac{\pi D^2}{4} = 0.785D^2 \quad \text{where } D \text{ is in ft}$$

$$V_0 = \frac{6.49 \times 10^{-5} Q_0}{0.785D^2} = 8.27 \times 10^{-5} \frac{Q_0}{D^2}$$

$$8.27 \times 10^{-5} \frac{Q_0}{D^2} = 2,660 \left(\frac{\gamma_w - \gamma_o}{\mu_0} \right) D_p^2$$

$$D_p = 500 \mu\text{m} = 500 \times 3.2808 \times 10^{-6} \text{ ft}$$

$$D_p = 1.64 \times 10^{-3} \text{ ft}$$

$$D = \left[\frac{8.27 \times 10^{-5} Q_0 \mu_0}{2,660(\gamma_w - \gamma_o) D_p^2} \right]^{0.5} = 4.15 \text{ ft} = 49.8 \text{ in.}$$

3. Calculate the total weight of oil and water in separator ($h_o + h_w$)

$$t_r = \frac{\text{Vol.}}{Q}$$

$$\text{Vol.} = \frac{\pi D^2}{4} h$$

$$Q = 6.49 \times 10^{-5} Q_L \text{ if } t \text{ is in min}$$

$$t_r 60 = \frac{\pi D^2 h}{4 \times 6.49 \times 10^{-5} Q_L} \quad Q_L (\text{bpd})$$

$$D^2 h = 4.958 \times 10^{-3} Q_L t_r$$

For two-phase separator design

$$D^2 h_o = 4.958 \times 10^{-3} Q_o(t_r)_o$$

$$D^2 h_w = 4.958 \times 10^{-3} Q_w(t_r)_w$$

$$h_o + h_w = 4.958 \times 10^{-3} \frac{Q_o(t_r)_o + Q_w(t_r)_w}{D^2}$$

where h_o = height of oil pad in ft

h_w = height from water outlet to interface in ft

Choose a nominal diameter from Table 6-36 considering minimum diameter in pts 2.54 in. (4.5 ft) is a proper choice. $(t_r)_o = (t_r)_w = 5$ min from Table 6-40.

$$h_o + h_w = 4.958 \times 10^{-3} \frac{500 \times 5 + 6,300 \times 5}{(4.5)^2} = 8.32 \text{ ft}$$

if $D = 5$ ft $h_o + h_w = 6.74$ ft

4. Calculate seam-to-seam length and slenderness ratios for $D = 4.5$ ft:

$$L_{ss} = h_o + h_w + \frac{76}{12} = 8.32 + 6.33 = 14.6 \text{ ft}$$

$$\frac{L_{ss}}{D} = \frac{14.6 \text{ ft}}{4.5} = 3.2 \quad \text{for } D = 5 \text{ ft}$$

$$L_{ss} = 6.74 + \frac{76}{12} = 13 \text{ ft}$$

$$\frac{L_{ss}}{D} = \frac{13 \text{ ft}}{5} = 2.6$$

Vertical three-phase separators have slenderness ratios on the order of 15 to 3. In this case both diameters are acceptable.

Example 4

Determine the size of a horizontal separator for data given in Example 3 and $F = 0.5$.

1. Gas capacity constraint: $t_g = t_d$

$$V_g = \frac{Q}{A_g}$$

$$Q = \frac{R \times Q_0}{86,400} \times \frac{14.7}{P} \times \frac{TZ}{520} = 2.1 \text{ ft}^3/\text{s}$$

$$A_g = \frac{\pi D^2}{4} \times F = 0.393 D^2$$

$$V_g = \frac{2.1 \text{ ft}^3/\text{s}}{0.393 D^2} = \frac{5.34}{D^2}$$

$$t_g = \frac{L_{\text{eff}}}{V_g} = \frac{L_{\text{eff}} D^2}{5.34}$$

$$t_d = \frac{D/2}{V_t} = \frac{D}{2V_t}$$

$$V_t = K \left(\frac{\gamma_L - \gamma_g}{\gamma_g} \right)^{0.5} \left(\frac{L_{\text{ss}}}{10} \right)^{0.56} = 0.33 \left(\frac{49.7 - 1.155}{1.155} \right)^{0.5} \left(\frac{L_{\text{eff}} + D}{10} \right)^{0.56}$$

$$= 0.589 (L_{\text{eff}} + D)^{0.56}$$

$$\frac{L_{\text{eff}} D^2}{5.34} = \frac{D}{0.589 (L_{\text{eff}} + D)^{0.56}}$$

$$L_{\text{eff}} D^2 = \frac{9.07 D}{(L_{\text{eff}} + D)^{0.56}}$$

For assumed D calculate L_{eff} :

D(ft)	L_{eff} (ft)
4.0	0.93
4.5	0.79
5.0	0.72

2. Calculate maximum oil pad thickness $(h_0)_{\text{max}}$. Use 500- μm droplet if no other information is available $t_w = t_0$:

$$t_w = \frac{h_0}{V_t} \quad V_t = 2,660 \frac{(\gamma_w - \gamma_0)}{\mu} D_p^2$$

$$t_w = \frac{h_0 \mu}{2,660(\gamma_w - \gamma_0) D_p^2}$$

$$t_0 = 60(t_r)_0 \quad t_r \text{ (min)}$$

$$\frac{h_0 \mu}{2,660(\gamma_w - \gamma_0) D_p^2} = 60(t_r)_0$$

$$h_0 = \frac{159,600(\gamma_w - \gamma_0) D_p^2 (t_r)_0}{\mu}$$

This is the maximum thickness the oil pad can be and still allow the water droplets to settle out in time $(t_r)_0$. If $D_p = 500 \mu\text{m} = 500 \times 3.2808 \times 10^{-6} \text{ ft} = 1.64 \times 10^{-3} \text{ ft}$

$$h_0 = \frac{0.43(\gamma_w - \gamma_0)(t_r)_0}{\mu}$$

For a given retention time (from Table 6-40 is equal 5 min) and a given water retention time (also 5 min) the maximum oil pad thickness constraint establishes a maximum diameter.

$$\gamma_w = 64.3 \text{ lb/ft}^3 \quad \gamma_0 = 49.7 \text{ lb/ft}^3 \quad \mu = 3 \text{ cp}$$

$$(h_0)_{\text{max}} = 10.46 \text{ ft}$$

3. Calculate the fraction of the vessel cross-sectional area occupied by the water phase (see Figures 6-181 and 6-185) A , A_w , A_0 (ft^2):

$$Q(\text{ft}^3/\text{s}) \quad t(\text{s}) \quad L_{\text{eff}}(\text{ft})$$

$$A = \frac{Q_t}{L_{\text{eff}}}$$

$$Q = 6.49 \times 10^{-5} Q_0, \quad \text{also } Q = 6.49 \times 10^{-5} Q_w$$

$$t_0 = 60(t_r)_0 \quad t = 60(t_r)_w$$

$$A_0 = 3.89 \times 10^{-3} \frac{Q_0(t_r)_0}{L_{\text{eff}}} \quad A_w = 3.89 \times 10^{-3} \frac{Q_w(t_r)_w}{L_{\text{eff}}}$$

$$A = 2(A_0 + A_w)$$

Hence

$$\frac{A_w}{A} = \frac{3.89 \times 10^{-3} Q_w(t_r)_w L_{\text{eff}}}{2L_{\text{eff}} 3.89 \times 10^{-3} [Q_w(t_r)_w + Q_0(t_r)_0]} = \frac{0.5 Q_w(t_r)_w}{Q_w(t_r)_w + Q_0(t_r)_0}$$

4. From Figure 6-185 determine the coefficient "d" and calculate D_{\max} for oil pad thickness constraint:

$$\frac{A_w}{A} = \frac{0.5(5)500}{500(5) + 6,300(5)} = 0.037$$

$$d = \frac{h_0}{D} = 0.43$$

$$D_{\max} = \frac{(h_0)_{\max}}{d} = \frac{10.46}{0.43} = 24.3 \text{ ft}$$

D_{\max} depends on Q_0 , Q_w , $(t_r)_0$ and $(t_r)_w$.

5. Liquid retention constraint:

$$t = \frac{\text{Vol.}}{Q}$$

$$\text{Vol.} = \frac{1}{2} \left(\frac{\pi D^2}{4} L_{\text{eff}} \right) = 0.393 D^2 L_{\text{eff}}$$

$$(\text{Vol.})_0 = 0.393 D^2 L_{\text{eff}} \left(\frac{A_0}{A_{\text{liq}}} \right)$$

$$(\text{Vol.})_w = 0.393 D^2 L_{\text{eff}} \left(\frac{A_w}{A_{\text{liq}}} \right)$$

Q_0 and Q_w are in bpd:

$$Q = 6.49 \times 10^{-5} Q_0 \quad Q = 6.49 \times 10^{-5} Q_w$$

$$t_0 = \frac{0.393 D^2 L_{\text{eff}} \left(\frac{A_0}{A_{\text{liq}}} \right)}{6.49 \times 10^{-5} Q_0}$$

$$\frac{Q_0 t_0}{D^2 L_{\text{eff}}} = 6,055 \frac{A_0}{A_{\text{liq}}}, \quad \text{also} \quad \frac{Q_w t_w}{D^2 L_{\text{eff}}} = 6,055 \frac{A_w}{A_{\text{liq}}}$$

$(t_r)_0$ and $(t_r)_w$ are in min.

$$\frac{Q_0 (t_r)_0}{D^2 L_{\text{eff}}} = 101 \frac{A_0}{A_{\text{liq}}} \quad \frac{Q_w (t_r)_w}{D^2 L_{\text{eff}}} = 101 \frac{A_w}{A_{\text{liq}}}$$

Adding by sides

$$\frac{Q_o(t_r)_o + Q_w(t_r)_w}{D^2 L_{\text{eff}}} = 101 \frac{A_o + A_w}{A_{\text{liq}}} = 101$$

$$D^2 L_{\text{eff}} = 0.0099 [Q_o(t_r)_o + Q_w(t_r)_w]$$

for given $(t_r)_o = (t_r)_w = 5$ min, and

$$Q_o = 6,300 \text{ bpd} \quad Q_w = 500 \text{ bpd}$$

$$D^2 L_{\text{eff}} = 0.0099 [500(5) + 6,300(5)] = 336.6$$

6. Compute combinations of D and L_{eff} :

$$L_{\text{ss}}, \quad \text{where} \quad L_{\text{ss}} = L_{\text{eff}} \frac{4}{3} \quad \text{and} \quad \frac{L_{\text{ss}}}{D}$$

D(ft)	L_{eff} (ft)	L_{ss}	L_{ss}/D
5.0	13.5	18.0	3.5
5.5	11.1	14.8	2.7
4.5	16.6	22.2	4.9

For three-phase horizontal separators, slenderness ratio is in the range of 3 to 5 usually, so $D = 4.5$ and 5 ft are proper choices.

As we can see, liquid retention constraint limits three-phase separator size, gas capacity and oil pad thickness does not govern.

Two-Stage Separation Systems

In high-pressure gas-condensate separation systems, it is generally accepted that a stepwise reduction of the pressure on the liquid condensate will appreciably increase the recovery of stock tank liquids. The calculation of the actual performance of the various separators in a multistage separation system can be made, using the initial wellstream composition and the operating temperatures and pressures of the various stages. Theoretically, three to four stages of separation would increase the liquid recovery over two stages; the net increase over two-stage separation will rarely pay out the cost of the second and/or third separator. Therefore, it has been generally accepted that two stages of separation plus the stock tank are the most optimum considered. The actual increase in liquid recovery for two-stage separation over single stage may vary from 3 to 15% (sometimes even more) depending on the wellstream composition, operating pressures and temperatures.

The optimum high stage or first separator operating pressure is generally governed by the gas transmission line pressure and operating characteristics of the well. This will generally range in pressures from 600 to 1,200 psia (41.4 to 82.7 bar). For each high or first-stage pressure there is an optimum low-stage separation pressure that will afford the maximum liquid recovery. This operating

pressure can be determined from an equation based on equal pressure ratios between the stages

$$R = \left(\frac{P_1}{P_s} \right)^{0.5} \quad \text{or} \quad P_2 = \frac{P_1}{R} = P_s R^{n-1} \quad (6-270)$$

where R = pressure ratio
 n = number of stages
 P_1 = first-stage separator pressure in psia
 P_2 = second-stage separator pressure in psia
 P_s = stock tank pressure in psia

Figure 6-182 illustrates a schematic flow diagram of a typical high-pressure well production equipment installation [125]. The basic equipment is illustrated for two-stage separation of the high-pressure stream. From the wellhead, the high-pressure wellstream flows through a high-pressure separator and indirect heater gas production unit. In this unit the inlet stream is heated prior to choking to reduce the wellstream pressure to sales line pressure. This is done to prevent the formation of hydrates in the choke or downstream of the choke in the separator or sales line. From the indirect heater the wellstream passes to the high-pressure separator where the initial separation of the high-pressure gas stream and produced well fluids occur.

From the high-pressure separator the gas flows through an orifice meter and to the sales line. The liquid from the high-pressure separator passes through a diaphragm motor valve where the pressure is reduced, and it is discharged to a low-pressure flash separator. In the low-pressure flash separator that would operate at approximately 100 psi (6.9 bar), a second separation occurs between the liquids and the lighter hydrocarbons in the liquids. The gas released from the low-pressure flash separator is returned back to the high-pressure unit where it may be used for both instrument and fuel gas for the indirect heater. As illustrated in Figure 6-175, a secondary makeup line is shown from the high-pressure separator, which would provide additional makeup gas for the instrument gas and fuel gas, if not enough gas was released from the low-pressure separator. Typically though, more gas is released than is required and the additional low pressure gas may be sold in a low-pressure gas gathering system and/or used for other utility purposes, such as fuel for compressor engines or other fired equipment in the area. This may be for reboilers for dehydrators or acid gas sweetening units, etc. From the low-pressure flash separator the liquid is discharged through another diaphragm motor valve into a storage tank that is generally operated at atmospheric pressure.

The additional features shown here that are different from a typical single-stage installation is the addition of the low-pressure flash separator between the liquid discharge from the high-pressure gas production unit and the storage tank. This provides for two stages of separation rather than one. This also provides a source of low-pressure gas that may be used for utility purposes with any excess sold, and increases the stabilization of the liquid product that in effect produces more liquid in the storage tank to be sold.

Example 5

Perform flash vaporization calculation to determine the increased recoveries that would be seen in both the low-pressure flash gas as well as increased liquid

recoveries in the storage tank. High-pressure gas $SG_g = 0.67$, the high-pressure separator pressures from 500 to 1,000 psi, the low-pressure separator $P = 100$ psi and the storage tank pressure $P_s = 14.7$ psia. Temperature for all vessels is the same, 70°F .

Results

Figure 6-183 illustrates the gas produced from the low-pressure flash separator for the above described wellstream at various high-pressure operating pressures (line pressure). The gas produced from the low-pressure flash separator in Mcf per year may be read from ordinate, based on the high-pressure gas stream flow rate in MMscfd and the high-pressure separator operating pressure.

Figure 6-184 illustrates the increase in stock tank liquid recovery that would be achieved by using the low-pressure flash separator. This chart is also based on the high-pressure gas flow rate in MMscfd and the high-pressure separator operating pressure. The increase in stock tank liquid recovery may be read from the chart in bbl/year.

This additional recovery not only gives profit, but prevents the unneeded waste of precious hydrocarbon energy that would normally be vented out the stock tank using only single-stage separation.

Crude Oil Treating Systems [119,126]

Water content of the untreated oil may vary from 1% to over 90%. Purchasers, depending on local conditions, accept a range of 0.2 to 3% of water in oil. When water forms a stable emulsion with crude oil and cannot be removed in conventional storage tanks, emulsion-treating methods must be used.

An emulsion is a heterogeneous liquid system consisting of two immiscible liquids with one of the liquids intimately disposed in the form of droplets in the second liquid (the water remaining is less than 10% of the oil). A common method for separating water-oil emulsion is to heat the stream. The use of heat in treating crude oil emulsions has four basic benefits

1. Heat reduces the viscosity of the oil, resulting in a greater force during collision of the water droplets.
2. Heat increases the droplets' molecular movement.
3. Heat can enhance the action of treating chemicals, causing the chemical to work faster to break the film surrounding the droplets of the dispersed phase of the emulsion.
4. Heat may increase the difference in density between the oil and the water, thus accelerating settling.

In general, at temperatures below 180°F (82°C), the addition of heat will increase the difference in density. Most light oils are treated below 180°F . For heavy crudes (below 20°API), heat may have a negative effect on difference in density.

In some cases, increased heat may cause the density of water to be less than that of oil, as it is shown in Figure 6-185. Adding heat changes the quality of the oil. The light ends are boiled off, and the remaining liquid has a lower API gravity and, thus, may have a lower value. Figure 6-186 illustrates typical gravity and volume losses for 33°API crude oil versus temperature. The molecules leaving the oil phase may be vented or sold. Heat can be added to the liquid by a direct heater, an indirect heater or any type of heat exchanger.

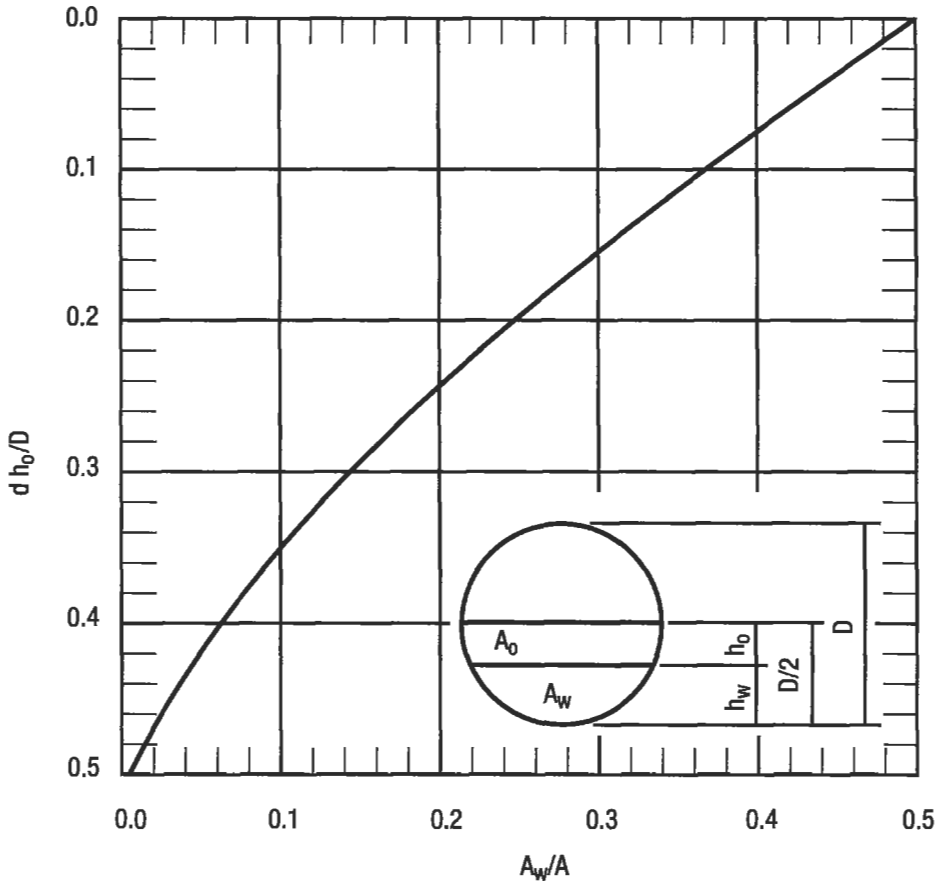


Figure 6-185. Coefficient "d" for a cylinder half filled with liquid [119].

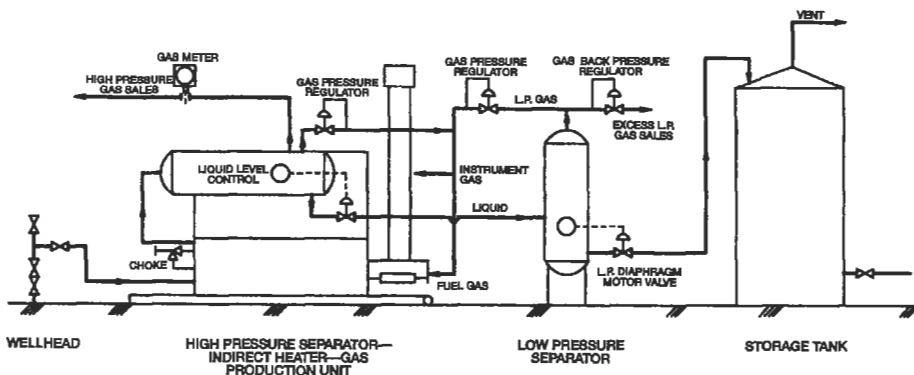


Figure 6-186. Two-stage separation system.

A direct fired heater is one in which the fluid to be heated comes in direct contact with the immersion-type heating tube or element of the heater. These heaters are generally used when large amounts of heat input are required and to heat low-pressure noncorrosive liquids. These units normally are constructed so that the heating tube can be removed for cleaning, repair or replacement.

An indirect fired heater is one in which the fluid passes through pipe coils or tubes immersed in a bath of water, oil, salt or other heat-transfer medium that, in turn, is heated by an immersion-type heating tube similar to the one used in the direct fired heater. Those heaters generally are used for high corrosive fluids, and are more expensive than direct fired heaters.

Heat exchangers are very useful where waste heat is recovered from an engine, turbine or other process stream or where fired heaters are prohibited.

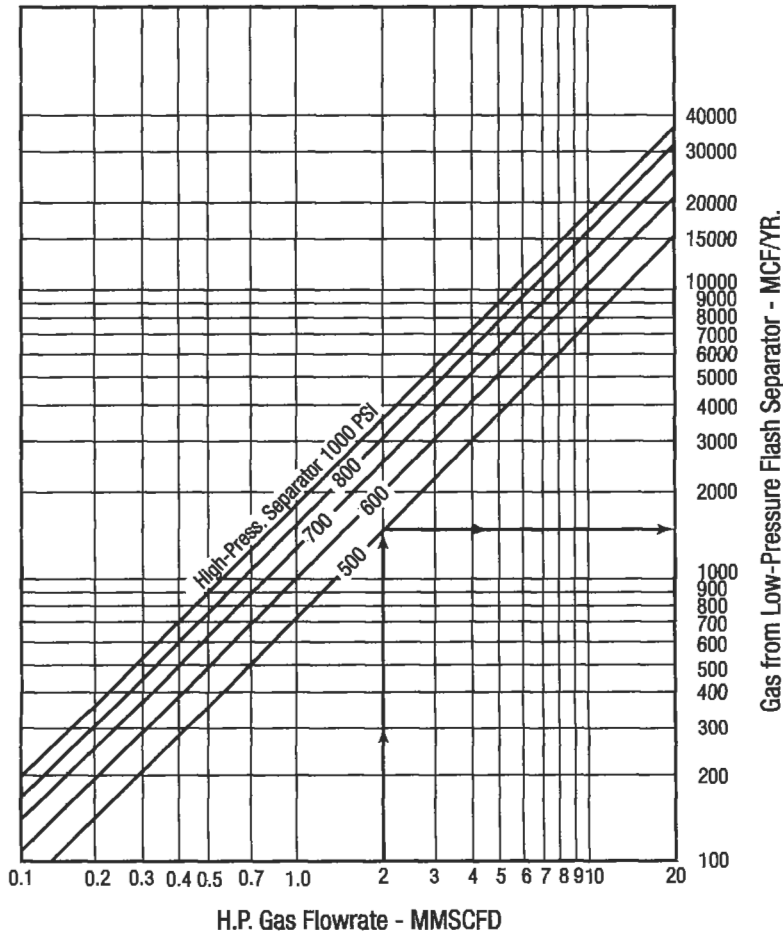


Figure 6-187. Low-pressure gas from flash separator [126].

Treating Equipment

All devices that accelerate the separation of two phases when the natural retention time is too long for commercial application, usually over 10 min., are called *treaters*. Emulsion treaters use some combination of heat, electricity, chemicals, retention time and coalescence to separate oil and water. Treater are designed as either vertical or horizontal vessels. The vertical treater is shown in Figure 6-188. Flow enters the top of the treater into a gas separation section. This section can be small if the treater is located downstream of a separator. The liquids flow through a downcomer to the base of the treater, which serves as a free-water knockout and water-wash section. If the treater is located downstream of a free-water knockout, the bottom section can be small. If the total wellstream is to be treated, this section should be sized for sufficient

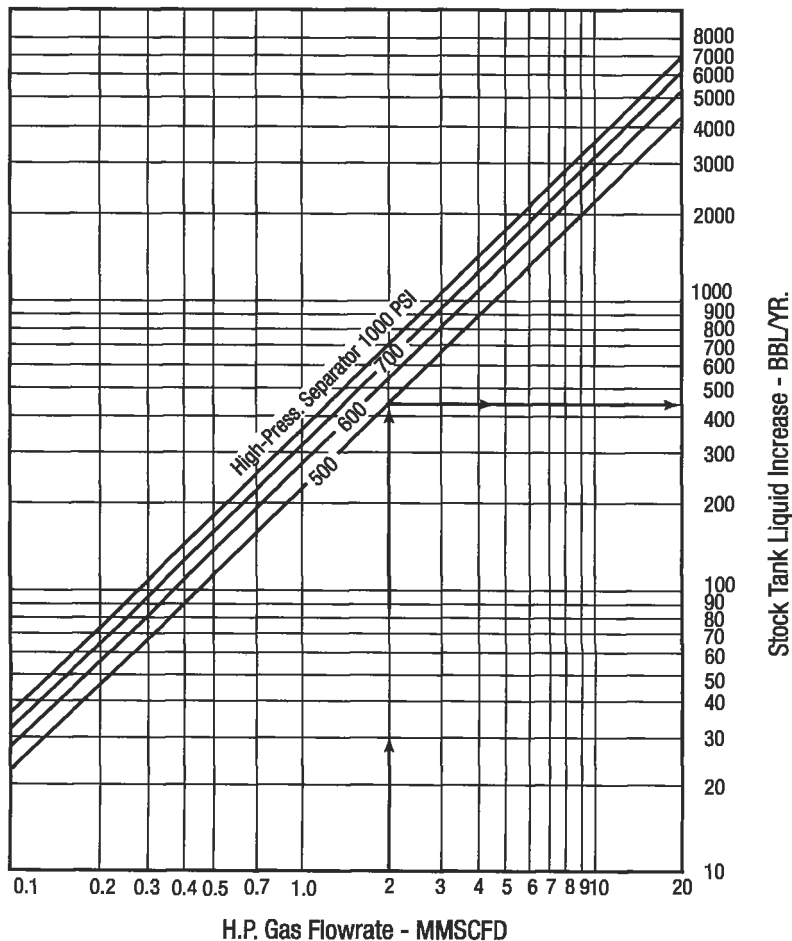


Figure 6-188. Stock tank liquid increase with flash separator [126].

retention time to allow the free water to settle out. This minimizes the amount of fuel gas needed to heat the liquid stream rising through the heating section. The oil and emulsion flows upward around the fire tubes to a coalescing section, where sufficient retention time is provided to allow the small water droplets to coalesce and to settle to the water section. Treated oil flows out the oil outlet. The oil level is maintained by pneumatic or lever-operated dump valves.

It is necessary to prevent steam from being formed on the fire tubes. This can be done by employing the "40° rule." That means that the operating pressure is kept equal to the pressure of saturated steam at a temperature equal to the operating temperature plus 40°F (4.5°C). The normal full-load temperature difference between the fire tube wall and the surrounding oil is approximately 30°F, allowing 10°F for safety; the 40° rule will prevent flashing of steam on the wall of the heating tube.

Low-pressure vertical flow treator, of large diameter, is called "gunbarrel" (Figure 6-189). Most gunbarrels are unheated, though it is possible to provide heat by heating the incoming stream external to the tank, installing heat coils in the tank, or circulating the water to an external heater in a closed loop

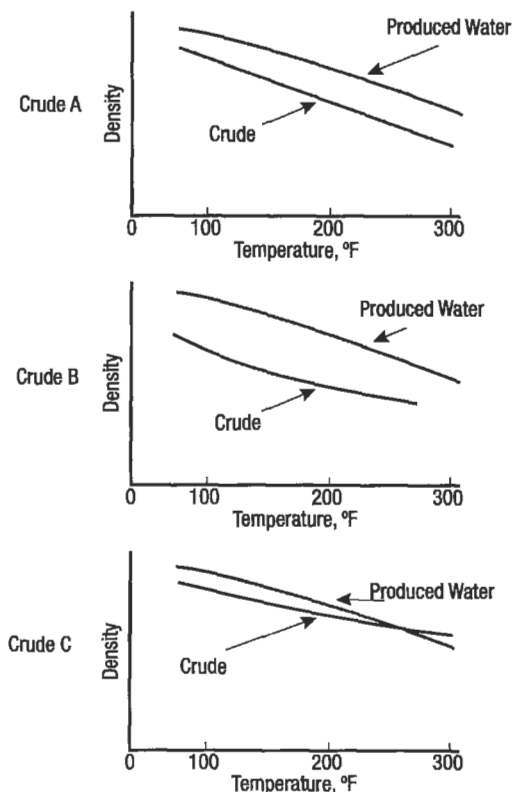


Figure 6-189. Relationship of specific gravity with temperature for three crude oils [126].

as shown in Figure 6-190. Heated gunbarrel emulsion treator is shown in Figure 6-191.

For higher flow inlet horizontal treators normally are preferred. A typical design of a horizontal treator is shown in Figure 6-192. Flow enters the front section of the treator where gas is flashed. The liquid flows downward to near the oil-water interface where the liquid is water-washed and the free water is separated. Oil and emulsion rises past the fire tubes and flows into an oil surge chamber. The oil-water interface in the inlet section of the vessel is controlled by an interface-level controller, which operates a dump valve for the free water. The oil and emulsion flows through a spreader into the back or coalescing section of the vessel, which is fluid-packed. The spreader distributes the flow evenly throughout the length of this section. Treated oil is collected at the top through a collection device used to maintain uniform vertical flow of the oil. Coalescing water droplets fall counter to the rising oil. The oil-water interface level is maintained by a level controller and dump valve for this section of vessel. A level control in the oil surge chamber operates a dump valve on the oil outlet line regulating the flow of oil out the top of the vessel and maintaining a liquid-packed condition in the coalescing section. Gas pressure on the oil in the surge section allows the coalescing section to be liquid-packed. The inlet section must be sized to handle separation of the free water and heating of the oil. The coalescing section must be sized to provide adequate retention time for coalescence to occur and to allow the coalescing water droplets to settle downward counter to the upward flow of the oil.

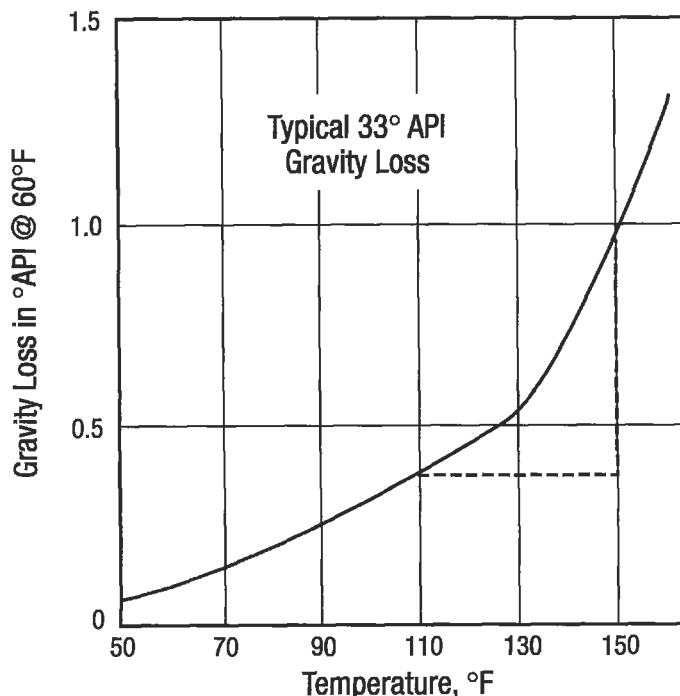


Figure 6-190. API gravity loss vs. temperature for crude oil [126].

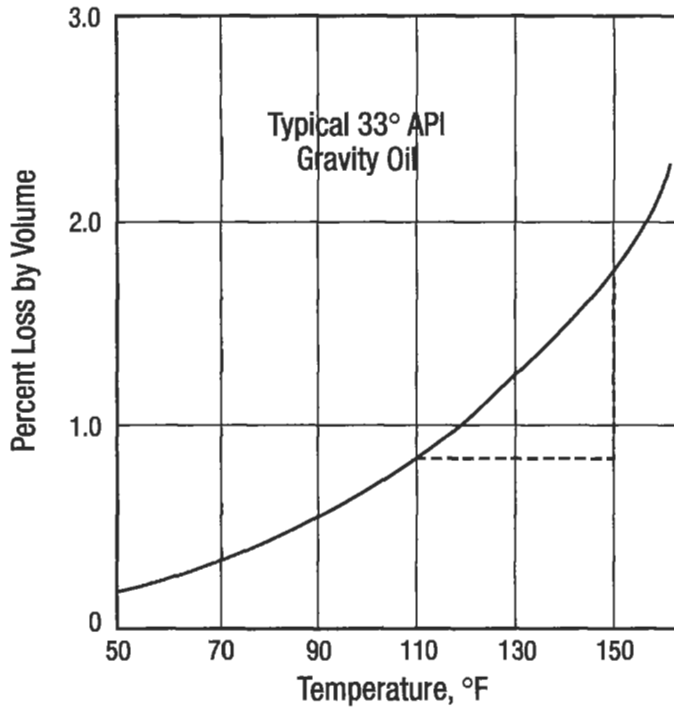


Figure 6-191. Percent loss by volume vs. temperature for crude oil [126].

Heat Input Requirement [122,127]

The required heat input for an insulated vessel can be calculated as

$$Q_{th} = \dot{w}c\Delta T$$

where Q_{th} = heat required in Btu/hr
 \dot{w} = weight flowrate in lb/hr
 c = specific heat constant at average temperature [Btu/(lb°F)] = 0.5 for oil and = 1.0 for water
 ΔT = temperature increase, assuming a water weight of 350 lb/bbl

$$Q_{th} = \frac{350}{24}q_o(SG_o)(0.5)\Delta T + \frac{350}{24}q_w(SG_w)(1.0)(\Delta T)$$

$$= 14.6\Delta T(0.5q_oSG_o + q_wSG_w)$$

If heat loss is assumed to be 10% of the heat input then

$$Q = \frac{Q_{th}}{0.9} = 16.2\Delta T(0.5q_oSG_o + q_wSG_w) \tag{6-271}$$

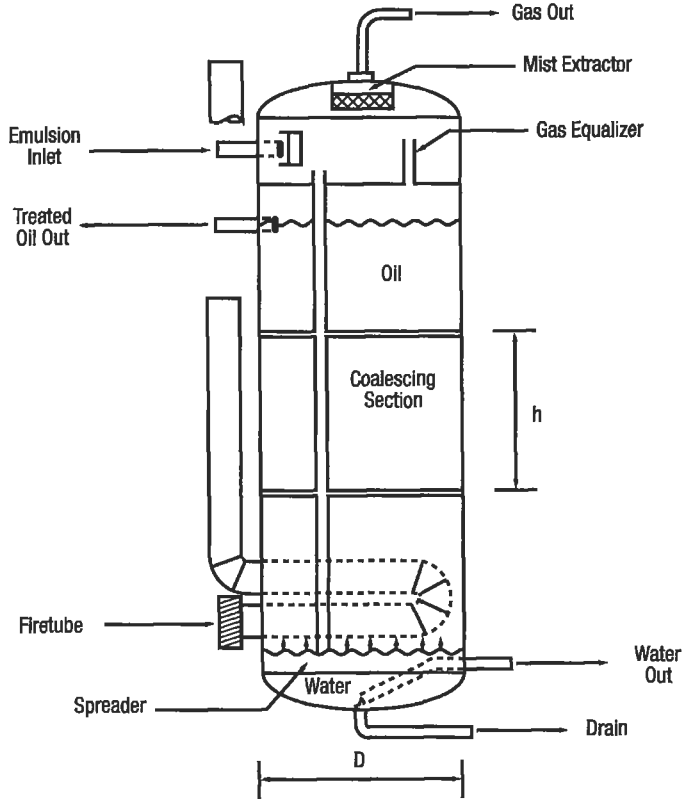


Figure 6-192. Vertical treater [119].

where q_o, q_w = oil and water flowrate in bpd
 SG_o, SG_w = specific gravity of oil and water

An alternative way is to employ the basic heat-transfer equation which is used in indirect heat sizing as follows:

$$Q = V_o A T_m \quad \text{or} \quad A = \frac{Q}{V_o T_m} \quad (6-272)$$

where Q = heat required in Btu/hr
 A = total heat transfer area (coil area) in ft^2
 T_m = log mean temperature difference in $^{\circ}F$

For low-pressure oil about 35°API and water liquid, streams, the heat required may be determined from the following equation:

$$Q = q_l [6.25 + 8.33(X)] \Delta T \quad (6-273)$$

where q_t = total liquid flowrate in bpd
 X = decimal water content in liquid
 ΔT = the difference between inlet and outlet temperature °F

The overall film or heat transfer coefficient for high-pressure gas streams may be found from Figure 6-193 using the gas flowrate and tube size selected. The overall film or heat transfer coefficient for water may be found from Figure 6-194 and the coefficient for oil from Figure 6-195, based on liquid flowrate and tube size. For liquid streams that are a mixture of oil and water, the overall coefficient may be averaged and calculated as

$$V_{0(\text{mix})} = V_{0(\text{oil})} + [V_{0(\text{water})} - V_{0(\text{oil})}]X \tag{6-274}$$

These film or heat-transfer coefficients are based on clean tubes; in other words, no allowance is made for any fouling factors. If any fouling is to be expected, excess coil area should be allowed in the heater selection.

$$T_m = \frac{GTD - LTD}{\ln \frac{GTD}{LTD}} \tag{6-275}$$

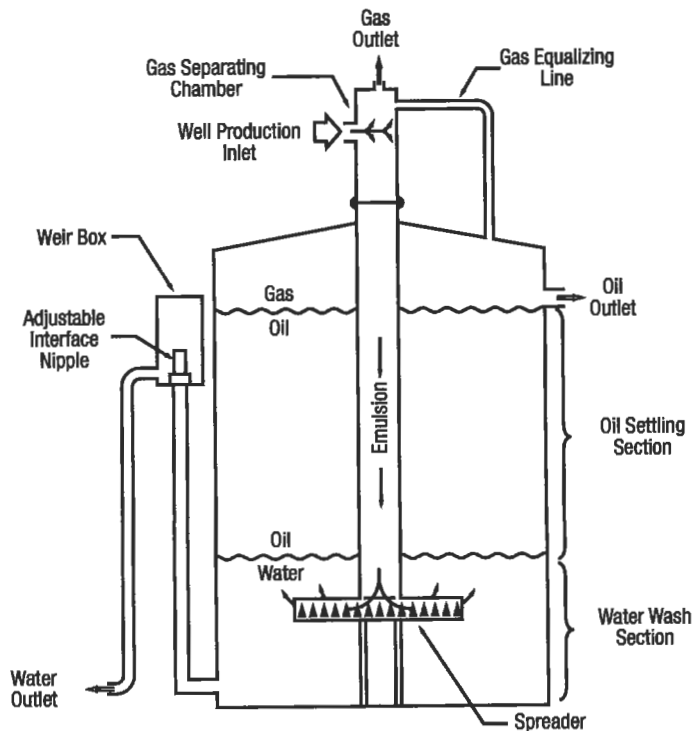


Figure 6-193. Low-pressure settling tank with internal flume [126].

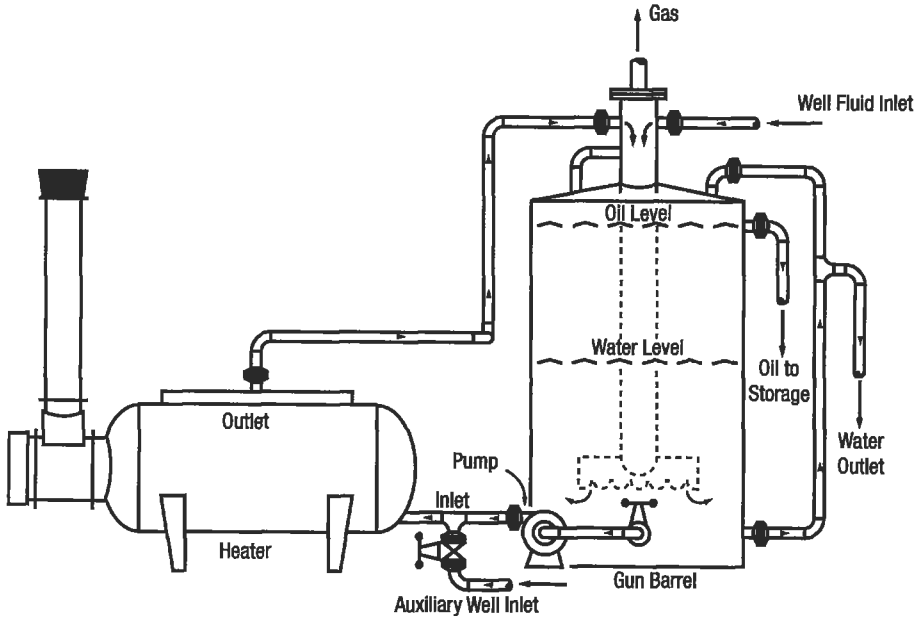


Figure 6-194. Heater and gunbarrel is forced circulation method of heating [126].

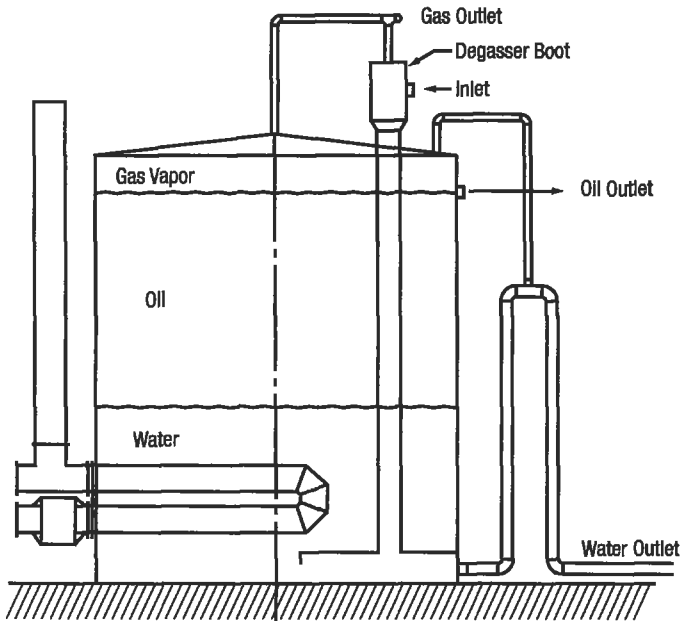


Figure 6-195. Heated gunbarrel emulsion treater [126].

- where T_m = log mean temperature difference in °F
 GTD = greater temperature difference
 = water bath temperature - inlet fluid temperature
 LTD = least temperature difference
 = water bath temperature - outlet fluid temperature in °F

A water bath temperature must be assumed for the calculations and as mentioned before. Usually 180°F is the maximum designed temperature recommended for indirect water bath heaters.

The coil area (A) required for indirect heater (Figure 6-196) can be calculated from the basic heat-transfer equation after all of the above factors have been determined. An indirect heater then may be selected from the standard models listed in Tables 6-41 and 6-42 based on the heat required and the coil area required. A heater should be selected that has a firebox rating and a coil area at least equal to or preferably slightly greater than that calculated.

By selecting a heater with a larger heat capacity and coil area than that calculated, sufficient excess will be provided to allow for heat loss from the vessel, any fouling that may occur within the tubes, and will allow the heater to be operated at less than the maximum design water bath temperature.

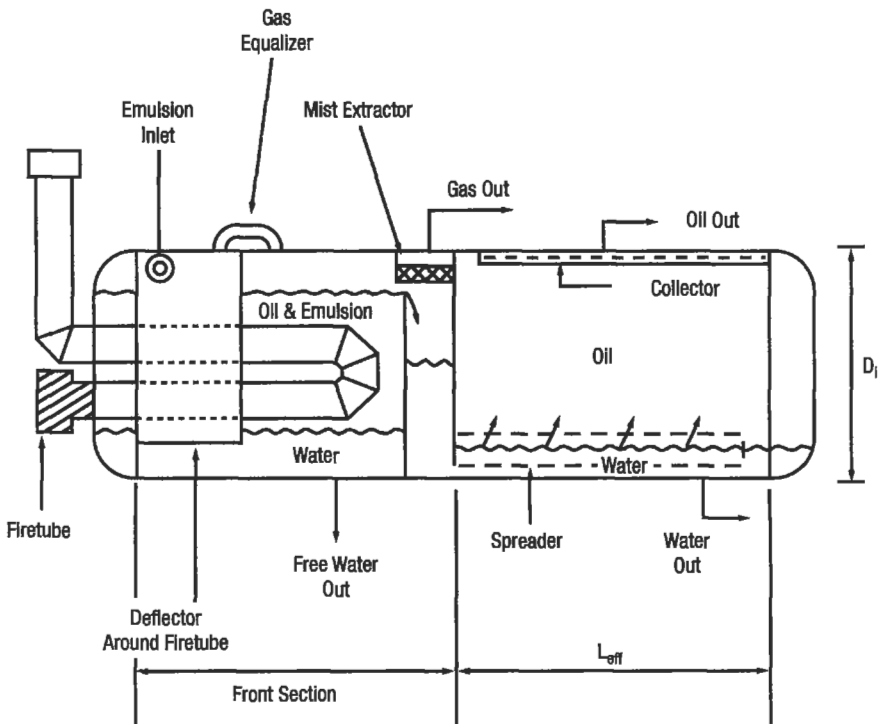


Figure 6-196. Horizontal heater-treater [126].

Table 6-41
Standard Indirect Heaters with Steel Pipe Coils [127]

Size Dia × Len.	Firebox Rating BTU/hr	No. of Tubes	Tube Size	Coil Area sq ft	Split Pass		Equivalent Len. of Pipe for Press. Drop, ft
					Tubes Split	Split Areas	
24" × 3'	100,000	Spiral	1" X	21.5	—	—	93.2
30" × 6'	250,000	14	1" X	26.2	8/6	15.0/11.2	96.4
		8	2" X or XX	28.9	4/4	14.5/14.4	68.3
30" × 10'	500,000	8	2" X or XX	48.8	4/4	24.4/24.4	100.3
36" × 10'	750,000	14	2" X or XX	85.3	8/6	48.7/36.6	177.7
		8	3" X or XX	72.3	10/4 4/4	60.9/24.4 36.1/36.2	112.7
48" × 10'	1,000,000	18	2" X or XX	109.7	12/6	73.1/36.6	229.3
		14	3" X or XX	126.4	8/6 10/4 12/2	72.2/54.2 90.3/36.1 108.3/18.1	200.7
60" × 12'	1,500,000	24	2" X or XX	176.1	16/8	117.4/58.7	354.7
		20	3" X or XX	217.1	12/8 14/6	130.3/86.8 152.0/65.1	328.7
		14	4" X or XX	196.4	8/6 10/4 12/2	112.2/84.2 140.3/56.1 168.3/28.1	243.8
72" × 12'	2,000,000	38	2" X or XX	278.7	20/18 28/10	146.7/132.0 205.4/73.3	563.3
		30	3" X or XX	325.6	30/8 22/8	220.0/58.7 238.8/86.8	495.4
		18	4" X or XX	252.5	26/4 12/6	282.2/43.4 168.3/84.2	315.1
60" × 20'	2,500,000	24	2" X or XX	295.5	16/8	197.0/98.5	546.7
		20	3" X or XX	363.7	12/8 14/6	218.2/145.5 254.6/109.1	488.7
		14	4" X or XX	328.4	8/6	187.7/140.7	355.8
					10/4 12/2	234.6/93.8 281.5/46.9	
60" × 24'	3,000,000	24	2" X or XX	355.2	16/8	236.8/118.4	642.7
		20	3" X or XX	437.0	12/8 14/6	262.2/174.8 305.9/131.1	568.7
		14	4" X or XX	394.3	8/6	225.3/169.0	411.8
					10/4 12/2	281.6/112.7 338.0/56.3	
72" × 24'	4,000,000	30	3" X or XX	655.4	22/8	480.6/174.8	855.4
		18	4" X or XX	507.0	26/4 12/6	568.0/87.4 338.0/169.0	531.1

Example 6

For a given date, calculate the heater size, such that

Oil flowrate = 2,500 bpd

Water flowrate = 1,400 bpd

Inlet temperature of liquids = 60°F

Outlet required temperature = 100°F

Coil size required = 3-in cast iron

Table 6-42
Standard Indirect Heaters with Cast Iron Coils [127]

Size Dia × Len.	Rating BTU/hr	No. of Tubes	Tube Size	Coil Area sq ft (outside tubes surface)	Equivalent Len. of Pipe for Press. Drop, ft
30" × 10'	500,000	6	2" C.I.	33.6	65.4
		4	3" C.I.	33.3	47.7
36" × 10'	750,000	14	2" C.I.	77.4	154.0
		8	3" C.I.	65.6	97.9
48" × 10'	750,000	20	2" C.I.	110.2	220.5
48" × 10'	1,000,000	18	2" C.I.	99.3	198.4
		12	3" C.I.	97.8	148.2
		18	3" C.I.	146.2	223.5
60" × 12'	1,500,000	24	2" C.I.	162.0	312.8
		24	3" C.I.	238.5	346.9
		16	4" C.I.	209.6	250.5
72" × 12'	2,000,000	38	2" C.I.	256.0	496.0
		38	3" C.I.	377.1	550.7
		20	4" C.I.	261.8	314.1

Heat required, from Equation 6-273, is

$$Q = q_i(6.25 + 8.33X)T$$

$$q_i = 2,500 + 1,400 = 3,900 \text{ bpd}$$

$$X = \frac{1,400}{3,900} = 0.36 = 36\%$$

$$\Delta T = 110 - 60 = 40^\circ\text{F}$$

$$Q = 3,900[6.25 + 8.33(0.36)]40 = 1,442,813 \text{ Btu/hr}$$

Heat transfer coefficient, from Equation 6-274, is

$$V_{0(\text{mix})} = V_{0(\text{oil})} + [V_{0(\text{water})} - V_{0(\text{oil})}]X$$

$$\text{Oil flowrate is } q_o = \frac{2,500}{24} = 104.2 \text{ bphr}$$

From Figure 6-199 $V_{0(\text{oil})} = 35.7 \text{ Btu}/(\text{hr ft}^2 \text{ }^\circ\text{F})$.

$$\text{Water flowrate is } q_w = \frac{1,400}{24} = 58.4 \text{ bphr}$$

from Figure 6-198 $V_{0(\text{water})} = 117.5 \text{ Btu}/(\text{hr ft}^2 \text{ }^\circ\text{F})$.

746 Production

$$V_{0(\text{mix})} = 35.7 + (117.5 - 35.7)0.36 = 65.15 \text{ Btu}/(\text{hr ft}^2 \text{ } ^\circ\text{F})$$

Log mean temperature difference, from Equation 6-275, is

$$T_m = \frac{\text{GTD} - \text{LTD}}{\ln \frac{\text{GTD}}{\text{LTD}}}$$

$$\text{GTD} = 180 - 60 = 120^\circ\text{F} \quad \text{LTD} = 180 - 100 = 80^\circ\text{F}$$

$$T_m = \frac{40}{\ln \frac{120}{80}} = 98.7^\circ\text{F}$$

Coil area, from Equation 6-272 is

$$A = \frac{Q}{V_0 T_m}$$

where

$$A = \frac{1,442,813}{117.5 \times 98.7} = 124.4 \text{ ft}^2$$

From Table 6-42

Heater size: 60 in. \times 12 ft
 Firebox capacity: 1,500,000 Btu/hr
 Coil data: 24-3 in. cast iron tubes
 Coil area: 238.5 ft²

Example 7

Size a horizontal treater for given data

Oil gravity: 33°API, $SG_o = 0.86$ at 60°F
 Oil flowrate: 6,000 bpd
 Inlet oil temperature: 100°F
 $SG_w = 1.03$.

Assume that 80% of the cross-sectional area is effective, retention time is 15 min and treating temperature is 120 or 150°F. Then oil viscosity = $\mu_o = 5.5$ cp at 100°F, 4 cp at 120°F and 2.5 cp at 150°F.

1. Settling equation:

$$V_t = V_o \text{ (terminal velocity of water = velocity of oil)}$$

Flow around settling oil drops in water or water drops in oil is laminar and thus Stokes law governs:

$$V_t = 2,600 \frac{\gamma_w - \gamma_o}{\mu_o} D_p^2 \text{ (ft/s)}$$

$$\gamma_w, \gamma_o \text{ (lb/ft}^3\text{)} \quad D_p \text{ (ft)} \quad \mu_o \text{ (cp)}$$

$$V_o = \frac{Q}{A}$$

$$Q = 6.49 \times 10^{-5} Q_o$$

$$Q \text{ (ft}^3\text{/s)} \quad A \text{ (ft}^2\text{)} \quad Q_o \text{ (bpd)}$$

$A = D \times L_{\text{eff}}$ is the highest cross-sectional area.

$$V_o = \frac{6.49 \times Q_o}{10^5 DL_{\text{eff}}} = 6.5 \times 10^{-5} \frac{Q_o}{DL_{\text{eff}}}$$

$$2,660 \frac{\gamma_w - \gamma_o}{\mu_o} D_p^2 = 6.5 \times 10^{-5} \frac{Q_o}{DL_{\text{eff}}}$$

$$DL_{\text{eff}} = 2.44 \times 10^{-8} \frac{Q_o \mu_o}{D_p^2 (\gamma_w - \gamma_o)} \quad \text{where } D_p \text{ is in ft}$$

or

$$DL_{\text{eff}} = 2,267 \frac{Q_o \mu_o}{D_m^2 (\gamma_w - \gamma_o)} \quad \text{where } D_m \text{ is in } \mu\text{m}$$

The diameter of water droplet to be settled from the oil (μm) is a function of viscosity of the oil (cp) and, according to Arnold and Stewart [119], can be expressed as

$$d_m = 500 (\mu_o)^{-0.675}$$

$$\text{at } 100^\circ\text{F } d_m = 500(5.5)^{-0.675} = 158 \mu\text{m}$$

$$120^\circ\text{F } d_m = 500(4)^{-0.675} = 196 \mu\text{m}$$

$$150^\circ\text{F } d_m = 500(2.5)^{-0.675} = 270 \mu\text{m}$$

$$\gamma_w = 1.03 \times 62.4 = 64.3 \text{ lb/ft}^3$$

Assume the same for the temperatures 60, 100, 120 and 150°F.

$$SG_o \text{ at } 60^\circ\text{F} = \frac{141.5}{\text{API} + 131.5} = \frac{141.5}{33 + 131.5} = 0.860$$

$$SG_o \text{ at } 100^\circ\text{F} = \frac{141.5}{(\text{API} - \text{loss}) + 131.5} = \frac{141.5}{32.8 + 131.5} = 0.861$$

where "loss" from Figure 6-190 is $0.3 - 0.1 = 0.2$:

$$SG_0 \text{ at } 120^\circ \text{ F} = \frac{141.5}{32.7 + 131.5} = 0.862$$

$$SG_0 \text{ at } 150^\circ \text{ F} = \frac{141.5}{32.2 + 131.5} = 0.864$$

Because specific gravity of oil as a function of temperature changes in a small range, assume constant values for oil and water specific weights:

$$\gamma_w = 64.3 \text{ lb/ft}^3$$

$$\gamma_o = 53.7 \text{ lb/ft}^3$$

$$\gamma_w - \rho_o = 106 \text{ lb/ft}^3$$

	T = 100°F	T = 120°F	T = 150°F
$\gamma_w - \gamma_o$ (lb _m /ft ³)	10.6	10.6	10.6
μ_o (cp)	5.5	4.0	2.5
d_m (μm)	158.0	196.0	269.0

Calculate d vs. L_{eff} :

$$\text{I. } DL_{\text{eff}} = 2267 \times \frac{6,000 \times 4}{(196)^2 10.6} = 133.6 \quad \text{if } T = 120^\circ \text{ F.}$$

$$\text{II. } DL_{\text{eff}} = 2267 \times \frac{6,000 \times 25}{(269)^2 10.6} = 44.3 \quad \text{if } T = 150^\circ \text{ F}$$

D(ft)	$L_{\text{eff}}(\text{I})$	$L_{\text{eff}}(\text{II})$
2.0	66.8	22.2
4.0	33.4	11.1
4.5	30.0	9.9
5.0	26.7	8.9
6.0	22.3	7.4
9.0	14.8	4.9
15.0	8.9	3.0
30.0	4.5	1.5

2. Calculate the retention time, such that

$$t = \frac{\text{Vol.}}{Q} \quad \text{Vol.} = \frac{\pi D^2}{4} L_{\text{eff}} \times 0.8 = 0.63 D^2 L_{\text{eff}}$$

$$Q = 6.49 \times 10^{-5} Q_0$$

$$t = \frac{0.63 D^2 L_{\text{eff}}}{6.49 \times 10^{-5} Q_0} = 9681 \frac{D^2 L_{\text{eff}}}{Q_0}$$

$$D^2 L_{\text{eff}} = 0.000103 Q_0 t$$

$(t_r)_0$ is in min

$$t = 60(t_r)_0$$

$$D^2 L_{\text{eff}} = 0.00618 Q_0 (t_r)_0$$

If the retention time $(t_r)_0 = 15$ min, then

$$D^2 L_{\text{eff}} = 0.00618 \times 6000 \times 15 = 556.2$$

D (ft)	2	4	4.5	5	6	9	15	30
L_{eff} (ft)	139	34	27.5	22.2	15.5	6.9	2.5	0.6

If the retention time $(t_r)_0 = 20$ min, then

$$D^2 L_{\text{eff}} = 0.00618 \times 6000 \times 20 = 741.6$$

and

D (ft)	2	4	5	6	9	15	30
L_{eff} (ft)	185	46	29.7	20.6	9.2	3.3	0.8

Plot Figure 6-201, D vs. L_{eff} gives the solution.

For settling temperature 150°F, the minimum effective length has to be 2.7 ft if $(t_r)_0 = 20$ min and 3.4 ft for $(t_r)_0 = 15$ min. At lower settling temperature L_{eff} should be 24 and 32 ft for $(t_r)_0 = 20$ and 15 min, respectively.

3. The heat required, from Equation 6-271, is

$$Q = 16.2 \Delta T (0.5 q_o SG_o + q_w SG_w)$$

or

$$Q_{\text{ch}} = 14.6 \Delta T (0.5 q_o SG_o + q_w SG_w)$$

$$q_w = 0.1\% \text{ of oil flow rate}$$

$$\Delta T = 150 - 100 = 50^\circ\text{F} \text{ and } 120 - 100 = 20^\circ\text{F}$$

If $\Delta T = 50^\circ\text{F}$, then

$$Q_{\text{ch}} = 14.6 \times 50 \times (0.5 \times 6000 \times 0.861 + 600 \times 1.03) = 2,336,730 \text{ Btu/hr}$$

(text continued on page 754)

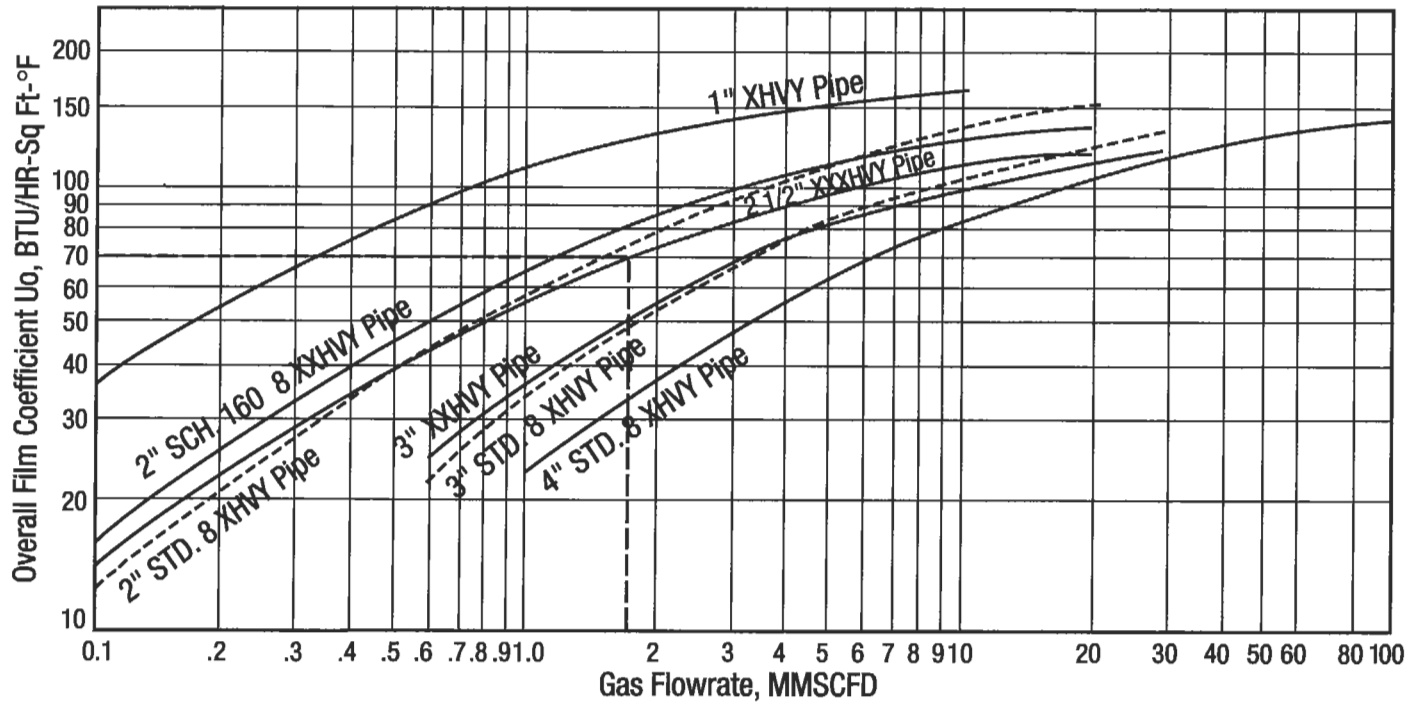


Figure 6-197. Overall film coefficient for natural gas in indirect heaters [127].

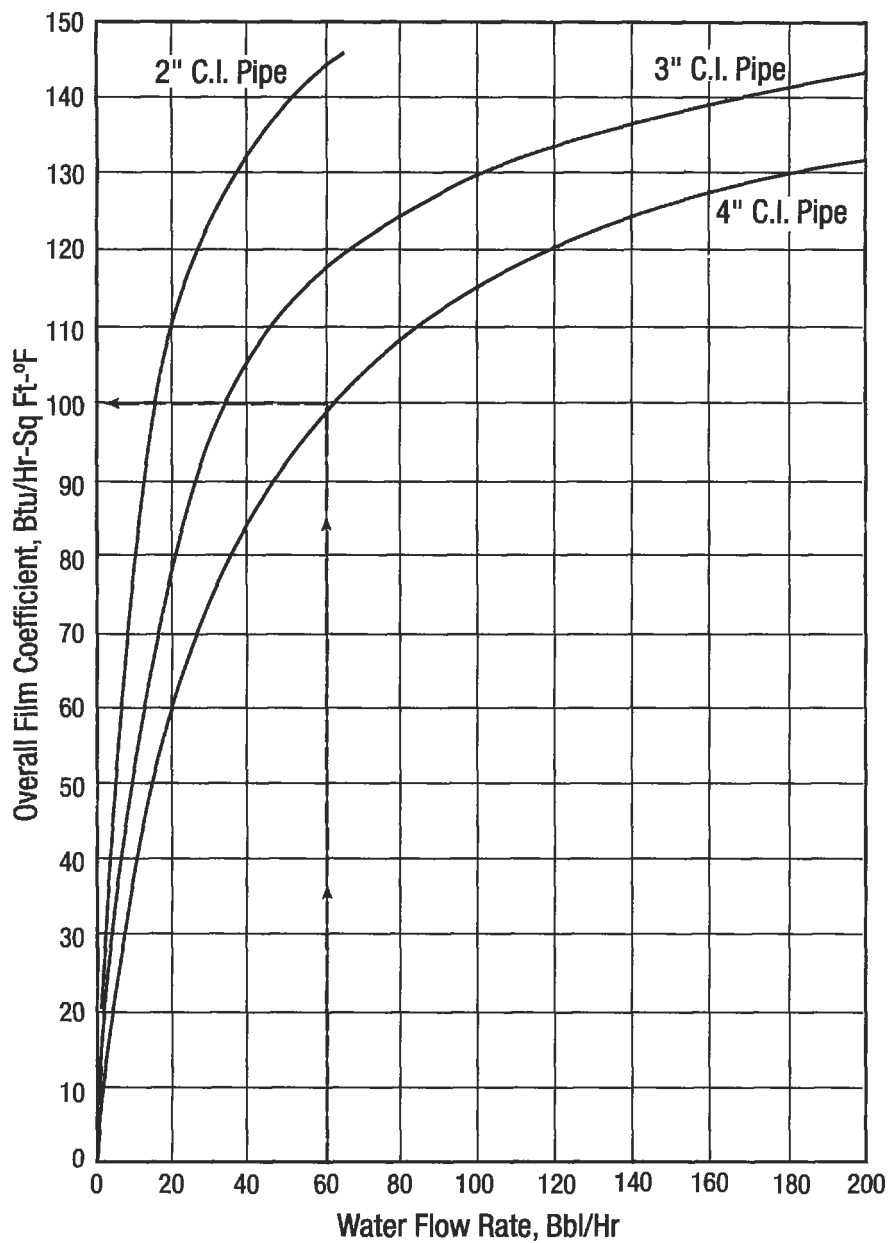


Figure 6-198. Overall film coefficient for water in indirect heaters [127].

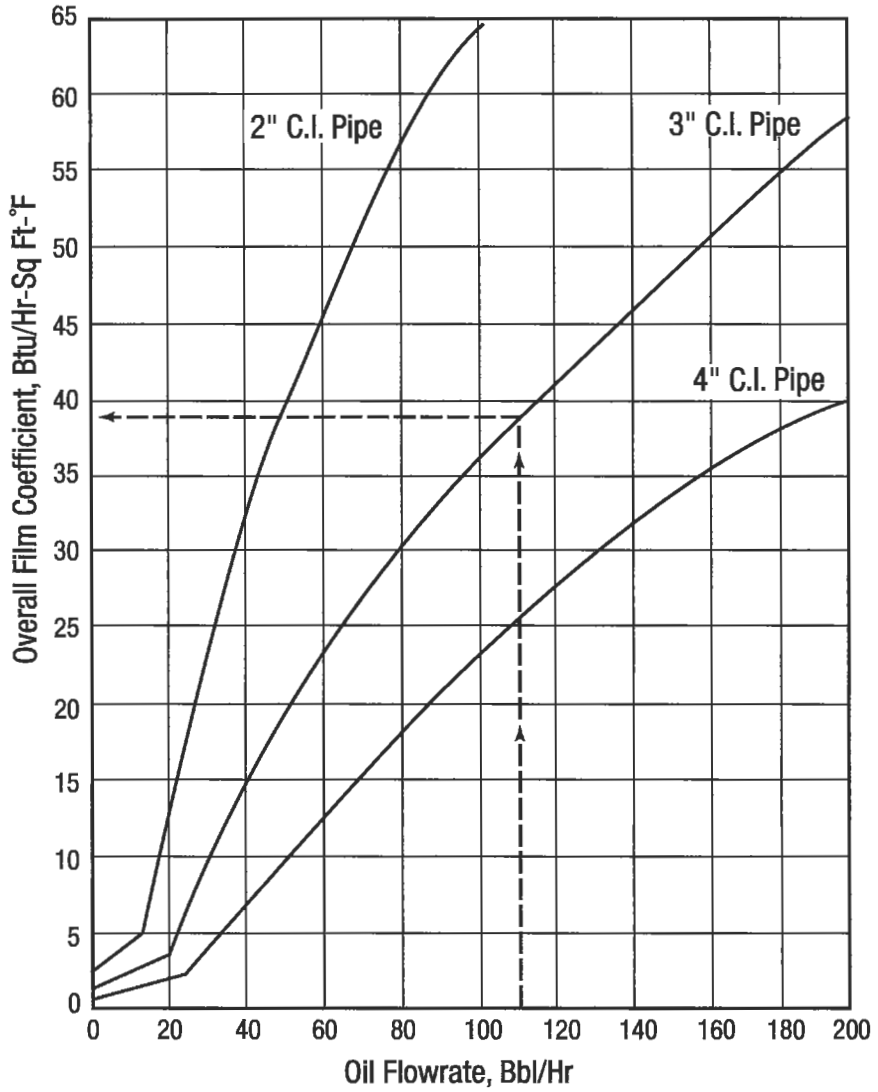


Figure 6-199. Overall film coefficient for oil in indirect heaters [127].

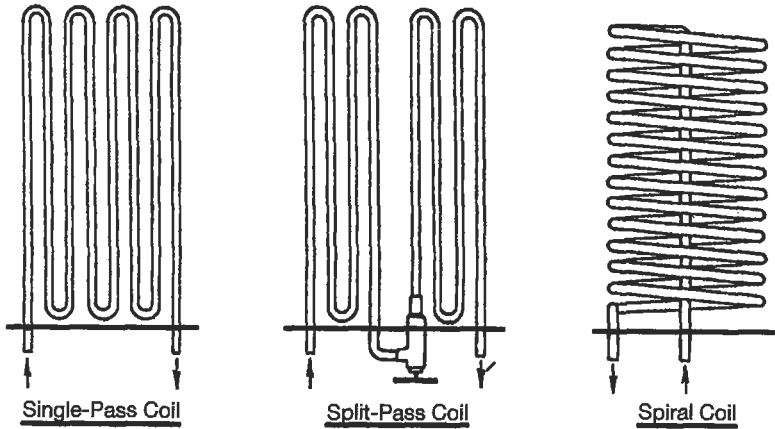


Figure 6-200. Indirect heater coils.

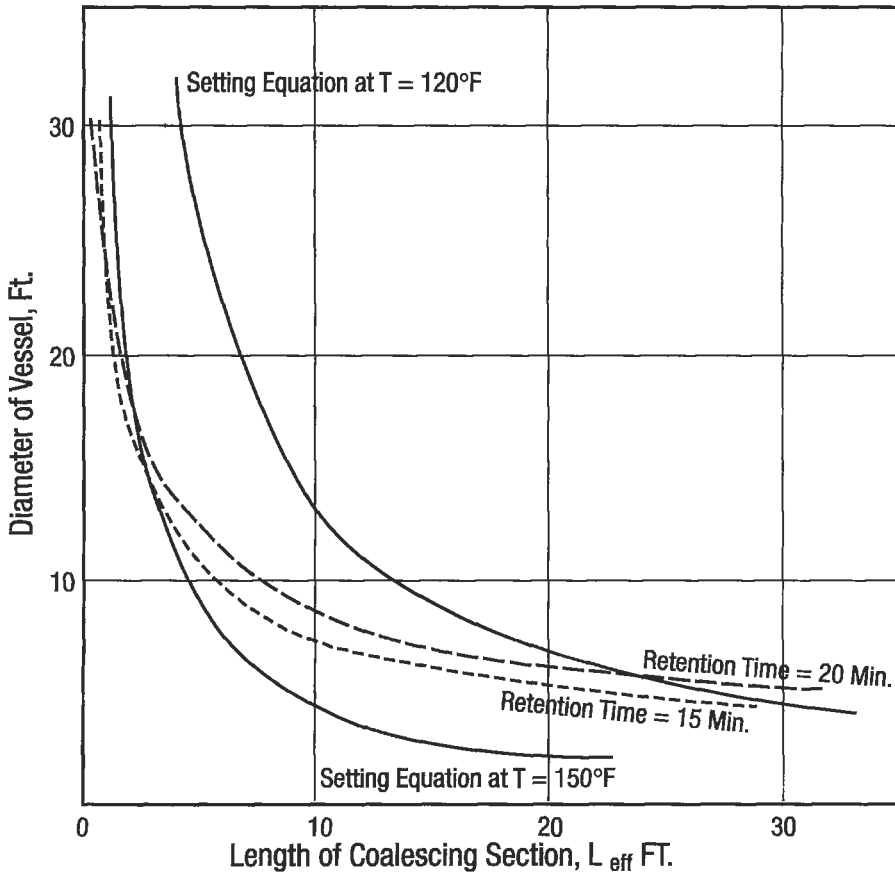


Figure 6-201. Horizontal treater example.

(text continued from page 749)

if $\Delta T = 20^\circ\text{F}$, then

$$Q_{\text{thf}} = 14.6 \times 20 \times (0.5 \times 6000 \times 0.861 + 600 \times 1.03) = 934,692$$

4. Conclusions are as follows. Treating temperature plays a more important role than retention time. For $T = 150^\circ\text{F}$ and $L_{\text{eff}} = 7.3$ ft any diameter above retention time curves is correct. The diameter of the front section has to be the same as the coalescing section.

An economical solution would be a 6×20 ft for the coalescing section and a 2.5-Btu/hr firebox rating.

GAS PRODUCTION ENGINEERING

Quality specifications for natural gas are individually negotiated and prescribed in the contracts between the purchaser or the pipeline companies and the producer. Gas contracts usually contain the following basic considerations:

- minimum, maximum and nominal delivery pressure
- water dew point or water content
- maximum condensable hydrocarbon content or hydrocarbon dew point
- minimum heating value
- contaminants
- maximum delivery temperature

Above quality parameters together with the price and quantity are the fundamental factors, and they determine producing equipments.

Gas–Water Systems and Dehydration Methods

Liquid water and water vapor are removed from natural gas to:

- prevent formation of hydrates in transmission lines
- meet a water dew point requirement of a sales gas contract
- prevent corrosion

Water vapor is the most common undesirable impurity in natural gas, usually in the range of 8,000 to 10,000 ppm by volume ($400\text{--}500$ lb_m water vapor/MMscf gas), while the pipeline specifications restrict the water content to a value no greater than 120 to 160 ppm by volume ($6\text{--}8$ lb_m/MMscf). In order to design and operate dehydration processes, a reliable estimate of the water content of natural gas is essential.

Water Content of Natural Gases

The water content of a gas is a function of pressure, temperature, composition and salt content of the free water [128]. The effect of composition increases with pressure. For lean, sweet natural gases containing over 70% methane and small amounts of “heavy ends,” pressure temperature correlations are suitable. Figure 6-202 is an example.

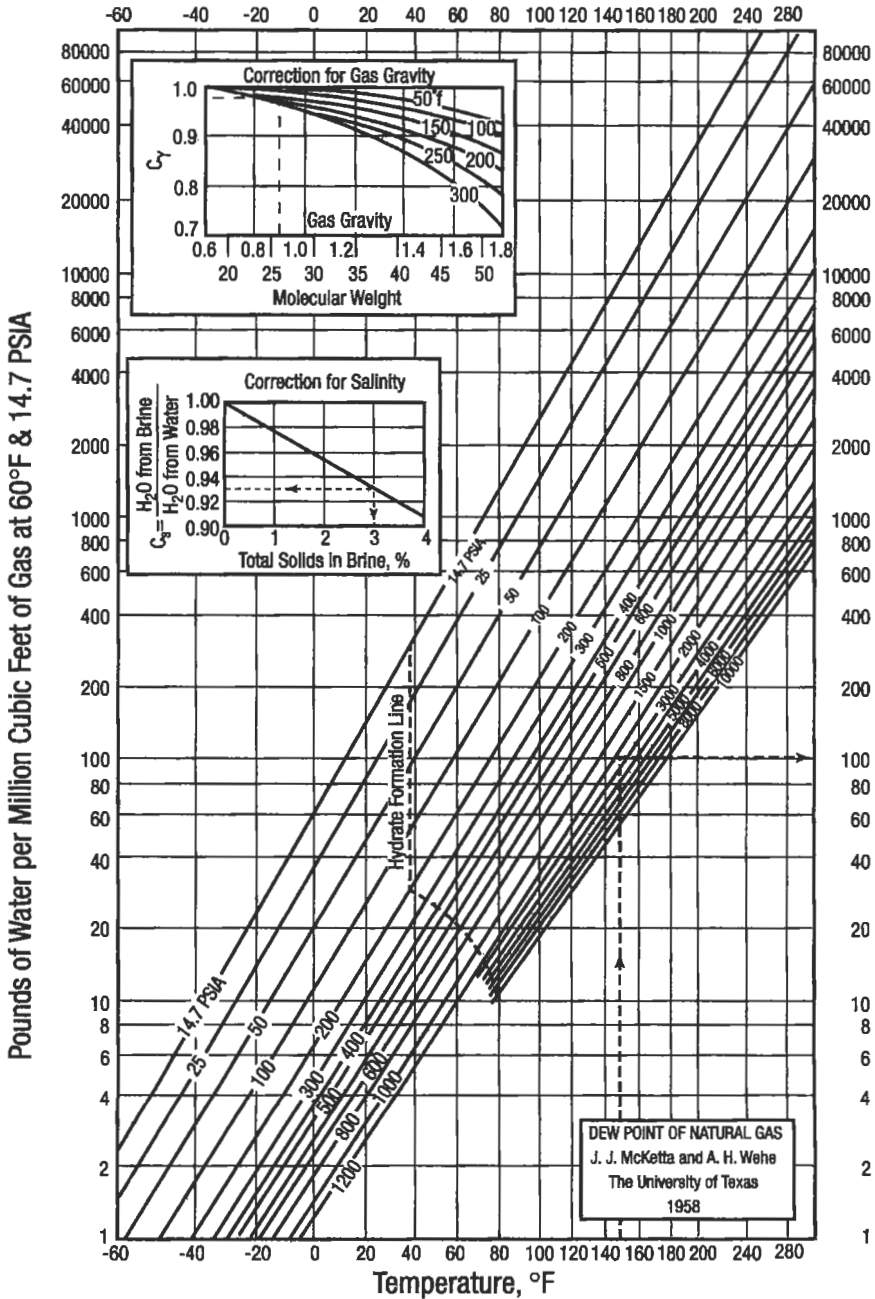


Figure 6-202a. Water content of natural gases with corrections for salinity and gravity [128].

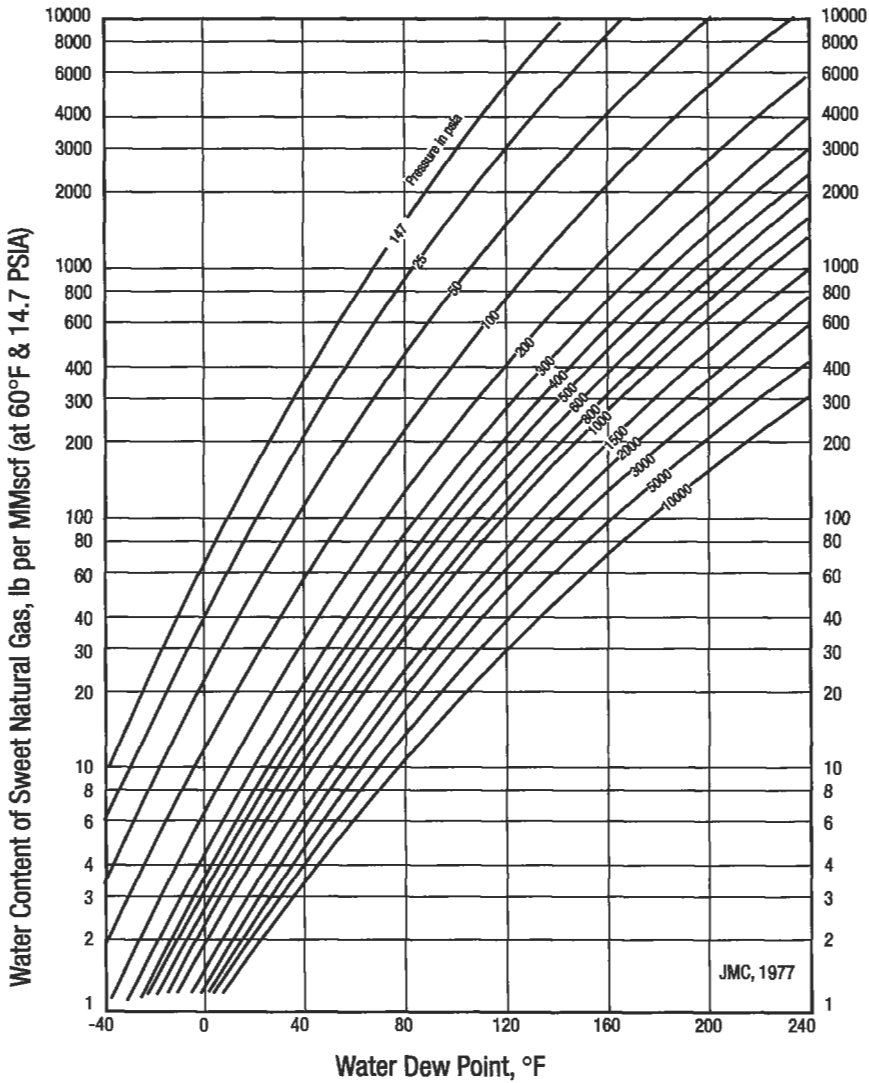


Figure 6-202b. Campbell's correlation for water content of sweet gases.

Example 1

A natural gas $SG_g = 0.9$ is with contact with brine in a reservoir. The brine contains 30,000 ppm solids (approximately 3% NaCl). The pressure of the gas is 3,000 psia and the gas temperature is 150°F. How much water is in the gas in pounds of water per million cubic feet of gas?

- a. Follow dashed lines on Figure 6-202a. From the general chart of Figure 6-202a at 3,000 psia and 150°F gas would contain 105 lb of water/MMscf of 0.6 gas if the gas had been in contact with pure water.
- b. Correction for gas gravity from 0.6 to 0.9. From the "correction chart for gravity" follow the dashed line from the abscissa where the desired gravity is 0.9, vertically, to the 150°F isotherm. Read horizontally, the correction factor for gas gravity C_g is 0.98.
- c. Correction for salinity of brine; see the second correction chart on the general Figure 6-202a. At a brine salinity of 3% go vertically to the correction line, and read on the ordinate the ordinate value of $C_s = 0.93$.

The final answer for water content W:

$$W = 105 \times C_g \times C_s = 105 \times 0.98 \times 0.93 = 95.6 \text{ lb water in the gas}$$

Experimental value for this gas was 96.2, which is satisfactory accuracy.

The McKetta and Wehe chart (Figure 6-202a) is not explicit for temperatures below the hydrate formation line. Because of this, it is better to use Campbell's correlation (Figure 6-203b). To determine the moisture within the pressure range of 1 to 690 bar (14.7 to 10,000 psia) and the temperature range of -40°C (-40°F) to 110°C (230°F), the following analytical expression is used:

$$W = \frac{A}{P} + B \quad \text{if} \quad SG_g = 0.6$$

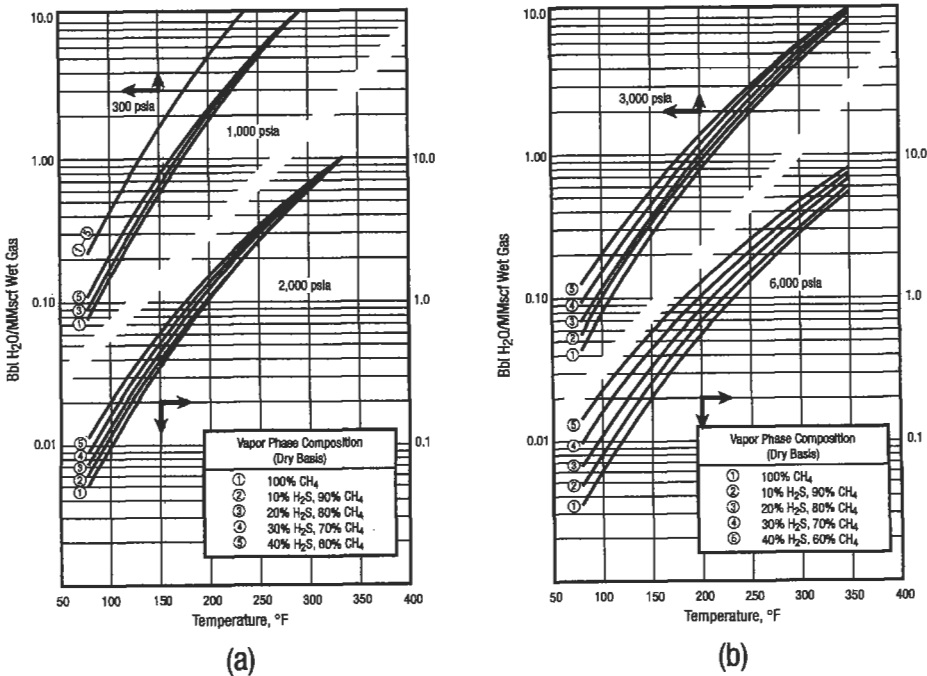


Figure 6-203. Campbell's correlation for water content of sweet gases [129].

or

$$W = \left(\frac{A}{P} + B \right) \times C_G \times C_s \quad \text{if } SG_g > 0.6 \quad (6-276)$$

where A,B = constants; see Table 6-43

SG_g = specific gravity of gas or relative densityW_g = water content in g/m³

P = gas pressure in atm

Table 6-43
Coefficients A and B in Equation 6-276 [133]

Temp., °C.	A	B	Temp., °C.	A	B
-40	0.1451	0.00347	+32	36.10	0.1895
-38	0.1780	0.00402	+34	40.50	0.207
-36	0.2189	0.00465	+36	45.20	0.224
-34	0.2670	0.00538	+38	50.80	0.242
-32	0.3235	0.00623	+40	56.25	0.263
-30	0.3930	0.00710	+42	62.70	0.285
-28	0.4715	0.00806	+44	69.25	0.310
-26	0.5660	0.00921	+46	76.70	0.335
-24	0.6775	0.01043	+48	85.29	0.363
-22	0.8090	0.01168	+50	94.00	0.391
-20	0.9600	0.01340	+52	103.00	0.422
-18	1.1440	0.01510	+54	114.00	0.454
-16	1.350	0.01705	+56	126.00	0.487
-14	1.590	0.01927	+58	138.00	0.521
-12	1.868	0.021155	+60	152.00	0.562
-10	2.188	0.02290	+62	166.50	0.599
-8	2.550	0.0271	+64	183.30	0.645
-6	2.990	0.3035	+66	200.50	0.691
-4	3.480	0.03380	+68	219.00	0.741
-2	4.030	0.03770	+70	238.50	0.793
0	4.670	0.04180	+72	260.00	0.841
+2	5.400	0.04640	+74	283.00	0.902
+4	6.225	0.0515	+76	306.00	0.965
+6	7.150	0.0571	+78	335.00	1.023
+8	8.200	0.0630	+80	363.00	1.083
+10	9.390	0.0696	+82	394.00	1.148
+12	10.720	0.767	+84	427.00	1.205
+14	12.390	0.0855	+86	462.00	1.250
+16	13.940	0.0930	+88	501.00	1.290
+18	15.750	0.1020	+90	537.50	1.327
+20	17.870	0.1120	+92	582.50	1.327
+22	20.150	0.1227	+94	624.00	1.405
+24	22.80	0.1343	+96	672.0	1.445
+26	25.50	0.1453	+98	725.0	1.487
+28	28.70	0.1595	+100	776.0	1.530
+30	32.30	0.1740	+110	1093.0	2.620

When natural gases contain substantial quantities of acid gases as H_2S and/or CO_2 , the water content of such sour natural gas mixtures can be considerably higher than the chart for sweet gas would indicate, especially at pressures above 70 bar (1,000 psi). Charts on Figure 6-203 expand the pressure and temperature ranges for determining the water vapor content for sour gases to data given for sweet gases [129].

Example 2

Determine the amount of water that will drop out in a plant inlet separator from a gas stream that consists of 16% H_2S , 13% CO_2 and 71% hydrocarbons. $T_{res} = 212^\circ F$, $P = 4675$ psia, $T_{sep} = 80^\circ F$ and $P_{sep} = 1,000$ psia.

(a) Reduce two-acid components CO_2 and H_2S to H_2S^* :

$$\begin{aligned} H_2S^* \text{ of pseudocomposition} &= H_2S + 0.75 \times CO_2 \\ &= 16 + 0.75 \times 13 = 25.75\% \end{aligned}$$

(b) Read water content from chart if $H_2S^* = 25.75$ (from Figure 6-203)

$$\begin{aligned} W &= 1.36 \text{ lb/MMscf at } 3,000 \text{ psia and } 212^\circ F \\ &= 1.13 \text{ bbl/MMscf at } 6,000 \text{ psia and } 212^\circ F \end{aligned}$$

By logarithmic interpolation with a pocket calculator (or by a plot on log-log paper), the water content at 4,675 psia is determined as follows:

$$\frac{\log 4,675 - \log 6,000}{\log 3,000 - \log 6,000} = \frac{\log x - \log 1.13}{\log 1.36 - \log 1.13}$$

$$\log x = 0.0820$$

$$x = 1.21 \text{ bbl/MMscf}$$

(c) The water content at the separator:

$$\text{if } P = 1,000 \text{ psia, } T = 80^\circ F, W = 0.11 \text{ bbl/MMscf}$$

(d) Water drop out in the separator:

$$1.21 - 0.11 = 1.10 \text{ bbl/MMscf}$$

Measurement of Water Content of Natural Gas

Many methods of measuring the amount of water in natural gases have been developed to fit various applications [130]. No single method of analysis can be utilized under all conditions (see Table 6-44).

Dew point sensors are devices for moisture detection utilizing the physical properties of water and the laws of physics and chemistry to effect a measurement. Some of them are applicable to gas samples only. Other instruments can be used to monitor moisture in both liquid and gas samples (see Table 6-45).

Table 6-44
Methods of Measuring Water Content [131]

Method	Measurement
Electrolysis for water	Electrolysis current of sample is measured.
Dielectric constant change	Capacitance of a sample is measured.
Electric impedance	Electric impedance of the vapor of a sample is measured.
Piezoelectric crystals	Frequency of crystal with sample moisture is measured.
Heat absorption	Energy absorption and desorption of a sample is measured.
Infrared absorption	Infrared electromagnetic radiation absorption of a sample is measured.
Microwave absorption	Microwave electromagnetic radiation absorption of a sample is measured.

Table 6-45
Summary of Moisture Detector Features [131]

Type	Range	Sample Phase	Sample System Required	Remarks
Electrolytic hygrometer	0-10 to 0-1,000 ppm	Clean gas. Special sampling for liquids	Yes	Sample flow must be constant
Change of capacitance	0-10 to 0-1,000 ppm	Clean gas or liquid	Yes	Sample temperature must be constant
Impedance type	0-20,000 ppm	Clean gas or liquid	For Liquids	Sample temperature of liquids must be constant
Piezoelectric type	0-5 to 0-25,000 ppm	Clean gas only	Yes	
Heat of adsorption type	0-10 to 0-5,000 ppm	Clean gas or liquid. Special sampling for liquids	Yes	Sample flow must be constant
Infrared absorption	0-0.05 to 0-50%	Liquids and slurries	Yes	
Microwave absorption	0-1 to 0-90%	Liquids, slurries and pastes	No	

For practice, two types of moisture detectors are recommended: first is the dew point tester (drilled mirror type) and second is the silicon chip hygrometer.

The dew point tester permits the visual determination of the temperature at which water will condense from a gas onto a silvered mirror (Figure 6-204), which is significant because it represents the actual equilibrium saturation temperature of the gas for temperatures above the hydrate-formation value. And, at temperatures below the equilibrium hydrate-formation conditions, it measures a reproducible metastable equilibrium condition between gas and liquid water.

Figure 6-204 presents a sectional view of the apparatus without lead lines and refrigerant source. Gas entering the apparatus through valve A is deflected by nozzle B so as to strike the cooled mirror C. The mirror is cooled through the copper cooling rod F by the evaporation of a refrigerant, such as propane, carbon dioxide or some liquefied gas, in chiller G. Pressure gages and a bulb thermometer are used to record the pressure and temperature conditions for the inception of condensation or fog formation on the silvered mirror.

In the absence of interfering substances, the accuracy of the determinations, given an experienced operator, is reported to be $\pm 0.1^{\circ}\text{C}$ down to 0°C , and $\pm 0.3^{\circ}\text{C}$ from 0 to -18°C .

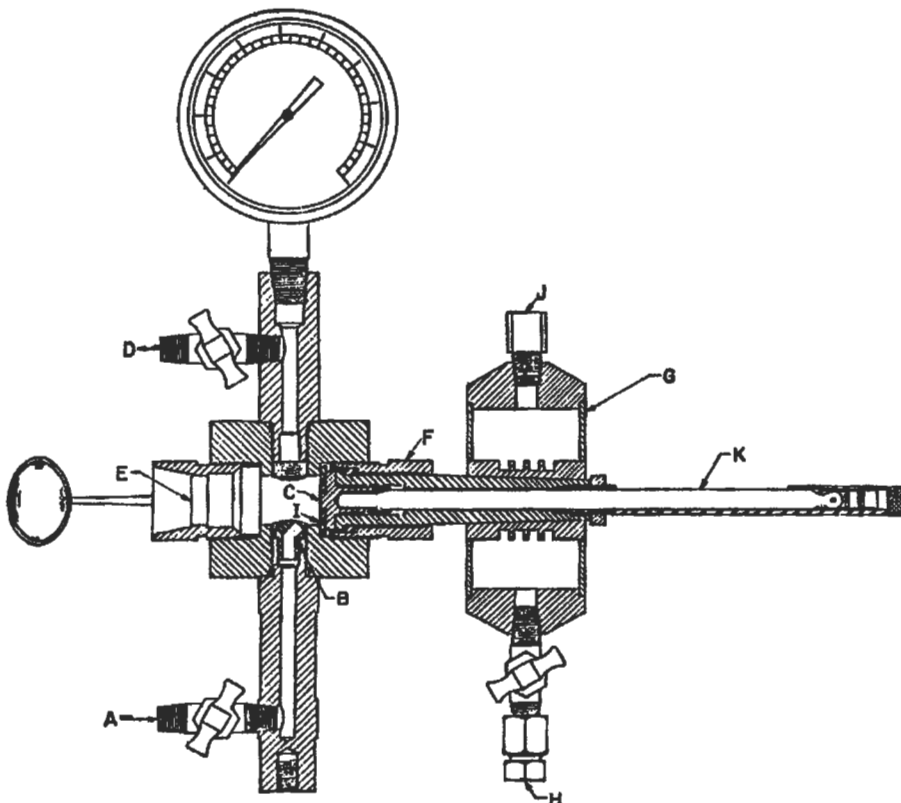


Figure 6-204. Bureau of Mines dew-point tester [144].

ASTM D1142-NGAA 2140 provides a detailed description of the apparatus. For technical details, see producer's catalog [131].

A silicon chip hygrometer [132] makes use of a tiny silicon chip to sense the presence of moisture. It can operate in environments ranging from -40°C to 45°C with no effect on accuracy, and gas flow rates from 50 to $1,500\text{ cm}^3/\text{min}$. It can also operate under static or vacuum conditions.

Example 3

A natural gas dew point is measured at -4°F at a pressure of 14.7 psia. Express this water content in terms of ppm and vpm if the relative density (specific gravity) of the gas is equal to 0.7.

(a) Water content W , in (g/m^3) and (lb/MMscf) , from Equation 6-276

$$W = \left(\frac{A}{P} + B \right) \times C_G \times C_S \quad -4^{\circ}\text{F} = -20^{\circ}\text{C} \quad 14.7\text{psia} = 1.03\text{atm}$$

$$A = 0.960 \quad B = 0.0134 \quad \text{from Table 6-43}$$

$$W = \frac{0.96}{1.03} + 0.0134 = 0.9454\text{g}/\text{m}^3 \quad \text{if } SG_g = 0.6$$

$$= 58.9\text{lb}/\text{MMscf} \quad \text{if } SG_g = 0.6$$

$$\text{for } SG_g = 0.7 \quad C = 1.0 \quad C_S = 1.0$$

$$W = 58.9\text{ lb water per } 10^6\text{ MMscf gas}$$

(b) Water content in terms of parts per million by weight (ppm)

$$1\text{ lb mol} = 0.7 \times 29 = 20.3\text{ lb}$$

$$= 379.3\text{ ft}^3 \text{ at } 14.7\text{ psia and } 60^{\circ}\text{F}$$

$$\frac{58.9\text{ lb}}{10^6\text{ scf}} = \frac{58.9\text{ lb}}{2,636.43\text{ lb mol}} = \frac{58.9\text{ lb}}{2,636.43 \times 20.3\text{ lb}}$$

(c) Water content in terms of parts per million by volume (vpm)

$$\begin{aligned} \frac{58.9\text{ lb}}{10^6\text{ scf}} &= \frac{58.9/18.00\text{ (lb/lb mol)}}{10^6\text{ scf}} = \frac{3.2722\text{ lb mol}}{10^6\text{ scf}} \\ &= \frac{3.2722\text{ lb mol} \times 379.4\text{ scf/lb mol}}{10^6\text{ scf}} = 1,241\text{vpm} \end{aligned}$$

(d) Water content W , from Figure 6-202*b* is 57.6 lb/MMscf.

Gas Hydrate

The amount of water soluble in a natural gas vapor is limited to temperature and pressure at dew point. If water will condense in the pipeline and accumulate in sufficient quantities, hydrate can be formed. A hydrate is a physical combination of water and other small molecules to produce a solid that has an "ice-like" appearance, which can be represented as:

- Methane = $\text{CH}_4 \cdot 6\text{H}_2\text{O}$
- Ethane = $\text{C}_2\text{H}_6 \cdot 8\text{H}_2\text{O}$
- Propane = $\text{C}_3\text{H}_8 \cdot 17\text{H}_2\text{O}$
- Isobutane i = $\text{C}_4\text{H}_{10} \cdot 17\text{H}_2\text{O}$
- Nitrogen = $\text{N}_2 \cdot 6\text{H}_2\text{O}$
- Carbon dioxide = $\text{CO}_2 \cdot 6\text{H}_2\text{O}$
- Hydrogen sulfide = $\text{H}_2\text{S} \cdot 6\text{H}_2\text{O}$

Normal butane does form a hydrate, but it is very unstable. Other components of a natural gas mixture do not form hydrate.

Several methods exist for determining the pressure and temperature at which hydrates begin to form: graphical, analytical and experimental. Rough data for determining the start of hydrate formation is obtained by the graphic method. With this method, for gas mixtures not containing H_2S , the curves shown in Figure 6-205 are appropriate.

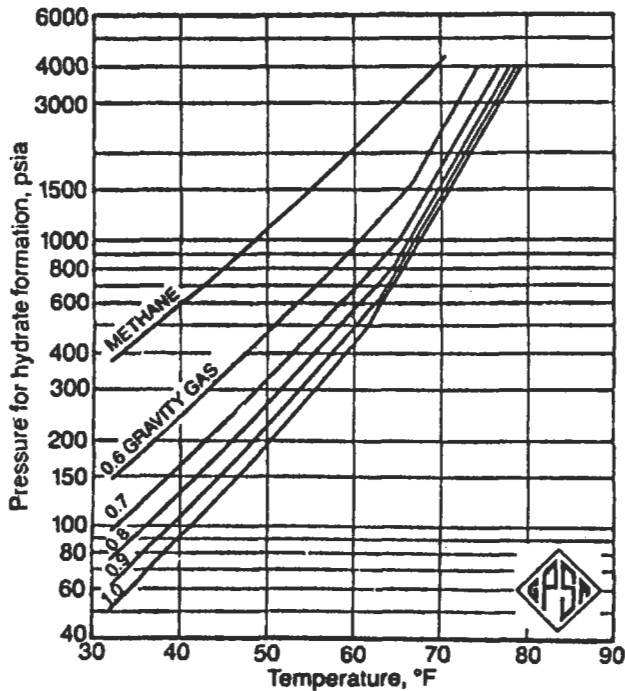


Figure 6-205. Hydrate-forming conditions for natural gases with various gravities [135].

Example 4

Find the pressure at which hydrate forms at $T = 40^\circ\text{F}$ for a gas with the following composition:

Component	Mole fraction in gas	M	lb/mole of mixture
C_1	0.88	16.04	14.12
C_2	0.09	30.07	2.71
C_3	0.02	44.10	0.88
C_4	0.01	58.12	0.58
			18.29

$$\text{Relative density} = \frac{M_{\text{gas}}}{M_{\text{air}}} = \frac{18.29}{28.97} = 0.631$$

From Figure 6-205 at 40°F :

$$P = 250 \text{ psia for } SG_g = 0.6$$

$$= 166 \text{ psia for } SG_g = 0.7$$

Using linear interpolation,

$$P = 250 - \left[(250 - 166) \times \left(\frac{0.631 - 0.6}{0.7 - 0.6} \right) \right] = 224 \text{ psia}$$

To solve technological design problems, it is simple to use an analytical method to express the relationship between pressure and temperature of hydrate formation. Usually, equations of such dependence are given in the form of $\log P = at + b$, that is, when the dependence of P vs. T has a linear character in semilog coordinates. However, as some experiments show [133], such dependence frequently does not have a linear character and may be more accurately expressed by

$$\log P = a(t + kt^2) + b \quad (6-277)$$

where P = pressure in atm

SG_g = relative density (specific gravity)

a, b, k = coefficients (see Table 6-46)

t = temperature in $^\circ\text{C}$ or T = temperature in K

Example 5

Find the pressure at which hydrate forms at $T = 40^\circ\text{F}$ for the gas from Example 4 using an analytical equation:

$$SG_g = 0.631$$

$$\log P = b + 0.0497 (t + kt^2)$$

Table 6-46
Equations for the Relationship between Pressure and Temperature
of Hydrate Formation for Several Gases [133]

Gas and its relative density	Temp. Interval °C	Equations
CH ₄	0 to -11	$\ln P = 5.6414 - 1154.61/T$
	0 to +23	$\ln P = 1.415 + 0.417(T + 0.01T^2)$
	+24 to +47	$\ln P = 1.602 + 0.0428T$
C ₂ H ₆	0 to -10	$\ln P = 6.9296 - 1694.86/T$
	0 to +14.5	$\ln P = 0.71 + 0.0547T$
C ₃ H ₈	0 to -12	$\ln P = 5.4242 - 1417.93/T$
	0 to +8.5	$\ln P = 0.231 + 0.0576T$
CO ₂	0 to -6	$\ln P = 13.4238 - 3369.1245/T$
	0 to +9.8	$\ln P = 1.08 + 0.056T$
H ₂ S	-32 to +29.6	$\ln P = 2.844 + 0.0466T$
C _n H _{2n+2} 0.6 to 1.0	0 to +25	$\ln P = \beta + 0.0497(T + kT^2)$

$$\beta = 0.91 \quad k = 0.006 \text{ from Figure 6-206}$$

$$t = 40^\circ\text{F} = 4.4^\circ\text{C}$$

$$\log P = 0.91 + 0.0497 [4.4 + 0.006 \times (4.4)^2]$$

$$\log P = 1.13445$$

$$P = 13.63 \text{ atm} = 13.19 \text{ atm} = 194 \text{ psia}$$

Using Figure 6-205 we got ≈ 224 psia, it is worst value overestimate 15%.

Example 6

The 0.631 specific gravity (relative density) gas is to be expanded from 1,500 psia to 500 psia. What is the minimum initial temperature that will permit the expansion without hydrate formation?

To solve this problem, use the charts in Figures 6-207 and 6-208.

From Figure 6-207 for $SG_g = 0.6$ $T_{\min} = 100^\circ\text{F}$.

From Figure 6-208a for $SG_g = 0.7$ $T_{\min} = 125^\circ\text{F}$.

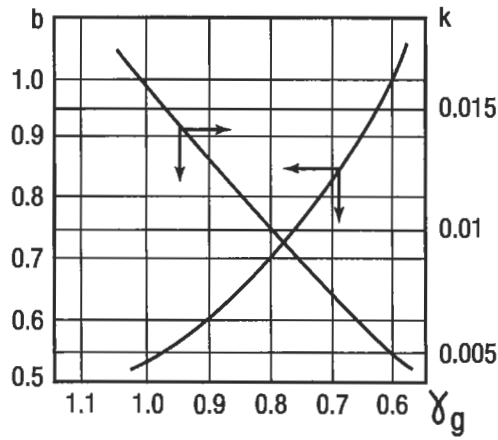


Figure 6-206. Dependence of coefficients β and k on the relative density (SG_g) [133].

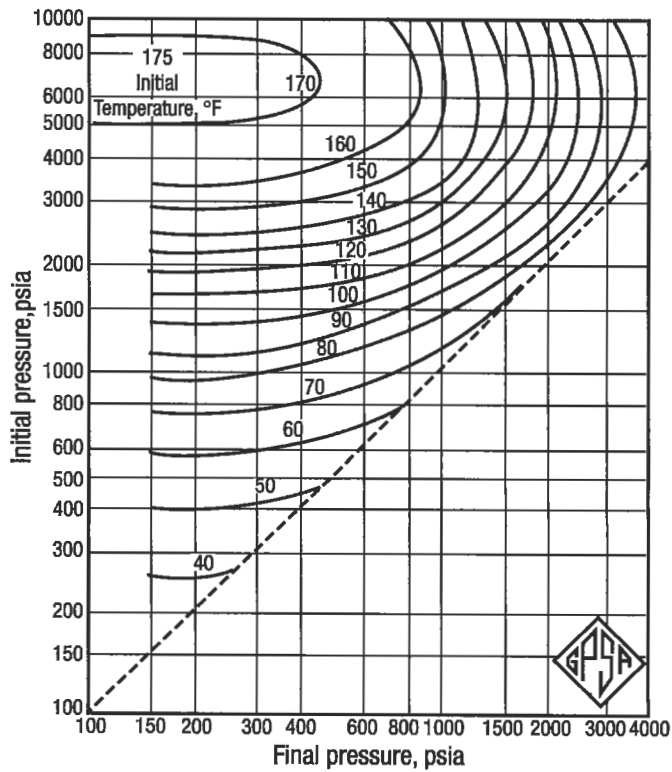


Figure 6-207. Permissible expansion of 0.6 gravity natural gas without hydrate formation [135].

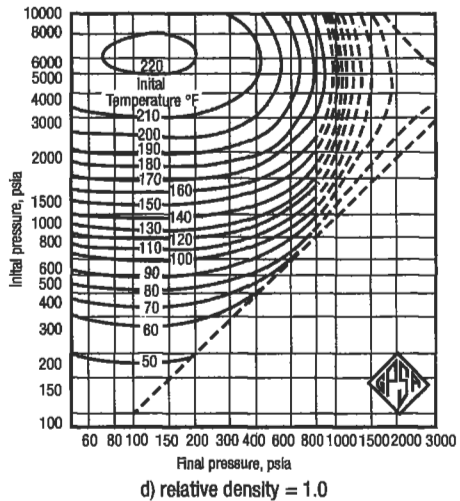
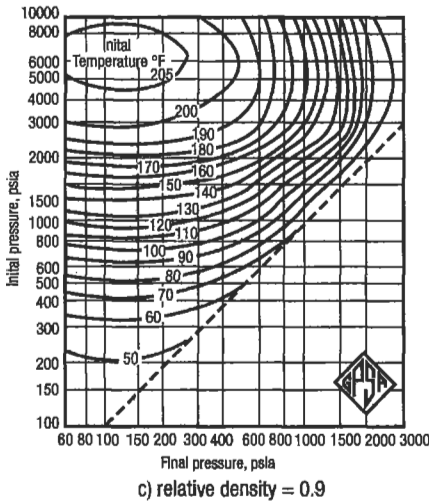
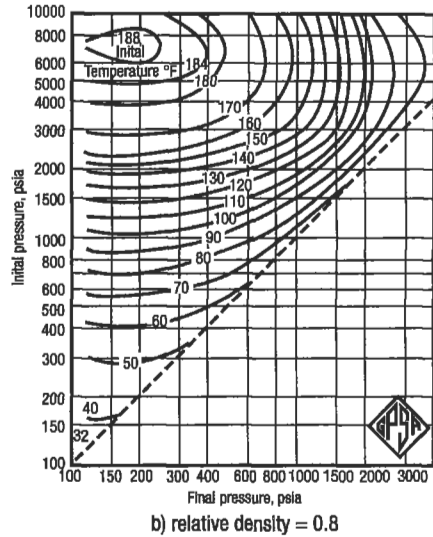
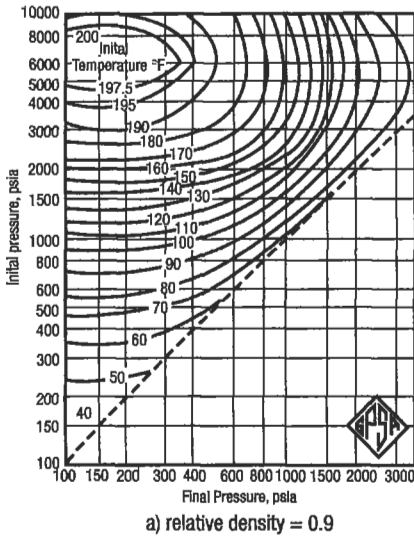


Figure 6-208. Permissible expansion of 0.7, 0.8, 0.9 and 1.0 gravity natural gas without hydrate formation [135].

For $SG_g = 0.631$

$$T_{min} = 100 + \left[(125 - 100) \left(\frac{0.631 - 0.6}{0.7 - 0.6} \right) \right] = 108^\circ \text{ F}$$

Example 7

How far may a 0.8 gravity gas at 2,500 psia and 100°F be expanded without hydrate formation?

On Figure 6-208b find the intersection of 2,500 psia initial pressure line with the 100°F initial temperature curve. Read on the x axis the permissible final pressure of 1,600 psia.

Example 8

How far may a 0.6 gravity gas at 2,500 psia and 144°F be expanded without hydrate formation?

On Figure 6-207 the 144°F initial temperature curve does not intersect the 2,500-psia initial pressure line; therefore, the gas may be expanded to atmospheric pressure without hydrate formation.

Figures 6-207 and 6-208 should only be used for first approximations of hydrate formation conditions.

Another graphical method was proposed by Katz. This procedure requires a gas analysis and utilizes vapor-solid equilibrium constant defined by the equation

$$K_{v-s} = \frac{y}{x} \quad \text{and} \quad \sum \left(\frac{y_i}{K} \right) = 1.0 \quad (6-278)$$

The applicable K-value correlations for the hydrate forming molecules (CH_4 , C_2H_6 , C_3H_8 , $i\text{-C}_4\text{H}_{10}$, $n\text{-C}_4\text{H}_{10}$, CO_2 and H_2S) are shown in Figure 6-209(a-g). All molecules too large to form hydrate, e.g., nitrogen and helium have a K-value of infinity.

Example 9

Calculate the temperature for hydrate formation at 435 psi for a gas with the following composition (%):

N_2 -5, C_1 -78, C_2 -6, C_3 -3, $i\text{C}_4$ -1, H_2 -1, CO_2 -4, C_{5+} -2.

Component	Mole fraction (y)	t = 59°F		t = 50°F		t = 54°F	
		K	$\frac{y_i}{K}$	K	$\frac{y_i}{K}$	K	$\frac{y_i}{K}$
N_2	0.05	inf	0	inf	0	inf	0
C_1	0.78	1.8	.433	1.65	0.473	1.74	0.448
C_2	0.06	1.3	0.046	0.475	0.126	0.74	0.081
C_3	0.03	0.27	0.110	0.066	0.454	0.12	0.250
$i\text{-C}_4$	0.01	0.08	0.125	0.026	0.384	0.047	0.213
H_2	0.01	inf	0	inf	0	inf	0
CO_2	0.04	~5	0.008	1.7	0.02	~3	0.011
C_{5+}	0.02	inf	0	inf	0	inf	0
		$\Sigma K = 0.722$		$\Sigma K = 1.457$		$\Sigma K = 1.003$	

Temperature at which hydrate will form is about 54°F.

Using Equation 6-203 gives

435 psia = 30.6 atm

(text continued on page 773)

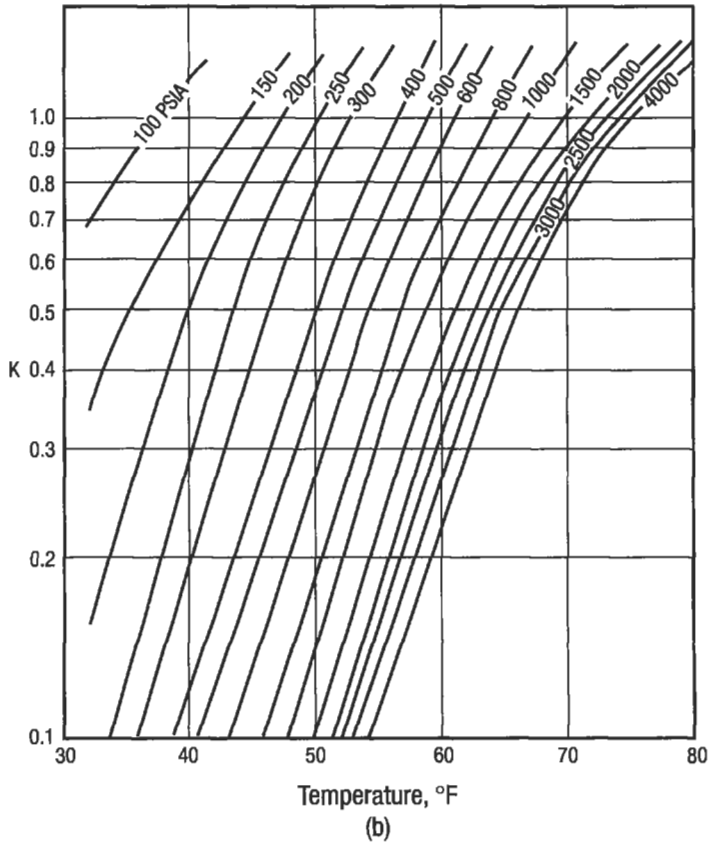
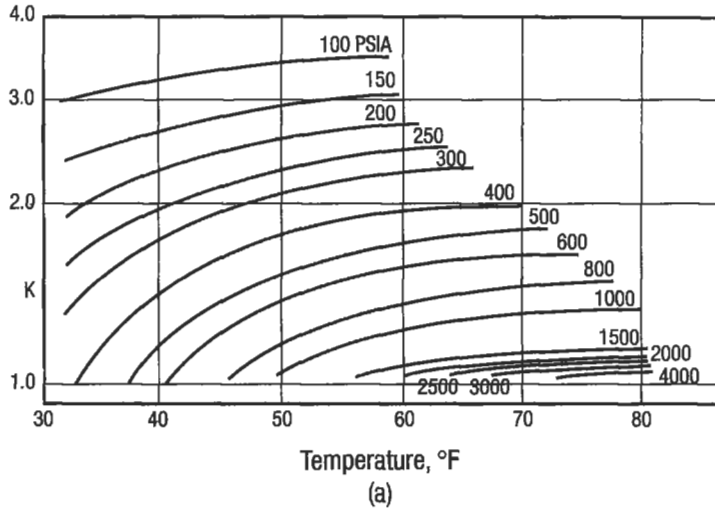


Figure 6-209. Vapor-solid equilibrium constants for CH_4 , C_2H_6 , C_3H_8 , $i\text{-C}_4\text{H}_{10}$, $\text{N-C}_4\text{H}_{10}$, H_2S and CO_2 [135,144].

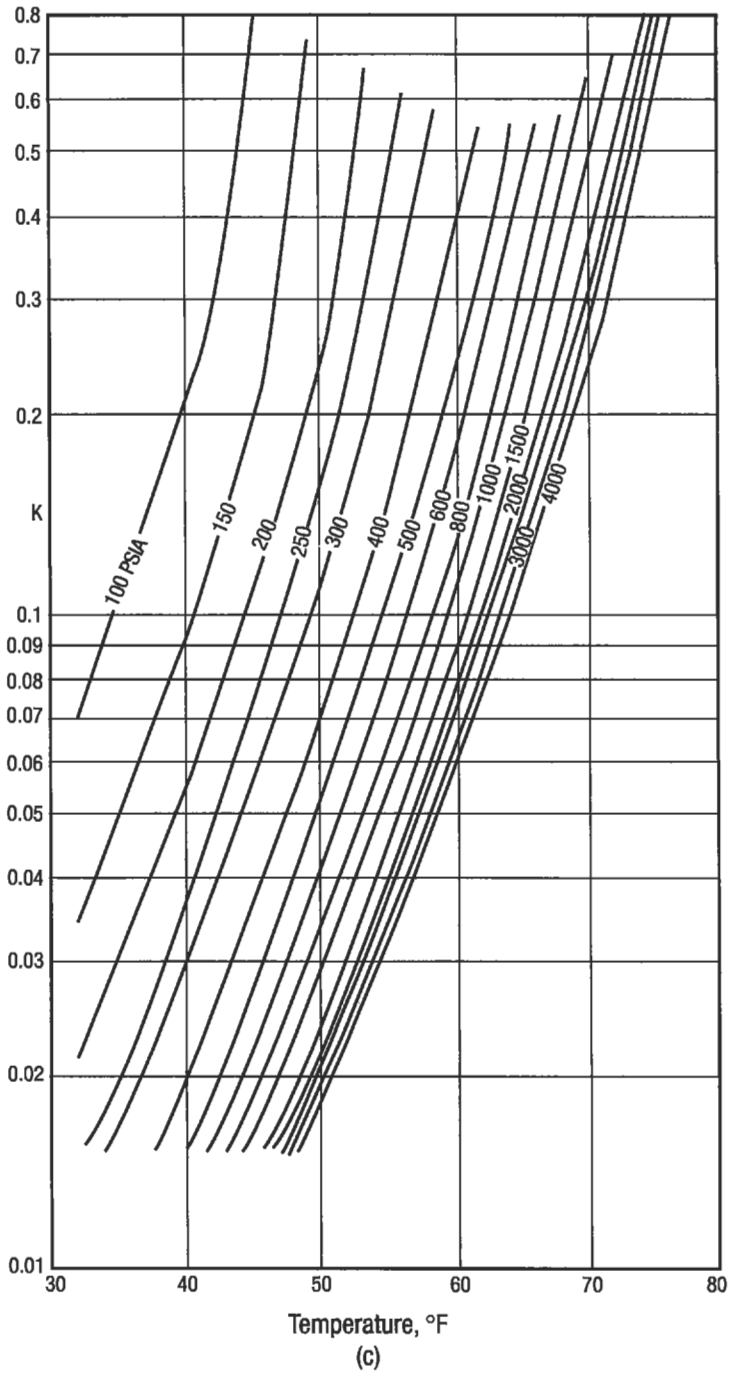
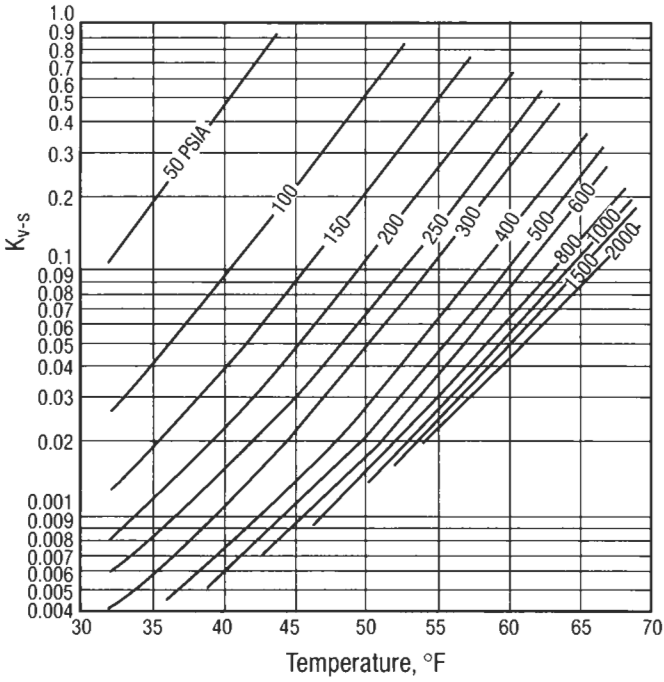
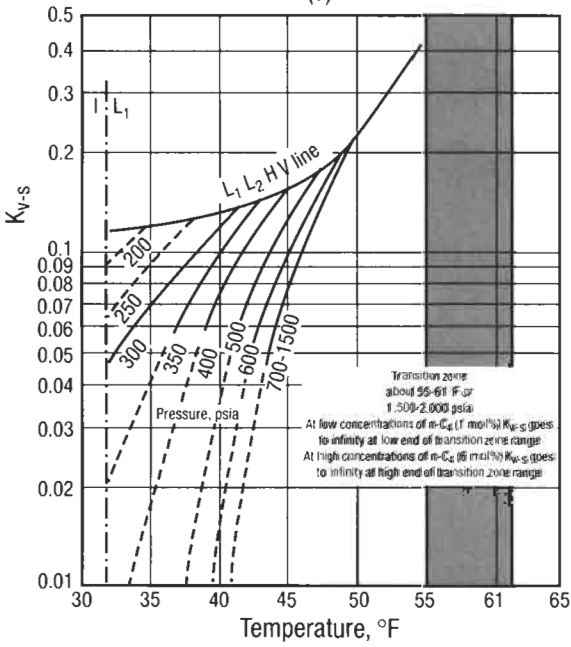


Figure 6-209. Continued



(d)



(e)

Figure 6-209. Continued

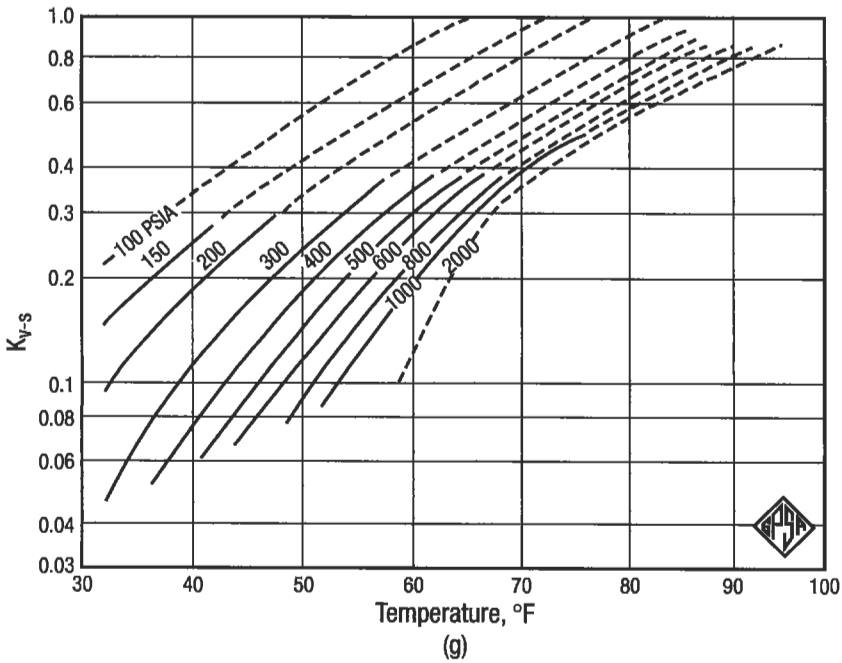
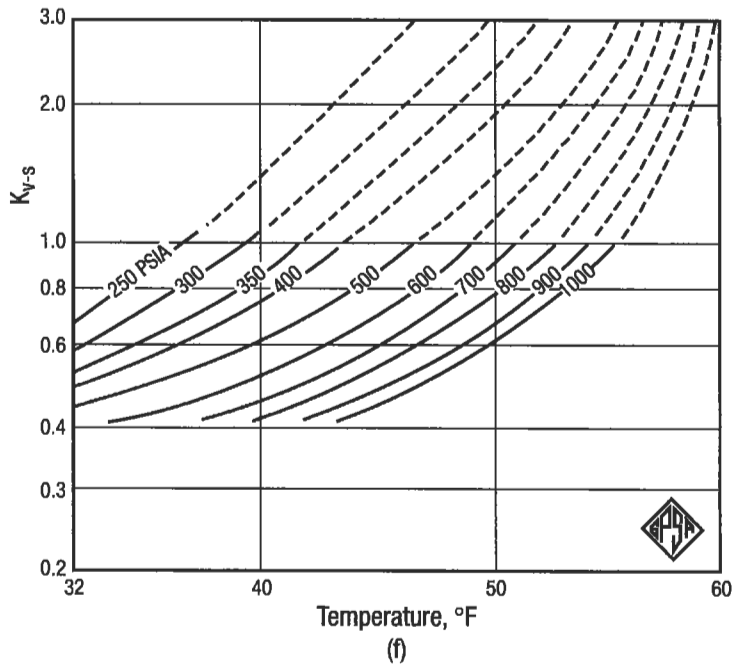


Figure 6-209. Continued

(text continued from page 768)

$$\log 30.6 = 0.8 + 0.0497 (t + 0.0077t^2)$$

$$0.000383t^2 + 0.0497t - 0.686 = 0$$

$$t = 12.57^\circ\text{C} = 54.6^\circ\text{F}$$

Both results are close enough.

Example 10

The gas with the composition below is at 3,500 psia and 150°F. What will be the hydrate conditions when this gas is expanded?

Solution

Step 1. Make several adiabatic flash calculations at different pressures and plot on a pressure versus temperature graph; see Figure 6-210.

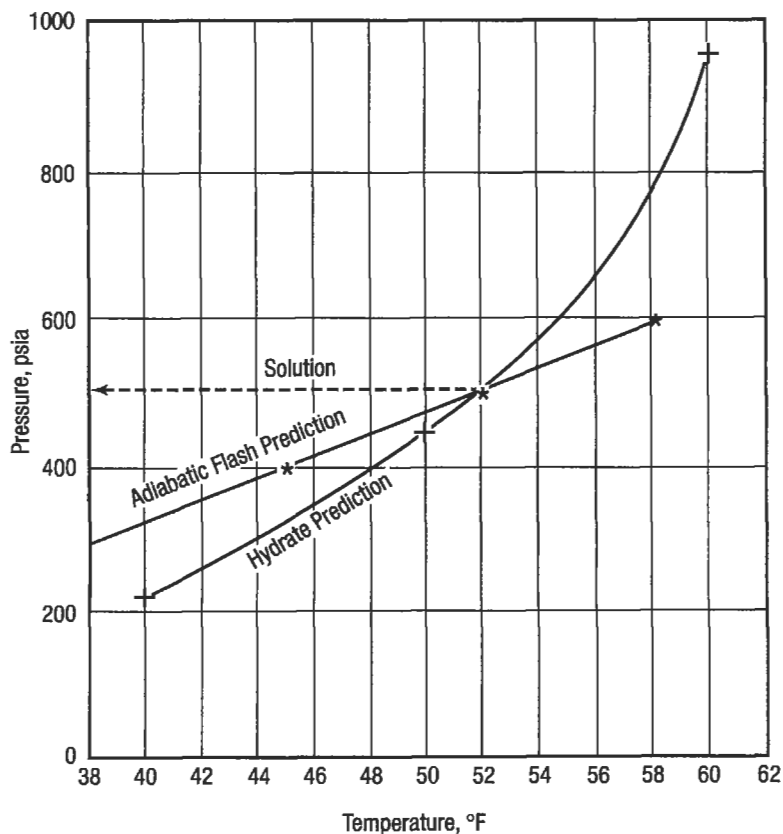


Figure 6-210. Solution sketch for example 10 [135].

Comp.	Mole fraction	Initial pressure (psia)	Initial temperature (°F)	Final pressure (psia)	Final pressure (°F)
C ₁	0.09267				
C ₂	0.529	3,500	150	300	38
C ₃	0.0138	3,500	150	400	45
iC ₄	0.0018	3,500	150	500	52
nC ₄	0.0034	3,500	150	600	58
nC ₅	0.0014	3,500	150	700	64
	= 1.000				

Step 2. Assume some temperatures (40°F, 50°F and 60°F) and predict the hydrate pressure for this gas using the solid-vapor K-data. Plot the results on Figure 6-210.

$$(y/K) = 1 \text{ at } 227 \text{ psia for } T = 40^\circ\text{F}$$

$$(y/K) = 1 \text{ at } 452 \text{ psia for } T = 50^\circ\text{F}$$

$$(y/K) = 1 \text{ at } 964 \text{ psia for } T = 60^\circ\text{F}$$

Step 3. The intersection of the lines in Figure 6-210 is the point at which hydrates start to form; in this example, 500 psia and 52°F.

The constants for H₂S shown in Figure 6-209g should be satisfactory at concentrations up to 15–20 mol% H₂S in the gas.

At this concentration of 30% or greater, hydrates may form at about the same conditions as for pure H₂S.

Slightly better results than the K-charts method will generally give computer solutions which have been developed for hydrate prediction applying P-V-T equations of state.

Hydrate Inhibition [135]

The formation of hydrates can be prevented by dehydrating to prevent a free-water phase or by inhibiting hydrate formation in the free water phase. Dehydration is usually preferable, but inhibition can often be satisfactory.

Inhibition utilizes injection of one of the glycols or methanol to lower the hydrate formation temperature at a given pressure.

Ethylene, diethylene and triethylene glycols have been used for glycol injection. The most popular has been ethylene glycol because of its lower cost, lower viscosity and lower solubility in liquid hydrocarbons.

Physical properties of the most common glycols are given in Table 6-47(a-c).

Estimation of properties for glycol-water mixtures can be achieved by a weight fraction average of the appropriate glycol curve and the water curve shown on each of the figures. To allow determination of mixture properties at lower temperatures, the pure glycol and water property curves have been extrapolated below their freezing points.

The inhibitor must be present at the very point where the wet gas is cooled to its hydrate temperature. Therefore, the inhibitor is sprayed upon the face of the feed gas chiller tube sheet where free water is present. Injection must be in

Table 6-47
Physical and Chemical Properties of Glycols [125]

	Ethylene Glycol	Diethylene Glycol	Triethylene Glycol
Molecular Weight	62.07	106.12	150.17
Specific Gravity @ 68°F	1.1155	1.1184	1.1255
Specific Weight, lb/gal.	9.292	9.316	9.375
Boiling Point @ 760 MMHg, °F	387.7	474.4	550.4
Freezing Point, °F	9.1	18.0	24.3
Surface Tension @ 77°F, dynes/cm	47.0	44.8	45.2
Heat of Vaporization @ 760 MMHg, BTU/lb	364	232	174

100% Diethylene Glycol

Temp °F	Sp Gr	Viscosity, cps	Sp Heat BTU/lb-F	Thermal Conductivity BTU/hr-sq ft-°F/ft
50	1.127	72	0.53	0.146
75	1.117	45	0.54	0.14
100	1.107	18	0.56	0.135
125	1.098	12.7	0.57	0.13
150	1.089	7.3	0.58	0.125
175	1.076	5.5	0.59	0.12
200	1.064	3.6	0.60	0.115
225	1.054	2.8	0.61	0.11
250	1.043	1.9	0.63	0.105
275	1.032	1.6	0.62	
300	1.021	1.3	0.66	

100% Triethylene Glycol

Temp °F	Sp Gr	Viscosity, cps	Sp Heat BTU/lb-F	Thermal Conductivity BTU/hr-sq ft-°F/ft
50	1.134	88	0.485	0.14
75	1.123	56	6.50	0.138
100	1.111	23	0.52	0.132
125	1.101	15.5	0.535	0.130
150	1.091	8.1	0.55	0.125
175	1.080	6.1	0.57	0.121
200	1.068	4.0	0.585	0.118
225	1.057	3.1	0.60	0.113
250	1.034	1.9	0.635	
300	1.022	1.5	0.65	

a manner to allow good distribution to every tube in chillers and heat exchangers operating below the gas hydrate temperature.

Glycol and its absorbed water are separated from the gas stream possibly along with liquid hydrocarbons. The glycol-water solution and liquid hydrocarbons can emulsify when agitated or when let down together from a high to a lower pressure. Careful separator design will allow nearly complete recovery of the glycol for regeneration and recycle.

The regenerator in a glycol injection system should be operated to produce a regenerated glycol solution that will have a freezing point below the minimum temperature encountered in the system.

Lowering of hydrate freezing point in natural gas system by an antifreeze compound may be calculated by

$$d = \frac{K_H(I)}{(100 - I)M_I} \tag{6-279}$$

where d = depression of gas hydrate freezing point in °F
 K_H = constant, for methanol = 2,335 for glycols = 4,000
 I = minimum inhibitor concentration in the free water in %
 M_I = molecular mass of solute inhibitor

Example 11

Estimate the methanol (MeOH) injection rate required to prevent hydrate formation in 2 MMscfd of 0.6 gravity natural gas at 800 psia and 40°F. The gas is water saturated at 1,000 psia and 100°F. No hydrocarbons are condensed.

Solution

From Figure 6-202b:

Water content at 100°F and 1,000 psia = 60 lb/MMscf

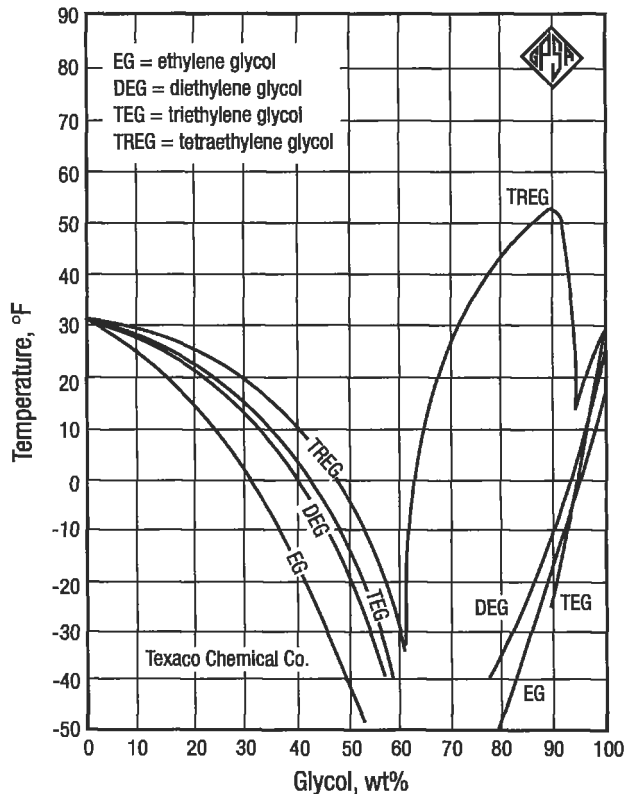


Figure 6-211. Freezing points of aqueous glycol solutions [135].

Water content at 40°F and 800 psia = 10.5 lb/MMscf

Condensed water = (60-10.5)2 = 99 lb/day

Hydrate temperature of gas = 57.5°F (Figure 6-206)

d = 57.5 - 40° = 17.5°F

From Equation 6-279:

$$17.5 = (2,335) (I) / [(100 - I) 32]$$

I = 19.4%

From Figure 6-212, find C:

$$C \left(\frac{\text{lb MeOH/MMscf}}{19.4 \text{ wt\% MeOH}} \right) = 0.975$$

so $\frac{19.4}{0.975}$ lb MeOH/MMscf → required for gas phase

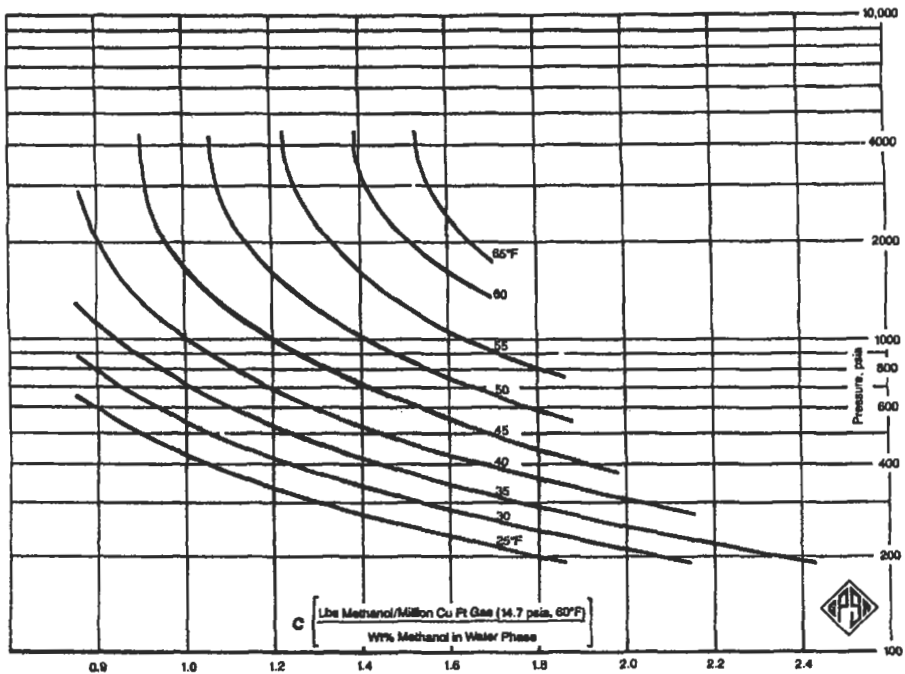


Figure 6-212. Ratio of methanol vapor composition to methanol liquid composition [135].

$$19.9 \times 2 + 39.8 \text{ lb MeOH/day}$$

$$\text{MeOH in liquid} = 99 \text{ lb/day } (0.194)/1.0 - 0.199 = 23.98$$

$$\text{Minimum MeOH injection rate} = 23.98 + 39.8 = 63.8 \text{ lb/day}$$

Gas Dehydration

In those situations where inhibition is not feasible or practical, dehydration must be used. Both liquid and solid desiccants may be used, but economics favors liquid desiccant dehydration when it will meet the required dehydration specification.

Liquid desiccant dehydration equipment is simple to operate and maintain. It can easily be automated for unattended operation; for example, glycol dehydration at a remote production well. Liquid desiccants can be used for sour gases, but additional precautions in the design are needed due to the solubility of the acid gases in the desiccant solution.

Solid desiccants are normally used for extremely low dew point specifications as required for expander plants to recover liquid hydrocarbons.

The more common liquids in use for dehydrating natural gas are triethylene glycol (TEG), diethylene glycol (DEG), and tetraethylene glycol (TREG). In general, glycols are used for applications where dew point depressions of the order of 15 to 50°C (59 to 120°F) are required. TEG is the most commonly used glycol.

For the following description of the process and flow through a typical glycol dehydration unit refer to the schematic flow diagram as shown in Figure 6-213. The wet inlet gas stream first enters the unit through a separate vertical inlet

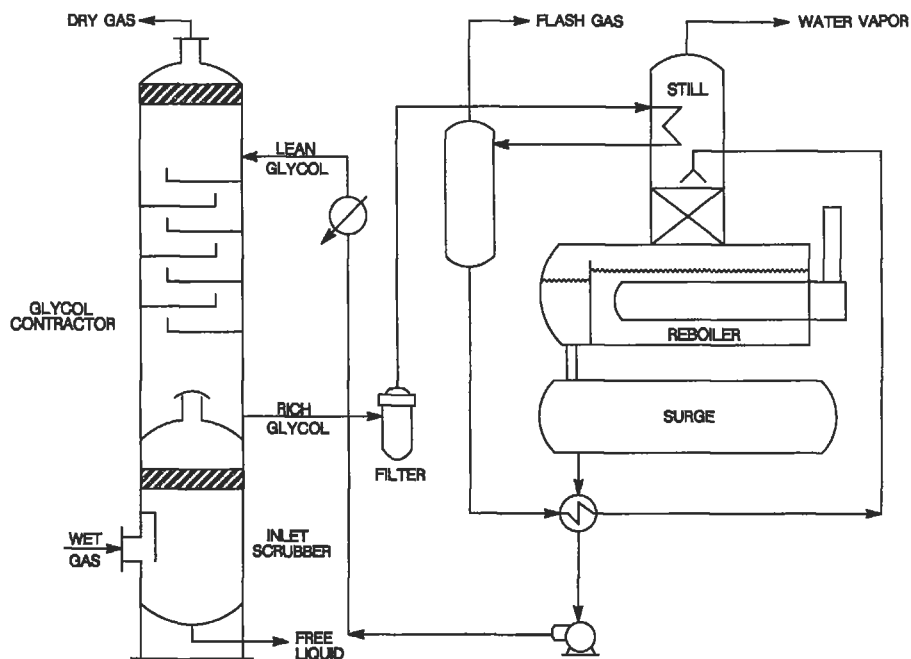


Figure 6-213. Flow sheets for TEG dehydration.

gas scrubber. In this scrubber any liquid accumulations in the gas stream are removed. The inlet scrubber is normally provided with a tangential inlet diverter that affects a circular flow of the well fluids around the wall of the vessel for centrifugal separation. The wet gas then passes out of the top of the scrubber through a high-capacity, high-efficiency, stainless steel wire mesh mist eliminator that allows for virtually no liquid carryover. The separated well fluids drain into a quiet settling chamber in the bottom of the vessel and are discharged through a diaphragm-operated motor valve operated by liquid level control. The vertical inlet gas scrubbers may be equipped for either a two-phase (oil-gas) operation or a three-phase (oil-gas-water) operation.

The wet gas leaves the top of the inlet scrubber and passes to the vertical glycol-gas contactor. The gas enters the bottom of this vessel and flows upward through the contact medium countercurrent to the glycol flow. The contact medium in the glycol-gas contactor may be valve-type trays or bubble cap trays. In smaller capacity units dumped packing may be used in the place of trays. The operation is the same in that the liquid glycol flows down through the packing and the gas vapor flows up through the packing contacting the glycol. In trayed columns the gas contacts the glycol on each tray as it passes through the vessel and the glycol absorbs the water vapor from the gas stream. Above the top tray in the contactor is an open space for entrainment settling where most of the entrained glycol particles in the gas stream will settle out. Any glycol not settling out will be removed by a high-efficiency mist eliminator in the top of the contactor vessel. The dry gas then leaves the contactor column at the top.

The incoming dry lean glycol from the surge tank is cooled in a heat exchanger before it enters the contactor for a maximum contacting efficiency. The lean concentrated glycol is picked up from the surge tank by the glycol pump and is pumped at the contactor operating pressure through the heat exchanger and into the top of the contactor column. The dry glycol enters the contactor on the top of the tray. The dry glycol flows downward through the contactor vessel by passing across each tray and spilling over the wire box on the tray, and then passing down through a downcomer to the next tray. By this countercurrent flow of gas and glycol, the driest incoming glycol on the top is in contact with the driest outgoing gas for maximum dehydration of the gas stream. The bottom tray downcomer is fitted with a seal to hold a liquid seal on the trays.

The wet rich glycol that has now absorbed the water vapor from the gas stream leaves the bottom of the glycol-gas contactor column and passes through a high-pressure glycol filter. The high-pressure glycol filter will remove any foreign solid particles that may have been picked from the gas stream in the contactor before the glycol enters the power side of the glycol pump. This is generally considered to be the ideal location for primary filtration of the glycol stream.

From the glycol filter water-rich glycol flows through the condenser coil, flashes off gas in the flash tank and flows through the glycol-glycol heat exchanger to the regenerator portion of the unit. The warmed water rich glycol enters the lower part of the tripping still column that is packed with ceramic saddles and is insulated. An atmospheric reflux condenser is integral with the stripping still at the top of the still column, and will condense any glycol vapors reaching the head of the still, plus some water vapor to provide the adequate reflux required for the stripping column. This reflux condenser is also packed with ceramic saddles to assure that all the vapor to be vented will come in contact with the cool wall of the condenser.

The wet glycol after entering the stripping still column will flow downward toward the reboiler contacting hot rising glycol vapors, water vapors and

stripping gas. The water vapor has a lower boiling point than glycol; therefore, any rising glycol vapors will be condensed in the stripping still and returned to the reboiler section. In the reboiler the glycol must travel a substantially horizontal path along the firebox to reach the liquid overflow exit at the opposite end. Here in the reboiler the glycol is heated to between 175 and 200°C to remove enough water vapor to reconcentrate it to 99.5% or more. For extra dry glycol (99% plus) it may be necessary to add some stripping gas to the reboiler.

The warm wet glycol stream flows from the reboiler to a low-pressure surge tank. Next, the regenerated glycol flows through the glycol heat exchangers for cooling and is recirculated to the contractor by the glycol pump.

Dehydrator Design [136]

Triethylene glycol dehydrators utilizing tray or packed column contactors may be sized from standard models by using the following procedures and associated graphs and tables. Custom-design glycol dehydrators for specific applications may also be designed using these procedures. The following information must be first available on the gas stream to be dehydrated.

- gas flowrate (MMscmd or MMscfd)
- composition or specific gravity of gas
- maximum working and operating pressure (bar or psig)
- gas inlet temperature (°C or °F)
- water dew point or water content required of the outlet gas (kg/MMscm or lb/MMscf)

From these, one can calculate:

1. the minimum concentration of TEG in the lean solution entering the top of the absorber required to meet outlet gas water specification.
2. the lean (dry) TEG circulation rate required to pick from the gas the needed amount of water.
3. the total heat load on reboiler.

To obtain the answer, it is necessary to have a vapor-liquid equilibrium correlation for TEG-water system.

The *minimum lean (dry) TEG concentration*, a TEG absorber, is essentially isothermal. The heat of the solution is about 21 kJ/kg (91 Btu/lb) of water absorbed in addition to the latent heat. But, the mass of water absorbed plus the mass of TEG circulated is trivial to the mass of gas, so the inlet gas temperature controls. The temperature rise seldom exceeds 2°C except when dehydrating at pressures below 10 bar (145 psia).

In Figure 6-214 diagonal lines represent % TEG in a TEG-water mixture entering the top of the absorber.

Example 12

What equilibrium water dew point could be obtained at 80°F with a lean glycol solution containing 99.5 wt% TEG?

In Figure 6-214 locate 80°F on the abscissa; go vertically to the 99.5% line and then horizontally to the ordinate. The answer is -26°F.

It is theoretical water dew point, which could be attained in a test cell, but not in a real absorber. The gas and TEG are not in contact for a long enough time to reach equilibrium.

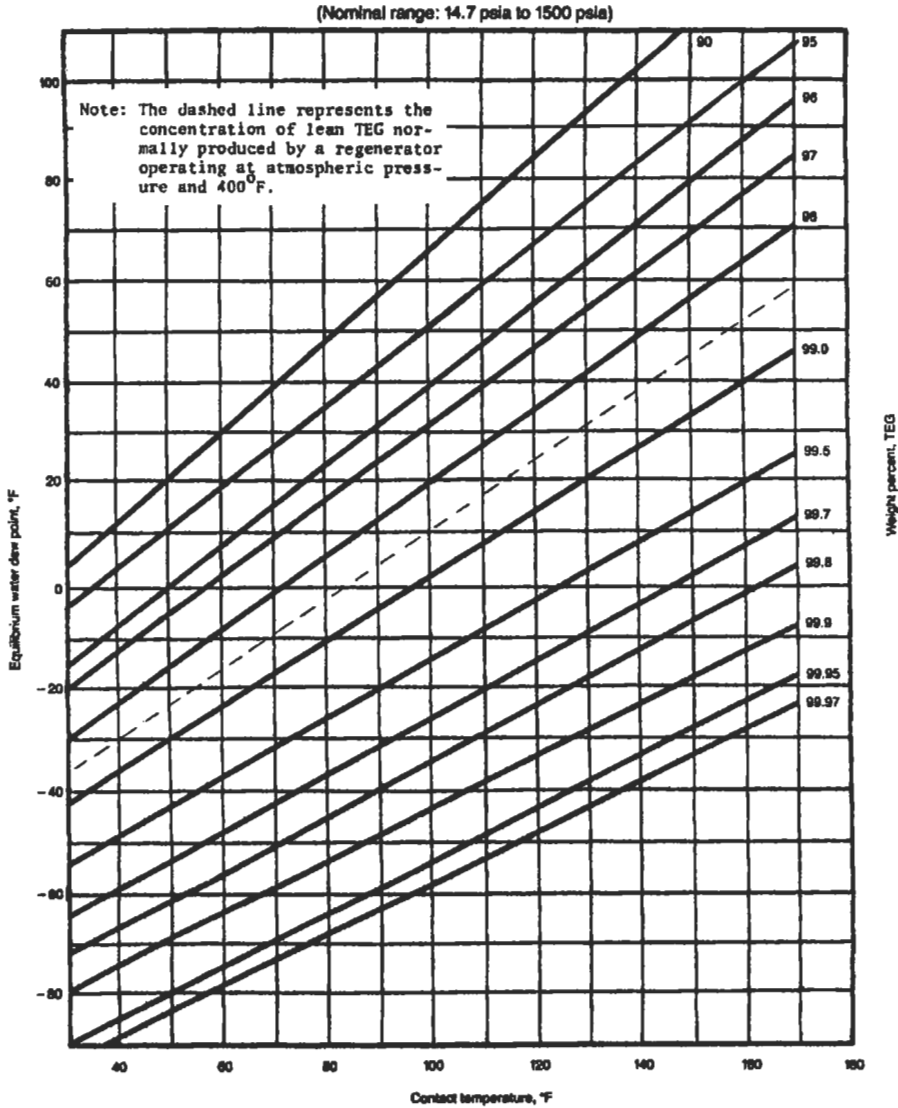


Figure 6-214. Equilibrium water dew points with various concentrations of TEG [137].

Practical tests show that a well-designed properly operated unit will have an actual water dew point $7 \pm 1.5^\circ\text{C}$ ($10 - 15^\circ\text{F}$) higher than the equilibrium dew point.

The procedure for calculation of minimum glycol concentration is as follows:

1. Establish the desired outlet dew point needed from sales contract specifications or from minimum system temperature.
2. Subtract the approach ($10 - 15^\circ\text{F}$) from the desired outlet dew point to find the corresponding equilibrium water dew point.

3. Enter the value in the second step on the ordinate of Figure 6-214 and draw a horizontal line.
4. Draw a vertical line from the inlet gas temperature on the abscissa.
5. The intersection of the lines in Steps 3 and 4 establishes minimum lean TEG concentration required to obtain the water dew point in Step 1.

If water content is specified or calculated in mass per unit gas volume, a water content–pressure dew point temperature correlation is required (see Figure 6-202*b*).

Example 13

The gas sales contract specifies an outlet water content of 5 lb/10⁶ scf at a pressure 1,000 psia. The inlet gas temperature is 100°F. What minimum TEG concentration is required?

For 5 lb/10⁶ scf and 1,000 psia, the equivalent dew point from Figure 6-202*b* is 25°F. Using 13°F approach the equilibrium dew point is 12°F. From Figure 6-214 at 12°F and 100°F contact temperature wt% TEG = 98.4%.

A given lean TEG concentration is produced in the reboiler and still column (regenerator) section by control of reboiler temperature, pressure and the possible use of a stripping gas. So long as no stripping gas is used, the concentration of the lean TEG leaving the reboiler is independent of the rich TEG entering. When stripping gas is used, the concentration of rich TEG leaving the absorber is found by a water material balance around the absorber. By definition

$$\text{Wt\% rich TEG} = \frac{(100) \text{ wt lean TEG}}{\text{Wt lean TEG} + \text{wt water absorbed} + \text{wt water in lean TEG}} \quad (6-280)$$

The weight quantities in this equation may be found per unit of time (or per unit of gas flow). In any case, the values used depend on circulation rate. This rate depends on dew point requirements, lean TEG concentration, amount of absorber contact and economics.

Economics dictates a rather low circulation rate. This rate usually will be a 7.5 to 22.5 L (2 to 6 gal) TEG solution per pound of absorbed water from the gas. The minimum rate is governed by the rate required for effective gas–liquid contact in the absorber; the maximum is limited by economics. Because regeneration takes place at low pressure, calculations are simple. Figure 6-215 has been prepared to predict regenerator performance based on Equation 2-280.

The minimum wt% lean TEG on the top abscissa is found from Figure 6-214. The wt% of rich TEG on the bottom abscissa is found from Equation 6-280. Neglecting the small amount of water in the lean TEG, the rich TEG concentration can be determined from

$$\text{Rich TEG} = \frac{8.34(SG_{gl})(\text{lean TEG})}{8.34(SG_{gl}) + 1/L_w} \quad (6-281)$$

where rich TEG = wt% TEG in rich TEG solution

8.34 = water specific weight in lb/gal

(SG_{gl}) = relative density of lean TEG solution at operating temperature of contractor

Lean TEG = wt% TEG in lean TEG solution

L_w = glycol to water circulation rate in gal TEG/lb H₂O

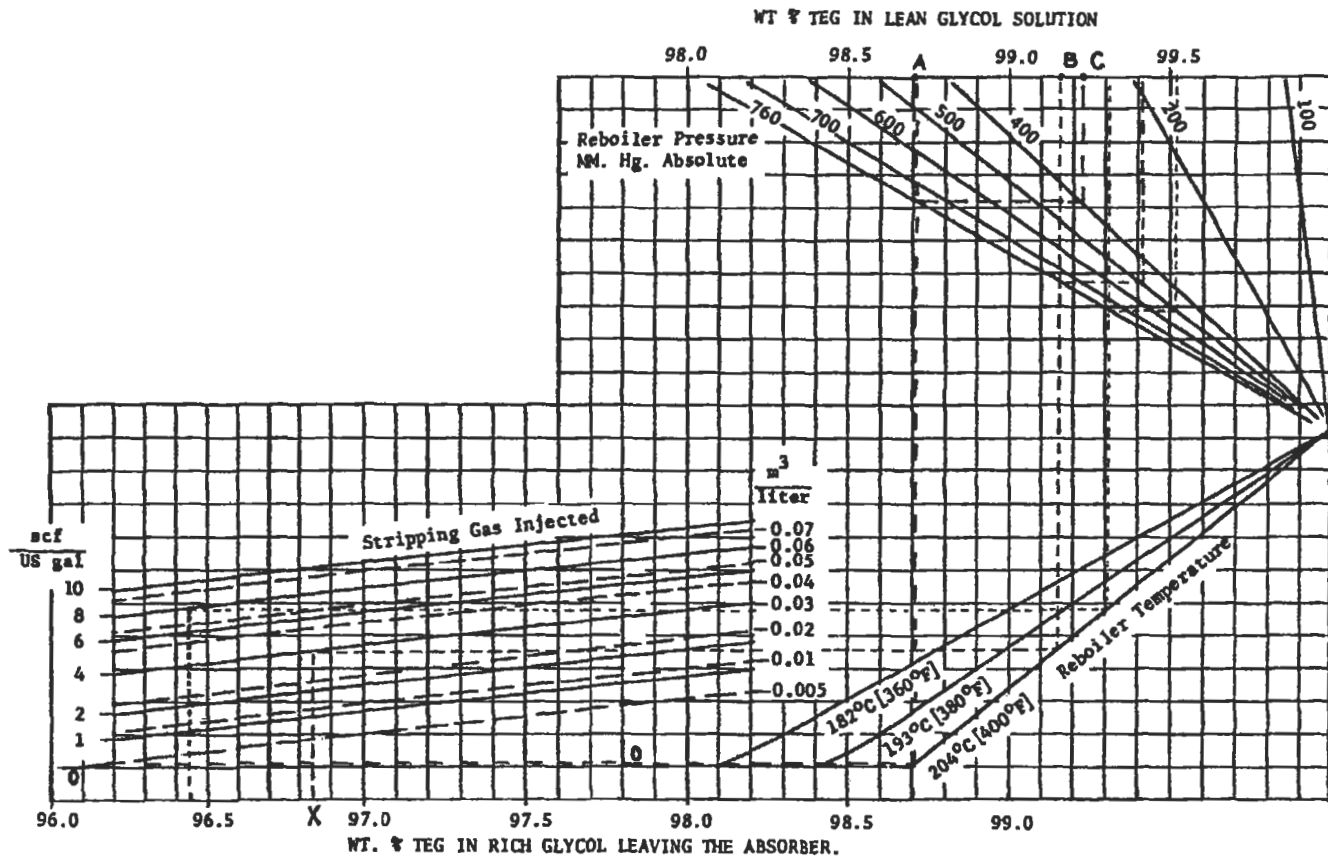


Figure 6-215. Nomograph for estimating regenerator performance as a function of pressure, reboiler temperature [137].

The diagonal lines in the lower left part of Figure 6-215 represent various amounts of stripping gas. Degree of regeneration depends on temperature regeneration, pressure and quantity of stripping gas. The general procedure for using nomogram (Figure 6-215) is as follows:

1. *Atm. Pressure, No Stripping Gas*
Wt% rich glycol is not a variable. Proceed vertically from 0 stripping gas and temperature line intersection. You will read 98.7 wt% TEG at 204°C; 98.4 wt% at 193°C.
 2. *Atm. Pressure, Stripping Gas*
 - a. Proceed vertically from B to temperature line and then horizontally.
 - b. Proceed vertically from X.
 - c. Intersection of two lines from (X) and (B) fixes amount of stripping gas.
 3. *Vacuum, No Stripping Gas*
 - a. Proceed vertically from intersection of 0 gas line and temperature line to atmosphere line (760 mmHg).
 - b. Proceed horizontally from point in (a) to pressure line necessary to fix value of point (C).
- If both stripping gas and vacuum are used, procedures 2 and 3 are combined.

99.0% to 99.9% lean TEG is available from most glycol reconcentrators. A value of 99.5 lean TEG is adequate for most design consideration.

Example 14

A 96.45 wt% rich glycol enters a regenerator using 8 scf of stripping gas per gallon of glycol solution. Reboiler temperature is 400°F. Find wt% TEG in lean glycol solution under atmospheric pressure and 400 mmHg absolute pressure.

From a bottom line for rich glycol at 96.45 flow to stripping gas we get an injected value of 8 scf/gal. Proceed to 400°F and then vertically to get a 99.31 wt% if atmospheric pressure is used. If a vacuum is employed, and the absolute pressure is 400 mmHg, the low glycol concentration is 99.52 wt%.

Calculate the required glycol circulation rate L :

$$L = \frac{L_w(W_r)G}{24} \quad (6-282)$$

and

$$W_r = \frac{(W_1 - W_0)G}{24} \quad (6-283)$$

where L = glycol circulation rate in gal/hr

L_w = glycol to water circulation rate in gal TEG/lb H₂O

W_1 = water content of inlet gas in lb H₂O/MMscf

G = gas flowrate in MMscfd

W_r = water removed from gas in lb/hr

W_0 = outlet water content in lb/hr

The required heat load, for the reboiler, can be estimated from

$$Q = 2,000(L) \quad (6-284)$$

where Q_t = total heat load on reboiler in Btu/hr

The above formula for determining the required reboiler heat load is an approximation that is accurate enough for most high-pressure glycol dehydrator sizing.

A more detailed determination of the required reboiler heat load may be made from the following procedure:

$$Q_t = Q_1 + Q_w + Q_r + Q_h \tag{6-285}$$

$$Q_1 = L\rho_{gl}C(T_2 - T_1) \tag{6-286}$$

$$Q_w = W_r \times 970.3(G) \tag{6-287}$$

$$Q_r = 0.25Q_w \tag{6-288}$$

Q_h = 5,000 to 20,000 Btu/hr depending on reboiler size

- where Q_1 = sensible heat required for glycol in Btu/hr
- Q_w = heat of vaporization required for water in Btu/hr
- Q_r = heat to vaporize reflux water in still in Btu/hr
- Q_h = heat lost from reboiler and stripping still in Btu/hr
- ρ_{gl} = glycol specific weight in lb/gal
- C = glycol specific heat at average temperature in reboiler in Btu/lb °F
- 970.3 = heat of vaporization of water at 212°F, 14.7 psia in Btu/lb
- T_2, T_1 = outlet and inlet temperatures in °F
- L, W_r, W_o, G = as in Equation 6-282

The size of the major components of a glycol dehydration unit may be estimated using the following procedures. The diameter of the inlet gas scrubber may be estimated using techniques in the section titled "Surface Oil Production Systems." The diameter of the glycol contactor can be estimated from Figure 6-216.

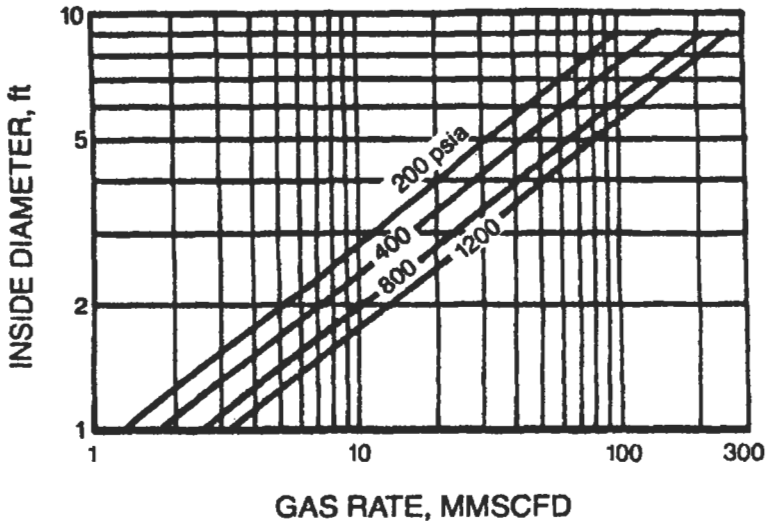
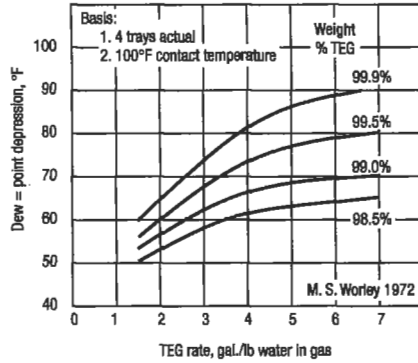
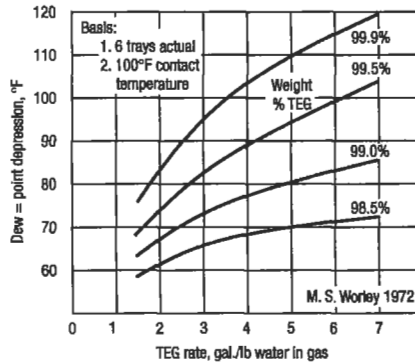


Figure 6-216. Glycol contactor capacity [135].

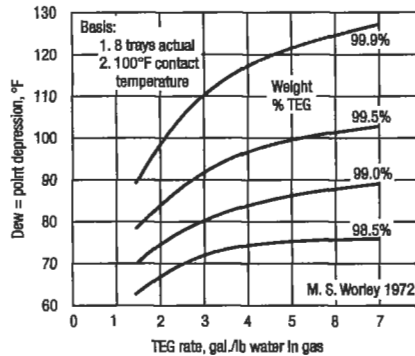
The height of the glycol contactor is based on the number of trays used in the column. The number of trays may be estimated using Figure 6-217, which is based on the dew point depression required and the glycol circulation rate. Typical field dehydration units use a value of 9 to 11 L (or 2.5 to 3 gal) of TEG per pound of water. Regardless of the type of tray, a spacing of 55 to 60 cm



a) four actual trays



b) six actual trays



c) eight actual trays

Figure 6-217. Approximate glycol flow rate [135].

(or 22–24 in.) is recommended. Therefore, the total height of the contactor column will be based on the number of trays required plus an additional 1.8 to 3 m (or 6–10 ft) to allow space for a vapor disengagement area above the top tray and an inlet gas area at the bottom of the column.

Bubble cap trays are normally used in glycol dehydrators to facilitate low liquid loadings and to offer a large turndown.

Example 14

Design the tower and reboiler for a glycol dehydration unit for these given data: gas flowrate 0.7 MMscf/hr at 1,000 psia and temperature of 100°F, and an exit dew point gas at 20°F. The inlet gas is fully water saturated with a molecular mass of 20.3. For gas reboiler $T_2 = 400^\circ\text{F}$, $T_1 = 280^\circ\text{F}$.

Solution

Inlet water content (see Figure 6-202a and b):

$$\left. \begin{array}{l} T = 100^\circ\text{F} \\ P = 1,000\text{ psia} \end{array} \right\} W_i = 60\text{ lb/Mscf} \quad \text{for } M = 17.4$$

$$W_{i(\text{at } M = 20.3)} = W_{i(M = 17.4)} \times C_G = 60 \times 0.99 = 59.4\text{ lb/MMscf}$$

Outlet water content:

$$\left. \begin{array}{l} T = 20^\circ\text{F} \\ P = 1,000\text{ psia} \end{array} \right\} W_o = 4.2\text{ lb/Mscf} \quad \text{for } M = 17.4$$

$$W_{i(\text{at } M = 20.3)} = 4.2 \times 1 = 4.2\text{ lb/Mscf}$$

Concentration of lean TEG (see Figure 6-214):

For 100°F inlet gas temperature and outlet dewpoint 20°F theoretical value for TEG is 97.9%, but we decrease this point 10–15°F. Let's take 12°F for a dew point 8°F actual concentration of lean TEG is equal 98.6 wt%.

Circulation rate glycol, from Equation 6-282:

$$L = \frac{L_w (W_r) G}{24}$$

L_w is assumed to be 3 gal TEG/lb H_2O ; a more accurate procedure is given by Campbell [136].

$$W_r = W_i - W_o = 59.4 - 4.2 = 55.2\text{ lb/MMscf}$$

$$G = 0.7\text{ MMscf/hr} = 16.8\text{ MMscfd}$$

$$L = \frac{3 \times 55.2 \times 16.8}{24} = 115.9\text{ gal/hr}$$

From Figure 6-217 find actual trays number if:

- dew point depression is $100 - 20 = 80^\circ\text{F}$
- lean glycol concentration 98.6%
- assume that $L_w = 3 \text{ gal/lb}$

Eight actual trays contactor with $L_w = 3 \text{ gal/lb}$, 80°F dew point depression and 99.1% lean TEG satisfy these conditions.

Next, the inside diameter of the contactor can be found from Figure 6-216 for $Q = 16.8 \text{ MMscfd}$, $P = 1,000 \text{ psia}$ and $D = 3 \text{ ft}$. Based on this diameter scrubber model DHT-3610 can be chosen from Table 6-49.

Glycol reboiler duty from Equation 6-285:

$$Q_r = Q_1 + Q_w + Q_r + Q_h$$

$$Q_1 = L \rho_g C (T_2 - T_1) = 115.9 \text{ gal/hr} \times 9.26 \text{ lb/gal} \\ \times 0.665 \text{ Btu/lb } ^\circ\text{F} \times (400 - 280) = 85,644 \text{ Btu/hr}$$

$$Q_w = 970.3 \text{ Btu/lb} \times 55.2 \text{ lb/MMscf} \times 16.8 \text{ MMscfd} \times \frac{1}{2} = 37,492 \text{ Btu/hr}$$

$$Q_h = 10,000 \text{ Btu/hr}$$

$$Q_r = 142,509 \text{ Btu/hr}$$

If $SG = 0.7$ and $T = 100^\circ\text{F}$, calculate the gas capacity of the gas-glycol contactor selected for the specific operating conditions:

$$G_0 = G_s(C_t)(C_g) \quad (6-289)$$

where G_0 = gas capacity of contactor at operating conditions in MMscfd
 G_s = gas capacity of contactor at $SG = 0.7$ and $T = 100^\circ\text{F}$, based on operating pressure in MMscfd

C_t = correction factor for operating temperature (Table 6-50a)

C_g = correction factor for gas specific gravity (Table 6-50b)

For more accurate calculation procedure, see Sivalls' *Glycol Dehydration Design Manual* [137].

Example 15

The sketch to Example 15 illustrates gas well surface facilities to reduce water content in gas stream. The well stream arrives at the well head at 2,000 psia and 123°F and separates water in two vessels. The first separator works at 123°F and $P = 2,000 \text{ psia}$, the second under pressure at $P = 800 \text{ psia}$.

Calculate the following:

1. Temperature in gas separator (approximately).
2. Heat removed or added (if one is necessary) by heat exchange before J-T expansion.
3. Does the well produce water (in liquid phase) in reservoir conditions? If the well does produce water, how much does it produce?

Table 6-48
Vertical Inlet Scubbers Specifications [125]

Model No.	Size O. D.	Nominal W.P. psig	Nominal Gas Capacity MMSCFD ¹	Inlet & Gas Outlet Conn	Std Oil Valve	Shipping Weight lb.
VS-162	18"	250	1.8	2"	1"	900
VS-202	20"		2.9	3"	1"	1000
VS-242	24"		4.1	3"	1"	1200
VS-302	30"		6.5	4"	1"	1400
VS-362	36"		9.4	4"	1"	1900
VS-422	42"		12.7	6"	2"	2600
VS-482	48"		16.7	6"	2"	3000
VS-542	54"		21.2	6"	2"	3500
VS-602	60"		26.1	6"	2"	4500
VS-165	16"	500	2.7	2"	1"	1000
VS-205	20"		4.3	3"	1"	1300
VS-245	24"		6.1	3"	1"	2100
VS-305	30"		9.3	4"	1"	2700
VS-365	36"		13.3	4"	1"	3800
VS-425	42"		18.4	6"	2"	4200
VS-485	48"		24.3	6"	2"	5000
VS-545	54"		30.6	6"	2"	5400
VS-605	60"		38.1	6"	2"	7500
VS-166	16"	600	3.0	2"	1"	1100
VS-206	20"		4.6	3"	1"	1400
VS-246	24"		6.3	3"	1"	2200
VS-306	30"		9.8	4"	1"	2800
VS-366	36"		14.7	4"	1"	3900
VS-426	42"		20.4	6"	2"	4500
VS-486	48"		27.1	6"	2"	5100
VS-546	54"		34.0	6"	2"	6000
VS-606	60"		42.3	6"	2"	5100
VS-1610	16"	1000	3.9	2"	1"	1100
VS-2010	20"		6.1	3"	1"	1600
VS-2410	24"		8.8	3"	1"	2500
VS-3010	30"		13.6	4"	1"	3200
VS-3610	36"		20.7	4"	1"	4400
VS-4210	42"		27.5	6"	2"	6300
VS-4810	48"		36.9	6"	2"	8400
VS-5410	54"		46.1	6"	2"	9700
VS-6010	60"		57.7	6"	2"	14500
VS-1612	16"	1200	4.2	2"	1"	1150
VS-2012	20"		6.5	3"	1"	1800
VS-2412	24"		10.0	3"	1"	2600
VS-3012	30"		15.3	4"	1"	3400
VS-3612	36"		23.1	4"	1"	4700
VS-4212	42"		31.0	6"	2"	6700
VS-4812	48"		40.5	6"	2"	8500
VS-5412	54"		51.4	6"	2"	11300
VS-6012	60"		62.3	6"	2"	14500
VS-1614	16"	1440	4.8	2"	1"	1500
VS-2014	20"		6.7	3"	1"	2100
VS-2414	24"		11.2	3"	1"	2800
VS-3014	30"		17.7	4"	1"	3900
VS-3614	36"		25.5	4"	1"	5400
VS-4214	42"		34.7	6"	2"	7800
VS-4814	48"		45.3	6"	2"	9200
VS-5414	54"		56.1	6"	2"	12900
VS-6014	60"		69.6	6"	2"	16000

1. Gas capacity based on 100°F, 0.7 sp gr, and vessel working pressure.

**Table 6-49
Tray-Type Glycol-Gas Contactors [125]**

Model No.	Size O. D.	Nominal W.P. psig	Nominal Gas Capacity MMSCFD ¹	Gas Inlet & Outlet Size	Glycol Inlet & Outlet Size	Glycol Cooler Size	Shipping Weight lb.
DHT-122	12½"	250	1.5	2"	½"	2" × 4"	800
DHT-162	16"		2.4	2"	¾"	2" × 4"	900
DHT-182	18"		3.2	3"	¾"	3" × 5"	1100
DHT-202	20"		4.0	3"	1"	3" × 5"	1400
DHT-242	24"		6.1	3"	1"	3" × 5"	2000
DHT-302	30"		9.9	4"	1"	4" × 6"	2400
DHT-362	36"		14.7	4"	1½"	4" × 6"	3200
DHT-422	42"		19.7	6"	1½"	6" × 8"	4400
DHT-482	48"		26.3	6"	2"	6" × 8"	6300
DHT-542	54"		32.7	6"	2"	6" × 8"	7700
DHT-602	60"	40.6	6"	2"	6" × 8"	9500	
DHT-125	12½"	500	2.0	2"	½"	2" × 4"	1000
DHT-165	16"		3.2	2"	¾"	2" × 4"	1200
DHT-185	18"		4.3	3"	¾"	3" × 5"	1500
DHT-205	20"		5.3	3"	1"	3" × 5"	1700
DHT-245	24"		8.3	3"	1"	3" × 5"	2900
DHT-305	30"		13.1	4"	1"	3" × 5"	3900
DHT-365	36"		19.2	4"	1½"	4" × 6"	6000
DHT-425	42"		27.4	6"	1½"	6" × 8"	7700
DHT-485	48"		35.1	6"	2"	6" × 8"	10000
DHT-545	54"		44.5	6"	2"	6" × 8"	12000
DHT-605	60"	55.2	6"	2"	6" × 8"	15300	
DHT-126	12½"	600	2.2	2"	½"	2" × 4"	1100
DHT-166	16"		3.4	2"	¾"	2" × 4"	1300
DHT-186	18"		4.5	3"	¾"	3" × 5"	1600
DHT-206	20"		5.5	3"	1"	3" × 5"	1800
DHT-246	24"		8.5	3"	1"	3" × 5"	3000
DHT-306	30"		14.3	4"	1"	3" × 5"	4000
DHT-366	36"		21.2	4"	1½"	4" × 6"	6300
DHT-426	42"		29.4	6"	1½"	6" × 8"	8400
DHT-466	48"		39.2	6"	2"	6" × 8"	11300
DHT-546	54"		49.3	6"	2"	6" × 8"	13400
DHT-606	60"	61.3	6"	2"	6" × 8"	16500	
DHT-1210	12½"	1000	2.7	2"	½"	2" × 4"	1300
DHT-1610	16"		4.3	2"	¾"	2" × 4"	1600
DHT-1810	18"		5.5	3"	¾"	3" × 5"	2100
DHT-2010	20"		7.3	3"	1"	3" × 5"	2600
DHT-2410	24"		11.3	3"	1"	3" × 5"	4200
DHT-3010	30"		18.4	4"	1"	3" × 5"	5500
DHT-3610	36"		27.5	4"	1½"	4" × 6"	8500
DHT-4210	42"		37.1	6"	1½"	6" × 8"	11800
DHT-4810	48"		49.6	6"	2"	6" × 8"	16200
DHT-5410	54"		62.0	6"	2"	6" × 8"	20200
DHT-6010	60"	77.5	6"	2"	6" × 8"	26300	
DHT-1212	12½"	1200	3.0	2"	½"	2" × 4"	1500
DHT-1612	16"		4.7	2"	¾"	2" × 4"	1900
DHT-1812	18"		6.0	3"	¾"	3" × 5"	2300
DHT-2012	20"		7.8	3"	1"	3" × 5"	3000
DHT-2412	24"		12.0	3"	1"	3" × 5"	4900
DHT-3012	30"		20.1	4"	1"	3" × 5"	6400
DHT-3612	36"		29.8	4"	1½"	4" × 6"	10000
DHT-4212	42"		41.4	6"	1½"	6" × 8"	13100
DHT-4812	48"		54.1	6"	2"	6" × 8"	18400
DHT-5412	54"		68.4	6"	2"	6" × 8"	23500
DHT-6012	60"	85.0	6"	2"	6" × 8"	29000	
DHT-1214	12½"	1440	3.1	2"	½"	2" × 4"	1800
DHT-1614	16"		4.9	2"	¾"	2" × 4"	2200
DHT-1814	18"		0.5	3"	¾"	3" × 5"	2800
DHT-2014	20"		8.3	3"	1"	3" × 5"	3500
DHT-2414	24"		13.3	3"	1"	3" × 5"	5800
DHT-3014	30"		22.3	4"	1"	3" × 5"	7500
DHT-3614	36"		32.8	4"	1½"	4" × 6"	11700
DHT-4214	42"		44.3	6"	1½"	6" × 8"	14400
DHT-4814	48"		58.3	6"	2"	6" × 8"	20000
DHT-5414	54"		74.0	6"	2"	6" × 8"	25800

¹Gas capacity based on 100°F, 0.7 sp gr and contactor working pressure.

What is the temperature in the gas separator? We calculate

$$527 \text{ vpm change in } \frac{\text{lb water}}{10^6 \text{ scf}}$$

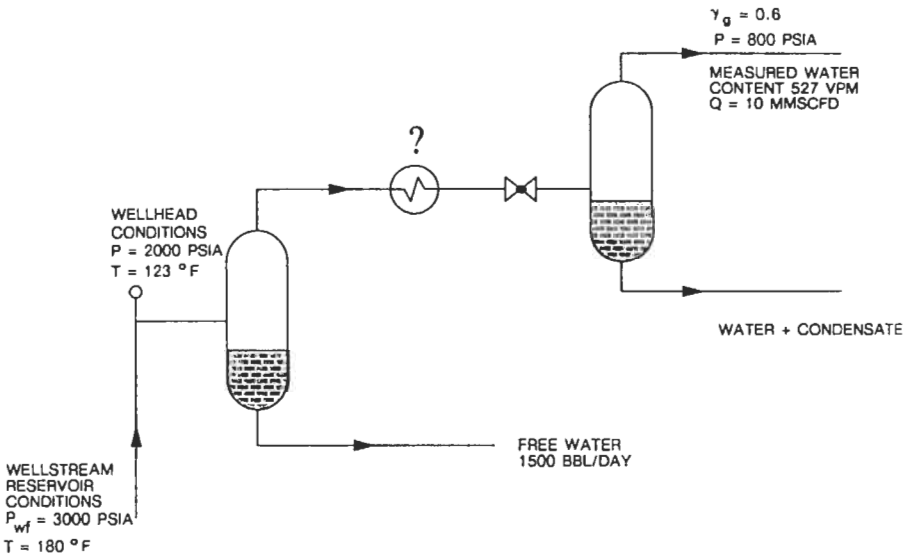
$$\frac{x \text{ lbmole H}_2\text{O} \times 379.4 \text{ scf/mole}}{10^6 \text{ scf}} = 527 \times 10^{-6}$$

$$x = \frac{527}{379.4} = 1.389 \text{ mole}$$

$$= 1.389 \text{ mole} \times 18 \text{ lb H}_2\text{O/lbmole} = 25 \text{ lb H}_2\text{O}/10^6 \text{ scf}$$

From Figure 6-202*b* for water content of 25 lb/10⁶ scf and P = 800 psia, T dew point = 67°F

Is heat added or removed?



Use any H-S diagram for natural gas with SG_g = 0.6. Starting from T = 67°F and 800 psia at constant enthalpy (J-T expansion) to P = 2,000 gives T = 123°F, so assuming constant enthalpy, no heat exchange is necessary.

Does the well produce water in reservoir conditions? The conditions are as follows:

Dissolved water in gas in reservoir conditions: T = 180°F and P = 3,000 psia, W = 195 lb/10⁶ scf.

Dissolved water in gas in separator no. 1: T = 123°F, P = 2,000 psia, W = 70/10⁶ scf.

Hence, an amount of water from gas stream is (195 - 70)10 = 1,250 lb/day. Separator no. 1 produces 1,500 lb/day water, which is more than can be

condensated from gas, which means the well produces water in liquid phase at a rate of 250 lb/day.

Solid Desiccant Dehydration (Adsorption)

Adsorption describes any process wherein molecules from the gas are held on the surface of a solid by surface forces. Solid desiccants that possess a total area of 500,000 to 800,000 m²/kg (2,400,000 to 3,900,000 ft²/lb) are used as adsorbents, and commercially use fall into one of three categories.

Alumina—a manufactured or natural occurring form of aluminum oxide that is activated by heating.

Gels—aluminum or silica gels manufactured and conditioned to have an affinity for water.

Molecular Sieves—manufactured or naturally occurring aluminosilicates exhibiting a degree of selectivity based on crystalline structure in their adsorption of natural gas constituents.

Each desiccant category offers advantages in different services. The best choice is not routine. The following discussion uses a molecular sieve to illustrate the design procedures.

Molecular sieves possess the highest water capacity, will produce the lowest water dew points (−90°C or −130°F), and can be used to simultaneously sweeten and dry gases and liquids. They also are usually much more expensive.

Molecular sieve dehydrators are commonly used ahead of NGL recovery plants where extremely dry gas is required. Cryogenic NGL plants designed to recover ethane produce very cold temperatures and require very dry feed gas to prevent formation of hydrates. Dehydration to approximately 1 ppmw is possible with molecular sieves. Typical desiccant properties are given in Table 6-51.

Figure 6-218 shows the simplest desiccant system. It consists of two towers of continuing desiccant; one is drying while the other is regenerating and cooling. During regeneration all adsorbed materials are dissolved by heat to prepare the tower for its next cycle on-stream.

The continuous process requires two (or more) vessels, with one on line removing water while the other is being regenerated. Generally a bed is designed to be on-line for 8 to 24 hr. When the bed is taken off-line, the water is removed by heating the sieve to 230–290°C (or 450–550°F). The regeneration gas used to heat the bed is usually a slipstream of dry process gas. The regeneration gas is returned to the process after it has been cooled and the free water removed.

Since solid desiccant units cost more to buy and operate than glycol units, their use is usually limited to applications such as very sour gases, very low water dew point requirements, simultaneous control of water and hydrocarbon dew points, and special cases such as oxygen-containing gases, etc. In cryogenic plants, solid desiccant dehydration usually is preferred over methanol injection to prevent hydrate and ice formation. Solid desiccants are also often used for the drying and sweetening of NGL liquids. Any host source can be used to heat the regeneration gas including waste heat from engines and turbines. Heat is a major operating cost and is a major design consideration.

Solid Desiccant Dehydrator Design [135]

The allowable superficial velocity through the bed is the first parameter that must be estimated. The pressure drop through the bed is related to the superficial velocity by a modified Ergun equation:

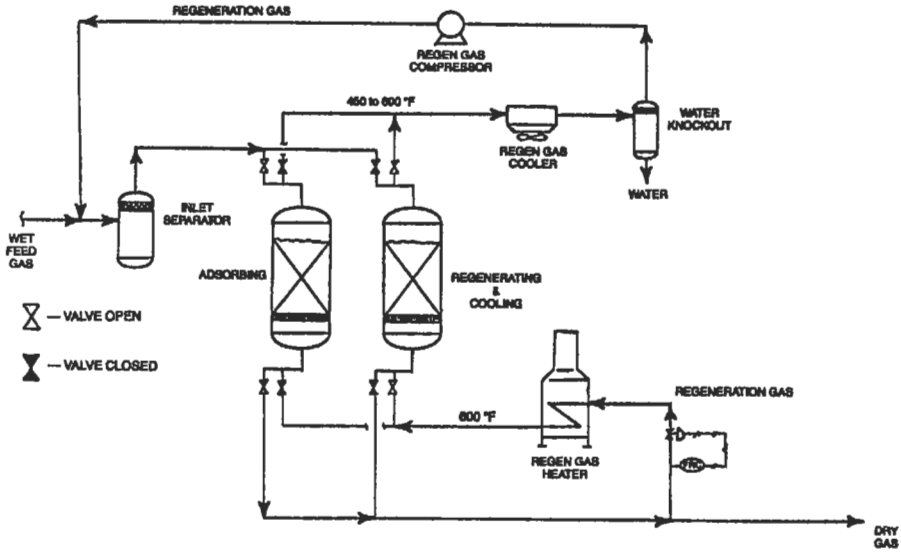


Figure 6-218. Flow sheet of a basic two-tower dry desiccant unit [135].

$$\frac{P}{L} = B\mu V + CpV^2 \tag{6-290}$$

where P = pressure drop in psi
 L = length of packed bed in ft
 μ = viscosity in cp
 V = superficial velocity in ft/min
 ρ = density in lb/ft³
 A,B = constants as below

Particle type	B	C
1/8 in bead	0.0560	0.0000889
1/8 in extrudate	0.0722	0.000124
1/16 in bead	0.152	0.000136
1/16 in extrudate	0.238	0.000210

Fire 6-219 was derived from this modified Ergun equation by assuming a gas composition and setting P/L equal to 0.333 psi/ft. The design pressure drop through the bed should be about 5 psi. A design pressure drop higher than 8 psi is not recommended. Remember to check the pressure drop after the bed height has been determined. Once the allowable superficial velocity is estimated, calculate the bed diameter:

$$D = \left[\frac{4(ACFM)}{3.14(V)} \right]^{1.2} \tag{6-291}$$

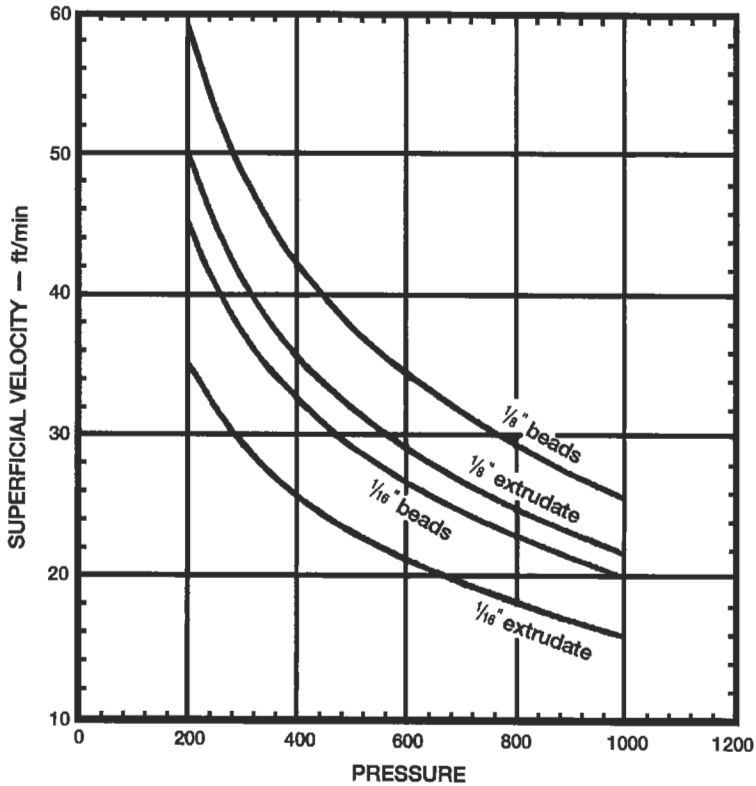


Figure 6-219. Allowable velocity for molecular sieve dehydrator [135].

where D = diameter in ft

ACFM = actual cubic feet per minute

The next step is to choose a cycle time and calculate the pounds of sieve required. Cycles for 8–12 hr are common. Cycles of greater than 12 hr may be justified especially if the gas is not water saturated. Long cycles mean less regenerations and longer sieve life, but larger beds and additional capital investment.

During the adsorption cycle, the bed can be thought of as operating with three zones. The top zone is called the saturation zone. The molecular sieve in this zone is in equilibrium with the wet inlet gas. The middle or mass transfer zone (MTZ) is where the water content of the gas is reduced from saturation to < 1 ppm. The bottom zone is unused sieve. If the bed operates too long, the mass transfer zone begins to move out the bottom of the bed causing a “breakthrough.”

Unfortunately, both the water capacity and the rate at which the molecular sieves adsorb water change as the molecular sieves age. The object of the design is to install enough sieve so that 3 to 5 years into the life of the sieve the mass transfer zone will be at the bottom of the bed at the end of the adsorption cycle.

In the saturation zone, the molecular sieve is expected to hold approximately 13 lb of water per 100 lb of sieve. This capacity needs to be adjusted when the

gas is not water saturated or the temperature is above 75°F. See Figures 6-220 and 6-221 for the correction factors. To determine the pounds of molecular sieve required in the saturation zone, calculate the amount of water to be removed during the cycle and divide by the sieve capacity:

$$S_s = \frac{W_r}{(0.13)(C_m)(C_T)} \tag{6-292}$$

$$L_s = \frac{(S_s)(\text{bulk density})(4)}{(3.14)(D^2)} \tag{6-293}$$

where S_s = amount of molecular sieve required in saturation zone in lb/hr
 W_r = water removed in lb/hr

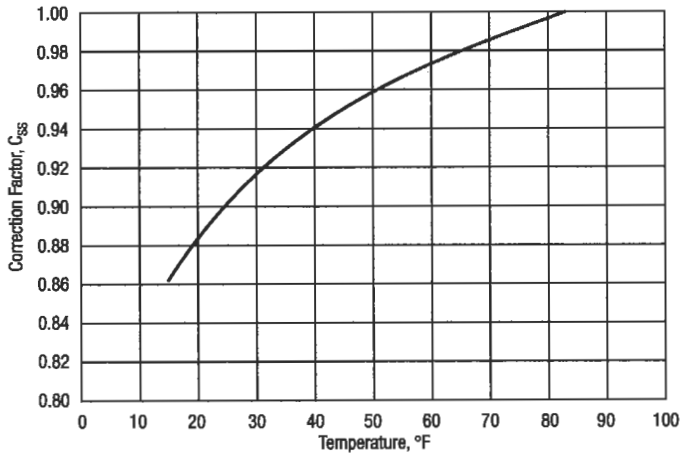


Figure 6-220. Mole sieve capacity correlation for undersaturated inlet gas [135].

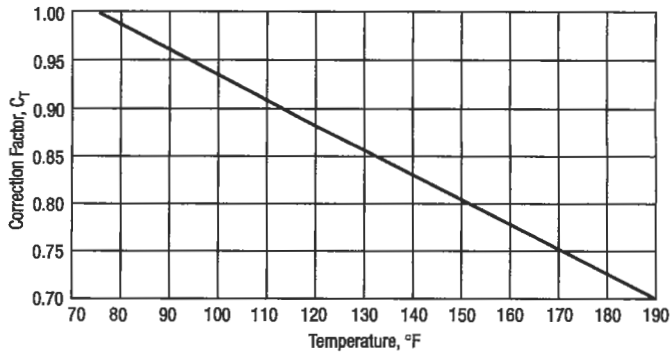


Figure 6-221. Mole sieve capacity correlation for temperature [135].

- C_s = saturation correction factor for sieve
- C_T = temperature correction factor
- L_s = length of packed bed saturation zone in ft

Bulk density is 42 to 45 lb/ft³ for spherical particles and 40 to 44 lb/ft³ for extruded cylinders.

Even though the MTZ will contain some water, the saturation zone is calculated assuming it will contain all the water to be removed.

Refer to Table 6-51 for bulk densities of common desiccants.

The length of the mass transfer zone can be calculated as

$$L_{MTZ} = (V/35)^{0.3}(Z) \tag{6-294}$$

Table 6-50
Correction Factors for Gas Capacity for Trayed Glycol-Gas
Contractors In Equation 6-289 [137]

(a)	
Operating Temp. °F	Correction Factor C_t
40	1.07
50	1.06
60	1.05
70	1.04
80	1.02
90	1.01
100	1.00
110	0.99
120	0.98
(b)	
Gas Specific Gravity	Correction Factor C_g
0.55	1.14
0.60	1.08
0.65	1.04
0.70	1.00
0.75	0.97
0.80	0.93
0.85	0.90
0.90	0.88

Table 6-51
Typical Desiccant Properties [137]

	Ethylene Glycol	Diethylene Glycol	Triethylene Glycol
Molecular Weight	62.07	106.12	150.17
Specific Gravity @ 68°F	1.1155	1.1184	1.1255
Specific Weight, lb/gal.	9.292	9.316	9.375
Boiling Point @ 760 MMHg, °F	387.7	474.4	550.4
Freezing Point, °F	9.1	18.0	24.3
Surface Tension @ 77°F, dynes/cm	47.0	44.8	45.2
Heat of Vaporization @ 760 MMHg, BTU/lb	364	232	174

$$Z = 1.70 \text{ for } \frac{1}{8}\text{-in sieve}$$

$$= 0.85 \text{ for } \frac{1}{16}\text{-in sieve}$$

The total bed height is the summation of the saturation zone and the mass transfer zone heights. Approximately 6 ft free space above and below the bed is needed.

Regeneration Calculations

The first step is to calculate the total Btus required to desorb the water and heat the sieve and vessel. A 10% heat loss is assumed, such that

$$Q_w = 1800 \frac{\text{Btu}}{\text{lb}_m} (\text{lb of water on bed}) \quad (6-295)$$

$$Q_{di} = (\text{lb of sieve}) \frac{0.22 \text{ Btu}}{\text{lb}^\circ \text{F}} (T_{rg} - T_i) \quad (6-296)$$

$$Q_{st} = (\text{lb of steel}) \frac{0.12 \text{ Btu}}{\text{lb}^\circ \text{F}} (T_{rg} - T_i) \quad (6-297)$$

$$Q_{hl} (\text{heat loss}) = (Q_w + Q_{di} + Q_{st})(0.10) \quad (6-298)$$

where Q_w = desorption of water heat duty in Btu/hr
 Q_{st} = duty required to heat mole sieve to regeneration temperature in Btu
 Q_{vt} = duty required to heat vessel and piping to regeneration temperature in Btu
 Q_{hl} = regeneration heat loss duty in Btu/hr
 T_{rg} = regeneration gas temperature in °F
 T_i = inlet temperature in °F

For the entire regeneration cycle, only about one-half of the heat put into the regeneration gas is utilized. This is because by the end of the cycle the gas is leaving the bed at about the same temperature at which it enters.

$$Q_{tr} = (2) (Q_w + Q_{st} + Q_{vt} + Q_{hl}) \quad (6-299)$$

= total regeneration heat duty in Btu

The heating time is usually $\frac{1}{2}$ to $\frac{5}{8}$ of the total regeneration time which must include a cooling period. For 8-hr adsorption cycles, the regeneration normally consists of $4\frac{1}{2}$ hr of heating, 3 hr of cooling and $\frac{1}{2}$ hr for standby and switching. For longer cycles the heating time can be lengthened as long as a minimum pressure drop of 0.1 psi/ft is maintained.

$$R_g (\text{lb/hr}) = \frac{Q_{tr}}{(C_p)(600^\circ \text{F} - T_i)(\text{heating time})} \quad (6-300)$$

where R_g = regeneration gas flow in lb/hr
 C_p = heat capacity in Btu/(lb °F)

Figure 6-222 can be used to estimate the required minimum velocity to meet 0.10 psi/ft.

The regeneration cycle frequently includes depressuring/repressuring to match the regeneration gas pressure and/or to maximize the regeneration gas volume to meet the velocity criterion. Some applications, termed pressure swing adsorption, regenerate the bed only with depressurization and sweeping the bed with gas just above atmospheric pressure.

Moisture analyzers for very low water contents require care to prevent damage to the probes. Sample probes and temperature probes must be installed to reach the center of the gas phase.

Mole sieve towers are insulated either internally or externally. Internal refractory requires careful dryout, usually before the mole sieve is installed.

Bed support and screens on top of the bed consist of three to five layers in graduated sizes. Since the flow is in both directions through the bed, both ends must be protected.

A layer of less expensive desiccant can be installed on the top of the bed to catch contaminants, such as amines. This may extend the bed life.

Since mole sieve can produce dust, filters are frequently installed downstream to protect subsequent equipment.

Operating data should be monitored to try to prevent permanent damage to the mole sieve. Performance tests are frequently scheduled on a routine basis, ranging from monthly during early operations to 6 months or longer. The size of the unit and the quantity of the expensive mole sieve also affect the frequency of performance tests.

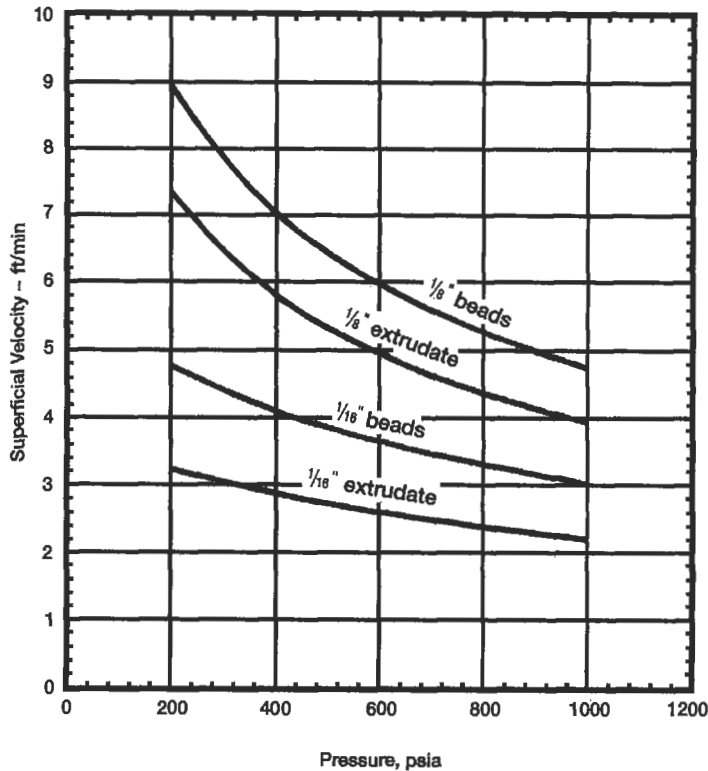


Figure 6-222. Minimum regeneration velocity for mole sieve dehydrator [137].

Gas Flow Measurement

For both sides, producers and gas users, measurement is very important; gas meters are, in fact, the cash register for gas companies. At two dollars per 1,000 ft³, a 1% error on 100 MMcfd of standard heating value is worth \$2,000 per day. $\frac{1}{10}$ % error, better than the capability of current technology, is still equal to \$73,000 per year.

An accuracy for measurement of technique, depends on:

- *Gas quality.* The best is the residue gas stream manufacturing facilities,
- *Stability gas flow.* The best measurement is for constant flowrate.
- *Pulsation and vibration.* Pulsation is defined as a variation that has a frequency of less than one cycle per second. Pulsation and vibration tend to force measurement to be interpreted too high. This is especially important during chart integration, where it becomes very difficult for the chart integrator operator to accurately interpret wide bands and highly variable flow on the charts, and for static and differential pressure measurement of pulsating flow where the recording devices tend to ride the top of the pulses and give high-volume indications.
- *Size of measuring system versus flowrate.* Systems are oversized.

- *Maintenance of metering systems especially in winter time.* All new systems for custody transfer measurement should have straightening vanes installed.
- *Proper calibration.* If we are trying to conduct gas measurement, there must be only a single-phase flow. Liquids or solids moving through the system can produce large errors and a great deal of uncertainty. In systems where two-phase flow is unavoidable, it may resort to wedge meters.

A flowmeter or measurement device is characterized using the following parameters:

- Accuracy is defined as the ratio of the difference between the actual and measured rates to the actual rate

$$\text{Accuracy} = \frac{\text{Abs. [Actual rate - measured rate]}}{\text{Actual rate}} \times 100\% \quad (6-301)$$

and it is reported in one of two ways: percent of full scale or percent of reading. For example, for a 80-MMscfd flowmeter, $\pm 1\%$ of full scale accuracy means that the measured flowrate is within ± 0.8 MMscfd of the actual flowrate, regardless of the value of the flowrate. Thus, for a measured flowrate of 15 MMscfd, the actual flowrate is between 14.2 and 15.8 MMscfd. The higher flowrate indicates more precise measurement. An accuracy of $\pm 1\%$ of reading, however, implies that the measured flowrate is within 14.85 to 15.15 MMscfd for a measured rate of 15 MMscfd and 79.2 to 80.8 MMscfd for a measured rate of 80 MMscfd.

- Rangeability is the ratio of the maximum flowrate to the minimum flowrate at the specified accuracy.
- Repeatability or precision is the ability of a meter to reproduce the same measured readings for identical flow conditions over a period of time. Repeatability does not imply accuracy; a flowmeter may have very good repeatability, but a lower overall accuracy.

Table 6-52 lists 19 different categories of flowmeters. In nearly every case each category further subdivides into several distinctly different variants.

Differential Pressure Method

This is undoubtedly the most widely used method of natural gas measurement. Some of the commonly used differential pressure devices are:

- Orifice meters, with a rangeability of about 3.5:1 and an accuracy up to $\pm 0.5\%$ [139].
- Venturi meters, with a rangeability of about 3.5:1 and an accuracy of $\pm 1\%$ [139].
- Flow nozzles, with a rangeability of 3.5:1 and an accuracy of $\pm 1.5 - 2\%$ [139].
- Pilot tube, which measures the difference between the static pressure at the wall of the flow conduit and the flowing pressure at its impact tip where the kinetic energy of the flowing stream is converted into pressure. Because of the relatively poor accuracy of this device, it is not used very often.

The Orifice Metering System

The orifice meter consists of static pressure and differential pressure recording gages connected to an orifice flange or orifice fitting. The orifice meter tube

Table 6-52
Orientation Table for Flow Sensors [130]

Type of Design	Applicable to Detect the Flow of					Direct Mass-Flow Sensor	Volumetric Flow Detector	Flow Rate Sensor	Inherent Transducer	Direct Indicator	Transmitter Available	Linear Output	Repeatability	Pressure Loss Through Sensor	Accuracy ± % Full Scale ± % Rate ± % Reproducibility	FLOW RANGE			
	Clear Liquids	Viscous Liquids	Slurry	Gas	Solids											cm ³ /min	ft ³ /min or Acm ³ /hr	SCFM or ACFM	gpm or m ³ /hr
Elbow Tap	/	L	L	/		/	/	/	/	/	SR	3:1	N	25/70	5:10 ⁴	gpm-m ³ /hr SCFM-Sm ³ /hr			
Jet Deflection				/		/	/	/	/	/	SR	35:1	M	20/5	3 ²	SCFM-Sm ³ /hr			
Laminar Flowmeters	/	/	/	/		/	/	/	/	/	/	10:1	H	15/5	1/2-5 ²	gpm-m ³ /hr SCFM-Sm ³ /hr			
Magnetic Flowmeters	/	/	/	/		/	/	/	/	/	/	10:1	N	N	1/2-10 ⁴	gpm-m ³ /hr SCFM-Sm ³ /hr			
Mass Flowmeters	/	/	/	/	SD	/	/	/	SD	SD	/	100:1	A	N	1/2-10 ⁴	gpm-m ³ /hr SCFM-Sm ³ /hr			
Metering Pumps	/	/	/	/		/	/	/	/	SD	/	20:1	-	N	1/2-1 ²	gpm-m ³ /hr			
Orifice (Plate or Integral Cell)	/	L	L	/		/	/	/	/	SR	3:1	H	20/5	1/2-2 ²	gpm-m ³ /hr SCFM-Sm ³ /hr				
Pitot Tubes	/			/		/	/	/	/	SR	3:1	L	20/70	3-5 ²	gpm-m ³ /hr SCFM-Sm ³ /hr				
Positive Displacement Gas Meters			/	/		/	/	/	/	SD	/	200:1	M	N	1/2-10 ⁴	SCFM-Sm ³ /hr			
Positive Displacement Liquid or Steam Meters	/	/		/		/	/	/	/	SD	/	10:1	H	N	1/2-10 ⁴	gpm-m ³ /hr			
Solids Flowmeters		SD	SD	/	SD	SD	/	/	SD	/	/	20:1	-	SD	1/2-10 ⁴	Sm ³ /hr			
Target Meters	/	/	L	/		/	/	/	SD	/	SR	4:1	H	15/5	1-5 ²	gpm-m ³ /hr SCFM-Sm ³ /hr			
Thermal Meters	/	L	L	/	/	/	/	/	/	/	L	20:1	A	SD	1-5 ²	gpm-m ³ /hr SCFM-Sm ³ /hr			
Turbine Flowmeters	/	L	SD	/		/	/	/	/	/	/	10:1	H	10/5	1/2-10 ⁴	gpm-m ³ /hr			
Ultrasonic Flowmeters																			
Transit Doppler	/	L	L	/		/	/	/	/	/	/	20:1	N	15/5	1-10 ⁴	gpm-m ³ /hr SCFM-Sm ³ /hr			
Variable Area Flowmeters	/	L	L	/		/	/	/	/	/	/	5:1	A	N	1/2-10 ⁴	gpm-m ³ /hr SCFM-Sm ³ /hr			
Venturi Tubes and Flow Nozzles	/	L	L	/		/	/	/	/	SR	3:1	M	20/5	1/2-3 ²	gpm-m ³ /hr SCFM-Sm ³ /hr				
Vortex Flowmeters	/			/		/	/	/	/	/	/	10:1	H	15/5	1/2-10 ⁴	gpm-m ³ /hr			
Shedding Processors	/	L	L	/		/	/	/	/	/	/	10:1	H	15/5	1-10 ⁴	ACFM-Acm ³ /hr			
Weirs, Flumes	/	L	L	/		/	/	/	/	SD	100:1	M			3-5 ²	gpm-m ³ /hr			

--- = Non Standard Range
 L = Limited
 SD = Some Designs
 H = High
 A = Average
 M = Mixed
 N = None
 SR = Square Root

⊙ = The data in this column is for general guidance only.
 ⊕ = Inherent Repeatability of Primary Device is substantially greater than shown. Value used reflects limitation of differential pressure sensing device, when maximum reading accuracy is desired.
 ⊖ = Pipe size establishes the upper limit.
 ⊗ = Practically indicated with the probe type design.
 ⊙ = Must be conductive.
 ⊕ = Can be re-ranged.
 ⊖ = Varies with upstream disturbance.
 ⊗ = Depends on application conditions.

If the thickness of the orifice plate must be greater than permitted by these limitations, the downstream edge shall be cut away (beveled or recessed) at an angle of 45° or less to the face of the plate, leaving the thickness of the orifice edge within those requirements. All orifice plates that are beveled should have the square-edge side stamped "inlet" or the beveled side stamped "outlet." The upstream edge of the orifice shall be square and sharp, so that it will not show a beam of light when checked with an orifice edge gage, or alternately will not reflect a beam of light when viewed without magnification. The orifice shall not have a burred or feathered edge; it shall be maintained in this condition at all times. Moreover, the orifice plate shall be kept clean at all times and free from accumulation of dirt, ice and other substances.

The magnitude of the measured pressure differential is affected by the location of the points across the orifice between which it is measured. The four types of pressure tap locations that have been used are as follows:

1. *Flange type.* In this type, the pressure is measured 1 in. upstream and 1 in. downstream of the orifice. This is the most common type of pressure tap.
2. *Pipe taps.* The pressure is measured 2.5 pipe IDs upstream and 8 pipe IDs downstream of the orifice.
3. *Vena contracta taps.* The upstream tap is one ID upstream of the orifice, and downstream tap is located at the plane of the vena contracta. Vena contracta location is determined from an experimental curve.
4. *Corner type.* The pressure taps are located immediately adjacent to the upstream and downstream faces of the orifice plate (see Figure 6-224).

The orifice is usually mounted between a pair of flanges. To avoid errors resulting from disturbance of the flow pattern due to valves, fittings, etc., a straight run of smooth pipe before and after the orifice is recommended. Required length depends on β ratio (ratio of diameter of orifice to inside diameter of pipe) and severity of the flow disturbance. The orifice to meter tube diameter ratio $\beta = d/D$ should be limited as follows: 0.15 to 0.70 with meters using flange taps and 0.20 to 0.67 with meters using pipe taps. The term "meter tube" shall mean the straight upstream pipe of the same diameter (of length A and A' on Figures 6-225 to Figure 6-229 and Table 6-53) between the orifice flanges or fittings and the similar downstream pipe (length B on the same figures) beyond the orifice.

The mean inside diameter of the meter tube should be determined. Measurements are to be made on at least four diameters equally spaced in a plane 1 in. upstream from the upstream face of the orifice plate. The mean of these four or more measurements is to be used in the calculation of the flow coefficient when minimum uncertainty of this variable is desired.

The difference between the maximum measured diameter and the minimum measured diameter of the inlet section shall not exceed the tolerance allowed by Figure 6-230 as a percent of the published diameter. The following equation may be used to calculate the variance of the upstream section of the meter tube:

$$\left(\frac{\text{Max } D - \text{Min } D}{D} \right) 100 \leq \% \text{ tolerance} \quad (6-302)$$

The meter tube diameter must agree with the published inside diameters within the tolerance allowed by Figure 6-230. The temperature at which the

(text continued on page 806)

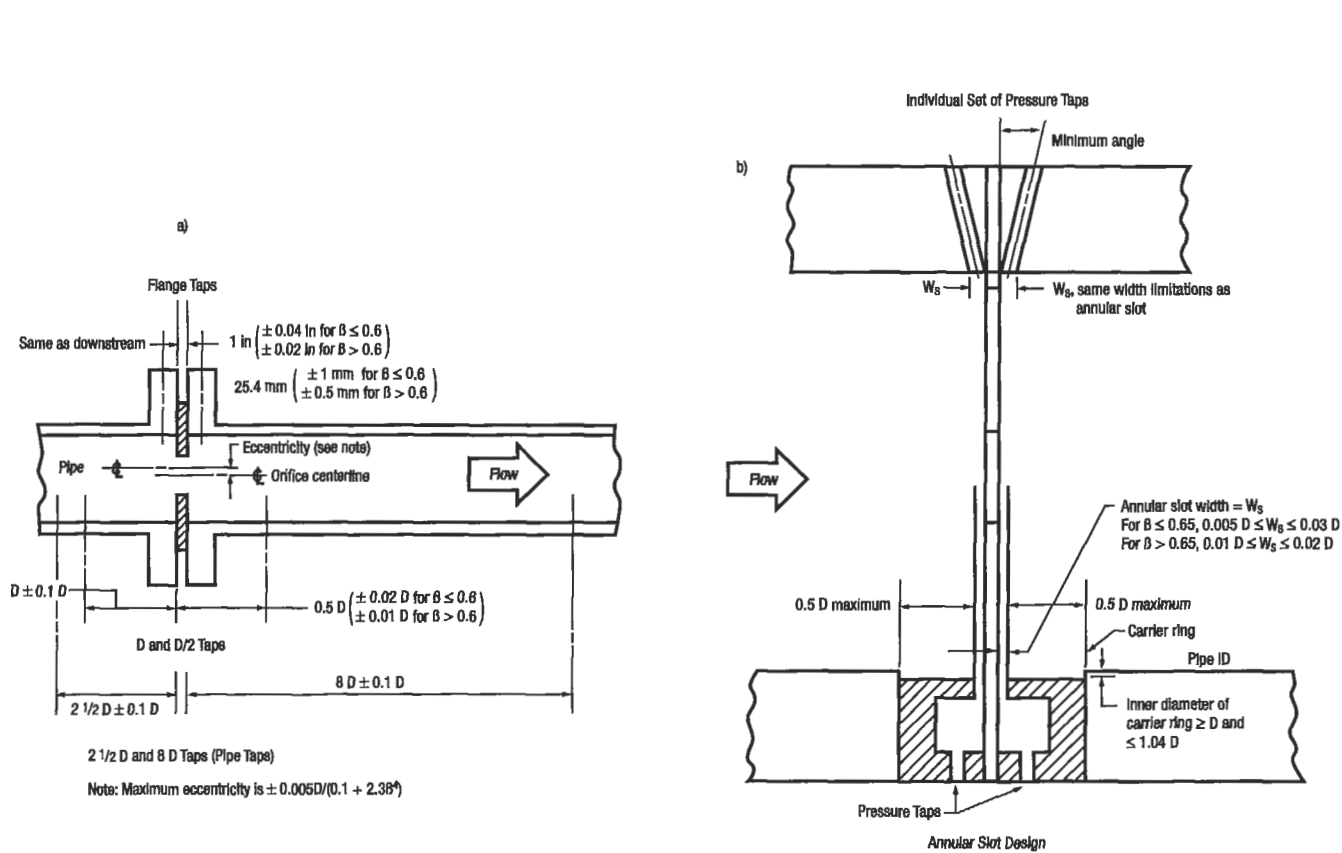


Figure 6-224. Pressure-tap spacing [141].

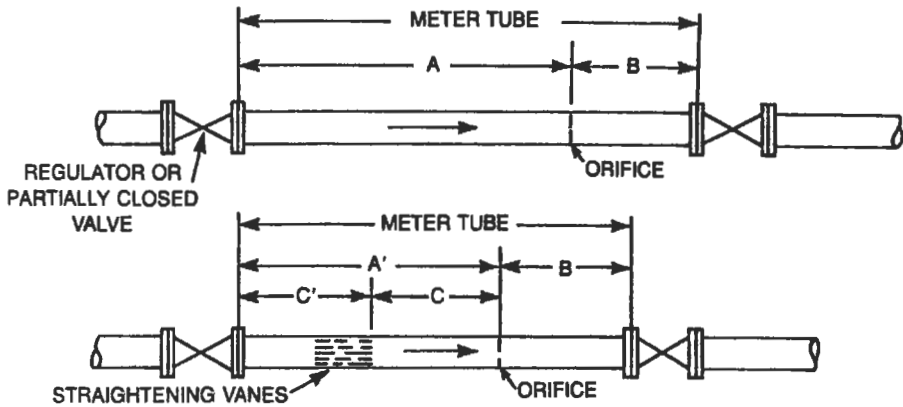


Figure 6-225. Partly closed valve upstream of meter tube [140].

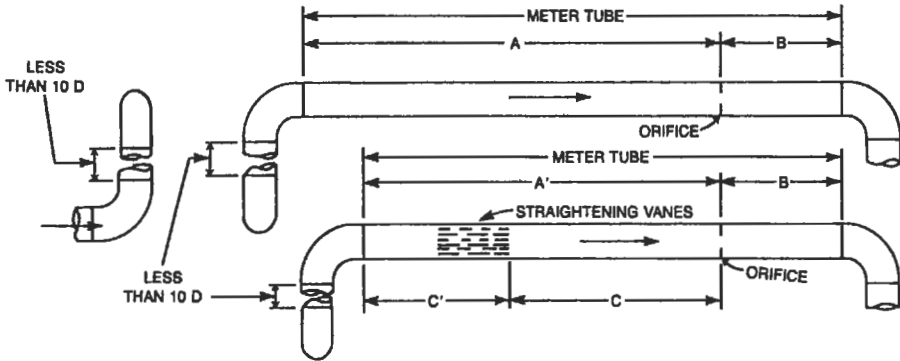


Figure 6-226. Two ells not in same plane upstream of meter tube [140].

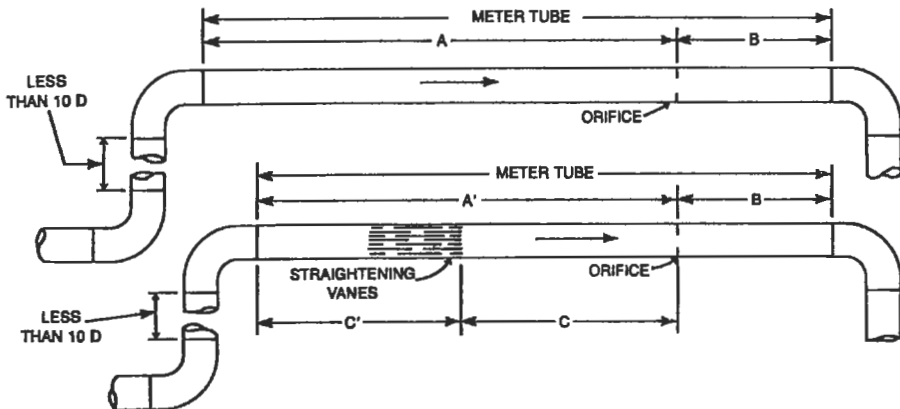


Figure 6-227. Less than ten pipe diameters D between two ells in same plane upstream of meter tube [140].

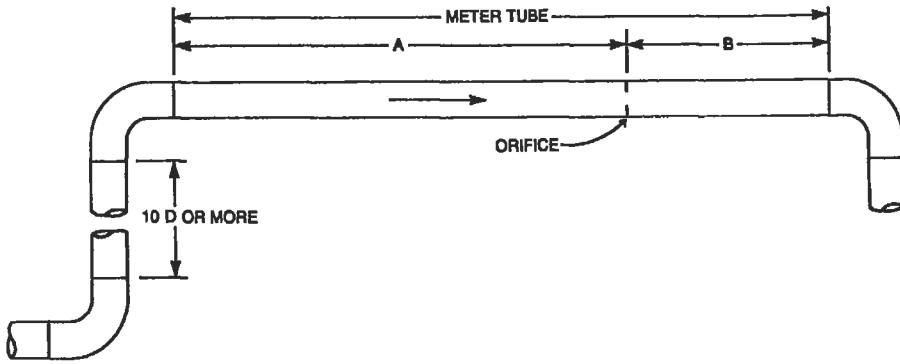


Figure 6-228. Greater than ten pipe diameters D between two ells in the same plane upstream of meter tube.
Source: after (13)

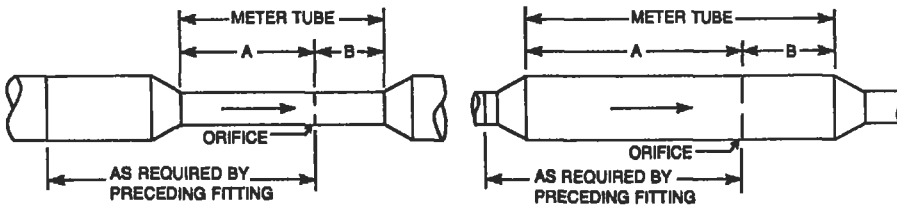


Figure 6-229. Reducer or expander upstream of meter tube [140].

(text continued from page 803)

motor tube measurements are made should be recorded for possible correction to operating conditions.

Gas Orifice Calculations [140,141]

In measurement of natural gas, the general practice is to express the flow in ft³/hr at some specified reference or base condition of pressure and temperature.

A convenient way of making this computation is to write flow equation using the orifice flow constant C':

$$Q_v = C'(h_w P_f)^{0.5} \tag{6-303}$$

where: Q_v = volume flowrate in ft³/hr at base conditions
 h_w = differential pressure in inches of water at 60°F
 P_f = static pressure in psia; use subscript 1 when P_f is measured at the upstream orifice tap and subscript 2 when the P_f is measured at the downstream orifice tap

and

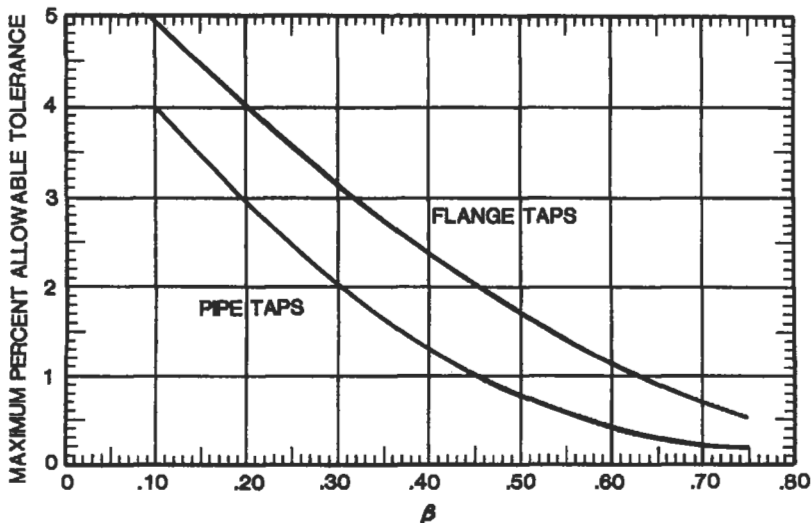
$$C' = F_b F_r Y F_{pb} F_{ub} F_{gr} F_{pv} F_m F_1 F_a \tag{6-304}$$

where C = orifice flow constant
 F_b = basic orifice factor
 F_r = Reynold's number factor

Table 6-53
Minimum Motor Tube Lengths in Terms of Pipe Diameters and Beta Ratio

Installation Figure	Dimension	Beta Ratio				
		0.5	0.6	0.67	0.70	0.75
6-225	A	25.0	30.0	36.0	38.6	43.5
	A'	10.2	12.2	14.2	15.3	17.5
	B	3.8	4.1	4.2	6.3	4.5
	C	5.0	5.5	6.2	6.4	7.0
	C'	5.2	6.7	8.0	8.9	10.5
6-226	A	20.8	25.0	28.8	31.0	35.2
	A'	10.0	11.4	12.8	13.5	15.0
	B	3.8	4.0	4.2	4.3	4.5
	C	5.0	5.5	6.2	6.5	7.2
6-227	C'	5.0	5.9	6.6	7.0	7.8
	A	10.0	13.8	17.4	19.0	22.0
	A'	9.0	10.3	11.7	12.3	13.8
	B	3.8	4.0	4.2	4.3	6.5
6-228	C	5.0	5.5	6.2	6.5	7.1
	C'	4.0	4.8	5.5	5.8	6.7
	A	6.9	9.3	12.5	13.9	16.7
	B	3.8	4.0	4.2	4.3	4.5
6-229	A	7.5	9.7	11.8	12.1	13.6
	B	3.8	4.1	4.2	4.3	4.5

Use for all pipe sizes. Based on flange taps. For pipe taps add 2 diameters to A, A', and C and 8 pipe diameters to B.



Note: Maximum percent allowable tolerance between measured upstream inside diameter and the published inside diameter refer to the published inside diameter.

Figure 6-230. Maximum percent allowable meter tube tolerance [140].

- Y = expansion factor
 F_{pb} = pressure base factor
 F_{tb} = temperature base factor
 F_{tf} = flowing temperature factor
 F_{gr} = real gas relative density factor
 F_{pv} = supercompressibility factor
 F_m = manometer factor (for mercury manometer)
 F_1 = gauge location factor
 F_a = orifice thermal expansion factor

The basic orifice factor F_b depends upon the type of pressure taps and the pipe and orifice diameters. F_b can be calculated from analytical equations as

$$F_b = 338.17d^2K_0 \quad (6-305)$$

where d = actual diameter of the orifice in in.

K_0 = coefficient of discharge for an infinite Reynolds number (which will be the minimum value for any particular orifice and pipe size)

and

$$K_0 = \frac{K_e}{1 + \frac{15E}{1,000,000d}}$$

where $E = d(830 - 500\beta + 9,000\beta^2 - 4,200\beta^3 + B)$

$B = 530/D^{0.5}$ (for flange taps)

$= 875/D + 75$ (for pipe taps)

$$\begin{aligned}
 K_e &= 0.5993 + \frac{0.007}{D} + \left(0.364 + \frac{0.076}{D^{0.5}}\right)\beta^4 + 0.4\left(1.6 - \frac{1}{D}\right)^5 \\
 &\quad \times \left[\left(0.07 + \frac{0.5}{D}\right) - \beta\right]^{3/2} - \left(0.009 + \frac{0.034}{D}\right)[0.5 - \beta]^{3/2} \\
 &\quad + \left(\frac{65}{D^2} + 3\right)[\beta - 0.7]^{3/2} \quad (\text{for flange taps}) \\
 &= 0.5925 + \frac{0.0182}{D} + \left(0.440 - \frac{0.06}{D}\right)\beta^2 + \left(0.935 + \frac{0.225}{D}\right)\beta^5 \\
 &\quad + 1.35\beta^{14} + \frac{1.43}{D^{0.5}}(0.25 - \beta)^{3/2} \quad (\text{for pipe taps})
 \end{aligned}$$

D = the actual internal pipe diameter in in.

β = the orifice diameter ratio, expressed as d/D

F_b should be rounded to four decimal places

In practice Tables 6-54 and 6-55 are used. The following conditions apply for F_b values: $T_b = 60^\circ\text{F}$, $T_f = 60^\circ\text{F}$, real gas relative density (specific gravity) = 1.0, $P_b = 14.73$ psia, $(h_w/P_f)^{0.5} = \infty$, $h_w/P_f = 0$.

(text continued on page 815)

**Table 6-54
(continued)**

Orifice Diameter Inches	Pipe Sizes, Nominal and Published Inside Diameters, in inches								
	10			12			16		
	9.562	10.020	10.136	11.374	11.938	12.090	14.688	15.000	15.250
1.000	200.20								
1.125	253.56	253.49	253.47						
1.250	313.32	313.21	313.18	312.95	312.86	312.84			
1.375	379.45	379.30	379.27	378.95	378.83	378.79			
1.500	451.96	451.77	451.73	451.31	451.15	451.11	450.54	450.49	
1.625	530.88	530.64	530.58	530.05	529.85	529.80	529.07	529.00	528.95
1.750	616.22	615.92	615.84	615.18	614.92	614.85	613.95	613.87	613.80
1.875	708.00	707.62	707.53	706.70	706.38	706.30	705.19	705.09	705.00
2.000	806.25	805.78	805.66	804.63	804.25	804.13	802.80	802.67	802.57
2.125	911.00	910.40	910.26	909.00	908.53	908.41	906.79	906.63	906.51
2.250	1022.3	1021.5	1021.4	1019.8	1019.2	1019.1	1017.2	1017.0	1016.8
2.375	1140.1	1139.2	1139.0	1137.1	1136.4	1136.2	1133.9	1133.7	1133.5
2.500	1264.5	1263.4	1263.2	1260.9	1260.0	1259.8	1257.1	1256.9	1256.7
2.625	1395.6	1394.3	1393.9	1391.2	1390.2	1389.9	1386.7	1386.4	1386.2
2.750	1533.4	1531.7	1531.4	1528.0	1526.8	1526.5	1522.7	1522.4	1522.1
2.875	1678.0	1675.9	1675.5	1671.4	1670.0	1669.7	1665.2	1664.8	1664.5
3.000	1829.5	1826.9	1826.4	1821.5	1819.8	1819.4	1814.2	1813.7	1813.4
3.125	1987.8	1984.8	1984.1	1978.2	1976.2	1975.7	1969.6	1969.1	1968.7
3.250	2153.3	2149.5	2148.7	2141.6	2139.2	2138.6	2131.5	2130.9	2130.4
3.375	2325.8	2321.3	2320.2	2311.8	2308.9	2308.3	2300.0	2299.3	2298.7
3.500	2505.7	2500.2	2498.9	2488.8	2485.4	2484.6	2475.0	2474.1	2473.5
3.625	2692.9	2686.3	2684.8	2672.7	2668.7	2667.8	2656.5	2655.6	2654.9
3.750	2887.7	2879.7	2878.0	2863.5	2858.9	2857.8	2844.7	2843.6	2842.8
3.875	3090.2	3080.7	3078.6	3061.5	3056.0	3054.7	3039.4	3038.2	3037.3
4.000	3300.7	3289.4	3286.8	3266.5	3260.1	3258.5	3240.9	3239.5	3238.4
4.250	3746.3	3730.3	3726.8	3698.6	3689.7	3687.6	3663.9	3662.0	3660.6
4.500	4226.3	4204.2	4199.3	4160.5	4148.5	4145.6	4114.0	4111.6	4109.8
4.750	4742.9	4712.9	4706.3	4653.6	4637.4	4633.6	4591.6	4588.5	4586.1
5.000	5298.9	5258.6	5249.7	5179.2	5157.5	5152.4	5097.3	5093.2	5090.2
5.250	5897.8	5843.8	5832.0	5738.7	5710.1	5703.3	5631.5	5626.2	5622.4
5.500	6543.6	6472.0	6456.4	6334.1	6296.8	6288.1	6194.9	6188.2	6183.2
5.750	7240.6	7147.1	7126.7	6967.3	6919.2	6908.0	6788.3	6773.8	6773.5
6.000	7994.1	7873.1	7846.9	7640.8	7579.2	7564.9	7412.5	7401.7	7393.8
6.250	8809.8	8655.0	8621.3	8357.8	8279.1	8260.9	8068.5	8054.9	8045.0
6.500	9694.3	9498.3	9455.5	9121.6	9021.9	8998.9	8757.5	8740.5	8728.1
6.750	10656	10409	10355	9935.9	9810.7	9781.8	9480.6	9459.6	9444.2
7.000	11713	11394	11327	10805	10649	10613	10239	10213	10194
7.250		12468	12381	11733	11540	11496	11035	11003	10980
7.500		13656	13541	12726	12489	12435	11870	11831	11803
7.750				13789	13500	13434	12745	12698	12664
8.000				14928	14579	14498	13664	13607	13566
8.250				16160	15730	15633	14629	14560	14511
8.500				17508	16963	16845	15642	15560	15501
8.750					18297	18148	16707	16610	16539
9.000						19566	17827	17711	17627
9.250							19005	18869	18770
9.500							20245	20086	19969
9.750							21553	21366	21229
10.000							22931	22713	22554
10.250							24385	24132	23948
10.500							25924	25628	25415
10.750							27567	27211	26961
11.000							29332	28900	28599
11.250								30711	30347

**Table 6-54
(continued)**

Orifice Diameter Inches	Pipe Sizes, Nominal and Published Inside Diameters, in inches								
	20			24			30		
	18.812	19.000	19.250	22.624	23.000	23.250	28.750	29.000	29.250
2.000	801.42	801.37	801.31						
2.125	905.13	905.08	905.00						
2.250	1015.2	1015.1	1015.0						
2.375	1131.6	1131.5	1131.4	1130.2	1130.1	1130.0			
2.500	1254.4	1254.3	1254.2	1252.8	1252.7	1252.6			
2.625	1383.6	1383.5	1383.3	1381.7	1381.6	1381.5			
2.750	1519.1	1519.0	1518.9	1517.0	1516.8	1516.7			
2.875	1661.1	1660.9	1660.8	1658.6	1658.4	1658.3	1656.0		
3.000	1890.4	1890.3	1890.1	1806.6	1806.4	1806.3	1803.7	1803.6	1803.5
3.125	1964.2	1964.0	1963.7	1961.0	1960.8	1960.6	1957.7	1957.6	1957.5
3.250	2125.3	2125.1	2124.8	2121.8	2121.5	2121.3	2118.0	2117.9	2117.8
3.375	2292.9	2292.7	2292.4	2288.9	2288.6	2288.4	2284.7	2284.6	2284.5
3.500	2466.9	2466.7	2466.3	2462.5	2462.1	2461.9	2457.8	2457.7	2457.5
3.625	2647.4	2647.1	2646.7	2642.4	2642.0	2641.8	2637.2	2637.1	2636.9
3.750	2834.3	2834.0	2833.5	2828.8	2828.3	2828.0	2823.0	2822.9	2822.7
3.875	3027.7	3027.3	3026.8	3021.5	3021.0	3020.7	3015.2	3015.0	3014.8
4.000	3227.6	3227.2	3226.6	3220.7	3220.2	3219.8	3213.8	3213.5	3213.3
4.250	3646.8	3646.3	3645.6	3638.4	3637.7	3637.3	3630.0	3629.8	3629.5
4.500	4092.2	4091.6	4090.7	4081.9	4081.1	4080.6	4071.8	4071.5	4071.2
4.750	4563.9	4563.0	4562.0	4551.2	4550.2	4549.6	4539.3	4538.9	4538.5
5.000	5062.0	5061.0	5059.7	5046.5	5045.3	5044.6	5032.4	5031.9	5031.5
5.250	5586.7	5585.5	5583.9	5567.9	5566.5	5565.6	5551.1	5550.6	5550.1
5.500	6138.4	6136.9	6134.9	6115.4	6113.8	6112.7	6095.7	6095.1	6094.5
5.750	6717.2	6715.4	6713.0	6689.3	6687.3	6686.1	6666.0	6665.4	6664.7
6.000	7323.6	7321.3	7318.3	7289.6	7287.3	7285.8	7262.3	7261.5	7260.7
6.250	7957.7	7954.9	7951.3	7916.6	7913.8	7912.1	7884.5	7883.6	7882.7
6.500	8620.2	8616.7	8612.4	8570.5	8567.1	8565.0	8532.7	8531.6	8530.6
6.750	9311.3	9307.1	9301.8	9251.3	9247.4	9244.9	9207.0	9205.8	9204.6
7.000	10032	10027	10020	9959.5	9954.8	9951.9	9907.6	9906.2	9904.8
7.250	10782	10776	10768	10695	10690	10686	10634	10633	10631
7.500	11563	11553	11546	11459	11452	11448	11388	11386	11384
7.750	12375	12366	12354	12251	12243	12238	12168	12165	12163
8.000	13218	13208	13194	13071	13062	13056	12974	12972	12969
8.250	14095	14082	14066	13921	13910	13903	13808	13805	13802
8.500	15006	14991	14972	14800	14787	14779	14668	14665	14662
8.750	15951	15933	15911	15709	15694	15685	15556	15552	15549
9.000	16932	16912	16885	16648	16631	16620	16471	16467	16463
9.250	17951	17927	17896	17619	17598	17586	17414	17409	17404
9.500	19008	18980	18944	18621	18597	18583	18385	18379	18374
9.750	20105	20072	20030	19656	19629	19612	19383	19377	19371
10.000	21244	21205	21157	20724	20692	20673	20411	20404	20397
10.250	22427	22382	22326	21826	21790	21767	21467	21459	21451
10.500	23655	23604	23539	22962	22921	22896	22552	22543	22534
10.750	24932	24872	24798	24133	24088	24059	23667	23656	23646
11.000	26259	26190	26104	25345	25291	25258	24811	24800	24788
11.250	27638	27559	27461	26593	26531	26493	25986	25973	25960
11.500	29072	28983	28870	27879	27809	27766	27192	27177	27162
11.750	30564	30462	30334	29206	29127	29078	28429	28411	28395
12.000	32118	32002	31856	30575	30485	30430	29697	29678	29659
12.500	35420	35271	35085	33445	33331	33260	32331	32307	32284
13.000	39006	38818	38582	36503	36358	36268	35100	35069	35040
13.500	42916	42674	42376	39764	39581	39468	38007	37969	37933
14.000	47248	46922	46524	43243	43016	42875	41060	41013	40969
14.500				46961	46680	46506	44264	44207	44153
15.000				50937	50593	50379	47628	47558	47491
15.500				55196	54775	54515	51161	51076	50995
16.000				59763	59252	58936	54873	54770	54672
16.500				64706	64062	63672	58774	58651	58533
17.000					69290	68794	62877	62729	62588
17.500							67195	67019	66850
18.000							71741	71532	71332
18.500							76530	76284	76048
19.000							81581	81291	81019
19.500							86910	86570	86246
20.000							92537	92142	91783
20.500							98493	98027	97586
21.000							104848	104285	103755
21.500								110986	110348

Table 6-55
Y₂ Expansion Factors for Flange Taps, Static
Pressure Taken From Downstream Taps [140]

Orifice Diameter Inches	Pipe Sizes, Nominal and Published Inside Diameters, in Inches									
	2			3				4		
	1.687	1.939	2.067	2.300	2.624	2.900	3.068	3.152	3.438	
0.250	12.850	12.813	12.800	12.782	22.765	12.754	12.748	12.745	12.737	
0.375	29.362	29.098	29.006	28.883	28.772	28.711	28.682	28.670	28.635	
0.500	53.713	52.817	52.482	52.020	51.594	51.354	51.244	51.197	51.065	
0.625	87.237	84.920	84.085	82.924	81.802	81.143	80.837	80.704	80.334	
0.750	132.29	126.87	124.99	122.45	120.08	118.67	118.00	117.70	116.87	
0.875	192.87	181.02	177.09	171.93	167.26	164.58	163.31	162.76	161.17	
1.000	275.73	251.11	243.28	233.30	224.61	219.77	217.53	216.55	213.79	
1.125	392.50	342.99	327.99	309.44	293.87	285.49	281.67	280.03	275.43	
1.250		466.00	438.00	404.53	377.50	363.41	357.13	354.45	347.04	
1.375			583.98	524.69	478.89	455.83	445.75	441.49	429.84	
1.500				679.11	602.80	565.80	549.95	543.32	525.41	
1.625					755.89	697.45	672.96	662.83	635.77	
1.750					947.87	856.39	819.07	803.79	763.59	
1.875						1050.4	994.01	971.22	912.00	
2.000						1290.7	1205.6	1171.9	1085.5	
2.125							1465.1	1415.0	1289.7	
2.250									1332.0	
2.375									1822.9	
Orifice Diameter Inches	Pipe Sizes, Nominal and Published Inside Diameters, in Inches									
	4		6				8			
	3.826	4.026	4.897	5.187	5.761	6.065	7.625	7.981	8.071	
0.250	12.727	12.723								
0.375	26.599	28.585								
0.500	50.987	50.887	50.740	50.707	50.653	50.629				
0.625	79.976	79.897	79.438	79.351	79.219	79.164				
0.750	116.05	115.79	114.81	114.62	114.32	114.20				
0.875	159.58	158.94	157.11	156.72	156.13	155.89	155.11	154.99	154.97	
1.000	211.03	209.92	206.63	205.92	204.85	204.41	203.01	202.80	202.76	
1.125	270.91	269.10	263.71	262.52	260.72	259.99	257.62	257.28	257.20	
1.250	339.88	337.06	328.73	326.87	324.03	322.87	319.10	318.57	318.44	
1.375	418.80	414.51	402.07	399.32	395.09	393.34	387.63	386.81	386.63	
1.500	508.77	502.39	484.21	480.26	474.21	471.70	463.40	462.20	461.93	
1.625	611.12	601.81	575.75	570.19	561.74	558.25	546.62	544.93	544.54	
1.750	727.55	714.17	677.99	669.69	658.09	653.34	637.52	635.20	634.67	
1.875	860.19	841.21	790.00	779.49	763.79	757.41	736.36	733.25	732.53	
2.000	1011.7	985.07	914.59	900.39	879.40	870.95	843.36	839.31	838.37	
2.125	1185.4	1148.4	1052.3	1033.4	1005.6	994.54	958.80	953.61	952.40	
2.250	1385.4	1334.5	1204.7	1179.6	1143.2	1128.9	1063.0	1076.4	1074.9	
2.375	1617.2	1547.4	1373.4	1340.5	1293.2	1274.6	1216.3	1206.0	1206.1	
2.500	1887.7	1792.3	1560.5	1517.5	1456.5	1432.8	1359.2	1348.9	1346.5	
2.625	2206.1	2076.0	1768.3	1712.6	1634.4	1604.3	1512.1	1499.3	1496.4	
2.750		2407.0	1999.9	1928.1	1828.3	1790.4	1675.4	1659.7	1656.1	
2.875			2258.6	2166.5	2040.0	1992.3	1849.9	1830.7	1826.3	
3.000			2548.6	2431.0	2271.2	2211.6	2036.1	2012.7	2007.4	
3.125			2875.3	2735.3	2524.3	2450.2	2234.7	2206.4	2200.0	
3.250			3244.9	3054.0	2801.9	2710.0	2446.6	2412.5	2404.8	
3.375			3665.7	3422.4	3106.9	2993.4	2672.6	2631.7	2622.4	
3.500				3837.6	3443.1	3303.1	2913.7	2864.8	2853.7	
3.625				4308.1	3814.5	3642.4	3171.2	3112.8	3099.6	
3.750					4226.4	4014.9	3446.1	3376.7	3361.1	
3.875					4685.0	4425.2	3739.9	3637.7	3639.3	
4.000					5197.9	4878.5	4034.3	3937.1	3935.3	
4.250							4751.6	4616.7	4586.7	
4.500							5534.8	5369.1	5328.1	
4.750							6485.5	6231.3	6175.4	
5.000							7571.6	7224.5	7148.8	
5.250							8850.5	8376.6	8274.2	
5.500								9724.0	9565.4	

Table 6-55
(continued)

Orifice Diameter Inches	Pipe Sizes, Nominal and Pinned Inside Diameters, in inches								
	10			12			16		
	9.562	10.020	10.136	11.374	11.938	12.090	14.688	15.000	15.250
1.000	202.16								
1.125	256.23	256.01	255.96						
1.250	316.90	316.57	316.49	315.82	315.57	315.51			
1.375	384.30	383.80	383.68	382.67	382.31	382.22			
1.500	458.53	457.80	457.64	456.17	455.85	455.53	453.93	453.79	
1.625	539.78	538.70	538.47	536.40	535.67	535.49	533.28	533.09	532.94
1.750	628.03	626.63	626.30	623.46	622.46	622.22	619.20	619.94	618.74
1.875	723.63	721.72	721.28	717.45	716.12	715.79	711.75	711.41	711.14
2.000	826.66	824.14	823.56	818.51	816.75	816.32	811.01	810.55	810.21
2.125	937.31	934.04	933.29	926.74	924.46	923.90	917.03	916.45	916.01
2.250	1055.8	1051.6	1050.7	1042.3	1039.4	1038.7	1029.9	1029.2	1028.6
2.375	1182.3	1177.0	1175.8	1165.3	1161.7	1160.8	1149.7	1148.8	1148.1
2.500	1316.9	1310.5	1309.0	1296.0	1291.4	1290.3	1276.6	1275.4	1274.5
2.625	1460.1	1452.2	1450.4	1434.4	1428.8	1427.4	1410.5	1409.1	1408.0
2.750	1611.8	1602.3	1600.1	1580.7	1573.9	1572.2	1551.7	1550.0	1548.6
2.875	1772.6	1761.1	1758.4	1735.2	1727.0	1725.0	1700.2	1698.1	1696.5
3.000	1942.6	1928.8	1925.6	1897.9	1888.2	1885.8	1856.1	1853.6	1851.7
3.125	2122.2	2105.8	2102.0	2069.1	2057.6	2054.7	2019.6	2016.6	2014.4
3.250	2311.8	2292.3	2287.8	2249.0	2235.4	2232.1	2190.7	2187.2	2184.6
3.375	2511.7	2488.7	2483.4	2437.8	2421.9	2418.0	2369.7	2365.6	2362.5
3.500	2722.5	2696.4	2689.2	2635.8	2617.2	2612.7	2556.5	2551.7	2548.1
3.625	2944.5	2912.8	2905.5	2843.2	2821.6	2816.4	2751.5	2743.9	2741.7
3.750	3178.4	3141.3	3132.8	3060.3	3035.4	3029.3	2954.6	2948.2	2943.4
3.875	3424.6	3381.4	3371.5	3287.5	3258.8	3251.8	3166.0	3158.7	3153.2
4.000	3683.9	3633.6	3622.2	3525.2	3492.1	3484.0	3385.8	3377.5	3371.3
4.250	4244.2	4176.9	4161.7	4033.1	3989.6	3979.1	3851.7	3841.0	3832.9
4.500	4865.6	4776.3	4756.2	4587.4	4530.9	4517.3	4353.5	4339.9	4329.7
4.750	5535.6	5438.0	5411.6	5191.9	5119.1	5101.6	4893.0	4875.9	4863.0
5.000	6282.1	6169.4	6135.0	5851.1	5737.9	5735.6	5472.1	5450.6	5434.5
5.250	7178.8	6979.1	6934.6	6570.1	6451.7	6423.4	6092.7	6066.0	6046.0
5.500	8135.5	7877.4	7820.2	7354.9	7205.3	7169.7	6757.2	6724.3	6699.6
5.750	9208.8	8876.6	8803.3	8212.4	8024.4	7979.8	7468.2	7427.8	7397.6
6.000	10418	9991.5	9898.0	9150.7	8915.6	8860.0	8228.7	8179.4	8142.5
6.250	11786	11240	11121	10179	9886.4	9817.5	9041.9	8981.9	8937.2
6.500	13344	12644	12493	11309	10946	10860	9911.4	9856.9	9784.9
6.750		14231	14038	12552	12103	11998	10842	10734	10689
7.000		16035	15790	13925	13371	13242	11837	11732	11654
7.250				15446	14763	14605	12902	12777	12684
7.500				17135	16295	16102	14044	13894	13784
7.750				19021	17986	17730	15269	15091	14959
8.000					19861	19572	16583	16372	16216
8.250					21948	21594	17996	17746	17562
8.500							19517	19221	19004
8.750							21157	20807	20551
9.000							22827	22515	22214
9.250							24842	24357	24004
9.500							26917	26347	25932
9.750							29173	28502	28015
10.000							31630	30840	30269
10.250							34316	33384	32714
10.500								36161	35373

Table 6-55
(continued)

Orifice Diameter Inches	Pipe Sizes, Nominal and Published Inside Diameters, in inches								
	20			24			30		
	18.812	19.000	19.250	22.624	23.000	23.250	28.750	29.000	29.250
2.000	806.73	806.59	806.42						
2.125	911.54	911.37	911.15						
2.250	1022.9	1022.7	1022.5						
2.375	1141.0	1140.7	1140.4	1136.8	1136.5	1136.3			
2.500	1263.7	1263.4	1263.0	1260.6	1260.2	1260.0			
2.625	1397.2	1396.8	1396.3	1390.9	1390.5	1390.2			
2.750	1535.5	1535.0	1534.4	1527.9	1527.4	1527.0			
2.875	1680.7	1680.1	1679.4	1671.6	1670.9	1670.5	1663.7		
3.000	1832.8	1832.1	1831.2	1821.9	1821.1	1820.6	1821.6	1812.3	1812.1
3.125	1991.9	1991.1	1990.0	1979.0	1978.1	1977.5	1968.0	1967.7	1967.4
3.250	2158.1	2157.1	2155.8	2142.9	2141.8	2141.1	2130.0	2129.7	2129.3
3.375	2331.4	2330.3	2328.8	2313.6	2312.9	2311.5	2298.6	2298.2	2297.8
3.500	2512.0	2510.6	2508.9	2491.2	2489.8	2488.8	2473.9	2473.4	2472.9
3.625	2699.8	2698.3	2696.8	2675.8	2674.1	2673.0	2655.8	2655.2	2654.7
3.750	2895.1	2893.3	2891.0	2867.4	2865.5	2864.2	2844.4	2843.7	2843.1
3.875	3097.8	3095.7	3093.1	3066.1	3063.8	3062.4	3039.7	3039.0	3038.3
4.000	3308.1	3305.7	3302.7	3271.9	3269.3	3267.7	3241.8	3241.0	3240.2
4.250	3751.8	3748.8	3744.9	3705.1	3701.8	3699.7	3666.5	3665.4	3664.4
4.500	4226.9	4223.1	4218.2	4167.7	4163.5	4160.8	4118.7	4117.4	4116.1
4.750	4734.3	4729.5	4723.4	4660.2	4654.9	4651.5	4598.9	4597.2	4595.5
5.000	5274.7	5268.8	5261.3	5183.1	5176.6	5172.4	5107.3	5105.2	5103.1
5.250	5849.2	5842.0	5832.8	5737.2	5729.2	5724.1	5644.3	5641.8	5639.3
5.500	6458.8	6450.1	6438.8	6323.1	6313.4	6307.2	6210.4	6207.3	6204.3
5.750	7104.7	7094.2	7080.6	6941.5	6929.8	6922.4	6806.0	6802.3	6798.7
6.000	7788.2	7775.5	7759.3	7593.1	7579.2	7570.3	7431.5	7427.1	7422.8
6.250	8510.8	8495.6	8476.2	8278.6	8262.2	8251.7	8087.5	8082.2	8077.1
6.500	9273.8	9255.8	9232.7	8999.1	8979.7	8967.3	8774.3	8768.1	8762.1
6.750	10079	10058	10031	9755.4	9732.6	9718.1	9492.6	9485.4	9478.4
7.000	10929	10903	10871	10548	10522	10505	10243	10234	10228
7.250	11824	11795	11757	11380	11349	11329	11026	11016	11007
7.500	12768	12733	12689	12250	12214	12191	11841	11830	11819
7.750	13763	13722	13671	13161	13119	13093	12691	12678	12666
8.000	14811	14764	14704	14113	14065	14036	13575	13560	13546
8.250	15915	15861	15791	15109	15055	15020	14494	14477	14461
8.500	17079	17016	16935	16150	16088	16048	15448	15429	15411
8.750	18306	18233	18140	17238	17166	17121	16439	16418	16398
9.000	19600	19515	19408	18374	18293	18241	17468	17444	17421
9.250	20964	20867	20744	19561	19468	19410	18535	18508	18482
9.500	22404	22293	22151	20801	20695	20629	19642	19612	19582
9.750	23925	23797	23635	22096	21976	21901	20780	20755	20722
10.000	25531	25384	25199	23448	23313	23228	21977	21939	21902
10.250	27229	27062	26850	24861	24708	24612	23208	23165	23124
10.500	29026	28834	28593	26387	26165	26057	24482	24435	24389
10.750	30928	30710	30435	27879	27686	27564	25802	25749	25698
11.000	32944	32695	32382	29492	29274	29137	27168	27109	27053
11.250	35082	34799	34444	31177	30933	30780	28582	28517	28454
11.500	37353	37031	36627	32941	32667	32495	30045	29973	29904
11.750	39766	39401	38942	34786	34479	34286	31559	31480	31403
12.000	42336	41921	41400	36717	36374	36158	33126	33038	32953
12.500	47998	47462	46791	40859	40430	40162	36426	36319	36216
13.000	54472	53779	52915	45410	44878	44545	39960	39830	39705
13.500				50425	49763	49353	43746	43590	43438
14.000				55965	55148	54640	47805	47617	47435
14.500				62106	61096	60469	52159	51933	51715
15.000				68938	67689	66917	56833	56563	56303
15.500				76572	75027	74075	61857	61535	61225
16.000					83233	82057	67263	66879	66511
16.500							73087	72632	72195
17.000							79372	78833	78315
17.500							86165	85527	84915
18.000							93522	92767	92044
18.500							101506	100614	99761
19.000							110192	109137	108130
19.500							119667	118420	117231
20.000							130036	128559	127153

(text continued from page 808)

The Reynolds number factor F_r accounts for the variation of the orifice discharge coefficient with Reynolds number. Tables 6-56 and 6-57 show the value of "b" flange taps and pipe taps, respectively, in an expression for F_r :

$$F_r = 1 + \frac{b}{(h_w P_f)^{0.5}} \quad (6-306)$$

Tables 6-56 and 6-57 have been calculated using the following average values: viscosity, 0.0000069 lb/ft-sec; temperature, 60°F, real gas relative density, $SG_g = 0.65$, applying particularly to natural gas. If the fluid being metered has viscosity, temperature and SG_g quite different from these, the value of "b" in the tables may not be applicable. However, for variation in viscosity of from 0.0000059 to 0.0000079 lb/(ft • s), in temperature from 30 to 90°F, or in specific gravity of from 0.55 to 0.75, the variations in the factor F_r would be well within the uncertainty limits.

The expansion factor Y is a function of beta ratio, the ratio of differential pressure to static pressure and the ratio of specific heats (the isentropic exponent). Values of the expansion factor Y can be calculated using analytical equations [140] or can be obtained from Tables 6-58 and 6-59. Y_1 corresponds to static pressure taken from upstream taps, Y_2 to static pressure taken from downstream taps.

The pressure base factor F_{pb} corrects for cases where the base (standard) pressure P_b in psia, at which flow is to be measured, is other than 14.73 psia.

$$F_{pb} = \frac{14.73}{P_b} \quad (6-307)$$

The temperature base factor F_{tb} is applied where the base temperature is other than 60°F and is calculated by dividing the required base temperature in °R by 519.67°R.

$$F_{tb} = \frac{T_b}{519.67} \quad (6-308)$$

The flowing temperature factor F_{tf} is required to change from the assumed flowing temperature of 60°F to the actual flowing temperature T_f (°R):

$$F_{tf} = \left(\frac{519.67}{T_f} \right)^{0.5} \quad (6-309)$$

The real gas relative density (or specific gravity) factor F_{gr} is to be applied to change from a real gas relative density of 1.0 to the real gas relative density G_r (or SG_g) of the gas flowing.

$$F_{gr} = \left(\frac{1}{G_r} \right)^{0.5} \quad (6-310)$$

(text continued on page 826)

Table 6-56
(continued)

Pipe Sizes, Nominal and Published Inside Diameters, in inches									
Orifice Diameter Inches	10			12			16		
	9.562	10.020	10.136	11.374	11.938	12.090	14.688	15.000	15.250
1.000	0.0788								
1.125	0.0685	0.0701	0.0705						
1.250	0.0635	0.0652	0.0656	0.0698	0.0714	0.0718			
1.375	0.0588	0.0606	0.0610	0.0654	0.0671	0.0676			
1.500	0.0545	0.0563	0.0567	0.0612	0.0631	0.0635	0.0706	0.0713	
1.625	0.0504	0.0523	0.0527	0.0573	0.0592	0.0597	0.0670	0.0678	0.0684
1.750	0.0467	0.0485	0.0490	0.0536	0.0555	0.0560	0.0636	0.0644	0.0650
1.875	0.0432	0.0450	0.0455	0.0501	0.0521	0.0526	0.0604	0.0612	0.0618
2.000	0.0401	0.0418	0.0423	0.0469	0.0488	0.0493	0.0572	0.0581	0.0587
2.125	0.0372	0.0389	0.0393	0.0438	0.0458	0.0463	0.0542	0.0551	0.0558
2.250	0.0346	0.0362	0.0366	0.0410	0.0429	0.0434	0.0514	0.0523	0.0529
2.375	0.0322	0.0337	0.0341	0.0383	0.0402	0.0407	0.0487	0.0495	0.0502
2.500	0.0302	0.0315	0.0319	0.0359	0.0377	0.0382	0.0461	0.0469	0.0476
2.625	0.0283	0.0296	0.0299	0.0336	0.0354	0.0358	0.0436	0.0443	0.0452
2.750	0.0267	0.0278	0.0281	0.0316	0.0332	0.0337	0.0413	0.0421	0.0428
2.875	0.0254	0.0263	0.0266	0.0297	0.0312	0.0317	0.0390	0.0399	0.0406
3.000	0.0242	0.0250	0.0252	0.0280	0.0294	0.0298	0.0370	0.0378	0.0385
3.125	0.0233	0.0239	0.0241	0.0265	0.0278	0.0282	0.0350	0.0358	0.0365
3.250	0.0226	0.0230	0.0231	0.0251	0.0263	0.0266	0.0331	0.0339	0.0346
3.375	0.0222	0.0223	0.0224	0.0239	0.0250	0.0253	0.0314	0.0322	0.0328
3.500	0.0219	0.0218	0.0218	0.0229	0.0238	0.0241	0.0298	0.0305	0.0311
3.625	0.0218	0.0214	0.0214	0.0220	0.0228	0.0230	0.0282	0.0290	0.0295
3.750	0.0218	0.0213	0.0212	0.0213	0.0219	0.0221	0.0268	0.0275	0.0281
3.875	0.0221	0.0213	0.0211	0.0208	0.0212	0.0213	0.0255	0.0262	0.0267
4.000	0.0225	0.0215	0.0213	0.0204	0.0206	0.0207	0.0243	0.0249	0.0254
4.250	0.0238	0.0222	0.0219	0.0200	0.0198	0.0198	0.0223	0.0228	0.0232
4.500	0.0256	0.0236	0.0232	0.0201	0.0195	0.0194	0.0206	0.0210	0.0213
4.750	0.0280	0.0254	0.0249	0.0207	0.0196	0.0194	0.0193	0.0196	0.0198
5.000	0.0307	0.0277	0.0270	0.0217	0.0202	0.0199	0.0184	0.0185	0.0187
5.250	0.0337	0.0303	0.0295	0.0232	0.0213	0.0208	0.0178	0.0178	0.0179
5.500	0.0370	0.0332	0.0323	0.0249	0.0226	0.0221	0.0176	0.0174	0.0174
5.750	0.0404	0.0363	0.0354	0.0271	0.0243	0.0237	0.0176	0.0174	0.0172
6.000	0.0439	0.0396	0.0386	0.0294	0.0263	0.0255	0.0180	0.0175	0.0173
6.250	0.0473	0.0429	0.0418	0.0320	0.0285	0.0277	0.0186	0.0181	0.0177
6.500	0.0506	0.0462	0.0451	0.0348	0.0309	0.0300	0.0195	0.0188	0.0183
6.750	0.0536	0.0494	0.0483	0.0376	0.0335	0.0325	0.0206	0.0198	0.0192
7.000	0.0569	0.0523	0.0513	0.0406	0.0362	0.0352	0.0230	0.0210	0.0203
7.250		0.0550	0.0541	0.0435	0.0390	0.0379	0.0235	0.0224	0.0216
7.500		0.0573	0.0564	0.0464	0.0418	0.0407	0.0252	0.0240	0.0230
7.750				0.0491	0.0446	0.0434	0.0271	0.0257	0.0247
8.000				0.0517	0.0473	0.0461	0.0291	0.0276	0.0264
8.250				0.0541	0.0499	0.0487	0.0312	0.0296	0.0288
8.500				0.0561	0.0523	0.0512	0.0334	0.0317	0.0304
8.750					0.0544	0.0534	0.0357	0.0338	0.0325
9.000						0.0553	0.0380	0.0361	0.0346
9.250							0.0402	0.0383	0.0368
9.500							0.0425	0.0406	0.0390
9.750							0.0448	0.0428	0.0412
10.000							0.0469	0.0450	0.0434
10.250							0.0490	0.0471	0.0455
10.500							0.0509	0.0491	0.0476
10.750							0.0526	0.0508	0.0495
11.000							0.0542	0.0526	0.0513
11.250								0.0541	0.0529

Table 6-56
(continued)

Orifice Diameter Inches	Pipe Sizes, Nominal and Published Inside Diameters, in inches								
	20			24			30		
	18.812	19.000	19.250	22.624	23.000	23.250	28.750	29.000	29.250
2.000	0.0667	0.0671	0.0676						
2.125	0.0640	0.0644	0.0649						
2.250	0.0614	0.0617	0.0623						
2.375	0.0588	0.0592	0.0597	0.0659	0.0665	0.0669			
2.500	0.0563	0.0567	0.0573	0.0636	0.0642	0.0646			
2.625	0.0540	0.0544	0.0549	0.0614	0.0620	0.0624			
2.750	0.0516	0.0521	0.0526	0.0592	0.0599	0.0603			
2.875	0.0494	0.0498	0.0504	0.0571	0.0578	0.0582	0.0664		
3.000	0.0473	0.0477	0.0483	0.0551	0.0557	0.0562	0.0645	0.0649	0.0652
3.125	0.0452	0.0456	0.0462	0.0531	0.0538	0.0542	0.0627	0.0631	0.0634
3.250	0.0432	0.0437	0.0442	0.0511	0.0518	0.0523	0.0610	0.0613	0.0616
3.375	0.0413	0.0418	0.0423	0.0492	0.0500	0.0504	0.0592	0.0596	0.0599
3.500	0.0395	0.0399	0.0405	0.0474	0.0481	0.0486	0.0575	0.0579	0.0582
3.625	0.0377	0.0382	0.0387	0.0457	0.0464	0.0468	0.0559	0.0562	0.0566
3.750	0.0361	0.0365	0.0370	0.0439	0.0447	0.0451	0.0542	0.0546	0.0550
3.875	0.0345	0.0349	0.0354	0.0423	0.0430	0.0435	0.0526	0.0530	0.0534
4.000	0.0329	0.0333	0.0339	0.0407	0.0414	0.0419	0.0511	0.0515	0.0518
4.250	0.0301	0.0305	0.0310	0.0376	0.0383	0.0388	0.0481	0.0485	0.0488
4.500	0.0275	0.0279	0.0284	0.0348	0.0355	0.0359	0.0452	0.0456	0.0460
4.750	0.0252	0.0256	0.0260	0.0322	0.0328	0.0333	0.0425	0.0429	0.0432
5.000	0.0232	0.0235	0.0239	0.0297	0.0304	0.0308	0.0399	0.0403	0.0407
5.250	0.0214	0.0217	0.0220	0.0275	0.0281	0.0285	0.0374	0.0378	0.0382
5.500	0.0199	0.0201	0.0204	0.0254	0.0260	0.0264	0.0351	0.0355	0.0359
5.750	0.0186	0.0188	0.0191	0.0236	0.0241	0.0245	0.0329	0.0333	0.0336
6.000	0.0175	0.0177	0.0179	0.0219	0.0224	0.0228	0.0308	0.0312	0.0315
6.250	0.0167	0.0168	0.0170	0.0204	0.0209	0.0212	0.0289	0.0292	0.0296
6.500	0.0161	0.0162	0.0163	0.0191	0.0195	0.0198	0.0270	0.0274	0.0277
6.750	0.0157	0.0157	0.0158	0.0179	0.0183	0.0185	0.0253	0.0257	0.0260
7.000	0.0155	0.0155	0.0154	0.0169	0.0172	0.0174	0.0237	0.0241	0.0244
7.250	0.0155	0.0154	0.0153	0.0161	0.0163	0.0165	0.0223	0.0226	0.0229
7.500	0.0157	0.0155	0.0154	0.0154	0.0156	0.0157	0.0209	0.0212	0.0215
7.750	0.0160	0.0158	0.0156	0.0148	0.0150	0.0151	0.0197	0.0199	0.0202
8.000	0.0166	0.0163	0.0160	0.0145	0.0145	0.0146	0.0185	0.0187	0.0190
8.250	0.0172	0.0169	0.0165	0.0142	0.0142	0.0142	0.0175	0.0177	0.0179
8.500	0.0181	0.0177	0.0172	0.0141	0.0140	0.0140	0.0165	0.0167	0.0170
8.750	0.0190	0.0186	0.0181	0.0141	0.0140	0.0139	0.0157	0.0159	0.0161
9.000	0.0201	0.0196	0.0190	0.0143	0.0141	0.0140	0.0150	0.0151	0.0153
9.250	0.0213	0.0208	0.0201	0.0146	0.0143	0.0141	0.0144	0.0145	0.0146
9.500	0.0226	0.0221	0.0213	0.0150	0.0146	0.0144	0.0138	0.0139	0.0141
9.750	0.0241	0.0234	0.0226	0.0155	0.0150	0.0147	0.0134	0.0135	0.0136
10.000	0.0256	0.0249	0.0240	0.0161	0.0155	0.0152	0.0130	0.0131	0.0132
10.250	0.0271	0.0264	0.0255	0.0168	0.0162	0.0158	0.0128	0.0128	0.0128
10.500	0.0288	0.0280	0.0270	0.0176	0.0169	0.0165	0.0126	0.0126	0.0126
10.750	0.0305	0.0297	0.0287	0.0185	0.0177	0.0173	0.0125	0.0125	0.0125
11.000	0.0323	0.0314	0.0303	0.0195	0.0186	0.0181	0.0125	0.0125	0.0124
11.250	0.0340	0.0332	0.0320	0.0205	0.0196	0.0191	0.0126	0.0125	0.0124
11.500	0.0358	0.0349	0.0336	0.0216	0.0207	0.0201	0.0127	0.0126	0.0125
11.750	0.0376	0.0367	0.0355	0.0228	0.0218	0.0211	0.0130	0.0128	0.0127
12.000	0.0394	0.0385	0.0373	0.0241	0.0230	0.0223	0.0133	0.0131	0.0129
12.500	0.0430	0.0420	0.0408	0.0268	0.0255	0.0248	0.0141	0.0138	0.0136
13.000	0.0463	0.0454	0.0442	0.0296	0.0283	0.0274	0.0151	0.0148	0.0145
13.500	0.0494	0.0485	0.0474	0.0326	0.0311	0.0302	0.0164	0.0161	0.0157
14.000	0.0520	0.0513	0.0503	0.0356	0.0341	0.0331	0.0179	0.0175	0.0171
14.500				0.0386	0.0370	0.0361	0.0197	0.0192	0.0187
15.000				0.0415	0.0400	0.0390	0.0215	0.0210	0.0205
15.500				0.0444	0.0429	0.0418	0.0236	0.0230	0.0224
16.000				0.0470	0.0456	0.0446	0.0257	0.0251	0.0244
16.500				0.0494	0.0481	0.0472	0.0280	0.0273	0.0266
17.000					0.0503	0.0495	0.0303	0.0296	0.0288
17.500							0.0327	0.0319	0.0312
18.000							0.0351	0.0343	0.0335
18.500							0.0375	0.0366	0.0358
19.000							0.0398	0.0390	0.0382
19.500							0.0421	0.0413	0.0405
20.000							0.0443	0.0435	0.0427
20.500							0.0463	0.0455	0.0448
21.000							0.0482	0.0475	0.0468
21.500								0.0492	0.0486

Table 6-57
Pipe Taps, Basic Orifice Factors, F_b [140]

Pipe Sizes, Nominal and Published Inside Diameters, in inches									
Orifice Diameter Inches	2			3			4		
	1.687	1.939	2.067	2.300	2.624	2.900	3.068	3.152	3.438
0.250	0.1106	0.1091	0.1087	0.1081	0.1078	0.1078	0.1079	0.1079	0.1081
0.375	0.0890	0.0878	0.0877	0.0879	0.0888	0.0898	0.0905	0.0908	0.0918
0.500	0.0738	0.0734	0.0729	0.0728	0.0737	0.0750	0.0758	0.0763	0.0778
0.625	0.0694	0.0647	0.0635	0.0624	0.0624	0.0634	0.0642	0.0646	0.0662
0.750	0.0676	0.0608	0.0586	0.0559	0.0546	0.0548	0.0552	0.0555	0.0568
0.875	0.0684	0.0602	0.0570	0.0528	0.0497	0.0488	0.0488	0.0489	0.0496
1.000	0.0702	0.0614	0.0576	0.0522	0.0473	0.0452	0.0445	0.0443	0.0443
1.125	0.0709	0.0635	0.0595	0.0532	0.0469	0.0435	0.0422	0.0417	0.0407
1.250		0.0630	0.0617	0.0552	0.0478	0.0454	0.0414	0.0406	0.0387
1.375			0.0629	0.0575	0.0496	0.0445	0.0418	0.0408	0.0379
1.500				0.0590	0.0518	0.0461	0.0431	0.0418	0.0382
1.625						0.0539	0.0482	0.0450	0.0392
1.750					0.0554	0.0504	0.0471	0.0456	0.0408
1.875							0.0521	0.0492	0.0477
2.000							0.0532	0.0508	0.0448
2.125								0.0519	0.0509
2.250									0.0483
2.375									0.0494

Pipe Sizes, Nominal and Published Inside Diameters, in inches									
Orifice Diameter Inches	4		6				8		
	3.826	4.026	4.897	5.187	5.761	6.065	7.625	7.981	8.071
0.250	0.1084	0.1085							
0.375	0.0932	0.0939							
0.500	0.0800	0.0810	0.0850	0.0862	0.0883	0.0893			
0.625	0.0685	0.0697	0.0747	0.0762	0.0789	0.0802			
0.750	0.0590	0.0602	0.0655	0.0672	0.0703	0.0719			
0.875	0.0513	0.0524	0.0575	0.0592	0.0625	0.0642	0.0716	0.0730	0.0734
1.000	0.0453	0.0461	0.0506	0.0523	0.0556	0.0573	0.0652	0.0668	0.0672
1.125	0.0408	0.0412	0.0448	0.0464	0.0495	0.0512	0.0593	0.0609	0.0613
1.250	0.0376	0.0377	0.0401	0.0414	0.0442	0.0458	0.0538	0.0555	0.0560
1.375	0.0358	0.0353	0.0363	0.0373	0.0397	0.0412	0.0489	0.0506	0.0511
1.500	0.0330	0.0341	0.0334	0.0341	0.0360	0.0372	0.0445	0.0462	0.0466
1.625	0.0331	0.0336	0.0313	0.0315	0.0329	0.0339	0.0405	0.0421	0.0425
1.750	0.0359	0.0340	0.0300	0.0298	0.0304	0.0311	0.0369	0.0384	0.0388
1.875	0.0372	0.0349	0.0293	0.0287	0.0285	0.0290	0.0338	0.0352	0.0355
2.000	0.0388	0.0363	0.0292	0.0281	0.0273	0.0273	0.0311	0.0323	0.0327
2.125	0.0407	0.0380	0.0297	0.0281	0.0265	0.0262	0.0288	0.0299	0.0301
2.250	0.0427	0.0398	0.0305	0.0285	0.0261	0.0256	0.0268	0.0277	0.0280
2.375	0.0445	0.0417	0.0316	0.0293	0.0262	0.0253	0.0252	0.0259	0.0261
2.500	0.0461	0.0435	0.0330	0.0304	0.0267	0.0254	0.0239	0.0244	0.0246
2.625	0.0472	0.0450	0.0345	0.0317	0.0274	0.0258	0.0230	0.0232	0.0233
2.750		0.0462	0.0362	0.0332	0.0284	0.0265	0.0224	0.0224	0.0224
2.875			0.0379	0.0348	0.0295	0.0274	0.0220	0.0218	0.0218
3.000			0.0395	0.0364	0.0306	0.0285	0.0219	0.0214	0.0213
3.125			0.0410	0.0380	0.0323	0.0297	0.0220	0.0213	0.0211
3.250			0.0422	0.0394	0.0338	0.0311	0.0223	0.0214	0.0212
3.375			0.0433	0.0408	0.0353	0.0325	0.0228	0.0217	0.0214
3.500				0.0419	0.0367	0.0339	0.0235	0.0221	0.0218
3.625				0.0428	0.0381	0.0354	0.0243	0.0227	0.0224
3.750					0.0393	0.0367	0.0252	0.0234	0.0230
3.875					0.0404	0.0380	0.0262	0.0243	0.0238
4.000					0.0413	0.0391	0.0273	0.0252	0.0248
4.250							0.0297	0.0278	0.0268
4.500							0.0321	0.0296	0.0290
4.750							0.0344	0.0320	0.0314
5.000							0.0364	0.0342	0.0336
5.250							0.0381	0.0361	0.0356
5.500								0.0377	0.0373

**Table 6-57
(continued)**

Orifice Diameter Inches	Pipe Sizes, Nominal and Published Inside Diameters, in inches								
	10			12			16		
	9.562	10.020	10.136	11.374	11.938	12.090	14.688	15.000	15.250
1.000	0.0728								
1.125	0.0674	0.0691	0.0695						
1.250	0.0624	0.0641	0.0646	0.0687	0.0704	0.0708			
1.375	0.0576	0.0594	0.0599	0.0645	0.0661	0.0666			
1.500	0.0532	0.0550	0.0555	0.0601	0.0620	0.0625	0.0697	0.0705	
1.625	0.0490	0.0509	0.0514	0.0561	0.0580	0.0585	0.0662	0.0670	0.0676
1.750	0.0452	0.0471	0.0476	0.0523	0.0543	0.0548	0.0628	0.0636	0.0642
1.875	0.0417	0.0436	0.0440	0.0488	0.0508	0.0513	0.0595	0.0603	0.0610
2.000	0.0385	0.0403	0.0407	0.0454	0.0475	0.0480	0.0563	0.0571	0.0578
2.125	0.0355	0.0373	0.0377	0.0423	0.0443	0.0449	0.0532	0.0541	0.0548
2.250	0.0329	0.0345	0.0349	0.0394	0.0414	0.0419	0.0503	0.0512	0.0519
2.375	0.0305	0.0320	0.0324	0.0367	0.0387	0.0392	0.0475	0.0485	0.0492
2.500	0.0283	0.0298	0.0301	0.0342	0.0361	0.0366	0.0449	0.0458	0.0466
2.625	0.0265	0.0277	0.0281	0.0319	0.0337	0.0342	0.0424	0.0433	0.0441
2.750	0.0248	0.0260	0.0263	0.0298	0.0316	0.0320	0.0400	0.0409	0.0417
2.875	0.0234	0.0244	0.0246	0.0279	0.0295	0.0300	0.0378	0.0387	0.0394
3.000	0.0222	0.0230	0.0233	0.0262	0.0277	0.0281	0.0356	0.0365	0.0372
3.125	0.0212	0.0218	0.0220	0.0246	0.0260	0.0264	0.0336	0.0345	0.0352
3.250	0.0205	0.0209	0.0210	0.0232	0.0245	0.0249	0.0317	0.0326	0.0333
3.375	0.0199	0.0201	0.0202	0.0220	0.0232	0.0235	0.0300	0.0308	0.0314
3.500	0.0195	0.0195	0.0196	0.0210	0.0220	0.0223	0.0283	0.0291	0.0297
3.625	0.0193	0.0191	0.0191	0.0200	0.0209	0.0212	0.0268	0.0275	0.0281
3.750	0.0192	0.0188	0.0188	0.0193	0.0200	0.0202	0.0254	0.0261	0.0267
3.875	0.0193	0.0187	0.0186	0.0187	0.0192	0.0194	0.0240	0.0247	0.0253
4.000	0.0195	0.0187	0.0186	0.0182	0.0185	0.0187	0.0228	0.0235	0.0240
4.250	0.0205	0.0192	0.0189	0.0176	0.0176	0.0177	0.0207	0.0213	0.0217
4.500	0.0215	0.0200	0.0197	0.0175	0.0172	0.0171	0.0190	0.0194	0.0198
4.750	0.0230	0.0212	0.0208	0.0178	0.0171	0.0170	0.0176	0.0180	0.0183
5.000	0.0248	0.0228	0.0223	0.0185	0.0175	0.0172	0.0166	0.0168	0.0171
5.250	0.0267	0.0245	0.0239	0.0195	0.0181	0.0178	0.0160	0.0161	0.0162
5.500	0.0287	0.0263	0.0257	0.0207	0.0190	0.0186	0.0156	0.0156	0.0156
5.750	0.0307	0.0282	0.0276	0.0221	0.0202	0.0197	0.0155	0.0154	0.0153
6.000	0.0326	0.0302	0.0295	0.0236	0.0215	0.0210	0.0157	0.0154	0.0153
6.250	0.0345	0.0320	0.0314	0.0253	0.0230	0.0224	0.0161	0.0157	0.0154
6.500	0.0368	0.0336	0.0331	0.0270	0.0246	0.0240	0.0167	0.0162	0.0159
6.750		0.0351	0.0346	0.0288	0.0262	0.0256	0.0175	0.0169	0.0164
7.000		0.0363	0.0359	0.0304	0.0279	0.0272	0.0184	0.0177	0.0172
7.250				0.0320	0.0295	0.0288	0.0195	0.0187	0.0181
7.500				0.0334	0.0310	0.0304	0.0206	0.0198	0.0191
7.750				0.0347	0.0325	0.0318	0.0219	0.0209	0.0202
8.000					0.0338	0.0332	0.0232	0.0222	0.0214
8.250					0.0349	0.0344	0.0246	0.0235	0.0227
8.500							0.0260	0.0249	0.0240
8.750							0.0275	0.0262	0.0253
9.000							0.0286	0.0276	0.0267
9.250							0.0299	0.0288	0.0280
9.500							0.0311	0.0301	0.0292
9.750							0.0322	0.0312	0.0304
10.000							0.0332	0.0323	0.0315
10.250							0.0341	0.0333	0.0326
10.500								0.0341	0.0335

**Table 6-57
(continued)**

Orifice Diameter Inches	Pipe Sizes, Nominal and Published Inside Diameters, in inches								
	20			24			30		
	18.812	19.000	19.250	22.624	23.000	23.250	28.750	29.000	29.250
2.000	0.0663	0.0667	0.0672						
2.125	0.0635	0.0639	0.0645						
2.250	0.0609	0.0613	0.0618						
2.375	0.0583	0.0588	0.0593	0.0658	0.0665	0.0669			
2.500	0.0558	0.0562	0.0568	0.0635	0.0642	0.0646			
2.625	0.0534	0.0538	0.0544	0.0613	0.0620	0.0624			
2.750	0.0510	0.0515	0.0520	0.0591	0.0598	0.0603			
2.875	0.0488	0.0492	0.0498	0.0570	0.0577	0.0582	0.0669		
3.000	0.0466	0.0470	0.0476	0.0549	0.0556	0.0561	0.0650	0.0654	0.0657
3.125	0.0443	0.0449	0.0455	0.0529	0.0536	0.0541	0.0632	0.0636	0.0639
3.250	0.0423	0.0429	0.0435	0.0509	0.0517	0.0521	0.0615	0.0618	0.0622
3.375	0.0405	0.0410	0.0416	0.0490	0.0497	0.0502	0.0597	0.0601	0.0604
3.500	0.0387	0.0391	0.0397	0.0471	0.0479	0.0484	0.0580	0.0584	0.0587
3.625	0.0369	0.0373	0.0379	0.0453	0.0461	0.0466	0.0563	0.0567	0.0571
3.750	0.0352	0.0356	0.0362	0.0436	0.0444	0.0449	0.0547	0.0551	0.0554
3.875	0.0336	0.0340	0.0346	0.0419	0.0427	0.0432	0.0530	0.0534	0.0538
4.000	0.0320	0.0324	0.0330	0.0403	0.0411	0.0416	0.0515	0.0519	0.0523
4.250	0.0291	0.0295	0.0301	0.0372	0.0380	0.0385	0.0484	0.0488	0.0492
4.500	0.0265	0.0269	0.0274	0.0343	0.0351	0.0356	0.0455	0.0459	0.0463
4.750	0.0242	0.0246	0.0250	0.0316	0.0324	0.0329	0.0427	0.0431	0.0435
5.000	0.0221	0.0225	0.0229	0.0292	0.0299	0.0303	0.0401	0.0405	0.0409
5.250	0.0203	0.0206	0.0210	0.0269	0.0276	0.0280	0.0376	0.0380	0.0384
5.500	0.0188	0.0190	0.0194	0.0248	0.0255	0.0259	0.0352	0.0356	0.0360
5.750	0.0175	0.0177	0.0180	0.0230	0.0236	0.0240	0.0330	0.0334	0.0338
6.000	0.0164	0.0165	0.0168	0.0213	0.0218	0.0222	0.0309	0.0313	0.0317
6.250	0.0155	0.0156	0.0158	0.0197	0.0203	0.0206	0.0289	0.0293	0.0297
6.500	0.0148	0.0149	0.0151	0.0184	0.0189	0.0192	0.0271	0.0274	0.0278
6.750	0.0144	0.0144	0.0145	0.0172	0.0176	0.0179	0.0253	0.0257	0.0261
7.000	0.0141	0.0141	0.0141	0.0162	0.0166	0.0168	0.0237	0.0241	0.0244
7.250	0.0140	0.0140	0.0139	0.0153	0.0156	0.0159	0.0223	0.0226	0.0229
7.500	0.0140	0.0140	0.0139	0.0146	0.0149	0.0150	0.0209	0.0212	0.0215
7.750	0.0143	0.0141	0.0140	0.0140	0.0142	0.0144	0.0196	0.0199	0.0202
8.000	0.0146	0.0144	0.0142	0.0136	0.0138	0.0139	0.0185	0.0187	0.0190
8.250	0.0151	0.0149	0.0146	0.0133	0.0134	0.0135	0.0174	0.0177	0.0179
8.500	0.0157	0.0154	0.0151	0.0132	0.0132	0.0132	0.0165	0.0167	0.0170
8.750	0.0163	0.0160	0.0157	0.0131	0.0130	0.0130	0.0156	0.0158	0.0161
9.000	0.0171	0.0168	0.0163	0.0131	0.0130	0.0130	0.0149	0.0151	0.0153
9.250	0.0180	0.0176	0.0171	0.0133	0.0131	0.0130	0.0142	0.0144	0.0146
9.500	0.0189	0.0185	0.0180	0.0136	0.0133	0.0132	0.0137	0.0138	0.0140
9.750	0.0198	0.0194	0.0189	0.0139	0.0136	0.0134	0.0132	0.0133	0.0135
10.000	0.0209	0.0204	0.0198	0.0143	0.0140	0.0138	0.0129	0.0129	0.0130
10.250	0.0219	0.0214	0.0208	0.0149	0.0144	0.0142	0.0126	0.0126	0.0127
10.500	0.0230	0.0225	0.0219	0.0154	0.0150	0.0147	0.0123	0.0124	0.0124
10.750	0.0241	0.0236	0.0229	0.0161	0.0155	0.0152	0.0122	0.0122	0.0122
11.000	0.0252	0.0247	0.0240	0.0168	0.0162	0.0158	0.0121	0.0121	0.0121
11.250	0.0263	0.0258	0.0251	0.0175	0.0169	0.0165	0.0121	0.0121	0.0121
11.500	0.0273	0.0268	0.0261	0.0183	0.0176	0.0172	0.0122	0.0122	0.0121
11.750	0.0284	0.0278	0.0272	0.0191	0.0184	0.0180	0.0124	0.0125	0.0122
12.000	0.0293	0.0288	0.0282	0.0200	0.0192	0.0188	0.0126	0.0124	0.0123
12.500	0.0312	0.0307	0.0301	0.0218	0.0210	0.0205	0.0131	0.0130	0.0128
13.000	0.0327	0.0323	0.0318	0.0236	0.0228	0.0222	0.0139	0.0137	0.0135
13.500				0.0255	0.0246	0.0240	0.0148	0.0146	0.0143
14.000				0.0272	0.0264	0.0258	0.0159	0.0156	0.0153
14.500				0.0289	0.0280	0.0275	0.0172	0.0168	0.0165
15.000				0.0304	0.0296	0.0291	0.0185	0.0181	0.0177
15.500				0.0318	0.0311	0.0306	0.0199	0.0194	0.0191
16.000					0.0323	0.0319	0.0213	0.0209	0.0205
16.500							0.0228	0.0223	0.0219
17.000							0.0242	0.0238	0.0233
17.500							0.0257	0.0252	0.0248
18.000							0.0270	0.0266	0.0261
18.500							0.0283	0.0279	0.0275
19.000							0.0296	0.0292	0.0288
19.500							0.0307	0.0303	0.0299
20.000							0.0317	0.0313	0.0310

Table 6-58
Y₁ Expansion Factors for Flange Taps, Static
Pressure Taken from Upstream Taps [140]

h ₀ /P ₀ Ratio	β = d/D												
	.1	.2	.3	.4	.45	.50	.52	.54	.56	.58	.60	.61	.62
0.0	1.000	1.000	1.000	1.000	1.000	1.000	1.000	1.000	1.000	1.000	1.000	1.000	1.000
0.1	0.9989	0.9989	0.9989	0.9988	0.9988	0.9988	0.9988	0.9988	0.9988	0.9988	0.9988	0.9987	0.9987
0.2	0.9977	0.9977	0.9977	0.9977	0.9976	0.9976	0.9976	0.9976	0.9976	0.9975	0.9975	0.9975	0.9974
0.3	0.9965	0.9965	0.9966	0.9965	0.9965	0.9964	0.9964	0.9965	0.9965	0.9965	0.9965	0.9962	0.9962
0.4	0.9954	0.9954	0.9954	0.9953	0.9953	0.9952	0.9952	0.9951	0.9951	0.9950	0.9949	0.9949	0.9949
0.5	0.9943	0.9943	0.9943	0.9942	0.9941	0.9940	0.9940	0.9939	0.9938	0.9938	0.9937	0.9936	0.9936
0.6	0.9932	0.9932	0.9931	0.9930	0.9929	0.9928	0.9927	0.9927	0.9926	0.9925	0.9924	0.9924	0.9923
0.7	0.9920	0.9920	0.9920	0.9919	0.9918	0.9916	0.9915	0.9915	0.9914	0.9913	0.9912	0.9911	0.9910
0.8	0.9909	0.9909	0.9908	0.9907	0.9906	0.9904	0.9903	0.9902	0.9901	0.9900	0.9899	0.9898	0.9897
0.9	0.9898	0.9897	0.9897	0.9895	0.9894	0.9892	0.9891	0.9890	0.9889	0.9888	0.9886	0.9885	0.9885
1.0	0.9886	0.9886	0.9885	0.9884	0.9882	0.9880	0.9879	0.9878	0.9877	0.9875	0.9874	0.9873	0.9872
1.1	0.9875	0.9875	0.9874	0.9872	0.9870	0.9868	0.9867	0.9866	0.9864	0.9863	0.9861	0.9860	0.9859
1.2	0.9863	0.9863	0.9862	0.9860	0.9859	0.9856	0.9855	0.9853	0.9852	0.9850	0.9848	0.9847	0.9846
1.3	0.9852	0.9852	0.9851	0.9849	0.9847	0.9844	0.9843	0.9841	0.9840	0.9838	0.9836	0.9835	0.9833
1.4	0.9841	0.9840	0.9840	0.9837	0.9835	0.9832	0.9831	0.9829	0.9827	0.9825	0.9823	0.9822	0.9821
1.5	0.9829	0.9829	0.9828	0.9826	0.9825	0.9820	0.9819	0.9817	0.9815	0.9813	0.9810	0.9809	0.9808
1.6	0.9818	0.9818	0.9817	0.9814	0.9811	0.9808	0.9806	0.9805	0.9803	0.9800	0.9798	0.9796	0.9795
1.7	0.9806	0.9806	0.9805	0.9802	0.9800	0.9796	0.9794	0.9792	0.9790	0.9788	0.9785	0.9784	0.9782
1.8	0.9795	0.9795	0.9794	0.9791	0.9788	0.9784	0.9782	0.9780	0.9778	0.9775	0.9772	0.9771	0.9769
1.9	0.9784	0.9783	0.9782	0.9779	0.9776	0.9772	0.9770	0.9768	0.9766	0.9763	0.9760	0.9758	0.9756
2.0	0.9772	0.9772	0.9771	0.9767	0.9764	0.9760	0.9758	0.9756	0.9753	0.9750	0.9747	0.9745	0.9744
2.1	0.9761	0.9761	0.9759	0.9756	0.9753	0.9748	0.9746	0.9744	0.9741	0.9738	0.9734	0.9733	0.9731
2.2	0.9750	0.9749	0.9748	0.9744	0.9741	0.9736	0.9734	0.9731	0.9729	0.9725	0.9722	0.9720	0.9718
2.3	0.9738	0.9738	0.9736	0.9732	0.9729	0.9724	0.9722	0.9719	0.9716	0.9713	0.9709	0.9707	0.9705
2.4	0.9727	0.9726	0.9725	0.9721	0.9717	0.9712	0.9710	0.9707	0.9704	0.9700	0.9697	0.9694	0.9692
2.5	0.9715	0.9715	0.9713	0.9709	0.9705	0.9700	0.9698	0.9695	0.9692	0.9688	0.9684	0.9682	0.9680
2.6	0.9704	0.9704	0.9702	0.9698	0.9694	0.9688	0.9686	0.9683	0.9679	0.9675	0.9671	0.9669	0.9667
2.7	0.9693	0.9692	0.9691	0.9686	0.9682	0.9676	0.9673	0.9670	0.9667	0.9663	0.9659	0.9656	0.9654
2.8	0.9681	0.9681	0.9679	0.9674	0.9670	0.9664	0.9661	0.9658	0.9654	0.9650	0.9646	0.9644	0.9641
2.9	0.9670	0.9669	0.9668	0.9663	0.9658	0.9652	0.9649	0.9646	0.9642	0.9638	0.9633	0.9631	0.9628
3.0	0.9658	0.9658	0.9656	0.9651	0.9647	0.9640	0.9637	0.9634	0.9630	0.9626	0.9621	0.9618	0.9615
3.1	0.9647	0.9647	0.9645	0.9640	0.9635	0.9629	0.9625	0.9622	0.9617	0.9613	0.9608	0.9605	0.9603
3.2	0.9636	0.9635	0.9633	0.9628	0.9623	0.9616	0.9613	0.9609	0.9605	0.9601	0.9596	0.9593	0.9590
3.3	0.9624	0.9624	0.9622	0.9616	0.9611	0.9604	0.9601	0.9597	0.9593	0.9588	0.9583	0.9580	0.9577
3.4	0.9613	0.9612	0.9610	0.9604	0.9599	0.9592	0.9589	0.9585	0.9580	0.9576	0.9570	0.9567	0.9564
3.5	0.9602	0.9601	0.9599	0.9593	0.9588	0.9580	0.9577	0.9573	0.9568	0.9563	0.9558	0.9554	0.9551
3.6	0.9590	0.9590	0.9587	0.9581	0.9576	0.9568	0.9565	0.9560	0.9556	0.9551	0.9545	0.9542	0.9538
3.7	0.9579	0.9578	0.9576	0.9570	0.9564	0.9556	0.9553	0.9548	0.9543	0.9538	0.9532	0.9529	0.9526
3.8	0.9567	0.9567	0.9564	0.9558	0.9552	0.9544	0.9540	0.9536	0.9531	0.9526	0.9520	0.9516	0.9513
3.9	0.9556	0.9555	0.9553	0.9546	0.9540	0.9532	0.9528	0.9524	0.9519	0.9513	0.9507	0.9504	0.9500
4.0	0.9545	0.9544	0.9542	0.9536	0.9529	0.9520	0.9516	0.9512	0.9506	0.9501	0.9494	0.9491	0.9487

h ₀ /P ₀ Ratio	β = d/D												
	.63	.64	.65	.66	.67	.68	.69	.70	.71	.72	.73	.74	.75
0.0	1.000	1.000	1.000	1.000	1.000	1.000	1.000	1.000	1.000	1.000	1.000	1.000	1.000
0.1	0.9987	0.9987	0.9987	0.9987	0.9987	0.9987	0.9986	0.9986	0.9986	0.9986	0.9986	0.9985	0.9984
0.2	0.9974	0.9974	0.9974	0.9974	0.9973	0.9973	0.9973	0.9973	0.9972	0.9972	0.9971	0.9971	0.9970
0.3	0.9961	0.9961	0.9961	0.9960	0.9960	0.9960	0.9959	0.9959	0.9958	0.9958	0.9957	0.9957	0.9956
0.4	0.9948	0.9948	0.9948	0.9947	0.9947	0.9946	0.9946	0.9945	0.9945	0.9944	0.9943	0.9943	0.9942
0.5	0.9935	0.9935	0.9934	0.9934	0.9933	0.9933	0.9932	0.9931	0.9931	0.9930	0.9929	0.9929	0.9928
0.6	0.9923	0.9922	0.9921	0.9921	0.9920	0.9919	0.9918	0.9918	0.9917	0.9916	0.9915	0.9914	0.9913
0.7	0.9910	0.9909	0.9908	0.9907	0.9907	0.9906	0.9905	0.9904	0.9903	0.9902	0.9901	0.9900	0.9899
0.8	0.9897	0.9896	0.9895	0.9894	0.9893	0.9892	0.9891	0.9890	0.9889	0.9888	0.9887	0.9886	0.9884
0.9	0.9884	0.9883	0.9882	0.9881	0.9880	0.9879	0.9878	0.9877	0.9875	0.9874	0.9873	0.9871	0.9870
1.0	0.9871	0.9870	0.9869	0.9868	0.9867	0.9865	0.9864	0.9863	0.9861	0.9860	0.9859	0.9857	0.9855
1.1	0.9858	0.9857	0.9856	0.9854	0.9853	0.9852	0.9851	0.9849	0.9848	0.9846	0.9844	0.9843	0.9841
1.2	0.9845	0.9844	0.9843	0.9841	0.9840	0.9838	0.9837	0.9835	0.9834	0.9832	0.9830	0.9828	0.9826
1.3	0.9832	0.9831	0.9829	0.9828	0.9827	0.9825	0.9823	0.9822	0.9820	0.9818	0.9816	0.9814	0.9812
1.4	0.9819	0.9818	0.9816	0.9815	0.9813	0.9812	0.9810	0.9808	0.9806	0.9804	0.9802	0.9800	0.9798
1.5	0.9806	0.9805	0.9803	0.9802	0.9800	0.9798	0.9796	0.9794	0.9792	0.9790	0.9788	0.9786	0.9783
1.6	0.9793	0.9792	0.9790	0.9788	0.9787	0.9785	0.9783	0.9781	0.9778	0.9776	0.9774	0.9771	0.9769
1.7	0.9780	0.9779	0.9777	0.9775	0.9773	0.9771	0.9769	0.9767	0.9764	0.9762	0.9760	0.9757	0.9754
1.8	0.9767	0.9766	0.9764	0.9762	0.9760	0.9758	0.9755	0.9753	0.9751	0.9748	0.9745	0.9743	0.9740
1.9	0.9755	0.9753	0.9751	0.9749	0.9747	0.9744	0.9742	0.9739	0.9737	0.9734	0.9731	0.9728	0.9725
2.0	0.9742	0.9740	0.9738	0.9735	0.9733	0.9731	0.9728	0.9726	0.9723	0.9720	0.9717	0.9714	0.9711
2.1	0.9729	0.9727	0.9725	0.9722	0.9720	0.9717	0.9715	0.9712	0.9709	0.9706	0.9703	0.9700	0.9696
2.2	0.9716	0.9714	0.9711	0.9709	0.9706	0.9704	0.9701	0.9698	0.9695	0.9692	0.9689	0.9685	0.9682
2.3	0.9703	0.9701	0.9698	0.9696	0.9693	0.9690	0.9688	0.9685	0.9681	0.9678	0.9675	0.9671	0.9667
2.4	0.9690	0.9688	0.9685	0.9683	0.9680	0.9677	0.9674	0.9671	0.9668	0.9664	0.9661	0.9657	0.9653
2.5	0.9677	0.9675	0.9672	0.9670	0.9667	0.9663	0.9660	0.9657	0.9654	0.9650	0.9646	0.9643	0.9639
2.6	0.9664	0.9662	0.9659	0.9656	0.9653	0.9650	0.9647	0.9643	0.9640	0.9636	0.9632	0.9628	0.9624
2.7	0.9651	0.9649	0.9646	0.9643	0.9640	0.9637	0.9633	0.9630	0.9626	0.9622	0.9618	0.9614	0.9610
2.8	0.9638	0.9636	0.9633	0.9630	0.9626	0.9623	0.9620	0.9616	0.9612	0.9608	0.9604	0.9600	0.9595
2.9	0.9625	0.9623	0.9620	0.9616	0.9613	0.9610	0.9606	0.9602	0.9598	0.9594	0.9590	0.9585	0.9581
3.0	0.9613	0.9610	0.9606	0.9603	0.9600	0.9596	0.9592	0.9588	0.9584	0.9580	0.9576	0.9571	0.9566
3.1	0.9600	0.9597	0.9593	0.9590	0.9586	0.9583	0.9579	0.9575	0.9571	0.9566	0.9562	0.9557	0.9552
3.2	0.9587	0.9584	0.9580	0.9577	0.9573	0.9569	0.9567	0.9561	0.9557	0.9552	0.9547	0.9542	0.9537
3.3	0.9574	0.9571	0.9567	0.9564	0.9560	0.9556	0.9552	0.9547	0.9543	0.9538	0.9533	0.9528	0.9523
3.4	0.9561	0.9558	0.9554	0.9550	0.9546	0.9542	0.9538	0.9534	0.9529	0.9524	0.9519	0.9514	0.9508
3.5	0.9548	0.9545	0.9541	0.9537									

Table 6-58
(continued)

h_g/F_g Ratio	$\beta = d/D$												
	.1	.2	.3	.4	.45	.50	.52	.54	.56	.58	.60	.61	.62
0.0	1.000	1.000	1.000	1.000	1.000	1.000	1.000	1.000	1.000	1.000	1.000	1.000	1.000
0.1	1.0007	1.0007	1.0006	1.0006	1.0006	1.0006	1.0006	1.0006	1.0006	1.0006	1.0005	1.0005	1.0005
0.2	1.0013	1.0013	1.0013	1.0013	1.0012	1.0012	1.0012	1.0012	1.0011	1.0011	1.0011	1.0011	1.0010
0.3	1.0020	1.0020	1.0020	1.0019	1.0019	1.0018	1.0018	1.0018	1.0017	1.0017	1.0016	1.0016	1.0016
0.4	1.0027	1.0027	1.0026	1.0026	1.0025	1.0024	1.0024	1.0023	1.0023	1.0022	1.0022	1.0021	1.0021
0.5	1.0033	1.0033	1.0033	1.0032	1.0031	1.0030	1.0030	1.0029	1.0029	1.0028	1.0027	1.0027	1.0026
0.6	1.0040	1.0040	1.0040	1.0039	1.0038	1.0036	1.0036	1.0035	1.0034	1.0034	1.0033	1.0032	1.0032
0.7	1.0047	1.0047	1.0046	1.0045	1.0044	1.0043	1.0042	1.0041	1.0040	1.0039	1.0038	1.0038	1.0037
0.8	1.0054	1.0053	1.0053	1.0052	1.0050	1.0049	1.0048	1.0047	1.0046	1.0045	1.0044	1.0043	1.0042
0.9	1.0060	1.0060	1.0060	1.0058	1.0057	1.0055	1.0054	1.0053	1.0052	1.0050	1.0049	1.0048	1.0048
1.0	1.0067	1.0067	1.0066	1.0065	1.0063	1.0061	1.0060	1.0059	1.0058	1.0056	1.0055	1.0054	1.0053
1.1	1.0074	1.0074	1.0073	1.0071	1.0069	1.0067	1.0066	1.0065	1.0063	1.0062	1.0060	1.0059	1.0058
1.2	1.0080	1.0080	1.0080	1.0078	1.0076	1.0073	1.0072	1.0071	1.0069	1.0068	1.0066	1.0065	1.0064
1.3	1.0087	1.0087	1.0086	1.0084	1.0082	1.0080	1.0078	1.0077	1.0075	1.0073	1.0071	1.0070	1.0069
1.4	1.0094	1.0094	1.0093	1.0091	1.0089	1.0086	1.0084	1.0083	1.0081	1.0079	1.0077	1.0076	1.0074
1.5	1.0101	1.0101	1.0100	1.0097	1.0095	1.0092	1.0090	1.0089	1.0087	1.0085	1.0082	1.0081	1.0080
1.6	1.0108	1.0107	1.0106	1.0104	1.0101	1.0099	1.0096	1.0095	1.0093	1.0090	1.0088	1.0087	1.0085
1.7	1.0114	1.0114	1.0113	1.0110	1.0108	1.0104	1.0103	1.0101	1.0099	1.0096	1.0094	1.0092	1.0091
1.8	1.0121	1.0121	1.0120	1.0117	1.0114	1.0111	1.0109	1.0107	1.0104	1.0101	1.0099	1.0098	1.0096
1.9	1.0128	1.0128	1.0126	1.0123	1.0121	1.0117	1.0115	1.0113	1.0110	1.0108	1.0105	1.0103	1.0102
2.0	1.0135	1.0134	1.0133	1.0130	1.0127	1.0123	1.0121	1.0119	1.0116	1.0114	1.0110	1.0109	1.0107
2.1	1.0142	1.0141	1.0140	1.0136	1.0134	1.0129	1.0127	1.0125	1.0122	1.0119	1.0116	1.0114	1.0112
2.2	1.0148	1.0148	1.0147	1.0143	1.0140	1.0136	1.0133	1.0131	1.0128	1.0125	1.0122	1.0120	1.0118
2.3	1.0155	1.0155	1.0154	1.0150	1.0146	1.0142	1.0140	1.0137	1.0134	1.0131	1.0127	1.0126	1.0124
2.4	1.0162	1.0162	1.0160	1.0156	1.0153	1.0148	1.0146	1.0143	1.0140	1.0137	1.0133	1.0131	1.0129
2.5	1.0169	1.0168	1.0167	1.0163	1.0159	1.0154	1.0152	1.0149	1.0146	1.0142	1.0139	1.0137	1.0134
2.6	1.0176	1.0175	1.0174	1.0170	1.0166	1.0161	1.0158	1.0155	1.0152	1.0148	1.0144	1.0142	1.0140
2.7	1.0182	1.0182	1.0180	1.0176	1.0172	1.0167	1.0164	1.0161	1.0158	1.0154	1.0150	1.0148	1.0146
2.8	1.0189	1.0189	1.0187	1.0183	1.0179	1.0173	1.0170	1.0167	1.0164	1.0160	1.0156	1.0154	1.0151
2.9	1.0196	1.0196	1.0194	1.0189	1.0185	1.0180	1.0177	1.0173	1.0170	1.0166	1.0162	1.0159	1.0157
3.0	1.0203	1.0203	1.0201	1.0196	1.0192	1.0186	1.0183	1.0180	1.0176	1.0172	1.0167	1.0165	1.0162
3.1	1.0210	1.0210	1.0208	1.0203	1.0198	1.0192	1.0189	1.0186	1.0182	1.0178	1.0173	1.0170	1.0168
3.2	1.0217	1.0216	1.0214	1.0209	1.0205	1.0198	1.0195	1.0192	1.0188	1.0184	1.0179	1.0176	1.0173
3.3	1.0224	1.0223	1.0221	1.0216	1.0211	1.0205	1.0202	1.0198	1.0194	1.0189	1.0184	1.0182	1.0179
3.4	1.0230	1.0230	1.0228	1.0223	1.0218	1.0211	1.0208	1.0204	1.0200	1.0195	1.0190	1.0187	1.0184
3.5	1.0237	1.0237	1.0235	1.0229	1.0224	1.0217	1.0214	1.0210	1.0206	1.0201	1.0196	1.0193	1.0190
3.6	1.0244	1.0244	1.0242	1.0236	1.0231	1.0224	1.0220	1.0216	1.0212	1.0207	1.0202	1.0199	1.0196
3.7	1.0251	1.0251	1.0248	1.0243	1.0237	1.0230	1.0226	1.0222	1.0218	1.0213	1.0207	1.0204	1.0201
3.8	1.0258	1.0258	1.0255	1.0249	1.0244	1.0236	1.0233	1.0229	1.0224	1.0219	1.0213	1.0210	1.0207
3.9	1.0265	1.0264	1.0262	1.0256	1.0250	1.0243	1.0239	1.0235	1.0230	1.0225	1.0219	1.0216	1.0213
4.0	1.0272	1.0271	1.0269	1.0263	1.0257	1.0249	1.0245	1.0241	1.0236	1.0231	1.0225	1.0222	1.0218

h_g/F_g Ratio	$\beta = d/D$												
	.63	.64	.65	.66	.67	.68	.69	.70	.71	.72	.73	.74	.75
0.0	1.000	1.000	1.000	1.000	1.000	1.000	1.000	1.000	1.000	1.000	1.000	1.000	1.000
0.1	1.0005	1.0005	1.0005	1.0005	1.0005	1.0004	1.0004	1.0004	1.0004	1.0004	1.0004	1.0004	1.0004
0.2	1.0010	1.0010	1.0010	1.0010	1.0009	1.0009	1.0009	1.0008	1.0008	1.0008	1.0008	1.0008	1.0007
0.3	1.0015	1.0015	1.0015	1.0014	1.0014	1.0014	1.0013	1.0013	1.0012	1.0012	1.0011	1.0011	1.0011
0.4	1.0021	1.0020	1.0020	1.0019	1.0019	1.0018	1.0018	1.0017	1.0017	1.0016	1.0016	1.0015	1.0014
0.5	1.0026	1.0025	1.0025	1.0024	1.0024	1.0023	1.0022	1.0022	1.0021	1.0020	1.0020	1.0019	1.0018
0.6	1.0031	1.0030	1.0030	1.0029	1.0028	1.0028	1.0027	1.0026	1.0025	1.0025	1.0024	1.0023	1.0022
0.7	1.0036	1.0036	1.0035	1.0034	1.0033	1.0032	1.0032	1.0031	1.0030	1.0029	1.0028	1.0027	1.0026
0.8	1.0042	1.0041	1.0040	1.0039	1.0038	1.0037	1.0036	1.0035	1.0034	1.0033	1.0032	1.0030	1.0029
0.9	1.0047	1.0046	1.0045	1.0044	1.0043	1.0042	1.0041	1.0040	1.0038	1.0037	1.0036	1.0034	1.0033
1.0	1.0052	1.0051	1.0050	1.0049	1.0048	1.0047	1.0045	1.0044	1.0043	1.0041	1.0040	1.0038	1.0037
1.1	1.0057	1.0056	1.0055	1.0054	1.0053	1.0051	1.0050	1.0049	1.0047	1.0046	1.0044	1.0042	1.0041
1.2	1.0062	1.0061	1.0060	1.0059	1.0058	1.0056	1.0055	1.0053	1.0052	1.0050	1.0048	1.0046	1.0044
1.3	1.0068	1.0066	1.0065	1.0064	1.0062	1.0061	1.0059	1.0058	1.0056	1.0054	1.0052	1.0050	1.0048
1.4	1.0073	1.0072	1.0070	1.0069	1.0067	1.0066	1.0064	1.0062	1.0060	1.0058	1.0056	1.0054	1.0052
1.5	1.0078	1.0077	1.0076	1.0074	1.0072	1.0070	1.0069	1.0067	1.0065	1.0063	1.0060	1.0058	1.0056
1.6	1.0084	1.0082	1.0081	1.0079	1.0077	1.0075	1.0073	1.0071	1.0069	1.0067	1.0065	1.0062	1.0060
1.7	1.0089	1.0088	1.0086	1.0084	1.0082	1.0080	1.0078	1.0076	1.0074	1.0071	1.0069	1.0066	1.0064
1.8	1.0094	1.0093	1.0091	1.0089	1.0087	1.0085	1.0083	1.0080	1.0078	1.0076	1.0073	1.0070	1.0068
1.9	1.0100	1.0098	1.0096	1.0094	1.0092	1.0090	1.0088	1.0085	1.0083	1.0080	1.0077	1.0074	1.0071
2.0	1.0105	1.0103	1.0101	1.0099	1.0097	1.0095	1.0092	1.0090	1.0087	1.0084	1.0081	1.0078	1.0075
2.1	1.0111	1.0109	1.0106	1.0104	1.0102	1.0100	1.0097	1.0094	1.0092	1.0089	1.0086	1.0083	1.0079
2.2	1.0116	1.0114	1.0112	1.0109	1.0107	1.0104	1.0102	1.0099	1.0096	1.0093	1.0090	1.0087	1.0083
2.3	1.0121	1.0119	1.0117	1.0114	1.0112	1.0109	1.0106	1.0104	1.0101	1.0098	1.0094	1.0091	1.0087
2.4	1.0127	1.0124	1.0122	1.0120	1.0117	1.0114	1.0111	1.0108	1.0105	1.0102	1.0098	1.0095	1.0091
2.5	1.0132	1.0130	1.0127	1.0125	1.0122	1.0119	1.0116	1.0113	1.0110	1.0106	1.0103	1.0099	1.0095
2.6	1.0138	1.0135	1.0133	1.0130	1.0127	1.0124	1.0121	1.0118	1.0114	1.0111	1.0107	1.0103	1.0099
2.7	1.0143	1.0140	1.0138	1.0135	1.0132	1.0129	1.0126	1.0122	1.0119	1.0115	1.0111	1.0107	1.0103
2.8	1.0148	1.0146	1.0143	1.0140	1.0137	1.0134	1.0131	1.0127	1.0124	1.0120	1.0116	1.0112	1.0107
2.9	1.0154	1.0151	1.0148	1.0145	1.0142	1.0139	1.0136	1.0132	1.0128	1.0124	1.0120	1.0116	1.0111
3.0	1.0160	1.0157	1.0154	1.0150	1.0147	1.0144	1.0140	1.0137	1.0133	1.0129	1.0124	1.0120	1.0116
3.1	1.0165	1.0162	1.0159	1.0156	1.0152	1.0149	1.0145	1.0141	1.0137	1.0133	1.0129	1.0124	1.0120
3.2	1.0170	1.0167	1.0164	1.0161	1.0158	1.0154	1.0150	1.0146	1.0142	1.0138	1.0133	1.0128	1.0124
3.3	1.0176	1.0173	1.0170	1.0166	1.0163	1.0159	1.0155	1.0151	1.0147	1.0142	1.0138	1.0133	1.0128
3.4	1.0181	1.0178	1.0175	1.0171	1.0168	1.0164	1.0160	1.0156	1.0151	1.0147	1.0142	1.0137	1.0132
3.5	1.0187	1.0184	1.0180	1.0177	1.0173	1.0169	1.0165	1.0160	1.0				

Table 6-59a
Y₁ Expansion Factors for Pipe Taps, Static
Pressure Taken from Upstream Taps [140]

h _v /P ₁ Ratio	β = d/D										
	.1	.2	.3	.4	.45	.50	.52	.54	.56	.58	.60
0.0	1.000	1.000	1.000	1.000	1.000	1.000	1.000	1.000	1.000	1.000	1.000
0.1	0.9960	0.9989	0.9988	0.9985	0.9984	0.9984	0.9982	0.9981	0.9980	0.9979	0.9977
0.2	0.9981	0.9979	0.9976	0.9971	0.9968	0.9964	0.9962	0.9961	0.9959	0.9957	0.9954
0.3	0.9971	0.9968	0.9964	0.9956	0.9952	0.9946	0.9944	0.9941	0.9938	0.9935	0.9931
0.4	0.9962	0.9958	0.9951	0.9942	0.9936	0.9928	0.9925	0.9921	0.9917	0.9913	0.9908
0.5	0.9952	0.9947	0.9939	0.9927	0.9919	0.9910	0.9906	0.9902	0.9897	0.9891	0.9885
0.6	0.9943	0.9937	0.9927	0.9913	0.9903	0.9892	0.9887	0.9882	0.9876	0.9870	0.9862
0.7	0.9933	0.9926	0.9915	0.9898	0.9887	0.9874	0.9869	0.9862	0.9856	0.9848	0.9840
0.8	0.9923	0.9916	0.9903	0.9883	0.9871	0.9857	0.9850	0.9843	0.9835	0.9826	0.9817
0.9	0.9914	0.9905	0.9891	0.9869	0.9855	0.9839	0.9831	0.9823	0.9814	0.9805	0.9794
1.0	0.9904	0.9895	0.9878	0.9854	0.9839	0.9821	0.9812	0.9803	0.9794	0.9783	0.9771
1.1	0.9895	0.9884	0.9866	0.9840	0.9825	0.9803	0.9794	0.9784	0.9773	0.9761	0.9748
1.2	0.9885	0.9874	0.9854	0.9825	0.9807	0.9785	0.9775	0.9764	0.9752	0.9739	0.9725
1.3	0.9876	0.9863	0.9842	0.9811	0.9791	0.9767	0.9756	0.9744	0.9732	0.9718	0.9702
1.4	0.9866	0.9853	0.9830	0.9796	0.9775	0.9749	0.9737	0.9725	0.9711	0.9696	0.9679
1.5	0.9857	0.9842	0.9818	0.9782	0.9758	0.9731	0.9719	0.9705	0.9690	0.9674	0.9656
1.6	0.9847	0.9832	0.9805	0.9767	0.9742	0.9713	0.9700	0.9685	0.9670	0.9652	0.9633
1.7	0.9837	0.9821	0.9793	0.9753	0.9726	0.9695	0.9681	0.9666	0.9649	0.9631	0.9610
1.8	0.9828	0.9811	0.9781	0.9738	0.9710	0.9677	0.9662	0.9646	0.9628	0.9609	0.9587
1.9	0.9818	0.9800	0.9769	0.9723	0.9694	0.9659	0.9643	0.9626	0.9608	0.9587	0.9565
2.0	0.9809	0.9790	0.9757	0.9709	0.9678	0.9641	0.9625	0.9607	0.9587	0.9566	0.9542
2.1	0.9799	0.9779	0.9745	0.9694	0.9662	0.9623	0.9606	0.9587	0.9566	0.9544	0.9519
2.2	0.9790	0.9768	0.9732	0.9680	0.9646	0.9605	0.9587	0.9567	0.9546	0.9522	0.9497
2.3	0.9780	0.9758	0.9720	0.9665	0.9630	0.9587	0.9568	0.9548	0.9525	0.9500	0.9473
2.4	0.9770	0.9747	0.9708	0.9650	0.9613	0.9570	0.9550	0.9528	0.9505	0.9479	0.9450
2.5	0.9761	0.9737	0.9696	0.9636	0.9597	0.9552	0.9531	0.9508	0.9484	0.9457	0.9427
2.6	0.9751	0.9726	0.9681	0.9621	0.9581	0.9534	0.9512	0.9489	0.9463	0.9435	0.9404
2.7	0.9742	0.9716	0.9670	0.9607	0.9565	0.9516	0.9493	0.9469	0.9443	0.9414	0.9381
2.8	0.9732	0.9705	0.9659	0.9592	0.9549	0.9498	0.9475	0.9449	0.9422	0.9392	0.9358
2.9	0.9723	0.9695	0.9647	0.9578	0.9533	0.9480	0.9456	0.9430	0.9401	0.9370	0.9335
3.0	0.9713	0.9684	0.9635	0.9563	0.9517	0.9462	0.9437	0.9410	0.9381	0.9348	0.9312
3.1	0.9704	0.9674	0.9623	0.9549	0.9501	0.9444	0.9418	0.9390	0.9360	0.9327	0.9290
3.2	0.9694	0.9663	0.9611	0.9534	0.9485	0.9426	0.9400	0.9371	0.9339	0.9305	0.9267
3.3	0.9684	0.9653	0.9600	0.9519	0.9469	0.9408	0.9381	0.9351	0.9319	0.9285	0.9244
3.4	0.9675	0.9643	0.9587	0.9505	0.9452	0.9390	0.9362	0.9331	0.9298	0.9261	0.9221
3.5	0.9665	0.9632	0.9574	0.9490	0.9436	0.9372	0.9343	0.9312	0.9277	0.9240	0.9198
3.6	0.9656	0.9621	0.9562	0.9476	0.9420	0.9354	0.9324	0.9292	0.9257	0.9218	0.9175
3.7	0.9646	0.9611	0.9550	0.9461	0.9404	0.9336	0.9306	0.9272	0.9236	0.9196	0.9152
3.8	0.9637	0.9600	0.9538	0.9447	0.9388	0.9318	0.9287	0.9253	0.9216	0.9175	0.9129
3.9	0.9627	0.9590	0.9526	0.9432	0.9372	0.9301	0.9269	0.9233	0.9195	0.9153	0.9106
4.0	0.9617	0.9579	0.9514	0.9417	0.9356	0.9283	0.9249	0.9213	0.9174	0.9131	0.9083

h _v /P ₁ Ratio	β = d/D									
	.61	.62	.63	.64	.65	.66	.67	.68	.69	.70
0.0	1.000	1.000	1.000	1.000	1.000	1.000	1.000	1.000	1.000	1.000
0.1	0.9976	0.9976	0.9975	0.9974	0.9973	0.9972	0.9971	0.9970	0.9969	0.9968
0.2	0.9953	0.9951	0.9950	0.9948	0.9947	0.9945	0.9943	0.9941	0.9938	0.9935
0.3	0.9929	0.9927	0.9925	0.9923	0.9920	0.9917	0.9914	0.9911	0.9907	0.9903
0.4	0.9906	0.9903	0.9900	0.9897	0.9893	0.9890	0.9886	0.9881	0.9875	0.9871
0.5	0.9882	0.9879	0.9875	0.9871	0.9867	0.9862	0.9857	0.9851	0.9845	0.9840
0.6	0.9859	0.9854	0.9850	0.9845	0.9840	0.9834	0.9828	0.9822	0.9814	0.9806
0.7	0.9835	0.9830	0.9825	0.9819	0.9813	0.9807	0.9800	0.9792	0.9784	0.9774
0.8	0.9811	0.9806	0.9800	0.9794	0.9787	0.9779	0.9771	0.9762	0.9753	0.9742
0.9	0.9788	0.9782	0.9775	0.9768	0.9760	0.9752	0.9742	0.9733	0.9722	0.9710
1.0	0.9764	0.9757	0.9750	0.9742	0.9733	0.9724	0.9714	0.9703	0.9691	0.9677
1.1	0.9741	0.9733	0.9725	0.9716	0.9707	0.9696	0.9685	0.9673	0.9660	0.9645
1.2	0.9717	0.9709	0.9700	0.9690	0.9680	0.9669	0.9657	0.9643	0.9629	0.9613
1.3	0.9694	0.9685	0.9675	0.9664	0.9653	0.9641	0.9628	0.9614	0.9598	0.9581
1.4	0.9670	0.9660	0.9650	0.9639	0.9627	0.9614	0.9599	0.9584	0.9567	0.9548
1.5	0.9646	0.9636	0.9625	0.9613	0.9600	0.9586	0.9571	0.9554	0.9536	0.9516
1.6	0.9623	0.9612	0.9600	0.9587	0.9573	0.9558	0.9542	0.9525	0.9505	0.9484
1.7	0.9599	0.9587	0.9575	0.9561	0.9547	0.9531	0.9514	0.9495	0.9474	0.9452
1.8	0.9576	0.9563	0.9550	0.9535	0.9520	0.9503	0.9485	0.9465	0.9443	0.9420
1.9	0.9552	0.9539	0.9525	0.9510	0.9493	0.9476	0.9456	0.9435	0.9412	0.9387
2.0	0.9529	0.9515	0.9500	0.9484	0.9467	0.9448	0.9428	0.9406	0.9381	0.9355
2.1	0.9505	0.9490	0.9475	0.9458	0.9440	0.9420	0.9399	0.9376	0.9351	0.9323
2.2	0.9481	0.9466	0.9450	0.9432	0.9413	0.9393	0.9371	0.9346	0.9320	0.9290
2.3	0.9458	0.9442	0.9425	0.9406	0.9387	0.9365	0.9342	0.9317	0.9289	0.9258
2.4	0.9434	0.9418	0.9400	0.9381	0.9360	0.9338	0.9313	0.9287	0.9258	0.9226
2.5	0.9411	0.9393	0.9375	0.9355	0.9333	0.9310	0.9285	0.9257	0.9227	0.9194
2.6	0.9387	0.9369	0.9350	0.9329	0.9307	0.9282	0.9256	0.9227	0.9196	0.9161
2.7	0.9364	0.9345	0.9325	0.9303	0.9280	0.9255	0.9227	0.9198	0.9165	0.9129
2.8	0.9340	0.9321	0.9300	0.9277	0.9253	0.9227	0.9199	0.9169	0.9134	0.9097
2.9	0.9316	0.9296	0.9275	0.9252	0.9227	0.9200	0.9170	0.9138	0.9105	0.9064
3.0	0.9293	0.9272	0.9250	0.9226	0.9200	0.9172	0.9142	0.9108	0.9072	0.9032
3.1	0.9269	0.9248	0.9225	0.9200	0.9173	0.9144	0.9113	0.9079	0.9041	0.9000
3.2	0.9246	0.9223	0.9200	0.9174	0.9147	0.9117	0.9084	0.9049	0.9010	0.8968
3.3	0.9222	0.9199	0.9175	0.9148	0.9120	0.9089	0.9056	0.9019	0.8979	0.8935
3.4	0.9199	0.9175	0.9150	0.9122	0.9093	0.9062	0.9027	0.8990	0.8948	0.8903
3.5	0.9175	0.9151	0.9125	0.9097	0.9067	0.9034	0.8999	0.8960	0.8918	0.8871
3.6	0.9151	0.9126	0.9100	0.9071	0.9040	0.9006	0.8970	0.8930	0.8887	0.8839
3.7	0.9128	0.9102	0.9075	0.9045	0.9013	0.8979	0.8941	0.8900	0.8856	0.8806
3.8	0.9104	0.9078	0.9050	0.9019	0.8987	0.8951	0.8913	0.8871	0.8825	0.8774
3.9	0.9081	0.9054	0.9025	0.8993	0.8959	0.8924	0.8884	0.8841	0.8794	0.8742
4.0	0.9057	0.9029	0.9000	0.8968	0.8933	0.8896	0.8856	0.8811	0.8763	0.8710

Table 6-59b
 Y_2 Expansion Factors for Pipe Taps, Static
Pressure Taken from Downstream Taps [140]

h_v/P_a Ratio	$\beta = d/D$										
	.1	.2	.3	.4	.45	.50	.52	.54	.56	.58	.60
0.0	1.000	1.000	1.000	1.000	1.000	1.000	1.000	1.000	1.000	1.000	1.000
0.1	1.0008	1.0008	1.0006	1.0003	1.0002	1.0000	0.9999	0.9998	0.9997	0.9996	0.9995
0.2	1.0017	1.0015	1.0012	1.0007	1.0004	1.0000	0.9999	0.9997	0.9995	0.9993	0.9990
0.3	1.0025	1.0023	1.0018	1.0010	1.0006	1.0000	0.9998	0.9995	0.9992	0.9989	0.9986
0.4	1.0034	1.0030	1.0024	1.0014	1.0008	1.0001	0.9997	0.9994	0.9990	0.9986	0.9981
0.5	1.0042	1.0038	1.0030	1.0018	1.0010	1.0001	0.9997	0.9992	0.9988	0.9982	0.9976
0.6	1.0051	1.0045	1.0036	1.0021	1.0012	1.0001	0.9996	0.9991	0.9985	0.9979	0.9972
0.7	1.0059	1.0053	1.0041	1.0025	1.0014	1.0002	0.9996	0.9990	0.9983	0.9975	0.9967
0.8	1.0068	1.0060	1.0047	1.0028	1.0016	1.0002	0.9995	0.9988	0.9980	0.9972	0.9962
0.9	1.0076	1.0068	1.0055	1.0032	1.0018	1.0002	0.9995	0.9987	0.9978	0.9969	0.9958
1.0	1.0085	1.0075	1.0059	1.0036	1.0021	1.0005	0.9994	0.9986	0.9976	0.9965	0.9954
1.1	1.0093	1.0083	1.0065	1.0039	1.0023	1.0003	0.9994	0.9984	0.9974	0.9962	0.9949
1.2	1.0102	1.0091	1.0071	1.0043	1.0025	1.0004	0.9994	0.9983	0.9972	0.9959	0.9945
1.3	1.0110	1.0098	1.0077	1.0047	1.0027	1.0004	0.9994	0.9982	0.9970	0.9956	0.9941
1.4	1.0119	1.0106	1.0083	1.0051	1.0030	1.0004	0.9993	0.9981	0.9968	0.9953	0.9939
1.5	1.0127	1.0113	1.0089	1.0054	1.0032	1.0005	0.9993	0.9980	0.9966	0.9950	0.9932
1.6	1.0136	1.0121	1.0096	1.0058	1.0034	1.0006	0.9993	0.9979	0.9964	0.9947	0.9928
1.7	1.0144	1.0128	1.0102	1.0062	1.0036	1.0006	0.9992	0.9978	0.9962	0.9944	0.9924
1.8	1.0153	1.0136	1.0108	1.0066	1.0039	1.0007	0.9992	0.9977	0.9960	0.9941	0.9920
1.9	1.0161	1.0144	1.0114	1.0070	1.0041	1.0008	0.9992	0.9976	0.9958	0.9938	0.9916
2.0	1.0170	1.0151	1.0120	1.0073	1.0044	1.0008	0.9992	0.9975	0.9956	0.9935	0.9912
2.1	1.0178	1.0159	1.0126	1.0077	1.0046	1.0009	0.9992	0.9974	0.9954	0.9932	0.9908
2.2	1.0187	1.0167	1.0132	1.0081	1.0048	1.0010	0.9992	0.9973	0.9952	0.9929	0.9904
2.3	1.0195	1.0174	1.0138	1.0085	1.0051	1.0010	0.9992	0.9972	0.9950	0.9927	0.9900
2.4	1.0204	1.0182	1.0144	1.0089	1.0053	1.0011	0.9992	0.9971	0.9949	0.9924	0.9896
2.5	1.0212	1.0189	1.0150	1.0093	1.0056	1.0012	0.9992	0.9971	0.9947	0.9921	0.9893
2.6	1.0221	1.0197	1.0156	1.0097	1.0058	1.0013	0.9992	0.9970	0.9945	0.9919	0.9889
2.7	1.0229	1.0205	1.0162	1.0101	1.0061	1.0014	0.9992	0.9969	0.9944	0.9916	0.9885
2.8	1.0238	1.0212	1.0169	1.0104	1.0063	1.0014	0.9992	0.9968	0.9942	0.9914	0.9883
2.9	1.0246	1.0220	1.0175	1.0108	1.0066	1.0015	0.9992	0.9968	0.9941	0.9911	0.9878
3.0	1.0255	1.0228	1.0181	1.0112	1.0068	1.0016	0.9993	0.9967	0.9939	0.9908	0.9874
3.1	1.0264	1.0235	1.0187	1.0116	1.0071	1.0017	0.9993	0.9966	0.9938	0.9906	0.9871
3.2	1.0272	1.0243	1.0193	1.0120	1.0074	1.0018	0.9993	0.9966	0.9936	0.9904	0.9867
3.3	1.0280	1.0250	1.0199	1.0124	1.0076	1.0019	0.9993	0.9965	0.9935	0.9901	0.9864
3.4	1.0289	1.0258	1.0206	1.0128	1.0079	1.0020	0.9994	0.9965	0.9935	0.9899	0.9860
3.5	1.0298	1.0266	1.0212	1.0133	1.0082	1.0021	0.9994	0.9964	0.9932	0.9896	0.9857
3.6	1.0306	1.0273	1.0218	1.0137	1.0084	1.0022	0.9994	0.9964	0.9931	0.9894	0.9854
3.7	1.0314	1.0281	1.0224	1.0141	1.0087	1.0024	0.9994	0.9963	0.9929	0.9892	0.9850
3.8	1.0323	1.0289	1.0230	1.0145	1.0090	1.0025	0.9995	0.9963	0.9928	0.9890	0.9847
3.9	1.0332	1.0296	1.0237	1.0149	1.0093	1.0026	0.9995	0.9963	0.9927	0.9888	0.9844
4.0	1.0340	1.0304	1.0243	1.0153	1.0095	1.0027	0.9996	0.9962	0.9926	0.9885	0.9840

h_v/P_a Ratio	$\beta = d/D$									
	.61	.62	.63	.64	.65	.66	.67	.68	.69	.70
0.0	1.000	1.000	1.000	1.000	1.000	1.000	1.000	1.000	1.000	1.000
0.1	0.9994	0.9994	0.9993	0.9992	0.9991	0.9990	0.9989	0.9988	0.9987	0.9986
0.2	0.9989	0.9988	0.9986	0.9985	0.9983	0.9981	0.9979	0.9977	0.9974	0.9972
0.3	0.9984	0.9982	0.9979	0.9977	0.9974	0.9972	0.9969	0.9965	0.9962	0.9958
0.4	0.9978	0.9976	0.9972	0.9969	0.9966	0.9962	0.9958	0.9954	0.9949	0.9944
0.5	0.9973	0.9970	0.9966	0.9962	0.9958	0.9953	0.9948	0.9942	0.9936	0.9930
0.6	0.9968	0.9964	0.9959	0.9954	0.9949	0.9944	0.9938	0.9931	0.9924	0.9916
0.7	0.9962	0.9958	0.9953	0.9947	0.9941	0.9935	0.9928	0.9920	0.9912	0.9902
0.8	0.9957	0.9952	0.9946	0.9940	0.9933	0.9926	0.9918	0.9909	0.9899	0.9889
0.9	0.9952	0.9946	0.9940	0.9932	0.9925	0.9917	0.9908	0.9898	0.9887	0.9875
1.0	0.9947	0.9940	0.9933	0.9925	0.9917	0.9908	0.9898	0.9887	0.9875	0.9862
1.1	0.9942	0.9935	0.9927	0.9918	0.9909	0.9899	0.9888	0.9876	0.9863	0.9848
1.2	0.9937	0.9929	0.9920	0.9911	0.9901	0.9890	0.9878	0.9865	0.9851	0.9835
1.3	0.9932	0.9924	0.9914	0.9904	0.9893	0.9881	0.9868	0.9854	0.9839	0.9822
1.4	0.9928	0.9918	0.9908	0.9897	0.9885	0.9872	0.9859	0.9844	0.9827	0.9809
1.5	0.9923	0.9912	0.9902	0.9890	0.9877	0.9864	0.9849	0.9833	0.9815	0.9796
1.6	0.9918	0.9907	0.9896	0.9883	0.9870	0.9855	0.9840	0.9822	0.9804	0.9783
1.7	0.9913	0.9902	0.9889	0.9876	0.9862	0.9847	0.9830	0.9812	0.9792	0.9770
1.8	0.9908	0.9896	0.9883	0.9870	0.9854	0.9838	0.9821	0.9801	0.9780	0.9757
1.9	0.9904	0.9891	0.9877	0.9863	0.9847	0.9830	0.9811	0.9791	0.9769	0.9744
2.0	0.9899	0.9886	0.9872	0.9856	0.9840	0.9822	0.9802	0.9781	0.9757	0.9732
2.1	0.9895	0.9881	0.9866	0.9849	0.9832	0.9813	0.9793	0.9770	0.9746	0.9719
2.2	0.9890	0.9876	0.9860	0.9843	0.9825	0.9805	0.9784	0.9760	0.9734	0.9706
2.3	0.9886	0.9870	0.9854	0.9836	0.9817	0.9797	0.9774	0.9750	0.9723	0.9694
2.4	0.9881	0.9865	0.9848	0.9830	0.9810	0.9789	0.9765	0.9740	0.9712	0.9681
2.5	0.9877	0.9860	0.9842	0.9823	0.9803	0.9780	0.9756	0.9730	0.9701	0.9669
2.6	0.9873	0.9855	0.9837	0.9817	0.9796	0.9772	0.9747	0.9720	0.9690	0.9657
2.7	0.9868	0.9850	0.9831	0.9811	0.9788	0.9764	0.9738	0.9710	0.9670	0.9634
2.8	0.9864	0.9846	0.9826	0.9804	0.9781	0.9757	0.9730	0.9700	0.9660	0.9622
2.9	0.9860	0.9841	0.9820	0.9798	0.9774	0.9749	0.9721	0.9690	0.9650	0.9610
3.0	0.9856	0.9836	0.9815	0.9792	0.9767	0.9741	0.9712	0.9681	0.9640	0.9598
3.1	0.9852	0.9831	0.9809	0.9786	0.9760	0.9733	0.9703	0.9671	0.9630	0.9586
3.2	0.9848	0.9826	0.9804	0.9780	0.9754	0.9725	0.9695	0.9661	0.9620	0.9574
3.3	0.9843	0.9822	0.9798	0.9774	0.9747	0.9718	0.9686	0.9652	0.9611	0.9572
3.4	0.9839	0.9817	0.9793	0.9768	0.9740	0.9710	0.9678	0.9642	0.9603	0.9561
3.5	0.9835	0.9812	0.9788	0.9762	0.9733	0.9702	0.9669	0.9633	0.9593	0.9549
3.6	0.9832	0.9808	0.9783	0.9756	0.9727	0.9695	0.9661	0.9623	0.9582	0.9537
3.7	0.9828	0.9803	0.9778	0.9750	0.9720	0.9688	0.9652	0.9614	0.9572	0.9526
3.8	0.9824	0.9799	0.9772	0.9744	0.9713	0.9680	0.9644	0.9605	0.9562	0.9514
3.9	0.9820	0.9794	0.9767	0.9738	0.9707	0.9673	0.9636	0.9596	0.9551	0.9503
4.0	0.9816	0.9790	0.9762	0.9732	0.9700	0.9665	0.9628	0.9586	0.9541	0.9491

(text continued from page 815)

where $G_r = G_i Z_b(\text{air})/Z_b(\text{gas})$ and $G_i = M_{\text{gas}}/M_{\text{air}}$.

In orifice meter measurement of gases, the effect of compressibility equates to the relationship $(1/Z)^{0.5}$; this has been termed the "supercompressibility" of the gas. The supercompressibility factor may be calculated from

$$F_{\text{pr}} = \left(\frac{Z_b}{Z_{\text{fl}}} \right)^{0.5} \quad (6-311)$$

The best way to obtain the Z calculation is to use the Hall-Yarborough equation [142], or figures of compressibility factors for natural gas (e.g., Figure 6-231). Also the supercompressibility factor F_{pv} may be taken from an AGA Report [143] and/or empirical equations as follows [141]:

$$F_{\text{pv}} = \left(1 + \frac{2.48 P_G \times 10^{5.0+2.025SG_g}}{T_f^{3.825}} \right)^{0.5} \quad (6-311a)$$

for $0.0601 \leq SG_g \leq 0.650$ and $P < 600$ psig

$$F_{\text{pv}} = \left(1 + \frac{3.32 P_G \times 10^{5.0+1.81SG_g}}{T_f^{3.825}} \right)^{0.5} \quad (6-311b)$$

for $SG_g \leq 0.600$ and $P < 600$ psig

$$F_{\text{pv}} = \left(1 + \frac{4.66 P_G \times 10^{5.0+1.68SG_g}}{T_f^{3.825}} \right)^{0.5} \quad (6-311c)$$

for $0.0651 \leq SG_g \leq 0.750$ and $P < 600$ psig

$$F_{\text{pv}} = \left(1 + \frac{7.91 P_G \times 10^{5.0+1.26SG_g}}{T_f^{3.825}} \right)^{0.5} \quad (6-311d)$$

for $0.751 \leq SG_g \leq 0.900$ and $P < 600$ psig

where P_G = gage pressure in psig
 SG_g = specific gas gravity
 T_f = flowing temperature in °R

Manometer factor F_m is used with mercury differential gages and compensates for the column of compressed gas opposite the mercury leg. Usually, it is not considered for pressures below 500 psia. It is also not required for mercuryless differential gages. F_m can be calculated as follows:

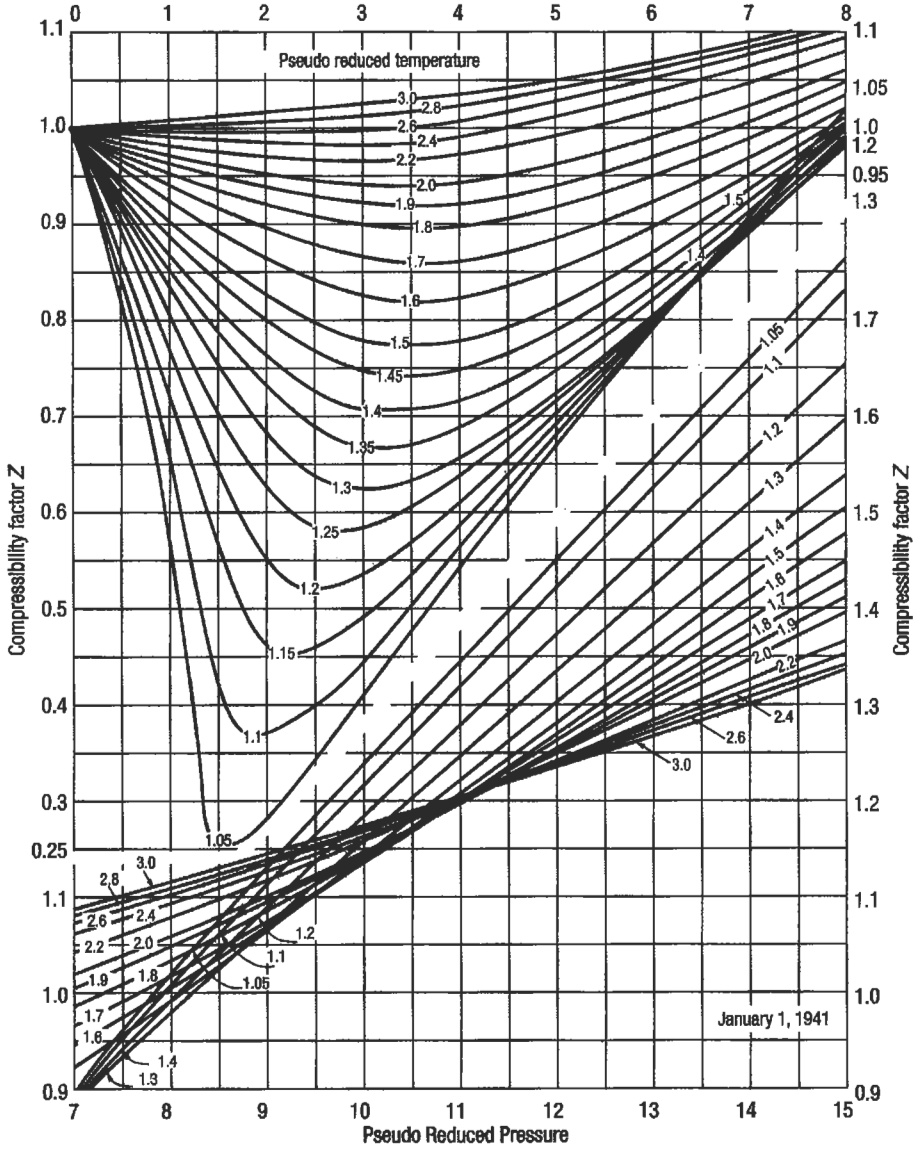


Figure 6-231. Compressibility factors for natural gas [144].

$$F_m = \left(\frac{Y_m - Y_g}{846.324} \right)^{0.5} \tag{6-312}$$

where $Y_m = 846.324 [1 - 0.000101(T_a - 520)]$

$Y_g = 2.699053SG(F_{pv})^2/T_a$

T_a = ambient temperature in degrees Rankine (air or atmospheric temperature surrounding the orifice meter)

SG_g = specific gravity of the flowing gas

F_{pv} = supercompressibility factor of the gas at ambient temperature, specific gravity and static gage pressure

The manometer factor can be read in Table 6-60.

The orifice thermal expansion factor F_a is introduced to correct for expansion or contraction of the orifice, when operating at temperatures appreciably different from the temperature at which the orifice was bored. It is calculated as

$$F_a = 1 + [0.0000185(T_f - 68)]$$

(for 304 and 316 stainless steel)

Table 6-60
 F_m Manometer Factors [140]

Specific Gravity, G	Flowing Pressure, psig						
	0	500	1000	1500	2000	2500	3000
Ambient Temperature = 0°F							
0.55	1.0000	0.9989	0.9976	0.9960	0.9943	0.9930	0.9921
0.60	1.0000	0.9988	0.9972	0.9952	0.9932	0.9919	0.9910
0.65	1.0000	0.9987	0.9967	0.9941	0.9920	0.9908	0.9900
0.70	1.0000	0.9985	0.9961	0.9927	0.9907	0.9896	0.9890
0.75	1.0000						
Ambient Temperature = 40°F							
0.55	1.0000	0.9990	0.9979	0.9967	0.9954	0.9942	0.9932
0.60	1.0000	0.9989	0.9976	0.9962	0.9946	0.9933	0.9923
0.65	1.0000	0.9988	0.9973	0.9955	0.9937	0.9923	0.9913
0.70	1.0000	0.9987	0.9970	0.9947	0.9926	0.9912	0.9903
0.75	1.0000	0.9986	0.9965	0.9937	0.9915	0.9902	0.9893
Ambient Temperature = 80°F							
0.55	1.0000	0.9991	0.9981	0.9971	0.9960	0.9950	0.9941
0.60	1.0000	0.9990	0.9979	0.9967	0.9955	0.9943	0.9933
0.65	1.0000	0.9989	0.9977	0.9963	0.9948	0.9935	0.9925
0.70	1.0000	0.9988	0.9974	0.9958	0.9940	0.9926	0.9915
0.75	1.0000	0.9987	0.9971	0.9951	0.9931	0.9916	0.9906
Ambient Temperature = 120°F							
0.55	1.0000	0.9992	0.9983	0.9974	0.9965	0.9956	0.9948
0.60	1.0000	0.9991	0.9981	0.9971	0.9960	0.9950	0.9941
0.65	1.0000	0.9990	0.9979	0.9967	0.9955	0.9944	0.9934
0.70	1.0000	0.9989	0.9977	0.9963	0.9950	0.9937	0.9926
0.75	1.0000	0.9988	0.9975	0.9959	0.9943	0.9929	0.9918

Note: Factors for intermediate values of pressure, temperature, and specific gravity should be interpolated.
Note: This table is for use with mercury manometer type recording gauges that have gas in contact with the mercury surface.

or

$$F_a = 1 + [0.0000159(T_f - 68)]$$

(for Monel)

where T_f = flowing temperature of the gas at the orifice in °F

The orifice thermal expansion factor is rounded to four decimal places. This factor is significant only where large quantities of gas are being measured.

The gage location factor F_1 is required when mercury orifice differential instruments are used. It compensates for differences in the weight of the gas column above the mercury reservoir for meter locations other than the standard of 45° latitude at sea level. It is a constant for any given metering location and can be combined with other flow constants or stored in the computer master file for use in calculating the orifice flow. The equation for determining the gauge location factor is

$$F_1 = \left(\frac{g_1}{980.665} \right)^{0.5} \quad (6-313)$$

where: g_1 = the ambient gravity value at the metering location can be obtained from U.S. Coast and Geodetic Survey data in reference to aeronautical data, from the Smithsonian Meteorological Tables, or calculated for midlatitudes, between 30° and 60°, as

$$g_1 = 980.665 + [0.087(^{\circ}L - 45)] - 0.000094H$$

where °L = degrees latitude

H = elevation in lineal feet above sea level

This gage location factor value can be read in Table 6-61.

Example 16

Compute the daily flowrate of natural gas through an orifice meter for the following condition:

Barometric pressure—14.5 psia

Diameter of pipe—11.938 in.

Orifice diameter—4.000 in.

Differential pressure across meter—27.0 in. of H₂O

Static pressure on meter—600 psig

Type of meter—flange taps

Temperature base (T_b)—60°F

Flowing temperature—75°F

Pressure base (P_b)—14.65 psia

Gas composition by volume: C₁—85%, C₂—5%, C₃—3%, i—C₄—1%, N₂—6%

Solution

1. Daily flowrate = $24 \times Q_v$
2. $(hP_v)^{0.5} = [27(600 + 14.5)]^{0.5} = 128.8$

**Table 6-61
Gauge Location Factors [140]**

Gauge elevation above sea level—lineal feet						
Degrees latitude	Sea level	2,000'	4,000'	6,000'	8,000'	10,000'
0 (Equator)	0.9987	0.9986	0.9985	0.9984	0.9983	0.9982
5	0.9987	0.9986	0.9985	0.9984	0.9983	0.9982
10	0.9988	0.9987	0.9986	0.9985	0.9984	0.9983
15	0.9989	0.9988	0.9987	0.9986	0.9985	0.9984
20	0.9990	0.9989	0.9988	0.9987	0.9986	0.9985
25	0.9991	0.9990	0.9989	0.9988	0.9987	0.9986
30	0.9993	0.9992	0.9991	0.9990	0.9989	0.9988
35	0.9995	0.9994	0.9993	0.9992	0.9991	0.9990
40	0.9998	0.9997	0.9996	0.9995	0.9994	0.9993
45	1.0000	0.9999	0.9998	0.9997	0.9996	0.9995
50	1.0002	1.0001	1.0000	0.9999	0.9998	0.9997
55	1.0004	1.0003	1.0002	1.0001	1.0000	0.9999
60	1.0007	1.0006	1.0005	1.0004	1.0003	1.0002
65	1.0008	1.0007	1.0006	1.0005	1.0004	1.0003
70	1.0010	1.0009	1.0008	1.0007	1.0006	1.0005
75	1.0011	1.0010	1.0009	1.0008	1.0007	1.0006
80	1.0012	1.0011	1.0010	1.0009	1.0008	1.0007
85	1.0013	1.0012	1.0011	1.0010	1.0009	1.0008
90 (Pole)	1.0013	1.0012	1.0011	1.0010	1.0009	1.0008

Note: While F_t values are strictly manometer factors, to account for gauges being operated under gravitational forces that depart from standard location; it is suggested that it be combined with other flow constants. In which instance, F_t becomes a location factor constant and F_m , the manometer factor agreeable with standard gravity remains a variable factor, subject to change with specific gravity, ambient temperature, and static pressure.

- 3. Basic orifice factor for taps F_b ; see Table 6-76 for $D = 12$ in. (11.938) and $D = 4,000$, $F_b = 3,260$
- 4. Reynolds number factor F_r :

$$F_r = 1 + \frac{b}{(hP)^{0.5}} = \frac{b}{128.8}$$

for b see Table 6-77 for given d and D

$$b = 0.0206$$

$$F_r = 1 + \frac{0.0206}{128.6} = 1.0001599 = 1.0002$$

(minimum four decimal places is required)

- 5. Expansion factor Y (function β and h/P)

$$\beta = \frac{d}{D} = \frac{4.000}{11.938} = 0.33506$$

$$\frac{h}{P} = \frac{27}{692.5} = 2.8989 \times 10^{-2} = 0.038989 = 0.039$$

from Table 6-58a $Y_1 = 0.9996$ by interpolation

6. Temperature base factor

$$F_{tb} = \frac{469.67 + 60}{519.67} = 1.0$$

7. Pressure base factor

$$F_{pb} = \frac{14.73}{14.65} = 1.0055$$

8. Flowing temperature factor

$$F_{tr} = \left(\frac{T_b}{T_f} \right)^{0.5} = \left(\frac{519.67}{459.67 + 75} \right)^{0.5} = 0.9859$$

9. Gas specific gravity factor F_g or $F_{gr} = (1/SG_g)^{0.5}$

Comp.	Concentr.	T_c (°R)	$Z_1 T_{cl}$	P_c (psia)	$Z_1 P_{cl}$	M	$Z_1 M_1$
C ₁	0.85	344	292.4	673	572.1	16	13.6
C ₂	0.05	550	27.5	712	35.6	30	1.5
C ₃	0.03	666	20.0	617	18.5	44	1.3
iC ₄	0.01	734	7.3	528	5.3	58	0.6
N ₂	0.06	227	13.6	492	29.5	28	1.7
		Σ	360.9°R		661 psia		18.7

$$SG_g = \frac{M_{gas}}{M_{air}} = \frac{18.7}{28.9625} = 0.646, \quad F_{gr} = \left(\frac{1}{SG_g} \right)^{0.5} = 1.2442$$

10. Supercompressibility factor

$$F_{pv} = \frac{1}{Z^{0.5}}$$

$$T_r = \frac{459.67 + 75}{360.9} = 1.481$$

$$P_r = \frac{692.5}{661} = 1.0477$$

from Figure 6-227 $Z = 0.895$

$$F_{pv} = \frac{1}{0.896^{0.5}} = 1.0564$$

or from Equation 6-311

$$F_{pv} = 1 + \frac{3.32 \times 600 \times 10^{5.0+1.81 \times 0.646}}{534.67^{3.825}} = 1.0526$$

11. Daily flowrate;

$$\begin{aligned} 24Q_v &= 24 (\times F_b F_r Y F_{pb} F_{tb} F_{tr} F_{gr} F_{pv} (h_w P_t)^{0.5}) \\ &= 24 \times 3260 \times 1.0002 \times 0.9996 \times 1.0055 \times 1.0 \times 0.9859 \\ &\quad \times 1.2442 \times 1.0526 \times 128.8 = 13.08 \text{ MMscfd} \end{aligned}$$

Example 17

A 1.6-MMscm daily flowrate at 0.63 relative density natural gas is to be metered at 27°C and 7 MPa in an orifice meter using flange taps. At this condition the compressibility factor $Z = 0.895$. What size orifice plate and meter run should be used? Assume that $h_w = 52$ in. of H_2O , $P_b = 14.5$ psia, $T_b = 59^\circ F$. Ignore F_r and Y_1 .

$$SG_g = 0.63$$

$$T = 27^\circ C = 80.6^\circ F$$

$$P_{\text{static on meter}} = 7 \text{ MPa} = 1,015.26 \text{ psig}$$

$$Z = 0.895$$

$$P_b = 14.5 \text{ psia} = 100 \text{ kPa} = 1 \text{ bar}$$

$$T_b = 59^\circ F = 15^\circ C$$

For P_{bar} assume it is the same as P_{base} if P_{bar} is unknown:

$$24 Q_v = F_b F_r Y F_{pb} F_{tb} F_{tr} F_{gr} F_{pv} (h_w P_t)^{0.5}$$

1° Flowrate Q_v (scf/hr) at 14.73 and $T = 60^\circ F$

$$24Q_v = 1.6 \text{ MMscm}/24 \text{ hr}$$

$$Q_v = 1.6 \text{ MMscm}/\text{hr}$$

Standard conditions for SI system:

$$P = 100 \text{ kPa}, T = 15^\circ\text{C} \text{ or } P = 101.325 \text{ kPa}, T = 0^\circ\text{C}$$

Use the first set, where molal volume = 23.96 scm/kmol; then our T_b and P_b are exactly the same.

$$P_b = 14.5 \text{ psia} = 100 \text{ kPa}$$

$$T_b = 59^\circ\text{F} = 15^\circ\text{C}$$

$$\text{Hence, } Q_w = 1.6 \times 10^6 \text{ (scm/day)}(1 \text{ kmol}/23.96 \text{ scm}) = 66,777.96 \text{ kmol}/24 \text{ hr}$$

$$= \frac{147217.73 \text{ lbmol}}{24 \text{ hr}}$$

Q_w is in the formula for orifice equations according to AGA Report [140] has standard conditions $P_{sc} = 14.73 \text{ psia}$ and $T_{sc} = 60^\circ\text{F}$. For those conditions the molal volume = 378.4 ft³/lb mol.

Flowrate Q_w (scf/h) at 14.73 psia and 60°F is equal to

$$Q_{v(\text{AGA})} = \frac{147,217.73 \text{ lbmol}}{24 \text{ h}} \times 378.4 \frac{\text{scf}}{\text{lbmol}} = 2.321133 \text{ scf/h}$$

2° Temperature base factor F_{tb}

$$F_{tb} = \frac{459.67 + 59}{519.67} = 0.9981$$

3° Pressure base factor F_{pb}

$$F_{pb} = \frac{14.73}{14.50} = 1.0159$$

4° Gas gravity factor F_{gr}

$$F_{gr} = \left(\frac{1}{SG_g} \right)^{0.5} = \frac{1}{0.63} = 1.2599$$

5° Supercompressibility factor F_{pv}

$$F_{pv} = \left(\frac{1}{Z_f} \right)^{0.5} = \left(\frac{1}{0.895} \right) = 1.057$$

6° Flowing temperature factor F_{tf}

$$F_{if} = \left(\frac{T_b}{T_f} \right)^{0.5} = \left(\frac{459.67 + 59}{459.67 + 80.6} \right)^{0.5} = 0.9798$$

$$7^\circ (h_w P_f)^{0.5} = [52 \times (1015.26 + 14.5)]^{0.5} = 231.4$$

8° Solve for F_b :

$$\begin{aligned} F_b &= \frac{Q_v}{F_{ib} F_{pb} F_{if} F_{gr} F_{pv} (h_w P_f)^{0.5}} \\ &= \frac{2,321,133}{(0.9981)(1.0159)(0.9798)(1.2599)(1.2599)(1.0570)(231.4)} \\ &= 6,017.6 \end{aligned}$$

9° Selection of meter run (see several combinations of orifice-to-pipe ratios) will fall within the recommended β ratio.

F_b	Pipe "D"		Orifice "d"	β
	Nominal	Size		
7579.2	12	11.938	6.0	0.5026
7564.7	12	12.090	6.0	0.4963
7640.4	12	11.374	6.0	0.5274
777.8	8	8.071	5.75	0.7124

The larger the run, the lower β but the higher the cost. Once a size has been chosen, the values of F_r and Y_1 could be calculated, but the effect on the choice is trivial.

Uncertainty Limits and Field Problems

No two orifice meters can be built, as a rule, to give exactly the same readings when the same amount of gas is flowing. For this reason, uncertainties are necessary for the values of the constants given in this standard. The commercial accuracy will be somewhat less than the accuracy indicated by the tolerance given for the orifice flow constants. Very exact duplication of orifice plates is not commercially possible. An example of the effect of uncertainties is provided below.

Example 18

Using the flow equation, find the overall measurement uncertainty of the flow, knowing percentage uncertainty of each variable. We use the equation

$$Q_v = F_b F_r Y F_{pb} F_{ib} F_{if} F_{gr} (h_w P_f)^{0.5}$$

Variable	% Uncertainty of variable (+)	Effect factor	
		Exponent	Square
F_b	0.5	1	0.25
F_r	0.1	1	0.01
Y	0.25	1	0.0625
F_{pb}	0.05	1	0.0025
F_B	0.03	1	0.0009
F_H	0.25	$\frac{1}{2}$	0.0156
F_{gr}	0.7	$\frac{1}{2}$	0.1225
F_{pv}	0.4	$\frac{1}{2}$	0.040
h_w	0.5	$\frac{1}{2}$	0.0625
P_t	0.5	$\frac{1}{2}$	0.0625
Sum of squares			0.6265
Square root of sum			0.7915%

As the table illustrates, the overall measurement uncertainty of the flow in this example is $\pm 0.7915\%$. The above analysis assumes constant flowrate, which is a rather theoretical case.

System design must consider monthly variations in flow, daily variations in flow and even very short form variation in flow. One of the most difficult metering conditions is when the producer has installed intermitters on the well production. Very often in these systems, the no-flow period (or low-flow period) is of a relatively long duration when compared to the flow periods. The result is a chart interpretation that is much higher than actual flow.

Sometimes in vacuum gathering systems, backflow may occur. In such a case it is possible to pay for gas twice. The gas flows through the metering system once as it is produced; it may flow backwards through the system into the reservoir when the compressor shuts down. When the compressor is restarted, it may be drawn through the system again and be remetered. For that reason, it is important to install check valves on the sublet of meter runs.

An Electronic Measurement—The primary considerations for going to electronic measurement includes the fact that it is more accurate. Electronic metering units are more capable of following highly variable flows than a mechanical chart recorder. After installation of electronic systems it is possible to reduce the imbalance between the plant inlets vs. the field volumes to less than 2% as compared with a balance that frequently runs 6–8% using mechanical recorders.

Gas Gathering

Gas gathering systems usually consist of the piping and processing equipment between individual wells in a gas field and the compressor station at the inlet of the transmission or distribution lines. The smallest gathering system consists simply of two or more gas wells interconnected by piping and tied directly into a distribution system. For large fields and for several interconnected fields involving hundreds of miles of piping, gathering systems may include such

equipment as drips, separators, meters, heaters, dehydrators, gasoline plant, sulfur plant, cleaners and compressors, as well as piping and valves.

Depending on local conditions, there are a few types of gathering systems. The basic systems are axial, radial, loop and their combinations (see Figures 6-232 and 6-233).

The choice between the gathering systems is usually economic, but technical feasibility is also important. Special attention is paid in the solution of complex transmission systems to express the various lengths and diameters of the pipe

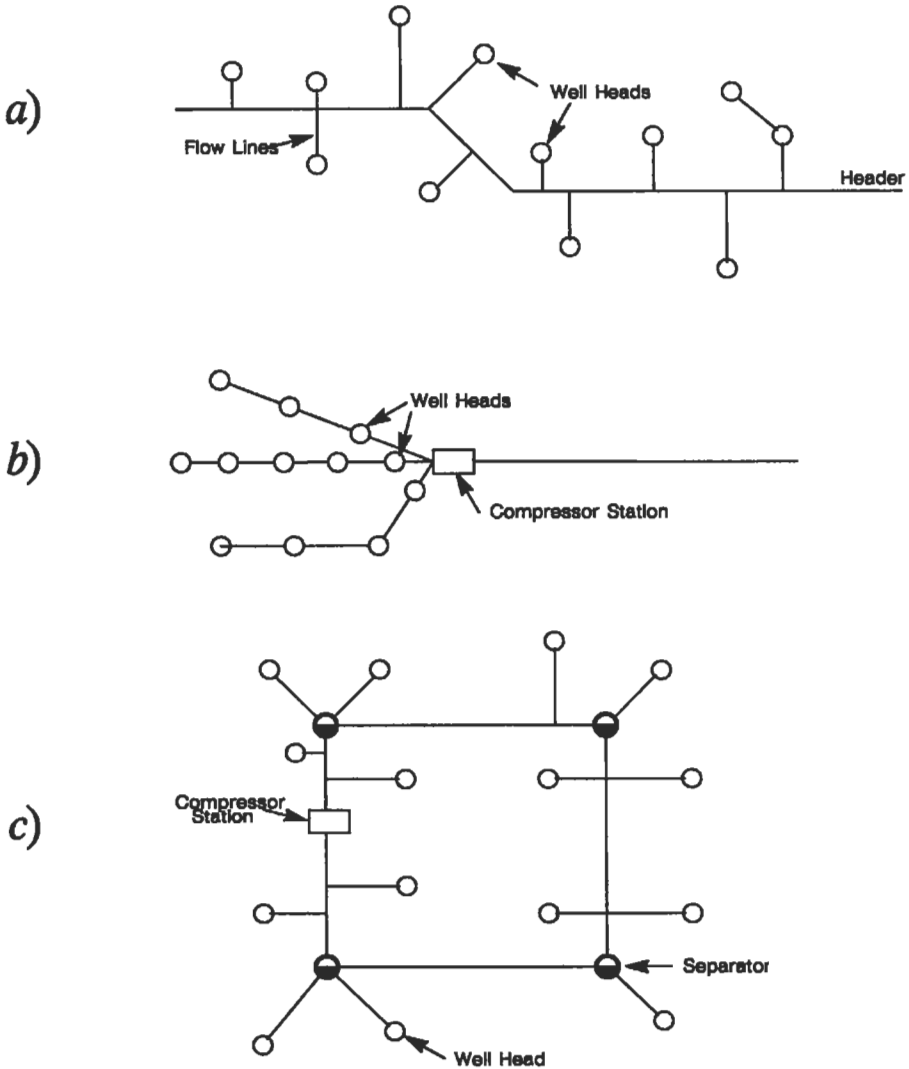


Figure 6-232. Simple gathering systems; a) an axial, b) a radial, c) loop.

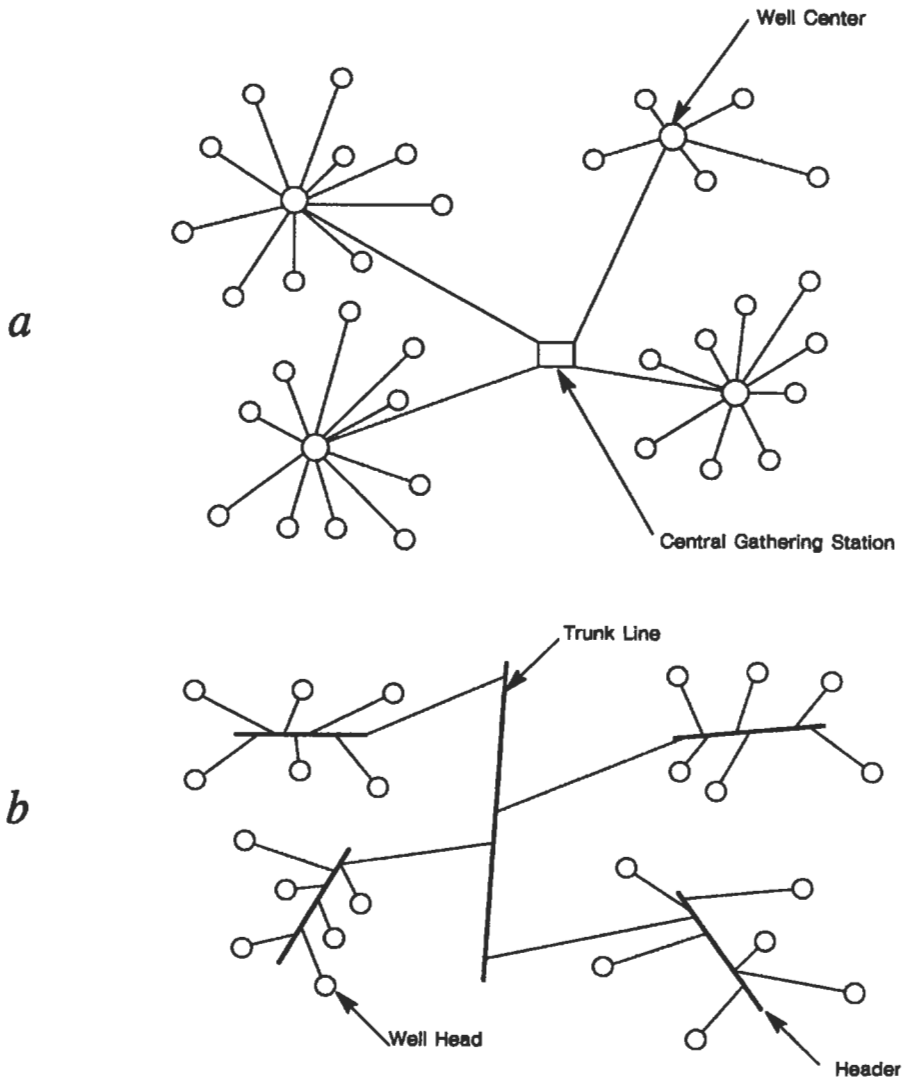


Figure 6-233. A combination of gathering systems: a) well-center, b) trunk-line.

in the system as equivalent lengths of a common diameter or equivalent diameters of a common length. Equivalent, in this case, means that both lines will have the same capacity with the same total pressure drop.

Flow Equations for Steady State

Commonly used equations for gas flow are given below:
 (a) Basic equation

$$Q_{sc} = K \left(\frac{T_{sc}}{P_{sc}} \right)^{1.000} \left[\frac{(P_1^2 - P_2^2) D^5}{8 SG_g L T_m Z_m} \right]^{0.5} \quad (E) \quad (6-314)$$

where $K = 38.774$ is in English units
 $= 5.62 \times 10^5$ is in SI units

(b) Weymouth equation

$$Q_{sc} = K \left(\frac{T_{sc}}{P_{sc}} \right)^{1.000} \left[\frac{(P_1^2 - P_2^2) D^{5.393}}{SG_g L T_m Z_m} \right]^{0.5} \quad (E) \quad (6-315)$$

where $K = 433.5$; $f = 0.008/D^{0.33}$ is in English units
 $= 1.162 \times 10^7$; $f = 0.0109/D^{0.33}$ is in SI units

(c) Panhandle A equation is

$$Q_{sc} = K \left(\frac{T_{sc}}{P_{sc}} \right)^{1.0788} \left[\frac{(P_1^2 - P_2^2) D^{4.854}}{SG_g^{0.854} L T_m Z_m} \right]^{0.5994} \quad (E) \quad (6-316)$$

where $K = 435.9$, $f = 0.0192/(Q_{sc} SG_g/D)^{0.1461}$ is in English units
 $= 1.198 \times 10^7$, $f = 0.0099/(Q_{sc} SG_g/D)^{0.1461}$ is in SI units

d) Panhandle B equation is

$$Q_{sc} = K \left(\frac{T_{sc}}{P_{sc}} \right)^{1.020} \left[\frac{(P_1^2 - P_2^2) D^{4.961}}{SG_g^{0.961} L T_m Z_m} \right]^{0.51} \quad (E) \quad (6-317)$$

where $K = 737$, $f = 0.00359/(Q_{sc} SG_g/D)^{0.03922}$ is in English units
 $= 1.264 \times 10^7$, $f = 0.0030/(Q_{sc} SG_g/D)^{0.03922}$ is in SI units

e) The Clinedinst equation in English units is

$$Q_{sc} = 288.7 \left(\frac{T_{sc}}{P_{sc}} \right) Z_{sc} P_{sc} \left[\frac{D^5}{SG_g T_m L f} \left(\int_0^{P_{r,1}} \frac{P_r}{Z} dP_r - \int_0^{P_{r,2}} \frac{P_r}{Z} dP_r \right) \right]^{0.5}$$

Values of the integral functions $\int_0^{P_r} (P_r/Z) dP_r$ are tabulated in Table A-6 of Katz [144] or in Table 7-1 of Kumar [145].

The constants in the equations of (a)-(e) are as follows:

Q_{sc} = gas flowrate at T_{sc} , P_{sc} , in scf/d or scm/d
 P , P_{sc} = absolute pressure at standard conditions in psia or kpa

- T_m, T_{sc} = mean absolute temperature of line at standard conditions in °R or K
 D = inside diameter of pipes in in. or m
 L = pipe length in mi or m
 μ = viscosity in lb/(ft • s) or Pa • s
 γ_g = relative gas density (air = 1.0)
 Z_m^g = mean compressibility factor
 E = pipeline efficiency
 R_c = Reynolds number
 P_r = pseudocritical pressure

Pipeline efficiency is a correction for small amounts of liquid, general debris, weld resistance, valve installations, line bends, and other factors that reduce the gas flowrate to a point below the basic equation of state. The design value of "E" in a new clean gas line usually is estimated as 0.92. Some companies arbitrarily use a graduated "E":

- E = 1.0, new straight pipe without bends, very seldom used in design
- = 0.95, excellent conditions (with frequent pigging)
- = 0.92, average to good conditions (normal design)
- = 0.85, adverse, unpigged, old dirty pipe

Equations 6-313 to 6-317 are equations for steady-state flow of gas through a horizontal pipe. These equations assume:

- no mechanical work is done on the gas between the points at which the pressures are measured
- negligible kinetic energy change

The Weymouth equation was devised for sizing gas lines operating at pressures from 35 to 100 psig if $Z = 1.0$. By including the compressibility factor, the Weymouth equation showed reasonable agreement with metered volumes, for field gathering lines operating at 1,000 to 3,200 psig. The Weymouth equation is used most often for designing gas gathering and transmission systems because it generally maximizes pipe diameter requirements for a given flowrate and pressure drop.

Example 18

A pipe line is to be designed to transmit 300 MMsf/d measured at 60°F and 15.025 psia. Specific gravity of the gas is 0.71. Flowing temperature is expected to average 60°F while barometric pressure is to average 14.3 psia. It has already been decided that 24-in. pipe will be used (ID = 23.2 in.) and that discharge and suction pressures at the compressed stations will be 800 psig and 350 psig, respectively. How far apart will the compressor stations be? Use the Weymouth and Panhandle equations, where $Z = 0.86$, $E = 0.92$.

From Equation 6-315

$$Q_{sc} = \left(\frac{T_{sc}}{P_{sc}} \right)^{1.000} K \left[\frac{(P_1^2 - P_2^2) D^{5.333}}{SG_g L T Z} \right]^{0.5} \quad (E)$$

Substituting the given values into the equation gives

$$300 \times 10^6 = \left(\frac{519.67}{15.025} \right)^{1.000} 433.5 \left[\frac{(814.3^2 - 364.3^2)(23.2)^{5.933}}{(0.71)L(519.67)(0.86)} \right]^{0.5} \quad (E)$$

$$2855.7 \times L = 228542E^2$$

$$= 80.03E^2$$

if $E = 1.0$, then $L = 80.03$ mi

if $E = 0.82$, then $L = 67.74$ mi

From Equation 6-316

$$Q_{sc} = K \left(\frac{T_{sc}}{P_{sc}} \right)^{1.0788} \left[\frac{(P_1^2 - P_2^2) D^{4.854}}{SG_g^{0.854} LTZ} \right]^{0.5594} \quad (E)$$

$$300 \times 10^6 = 435.87 \left(\frac{519.67}{15.025} \right)^{1.0788} \left[\frac{530,370 \times 23.2^{4.854}}{(0.71)^{0.854} L(519.67)(0.86)} \right]^{0.5594}$$

$$\left[\frac{530,370 \times 4,246,964.97}{33.58L} \right]^{0.5594} \quad (E)$$

$$L^{0.5594} = 13.317E$$

If $E = 1.0$, then $L = 121.5$ mi

If $E = 0.92$, then $L = 104.1$ mi

From Equation 6-317

$$300 \times 10^6 = 737 \left(\frac{519.67}{15.025} \right)^{1.02} \left[\frac{(814.3^2 - 364.3^2) 23.2^{4.861}}{(0.71)L(519.67)(0.86)} \right]^{0.51} \quad (E)$$

$$L = 99.4$$

Panhandle equations "A" and "B" give good results for pressures higher than 100 psia and diameters larger than 8 in. and for systems operating at $R_e > 10^5$.

In our example, because of the large diameter of pipe being used, $L = 104.1$ mi is the correct answer.

Example 19

Suppose that the pipeline of example 18 has been built and that at some later date the capacity of the line is to be increased to 320 MMcf/d by lowering the suction pressure at the stations. If $E = 0.95$, what suction pressure would be required? Use the Panhandle "A" and "B" equations.

Using Panhandle "A" equation

$$\begin{aligned}
 P_2^2 &= P_1^2 - \frac{Q_{sc}^{2/0.5394} P_1^2 T_m Z_m \gamma_g^{0.854} L}{(KE)^{1/0.5394} (520)^2 (23.2)^{4.854}} \\
 &= (84.3)^2 - \frac{(320)(10^6)^{1.8539} (15.025)(520)(0.86)(0.71)^{0.854} (104.1)}{(0.95)^{1.8539} (435.87)^{1.8539} (520)^2 (23.2)^{4.854}} \\
 &= 100,183
 \end{aligned}$$

$$P_2 = 316.5 \text{ psia}$$

Using Panhandle "B" equation

$$\begin{aligned}
 P_2^2 &= (814.3)^2 - \frac{(320)(10^6)^{1.96} (15.025)^2 (520)(0.86)(0.71)^{0.961} (99.4)}{(0.95)^{1.96} (737)^{1.96} (520)^2 (23.2)^{4.961}} \\
 &= 100,183
 \end{aligned}$$

$$P_2 = 313.1 \text{ psia}$$

Complex Gas Flow Systems

A situation often required to increase the flowrate per unit pressure drop in a system. The common way to solve this problem is to place one or more lines parallel to the original, either partially or throughout the entire length of the system (see Figure 6-234a). If the lines are of equal length $(\Delta P/L)_A = (\Delta P/L)_B$ and if a line 1-2 is partially looped with B length, $L_A = L_B$

$$\begin{aligned}
 Q_A + Q_B &= Q_C = Q_{\text{total}} \\
 \Delta P_A &= \Delta P_B
 \end{aligned}$$

The pressure loss due to friction in the looped position plus that in the unlooped portion must equal the total friction loss:

$$\left(\frac{\Delta P_f}{L_n}\right)_A (x) + \left(\frac{\Delta P_f}{L_n}\right)(L - x) = \text{total } \Delta P_f$$

The purpose of the second line B is to decrease the pressure drop between points 1 and 3, compensating for the increased pressure between points 3 and 2, the unlooped portion, with the required increased flow.

The basic equations (6-314) may be used to anticipate rates and sizing of lines, which could be expressed as

$$Q = K' \left(\frac{D_b}{f_L}\right)^{0.5} (E)$$

The flow of gas in "n" number of horizontal parallel looped lines is

$$Q = K \left(\frac{T}{P}\right)_{sc} \left(\frac{P_1^2 - P_2^2}{SG_g TLZ}\right) \underbrace{\left(\frac{D_A^{2.5}}{f_A^{0.5}} + \frac{D_B^{2.5}}{f_B^{0.5}} + \dots + \frac{D_n^{2.5}}{f_n^{0.5}}\right)}_{D_e} E$$

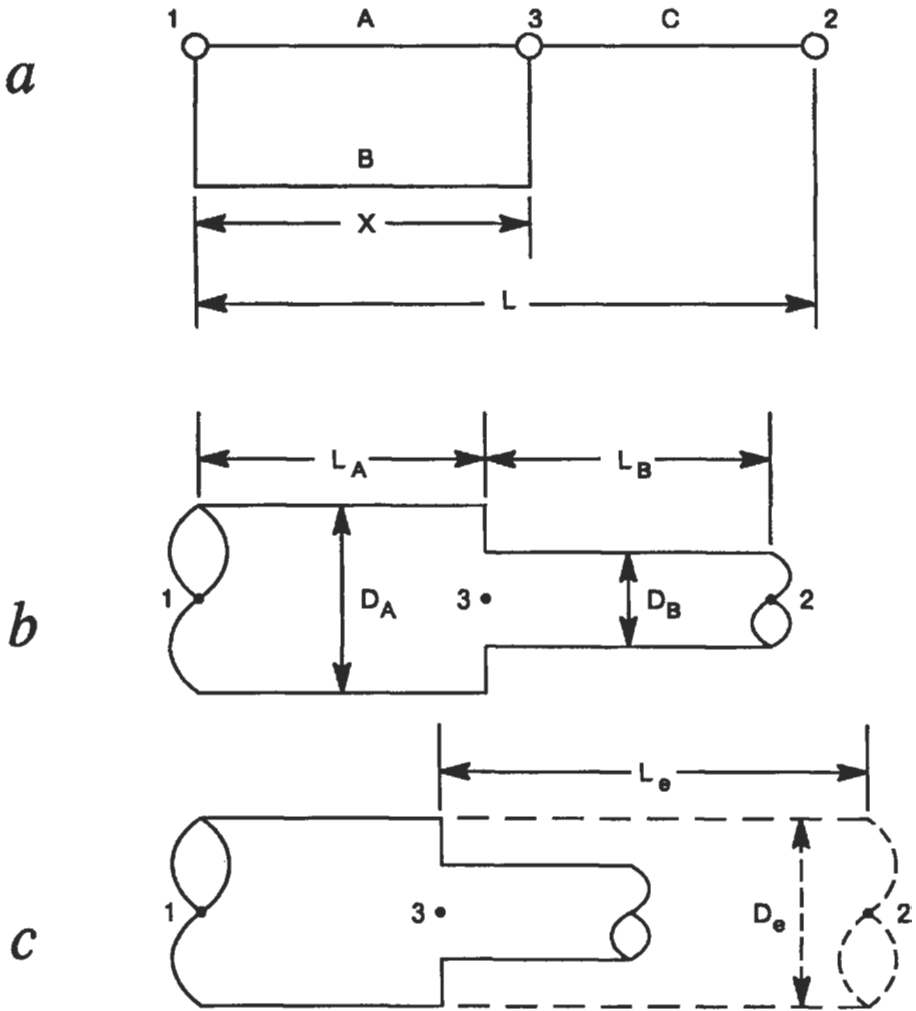


Figure 6-234. Complex pipelines: a) the looped pipeline system, b) the series pipeline system, c) the equivalent length and diameter.

The equivalent diameter D_e of a single line having the same capacity as the foregoing set of parallel lines is

$$D_e^{2.5} = \left(\frac{f_e}{f_A}\right)^{0.5} D_A^{2.5} + \left(\frac{f_e}{f_B}\right)^{0.5} D_B^{2.5} + \dots + \left(\frac{f_e}{f_n}\right) D_n^{2.5}$$

Combining both an equivalent length, L_e , and equivalent diameter, D_e , terms:

$$\frac{D_e^{2.5}}{(f_e L_e)^{0.5}} = \frac{D_A^{2.5}}{(f_A L_A)^{0.5}} + \frac{D_B^{2.5}}{(f_B L_B)^{0.5}} + \dots + \frac{D_n^{2.5}}{(f_n L_n)^{0.5}} \tag{6-319}$$

In Equation 6-319, one usually chooses a diameter D_c , equal in size to the unlooped portion, then calculates the equivalent L_c (corresponding to that ΔP characteristic of the actual looped section). This L_c is added to the length of the unlooped portion. Table 6-62 summarizes other complex gas flows. For more details see books [136,144-146].

Example 20

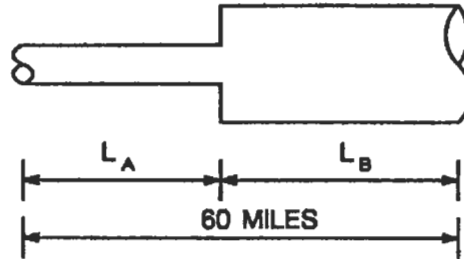
A brand line is laid to move gas a distance of 60 mi from a junction on the main line to a city. The line is to transmit 23 MMcf/d of 0.73 gravity gas, measured at 60°F and 14.65 psia. Flowing temperature will be 65°F at 14.65 psia. Pressure at the junction is 620 psia and the gas is to be delivered to the city gate at 100 psia. The objective is to minimize the investment in pipe by laying a line consisting of two sizes in series. The following sizes are available:

Nominal Size (in.)	Internal diameter (in.)
6	6.065
8	8.071
10	10.192
12	12.090

Table 6-62
Equations for Complex Gas Flow

Equation	Basic	Weymouth	Panhandle A
For Two Lines in Series			
Equivalent Diameter D_c	$D_B \left(\frac{L_A}{L_B} \right)^{1/3} \left(\frac{f_A}{f_B} \right)^{1/5}$	$D_B \left(\frac{L_A}{L_B} \right)^{3/16}$	$D_B \left(\frac{L_A}{L_B} \right)^{0.2060}$
Equivalent Diameter L_c	$L_B \left(\frac{D_A}{D_B} \right)^5 \left(\frac{f_B}{f_A} \right)$	$L_B \left(\frac{D_A}{D_B} \right)^{16/3}$	$L_B \left(\frac{D_A}{D_B} \right)^{4.264}$
For Two Lines in Series			
Equivalent Diameter or Length-Loops D_c or L_c	$\frac{D_c^{2.5}}{(f_c L_c)^{0.5}} = \frac{D_A^{2.5}}{(f_A L_A)^{0.5}} + \frac{D_B^{2.5}}{(f_B L_B)^{0.5}}$	$\frac{D_c^{8/3}}{L_c^{0.5}} = \frac{D_A^{8/3}}{L_A^{0.5}} + \frac{D_B^{8/3}}{L_B^{0.5}}$	$\frac{D_c^{2.616}}{L_c^{0.5394}} = \frac{D_A^{2.616}}{L_A^{0.5394}} + \frac{D_B^{2.616}}{L_B^{0.5394}}$
Loops-Diameters and Flows Vary X_f - Fraction Looped	$x_f = \frac{\left(\frac{Q_1}{Q_2} \right)^{0.5} - 1}{\left[\frac{1}{(1 + D_R)^2} - 1 \right]}$	$x_f = \frac{1 - \left(\frac{Q_1}{Q_2} \right)^2}{1 - \left[\frac{D_1^{8/3}}{D_2^{8/3} + D_1^{8/3}} \right]^2}$	$x_f = \frac{1 - \left(\frac{Q_1}{Q_2} \right)^{1.86}}{1 - \frac{1}{\left[1 - \left(\frac{D_2}{D_1} \right)^{2.62} \right]^{1.86}}}$
Entire Line Looped		$\frac{Q_2}{Q} = 1 + \left(\frac{D_2}{D_1} \right)^{8/3}$	$\frac{Q_2}{Q} = 1 + \left(\frac{D_2}{D_1} \right)^{2.616}$
Diameters of Original and Parallel Lines are the same X_f = Fraction Looped	$x_f = \frac{4}{3} \left[1 - \left(\frac{Q_1}{Q_2} \right)^2 \right]$	$x_f = \frac{4}{3} \left[1 - \left(\frac{Q_1}{Q_2} \right)^2 \right]$	$x_f = \frac{4}{3} \left[1 - \left(\frac{Q_1}{Q_2} \right)^{1.86} \right]$

Which two of the above pipe sizes should be used, and how much of each should be laid? Disregard the compressibility factor and pipeline efficiency in this problem.



Find D_c from Weymouth Equation 6-315:

$$D_c = \left[\frac{SG_g T_m Z_m L}{(P_1^2 - P_2^2)} \left(\frac{Q_{sc} E P_{sc}}{KT_{sc}} \right)^2 \right]^{1/5.333}$$

$$Z_m = E = 1.0$$

$$D_c = \left[\frac{0.73 \times 525 \times 60}{620^2 - 100^2} \left(\frac{23 \times 10^6 \times 14.65}{433.5 \times 520} \right)^2 \right]^{1/5.333}$$

$$= 9.19023$$

For Case I, assume $D_A = 8.071$, $D_B = 10.192$, $L_A + L_B = 60$, $L_A = 60 - L_B$, $L_B = 60 - L_A$ or

$$D_c = D_B \left(\frac{L_A}{L_B} \right)^{5/16} = D_B \left(\frac{L_A}{60 - L_A} \right)^{5/16}$$

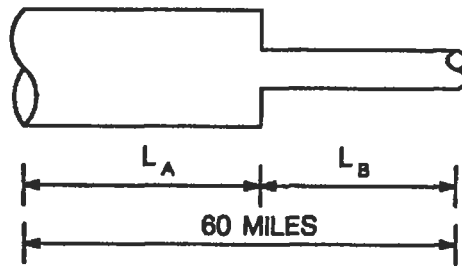
$$9.19023 = 10.192 \left(\frac{L_A}{60 - L_A} \right)^{5/16}$$

$$L_A = 21.92 (D_A = 8 \text{ in.})$$

and

$$L_B = 38.08 (D_B = 10 \text{ in.})$$

For Case II, assume $D_A = 10.192$, $D_B = 8.071$



$$D_c = D_B \left(\frac{L_A}{L_B} \right)^{3/16}$$

$$9.19023 = 8.071 \left(\frac{L_A}{60 - L_A} \right)^{3/16}$$

$$1.9989 = \frac{L_A}{60 - L_A}$$

$$L_A = 39.99 = 40 \text{ mi } (D_A = 10 \text{ in.})$$

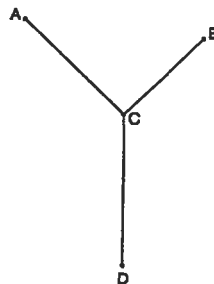
$$L_B = 20 \text{ mi } (D_B = 8 \text{ in.})$$

Both cases, more or less, in given conditions give similar results. As a solution, it is better to take $L_A = 21.92$ with $D_A = 8$ in. and $L_B = 38.08$ with $D_B = 10$ in.

Example 21

Two lines, AC (5-in. ID, 4.5 mi long) and BC (5 in. ID, 3.8 mi long), emanating from leases A and B, respectively, terminate at the gathering station at C. From C a single 11.5-mi, 8-in. ID pipeline leads into the regional trunk line at D, where the gas must be delivered at 520 psig. Lease A produces 5 MMscfd of 0.65 gravity gas, while lease B produces 7 MMscfd of 0.68 gravity gas. What pressure should the gas be compressed to at (a) lease A and (b) lease B to enable delivery of gas to the trunk line? $E = 0.92$.

Assume a flowing temperature of 85°F, and horizontal flow system. $P_{sc} = 14.73$ psia, $T_{sc} = 60^\circ\text{F}$.



AC = 4.5 mi, ID = 5 in.,

Q = 5 MMscfd

BC = 3.8 mi, ID = 5 in.,

Q = 7 MMscfd

CD = 11.5 mi, ID = 8 in.

First, the pressure at point C is necessary to find:

$$SG_{gv} = \frac{5 \times 0.65 + 7 \times 0.68}{12}$$

$$= 0.6675$$

Apply the Weymouth equation for section C-D;

$SG_{gv} = 0.6675$, $T_{pc} = 378^\circ R$, $P_{pc} = 668$ psia

$Z = 0.91$

$$12 \times 10^6 = 433.5 \left(\frac{520}{14.73} \right) \left[\frac{P_1^2 - (534.73)^2 8^{16/3}}{(0.6675)(11.5)(545)(0.91)} \right]^{0.5} 0.92$$

P_1 corresponds to P_c

$P_c = 572.8$

Section B-C

$SG_g = 0.68$, $T_{pc} = 384^\circ R$, $P_{pc} = 668$ psia

$Z = 0.9$

$$7 \times 10^6 = 433.5 \left(\frac{60 + 460}{14.73} \right) \left[\frac{(P_B^2 - 572.8^2) 5^{16/3}}{(0.68)(0.9)(545)(3.8)} \right]^{0.5} 0.92$$

$P_B = 621.8$ psia

Section A-C

$SG_g = 0.65$, $T_{pc} = 373^\circ R$, $P_{pc} = 670$ psia, $Z = 0.9$

$$5 \times 10^6 = 433.5 \left(\frac{60 + 460}{14.73} \right) \left[\frac{(P_A^2 - 572.8^2) 5^{16/3}}{(0.65)(0.9)(545)(4.5)} \right]^{0.5} 0.92$$

$P_A = 601.6$ psia

Example 22

A portion of a large gas-gathering system consists of a 6.067-in. ID line 9.4 mi long, handling 7.6 MMscfd of gas 0.64 gravity. The pressure at the upstream

end of this section is 375 psig and the average delivery pressure is 300 psig. The average temperature is 73°F. Due to new well completions, it is desired to increase the capacity of this line by 20% by looping with additional 6.067-in. pipe. What length is required?

From Table 6-61, if the Weymouth equation is used, then

$$X_f = \frac{1 - \left(\frac{Q_1}{Q_2}\right)^2}{1 - \left(\frac{D_1^{9.5}}{D_1^{9.5} + D_2^{9.5}}\right)^2} = \frac{1 - \left(\frac{1}{1.2}\right)^2}{1 - \left(\frac{6.067}{6.067 + 6.067}\right)^2} = 0.4014$$

The length of looping pipe required = $0.4074 \times 9.4 = 3.83$ mi

Compressor Stations

A compressor station is one of the most important elements in a natural gas pipeline system. Compressor stations supply the energy to pump gas from production fields, overcome frictional losses in transmission pipelines and pump gas into storage reservoirs.

Depending on its purpose, a compressor station generally falls into one of three distinct classifications: production, storage and transmission.

Production stations are used in the natural gas production field to pump gas from the well head to the pipeline system. They usually are designed for unattended operation with a life expectancy comparable to that of the production field. Unitized, skid-mounted, medium to high-speed, packaged compressor units in the 50 to 1,000 hp (35 to 745 kW) range often are utilized for this type of service. Operating pressures in production stations vary widely. The suction pressure may be required to go subatmospheric, while the discharge pressure could be as high as 1,000 psig (6,900 kPa).

Storage stations are used primarily to pump gas from a transmission pipeline into an underground gas storage field during the injection period. In addition to injecting gas during the storage season, some are used to pump gas from the storage field to the pipeline during the withdrawal period. Most storage field compressors are designed to operate over a broad range of volumes and pressures. A typical storage station would contain several reciprocating compressor units ranging in size from 1,000 to 6,000 hp (745 to 4,475 kW) each.

Transmission stations are the most common type. They generally contain several large compressor units at one location, each having a power rating or 1,000 to 20,000 hp transmission pipeline. Their purpose is to move gas from one station to the next. Operating pressure seldom exceeds 1,000 psig (6,900 kPa). Designed for long life, 50 years or more, and intended to operate year-round.

Independent of compressor station sort, three types of compressors are used: reciprocating, centrifugal and axial. See Figure 6-235. Reciprocating compressors are considered for applications where the inlet gas rate is about 3000 acfm or less. They are favored for low-flow, high-pressure service, compression ratio 2:1 to 4:1. They are available in sizes up to 15,000 hp (11,190 kW).

Centrifugal compressors are used for the inlet gas rate 500–200,000 acfm, low compression ratio 1.1:2 and range power 1,000 to 30,000 up (746–22,380 kW).

For axial-flow compressors, with the inlet gas rate at 75,000 to 600,000 acfm, smaller axials are available (down to 20,000 acfm), but centrifugal compressors

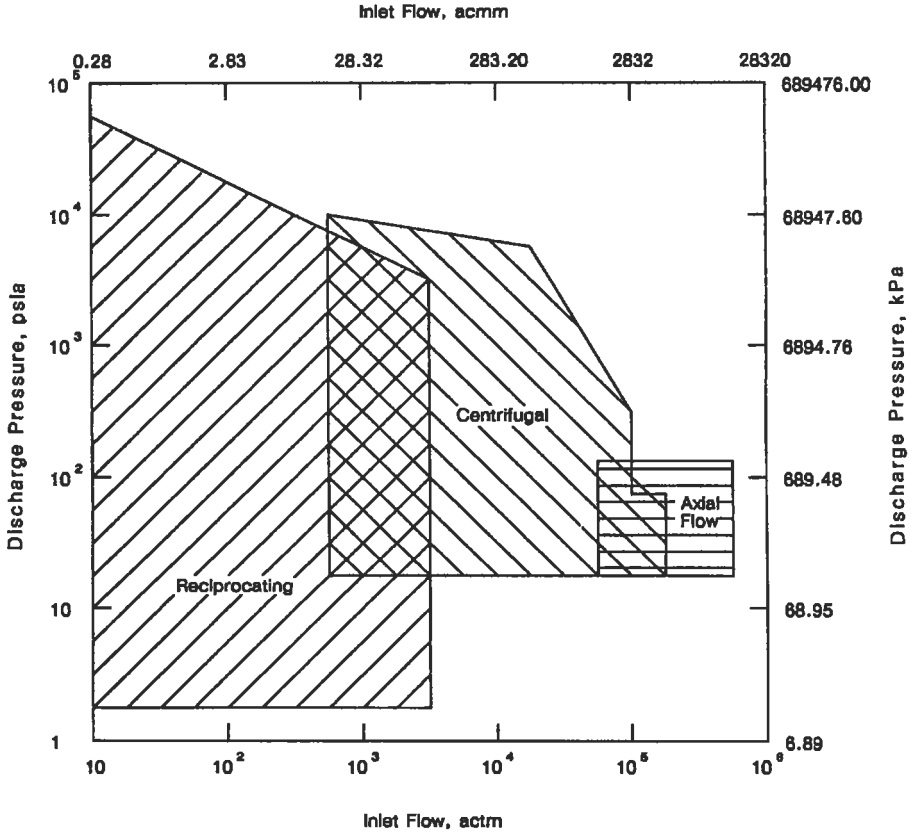


Figure 6-235. Approximate ranges of application for reciprocating, centrifugal and axial flow compressors.

are preferred at these capacities. Axial compressors are more efficient than centrifugal compressors.

Reciprocating Compressor Calculations

Figure 6-236 illustrates an ideal compression cycle on a pressure-volume cycle. The events during this cycle are as follows:

- *Compression (points 1 to 2).* The piston has moved to the left, reducing the original volume of gas with an accompanying rise in pressure. Valves remain closed. The P-V diagram shows compression from point 1 to point 2 and the pressure inside the cylinder has reached that in the receiver.
- *Discharge (points 2 to 3).* The discharge valves are opened just beyond point 2. Compressed gas is flowing out throughout the discharge valves to the receiver. After the piston reaches point 3, the discharge valves will close, leaving the clearance space filled with gas at discharge pressure.
- *Expansion (points 3 to 4).* During the expansion stroke, both the inlet and discharge valves remain closed and gas trapped in the clearance space

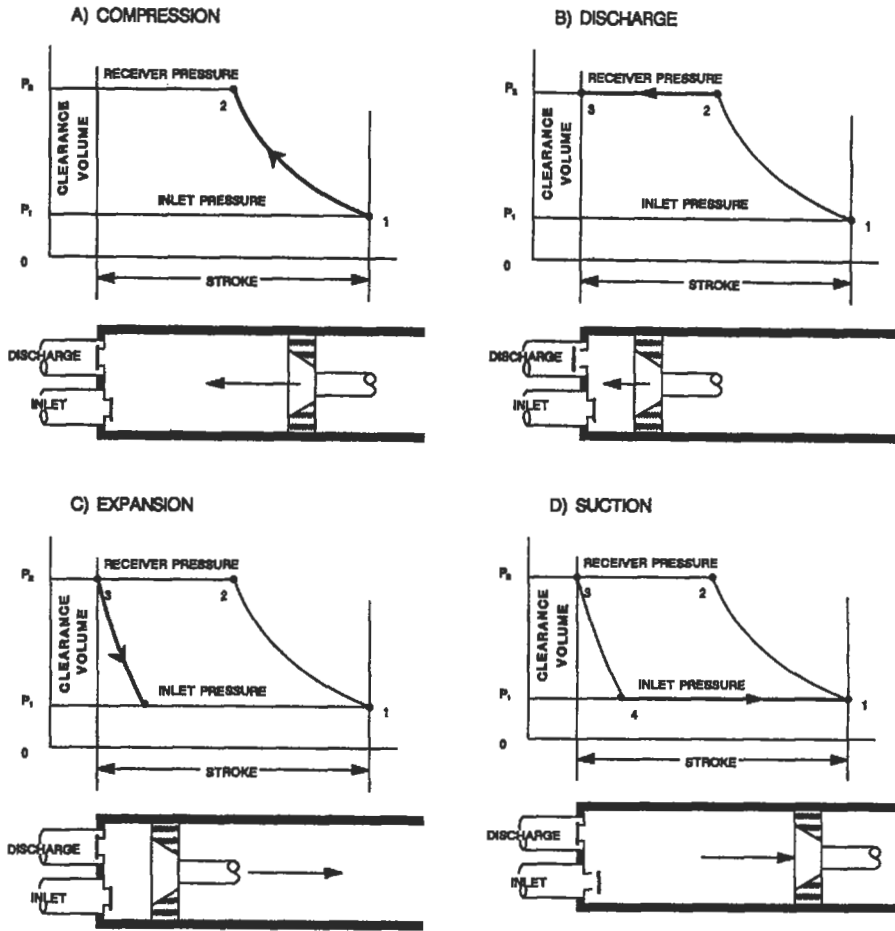


Figure 6-236. P-N diagram illustrating ideal reciprocating compression of gases.

increases in volume, causing a reduction in pressure. This continues as the piston moves to the right, until the cylinder pressure drops below the inlet pressure at point 4.

- *Suction (points 4 to 1).* At point 4 the suction valve opens and permits gas at suction pressure to enter the cylinder as the piston moves from point 4 to point 1.

To determine the quantity of gas that a specific compressor can pump, the displacement volume of gas at suction conditions and suction volumetric efficiency must be known.

The displacement of a compressor is expressed in cubic feet per minute (ft³/min), cubic feet per second (ft³/s) or in cubic meters per second (m³/s). Figure 6-236 shows the cycle as related to a single-acting compressor (compression occurs only on one end of the piston). Most reciprocating compressors in

the gas industry are double-acting. Gas is compressed alternately on each end of the piston. For single-acting compressors:

$$PD = \frac{A_H \times L \times M}{1,728} \quad (\text{ft}^3/\text{min}) \quad (6-320)$$

or

$$PD = \frac{A_H L N}{6 \times 10^9} \quad (\text{m}^3/\text{s})$$

and for double-acting compressors

$$PD = \frac{(A_H + A_c) \times L \times N}{1,728} \quad (\text{ft}^3/\text{min}) \quad (6-321)$$

or

$$PD = \frac{(A_H + A_c) \times L \times N}{6 \times 10^9} \quad (\text{m}^3/\text{s})$$

where PD = piston displacement in ft³/min or m³/s

A_H = area of head end of the piston in in.² or mm²

L = length of stroke in in. or mm

N = compressor rotation speed in rpm

A_c = area of crank end of the piston in in.² or mm²

Most compressor manufacturers publish data listing displacement at full compressor speed for each size cylinder that is manufactured.

Volumetric efficiency E_v is the ratio (%) of the actual delivered volume flowrate (at inlet conditions) to the piston displacement. The volumetric efficiency factor may be calculated as follows:

$$E_v = 100 - L - Cl \times \left[\frac{Z_s}{Z_d} \left(\frac{P_d}{P_s} \right)^{1/k} - 1 \right] \quad (6-322)$$

where E_v = volumetric efficiency factor in %

Cl = cylinder clearance expressed as a percentage of piston displacement

P_d = pressure at the discharge flange in psia or kPa

P_s = pressure at the suction flange in psia or kPa

k = ratio of specific heat capacities (adiabatic exponent), C_p/C_v

L = volumetric efficiency correction factor in %, $L = P_d/P_s$

Z_s = compressibility factor at suction conditions

Z_d = compressibility factor at discharge conditions

$P_d/P_s = r$, the compression ratio

Compressor cylinder capacity Q may be found from the following:

$$Q = PD \times E_v \times P_i/P_a \times 14.4 \times 10^{-6} \quad (\text{MMcf/d}) \quad (6-323)$$

or

$$Q = PD \times E_v \times P_i/P_a \times 864 \quad (\text{m}^3/\text{d})$$

where Q = cylinder capacity in desired units at the prevailing inlet temperature and the base suction pressure in MMcf/d or m^3/d

P_a = base reference pressure in psia or kPa

PD , E_v , P_i are as in Equation 6-322.

If the base reference pressure is 14.4 psia (99 kPa), the cylinder capacity at this base reference pressure and prevailing temperature is

$$Q = PD \times E_v \times P_i \times 10^{-6} \quad (\text{MMcf/d}) \quad (6-324)$$

or

$$Q = PD \times E_v \times P_i \times 8.73 \quad (\text{m}^3/\text{d})$$

Q represents the actual displaced quantity of gas in MMcf/d (m^3/d), corrected only for pressure to a base of 14.4 psia (99 kPa) at the prevailing suction temperature. According to ISO 5024 scm has only one set of reference conditions: $P_a = 101.325$ kPa and $T = 15^\circ\text{C}$. In the United States, $T = 15.5^\circ\text{C}$ (60°F) and pressures differ in the various industries.

$$Q_{\text{std}} = \frac{Q \times P_a \times T_b}{Z_i \times P_b \times T_i} \quad (6-325)$$

where Q_{std} = rate of flow in MMscf/d or scm/d

Q = rate of flow in MMcf/d or m^3/d

P_a = reference base pressure in psia or kPa

P_b = pressure base or standard pressure in psia or kPa

T_b = temperature base or standard in $^\circ\text{R}$ (K)

T_i = suction temperature in $^\circ\text{R}$ (K)

Z_i = compressibility factor at inlet conditions

For power P many methods are available to determine the power required to compress a given volume rate of gas between two pressure levels. The theoretical adiabatic power requirement, taking volumetric efficiency into account, can be calculated as follows:

$$P_{\text{ad}} = 4.3636 \times 10^{-5} \times P_i \times PD \times k/k-1 [r^{(k-1)/k} - 1]E_v \quad (6-326a)$$

where P is in hp or, in the SI System,

$$P_{\text{ad}} = 1.6672 \times 10^{-4} \times P_i \times PD \times k/k-1 [r^{(k-1)/k} - 1]E_v \quad (6-326b)$$

where P is in kW

If compressor capacity is given in mass flowrate, then for Case I

$$v_1 = v_i \rightarrow z_1 = z_i = 1$$

852 Production

$$P_{ad} = 0.2618 P_s V_s k / k - 1 [r^{(k-1)k} - 1] \quad (6-327a)$$

where P_{ad} power is in hp
 P_s suction pressure is in psia
 V_s flow rate at suction is in scf/s

and in the SI System

$$P_{ad} = P_s V_s k / k - 1 [r^{(k-1)/k} - 1] \quad (6-327b)$$

where P_{ad} (kW) = power in kW
 P_s (kPa) = suction pressure in kPa
 V_s = (scm/s) = flow rate at suction (scm/s)
 $V_s = V_s m(k_g/s \times m^3/k_g) \rightarrow (m^3/s)$

For Case II

$$V_1 \neq V_2 \rightarrow z_1 \neq z_2$$

$$P_{ad} = \text{const } V_s (P/T)_{sc} T_s Z_{avg} (k/k-1) (r^{(k-1)/k} - 1) \quad (6-328)$$

where const = 0.2618 for the English System
 = 1.0 for the SI System
 V_s = is in scf/s or scm/s
 P, T_s = standard conditions in psia, °R or kPa, K
 T_s = suction temperature in °R or K
 $Z_{avg} = (Z_1 + Z_2) / 2$
 $T_D = T_s [(P_d/P_s)^{k-1/k}]$

The actual brake horsepower (ABHP), or the power to the shaft, is calculated as

$$ABHP = \frac{P_{ad}}{\eta_{ad} \eta_m} = \frac{P_{ad}}{\eta_t} \quad (6-329)$$

The adiabatic efficiencies for commercial machines are as follows [147]:

- 0.83 to 0.94 for a cylinder of a reciprocating compressor
- 0.60 to 0.65 for Roots blowers
- 0.80 to 0.85 for screw-type rotary compressor

Compression ratio $r = P_d/P_s$ when this value is higher than 3.5; a multiple-stage machine may have to be used. There are several reasons for considering multistage compression systems:

- to avoid high temperatures [350–380°F (180–200°C)]
- to optimize the mechanical design of the compressor
- to minimize compression power

The total power is a minimum when a ratio in each stage is the same.

$$r_{opt} = (r_t)^{1/s} = (P_d/P_s)^{1/s}$$

where S = number of stages required

r_{opt} = optimum compression ratio per stage

If intercoolers are provided between the stages, reduce the theoretical intake pressure of each stage by about 3%, so

$$r_{opt} = (r_i/0.97)^{1/s} \quad (6-330)$$

Example 23

A compressor station is to handle 54 MMscfd of 0.65 relative density gas. Suction temperature will be 70°F and suction pressure 190 psia. Discharge pressure will be 1,500 psia. Calculate the brake horsepower required for two-stage compression with intercooling at 70°F. Other data observed: $\eta_{ad} = 0.85$, $\eta_m = 0.97$, $T_{sc} = 60^\circ\text{F}$, $P_{sc} = 14.5$ psia.

$$\text{Flowrate } V = 54 \times 10^6 \text{ scf/day} = 625 \text{ scf/s}$$

$$SG_g = 0.65$$

$$T_s = 70^\circ\text{F} = 530^\circ\text{R}$$

$$P_s = 190 \text{ psia} \quad P_d = 1,500 \text{ psia}$$

1. Single-stage compression, from Equation 6-328, is calculated by

$$P_{ad} = 0.2618V(P/T)_{sc} T_s Z_{avg} k/k-1 [(P_d/P_s)^{k-1/k} - 1]$$

$$Z_{avg} = (Z_s + Z_d)/2$$

$$M = 28.96 \times 0.65 = 18.8$$

For the given molecular mass, from Figure 6-231,

$$P_{pc} = 674 \text{ psia}, T_{pc} = 324^\circ\text{R}$$

$$P_r = 190/674 = 0.282, T_r = 530/324 = 1.64, Z_s = 0.97$$

$$T_d = 530(1500/190)^{(k-1)/k} \quad k = 1.26 \text{ (from Figure 6-237) if } T = 530^\circ\text{R}$$

$$T_d = 811.8^\circ\text{R}$$

$$P_r = 1500/674 = 2.23, T_r = 811.8/324 = 2.51, Z_d = 0.99$$

$$Z_{avg} = \frac{0.97 + 0.99}{2} = 0.98$$

$$T_{avg} = \frac{70 + 352}{2} = 211^\circ\text{F}$$

$k = 1.23$ (from Figure 6-237)

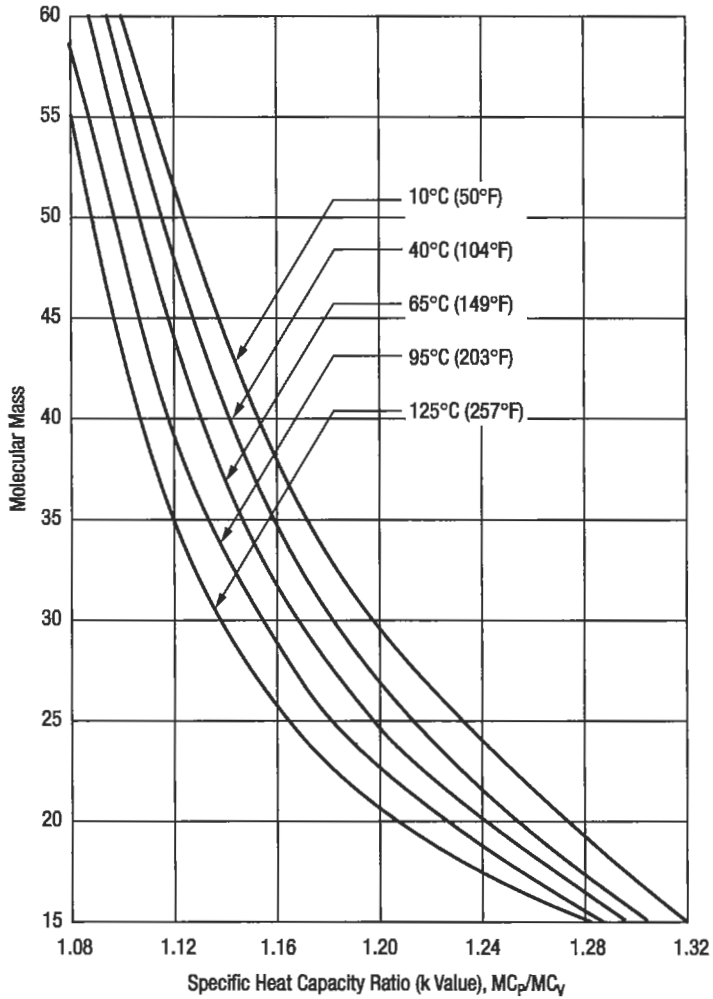


Figure 6-237. Approximate specific heat capacity ratios of hydrocarbon gases.

$$P_{ad} = 0.2618 \times 625 \left(\frac{14.5}{520} \right) 530(0.98) \frac{1.23}{1.23 - 1} \left[\left(\frac{1,500}{190} \right)^{0.23/1.23} - 1 \right] = 5,977$$

$$ABHP = \frac{5,977}{\eta_{ad}\eta_m} = \frac{5,977}{(0.85)(0.97)} = 7,249$$

2. Two-stage compression is calculated by

$$r_t = \frac{1,500}{190} = 7.89 \text{ total compression ratio}$$

$$r_{\text{opt}} = (7.89/0.97)^{0.5} = 2.85 \text{ compression ratio per stage with intercoolers}$$

The calculation for the first stage:

$$P_{d1} = rP_{s1} = 2.85 \times 190 = 541.9$$

For

$$T_s = 70^\circ\text{F} \quad k = 1.26$$

$$T_d = 530 \left(\frac{541.9}{190} \right)^{0.29/1.26} = 658^\circ\text{R} = 198^\circ\text{F}$$

For

$$T_m = \frac{70 + 198}{2} = 134^\circ\text{F} (294^\circ\text{R}) \quad k \cong 1.26$$

$$Z_s = 0.97 \text{ (from Figure 6-231)}$$

$$P_{ad} = 0.2618 \times 6.25 \left(\frac{14.5}{520} \right) 530 (0.97) \frac{1.26}{0.26} \left[\left(\frac{541.9}{190} \right)^{1.26-1} - 1 \right]$$

$$= 2,744.4 \text{ hp}$$

$$\text{ABHP} = \frac{P_{ad}}{\eta_{ad}\eta_m} = \frac{2,744.4}{(0.85)(0.97)} = 3,328.6 \text{ hp}$$

The calculation for the second stage:

Because of intercooling

$$T_s = 70^\circ\text{F} = 530^\circ\text{R} \quad P_s = 541.9 \quad k = 1.24$$

$$T_d = T_s \left(\frac{1,500}{541.9} \right)^{(1.24-1)/1.24} = 85.2^\circ\text{F}$$

$$T_{\text{avg}} = \frac{85.2 + 70}{2} = 77.6 \quad k = 1.27$$

$$P_r = \frac{(1,500 + 541.9)/2}{674} = 1.515 \quad T_r = \frac{77.6 + 460}{324} = 1.66$$

$$Z_{\text{avg}} = 0.9$$

$$H_{ad} = 0.2618 \times 625 \left(\frac{14.5}{520} \right) 530 (0.9) \frac{1.27}{1.27-1} \left[\left(\frac{1,500}{541.9} \right)^{0.27/1.27} - 1 \right] = 2,473.9 \text{ hp}$$

$$\text{ABHP} = \frac{2,473.9}{0.85 \times 0.97} = 3,000.54$$

$$\text{Total ABHP} = 3,000.54 + 3,328.6 = 6,329.1 \text{ hp}$$

Example 24

A branch pipeline is to move 40.0 MMscf/d of 0.69 relative density gas from a junction on the main line to a city, a distance of 100 mi. The line will be a 10-in. line (internal diameter 9.562 in.). The gas will enter the branch line at a pressure of 750 psia and is to be delivered to the city gate at a pressure of 80 psia. The flowing temperature will be 50°F. Pressure on the pipeline is not to exceed 1,000 psia. One compressor station will be needed. If the compressor station should be located at the midpoint of the branch line, what would the required brake horsepower be? Where should the compressor station be located for the minimum horsepower requirements? Assume that $Z = 1.0$, $k = 1.30$, $E = 1.0$, $\eta_{ad} = 0.85$, $\eta_m = 0.97$, $T_{ic} = 60^\circ\text{F}$, $P_{sc} = 14.696$ psia.

1. Solve the Weymouth equation if the compressor is in the midpoint:

$$P_i = ?$$

$$40 \times 10^6 = 433.5 \left(\frac{519.67}{14.696} \right) \left[\frac{(9.562)^{14/3} (750^2 - P_i^2)}{0.69100(509.67)(1)} \right]^{0.5} \times 1.0$$

$$(1,188.16)^2 = 750^2 - P_i^2$$

It is impossible.

2. At what point downstream reaches 80 psia?

$$40 \times 10^6 = 433.5 \left(\frac{519.67}{14.696} \right) \left[\frac{(9.562)^{14/3} (750^2 - 80^2)}{0.69(509.67)(X) \times 1} \right]^{0.5}$$

$$X = 39.4 \text{ mi}$$

3. What is the minimum discharge pressure for compressors?

$$40 \times 10^6 = 433.5 \left(\frac{519.67}{14.696} \right) \left[\frac{(9.562)^{14/3} (P_d^2 - 80^2)}{0.69(509.67)(100 - 39.4)} \right]^{0.5} \quad (1)$$

$$P_d = 928.3 \text{ psia}$$

$$\text{ABHP} = \frac{0.2618(1.3)463 \times 14,696 \times 509.67}{(0.3)(0.85)(0.97)(519.67)} \left[\left(\frac{928.3}{80} \right)^{0.3713} - 1 \right]$$

$$= 6,984.6 \text{ hp}$$

To minimize ABHP it is necessary to use stage-2 compressors because $r = 11.6$ and maximum r should not be higher than 6.

Alternative Solution

The equation for the upstream section is

$$40 \times 10^6 = \frac{433.5(519.67)}{14.696} \left[\frac{(9.562)^{1.93}(750^2 - P_s^2)}{(0.69)(509.67)(1)X} \right]^{0.5} \quad (1.0)$$

$$6,800,709X = 482.14(750^2 - P_s^2)$$

$$14,105.3X = 750^2 - P_s^2$$

The equations for the downstream section are

$$40 \times 10^6 = 14,338.5 \left[482.14 \frac{P_d^2 - 80^2}{100 - X} \right]^{0.5} \quad (1.0)$$

$$14,105.3(100 - X) = P_d^2 - 80^2$$

$$P_d^2 = 1,416,930 - 14,105.3X$$

Solving these two equations gives

$$14,105.3X = 1,416,930 - P_d^2$$

$$= 750^2 - P_s^2$$

$$\text{If } P_s = 80, P_d = 927.8$$

$$\text{If } P_d = 1,000, P_s = 381$$

$$\begin{aligned} \text{ABHP} &= \frac{0.2619(1.3)(463)(14,696)(509.67)}{(0.3)(0.85)(0.97)(519.67)} \left[\left(\frac{1,000}{381} \right)^{0.971.3} - 1 \right] \\ &= 2,790 \end{aligned}$$

The minimum hp requirement for suction pressure to compressor will be 381 psia. It corresponds to X equal to

$$14,105.3X = 750^2 - 381^2 = 417,339$$

$$X = 29.58 \text{ mi}$$

Using Mollier Charts for Compressor Calculations

Mollier charts are forms in which gas properties such as pressure, specific volume, temperature, entropy and enthalpy are presented. Gases are generally plotted as pressure against enthalpy or enthalpy-entropy. The enthalpy-entropy plot is a good technique for solving compression problems (isentropic compression). The key assumptions in this approach are that the process is adiabatic,

$Q = 0$, reversible, $S = \text{const}$, and lost work due to friction and kinetic energy changes are neglected.

$$W = \Delta H = n(h_2 - h_1) \quad (6-331)$$

where W = work done by the compressor on the gas in Btu or kJ

ΔH = change in enthalpy of the gas in Btu or kJ

n = number of moles of gas being compressed in lb mole or kmol

h_1, h_2 = enthalpies of the gas at the compressor inlet and discharge, respectively, in Btu/lb mole or kJ/kmol

Necessary data include inlet gas rate, pressure, temperature and composition, plus outlet pressure. The corresponding outlet temperature is found from these data by assuming $S_2 = S_1$, using an iterative process.

Figure 6-238 shows a qualitative sketch of an enthalpy-entropy chart, illustrating two-stage compression with intercoolers and aftercoolers. Point 1 is the initial state of the gas as it enters the compressor. Path 1-2 shows the first stage of compression. The gas is then cooled in the intercoolers at constant pressure 2-3; the difference in enthalpy along this path is equal to the heat removed in the intercoolers. Path 3-4 shows the second stage of compression. Path 4-5 shows cooling at constant pressure in aftercoolers. The temperatures at points 2 and 4 are the temperatures of the gas at the end of the first and second stages of compression. The temperatures at points 3 and 5 are the temperatures to which the gas is cooled in the intercoolers and aftercoolers. The ideal compression power (or rate of work) required is given by

$$P = \frac{W}{t} = \frac{n(h_2 - h_1)}{t} \quad (6-332)$$

where P = compression power required in Btu/day or kJ/day
 t = time for compression in days

Power requirement = Btu/day \rightarrow HP

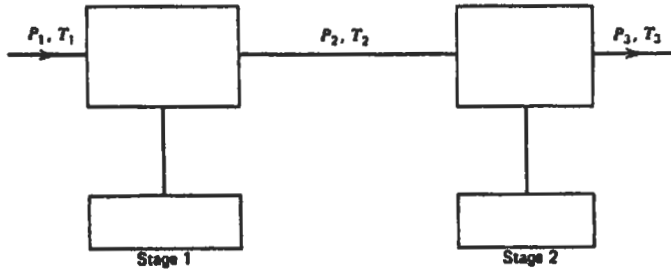
$$\begin{aligned} \text{HP} &= \frac{1 \text{ hp}}{33,000 \text{ ft lb}_t/\text{min}} \frac{778.2 \text{ ft lb}_t/\text{min}}{\text{Btu/min}} \frac{n(h_2 - h_1)/t \text{ Btu/day}}{1,440 \text{ min/day}} \\ &= 1.6376 \times 10^{-5} \frac{n(h_2 - h_1)}{t} \end{aligned}$$

Example 25

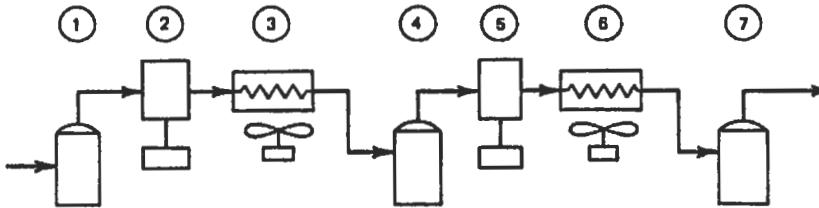
A reciprocating compression system is to be designed to compress 10 MMscfd from 100 psia and 80°F to 2,200 psia of the gas as follows: $C_1 = 0.9233$, $C_2 = 0.0488$, $C_3 = 0.0185$, $i\text{-}C_4 = 0.0039$, $n\text{-}C_4 = 0.0055$. The gas is cooled with intercoolers and aftercoolers to 120°F.

Find:

- molecular mass of gas and compression ratio
- brake hp using the analytical method
- brake hp using Mollier diagram method

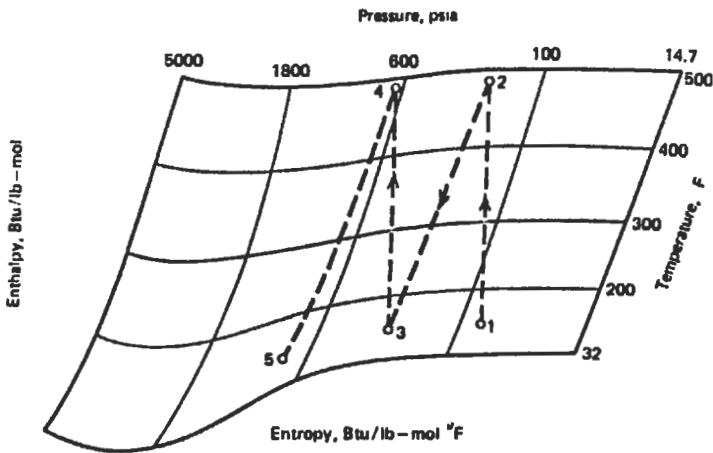


a) Arrangement



- ① ④ ⑦ Knockout drums (to remove condensed liquids)
- ② ⑤ Compressors (first and second stages)
- ③ Interstage cooler / intercooler (air-type)
- ⑥ Aftercooler (air-type)

b) Arrangement with intercoolers and after coolers



c) Enthalpy-Entropy diagram

Figure 6-238. Two-stage compression.

- d. estimate the cooling requirements from the results of part (c)
 e. From the results of part (c), determine whether the first stage can be handled by a compressor with a speed of 1,200 rpm, piston diameter of 12 in. and stroke length of 3 ft. Assume that $\eta_c = 0.82$, $CL = 0.08$, $Z_s = Z_d = 1.0$

(A) For given composition calculate molecular mass

$$M = \sum Y_i M_i = 17.64 \text{ lb}_m/\text{lb mole}$$

$$SG_g = \frac{17.64}{28.97} \cong 0.61$$

$$T_{pc} = 363^\circ\text{R} \quad P_{pc} = 668$$

Using $P_s = 100$ psia, $T_s = 80^\circ\text{F}$, we find T_r and P_r and use charts

$$Z_s = 0.985, k = 1.28 \text{ at } T = 80^\circ\text{F} \text{ (from Figure 6-36)}$$

Compression ratio is calculated from

$$r = \frac{P_d}{P_s} = \frac{2,200}{100} = 22$$

Assuming two-stage compression

$$r_{opt} = (22)^{0.5} = 4.69$$

if intercooling is not provided or

$$r_{opt} = (22/0.97)^{0.5} = 4.76$$

if intercooling is provided.

(B) Brake horsepower using the analytical method, two-stage compression with intercooling, is calculated:

$$P_{ad} = 0.2618Q \left(\frac{P}{T} \right)_c T_s Z_{avg} \left(\frac{k}{k-1} \right) (r^{(k-1)/k} - 1)$$

$$Q = 10 \text{ MMscfd} = 115.7 \text{ scf/s}$$

$$P = 14.7 \quad T = 520$$

$$T_d = T_s \left(\frac{P_d}{P_s} \right)^{(k-1)/k} = 540 \left(\frac{476}{100} \right)^{0.28/1.28} = 760$$

$$T_{avg} = \frac{540 + 760}{2} = 650^\circ\text{R} = 190^\circ\text{F}$$

for $T_{avg} = 190^\circ\text{F}$ $k = 1.26$

$$P_{ad} = 0.2618(115.7) \left(\frac{147}{520} \right) 540(1) \left(\frac{1.26}{1.26-1} \right) (4.76^{0.26/1.26} - 1)$$

$$= 851.1 \text{ hp}$$

Stage II

$$T_D = 580 \left(\frac{2,200}{476} \right)^{0.26/1.26} = 795^\circ\text{R}$$

$$T_{avg} = \frac{580 + 795}{2} = 688^\circ\text{R} = 228^\circ\text{F}$$

$k = 1.25$ for $T_{avg} = 228^\circ\text{F}$

$$P_{ad} = 0.2618(115.7) \left(\frac{14.7}{520} \right) (580)(1) \left(\frac{1.25}{0.25} \right) (4.62^{0.26/1.25} - 1)$$

$$= 922.4 \text{ hp}$$

$$\text{ABHP} = \frac{851.1 + 922.4}{\eta_c} = \frac{1,773.5}{0.82} = 2,163 \text{ hp}$$

(C) Brake horsepower using the Mollier diagram (use any H-S chart for natural gas with $\gamma_g = 0.61$) is calculated.

At the first stage:

$$P_1 = 100 \text{ psia at } 80^\circ\text{F and } P_2 = 476 \text{ psia}$$

$$\text{when } \Delta h_{1-2} = h_2 - h_1 = 2,200 - 400 = 1,800 \text{ Btu/lb mol}$$

Cooling in intercoolers at constant pressure of 476 psia to $T = 580^\circ\text{R}$ (120°F) is calculated as

$$\Delta h_{2-3} = h_3 - h_2 = 600 - 2,200 = -1,600 \text{ Btu/lb mol}$$

At the second stage:

$$P_3 = 2,200/4.76 = 462 \text{ at } 120^\circ\text{F} \quad P_D = 2,200 \text{ psia}$$

$$\Delta h_{3-4} = h_4 - h_3 = 2,900 - 600 = 2,300 \text{ Btu/lb mol.}$$

Cooling in aftercooler at constant pressure of 2,200 psia is

$$\Delta h_{5-4} = h_5 - h_4 = -200 - 2,900 = -3,100 \text{ Btu/lbmol}$$

Gas flow in number of moles is

$$\frac{h}{t} = \frac{10 \times 10^6 \text{ scf}}{\text{day}} \frac{\text{lb mol}}{379.3 \text{ scf}} = 26,364 \frac{\text{lb mol}}{\text{day}}$$

$$\text{HP} = 1.6376 \times 10^{-5} \left(26,364 \frac{\text{lb mol}}{\text{day}} \right) \left(1,800 \frac{\text{Btu}}{\text{lb mol}} + 2,300 \frac{\text{Btu}}{\text{lb mol}} \right) = 1,770$$

$$\text{ABHP} = \frac{1,700}{0.82} = 2,159$$

(D) The cooling requirements are the following:
Heat load on intercooler is

$$\begin{aligned} \Delta h_{2-3}(n) &= \left(-1,600 \frac{\text{Btu}}{\text{lb mol}} \right) \left(26,364 \frac{\text{lb mol}}{\text{day}} \right) \\ &= -4.218 \times 10^7 \text{ Btu/day} = -691 \text{ hp} \end{aligned}$$

Heat load aftercooler is

$$\begin{aligned} \Delta h_{4-5}(n) &= \left(-3,100 \frac{\text{Btu}}{\text{lb mol}} \right) \left(26,364 \frac{\text{lb mol}}{\text{day}} \right) \\ &= -8.173 \times 10^7 \text{ Btu/day} = -1,338 \text{ hp} \end{aligned}$$

Total cooling requirements are

$$-691 - 1,338 = -2,029 \text{ hp}$$

(E) From the results of part (D), determine whether the first stage can be handled by a compressor with a speed of 1,200 rpm from Equation 6-322:

$$E_r = 100 - L - C1 \left[\frac{Z_s}{Z_d} \left(\frac{P_d}{P_s} \right)^{1/k} - 1 \right]$$

$$L = \frac{P_d}{P_s} = 4.76$$

$$E_r = 100 - 4.76 - 8 \left[\left(\frac{476}{100} \right)^{1/1.26} - 1 \right] = 75.6\%$$

From Equation 6-327a

$$\text{HP} = 4.3636 \times 10^{-5} \times 100 \times \text{PD} \times \frac{1.26}{0.26} (4.76^{0.26/1.26} - 1) 76\% = 1,726.2$$

$$\text{PD} = \frac{A_H \times L \times N}{1,728} = \frac{\pi r^2 \times 36 \times 1,200}{1,728} = 2,827.4 \text{ ft}^3/\text{min}$$

Answer

Yes, it can easily handle the necessary rate. The first-stage theoretical power needed is 851.1 hp using the analytical method; it is 777.1 hp using Mollier charts.

Centrifugal Compressors

Centrifugal compressors have become very popular because they offer more power per unit weight and are essentially vibration free. This makes them particularly attractive for offshore locations or where air transportation to remote locations is necessary. The performance of a centrifugal compressor usually is measured and described in terms of head, volume flow, efficiency and power.

Head is a measure of the energy input per unit mass into the gas stream by the compressor. It is produced by the velocity changes in the gas flow resulting from the action of the impeller. Since the compressor geometry remains constant (as contrasted with a reciprocating or positive-displacement compressor), a variation of flow will cause changes in velocity. This, in turn, causes a varying head. A compressor operating on a given gas at a fixed speed will produce a head versus volume flow relationship that essentially remains constant; that is, for each value of flow there is a corresponding value of head. Since head is produced by velocity changes that are dependent upon volume rather than gas properties or conditions, the characteristic head versus volume curve is independent of the gas involved. Although the head versus volume characteristic can be considered constant, the pressure ratio and volume changes vary greatly from one gas to another. Theoretical head may be calculated as follows:

$$H_{ad} = Z_s RT_s \frac{k}{k-1} \left[\left(\frac{P_d}{P_s} \right)^{(k-1)/k} - 1 \right]$$

where H_{ad} = adiabatic head is in desired units, ft \times lb/lb or J/kg
 Z_s = compressibility factor at compressor suction conditions
 k = mean ratio of specific heat capacities, c_p/c_v , where $k = (k_s + k_d)/2$
 R = specific gas constant for a particular gas:
 1545.3/M [ft \times lb/lb $^\circ$ R] or 8.314/M [J/(kg \times K)]
 M = molecular mass of gas in lb/(lb mol) or kg/kmol

In the above equation, the value of the polytropic exponent n may be substituted for k . This will yield a polytropic head, which more closely will represent the actual process. The polytropic exponent must be developed experimentally. It

can be seen from the above equation that the head is dependent upon the ratio of specific heat capacities, molar mass of the gas, inlet temperature, and compression ratio. Conversely, the molar mass of the gas, inlet temperature, compressibility factor and k-value determine the pressure ratio resulting from the head developed by a stage of compression.

Volume Flowrate. Variations in volume flowrate affect the head developed by an impeller. The specific shape of the head-flow curve is a function of the stage geometry, that is, the inlet guide vane angle, impeller blade angle, and outlet diffuser construction. When describing centrifugal compressor performance it is necessary to convert the mass flow in lb/h (kg/h), or volume flow in MMscf/d (scm/d), to actual volumetric rate at the inlet conditions. This is the volume of gas that actually is entering the eye of the impeller.

To convert the volumetric flowrate from reference conditions to suction conditions, the following is used:

$$Q_{act} = 694 Q_{std} \frac{P_b}{P_s} \frac{T_s}{T_b} \quad (\text{ft}^3/\text{min}) \quad (6-333a)$$

or

$$Q_{act} = 1.1574 \times 10^{-5} Q_{std} Z_s \frac{P_b}{P_s} \frac{T_s}{T_b} \quad (\text{m}^3/\text{s}) \quad (6-333b)$$

where Q_{act} = actual inlet volumetric flowrate in desired units: ft³/min or m³/s at T_s, P_s
 Q_{std} = volumetric flowrate at base conditions in MMscf/d or scm/d at T_b, P_b

When the original data are reported as mass flow per hour, the actual volumetric flowrate can be determined by multiplying the mass flowrate by the specific volume value [ft³/lb (m³/kg)] and dividing it by the appropriate factor to account for differences in time base [60 min/hr (3,600 s/hr)].

Power. The theoretical equation for gas hp or kW for centrifugal compressor is

$$P_{ad} = 8.179 \times 10^{-5} H_{ad} Q_{act} \gamma_g \frac{P_s}{A_s T_s} \quad (6-334a)$$

and in the SI unit system

$$P_{ad} = H_{ad} Q_{act} S G_g \frac{P_s}{287 Z_s T_s} \quad (6-334b)$$

where P_{ad} = input power to the gas stream in desired units, hp or kw
 $S G_g$ = gas relative density

To account for the aerodynamic losses, it is necessary to replace H_{ad} with H'/η' , where H'/η' is the adiabatic or polytropic head divided by the corresponding adiabatic or polytropic efficiency.

In addition to the aerodynamic losses, there are mechanical losses due to seal and bearing friction. For service design purposes, the mechanical losses for centrifugal and rotary compressors over 1,000 hp (746 kW) can be assumed to be 35 hp (26 kW) for bearings and 35 hp (26 kW) for oil-type shaft seals; below that size, losses will amount to 1 to 3%. In any case, these losses are included in the mechanical efficiency factor. Therefore, the required shaft power is

$$P_{\text{shaft}} = P/\eta_m \quad (6-335)$$

where P_{shaft} = compressor shaft input power in desired units, hp or kw
 η_m = mechanical efficiency (0.97 to 0.99)

Comparison of Reciprocating and Centrifugal Compressors

The advantages of a centrifugal compressor over a reciprocating machine are:

- lower installed first cost where pressure and volume conditions are favorable
- lower maintenance expense
- greater continuity of service and dependability
- less operating attention
- greater volume capacity per unit of plot area
- adaptability to high-speed low-maintenance-cost drivers

The advantages of a reciprocating compressor over a centrifugal machine are

- greater flexibility in capacity and pressure range
- higher compressor efficiency and lower power cost
- capability of delivering higher pressures
- capability of handling smaller volumes
- less sensitive to changes in gas composition and density

Example 26

Perform centrifugal compressor calculations using the following data: $M = 18.3$, $P_{\text{inlet}} = 156$ psia, $T_{\text{inlet}} = 105^\circ\text{F}$, $Q_{\text{std}} = 12,000$ scfm, $P_{\text{discharge}} = 310$ psia. The base conditions are $P = 14.73$ psia, $T = 60^\circ\text{F}$

- Calculation of the compressibility factor Z_s and k

$$T_s = 105^\circ\text{F} = 565^\circ\text{R}$$

$$M = 18.3 = SG_g = 0.63$$

$$T_{pc} = 370^\circ\text{R}, P_{pc} = 670 \text{ psia (from Figure 6-231)}$$

$$T_r = 565/370 = 1.53, P_r = 156/670 = 0.233$$

$$Z_s = 0.98 \text{ (from Figure 6-231)}$$

$$k_s = 1.27 \text{ at } 565 \text{ (from Figure 6-235)}$$

$$T_d = T_s(P_d/P_s)^{(k-1)/k} = 565(1.99)^{0.27/1.27} = 654^\circ\text{R} = 194^\circ\text{F}$$

$$k_d = 1.25 \text{ at } 194^\circ\text{F}$$

$$k = (k_s + k_d)/2 = 1.26$$
- The actual inlet capacity, using Equation 6-335a, is

$$Q_{\text{act}} = 694 \times 17.28 \times \frac{14.73}{156} \frac{565}{520} = 1,230.3 \text{ acfm}$$

- The theoretical head, using Equation 6-334, is

$$H_{ad} = Z_s R T_s (k/k-1) [r^{(k-1)/k} - 1]$$

$$R = \frac{1,545.3}{M} = \frac{1,545.3}{18.3} = 84.44$$

$$\begin{aligned} H_{ad} &= 0.98 \times 84.44 \times 565 \times \frac{1.26}{1.26 - 1} (1.99^{0.26/1.26} - 1) \\ &= 34,570 \end{aligned}$$

- The theoretical power, using Equation 6-336a, is

$$\begin{aligned} P_{ad} &= 8.179 \times 10^{-5} H_{ad} Q_{act} \gamma \frac{P_s}{Z_s T_s} \\ &= 8.179 \times 10^{-5} \times 34,570 \times 1,230.3 \times 0.63 \frac{156}{0.98 \times 565} = 617 \text{ hp} \end{aligned}$$

- Adiabatic efficiency $\eta_{ad} = 0.7$ (from Table 6-61) mechanical efficiency assuming 0.98.
- The required shaft power is

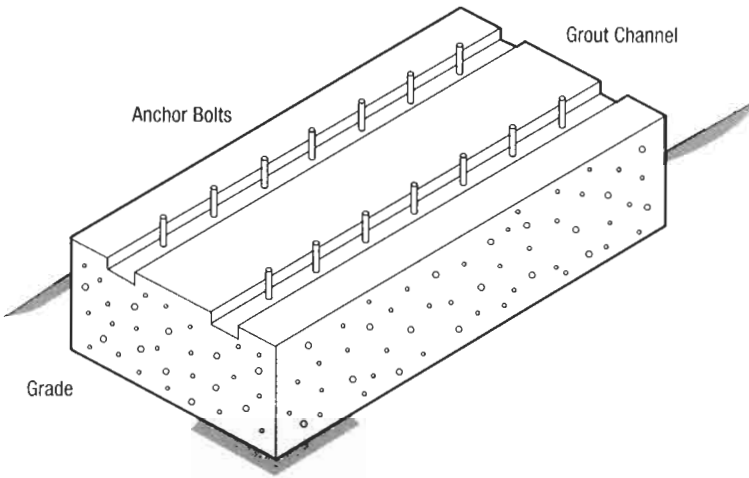
$$P_{shaft} = \frac{P_{ad}}{\eta_{ad} \eta_m} = \frac{617}{0.7 \times 0.98} = 899.4 \text{ hp}$$

Engine and Compressor Foundations [148]

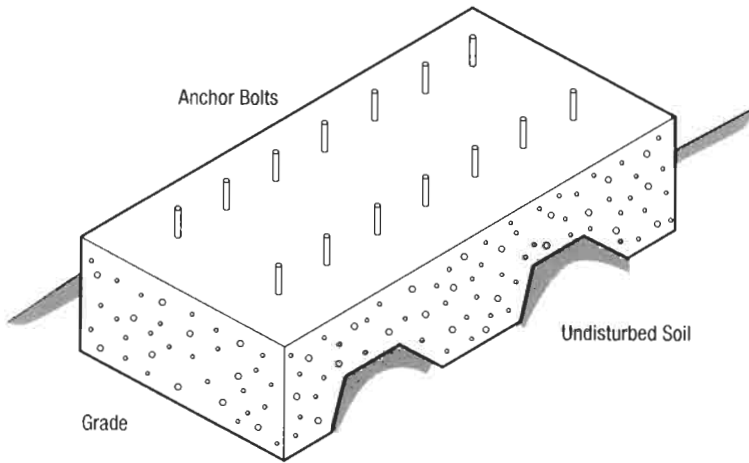
Machinery foundations are one of the most important aspects of compressor station engineering. Such factors as soil analysis, reinforced concrete design, and dynamics of foundation systems require particular attention. There are two basic types of foundations used for compressor units in the gas industry (see Figures 6-239 and 6-240). The first is a simple concrete pad that is used for most small skid-mounted reciprocating units and for high-speed centrifugal compressors. The second incorporates a combination of reinforced block and mat concepts. The block and mat design is common for large, low or medium-speed reciprocating compressors. The block provides the required load distribution so that the allowable soil-bearing capacity is not exceeded. The following minimum data should be available to the foundation designer: total weight of the package, base dimensions of the package, operating speed of the machine, radius of the crankshaft throws, weight of the reciprocating parts, length of connecting rod, distance required to remove engine and compressor pistons and connecting rods and the weight of unbalanced rotating parts.

The base dimensions of the concrete pad or block should be such that there is 6 to 12 in. of concrete beyond all sides of the base of the unit. Manufacturers have recommended from 0.091 to 0.141 yd³ of concrete per engine hp (0.093 to 0.144 m³/kW) for low-speed machines. Manufacturers recommend a foundation weight that is two to five times the weight of the machine.

The combined resonant frequency of the machine, foundation, and soil system is next in importance.



a. Continuous Pad Foundation



b. Waffle Type Pad Foundation

Figure 6-239. Typical concrete pad compressor foundations.

$$f_n = \frac{1}{2\pi} \left(\frac{K \times g}{W_f + W_s} \right) \quad (6-336)$$

where f_n = natural frequency of the foundation and soil system in Hz
 K = spring constant of soil mass in lb/ft or kN/m

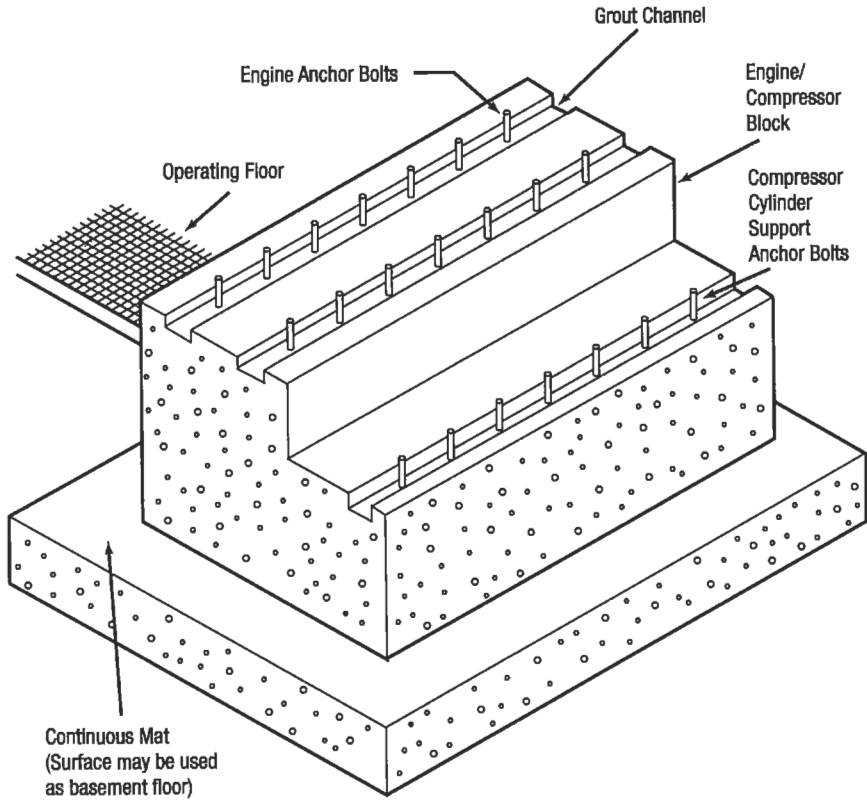


Figure 6-240. Concrete block and mat compression.

W_f = weight of machine and foundation in lb/ft or kN

W_s = weight of soil system in lb or kN

g = acceleration of gravity in 32.174 ft/s or 9.81 m/s²

The spring constant k is a function of Poisson's ratio, shear modulus and the radius of the loading area. In general, the natural frequency of the system should be at least twice the frequency of the applied forces for low-speed units, or less than one-half of the resonant frequency for machines that operate at a frequency greater than the natural frequency of the system. The natural frequency of the foundation system can be decreased by (1) increasing the weight of the foundation, (2) decreasing the base area of the foundation, (3) reducing the shear modulus of the soil, (4) placing the foundation deeper into the soil.

The Gas Piping System

The gas piping system in a compressor station includes the valving, pulsation control equipment, overpressure protection devices, cathodic protection facilities and structural supports to route the gas through the compressor and gas conditioning facilities. Figure 6-241 shows a schematic diagram of such system at a small compressor station. Figure 6-242 gives a general flow diagram for a

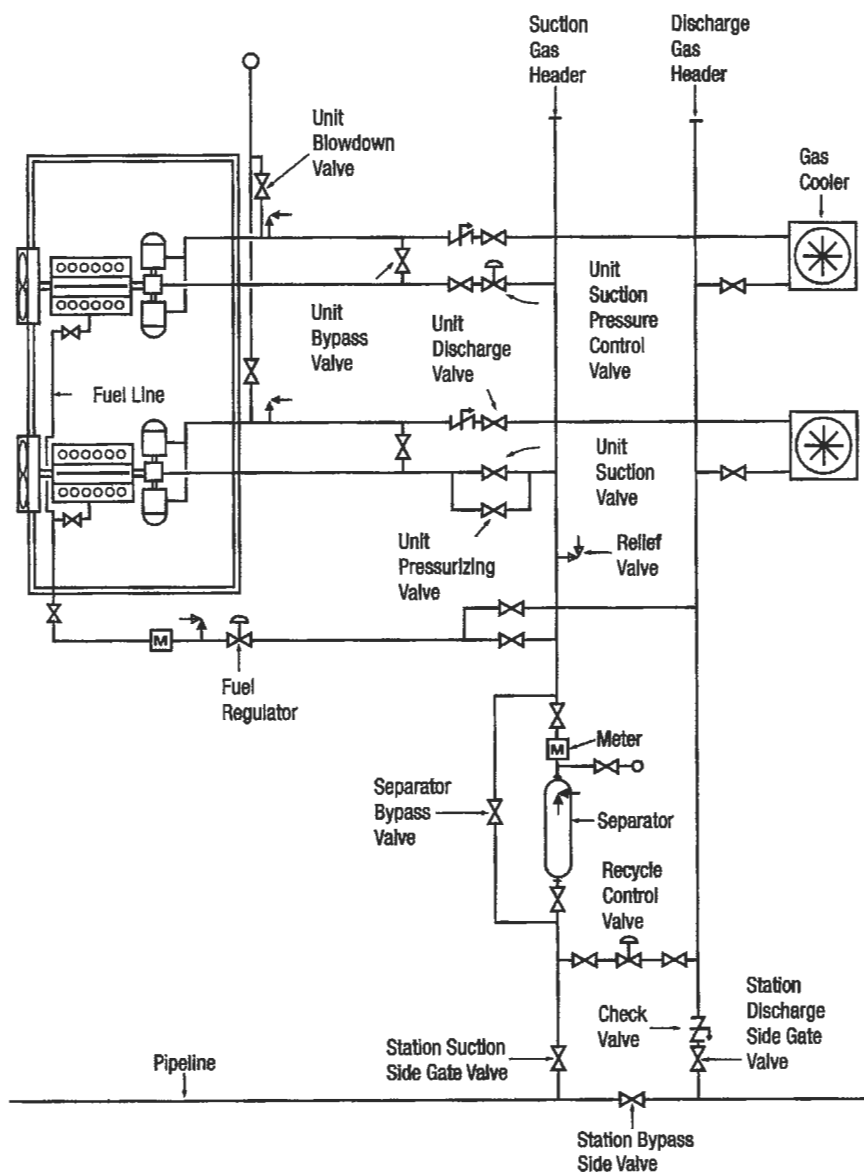


Figure 6-241. Foundation typical reciprocating compressor station piping.

storage/withdrawal compressor operation. In designing the piping system the following items must be taken into consideration: operating pressure and capacity, pressure drop, gas velocity, mechanical strength and composition of pipe materials, temperatures, effects of corrosion, safety, efficiency of operations, and economy of installation.

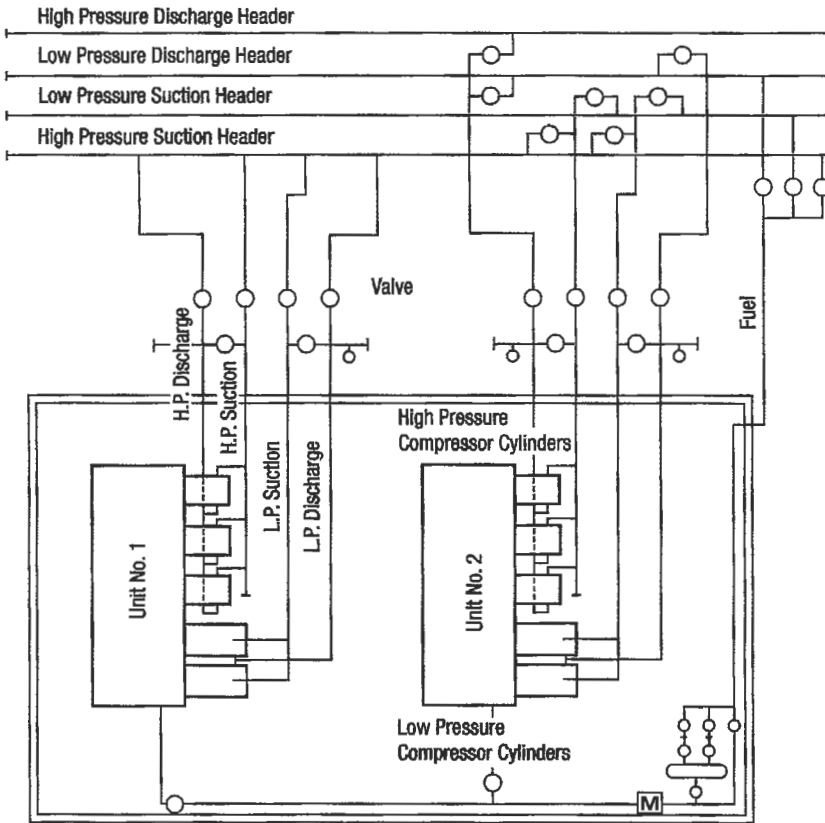


Figure 6-242. Compressor unit gas flow diagram for storage injection and withdrawal service.

Table 6-63
Centrifugal Compressor Flow Range

Nominal flow range (inlet acfm)	Average polytropic efficiency	Average adiabatic (isentropic) efficiency	Speed to develop 10,000 ft head/wheel
100– 500	0.63	0.60	20,500
500– 7,500	0.74	0.70	10,500
7,500– 20,000	0.77	0.73	8,200
20,000– 33,000	0.77	0.73	6,500
33,000– 55,000	0.77	0.73	4,900
55,000– 80,000	0.77	0.73	4,300
80,000–115,000	0.77	0.73	3,600
115,000–145,000	0.77	0.73	2,800
145,000–200,000	0.77	0.73	2,500

Pressure drops in compressor station piping result from energy losses caused by friction between the gas and pipe wall should not exceed 1 to 2% of the total station power requirements.

Gas velocity can be determined as follows:

$$V = \frac{127.3 \times 10^3 Q P_b T_r Z}{D^2 P_m T_b} \quad (6-337a)$$

or in the SI System

$$V = \frac{14.73 Q P_b T_r Z}{D^2 P_f T_b} \quad (6-337b)$$

where V = velocity in desired units in ft/min or m/s

Q = volume rate of flow in MMcf/d or m³/d

P_b = base pressure in lb/in.² or kPa absolute

T_f = flowing temperature in °R or K

Z = compressibility

D = diameter of pipe in in. or mm

P_f = flowing pressure in lb/in.² or kPa absolute

T_b = base temperature in °R or K

Gas piping used in compressor stations now be manufactured in compliance with the standards (DOT) Code, Title 49, Part 192 (see Table 6-64).

Gas Cooling

Gas cooling equipment is necessary in compressor stations to remove heat from the gas stream between stages of compression intercoolers or after the final stage of compression (aftercoolers). Heat exchangers are used to remove heat from gas streams, reduce cooling water temperature, lower oil temperature or to cool compressed air. Several types of gas coolers are available, but the aerial cooler is one of the most common. Aerial coolers make use of air to cool hot gas. There are two kinds: forced draft and induced draft (see Figure 6-243).

Advantages of forced draft are:

- Slightly lower horsepower since the fan is in cold air. Horsepower varies directly as the absolute temperature.
- Better accessibility of mechanical compounds for maintenance.
- Easily adaptable for warm air recirculation for cold climates.

Disadvantages are as follows:

- Poor distribution of air over the section.
- Greatly increased possibility of hot air recirculation, due to low discharge velocity from the sections and absence of stack.
- Low natural draft capability on fan failure due to small stack effect.
- Total exposure of tubes to sun, rain and hail.

(text continued on page 884)

Table 6-64
Codes and Standards

Codes and standards governing the design, construction, and maintenance of compressor station facilities are found in publications issued by various regulatory and governing agencies.

It is not the intent of this book to provide a comprehensive explanation of each code that is applicable to compressor station design and operation, but instead provide a listing by agency and professional society of all codes that may apply to compressor stations.

Below is a list of codes and standards established by various federal, state, and other agencies. When a question concerning design or operation arises, the engineer can refer to this listing to determine which codes and standards apply to the point in question.

U.S. Government regulations are printed in the Code of Federal Regulations (CFR) published by the U.S. Government Printing Office. Mail orders should be addressed to: Superintendent of Documents, U.S. Government Printing Office, Washington, DC 20402; phone orders may be placed by calling (202) 783-3238.

**U.S. Department of Transportation (DOT), Materials Transportation Bureau (MTB),
Office of Pipeline Safety Regulation (OPSR), Part 192, Title 49 of the Code of
Federal Regulations**

DOT Code, Part 192, Title 49, Subpart C—Pipe Design

- Section 192.111—Design Factor (F) for Steel Pipe
- Section 192.115—Temperature Derating Factor (T) for Design of Steel Pipe

DOT Code, Part 192, Title 49, Subpart D—Design of Pipeline Components

- Section 192.163—Compressor Station—Design and Construction
 - Location of Compressor Building
 - Building Construction
 - Exits
 - Fenced Areas
 - Electric Facilities
- Section 192.165—Compressor Stations—Liquid Removal
- Section 192.167—Compressor Stations—Emergency Shutdown
- Section 192.169—Compressor Stations—Pressure Limiting Devices
- Section 192.171—Compressor Stations—Additional Safety Equipment
- Section 192.173—Compressor Stations—Ventilation
- Section 192.201—Required Capacity of Pressure Relieving and Limiting Stations

DOT Code, Part 192, Title 49, Subpart J—Test Requirements

- Section 192.505—Strength Test Requirements for Steel Pipeline to Operate at a Hoop Stress of 30 Percent or More of SMYS

DOT Code, Part 192, Title 49, Subpart M—Maintenance

- Section 192.729—Compressor Stations: Procedures for Gas Compressor Units
- Section 192.731—Compressor Stations: Inspection and Testing of Relief Devices
- Section 192.733—Compressor Stations: Isolation of Equipment for Maintenance or Alterations
- Section 192.735—Storage of Combustible Materials

- Section 192.751—Prevention of Accidental Ignition
NOTE: *The above DOT Regulations are also published in the ASME Guide for Gas Transmission and Distribution Piping Systems (see Bibliography).*

U.S. Department of Labor Occupational Safety and Health Administration (OSHA)

See Code of Federal Regulations, 29 CFR Parts 1900–1990.

U.S. Environmental Protection Agency (EPA)

Regulations under the Clean Air Act as amended

- 40 CFR 50—Air Quality Standards
- 40 CFR 60—New Source Standards of Performance for Turbines and Reciprocating Engines
- 40 CFR 51 and 52—Prevention of Significant Deterioration (Best Available Control Technology) in Attainment Areas
- 40 CFR 51—Visibility Protection—The prevention of any future, and remedying of any existing impairment of visibility in Federal Class I areas.
- 40 CFR 51 and 52—Requirements for Offsets and Lowest Achievable Emission Rates for New or Modified Sources in Nonattainment Areas

Regulations under the Clean Water Act of 1977 as amended

- 40 CFR 112—Spill Prevention, Control and Countermeasure Plan for Oil and Hazardous Substances Storage
- 40 CFR 125—National Pollution Discharge Elimination System for Waste Water Discharges to Surface Waters

Regulations under the Resource Conservation and Recovery Act as amended

- 40 CFR 262—Standards for Generators of Hazardous Wastes
- 40 CFR 264 and 265—Standards for Hazardous Waste Treatment, Storage, and Disposal Facilities

LOCAL CODES AND ORDINANCES

Facilities within incorporated areas are regulated by individual city, municipal, county, and state codes administered by various agencies including, but not limited to, the following:

Department of Buildings and Safety (City)

- General Building Requirements and Permits
- Zoning Requirements
- Grading Requirements and Permits

Building and Safety Commission

- Electrical Requirements and Permits
- Heating and Air Conditioning Requirements and Permits
- Plumbing Requirements and Permits
- Boiler and Pressure Vessel Inspections and Permits

**Table 6-64
(continued)**

- Elevator Inspections and Permits

Department of Public Works

- Environmental Impact Reports
- Driveway and Sidewalk Requirements and Permits
- Sewer Requirements and Permits
- Excavation Permits

Department of Water and Power

- Electrical Service
- Water Service

Planning Commission

- Zone Changes

County Building and Safety (Unincorporated Areas)

- General Building Permits
- Grading Permits
- Electrical Permits
- Plumbing Permits
- Compaction Requirements

County Engineer

- Geological Reports
- Sewers

County Regional Planning (Unincorporated Areas)

- Zoning Requirements
- Environmental Impact Studies

County Air Pollution Control District

- Engine Exhaust Emissions
- Tank and Pond Vapors
- Other Discharges Into the Atmosphere

County Flood Control District

- Water Discharges

County Health Department

- Septic Systems
- Water Wells

Public Utilities

- Compressor Station Design and Construction

- Liquid Removal
- Bottle-Type and Pipe-Type Holders
- Material Selection
- Welding
- Instrumentation
- Regulation
- Compressor Station Operation and Maintenance
 - Procedures for Gas Compressor Units
 - Inspection and Testing of Relief Devices
 - Isolation of Equipment for Maintenance and Alteration
 - Inspection and Testing of Pipe-Type and Bottle-Type Holders
 - Storage of Combustible Materials
 - Inspection and Testing of Pressure Limiting and Regulating Stations
 - Prevention of Accidental Ignition

State Air Resources Board

- Engine Exhaust Emissions

State Fish and Game Department

- Oil Spills in Rivers, Streams, and Oceans Along the Coast
- Threats to Rare and Endangered Species of Wildlife

State Water Quality Control Board

- Water Discharges

State Coastal Commission

- Facilities Constructed in the Coastal Zone, in Addition to Regulations Imposed by Cities and Counties

AMERICAN NATIONAL STANDARDS INSTITUTE (ANSI)

1430 Broadway
 New York, NY 10018
 Phone: (212) 354-3300

ANSI B1.1—Unified Inch Screw Threads

ANSI/ASME B1.20.1—Pipe Threads, General Purpose (Inch)

ANSI B16.5—Steel Pipe Flanges and Flanged Fittings, Including Ratings for Class 150, 300, 400, 600, 900, 1500, and 7500

ANSI B16.10—Face-to-Face and End-to-End Dimensions of Ferrous Valves

ANSI B16.11—Forged Steel Fittings, Socket Welding and Threaded

ANSI B16.15—Cast Bronze Threaded Fittings, Class 125 and 250

ANSI B16.20—Ring-Joint Gaskets and Grooves for Steel Pipe Flanges

**Table 6-64
(continued)**

- ANSI B16.21—Nonmetallic Flat Gaskets for Pipe Flanges**
- ANSI B16.22—Wrought Copper and Bronze Solder-Joint Pressure Fittings**
- ANSI B16.25—Butt Welding Ends**
- ANSI B16.34—Steel Valves, Flanged and Butt-Welding**
- ANSI B18.2.1—Square and Hex Bolts and Screws**
- ANSI B18.2.2—Square and Hex Nuts**
- ANSI B18.22.1—Plain Washers**
- ANSI B19.1—Air Compressor (Draft Safety Standards)**
- ANSI B19.3—Compressors for Process Industries (Safety Standards)**
- ANSI B31.1—Power Piping**
- ANSI B31.3—Chemical Plant and Petroleum Refinery Piping**
- ANSI B31.8—Gas Transmission and Distribution Piping Systems**
- ANSI C2—National Electrical Safety Code**
- ANSI/ASME PTC9—Performance Test Code—Displacement Compressors, Vacuum Pumps, and Blowers**
- ANSI/ASME PTC10—Performance Test Code—Compressors and Exhausters**

AMERICAN PETROLEUM INSTITUTE (API)

1200 L Street, N. W.
Washington, D.C. 20005
Phone: (202) 682-8000

- API 7B-11C—Internal Combustion Reciprocating Engines for Oil Field Service**
- API SPEC 11P—Packaged, High Speed, Separable, Engine-Driven, Reciprocating Gas Compressors**
- API RP 550—Installation of Refinery Instruments and Control Systems**
- API 616—Type H Industrial Combustion Gas Turbines for Refinery Services**
- API 617—Centrifugal Compressors for General Refinery Services**

API 618—Reciprocating Compressors for General Refinery Services

API 650—Welded Steel Tanks for Oil Storage

API 2000—Venting Atmospheric and Low Pressure Storage Tanks (Nonrefrigerated and Refrigerated)

AMERICAN SOCIETY FOR TESTING AND MATERIALS (ASTM)

1916 Race Street
Philadelphia, PA 19103
Phone: (215) 299-5400

ASTM A-36—Structural Steel

ASTM A-53—Pipe, Steel, Black, and Hot-Dipped Zinc Coated, Welded and Seamless

ASTM A-106—Seamless Carbon Steel Pipe and High-Temperature Service

ASTM A-134—Pipe Steel Electric-Fusion (Arc)—Welded (size NPS 16 and over), Spec for

ASTM A-135—Electric-Resistance-Welded Steel Pipe

ASTM A-139—Electric-Fusion (Arc)-Welded Steel Pipe (Sizes 4-inch and over)

ASTM A-155—Electric-Fusion-Welded Steel Pipe for High-Pressure Service
Discontinued—See A671, A672, A691

ASTM A-181—Forgings, Carbon Steel for General-Purpose Piping

ASTM A-193—Alloy-Steel and Stainless Steel Bolting Materials for High-Temperature Service

ASTM A-194—Carbon and Alloy Steel Nuts and Bolts for High-Pressure and High-Temperature Service

ASTM A-197—Cupola Malleable Iron

ASTM A-216—Carbon Steel Castings Suitable for Fusion Welding for High-Temperature Service

ASTM A-234—Piping Fittings of Wrought Carbon Steel and Alloy Steel for Moderate and Elevated Temperatures

ASTM A-307—Carbon Steel Externally Threaded Standard Fasteners

ASTM A-325—High-Strength Bolts for Structural Steel Joints

ASTM A-381—Metal Arc-Welded Steel Pipe for Use with High-Pressure Transmission Systems

**Table 6-64
(continued)**

ASTM A-395—Ferritic Ductile Iron Pressure-Retaining Casting for Use at Elevated Temperatures

ASTM A-490—Heat-Treated Steel Structural Bolts, 150 ksi (1035 MPa) Minimum Tensile Strength

ASTM A-539—Electric-Resistance-Welded Coiled Steel Tubing for Gas and Fuel Oil Lines

ASTM A-605—Pressure Vessel Plates, Alloy Steel, Quenched and Tempered Nickel-Cobalt-Molybdenum-Chromium

ASTM A-615—Deformed and Plain Billet—Steel Bars for Concrete Reinforcement

ASTM A-671—Electric Fusion-Welded Steel Pipe for Atmospheric and Lower Temperatures

ASTM A-672—Electric-Fusion-Welded Steel Pipe for High-Pressure Service at Moderate Temperatures

ASTM A-691—Carbon and Alloy Steel Pipe, Electric-Fusion-Welded for High-Pressure Service at High Temperatures

ASTM B-42—Seamless Copper Pipe, Standard Sizes

ASTM B-62—Composition Bronze or Ounce Metal Castings

ASTM B-75—Seamless Copper Tube

ASTM C-31—Making and Curing Concrete Test Specimens in the Field

ASTM C-33—Concrete Aggregates

ASTM C-39—Compressive Strength of Cylindrical Concrete Specimens

ASTM C-76—Reinforced Concrete Culvert, Storm Drain, and Sewer Pipe

ASTM C-94—Ready-Mix Concrete

ASTM C-150—Portland Cement

ASTM D-1751—Preformed Expansion Joint Fillers for Concrete Paving and Structural Construction (Nonextruding and Resilient Bituminous Types)

AMERICAN SOCIETY OF MECHANICAL ENGINEERS (ASME)

345 East 47th Street
New York, NY 10017
Phone: (212) 705-7722

ASME Boiler and Pressure Vessel Code, Section VIII, Division 1—Unfired Pressure Vessels

- UG 126—Pressure Relief Valves
- UG 127—Nonreclosing Pressure Relief Devices
- UG 131—Certification of Capacity of Pressure Relief Valves
- UG 133—Determination of Pressure Relieving Requirements
- UG 135—Installation
- Appendix M-5—Stop Valves between Pressure Relieving Device and Vessel
- Appendix M-6—Stop Valves on the Discharge Side of a Pressure Relieving Device

ASME PTC7.1—Performance Test Code—Displacement Pumps

ASME PTC8.2—Performance Test Code—Centrifugal Pumps

ASME PTC9—Performance Test Code—Displacement Compressors, Vacuum Pumps, and Blowers

ASME PTC10—Performance Test Code—Compressors and Exhausters

INSTITUTE OF ELECTRICAL AND ELECTRONICS ENGINEERS (IEEE)

345 East 47th Street
New York, NY 10017
Phone: (212) 705-7900

IEEE Std. 80-1976—IEEE Guide for Safety in Substation Grounding

INSTRUMENT SOCIETY OF AMERICA (ISA)

67 Alexander Drive
P.O. Box 12277
Research Triangle Park, NC 27709
Phone: (919) 549-8411

S75.01—Control Valve Sizing Equations (Replaces S39.3 Control Valve Sizing Equations for Compressible Fluids)

NATIONAL FIRE PROTECTION ASSOCIATION (NFPA)

Batterymarch Park
Quincy, Massachusetts 02269
Phone: (617) 770-3000

NFPA Code 1—Fire Prevention Code

NFPA Code 3M—Health Care Emergency Preparedness

NFPA Code 9—Training Reports and Records, Recommended Practice

NFPA Code 10—Portable Fire Extinguishers

**Table 6-64
(continued)**

- NFPA Code 10L—Model Enabling Act, Portable Fire Extinguishers**
- NFPA Code 11—Low Expansion Foam and Combined Agent Systems**
- NFPA Code 11A—Medium and High Expansion Foam Systems**
- NFPA Code 12—Carbon Dioxide Extinguishing Systems**
- NFPA Code 12A—Halon 1301 Fire Extinguishing Systems**
- NFPA Code 12B—Halon 1211 Fire Extinguishing Systems**
- NFPA Code 13—Sprinkler Systems, Installation**
- NFPA Code 13A—Inspection, Testing and Maintenance of Sprinkler Systems**
- NFPA Code 13E—Fire Department Operations in Properties Protected by Sprinklers and Standpipe Systems**
- NFPA Code 14—Standpipe and Hose Systems, Installation of**
- NFPA Code 15—Water Spray Fixed Systems for Fire Protection**
- NFPA Code 16—Deluge Foam-Water Sprinkler System**
- NFPA Code 17—Dry Chemical Extinguishing Systems and Foam-Water Spray Systems**
- NFPA Code 18—Wetting Agents**
- NFPA Code 19B—Respiratory Protective Equipment for Fire Fighters**
- NFPA Code 20—Centrifugal Fire Pumps**
- NFPA Code 22—Water Tanks for Private Fire Protection**
- NFPA Code 24—Installation of Private Fire Service Mains and their Appurtenances**
- NFPA Code 30—Flammable and Combustible Liquids Code**
- NFPA Code 31—Oil Burning Equipment**
- NFPA Code 33—Spray Application**
- NFPA Code 34—Dipping and Coating Processes Using Flammable or Combustible Liquids**
- NFPA Code 37—Stationary Combustion Engines and Gas Turbines**

NFPA Code 49—Hazardous Chemicals Data

NFPA Code 51B—Cutting and Welding Processes

NFPA Code 54—National Fuel Gas Code

NFPA Code 58—Liquefied Petroleum Gases, Storage and Handling

NFPA Code 59—Liquefied Petroleum Gases at Utility Gas Plants, Storage and Handling

NFPA Code 59A—Liquefied Natural Gas, Storage and Handling

NFPA Code 68—Explosion Venting, Guide

NFPA Code 69—Explosion Prevention Systems

NFPA Code 70—National Electrical Code (NEC)

- NEC Chapter 1—General
 - Article 100—Definitions
 - Article 110—Requirements for Electrical Installations
- NEC Chapter 2—Wiring Design and Protection
- NEC Chapter 3—Wiring Methods and Materials
- NEC Chapter 4—Equipment for General Use
- NEC Chapter 5—Special Occupancies
- NEC Chapter 6—Special Equipment
- NEC Chapter 7—Special Conditions
- NEC Chapter 8—Communications Systems
- NEC Chapter 9—Tables and Examples

NFPA Code 70B—Electrical Equipment Maintenance

NFPA Code 70L—Model State Law Providing for Inspection of Electrical Installations

NFPA Code 71—Central Station Signaling Systems, Installation, Maintenance, and Use of

NFPA Code 72A—Local Protective Signaling Systems, Installation, Maintenance and Use of

NFPA Code 72B—Auxiliary Protective Signaling Systems for Fire Alarm Service Installation, Maintenance, and Use of

NFPA Code 72C—Remote Station Protective Signaling Systems Installation, Maintenance and Use of

NFPA Code 72D—Proprietary Protective Signaling Systems, Installation, Maintenance and Use of

**Table 6-64
(continued)**

NFPA Code 72E—Automatic Fire Detectors

NFPA Code 77—Static Electricity

NFPA Code 78—Lightning Protection Code

NFPA Code 80—Fire Doors and Windows

NFPA Code 85A—Prevention of Furnace Explosions in Fuel Oil and Natural Gas-Fired Single Burner Boiler-Furnaces

NFPA Code 85B—Prevention of Furnace Explosions in Natural Gas-Fired Multiple Burner Boiler-Furnaces

NFPA Code 214—Water Cooling Towers

NFPA Code 220—Building Construction, Standard Types

NFPA Code 231—General Storage, Indoor

NFPA Code 321—Basic Classification of Flammable and Combustible Liquids

NFPA Code 325M—Properties of Flammable Liquids, Gases, and Volatile Solids

NFPA Code 327—Cleaning or Safeguarding of Small Tanks and Containers Using Flammable and Combustible Materials

NFPA Code 385—Tank Vehicles for Flammable and Combustible Liquids

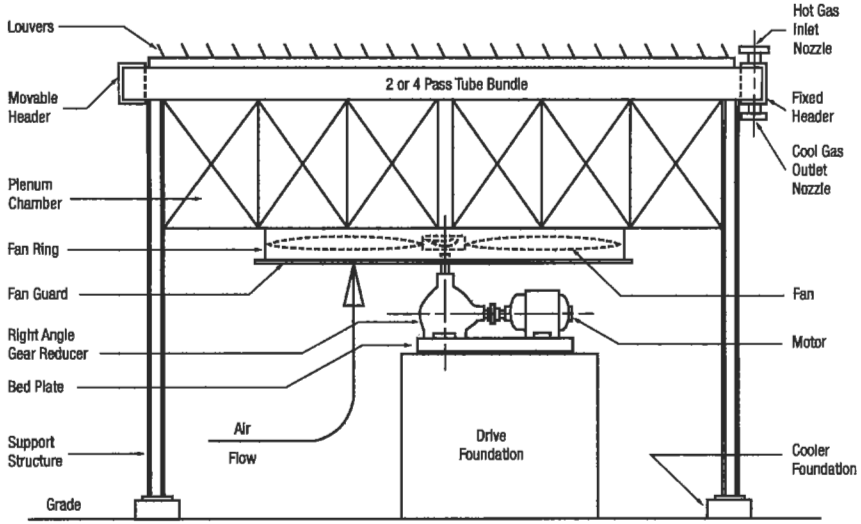
NFPA Code 491M—Hazardous Chemical Reactions

NFPA Code 493—Intrinsically Safe Apparatus and Associated Apparatus for Use in Class I, II, and III, Division 1 Hazardous Locations

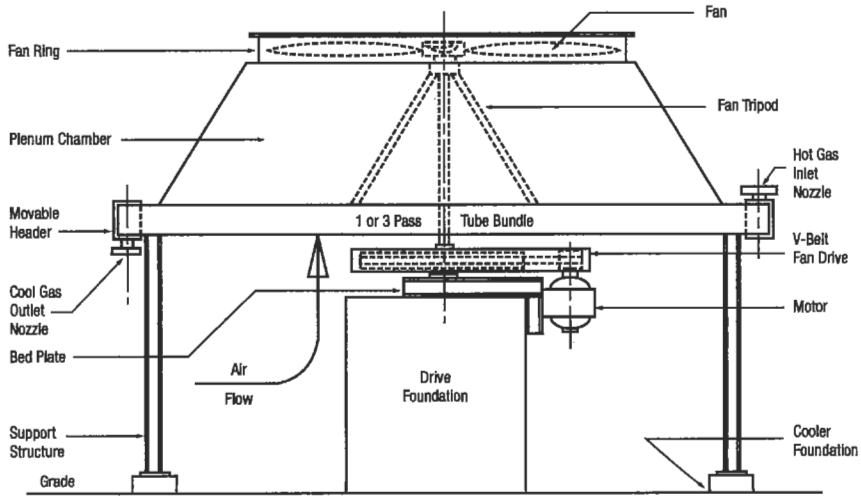
NFPA Code 495—Manufacture, Transportation, Storage and Use of Explosive Materials

NFPA Code 496—Purged and Pressurized Enclosures for Electrical Equipment in Hazardous (Classified) Locations

NFPA Code 498—Explosives, Motor Vehicle Terminals



a. Forced Draft Cooler



b. Induced Draft Cooler

Figure 6-243. Types of aerial heat exchanges [149].

(text continued from page 871)

The advantages of induced draft are:

- Better distribution of air across the section.
- Less possibility of the hot effluent air recirculating around to the intake of the sections. The hot air is discharged upward at approximately 2.5 times the velocity of intake or about 1,500 ft/min.
- Less effect of sun, rain and hail, since 60% of the face area of the sections is covered.
- Increased capacity in the event of fan failure, since the natural draft stack effect is much greater with induced draft.

The disadvantages of induced draft are:

- Higher horsepower since the fan is located in the hot air.
- Effluent air temperature should be limited to 200°F to prevent potential damage to fan blades, bearings, V-belts, or other mechanical components in the hot airstream.
- The fan drive components are less accessible for maintenance, which may have to be done in the hot air generated by natural convection.
- For inlet process fluids above 350°F forced draft design should be used: otherwise, fan failure could subject the fan blades and bearings to excessive temperatures.

In sizing gas coolers the most important parameters are the actual heat load and design air temperature. The heat load may be found from the following:

$$Q_H = Q_{std} \rho c_p (t_1 - t_2) \text{ for SI and } Q_H = Q_{std} \gamma c_p (t_1 - t_2) \text{ for English System}$$

where Q_H = heat load in desired units: Btu/n or W

Q_{std} = gas flowrate in scf/n or scm/s

c_p = specific heat capacity at average temperature
($T_1 + T_2$)/2 in Btu/(lb °F) or J/(kg °C)

t_1, t_2 = inlet and outlet temperatures in °F or °C

ρ = density (kg/scm)

γ = specific weight (lb/scf)

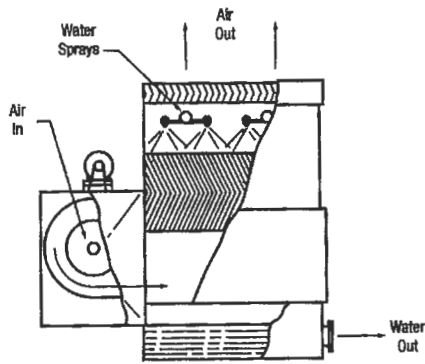
The design air temperature is usually the average daily maximum temperature for the hottest month of the year at the gas cooler location plus 3 to 5°F (1.5 to 2.5°C) correction value for the location environmental conditions.

Cooling Towers [149]

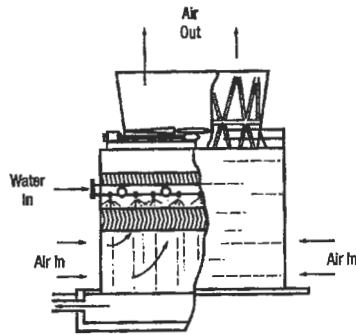
Cooling towers allow water to be cooled by ambient air through evaporation. They have two types of air flow, crossflow and counterflow. In crossflow towers, the air moves horizontally across the downward flow of water. In counterflow towers, the air moves vertically upward against the downward fall of the water. There are a few types and sizes of cooling towers:

Mechanical draft towers (see Figure 6-244) are characterized as follows:

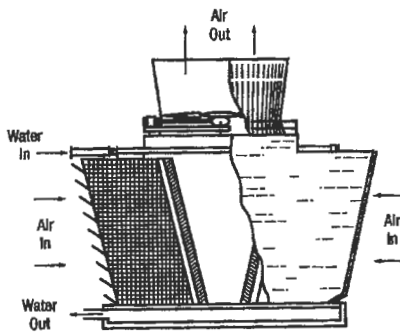
- Forced draft towers, where the fan is located on the airstream entering the tower.
- Induced draft tower, where the fan is located on the airstream leaving the tower.



a) Forced draft, counterflow, blower fan tower.



b) Induced draft counterflow tower.



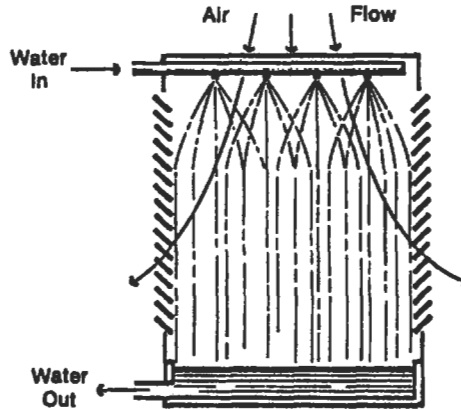
c) Double-flow, crossflow tower.

Figure 6-244. Mechanical draft towers [149].

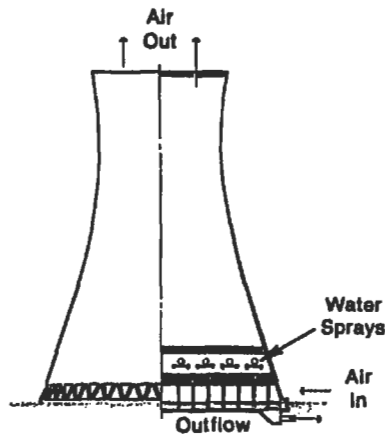
- Coil shed towers, where the atmospheric coils or sections are located in the basin of the cooling tower.

Natural draft towers (see Figure 6-245) are as follows:

- Atmospheric spray towers are dependent upon atmospheric conditions; no mechanical devices are used to move the air.
- Hyperbolic natural draft towers, where a chimney or stock is used to induce air movement through the tower.



a) Atmospheric spray tower.



b) Counterflow natural draft tower.

Figure 6-245. Natural draft towers [149].

The performance characteristics of various types of towers will vary with height, fill configuration and flow arrangement: crossflow or counterflow. When rough characteristics of a specific tower are required the performance characteristic nomograph (Figure 6-246) can be used.

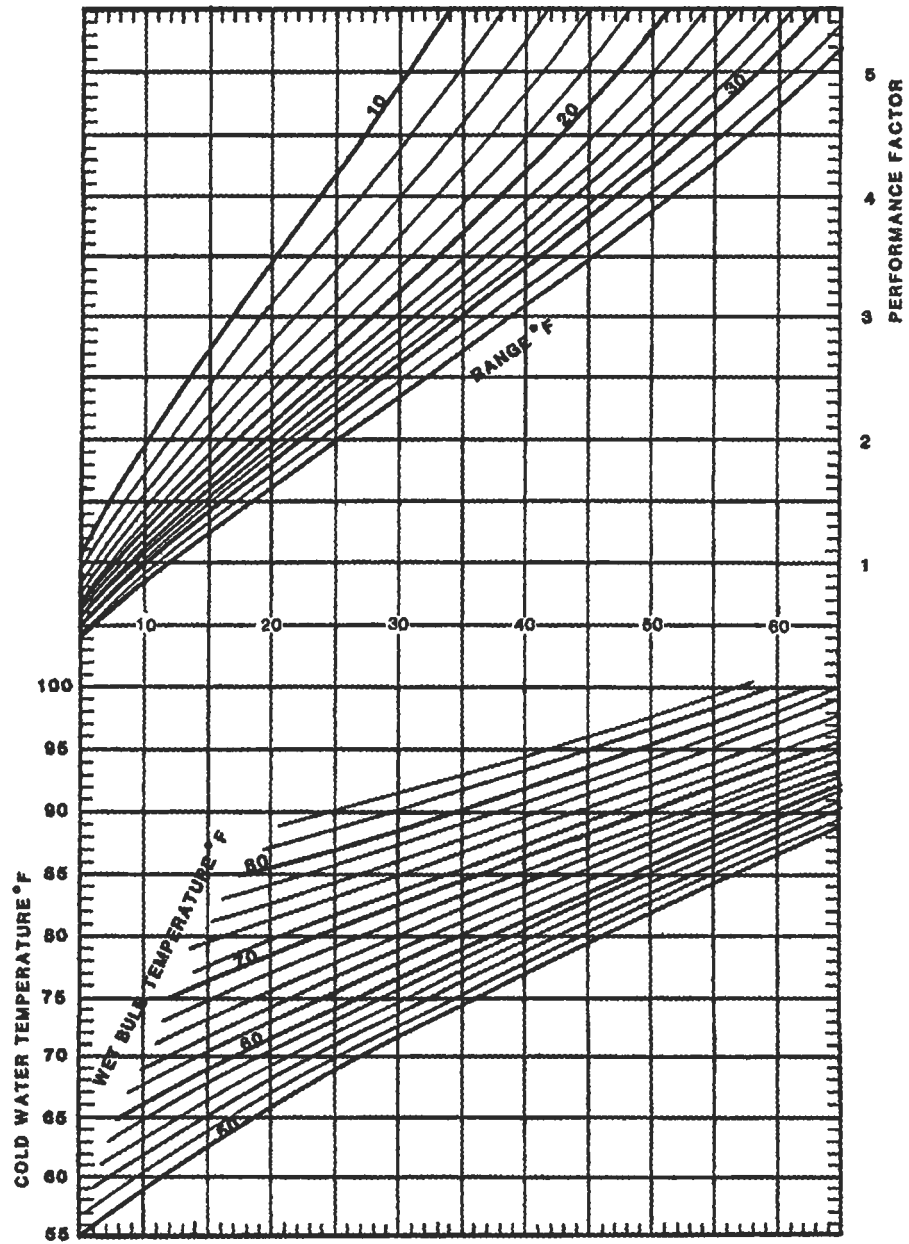


Figure 6-246. Pressure characteristic nomograph.

Example 27

The use of the nomograph is illustrated by the following examples covering typical changes in operating conditions. Assume a cooling tower is operating at these known conditions: flow = 1,000 gal/min, hot water at 110°F, cold water at 86°F, wet bulb temperature = 70°F. This is commonly referred to as 110 - 86 - 76 or 24° range (110° - 86°) and 10° approach (86 - 76°).

- a. What is the effect of varying wet bulb temperature (WB) on cold water temperature (CWT)? What is new CWT when WB changes from 76 to 65°F with gal/min and the range remains constant? Enter the nomograph at 86° CWT, go horizontally to 76°F WB, then vertically down to 65°F WB, then read new CWT of 79.5°.
- b. What is the effect of varying the cooling range on the cold water temperature? What is the CWT now when the cooling range is changed from 24° to 30° (25% increase in heat load) with gal/min and WB held constant? Enter the nomograph at 86° CWT, go horizontally to 76° WB, vertically to 24°R, horizontally to 30°R, vertically downward to 76° WB, then read new CWT 87.4°.
- c. What is the effect of varying water circulating rate and heat load on cold water temperature? What is the new CWT when water circulation is changed from 1,000 to 1,200 gal/min (50% change in heat load at constant range)? Varying the water rate, particularly over wide ranges, may require modifications to the distribution system. Enter the nomograph at 86°F CWT, 90 horizontally to 76°F WB, vertically to 24°R, horizontally to performance factor of 2.88. Obtain a new performance factor (PF), multiplying $(2.88)(1,200/1,000) = 3.46$, then enter the nomograph at PF = 3.46, go horizontally to 24°R, vertically down to 76°F WB, then read new CWT 88.5°F.
- d. What is the effect of varying the WB temperature, range and water circulating rate on the cold water temperature? What is the new CWT when the WB changes from 76° to 65°, R changes from 24° to 25°, gal/min changes from 1,000 to 1,500³. Enter the nomograph at 86° CWT, go horizontally to 76 WB, vertically to 24°R, horizontally read PF = 2.88, then multiply $(2.88)(1,500/1,000) = 4.32$ (new PF). Enter the nomograph at PF = 4.32, go horizontally to 25°R, vertically down to 65° WB, then read 86.5° as the new CWT.
- e. What is the effect of varying the fan hp input on the cold water temperature? What is the new CWT if the motor is changed from 25 to 30 hp in example (d)? The air flowrate varies as the cube root of the horsepower and performance varies almost directly with the ratio of water rate to air rate; therefore, the change in air flowrate can be applied to the performance factor. Increasing the air flowrate (or hp) decreases the performance factor. PF correction factor = $(30/25)^{1/3} = 1.0627$.
Divide PF by the PF correction factor to get the new PF. Applying this to example (d), we get $4.32/1.0627 = 4.07$. Enter the nomograph to 4.07 PF (instead of 4.32), go horizontally to 25°R, vertically down to 65 WB, then read 85.5 CWT.
- f. The correction factor shown in example (e) could also be used to increase the gal/min instead of decreasing the CWT, as was done in example (e). In example (d) we developed a new CWT of 86.5 when circulating 1,500 gal/min at 25°R and 65 WB. If the motor hp is increased from 25 to 30 under these conditions, with a PF correction factor of 1.0627 (as shown above), gal/min could be increased from 1,500 to $1,500 \times 1.0627 = 1,594$ gal/min.

- g. Calculate the concentrations and blowdown rate for the following cooling tower.

Circulation rate = 8,000 gal/min

Water temperature drop through tower = 20°F

Type of tower = mechanically induced draft

Blowdown rate = 20 gal/min or 0.2% of circulation rate

Solution

Evaporation loss = 2% (1% for each 1° temperature drop) (All rates are based on a percent of circulation rate.) Windage loss = 0.3% (maximum for mechanical draft tower) Number of concentrations (cycles) is

$$N = (E + B)/B = \frac{2.0 + (0.2 + 0.3)}{(0.2 + 0.3)} = 5.0$$

If the resultant concentrations are excessive and a desired concentration of 4.0 is required, what must the blowdown rate be?

$$B = \frac{E}{\text{cycles} - 1} = \frac{2.0}{4.0 - 1} = 0.67\%$$

The windage component of B is 0.3%, therefore, the blowdown rate required would be 0.67 - 0.3 = 0.37% or (8,000 gal/min)(0.0037) = 29.6 gal/min.

CORROSION AND SCALING

Production Operations

The increasing cost of tubular goods failures due to corrosion in the oil and gas industry has increased interest in and importance of corrosion problems and their solutions. Metal dissolution and sudden cracking of tubing and casing are mainly caused by the presence of carbon dioxide, hydrogen sulfide, oxygen, and water. The presence of larger volumes of water in aggressive environments intensifies the severity of corrosion, while oil tends to form a protective oily film on the metal surfaces. Therefore, one of the criteria for predicting the severity of corrosion in an oil and gas environment is the water/oil ratio [150]. The majority of field experience has shown that in wells producing 0-25% water, corrosion does not likely occur if there are not significant amounts of corrosive gases; 25-40% water cut indicates the probable occurrence of corrosion, and the degree of corrosivity depends on carbon dioxide, hydrogen sulfide, pressure and temperature. Above 40% water cut most of the oil and gas fields have shown very potent corrosive environments [151,152]. Figure 6-247 illustrates a relationship between the water cut and number of corroded oil and gas wells.

There are a number of corrosion prevention methods used in the oil and gas industry. The most useful methods are those with high efficiency and favorable economics. Corrosion inhibitors have been used to minimize the problems encountered by aggressive environments. Some inhibitors are used as the sole corrosion prevention method; some others are used in conjunction with coatings; and finally, there are some problems in oil and gas production where their use is not recommended [153].

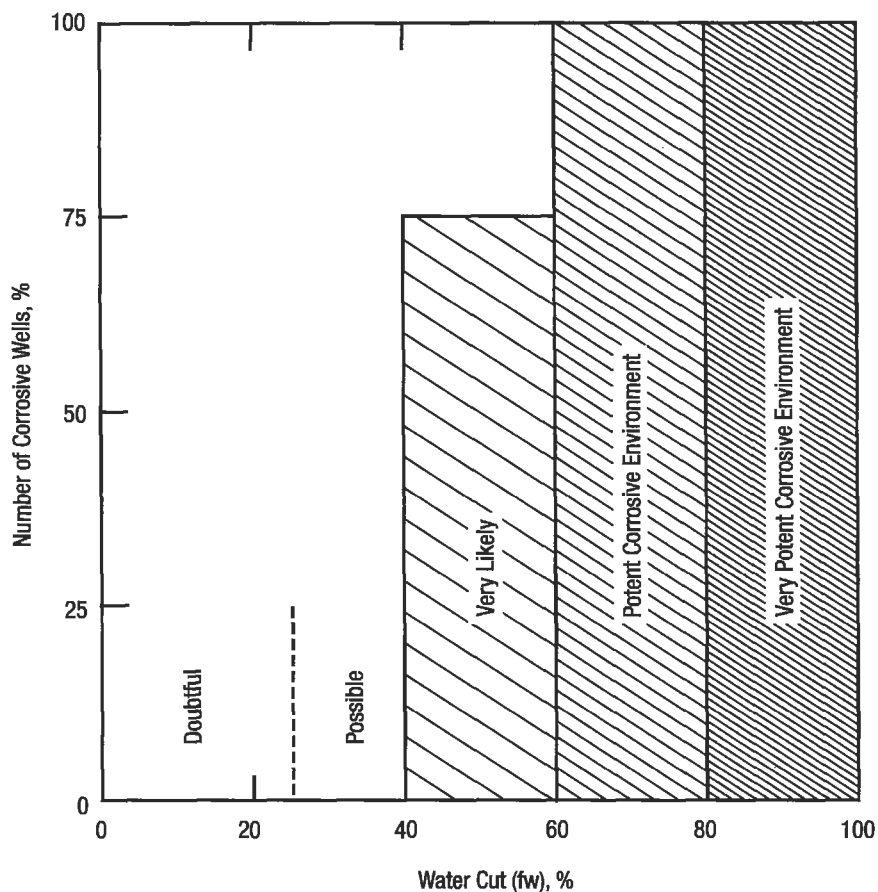


Figure 6-247. Relationship between water cut, and number of corrosive wells [151,152]

Generally, corrosion inhibitors show poor results in the absence of an oil film on the metal surface. However, this problem can be solved by the use of water-soluble inhibitors rather than oil-soluble inhibitors. The selection of proper corrosion inhibitors in deep, high-pressure, high-temperature wells with a high percentage of corrosive gases, such as in sour gas wells, has required extensive laboratory study to find oil-inhibitor systems that do not vaporize into the dry gas at bottomhole conditions. The conditions of an ineffective inhibitor action in high pressure and temperature sour gas wells is shown in Figure 6-248. The principal approach to prevent oil vaporization under bottomhole conditions is to select an oil-inhibitor system with a dew point greater than bottomhole flowing condition, i.e., by duplicating bottom-hole conditions in surface test facilities and examining the inhibitor performance with various oils until one is found that yields sufficient liquid phase at acceptable ratios of circulated-carrier oil to gas [154-157].

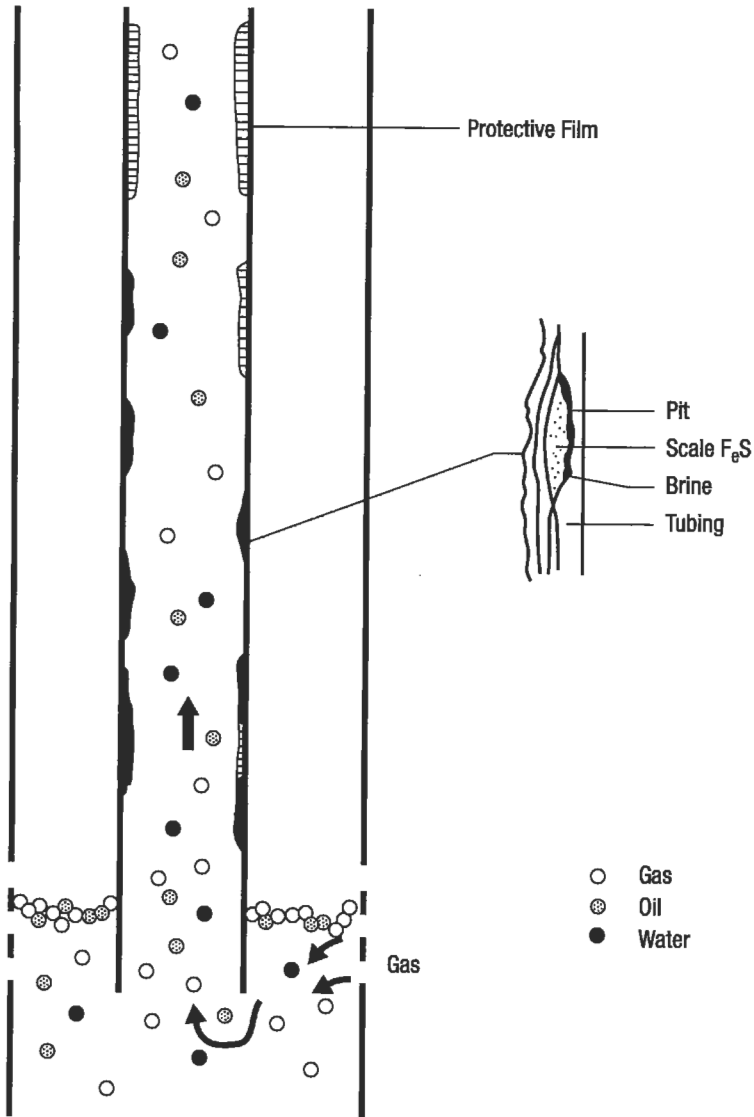


Figure 6-248. Vaporization of oil-inhibitor mixture [156].

Hydrogen Sulfide Corrosion

Stress corrosion cracking (SCC) and sulfide stress cracking (SSC) are the most common types of corrosion in sour oil and gas environments. Failures due to hydrogen sulfide are usually sudden with no warning. Generally, corrosion in sour environments is a combination of a small and apparently insignificant amount of localized corrosion combined with tensile stresses.

Stress corrosion cracking occurs at the metal surface in the form of pitting corrosion, which is the result of iron sulfide (FeS) deposits on the metal surface. The iron sulfide is cathodic to steel, contributing to pitting corrosion of scale-free areas. Basically, stress corrosion cracking susceptibility is a function of hydrogen sulfide concentrations, alloy compositions, hydrogen sulfide partial pressure, residual and applied stresses, and temperature. Very high-strength alloys can crack almost instantly when subjected to a sour environment [158,159].

Sulfide stress cracking is the worst type of corrosion in the presence of hydrogen sulfide. Sulfide stress cracking is a function of hydrogen sulfide concentration (as low as 1–3 ppm), hydrogen sulfide partial pressure, stresses, material yield strength, temperature and pH. Sulfide stress cracking mostly occurs in very highly acidic environments. The mechanism of sulfide stress cracking involves a combination of stress corrosion cracking and hydrogen embrittlement.

Hydrogen embrittlement is a function of the hydrogen absorption characteristics of the metal in the aggressive environment, which is the formation of molecular hydrogen from atomic hydrogen within the metal structure [160].

The atomic hydrogen created at the surface of the metal will either combine to form hydrogen gas or will be absorbed at grain boundaries. Trace amounts of sulfur, arsenic, antimony, phosphorus and tellurium act to promote absorption of atomic hydrogen by the surface [157,160].

Once the atomic hydrogen has been absorbed by the metal, it diffuses through the material until it comes in contact with the metal structure's discontinuities or defects, such as inclusions, carbides or grain boundaries. The atomic hydrogen then combines to form molecular hydrogen, which puts additional pressure on the metal discontinuities or defects.

Hydrogen embrittlement occurs below the metal surface. pH strongly influences hydrogen embrittlement, since sour environments may contain significant traces of hydrogen sulfide as well as HCl. Therefore, hydrogen sulfide alters hydrogen embrittlement by enhancing additional atomic hydrogen at the cathode. This combined action of hydrogen embrittlement and hydrogen sulfide contributes to sulfide stress cracking. The formation of atomic and molecular hydrogen is shown as



Metallurgical factors and alloying elements are the most important considerations for tubular goods selection in sour oil and gas environments. High-alloy metals, and steels below 80,000 psi yield and 90,000 psi tensile strength are reported to be relatively resistant to cracking due to hydrogen sulfide [161,162].

Filming amines and organic phosphates such as amine phosphates are reported to be effective corrosion inhibitors in sour environments. These inhibitors are usually prepared as oil-soluble for lower-pressure and temperature, flowing wells, while water-soluble inhibitors are mostly recommended at higher temperatures and pressures [163–168]. Table 6-65 gives inhibitors for hydrogen sulfide corrosion.

Carbon Dioxide Corrosion

Corrosion due to carbon dioxide is primarily a function of carbon dioxide partial-pressure and temperature. The following equation indicates the corrosion rate due to CO₂ as a function of temperature and CO₂ partial pressure [169,170]:

Table 6-65
Commercial Inhibitors In Presence of Hydrogen Sulfide

INHIBITOR MIXTURE	CON, ppm	TEMP, °F	EFFECTIVENESS, %
Imidazoline-Amino tri (methyl phosphonic acid)	83	165	95
Imidazoline-carboxylic acid salts	30	170	90
Alkylenediamine-phosphate ester	120	200	90

$$\log(r) = 8.78 - \frac{2,320}{T + 273} - 5.55 \times 10^{-5} T - 0.67 \log P_{CO_2} \tag{6-339}$$

where r = corrosion rate due to CO₂ in mpy

T = temperature in °C

P_{CO₂} = partial pressure of CO₂ in psi

The overall results of the corrosion rate due to carbon dioxide as a function of temperature and carbon dioxide partial pressure are shown in Figure 6-249.

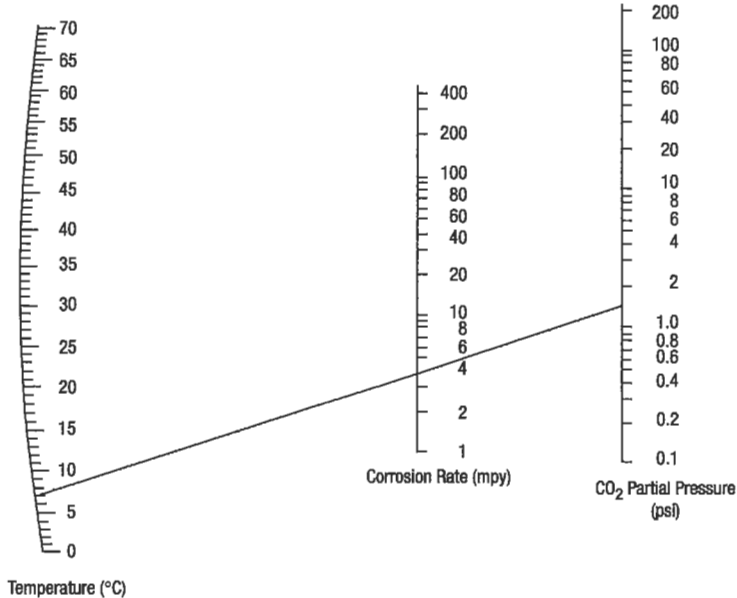


Figure 6-249. Nomograph for calculation of corrosion rates as a function of carbon dioxide partial pressure and temperature [169].

Corrosion due to carbon dioxide in primary, secondary and/or tertiary recovery can occur from carbon dioxide-transporting pipelines to production wells, and surface facilities. Basically, carbon dioxide in the presence of water produces carbonic acid, which may cause uniform, but mainly pitting, corrosion. Pitting and weight-loss corrosion can be minimized by (1) using corrosion-resistant alloys for critical components; (2) ensuring metallurgically-uniform grain structures; (3) keeping flow velocities below the erosional velocity to reduce erosion and/or corrosion and (4) application of corrosion inhibitors [171-173].

The most effective and economical corrosion inhibitors in presence of carbon dioxide are reported to be variations of filming amines [172]. These inhibitors are usually prepared as water-soluble solutions. The use of oil-soluble solutions. The use of oil-soluble corrosion inhibitors is not recommended due to high fluid levels in the well bore that may prevent the inhibitors' circulation [173]. In addition, the inhibitors in Table 6-66 have been recommended in presence of carbon dioxide [167,168,174-176].

The inhibitors listed in Table 6-66 are diluted with water. These chemical inhibitors have been applied by batch-treating methods on weekly schedules [153].

Methods of Corrosion Inhibitor Application

There are two principal requirements for successful corrosion mitigation in oil and gas wells: selecting a suitable inhibitor, and specifying a method of inhibitor application that assures the filming of the producing equipment. Many corrosion treatment methods are used in the oil industry. These are [150]:

1. batch treatment
2. continuous treatment
3. formation squeeze

Table 6-66
Commercial Inhibitors in Presence of Carbon Dioxide

INHIBITOR MIXTURE	CON, ppm	TEMP, °F	EFFECTIVENESS, %
Imidazoline-carboxylic acid salts.	25	170	89-91
Imidazoline compound and hydrazine.	100	< 210	97
Fatty acid-ester-Aminoethyl Ethanolamine Reaction product	100	200	97
Phosphate of cyclic Amidine salts	50	< 200	90
Alkylenediamine-Phosphate Ester	120	< 225	90

Each method is applicable to specific conditions. The latest investigations related to the effectiveness of various treatment methods imply that when it can be employed, the continuous downhole application of a corrosion inhibitor is a more economical and favorable method of application than others. However, the reliability of each method depends on conditions such as well completion, the specific corrosion inhibitor employed and tubing string parameters. The following sections compare economics and effectiveness of various methods of application.

Batch Treatment. Batch-treating techniques can be used in oil and gas wells to form protective films on metal surfaces. The majority of batch-treated wells are treated with oil-soluble, and oil-soluble/water-dispersible, corrosion inhibitors mixed with hydrocarbon solvents. In some cases the use of water-soluble corrosion inhibitors by batch-treating techniques is reported [177,178]. The use of water-soluble corrosion inhibitors can be associated with the following problems:

1. less-tenacious, inhibitor film
2. scale and contamination problems with the carrier water
3. increased hydrostatic pressure on the well
4. foaming and emulsion problems

Scale and contamination problems can be solved by using a suitable carrier-water compatible with produced water. The carrier water should be clean (solids-free) to avoid plugging, emulsions and loss of inhibitor due to adsorption onto the solids present in the water. Waters with high pH have a tendency to increase scaling. Also, waters containing barium or strontium should not be applied to treat wells where produced water contains sulfates.

Increased hydrostatic pressure can be reduced by using smaller water-volumes.

Emulsions can cause blocks in the tubing, resulting in the decreased ability of the inhibitor to fall to the bottom where it is needed. If the inhibitor cannot separate from the emulsion, then it cannot film the tubing wall. Emulsions also can cause fouling in surface vessels and gas-treating units. Emulsions can be controlled in batch-treating systems by selecting a proper corrosion inhibitor and water carrier. Demulsifiers can be added to corrosion inhibitor and carrier water to decrease emulsion tendency [177,178].

Foaming can prevent the corrosion inhibitor mixture from falling to the level desired in the tubing. Foaming can be controlled by using a corrosion inhibitor that shows low-foaming tendency with carrier water. Foaming is also controlled by adding antifoam compounds to the batch-treatment mixture [159,160]. Several batch-treating techniques are used for treating oil and gas wells, including:

- tubing displacement
- periodic batch
- extended-period batch
- periodic batch with inhibitor emulsion
- batch with weighted inhibitor

Tubing Displacement. A concentration of about 5–12% inhibitor as material received is either dispersed or dissolved in water or a hydrocarbon. The desired amount of this mixture is displaced through the tubing to the bottom of the well by pumping produced fluids in behind the mixture. The amount of displacing liquid is calculated by determining the volume of the tubing and subtracting the volume of inhibitor mixture. In the tubing displacement method 2 to 15 hr shut-in time is required to build up pressure. The tubing displacement method

becomes less satisfactory as reservoir pressures decline. The tubing displacement is recommended for wells equipped with packers and gas lift [179].

Periodic Batch. The periodic batch treatment is recommended for open-annulus completion with both high and low fluid-level wells. The occasional failures with this treatment in high fluid-level wells can generally be attributed either to the improper selection of inhibitors or the improper circulation of the wells. The application of the treatment in low fluid-level wells depends on the fluid level maintained in the annulus. It is estimated that a fluid level of at least 150 ft should be maintained in the annulus to achieve better effectiveness.

Extended-Period, Batch Treatment. The extended-period, batch treatment is a variation of the standard, periodic-batch treatment. This treating method has been used successfully in high fluid-level wells. The procedure consists of calculating the total volume of inhibitor required for a 3 to 8-month period and batching that quantity into the annulus. The well is put on complete circulation and circulated until the inhibitor goes down the annulus, up the tubing and back into the annulus. Extended-period, batch treatment can last up to 6 months [150].

Periodic Batch with Inhibitor Emulsion. Periodic batch with inhibitor-emulsion treatment can be applied with both low and high-level wells, as well as wells set on packers. This treatment consists of creating a semipermanent emulsion with inhibitor and water, dumping the mixture into the tubing or annulus and shutting the well off for a time sufficient for the mixture to fall to the well bottom. The effectiveness of this method depends on the emulsion being sufficiently stable to remain dispersed until the mixture has reached bottom. The emulsion must be of a semipermanent nature that will allow the inhibitor to slowly coalesce and enter the oil column. The mixture is required to remain relatively stable for several hours [180].

Batch with Weighted Inhibitor. The inhibitor is chemically coupled to a weighting agent. These chemicals are available in various densities to assure that the chemicals will fall through either the oil or water in the annulus or tubing. The weighted inhibitors have frequently been applied successfully where other types of treatment have been ineffective. It is noted that certain weighting agents are not suitable in sour operations; therefore, sweet or sour production should be considered to select the chemical [180].

Continuous Treatment. The continuous injection of inhibitor into the fluid stream has been recognized as the optimum treating method since the inception of corrosion control by chemical injection [181–183]. Continuous downhole injection is reported to increase the functional life of the tubing 10 to 20-fold, where no other treating methods could increase the functional life of the tubing more than three to fivefold [184]. The continuous treating method generally involves introducing the inhibitor on a continuous basis at sufficient concentrations to form a protective film on the tubing. This concentration may vary from 20 to 130 ppm depending on several factors, such as:

1. the degree of oil and gas well corrosivity
2. well-stream fluid velocity
3. well completion design
4. depth of corrosive oil and gas wells

To reduce corrosion rates, higher concentrations of corrosion inhibitor are necessary. Since the major objective of corrosion inhibitors in oil and gas wells is to form a protective film on the tubing surface, wellstream fluid velocity plays a significant role in maintaining this film at constant inhibitor concentration for a longer period of time in continuous, downhole, treating methods. Generally, the criterion is erosional velocity, i.e., the selection of the proper tubing ID to keep the well-stream fluid velocity below erosional velocity. Erosional velocity can be determined by the following relationship [184]:

$$V_e = K/\gamma_m \quad (6-340)$$

where K = empirical constant (generally 100)

V_e = erosional velocity in ft/s

γ_m = specific weight of wellstream in lb/ft³

The values for K , which is a function of solids present in fluid, vary from 50 to 500. The continuous downhole injection technique can be applied with the following three, completion designs [164,167]:

1. open-annulus injection
2. dual completion
3. closed-annulus injection

For wells completed with no packers, the annular space can be used to carry corrosion inhibitors to the bottom of the tubing string up to the production string as shown in Figure 6-250.

In wells completed with a "dual" or "kill string" completion, corrosion inhibitors can be injected through injection tubing (1.0 in., generally, but can be up to 2 $\frac{7}{8}$ in. OD). Generally, when "kill string" inhibition is used, the bottom will be equipped with a valve or flow-restricting device, and the mixture is then continuously pumped into the injection tubing, building sufficient pressure to open the downhole valve. Figures 6-251 through 6-253 illustrate typical dual completion designs [184,187].

For a well completed with a packer, an injector valve that operates on a predetermined pressure differential in the tubing string is employed. Generally the annulus is filled with corrosion inhibitors, and a pump is used to apply the necessary pressure to open the injection valve. The latest investigations on the application of continuous treating methods with a closed-annulus injection system show many problems with the technique [187]. The principal cause of failure is the plugging of the small-diameter injection ports due to solids present in the annulus fluid and/or microbiological corrosion as well as inhibitor separation or polymerization. Weighting agents must be added to inhibitors in high-pressure wells in order to apply adequate backpressure at the packer and injection valve. The wells completed with gas-lift can be treated by injecting corrosion inhibitors down the annulus through the operating gas-lift valve as shown in Figure 6-254.

Based on observed field results, the continuous treating method in gas-lift wells has shown that [186]:

1. Corrosion-inhibitor transport in the gas-lift gas stream is a feasible treating technique.
2. Operating problems do not result from the presence of liquid inhibitors in the gas-lift system.

(text continued on page 903)

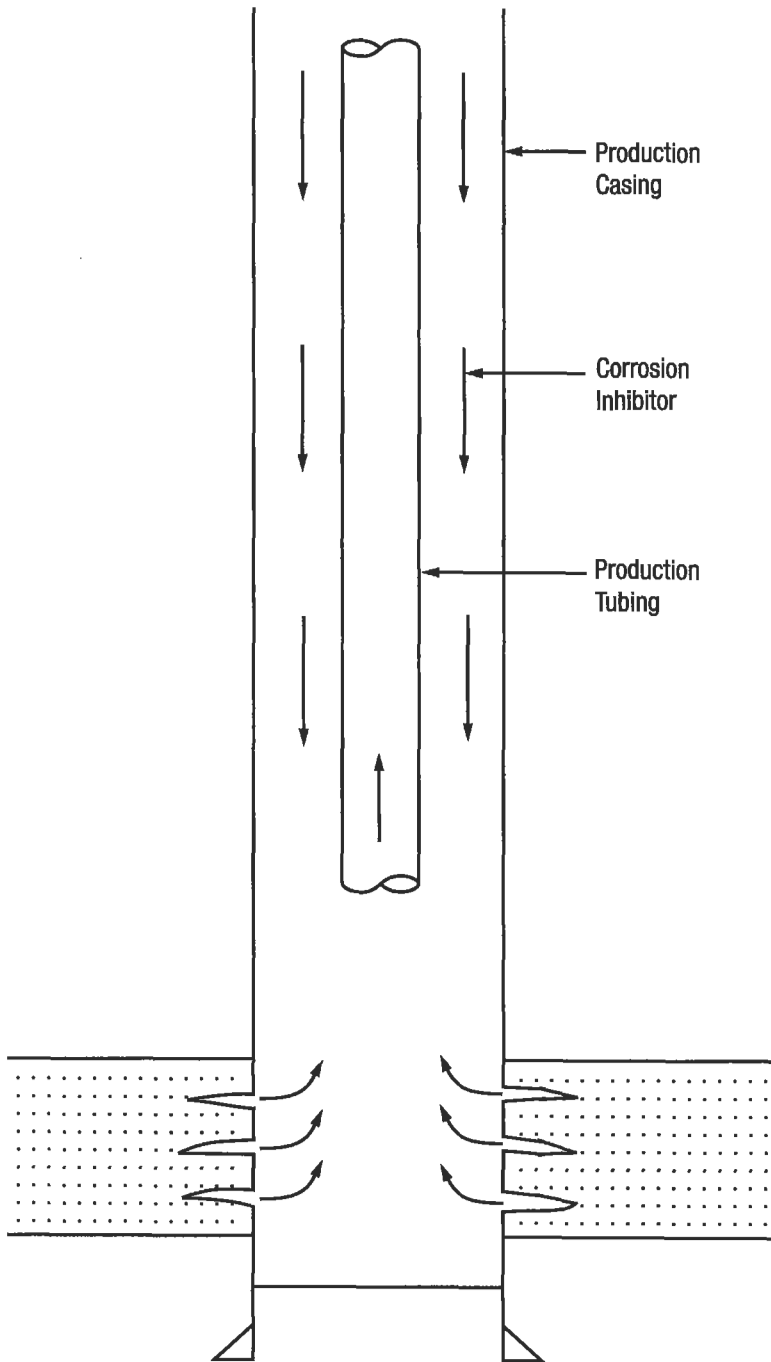


Figure 6-250. Open-annulus completion [184].

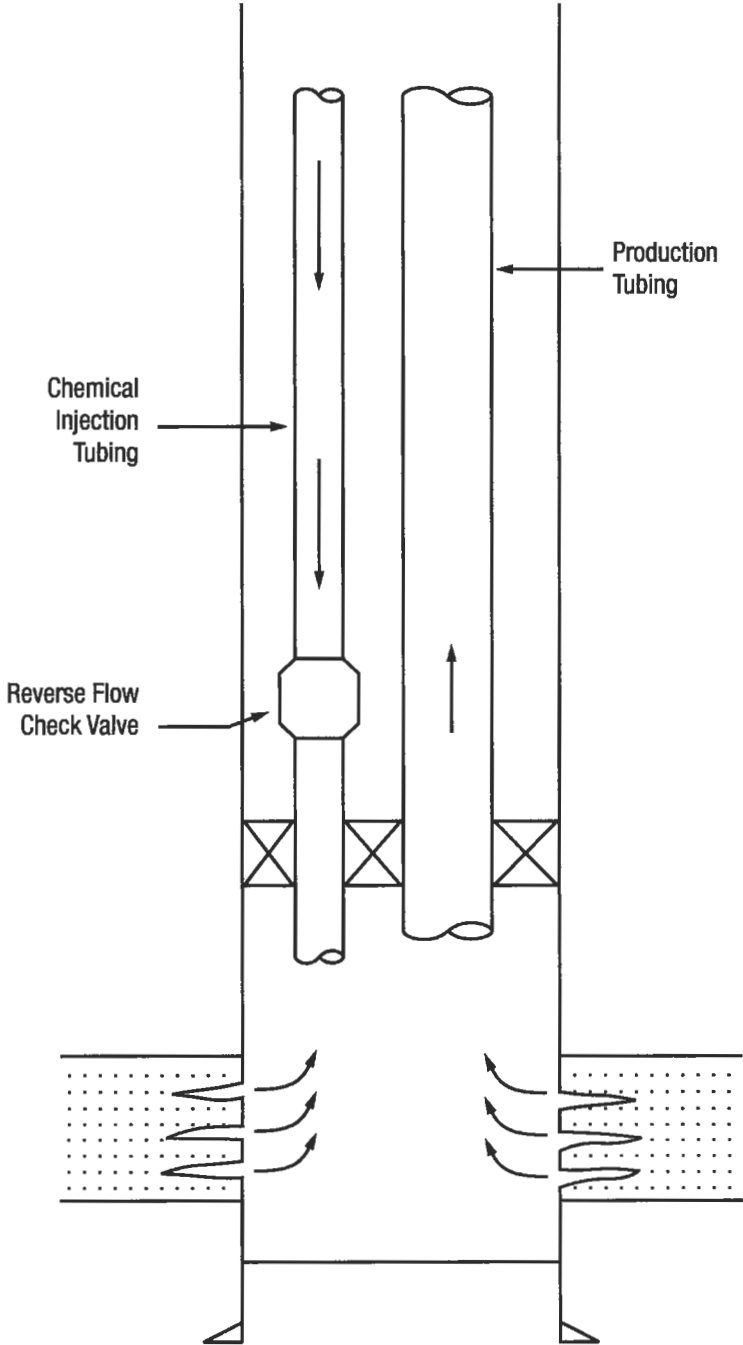


Figure 6-251. Dual completion [184].

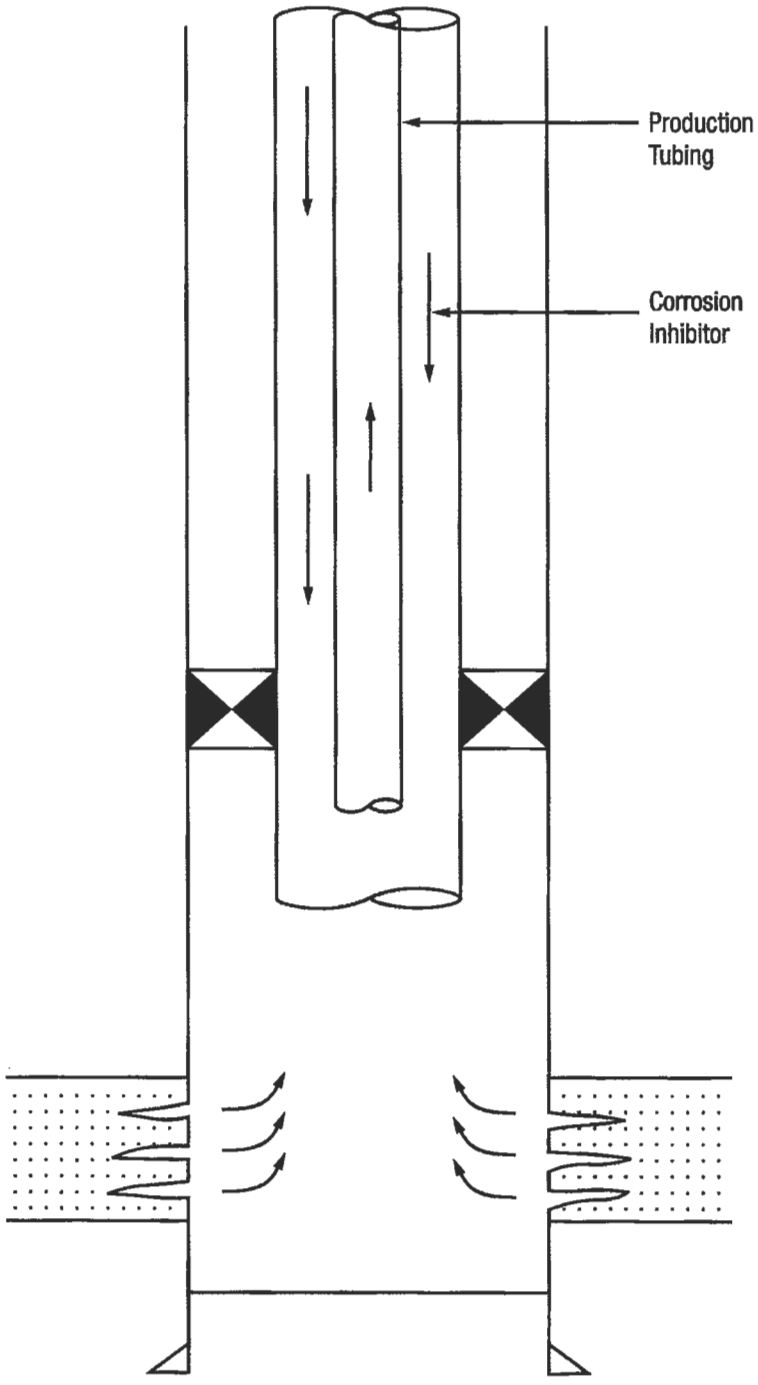


Figure 6-252. Concentric completion [184].

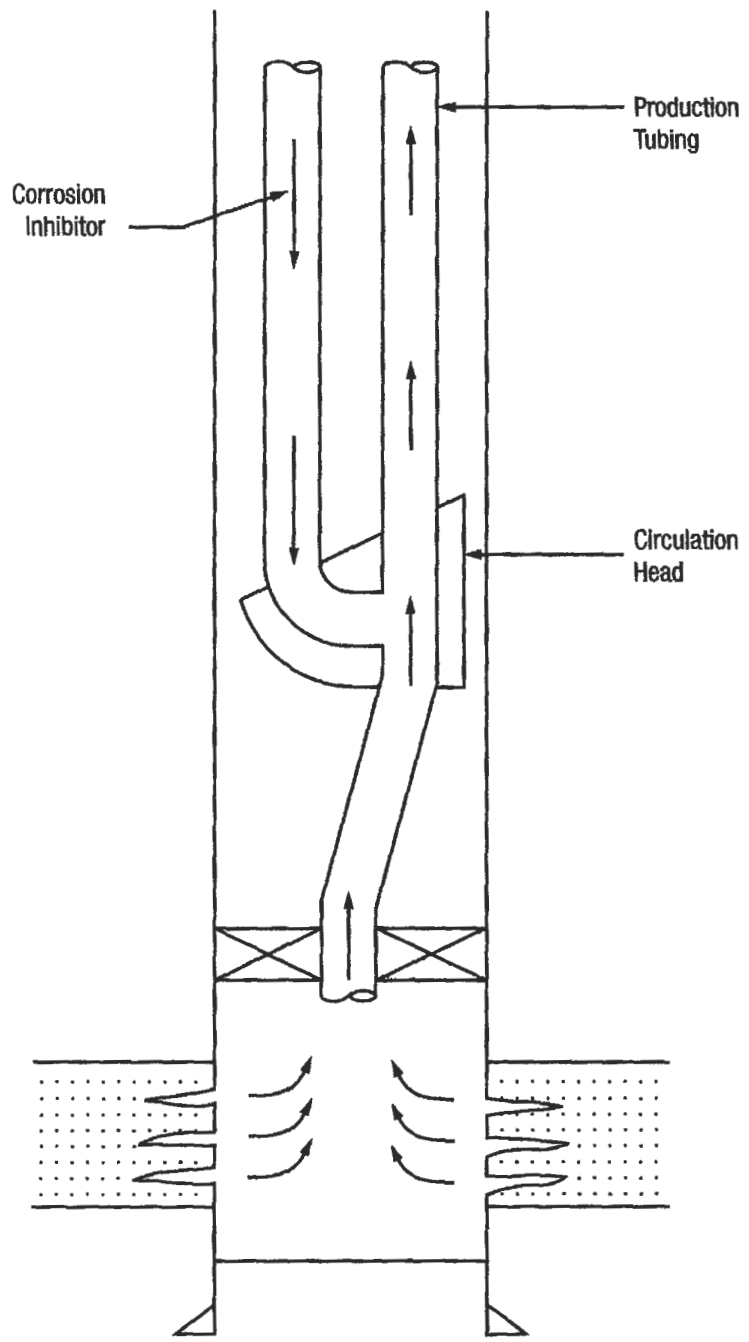


Figure 6-253. Y-block completion [184].

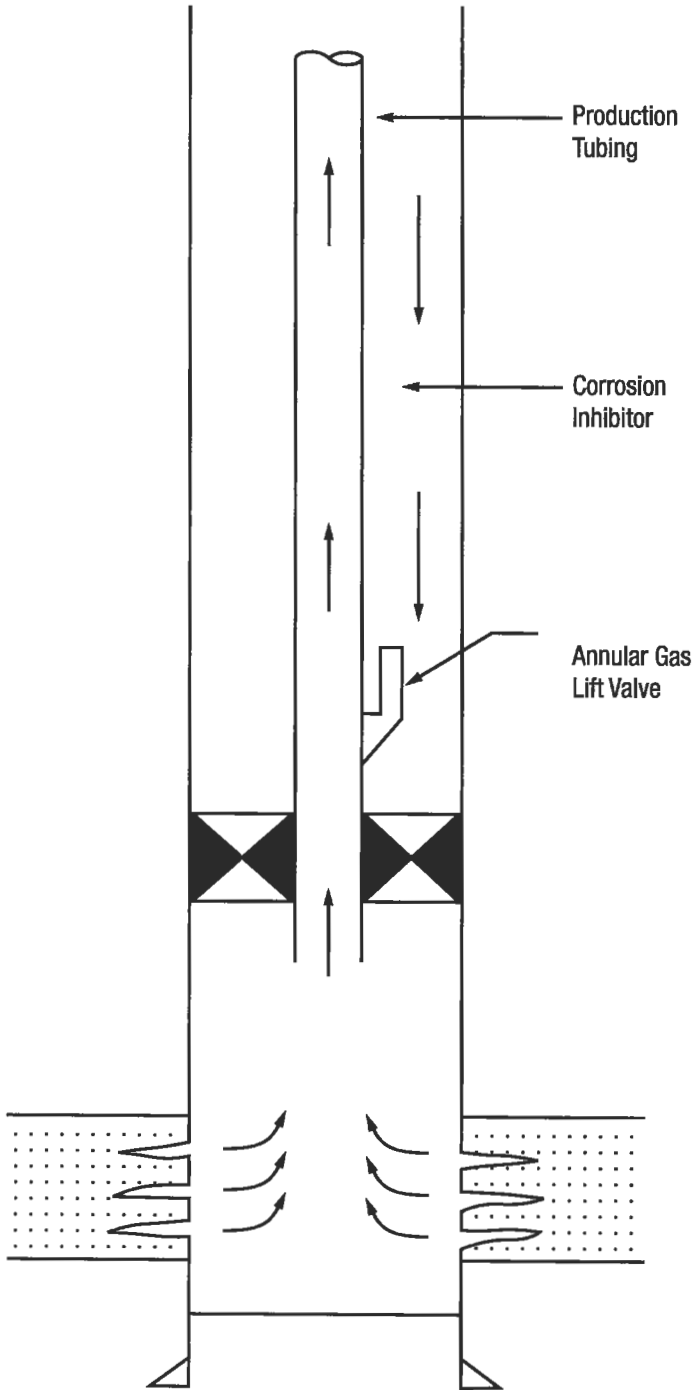


Figure 6-254. Gas-lift well completion [184].

(text continued from page 897)

3. The continuous-inhibitor, treating method offers corrosion prevention of gas-lift well tubulars at least equivalent to that afforded by a well-managed, conventional batch-treating program.

Continuously transmitting inhibitors downhole through capillary tubing has overcome many problems caused by other techniques. The philosophy behind the development of this method was to design a continuous, downhole-injection system that would not effect major changes in the drilling or completion program of a well, but would offer a higher degree of flexibility and reliability. A well completion with this technique is shown in Figure 6-255. It requires (1) a modified side-pocket, gas-lift mandrel and valve; (2) a required length of injection tubing (0.25 in. OD with a 0.049-in. wall); (3) special clamps to support and protect the injection tubing; and (4) a tubing hanger bored to accept the injection tubing. The amount of corrosion inhibitor required for continuous transmission downhole can be determined by the following relationship [181,182,184]:

$$V_i = \frac{(5.82 \times 10^{-5})(d)(D_m)}{C_i} \quad (6-341)$$

where C_i = corrosion inhibitor concentration in %
 d = production tubing (ID) in in.
 D_m = production tubing measured depth in ft
 V_i = volume of corrosion inhibitor in gal/day

Laboratory and field comparison of continuous inhibitor injection by the capillary system, bottomhole valve and other techniques has shown the following advantages of transmitting inhibitor downhole through an annular-mounted capillary [181,182].

1. Assures delivery of clean, debris-free inhibitor to downhole-injection chamber.
2. Capillary volume is small, minimizing time and well-temperature effects on inhibitor.
3. Inhibitor formulas and injection rates can be changed quickly.
4. Design of capillary system minimizes the possibility of communication between the tubing and casing-annulus.
5. Capillary can be used for batching of combination treatments, such as corrosion and scale inhibitors, foaming agents and cleaning agents.
6. More efficient production is achieved.
7. Capital investments, chemical costs and manpower requirements are reduced.

Formation Squeeze Treating Techniques. The squeeze-treating technique consists of forcing corrosion or scale inhibitors into an oil, gas, or water-bearing formation. The squeeze technique can be successful when treating a producing formation with sufficiently porous strata [185]. In the squeeze treatment, the mixture of corrosion and/or scale inhibitor and a compatible diluent is injected down the tubing and into the formation. Generally, an "overflush" of oil or brine of the required volume is necessary to push the mixture further into the formation. The frequency of the squeeze treatment and the type of chemical required often is difficult to simulate in the laboratory. Frequency usually is assessed by monitoring the residual inhibitor found in the production effluent. The dynamic, laboratory test is used to determine initial inhibitor concentration

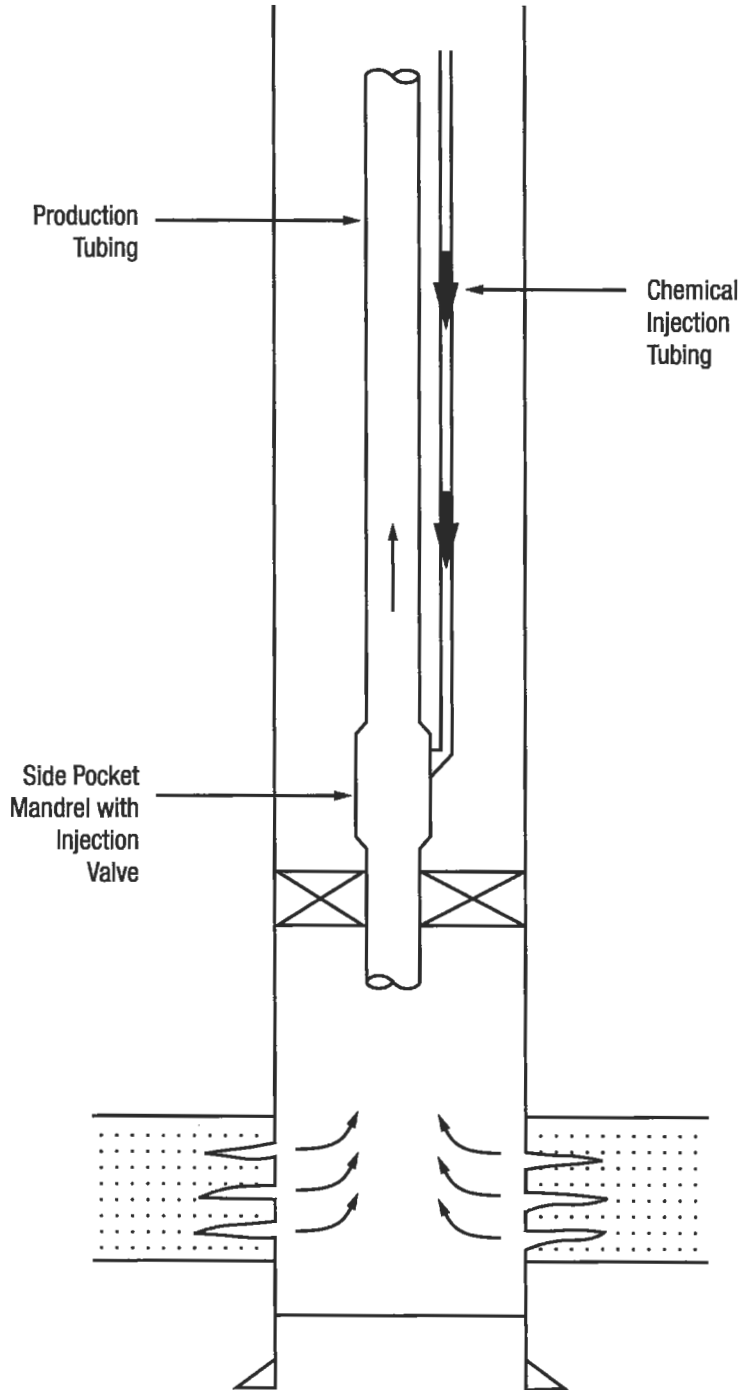


Figure 6-255. Continuous downhole injection system (CDIS) [182].

at certain given conditions [181,184]. When initial inhibitor concentrations are found by this test, the mixture of inhibitor and its diluent (generally 10 to 25% inhibitor) is squeezed into the formation. This initial squeeze is applied only to treat the well for short periods of time, approximately 2 to 3 weeks. The main purpose of initial squeeze treatment is a study of actual inhibitor performance. Generally, the amount of inhibitor concentration flowback with production should be known to calculate the quantity of chemical needed to treat the well for longer periods of time (usually 3 to 18 months).

The following relationship has been used in several cases to calculate the volume of inhibitor needed [184]:

$$V_i = \frac{(q)(f_w)(t)(C_i)}{1,000,000} \quad (6-342)$$

where C_i = inhibitor concentration in ppm

f_w = water cut in %

q = production rate in bpd

t = desired treatment life in days

V_i = amount of inhibitor without diluent in bbl

The inhibitor concentration (C_i) is dependent on inhibitor concentration flowback as mentioned earlier. It has been found experimentally that in initial squeeze treating, an inhibitor concentration can be based on laboratory dynamic tests, but most operators try to use higher concentration of the inhibitor for the initial squeeze job. The majority of actual field squeeze jobs shown that the actual (C_i) is three times greater than inhibitor concentration flow-back. Then

$$C_i = 3 \times C_{fb} \quad (6-343)$$

where C_{fb} = flow-back inhibitor concentration in ppm

It is believed that one-third of the inhibitor is lost due to adsorption in the formation, and that one-third flows back immediately after the well is returned to production. The remaining one-third flows back with the produced fluids, giving protection for a period of time.

Any squeeze-treatment job requires extensive laboratory study. For example, if the design of the squeeze job is based on adsorption characteristics, and if the liquids do not contact the assumed surface area inside the formation because of fractures and cavities, the life-span of the job will be short. Therefore, Equations 6-342 and 6-343 are only practical assumptions of the life-span and quantity of inhibitors. As is shown in Equation 6-342, expected treatment life tends to decrease with increased water production.

One of the factors influencing the effectiveness and economic aspects of squeeze treatments in water flooding is proper timing for starting the process. This should begin as soon as water breakthrough is accomplished. If the squeeze treatments are started too late, the well will plug, and, if too early, expensive chemical will be wasted [186]. The squeeze-treating technique can be a very effective inhibitor injection method when applied in producing formations with sufficiently porous strata. One of the disadvantages with the squeeze technique compared to other techniques is the longer shut-in time required to inject the chemical into and through the formation [181].

Comparison of Treating Techniques. The comparison between the mentioned inhibitor injection techniques has indicated that continuous, downhole-inhibitor injection is the most reliable and effective treatment method to mitigate corrosion problems in oil and gas wells. Table 6-67 is an effective comparison of various treating techniques [181,182,184].

The comparison of annual chemical injection costs for squeeze job, continuous injection and tubing displacement in Ekofish (North Sea) Field is shown in Table 6-68 [181,182].

Table 6-68 shows three, inhibitor-treating methods (cost of diluent = \$1.25/gal) ($C_{in} = 40$ ppm; chemical injection is based on the 5% and 10% inhibitor/diesel oil solution) (cost of inhibitor = \$8/gal). Squeeze costs are based on four treatments per year; tubing displacement is based on a monthly well treatment (12 treatments per year).

As shown in Tables 6-67 and 6-68, the advantages of continuous treatment over other treating techniques are well demonstrated by actual field work and literature surveys. The advantages of continuous, downhole injection of inhibitors over batch and squeeze jobs can be summarized as follows:

1. Continuous injection of inhibitors assures optimum corrosion control.
2. Corrosion-erosion attack is minimized by continuously applying inhibitor.
3. Inhibitor does not contact producing formation.
4. Shut-in time is not required.
5. Volume of inhibitor can be adjusted for changes in production rates.
6. Cost is minimized.

Corrosion in Water Floods

Water flood operation is a common enhanced oil recovery method used to increase the amount of oil recovered. Water can be used from natural sources, or produced water can be used for injection into the injection well. Sometimes the volume of water needed to inject and flood the reservoir exceeds as much

Table 6-67
Comparison of Corrosion Treatment Methods

Production				Efficiency %	Frequency (Days)	Formation Damage	Shut-In Time
Gas	Gas Cond.	Oil	Flow V				
Batch Treatment							
yes	yes	no	<Ve	60 to 80	<30	very unlikely	yes
Tubing Displacement							
yes	yes	yes	<Ve	80 to 90	<30	unlikely	yes
Formation Squeeze							
yes	yes	yes	>Ve	80 to 90	>30	possibly	yes
Continuous Treatment							
yes	yes	yes	>Ve	95 to 100	—	none	no

(Ve = erosional velocity ft/sec)

Table 6-68
Comparison of Annual Chemical Costs [181, 182]

Well Production/GOR Squeeze Continuous Tubing-Displacement			
100 bpd/5,000	\$123,000 (5%)	\$23,000 (10%)	\$110,000 (10%)
Cost Ratio	3.5	1	3.1
5,000 bpd/5,000	\$350,000 (5%)	\$60,000 (10%)	\$110,000 (10%)
Cost Ratio	5.8	1	1.8
10,000 bpd/5,000	\$415,000 (10%)	\$120,000 (10%)	\$110,000 (10%)
Cost Ratio	3.8	1	0.9
1,000 bpd/12,500	\$209,000 (5%)	\$35,000 (10%)	\$110,000 (10%)
Cost Ratio	6.0	1	3.1
5,000 bpd/12,500	\$502,000 (10%)	\$60,000 (10%)	\$110,000 (10%)
Cost Ratio	8.2	1	1.8

as ten times the oil produced. Briefly, the water-flooding process entails a number of steps as follows:

1. Locating a satisfactory source of water.
2. Treating water to prevent corrosion and scaling or to improve water quality.
3. Moving the high-pressure water through distribution lines to well-heads of injection wells and down the tubing to the formation.

The objective of this section related to the water-flooding operation is to explain the effect of injection water on corrosion and scale formation, and to decrease the use of corrosion and scale inhibitors in minimizing corrosion and scaling tendencies. As was pointed out earlier, oxygen is a potent corrosive, even in very low concentrations. Obviously, injected water contains considerable dissolved oxygen if the source of injection water is open to atmosphere. Injection water treatment can be divided into four problem areas that are classified as follows:

1. filtration
2. corrosion
3. scale
4. bacteria

Water quality is a function of the quantity and the nature of suspended solids. The water must be of such quality that it can flow into and through the formation at acceptable volumes and pressure without restrictive plugging. Some of the characteristics of solids and formations that enter into water quality are summarized as follows [180]:

Water	Rock
Turbidity	Porosity
Suspended particles	Pore size
Quantity	Pore size distribution
Shape	Tortuosity
Form	Permeability
Size	Fractures

Filtration is commonly employed to remove suspended solids and make water acceptable for injection. There are several types of filtration.

Both produced water and water from natural sources are carriers of dissolved gases, such as oxygen, carbon dioxide and hydrogen sulfide. Corrosion cells will not be established without presence of moisture or liquid water. Therefore, water-flooding operations deal with more corrosive environments than does primary production [187,188]. Although pure water, free of minerals and dissolved gases, is known to be practically noncorrosive, it is impractical in field operations to prepare water of such a quality. Basically, corrosion in water flooding is caused by organic or inorganic acids and oxygen.

Oxygen Scavengers. The film-forming amines as corrosion inhibitors have little effect in decreasing the concentration of oxygen. The most effective method to decrease dissolved oxygen is believed to be scavengers, which are applied to remove oxygen from water by chemical reaction. Chemical scavenging can be economically unacceptable when large quantities of oxygen are to be removed [189]. There are different kinds of chemical materials that are used as oxygen scavengers in the produced water and injection water. Commonly, sulfite ions such as sodium sulfite, sodium bisulfite, ammonium bisulfite and sulfur dioxide, as well as hydrazine, aided by metal catalysts such as Fe, Ni, Co, Cu and Mn are known as the most effective oxygen scavengers in the oil field. Sulfur dioxide (SO_2) is supplied in cylinders as a liquid under pressure. The oxygen removal reaction with SO_2 is



The amount of SO_2 required to remove oxygen is four times by weight the amount of oxygen present. Application of SO_2 is achieved by the use of a by-pass line. The scavenger is added to the by-pass fluids and returned to the system by a pump. Commonly, the material used for the by-pass system should be resistant to acid attack. A catalyst can be applied to accelerate oxygen removal. Precipitation of sulfate can occur as a result of reaction products in the presence of barium, strontium or calcium [150,172].

Ammonium bisulfite $[(\text{NH}_4)\text{HSO}_3]$ requires a 5:1 ratio by weight for reaction [172]. The ammonium bisulfite is injected directly into the system. A catalyst is not usually needed in oilfield brine, but usually is in fresher water. Sodium sulfite (Na_2SO_3) is also used to remove dissolved oxygen and is commercially available as a powder. The chemical reaction between sodium sulfite and oxygen can be written as



The amount of Na_2SO_3 required to react is eight times by weight the amount of dissolved oxygen present. A catalyst such as cobalt (Co^{2+}) is used in the range of 1 to 5 ppb based on the total fluids. A catalyst can be added directly to the Na_2SO_3 . Because a sodium sulfite solution will react readily with atmospheric oxygen, an inert atmosphere should be used during mixing and application. Metal ions, such as Fe^{2+} , Ni^{2+} , Co^{2+} , Cu^{2+} and Mn^{2+} , catalyze the sulfite-oxygen reaction [150,189].

Hydrazine is the most effective oxygen removal agent at higher temperatures of approximately 200°F. When the reaction must be catalyzed, the catalyst is most often added as the metal chloride. Hydrazine reacts with oxygen on a 1-to-1 basis on stoichiometry. Actually, hydrazine is shipped as a 35% liquid. The reaction equation is



One of the most practical oxygen scavengers that has a great deal of application in recent years in water flooding and steam generation is characterized by (1) a catalyst comprising an anthraquinone-disulfonic acid (AQ) and a vanadate salt, for example, sodium vanadate (Na_3VO_4), and (2) a reducing agent such as H_2S or hydrazine. The oxygen scavenging reaction can be written as [190]



and



Other sodium salts, such as sodium bisulfite, sodium meta-bisulfite and sodium hydrosulfite can be used as oxygen scavengers. Amine sulfites have had some success both as scavengers and as conventional corrosion inhibitors. Factors such as their cost, high ratio of scavenger-to-oxygen requirement, solubility, stability and compatibility have hindered increased field application.

The effective inhibition of oxygen corrosion usually involves passivating inhibitors such as chromates, nitrites, inorganic barrier formers such as calcium plus bicarbonate, zinc salts, phosphate combinations or silicates [191].

The majority of corrosion inhibitors employed to decrease the rate of corrosion by dissolved oxygen appear to be centered on variations of the zinc phosphate and organic components. A mixture of 0.1 to 1.0 ppm of hydrazine and film-forming, long-chain nitrogenous compounds such as imidazoline is reported to be very effective at concentrations of 5 to 200 ppm in water-flooding operations to minimize corrosion due to oxygen and dissolved gases [150,179,191].

Inhibition of Water-Flood Corrosion. Inhibitors used in water-flood operation are substantially like those inhibitors that are applied in primary production. Hydrogen sulfide, carbon dioxide, oxygen and other low-molecular-weight organic acids are believed to be the most important constituents that accelerate corrosion in water-flood operation. The use of oil-soluble, film-forming organic compounds as corrosion inhibitors is not practically recommended in water-flood operations because of the water-wetting phase on the metal surface and lack of oil phase. In the case of water-wetting phase in injection and production well

facilities, extensive attention should be given to the selection of the proper inhibitor that gives the desirable inhibition effectiveness. Generally, water-soluble organic compounds as corrosion inhibitors have reverse-wetting characteristics that can convert the water-wet phase on metal surfaces to oil wetting in the producing wells [178,179].

Because of the water-wetting phase factor, the use of water-soluble, film-forming organic corrosion inhibitors is becoming more acceptable in water-flooding operations. However, use of water-soluble inhibitors requires extensive laboratory investigation to establish effective inhibitors. Generally, water solubility of the basic, filming-amine type of inhibitor with molecules consisting of a carbon chain and a polar group, can be increased by increasing the solubility of the hydrophilic portion of the molecule. Also, it is noted that multiple polar groups such as diamines or imidazolines instead of monoamines will increase hydrophilicity. The most practical corrosion inhibitors in water-flood operation are variations of the following materials:

- primary monoamines
- polysubstituted monoamines
- diamines
- polyamines
- imidazolines
- quaternary ammonium compounds

Aminotri (methyl phosphonic acids) as corrosion and scale inhibitors are widely applied in water-flooding operations because of their high water-solubility [166]. The imidazoline-aliphatic acids salts are known to be applicable corrosion inhibitors in water-flood operation due to their high water-solubility [167]. The mixture of 5 to 200 ppm imidazoline and about 0.01 to 1 ppm hydrazine is noted to protect oilfield metals in water-flood operations [175].

Cyclic amidine salts as corrosion inhibitors are applied in environments with high concentrations of CO_2 , H_2S and O_2 . Inhibitors can be prepared either oil-soluble, water-dispersible or water-soluble. These materials as inhibitors are very effective in concentrations of 40 to 80 ppm in water-flood and primary production operations at 200°F [176,179].

Scale Deposition and Scale Inhibition. Scaling is the precipitation of dense, adherent material on metal surfaces and other materials. Normally, precipitation of scale-forming salts occurs when solubilities are exceeded because of high concentrations or unfavorable temperatures. The problem of scale in water flooding occurs all the way from the water injection facilities to the producing well. Generally, there are six important regions where scaling can occur during and after injection operations [152,186,192]. These are:

1. in the injector wellbore
2. near the injection-well bottomhole
3. in the reservoir between the injector and the producer
4. at the skin of the producer well
5. in the producer wellbore
6. at the surface facilities

Wide variations in temperature, total pressure and changes in pressure during production make practical control of scale deposition difficult in water-flooding operations. CaSO_4 (calcium sulfate), CaCO_3 (calcium carbonate), BaSO_4 (barium

sulfate), SrSO_4 (strontium sulfate), FeCO_3 (iron carbonate) and iron hydroxides are the most common scales in oilfield environments. Injection-water incompatibility with reservoir formation and brine, changes of the thermodynamic, kinetic, and hydrodynamic conditions under which the waters are found, injected and produced are the major causes of scale deposition in oil and gas wells.

There are some scale deposits in oilfield environments that are called *pseudoscale*; that is, the deposit of a reaction product between two or more human-introduced chemicals, or between a naturally occurring fluid and one or more human-introduced chemicals. For example, most water-soluble corrosion inhibitors have a tendency to establish pseudoscale. Also, scale inhibitors such as phosphonates and polymers react with Ca^{2+} and/or Mg^{2+} ions in oilfield brines, thus forming pseudoscales that look and behave exactly like "real" scale [179,192].

There are a number of reasons for precipitating scale. Temperature, pressure and water incompatibility are known to be the major causes of scale deposition in oilfield environments. Scales are usually formed in a supersaturation condition; that is, when the solubility product of a deposit-forming material is exceeded, it precipitates. Each scale is deposited under certain conditions that depend on temperature, pressure and mineral content.

A supersaturated solution is a solution that contains a higher concentration of a particular mineral than the solution can hold under the same set of conditions with its solute in equilibrium [179,193].

There are two states of supersaturation: metastable and labile. Figure 6-256 represents a normal solubility curve and two different states of supersaturation.

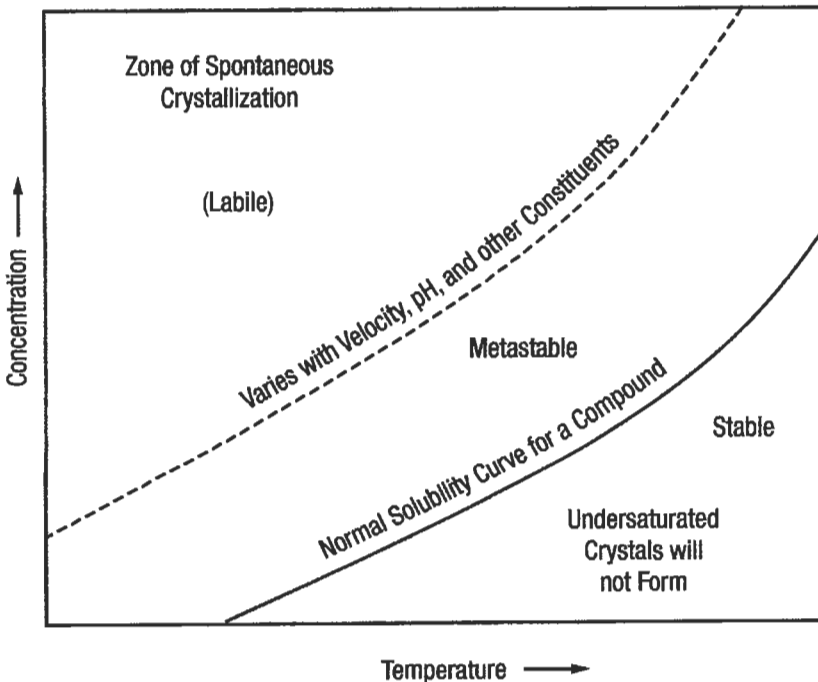


Figure 6-256. Variation of solubility and supersaturation with temperature [152].

It should be mentioned that a scale inhibitor tends to shift the dotted line, which is a function of fluid velocity, hydrocarbon content, agitation, temperature, pressure and pH, toward the solid line that represents the normal solubility curve. Normally, crystallization of scale will not occur in the stable region (unsaturated). In the metastable region, spontaneous crystallization does not occur nor do scales form rapidly. In the upper portion, above the dotted line that represents the unstable, or labile region, spontaneous crystallization is probable [152,192,193].

Barium sulfate crystallization and adherence will increase with decreasing temperature. Other factors that have direct influence on the solubility of BaSO_4 are increasing pressure and increasing salt content of the brine. Figure 6-257 shows solubility of barium sulfate as a function of temperature.

Ethylenediaminetetraacetic acid (EDTA) and nitrilotriacetic acid (NTA) are known to be the common solvents for barium sulfate. These solvents and some other similar chelating compounds break down the BaSO_4 crystals by tying up the Ba^{2+} ions. The dissolved Ba^{2+} ions are masked or chelated. Therefore, they become incorporated into new chemical compounds that are soluble [192-194].

The mechanism of scale inhibitors in preventing scaling tendency is very difficult to predict under a given set of conditions. Some scale inhibitors are believed to prevent the crystallization of a scale, and others are believed to prevent the adherence of crystals to themselves or to metal surfaces in the field. Obviously, if there is a scale inhibitor that can prevent crystallization of scale,

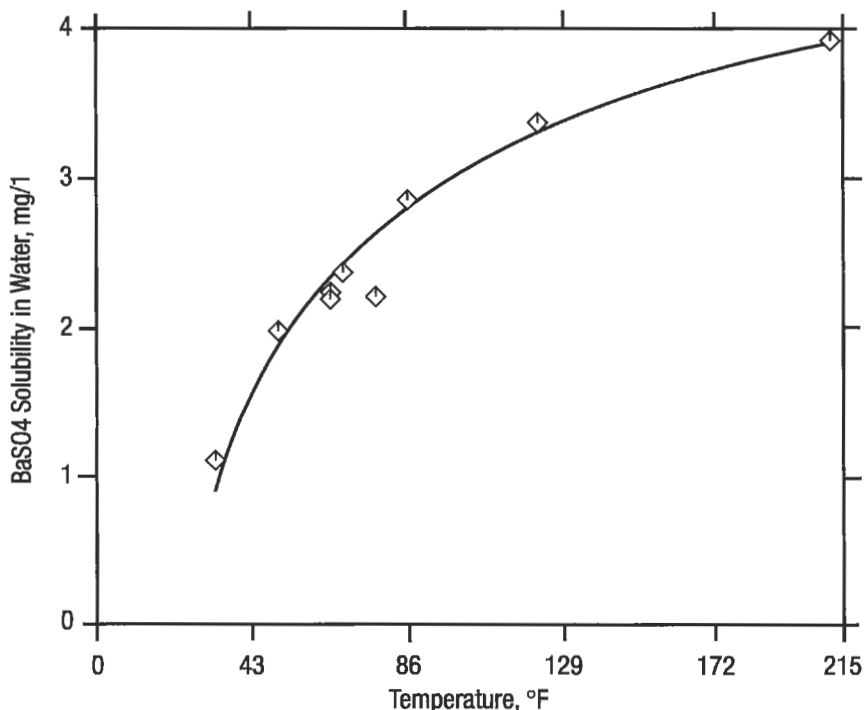


Figure 6-257. Barium sulfate solubility in water [236].

it can be sufficiently effective to minimize scale adherence tendencies. Commonly, the most effective scale inhibitors are the derivatives of one of the following chemicals:

1. polymers (polymaleic acids, polyacrylates)
2. esters of phosphoric acid
3. phosphonates, such as triethylenediaminetetra (methylene phosphonic acid)

The necessary concentration of scale inhibitor is a function of three variables—supersaturation, temperature and the chemical composition of the scale. The higher the supersaturation and the higher the temperature, the higher will be the inhibitor concentration required to prevent the precipitation of a given amount of scale per unit volume of solution. Extensive laboratory and field experiments indicate the inhibitors listed in Table 6-69 are effective against the BaSO_4 scale [179,196].

There are a few disadvantages of some of the scale inhibitors that lead to formation of emulsions and pseudoscale. Basically, the inhibitor reactions with dissolved ions in oilfield brines are believed to be the main causes of pseudoscale. The pseudoscales are mostly caused by interactions between the dissolved ions such as Ba^{2+} , Ca^{2+} and Mg^{2+} ions in the brine and the applied inhibitors. The pseudoscales act like a real scale. Therefore, additional problems caused by deposition of pseudoscales can be encountered with the application of improper inhibitors. Normally most oilfield operators try to solve emulsion problems by raising the temperature in the heater-treater. However, as temperature increases in the heater-treaters, more scaling is encountered. Therefore, the application of an effective inhibitor under specific conditions requires laboratory studies and field tests. To predict the emulsification tendency of an inhibitor with crude oil, a dynamic test is usually required under specific given conditions employing kerosene and/or the specific crude oil [179,192,193].

Strontium sulfate (SrSO_4) follows the same behavior and role as BaSO_4 . The strontium sulfate scale results mostly from mixing incompatible waters. As shown in Figure 6-258, solubility of SrSO_4 is a function of temperature. Most operators try to avoid strontium sulfate scale problems by preventing crystal growth and adherence of crystals to one another or to metal and/or porous media by applying an effective chemical. Field experiences indicate that phosphonate salts rather than polymers and phosphate esters show very good inhibition efficiency [179,192,193,196].

The phosphonate inhibitor in acid solution is injected into the producing zone by a squeeze treatment. Bottle tests of phosphonate inhibitors indicate that 95% protection can be provided at 10 ppm of inhibitor. The use of phosphate ester

Table 6-69
List of Some Effective Inhibitors for Barium Sulfate

Scale Inhibitor Type	Inhibitor Concentration ppm	Maximum Temperature °F
Esters	10 to 25	250
Phosphonates	10 to 25	350
Polyelectrolytes (polymer)	15 to 45	350

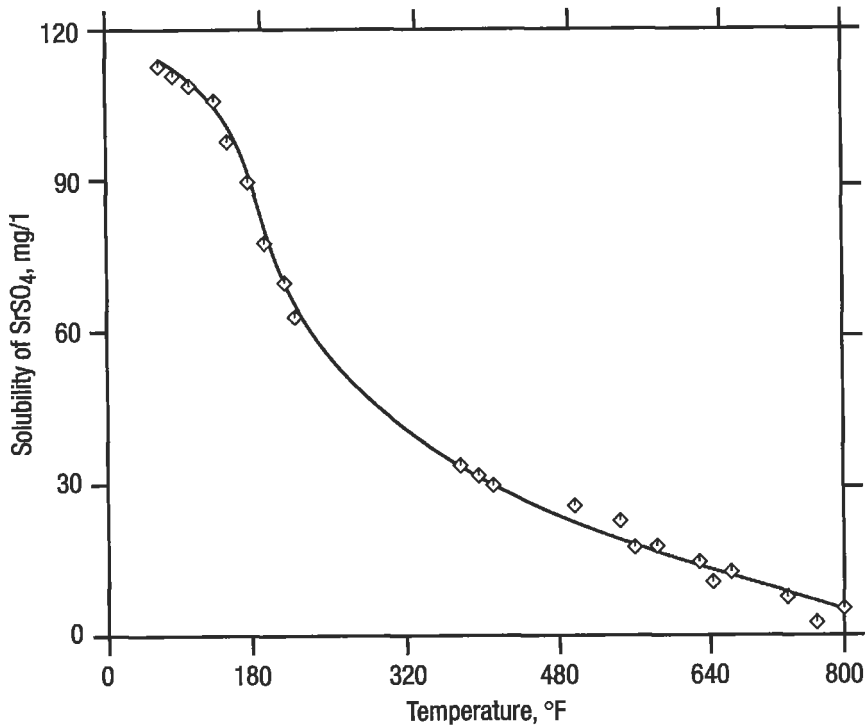


Figure 6-258. Strontium sulfate solubility in water [198].

for preventing crystallization or adherence of SrSO_4 is usually ineffective at temperatures above 200°F [196–198]. Strontium sulfate control by phosphonates salts has shown good results by squeezing these chemicals after acidification with HCl to form phosphonic acids in the Fateh field, where the strontium sulfate scale was found in water-flood operation because of incompatibility of injected water and brine [192,197,198].

Calcium sulfate (CaSO_4) is also known as one of the most common scales in oilfield environments. The main reason for the scaling difficulties experienced with calcium sulfate is the solubility behavior of calcium sulfate in its three forms: dihydrate or gypsum ($\text{CaSO}_4 \cdot 2\text{H}_2\text{O}$), anhydrite (CaSO_4) and hemihydrate ($\text{CaSO}_4 \cdot \frac{1}{2}\text{H}_2\text{O}$). Gypsum is less soluble at low temperatures but anhydrite is formed at higher temperatures. Pressure drops play a major role in deposition of gypsum and anhydrite scales. Figure 6-259 shows solubility of calcium sulfate as a function of temperature [192,199]. Some water-flooding operations in Texas and Wyoming have indicated significant production declines due to deposition of calcium sulfate. One of the major causes of calcium sulfate scale deposition in oil fields is known to be the presence of high quantities of native anhydrite in the reservoir formation as well as incompatibility of injection and reservoir waters [166,192,197].

Normally, fracturing jobs will increase the scale problem unless scale deposition is effectively prevented. The squeeze treatment is known to be the most effective method for application of scale inhibitors to prevent calcium sulfate deposition. One of the most effective scale inhibitors to prevent CaSO_4 scale is a water solution of imidazolines and aminotri(methylphosphonic acids) [166].

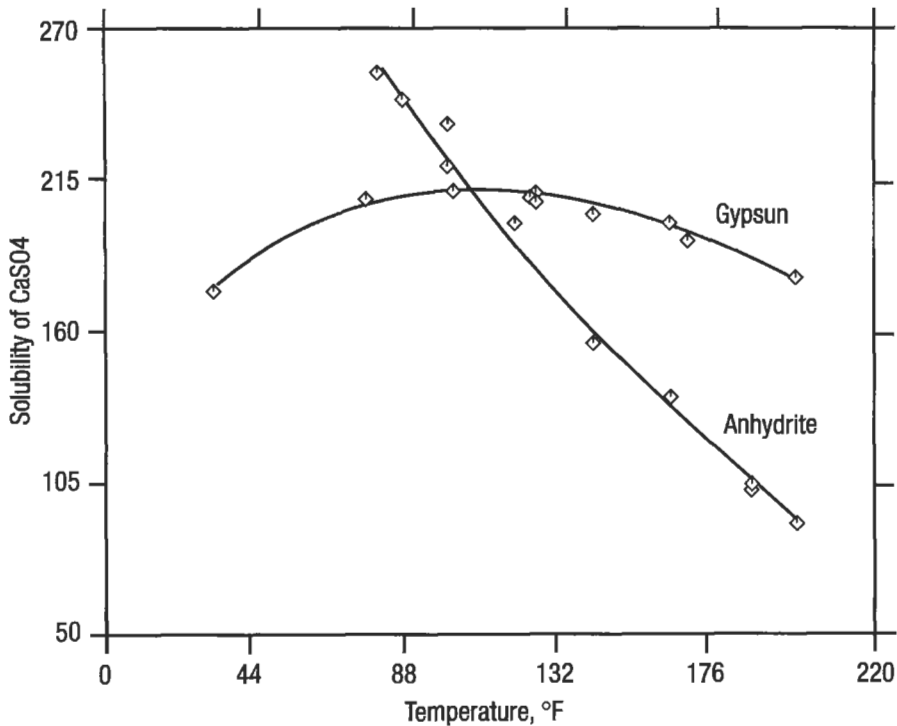


Figure 6-259. Calcium sulfate solubility in water [236].

This chemical composition as a scale inhibitor was tried in a well near Powell, Wyoming, in which calcium sulfate scale problems were known to be the only cause of the production decline of a well from 380 to 42 bpd. After physically breaking up the scale with explosives, the scale inhibitor at 130 ppm concentration was injected by a squeeze treatment. Table 6-70 is the production performance of the treated well with the mentioned inhibitor [166].

The majority of laboratory and field experiments show that phosphonates and low-molecular-weight polyacrylate scale inhibitors are effective in preventing the formation of calcium sulfate scale at temperatures up to 300°F. Experiments using phosphonates and polyacrylates have shown that metastable compounds such as gypsum scale were dehydrated to anhydrous calcium sulfate within the deposit. The additional influence of a phosphonate-type scale inhibitor at high temperature in a supersaturated calcium sulfate solution reduces the growth rate of all three forms of calcium sulfate crystals, but at 265°F the phosphonate-type scale inhibitors accelerate formation of anhydrite. To prevent the formation of anhydrite the application of a low-molecular-weight polyacrylic acid is suggested [196,200-202].

Calcium carbonate (CaCO_3) scale is normally encountered in primary oil production, water flooding, and carbon dioxide flooding. For a low carbon dioxide partial pressure, calcium carbonate shows lower solubility than it does at higher partial pressures. However, the temperature fluctuation, pH alteration, injection and produced water are the most influential factors in precipitation of calcium carbonate. Figure 6-260 shows the limiting pH level for CaCO_3

Table 6-70
Effect of Amino-Tri-(Methyl Phosphonic Acid)
as a Scale Inhibitor of Calcium Sulfate [166]

Days After Treatment	Inhibitor Concentration (in Production)	Production Rate bbl/day	
		Oil	Water
—	—	42	24
2	130	196	186
5	130	408	161
11	130	312	172
35	130	219	135
46	60	219	135
62	40	219	135
74	40	204	138
77	80	204	138
89	60	204	120
102	60	237	120
103	40	237	120
117	50	237	120
122	50	198	132

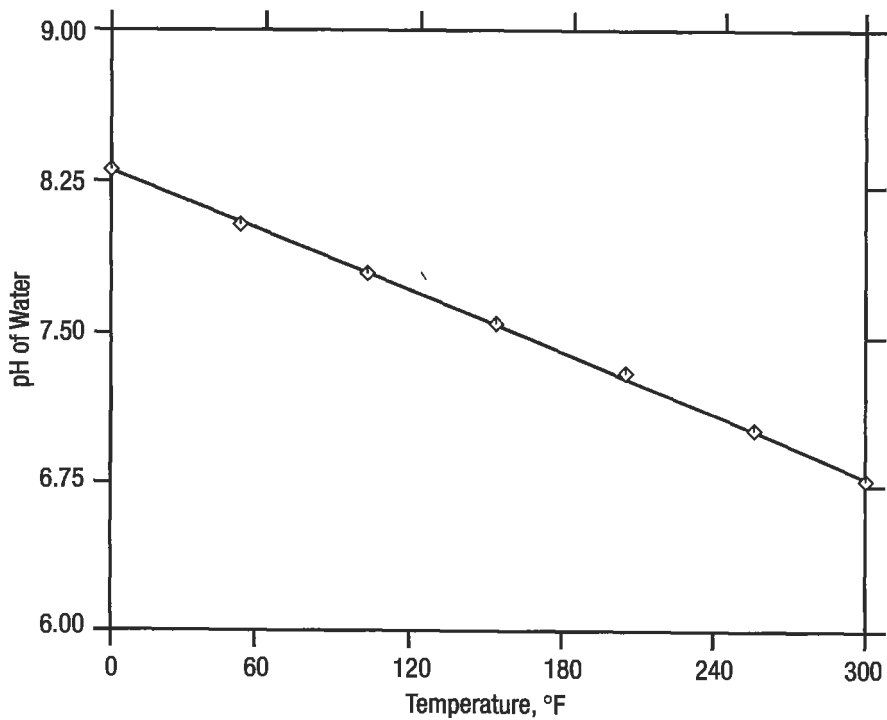


Figure 6-260. Calcium carbonate scaling threshold in normal seawater [163].

precipitation from normal seawater as a function of temperature. Other waters will have similar responses. Deposition of CaCO_3 scale results from precipitation of calcium carbonate according to the following equation [180]:



The solubility of calcium carbonate decreases with increasing temperature. Normally, when carbon dioxide comes in contact with water, it dissolves and forms carbonic acid, and carbonic acid is ionized by the following reactions:



The effect of carbon dioxide pressure on calcium carbonate solubility is shown in Figure 6-261 [203]. Normally, as the water is produced, the carbon dioxide

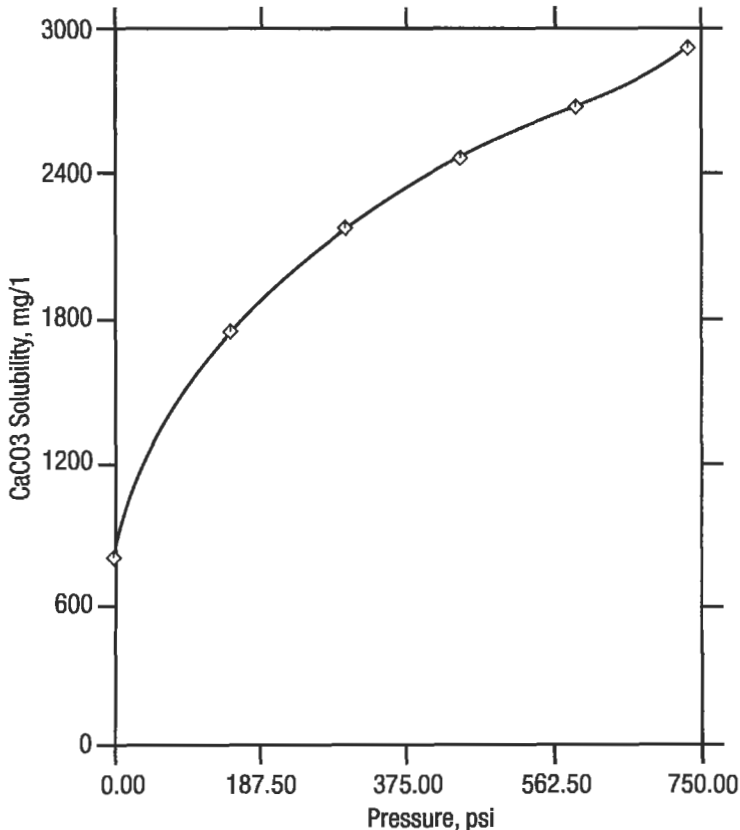


Figure 6-261. Influence of carbon dioxide partial pressure on solubility of calcium carbonate [203].

pressure decreases as the water reaches the surface. This phenomenon upsets the chemical equilibrium, and scale deposits. As was pointed out earlier, at lower temperatures calcium carbonate has higher solubility as shown by Figure 6-262 [203]. Therefore, calcium carbonate scaling tends to be lower at the surface facilities than at the production wellbore as predicted from temperature change. Table 6-71 shows solubility of calcium carbonate at different CO_2 partial pressures and temperatures [204].

The use of scale inhibitors is necessary to prevent calcium carbonate (CaCO_3) crystallization and adherence in water-flooding and carbon dioxide-flooding operations. Generally, the majority of scale inhibitors for prevention of calcium carbonate deposition are derivatives of phosphonates, phosphate esters and polymers such as polyacrylates and polymaleic acids derivatives [205]. One of the most useful scale inhibitors for reducing the growth rate of calcium carbonate crystallization at 215°F is hydroxyethylidene 1,1-diphosphonic acid (HEDP). Inorganic polymetaphosphates have a successful history of being applied as scale inhibitors. Normally, the original polymetaphosphates used as scale-prevention chemicals are sodium salts of metaphosphoric acid. Dimetallic

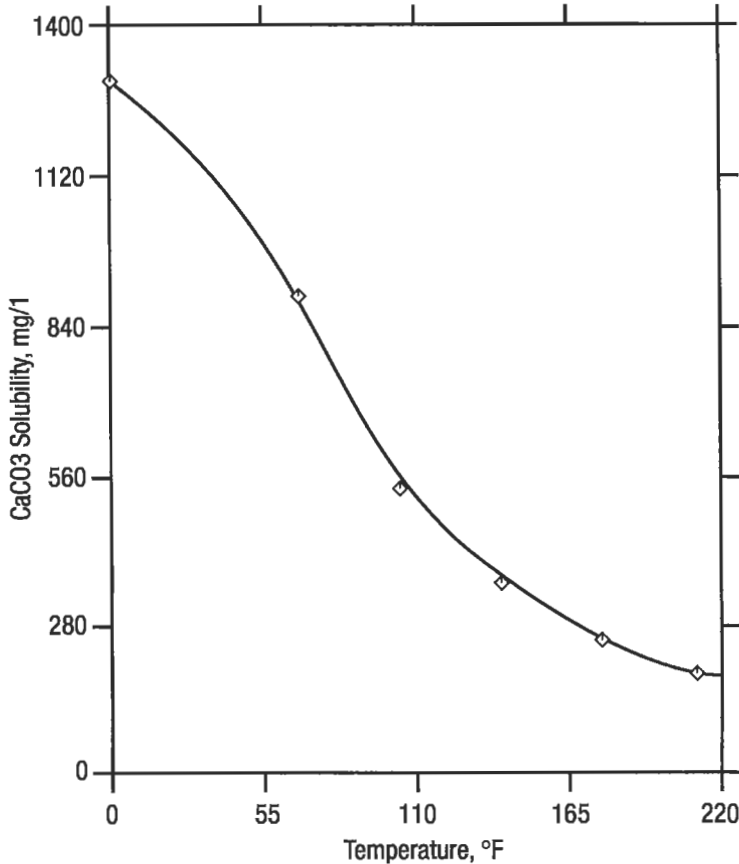


Figure 6-262. Effect of temperature on the solubility of calcium carbonate [203].

Table 6-71
Solubility of Calcium Carbonate at Different Temperatures
and Carbon Dioxide Partial Pressures [204]

Partial Pressure of CO ₂ , atm	Temperature F				
	100°F	150°F	200°F	250°F	300°F
1	0.261	0.094	0.040	0.015	0.006
4	0.360	0.158	0.063	0.024	0.009
12	0.555	0.221	0.091	0.036	0.012
62	—	0.405	0.152	0.051	0.014

(solubilities in g CaCO₃/1,000 g solution)

phosphates are known to be very effective in preventing calcium carbonate deposition. The concentration of dimetallic phosphate in order to stop and/or decrease scale deposition of calcium carbonate depends on amounts of carbonate dissolved in water. For example, for every 100 ppm of calcium carbonate, 2 ppm of dimetallic phosphate is necessary to prevent the precipitation [197,202-206].

Table 6-72 shows some typical phosphates used for preventing CaCO₃ scale formation in producing and injection wells. Normally, the concentration of these phosphates ranges between 5 and 60 ppm, depending upon water-cut, treatment application, water compatibility and type of scale formation [187].

Other scale inhibitors, such as organic compounds, have shown better results in inhibition of calcium carbonate and other scales formed at higher temperatures. Within these organic scale inhibitors, phosphonate materials are the most effective. The majority of experience in actual field environments indicates that the general types of organic materials used as scale inhibitors such as phosphonates, disphosphonates, phosphate esters and polyacrylates in concentration of 10 to 100 ppm, are effective in stopping scale deposition through squeeze

Table 6-72
Typical Phosphates as Scale Inhibitors of Calcium Carbonate [187]

Names of Phosphate	Formula
Tetrasodium Pyrophosphate	Na ₄ P ₂ O ₇
Sodium triphosphate	Na ₅ P ₃ O ₁₀
Trisodium tripolyphosphate	Na ₃ P ₃ O ₉
Hexasodium hexametaphosphate	Na ₆ P _{6c} O ₁₈
Sodium-calcium phosphate	Na ₂ O CaO P ₂ O ₅
Sodium-magnesium phosphate	Na ₂ O MgO P ₂ O ₅
Sodium-zinc phosphate	Na ₂ O ZnO P ₂ O ₅

treatments. Table 6-73 shows some typical phosphonates used as inhibitors against calcium carbonate scale [207]. Recently organic chelating agents have been widely used to complex with metal ions in water to stop scaling. One of the most common organic chelating agents is ethylenediaminetetraacetic acid (EDTA) or its sodium salts. EDTA forms stable soluble complexes with magnesium, calcium, strontium, barium, etc. When these metal ions have formed the soluble complex with EDTA, they cannot combine with the carbonate and/or sulfate ions in the water to form a scale. The use of chelating agents as scale inhibitors can be prohibitive in water-flooding operations because of their expense in the high volumes of water necessary for water-flood operations [192,206].

Microbiological Corrosion. Bacteria in injection water and produced water can contribute to corrosion. Bacteria may best be classified according to their oxygen requirement in order to grow. Obligate aerobes grow only in an aerobic environment where the presence of molecular oxygen is required. Obligate anaerobes grow only in an anaerobic environment in the absence of oxygen [208]. Bacteria present in injection water or other oilfield water generally grow best in the pH range between 5 and 9 and in the temperature range of 0°F to 180°F [208]. Normally, bacteria tend more to grow in freshwater, but some are capable of growth in brines. The establishment of oxygen concentration cells by microorganisms is very common in oilfield environments. Any species or mixed population of bacteria, algae or other microorganic growth that produces nonconducting layers on the metal surface would increase potential for differential oxygen cells as explained earlier [187,208].

Slime-forming microorganisms such as the iron bacteria (*Crenothrix* and *Gallionella*), which function only in the presence of air, can result in unwanted accumulations of iron oxide solids. Once an accumulation is established, the organisms increase the size and amount of deposit by their own growth and

Table 6-73
Typical Phosphonates as Scale Inhibitors of Calcium Carbonate [207]

Inhibitor	Formula
Aminotri (methylene phosphonic acid)	$N(CH_2PO_3H_2)_3$
1-Hydroxyethylidene-1,1-diphosphonic acid	$HOC(PO_3H_2)_2CH_3$
Ethylenediaminetetra (methylene phosphonic-acid)	$(H_2O_3PCH_2)_2NCH_2CH_2N(CH_2PO_3H_2)_2$
Hexamethylenediaminetetra (methylene phosphonic-acid)	$(H_2O_3PCH_2)_2N(CH_2)_6N(CH_2PO_3H_2)_2$
Diethylenetriaminepenta (methylene phosphonic-acid)	$H_2O_3PCH_2N[CH_2CH_2N(CH_2PO_3H_2)_2]_2$

by entrainment and absorption of suspended solids in the water. Since the microbial-debris mass is usually semipermeable, it separates the area immediately under the mass from the main water-stream. Oxygen concentration under the mass becomes lower than in the main water-body. This differential in oxygen concentration increases the cathodic area, and corrosion takes place in anodic areas under the deposit mass, causing pitting. Usually, the outer surface of the microbial-debris mass is reddish or tan colored due to the presence of oxides and hydroxides of iron. The mass itself may be slimy or hard and brittle, especially if carbonate or sulfate deposits are present. Sulfate-reducing bacteria, which are viable in the absence of air, produce hydrogen sulfide in the water, resulting in corrosion. Sulfate-reducing bacteria (*Desulfovibrio*) are the most important and damaging microorganisms in oil-producing operations. They are extremely efficient and active cathodic depolarizers. They react with the hydrogen available in water to produce hydrogen sulfide by the following reactions:



As is shown in the above reaction, for each molecule of sulfate ion that is reduced to a molecule of H_2S , about 10 atoms of hydrogen are needed. This explains the high rate of depolarization of the cathodes by sulfate-reducing bacteria. Another factor in acceleration of corrosion by sulfate reducers in a closed, air-free system is the production of insoluble iron sulfide as follows:



Iron sulfide (FeS) is cathodic to iron or steel surfaces. Therefore, when sulfate-reducing bacteria are localized and grow under debris, scale, or other bacterial masses in cracks or crevices where oxygen cannot penetrate, they accelerate corrosion rates. Sulfate-reducing bacteria and iron bacteria can produce masses that will plug water-injection wells and reduce flow in lines. Control of microorganisms requires extensive attention to the quality of water handling and treatment. Chemical treatment is the most effective and certain method to assure control of microbiological problems. Chemical products can be subdivided into two categories:

1. bactericides (biocides)
2. bacteristats (biostats)

Bactericidal (biocidal) chemicals are capable of killing various microorganisms, while bacteristats inhibit or retard the growth of bacteria, but do not kill the microorganisms at applied concentrations [188,208-210]. Some typical chemical compounds used as bactericides are shown in Table 6-74. Biocidal materials at high concentrations may often act as biostats at lower concentrations.

In addition, the following chemical compositions are recommended as biocides and corrosion inhibitors [211]:

1. acridine phosphonic compounds
2. dihydroacridine phosphonates
3. dihydrophenanthridine phosphonates
4. dihydro-aromatic nitrogen-heterocyclic phosphonates
5. nitrogen heterocyclic phosphonic acid
6. nitrogen heterocyclic phosphates
7. quaternary "full" nitrogen-heterocyclic phosphonates

Table 6-74
List of Some Bactericidal Chemicals [212]

Type of Chemical Compound	Name of Chemical	Formula	Physical Form	Concentration Employed, ppm
Chromium	Sodium chromate	$\text{Na}_2 \text{CrO}_4$	Solid	500
Mercury	Mercury chloride	Hg Cl_2	Solid	50-300
Silver	Silver nitrate	Ag NO_3	Solid	0.05
Amine	Coco primary amine acetate	$(\text{R-NH}_3)^+$ $(\text{CH}_3\text{COO})^-$	Solid	10-40
Diamine	Coco trimethylene diamine		Liquid	5-25
Quaternary Ammonium	Alkyl trimethyl quaternary ammonium chloride	$\text{RN} (\text{CH}_3)_3 \text{Cl}$	Liquid	25-100
Imidazolines	1-Pheny-4, 4-dimethyl-imidazoline	$\text{C}_6\text{H}_5\text{NCHNC}(\text{CH}_3)_2\text{CH}_2$	Solid	75-100
Chlorinated Phenols	Sodium tetrachloro phenate	$\text{NaOC}_6\text{HC}_{14}$	Liquid	10-85
Aldehydes	Acrolein	$\text{CH}_2=\text{CH-CHO}$	Liquid	10-85
Peroxygens	Peracetic acid	$\text{CH}_3\text{COO}_2\text{H}$	Liquid	>10

Commonly, bacteristats should be applied in injection and/or production wells by continuous treatment. Other treatments, such as slug treatment and intermittent and squeeze treatments, are not suggested for application of bacteristats. There is not any restriction on application methods of biocides except from an economic point of view. There are some factors that should be considered when chemical treatment is employed [212]:

1. Cleaning a system is of primary importance in treating microbiological problems. The system can be cleaned by acidizing, scrapers, applying detergents and solvents, and other cleaning methods.
2. Chemicals selected for treatment should be evaluated in the laboratory for effectiveness of kill at various concentrations. The upper limitations on concentration of bactericide are determined by cost as well as on kill requirements.

3. The uses of biological control agents are covered by different laws and regulations. The Federal Insecticide, Fungicide, and Rodenticide Act requires the registration of all materials that claim biological control capability. With this registration, the manufacturer must not only provide proof of effectiveness, but also must relate environmental effects that could occur as a result of the use of the material.

Recommended Procedures for Corrosion Control

During production operations, failures of tubular goods and equipment are mainly caused by the presence of carbon dioxide, hydrogen sulfide, oxygen and water. The following general procedures for a new design are recommended.

1. Evaluate the type of corrosion that might occur. In production operation, hydrogen sulfide, carbon dioxide, oxygen and water are the main causes of corrosion.
2. Unless unavoidable, use high-alloy metal steels with a yield of below 80,000 psi and 90,000 psi tensile strength for "sour" environment. While designing the tubular goods and equipment most compatible to the environment encountered consider the metallurgical factors and alloying elements for "sweet" and "sour" oil and gas environment.
3. Select the best and economically feasible inhibitor by considering similar situations and past experience with conditions close to those encountered. In the case of an unique condition, extensive lab tests should be performed to confirm the effectiveness of the inhibitor.
4. Determine a method of application by considering its effectiveness, economy and frequency of application.
5. Monitor and inspect the equipment if possible and keep track of the performance to evaluate and update the program treatment.

To control the corrosion in the tubing, casing and surface equipment for a system already in operation, the material cannot be chosen since it is already in use. In this situation, corrosion can be controlled by a judicious selection of inhibitors and practical method of applying the inhibitor. A general procedure in existing system is as follows:

1. Select the most effective inhibitor for the case. If possible, investigate its performance for similar situations in the field and in the lab. For hydrogen sulfide, filming amines and organic phosphates are reported to be effective corrosion inhibitors. Filming amines are also reported to be effective for carbonate dioxide.
2. Determine the most effective concentration and amount of the inhibitor.
3. Use a practical method to apply the inhibitor to the system. Since the continuous method, especially with a capillary system, is reported to be the most effective and economical, this method should be considered strongly if applicable.
4. Determine the frequency of application.
5. Monitor and evaluate the performance of the system and adjust the treatment program according to the observation.

In water flooding not only is corrosion more severe than in primary production, but also there are scale problems. Since water is open to atmosphere, it dissolves more oxygen. Necessary water treatments include:

1. Filtration: to remove the suspended solids from water.
2. Oxygen scavengers: to reduce the oxygen concentration.
3. Scale inhibitors: either to prevent crystallization or prevent the adherence of crystals to the surface. It should be mentioned that improper use of scale causes pseudoscale; therefore, extensive field and lab tests should be performed to prevent this problem.
4. Chemical treatment for bacteria: to reduce or eliminate the bacteria population.
5. Corrosion inhibition: basically this is the same as primary production. It is more desirable to use inhibitors that reduce scale and are effective corrosion controllers.

Transportation and Storage Equipment

Surface equipment that is used to transport and store crude oil, refined liquid product and natural gas are quite prone to corrosion since they exist and operate in constantly changing environments (i.e., temperature and humidity).

Crude Oil and Liquid-Product Pipelines

Internal corrosion in product pipelines, in most cases, is caused by water and oxygen dissolved in the product. Dry refined products with normal additives are noncorrosive to steel pipelines. The products are corrosive because of associated water and air. A film of liquid water adheres to the pipeline surface, and oxygen is available from air dissolved in the product. The solubility of air in products varies, but there seems little doubt that refined products carry sufficient oxygen to support corrosion. Air is introduced into the products by tank mixers, turbulence, normal tank breathing, etc.

Even though the product is clear when it is placed in the pipeline, indicating absence of free water, temperature drops may occur during transit and cause water to separate. Table 6-75 shows increasing solubility of water in gasoline as temperature increases. Table 6-76 indicates the range of solubility of water in some pure hydrocarbons. The important factor is the change in solubility per increment of temperature change. From Table 6-76 a 17°F increase in temperature doubles the solubility of water in n-pentane.

Table 6-75
Solubility of Water In Gasoline

Temperature F	Solubility Gal/1000 bbl
40	1.8
50	2.1
60	2.4
70	2.7
80	3.0
90	3.3
100	3.6
110	4.0

Table 6-76
Solubility of Water in Specific Hydrocarbons

Hydrocarbon	C	F	Solubility	
			mg/100g	Gal/1000 Bbl
n-butane	20	68.0	6.5	1.5
isobutane	19	66.2	6.5	1.7
n-pentane	15	59.0	6.1	1.6
	24.8	76.6	12.0	3.2
isopentane	20	68.0	9.4	2.4
n-hexane	20	68.0	11.1	3.1
cyclohexane	20	68.0	10.0	3.3
n-heptane	20	68.0	12.6	3.6
n-octane	20	68.0	14.2	4.2
benzene	20	68.0	43.5	16.1
heptene-1	20.5	68.9	104.7	30.8
butene-1	20	68.0	39.7	11.1

Water is often carried into the pipeline as a separate phase. For example, where conventional floating roof tanks are used during heavy rains, it is difficult to keep water from entering the product while it is being pumped to the pipeline. Covered floating roof tanks practically eliminate rain as a source of water [213].

Methods of Control. Internal corrosion can be controlled by removing one of the active ingredients, water or air; by adding an inhibitor which will make the steel inactive; or using a barrier coating on the steel.

Deaeration. Deaeration alone is probably not a practical method for controlling corrosion. However, if large amounts of oxygen are present in the product, it is desirable to reduce the oxygen content to an acceptable level.

Dehydration. Dehydration can be used to control corrosion if the water is kept at a low level. This method requires considerable equipment and manpower for maintenance, so the cost is high for control. Free water can be removed in the storage tank by allowing the water to settle out of the product. Free and entrained water can be removed by using water separators and coalescers. This is best done by filtering the products entering the system.

Rust particles, dirt, etc., in the product will settle out in the low section of the pipeline if the flow velocity is not sufficient to keep the particles entrained. These particles, being of dissimilar electrochemical properties to the underlying metal, will form local corrosion cells in the presence of water. They will be filmed with a chemical inhibitor the same as the pipe, and this causes depletion of available inhibitor to protect the line. Most filters are designed to prevent free water from entering the system. Some of the common types of filters used include (a) hay tanks, (b) cartridge type, (c) centrifugal type. Selection of the filter will depend upon the application and design of each pipeline.

Inhibitors. Chemical inhibitors can be divided into inorganic and organic compounds. Inorganic inhibitors, such as sodium nitrate, are usually water soluble; sodium nitrate was used with good results [213]. When using sodium nitrate, the pH must be above 6 because in an acid environment it decomposes, forming volatile nitric oxide and nitrogen peroxide.

The most common method employed today in controlling internal corrosion is the use of organic or oil-soluble inhibitors. These inhibitors are generally hydrocarbons (with polar group attached) that tend to form a protective film on the pipeline's internal surface [213].

Water-Soluble Inhibitors. Water-soluble corrosion inhibitors are widely used to solve internal pipeline corrosion problems. Because of the relatively short film life of water-soluble corrosion inhibitors, they are continuously injected as opposed to the batch-treatment method.

Because water on the bottom of the pipe is the primary source of the corrosion problem, one might assume a water-soluble inhibitor to be the answer to treating a pipeline carrying crude oil and water. However, another problem must be considered. The portion of pipe occupied by the oil and water emulsion is also a corrosive environment. Under such conditions, a water-soluble inhibitor will probably not provide adequate protection. However, there is laboratory evidence that a portion is absorbed into the oil, and this can provide some protection in the oil phase (see Figures 6-263 and 6-264) [214].

Oil-Soluble Inhibitors. The use of oil-soluble corrosion inhibitors is widespread in systems handling both oil and water. This type of inhibitor may do a good job protecting small-diameter pipelines because high velocity or turbulent flow prompts mixing of the inhibitor and produced fluids. However, due to reduction in velocity or turbulence, it may not provide the desired protection in large flowlines or pipelines carrying these same fluids.

The oil-soluble inhibitors have the advantage that they may be injected at the refinery during the normal blending operations and will protect the refinery piping, the pipeline, the gasoline station tanks, etc. This advantage is fully realized when a company operates its own pipeline and handles its own products. Similarly, common-product pipelines can inject inhibitor at source points only, or can require shippers to supply inhibited products [215].

Mechanics of Inhibitor Application

Inhibition can be accomplished by one of two general methods—by batch (intermittent) treatment or by continuous injection. Batch treatment normally entails pumping a suitable-size slug of pure or high-concentration inhibitor solution through the line. Frequency of the treatment is governed by the effectiveness of the inhibitor remaining after a given time or after a specified amount of product has been moved through the line.

Continuous injection consists of adding a constant volume of inhibitor to the product being transported through the pipeline. This method is probably the most desirable and widely used.

Injection facilities vary greatly in design and operation, and in general the installation consists of the following equipment units:

1. inhibitor storage vessel
2. injection pump
3. measurement device (meter or calibrated sight glass)
4. connection to the pipeline

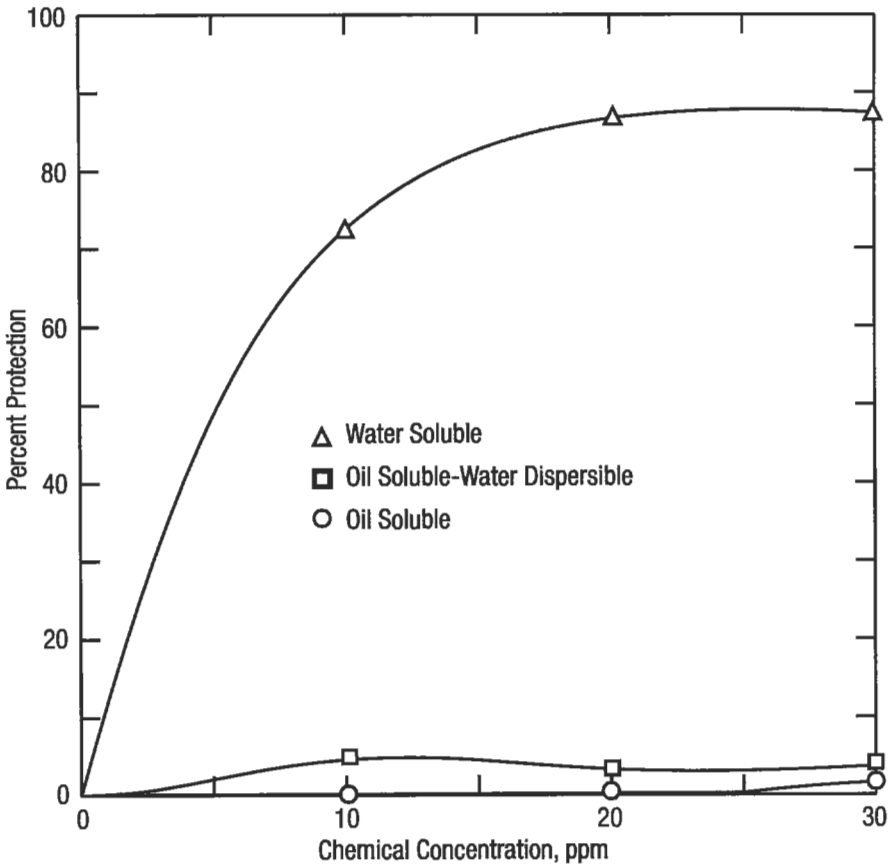


Figure 6-263. Sweet corrosion wheel test [214].

Positive-displacement chemical pumps, with adjustable capacity, are probably the most widely used on product pipelines [216].

Construction materials for the equipment should be suitable for continuous service when in contact with the inhibitor. Plain carbon steel or stainless steel should be suitable for most applications. Stainless steel should be considered for small-diameter piping or tubing where even minor rusting could cause plugging and make pumping of more viscous liquids difficult. When handling nitrogen-based inhibitors (amines, amides, nitrites, etc.) the use of copper or copper-based alloys should be avoided, as stress corrosion cracking might result. Nonmetallic seals and packing materials should be checked for compatibility with the inhibitor formulation [217].

Points of injection should be chosen to provide maximum benefit in the pipeline system. Injection on the suction side of pumps takes advantage of pump turbulence to promote mixing of the inhibitor with product. Injection through a tube into the center of the pipeline also aids mixing.

Premixing or dilution of the inhibitor can improve handling and promote a more rapid phase-contact. Viscous inhibitors can be diluted with compatible hydrocarbon carriers to decrease viscosity, making pumping easier and metering more accurate, especially at low-dosage rates. Premixing water-phase inhibitors

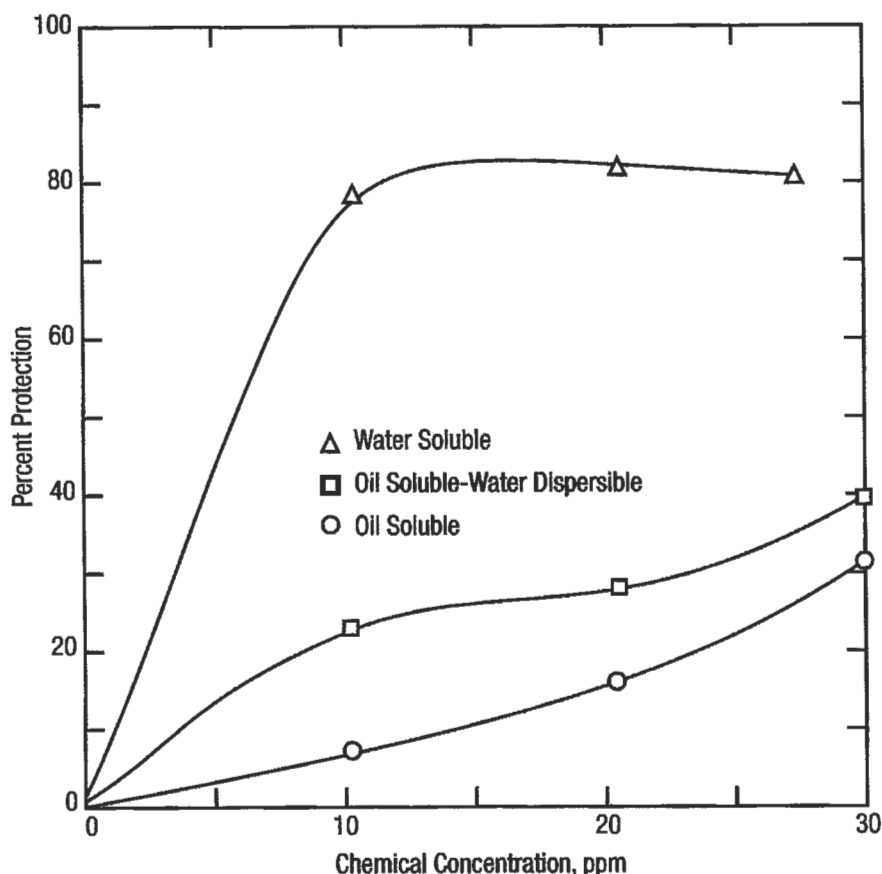


Figure 6-264. Sour corrosion wheel test [214].

with water prior to injection greatly facilitates phase contact of inhibitor with entrained water.

A typical dosage of oil-soluble inhibitor in refined products is in the range of 3 to 6 ppm. This amounts to 1 to 2 lb per 1,000 bbl.

When using an inhibitor, it should be remembered that all the natural protection, such as iron oxide, is removed and a protective film is put on the pipe's surface. If this film is removed by uninhibited products, the pipe's surface is very susceptible to the water and oxygen in the product, and corrosion begins immediately. It is important that the film remain intact so this condition cannot exist. Tests have shown that uninhibited products can be pumped up to 30% of the time without serious corrosion problems if the products pumped before and after the uninhibited product contain an adequate amount of inhibitor [213,218].

Use of Protective Coatings. Internal pipe coatings, no matter how applied, definitely provide a benefit by reducing power costs, increasing flow and eliminating corrosion [219]. Rehabilitating a pipeline with in-place internal coating versus replacement returns the line to active service. During research of flow improvement due to pipe cleaning, additional studies were made to

determine the improvements in pipeline flow and corrosion protection with the use of coatings [220]. The conclusion was that both flow improvement and corrosion protection were evident.

There is no present limit to the pipeline services that can benefit from coatings [221]. Typical services include crude oil, natural gas and petroleum-product pipelines. It is essential that a pipe coating perform the service of corrosion prevention for which it is designed to attain the safety and economic standards of the pipeline. McConkey has listed the following properties required of a pipeline coating [222]:

- ease of application
- good adhesion to pipe
- good resistance to impact
- flexibility
- resistance to soil stress
- resistance to flow
- water resistance
- electrical resistance
- chemical and physical stability
- resistance to soil bacteria
- resistance to cathodic disbandment

These properties all relate either to the economic viability of the coating or to the ability of the coating to protect the pipeline from damage and possible failure due to corrosion.

The coatings that best meet the needs of the pipeline industry are the polyamide epoxies and amine-adduct-type coatings [223]. A comparison of the two types is presented in Table 6-77.

Control Criteria. The ultimate criterion for control is securing the maximum volume per horsepower unit. This is accomplished by obtaining the smoothest possible internal pipe section; that is, the least possible friction. The friction factor is expressed as the modified Hazen-Williams C factor:

$$C = \frac{162.04QS^{0.54}}{P^{0.54}D^{2.63}} \quad (6-355)$$

where Q = barrels per hour
 P = pressure drop per mile in psi
 S = specific gravity at operational temperature
 D = internal diameter of pipe in inches

which can be rewritten as

$$C = Q \frac{162.04}{D^{2.63}} \times (S/P)^{0.54} \quad (6-356)$$

This concept can also be expressed as efficiency. This is

$$e = \frac{B}{4.06(d^5 I/s)^{1.2} (\log d^3 sI/z^2 + 4.35)} \quad (6-357)$$

Table 6-77
Coating Comparison [223]

Property	Coating	
	Amine	Polyamide
Hardness	5H to 6H pencil hardness, Faster initial cure.	4H to 5H pencil hardness, Slower initial cure.
Tolerance to inadequately prepared surface	Good	Very good
Brittleness	Very brittle in a few months	Same resiliency remains after a few months
Sag resistance (5-7 mil wet)	Good	Good
Adhesion	Good	Good
Application characteristics	Very good	Excellent
Flexibility	—	Best
Abrasion resistance	Equal	Equal
Water resistance	—	Best

where e = line efficiency factor

B = barrels per day

d = internal diameter of pipe in in.

I = pressure drop per mile in psi

s = specific gravity of product at operating temperature

z = absolute viscosity in centipoises at operating temperature

The generalized values shown in Table 6-78 can be used for absolute viscosity without introducing too much error. A pipeline constructed of new pipe and that has been efficiently inhibited or dehydrated will have C factors of 155 to 160 or efficiency factors of 95 to 99% [224].

Natural Gas Pipelines

Oxygen, carbon dioxide and hydrogen sulfide are the main corrosives in natural gas pipelines, and they are aggressive only when they are absorbed into water or condensed moisture in the lines. Most pipeline gas has been sweetened and dehydrated as well as treated otherwise before it is pumped into transmission lines. Consequently, most of the corrosion problems in gas systems occur in the various gathering lines and in the piping and equipment used for removing liquid hydrocarbons and sulfur.

While inhibitors may be slugged, injected or sprayed into a gas stream, they function only to the extent that they are adsorbed onto or react with the steel to set up a barrier between it and the aggressive agents [224].

Natural gas pipelines can be classified as either wet or dehydrated. Most of the internal corrosion problems discussed thus far are characteristic of wet-gas pipelines.

Dehydrated systems are usually characterized by a water vapor content in the gas less than saturation and the sporadic movement of fluids through the system. The corrosive contaminants, particularly carbon dioxide, may still be present in the gas, but if there is no liquid water into which they can absorb, they are not corrosive [225].

Types of Corrosion. Natural gas pipeline corrosion is an electrochemical reaction. To have corrosion, there must be an electrolyte, as well as a cathode and an anode, present; also there must be direct current flow between them. Corrosion can be inhibited by blocking the action of any of these components.

The three most common types of internal corrosion are "sweet" corrosion, caused by CO_2 or organic acids, plus water; "sour" corrosion due to the presence of H_2S and water; and oxygen corrosion, caused by the interaction of O_2 and water.

The "sweet" variety causes general loss of metal and shallow areas of localized attack. "Sour" corrosion results in pitting and cracking of internal pipeline surfaces, and forms insoluble iron sulfide. It can occur quickly and may often result in metal loss of considerable magnitude during a relatively short time.

Oxygen corrosion causes loss of metal and creates an iron oxide film. It results in extreme pitting.

With reservoir gas quality diminishing due to increasing production of sour gas fields, it is probable that most gathering and transmission lines are subject to any or all of these corrosion types—some severely, others to a more subtle degree. However, either way, all are materially and economically destructive [224,226,227].

Inhibition of Natural Gas Pipelines. The inhibition of corrosion in gas pipelines is a very complex subject, due to many varied conditions in gas pipelines; however, recent research has shown that under many pipeline conditions, inhibition may be simpler and more effective than previously believed possible. The major problem in treating these lines is the distribution of inhibitor to the corrodible areas. How do we get an effective, nonvolatile inhibitor to the top and sides of a pipeline? How do we get a nonvolatile

inhibitor to carry through the entire length of a pipeline? Under proper conditions, these are all possible using the simplest of application methods. According to EnDean all we need to know are [228]:

1. diameter of the line
2. length of the line
3. volume of gas in MMcfd
4. pressure
5. pressure drop
6. temperature
7. volume of liquid water through the pipe
8. volume of liquid hydrocarbons

From these data, we can predict if there is annular flow in the pipeline. If there is annular flow, then all that is necessary is to add the inhibitor as a solution. Transport and distribution of the inhibitor along the pipeline is assumed. The eight variables listed define the flow conditions in a pipeline and thus determine the method and type of inhibitor treatment that is required [229]. Other useful information is [230]:

1. gas analysis to help predict the severity of corrosion, particularly the percent CO₂ and H₂S
2. water content of the gas at entry and exit from the pipeline
3. oxygen content
4. presence of any solids

Selection and Application

System analysis. There is no panacea for inhibiting corrosion; therefore, we need to evaluate what it is we want to do, and where it is we need to protect. It is a safe assumption that anywhere water is present, there is a potentially corrosive environment. It is also safe to assume that anywhere free water is removed, a water-soluble inhibitor will also be removed (i.e. drips, separators, slug catches). Downstream water condensation presents a whole new problem. A complete understanding of the system to be treated allows one to determine where and how many injection points are required.

Corrosivity encountered or expected. Simply stated, do we have a corrosive situation, and if so, how severe is it? In the case of existing systems, what sort of monitoring background do we have in the worst case, and what is the leak frequency? It is interesting to note that even if it takes 5 years to experience the first leak, it almost never takes as long a time to have another.

In designing new systems, it is important to include a treatment program for immediate use or use when the system becomes corrosive.

Water behavior and quality. By behavior we mean: Is water an ever-present phase of the system, or is it present only as a result of system upset or downstream condensation? In either case, pigging can be most effective because of water accumulation in low spots.

In the case of continuously flowing water, a continuous injection program is desirable and quite effective. This approach is desirable and quite effective. This approach affords continuous feed to the water, and, thus, continuous filming of the inhibitor from the water traversing the system.

The selection of an inhibitor for continuous injection is crucial in that certain determinations are required before selecting the proper inhibitor.

The chemistry of inhibitors is such that they can exhibit different solubility characteristics in different waters. For best results an inhibitor needs to be dispersible in water, thereby filming from the water phase and not readily removed by water flowing past it. Some inhibitors, although dispersible in one water, can be affected by certain cations in another, to render them insoluble or to form insoluble additional products or solids (salts).

Chemical selection and use rate. Factors in chemical selection are summarized as:

1. solubility
2. compatibility with process equipment
3. effectiveness in similar systems
4. stability
5. selection based on application

One of the most difficult aspects of treating pipelines is determining the most economical amount of inhibitor to use. Knowing the liquid volumes in a line, especially the water, makes it easier for one to select the proper chemical.

Determination of cost versus effectiveness. To determine whether the concentration, based on gas volume, is more than adequate, or inadequate, there are tests to determine chemical concentrations in water; these are called *residuals*. This information, combined with comprehensive monitoring, allows for maximum protection at minimum cost. It should be realized that residuals can fluctuate widely in systems where water volumes are subject to great fluctuations. These residuals are still very useful when monitored over a period of time and a statistical average determined.

Proof of the treatment. Once an inhibitor program has been selected and the appropriate application initiated, a very crucial step still remains before a complete program can be initiated. This is a method of monitoring the efficiency of the proposed treatment. Although the complete effect-revealing, monitoring program has not been developed, there are many tools available to strive for perfection. These range from wet analysis of fluids to on-line continuous recording devices for corrosion rate termination [231].

Types of Inhibitors. Most inhibitors are classified as:

1. oil soluble
2. oil soluble/water dispersible
3. water soluble
4. oil/water dispersible (but insoluble)

The most common gas pipeline inhibitors are as follows:

Petrolite Corporation

KG-2. Water-soluble, oil-insoluble. Organic filming inhibitor designed to flow in dehydrated gas pipelines and systems. KG-2 is best applied continuously and is recommended for any gas system where the following conditions are present:

1. dehydrated gas lines
2. injection into hot gas (above water dew point), which will cool to dew point in the pipeline
3. immediately downstream from compressors

KG-6 is oil soluble, water-dispersible and is a combination of a volatile amine and organic filming inhibitor. It is best applied continuously in wet, sweet (CO₂) and sour (H₂S) gas systems to utilize its volatile portion.

KG-7. Water dispersible, oil-insoluble. KG-7 is an organic filming inhibitor designed to flow in dehydrated gas pipelines and systems. Applications are same as KG-2.

KG-8. Water dispersible, oil-insoluble. KG-8 is an organic, filming inhibitor, best applied in a continuous injection for both sweet and sour "wet" systems.

KG-9. Highly water soluble; oil-insoluble. KG-9 is an organic filming inhibitor. Designed primarily for application in high salinity brine waters; applied continuously in both wet, sweet and sour systems.

KG-10. Oil-soluble; water-dispersible. KG-10 is an organic filming inhibitor. Excellent for batch treating or continuous treating. Very effective in emulsion prevention. KG-10 can be applied:

1. continuously
2. by batch treatment
3. in combination with pigs

KG-11. Oil soluble; water dispersible. KG-11 is a heavy organic filming inhibitor recommended for batch treating, preferably between two pits or in front of one pit. Application should allow for a 2 to 3-ml-thick film of KG11/diluent solution throughout the entire surface of the pipeline.

KG-15. Oil-soluble; water dispersible. KG-15 is a concentrated combination of volatile amine and filming inhibitor (a three-phase type inhibitor) applied on a continuous basis, to utilize the volatile portion and maintain the protective inhibitor film.

KG-18. Oil-soluble, water-dispersible. KG-18 is a combination of an organic film-former and a quaternary ammonium compound. This product can be used for continuous treatment and for batch treatment, before or between pigs or line balls.

KG-19. Oil-soluble, water-dispersible, hydrocarbon-based volatile amine. The volatility of KG-19 is such that in most systems it will vaporize and be carried along with whatever acid gases are present in the vapor phase. When water is encountered and the acid gas dissolves in it to form a corrosive acid liquid, the amine is present to dissolve in the water, neutralize the acid, and reduce the corrosivity of the water. The amount of KG-19 required is largely dependent on the amount of acid gas and water present, but generally $\frac{1}{2}$ to 2 pints of KG-19 per MMcf gas are adequate.

KG-20. Oil-soluble; water-dispersible. KG-20 is a combination of volatile amine and organic filming inhibitor (a three-phase type inhibitor with a nonvolatile solvent system). This product is best applied continuously where a three-phase inhibitor is desired, but where periodically the line contacts no fluids. KG-20 has particular application in natural gas storage wells in a continuous treatment during the gas injection cycle [225].

Products by Nalco

Gas-cor 969 is a cationic filming amine effective in controlling corrosion in gas pipelines.

Gas-cor 970 is effective in reducing corrosion attack by H_2S , CO_2 , organic acids and limited amount of O_2 .

Gas-cor 4,944 is a cationic filming amine formulated to inhibit corrosion caused by hydrogen sulfide, CO_2 , organic acids [226].

Similar materials are available from other service companies involved in the petroleum industry and who advertise in the trade literature (e.g., Baker-Hughes, Champion and Halleburton).

Storage Tanks

Crude petroleum ordinarily is considered much less corrosive than refined products of petroleum. This difference is mainly the result of the tendency of oil to plate out on metal surfaces, on the protective properties of the scale and deposits formed on surfaces contacted by crude oil and to the inhibitive properties of some of the constituents found in the oil. However, sour crudes such as those from the Middle East and some from the Permian Basin may be very corrosive.

There are, however, environments in which crude oil becomes corrosive, and inhibition is necessary. There are also related environments, such as tankships, in which the corrosion damage occurs as a result of the necessity to clean cargo space and from the alternate loadings, such as when seawater is used as ballast. Most of the corrosion suffered by tankships, however, occurs in tanks carrying "clean," that is, refined petroleum products.

Vapor Space Corrosion In Tanks. There is conflicting information on the effectiveness of using ammonia to control corrosion in the vapor space of tanks holding crude petroleum. Gardner, Clothier and Coryell reported as the result of using ammonia reductions up to 99% in corrosion rates of oil-storage tanks handling crude containing hydrogen sulfide [232]. Ammonium carbonate and anhydrous ammonia both produced good results in tankage when metered into the vapor space at a rate of about 12 ppd for a 55,000-bbl cone roof tank. Table 6-79 shows the record on a 55,000-bbl tank protected with anhydrous ammonia.

Table 6-79
Results of Anhydrous Ammonia Treatment of
a 55,000-Barrel Sour Crude Storage Tank [232]

Date	Exposure Days	Injection Rate, Lb/Day	Corrosion Mdd	Percent [1] Reduction
October–December	57	15	45	85
December–February	62	15	[2]	
February–March	30	15	30	90
March–April	28	15	3	99
April–May	31	15	11	96
May–June	32	15	7	96

[1] Referred to yearly average corrosion rate of 289 mdd determined in this area prior to the start of routine inhibitor treatment.

[2] Not determined. Weights lost.

Field Results. Rogers discussed tests made by his company involving injection of anhydrous ammonia into the vapor spaces of 13 tanks with capacities from 55,000 to 80,000 bbl [233]. Protection in the vapor space from attack by hydrogen sulfide was only temporary. When coupons and new steel were exposed to vapors containing hydrogen sulfide and ammonia, protection lasted 4 to 8 months. After this period, the corrosion rate increased to about the same as that for unprotected steel.

The pH of water collected on the decks of tanks was in the 10 to 11.5 range at all times during the tests. But because iron sulfide surfaces are cathodic to steel and difficult to polarize, the result is high corrosion rates in hydrogen sulfide environments. Changes in fluid pH from 4.5 to 9.5 such as result from ammonia treatment do not greatly change the polarization characteristics of an iron sulfide cathode. These data support the conclusion that treatments with ammonia of a tank having already developed iron sulfide surfaces would not reduce the corrosion rate appreciably [233].

Inhibition of Crude Oil Tanks. Problems in tankers used in marine service are in many ways quite similar to those in storage tanks as previously described. An exception is that tankers in marine service usually are loaded intermittently with hydrocarbons (crude oils or refined products) on one leg of their trip and with corrosive seawater ballast on the other. An additional important concept is that responsibility for alleviation of corrosion in a given company is often split between two or more different company divisions which may not communicate about problems and solutions that are really quite similar.

According to Quimby, marked benefits were obtained when a polar-type oil-soluble inhibitor was metered at a rate of 24 lb per 1,000 bbl into crude oil being loaded into a tank [234]. The 3-year old ships has suffered significant pitting corrosion damage on bottom plates, cargo piping and heating coils.

Annual inspection for 6 years after the inhibition program started showed marked improvement and much better conditions compared to ships without the inhibitor program. Pitting rate was reduced. Most pits ranged from 0.3 to 0.6 in. deep in upward-facing horizontal surfaces. There was little or no bulk.

Relatively little rust was removed from the tanks, the residue being mainly waxy material that tended to settle from the crude oil. While pitting was reduced, it was not brought to an acceptably low value because the pits tended to be filled with water and were not affected by the inhibitor in the oil.

Inhibition of Product Tanks. Tankships carrying refined petroleum products can enjoy marked benefits from effective inhibition practices in their cargo tanks. As is the case with other hydrocarbon environments, major corrosion damage occurs in the vapor phase or as the result of a water phase developed from water absorbed in and/or aspirated into the hydrocarbons from the environment.

The high initial cost and usual long service life of tankships, added to the expense involved in tying up a ship to make repairs of corrosion damage, make inhibitors attractive. Because sides of cargo tanks of tankships also make up the hull and decks, the consequences of catastrophic corrosion attack are too serious to be ignored.

Oil-Soluble Inhibitors. As reported by Quimby, a 5-year test of several ships engaged in coastwide, clean-cargo service revealed that approximately 24 lb/1,000 barrels of an oil-soluble inhibitor was effective in reducing corrosion of tank surfaces to reasonable limits [234]. Micrometer-thickness measurements, as shown in Table 6-80, showed an indicated rate of 6.6 mil a year over the 5 years.

Table 6-80
5-Year Corrosion Rates on Inhibited Tanks [234]

Member	Average Rate, mpy
Shell Longitudinals	5.4
Transverse Wet Frames	4.5
Vertical Keels	1.8
Bulkhead Stiffeners	8.3
Stringers	7.6
Bulkheads	9.3
Shell Stringers	9.2
<hr/>	
Average of members below cargo level	6.6

This was a considerable reduction from the estimated 14 to 16 mpy that would have been suffered if the inhibitor had not been used. Published industry figures of 23 to 25.6 mpy indicate that the savings may have been even greater.

Weights of rust removed from tanks in these ships were significantly less than those from similar ships operated without inhibition. The annual average rust weight from the four ships tested was 52,000 lb, while uninhibited ships in the same trade between 5th and 10th years of service would have 150,000 to 200,000 lb of rust a year removed from tanks.

Vapor Space Corrosion. There is about 18 in. of space between the top of ladings and the bottoms of decks. Condensation in these spaces can result in corrosion at rates up to 40 mpy. When an inhibitor was brushed or sprayed on the exposed areas, corrosion was substantially reduced in 5-year tests.

Flotation and Fogging Techniques. Because of large volumes of fluids handled, every effort must be made to find techniques of inhibitor application that economize on the quantities necessary. Oosterhout, Stanley and Quimby discuss the flotation and fogging techniques for applying inhibitors in tankships [235].

Flotation technique. Flotation inhibitors are applied in an oil solution that is floated on top of water in a relatively thin layer. The exposed steel makes contact with the inhibitor both when the tank is being filled with water and when the water is pumped out. The effect of flotation inhibitors can be demonstrated by the following procedure, as reported by Oosterhout, Stanley and Quimby [235]:

1. A layer of inhibitor is deposited on water in a jar.
2. Coupons are suspended in the jar.
3. The amount of water in the jar is increased until the tops of the coupons are covered.
4. The coupons are withdrawn and then suspended in saltwater for varying periods to determine the effectiveness of the adsorbed layer.

When about 2 gal of inhibitor per 1,000 bbl capacity were poured onto the rising surface of water in a tank being filled to the top with ballast water, a

layer of inhibitor was deposited on the sides of the tank and on all areas of the vapor space [234,235]. Table 6-81 shows corrosion data.

Fogging technique. Empty tanks (nonballast) were protected by "fogging" the inhibitors into them. A finely atomized spray or fog of the inhibitor concentrate in air or steam covered all of the underside area [235]. The injection rate was 2 gal per 1,000 barrels of tank capacity in about 10 min. Injection was done as soon as practical after cargo was discharged. Inspection and corrosion data showed protection comparable to that achieved with the flotation treatment. Table 6-82 shows results.

Oil-soluble polar compounds used as inhibitors in refined products cargoes are applicable to flotation and fogging techniques.

Oosterhout, Stanley and Quimby reported tests of tankship fogging inhibitors using a 300-barrel tank in which the coupons to be tested were suspended from the top in such a way that the fogging spray impinged on them [235].

Recommended Procedure

Pipelines and equipment that are used for storage and transportation are subjected to corrosion due to water and oxygen dissolved in crude or refined products. The following procedure is recommended for pipelines and equipment [237].

1. Use plain carbon steel or stainless steel for equipment. For small pipes, use stainless steel if possible.
2. Remove oxygen and air (deacrate and dehydrate) from products.

Table 6-81
2-Year Corrosion Rates on Coupons Exposed
to Flotation Inhibitors [234]

Tank Corrosion	Corrosion	
	Center Tanks	Wing Tanks
Ballast-Average	20	8.5
Ballast + Flotation-Average	4	2

Table 6-82
2-Year Corrosion Rates on Coupons
Exposed to Fogging Inhibitors [234]

Tank Corrosion	Corrosion	
	Center Tanks	Wing Tanks
Empty-Average	23	6
Empty + Fogging-Average	4.2	6

3. Use organic and inorganic inhibitors. Water-soluble inhibitors solve internal pipeline corrosion, but they should be injected continuously. Oil solubles are common for systems handling both oil and water.
4. For better results, make sure that the inhibitor and product are mixed; it may be necessary to pre-mix.
5. Use coating for pipelines to protect them from corrosion. Coating also has the advantage of improving flow through the pipeline.

For pipelines transferring natural gas the procedure may be as follows:

1. Determine the severity and type of corrosion.
2. Evaluate the percentage of hydrogen sulfide, oxygen, solids and amount of water in the natural gas.
3. Determine the type of flow in the pipe, because the application of an inhibitor depends on the type of flow.
4. Select the inhibitor.
5. Consider a method of application of the inhibitor. Inhibitors may be slugged, injected or sprayed into a gas stream, depending on the flow type. In case of a continuous water flow, a continuous injection program is more effective.
6. Monitor the program and inspect the equipment for effective corrosion control.

ENVIRONMENTAL CONSIDERATIONS

Introduction

The average well requires minor human support on a daily basis. The pumper or switcher may visit the site for a few minutes, confirm normal operations, and move on to the next location. Occasionally, the well may be worked over for repair or stimulation and the activity around the wellsite increased for a short period of time. Because of the lessened activity involved in production operations, the environmental impacts associated with it are also decreased.

Hydrocarbon Contamination

Spills and leaks are the most common accidents encountered at the production site. The spill of condensate, oil or produced water onto the lease and the surrounding areas exhibits the greatest liability to the producer. Chemicals associated with operations may also leak and create an undesirable situation. Sometimes, leaks and spills are unpreventable due to equipment failure or unpredictable production. Because of this, the operator may choose to alleviate the consequences of these possible situations based on probability (see Equation 4-373) and liability.

Containment of a spill is one preventative measure. The berm design around a tank battery is based on the produced flowrate multiplied by frequency of inspection. This is

$$S_{\text{vol}} = 5.61QF_1(SF) \quad (6-358)$$

$$B_b = \frac{S_{\text{vol}}}{\left(B_l B_w - n \frac{\pi}{4} D_i^2 \right)} \quad (6-359)$$

where S_{vol} = spill volume in ft³
 SF = safety factor (2.0-3.0)
 Q = liquid flowrate to tank in bpd
 F_i = frequency of inspection in days
 B_h = height of berm in ft
 B_l = length of berm in ft
 B_w = width of berm in ft
 n = number of tanks in battery
 D_t = tank diameter of n tanks in ft

Soil contaminated by a spill or leak may be treated as an exempt waste provided the leaking substance is listed as an exempt waste [238; refer also to the section titled "Drilling-Environmental Section"]. The hydrocarbon/soil mixture may be left in place provided that all petroleum products stay on location. Operators have found that a mixture of crude and raw materials make an excellent road base, and if properly designed and create less of an environmental hazard than the traditional asphalt road base (see Table 6-83). A typical mixture of 13.0% heavy oil, 7.5% liquid (H_2O) and 79.5% solids make a road surface that can endure heavy road traffic [239]. This road application has tested in northern climates where reduced volatilization of the hydrocarbons is realized. In warmer climates the appearance of a sheen during runoff conditions may be apparent, thus increasing the likelihood of hydrocarbon contamination to the immediate area. To decrease the likelihood of hydrocarbons migrating from the wellsite during periods of heavy rain, the perimeter of the location should have a berm allowing for drainage away from the location. Water collecting on location should be diverted to an onsite catchment. It has been recognized that hydrocarbon contents above 20% in soil mixtures have a lasting detrimental effect on plant life with 1% showing no adverse effects [240]. In landfarming, applications of 2-3% liquid hydrocarbon are common.

As a result of a spill, a hydrocarbon may impose a hazard to groundwater, flora, fauna, and humans. While many wastes produced at the wellsite are exempt, the operator is responsible for degradation of the surroundings due to imprudence, neglect, and accidental release. Hydrocarbon content in the soil

Table 6-83
Comparative Samples of Oil Waste Road Material and Asphalt [639]

Parameter	Oil Waste (ppm)	Asphalt (ppm)
Arsenic	0.04	0.10
Boron	0.1	0.38
Cadmium	0.001	0.01
Chromium	0.6	0.16
Lead	0.057	0.63
Zinc	0.14	0.99
Mercury	0.0001	0.0001
Selenium	0.0017	0.0002
Barium	0.55	2.80
Copper	0.06	0.36
Phenol	0.035	0.24

in excess of the saturation limit may be transmitted to the surrounding environment through runoff and gravity. These hydrocarbons are loosely categorized as dense or light nonaqueous phase liquids (LNAPL and DNAPL, respectively) with DNAPLs being heavier than water. In the field, both of these species are present. The LNAPL is more mobile. This mobility translates to greater relative conductivity in the soils and lesser adsorption onto the soil. However, the LNAPL possesses a lower vapor pressure allowing the liquid to more rapidly dissipate into the gaseous phase leaving only traces of its product. Table 6-84 shows how the hydrocarbon's partition among the phases with Figure 6-265 showing the divisions graphically. An approximation for the volume of liquid hydrocarbon that may be retained by a volume of soil, the depth of infiltration plus the lateral spread of the oil onto the top of the water table is given in the following equations [241]:

$$V_s = \frac{0.2 V_{hc}}{\phi S_{wr}} \quad (6-360)$$

where V_s = soil require to obtain residual saturation in yd^3

V_{hc} = volume of spilled hydrocarbon in bbl

ϕ = soil porosity

S_{wr} = residual oil saturation capacity of the soil (see Table 6-85)

Table 6-84
Phase Distribution of Certain Petroleum Products
in Percentages in Air, Soil and Water [283]

Compound	Adsorbed to Soil	Volatilization	Soluble in groundwater
Aromatics			
Benzene	5	60	35
Toluene	5	75	20
Ethylbenzene	20	60	20
Xylenes	15	55	30
Aliphatics		95	
n-Pentane	< 1	95	4
iso-Pentane	< 1	95	4
n-Hexane	< 1	95	4
n-Heptane	< 1	95	4
Cyclohexane	1	90	4
PAHs			
Napthalene	60	10	30
Benzo(a)pyrene	100	0	0
Anthracene	100	0	0
Phenanthrene	90	3	7
Alcohols			
Methanol	0	2	98
Ethanol	0	2	98
Phenol	9	> 1	90

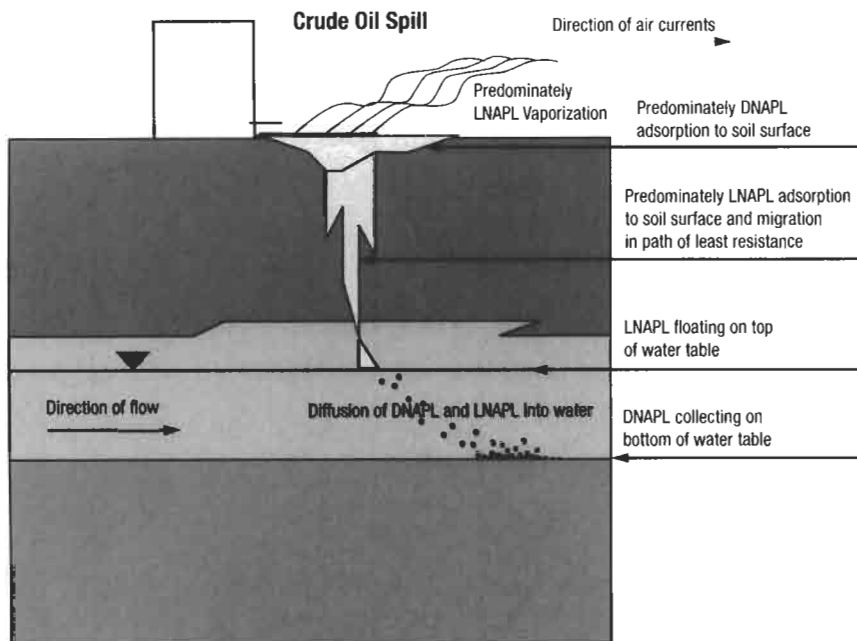


Figure 6-265. Partitioning of hydrocarbons during a spill.

Table 6-85
Kerosene Retention Capacities in Unsaturated Soils [281]

Soil Type	Kerosene Retention Capacity	
	L/m ³	gal/yd ³
Stone, coarse sand	5	1
Gravel, coarse sand	8	2
Course sand, medium sand	15	3
Medium sand, fine sand	25	5
Fine sand, silt	40	8

and knowing the area of infiltration of the soil, the depth of the spill may be determined by

$$D = \frac{27V_s}{A} \tag{6-361}$$

where D = depth in ft
A = observed area of infiltration in ft²

In the event the spill has been determined to reach the water table, the lateral spreading onto the top of the water table may be estimated as [242]

$$S = \left(\frac{1,000}{F} \right) \left(V - \frac{Ad}{K} \right) \quad (6-362)$$

where S = maximum spread of pancake shaped layer in m^2
 V = volume of infiltrating hydrocarbons in m^3
 A = area of infiltration
 d = depth to water table in m
 K = constant in see Table 6-86

Oil, being immiscible in water, will either float on top of the water table in the case of the LNAPL or sink to the bottom. The amount of hydrocarbon that is dissolved in the water depends primarily on the solubility and mass of the component. Only a few hydrocarbons are readily soluble in water such as benzene, toluene and xylene. Table 6-87 shows the solubilities for several hydrocarbons.

When a land spill occurs, the liquid petroleum will simultaneously spread over the top of the site and seep into the soil. In the event the water table is shallow, the liquid will rest on top of or below the water table and will migrate at a rate proportional to the groundwater flow.

The evaporation rate of the spilled hydrocarbon may be inferred from Fick's law:

$$N_A = D_A A \frac{dC}{dX} \quad (6-363)$$

where N_A = rate of mass transport in mol/s
 D_A = mass diffusivity of hydrocarbon in air in ft^2/s
 A = transport area in ft^2
 C = concentration in M
 X = length of path traveled in ft

In a stagnant system, the length of the diffusing path is often unknown for a given field spill. In the event advection also is taking place in the presence of wind currents, the boundary layer may be inferred to be this length. For a finite flat plate in laminar flow, the thickness of the boundary layer is [243]

$$\delta = 5(x)(N_{Re})_x^{-0.5} \quad (6-364)$$

Table 6-86
K-Values for Equation 6-362

Soil Type	Gasoline	Kerosene	Light Gas Oil
Stone, coarse sand	400	200	100
Gravel, coarse sand	250	125	62
Course sand, medium sand	130	66	33
Medium sand, fine sand	80	40	20
Fine sand, silt	50	25	18

Table 6-87
Aqueous Solubility Data for Selected Petroleum Products [282]

Product	Solubility (mg/L of H ₂ O)
Gasoline	50-100
1-Pentene	150
Benzene	1,791
Toluene	515
Ethylbenzene	75
Xylenes	150
n-Hexane	12
Cyclo-Hexane	210
i-Octane	8 ppb
JP-4 Jet Fuel	< 1
Kerosene	< 1
Diesel	< 1
Light Fuel Oil (#1 & #2)	< 1
Heavy Fuel Oil (#4, #5, and #6)	< 1
Lubricating Oil	< 1 ppb
Used Oil	< 1 ppb
Methanol	> 100,000

$$(N_{re})_x = \frac{Vxp}{\mu} \quad (6-365)$$

where δ = the thickness of the boundary layer in cm

x = the length of the spill in cm

N_{re} = Reynolds number

V = free stream velocity of the wind in cm/s

ρ = density of air in g/cm³

μ = viscosity of air in g s⁻¹/cm

The concentration of the hydrocarbon is evaluated at the equilibrium concentration of the vapor in the pores (C_p) and the concentration of the vapor at the air-soil interface (C_{ai}). In the presence of wind, C_{ai} may be assumed to be zero. The concentration of the vapor in the pores is estimated from Dalton's law:

$$P_i = y_i P_T \quad (6-366)$$

and Raoult's law

$$P_i = x_i P_i^0 \quad (6-367)$$

where P_i = partial pressure of the hydrocarbon in atm

y_i = mol fraction of the hydrocarbon in the gas phase

x_i = mol fraction of the hydrocarbon in the liquid phase

P_T = total pressure (1 atm for most cases)

P_i^0 = vapor pressure of the hydrocarbon in atm

Knowing the mass of hydrocarbon at the surface, the time for disappearance of the hydrocarbon from the surface may be determined by using Equation 6-363. In turn, the time for the spill to evaporate from the pore space may be estimated by Equation 6-369 using a correlation between the diffusivity in air and the hydrocarbon's diffusivity in the pore space [244]. Figure 6-266 illustrates this analogy.

$$D_p = D_a \frac{\phi}{\tau} \tag{6-368}$$

where D_p = mass diffusivity of the hydrocarbon in the pore space in cm^2/hr
 ϕ/τ = ratio of porosity to tortuosity (typically 1.5-3.0)

The time for the spill to evaporate from the pore space may be estimated by

$$T = \frac{hM}{2AD_p(C_p - C_{ai})} \tag{6-369}$$

where T = time in hr
 M = mass of hydrocarbon in mol
 h = initial thickness of the contaminated soil in cm
 A = area perpendicular to flux in cm^2

To accurately infer the results of a spill, an onsite and laboratory study should be made for each representative site. The onsite investigation would take inventory on the effects of a worst case scenario such as the total evacuation of a holding tank. The inventory would include the likely migration path of a spill in accordance to topography, potential threats to humans, livestock, and plants, and the relationship of spill area to groundwater and surface water supplies. A laboratory analysis will include hydrocarbon quantitative analysis for constituents creating potential health risks, soil analysis and volatilization parameters.

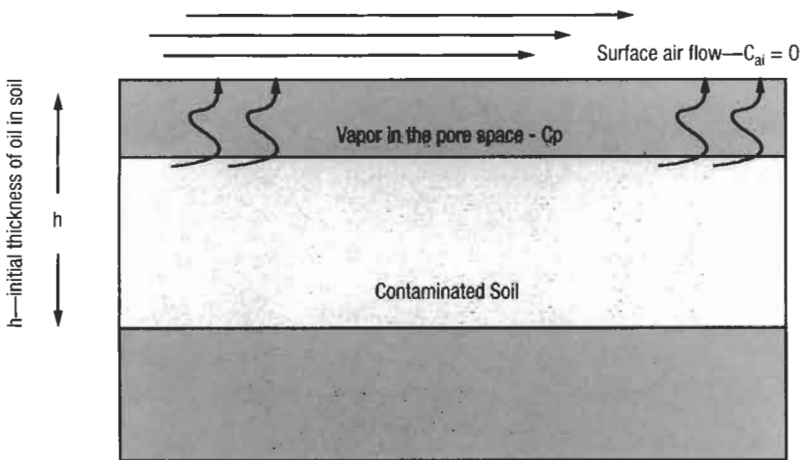


Figure 6-266. Vapor migration through soil pore space.

The soil analysis determines the conductivity of the soil in regards to the liquid hydrocarbon and the absorption/desorption potential of the soil. Knowledge of this conductivity will help in determining the consequences of a spill and may in some cases divert an unwarranted emergency cleanup operation. Many times, the heavier crudes will only penetrate the surface a few inches. The process of determining conductivity is analogous to determining relative permeabilities in a reservoir core sample. In the present analysis, a soil core is taken and left in place in the core barrel with the soil water content undisturbed. The site's liquid hydrocarbon is then allowed over the sample at constant representative head. The time to exit the barrel will infer the flux of the hydrocarbon at partial saturation. This time is critical due to fingering of hydrocarbons. The area affected initially may be much less than the total area of the barrel. The test is continued until the sample is saturated. The conductivity is then estimated through Darcy's law (Equation 6-370). The mass flowrate may then be estimated from this conductivity relationship.

$$q = K \frac{dH}{dL} \quad (6-370)$$

where q = hydrocarbon flux in m/s
 K = conductivity in m/s
 dH = differential head on core in m
 dL = length of core in m

After the conductivity is found, all residual oil is allowed to drain from the sample. The residual left in the core is the absorption capacity of the soil sample. The saturation level of a particular soil may also be found by plotting the data in the form of a sorption isotherm. After the residual oil is drained, the soil sample is washed at constant temperature with water until the hydrocarbon exists only in trace amounts in the product stream. The difference in hydrocarbon mass introduced initially and the displaced hydrocarbon is the total residual saturation for that soil. Depending on the wellsite conditions, this amount of oil may be safely left in place without harm to the surroundings and will continue to decrease in quantity due to *in situ* microbial populations and through diffusion. The desorption isotherm may be constructed through the Freundlich equation. This is

$$C_s = KC_e^n \quad (6-371)$$

or

$$\ln C_s = \ln K + n \ln C_e \quad (6-372)$$

where C_s = mass of oil/mass soil in g/g
 C_e = effluent concentration of oil/volume of water in g/cm³
 K = constant in L/g
 n = constant (unitless—often equal to one for hydrocarbons)

In the linearized form of the equation, $\ln K$ is recognized as the residual oil saturation for the soil sample (see Figure 6-267).

The constant K is a measure of the soils' volumetric capacity of hydrocarbon saturation, while the constant $1/n$ is measure of the mutual attraction between the constituents. Once the isotherm is defined, it may then be used to predict effluent concentrations of hydrocarbons that may be transported into groundwater.

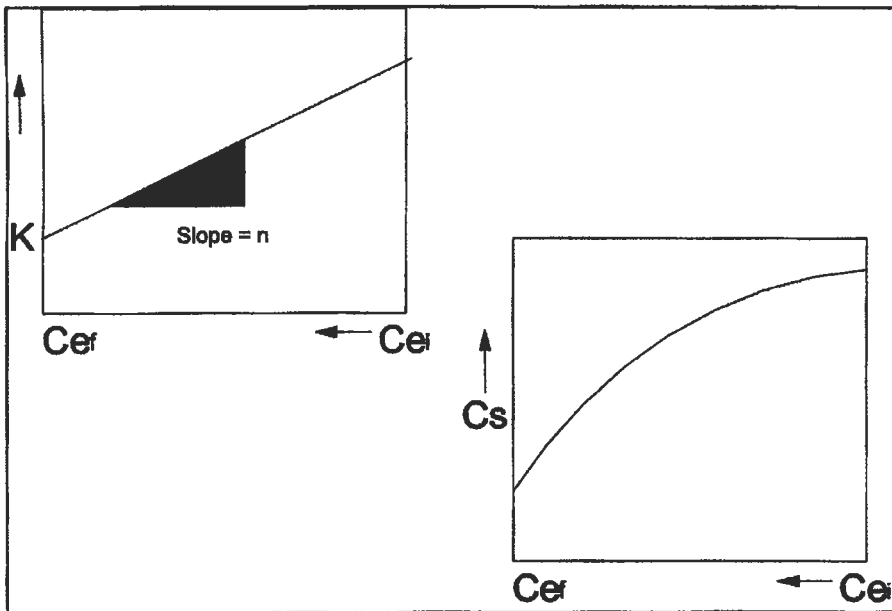


Figure 6-267. Freundlich type isotherms.

In general, due to the nonpolar nature of hydrocarbons, a soil comprised of a high percentage of organic matter will absorb more liquid hydrocarbons. Less soluble, heavier hydrocarbons will absorb better than lighter soluble hydrocarbons and are considerably less mobile than LNAPLs.

Solutions of gases and crude oil follow Henry's law at atmospheric pressures. Henry's constant, more commonly referred to as an equilibrium constant in the petroleum industry, may be used to find the distribution of a hydrocarbon in the aqueous and the atmospheric phases by using

$$K_H = \frac{y_i}{x_i} \quad (6-373)$$

where K_H = Henry's law constant (unitless)
 y_i = mole fraction of the hydrocarbon in air
 x_i = mole fraction of the hydrocarbon in the liquid

Henry's constant is most often referred to in the environmental industry in units of atm. In one liter of water there are 55.6 mols and 22.4 L of air per mol of air, such that

$$K_H = \frac{\text{partial pressure of gas in air}}{\text{mol hydrated gas/mol water}} \quad (6-374)$$

Table 6-88 gives some values of Henry's constants for gases in contact with air at 20°C.

Table 6-88
Henry's Constant for Gases at 1 Atm, 20°C [262]

Component	Henry's Constant (water)
Methane	3.8×10^4
Benzene	2.4×10^2
H ₂ S	5.15×10^2
CO ₂	1.51×10^2
Toluene	3.4×10^2 (25°C)

Other Sources of Waste and Contamination

Glycol and other liquids used for dehydration may occasionally leak or be spilled on the ground. They also may become contaminated, whereby the product must be replaced. Due to the inherent physical properties, i.e. viscosity, of dehydration liquids such as triethylene glycol (TEG), significant losses are not realized to soil seepage or evaporation. The desiccants on the whole are very toxic and completely miscible in water. Unless treated, ethylene glycol is colorless and odorless, and may be mistaken for water upon casual analysis. The greatest potential danger is then contamination of surface runoff. Any spillage should be retrieved and properly disposed of. Waste liquid desiccants should be recycled when possible; otherwise they must be properly disposed of. Class II injection is the most cost-effective disposal method. Solid desiccants, such as alumina, molecular sieves and silica become uneconomically regenerable with time. There is also loss due to structural failure. When exhausted, these materials may be sent to a disposal site or buried on site.

In the sweetening processes, amine treatment is the most prevalent. The amines, such as monoethanoamine (MEA), DEA, and sulfinol combine with CO₂ and H₂S at moderate temperatures and are released when the combined solution temperature is slightly raised.

The wasted H₂S may then be flared and the CO₂ vented. H₂S may be recycled into sulfur products while the CO₂ may be collected and used in recovery projects. These gases may also be trapped in caustic solutions (see Equations 6-375, 6-376). In this case, the pH of the solution is lowered and a salt is formed. These salt solutions, as with most liquid wastes, may be disposed of in Class II injection wells when recycling is not feasible. The pertinent chemical reactions involved here are



Production Site Remediation

In remediation, a site's contaminated material is reduced by either relocating the contaminated material to disposal area or onsite treatment. Physical treatment methods may include [245]

Gravity Separation
 Sedimentation
 Centrifugation

Phase Change
 Evaporation
 Air Stripping

Flocculation
Oil/Water Separation
Dissolved Air Flotation
Heavy Media Separation

Steam Stripping
Distillation

Dissolution
Soil Washing/Flushing
Chelation
Super Critical Solvent Extraction
Liquid/Liquid Extraction

Size/Adsorptivity/Ionic Characteristics
Filtration
Carbon Adsorption
Ion Exchange
Reverse Osmosis

In addition to these physical methods, chemical alterations and biotransformation are also used in site remediation. Table 6-89 shows a relative cost comparison between selected treatment techniques.

Landfarming

Landfarming utilizes *in situ* and introduced microbes such as *Bacillus cereus*, *Bacillus polymixa*, *Arthrobacter globiformous* and *Alcanigenes paradoxus* to degrade contaminants. Heterotrophic bacteria use organic compounds as energy and the carbon source for synthesis. The heterotrophs are classic oil spill degraders. Autotrophic bacteria use carbon dioxide as a carbon source and oxidize inorganic compounds for energy. They are most useful in drilling mud degradation.

In some instances biodegradation of contaminants may result in harmful intermediates, as with mercury. Mercury and other minerals, in their pure metal form, may remain immobile until the introduction of reducing microbes. The altering of conditions, pH and organic content, may change the redox state of the metal. Under such conditions, the metal may then be prone to migration and thus be leached into the groundwater. Also, anaerobic microbes may reduce the metal to a sulfide whereby solubility is enhanced.

In the case of oil spills, on-site bioremediation has proven successful. *In situ* microbial strains are active in most soils. If a previous spill has been documented, a culture from the older site may be introduced in addition to other cometabolites. The successive strains have shown to genetically adapt and become more successful in regards to rate and mass consumed. Composting of contaminated material has also proven effective [246]. Assuming equivalent environments, these successive strains of biomass may be compared quantitatively by

Table 6-89
Comparison of Treatment Processes [246]

Type of Treatment	Cost per Cubic Yard	Time required months	Addition Factors	Safety Issues
Incineration	250-800	6-9	Energy	air pollution
Fixation	90-125	6-9	Transport/monitoring	leaching
Landfill	150-250	6-9	monitoring	leaching
Biotreatment	40-100	18-60	time	intermediary metabolites and polymerization

$$\frac{dM}{dT} = \phi V_b K_b C_p \quad (6-377)$$

where K_b = biorate constant in hr^{-1}

C_p = concentration of petroleum in the pore space in mol/yd^3

In this method, it is assumed that the soil is homogeneously distributed with hydrocarbons, nutrients, and biomass and that the degradation occurs in a uniformly distributed manner. The biodegradation rate constant, assumed pseudo first-order, may then be used comparatively between sites. In the event that the addition of a cometabolite results in a slower rate constant, it is assumed that the previous biomass was more efficient.

In landfarming, drilled solids, mud and contaminated soil are distributed over an area in addition to microbial nutrients (fertilizer). The mixture may be turned and fertilized periodically to enhance degradation. The microbial growth can be quantified by a number of methods. The microcosm turbidity method can be used to estimate the viability of the indigenous species to degrade the hydrocarbons present. A sample of soil or cuttings is taken and allowed to grow. A turbidimeter is then used to quantify growth periodically and mass is calculated as a function of time [247]. CO_2 , generated by the microbes, collected in a caustic solution and the use of a respirometer are yet other growth measurement methods. Both of these use the mass of gas produced or consumed as a measure of cell growth. Figure 6-268 shows the characteristic growth phase of a pure culture of bacteria. Bacterial growth is typically substrate limited.

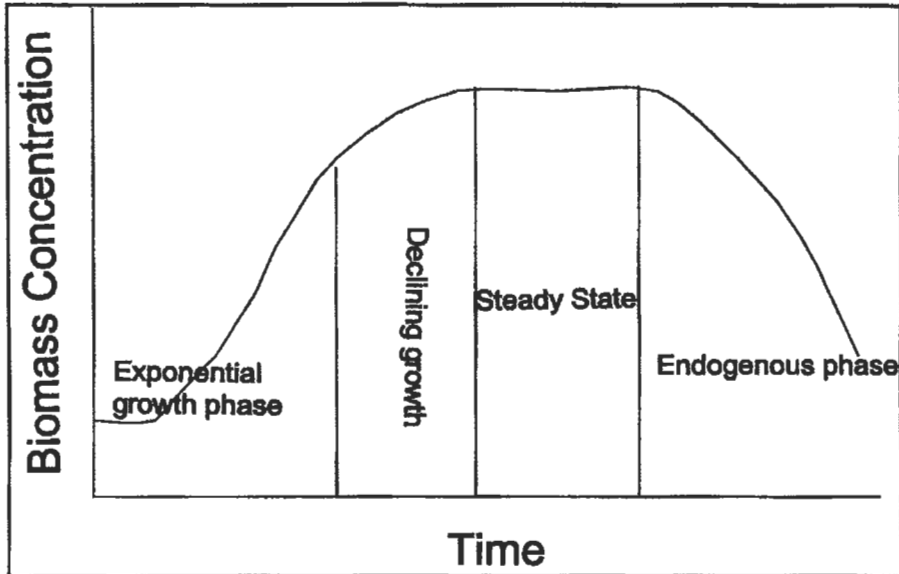


Figure 6-268. Growth phases of bacteria.

In the case of oil-based muds, several mixtures of hydrocarbon-to-fertilizer ratios have been tested for microbial response. The microbes have been found to react favorably to certain conditions. A hydrocarbon:ammonia-nitrogen:phosphate level ratio of 100:2.0:1.0 with the addition of trace minerals, improved moisture retention properties, and adjustment of pH to neutral levels was found to increase the half-life reduction of naphthenic crude from more than 2 years to approximately 8 weeks [248]. In this same set of experiments, a hydrocarbon:ammonia-nitrogen:phosphate level of 100:1:0.02 had only marginal hydrocarbon biodegradation rates, and increasing this ratio to 100:2.0:0.15 while controlling pH and tilling did not significantly raise the rate. Another study concluded the most productive carbon-to-phosphorus ratio was 120:1 with a pH of 7.7 at 77-95°F. The soil was treated with water spray loaded with common fertilizers. The initial hydrocarbon contents were at 600-700 ppm and degraded to 415 ppm within 2 months ($k = 0.0033 \text{ mg L}^{-1} \text{ min}^{-1}$) [249].

Slurry phase bioreactors may be used to decrease the oil and grease levels in soil or drill cuttings. Here, drill cuttings are introduced to a tank in the presence of nutrients, oxygen and hydrocarbon degrading microbes. The vessels are operated at pH levels from 5 to 9 and nitrogen to phosphorus levels of 10:20. Oil and grease pseudo-first-order degradation rates of $0.60 \text{ mg L}^{-1} \text{ min}^{-1}$ (k) have been recorded with pH levels below 6.5 where phosphorus is more readily soluble [250]. The slurry reactor parameters are typically designed as batch mixed at constant pressure using these design equations:

$$-r_a = kC_a \quad (6-378)$$

$$T_R = \int_{N_{a0}}^{N_{af}} \frac{dN_a}{V_R(-r_a)} \quad (6-379)$$

$$T_R = N_{a0} \int_0^{X_{af}} \frac{dX_a}{V_R(-r_a)} \quad (6-380)$$

where $-r_a = -(dC_a/dt)$ = the degradation rate of species "a" (hydrocarbon)

- C_a = concentration of "a" in M
- k = first-order-rate constant in Ms^{-1}
- N_a = mols of "a" at time t
- N_{a0} = initial mols of "a"
- T_R = reactor residence time in s
- V_R = reactor volume in L
- X_a = fractional conversion of "a"

Here all the reactants are fed into the reactor initially and remain there for a mean residence time (T_R). Nutrients may be added occasionally until desired degradation is met. The volume attributed by the additional nutrients can usually be neglected. Equations 6-378 through 6-380 are valid for any batch-mix operation. Usually the kinetics of system are established and then the reactor optimized to facilitate the operation [243].

Kinetics are controlled by oxygen levels, moisture content, temperature, nutrients, pH, and concentration [251]. Soils may have hydrocarbons up to 5% by weight without harmful effects and half-lives of only 2 years may be realized for soils containing up to 14% [252,253].

Landspreading

Landspreading is differentiated from landfarming in that the area over which the contaminated soil or liquid is spread is not actively manipulated to increase degradation rates. One study showed that by spreading oil-based cuttings over an area of soil at thicknesses not over 2 in. has lead to natural degradation rates of approximately 80% in the first year and 95% of the hydrocarbons had been eliminated after 3 years. Further analysis proved no significant migration or leaching of the hydrocarbons had taken place [254]. Another method of landspreading includes reliquidifying the solids and then spreading them evenly over an area. Here, the loading factors take into consideration the soil and contaminant characteristics. A cumulative salt burden of 6,000 lb/acre (3,000 ppm) is considered a safe level with a hydrocarbon loading of 40,000 lb/acre (2%). These numbers are based on a 2,000,000-lb_m/acre soil horizon [255]. The total salt burden of the soil is calculated from the total dissolved solids contained in the contaminant/soil mixture. Applications of freshwater gels may be added at 1,000 kg Cl/ha (KCl form) and 1,400 kg Cl/ha (NaCl form) and present no limitation to the soils and may actually enhance soil characteristics for plant growth. Chloride concentrations of 1,000–2,600 ppm have been safely used without loss of yield in grass growth [256]. Where sodium activity ratios (SAR) levels increase, the addition of gypsum is added to relieve the problem [257].

Hydrocarbons and salts inherent in some production water and drilling muds may pose threats to the local ecosystem if not properly managed. The salt concentration may be estimated for a liquid from the electrical conductivity of the solution by

$$\text{TDS} \doteq \text{B}(\text{EC}) \quad (6-381)$$

$$\text{I} = 0.016(\text{EC}) \quad (6-382)$$

Electrical conductivity (EC) is measured in mmhos/cm, TDS as mg/L and ionic strength (I) as molarity. The values for B are held closely in agreement by several sources as 640 [258] and 613 [259]. While Equations 6-381 and 6-382 are only used as an estimate of ionic content in the soil or solution they are accepted due to their general use in the soil sciences. EC values less than 4 mmhos/cm are generally satisfactory for crop yields. The additions of drilling mud-showing an EC of 1.3–5.3 mmho/cm showed no adverse effects on Bermuda grass [260]. Generally an SAR < 12 and ESP < 15% is acceptable for land disposal [259]. The ESP is another measure of sodium contained in the soil. Israel has developed crops and technologies that allow for 10% seawater at 4,000 ppm (6.5 mmhos/cm) TDS [261]. This is

$$\text{ESP} \doteq \frac{[\text{NaX}]}{\text{CEC}} (100) \quad (6-383)$$

$$\text{SAR} = \frac{[\text{Na}]}{\sqrt{\frac{[\text{Ca}] + [\text{Mg}]}{2}}} \quad (6-384)$$

where NaX = the sodium in the solid phase
 CEC = the cation exchange capacity of the soil phase in meq/100 g
 [] = molarity

Table 6-90 shows the oil tolerance for selected grasses and plants [260]. API recommends a one-time application of <1% [259].

Table 6-90
Oil Tolerance for Selected Grasses and Plants [260]

Grass/Plant Type	Oil and Grease for 1 Application
lawngrasses	< 0.5%
ryegrass, oats, wheat, corn	< 1.5%
red clover	< 3.0%
perennial grasses, trees	> 3.0%

Airstripping

In phase transformation, most often the liquid phase is let to a gaseous phase, through the addition of heat, a reduction in pressure or concentration, or any combination thereof. Evaporation may be used as applied through variations of Equation 4-390. The two film theory states the basis for most air stripping operations, and is mathematically defined by

$$\frac{dC}{dt} = -K_L a (c_s - c_l) \tag{6-385}$$

where C = concentration of the hydrocarbon in M
 $K_L a$ = overall rate constant in hr^{-1}
 c_s = concentration of the hydrocarbon in the gas phase at time (t) in M
 c_l = concentration of the hydrocarbon in the liquid bulk at time (t) in M

Here, a gas (air) is passed through the contaminated liquid phase and the resulting equilibrium concentration difference between the phases drives the vaporization of the liquid. The airstripping design may be a simple bubbling of air through an open tank (see Equation 6-385) or the more efficient and costly packed tower that uses these design equations [262]:

$$(HTU)(NTU) = \frac{L(C_i - C_e)}{K_L a} \frac{\ln \frac{DF_e}{DF_i}}{DF_e - DF_i} \tag{6-386}$$

$$HTU = \frac{L}{K_L a} \tag{6-387}$$

$$NTU = \frac{R}{R-1} \ln \frac{\frac{C_i}{C_e} (R-1) + 1}{R} \tag{6-388}$$

$$R = \frac{K_H G}{L} \quad (6-389)$$

where HTU = height of transfer unit in m

NTU = number of transfer units

L = liquid velocity through empty diameter of transfer unit in m/s

G = gas velocity through empty diameter of transfer unit in m/s

C_i = inlet concentration of contaminant in gas in M

C_e = exit concentration of contaminant in gas in M

Df_i = driving force at the inlet in M

Df_e = driving force at the outlet in M

R = stripping factor

K_H = unitless Henry's constant for contaminant

$K_L a$ = (s^{-1})

In the stripping tower design, determination of $K_L a$ is most important. This value is particular to the type of packing used in the tower, the type of contaminant and a number of other parameters. The Sherwood-Holloway equation may be used to determine $K_L a$ for a given packing, liquid and gas. This is

$$K_L a = D_L m \left(\frac{L}{u_L} \right)^{1-n} \frac{u_L^{0.5}}{r_L D_L} \quad (6-390)$$

where $K_L a$ = hr^{-1}

D_L = diffusion coefficient for gas of interest in water in ft^2/h

L = liquid velocity in lb water/hr-ft²

u_L = liquid viscosity in lb/hr-ft

r_L = liquid density in lb/ft³

Tables 6-91 and 6-92 give values for the diffusion coefficient and the constants m and n, respectively.

Table 6-91
Diffusion Coefficients for Some Petroleum-Related Contaminants [262]

Contaminant	Diffusion coefficient x 10^{10} m ² /s at 20°C
Methane	18.1
Trichloroethylene	8.37
Chloromethane	13.1
Benzene	8.91
Carbon Dioxide	19.6 (25°C)
Oxygen	16.1 (25°C)
Hydrogen Sulfide	20.3

Produced Water

Produced water varies widely in composition with dissolved ions being the major component in these waters. The total dissolved solid (TDS) content may be close to saturation at more than 300,000 mg/L TDS or be considered fresh

Table 6-92
Sherwood-Holloway Constants for Packing Materials as Based
on the Desorption of Hydrogen, Oxygen and Carbon Dioxide [262]

Packing	Size (mm)	m	n
Raschig rings	50	80	0.22
Raschig rings	38	90	0.22
Raschig rings	25	100	0.22
Berl saddles	38	160	0.28
Berl saddles	25	170	0.28

at less than 500 mg/L TDS. The composition of the water depends on a number of factors. Some waters are the remains of the ancient seas held in formations thousands of feet below the surface. Some water may have been fresh originally, but through geologic time has become saturated with the minerals contained in the surrounding rock. Still other water has changed in composition through migration through pore space and fractures, solubilizing minerals in the pathway. In a study characterizing production of produced waters from natural gas wells it was found that that less than 60% had any concentration of the heavier volatile constituents, but instead the bulk was composed of lighter hydrocarbons [263]. Table 6-93 shows average water analyses for 19 natural gas wells. The components shown were found in 80% of the surveyed wells.

Knowing the composition of the reservoir rock and assuming freshwater was in place at time of deposition, a water's TDS may be forecast with some accuracy from equilibrium equations. Produced water of course also carries a certain amount of hydrocarbons. These concentrations may also be calculated from equilibrium equations. For a water being in contact with the gas phase, Henry's law then is used to predict the concentration of certain hydrocarbons. These gas-phase constituents, however, maintain equilibrium with the atmosphere when exposed. Thus the organics may be stripped from the water by means of a packed tower, diffused aeration or other means.

Solubility

Because of the dissolved mineral content in the water and residual hydrocarbons, produced water must be treated for use or disposed of. Safe disposal of this water is secured through injection into a secure geologic formation, evaporation in lined pits, or other approved means [264,265]. The use of lined pits as the sole means for disposal has been eliminated in all but a few cases where the evaporation rates are competitive with the wells' production. Unlined pits are not considered a sound environmental approach in today's political climate. In the past, the percolation in such pits has allowed for a cost-effective means of disposal. In some cases, however, this practice has led to local groundwater contamination [266].

Guidelines have been made for the production water pit construction, including the following [265]:

- A minimum freeboard of 2 ft must be maintained in the pits.
- Life expectancy and pertinent characteristics of the liner material
- Monthly evaporation/precipitation rates
- Method and schedule for removal of residual solids and saturated brine.

Table 6-93
Produced Water from Natural Gas Sites [263]

Compound	Average Value
TDS	93000 mg/L
TSS	132 mg/L
BOD ₅	1486 mg/L
Chloride	55000 mg/L
COD	11200 mg/L
Ammonia as N	72.3 mg/L
Oil and Grease (62.5%)	15.6 mg/L
pH	5.83 mg/L
TOC	2280 mg/L
Barium	87.0 mg/L
Calcium	6424 mg/L
Iron	100 mg/L
Magnesium	683 mg/L
Manganese	7.47 mg/L
Sodium	18800 mg/L
Lithium	91.3 mg/L
Potassium	539 mg/L
Silicon	9.86 mg/L
Strontium	10 mg/L
Sulfur	25.9 mg/L
Phenols (62.5%)	330 ppb
Naphtalene (62.5%)	39.8 ppb
Benzene	5980 ppb
Toluene	6440 ppb
Total Xylenes (75%)	3420 ppb

Pits used as a means of storage for treatment may be preferred over manufactured tanks due to volume considerations. Evaporation may be used in these wells and may in some instances be considerable in arid climates as calculated through the Meyer equation.

In the case of injection, steel tank storage is preferred to eliminate any contamination of the water supply by dust and other particles. In the case of Class II injection, the water is often pumped into subsurface formations at less than the fracture pressure. Thus the water must be free of particulate matter to avoid pore plugging. Pretreatment with biocides is for this same reason. The construction of properly designed Class II injection wells often cost in excess

of a million dollars. Thus, considerable planning is necessary to prevent early decline of injectivity.

In planning a Class II well, the geology of the area must be considered as well as the number of viable injection zones presented. These zones must be separated from each other; at least one zone must be permeable and the other must be impermeable from the USDW and be free of commercial quantities of oil or gas. The area must also be proven free of faults. Crossbedding, tonguing and other permeability hindrances should be considered. Most states allow a radial extent of $\frac{1}{4}$ to $\frac{1}{2}$ mi. The area then available for storage is

$$V = C_t(\nabla_f - \nabla_i)D_{avg}Ah\phi \quad (6-391)$$

where ∇_f = final pressure gradient in less than frac pressure - psi/ft

∇_i = initial pressure gradient in psi/ft

A = areal extent in ft

D_{avg} = average depth of injection zone

C_t = total compressibility in psi^{-1}

h = thickness of zone in ft

ϕ = porosity

NORMS in Produced Water/Gas

Radioactive contamination of production equipment is an emerging concern in the petroleum industry. Radiation is normally reported in curies (Ci), rads, rems, or bequerels (Bq). The commonest way of reporting is pCi or 10^{-12} curies. One curie is equal to $3.7 \times 1,010$ nuclear transformations per second or 1 gram of radium. In contrast, 1 gram of uranium has 0.36×10^{-6} Ci of activity. A rad quantifies an absorbed dose and a rem a dose effect ($0.1 \text{ mrem/year} = 10^{-6}$ excess lifetime cancer risk).

$$\text{Xrems} = Q(\text{Yrads}) \quad (6-392)$$

The Q here is a quality factor based on the source of activity. Alpha particles inflict much more damage to human tissue than do beta emissions. The generation of these two particles causes the decay of the parent isotope and leads to production of the progeny which are sometimes referred to as daughters. Isotopes with larger half-lives usually present lower radioactive risks. Gamma ray emission does not produce progenies. Elements that have very short half-lives are not significant in that they change rapidly in transport. Radium-228 emits beta particles, whereas uranium, radon and radium-226 are alpha emitters. The average annual dose received by humans in the United States is 200 mrem of which only 4 mrem are attributed to drinking water. Some public water supplies have shown radioactivity in excess of 10,000 pCi/L, equivalent to a dose of 100 mrem/yr [267].

Contamination may be caused by natural sources, and as such is termed NORM (naturally occurring radioactive material). Radioactivity is a concern due to the widespread occurrence of radium, uranium and radon and the inherent carcinogenicity attributed to them. A national survey of 1,200 drinking water supplies showed that 72% had positive readings for radon with a mean of 881 pCi/L with a maximum of 26,000 pCi/L. Using data compiled from uranium miner incidences, radon probably constitutes the greatest health risk of any substance found in drinking water. Under the SWDA of 1986, radium-228, and radium-226, radon, uranium, gross alpha, beta, and photon particle activity are

regulated. The national interim primary drinking water standards are given in Table 6-94.

In Canada, the maximum acceptable concentration of Ra-226 is 27 pCi/L (1 Bq/L) and for strontium-90 270 pCi/L (10 Bq/L). The World Health Organization sets a guideline value of 2.70 pCi/L (0.1 Bq/L) for the gross alpha activity and 27 pCi/L (1.0 Bq/L) for the gross beta activity.

Radon gas is common to natural gas production. It has long-lived decay products that contribute to the contamination of production equipment. Radon-222 is a highly mobile inert gas produced from radium-226. Other radon isotopes exist (thoron) but are rare and have extremely short half-lives which cause decay even before the gas is produced at the wellhead. Due to radon's characteristics, it freely travels in groundwater, oil, and natural gas without chemical reaction. Once produced at the wellhead, the radon (222) is coprocessed with the natural gas. In the refinery, radon may become concentrated in the production of propylene or ethane with a boiling point being intermediate to these two. On the wellsite, concentrated radon gas is not expected. Table 6-95 gives radon concentrations found worldwide at the wellhead.

Radon-222 has a short half-life at 3.8 days. Being inert, it does not accumulate in the body. 99% of radon-222 decays into lead-210 within 25 days. Figure 6-269 shows the complete decay series of uranium-238. In the wellsite facilities the

Table 6-94
U.S. Interim Primary Drinking Water Regulations for Radionuclides [262]

Contaminant	MCL (enforceable)
Radium 228 and 226	5 pCi/L (0.185 Bq/L)
Gross alpha particle activity	15 pCi/L (0.56 Bq/L)
Beta, and photon particle activity	4 mrem (annual dose equivalent)

Table 6-95
Radon Concentrations Found at the Wellhead [268]

Location of Well	Radon Concentration (pCi/L)
Borneo	1 - 3
Canada	
Alberta	10 - 205
British Columbia	390 - 540
Ontario	4 - 800
Germany	1 - 10
The Netherlands	1 - 45
Nigeria	1 - 3
North Sea	2 - 4
U.S.	
Colorado, New Mexico	1 - 160
Texas, Oklahoma, Kansas	1 - 1450
California	1 - 100

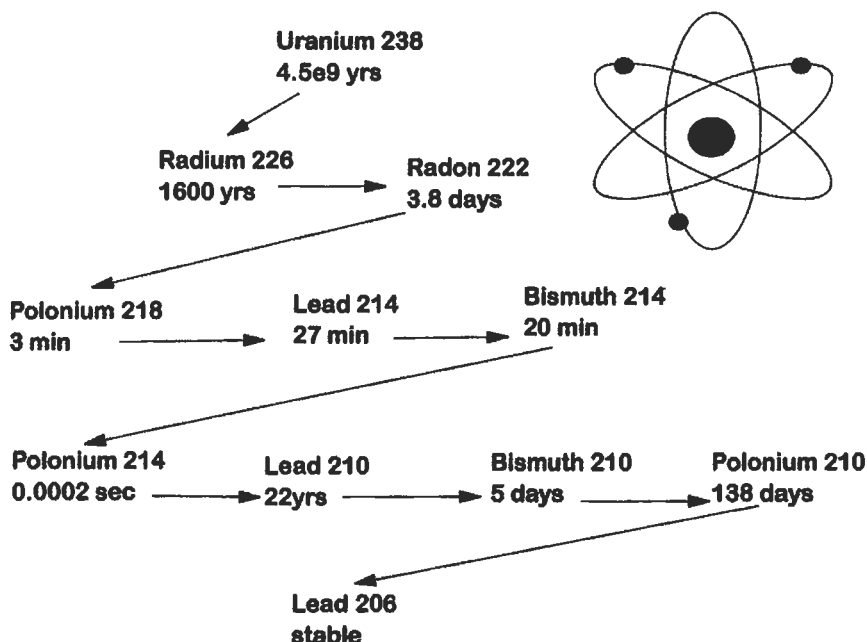


Figure 6-269. Uranium-235 decay series [284].

daughter products of radon accumulate inside the containing vessels. Due to the low concentrations, it may be difficult to measure the radioactivity from outside the vessels. Usually, laboratory analysis or specialized probes are needed to detect these quantities. An alpha/beta probe may register positive if held to the internal surface. Radon gas does have sufficient gamma energies to register on a gamma survey meter. These radioactive materials are not considered hazardous unless inhaled or ingested [268].

Ra-228 comes from the decay of thorium-232. Ra-228 has a beta intensity of 4.71 MeV and Ra-226 emits an alpha intensity of 0.024 MeV. Ra-226 has an initial registered gamma energy of 185.7 keV compared to Ra-228's 10.3 keV. A coal gas well in New Mexico (see Table 6-96) portrays radium levels in excess of present drinking water standards in addition to a high level of strontium-90, which has a lifetime of 28 years and a beta particle energy of 0.55 MeV. This isotope is rare in nature, whereas the stable isotope Sr-88 is quite abundant with 82.6% of strontium's isotopes being in this form. Isotopes such as Sr-90 are most frequently encountered in tracer surveys. Table 6-97 shows Wyoming's produced water characteristics.

Tracer surveys are an important technology used in today's petroleum industry. The injection of low-level radioactive elements downhole allows us to follow fluid migration downhole through gamma ray logs. The federal government in fact allows their use in the confirmation for mechanical integrity in Class II injection wells 40 CFR 146.8 [269]. The low level radioisotopes are prepared in the lab and transported in approved containers to the site. Several different isotopes may be injected into any one well depending on the number of fluids needing to be traced. The isotopes of strontium, antimony, gold and others are frequently used. Each isotope registers a different signature on the gamma ray log.

Table 6-96
Water Analysis from Fruitland Coal Well [285]

Component	mg/L	meq/L
Aluminum	< 1	
<i>Arsenic</i>	<i>0.003</i>	<i>0.0001</i>
Barium	61.9	1.3521
<i>Cadmium</i>	<i>< 0.005</i>	
Calcium	29.6	1.4770
<i>Chromium</i>	<i>< 0.01</i>	
Cobalt	< 0.02	
<i>Copper</i>	<i>< 0.25</i>	
Iron	4.2	0.2256
<i>Lead</i>	<i>0.27</i>	<i>0.0026</i>
Magnesium	18.4	1.5138
<i>Mercury</i>	<i>< 0.001</i>	
<i>Nickel</i>	<i>< 0.03</i>	
Potassium	48.4	1.2378
<i>Selenium</i>	<i>< 0.0001</i>	
Sodium	5370.0	233.59
Strontium	NR	
Vanadium	< 0.1	
<i>Zinc</i>	<i>0.39</i>	<i>0.0119</i>
Total Cations		239.411
Bicarbonate as CaCO ₃	14700.0	240.944
Carbonate as CaCO ₃	0.0	
Boron	1.6	0.4440
Chloride	905.0	25.528
Fluoride	0.94	0.0495
Nitrate/Nitrite as N	0.14	0.0030
Total Anions		266.96
<i>Oil and Grease</i>	<i>70.0</i>	
<i>Phenols</i>	<i>0.027</i>	
Sulfate	< 20	
<i>Benzene</i>	<i>< 0.01</i>	
<i>Toluene</i>	<i>0.03</i>	
<i>Ethyl Benzene</i>	<i>< 0.01</i>	
Total Xylene	< 0.01	
Alkalinity as CaCO ₃	14700.0	
pH	8.07	
T. Dissolved Solids	16300	
Radium-226	4.3 +/- 1.0	pCi/L
Radium-228	8.6 +/- 2.2	pCi/L
Strontium - 90	70.7 +/- 1.1	pCi/L

Table 6-97
Concentration of Ra-226 in Wyoming Produced Waters [286]

Parameter	Value
No. of Wells Tested	373
Maximum Recorded Value of Ra 226	2152 pCi/L
Minimum Recorded Value of Ra 226	0 pCi/L
Average Value	21.5 pCi/L
Median Value	3.7 pCi/L
Number of Wells above 5 pCi/L	167

Water or gas contaminated by radioactive tracers is to be expected. In the case of an injection well, the contamination should be documented with no further considerations. In the case of a producing gas well, precautions must be taken to protect workers from inhalation of vented gas that may contain radioactive vapor. The completion or workover fluid retrieved from the tracer operation are nonexempt subtitle "C" hazardous wastes. As such it must be properly contained, labeled, and transported to a specially permitted TSD facility authorized to dispose of low-level radioactive waste. Low amounts of waste may be stored onsite for extended periods of time.

Cation exchange is a very effective means of radium removal because it is preferred above all other common cations found in water. An even more efficient exchange mechanism is BaSO₄ located in an alumina or SAC resin. A resin impregnated with barium sulfate was used to decontaminate the spent regenerant solution from a conventional cation exchange process of radim. The process was tested on a small municipal system and was very successful and was still removing radium when the resin was loaded at 2.7 million pCi/L. This level, however, posed a far greater disposal problem than the initial brine solution [270].

NORMS frequently enter the production system in the form of scale. This scale may be found in the tubing, wellhead, and any of the surface equipment. The concentrations have been found up to 30,000 pCi/gm in the production equipment scale and 250 pCi/gm in associated sediments such as BS&W. Soils surrounding locations may show radium levels up to 2000 pCi/gm [271].

The radioactive scale is often found in association with precipitates of barium, strontium, and calcium. Equilibrium calculations favor the formation of radium sulfate in excess of barium sulfate. The prevention of NORM contamination then may be prevented through scale inhibition. An equal mixture at 1 mg/L of aminotrimethylene phosphonic acid and phosphinopoly-carboxylate has been found effective in eliminating radioactive scale.

The greatest health risk attributed to NORM-contaminated production equipment comes from the cleaning or repair. The radioactive materials are not health hazards unless ingested or inhaled into the body. In the event of inhalation, dustborne particles containing NORM or a gas such as radon attach to the lung tissue where they emit alpha particles into the lung tissue, which may lead to cancer.

Class II Injection Wells

Class II injection wells afford an economic means of disposal of produced brine water. They are regulated through the Underground Injection Control

Program (UIC) under the provisions of the SDWA. State and local governments may be granted primacy over UIC programs by the federal government. The underlying rules for the UIC program are found in 40 CFR 144 and 146.

UIC Criteria and Standards

An underground source of drinking water (USDW) includes an aquifer and its portion which supplies a public water system, or contains a sufficient amount of water to supply a public water system, or contains less than 10,000 ppm TDS, and is not an exempted aquifer (40 CFR 146.3). An exempted aquifer or portion of such must meet the following criteria: does not currently serve as source of drinking water, and it cannot or will not serve as source of drinking water due to (1) commercial quantities of minerals, hydrocarbons, or geothermal energy, (2) situated at a depth or location making recovery of water technically or economically impractical, (3) so contaminated that making recovery of water is technically or economically impractical for drinking water purposes, (4) contains more than 3,000 ppm TDS but less than 10,000 ppm TDS and is not reasonably expected to supply drinking water, (5) is located over a Class III well mining area subject to collapse or subsidence (40 CFR 146.4).

A Class II injection well injects fluids (1) that are brought to the surface in connection with conventional oil and natural gas production and may be commingled with wastewaters from integral gas plants (2) for enhanced recovery of oil or natural gas, or (3) for storage of hydrocarbons which are liquid at standard temperature and pressure (40 CFR 146.5).

Class II injection wells are to be located in a formation separated from any USDW by a confining zone and be free of known open faults within the area of review. The area of review may be computed from a modified Theis equation:

$$r = \left[\frac{(2.25KHt)}{S10^x} \right]^{0.5} \quad (6-393)$$

$$x = \frac{4\pi KH(h_w - h_{bo}S_pG_b)}{23Q} \quad (6-394)$$

where r = radius of endangering influence from injection well (length)

K = hydraulic conductivity (length/time)

H = thickness of injection zone (length)

t = time of injection

S = storage coefficient

h_{bo} = observed original hydrostatic head of injection zone as measured from the base of the lowermost USDW (length)

h_w = hydrostatic head height of USDW zone as measured from the base of the lowermost USDW (length)

S_pG_b = specific gravity of fluid in the injection zone

These equations assume homogeneous, unconfined, isotropic, and total penetration of the aquifer with $r_w \ll r_e$ (40 CFR 144.6).

Some states question the use of Equations 6-393 and 6-394 in determining the range of influence of an injection well and require a set radius. New Mexico requires a set radius of influence of $\frac{1}{2}$ mi.

The requirements do not apply to those wells that were previously drilled under a state or federal regulatory system in compliance with these controls

provided well injection will not contaminate a USDW. Remedial work may be approved to bring newly drilled wells (dryholes) into compliance. Currently, amendments to 40 CFR 144 and 146 are proposed for modifying well construction and extending the scope of wells necessitating documentation for "area of review" [272]. Under the new rulings, with some allowances, all new Class II wells will be required to:

- run surface casing through all USDWs containing $\leq 3,000$ mg/l TDS and cement same to surface,
- cement the long string to prevent the migration of fluid from the injection zone,
- have the tubing string landed with a packer.

UIC Permitting Process

To be granted a permit for a Class II injection well, the operator must file an application to the ruling UIC program at the state, local, or EPA office. On federal leases, the BLM must also grant approval. The permit will address the following as stipulated in 40 CFR 146:

1. depth of well
2. depth to base of USDW
3. estimated maximum and average injection pressures
4. nature of injected fluid
5. lithology of injection and confining zones
6. external pressure, confining pressure and axial loading
7. hole size
8. size and grade of all casing strings
9. class of cement

The permit is then reviewed and once accepted is let to the public for comment. After this comment period, the final permit decision is issued. Once completed, the well then may be used to dispose of:

- produced water
- waste fluids from the drilling operation
- pigging fluids from within the field
- used workover, and stimulation fluids from injection, exploration, and recovery wells
- any gas used for enhanced recovery or pressure maintenance
- brine reject associated with enhanced recovery
- waste fluids from sweetening and dehydration of methane as long as the fluid is not hazardous at the point of injection
- waste oil and fluids from cleanup operations associated with primary production of oil within the field
- waste fluids from cementing operations
- fresh water used as an enhanced recovery base
- water containing chemicals used for enhanced recovery.

Monitoring of fluid composition, injection pressure, annulus pressure, flowrate, and volume is required. Reporting of regular activities is required annually and a mechanical integrity test must be performed every 5 years and each time the tubing is moved.

OFFSHORE OPERATIONS

The oil and gas industry drilling and production technology have advanced from producing oil and gas from onshore locations to producing from distant offshore locations in water depths up to 1,000 ft or more.

Some 50 years ago, locations in the marshlands were built up above the water level with oyster shells. Lumber measuring 3 in. × 8 ft and random lengths were laid as matting over the shell fill. A land rig was then moved in by tug and barge in a freshly dug canal to the location where the derrick and drilling equipment was unloaded and rigged up. Drilling and completion was accomplished as on land locations.

Later a barge rig was used. This was a derrick with drilling machinery mounted on a steel barge. This barge was sunk on location in water depth limited by the freeboard of the barge prior to sinking.

Since the barge rig was limited to very shallow depths, a posted barge was developed (drilling deck separated from the barge by I-beams supporting the drilling deck). With this unit, the barge could be sunk completely below the surface of the water as long as the drilling deck was above the water. The barge rig and posted barge rig were used mostly in marshlands and shallow lakes. They are still used in such areas today.

Offshore drilling started in shallow water near the shore line on concrete structures. Concrete prestressed pilings were driven in the ocean floor and a concrete platform was installed on the piling to support the land-type rig. After the well was completed, the rig was moved off the structure and production equipment moved in.

Steel structures were later fabricated onshore and moved to offshore locations by tug and crane barge. At location, the crane was used to lift the structure, swing it to one side and lower it onto the ocean floor. Large-diameter pipe was hammered down through the larger steel casing legs into the ocean floor. Cement was then circulated between the two casing legs. After the platform was installed on the structure, the drilling rig was unloaded onto the platform and rigged up for drilling. This method of drilling offshore was used in water depths of 100 ft or more. After the well was drilled, cased and completed, including the Christmas tree, the rig would move to another location that was ready to be drilled. Once the drilling rig left the completed well, flow lines were laid and all necessary equipment installed to transport the production either directly to a purchaser's line, to an onshore separation facility, or to a centrally located production platform before being transported to land. On Lake Maracaibo, in Venezuela, all production was directed to a production platform and then to an offshore separation and storage facility.

Then came the mobile drilling rigs. These were the submersibles, jack-ups, semisubmersibles, and floating drillships. Both the semisubmersibles and drillships have drilled in over 3,000 ft of water.

At the present time, drilling in the Gulf of Mexico has been in water depths of 1,000 ft. In Lake Maracaibo in Venezuela, the water depths near the center of the lake are about 100 ft. Off Norway, the water depths are 500–600 ft.

Production platforms in 600–700 ft of water are being anchored on the ocean floor. The structures are massive to withstand all external forces. As water depth increases, the weight and cost of the structure escalates. The taller the structure, the greater the moment around the base. This greater moment is caused by the greater force (same force per unit length but acting over a longer distance), and this force is concentrated at a greater distance from the ocean floor. The forces

include currents, wind, tides, earthquakes and floating material such as ice. Because of the escalating cost of ocean-floor-anchored structures, other types of platforms are under study.

Systems under study at the present time are (1) guyed tower, (2) tension leg, and (3) catenary anchoring systems. Technology is growing rapidly and, no doubt, platforms above the water will function economically and safely at still greater depths. Exxon has set a guyed tower in 1,000 ft of water in the Gulf of Mexico off the state of Louisiana. Since there are only about 250 underwater production systems around the world today, these systems will not be discussed.

Multiple Use of Structures

The structure for use offshore may be constructed as a drilling platform but may also be used as a production platform. The structure will act as a stabilizer for the well casing above the ocean floor to the Christmas tree located above the surface of the water. Flowline risers, helicopter landing pads, and mooring facilities for crew boats and work boats are necessities that must be supported by the structure.

Primary Considerations

The entire next section is excerpted from API RP 2A, "API Recommended Practice for Planning, Designing and Constructing Fixed Offshore Platforms," July 10, 1984 [279].

One of the primary considerations in the design of a structure used in drilling and production is for the safety of personnel. Other considerations that must be built into the structure with adequate safety factors are the loads applied on the structure that may be summarized as follows:

1. Total weight of structure. This is the total weight in air minus the buoyancy on the part of the structure below the water line.
2. Drilling equipment weight. This load shall be the weight of the drilling equipment placed on the platform, including such items as derrick, drawworks, mud pumps, and mud tanks.
3. Production equipment weight. Production equipment load shall be the weight of production equipment, which includes separators, compressors, tanks and production manifolds.
4. Drilling supply weights. This load, which includes such things as mud weights, water, diesel fuel, and casing, will vary during production.
5. Production supply weight. Production supply weight will vary during production including such things as fluid in tanks and separators.
6. Drilling load. The drilling load shall consist of any appropriate combination of derrick corner load, set-back, or rotary load.
7. Dynamic loads. Those loads, which act in addition to the equipment weight taken statistically, shall include due consideration of the following: (a) dynamic amplification of cyclic loads that excite the platform (or some component) or near natural frequency; (b) impact from loads that are suddenly or dynamically applied.
8. Installation loads. Those are loads experienced during platform construction. They generally are forces that occur during loading out, launching or lifting operations.

9. Environmental loads. Those loads are imposed on the platform by the environment. Combinations and severity of environmental loads used for the design shall be consistent with the probability of occurrence in particular location. Loads to be considered are (a) Wave loads, (b) Current load, (c) Wind load, (d) Ice or debris loads, and (e) Earthquake load.
10. Natural simultaneous occurrence of those phenomena shall be recognized by proper superposition of items (a) through (d). Item (e), earthquake load, when applied, shall be in lieu of items (a) through (d).

Environmental Considerations

The following section is excerpted from API RP 2G, "API Recommended Practice for Production Facilities on Offshore Structures," January, 1974 [280].

In establishing structure orientation, prevailing seas, swells, currents, and winds should be considered. Likewise, when planning for heliports, docking facilities, flare and relief systems, support cranes and hoists, and escape systems, oceanographic and meteorological influences should be introduced.

Weather conditions, such as temperature, precipitation, humidity and winds, have a significant effect upon the overall arrangement of the structure production facilities. For example, in cold climates, enclosed structures are desirable. Enclosures in turn affect the design considerations such as ventilation and communication systems.

General information on the various types of storms that might affect the platform site should be used to supplement other data developed for operational conditions. Statistics can be compiled giving the expected occurrence of storms by the seasons, direction of approach, etc. Of special interest for construction planning are the duration, the speed of movement and development, and the extent of these conditions. Also of major importance is the ability to forecast storms in the vicinity of a platform.

The probability of personnel being quartered on the platform should be considered, and available transportation to remove personnel from the platform on short notice.

Geographical Considerations

This section is excerpted from API RP 2A, "API Recommended Practices for Planning, Designing and Construction Fixed Offshore Platforms," July 1984 [279].

Knowledge of the soil conditions at the site of construction of any sizable structure is necessary for safe and economical design. On-site soil investigations that outline the various soil strata and strength parameters should be made if sufficient knowledge has not been gained in a particular locality from previous soil investigations. Soundings should also be gathered during the on-site studies. These data should be combined with an understanding of the geology of the region to develop the required foundation design parameters. These studies should extend throughout the depth of the soil to be affected by installation of the foundation elements. The bearing capacity of mat and spread footing foundations and the lateral capacity of the pile foundations are largely determined by the strength of the soil close to the sea floor. Consequently, particular attention should be paid to developing complete information on these soils.

The distance between the platform and shoreside terminal will be a definite consideration when planning pipelines, shipping pumps, gas compressors, storage requirements and waste water-handling facilities.

Operational and Design Considerations

The following is excerpted from API RP 2G, API "Recommended Practice for Production Facilities on Offshore Structures," January 1974 [280].

Space is an important factor in promoting a safe operation. As the density of production facilities on a structure increases, operating and maintenance problems and the chance of failure also increase. The use of other productive measures should be considered.

Adequate space should be provided around machinery, tanks, vessels, and pipe headers to permit easy access for maintenance. Craneways or lifting points should be provided for the ease of handling of equipment and supplies. Work areas should be well lighted and ventilated with adequate provisions for communication between personnel.

In determining spacing production facilities on an offshore structure, many factors should be considered. Some of the major items to be considered are:

- space of operation and operating personnel
- space for maintenance access
- space to provide safety from inadvertent mechanical damage
- space to protect against sources of ignition
- space to provide access for control of fires
- space to limit exposure of important equipment and utilities to possible fire.

It is recognized that the space limitations imposed by the very nature of offshore structures will make many compromises necessary. However, production facilities can be arranged to provide a safe, pollution-free operation.

All equipment should be designed in accordance with the latest standards and in compliance with correct government regulations.

Piping in all areas should be planned to minimize the number of bends, corrosion, and erosion and also provide easy access and egress from the functional parts of each piece of equipment.

The safety of operating personnel is the primary consideration in designing producing facilities. Requirements for means of escape, personnel landings, guards, rails, and lifesaving appliances are specified in U.S. Coast Guard Rules and Regulations for "Artificial Islands and Fixed Structures on the Outer Continental Shelf."

Equipment should be arranged to provide well-defined corridors of egress from all structural areas. Two exit routes in opposite directions from each area should be provided where possible. Enclosed areas containing a source of fuel should have at least two exits opening to a nonhazardous area.

There are many different types of structures utilized in offshore operations. These vary from single-well structures to multiwell completely self-contained drilling and production handling structures. Similarly, the utilities and quarters required vary with the type of structure and how it is utilized.

In planning the utility systems, consideration should be given to number and type of wells, oil and gas processing facilities, remoteness from shore, anticipated production volume, number of people to be housed on the structure, type of fire fighting system, type of control system and electric power source. For example, the single well structure may not require the installation of any utility system; whereas, the self-contained manned structure may require all utilities listed.

Safety Shut-Down Systems

A properly designed safety shut-down system will sense an abnormal operational or equipment condition and react to this condition by shutting in or isolating necessary system components, or even the entire system. Other actions, such as sounding alarms, starting fire extinguishing systems, and depressuring all piping and pressure vessels, may also be initiated by the shut-down system. The actions to be taken will depend on the level of criticality of the abnormal conditions. The three primary purposes for installing shut-down systems are to:

- protect human life
- prevent ecological damage
- protect the investment

In planning and designing shut-down systems, it is first necessary to determine which events could endanger life, environment, or investment. Inspection, maintenance and failure documentation are definite considerations in planning shut-down systems. Inspection procedures that call for in-place functional tests or component removal should be carefully planned. Production facilities arrangements should include locating shut-down system components for easy access for the inspection and test. The personnel who perform inspections should be educated and trained on a formal basis.

Flare and Emergency Relief Systems

Flare and emergency relief systems associated with process equipment should be designed and located with consideration of the amount of combustibles to be relieved, prevailing winds, location of other equipment (including rigs, personnel quarters, fresh air intake systems and helicopter approaches) and other factors affecting the safe, normal flaring or emergency relieving of the process fluids and gases.

Relief System

The relief system is an emergency system for discharging gas by manual or controlled means or by an automatic pressure relief valve from a pressured vessel or piping system to the atmosphere for the purpose of relieving pressures in excess of rated working pressures. The relief system may include the relief valve or rupture disc, the collection piping, a gas scrubber for liquid separation and a gas vent.

Flare System

The flare system is a system for discharging gas through a control valve from a pressured system to the atmosphere during normal operations. This discharge may be either continuous or intermittent. The flare system may include the flare control valve, collection piping, the gas liquid scrubber, and gas vent.

Normally, gases discharged into the flare system are at low pressures and low flowrates. The back pressure requirements are not defined; however, flare systems should be designed to ensure that vessels and tanks will not be over-pressured and to accommodate the maximum volume that could be vented.

Ventilation

Enclosed structures require a thorough review to ensure adequate ventilation. Areas enclosed on all sides that contain equipment considered a source of ignition should be pressurized to prevent hydrocarbons entry. The air intake for the pressurizing system should be located to preclude entry of hydrocarbons into that system. Enclosed areas containing hydrocarbon fuel sources should be vented with an exhaust system to ensure removal of any escaping hydrocarbons. Also, enclosed areas where welding is to be conducted should be ventilated with an exhaust system to ensure removal of gas evolved during welding operations. Air intake for this system should be located to preclude entry of hydrocarbons.

Equipment areas located on open-type structures should be arranged to allow the natural ventilation caused by winds and convection currents. Care should be taken around fired process equipment to ensure that adequate draft for the equipment is provided. Also, the equipment should be arranged to take advantage of the prevailing winds to keep escaping hydrocarbons from being carried toward equipment considered to be a source of ignition. Special care should be taken in the use of protective walls to ensure proper ventilation. Special consideration should be given to ventilation of the wellhead areas. This area should be as open as possible, with a minimum of two sides of the structure open. The interior of the quarters building should have an adequate exhaust system to preclude accumulation of smoke and odors.

Transportation

In designing support facilities for the transportation of personnel and equipment on offshore structures, one must consider the prevailing meteorological and oceanographic conditions. The location of transportation facilities relative to prevailing wind, waves and currents may control the orientation and layout of the entire structure.

Boat landings and docks should be located on the lee side of the structure. Cranes in turn must be located over the boat landing for convenience in loading and offloading equipment. Storage areas for pipe and bulk materials should be located within or adjacent to the area covered by the crane boom.

On manned structures the primary means of escape will be the stairway from the cellar and main decks to the personnel landing. Location of the personnel landing and primary escape route should be taken into consideration when arranging the production facilities and quarters.

Helicopter pads should be located so as to give clear landing approaches for the helicopters. Stacks, guy wires, crane booms, antennas, etc., should be arranged so as not to intrude into the approach or departure paths of the helicopters. The lack of other structures in the area may dictate the need for landing space for two or more helicopters.

Pollution Prevention

Offshore production facilities must include methods for containment and proper disposal of any contaminants (which may be defined as any foreign or undesirable substance, but as used here these substances are meant to be liquids or solids containing liquid hydrocarbons, relatively high concentrations of austic or acidic chemicals, raw sewage, trash and inedible garbage).

Methods must be provided for collecting spilled hydrocarbons from all deck areas. For example, solid deck areas may be drained to a gutter and routed

through a system of gutters or piping to a central point. This may also be done by providing a number of drain openings in the decks that are then piped to a central point. From the central point, the collected liquid material may be discarded into a tank or container where separation takes place due to a specific gravity difference. Liquid hydrocarbons may then be skimmed off and routed into the production system and the remaining water treated by further separation, filtration, etc., as needed.

All deck areas that have a source of oil leakage, spills, or drips must be surrounded by a curbing or a continuous gutter. Alternatively, drip pans may be installed under equipment, provided liquids are routed to a central point and treated as just described.

In installations where toilets are installed and human waste is discharged into surrounding waters, the effluent must meet requirements of applicable government agencies.

Combustible solid wastes such as paper or wood products or other organic material such as garbage may be disposed of by incineration in a suitable container in an area which permits an open fire. Alternatively, the waste may be placed in containers and transported to shore for proper disposal.

Basic Service Safety Systems

The primary reason to have a service safety system on an offshore production platform is for maximum protection of personnel, to minimize chances of fire and reduce chances of explosion and pollution as a result of equipment failure.

The design of each safety system must be engineered for the type of well or wells coming onto the platform. The design must be within guidelines established by the regulatory agency. In the United States, the U.S. Geological Survey is the regulatory agency that enforces periodic testing of the various parts of the shut-down system; that is, provided the platform in question is in federal waters. Platforms in state waters fall within the jurisdiction of the bordering state.

To learn the requirements of the safety shut-down system, refer to the American Petroleum Institute, API RP 14C.

Regulatory Agencies Most Involved with Production Operations

In the United States, a permit is required from the U.S. Army Corps of Engineers to set a structure on or build on manmade islands in any federal or state waters. A dredging permit may be needed for digging a canal in the marshlands.

The U.S. Coast Guard must be notified well in advance of any structural movement in state or federal waters beyond the coast line. This requirement is so the Coast Guard may inform all vessels navigating in the area of such movement and hazard.

The regulatory agency in the United States responsible for drilling and production operations in federal waters is the Minerals Division of the U.S. Geological Survey.

On August 7, 1953, the Outer Continental Shelf Lands Act was enacted, which authorized the Secretary of the Interior, at any time, to prescribe and amend such rules and regulations to be applicable to all operations conducted under a lease or maintained under the provision of the Act, as he determines to be necessary and proper to provide for the prevention of waste and conservation of natural resources of the outer continental shelf, and the protection of correlative rights therein; subject to the supervisory authority of the Secretary of the Interior, the regulations shall be administered by the Director of the

Geological Survey through the Chief of the Conservation Division.

The U.S. Geological Survey regulates drilling and production under fourteen (14) OCS Orders, which are listed below. These orders are subject to revision at any time.

- OCS Order #1 Identification of Well Platforms, Structures, Mobile Drilling Units, and Sub-sea Objects.
- OCS Order #2 Drilling Operations.
- OCS Order #3 Plugging and Abandonment of Wells.
- OCS Order #4 Determination of Well Productivity.
- OCS Order #5 Production Safety Systems.
- OCS Order #6 Completion of Oil and Gas Wells.
- OCS Order #7 Pollution Prevention and Control.
- OCS Order #8 Platforms and Structures.
- OCS Order #9 Oil and Gas Pipelines.
- OCS Order #10 Sulfur Drilling Operations.
- OCS Order #11 Oil and Gas Production Rates, Prevention of Waste, and Protection of Correlative Rights.
- OCS Order #12 Public Inspection of Records.
- OCS Order #13 Production Measurement and Commingling.
- OCS Order #14 Approval of Suspension of Production.

REFERENCES

Properties of Hydrocarbon Mixtures

1. Katz, D. L., *et al.*, *Handbook of Natural Gas Engineering*, McGraw-Hill Book Co., New York, 1959.
2. *Engineering Data Book*, Vols. 1 and 2, GPSA, Tenth Edition, Tulsa, OK, 1987.
3. SPE Reprint No. 13, Vol. 1, pp. 233-235.
4. Soave, G., "Equilibrium constants from a modified Redlich-Kwong equation of state," *Chemical Engineering Science*, 1972.
5. Peng, O. Y., and D. B. Robinson, "A new two constant equation of state," *Industry and Engineering Chemistry Fundamentals*, 1976.
6. *The Phase Behavior of Hydrocarbon Reservoir Fluids*, course given at Core Laboratories Inc., Dallas, TX.
7. MacDonald, R. C., "Reservoir simulation with interface mass transfer," Report No. UT-71-2, University of Texas, Austin, 1971.
8. Moses, P. L., "Engineering applications of phase behavior of crude oil and condensate systems," *Journal of Petroleum Technology*, July 1986.
9. API 811-08800 Standard, RP 44: "Recommended Practice for Sampling Petroleum Reservoir Fluids."
10. Amex, J. W., D. M. Bass and R. L. Whiting, *Petroleum Reservoir Engineering*, McGraw-Hill Book Co., New York, 1960.
11. Weatherly Laboratories, Inc., *Manual 1984*, Lafayette, LA, 1984.
12. Maddox R. N., and J. H. Erbar, *Gas Conditioning and Processing*, Campbell CPS, Norman, OK, 1982.
13. Edmister, W. C., and B. I. Lee, *Applied Hydrocarbon Thermodynamics*, Vol. 1, Gulf Publishing Co., Houston, 1984.
14. Danbert, T. E., and R. P. Danner, *Technical Data Book*, API Washington, D.C., 1980.
15. Danbert, T. E., "Property predictions," *Hydrocarbon Processing*, March 1980.
16. Starling, E., *Fluid Thermodynamic Properties for Light Petroleum Systems*, Gulf Publishing Co., Houston, 1973.

17. Asselineau, L., G. Bogdanic, and J. Vidal, *Fluid Phase Equilibrium*, 1979.
18. Gundersen, T., *Computer and Chemical Engineering*, 1982.

Fluid Flow Performance

19. Brown, K. E., *The Technology of Artificial Lift Methods*, Pennwell Books, Tulsa, Vol. 1, 1977.
20. Golan, M., and C. H. Whitson, *Well Performance*, IHRDC, Boston, 1986.
21. Wallis, G. B., *One-Dimensional Two-phase Flow*, McGraw-Hill Book Co., New York, 1969.
22. Crowley, Ch. J., G. B. Wallis, and P. H. Rothe, *State of the Art Report on Multiphase Methods for Gas and Oil Pipelines*, Vols. 1-3, AGA Project, PR-172-609, December 1986.
23. Duns, H., Jr., and N. C. J. Ros, "Vertical flow of gas and liquid mixture in wells," Proc. 6th World Petroleum Congress, 1963.
24. Orkiszewski, J., "Predicting two-phase pressure drops in vertical pipe," *Journal of Petroleum Technology*, June 1967.
25. Boyd, O. W., *Petroleum Fluid Flow Systems*, Campbell Petroleum Series, 1983.
26. Griffith, P. G., and B. Wallis, "Two-phase Slug Flow," *ASME Journal of Heat Transfer*, 1967.
27. Moody, L. F., "Friction factors in pipe flow," *Transactions of ASME*, November 1941.
28. Barker, A., K. Nielsen, and A. Galb, "Pressure loss, liquid-holdup calculations developed," *Oil & Gas Journal*, March, 1988 (three parts).
29. Hagedorn, A. R., and K. E. Brown, "The effect of liquid viscosity in vertical two-phase flow," *Journal of Petroleum Technology*, February 1964.

Natural Flow Performance

30. Jones, L. G., E. M. Blount, and O. H. Glaze, "Use of short term multiple rate flow tests to predict performance of wells having turbulence," paper SPE 6183, prepared for the 51st Annual Fall Technical Conference and Exhibition of the SPE of AIME, New Orleans, October 3-6, 1976.
31. Crane Company Industrial Products Group, "Flow of Fluids Through Valves, Fittings and Pipe," Chicago Technical Paper No. 410.
32. Rawlins, E. L., and M. A. Schellhardt, "Back-pressure data on natural gas wells and their application to production practices," Monograph 7, USBM, 1936.
33. Mishra, S., and B. H. Caudle, "A simplified procedure for gas deliverability calculations using dimensionless IPR curves," paper SPE 13231, presented at the 59th Annual Technical Conference and Exhibition, Houston, TX, Sept. 16-19, 1984.
34. Dake, L. P., "Fundamentals of reservoir engineering," Elsevier Scientific Publishing Co., Amsterdam, 1978.
35. Chase, R. W., and T. M. Anthony, "A simplified method for determining gas well deliverability," paper SPE 14507, presented at the SPE 1985 Eastern Regional Meeting, Morgantown, WVA, November 6-8, 1985.
36. Cullender, M. H., "The isochronal performance method of determining flow characteristics of gas wells," *Transactions of AIME*, 1955.
37. Cullender, M. H., and R. V. Smith, "Practical solution of gas-flow equations for wells and pipe lines with large temperature gradients," *Transactions of AIME*, 1956.
38. Peffer, J. W., M. A. Miller, and A. D. Hill, "An improved method for calculating bottomhole pressure in flowing gas wells with liquid present," paper SPE 15655, prepared for presentation at the 61st Annual Technical Conference and Exhibition of the SPE, New Orleans, LA, October 5-8, 1986.

39. Katz, D. L., *et al.*, *Handbook of Natural Gas Engineering*, McGraw-Hill Book Co., New York, 1959.
40. Nind, T. E. W., *Principles of Oil Well Production*, Second Edition, McGraw-Hill Book Co., New York, 1981.
41. Ikoku, C. U., *Natural Gas Production Engineering*, John Wiley & Sons, Inc., New York, 1984.
42. Vogel, J. V., "Inflow performance relationships for solution-gas drive wells," *Journal of Petroleum Technology*, January 1968.
43. Fetkovich, M. J., "The isochronal testing of oil wells," paper SPE 4529, prepared for the 48th Annual Fall Meeting of the SPE of AIME, Las Vegas, NV, September 30–October 3, 1973.
44. Standing, M. B., "Inflow performance relationships for damaged wells producing by solution-gas drive," *Journal of Petroleum Technology*, November 1970.
45. Camacho, V., R. G. Raghavan, and R. Raghavan, "Inflow performance relationships for solution-gas-drive reservoirs," *Journal of Petroleum Technology*, May 1989.
46. Standing, M. B., "Concerning the calculation of inflow performance of wells producing from solution-gas drive reservoirs," *Journal of Petroleum Technology*, September 1971.
47. Kelkar, B. G., and R. Cox, "Unified relationship to predict future IPR curves for solution-gas-drive reservoirs," paper SPE 14239, prepared for Conference of the SPE, Las Vegas, NV, September 22–25, 1985.
48. Brown, K. E., *The Technology of Artificial Lift Methods*, Vols. 3a and 3b, Petroleum Publishing Co., Tulsa, OK, 1980.
49. Gilbert, W. E., "Flowing and gas-lift well performance," *Drilling and Production Practices*, 1954.
50. Poettmann, F. E., and R. L. Beck, "New charts developed to predict gas-liquid flow through chokes," *Worlds Oil*, March 1963.
51. Ashford, F. E., "An evaluation of critical multiphase flow performance through wellhead chokes," *Journal of Petroleum Technology*, August 1974.
52. Sachdeva, R., Z. Schmidt, J. P. Brill, and R. M. Blais, "Two-phase flow through chokes," paper SPE 15657, prepared for presentation at the 61st Annual Technical Conference and Exhibition of the SPE, New Orleans, LA, October 5–8, 1986.
53. Richardson, J. M., and A. H. Shaw, "Two-Rate IPR testing—A practical production tool," *The Journal of Canadian Petroleum Technology*, March–April 1982.

Artificial Lift Methods

54. API Recommended Practice 11AR, "Recommended Practice for Care and Use of Subsurface Pumps," Third Edition, June 1, 1989.
55. Brown, K. E., *The Technology of Artificial Lift*, Vol. 2a, Petroleum Publishing Co., Tulsa, OK, 1980.
56. Curtis, S., and E. Showalter, in *Petroleum Engineering Handbook*, H. B. Bradley, Ed., Society of Petroleum Engineers, Richardson, TX, 1987.
57. API Recommended Practice 11L, "API Recommended Practice for Design Calculations for Sucker Rod Pumping Systems," Third Edition, February 1977.
58. Vogel, J. V., "Inflow performance relationships for solution gas drive wells," *Journal of Petroleum Technology*, January 1968.
59. Gibbs, S. G., "Predicting the behavior of a sucker rod pumping system," SPE of AIME paper No. 588, Denver, CO, May 1963.

60. 6.4.1.2 Craft, B. C., W. R. Holden and E. D. Graves, Jr., *Well Design: Drilling and Production*, Prentice-Hall, Englewood Cliffs, NJ, 1962.
61. 6.4.1.3 Atlantic Richfield Co., *Artificial Lift-Sucker Rod Pumping* (manual).
62. 6.4.1.4 API Specification 11E, "Specification for Pumping Units," Sixteenth Edition, October 1, 1989.
63. 6.4.1.6 API Specification 11B, "Specification for Sucker Rods (Pony Rods, Polished Rods, Couplings and Subcouplings)," Twenty-third Edition, October 1, 1989.
64. 6.4.1.7 API Specification 11C, "Specification for Reinforced Plastic Sucker Rods," Second Edition, June 1, 1988.
65. 6.4.1.8 Norris Sucker Rods, Tulsa, OK.
66. 6.4.1.9 API Recommended Practice 11BR, "Recommended Practice for Care and Handling of Sucker Rods," Eighth Edition, October 1, 1989.
67. 6.4.1.13 Bethlehem Steel Co., *Sucker Rod Handbook*, Handbook 489, 1958.
68. 6.4.1.15 Griffin, F. D., in *Petroleum Engineering Handbook*, H. B. Bradley, Ed. Society of Petroleum Engineers, Richardson, TX, 1987.
69. Brill, J. P., and H. D. Beggs, *Two-Phase Flow in Pipes*, University of Tulsa, Tulsa, OK, 1978.
70. Sage, B. H., and W. N. Lacy, *Thermodynamic Properties of the Lighter Hydrocarbons and Nitrogen*, American Petroleum Institute, 1950.
71. Buthod, P., and B. W. Whitley, "Graphic solutions of design problems—Flow of gases in vertical pipes," *The Oil and Gas Journal*, December 1945.
72. Petrie, H., P. Wilson and E. E. Smart, "The theory, hardware, and application of the current generation of oil well jet pumps," Southwestern Petroleum Short Course Association, Lubbock, TX, 1983.
73. Baily, M. C., et al., "The Electrical Submersible Pump," *Petroleum Engineer International*, Parts 1–7, August 1982 through November 15, 1983.

Stimulation and Remedial Operations

74. Economides, M. J., and K. G. Nolte, (Eds.), *Reservoir Stimulation*, Second Edition, Prentice-Hall, Englewood Cliffs, NJ, 1989.
75. Hubbert, M. K., and D. G. Willis, "Mechanics of hydraulic fracturing," *Transactions of AIME*, 1957.
76. Roegiers, J.-C., and E. Detournay, "Considerations on failure initiation in inclined boreholes," Proc. 29th U.S. Symp. on Rock Mech., Minnesota University, 1988.
77. Terzaghi, K., "Die berechnung der durchlässigkeitsziffer des tones aus dem verlauf der hydrodynamischen spannungerscheinungen," *Sber. Akad. Wiss.*, Wien, 1923.
78. Nolte, K. G., "Determination of fracture parameters from fracturing pressure decline," paper SPE 8341, 1979.
79. Nolte, K. G., "A general analysis of fracturing pressure decline with applications to three models," *SPEFE*, December 1986.
80. Castillo, J. L., "Modified fracture pressure decline analysis including pressure-dependent leakoff," paper SPE 16417, 1987.
81. Mayerhofer, M. J., M. J. Economides, and K. G. Nolte, "Experimental study of fracturing fluid loss," CIM/AOSTRA 91–92 presented at the Annual Technical Conference of the Petroleum Society of CIM and AOSTRA, Banff, 1991.
82. Mayerhofer, M. J., M. J. Economides, and K. G. Nolte, "An experimental and fundamental interpretation of filtercake fracturing fluid loss," paper SPE 22873, 1991.

83. Doerler, N., and L. P. Prouvost, "Diverting agents: Laboratory study and modeling of resultant zone injectivities," paper SPE 16250, 1987.
84. Economides, M. J., *A Practical Companion to Reservoir Stimulation*, Elsevier Scientific Publishing, New York, 1992.
85. Gulbis, *et al.*, "Encapsulated breaker for aqueous polymeric fluids," paper SPE 19433, 1990.
86. Montgomery, C. T., and R. E. Steanson, "Proppant selection: The key to successful fracture stimulation," *Journal of Petroleum Technology*, December 1985.
87. Meng, H-Z., and K. E. Brown, "Coupling of production forecasting, fracture geometry requirements and treatment scheduling in the optimum hydraulic fracture design," paper SPE 16435, 1987.
88. Balen, R. M., H-Z. Meng, and M. J. Economides, "Applications of the net present value (NPV) in the optimization of hydraulic fractures," paper SPE 18541, 1988.
89. Perkins, T. K., and L. R. Kern, "Widths of hydraulic fracture," *Journal of Petroleum Technology*, September 1961.
90. Nordgren, R. P., "Propagation of vertical hydraulic fractures," *SPEJ*, August 1972.
91. Khristianovich, S. A., and Y. P. Zheltov, "Formation of vertical fractures by means of highly viscous liquid," Proc. 4th World Petroleum Congress, Section II, 1959, pp. 579-586.
92. Geertsma, J., and R. de Klerk, "A rapid method of predicting width and extent of hydraulically induced fractures," *Journal of Petroleum Technology*, December 1969.
93. Cinco-Ley, H., F. Samaniego, and N. Dominquez, "Transient behavior for a well with a finite-conductivity vertical fracture," *SPEJ*, August 1978.
94. Carter, R. D., Appendix to "Optimum fluid characteristics for fracture extension," by G. C. Howard and C. R. Fast, *Drilling and Production Practices*, 1957.
95. Kemp, L. F., "Study of Nordgen's equation of hydraulic fracturing," *SPEPE*, August 1990.
96. Simonson, E. R., A. S. Abu-Sayed, and R. J. Clifton, "Containment of massive hydraulic fractures," *SPEJ*, February 1978.
97. Ben-Naceur, K., "Modeling of hydraulic fractures," in *Reservoir Stimulation*, Second Edition, M. J. Economides, and K. G. Nolte (Eds.), Prentice-Hall, Englewood Cliffs, NJ, 1989.
98. Palmer, I. D., and R. W. Veatch, Jr., "Abnormally high fracturing pressures in step-rate tests," *SPEPE*, August 1990; and *Transactions of AIME*, month year.
99. Valkó, P., and M. J. Economides, "A continuum damage mechanics model of hydraulic fracturing," *Journal of Petroleum Technology*, March 1993.
100. Valkó, P., and M. J. Economides, "Applications of a continuum damage mechanics model to hydraulic fracturing," paper SPE 25887, 1993.
101. Nierode, D. E., B. B. Williams, and Bombardieri: "Prediction of stimulation from acid fracturing treatments," *Journal of Canadian Petroleum Technology*, October-December 1972.
102. Nierode, D. E., and K. F. Kruk, "An evaluation of acid fluid-loss additives, retarded acids, and acidizing fracture conductivity," paper SPE 4549, 1973.
103. Ben-Naceur, K., and M. J. Economides, "The effectiveness of acid fractures and their production behavior," paper SPE 18536, 1988.
104. Mukherjee, H., and M. J. Economides, "A parametric comparison of horizontal and vertical well performance," paper SPE 18303, 1988.

105. Ben-Naceur, K., and M. J. Economides, "Production from naturally fissured reservoirs intercepted by a vertical hydraulic fracture," *SPEFE*, December 1989.
106. McLennan, J. D., J-C. Roegiers, and M. J. Economides, "Extended reach and horizontal wells," in *Reservoir Stimulation*, Second Edition, M. J. Economides and K. G. Nolte (Eds.), Prentice-Hall, Englewood Cliffs, NJ, 1989.
107. Owens, K. A., S. A. Andersen, and M. J. Economides, "Fracturing pressures for horizontal wells," 1992.
108. Cinco-Ley, H., H. J. Ramey, Jr., and F. G. Miller, "Pseudoskin factors for partially penetrating directionally drilled wells," paper SPE 5589, 1975.
109. Karakas, M., and S. Tariq, "Semi-analytical productivity models for perforated completions," paper SPE 18271, 1988.
110. Piot, B. M., and O. M. Lietard, "Nature of formation damage," in *Reservoir Stimulation*, Second Edition, M. J. Economides and K. G. Nolte (Eds.), Prentice-Hall, Englewood Cliffs, NJ, 1989.
111. Piot, B. M., and H. G. Perthuis, "Matrix acidizing of sandstones," in *Reservoir Stimulation*, Second Edition, M. J. Economides and K. G. Nolte (Eds.), Prentice-Hall, Englewood Cliffs, NJ, 1989.
112. Gidley, J. L., J. C. Ryan, and T. D. Mayhill, "Study of the field application of matrix acidizing," paper SPE 5693, 1976.
113. Daccord, G., E. Touboul, and R. Lenormand, "Carbonate acidizing: A quantitative study of wormholing phenomenon," paper SPE 16887, 1987.
114. Frick, T. P., and M. J. Economides, "Horizontal well damage characterization and removal," paper SPE 21795, 1991.
115. Paccaloni, G., "New method proves value of stimulation planning," *Oil & Gas Journal*, November 1979.
116. Prouvost, L. P., and M. J. Economides, "Applications of real-time matrix acidizing evaluation method," paper SPE 17156, 1988.

Surface Oil Production Systems

117. GPSA, *Engineering Data Book*, Vols. 1 and 2, Tenth Edition, Tulsa, OK, 1987.
118. Perry, R. H., and D. Green, *Perry's Chemical Engineers Handbook*, Sixth Edition, McGraw-Hill, Inc., New York, 1984.
119. Arnold, K., and M. Steward, *Surface Production Operation*, Gulf Publishing Co., Houston, 1986.
120. Robertson, J. A., and T. C. Clayton, *Engineering Fluid Mechanics*, Houghton-Mifflin Co., Boston, 1985.
121. API Specification 12J, Sixth Edition, Washington, D.C., June 1, 1988.
122. API Specification 12K, Sixth Edition, June 1, 1988.
123. Bizanti, M. S., and Yu. Hancheny, *Oil & Gas Journal*, 1987.
124. Campbell, J. M., *Gas Conditioning and Processing*, Vols. 1 and 2, OK, 1984.
125. Sivalls, C. R., *Oil and Gas Separation Design Manual*, Sivalls, Inc., Box 2792, Odessa, TX.
126. Bradley, B. H., *Petroleum Engineering Handbook*, SPE, Richardson, TX, 1987.
127. Sivalls, C. R., Tech. Bull. No. 113, Sivalls, Inc., Box 2792, Odessa, TX.

Gas Production Engineering

128. McKetta, J. J., and A. H. Wehe, *Hydrocarbon Processing*, August 1958.
129. Robinson, J. N., and E. Wichert, *Oil & Gas Journal*, February 1978.
130. Liptak, B. G., and K. Venczel, *Instrument Engineers' Handbook*, Chilton Book Co., Rodnor, 1982.
131. Carr-Brion, K., *Moisture Sensors in Process Control*, Elsevier Scientific Publishers, New York, 1986.

132. E. G. & G. Chandler *Engineering Catalog*, Tulsa, OK.
133. Makogon, Y. F., *Hydrates of Natural Gas*, Pennwell, Tulsa, OK, 1981.
134. *Moisture Control and Measurement Limited Catalog*, Wetherby, WY, England LS23 7BJ.
135. *Engineering Data Book*, Tenth Edition, 1987: GPSA, 6526 East 60th Street, Tulsa, OK 74145.
136. Campbell, J. M., *Gas Conditioning and Processing*, Vols. 1 and 2, CPS Series 1984, Norman, OK.
137. Sivalls, R., *Glycol Dehydration Design Manual*, Sivalls, Inc., Odessa, TX, 1982.
138. Orsdol, F. G., 1988 SPE Gas Technology Symposium Proceedings, Dallas, TX, June 13-15, SPE 17753.
139. Corcoran, W. S., and J. Honeywell, *Chemical Engineering*, July 1975.
140. *Manual of Petroleum Measurement Standards*, Chap. 14, Sec. 3, API, Washington, D.C., 1985.
141. Miller, R. W., *Flow Measurement Engineering Handbook*, McGraw-Hill, Inc., 1983.
142. Yarborough, L., and K. R. Hall, SPE publ. No. 13, Vol. 1, pp. 233-235.
143. "Compressibility and supercompressibility for natural gas and other hydrocarbon gases transmission measurement," Report No. 8, AGA Manual XQ 1285, Arlington, VA, 1986.
144. Katz, D. L., et al., *Handbook of Natural Gas Engineering*, McGraw-Hill Book Co., New York, 1959.
145. Kumar, S., *Gas Production Engineering*, Gulf Publishing Co., Houston, TX, 1987.
146. Ikoku, Chu U., *Natural Gas Production Engineering*, John Wiley & Sons, New York, 1984.
147. Pichot, P., *Compressor Application Engineering*, Vols. 1 and 2, Gulf Publishing Co., Houston, TX, 1986.
148. The American Gas Association, GEOP Book T-2 *Compressor Station Operations*, Arlington, VA, 1985.
149. The Marley Cooling Tower Co., *Cooling Tower Fundamentals*, Kansas City, MO, 1982.

Corrosion and Scaling

150. Nestle, A. C., *Corrosion Inhibitors in Petroleum Production Primary Recovery*, NACE, Houston, TX, 1973.
151. EnDean, E. J., "Corrosion control in the well bore," *Petroleum Engineering International*, August 1976.
152. Weintritt, D. J., "Criteria for scale and corrosion," *Petroleum Engineering International*, August 1980.
153. Milligan, M. R., "Sour gas well completion practices in the foothills, western Canada," *Journal of Petroleum Technology*, September 1982.
154. Hamby, T. W., and R. N. Tuttle, "Deep, high pressure sour gas is challenge," *Oil & Gas Journal*, May 12, 1975.
155. Hamby, T. W., and R. N. Tuttle, "Deep wells—A corrosion engineering challenge," *Material Performance*, October 1977.
156. Tyler, W., and T. W. Hamby, "Development of high pressure sour gas technology," paper SPE 8309, presented in 54th Annual Fall Technical Conference and Exhibition of Society of Petroleum Engineers of AIME, Las Vegas, NV, September 23-26, 1979.
157. Huntoon, G. G., "Completion practices in deep sour Tuscaloosa wells," *Journal of Petroleum Technology*, January 1984.
158. Greer, J. B., and M. Watkins, "Corrosion testing of highly alloyed materials for deep, sour gas well environments," *Journal of Petroleum Technology*, June 1976.

159. Kilstrom, K. J., "Whitney Canyon sour gas well completion techniques," *Journal of Petroleum Technology*, January 1983.
160. Uhlig, H. H., *Corrosion and Corrosion Control*, Second Edition, John Wiley & Sons, Inc., New York, 1971.
161. Lyle, F. F., S. Lechler, J. Brandt, F. E. Blount, and E. S. Snaveley, "Inhibition of steel corrosion in sour gas well environments containing sulfur and ethylamine," *Material Performance*, 1978.
162. Kane, R. D., and J. B. Greer, "Sulfide stress cracking of high-strength steels in laboratory and oilfield environments," *Journal of Petroleum Technology*, November 1977.
163. Place, M. C., "Corrosion control-deep sour gas production," presented at The 54th Annual Fall Technical Conference of Exhibition of The Society of Petroleum Engineers of AIME, Las Vegas, NV, September 1979.
164. Chin, C. L., and L. M. Cenegy, "A test for corrosion inhibitors to be used in oilfield capillary injection system," *Materials Performance*, April 1983.
165. Gatlin, W. G., "Evaluation of inhibitors for wet, sour gas gathering system," *Material Performance*, May 1978.
166. Donham, J. E., U.S. Pat. 3,699,118 (Oct. 17, 1972), assigned to Amoco Production Co.
167. Maddox, Jr., J., U.S. Pat. 3,758,493 (Sept. 11, 1973), assigned to Texaco, Inc.
168. Larsen, A. L., U.S. Pat. 3,787,319 (Jan. 22, 1974), assigned to Marathon Oil Co.
169. DeWaard, C., and D. E. Milliams, Paper F-1, First Int. Conf. on Internal and External Prot. of Pipes, September 1975, Univ. of Durham.
170. Shock, D. A., and J. D. Sudbury, *Corrosion*, 1952.
171. Patterson, K. W., "Downhole corrosion encountered in the carbon dioxide flood at the Sacroc unit," South West Petroleum Short Course, pp. 608-615, Chevron U.S.A. Inc., Houston, TX, 1979.
172. McClay, R. A., and L. E. Newton, "Corrosion and operational problems, CO₂ Project, Sacroc Unit, paper SPE 6391, prepared for the 1977 Permian Basian Oil and Gas Recovery Conference of the Society of Petroleum Engineers of AIME, Midland, TX, March 10-11, 1977.
173. Macon, R. B., "Design and operation of the Levelland unit CO₂ Injection Facility," paper SPE 8410, presented at the 54th Annual Fall Technical Conference and Exhibition of the Society of Petroleum Engineers of AIME, Las Vegas, NV, September 23-26, 1979.
174. Nimerick, K. H., U.S. Pat. 3,692,675 (Sept. 19, 1972), assigned to the Dow Chemical Co.
175. Larsen, A. L., U.S. Pat. 3,770,055 (Nov. 6, 1973), assigned to Marathon Oil Co.
176. Redmore, D., U.S. Pat. 3,846,071 (Nov. 5, 1974), assigned to Petrolite Corp.
177. Bufkin, L. B., and J. L. Houk, "Batch treatments of deep gas wells using water-soluble corrosion inhibitors," paper SPE 9699, presented at the 1981 Deep Drilling & Production Symposium of the Society of Petroleum Engineers of AIME, Amarillo, TX, April 5-7, 1981.
178. Maxwell, R., "System soothes downhole indigestion," *Production Chemicals*, Midland, TX, September 1983.
179. "Corrosion Inhibitors in Secondary Recovery," A. K. Dunlop Corrosion Inhibitors, NACE, Houston, TX, 1973.
180. Carlberg, B. L., "Water quality for trouble-free injection," *Petroleum Engineer International*, August 1980.
181. Mitchell, R. W., D. M. Grist, and M. J. Boyle, "Chemical treatment associated with North Sea projects," *Journal of Petroleum Technology*, May 1980.

182. Cannon, J. H., H. J. EnDean, R. B. Todd, and K. Belanus, "Corrosion protection by downhole continuous inhibitor transmission via external capillary," *Material Performance*, February 1981.
183. LaFayette, C. R., A. U. Landrum, J. E. Atwood, and D. H. Mutti, "Corrosion control of gas-lift well tubulars by continuous inhibitor injection into the gas-lift gas stream," *Journal of Petroleum Technology*, June 1976.
184. Karla, S. K., and J. B. Bradburn, "Corrosion mitigation-critical facet of well-completion design," *Journal of Petroleum Technology*, September 1983.
185. Vetter, O. J., "The chemical squeeze process—Some new information on some old misconceptions," *Journal of Petroleum Technology*, March 1973.
186. Hover, G. W., and D. M. Spriggs, "Field performance of a scale inhibitor squeeze program," *Journal of Petroleum Technology*, July 1972.
187. Ostroff, A. G., *Introduction to Oilfield Water Technology*, National Association of Corrosion Engineers, Houston, TX, 1979.
188. Munger, C. G., "Sulfides—Their effect on coating and substrates," *Material Performance*, 1978.
189. Snavelly, E. S., "Chemical removal of oxygen from natural waters," *Journal of Petroleum Technology*, April 1971.
190. Redmore, D., U.S. Pat. 3,764,548 (Oct. 9, 1973), assigned to Petrolite Corp.
191. Recommended Practice RP-04-75, "Recommended practice for selection of metallic materials to be used in all phases of water handling for injection into oil bearing formations," N.A.C.E., Houston, TX, 1976.
192. Vetter, O. J., "Oilfield scale—Can we handle it?," *Journal of Petroleum Technology*, December 1976.
193. Vetter, O. J., "An evaluation of scale inhibitors," *Journal of Petroleum Technology*, August 1972.
194. Vetter, O. J., "How barium sulfate is formed: An interpretation," *Journal of Petroleum Technology*, December 1975.
195. Liu, S. T., and G. H. Nancollas, "Crystal growth and dissolution of barium sulfate," paper SPE 5300, presented at the SPE-AIME Oilfield Chemistry Symposium, Dallas, January 16–17, 1975.
196. Kandarpa, U., and O. J. Vetter, "Scale inhibitors for injection of incompatible waters," paper SPE 10595, presented at the SPE Sixth International Symposium on Oilfield and Geothermal Chemistry, Dallas, January 25–27, 1982.
197. Mitchell, R. W., "The forties field sea-water injection system," *Journal of Petroleum Technology*, June 1978.
198. Essel, A. J., and B. L. Carlberg, "Strontium sulfate scale control by inhibitor squeeze treatment in the Fateh field," *Journal of Petroleum Technology*, June 1982.
199. Phillips, R. C., and O. J. G. Vetter, "Prediction of deposition of calcium sulfate scale under down-hole conditions," paper SPE 2620, presented at SPE-AIME, 44th Fall Meeting, Denver, September 28–October 1, 1969.
200. Ralston, P. H., "Scale control with aminomethylene-phosphonates," *Journal of Petroleum Technology*, August 1969.
201. Gill, J. S., and G. H. Nancollas, "Formation and dissolution of high-temperature forms of calcium sulfate scales: The influence of inhibitors," paper SPE 7861, SPE-AIME, Houston, January 22–24, 1979.
202. Sawada, K., and G. H. Nancollas, "Formation of scales of calcium carbonate polymorphs: The influence of magnesium ion and inhibitors," *Journal of Petroleum Technology*, March 1982.
203. Miller, J. P., "A portion of the system calcium carbonate, carbon dioxide, water," *American Journal of Solids*, 1952.
204. Ellis, A. S., "The solubility of calcium carbonate in sodium chloride solutions at high temperatures," *American Journal of Solids*, 1963.

205. Legezin, N. E., and K. S. Zarembee, Mater. Nach. Tekh. Soveshch. Zashch. Korroz. Oborudouaniya Neft. Gazav. Shvazhin, Baku, 1964.
206. Englander, H. E., "Conductometric measurement of carbonate scale deposition and scale inhibitors effectiveness," *Journal of Petroleum Technology*, July 1975.
207. Martin, R. L., and W. P. Evelyn, U.S. Pat. 4,339,349 (Feb. 11, 1980), assigned to Petrolite Corp.
208. Baumgartner, A. W., "Microbiological corrosion—What causes and how it can be controlled," paper SPE, presented at 5th Biennial Secondary Recovery Symposium, Wichita Falls, TX, May 7–8, 1962.
209. Allred, C. R., "Use of chemical pesticides and the effect on production and cost of crude oil," *Materials Performance*, Betz Laboratories, Inc., March 1979.
210. *Handbook of Industrial Water Conditioning*, Sec. 5, p. 456, Trevoze, PA, 1980.
211. Redmore, D., U.S. Pat. 3,888,626 (June 10, 1975) assigned to Petrolite Corp.
212. "The role of bacteria in the corrosion of oilfield equipment," TPC Publication No. 3, National Association of Corrosion Engineers, Houston, 1976.
213. Taylor, R. E., "How to control corrosion in product pipelines," *Pipeline & Gas Journal*, February 1980.
214. Pettus, P. L., and L. N. Strickland, "Water soluble corrosion inhibitors help solve internal corrosion problems," *Pipeline and Gas Journal*, February 1979.
215. Congram, G. E., "Organic inhibitors help control internal pipeline corrosion," *Oil & Gas Journal*, December 12, 1974.
216. Carradine, W. R., G. J. Hanna, G. F. Pace, and R. N. Grabois, "High-performance flow improves for products Lines," *Oil & Gas Journal*, August 8, 1983.
217. Bauman, T. C., and L. T. Overstreet, "Corrosion and piping materials in the CPI," *Chemical Engineering*, August 3, 1978.
218. Popan, V. A., "Cleaning and drying pipelines," *Pipeline & Gas Journal*, December 1979.
219. O'Donnell, P., "Offshore pipeline internally coated in place," *Oil & Gas Journal*, October 21, 1975.
220. Senkovski, Jr., E., "Standard laboratory test for Pipeline Coatings," *Materials Performance*, August 1979.
221. Carlson, R. E., "Internal coatings of welded on offshore line," *Pipeline & Gas Journal*, January 1982.
222. McConkey, S. E., "Fusion-bonded epoxy pipe coatings are economical, practical," *Oil & Gas Journal*, July 19, 1982.
223. Kipin, P., "Internal pipe coatings pay off," *Oil & Gas Journal*, August 3, 1982.
224. Nathan, C. C., "Corrosion inhibitors," N.A.C.E., Houston, TX, 1974.
225. "Corrosion in gas sweetening units," *Petrolite Corporation Manual*, St. Louis, MO, 1982.
226. "Multi-Purpose products for gas systems corrosion control," *Nalco Manual*, Houston, 1983.
227. Robertson, G. A., "Gas lines find inhibitors increase flow reduce internal corrosion," *Pipeline & Gas Journal*, March 1982.
228. EnDean, H., "Design corrosion control treatments," *Champion Chemical Inc. Manual*, Houston, TX, 1982.
229. "Corrosion inhibition of gas pipelines by Chemical treatment," SPE 6596, 1977.
230. Johns, T. G., "Pipeline corrosion still major problem," *Corrosion*, September 1979.
231. "Ultrasonic treatment enhances pipe corrosion monitoring," *Oil & Gas Journal*, September 6, 1983.
232. Gardner, F. T., A. T. Clothier, and F. Coryell, "The use of ammonia in control of vapor space corrosion of storage tanks," *Corrosion*, March 1950.

233. Rogers, W. F., "A note on the value of ammonia treatment for tank and casing annulus corrosion by hydrogen sulfide," *Corrosion*, November 1955.
234. Quimby, W. S., "Oil soluble inhibitors for controlling corrosion in tankers and pipe lines," *Corrosion*, March 1960.
235. Oosterhout, J. C. D., M. E. Stanley, and W. S. Quimby, "Corrosion prevention in tankers and storage tanks by fogging or flotation with an inhibitor solution," *Corrosion*, May 1959.
236. Linke, W. F., "Seidell's solubilities," The American Chemical Society, Fourth Edition, Vol. 2, pp. 1452-1455, Washington, D.C., 1965.
237. *NACE Corrosion Engineer's Reference Book*, Second Edition, National Association of Corrosion Engineers, 1991.

Environmental Considerations

238. American Petroleum Institute, "API environmental guidance document—Onshore solid waste management in exploration and production operations," API, Washington, D.C., 1989.
239. Kennedy, A. J., Esso Resources Canada LTD., "Oil waste road application practices at the Esso Resources LTD Cold Lake Project," Proceedings from the 1st International Symposium on Oil and Gas Exploration Waste Management Practices, pp. 689-701, 1990.
240. Deuel, L. E., "Evaluation of limiting constituents suggested for land disposal of exploration and production wastes," Proceedings from the 1st International Symposium on Oil and Gas Exploration Waste Management Practices, pp. 411-430, 1990.
241. American Petroleum Institute, "The migration of petroleum in soil and groundwater, principles and countermeasures," paper 4149, API, Washington, D.C., 1972.
242. CONCAWE Secretariate, "Inland oil spill clean-up manual," Report No. 4/74. The Hague, Netherlands, 1974.
243. Perry, R., and D. Green, *Perry's Chemical Engineering Handbook*, McGraw-Hill, Inc., New York, 1984.
244. Nirmalakhandan, N., *Fate and Transport of Environmental Contaminants*, New Mexico State University Printing Press, Las Cruces, NM, 1994.
245. EPA, "A compendium of technologies used in the treatment of hazardous wastes," Office of Research and Development, EPA/625/8-87/014, 1987.
246. Levin, M. A., and M. A. Gealt, *Biotreatment of Industrial and Hazardous Waste*, McGraw-Hill, Inc., New York, 1993.
247. Wolfram, J. H., *et al.*, "Method development using field samples for assessing bioremediation potential," SPE 25994, SPE/EPA Exploration and Production Environmental Conference, San Antonio, TX, March 7-10, 1993.
248. McMillen, S. J., J. M. Kerr, and N. R. Gray, "Microsm studies of factors that influence biremediation of crude oils in soils," SPE 25981, SPE/EPA Exploration and Production Environmental Conference, San Antonio, TX, March 7-10, 1993.
249. Ratliff, M., "Construction and operation of a biological treatment cell for the treatment of hydrocarbon-contaminated soil in Alaska," SPE 25998, SPE/EPA Exploration and Production Environmental Conference, San Antonio, TX, March 7-10, 1993.
250. Crews, B., and E. Malachosky, "The effect of pH on microbial degradation of oil based drilling mud in a slurry phase reactor," SPE 25992, SPE/EPA Exploration and Production Environmental Conference, San Antonio, TX, March 7-10, 1993.
251. Bleckman, *et al.*, "Landtreatment of oil base drill cuttings," SPE/IADC Drilling Conference, New Orleans, pp. 529-536, 1989.

252. Whitfield, D. L., "Soil farming of oil mud drill cuttings," SPE/IADC Drilling Conference, New Orleans, pp. 429-438, 1987.
253. Streebe, L. E., "Landtreatment of petroleum refinery sludges," EPA Doc. No. 600/2-84-193, 1985.
254. Ashworth, J., R. P. Scroggins, and D. McCoy, "Feasibility of land application as a waste management practice for the disposal of residual diesel invert base muds and cuttings in the foothills of Alberta," Proceeding from the International Conference on Drilling Waste, Calgary, 1988.
255. Shirazi, G. A., "Landfarming of drilling muds in conjunction with pit site reclamation: A case history," Proceedings from the 1st International Symposium on Oil and Gas Exploration Waste Management Practices, pp. 553-564, 1990.
256. Mayk, T. M., F. I. Nikiforuk, and D. K. Weiss, "Drilling waste landspreading field trail in the cold Lake Heavy Oil Region," Proceeding from the 1st International Symposium on Oil and Gas Exploration Waste Management Practices, pp. 267-279, 1990.
257. Zimmerman, P. K., and J. D. Robert, "Landfarming of drilling muds in conjunction with pit site reclamation: A case history," Proceeding from the 1st International Symposium on Oil and Gas Exploration Waste Management Practices, pp. 565-573, 1990.
258. U.S. Salinity Laboratory, "Diagnosis and improvement of saline and alkaline soils," *Handbook 60*, USDA, USGPO, Washington, D.C., 1954.
259. American Petroleum Institute, "Oil and gas industry exploration and production wastes," Doc. No. 471-01-09, July 1987.
260. Deuel, L. E., "Evaluation of limiting constituents suggested for land disposal of exploration and production wastes," Proceeding from the 1st International Symposium on Oil and Gas Exploration Waste Management Practices, pp. 411-430, 1990.
261. Pasternak, D., and Y. Malach, "Saline irrigation in the Negev desert," Publications Section, The Institute of Applied Research, Ben-Gurion University of Negev, Beer-Shiva, Israel, 1987.
262. American Water Works Association, *Water Quality and Treatment*, Fourth Edition, McGraw-Hill, Inc., New York, 1990.
263. Wesolwski, A., *et al.*, "Characterization of produced waters for natural gas production operations," December 1987, Topical Report For Gas Research Institute, Chicago, IL.
264. MacDonald, C., "BLM issues proposed guidance on the disposal of water produced from oil and gas production," Department of the Interior News Release, January 19, 1990.
265. Bureau of Land Management, Onshore Order No. 7, 43 CFR 3160.
266. Bureau of Land Management, "Unlined surface impoundment remediation and closure for approximately 47,175-62,900 unlined surface impoundments" (under the jurisdiction of the Farmington and Albuquerque Districts), Environmental Assessment NM-070-3004, December 1993.
267. Federal Register, title 51, part 189, September 30, 1986, p. 34836.
268. Gray, P. R., "Norm contamination in the petroleum industry," *Journal of Petroleum Technology*, January 1993.
269. Osborne, P., "Program overview—Underground injection control, Region VIII Second Edition, EPA Region VIII, Denver, 1991.
270. Mangelson, K., "Radium removal for small community water supply systems," EPA/600/52-88/039, USEPA.
271. Miller, H. T., and E. D. Bruce, "Pathway exposure analysis and the identification of waste disposal options for petroleum production wastes containing

- naturally occurring radioactive materials," First International Symposium on Oil and Gas Exploration Waste Management Practices, pp. 731-744, 19XX.
272. Smith, J. B., and L. A. Browning, "Proposed changes to EPA Class II well construction standards and area of review procedures," SPE 25961, SPE/EPA Exploration and Production Environmental Conference, San Antonio, TX, March 7-10, 1993.

Offshore Operations

279. API Recommended Practice RP 2A, "API Recommended practice for planning, designing and construction fixed offshore Platform," Fourteenth Edition, July 1984.
280. API Recommended Practice RP 26, "API Recommended practice for production facilities on offshore structures, First Edition, January 1974.
281. CONCAWE, "Protection of groundwater from oil pollution," NTIS PB82-174608, The Hague, Netherlands, 1979.
282. Riddick, J. A., W. B. Bunger, and T. K. Sakano, *Organic Solvents Physical Properties and Methods of Purification*, Fourth Edition, John Wiley and Sons, New York, 1986.
283. Cole, G. M., *Assessment and Remediation of Petroleum Contaminated Sites*, Lewis Publishers (CRC Press), Boca Raton, FL, 1994.
284. *Handbook of Chemistry and Physics*, CRC Press, Cleveland, 1977.
285. Ray, J., and F. Engelhardt, *Produced Water, Technological/Environmental Issues and Solutions*, Plenum Press, New York, 1992.
286. Wagner, J. F., "Toxicity and radium 226 in produced water," Wyoming's Regulatory Approach Proceeding from the First International Symposium on Oil and Gas Exploration Waste Management Practices, pp. 987-994, 1990.

7

Petroleum Economics

Richard J. Miller

Richard J. Miller and Associates, Inc.
Huntington Beach, California

Estimating Oil and Gas Reserves	987
Classification of Petroleum Products	989
Methods for Estimating Reserves	990
Non-Associated Gas Reservoirs	997
Production Stimulation	1005
Determining the Value of Future Production	1011
The Market for Petroleum	1011
Economics and the Petroleum Engineer	1013
Preparation of a Cash Flow	1014
Valuation of Oil and Gas Properties	1024
Risk Analysis	1027
References	1030

Chapter 7

Petroleum Economics

The purpose of petroleum engineering is to examine, define and implement the methods and procedures for developing and producing oil, gas and associated products so as to optimize profits and return on investment. In other words—to make money. We say optimize because there are factors other than financial considerations that influence a return. The purpose of this chapter is to outline the methods and procedures used to evaluate an oil and/or gas property. Evaluation consists of two major steps:

- determination of the amount of producible oil and/or gas and the schedule of recovery
- determination of the economic value of the future production

These are not separate functions, but meld at the boundary so that one influences the other.

ESTIMATING OIL AND GAS RESERVES

What are reserves? The USGS and DOE define the relationship between petroleum resources and reserves in fairly simple terms. The total resource base of oil and gas, the amount that exists prior to production, consists of the total volume that was formed and later trapped within the earth. A portion of this resource base is nonrecoverable by current or foreseeable technology because either it is dispersed in low concentrations or it simply cannot be extracted due to economics, intractable physical forces or both. The recoverable resource base consists of discovered and undiscovered resources. Discovered resources include recoverable and nonrecoverable resources, while the recoverable resources include cumulative production and reserves. If there has been no production, then all the recoverable resource is classed as reserves. DOE describes reserves as “volumes, estimated to exist in known deposits, that are believed to be recoverable in the future through the application of anticipated technology” (Figure 7-1).

Industry applies a more restrictive definition by including a concern for economics. The Society of Petroleum Engineers (SPE) defines reserves [1] as “estimated volumes of crude oil . . . and other products . . . anticipated to be commercially recoverable . . . from a given date forward, under existing economic conditions, by established operating practices, and under current government regulations.” Within the term “reserves” are subcategories from *proved producing reserves* currently being produced and likely to continue to be produced—to *proved undeveloped*—reserves requiring capital expenditures to drill a well or otherwise initiate production—to *probable and possible reserves*. Probable reserves are less certain of recovery than proved reserves and possible reserves are less certain than probable reserves (Figure 7-2).

Reserves are a volume of future production estimated as of a given point in time, such as December 31 for many public companies. The estimator must consider the conditions that exist at that time, not the year before or a year hence. The volume must be estimated based on currently established operating

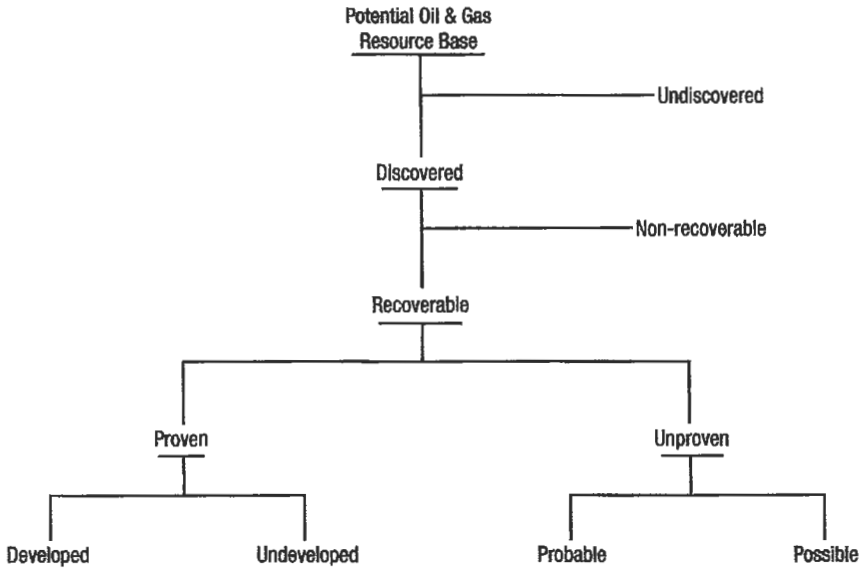


Figure 7-1. Table of resources and reserves.

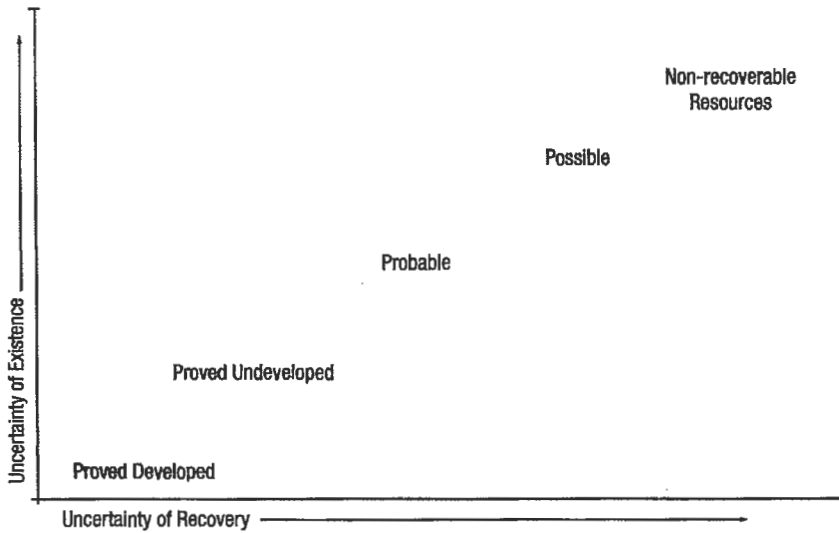


Figure 7-2. Reserve class vs. uncertainty.

practices that are in use on the property, or which can reasonably be expected to be applicable to the property. This gives some latitude to the estimator but, as the range of possible operating methods is broadened, there is a strong probability that the classification of the reserves will have to be changed as the certainty of recovery changes. Finally, the volume must be recoverable under current prices and costs with due consideration for the interaction of prices and costs. Thus, if oil price declines and costs do not, the volume of reserves could be reduced as the "economic life" of the property is shortened. There is some debate whether current economic conditions should include the expectation that prices and/or costs will change in the future. The SPE definition says that current economic conditions "include prices and costs prevailing at the time of the estimate" but does not rule out the inclusion of price/cost escalators. It is common practice in today's industry to escalate or deescalate prices and costs based on the expectation of future events as deemed appropriate at the time of the evaluation.

Definitions for reserves such as those published by the SPE and other organizations and agencies may vary in terminology but not in general practice. There are also special case definitions used by government agencies. The Securities and Exchange Commission requires reserve estimates filed with that agency to be done with prices and costs held constant at the then current levels and using a discount rate of 10%. This definition is intended to allow comparison on a common basis between companies and from year to year. The SEC method has no practical value. Some taxing agencies, particularly those with *ad valorem* taxing authority, use reserve definitions that allow the assessor wide latitude in determining reserves and property values.

CLASSIFICATION OF PETROLEUM PRODUCTS [2-4]

The petroleum products that may be subject to evaluation can be grouped as:

- crude oil
- natural gas
- associated products

Crude oil is a liquid composite of many hydrocarbon compounds that, depending on the composition, has differing properties such as oil gravity, viscosity, and pour point which, at least in part, define the quality of the oil for end use and also influence the methods that would be used to develop and produce the oil. Crude that has a high API gravity and low viscosity is generally easier to produce than low gravity, high viscosity oil that may require stimulation to maintain production rates. The characteristics of the oil can, and often does, influence everything from well spacing to pump size to life of production—all of which has an impact on the economic value of the producing property.

Crude oil is a market commodity and is subject to considerable variation in its economic value. Oil price varies based on location, gravity, sulfur content and competition from other fuel sources. As an example, crude oil produced in California is consistently priced \$3-4/bbl below similar oil in the mid-continent in part because of oil gravity but also because of the sulfur content and the lack of access to other markets. At times, such as under the WPT, crude oil has been economically stratified based on when it was put on production and the status of the producing company.

Natural gas is a fluid also composed of many hydrocarbon compounds although generally not as complex as crude oil. The primary differences between

gases are (1) the heating value (generally the methane content), (2) the non-hydrocarbon gas (N_2 , O_2 , H_2S , etc.) content and (3) the amount of liquid or heavy ends that can be obtained as natural gas liquids (NGL).

The economic value of natural gas is directly related to its composition. A gas with no nonhydrocarbons and which is entirely methane and ethane has a high heating value. If it contains propanes and other stripable ends, the value increases. Natural gas enjoys a relatively high economic value because it has a low cost of production. However, it is highly regulated through pipeline and utility controls on transportation and pricing so that it rarely achieves equivalent value with crude oil on a \$/Btu basis. In addition, due to the ease of transporting gas, there is substantial competition among gas producing regions, which acts as a control on gas prices.

Associated products include (a) natural gas liquids (NGL) that can include propane, butane, natural gasoline and virtually any other hydrocarbon that can be stripped from gas, (b) sulfur, (c) nonhydrocarbon gases. The NGLs can have substantial economic value but require investment in specialized stripping plants. Pricing tends to be driven by the local market and can be volatile with demand. Sulfur is a common by-product in many Canadian fields and in some areas of the United States. The economic value tends to fluctuate considerably, and sulfur production may often be more of a nuisance than an economic benefit. Non-hydrocarbon gases such as nitrogen and helium can be economic by-products, but in most cases where this occurs the nonhydrocarbon becomes the primary product and the natural gas is secondary.

The economics of crude oil, natural gas and associated products can differ significantly depending on market conditions.

METHODS FOR ESTIMATING RESERVES [5,6]

The true reserves of a well are known only after it has been plugged and abandoned. Reserves determination is never more than an estimate. Some estimates are based on more knowledge and analysis than others, but a large part of the estimate is the evaluator's perception of future production and economic conditions. Information is critical and the proper usage of that data is vital.

Primary Production. Primary production uses the natural reservoir energy of dissolved gas, encroaching water, gravity or other source as the recovery mechanism. There are a number of methods available for reserves estimation, which can be used alone or in concert. The use of the methods depends on the stage of life of the property and the amount and quality of data that are available. These methods can be generally grouped as (1) volumetric, (2) material balance, (3) production performance. Each method has its attributes and drawbacks.

Volumetric methods [7,8] are used early in the life of a property, before significant production has occurred. This is a subjective criteria; volumetric methods can be and often are used long after production has reached maturity. Volumetric methods attempt to determine the amount of oil and/or gas-in-place and reserves by calculating a volume from the physical properties of the reservoir(s). The method requires a knowledge of the size of the reservoir, and the physical properties of the reservoir rock(s) and fluid(s). The volume of original oil in place (OOIP) in a segment of the reservoir is equal to:

Volume V = Amount of pore space \times (amount of oil - amount of water)

$$OOIP = V_0 = V(\phi) \times S_h \quad (7-1)$$

where V = specified volume of reservoir measured in acre feet
 ϕ = porosity—% of void space in V
 S_h = hydrocarbon saturation as a % of fluid content
 $= 1 - S_w$, where S_w is the water saturation as a % of fluid content
 $= S_o + S_g$ if there is a free gas cap

In practical use, the equation is

$$V_o = \frac{7758V(\phi)(1 - S_w)}{B_{oi}} \quad \text{bbl STO} \quad (7-2)$$

in which 7,758 is the conversion from acre-feet to barrels and B_o is a factor to convert the fluid volume at reservoir pressure and temperature to stock tank barrels.

In free-gas reservoirs or in the gas cap of oil reservoirs, the volume of gas-in-place is

$$V_g = \frac{43,560V(\phi)(1 - S_w)}{B_{gi}} \quad \text{scf} \quad (7-3)$$

where 43,560 is the conversion from acre-feet to cubic feet. The gas formation volume factor (B_g) may be estimated for various combinations of pressure, temperature and gas gravity from published tables.

The volume of dissolved gas in an oil reservoir is given by

$$V_g = \frac{7758V(\phi)(1 - S_w)R_s}{B_g} \quad (7-4)$$

where R_s is the volume of dissolved gas per barrel of oil at reservoir conditions.

The volumetric method can be subject to considerable error because (1) it is often used to evaluate a property when little specific data may be available and (2) it requires the estimation of reservoir rock and fluid properties and reservoir volumes from spot measurements of the properties that are then applied to the entire reservoir. Porosity and water saturation are obtained from well logs and/or core samples that are measured from a small volume of the reservoir and that, under the best circumstances, only approximate the conditions in the reservoir. The areal extent of the reservoir is rarely known until many wells are drilled, while volume is estimated using a zone thickness measured at one or more points in the reservoir. While techniques of core analysis and, especially, electric and other well log measurement and analysis have become very sophisticated, the volumetric method remains only a gross estimate of oil-in-place.

Conversion of a volumetric oil-in-place to ultimate recovery requires the use of a *recovery factor*, R_f , which can be either a unit recovery (bbl or Mcf/acre ft) or a percentage of OOIP.

Recovery factors can be determined from the performance of similar reservoirs, from laboratory analysis of cores, or computer simulation of anticipated performance. Unit recovery can also be calculated assuming information is available from reservoir fluids and core analysis.

Ultimate recovery = $V_o \times$ recovery factor

For solution gas drive or depletion drive reservoirs:

$$N = 7758(\phi) \left(\frac{1 - S_w}{B_{oi}} - \frac{1 - S_w - S_g}{B_{oa}} \right) \text{ STB/acre ft} \quad (7-5)$$

where recovery is the difference between OOIP at initial reservoir conditions and OIP at abandonment conditions.

In a water drive reservoir:

$$N = 7758(\phi) \left(\frac{1 - S_{oi}}{B_{oi}} - \frac{S_{or}}{11B_{oa}} \right) \text{ STB/acre ft} \quad (7-6)$$

The volumetric method has certain data requirements. In checklist form:

Reservoir volume:

- accurate mapping of gross and net sand
- determination of oil-water and gas-oil contacts
- calculation of reservoir volume (acre/ft)

Rock properties:

- determine porosity—from logs, cores or both
- determine water saturation—from logs, cores or both
- determine residual S_o and S_w —from core tests

Fluid properties:

- determine B_o at initial and abandonment conditions from PVT analysis

The *material balance* [9–12] is a more complex method of estimating reserves, but has the advantage of providing an estimate of production over time under certain conditions. The method has several forms and requires both an extensive pressure–volume–temperature (PVT) analysis of reservoir fluids and an accurate pressure history of the reservoir. The latter obviously requires that some production (5–10% of ultimate recovery) occur before the method can be used. The method is not a substitute for the volumetric method but can be used along with the volumetric method later in the life of the property and is often used to obtain a recovery factor for volumetric calculations. The material balance method could also be used if reliable pressure history data can be obtained for a reservoir with similar rock and fluid properties.

The material balance is a practical application of conservation of mass and energy principles used to balance the withdrawals from a reservoir with changes in volume of the original reservoir fluids and the influx of additional fluids. The method has been modified, adapted and simplified by many authors. The several forms attempt to model reservoir performance over time by equating the expansion of reservoir fluids, as pressure decline occurs during production, to the change in voidage of the reservoir caused by withdrawal of oil, gas and water (less any water influx). The method requires an iterative solution of sequential pressure drops caused by production. The values for each successive step in the analysis are taken from PVT analysis of the reservoir fluids.

The general equation is:

$$N = \frac{N_p [B_t + 0.1781 B_g (R_p - R_{si})] - (W_c - W_p)}{B_{oi} \left[m \left(\frac{B_g}{B_{gi}} \right) + \frac{B_t}{B_{oi}} - (m + 1) \left(1 - \frac{\Delta p (C_f + S_w C_w)}{1 - S_w} \right) \right]} \quad (7-7)$$

where N is the OOIP, which, by definition, must remain the same through each step of pressure decline. The general equation assumes that all components of the reservoir react to production. By using the pressure-production history of the reservoir to obtain a relation of $N_p / \Delta P$ (production) to ΔP (change in reservoir pressure), a projection of $N_p / \Delta P$ can be used as the basis for a material balance estimate of future production to the point of pressure depletion. At that point, ultimate *primary* recovery is obtained and

$$R_r = N_p / N$$

The material balance may be thought of as:

$$\text{Initial oil in place} = \text{oil remaining} + \text{oil produced at time (t)}$$

However, it is more convenient to treat the balance as:

$$\text{Initial gas in place} = \text{gas remaining} + \text{gas produced}$$

In this form the general equation becomes:

$$N = \frac{N_p [B_o + B_g (R_p - R_s)] - B_w (W_c - W_p)}{m B_{oi} \left(\frac{B_g}{B_{gi}} - 1 \right) + B_g (R_{si} - R_s) - (B_{oi} - B_o)} \quad (7-8)$$

where $N_p [B_o + B_g (R_p - R_s)]$ is the reservoir volume of produced oil and gas; $B_w (W_c - W_p)$ is the total amount of water influx retained in the reservoir; $m B_{oi} (B_g / B_{gi} - 1)$ is the expansion of the gas cap; and $B_g (R_{si} - R_s)$ is the reduction in the amount of solution gas at reservoir conditions occurring with production of N_p barrels of oil [13,14].

If there is no gas cap and no water influx, then:

$$N = \frac{N_p [B_o + B_g (R_p - R_s)] + B_w W_p}{B_g (R_{si} - R_s) - (B_{oi} - B_o)} \quad (7-9)$$

If the reservoir is above the bubble point [15], then B_g remains constant; R_p , R_s and R_{si} are equal and:

$$N = \frac{N_p B_o + W_p B_w}{B_o - B_{oi}} \quad (7-10)$$

B_w can often be ignored if reservoir pressure is low; however, data on water compressibility are readily available. Where reservoir fluid property data indicate measurable change in the compressibility of oil, water and rock with changes in pressure, then the equation(s) would be modified by using an effective oil compressibility term:

$$N = \frac{N_p B_o + W_p B_o}{C_{oe} B_{oi} (P_i - P)} \tag{7-11}$$

where:

$$C_{oe} = C_o + \left(\frac{S_w}{1 - S_w} \right) C_w + \left(\frac{1 - \phi}{\phi(1 - S_w)} \right) C_r \tag{7-12}$$

In water drive reservoirs [16,17]:

$$N = \frac{N_p [B_o + B_g (R_p - R_s)] + B_w W_p}{D_i} - \frac{W_c B_w}{D} = N_i - \frac{W_c B_w}{D_i} \tag{7-13}$$

where:

$$D_i = B_g (R_{si} - R_s) - (B_{oi} - B_o) \tag{7-13a}$$

Water influx (W_w) is rarely known or measurable; however, where water influx occurs, calculated values of N_i over time would increase. N could be estimated by plotting N_i vs. time and extrapolating back to $t = 0$ where $N_i(t = 0) = N$. This approach includes a significant potential for error if the plotted points are not a straight line. Several authors have presented means of improving this approach (Figure 7-3).

In reservoirs with an active gas cap and no active oil/gas segregation with production:

$$N = \frac{N_p [B_o + B_q (R_p - R_s)] + B_w W_p}{mB_{ob} \left(\frac{B_g}{B_{gt}} - 1 \right) + B_g (R_{tb} - R_s) - (B_{ob} - B_o)} \tag{7-14}$$

where subscript b refers to the bubble point (BP).

In reservoirs with a combination of drives:

$$N = \frac{N_p [B_o + B_g (R_p - R_s)] - B_w (W_c - W_p)}{mB_{ob} \left(\frac{B_g}{B_{gt}} - 1 \right) + B_g (R_{tb} - R_s) - (B_{ob} - B_o)} \tag{7-15}$$

or

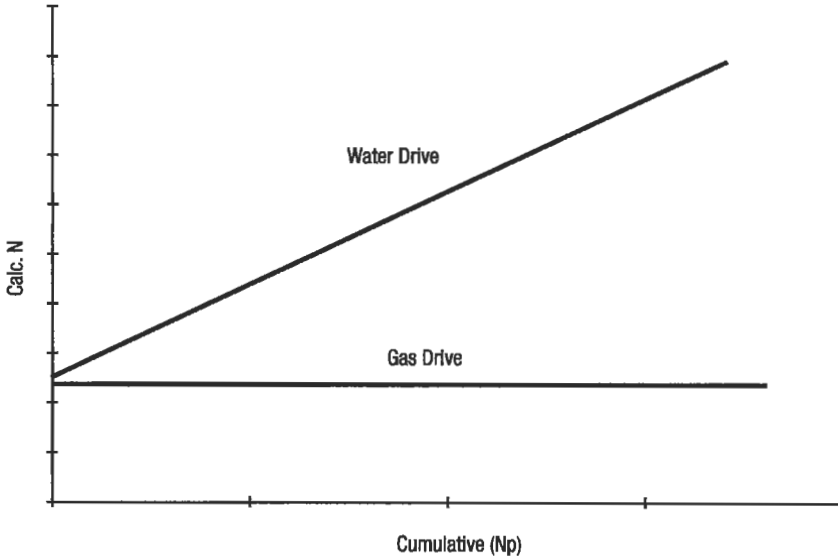


Figure 7-3. Calculated N vs. cumulative Np.

$$N = \frac{N_p [B_o + B_g (R_c - R_s)] + B_w W_p}{D_i} - \frac{B_w W_e}{D_i} \quad (7-16)$$

where

$$D_i = mB_{ob} \left(\frac{B_g}{B_{gi}} - 1 \right) + B_g (R_{ob} - R_s) - (B_{ob} - B_o) \quad (7-17)$$

Several authors have presented variations in the calculation procedure to obtain material balance recovery factors. Muskat's method [18-20] calculates the change in oil saturation with change in pressure as production occurs:

$$\frac{\Delta S_o}{\Delta p} = \frac{S_o \left(\frac{B_g dR_s}{B_o dp} \right) + (1 - S_o - S_w) \left[B_g \frac{d(1/B_g)}{dp} \right] + S_o \left(\frac{\mu_o k_{rq}}{\mu_g k_{ro}} \frac{dB_o}{B_o dp} \right)}{1 + \frac{\mu_o k_{rq}}{\mu_g k_{ro}}} \quad (7-18)$$

At depletion,

$$S_{oa} = S_{oi} - \Delta S_o \quad (7-19)$$

$$R_f = \frac{S_{oi} - S_{oa}}{S_{oi}} (\%) \quad (7-20)$$

Muskat's method assumes uniform oil saturation (no gas segregation) and relatively low permeability. The method requires small pressure increments but is readily adapted to computer analysis, thereby reducing the tedium of the calculation. The results are converted into recovery per acre foot by:

$$N_p = 7758(\phi) \left(\frac{1 - S_w}{B_{oi}} - \frac{S_o}{B_o} \right) \text{ STB/acre ft} \quad (7-21)$$

Cumulative recovery as a percentage of OOIP can be determined by:

$$\frac{N_p}{N} = 1 - \left(\frac{S_o}{1 - S_w} \right) \left(\frac{B_{oi}}{B_o} \right) \quad (7-22)$$

and gas/oil ratio performance by:

$$R = R_s + 5.615 \left(\frac{B_o}{B_{oi}} \frac{\mu_o}{\mu_g} \frac{k_{rg}}{k_{ro}} \right) \text{ SCF/STB} \quad (7-23)$$

Relative production can be calculated from:

$$q_o = q_{oi} \left(\frac{k_o}{k_{oi}} \frac{\mu_{oi}}{\mu_o} \frac{p}{P_i} \right) \text{ STB/Day} \quad (7-24)$$

Turner's method [21,22] for use in solution gas reservoirs below the bubble point (BP), requires a simultaneous solution of the material balance equation and the instantaneous gas/oil ratio equation. The procedure is to calculate the cumulative oil (N_p) and gas (G_p) for a pressure drop ($p_1 - p_2$) as follows:

1. $N_p = 0$ at the bubble point.

$$2. \quad (G_p)_2 = (N_p)_2 (R_p)_2 = N \left[(R_s - R_s) - 5.615 \left(\frac{B_{oi} - B_o}{B_g} \right) \right] - (N_p)_2 \left(5.615 \frac{B_o}{B_g} - R_s \right) \quad (7-25)$$

$$3. \quad (S_i)_2 = S_w + (1 - S_w) \frac{B_o}{B_{oi}} \left[1 - \frac{(N_p)_2}{N} \right] \quad (7-26)$$

4. Determine k_{rg}/k_{ro} at $(S_i)_2$:

$$R_2 = R_s + 5.615 \left(\frac{B_o}{B_g} \right) \left(\frac{\mu_o}{\mu_g} \right) \left(\frac{k_{ro}}{k_{rg}} \right) \text{ at } p_2 \quad (7-27)$$

$$5. \quad \text{Compute } (G_p)_2 = (G_p)_1 + \frac{R_1 + R_2}{Z} [(N_p)_2 - (N_p)_1] \text{ @ } p_2 \quad (7-28)$$

6. Make three good estimates of $(N_p)_2$ and the corresponding $(G_p)_2$ from steps 2 and 5. Plot $(N_p)_2$ vs. $(G_p)_2$ for step 2 and for step 5 and take the intersection of the curves as satisfying both equations.

Published tables of recovery factors, calculated using the Muskat and Tarnier methods, can be used where no detailed data regarding reservoir fluids or rock properties is available.

NON-ASSOCIATED GAS RESERVOIRS [23,24]

$$\text{OGIP} = G = \frac{43560V_g(\phi)(1-S_w)}{B_g} \quad \text{SCF} \quad (7-29)$$

$$\Delta G_p = 43,560(\phi)(1-S_w) \left(\frac{1}{B_{gi}} - \frac{1}{B_{ga}} \right) \quad \text{SCF/acre ft} \quad (7-30)$$

The gas formation volume factor (B_g) at abandonment (B_{ga}) is calculated at abandonment pressure (P_a), which can be based on pipeline pressure or the minimum pressure to which the reservoir can be reduced for the conditions of reservoir depth, tubing size or other constraint(s).

Production Performance. The volumetric and material balance methods of estimating reserves are valuable tools but are often limited by paucity of data; mathematical calculations that, in being simplified, leave out or assume certain reservoir conditions to be true; and/or the assumption of uniformity of conditions throughout the reservoir. In contrast, the *production performance* [25-28] *approach* implicitly includes all reservoir and production operating conditions that would effect performance. When production is not curtailed by regulatory or other artificial conditions, the volume of production from the well is a direct result of the interaction, however great or small or uniformly dispersed, of all reservoir rock and fluid properties with the existing wellbore and operating conditions. Since oil reservoirs are finite in volume, production over time causes a reduction in pressure that, in turn, causes a decline in the rate of production per unit time. The combination of time, production rate and cumulative production can be used to determine both remaining reserves and productive life.

When there has been sufficient history to establish a production trend for a property, the three variables may be plotted as graphs, commonly known as *decline curves*, which can then be extrapolated to determine future production and reserves. The most common approach is the rate-time plot where time is plotted as the independent variable (X) and production rate is plotted as the dependent variable (Y). This curve, with sufficient definition, can be extrapolated into the future to estimate future production and reserves.

The only requirements for extrapolation are that the curve demonstrate uniformity of shape and that there be an end point. The uniformity of shape is required to ensure that performance is the result of interaction of reservoir and operating condition and is not being altered by changing operating or other artificial conditions. It is important to carefully analyze all data used to define production performance and to equate production during short production periods (February) and downtime (during pump changes or other well work) to

production during "normal" periods. Changes in production caused by mechanical alterations, such as opening or closing flow valves, pump changes or pump speeds, must be equated and may require additional graphical analysis. The use of sales data must equate the time between sales to the production time. Often sales occur when a certain tank volume is accumulated, not on a strict time basis, so that, over time, the period between sales may increase while the volume appears to be constant. The production rate, however, may well be declining.

The decline curve may generally demonstrate one of three forms: *exponential*, essentially a straight line of constant slope; *hyperbolic*, a continuously flattening curve that can be described mathematically; and *harmonic*, a special case of the hyperbolic decline (Figure 7-4).

The decline can be described in two ways: the nominal decline rate is the negative slope of the curve of the natural log of the production ratio (q) at time (t), or

$$D = -\frac{d \ln q}{dt} = -\frac{dq/dt}{q} \tag{7-31}$$

The effective decline rate is more common in actual practice and has the form of a loss rate:

$$D_e = \frac{q_i - q_1}{q_i} \tag{7-32}$$

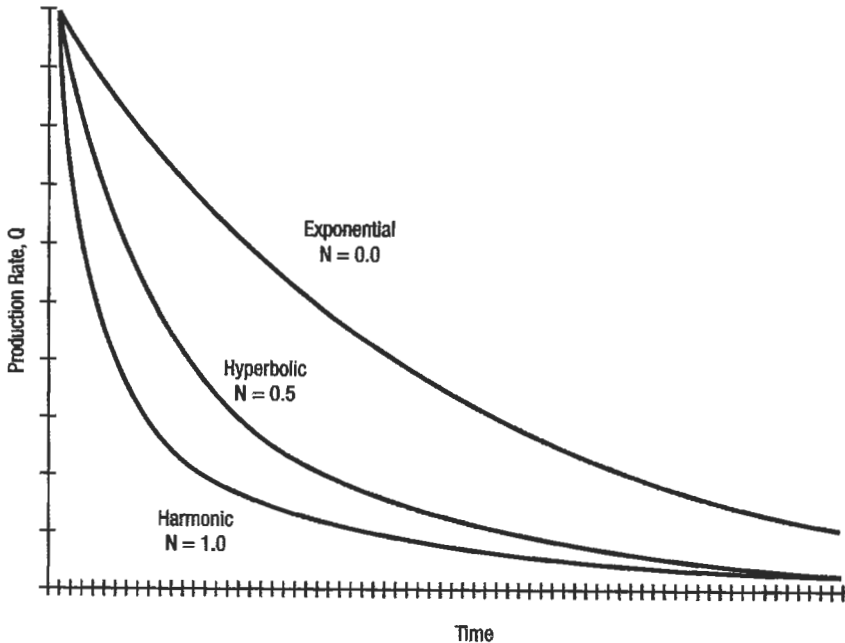


Figure 7-4. Decline curve—Rate/Time (exponential, harmonic, hyperbolic).

Decline rate is normally expressed as an annual rate for comparison among properties.

For exponential or constant-percentage decline, the nominal rate is

$$D = -\frac{dq/dt}{q} \quad (7-33)$$

where, after integration,

$$q = q_1 e^{-Dt} \quad (7-34)$$

where t is the time period over which q is to be calculated and to which D must conform. Further integration yields

$$N_p = \frac{q_i - q}{D} \quad (7-35)$$

where N_p is the cumulative production during the period between q_i and q . If q_u at abandonment is substituted for q , then N_p is the ultimate recovery at decline rate D .

Hyperbolic decline may only become evident later in the life of a property and may require careful analysis to be discerned. In fact, most primary production occurs as hyperbolic decline but, in practice, constant rate decline is often used to approximate future production. In the late life of production, hyperbolic decline approaches asymptotic conditions and can very well be approximated by an exponential decline. For the early life:

$$D = \frac{-dq/dt}{q} = bq^n \quad (7-36)$$

where n is a fractional power of the production rate between 0 and 1 and b is a constant determined at initial conditions:

$$b = \frac{D_1}{q_1^n} \quad (7-37)$$

$$q = q_1(1 + nD_1 t)^{-1/n} \quad (7-38)$$

$$N_p = \frac{q_1^n (q_1^{1-n} - q^{1-n})}{(1-n)D_1} \quad (7-39)$$

For harmonic decline:

$$D = -\frac{dq/dt}{q} = bq \quad (7-40)$$

where:

$$b = \frac{D_i}{q_i} \quad (7-41)$$

and, after integrating,

$$q = \frac{q_i}{1 + D_i t} \quad (7-42)$$

$$N_p = \frac{q_i}{D_i} \ln \frac{q_i}{q} = \frac{q_i}{D_i} \ln r \quad (7-43)$$

Nominal and effective declines can be related:

$$\text{Exponential: } D_e = 1 - e^{-D} \quad (7-44)$$

$$D_n = -\ln(1 - D_e) \quad (7-45)$$

$$\text{Hyperbolic: } D_{ei} = 1 - (1 + nD_i)^{-1/n} \quad (7-46)$$

$$D_{ni} = \frac{1}{n} [(1 - d_{ei})^{-n} - 1] \quad (7-47)$$

$$\text{Harmonic: } D_{ei} = \frac{D_i}{1 + D_i} \quad (7-48)$$

$$D_{ni} = \frac{D_{ei}}{1 - D_{ei}} \quad (7-49)$$

Most decline curves are hyperbolic with values of $n = 0.0$ and 0.7 , while the majority are between 0.0 and 0.4 . Published tables relating time to loss rate and N_p for various decline rates may be useful.

In addition to the requirement for a uniform trend, estimation of reserves from production performance requires an end point. This can be an imposed limit, such as the flowrate at a certain wellhead pressure for gas wells, but is most commonly an *economic limit*.

The economic limit is the production rate at which the revenue from sale of production equals the cost of production at the same time. Continued production at or below the economic limit rate creates no economic gain and would serve no economic purpose. Of course, there may be other reasons to continue production—as many operators did after the price declines of 1986–1990—but the estimated amount of that production is not, by definition, reserves.

Economic limit = production × product price
 minus royalty
 minus production and *ad valorem* tax
 minus operating costs
 = zero

or

$$\text{Economic limit} = \frac{\text{Costs of production/unit time}}{\text{Product price/bbl or Mcf}} = \text{Production/unit time}$$

Other forms of production performance analysis may be useful as an adjunct to the time-rate curve.

Rate—Cumulative. A plot of exponential production rate versus cumulative production on cartesian scale often yields a straight line. Extrapolation of this line to the economic limit production rate yields the ultimate oil or gas recovery (under the assumed economic conditions).

$$\text{Reserves} = \text{ultimate recovery} - \text{cumulative recovery}$$

WOR—Cumulative Production. In water drive reservoirs or in most waterflood or steamflooding operations, ultimate recovery can be estimated by plotting the WOR against cumulative recovery (Figure 7-5). The maximum WOR that can be sustained under the assumed economic conditions can be used as an economic limit. The cumulative production at that point is ultimate recovery and reserves can be estimated as above. A variation on this method is to use water cut (water as a % of total fluid) rather than WOR (Figure 7-6).

GOR—Cumulative Oil Production. Use of a rate-cum or WOR-cum analysis can be used to estimate periodic and ultimate GOR, which can then be converted to gas production. Conversely, if gas volume is a limitation on production (such as where gas cannot be sold) then GOR versus cumulative oil can be used to estimate recovery.

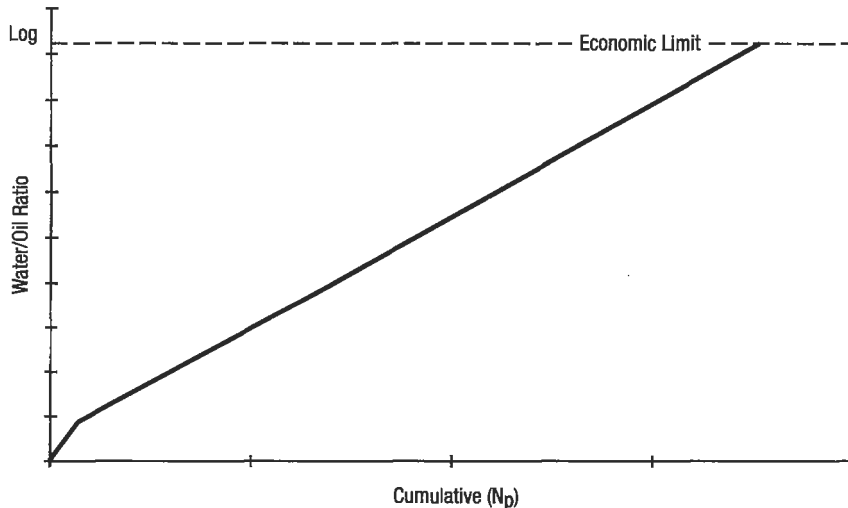


Figure 7-5. Water/oil ratio and cumulative decline curve.

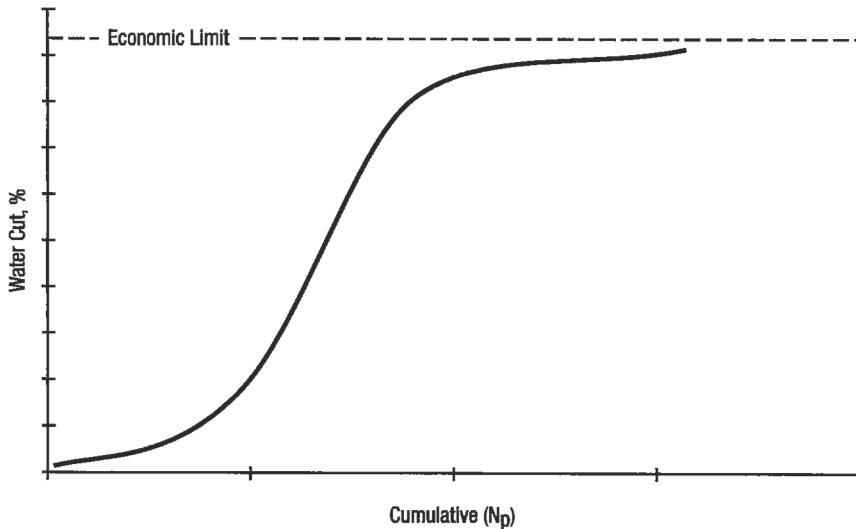


Figure 7-6. Water cut and cumulative decline curve.

Analysis of rate-cum and other variations using hyperbolic or harmonic decline trends may require semi-log or log-log treatment.

In the instance where the property being valued does not have sufficient history to be fully definitive, the *performance of similar properties* may be used to estimate reserves for the subject property. The similar property may be another well on the same lease if the subject property is a new well, or it may be a group of wells on an adjacent lease, or even a group of wells in a nearby field that produces from the same reservoir. "Similar" is a broad term and must be used with care. Similar does not necessarily mean identical—no two wells or fields are identical. The properties must, however, share the reservoir rock and fluid characteristics and operating conditions that would allow the evaluator to expect that they would perform much the same way over time. Wells in the same field (or portions thereof) and reservoir should perform in a similar manner, whereas wells in different reservoirs may perform very differently. In some cases, however, even wells in the same reservoir may perform differently if the conditions are changed. The performance of infill wells may be very different from the original wells if the infill wells reduce the drainage areas of all wells.

Single-well comparisons require extreme care, but can be used by imposing the historical performance decline of one well on a new well. Multiwell or "family" curves combine the performance of several wells by overlaying the decline curve of each well and defining a composite curve through the set. The steps to this are:

1. Select the comparable wells or leases.
2. Plot the decline curves for each well or lease with initial production points set at (a) a common zero point of the wells that went on production at near the same time or (b) at date of first production. Some judgment is needed here.
3. Define a composite decline curve through the curve set.
4. Use the family curve to project the new well or lease.

Slider [29], Fetkovich [30,31] and others [32] have developed methods of decline curve (rate-time) analysis that are described as "type-curve" analysis. The methods are based on the idea that wells or groups of wells with similar reservoir characteristics will describe similar decline curves over time when compared on a dimensionless time-rate basis. The method requires production history sufficient to demonstrate some depletion but can then be used to determine (a) the form of the decline (including the hyperbolic constant), and (b) certain reservoir properties (assuming other data are available). Type-curve matching requires an overlay of actual rate-time data on a set of dimensionless time-rate curves. The dimensionless decline trend that best fits the actual rate-time curve can then be transferred directly to the actual curve to define the future decline trend. The method can employ a number of forms of dimensionless curves.

The match points can then be used to calculate certain reservoir properties, such as kh, using the dimensionless equations:

$$q_{Da} = \frac{q(t)}{q_i} = q_D \left[\ln \left(\frac{r_e}{r_w} \right) - \frac{1}{2} \right] = \frac{\frac{q(t)}{kh(P_i - P_{wf})}}{141.3 \mu B \left[\ln \left(\frac{r_e}{r_o} \right) - \frac{1}{2} \right]} \quad (7-50)$$

$$t_{Da} = \frac{t_d}{\frac{1}{2} \left[\left(\frac{r_e}{r_w} \right)^2 - 1 \right] \left[\ln \left(\frac{r_e}{r_w} \right) - \frac{1}{2} \right]} = \frac{\frac{0.00634kt}{\phi \mu C_r r_w^2}}{\frac{1}{2} \left[\left(\frac{r_e}{r_w} \right)^2 - 1 \right] \left[\ln \left(\frac{r_e}{r_w} \right) - \frac{1}{2} \right]} \quad (7-51)$$

Type-curve matching is similar-well analysis on a highly technical level. The method has a potential advantage in allowing an evaluator to define a decline form and quantify the hyperbolic constant earlier in the life of a property than would be the case using "eyeball" methods.

For primary reserves estimation, the production performance method is the most reliable method assuming the data are available and are properly analyzed. The characteristics of the various methods allow them to be used in progression from volumetric to performance with increasing accuracy and reliability. In practice, the methods can be shown to be complementary over time so that one method may be used as a check on another method, all other things being equal.

Gas Reservoirs. Estimation of future recovery from natural gas reservoirs uses the same rate-time and rate-cumulative relations as discussed for oil reservoirs, however, the fluid characteristics of gas gives greater effect to pressure. A useful relation for estimating gas reserves is the P/Z-cumulative relation (Figure 7-7) which plots reservoir pressure divided by the compressibility factor, Z, at time t against cumulative gas Ng. Extrapolation to the economic limit yields an estimate of ultimate recovery.

A Note on Production Data. Use of the production performance methods of evaluation, either alone or in combination with other methods, requires the collection and analysis of historical production data to formulate a trend that

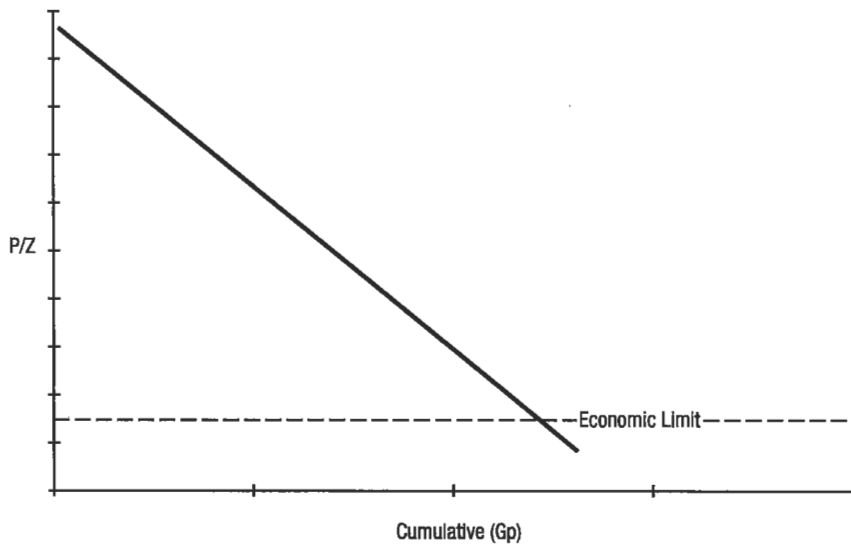


Figure 7-7. Nonassociated gas—Pressure/cumulative decline.

can be extrapolated into the future in the form of a production schedule. There are numerous sources of data, including, but not limited to, company production records, sales records, well tests, reports to regulatory agencies and public data gathering and reporting firms. All data, regardless of the source, must be carefully reviewed for accuracy and to define any variations that may have occurred.

The most common variations in performance are those caused by (a) short producing periods, (b) mechanical changes, (c) regulatory restrictions, (d) capacity restrictions.

Review and check production data for:

Duration of producing period:

- short months (February)
- wells produced less than full month

Mechanical changes:

- production reductions due to well downtime for repairs, etc.
- increase production due to change in flow valves; pump size, stroke length, or speed; workovers
- decline in production due to increasing fluid levels, etc.

Regulatory restrictions:

- proration
- limits on gas disposal
- limits on water disposal
- air emission requirements

Capacity restrictions:

- limited pipeline or other shipping facilities

PRODUCTION STIMULATION

A subset of the estimation of primary oil (and gas) reserves is the evaluation of properties that are subject to production stimulation techniques. These are methods such as cyclic steaming, fracturing, and acidizing, among others, that alter the reservoir and, possibly, operating conditions of a property but continue to rely on the natural reservoir energy to cause production to occur. These methods add no new energy and are therefore not secondary or enhanced recovery methods and, except in some arguable cases, do not add reserves; they simply act to speed the recovery of oil and/or gas that would be ultimately recovered at some time in the future. On the other hand, the stimulation of eventual production sooner rather than later *can* have important economic benefits and may result in additional reserves being credited to the property where *economic conditions* alone would suggest that the property should be shut-in or abandoned.

Cyclic steaming [33–36] is a common method in oil fields where the oil is high viscosity or has a physical composition that causes production to occur at low rates. Steam is injected into a producing well for periods of up to several days. The well is then returned to production after a period of time. The steam is used to transfer heat to the reservoir where the heat serves two primary purposes in varying degrees. Heat reduces the viscosity of the oil. It also “cleans up” the wellbore by steam cleaning the perforations and/or liner slots and the sand face of accumulated tar and sand thereby improving permeability near the wellbore.

The combination of effects may cause production to increase as much as 10 to 20 times the presteam rate. Wells that have been steamed generally increase to a peak immediately following the steaming and then decline in a definable manner over time. The production cycle may last from a few months to as much as 2 years. Wells can be steamed repeatedly, but the stimulation effect will noticeably diminish with repeated cycles as reservoir energy in the near wellbore region depletes. Eventually, the production declines to a point where the cost of steaming is equal to the incremental return and cycling steaming is stopped.

Fracturing [37–40] The use of hydraulic energy to create fractures in the reservoir—and acidizing—the use of acid to improve near wellbore permeability—are production stimulation methods that alter the reservoir characteristics, permanently or temporarily, in such a way as to cause production to increase over a period of time. As with cyclic steaming, the methods generally increase the rate of production and, thereby, have an economic benefit but do not usually add reserves.

Estimation of reserves and future production from stimulated wells generally requires an overlay of production performance and volumetric methods. Some experience with performance using a stimulation method is necessary before a reliable projection method can be defined. Estimation of recovery from cyclic steaming must be based solely on experience and analysis of actual performance of the same or similar properties. The construction of “family” curves of wells, grouped according to the number of cycles common to the wells, can be used to estimate the change in q_p to q_s with each cycle and the point on the decline curve where the stimulated production will begin. Several authors have published methods of estimating production performance from fractured and acidized wells and these may be used as part of an estimation of reserves.

Secondary Recovery and EOR Methods. There are many differing definitions of secondary recovery and enhanced oil recovery (EOR). As used in this discussion, EOR will include recovery methods that might also be described as

secondary or tertiary depending on the timing of the project and the circumstances of the reservoir. The essential difference between these methods and primary recovery is that EOR methods result in additional production by adding energy to the reservoir, while primary recovery uses only the natural energy of the reservoir. The purpose of EOR is to increase the reserves and production from reservoirs that can be, or have been, produced by primary means.

EOR methods can be put in three general groups:

1. Gas injection—the use of natural gas or other gas as an injection fluid
2. Water injection—use of unheated water as an injection fluid
3. Thermal methods including
 - steam injection
 - *in situ* combustion

These basic methods have many variants depending on reservoir conditions and the use of additives in the injection fluids. Indeed, each project design can be considered a unique method if the design is based on specific reservoir characteristics. Only the basic methods are discussed.

In virtually all EOR methods, a fluid is injected into the reservoir at one point with the intention of sweeping or flushing oil from that point to other points in the reservoir where the oil can be produced. For analysis purposes, this is most often pictured as a piston-type mechanism where the injected fluid occupies an increasingly larger part of the reservoir pushing a “bank” of oil ahead of it to producing wells.

The success or failure of an EOR project generally depends on:

1. The mobility ratio (M), where:

$$M = \frac{\text{Mobility of displacing fluid}}{\text{Mobility of displaced fluid}} = \frac{\lambda_1}{\lambda_2} \quad (7-52)$$

and where

$$\lambda = K/\mu = \frac{\text{permeability}}{\text{viscosity}} \quad (7-53)$$

If $M = 1$, the fluid mobilities are identical

Favorable $\langle M = 1 \rangle$ Unfavorable

2. Areal and vertical sweep efficiency—The relative proportion (%) of reservoir area and net thickness that is swept by the displacing fluid. This is largely a function of geology although mobility also plays a part.

Regardless of the EOR method used, the project must be designed to consider and account for both mobility and sweep efficiency. Most of the variations in the basic methods result from attempts to alter and improve mobility or sweep efficiency or both.

Gas Injection. The injection of natural gas either as a pressure maintenance or EOR method is by far the oldest form of injection method for increasing oil recovery. Prior to the time when natural gas became a major fuel source and

could be transported, most produced gas was either burned off or injected into the same or another reservoir. Gas injection is virtually unknown in the United States today.

Gas can be a very efficient injection medium but is generally limited (by mobility ratio) to light oil reservoirs with thin sand sections. The method is most efficient when injection can occur in the top of a structure or into an existing gas cap where it then performs as a piston moving downward, pushing oil down or out to producing wells.

Water Injection. Water injection or waterflooding has been around for a long time. Waterflooding may be done by reinjecting produced water from the reservoir; injecting water from other reservoirs; or by mixing produced waters from various sources. Freshwater and seawater have also been used. In addition, there are many varieties of materials such as soap, carbon dioxide and other more exotic material that may be added to the water to improve mobility and/or sweep efficiency. Some of these agents act to reduce the viscosity of the oil or to increase the viscosity of the water while others act to improve the relative permeability to water which often results in stripping more oil off of such surfaces. Various mechanical methods are also used to improve sweep efficiency.

The basis for most waterflooding recovery methodologies is the Buckley-Leverett [41-43] or *frontal advance method*. The Buckley-Leverett method assumes a linear oil-bearing zone in a depleted state. The method requires a knowledge of the change in reservoir properties of k_o , k_w , μ_o and μ_w with change in water saturation S_w . Assuming immiscible, steady-state conditions the flow through a linear block of reservoir can be modeled where

$$f_D = \frac{1 - \frac{1.127k_o}{q_t \mu_o} \left[\frac{\partial Pc}{\partial \mu} + 0.434(\Delta p) \sin \alpha \right]}{1 + \left(\frac{k_o}{k_w} \cdot \frac{\mu_w}{\mu_o} \right)} \quad (7-54)$$

where f_D is the fraction of displacing fluid flowing at a given point in the system and q_t is the total flowrate per cross-sectional area. If the capillary pressure gradient $\partial Pc/\partial u$ is small and the zone is essentially flat, so that the gravitational function can be dropped, the equation can be simplified to

$$f_D = \frac{1}{1 + \left(\frac{k_o}{k_w} \cdot \frac{\mu_w}{\mu_o} \right)} \quad (7-55)$$

The distance (u) that a plane of constant S_w has advanced at time (t), can be calculated as

$$u = \frac{Q_i}{A\phi} \left(\frac{\partial f_D}{\partial S_D} \right) t \quad (7-56)$$

where Q_i is the injection rate which is assumed constant. The slope $\partial f_D/\partial S_D$ is obtained by plotting f_D for various values of S_D . The time to water breakthrough is then

$$t_B = \frac{AL\phi(\overline{S_{wf}} - S_{wi})}{Q_i}$$

where S_{wf} is the mean water saturation in the system. S_{wf} is obtained by projecting a line from S_{wi} tangent to the $\partial f_D / \partial S_D$ curve to $f_D = 1$. If water is the displacing fluid and S_{wi} is the irreducible saturation, then oil production (q_o) until breakthrough is equal to water injected (q_{wi}).

If water is mobile, then $q_i = q_o + q_w = q_{wi}$ and the water/oil ratio is

$$WOR_{surf} = \frac{k_w \mu_o B_o}{k_o \mu_w B_w} \quad (7-57)$$

and

$$q_o = \frac{(1 - f_w) Q_i}{B_o} = \frac{Q_i}{B_o + (WOR) B_w} \quad \text{at time } t \quad (7-58)$$

After breakthrough, oil production is determined by obtaining values of S_{wf} at various values of f_w up to an abandonment f_w ; calculating t for each value of S_{wf} ; determining WOR at each f_w ; and calculating q_o for each value of WOR.

The Stiles [44] method takes a frontal advance approach but assumes the zone is composed of layers of constant thickness but each layer may have a different permeability. Stiles requires a constant q_i and predetermined S_o after flooding. The method extends the frontal advance approach to determine ultimate recoverable oil and then uses f_w to determine the recovered fraction as a function of time. The method allows a direct derivation of q_o , cumulative oil and WOR.

Suder and Calhoun presented another frontal advance method that allows calculation of injection rates and assumes radial flow up to a point. The method requires a predetermined value for S_{or} .

Dykstra and Parsons [45] also presented a method based on permeability stratification and Johnson [46] converted the method to a graphical approach. The method allows a consideration of permeability variation. The Johnson graphical approach is particularly useful for quick estimates before engaging in one of the more detailed calculations. The set of four graphs is defined at producing WOR of 1, 5, 25 and 100 and result in values of recovery factor R_r for each WOR. Assuming recoverable oil and injection rate can be estimated, the method allows calculation of production rates and cumulative recovery over time. The method works well as a first approximation and is simple enough to use that several analyses can be done for varying conditions.

There have been many variations of these methods proposed and used. In addition, the inclusion of variations in reservoir fluid or rock conditions is only a matter of how much work the evaluator is willing to do. These basic methods underlie most if not all computer models used to simulate waterflooding.

Heat Injection Methods. The primary purpose of heat injection using steam or hot water is to transfer heat from the injected fluid to the crude oil and reservoir rocks to reduce oil viscosity. Reduction of viscosity in the oil—at least at the water–oil contact—results in an improved mobility ratio, thereby allowing high viscosity oils to be recovered.

Steam is particularly useful for this purpose because steam can carry a much greater quantity of heat per unit volume than can hot water or heated gasses.

Although some attempts to use superheated steam have occurred, in practice steam at about 80% quality (80% vapor/20% liquid) is most commonly used. Heat injection is a costly process due to the requirement to burn fuel to generate steam or hot water. The major limitation on heat injection methods is heat loss in surface facilities, distribution lines, wellbores, and in the reservoir, to over and underlying rocks and to water in the reservoir. Because of the heat losses in the wellbore, steam injection is normally limited to 3,000 ft or less in depth. Reservoir heat losses cause the injected fluid to continually cool as the steam front advances from the injection sand face. Continual steam injection is required to attempt to maintain a heated oil-water interface at the flow front. Many authors have described and quantified the heat losses in surface, wellbore and reservoir rocks and reference should be made to those sources.

Marx and Langenheim [47] have presented a series of equations designed to determine the radial distance at which the heat loss ratio in the reservoir equals the heat injection rate.

The inclusion of cost factors (\$h and \$0) allows the calculation to be thought of as an economic limit as well as a physical limit. The calculation assumes no breakthrough but otherwise could be used to define well spacing for a continuing flood.

$$[e^{x^2} \operatorname{erfc} x]_1 = (5.618 \times 10^{-6}) \left[\frac{\$h M(\Delta T)}{\$0 \phi (S_o - S_{or})} \right] \quad (7-59)$$

where

$$x = \frac{2k_{ob} t^{1/2}}{Mh \sqrt{a_D}}, \quad \text{dimensionless time} \quad (7-60)$$

and

$$M = (1 - \phi) \rho_f C_r + S_w \phi \rho_w C_w + S_o \phi \rho_o C_o \quad (7-61)$$

The cumulative heated area (ft²) can be calculated at time (t):

$$A(t) = \frac{H_o M h \alpha_p}{4k_{ob}^2 (\Delta T)} \left(e^{x^2} \operatorname{erfc} x + \frac{2x}{\sqrt{\pi}} - 1 \right) \quad (7-62)$$

where H_o = constant injection rate in Btu/hr

Several approaches have been presented for estimating steam drive performance. In essence, steamflooding is analogous to cold waterflooding and the same principles apply with additional recovery due to:

1. thermal expansion of the oil
2. viscosity reduction, which improves mobility
3. steam distillation of some light oil components

Thermal expansion and viscosity reduction can be determined in laboratory analysis and the effects can be built into the calculation. Estimation of results from distillation are more difficult to assess and include.

Willman et al. [48] has proposed methods of determining steam drive performance that envisions a series of displacements occurring. A cold water-oil displacement front; a hot water and condensate oil front; and a steam-condensate and hot water displacement which is partially miscible.

The radial position of the steam front is calculated as

$$R_{ST}^2 = \frac{14.6 i_w H_{fg}}{k(T_{ST} - T_f)} \sqrt{\frac{\alpha}{\pi}} \left[\frac{\sqrt{t}}{2} - \frac{h}{8} \sqrt{\frac{\pi}{K}} \frac{(\rho C_p)_f}{(\rho C_p)_{OB}} \times \ln \left(\frac{4}{h} \sqrt{\frac{\alpha}{\pi}} \frac{(\rho C_p)_{OB}}{(\rho C_p)_f} \sqrt{t} + 1 \right) \right] \quad (7-63)$$

The steam injection rate must increase as the flood front expands in order to maintain temperature. The required steam rate is

$$i_w = \frac{\pi R_{ST}^2 (T_{ST} - T_f)}{14.6 H_{fg} t} \left[h(\rho C_p)_f + 4k \sqrt{\frac{t}{\pi \alpha}} \right] \quad (7-64)$$

In general, however, the Buckley-Leverett approach used for waterflood can be modified for steamflood. For a radial system,

$$\left[\frac{\partial (R^2)}{\partial t} \right]_{S=\text{const}} = \frac{i_w}{13.43} \left(\frac{\partial f_w}{\partial S_w} \right)_{S=\text{const}} \quad (7-65)$$

where i_w = effective injection rate in bbl/day of steam, and

$$f_w = \frac{1}{1 + \frac{k_o \mu_w}{k_w \mu_o}} \quad (7-66)$$

Both i_w and f_w (as a function of S_w) are functions of temperature; therefore, the above equation is modified to

$$(R^2)_{S=\text{const}} = \frac{1}{13.43} \int_0^t i_w \left(\frac{\partial f_w}{\partial S_w} \right)_{S=\text{const}} dt \quad (7-67)$$

which is amenable to graphical solution as outlined above for waterflood, assuming isothermal steps.

Given the complexity of these calculations and the many variations presented by authors, the evaluator is well advised to make maximum use of data from heat injection projects in similar fields to determine reservoir and production performance over time. Data on many EOR projects have been published in the 1970s and 1980s as the result of DOE projects and a high level of interest in industry.

In 1980, Gomaa [49] presented a method of estimating steamflood performance based on correlations of reservoir characteristics with steamflood injection rates, pattern sizes and shapes, and other factors from existing projects and laboratory studies. The method uses a series of graphical correlations to provide an estimate of reserves and recovery rate. The method is useful in quick evaluations of steamflood project potential.

Heat injection methods of EOR have numerous advantages and disadvantages.

Advantages:

- increase recovery from high viscosity oil reservoirs
- increase production rates from high viscosity reservoirs

Disadvantages:

- requires extensive reservoir, rock, and fluid analysis
- high capital investment of steam generators, new injection wells, and surface systems
- high operating costs for steam or hot water generation, hot fluid and feedwater treating, and personnel
- subject to environmental and other regulatory constraints

DETERMINING VALUE OF FUTURE PRODUCTION

The earlier discussion of the various definitions of reserves included the reference to economics. Reserves are, by definition, not simply a physical volume but an economically recoverable volume. No property evaluation for any purpose is complete without a determination of the economic value of future production.

THE MARKET FOR PETROLEUM

Petroleum—oil, gas and derivatives—are the primary sources of energy in the world today. There are other major fuel sources, such as coal and nuclear power, but petroleum remains the major source in the United States, Europe and Japan. These markets together account for about 45% of world energy usage and petroleum provides over 60% of energy in these areas. Petroleum is likely to retain this position because there are very large volumes of oil and gas already discovered and available at relatively low prices. The combined reserves of the Persian Gulf states alone are sufficient to supply current world demand for 50–100 years. Moreover, these reserves can be produced at low cost when compared to production in the United States and other parts of the world. Persian Gulf reserves are large enough and production sufficiently controlled, even though somewhat erratically, by the Gulf countries, that the increase in usage of higher-cost energy sources such as nuclear or environmentally acceptable coal would be very difficult unless heavily subsidized.

In the United States and other areas where similar industry conditions exist, petroleum economics will be controlled, indirectly and directly, for the foreseeable future by the baseline oil price either set by or derived by major producing countries. Under market conditions, oil priced in the United States cannot rise much above the world market level but can readily fall below that level. Production in the United States is generally in decline so that the United States, along with Europe and Japan, is a net importer of over 50% of crude oil demand, thereby tying the United States market more closely to world markets. In addition, United States production is very high cost relative to the Persian Gulf or anywhere else so that the difference between price (revenue) and cost of production can be, and often is, very narrow. As shown by the events of 1985–1986, a decrease in oil price is often enough to render a large volume of U.S. production uneconomic, causing wells to be shut in and abandoned; resulting in the cancellation or deferment of new drilling, exploration and other capital investment

projects; and bringing about the financial collapse of oil companies, service companies, and whole regions that depend on the oil industry.

The primary impact of the market for petroleum is, of course, on price. Throughout history, prices for oil and natural gas have varied with demand and supply. In the United States, there have been periods of high production relative to demand causing prices to drop; as well as periods of high demand relative to production that resulted in price increases. For a long period, however, from the early 1930s until 1971, oil production was controlled by proration that limited production, particularly in Texas but also in other areas, to a certain "allowable" each month that was expected to fulfill, but not exceed, demand. The allowable production was set as a percentage of productive capacity. This regulation resulted in stable and relatively low oil prices for most of that period. The increase in allowables over time to 100% in the early 1970s was one of the major reasons that control of the world market passed from the United States to OPEC and from industry to governments in the mid-1970s.

The U.S. economy is, among other things, energy intensive. In this situation, changes in oil and gas prices take on national significance and can have immediate and serious impacts on the economy of regions and the country as a whole. The demonstration of this is in the relation between oil price and inflation. Since 1928, the first year that reliable inflation data in the form of the Consumer Price Index was kept, changes in oil price can be shown to be closely followed by changes in CPI or, more broadly, inflation. Major price increases such as 1971-1973 and 1979-1980 resulted in serious increases in inflation in those and following years. For most of the period from 1928 to 1994, however, oil production exceeded demand. Price was regulated through proration and in many years oil price declined. Inflation, however, being caused by many factors, continued even though at low rates so that, while the nominal or actual oil price may have increased slightly or remained essentially constant, the "real" price—the nominal price minus inflation—actually declined for many years and has, in fact, declined significantly since 1982 (Figures 7-8 and 7-9).

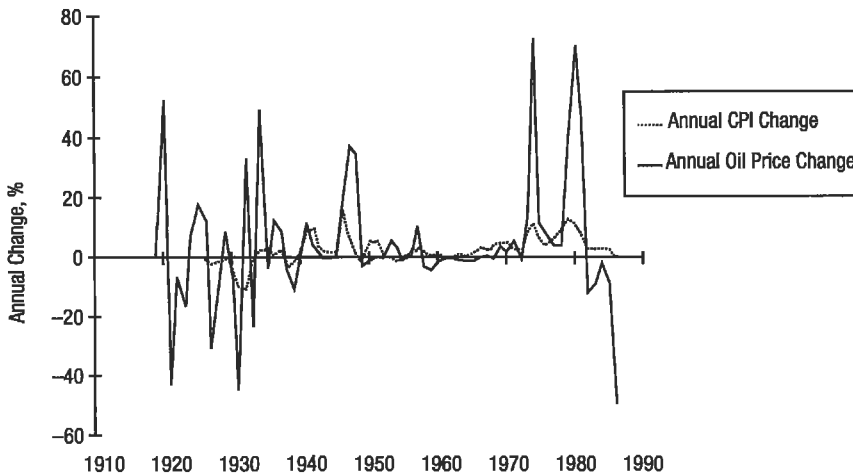


Figure 7-8. Oil price history vs. inflation.

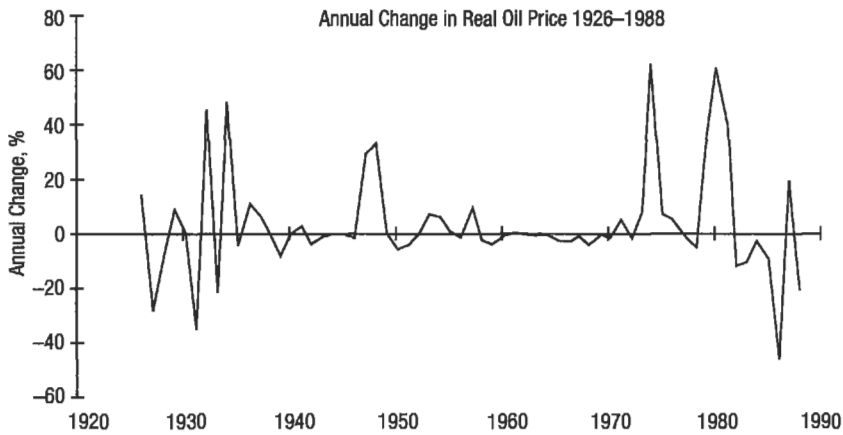


Figure 7-9. Annual change in real oil price.

Economics and the Petroleum Engineer [50,51]

The function of the petroleum engineer is to determine how to produce the most oil and/or gas from a property in the most efficient manner and at the least cost to optimize the economic return from that production. Producing the most oil from a property in the most efficient manner explicitly includes production and reservoir management so as to optimize *both* production rate and ultimate recovery from the reservoir. The petroleum engineer has little or no control over oil price. Therefore, he or she must attempt to minimize production costs and investment over the life of the property so that, whatever the price, the economic return is optimized. This means that virtually every decision made regarding the development and maintenance of production must consider the *economic costs and benefits* of the decision. This is true regardless of whether the project is drilling a new well, changing a pumping unit, considering a stimulation method, installing an EOR project or buying a property. The benefits may be increased production rate, increased reserves, or a reduction in costs, or some combination; while the costs may include new capital investment or increased operating costs.

The relation between benefits and costs can be measured in various ways. Among these are the undiscounted net profit, the net present value, the (internal) rate of return and various other methods as will be discussed later. Each of these approaches provides a somewhat different perspective on project evaluation and allows the engineer or other decision maker to not only evaluate a particular project, but allows comparisons when selecting projects for completion. As an example, if a new well is proposed that would result in a net profit of \$1 million and a ROR of 19%, this project must be compared to other projects and to company criteria for net profit and ROR. If the company requires a minimum ROR of 15%, the project might be accepted. If, on the other hand, the net profit was \$1 million but ROR was only 9%, the project ROR would not only fail to

meet company guidelines, but might be less than could be obtained on investments where there is no risk.

Reserves are a function of economic conditions—both by definition and in practice. Any determination of reserves must be bounded by a reasonable set of economic conditions. The vehicle for this analysis is the cash flow.

Preparation of a Cash Flow [52]

A cash flow consists of five basic elements: (1) production schedule, (2) product prices, (3) ownership interests, (4) costs of production and (5) capital investments. The cash flow can be expanded in any of these segments and through the addition of income tax considerations. The cash flow is designed to model the production, price and cost expectations of the evaluator to an economic limit.

A *production schedule* must be estimated for oil and gas production plus any associated production such as NGL or condensate. Previous discussion has described the methods of estimating future reserves and production. Extrapolation of existing or similar property production decline is the most direct method of estimating future production when either oil or nonassociated gas is the primary production stream. Associated gas may be projected as a function of oil production using a fixed or variable gas-oil ratio (GOR). Nonassociated gas may have associated condensate production that can be projected as a fixed or variable yield.

Where decline curve extrapolation is used, the form of the decline, whether exponential, hyperbolic or harmonic, must be defined and applied. It is always a good idea to compare the reserves obtained from production decline with reserves obtained from other methods such as rate-cum or WOR-cum curves or to volumetric and/or material balance calculations. When decline curve extrapolation may not be appropriate, such as when projecting future production from a new field or reservoir or for an EOR project, production estimates can be obtained by converting the volume results of the material balance, frontal advance, or other method into annual or monthly production. This may require determining a limiting condition that can be identified, such as lifting capacity or injection rates and back-calculating a production rate. However it is done, be sure to compare the production schedule with other similar projects or fields and with good reservoir and operating practice. Also, the selection of a schedule may have economic impacts, such as the requirement for investment, increased operating costs, or in some circumstances royalties and/or taxes that may cause an alteration of the selected production schedule. Finally, as noted earlier, the proper analysis of the source and form of the production data is very important to a valid cash flow analysis.

Product prices are the market price of oil, gas, condensate, or NGL. A cash flow is usually done as of a point in time so the prices would be those in effect at that date. Two basic sources for product prices are actual sales and posted prices. The actual price for oil and/or gas being received on the property to be evaluated is the best source of a price for a cash flow. In using *actual prices*, determine if there are any shipping, pipeline, dehydration or other deductions that would reduce the price actually received for the oil or gas produced. These charges must be accounted for in the cash flow. Also, *gas sales* prices are often based on the heating or Btu value of the gas *not* on the Mcf or volume of gas. Since gas production is normally expressed in Mcf, a correction must be made if the gas price is in \$/Btu. *Posted prices* (Figure 7-10) are the prices offered in the market by large purchasers of crude oil, such as major refiners. These posted prices are readily available for oil from various fields or for regions of the



Amoco Production Company
 200 East Randolph Drive
 P.O. Box 87689
 Chicago, Illinois 60680-0689

Crude Oil Price Bulletin 90-50
 (Supersedes Crude Oil Price Bulletin 90-49)

September 27, 1990

This bulletin shows prices and gravity adjustments posted by Amoco Production Company (Amoco) for purchases of crude oil and condensate. Prices are based on the use of 100% tank tables or mutually acceptable automatic measuring equipment with customary adjustment of volume and gravity for temperature and full deduction for basic sediment and water.

Subject to change without notice, Amoco will pay the prices shown for merchantable crude oil and condensate delivered for its account into the facilities of its authorized receiving agency. Merchantable crude and condensate is defined as virgin crude and/or condensate produced from wells which is free of injected or outside foreign contamination, added chemicals containing but not limited to halogenated organic compounds and oxygenated compounds and which is fit for normal refinery processing. Seller warrants that the crude oil and condensate delivered to Amoco shall be of merchantable quality as defined above and fit for normal refinery use. Prices are shown for 40 gravity and above, except as noted.

All prices may be subject to deductions for trucking and other charges where applicable. In the event government regulations require adjustment to Amoco's prices or effective dates, Amoco reserves the right to amend these prices and recover any excess payments by withholding payments from future settlements or by separate invoicing.

Effective September 27, 1990

Areas		Price: \$/Barrel	For Gravity Adjustment See Column
Colorado	Western	39.00*	5
	Eastern	38.00*	7
Kansas	Sweet	37.75*	3
Louisiana	Southern Louisiana Light	38.75*	3
	Hackberry, Charenton, Edgerly (30° Lowest Price)	38.10*	3
	Southern Louisiana Sour—Eugene Island	37.25*	3
Nebraska	West Panhandle Sweet	37.75*	1
North Dakota	Incl. Sheridan, Roosevelt, Richland Counties, Montana	37.65*	1
	Fryburg-Medora (Flat Price)	36.75*	None
Oklahoma	Sweet	38.25*	8
	Sour	37.50*	5
Texas	East—Asphaltic (32° Top Price)	38.00*	4
	—East Texas Field (Flat Price)	38.25*	None
	—Quitman Light	36.25*	5
	Gulf Coast—Sweet (Flat Price)	38.25*	None
	—Fairbanks Area, Gillock, High Island	38.25*	1
	North	38.25*	1
	West Central—Including King & Knox Counties	38.25*	1
	West Texas & New Mexico—Intermediate	38.25*	1
—Sour (34° Top Price)	36.25*	6	
Utah	Black Wax	38.75*	5
	Yellow Wax	38.00*	5
Wyoming	Southwestern Sweet (Carbon, Lincoln, Sublette, Sweetwater, Uinta Counties)	38.75*	5
	Sweet (Other)	38.00*	1
	Sour (including Montana fields)	37.00*	2
	Sweet (Salt Creek Field)	38.50*	1

*Indicates change

A recorded message containing information on Amoco Production Company's latest Crude Oil Price Bulletin is available by calling (312) 856-3114

Figure 7-10. Example of posted prices.

country or state. The posted price changes as economic conditions change. The posted price is listed as \$/bbl for a certain gravity of oil, with a correction factor for gravity differentials.

The appropriate price for the oil in the property being evaluated can be estimated by obtaining one or more posted prices for oil of a similar gravity in or near the same field and making necessary adjustments for gravity. Gas prices can be estimated from standard prices offered by pipelines in the area. Gas sales are not always as straightforward as oil sales. During periods of high demand, the purchaser may be willing to take all the gas that can be produced and will build the connection lines to the property. At other times, however, the purchaser may limit sales to a percent of capacity and may not be willing to provide connection. These conditions could not only reduce revenue from sales but could require additional investment and may have the effect of reducing production of other products if the gas is associated gas. Whatever the conditions, they must be considered in the production schedule and cash flow.

Condensate is generally treated and priced as crude oil. NGL is generally treated as a by-product of gas sales where "wet" gas containing NGL is sold to a "gas plant" that strips out the liquids and sells the "dry" gas and liquids. The producer may receive revenue from the dry gas sales and a share of NGL sales or he or she may receive a wet gas price.

The *projection of product prices* into the future depends on the perspective of the evaluator regarding future economic conditions and, to some extent, the purpose of the cash flow. The simplest approach is to determine the appropriate price(s) as of the date of evaluation and hold those prices constant for the life of production. This was virtually the only way projections were done prior to the price increases of the 1970s and is still relatively common. Constant pricing is required for SEC evaluations. Since the 1970s it has become more common to attempt to estimate whether oil and/or gas prices would change over the expected life of production and to build those anticipated changes into the cash flow by escalating or deescalating oil prices at certain rates over time.

The question of whether or not to escalate prices in a cash flow depends on the information available to the evaluator and how well the evaluator can translate information into expectation. Major companies often have economics departments whose purpose is to estimate future oil prices that are often implemented in cash flows. Smaller companies and others are generally without such resources and must rely on other, published and unpublished sources and their own intuition. Since the early 1970s, oil and, to a lesser extent, gas have been open market commodities subject to a wide range of forces causing prices to rise and fall. Most price projections that extend for more than a year or two will probably be wrong except that over time, because oil and gas are finite resources, the price must eventually increase. As will be discussed below, the use of several cash flows with differing price projections may serve to reduce "price risk."

The prices used in cash flow projections are normally "nominal" prices that include expected inflation. In making projections of oil prices, it is important to keep in mind that the rate of increase of oil prices, the escalation rate, has rarely exceeded the rate of inflation for more than 2-3 years (Figure 7-8) and that, after that time, the escalation rate may be equal to or less than the rate of inflation. On average the "real" price of oil (real = nominal minus inflation) has increased by an average of 1.1% over the 60 years from the late 1920s to the late 1980s, including the major increases of the 1970s (Figure 7-9). Most oil field operating costs are directly influenced by inflation so that *price escalation should not exceed cost escalation for any extended period of time.*

Ownership interests are the percentages of the production revenue and cash flow from a property owned by various parties. Ownership can be broadly divided into two classes: working and royalty interests. The basic difference is that the *working interest* pays all the operating costs and makes the investments and then receives a share of the revenue. The *royalty interest* receives a percentage of the revenue but pays no costs and makes no investment. The share of revenue received by the working interest is called the net revenue interest. If the WI is 100% or 8/8 and the royalty is 12.5% or one-eighth.

$$\begin{aligned} \text{Net revenue interest (NRI)} &= \text{working interest} - \text{royalty interest} \\ &= 100.0\% - 12.5\% = 87.5\% \end{aligned}$$

There are several types of royalty interest including landowner, overriding, and sliding scale. The latter are most common on federal or state government leases but may occur on private leases and are very common in foreign countries. The royalty interest is paid directly out of sales, often by the production purchaser, so that the WI pays all operating costs, etc., out of the NRI. If there is more than one working interest owner, the WI and NRI will generally be divided proportionately. Whatever the type of royalty, the effect on the cash flow is the same.

In some cases, the ownership interest may change during the expected life of production. These "reversionary" interests may occur when a certain cumulative volume of production is obtained but more commonly occur when a predetermined amount of net cash flow has been obtained by the WI. The situation often occurs in new drilling projects when a WI owner, generally an investor, receives a certain WI until his or her investment is recovered or "paid out" at which time the WI reverts to a reduced percentage. At that time the other WI owner(s) share would increase. For example, assume the operator (A) of a property wants to drill a new well and an investor (B) agrees to provide the \$100,000 needed to drill the well and to accept a 75% WI reverting to 35% at payout. Assume a 12.5% royalty (Table 7-1).

In constructing a cash flow it is very important that the ownership interests be determined and accurately applied. The best source is your land department and/or the division orders issued by product purchasers in most states.

The *costs of production* include all the costs, except royalty and investment, required to produce, treat and sell the oil, gas and any other products from the property being evaluated. There are a great many different types of costs

Table 7-1
Example of Working Interest Reversion

	Before Payout		After Payout	
	WI	NRI	WI	NRI
A	25%	21.875%	65%	56.875%
B	75%	65.625%	35%	30.625%

and companies may account for them in various ways but they must be included in the cash flow. Costs of production can be broadly divided into (1) operating or lifting costs and (2) production taxes and charges.

Operating costs can be further subdivided into (a) fixed, (b) variable, (c) periodic and (d) overhead. *Fixed costs* include those costs that remain generally the same regardless of the volume of production, such as lease labor (pumper, treater), well pulling, maintenance, engineering, and/or supervisory staff); some fuel and power costs; lease maintenance and repair. While these costs may change over a long period of time, for cash flow purposes they may be considered fixed costs in dollars per month or per year. *Variable costs* are those that vary with the volume of gross (oil plus water) production or with the number of wells. Such costs are chemical treating, some fuel and power costs, water disposal and some labor costs. *Periodic costs* are those that do not occur constantly but recur with sufficient regularity that they can be scheduled in a cash flow. Such costs might be pump changes, hot oiling, dewaxing, acidizing or other stimulation or maintenance requirements. *Overhead* is often an indirect cost that is incurred off the lease but is then allocated to the property. Such costs might be district or head office supervisory and engineering staff. *Other costs* might include distributed costs of environmental, regulatory or other programs that are applied across several properties or that have no property-specific application.

The best source of operating cost data is the historical cost records for the property being evaluated or a similar property. It is important to review at least 12–24 months of previous costs to properly define the full range of costs and the variation of those costs with time and production changes, and to define any recurring costs. If certain costs remain essentially the same over time, they should be treated as fixed costs in the cash flow. On the other hand, costs that can be shown to vary with total fluid or oil production or the number of wells or some other criteria should be treated as variable costs in the cash flow. Periodic costs can be included in the cash flow as occurring at specific time intervals or can be spread over the cash flow as a monthly or annual charge.

Certain special cases require mention. If produced oil and/or gas is retained for use as *lease fuel*, the volume used for fuel can be included in the cash flow by (a) reducing the amount of production, or (b) by deducting the equivalent value of the fuel volume as an operating cost. The choice of treatment depends on such things as whether or not the lease requires payment of royalty on production used as lease fuel (most leases do not) or whether fuel usage can be deducted for production tax calculation (generally no). Deduction of fuel usage from production may distort the cash flow; therefore, it is probably best to treat fuel usage as an operating cost at the prevailing price for oil or gas used.

Production taxes and charges include, but are not limited to (a) severance taxes, (b) wellhead taxes, (c) *ad valorem* taxes, (d) regulatory impositions and (e) certain charges based on income such as the *windfall profit tax*. These taxes not only occur individually but, in many areas, one or more of the taxes occur and are cumulative. It is important to identify the taxes applicable to the property being evaluated and to include them in the cash flow. Most major producing states (Texas, Oklahoma, Louisiana) impose a *severance* tax on oil and gas production, which is a percentage of the sales price before any costs, including royalty or other taxes, are deducted. The tax may be a different percentage for oil and gas. They are normally paid to the state by the purchaser of the oil and gas. While some states have relatively high severance tax rates (7–8%), the tax is a fixed share of the price and fluctuates with the price. *Wellhead* taxes, on the

other hand, are generally a fixed amount such as \$/bbl or Mcf, which, while generally small, become a larger percentage of revenue if prices decline.

Ad valorem taxes are based on the value of the property as determined by the taxing authority such as a county tax assessor. The *ad valorem* tax is relatively minor in most states. The exception is California where there is no severance tax and the *ad valorem* tax can equate to as much as 3-5% of gross revenue. The difficulty with *ad valorem* taxes is that the assessed property values do not always follow changes in property value caused by changing economic conditions. For use in a cash flow, *ad valorem* taxes can be converted to a percentage of gross revenue. *Regulatory taxes* can consist of either percentage or fixed amount per unit taxes that are similar to severance or wellhead taxes but are directed toward specific uses, such as funding a state agency or environmental fund. These taxes vary greatly from one jurisdiction to another and may only occur for fixed time periods.

Some taxes are based on income but are not income taxes per se. The so-called *windfall profit tax*, which did not tax profits, is one example. The WPT imposed a percentage tax, which varied depending on differing classes of sellers and types of oil production, on the adjusted difference between a so-called base price and the actual sales prices. At some points during the time it was effective, the WPT attained a large percentage of the price differential. The tax remained long after the profits had evaporated.

Capital investments are not operating costs. While the difference between periodically recurring costs and capital investments is not always clear and each company may have its own definition, capital investments can be broadly defined as relatively major expenditures, which may or may not be predictable, and which generally result in an increase in production or a decrease in costs or both as a direct result of the investment. Changing a pump might be operating cost while changing a pumping unit is an investment. Cyclic steaming might be a periodic cost but fracing might be an investment. There is a certain amount of subjectivity involved here and company policy should be consulted. In any event, any anticipated capital investment including eventual abandonment should be included in the cash flow and evaluated for appropriate return. Investment is deducted after all royalties, operating costs, production taxes.

The components discussed to this point are sufficient to develop a more or less detailed cash flow for any property which will allow the property to be evaluated for virtually any purpose for which a cash flow is used (Figure 7-11). In model form:

$$\begin{aligned}
 \text{Production} \times \text{product price} &= \text{gross revenue} \\
 \text{Net operating income} &= \text{gross revenue} \\
 &\quad - \text{royalty} \\
 &\quad - \text{production taxes} \\
 &\quad - \text{operating costs} \\
 \text{Cash flow} &= \text{net operating income} \\
 &\quad - \text{investment}
 \end{aligned}$$

When calculated on a monthly or annual basis to the *economic limit* of production, the cash flow provides a foundation for determining the value of the property and/or the profitability of capital expenditures; or, simply, the future flow of cash from the property. The economic limit is the minimum production rate which, at a given price, is required to exactly offset all the costs of production.

Run Date: 08 50 1990
Run Time: 13:45:55

Evaluation Texas, I

As of Date: Jan 84

Name: Gusher 1-1
Field: Oil Dorado Field
Location: Oz County
Formation: Yellow Brick Lime
Operator: Oyl Bidness, Inc.

NPV 10.0% 632.053 BFIT
NPV 15.0% 445.028 BFIT
NPV 25.0% 158.646 BFIT
NPV 30.0% 56.478 BFIT
NPV 35.0% -27.553 BFIT
IRR 33% BFIT

Interest and Effective Date			Prices			Gross Reserves					
Cost	Revenue	Date	Beginning	Ending	Average	Cumulative	Remaining	Ultimate	%Remaining		
1.000000	0.850000	Jan84	Oil	19.00	29.48	21.79	543.000	226.976	769.976	29.48	Oil
0.900000	0.800000	Jan85	Gas	1.30	1.92	1.42	1629.000	680.927	2509.927	29.48	Gas
0.500000	0.400000	Jan86	Cond	0.00	0.00	0.00	0.000	0.000	0.000	0.00	Cond
0.500000	0.300000	Jan91									

Year	Gross Oil Production MMBLS	Gross Gas Production MMSCF	Net Oil Production MMBLS	Net Gas Production MMSCF	Average Oil Price \$/B	Average Gas Price \$/MSCF	Net Oil Sales M\$	Net Gas Sales M\$	Net Other Rev M\$	Net Total Revenue M\$
1984 (12Mo)	84.168	102.505	20.043	87.129	19.000	1.300	851.813	113.268	0.000	665.081
1985	90.752	92.255	24.602	75.804	19.000	1.300	467.430	95.945	0.000	563.376
1986	27.676	83.029	11.070	33.212	19.475	1.300	215.596	43.175	0.000	258.771
1987	24.909	74.726	9.964	29.890	20.449	1.300	203.743	38.858	0.000	242.601
1988	22.418	67.254	8.967	26.902	21.471	1.365	192.536	36.721	0.000	229.257
1989	20.176	60.528	8.070	24.211	22.545	1.433	181.945	34.701	0.000	216.646
1990	18.158	54.475	7.263	21.790	23.672	1.505	171.934	32.792	0.000	204.726
1991	15.433	46.298	4.650	13.889	24.856	1.580	115.079	21.947	0.000	137.026
1992	12.346	37.039	3.704	11.112	26.098	1.659	96.663	18.436	0.000	115.099
1993	9.877	29.651	2.963	8.889	27.403	1.742	61.199	15.486	0.000	96.685
1994	7.902	23.705	2.371	7.112	28.773	1.829	68.210	13.003	0.000	81.219
1995 (6Mo)	3.161	9.482	0.948	2.845	29.475	1.921	27.947	5.464	0.000	33.411
1996	0.000	0.000	0.000	0.000	0.000	0.000	0.000	0.000	0.000	0.000
1997	0.000	0.000	0.000	0.000	0.000	0.000	0.000	0.000	0.000	0.000
1998	0.000	0.000	0.000	0.000	0.000	0.000	0.000	0.000	0.000	0.000
Sub Total	226.976	680.927	113.595	340.785	21.786	1.420	2374.097	469.801	0.000	2843.897
Remaining	0.000	0.000	0.000	0.000	0.000	0.000	0.000	0.000	0.000	0.000
Tot 11.5Yr	226.976	680.927	113.595	340.785	21.786	1.420	2374.097	469.801	0.000	2843.897

Year	Net Total Prod Tax M\$	Net Total Loc M\$	Net Total Oper Exp M\$	Net Oper Revenue M\$	Net Leasehold M\$	Net Total Investments M\$	Net BFIT Cashflow M\$	Cum BFIT Cashflow M\$	BFIT CF Disc @ 20% M\$	Cum BFIT CF Disc @ 20% M\$
1984 (12Mo)	19.952	24.000	43.952	621.129	0.000	1250.000	-628.871	-628.871	-667.658	-667.650
1985	16.901	22.680	39.581	523.794	0.000	0.000	523.794	-105.077	893.992	-271.666
1986	7.763	13.230	20.983	237.778	0.000	0.000	237.778	132.701	149.655	-122.010
1987	7.278	13.891	21.170	221.431	0.000	0.000	221.431	354.132	116.136	-5.873
1988	6.878	14.586	21.464	207.793	0.000	0.000	207.793	561.926	90.820	84.946
1989	6.499	15.315	21.815	194.831	0.000	0.000	194.831	766.757	70.961	155.908
1990	6.142	16.081	22.223	182.503	0.000	0.000	182.503	939.260	55.392	211.300
1991	4.111	16.885	20.996	116.030	0.000	0.000	116.030	1055.290	29.346	240.646
1992	3.453	17.729	21.182	93.917	0.000	0.000	93.917	1149.207	19.793	260.439
1993	2.901	18.616	21.516	75.168	0.000	0.000	75.168	1224.376	13.201	273.640
1994	2.437	19.547	21.983	59.236	0.000	0.000	59.236	1283.611	8.868	282.509
1995 (6Mo)	1.002	10.262	11.264	22.146	0.000	0.000	22.146	1305.757	2.827	285.186
1996	0.000	0.000	0.000	0.000	0.000	0.000	0.000	0.000	0.000	0.000
1997	0.000	0.000	0.000	0.000	0.000	0.000	0.000	0.000	0.000	0.000
1998	0.000	0.000	0.000	0.000	0.000	0.000	0.000	0.000	0.000	0.000
Subtotal	85.317	202.823	288.140	2555.757	0.000	1250.000	1305.757	1305.757	285.136	285.136
Remaining	0.000	0.000	0.000	0.000	0.000	0.000	0.000	0.000	0.000	0.000
Tot 11.5Yr	85.317	202.823	288.140	2555.757	0.000	1250.000	1305.757	1305.757	285.136	285.136

Figure 7-11. Example of cash flow.

$$\text{Costs of production/unit time} = \text{Production taxes + operating costs} \\ \text{Price per Bbl or Mcf} = \frac{\text{Production taxes + operating costs}}{\text{Production/unit time}} \\ = \text{Economic limit (Bbls or Mcf/unit time)} \quad (7-68)$$

Income taxes, both state and federal, exist and should be considered in any cash flow evaluation particularly where large capital investments are involved.

Even with the tax reductions of the 1980s, corporate and individual tax rates are 33-51% of taxable income that can be substantial depending on the deductions available at the time. The tax code is complex, is subject to rapid change, and to individual case application so that a comprehensive treatment in a handbook is not appropriate. Consult your company policy regarding income tax analysis.

Present Value of Future Income

A cash flow is a stream of income expected to be received over a period of time into the future. For example, if a cash flow consisted of equal amounts of \$5,000 over 5 years, the total income would be \$25,000 (Table 7-2).

However, from the perspective of the date of valuation, the \$5,000 to be earned in years 2, 3, 4 and 5 does not have the same value as the \$5,000 to be earned in the first year. Because of inflation and other financial risks, the *present value* of future income is reduced or discounted by an amount that varies with the evaluator's perceptions of the risks involved in waiting. To equate future cash flow to present value, a discount rate or present value factor is applied to the cash flow. Present value calculation can be thought of as the reverse of compounding interest where, instead of increasing the value of a currently held amount over time, the present value factor or discount rate decreases future amounts to a present value. For example, if a principal sum P is invested at an annual interest rate i for n years, the accumulated interest would increase P to a total future amount S as follows:

$$S = P(1 + i)^N \tag{7-69}$$

On the other hand, if, for example, S is the amount of income to be received in year 10, then the present value of S would be

$$P = \frac{S}{(1 + i)^N} \tag{7-70}$$

where N = 10

**Table 7-2
Example of Uniform Cash Flow**

<u>Year</u>	<u>Cash Flow, \$</u>
1	\$ 5,000
2	5,000
3	5,000
4	5,000
5	<u>5,000</u>
	\$25,000

These equations may be modified to reflect real interest rates by deducting an amount equal to anticipated inflation.

A cash flow is a series of payments received over time. These successive payments are discounted to present value by setting each annual amount equal to S and setting N at the appropriate amount in years. The selection of an appropriate N and i is very important. Cash flows for oil and gas production are rarely constant and generally decline over time. In addition, cash flows are often calculated on a monthly basis. The basic equation then must be modified to reflect the condition of the evaluation. A mid-year discount is probably more common than year-end. In this case,

$$P = S \left(\frac{1}{\left(1 + \frac{i}{2}\right)^{-0.5}} \right) \text{ in year 1} \quad (7-71)$$

and

$$P = S \left(\frac{1}{(1+i)^{N-0.5}} \right) \text{ in later years} \quad (7-72)$$

If discounting is done monthly, then

$$P = S \left(\frac{1}{\left(1 + \frac{i}{12}\right)^N} \right) \quad (7-73)$$

where S = monthly cash flow

N = no. of months from start of cash flow

This method is most commonly used in computer programs that calculate on a monthly basis. There are many convenient tables of present value factors published, and specialized tables are readily generated using the basic formulas.

The choice of the discount rate (DCR) is one of the most important elections made in evaluating a property or project. This is easily illustrated by comparing the present value of a cash flow that provides \$100,000 every year for 10 years. At increasing DCR, the present value declines significantly as shown in Table 7-3. If, as in most oil and gas cash flows, the cash flow declines, the effect of the DCR is even more pronounced as shown in Table 7-3.

As noted above, the DCR is a factor to account for the perceived risk associated with the deferral of income to some time in the future or, more commonly, making an investment with the expectation of future returns. The DCR can be thought of as being composed of four elements [53] of various types of risks: (1) real return on investment, (2) inflation, (3) liquidity and (4) specific investment risk. The first three are financial factors. Any investor requires the return of and on his investment which, net of inflation, is a real rate of return. Inflation is a risk that must be considered because it has the effect of diminishing the

Table 7-3
Effect of Discount Rate on Uniform and Declining Cash Flow

DCR, %	No Decline Present Value, \$	Decline @ 10%/yr. Present Value, \$
0 (undisc)	1,000,000	651,322
5	772,173	523,961
10	614,457	432,785
15	501,877	365,525
20	419,247	314,562
25	357,050	275,017
30	309,154	243,677

value of long-term investments. Liquidity is the risk associated with the length of time required to obtain the return; for example, long-term certificates of deposit generally pay a higher rate of interest than short-term accounts because the deposit is unavailable to the depositor for a longer time. Finally, specific investment risk is the risk associated with particular industries, businesses and projects. Government bonds are generally considered riskless while corporate stocks carry substantial risk. Investment in certain industries such as oil and gas production has higher than average risk compared to other industries—so-called business risk. In addition, investments in oil and gas projects have varying, but generally high, risks associated with them. Drilling exploratory wells is very high risk, while purchasing a new pumping unit may be relatively low risk. All these components must be considered in selecting a DCR for property or project valuation.

There are two basic sources for discount rates: (1) cost of capital, (2) market place. The *cost of capital* [54-56] is the cost to an investor of the funds available for the investment, generally consisting of debt and equity. The *cost of capital* includes real return, inflation, liquidity and general business risk. A risk premium for specific risk must be added. Reference should be made to the many textbooks and articles on this subject.

The marketplace is an indirect source of DCR through publications by banks and other financial institutions regarding DCR used for valuing oil and gas properties for lending or other purposes. *In no case should the evaluator confuse cost of capital or market DCR with the so-called prime rate or other single-issue, low-risk interest rate.* The cost of capital in the oil and gas industry since the early 1980s has averaged 12-16% after income tax, or about 20-24% before income tax [57,58,66]. At the same time, analysis of oil and gas property acquisitions indicates discount rates in the 20-30% range—averaging around 25% for the same period. Unless a company or individual consistently invests only 100% debt capital, the DCR must consist of a base interest rate plus an equity return premium plus a project risk premium.

However the DCR is chosen, it is applied to the cash flow to determine the present value of a future stream of income from a particular property or project.

If the DCR is properly chosen, the present value cash flow from that property or project is directly comparable with the present value cash flow from another property or project.

VALUATION OF OIL AND GAS PROPERTIES

Purpose of Valuation [59]

There are almost as many reasons and methods for determining the economic value of an oil and gas property or project as there are people who wish to do it. However diverse the reasons, they can generally be placed in two groups; investment analysis and regulatory compliance. The latter are special cases for SEC filings, *ad valorem* tax valuation, or other tax requirements such as estate taxes. In most cases, valuation is done for investment analysis. This could be anything from evaluation of the return from a workover or equipment upgrade to drilling a new well to purchasing producing properties. Whatever the purpose, the practical aspects are identical. In investment analysis, the evaluator is seeking to determine the additional benefit in terms of cash flow, profit and return on investment that can be obtained by making the investment. If it will *cost* \$10,000 to work-over a well to acidize or to open a new zone, will the additional production *increase revenues* sufficiently to pay back the \$10,000 in a reasonable time and provide a return beyond simple payback that *compensates for the risk* incurred in making the investment? If payback takes 3 years, there is some risk associated with waiting 3 years that must be compensated—otherwise the company could as well put its money in CDs and avoid the risk.

Fair Market Value. Many investments, such as purchasing properties or valuations done for *ad valorem* or estate taxes, require a determination of fair market value as the goal of valuation. The most common definition of FMV is:

“The price that would be paid by a knowledgeable and willing buyer and which would be accepted by a knowledgeable and willing seller neither being under any pressure to conclude a transaction.”

This definition, in various forms, means that the real value of a property can only be established in the marketplace by the free interaction of buyers and sellers. The true FMV will only be known after a property has been sold. However, it can be (and often must be) estimated through property valuation. FMV evaluations require the use of price/cost projections and DCRs that reasonably approximate the marketplace for property sales.

Profitability of Ventures

Profit is the amount of revenue remaining after payment of royalty, operating costs, investments and taxes, including income taxes. A distinction is often made between before-income tax (BFIT) profit and after-income tax (AFIT) profit for analysis purposes. If a firm has a large number of investments to evaluate and compare, use of pretax profit analysis may be useful if the investments have differing tax characteristics or benefits. However, comparison on only a BFIT basis may distort the ultimate profit and return because taxes do have to be paid.

Investment Analysis. As noted above, many evaluations are done to determine the economic value of an investment. To that end, there are many methods avail-

able to determine and compare the value of investments. These can be grouped as undiscounted methods and discounted methods.

Undiscounted methods are based on an undiscounted cash flow that can be BFIT or AFIT or both. In 1985, Boyle and Schenck [61] published a study of investment evaluation methods used in the oil and gas industry. The study found that most companies (a) allocate capital to investments in a systematic manner and (b) tend to use certain basic methods of investment analysis. The study also defined the methods in most common use by companies. The most common of these methods are:

Payout. The time required to accumulate an amount equal to the investment from the incremental cash flow created by the investment is the payout or payback. A common rule of thumb is 2–4 years subject to the conditions of the cash flow. It is important to measure payout using only the *incremental cash flow* created by the investment, not cash flow that would have been obtained anyway.

Profit/investment. The ratio of AFIT cumulative cash flow derived from an investment to the amount of the investment is

$$P/I = \frac{\text{AFIT cash flow}}{\text{Investment}}$$

There are several variations on this ratio that include using BFIT cash flow, discounted investment, and other combinations. Whichever is chosen, it must be used consistently from one cash flow to another. There are a large number of special-purpose rules of thumb that have been developed over time, particularly for property acquisitions. These include, but are not limited to:

\$/BOE. According to this rule, a property has a value of X\$ per bbl of recoverable reserves. At the time the rule enjoyed general use (1940–1960s), the ratio ranged from 25 to 40% of the wellhead price of oil depending on the section of the country.

\$/BOPD. Property value was X\$ per bopd of production at the time of purchase. Values ranged from \$5,000–15,000/bopd depending on location, etc.

Other rules of thumb are variations on the above. In practice, the development and use of such methods, including payout, held some benefit simply because they were easy to use and did not necessarily require a cash flow. However, as production has changed from declining primary to variable secondary and enhanced recovery and as economics have become less predictable, the validity of most rules of thumb has diminished considerably. In addition, the rapid growth in computers and software allows even the smallest operator to do relatively sophisticated evaluations so that reliance on generalizations are no longer necessary.

There are two basic discounted methods of defining project profitability, both of which have numerous variations [60]. Either method can be used BFIT or AFIT.

Net Present Value. Cumulative present value cash flow discounted at a specific rate. When calculated prior to deduction of investment, the NPV can be compared to the amount of investment. If NPV exceeds investment, the project should be profitable.

Rate of Return. ROR or internal rate of return is the discount rate that would reduce the cash flow to the amount of the investment or to zero if investment is included in the cash flow. Many authors have suggested modifications on this method and many variations are in use depending on individual or company preference. In general, the method requires a trial-and-error approach of discounting the cash flow at various DCRs (Table 7-3) until a match with the investment is achieved. The method can also be done graphically by calculating the PV of the cash flow at various DCRs defining a curve through the points, and finding the DCR at the point on the curve where PV cash flow equals the planned investment (Figure 7-12).

Investment Decision Making. Every company and individual has a unique approach to making investment decisions. As shown by Dougherty [62], many companies use two or more methods together. Companies often use a certain DCR that may be known as a "hurdle" rate or *minimum required return* (MRR) [63] to discount all cash flows. Assuming some consistency in other cash flow parameters, the various projects may then be compared to each other and the most favorable projects selected. As an example, a company has six projects in which it can invest funds but does not have sufficient funds for all six. The company has a cost of capital of 18% BFIT and an MRR of 20% BFIT. The company requires all cash flows to be discounted at MRR to determine NPV net of investment and also requires that IRR on each project meet or exceed MRR. The results are as shown in Table 7-4.

In this comparison, Project D has the highest NPV but the IRR of 19% is less than MRR and only 1% above the cost of funds and, therefore, has little margin for risk. Project B has a considerably lower NPV but a high IRR. A combination of Projects A, B and C would have a total NPV greater than D and also a higher composite IRR. Depending on budget constraints, a ranking of A, B, C, E and F would be appropriate. There are circumstances when D

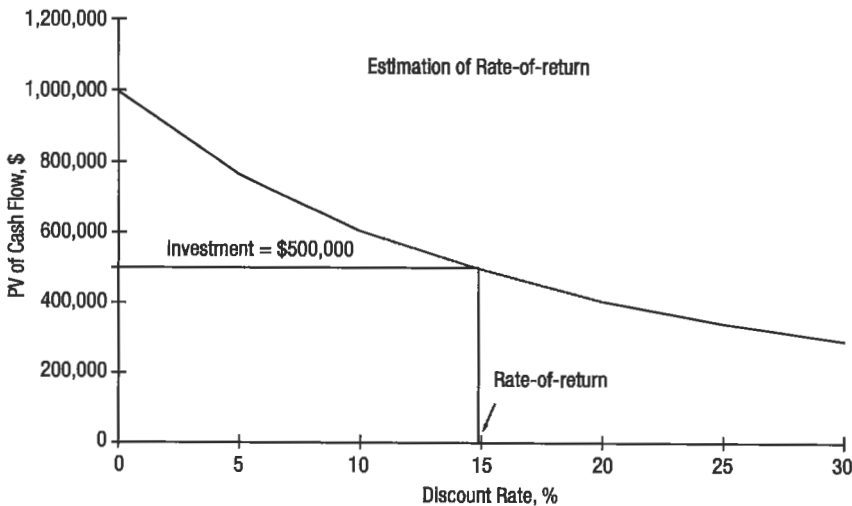


Figure 7-12. Graphical rate-of-return solution.

Table 7-4
Comparison of Net Present Value
and Internal Rate-of-Return

	NPV	IRR
A	\$300,000	22%
B	\$150,000	26%
C	\$100,000	24%
D	\$500,000	19%
E	\$200,000	21%
F	\$ 20,000	25%

would be accepted despite its low(er) IRR such as when intangible values come into play. In this example, all the projects were assumed to have the same level of risk. That may not always be the case and, if not, differing threshold levels of IRR may be used to account for the variance in risk.

Risk Analysis

Risk is the possibility that events or conditions in the future may not occur as expected. When flipping a coin you may expect it to turn up heads, but there is a 50% possibility that it will be tails. In drilling a purely exploratory well, there is a very high possibility that the well will be dry. In projecting future oil prices, there is a very good chance that your projection will be wrong both as to direction and timing. Each example contains risk, but the ability to quantify that risk ranges from a fixed 50% to a statistical value for wildcat drilling to virtually unquantifiable for the price projection.

Risk has a significant impact on valuation of oil and gas properties [64]. The oil business is a relatively high-risk endeavor to begin with, and within any property evaluation there are numerous opportunities for risk to impact the value. The production projection and reserves determination can be done using all available data and the best methods, but the actual production is still subject to the vagaries of a natural system—the reservoir rocks and fluids—that cannot even be sampled and measured to any major extent, let alone be accurately modeled to eliminate the potential for variance from expectations. Reserves are classified as *proved*, *probable* and *possible* on the basis of the ability to estimate those reserves and likelihood of recovery. Added to that are various potential mechanical problems that impose uncertainty on any projection of production.

There is substantial risk in projecting future prices and operating costs because of the inherent uncertainties of trying to determine how economic conditions that affect oil and gas prices and operating costs over the often

several year period of an oil property evaluation. In July–August, 1990, oil prices suddenly increased by over \$10 per barrel in the space of 30 days after generally declining for over 3 years. The increase was totally unexpected—as was, to a large extent, the major price drop in early 1986.

A property valuation should attempt to recognize and account for risk. There are several methods of analyzing risk and applying adjustments. The process has steps which can be generalized:

1. Define the risk.
2. Determine if the risk is measurable.
3. Define a range of values for the risk.
4. Select a risk evaluation method(s).
5. Apply risk adjustments to the evaluation.

Define the Risk

Any evaluation of an oil and gas property has a wide range of risks associated with it, starting with the geologic risk that recoverable hydrocarbons exist to the economic risk posed by price/cost projections and selection of discount rate.

Geologic risk is very important in assessing drilling prospects but is much reduced in production development projects. There have been several treatises written on a drilling project risk that allows the risk to approach quantification.

Geologic risks:

- Does the zone exist?
- Field size?
- Sufficient recoverable hydrocarbons?

Performance risk:

- reservoir properties (S_w , ϕ , K , μ , etc.)
- zone thickness
- areal extent
- drive mechanism (effects R_p)
- decline rate
- depth
- production method needed
- well spacing required
- stimulation needed?

Economic risks:

- Price projection depends on gravity of oil and composition
- Operating costs projection depends on gravity and composition, depth, number of wells, etc.
- Royalty and production taxes.
- Required investment.
- Cost-of-capital.
- Income tax treatment.

Measurement of Risk

Each of these risk elements and many others can be measured to some degree although the degree of real quantification varies considerably. Geologic risk has been addressed by many authors to the point that such factors as field size

distributions are quantified based on normal or log-normal analysis. Reservoir properties such as S_v and ϕ can generally be estimated from similar properties and fields and can be analyzed statistically as data are available. Areal extent can be estimated from mapping depending on the quality of control data. Economic data can be well known, such as current price, within very narrow boundaries but future trends can be highly variable. Each factor must be reviewed to determine the error potential, degree of uncertainty and range of possible but realistic values.

Define Range of Values

Most of the risk factors that may occur in an evaluation and that can be measured can be quantified on a range of values about the most likely value. Porosity may be $20 \pm 5\%$, or areal extent might be expressed as drainage radius of 20 acres $\pm 20\%$, whereas an overall field size of 100,000 barrels might have a $10 \pm 10\%$ probability of occurring.

Each risk element must be assessed for the range of possible values that may occur or the likelihood that a certain value would occur. Selection of those values should be based on objective measurement where possible supplemented by analysis of similar field (property) data and tempered by subjective experience.

Select Risk Evaluation Method

The method used for evaluation of risk often depends on (a) the relation to the risk element to the overall evaluation and (b) the degree to which a probability can be assigned to the value or values in the range of values. As an example, such factors as porosity, S_w , zone thickness; areal extent; and starting prices and costs could have as much probability of being one value as another within the range of values, in which case sensitivity analysis or Monte Carlo analysis would provide sufficient consideration of the risk factors. On the other hand, where probabilities of occurrence can be assigned to such factors as field size or price/cost escalations an expected value approach might be more appropriate.

Of course, each risk element can be evaluated either on its own or in combination with other factors. Oil-in-place might be calculated using a range of equally likely values for ϕ , S_w , etc., which would result in a range of values for OOIP that could then be tested for field size distribution and assigned a probability. A set of production projections could be evaluated using a range of price escalations to determine the sensitivity of project value or return to various prices.

Apply Risk Evaluation Methods

Sensitivity Analysis

1. Select one risk element and measure the range of equally likely values.
2. Apply the range of values, with appropriately selected intervals, to the part of the evaluation which is sensitive to that element; i.e., how is OOIP affected by changing ϕ from 18% to 30% at 1% intervals.
3. Combine compatible risk elements to determine if the elements offset or enhance each other.
4. Determine a range of outcomes and analyze statistically to determine the most likely outcome and range of probabilities.

Monte Carlo Analysis

This method essentially combines the sensitivity analysis approach with a system of randomly selecting the values to be used. The method is most effective

in analyzing the interrelation of a large number of variable factors. The outcomes can be statistically analyzed for assignment of probabilities.

Expected Value Theory [65]

Expected value is similar to sensitivity analysis with the major difference that the values used are considered to have a probability of occurrence and to be mutually exclusive. As an example, if ϕ were the element being evaluated, the range of values might be:

Table 7-5
Probability Assignment

<u>Test#</u>	<u>$\phi, \%$</u>	<u>Probability</u>
1	20	40%
2	18	20%
3	22	20%
4	17	15%
5	24	10%
6	16	5%

Assuming that all the other components of the OOIP calculation are fixed, an expected value of OOIP would be determined by calculating OOIP using each value of ϕ and then multiplying that OOIP by the probability. The sum of the adjusted OOIP is the expected value of OOIP.

In another example, probabilities could be assigned to a range of oil price escalation rates than an expected value of a property could be calculated by calculating a value using each escalation rate, multiplying the result by the probability and taking the sum as the expected value of the property.

These methods are relatively easy to apply once the risks (also read variables) have been analyzed and defined. They are particularly adaptable to computer analysis.

REFERENCES

The references cited here are primarily basic text references that provide an expansion of the information presented in the chapter sections of this handbook. Each such text reference contains numerous specific references and citations for specific topics. Also, specific references are listed below for certain chapter sections. The text references are basic sources that have been augmented over time. Neither the text nor the specific references are intended to be exhaustive and recourse to other publications should be pursued.

Estimating Oil and Gas Reserves

Primary Reserves

1. Society of Petroleum Engineers, *Definitions of Oil and Gas Reserves*, 1988.
2. Frick, Thomas C., *Petroleum Production Handbook*, McGraw-Hill Book Co., New York, (1962), pp. 17-3 to 18-23.
3. Standing, M. B., *Volumetric and Phase Behavior of Oil Field Hydrocarbon Systems*, Reinhold Publishing Co., (1952), pp. 1-9.
4. Gatlin, Carl, *Petroleum Engineering*, Prentice-Hall, Inc., Englewood Cliffs, NJ, (1964), pp. 1-5.
5. Frick, Thomas C., *Petroleum Production Handbook*, McGraw-Hill Book Co., New York, (1962), pp. 37-1 to 37-56.
6. Campbell, John M., *et al.*, *Mineral Property Economics*, Campbell Petroleum Series, (1978), pp. 1-122.
7. Frick, Thomas C., *Petroleum Production Handbook*, McGraw-Hill Book Co., New York, (1962), pp. 37-8 to 37-10.
8. Campbell, John M., *et al.*, *Mineral Property Economics*, Campbell Petroleum Series, (1978), pp. 3-23.
9. Frick, Thomas C., *Petroleum Production Handbook*, McGraw-Hill Book Co., New York, (1962), pp. 37-10 to 37-20.
10. Craft, B. C., and M. F. Hawkins, *Applied Petroleum Reservoir Engineering*, Prentice-Hall Inc., Englewood Cliffs, NJ, (1959), pp. 110-138.
11. Campbell, John M., *et al.*, *Mineral Property Economics*, Campbell Petroleum Series, (1978), pp. 23-44.
12. Amyx, Bass & Whiting, *Petroleum Reservoir Engineering*, McGraw-Hill Book Co., New York, (1960), pp. 561-598.
13. Wahl, W. L., L. D. Mullins, and E. B. Elfrink, "Estimation of ultimate recovery from solution gas drive reservoirs," *Journal of Petroleum Technology*, June 1958.
14. Higgins, R. V., "Calculating oil recoveries for solution-gas drive reservoirs," RI 5226, USBM, April 1956.
15. "Material balances in expansion type reservoirs above bubble point," *Journal of Petroleum Technology*, October 1955.
16. Buckley, S. E., and M. C. Leverett, "Mechanism of fluid displacement in sand," *Transactions of AIME*, 1942.
17. Welge, H. J., "A simplified method of calculating recovery by gas or water drive," *Transactions of AIME*, 1952.
18. Woods, W. W., and M. Muskat, "An analysis of material balance calculations," *Transactions of AIME*, 1945.
19. Muskat, M., and M. O. Taylor, "Effect of reservoir fluid and rock characteristics on production histories of gas drive reservoirs," *Transactions of AIME*, 1946.
20. Muskat, M., *Physical Principles of Oil Production*, McGraw-Hill Book Co., New York, (1949), p. 177.
21. Tarner, J., "How different size gas caps and reserve maintenance programs affect amount of recoverable oil," *Oil Weekly*, June 12, 1944.
22. Frick, Thomas C., *Petroleum Production Handbook*, McGraw-Hill Book Co., New York, (1962), pp. 27-15.
23. Frick, Thomas C., *Petroleum Production Handbook*, McGraw-Hill Book Co., New York, (1962), pp. 37-32 to 37-41.
24. Craft, B. C., and M. F. Hawkins, *Applied Petroleum Reservoir Engineering*, Prentice-Hall Inc., Englewood Cliffs, NJ, (1959), pp. 14-48.

25. Frick, Thomas C., *Petroleum Production Handbook*, McGraw-Hill Book Co., New York, (1962), pp. 37-41 to 37-54.
26. Arps, J. J., "Estimation of primary oil reserves," *Transactions of AIME*, 1956.
27. Arps, J. J., "Analysis of decline curves," *Transactions of AIME*, 1945.
28. Campbell, John M., *et al.*, *Mineral Property Economics*, Campbell Petroleum Series, (1978), p. 177.
29. Slider, H. C., "A simplified method of hyperbolic decline curve analysis," *Journal of Petroleum Technology*, March 1968.
30. Fetkovich, M. J., "Decline curve analysis using type curves," *Journal of Petroleum Technology*, June 1980.
31. Fetkovich, M. J., *et al.*, "Decline curve analysis using type curves: Case histories," SPE No. 13169, 59th Annual Technical Conference, Houston, TX, September 1984.
32. "The ability of rate-time decline curves to predict future production rates," MS Thesis, University of Tulsa, Tulsa, OK, 1968.

Production Stimulation

33. "Review of steam soak operations: California," *Journal of Petroleum Technology*, August 1972.
34. "Cyclic steam injection: Optimization of process using penalty functions," *SPEJ*, December 1971.
35. "Steam stimulation: Correlation of performance," *Journal of Petroleum Technology*, November 1972.
36. Smith, Charles Robert, *Mechanics of Secondary Oil Recovery*, Reinhold Publishing Co., (1966), pp. 471-476.
37. Van Poolen, H. K., *et al.*, "Hydraulic fracturing—Fracture flow capacity vs. well productivity," *Transactions of AIME*, 1958.
38. Allen, Thomas O., and Alan P. Roberts, Oil and Gas Consultants, Inc., *Production Operations*, pp. 141-169.
39. Tinsley, J. M., *et al.*, "Vertical fracture height—Its effect on steady state production increase," *Journal of Petroleum Technology*, May 1969.
40. McGuire, W. J., and V. J. Sikora, "The effect of vertical fractures on well productivity," *Journal of Petroleum Technology*, October 1960.

Secondary and EOR Methods

41. Smith, Charles Robert, *Mechanics of Secondary Oil Recovery*, Reinhold Publishing Co., (1966), Chap. 9, p. 282.
42. Smith, Charles Robert, *Mechanics of Secondary Oil Recovery*, Reinhold Publishing Co., (1966), Chap. 5, p. 148.
43. Buckley, S. E., and M. C. Leverett, "Mechanism of fluid displacement in sands," *Transactions of AIME*, 1942.
44. Stiles, W. E., "Use of permeability distribution in water flood calculations," *Transactions of AIME*, 1942.
45. Dykstra, H., and R. L. Parsons, "The prediction of waterflood performance with variation in permeability profile," *Production Monthly*, 1950.
46. Johnson, J. P., "Predicting waterflood performance by graphical representation of porosity and permeability distribution," *Journal of Petroleum Technology*, November 1965.
47. Marx, J. W., and R. H. Lagenhiem, "Reservoir heating by hot fluid injection," *Petroleum Transactions of AIME*, 1959.
48. Willman, B. T., *et al.*, vol. 222, p. 681, *Petroleum Transactions of AIME*, 1961.
49. Gomma, Ezzat E., "Correlations for predicting oil recovery by steamflood," *Journal of Petroleum Technology*, 1980.

Determining the Value of Future Production

50. Frick, Thomas C., *Petroleum Production Handbook*, McGraw-Hill Book Co., New York, (1962), Chap. 38, pp. 38-1.
51. Campbell, John M., *et al.*, *Mineral Property Economics*, Campbell Petroleum Series, (1978), Vol. 1, Chap. 5.
52. Campbell, John M., *et al.*, *Mineral Property Economics*, Campbell Petroleum Series, (1978), Chap. 6, p. 196.
53. Weston, J. Fred, and Thomas E. Copeland, *Managerial Finance*, The Dryden Press, (1986), Chap. 7, p. 139.
54. Weston, J. Fred, and Thomas E. Copeland, *Managerial Finance*, The Dryden Press, (1986), Chap. 21, p. 579.
55. Campbell, John M., *et al.*, *Mineral Property Economics*, Campbell Petroleum Series, (1978), Chap. 3, p. 66.
56. Bierman, Jr., Harold, and Seymour Smidt, *Financial Management for Decision Making*, MacMillan, New York, (1986), Chap. 14, p. 420.
57. Miller, R. J., and R. Vasquez, "Analysis of oil and gas property sales transactions and sales in California," *Journal of Petroleum Technology*, March 1988.
58. Miller, R. J., and R. Vasquez, "Discount rates, cost of capital and property acquisition evaluations," 63rd Annual Technical Conference, Houston, TX, October 2-5, 1988.
59. McCray, Arthur W., *Petroleum Evaluations and Economic Decisions*, Prentice-Hall Inc., Englewood Cliffs, NJ, (1975), Chap. 1, p. 4.
60. Weston, J. Fred, and Thomas E. Copeland, *Managerial Finance*, The Dryden Press, (1986), Chap. 6, p. 99.
61. Boyle, Hugh F., Jr., and George K. Schenck, "Investment analysis: U.S. oil and gas producers score high in university survey," *Journal of Petroleum Technology*, April 1985.
62. Dougherty, E. L. and Sarkar, Jayati, "Current Investment Practices and Procedures: Results of a Survey of U.S. Oil and Gas Producers and Petroleum Consultants," SPE Hydrocarbon Economics and Evaluation Symposium, Dallas, TX, March 29-30, 1993.
63. Text P, Chap. 3, p. 67.
64. Newendorp, Paul D., *Decision Analysis for Petroleum Exploration*, Petroleum Publishing Co., (1976), , Chap. 1, p. 1.
65. Newendorp, Paul D., *Decision Analysis for Petroleum Exploration*, Petroleum Publishing Co., (1976), , Chap. 3, p. 58.
66. Miller, Richard J., "Fair Market Value Discount Rates: Analysis of Market Sales Data," SPE Hydrocarbon Economics and Evaluation Symposium, Dallas, TX, March 26-28, 1995.
67. Campbell, John M., *et al.*, *Mineral Property Economics*, Campbell Petroleum Series, (1978), Chap. 3, p. 67.

Appendix

Units and Conversions

Table A-1
Alphabetical List of Units
(symbols of SI units given in parentheses)

To Convert From	To	Multiply By**	
abampere	ampere (A)	1.0*	E+01
abcoulomb	coulomb (C)	1.0*	E+01
abfarad	farad (F)	1.0*	E+09
abhenry	henry (H)	1.0*	E-09
abmho	siemens (S)	1.0*	E+09
abohm	ohm (Ω)	1.0*	E-09
abvolt	volt (V)	1.0*	E-08
acre-foot (U.S. survey) ⁽¹⁾	meter ³ (m ³)	1.233 489	E+03
acre (U.S. survey) ⁽¹⁾	meter ² (m ²)	4.048 873	E+03
ampere hour	coulomb (C)	3.6*	E+03
are	meter ² (m ²)	1.0*	E+02
angstrom	meter (m)	1.0*	E-10
astronomical unit	meter (m)	1.495 979	E+11
atmosphere (standard)	pascal (Pa)	1.013 250*	E+05
atmosphere (technical = 1 kgf/cm ²)	pascal (Pa)	9.808 650*	E+04
bar	pascal (Pa)	1.0*	E+05
barn	meter ² (m ²)	1.0*	E-28
barrel (for petroleum, 42 gal)	meter ³ (m ³)	1.589 873	E-01
board foot	meter ³ (m ³)	2.359 737	E-03
British thermal unit (International Table) ⁽²⁾	joule (J)	1.055 056	E+03
British thermal unit (mean)	joule (J)	1.055 87	E+03
British thermal unit (thermochemical)	joule (J)	1.054 350	E+03
British thermal unit (39°F)	joule (J)	1.059 67	E+03
British thermal unit (59°F)	joule (J)	1.054 80	E+03
British thermal unit (60°F)	joule (J)	1.054 68	E+03
Btu (International Table)-ft/(hr-ft ² -°F) (thermal conductivity)	watt per meter kelvin [W/(m-K)]	1.730 735	E+00
Btu (thermochemical)-ft/(hr-ft ² -°F) (thermal conductivity)	watt per meter kelvin [W/(m-K)]	1.729 577	E+00
Btu (International Table)-in./(hr-ft ² -°F) (thermal conductivity)	watt per meter kelvin [W/(m-K)]	1.442 279	E-01
Btu (thermochemical)-in./(hr-ft ² -°F) (thermal conductivity)	watt per meter kelvin [W/(m-K)]	1.441 314	E-01

Btu (International Table)-in./(s-ft ² -°F) (thermal conductivity)	watt per meter kelvin [W/(m·K)]	5.192 204 E+02
Btu (thermochemical)-in./(s-ft ² -°F) (thermal conductivity)	watt per meter kelvin [W/(m·K)]	5.188 732 E+02
Btu (International Table)/hr	watt (W)	2.930 711 E-01
Btu (thermochemical)/hr	watt (W)	2.928 751 E-01
Btu (thermochemical)/min	watt (W)	1.757 250 E+01
Btu (thermochemical)/s	watt (W)	1.054 350 E+03
Btu (International Table)/ft ²	joule per meter ² (J/m ²)	1.135 653 E+04
Btu (thermochemical)/ft ²	joule per meter ² (J/m ²)	1.134 893 E+04
Btu (thermochemical)/(ft ² -hr)	watt per meter ² (W/m ²)	3.152 481 E+00
Btu (thermochemical)/(ft ² -min)	watt per meter ² (W/m ²)	1.891 489 E+02
Btu (thermochemical)/(ft ² -s)	watt per meter ² (W/m ²)	1.134 893 E+04
Btu (thermochemical)/(in. ² -s)	watt per meter ² (W/m ²)	1.634 246 E+06
Btu (International Table)/(hr-ft ² -°F) (thermal conductance)	watt per meter ² kelvin [W/(m ² ·K)]	5.678 263 E+00
Btu (thermochemical)/(hr-ft ² -°F) (thermal conductance)	watt per meter ² kelvin [W/(m ² ·K)]	5.674 466 E+00
Btu (International Table)/(s-ft ² -°F)	watt per meter ² kelvin [W/(m ² ·K)]	2.044 175 E+04
Btu (thermochemical)/(s-ft ² -°F)	watt per meter ² kelvin [W/(m ² ·K)]	2.042 808 E+04
Btu (International Table)/lbm	joule per kilogram (J/kg)	2.326 ^a E+03
Btu (thermochemical)/lbm	joule per kilogram (J/kg)	2.324 444 E+03
Btu (International Table)/(lbm-°F) (heat capacity)	joule per kilogram kelvin [J/(kg·K)]	4.186 8 ^a E+03
Btu (thermochemical)/(lbm-°F) (heat capacity)	joule per kilogram kelvin [J/(kg·K)]	4.184 000 E+03

^a See footnote on Page 13.

⁽¹⁾ Since 1893 the U.S. base of length measurement has been derived from metric standards. In 1959 a small refinement was made in the definition of the yard to resolve discrepancies both in this country and abroad, which changed its length from 3600/3937 m to 0.9144 m exactly. This resulted in the new value being shorter by two parts in a million. At the same time it was decided that any data in feet derived from and published as a result of geodetic surveys within the U.S. would remain with the old standard (1 ft = 1200/3937 m) until further decision. This foot is named the U.S. survey foot. As a result, all U.S. land measurements in U.S. customary units will relate to the meter by the old standard. All the conversion factors in these tables for units referenced to this footnote are based on the U.S. survey foot, rather than the international foot. Conversion factors for the land measure given below may be determined from the following relationships:

- 1 league = 3 miles (exactly)
- 1 rod = 16 1/2 ft (exactly)
- 1 chain = 66 ft (exactly)
- 1 section = 1 sq mile
- 1 township = 36 sq miles

⁽²⁾ This value was adopted in 1956. Some of the older International Tables use the value 1.055 04 E+03. The exact conversion factor is 1.055 055 852 62^a E+03.

Table A-1
(continued)

To Convert From	To	Multiply By**
bushel (U.S.)	meter ³ (m ³)	3.523 907 E-02
caliber (inch)	meter (m)	2.54* E-02
calorie (International Table)	joule (J)	4.186 8* E+00
calorie (mean)	joule (J)	4.190 02 E+00
calorie (thermochemical)	joule (J)	4.184* E+00
calorie (15°C)	joule (J)	4.185 80 E+00
calorie (20°C)	joule (J)	4.181 90 E+00
calorie (kilogram, International Table)	joule (J)	4.186 8* E+03
calorie (kilogram, mean)	joule (J)	4.190 02 E+03
calorie (kilogram, thermochemical)	joule (J)	4.184* E+03
cal (thermochemical)/cm ²	joule per meter ² (J/m ²)	4.184* E+04
cal (international Table)/g	joule per kilogram (J/kg)	4.186* E+03
cal (thermochemical)/g	joule per kilogram (J/kg)	4.184* E+03
cal (International Table)/(g·°C)	joule per kilogram kelvin [J/(kg·K)]	4.186 8* E+03
cal (thermochemical)/(g·°C)	joule per kilogram kelvin [J/(kg·K)]	4.184* E+03
cal (thermochemical)/min	watt (W)	6.973 333 E-02
cal (thermochemical)/s	watt (W)	4.184* E+00
cal (thermochemical)/(cm ² ·min)	watt per meter ² (W/m ²)	6.973 333 E+02
cal (thermochemical)/(cm ² ·s)	watt per meter ² (W/m ²)	4.184* E+04
cal (thermochemical)/(cm·s·°C)	watt per meter kelvin [W/(m·K)]	4.184* E+02
capture unit (c.u. = 10 ⁻³ cm ⁻¹)	per meter (m ⁻¹)	1.0* E-01
carat (metric)	kilogram (kg)	2.0* E-04
centimeter of mercury (0°C)	pascal (Pa)	1.333 22 E+03
centimeter of water (4°C)	pascal (Pa)	9.806 38 E+01
centipoise	pascal second (Pa·s)	1.0* E-03
centistokes	meter ² per second (m ² /s)	1.0* E-06
circular mil	meter ² (m ²)	5.067 075 E-10
clo	kelvin meter ² per watt [(K·m ²)/W]	2.003 712 E-01
cup	meter ³ (m ³)	2.365 882 E-04
curie	becquerel (Bq)	3.7* E+10
cycle per second	hertz (Hz)	1.0* E+00
day (mean solar)	second (s)	8.640 000 E+04
day (sidereal)	second (s)	8.616 409 E+04

degree (angle)	radian (rad)	1.745 329 E-02
degree Celsius	kelvin (K)	$T_K = T_C + 273.15$
degree centigrade (see degree Celsius)		
degree Fahrenheit	degree Celsius	$T_C = (T_F - 32)/1.8$
degree Fahrenheit	kelvin (K)	$T_K = (T_F + 459.67)/1.8$
degree Rankine	kelvin (K)	$T_K = T_R/1.8$
°F-hr-ft ² /Btu (International Table) (thermal resistance)	kelvin meter ² per watt [(K-m ²)/W]	1.781 102 E-01
°F-hr-ft ² /Btu (thermochemical) (thermal resistance)	kelvin meter ² per watt [(K-m ²)/W]	1.782 250 E-01
denier	kilogram per meter (kg/m)	1.111 111 E-07
dyne	newton (N)	1.0° E-05
dyne-cm	newton meter (N-m)	1.0° E-07
dyne/cm ²	pascal (Pa)	1.0° E-01
electronvolt	joule (J)	1.602 19 E-19
EMU of capacitance	farad (F)	1.0° E+09
EMU of current	ampere (A)	1.0° E+01
EMU of electric potential	volt (V)	1.0° E-08
EMU of inductance	henry (H)	1.0° E-09
EMU of resistance	ohm (Ω)	1.0° E-09
ESU of capacitance	farad (F)	1.112 650 E-12
ESU of current	ampere (A)	3.335 6 E-10
ESU of electric potential	volt (V)	2.997 9 E+02
ESU of inductance	henry (H)	8.987 554 E+11
ESU of resistance	ohm (Ω)	8.987 554 E+11
erg	joule (J)	1.0° E-07
erg/cm ² -s	watt per meter ² (W/m ²)	1.0° E-03
erg/s	watt (W)	1.0° E-07
faraday (based on carbon-12)	coulomb (C)	9.648 70 E+04
faraday (chemical)	coulomb (C)	9.649 57 E+04
faraday (physical)	coulomb (C)	9.652 19 E+04
fathom	meter (m)	1.828 8 E+00
fermi (femtometer)	meter (m)	1.0° E-15
fluid ounce (U.S.)	meter ³ (m ³)	2.957 353 E-05
foot	meter (m)	3.048° E-01
foot (U.S. survey) ⁽¹⁾	meter (m)	3.048 006 E-01

Table A-1
(continued)

To Convert From	To	Multiply By**
foot of water (39.2°F)	pascal (Pa)	2.988 98 E + 03
sq ft	meter ² (m ²)	9.290 304* E - 02
ft ² /hr (thermal diffusivity)	meter ² per second (m ² /s)	2.580 640* E - 05
ft ² /s	meter ² per second (m ² /s)	9.290 304* E - 02
cu ft (volume; section modulus)	meter ³ (m ³)	2.831 685 E - 02
ft ³ /min	meter ³ per second (m ³ /s)	4.719 474 E - 04
ft ³ /s	meter ³ per second (m ³ /s)	2.831 685 E - 02
ft ⁴ (moment of section) ⁽³⁾	meter ⁴ (m ⁴)	8.630 975 E - 03
ft/hr	meter per second (m/s)	8.468 667 E - 05
ft/min	meter per second (m/s)	5.080* E - 03
ft/s	meter per second (m/s)	3.048* E - 01
ft/s ²	meter per second ² (m/s ²)	3.048* E - 01
footcandle	lux (lx)	1.076 391 E + 01
footlambert	candela per meter ² (cd/m ²)	3.426 259 E + 00
ft-lbf	joule (J)	1.355 818 E + 00
ft-lbf/hr	watt (W)	3.766 161 E - 04
ft-lbf/min	watt (W)	2.259 697 E - 02
ft-lbf/s	watt (W)	1.355 818 E + 00
ft-poundal	joule (J)	4.214 011 E - 02
free fall, standard (g)	meter per second ² (m/s ²)	9.806 650* E + 00
cm/s ²	meter per second ² (m/s ²)	1.0* E - 02
gallon (Canadian liquid)	meter ³ (m ³)	4.546 090 E - 03
gallon (U.K. liquid)	meter ³ (m ³)	4.546 092 E - 03
gallon (U.S. dry)	meter ³ (m ³)	4.404 884 E - 03
gallon (U.S. liquid)	meter ³ (m ³)	3.785 412 E - 03
gal (U.S. liquid)/day	meter ³ per second (m ³ /s)	4.361 264 E - 08
gal (U.S. liquid)/min	meter ³ per second (m ³ /s)	6.309 020 E - 05
gal (U.S. liquid)/hp-hr (SFC, specific fuel consumption)	meter ³ per joule (m ³ /J)	1.410 089 E - 09
gamma (magnetic field strength)	ampere per meter (A/m)	7.957 747 E - 04
gamma (magnetic flux density)	tesla (T)	1.0* E - 09
gauss	tesla (T)	1.0* E - 04
gilbert	ampere (A)	7.957 747 E - 01

gill (U.K.)	meter ³ (m ³)	1.420 654	E - 04
gill (U.S.)	meter ³ (m ³)	1.182 941	E - 04
grad	degree (angular)	9.0°	E - 01
grad	radian (rad)	1.570 796	E - 02
grain (1/7000 lbm avoirdupois)	kilogram (kg)	6.479 891*	E - 05
grain (lbm avoirdupois/7000)/gal (U.S. liquid)	kilogram per meter ³ (kg/m ³)	1.711 806	E - 02
gram	kilogram (kg)	1.0°	E - 03
g/cm ³	kilogram per meter ³ (kg/m ³)	1.0°	E + 03
gram-force/cm ²	pascal (Pa)	9.806 650*	E + 01
hectare	meter ² (m ²)	1.0°	E + 04
horsepower (550 ft-lbf/s)	watt (W)	7.456 999	E + 02
horsepower (boiler)	watt (W)	9.809 50	E + 03
horsepower (electric)	watt (W)	7.460*	E + 02
horsepower (metric)	watt (W)	7.354 99	E + 02
horsepower (water)	watt (W)	7.460 43	E + 02
horsepower (U.K.)	watt (W)	7.457 0	E + 02
hour (mean solar)	second (s)	3.600 000	E + 03
hour (sidereal)	second (s)	3.590 170	E + 03
hundredweight (long)	kilogram (kg)	5.080 235	E + 01
hundredweight (short)	kilogram (kg)	4.535 924	E + 01
inch	meter (m)	2.54°	E - 02
inch of mercury (32°F)	pascal (Pa)	3.386 38	E + 03
inch of mercury (60°F)	pascal (Pa)	3.376 85	E + 03
inch of water (39.2°F)	pascal (Pa)	2.490 82	E + 02
inch of water (60°F)	pascal (Pa)	2.488 4	E + 02
sq in.	meter ² (m ²)	6.451 6°	E - 04
cu in. (volume; section modulus) ⁽⁴⁾	meter ³ (m ³)	1.638 706	E - 05
in. ³ /min	meter ³ per second (m ³ /s)	2.731 177	E - 07
in. ⁴ (moment of section) ⁽³⁾	meter ⁴ (m ⁴)	4.162 314	E - 07
in./s	meter per second (m/s)	2.54°	E - 02
in./s ²	meter per second ² (m/s ²)	2.54°	E - 02
kaysar	1 per meter (1/m)	1.0°	E + 02
kelvin	degree Celsius	$T_c = T_K - 273.15$	

⁽³⁾ This sometimes is called the moment of inertia of a plane section about a specified axis.

⁽⁴⁾ The exact conversion factor is 1.638 706 4°E - 05.

Table A-1
(continued)

To Convert From	To	Multiply By**
kilocalorie (International Table)	joule (J)	4.186 8* E+03
kilocalorie (mean)	joule (J)	4.190 02 E+03
kilocalorie (thermochemical)	joule (J)	4.184* E+03
kilocalorie (thermochemical)/min	watt (W)	6.973 333 E+01
kilocalorie (thermochemical)/s	watt (W)	4.184* E+03
kilogram-force (kgf)	newton (N)	9.806 65* E+00
kgf·m	newton meter (N·m)	9.806 65* E+00
kgf·s ² /m (mass)	kilogram (kg)	9.806 65* E+00
kgf/cm ²	pascal (Pa)	9.806 65* E+04
kgf/m ²	pascal (Pa)	9.806 65* E+00
kgf/mm ²	pascal (Pa)	9.806 65* E+06
km/h	meter per second (m/s)	2.777 778 E-01
kilopond	newton (N)	9.806 65* E+00
kilowatthour (kW·hr)	joule (J)	3.6* E+06
kip (1000 lbf)	newton (N)	4.448 222 E+03
kip/in. ² (ksi)	pascal (Pa)	6.894 757 E+06
knot (international)	meter per second (m/s)	5.144 444 E-01
lambert	candela per meter ² (cd/m ²)	1/π* E+04
lambert	candela per meter ² (cd/m ²)	3.183 099 E+03
langley	joule per meter ² (J/m ²)	4.184* E+04
league	meter (m)	(see Footnote 1)
light year	meter (m)	9.460 55 E+15
liter ⁽⁹⁾	meter ³ (m ³)	1.0* E-03
maxwell	weber (Wb)	1.0* E-08
mho	siemens (S)	1.0* E+00
microinch	meter (m)	2.54* E-06
microsecond/foot (μs/ft)	microsecond/meter (μs/m)	3.280 840 E+00
micron	meter (m)	1.0* E-06
mil	meter (m)	2.54* E-05
mile (international)	meter (m)	1.609 344* E+03
mile (statute)	meter (m)	1.609 3 E+03
mile (U.S. survey) ⁽¹⁾	meter (m)	1.609 347 E+03
mile (international nautical)	meter (m)	1.852* E+03

mile (U.K. nautical)	meter (m)	1.853 184* E + 03
mile (U.S. nautical)	meter (m)	1.852* E + 03
sq mile (international)	meter ² (m ²)	2.589 988 E + 06
sq mile (U.S. survey) ⁽¹⁾	meter ² (m ²)	2.589 998 E + 06
mile/hr (international)	meter per second (m/s)	4.470 4* E - 01
mile/hr (international)	kilometer per hour (km/h)	1.609 344* E + 00
mile/min (international)	meter per second (m/s)	2.682 24* E + 01
mile/s (international)	meter per second (m/s)	1.609 344* E + 03
millibar	pascal (Pa)	1.0* E + 02
millimeter of mercury (0°C)	pascal (Pa)	1.333 22 E + 02
minute (angle)	radian (rad)	2.908 882 E - 04
minute (mean solar)	second (s)	6.0* E + 01
minute (sidereal)	second (s)	5.983 617 E + 01
month (mean calendar)	second (s)	2.628 000 E + 06
oersted	ampere per meter (A/m)	7.957 747 E + 01
ohm centimeter	ohm meter (Ω·m)	1.0* E - 02
ohm circular-mil per ft	ohm millimeter ² per meter [(Ω·mm ²)m]	1.662 426 E - 03
ounce (avoirdupois)	kilogram (kg)	2.834 952 E - 02
ounce (troy or apothecary)	kilogram (kg)	3.110 348 E - 02
ounce (U.K. fluid)	meter ³ (m ³)	2.841 307 E - 05
ounce (U.S. fluid)	meter ³ (m ³)	2.957 353 E - 05
ounce-force	newton (N)	2.780 139 E - 01
ozf·in.	newton meter (N·m)	7.061 552 E - 03
oz (avoirdupois)/gal (U.K. liquid)	kilogram per meter ³ (kg/m ³)	6.236 021 E + 00
oz (avoirdupois)/gal (U.S. liquid)	kilogram per meter ³ (kg/m ³)	7.489 152 E + 00
oz (avoirdupois)/in. ³	kilogram per meter ³ (kg/m ³)	1.729 994 E + 03
oz (avoirdupois)/ft ²	kilogram per meter ² (kg/m ²)	3.051 517 E - 01
oz (avoirdupois)/yd ²	kilogram per meter ² (kg/m ²)	3.390 575 E - 02
parsec	meter (m)	3.085 678 E + 16
peck (U.S.)	meter ³ (m ³)	8.809 768 E - 03
pennyweight	kilogram (kg)	1.555 174 E - 03
perm (°C) ⁽²⁾	kilogram per pascal second meter ² [kg/(Pa·s·m ²)]	5.721 35 E - 11

⁽¹⁾In 1984 the General Conference on Weights and Measures adopted the name liter as a special name for the cubic decimeter. Prior to this decision the liter differed slightly (previous value, 1.000 028 dm³) and in expression of precision volume measurement this fact must be kept in mind.

⁽²⁾Not the same as reservoir "perm."

Table A-1
(continued)

To Convert From	To	Multiply By**
perm (23°C) ⁽⁶⁾	kilogram per pascal second meter ² [kg/(Pa·s·m ²)]	5.745 25 E - 11
perm·in. (0°C) ⁽⁷⁾	kilogram per pascal second meter [kg/(Pa·s·m)]	1.453 22 E - 12
perm·in. (23°C) ⁽⁷⁾	kilogram per pascal second meter [kg/(Pa·s·m)]	1.459 29 E - 12
phot	lumen per meter ² (lm/m ²)	1.0* E + 04
pica (printer's)	meter (m)	4.217 518 E - 03
pint (U.S. dry)	meter ³ (m ³)	5.506 105 E - 04
pint (U.S. liquid)	meter ³ (m ³)	4.731 765 E - 04
point (printer's)	meter (m)	3.514 598* E - 04
poise (absolute viscosity)	pascal second (Pa·s)	1.0* E - 01
pound (lbm avoirdupois) ⁽⁸⁾	kilogram (kg)	4.535 924 E - 01
pound (troy or apothecary)	kilogram (kg)	3.732 417 E - 01
lbm·ft ² (moment of inertia)	kilogram meter ² (kg·m ²)	4.214 011 E - 02
lbm·in. ² (moment of inertia)	kilogram meter ² (kg·m ²)	2.926 397 E - 04
lbm/ft·hr	pascal second (Pa·s)	4.133 789 E - 04
lbm/ft·s	pascal second (Pa·s)	1.488 164 E + 00
lbm/ft ²	kilogram per meter ² (kg/m ²)	4.882 428 E + 00
lbm/ft ³	kilogram per meter ³ (kg/m ³)	1.601 848 E + 01
lbm/gal (U.K. liquid)	kilogram per meter ³ (kg/m ³)	9.977 633 E + 01
lbm/gal (U.S. liquid)	kilogram per meter ³ (kg/m ³)	1.198 264 E + 02
lbm/hr	kilogram per second (kg/s)	1.259 979 E - 04
lbm/(hp·hr) (SFC, specific fuel consumption)	kilogram per joule (kg/J)	1.689 659 E - 07
lbm/in. ³	kilogram per meter ³ (kg/m ³)	2.767 990 E + 04
lbm/min	kilogram per second (kg/s)	7.559 873 E - 03
lbm/s	kilogram per second (kg/s)	4.535 924 E - 01
lbm/yd ³	kilogram per meter ³ (kg/m ³)	5.932 764 E - 01
poundal	newton (N)	1.382 550 E - 01
poundal/ft ²	pascal (Pa)	1.488 164 E + 00
poundal·s/ft ²	pascal second (Pa·s)	1.488 164 E + 00
pound-force (lbf) ⁽⁹⁾	newton (N)	4.448 222 E + 00

lbf-ft ⁽¹⁰⁾	newton meter (N·m)	1.355 818 E + 00
lbf-ft/in. ⁽¹¹⁾	newton meter per meter [(N·m)/m]	5.337 868 E + 01
lbf-in. ⁽¹¹⁾	newton meter (N·m)	1.129 848 E - 01
lbf-in./in. ⁽¹¹⁾	newton meter per meter [(N·m)/m]	4.448 222 E + 00
lbf-s/ft ²	pascal second (Pa·s)	4.788 026 E + 01
lbf/ft	newton per meter (N/m)	1.459 390 E + 01
lbf/ft ²	pascal (Pa)	4.788 026 E + 01
lbf/in.	newton per meter (N/m)	1.751 268 E + 02
lbf/in. ² (psf)	pascal (Pa)	6.894 757 E + 03
lbf/lbm (thrust/weight [mass] ratio)	newton per kilogram (N/kg)	9.806 650 E + 00
quart (U.S. dry)	meter ³ (m ³)	1.101 221 E - 03
quart (U.S. liquid)	meter ³ (m ³)	9.463 529 E - 04
rad (radiation dose absorbed)	gray (Gy)	1.0* E - 02
rhe	1 per pascal second [1/(Pa·s)]	1.0* E + 01
rod	meter (m)	(see Footnote 1)
roentgen	coulomb per kilogram (C/kg)	2.58 E - 04
second (angle)	radian (rad)	4.848 137 E - 06
second (sidereal)	second (s)	9.972 696 E - 01
section	meter ² (m ²)	(see Footnote 1)
shake	second (s)	1.000 000* E - 08
slug	kilogram (kg)	1.459 390 E + 01
slug/(ft·s)	pascal second (Pa·s)	4.788 026 E + 01
slug/ft ³	kilogram per meter ³ (kg/m ³)	5.153 788 E + 02
statampere	ampere (A)	3.335 640 E - 10
statcoulomb	coulomb (C)	3.335 640 E - 10
statfarad	farad (F)	1.112 650 E - 12
stathenry	henry (H)	8.987 554 E + 11
statmho	siemens (S)	1.112 650 E - 12
statohm	ohm (Ω)	8.987 554 E + 11
statvolt	volt (V)	2.997 925 E + 02
stere	meter ³ (m ³)	1.0* E + 00

⁽⁷⁾Not the same dimensions as "mildarcy-foot."

⁽⁸⁾The exact conversion factor is 4.535 923 7*E - 01.

⁽⁹⁾The exact conversion factor is 4.448 221 615 260 5*E + 00.

⁽¹⁰⁾Torque unit; see text discussion of "Torque and Bending Moment."

⁽¹¹⁾Torque divided by length; see text discussion of "Torque and Bending Moment."

Table A-1
(continued)

To Convert From	To	Multiply By**	
stilb	candela per meter ² (cd/m ²)	1.0*	E + 04
stokes (kinematic viscosity)	meter ² per second (m ² /s)	1.0*	E - 04
tablespoon	meter ³ (m ³)	1.478 676	E - 05
teaspoon	meter ³ (m ³)	4.928 922	E - 06
tex	kilogram per meter (kg/m)	1.0*	E - 06
therm	joule (J)	1.055 056	E + 08
ton (assay)	kilogram (kg)	2.916 667	E - 02
ton (long, 2,240 lbm)	kilogram (kg)	1.016 047	E + 03
ton (metric)	kilogram (kg)	1.0*	E + 03
ton (nuclear equivalent of TNT)	joule (J)	4.184	E + 09 ⁽¹²⁾
ton (refrigeration)	watt (W)	3.516 800	E + 03
ton (register)	meter ³ (m ³)	2.831 685	E + 00
ton (short, 2000 lbm)	kilogram (kg)	9.071 847	E + 02
ton (long)/yd ³	kilogram per meter ³ (kg/m ³)	1.328 939	E + 03
ton (short)/hr	kilogram per second (kg/s)	2.519 958	E - 01
ton-force (2000 lbf)	newton (N)	8.896 444	E + 03
tonne	kilogram (kg)	1.0*	E + 03
torr (mm Hg, 0°C)	pascal (Pa)	1.333 22	E + 02
township	meter ² (m ²)	(see Footnote 1)	
unit pole	weber (Wb)	1.256 637	E - 07
watthour (W-hr)	joule (J)	3.60*	E + 03
W-s	joule (J)	1.0*	E + 00
W/cm ²	watt per meter ² (W/m ²)	1.0*	E + 04
W/in. ²	watt per meter ² (W/m ²)	1.550 003	E + 03
yard	meter (m)	9.144*	E - 01
yd ²	meter ² (m ²)	8.361 274	E - 01
yd ³	meter ³ (m ³)	7.645 549	E - 01
yd ³ /min	meter ³ per second (m ³ /s)	1.274 258	E - 02
year (calendar)	second (s)	3.153 600	E + 07
year (sidereal)	second (s)	3.155 815	E + 07
year (tropical)	second (s)	3.155 693	E + 07

⁽¹²⁾Defined (not measured) value.

Courtesy of Society of Petroleum Engineers

Table A-2
Conversion Factors for the Vara*

Location	Value of Vara in Inches	Conversion Factor, Varas to Meters	
Argentina, Paraguay	34.12	8.666	E-01
Cadiz, Chile, Peru	33.37	8.476	E-01
California,			
except San Francisco	33.3720	8.476 49	E-01
San Francisco	33.0	8.38	E-01
Central America	33.87	8.603	E-01
Colombia	31.5	8.00	E-01
Honduras	33.0	8.38	E-01
Mexico		8.380	E-01
Portugal, Brazil	43.0	1.09	E+00
Spain, Cuba, Venezuela, Philippine Islands	33.38**	8.479	E-01
Texas			
Jan. 26, 1801, to Jan. 27, 1838	32.8748	8.350 20	E-01
Jan. 27, 1838 to June 17, 1919, for surveys of state land made for Land Office	33-1/3	8.466 667	E-01
Jan. 27, 1838 to June 17, 1919, on private surveys (unless changed to 33-1/3 in. by custom arising to dignity of law and overcoming former law)	32.8748	8.350 20	E-01
June 17, 1919, to present	33-1/3	8.466 667	E-01

* McElwee, P. G., *The Texas Vara*, available from commissioner, General Land Office, State of Texas, Austin, Texas (April 30, 1940).

Courtesy of Society of Petroleum Engineers.

Table A-3
"Memory Jogger"—Metric Units

Customary Unit	"BallPark" Metric Values; (Do Not Use As Conversion Factors)
acre	{ 4000 square meters
	{ 0.4 hectare
barrel	0.16 cubic meter
British thermal unit	1000 joules
British thermal unit per pound-mass	{ 2300 joules per kilogram
	{ 2.3 kilojoules per kilogram
calorie	4 joules
centipoise	1 [*] millipascal-second
centistokes	1 [*] square millimeter per second
darcy	1 square micrometer
degree Fahrenheit (temperature difference)	0.5 kelvin
dyne per centimeter	1 [*] millinewton per meter
foot	{ 30 centimeters
	{ 0.3 meter
cubic foot (cu ft)	0.03 cubic meter
cubic foot per pound-mass (ft ³ /lbm)	0.06 cubic meter per kilogram
square foot (sq ft)	0.1 square meter
foot per minute	{ 0.3 meter per minute
	{ 5 millimeters per second
foot-pound-force	1.4 joules
foot-pound-force per minute	0.02 watt
foot-pound-force per second	1.4 watts
horsepower	750 watts (¾ kilowatt)
horsepower, boiler	10 kilowatts
inch	2.5 centimeters
kilowatthour	3.6 [*] megajoules
mile	1.6 kilometers
ounce (avoirdupois)	28 grams
ounce (fluid)	30 cubic centimeters
pound-force	4.5 newtons
pound-force per square inch (pressure, psi)	7 kilopascals
pound-mass	0.5 kilogram
pound-mass per cubic foot	16 kilograms per cubic meter
section	{ 260 hectares
	{ 2.6 million square meters
	{ 2.6 square kilometers
ton, long (2240 pounds-mass)	1000 kilograms
ton, metric (tonne)	1000 [*] kilograms
ton, short	900 kilograms

^{*}Exact equivalents

Courtesy of Society of Petroleum Engineers

Index

- AAD. *See* Average absolute deviation
- Absolute open flow potential (AOF), 545-546, 550
- Acceleration element, 429
- Acoustic log. *See* Sonic log
- Actual brake horsepower, 852
- Actual maximum flow potential (AOF), 589
- Ad valorem* tax, 1018, 1019
- Additives, wettability effects of, 66-67
- Aerial cooler, forced draft, 871
- Aerial heater, 883
- inducted draft, 884
- Afterflow. *See* Wellbore storage
- Airstripping, 952-953
- two film theory, 953
- Alkaline flooding, 323
- description, 333-334
- laboratory design, 343
- limitations and problems, 334
- mechanisms, 334
- A
- n-Alkanes, physical properties, 410
- Alumina as a desiccant, 792
- American National Standards Institute (ANSI), compressor station regulations, 875-876
- American Petroleum Institute (API) compressor station regulations, 876-877
- Offshore Platform regulations, 965, 966
- Recommended Practice for Core-Analysis Procedure, 92-93
- RPIL calculation procedure, 615, 620, 625-631
- American Society for Testing and Materials (ASTM), compressor station regulations, 877-878
- American Society of Mechanical Engineers (ASME), compressor station regulations, 878-879
- Amidine salts, cyclic, as corrosion inhibitors, 910
- Amines, contamination by, 948
- Aminotri as corrosion inhibitor, 910
- Ammonia, anhydrous, as corrosion inhibitor, 936
- Ammonium bisulfite as oxygen scavenger, 908
- Amott method of inferring reservoir wetting, 64
- Annular-slug transition, 450
- Anthony, T. M., 547, 549
- AOF. *See* Absolute open flow potential (AOF)
- Archie equation
- to calculate water saturation, 147-148, 151
- cementation exponent, 46
- modified, 43
- saturation exponent, 54-58, 84
- Areal sweep efficiency, 281-284
- direct and staggered line drives, 281
- polymer treatment and improvement in, 321
- vs. vertical sweep efficiency, 283
- Arnold, K., 747
- Arps Equation, 122, 249
- Artificial lift methods. *See also* Gas lift; Sucker rod pumping
- electrical submersible pumps, 662-664
- oil well jet pumps, 658-662
- Ashford, F. E., 585
- ASTM analysis, 412
- Atmospheric reflux condenser, 779
- Attic oil recovery, 260
- Average absolute deviation, 410, 412
- B
- Bacteria
- in oilfield water, 920
- sulfate-reducing, corrosion from, 921
- used in landfarming, 949

- Bactericides, 921
 laws and regulations, 923
 Bacteristats
 application of, 922
 laws and regulations, 923
 Barge rig, 964
 Barium sulfate
 crystallization, 912
 inhibitors for, 913
 Bateman, R. M., 190
 Bauxite as a proppant, 674
 Beal's correlation, 31
 Beck, R. L., 571
 Beggs empirical correlation, 33-35
 Beggs-Brill method, 522-533
 Bellows pressure, 649
 Benedict-Webb-Rubin equation, 422
 Ben-Naceur, K., 692
 BHC. *See* Borehole compensated
 sonic (BHC) log
 Bioremediation, on-site, 949
 Biot's poroelastic constant, 666
 Black-oil model, 431
 Bleeding, 92
 Bond index, 194-196
 Borehole compensated sonic (BHC)
 log, 172
 Borehole viewers, 202
 Bossler, D. P., 351
 Botset, H. G., 76
 Boundary layer, thickness of, 943-944
 Breakers, encapsulated, 674, 676
 Brigham, W. E., 287
 Brown, K. E., 613, 645
 Bruce, W. A., 70
 Bubble point/dew point
 calculations, 405-406
 Bubble-point pressure (saturation
 pressure), 3
 Buckley, S. E., 76, 242
 Buckley-Leverett equations, 269-272
 for steamflooding, 1010
 for waterflooding, 1007-1008
 Burrows correlation, 31
 Buthod, P., 650
- C**
- Calcium carbonate scale, 915-918
 inhibition of, 918-920
 Calcium sulfate scale, 914-915
 Calhoun, J. C., Jr., 83
 Camacho, V. R. G., 564
 Campbell's correlation, 757-758
 Capacity of reservoir rock, 38
 Capillary pressure, 68-72
 to determine fluid saturation, 70
 to indicate pore size distribution,
 70
 oil-water, 83
 reduced function, 70
 water saturation and, 69-70
 wettability effects, 83
 Carbon dioxide
 corrosion, 892-894
 flooding, 324, 327
 description, 331
 laboratory design, 343
 mechanisms, 331
 limitations and problems, 331
 Carbonate reservoirs, acid
 fracturing in, 691
 Carbon-oxygen log, 312-313, 314, 316
 Carbon-oxygen ratio, 190, 191, 192
 Carothers, J. E., 43
 Carpenter, C. B., 50
 Carr correlation, 31
 Carter equation, 686
 Cash flow
 capital investment, 1019-1021
 discount rate, 1022-1024
 income tax considerations,
 1020-1021
 ownership interests, 1017
 present value factor, 1021-1024
 product prices, 1014, 1016
 production costs, 1017
 production schedule, 1014
 projection of product prices, 1016
 Casing
 for beam pumping unit, 619
 -cement formation bonding, 197-199
 Casing-operated valve
 mechanics, 647, 648
 in unloading process, 653, 656-658
 Castillo, J. L., 669
 Cation exchange in radium
 removal, 961
 Caudle, B. H., 546, 547, 549, 557
 Caustic flooding. *See* Alkaline
 flooding
 Cavitation
 avoiding, 661
 zone in jet pumps, 659
 CBE. *See* Counterbalance effect

- CDIS. *See* Continuous downhole injection system
- CDM. *See* Continuum damage mechanics
- Cement bond log
interpretation, 197-199
presentations, 196-197
theory, 193-196
- Cement, microannulus in, 200-201
- Cementation factor, 39
- Central flooding, well placement, 264-265
- Centrifugal compressor, 847-848
head vs. volume flow relationship, 863
polytropic exponent, 863-864
power, 864-865
vs. reciprocating compressor, 865-866
volume flowrate, 864
- Centrifugal force in separation process, 722
- Channeling, 200-201, 284
- Chase, R. W., 547, 549
- Chemical flooding
alkaline, 322-323
alkaline/surfactant/polymer, 323
polymer-augmented
waterflooding, 320-322
surfactant, 322-323
- Chew correlation, 32
- Choke
adjustable, 537
positive, 537
reasons for installing, 537
subsurface, 554
surface, 554
- Choke performance
gas wells, 554-555
subsonic vs. sonic flow, 554-555
two-phase
Ashford's correlations, 585-586
Gilbert's correlation, 571
Poetmann-Beck's correlation, 571, 585
- Chromatographic analysis, 412
- Claridge, E. L., 283
- Class II injection well
contamination by, 961-962
location of, 962
produced water contamination, 956
UIC criteria and standards, 962-963
- UIC permitting process, 963
- Clinedinst equation, 838
- Clothier, A. T., 935
- CNL. *See* Compensated neutron log (CNL)
- Coates, G. R., 46, 57
- Combination of forward combustion and waterflooding (COFCAW), 334
- Combination reservoir
material balance, 233-234
reserve estimation, 994-995
- Compaction correction factor, 159
- Compensated neutron log (CNL), 163
- Composting of contaminants, 949
- Compressibility
gas, 20-23
of multiple-fluid-containing reservoir rock, 52-53
of natural gas, equation for, 32
oil, 23-27
water, 27
- Compressibility factor
depletion study, 386
direct calculation of Z factors, 368-371
using principle of corresponding states, 365-368
- Compressive-wave attenuation-rate, 194
- Compressor. *See also* Centrifugal compressor; Reciprocating compressor
axial-flow, 847-848
calculations, Mollier charts, 857-863
multistage systems, 852
storage/withdrawal operation, 868-869
- Compressor station
block and mat design, 866
codes and standards, 872-882
combined resonant frequency, 866
compressor types, 847-848
gas cooling equipment, 871, 884
gas piping system, 868-871
pressure drops in, 871
machinery foundations, 866-868
production, 847
spring constant, 868
storage, 847
transmission, 847
- Compton scattering, 161

- Condensate, 225
- Conductive solids, 46
- Conformance factor, 306-307
- Connally correlation, 32
- Connate water, 225
- Contact angle
 - receding vs. advancing, 63-64
 - of reservoir rock, 61, 63-68
- Contamination
 - diffusion coefficients for
 - petroleum-related, 954
 - hydrocarbon, 939-948
 - nonhydrocarbon sources, 948
 - radioactive, 957-961
 - site remediation, 949-954
- Continuous downhole injection
 - system, 902, 904
- Continuum damage mechanics, 687
- Conventional pumping unit
 - crank balanced, 595
 - maximum practical pumping
 - speed, 622-623
- Cooling towers, 884-889
 - performance characteristics, 887-889
- Core analysis
 - to estimate residual oil, 307-309
 - laboratory core flooding, 308-309
 - measurements, 308
 - fluid saturation, 91-93
 - grain density and core
 - description, 93
 - permeability, 91
 - porosity, 90-91
 - procedures, 87-88
 - results of, 92-107
 - routine tests, 86-87
 - specialized, 87, 89, 108
- Cores
 - handling
 - conventional cores, 307-308
 - pressure cores, 308
 - methods of preservation, 89
 - preparation, 90
 - preserved, 67-68, 88-89, 307
 - restored-state, 68, 89, 307
 - rubber sleeve, 304
 - storage of, 89
- Corey, A. T., 79
- Coring, 88
 - to determine residual oil, 304
 - flushing during, 304-305
 - pressure, 88, 90
 - rubber sleeve, 88
- Corrected pressure. *See* Fugacity of component *i*
- Corresponding states principle (CSP), 365-368
- Corrosion. *See also* Pitting
 - carbon dioxide, 892-894
 - hydrogen sulfide, 891-892
 - microbiological
 - inhibition of, 921-922
 - in waterflooding operations, 920-921
 - pipeline
 - crude oil and liquid-product, 924-930
 - natural gas, 930-935
 - prevention methods, 889
 - in production operations, design
 - recommendations, 923
 - in storage tanks
 - crude oil, 936
 - product tank, 936-938
 - recommended procedure, 938-939
 - vapor space, 935-936
 - in sucker rod pumps, 600, 610
 - from sulfate-reducing bacteria, 921
 - in waterflooding operations, 906-923
- Corrosion inhibitors, 889-890
 - application methods, 923, 926-930
 - comparing techniques, 906, 907
 - cost vs. effectiveness, 933
 - equipment units, 926-927
 - point of injection, 927
 - proof of treatment, 933
 - system analysis, 932
 - batch treatment, 894-896, 926
 - extended-period, 896
 - with inhibitor emulsion, 896
 - periodic, 896
 - tubing displacement, 895-896
 - with weighted inhibitor, 896
 - calculating volume needed, 896
 - carrier water, 895
 - chemical, 924, 926
 - continuous treatment, 893, 926
 - closed-annulus injection, 897
 - concentric completion, 900
 - determining concentrations, 896, 905
 - dual completion, 897, 899

- in gas-lift wells, 897, 902, 903
 - open-annulus injection, 897, 898
 - Y-block completion, 901
 - control criteria, 929-930
 - in crude oil and product tankers
 - flotation technique, 937-938
 - fogging technique, 938
 - oil-soluble, 936-937
 - filming amines, 893, 894, 910
 - formation squeeze treating, 903, 905
 - oil-soluble, 890, 926
 - oxygen scavengers, 908-909
 - in pipelines
 - crude oil and liquid-product, 926-930
 - natural gas, 931-935
 - premixing or dilution, 927-928
 - protective coatings, 928-929
 - in sour environments, 890, 891, 892
 - water-soluble, 890, 910, 926
 - problems with, 895
 - Coryell, F., 935
 - Counterbalance effect, 636, 641
 - Cox, R., 567
 - Craig, F. F., Jr., 82, 269, 277, 287
 - waterflooding performance prediction method, 293
 - Crawford, P. B., 281
 - Craze, R. C., 242
 - Crossflow index, 289
 - Crude oil. *See also* Primary oil recovery
 - defined, 249, 987
 - economic value, 987
 - PVT properties, 17, 33-35
 - surface tension, 60
 - effect of dissolved gases on, 58
 - treating systems, 733-735
 - equipment, 736-739
 - heat input requirement, 739-754
 - viscosity of, 7-10, 11, 12
 - undersaturated, 35
 - Crude oil pipelines
 - corrosion in, 924-925
 - control methods, 925-926
 - protective coatings, 928-929
 - CSP. *See* Corresponding states principle (CSP)
 - Cullender, M. H., 548, 550, 553
 - Curtis, S., 613, 614
 - Curve separation, 151
 - Cyclic steaming, 1005
- D**
- Dalton's law, 944
 - Damage ratio (DR), 701
 - Darcy equation, 643, 664-665, 672, 946
 - for linear displacement, 36-37
 - for radial flow, 37-38
 - for turbulent flow, 535-536
 - DCR. *See* Discount rate (DCR)
 - Deaeration, 925
 - Dean Stark method, 308
 - Deans, H. A., 310
 - Decline
 - effective, 1000
 - exponential, 998, 999
 - harmonic, 998, 999-1000
 - hyperbolic, 998, 999
 - nominal, 1000
 - Decline curve analysis, 244-246
 - classification of, 247
 - cumulative production
 - vs. exponential production rate, 1001
 - vs. gas-oil ratio, 1001-1002
 - vs. water-oil ratio, 1001
 - in developing production schedule, 1014
 - exponential decline, 246-247
 - harmonic decline, 248
 - hyperbolic decline, 247-248
 - production decline curves, 258
 - production type-curve, 248-249, 1003
 - rate-time plot, 997-1000
 - Dehydration liquids
 - contamination by, 948
 - to control corrosion, 925
 - recycling, 948
 - Dehydrators
 - design, 780-792
 - height of glycol contactor, 786-787
 - molecular sieve, 792
 - mass transfer zone, 794, 796-797
 - saturation zone, 794-796
 - solid desiccant
 - allowable superficial velocity, 797
 - design, 792-797
 - regeneration calculations, 797-798
 - triethylene glycol, 780-792
 - bubble cap trays in, 787
 - gas capacity, 788
 - tray-type, 787-788, 790

- Dense nonaqueous phase liquids (DNAPL), 941
- Density log, 160-161
interpretation, 162
long-spacing vs. short-spacing detector, 161-162
spine and ribs plot, 161-162
theory, 161-162
- Desbrandes, R., 169
- Desiccants
liquid, 778
recycling, 948
solid, 778, 792
waste liquid contamination, 948
- Desorption isotherm, 946-947
- DeSouza, A. O., 287
- Deviated well
fracturing, 692-696
nonvanishing shear stress component, 694
- Dew point
calculations, 401, 402-403
pressure determination, 384
sensor, 759, 761
- Dielectric constant, 312-313, 315
- Dielectric measurement tools, 170-179
interpretation, 175-179
theory, 172-174
types of, 171
- Differential condensation. *See* Differential liberation
- Differential liberation, 17-18, 374, 377-379, 397
laboratory measurements, 381
material balance equations, 394
in reservoir conditions, 379
- Differential vaporization. *See* Differential liberation
- Dimetallic phosphates as scale inhibitors, 918-919
- Dipmeter, 179
- Discount rate (DCR), 1022-1024
in calculating rate of return, 1026
cost of capital, 1023
market, 1023-1024
- Displacement sweep efficiency, 279
- Distillate, 225
- Distillation-extraction method, 92
- DNAPL. *See* Dense nonaqueous phase liquids (DNAPL)
- DNLL. *See* Dual neutron lifetime log (DNLL)
- Dorfman, M. H., 57-58
- Dougherty, E. L., 1026
- Drag coefficient, 706, 708
for turbulent flow, 709
- Drawdown pressure test, 180
- Drill stem test
interpretation of results, 108-115
tool assembly, 108
- Drilling mud
bacterial degradation, 949
oil-based, bioremediation methods, 951
resistivity tools affected by, 118-120
- Drilling rig
mobile, 964
offshore operations, 964
- Drillship, 964
- Drinking water
radon in, 957-958
regulations for radionuclides in, 958
underground sources, 962
- DST. *See* Drill stem test
- Dual neutron lifetime log (DNLL), 182, 183
- Dumanoir, J. L., 46, 57
- Duns-Ros method, 488-504
- Dupre's equation for wetting tension, 63
- Dykstra, H., 1008
- Dykstra-Parsons coefficient, 284-289, 293
- Dynagraph card, 638-639
- Dynamometer, 638-639
standing valve check, 641
traveling valve check, 640-641

E

- Earlougher, R. C., Jr., 299
- Early-time region (ETR), 220-222
- Economic limit of production, 1000-1001, 1019
- Economic risk, 1028
- Economics of petroleum. *See* Petroleum economics
- Economides, M. J., 671, 692, 700, 701
- Elasticity relation, 684
- Electrical conductivity
of reservoir rock, 38
salt concentration estimated from, 952

- Electrical potential logs, 202
 - Electrical resistivity, residual oil saturation and, 312-313
 - Electrical submersible pump
 - environmental variables affecting performance, 662
 - motor controller, 662-663
 - pump stages required, 662
 - recommended operating range, 664
 - seal section, 662
 - surface and subsurface components, 662
 - Electromagnetic inspection logs, 201-202
 - Electromagnetic propagation tool (EPT), 171
 - interpretation, 175-179
 - uses, 172
 - Emulsions
 - caused by scale inhibitors, 913
 - formed during corrosion treatments, 895
 - fracturing fluids, 674
 - treating methods, 733, 736
 - Energy conservation, 426
 - Engineering, reservoir, 3
 - Enhanced oil recovery (EOR), 260, 1005-1006. *See also* Chemical flooding
 - chemical methods, criteria for, 337-338
 - definition, 319-320
 - depth requirements, 340, 341
 - economic factors, 327
 - gas injection, 323-325, 1006
 - criteria for, 336-337
 - heat injection, 1008-1011
 - laboratory design
 - carbon dioxide flooding, 343
 - polymer testing, 342-343
 - preliminary tests, 342
 - surfactant and alkali testing, 343
 - thermal recovery, 343-344
 - permeability ranges, 342
 - technical guides, 327-329
 - graphical representation, 339-341
 - thermal methods, 326-327, 338-339
 - viscosity ranges, 339, 340
 - water injection, 1007-1008
 - Enriched gas drive, 329
 - Enthalpy-entropy plot, 857-858
 - Environmental considerations
 - in offshore production, 969-970
 - in production operations, 939-963
 - Class II injection wells, 961-962
 - hydrocarbon contamination, 939-947
 - produced water, 954-961
 - site remediation, 948-954
 - EOR. *See* Enhanced oil recovery (EOR)
 - EPT. *See* Electromagnetic propagation tool (EPT)
 - Ergun equation, 792-793
 - ESP. *See* Electrical submersible pump
 - Ethylenediaminetetraacetic acid (EDTA), as scale inhibitor, 912, 920
 - ETR. *See* Early-time region (ETR)
 - Excavation effect, 163
 - Expansion vessel, 705
 - Exponential decline, 244, 246-247
- F**
- Fair market value, 1021
 - Fassihi, M. R., 283, 286
 - Fatt, I., 50
 - Fetkovich, M. J., 1003
 - IPR equation, 213, 564, 567, 644
 - type-curve, 249
 - FFI. *See* Free fluid index (FFI)
 - Fick's law, 943
 - Fifadara gas deviation factor
 - estimation program, 33
 - Filtercake
 - hydraulic resistance, 671-673
 - viscoelastic relaxation, 672-673
 - Filtration, 924, 925
 - in waterflooding operations, 908
 - Fireflooding. *See* In-situ combustion
 - Flare system, offshore production operations, 968
 - Flash equation/convergence algorithm, 406
 - Flash liberation *See* Flash vaporization
 - Flash tank, 704-705
 - Flash vaporization, 17-18, 374, 376, 377-379, 388, 390
 - calculations, 403-408
 - laboratory measurements, 381
 - Floating rods, 620
 - Flow behind casing, 203

- Flow regimes. *See also* Gas flow
- annular
 - liquid entrainment fraction, 471, 472
 - liquid holdup, 471, 473, 474-477, 478
 - pressure gradient, 473
 - annular-slug transition, 449
 - bubbly
 - liquid holdup, 481
 - pressure gradient, 483
 - downcomers, 447-449
 - horizontal, 433
 - late-transient region, 214, 215
 - limitations on, 484-488
 - region of occurrence, 491
 - risers and wells
 - dimensionless parameters, 437, 447
 - map, 447, 448
 - selection of, 447
 - semisteady-state region, 214, 215, 216
 - slightly inclined pipes
 - dimensionless parameters, 436-437
 - map, 437, 438-446
 - selection of, 437
 - slug
 - drift-flux parameters, 480
 - liquid film thickness, 481, 482
 - liquid holdup, 478, 479
 - optional correction, 481
 - pressure gradient, 478, 480
 - slug velocity, 478
 - slug-bubbly transition, 449
 - steady-state, 216
 - steps in determination of, 435
 - stratified
 - dimensionless parameters, 465-469
 - friction factor ratio, 449, 456-463
 - liquid holdup, 449, 452-455, 470, 478
 - pressure gradients, 464, 470
 - transient region, 214, 215
 - vertical, 433
- Flowline performance
- multiphase fluids, 586-594
 - oil, 541-544
- Flowmeter
- accuracy, rangeability, and repeatability, 800
 - continuous, 207
 - fullbore-spinner, 206-207
 - packer, 207
- Flue gas flooding, 324, 330
- Fluid compressibility. *See* Compressibility
- Fluid flow. *See also* Flow regimes;
- Oil flow performance
 - categories of, 426
 - formulas, 426, 428
 - friction loss, 426
 - two-phase, engineering analysis, 429, 431
- Fluid pound, 639
- in sucker rod pumps, 611-612
- Fluid saturation
- core analysis, 91
 - distillation-extraction method, 92
 - solvent extraction method, 93
 - sources of error, 93
 - vacuum distillation method, 92-93
 - oil recovery and, 79-80
- Fluid velocity, radioactive tracers, 207
- Fluid-flow equation, 684
- Fluid-rock properties. *See also* Reservoir rock
- capacity, 38
 - compressibility, 49-52
 - electrical conductivity, 38
 - formation resistivity factor, 39-48
 - linear flow, 36-37
 - of multiple-fluid containing rocks, 52-86
 - permeability, 36
 - pore volume, 35-36
 - porosity, 35
 - radial flow, 37-38
 - resistivity, 38-39
 - transmissibility, 38
 - wettability effects, 79-86
- Flushing
- chlorinated oil, 313-314
 - during coring, 304-305
- Foam
- as diverting agent, 699
 - fracturing fluids, 674
- Foaming
- in corrosion treatments, 895
 - in separators, prevention of, 722
- Formation evaluation. *See also* Logs
- in cased holes, 181-192
 - coring and core analysis, 86-108

- drill stem tests, 108–115
 - Formation resistivity factor
 - effect of clay on, 46, 48
 - of limestone, 43
 - permeability property, 48
 - porosity and, 39, 41, 44, 47
 - of reservoir rock, 39–48
 - of sandstone, 46
 - Formation volume factor, 4, 12–20
 - correlations for estimating, 19–20
 - flash vs. differential liberation processes, 17–18
 - gas, 13–15, 34
 - oil, 15–20, 28, 34
 - changes with pressure for, 16–17
 - single-phase, 33
 - two-phase, 17
 - water, 20, 21
 - Forty-degree rule, 737
 - Fouling, heater, 741, 743
 - Fracturing, 1003
 - acid, 665, 691–692
 - breakdown pressure, 667–668
 - closure pressure, 668–669
 - flowback period, 669
 - design evaluation, 688–690
 - desired lengths, 694
 - of deviated vs. horizontal wells, 692–694
 - dimensionless conductivity, 682
 - hydraulic, 665, 686
 - pressure decline analysis, 669–673
 - propagation modeling, 686–688
 - CDM-PKN model, 687–688
 - fracture toughness concept, 686–687
 - material balance, 684–686
 - stress intensity factor, 686–687
 - width equations, 683–684
 - propagation simulator, 677
 - propped, 676–683
 - KGD model, 677, 679
 - optimizing, 676–677
 - PKN model, 677, 678
 - stress distribution, 665, 666
 - vertical horizontal, 666–667
 - Fracturing fluids
 - breakers, 674
 - emulsions, 674
 - foam, 674
 - oil-base, 674
 - properties of, 673–674
 - water-base, 673–674
 - Free fluid index (FFI), 168, 169, 314–315
 - Frick, T. P., 700
 - Friction factor ratio for stratified flow regime, 449, 456–463
 - Friction loss, 426, 429
 - Froehlich equation, 946
 - Fugacity of component *i*, 418–419
- ## G
- Gamma ray log
 - interpretation, 157–158
 - theory, 157
 - Gamma spectroscopy tools (GST), 190–191
 - Gardner, F. T., 935
 - Gardner, J.S., 159
 - Gas
 - compressibility, 20–23
 - condensate, 372
 - dry, 372
 - formation volume factor, 13–15
 - nonassociated, 251
 - recovery, volumetric calculations, 241
 - solubility of water in, temperature effects, 924–925
 - superficial velocities, 435–436
 - viscosity of, correlations for, 31
 - wet, 372
 - Gas cap reservoir, 225, 251, 374
 - estimating gas-in-place, 989
 - oil saturation, 243
 - reserve estimation, 992
 - Gas contract, 754
 - Gas coolers, 871
 - sizing, 884
 - Gas dehydration, 778–780
 - dehydrator design, 780–792
 - regenerator performance, 782–784, 797–798
 - required reboiler heat load, 784–785
 - solid desiccant, 792
 - dehydrator design, 792–797
 - Gas deviation factor, 232
 - estimating, 33
 - Gas, dissolved, 251
 - formation volume factor, 34
 - in reservoir fluids, 3–4
 - viscosity and gravity effects, 4

- Gas flow
 complex systems, 841-847
 electronic metering units, 835
 equations for steady state, 837-841
 gathering systems, 835-837
 measurement
 accuracy of, 799-800
 calibration, 800
 differential pressure method, 800
 maintenance of metering systems, 800
 orifice, 800, 802-834
 saturation pressure, 379
 Gas flow performance, 544
 choke, 554-555
 flowline, 556-561
 inflow, 545-551
 tubing, 551-554
 Gas Froude number, 436-437
 Gas hydrate formation
 inhibition of, 774-778
 pressure and temperature of, 763-774
 Gas in solutions curve, adjustment to separator conditions, 399
 Gas injection, 1006-1007
 carbon dioxide flooding, 324-325
 criteria for, 336-337
 hydrocarbon miscible flooding, 323-325
 nitrogen and flue gas flooding, 324
 Gas lift
 continuous vs. intermittent methods, 642-643
 corrosion treatment, 897, 902, 903
 gradient curves, 645-647
 inflow performance, 643-645
 unloading the well, 650-654
 utilization of, 642
 valve mechanics, 647-650
 for small pipes, 650
 Gas pound, 640
 in sucker rod pumps, 612
 Gas rate, calculation of, 382
 Gas reservoir reserve estimation
 material balance approach, 231-233
 production performance approach in nonassociated, 997-1004
 Gas-condensate reservoir, 225
 Gas/liquid ratio
 flowing gradients and, 570
 saturation pressure effects, 387
 Gas-oil ratio (GOR)
 producing, 262
 in production projections, 1014
 Geffen, T. M., 293
 Gels as desiccants, 792
 Gentry, R. W., 248-249
 Geologic risk, 1028
 Geophysical well logging
 accuracy of methods, 316-317
 carbon-oxygen, 314
 dielectric constant, 315
 electrical resistivity, 312-313
 nuclear magnetism, 314-315
 pulsed-neutron capture, 313-314
 reservoir volume sampled, 315-316
 Gibbs free energy, 418, 419
 Gibbs phase rule, 378
 Gibbs, S. G., 639
 Gilbert, W. E., 568
 flowline performance correlation, 544, 571, 587, 590
 Glycol
 contamination, 948
 as a desiccant, 778
 calculating minimum concentration, 781-782
 in hydrate formation, 774-775
 injection system, regeneration in, 775, 782
 physical and chemical properties, 774-776
 required circulation rate, 784
 Glycol-gas contactor, 779
 Gomaa, Ezzat E., 1010
 Gradiomanometer, 203-206
 Grain density, core analysis, 93
 Gravity drainage reservoir, 260
 oil saturation, 243
 Gregory, A. R., 42
 Gringarten, A. C., 224
 Ground loops, 134
 GST. *See* Gamma spectroscopy tools (GST)
 Guerrero, E. T., 77
- H**
- Hagedorn-Brown method, 513-522
 Hall, H. N., 50, 298-299
 Hall's correlation, 52
 Hall-Yarborough equation, 368, 826

- Harmonic decline, 244, 246, 248
 Hassler, G. L., 76
 Hawkins' formulation for vertical wells, 700
 Hazen-Williams C factor, 929-930
 HCPV. *See* Hydrocarbon pore volume
 Hearn, C. L., 298
 Heat exchangers, 871
 Heat injection
 advantages and disadvantages, 1011
 cost factors, 1009
 limitations of, 1009
 Heater
 direct fired, 735
 indirect fired, 735
 coil area, 743
 heat-transfer equation in sizing, 740-743
 Henry's constant, 947-948
 Hexane
 analysis categories, 414-415
 physical properties, 408-413
 state-of-the-art equation, 412-413
 Higgins, R. V., 77
 Higgins-Leighton streamtube model, 293
 High pressure gas drive, 329
 Hilchie, D. W., 120-121
 Hilchie equation, 162
 Hill, A. D., 553
 Hill, H. J., 43
 Hollo gas deviation factor
 estimation program, 33
 Horizontal wells
 drilled in direction of minimum vs. maximum stress, 695
 fracturing, 692-696
 matrix stimulation in, 700
 Horner plot, 217-218
 HPAM. *See* Partially hydrolyzed polyacrylamides
 Hudson, E. J., 258
 Huff and puff. *See* Steamflooding
 Humble relation, 39, 42, 46
 Hunt, E. R., 159
 Hurst, W., 241
 Hydrazine as oxygen scavenger, 909
 Hydrocarbon miscible flooding, 260, 327
 description, 329
 limitations, 329-330
 mechanisms, 329
 Hydrocarbon pore volume, 378
 Hydrocarbons
 classification, 372-374
 contamination
 air, 943-945
 in offshore operations, 969-970
 preventive measures, 939-940
 soil, 940-941, 946
 water, 941-943
 evaporation rate of spilled, 943
 GPM content, 385, 389
 physical properties, 365-371
 light, 408-413
 in produced water, 955-957
 solubility of water in, temperature effects, 924-925
 surface tension, 58, 59
 Hydrocarbon-to-fertilizer ratio, 951
 Hydrogen embrittlement, 892
 Hydrogen sulfide corrosion, 891-892
 Hydrostatic pressure, 429
 Hydroxyethylidene-1,
 1-diphosphonic acid (HEDP),
 as scale inhibitor, 918-919
 Hydroxypropyl guar (HPG), 673
 Hyperbolic decline, 244, 246, 247-248
- I
- Ikoku, C. U., 557
 Imbibition curve, 70
 Imidazoline-aliphatic acids as corrosion inhibitors, 910
 Immiscible gas injection, 260
 Inflow performance relationship (IPR), 210-213
 four-point test, 545
 gas, 545-551, 643-645
 flowing vs. static bottomhole pressure, 550-551
 isochronal prediction method, 548
 low-permeability well tests, 548
 predicting future, 548-551
 numerical integration technique, 547
 oil, 536-537
 predicting future, 536-537
 combined Fetkovich-Vogel method, 567
 Fetkovich method, 593-594
 Standing's method, 566-567
 unified method, 567-568

- IPR (*continued*)
 pseudopressure function, 547
 for single-phase liquid flow, 534
 single-point test, 546
 for sucker rod pumping, 617
 two-phase
 constant J equation, 562-564
 Fetkovich method, 864
 modified Standing's method, 564-565
 Vogel's method, 561-564
- Injection wells. *See also* Class II
 injection well; Waterflooding
 gas, 260-262, 1004
 volumetric calculations, 261-262
 heat, 1008-1011
 logging, 203
 placement of, 263-264
 pattern flooding, 265-268
 peripheral or central flood, 264-265
 water, 1007-1008
- Injectivity
 into depletion drive reservoirs, 295-298
 for different flood patterns, 294-298
 index, 293-294
 monitoring, 298-299
 for unit mobility ratio, 295
 values of, 293-294
- In-situ combustion, 326
 criteria for, 338-339
 description, 334-335
 limitations and problems, 335
 mechanisms, 335
- Instrument Society of America (ISA), compressor station regulations, 878-879
- Interfacial tension
 additives lowering, 91-92
 effect of dissolved gas and pressure on, 60, 62
 of reservoir rock, 58-61
 temperature effects, 58, 60, 61, 62
- Intermediate Strength Proppant, 676
- Interstate Oil Compact Commission, on waterflooding, 269
- Invasion sweep efficiency. *See* Vertical sweep efficiency
- Investment analysis
 net present value, 1025
 payout, 1025
 profit/investment, 1025
 property value, 1025
 rate of return, 1026
- IPR. *See* Inflow performance relationship (IPR)
- Iron oxide deposition in waterflooding operations, 920-921
- Iron sulfide corrosion, 892, 921
- Isopach map, 255
- Isothermal retrograde condensation, 372-373
- Isothermal rock compressibility, 49-52
- Isovol map, 255
- ISP. *See* Intermediate Strength Proppant
- J**
- Jennings, S. Y., Jr., 83, 85
 Johnson, C. E., Jr., 286
 Johnson, E. F., 76
 Johnson, J. P., 1008
 Jones flow correlation, 537
 Jones, S. C., 77
- K**
- Kachanov law of damage growth, 687
- Katz, D. L., 551, 768
- Kelkar, B. G., 567
- Kemp, L. F., 686
- Kern, L. R., 684
- Kerosene retention capacity in unsaturated soils, 942
- KGD model. *See* Khristianovich, Geertsma, and de Klerk model
- Khristianovich, Geertsma, and de Klerk model, 677, 679, 681, 686
- Killins, C. R., 83
- Klinkenberg effect, 73-74
- Klinkenberg, L. J., 72
- Knockout vessel, 702
- Kobayashi correlation, 31
- Kruk, K. F., 691
- L**
- Laminar flow coefficient, 536
- Landfarming
 microcosm turbidity method, 950
 on-site bioremediation, 949
 slurry phase bioreactors, 951

- Landspreading, 952-953
 Langenheim, R. H., 1009
 Larmor proton frequency (LFRE), 167, 168
 Laterologs, 134-135
 Late-time region (LTR), 220-222
 LDT. *See* Lithodensity tool (LDT)
 Lease fuel, 1018
 Leeman, E. H., 76
 Leverett J function, 70
 Leverett, M. C., 76
 Light nonaqueous phase liquids (LNAPL), 941, 947
 Limestone, formation factor, 43
 Line drip, 704
 Linear elasticity theory, 683
 Linear flow for reservoir rock, 36-37
 Liquid holdup
 for annular flow regime, 471, 473, 474-477, 478
 for bubbly flow regime, 481
 calculations, 435-436
 drift-flux model, 481
 pressure gradient for low and high, 470, 478
 for slug flow regime, 478, 479
 for stratified flow regimes, 449, 452-455, 470, 478
 Liquefied petroleum gas (LPG), 329
 Lithodensity tool (LDT), 166
 Lithology, log estimation, 117-118
 LNAPL. *See* Light nonaqueous phase liquids (LNAPL)
 Log-flush technique, 314
 Log-inject-log procedure, 313, 315, 316, 318
 Log-log type-curve, 249
 Logs
 cased hole, 116
 completion tools, 192-202
 gamma spectroscopy tools, 190-192
 production, 202-207
 pulsed neutron, 181-190
 free gas in place, 209
 influences on
 mud relationships, 118-120
 temperature relationships, 120-122
 initial gas in place, 209
 initial oil in place, 208-209
 mud cake effects, 146, 149
 openhole, 116
 density, 160-161
 dielectric measurement tools, 170-179
 gamma ray, 157-158
 microresistivity tools, 151-157
 multiple-porosity, 164-167
 neutron, 162-163
 nuclear magnetic resonance, 167-170
 resistivity tools, 127-151
 sonic, 158-160
 special, 179-181
 spontaneous potential, 122-127
 parameters estimated from, 116-118
 Lorenz coefficient, 284
 LPG. *See* Liquefied petroleum gas (LPG)
 LTR. *See* Late-time region (LTR)
 Lufkin Mark II pumping unit, 595
- M**
- McKetta and Wehe chart, 755-757
 McKinley, R. M., 224
 McLennan, J. D., 694
 Manometer, 203-206
 Martin, J. C., 52
 Martinelli parameter, 436
 Marx, J. W., 1009
 Material balance equations, 228
 to estimate residual oil saturation, 317
 for gas reservoirs, 231-233
 generalized, 234, 236-237
 graphical form, 232
 Muskat's method, 993-994
 nomenclature, 230
 in oil or combination reservoirs, 233-234
 in reserve estimation, 257
 primary production, 992-997
 for solution-gas drive reservoirs with gas liberation, 238
 with liquid expansion, 237-238
 Turner's method, 996
 for waterflooding recovery, 301
 Matrix stimulation, 665, 696-697
 fluid volume requirements, 698
 in horizontal wells, 700
 matrix acidizing
 design, 698
 diversion in, 698-699
 evaluation of, 701-702, 703

- Maximum allowable superficial velocity for separators, 714
 Mayerhofer, M. J., 671
 Mechanical draft tower
 coil shed, 886
 forced draft, 884
 induced draft, 886
 Mercury porosimeter, 90
 Methanol tracer, 310
 Meyer equation, 956
 Micellar/polymer flooding. *See*
 Surfactant/polymer flooding
 Micro spherically focused log
 (MSFL), 157
 Microannulus in cement, 200-201
 Microemulsion flooding. *See*
 Surfactant/polymer flooding
 Microlaterolog, 157
 Microresistivity tools
 disadvantage of, 155
 electrode arrangements, 154
 to identify permeable zones, 156
 interpretation, 157
 microinverse reading, 156-157
 micronormal reading, 157
 proximity log, 155-156
 theory, 151, 155-157
 Middle-time region (MTR), 220-222
 Milburn, J. D., 43
 Miller, M. A., 553
 Miller-Dyes-Hutchinson (MDH) plot,
 217
 Minimum miscibility pressure,
 324-325
 Minimum polished rod load
 (MPRL), 632, 636
 Mishra, S., 546, 547, 549, 557
 MMP. *See* Minimum miscibility
 pressure
 Mobility
 defined, 276
 oil, 277
 water, 277
 Mobility ratio, 276-277, 1004
 crossflow and, 289, 290
 displacement and sweep
 efficiency and, 320-321
 Moisture analyzers, 798
 Mole sieve towers, 798
 Molecular sieves as desiccants, 792
 Moment, height of structure and,
 964-965
 Moore, E. J., 84, 85
 Morgan, W. B., 85
 Morrow, N. R., 65
 Morse, R. A., 293
 MPRL. *See* Minimum polished rod
 load (MPRL)
 MSFL. *See* Micro spherically focused
 log (MSFL)
 MTR. *See* Middle-time region (MTR)
 Multifingered caliper logs, 201
 Multiphase flow, parameters,
 432-435
 Multiple-porosity log, 164-167
 correction for gas effect, 165
 Mungan, N., 84, 85
 Muskat, M., 20
 material balance method, 240,
 257-258, 993-994
- N
- Nalco, gas pipeline inhibitors,
 934-935
 National Electrical Manufacturers
 Association (NEMA), electric
 motor classes, 613
 National Fire Protection Association
 (NFPA), compressor station
 regulations, 879-882
 National Petroleum Council (NPC),
 Enhanced Recovery report, 327
 Natural draft tower
 atmospheric spray, 886
 hyperbolic, 886
 Natural gamma spectroscopy, 191
 Natural gas
 compressibility of, equation for, 32
 defined, 251, 989-990
 dew point, 762
 economic value, 990
 physical properties, 365
 pressure temperature correlations,
 754-757
 produced water from, 956
 reserves, 252
 reservoirs, mechanisms and
 recovery, 225
 water content, 754-759
 measurement of, 759-762
 sour gases, 759
 Natural gas liquid (NGL), 251
 economic value, 990
 recovery plants, molecular sieve
 dehydrators for, 792
 sales, 1016

- Natural gas pipelines
 corrosion in, 930-931
 inhibition of, 931-935
 types of, 931
 wet vs. dehydrated, 931
- Naturally occurring radioactive material (NORM) in produced water, 957-961
 prevention of, 961
 in scale form, 961
- Naumann, V. O., 76
- Near-critical oil, 374
- Net pay volume, 256
- Net present value (NPV)
 calculations, 695
 in fracture design, 676, 682-683
- Neuse, S. H., 258
- Neutron log
 interpretation, 163
 theory, 162-163
- Newman, G. H., 51-52
- Newton-Raphson iterative technique, 369
- NGL. *See* Natural gas liquid (NGL)
- Nielsen, R. F., 83
- Nierode, D. E., 691
- Nind, T. E. W., 555
- Nitriiotriacetic acid (NTA) as scale inhibitor, 912
- Nitrogen flooding, 324, 330
- Nitrogen, gas deviation factor, 649
- NMR. *See* Nuclear magnetic resonance (NMR)
- Nolte, K. G., 671, 680
 decline analysis, 668, 669
- Nordgren, R. P., 686
- NORM, 957-961
- NPE, 327
- NPV, 676, 682-683, 695
- Nuclear magnetic resonance (NMR), 167-170
 log modes, 168-169
 uses of, 169-170
- Nuclear magnetism log
 accuracy of, 317
 to estimate residual oil saturation, 312-315, 318
- O**
- Offshore production operations
 design and operation, 967
 environmental considerations, 966
 pollution prevention, 969-970
 flare system, 968
 geographical considerations, 966
 platform design, 965-966
 regulatory agencies, 970-971
 relief system, 968
 safety shut-down system, 968
 service safety system, 970
 technological history, 964
 transportation, 969
 utility systems, 967
 ventilation, 969
- Oil. *See also* Crude oil
 compressibility, 23-27
 displaced during coring, factors affecting, 91-92
 dissolved gas in, 3-4
 viscosity and gravity effects, 4
 formation volume factor, 15-20, 28, 34
 heavy, 374
 physical properties, 365
 relative volume curve, 398, 400
 reservoirs, material balance, 233-234
 saturated, 3
 saturation changes during core recovery, 92
 superficial velocities, 435-436
 undersaturated, 3
 viscosity of dead, correlation for, 31-32, 33
- Oil flow performance
 choke, 537, 541
 flowline, 541-544
 for incompressible fluids, 537
 inflow, 534-536
 possibility of changes in, 538
 tubing
 performance, 537
 size and head pressure effects, 539
- Oil in place (OIP), 992
- Oil recovery
 residual, from waterflooding, 301-318
 water-wet vs. oil-wet cores, 79-80
- Oil saturation
 for gas cap drive reservoirs, 243
 for gravity drainage reservoirs, 243
- Oil zone, 225
- Oil-shrinkage curve, 399
- Oil/water ratio, inflow performance and, 643

- OIP. *See* Oil in place (OIP)
 OOIP. *See* Original oil in place (OOIP)
 Oosterhout, J. C. D., 937
 Organometallic crosslinkers, 674
 Orifice meter, 800, 802-806
 flange tap
 expansion factors, 812-814, 822-823
 orifice factors, 809-811
 Reynolds number, 816-818
 gas flow calculations, 806-834
 expansion factor, 815
 flowing temperature factor, 815
 gage location factor, 829, 830
 gas relative density factor, 815
 manometer factor, 826-828
 orifice flow constant, 806
 pressure base factor, 815
 Reynolds number, 815, 816-818
 supercompressibility factor, 826
 temperature base factor, 815
 thermal expansion factor, 828-829
 meter tube measurements, 803, 805-806, 807
 pipe taps
 expansion factors, 824-825
 orifice factors, 819-821
 pressure tap locations, 803, 804
 uncertainty limits and field problems, 834-835
 Original oil in place (OOIP), 992, 993
 estimating, 990-991
 risk analysis, 1030
 Orkiszewski method, 504-513
 bubble flow, 506
 mist flow, 508
 slug flow, 506-507
 transition flow, 508
 Outer Continental Shelf Lands Act, 970
 Overbalance pressure, oil displaced by, 91, 305
 Ownership, working vs. royalty interests, 1017
 Oxygen
 corrosion, 924, 931
 scavengers, 908-909, 924
- P**
- Pacaloni, G., 703
 Panhandle equations, 556-557, 838, 840-841
 Parsons, R. L., 1008
 Partially hydrolyzed polyacrylamides (HPAM), 321, 322
 Patnode, H. W., 55
 Pattern flooding, well placement, 265-268
 Pattern sweep efficiency. *See* Areal sweep efficiency
 Pay thickness, log estimation, 117
 Peak polished road load (PPRL), 631, 636
 Peffer, J. W., 553
 Peng-Robinson equation, 370, 419, 420, 422
 Penn State steady-state method, 76, 81
 Perez-Rosales, C., 46
 Performance. *See also* Gas flow performance; Oil flow performance
 posttreatment, 688-690
 risk, 1028
 waterflooding
 monitoring, 293-300
 prediction, 293
 Peripheral flooding, well placement, 264
 Perkins, Kern, and Nordgren model, 669, 677, 678, 681, 684
 short-cut, 686
 Perkins, T. K., 684
 Permeability
 absolute, 36
 air, connate water saturation and, 74, 75
 core analysis, 91
 crossflow and, 290
 effective
 vs. absolute, 76
 overburden effects, 74
 log estimation, 118
 micrologs, 156
 relative
 dynamic vs. static determination methods, 76-77
 empirical equations, 79
 fluid property effects, 79
 gas-oil, 78
 oil-water, 77-78

- three-phase, 79
 - wettability and, 80-83
- of reservoir rock, 36, 48
 - effective, 72-76
 - relative, 76-79
- reservoir stimulation and, 665
- resistivity logs, 151
- stratification
 - crossflow and, 289
 - quantitative extent of, 284-291
 - vertical, 286
 - waterflooding and, 284
- Permeability anisotropy, 700
 - vertical-to-horizontal, 692, 694
- Petroleum economics. *See also* Cash flow
 - controlled by baseline oil price, 1012
 - cost/benefit factors, 1013
 - function of petroleum engineer in, 1013
 - market for petroleum, 1011-1012
 - inflationary effects, 1012
 - price impact, 1012
- Petroleum engineer, economic function, 1013
- Petroleum products, classification of, 989-990
- Petroleum reservoir, definitions, 225
- Petrolite Corporation, gas pipeline inhibitors, 933-934
- Phase behavior
 - multicomponent vs. pure component systems, 370-371
 - in production tubing, 431
 - reservoir conditions, 374-380
- Phasor Induction SFL, 134
- Phosphates as scale inhibitors, 919-920
- Phosphonates as scale inhibitors, 913-914, 915, 920-921
- Photoelectric absorption effect, 161
- Pipelines. *See* Crude oil pipelines; Natural gas pipelines
- Pirson, S. J., 85
- Pits, production water, construction guidelines, 955-956
- Pitting, 892, 894
- PKN. *See* Perkins, Kern, and Nordgren model
- Platform. *See* Production platform, offshore
- Poetman, F. H., 571
- Poisson's ratio, in stress calculation, 666
- Polished rod horsepower (PRHP), 634, 636, 637-638
- Polyacrylates as scale inhibitors, 915
- Polymer flooding
 - criteria for, 337
 - description, 332-333
 - injection rates, 338
 - laboratory design, 342-343
 - limitations and problems, 333
 - mechanisms, 333
- Polymers
 - crosslinked or gelled, 322
 - in fracturing fluid, 673
 - in-situ polymerization, 322
 - polymer-augmented waterflooding, 320-322
- Pore volume of reservoir rock, 35-36
- Porosity
 - absolute vs. effective, 35
 - core analysis, 90-91
 - formation resistivity factor and, 47
 - irreducible water saturation and, 118
 - log estimations, 116
 - of reservoir rock, 35
 - formation factor and, 39, 41, 44
 - sonic travel time and, 159
- Porter, C. R., 43
- Positive separation, 157
- Positive-displacement chemical pumps, 927
- PPRL. *See* Peak polished road load (PPRL)
- PR equation, 408
- Present value of future income, 1021-1024
- Pressure
 - buildup test, 216
 - falloff test, 216
- Pressure core barrel, 307
- Pressure coring, 317-318
- Pressure decline analysis, 669-673
 - Castillo's time function, 669
 - dimensionless resistance, 672
 - to estimate fluid efficiency, 671
 - Kelvin model, 672
 - Nolte's techniques, 669
 - Perkins and Kern model, 669
 - Voight model, 672

- Pressure drawdown
 - defined, 643
 - reducing, 381
 - test, 216
- Pressure gradient
 - due to acceleration, 429
 - for annular flow regime, 473
 - for bubbly flow regime, 483
 - in complete systems, 429
 - correction for acceleration
 - effects, 483-484
 - due to elevation, 429
 - frictional and gravitational, 470
 - liquid gas/oil ratio and, 645
 - for multiphase flow, 645
 - in production systems, 427
 - for slug flow regime, 478, 480
 - for stratified flow regimes, 464, 470
 - in tubing, 430
 - two-phase flow, semiempirical
 - calculation methods, 488-533
 - due to viscous forces, 429
- Pressure maintenance, 260
- Pressure transient tests
 - concepts, 219-222
 - definitions, 214-219
 - equations, 222-223
 - interference, 216-217
 - multiple-rate, 216
 - nomenclature, 223
 - type-curves, 223-224
- Pressure traverse, 429
- Pressure-volume-temperature (PVT)
 - analysis, 17, 992
- Pressurization/repressurization
 - cycle, 668
- PRHP. *See* Polished rod horsepower (PRHP)
- Price/cost escalator, 989
- Primary oil recovery, 225-226. *See also* Secondary recovery
 - empirical estimates, 227-228
 - volumetric calculations, 242-243
 - material balance equations, 228-241
 - reserve estimation
 - material balance, 992-997
 - volumetric methods, 990-992
 - in solution gas drive reservoirs, 228, 242-243
 - predicting, 238-240
 - statistical analysis, 226
 - in water drive reservoirs, 243
 - predicting, 240-241
- Prime mover factor (PMF), 614
- Prime mover for pumping units
 - electric motors, 613
 - horsepower, 637-638
 - internal combustion engine, 612, 613
 - selecting size of, 613-614
- Produced water
 - disposal of, 955-956
 - hydrocarbons in, 955
 - from natural gas sites, 956
 - NORMS in, 957-961
 - solubility, 955-957
 - total dissolved solid content, 954-955
- Product prices
 - actual, 1014
 - gas sales, 1014
 - posted, 1014, 1016
 - projection of, 1016
- Production decline. *See* Decline curve analysis
- Production logs
 - flow behind casing, 203
 - manometers and
 - gradiomanometers, 203-206
 - temperature, 203
- Production operations. *See also* Surface production systems
 - corrosion and scaling, 889-939
 - cost of, 1017-1018
 - environmental impacts, 939-963
 - equipment, radioactive
 - contamination, 957-961
 - offshore, 964-971
 - possible system pressure losses, 427
 - site remediation, 948-954
- Production performance analysis
 - data evaluation, 1003-1004
 - economic limit, 1000-1001
 - for nonassociated gas reservoirs, 997-1004
- Production platform, offshore, 964
 - design, 965
 - environmental considerations, 966
 - geographical considerations, 966
 - multiple use of, 965
 - operation and design, 967
 - safety factors, 965-966
- Production stimulation, 1005
 - secondary and enhanced oil

- recovery, 1005-1008
 - Productivity index
 - estimating from subsurface data, 570
 - inflow performance relationship, 210-213
 - J, 563, 589
 - pressure drawdown vs. flow rate, 210
 - in pump selection, 663
 - straight line, 643
 - vertical vs. horizontal well, 692
 - for well performance, 534-535
 - Proppants, 674, 676
 - continuous addition, 680
 - stairstep addition, 680-681
 - Prouvost, L. P., 701
 - Pseudoscale, 911, 913
 - Pulse test, 217
 - Pulsed neutron log
 - applications, 187, 190
 - to estimate residual oil saturation, 312-314
 - interpretation, 182, 184-187
 - presentation, 182
 - theory, 181-182
 - Pump displacement (PD), 615-616
 - stroke length and plunger diameter and, 629
 - Pump-in/flowback test, 668-669
 - PVT. *See* Pressure-volume-temperature (PVT) analysis
- Q**
- Quimby, W. S., 936, 937
- R**
- Radial diffusivity equation, 241
 - Radial flow of reservoir rock, 37-38
 - Radioactive contamination of
 - production equipment, 957-961
 - Radioactive tracers, 207-208
 - contamination by, 959, 961
 - corrections for tracer loss, 311
 - to estimate residual oil, 309-311, 318
 - reservoir heterogeneity factor, 311
 - single-well technique
 - accuracy, 311
 - field application, 311
 - interpretation, 311
 - procedure, 310
 - theory, 309-310
 - Radium
 - in produced water, 959
 - removal, 961
 - Radon
 - detection of, 959
 - in drinking water, 957
 - on wellsite, 958-959
 - Raghavan, R., 564
 - Rahme, H. D., 284
 - Ramey, H. J., Jr., 27, 52, 53, 224
 - Ransome, R. C., 57
 - Rawlins, E. L., 545
 - Raymer, L. L., 159
 - Reciprocating compressor, 847
 - adiabatic power requirement, 851-852
 - calculations, 848-857
 - vs. centrifugal compressor, 865-866
 - compression cycle, 848-849
 - compressor cylinder capacity, 850-851
 - displacement of, 849-850
 - intercooling effects, 853, 855, 858
 - volumetric efficiency, 850
 - Recoverable oil (RO), solution gas vs. water drive reservoirs, 227
 - Recovery. *See also* Enhanced oil recovery (EOR); Primary oil recovery; Secondary recovery improved, 251, 252
 - tertiary, 260, 301
 - economic factors, 317
 - method comparison, 317-318
 - waterflood, 277-279
 - Recovery estimation
 - material balance, waterflooding, 292-293, 301
 - well test analyses
 - applicability, 304
 - production data, 302-303
 - transient tests, 303-304
 - Recovery factor, 991
 - Recycling of contaminants, 948
 - Regeneration
 - in glycol injection systems, 775, 782
 - performance of regenerators, 782-784, 797-798
 - pressure swing adsorption, 798

- Regulation
 - of air and water, 873
 - bacteristats and bactericides, 923
 - of compressor stations, 875-882
 - of offshore production
 - operations, 965, 966, 970-971
 - pipelines, 872-873
 - radionuclides, 958
- Regulatory tax, 1018, 1019
- Relative-oil-volume curve in
 - separator conditions, 388, 398
- Relief system in offshore
 - operations, 968
- Remediation
 - airstripping, 953
 - landfarming, 949-951
 - landspreading, 951-953
 - physical treatment methods, 948-949
- Repeat formation tester, 180
- Reserve estimation
 - economic factors, 251-252
 - gas in place, 256
 - material balance, 257
 - in combination reservoirs, 994-995
 - in gas cap reservoirs, 994
 - general equation, 993-994
 - methods of determining, 254
 - analogy, 255
 - volumetric, 255-256
 - model studies, 257-258
 - nonassociated gas reservoirs, 997-1004
 - oil in place, 256
 - performance of similar
 - properties, 1002
 - primary production
 - material balance method, 992-997
 - volumetric methods, 990-992
 - production decline curves, 258
 - production performance
 - approach, 997-1004
 - production stimulation methods, 1005-1011
 - quality of, 258-259
 - uncertainty factor, 252
- Reserves
 - classification of, 252-254, 986-987
 - definitions, 249-252
 - developed, 254
 - economic factors, 987, 1014
 - nonproducing, 254
 - producing, 254
 - proved, 252-253, 985
 - vs. resources, 985
 - status categories, 254
 - undeveloped, 254
 - unproved
 - possible, 253-254
 - probable, 253, 987
- Reservoir
 - defined, 251
 - engineering, 3
- Reservoir fluids
 - depletion studies, 385, 390-393, 395
 - constant volume, 382
 - retrograde condensation, 394
 - equilibrium cell determinations, 384-385
 - equilibrium flash calculations, 385-394, 395, 396
 - fluid viscosities
 - gas, 7
 - oil, 7-10, 11, 12
 - water, 10, 12, 13, 14
 - oil and gas, 7
 - physical properties, 4
 - estimating with programmable calculators and computers, 27-35
 - pressure-volume relations, 384, 385
 - sample collection, 380-394
 - subsurface vs. surface, 381
 - shrinkage of, 92
 - water, 7
 - wellstream compositions, 384-385, 388
- Reservoir rock
 - compressibility of, 49-52
 - multiple-fluid-containing
 - capillary pressure, 68-72
 - effective permeability, 72-76
 - relative permeability, 76-79
 - resistivity index, 53-58
 - surface and interfacial tensions, 58-61
 - total reservoir compressibility, 52-53
 - wettability and contact angle, 61, 63-68
- Reservoir stimulation, 664-665
 - fracturing, 665-696
- Reservoir volume factor. *See* Formation volume factor

- Residual oil saturation
 coring and core testing, 304-309
 estimation methods
 existing wells, 318
 new wells, 319
 geophysical well logging
 techniques, 312-317
 material balance equations, 301
 tracer tests, 309-311
 well test analyses, 302-303
 applicability, 304
 transient tests, 303-304
- Resistivity
 mud, temperature and, 120-121
 of reservoir rock, 38-39
 containing multiple fluids, 53-58
 variables affecting, 46
 water saturation effects, 54-58
 of saline solutions, 40
 saturation effects, 83, 84-86
- Resistivity tools
 affected by drilling mud, 118-120
 correction charts, 135-146,
 147-150
 electrode arrangement, 132-133
 focused, 134-135
 to identify permeable zones, 151
 induction, 134
 interpretation, 146-151
 nonfocused, 130, 134
 phasor induction, 134, 146
 purpose of, 127-128
 service company nomenclature,
 131-132
 types of, 128-129
- Resources
 discovered vs. undiscovered, 987
 vs. reserves, 987
- Reynolds number
 for drag coefficient, 708
 for orifice meters, 815, 816-818
- Rice, R. R., 76
- Risk analysis, 1027-1028
 defining range of values, 1028
 defining risk, 1028
 evaluation method
 expected value theory, 1030
 Monte Carlo analysis, 1029-
 1030
 selecting, 1029
 sensitivity analysis, 1029
 measurement of risk, 1028-1029
 RO, 227
- Roads, hydrocarbon/soil mixtures
 as base for, 940
- Robinson correlation, 33
- Rod pump, downhole components, 596
- Rose, W. R., 70
- Rozelle, W. O., 77
- Rust, C. F., 85
- S**
- Safety factors in offshore
 production, 965-966
 measurement of risk
 service safety system, 970
 shut-down system, 968
- Sand
 accumulation in sucker rod
 pumps, 612
 as a proppant, 676
- Sandstone
 acidizing, 696, 698
 formation resistivity factor, 46
- SAR, 952
- Saturation. *See also* Fluid saturation;
 Oil saturation; Water saturation
 capillary pressure and, 70
 changes during core recovery, 92
 effect of gas/liquid ratio on, 387
 effect on resistivity factors, 83,
 84-86
 irreducible, 70
 gas, 78-79
 water, 77, 91
 pressure, 3
 residual oil, 70, 91
 resistivity and, 54-58
 waterflood residual oil, 78
- Scale inhibitors, 924
 emulsification tendency, 913
 squeeze treatment, 914-915
 in waterflooding operations,
 912-920
 concentrations, 913
 disadvantages of, 913
- Scaling
 radioactive, 961
 in sucker rod pumps, 612
 supersaturation and, 911-912
 in waterflooding operations,
 910-920
 causes of, 911
 regions of occurrence, 910

- SCC. *See* Stress corrosion cracking
 Schellhardt, M. A., 545
 Schilthuis, R. J., material balance equation, 233, 238-239, 257
 Schlumberger, Ltd., 184, 202
 electromagnetic propagation tool, 171
 induction tool, 134
 permeability estimation chart, 118, 120
 Schmalz, J. P., 284
 Scrubber, 702
 vertical inlet, 778-779, 789
 Secondary recovery, 1005-1008
 definitions, 259-260
 gas injection, 260-262
 injection well placement, 263-268
 pressure maintenance, 260
 saturation distribution and, 272
 water injection, 262
 well spacing, 262-263
 Securities and Exchange Commission (SEC), definition of reserves, 987
 Semilog plots, 248-249
 Semisubmersible, 964
 Separation
 gas-oil-water, 722-731
 momentum for bulk, 706
 two-stage, 731-733
 Separator gas
 equilibrium cell determinations, 384-385
 hydrocarbon analysis, 383
 Separator liquid
 equilibrium cell determinations, 384-385
 hydrocarbon analysis, 383
 Separator sampling, 381
 Separators, 702
 collection efficiency, as function of pressure drop, 720-721
 design and construction
 horizontal, 709, 711, 716-720
 spherical, 711
 vertical, 709, 710-716
 filter, 704
 gas capacity constraint, 716, 717-718, 719
 impingement type-mist-extraction elements, 720, 722
 with knitted wire mesh extractors, 721
 liquid capacity constraint, 718, 719-720
 liquid-liquid, 704
 low-pressure flash, 732, 733
 metal used in, 721
 retention time, 724
 stem, 722
 three-phase, 704, 724-731
 two-phase, retention time, 714-715, 718, 720
 vane type mist extractor, 720
 vessel carryover problems, 722
 vessel internals, 720-722
 Severance tax, 1018
 Sherwood-Holloway equation, 954, 955
 Showalter, E., 613
 Shrinkage curve, 388
 Shut-in period, 381
 Sidewell neutron tools (CNL), 163
 Signal-to-noise ratio (STNR), 168
 Silicon chip hygrometer, 761, 762
 Silicon-calcium ratio, 190, 192
 Simpson's rule, 256
 Simulators
 black oil, 431
 classification of, 258
 Skin effect, 212, 218-219, 221-222, 223
 damage-induced, 696
 evolution of, 703
 due to flow impairment around wellbore, 696
 reservoir stimulation and, 665
 total, 696
 Slider, H. C., 79, 237, 248, 1003
 Slime-forming microorganisms, 920-921
 Slug catcher, 704
 Slug-bubbly transition, 451
 Slurry phase bioreactor, 951
 Smith, C. R., 269
 Smith, R. V., 550, 553
 SNP. *See* Sidewell neutron tools (CNL)
 Soave equation, 369-370, 408, 419
 Society of Petroleum Engineers (SPE), definition of reserves, 987
 Sodium activity ratio (SAR), in landspreading operations, 952
 Sodium sulfite as oxygen scavenger, 908
 Soil contamination by hydrocarbons, 940-941

- conductivity of liquid hydrocarbons, 946
- saturation level and type of, 946-947
- Solution gas drive reservoir, 226
 - material balance
 - with gas liberation, 238
 - with liquid expansion, 237-238
 - oil recovery, 227, 228
 - predicting, 238-240
 - reserve estimation, 994
- Solution gas-oil ratio, 4, 19-20
- Solvent extraction method, 93
- Sonic flow, 554-555
 - upstream pressure effect, 555
- Sonic log
 - interpretation, 158-160
 - theory, 158
 - travel-time to porosity transform, 159-160
- SP log. *See* Spontaneous Potential log
- Spangler, M. B., 56
- Spencer, G. B., 50
- Spills
 - bacterial degraders, 949
 - containment of, 939-940
 - evaporation from pore space, 945
 - offshore, 969-970
 - results of, onsite and laboratory study, 945-947
 - treated as exempt waste, 940
- Sponge coring, 307, 317-318
- Spontaneous Potential log
 - electrochemical component, 124-125
 - electrokinetic component, 123-124
 - interpretation, 125-127
 - liquid-junction potential, 124-125
 - membrane potential, 125
 - theory, 123-125
 - uses, 122-123, 126
- Spurt loss, 305
- SRK equation. *See* Soave equation
- SSC. *See* Sulfide stress cracking
- Standing, M. B., 4
 - correlation for estimating formation volume factor, 19, 27, 31-33
 - IPR curve modification, 212-213, 564-567
- Stanley, M.E., 937
- Starling modification, 421-422
- Steamflooding, 326-327
 - Buckley-Leverett approach, 1010
 - criteria for, 338-339
 - description, 335
 - estimating steam drive performance, 1009-1010
 - limitations and problems, 336
 - mechanisms, 336
- Steward, M., 747
- Stewart, F. M., 77
- Stiles recovery method, 293, 1008
- Stimulation. *See* Matrix stimulation; Reservoir stimulation
- STNR. *See* Signal-to-noise ratio (STNR)
- Stokes law, 726
- Storage effect, 221-222
- Storage tanks
 - classification, 705
 - corrosion in
 - field results, 936
 - inhibition program, 936-939
 - vapor space, 935
- Streamtube model, 289, 293
- Stress
 - absolute, 666
 - effective, 666
 - effective vertical, 666
 - horizontal, 666
 - effective minimum, 666
 - maximum, 666, 695
 - minimum, 668, 695
 - intensity factor, 686-687
 - principal direction, 667
 - in sucker rods, 600, 602, 605-607
- Stress corrosion cracking, 891
- Stripping towers, design of, 953-954
- Strontium sulfate scale, control of, 913-914
- Subsonic flow, 554-555
- Subsurface geological contour map, 255
- Sucker rod pumping
 - beam pumping unit
 - casing size, 619
 - expected fluid production, 615-619
 - performance computation procedures, 914-915
 - setting depth, 619
 - tubing anchor, 619
 - design data, 619-625

- Sucker rod pumping (*continued*)
 API RP1L calculations, 625-631
 peak torque, 633, 635, 637
 plunger diameter, 620
 prime mover horsepower,
 637-638
 pumping speed, 620
 rod stress, 636
 string selection, 623-625
 stroke length, 621, 637
 structural capacity, 637
 testing, 631, 634-638
 fluid pound condition, 611-612,
 639
 gas pound, 612, 640
 primer movers
 electric-motor types, 613
 internal combustion engines, 613
 selecting size of, 613-614
 pumping units
 dynamometer tests, 638-641
 operating characteristics,
 630-631
 operation, 594-595
 system components, 594
 types and specifications, 595-598
 well pumping off, 612, 640
 pumps
 API designations, 607-609
 obtaining optimum
 performance, 610
 problems and solutions, 610-612
 rod, 610
 tubing, 609-610
 sand accumulation, 612
 scale formation, 612
 sucker rods
 allowable stress, 600, 602,
 605-607
 API selection, 600
 determining percent of rod
 size, 625
 dimensions and tolerances, 601
 reinforced plastic, 600, 604
 steel, 605
 types, sizes, and grades, 599-600
 Sulfide stress cracking, 891
 in sucker rods, 600
 Sulfur dioxide as oxygen scavenger,
 908
 Supersaturation, 911-912
 Surface production systems
 crude oil treating systems, 733-754
 gas-oil-water separation, 722-731
 gravity setting, 706, 708-709
 momentum, 706
 phase separation, 705-709
 purpose of, 702
 separating vessels
 design and construction,
 709-720
 nomenclature, 702-705
 storage classification, 705
 two-stage separation, 731-733
 vessel internals, 720-722
 Surface tension
 of reservoir rock, 58-61
 between water and natural gas,
 57, 59
 Surfactant flooding, laboratory
 design, 343
 Surfactant/polymer flooding, 323
 criteria for, 337
 description, 332
 mechanisms, 332
 problems and limitations, 332
 Surge tank, 779
 Sweeny, S. A., 83, 85
- T
- Taber, J. J., 323
 Tankship corrosion
 flotation inhibitors, 937-938
 inhibition program, 938-939
 oil-soluble inhibitors, 936-937
 vapor-space, 937
 Tapered rods, 624, 625
 Tarner material balance method,
 239, 257-258, 994
 Taxes, production, 1018-1019
 TBP, 413
 TDH, 663
 TDS, 954-955
 TEG, 778
 Temperature log, 203, 205, 206
 Terzaghi's criterion, for fracture
 initiation pressure, 667
 Texas-Louisiana Gulf Coast logs, 43
 Theis equation, 962
 Timmerman, E. H., 239
 Timur, A., 43
 chart for permeability estimation,
 118, 119
 Tornado Charts, 141-146

Total dissolved solids (TDS), 954-955
 Total dynamic head (TDH), 663
 T_{po} method, 175-177
 TPR. *See* Tubing performance relationship
 Transition zone, 70, 72
 Transmissibility of reservoir rock, 38
 Treater
 emulsion, 736
 gunbarrel, 737-738
 horizontal, 738
 sizing, 746
 oil-water interface control, 738
 vertical, 736
 Triethylene glycol
 as a desiccant, 778
 minimum lean concentration, 778
 Trube's correlation, 22, 23, 25, 26
 True boiling point, partial vs.
 complete analysis, 413
 Tubing anchor for beam pumping unit, 619
 Tubing performance relationship (TPR)
 gas, 551-554
 oil, 537, 542
 two-phase, 568-571
 flowing pressure gradients, 568, 572-584
 multiphase flow equation, 568
 predicting flowing life, 570-571
 vertical pressure gradients, 570
 water content, 570
 wellhead pressure, 570
 Tubing pump, downhole
 components, 596
 Tubing-operated valve
 mechanics, 647, 649
 in well unloading process, 653, 654-656
 Turbidimeter, 950
 Turbulent factor, 536
 Type-curve analysis, 303
 in pressure transient tests, 223-224
 production, 248-249, 1003

U

U.S. Army Corps of Engineers,
 regulation of offshore operations, 970
 U.S. Bureau of Mines wettability test, 65

U.S. Coast Guard, regulation of offshore operations, 970
 U.S. Department of Energy,
 definition of reserves, 987
 U.S. Department of Transportation (DOT), pipeline regulations, 872-873
 U.S. Environmental Protection Agency (EPA), clean air and water regulations, 873
 U.S. Geological Survey, Minerals Division, regulation of offshore operations, 970
 UHF sondes, 171
 Underground Injection Control Program (UIC), 961
 criteria and standards, 962-963
 permitting process, 963
 Underground source of drinking water (USDW), 962

V

Vacuum distillation method, 92-93
 Valuation of oil and gas properties
 profitability of, 1024-1027
 purpose of, 1024
 risk analysis, 1027-1030
 Valve spread, 6481508
 Van der Knapp, W., 50
 Van Everdingen, A. F., 241
 Vapor-liquid equilibrium
 calculations, 394, 400-408
 bubble point/dew point, 405-406
 vs. calculated phase compositions, 406
 dew point, 401, 402-403
 by equations of state, 413, 416, 418-426
 to determine physical properties, 431
 objectives of, 422
 solutions for cubic, 422-426
 flash, 403-408
 Vasquez empirical correlation, 33-35
 Velocity
 fluid, 207
 in separation process, 722
 Vertical sweep efficiency, 284
 vs. areal sweep efficiency, 283
 VHF sondes, 171

- Viscosity
 of crude oil, 7-10, 11, 12
 effect of pressure on, 7
 temperature and, 7
 undersaturated, 35
 of dead oil, 7
 correlation for, 31-32, 33
 of fracturing fluids, 673
 of gas, correlations for, 31
 of water, 10, 12, 13, 14
 correlation for, 29-30
 salinity and, 12
 Viscous fingering, 275-276, 330
 Vogel, J. V., 210-213
 inflow performance equation,
 212, 561, 567, 587, 617, 644
 Volatile oil. *See* Near-critical oil
 Volumetric efficiency of sucker rod
 pumps, 617
 Volumetric reservoir, 225
 Volumetric sweep efficiency, 279-280
 estimates of, 289, 291, 292
- W**
- Water. *See also* Produced water
 compressibility, 27
 content of natural gas, 754-762
 formation volume factor, 20, 21
 superficial velocities, 435-436
 surface tension, 58
 viscosity of, 10, 12, 13, 14
 correlation for, 29-30
 Water drive reservoir
 recoverable oil, 227
 predicting primary recovery,
 240-241
 reserve estimation, 990
 Water saturation
 calculating, 147-148, 151
 irreducible, 77, 91
 porosity and, 118
 log estimations, 116-117
 Water table, hydrocarbon
 contamination of, 941-943
 Waterflooding, 260, 1007-1008
 areal sweep efficiency, 281-284
 corrosion problems, 906-923
 inhibition of, 923-924
 microbiological, 920-923
 water quality factor, 907-908
 crossflow effects, 289
 displacement mechanisms,
 269-275
 displacement sweep efficiency, 279
 frontal advance method,
 1007-1008
 inhibitors used in, 909-910
 injectivity and injectivity index,
 293-299
 Johnson graphical approach, 1008
 mobility ratio, 276-277
 monitoring performance, 293-299
 parameters, 300
 performance prediction methods,
 293
 polymer-augmented, 320-322,
 332-333
 production curves, 299-300
 recovery efficiency, 277-279
 residual oil recovery
 coring and core testing, 304-309
 corrections for shrinkage and
 bleeding, 305-307
 geophysical well logging,
 312-317
 material balance, 292-293, 301
 method comparison, 317-318
 tracer tests, 309-311
 well test analyses, 302-304
 scaling and scale inhibitors,
 910-920
 Stiles method, 1008
 viscous fingering, 275-276
 volumetric sweep efficiency,
 279-280, 289, 291, 292
 Water-holdup meter, 206
 Water-oil ratio, 286
 corrosion and, 889
 vs. oil recovery, 286-287
 Welge, H. J., 76
 graphical technique, 272-275, 277
 Well coring. *See* Coring
 Wellbore storage, 219, 222
 Wellhead pressure, 429
 Wellhead tax, 1018-1019
 Wettability
 changes during handling and
 storage, 67
 effect of mud additives on, 66-67
 effect on fluid-rock properties
 capillary pressure, 83
 oil recovery and fluid
 saturation, 79-80
 relative permeability, 80-83

- resistivity factors and saturation exponents, 83, 84-86
 - fractional, 65
 - preventing changes in, 89
 - quantitative indication, 64-65
 - of reservoir rock, 61
 - distribution by lithology, 65
 - role in crude oil recovery, 63-68
 - residual oil determination and, 309
 - speckled, 66
 - spotted or Dalmatian, 65
 - Weymouth equation, 838, 839-840, 844, 846, 847
 - Whiteley, B. W., 650
 - Willman, B. T., 1010
 - Windfall profit tax, 1018, 1019
 - WOR. *See* Water-oil ratio
 - Wormholes, 698
 - Wyckoff, R. D., 76
 - Wyllie, M. R. J., 42, 55, 56, 79
 - porosity equation, 159, 160, 162
- X
- Xanthan gum, 321
- Y
- Young's equation for wetting tension, 63

PETROLEUM ENGINEERING

from
 Gulf
Publishing
Company

Classics

STANDARD HANDBOOK OF PETROLEUM AND NATURAL GAS ENGINEERING Volume 1

William C. Lyons, Editor

Volume 1 presents the mathematics and general engineering and science of petroleum engineering. This first volume examines the auxiliary equipment and provides complete coverage of all aspects of drilling and well completion.

1996. 1,382 pages, figures, index, 6" x 9" jacketed hardcover.
ISBN 0-88415-642-7 #5642 \$195



ENVIRONMENTAL CONTROL IN PETROLEUM ENGINEERING

John C. Reis

This book assembles a tremendous amount of practical information to show how to plan and manage production activities to minimize and even eliminate some environmental problems without severely disrupting operations. It focuses on ways to treat drilling and production wastes to reduce their toxicity and/or volume before their ultimate disposal.

1996. 400 pages, tables, figures, appendices, index, 6" x 9" hardcover.
ISBN 0-88415-273-1 #5273 \$65

SURFACE PRODUCTION OPERATIONS Volumes 1 and 2

Ken Arnold and Maurice Stewart, Jr.

These two volumes are thorough, practical references for specifying, designing, operating, and troubleshooting surface production equipment.

Volume 1: Design of Oil-Handling Systems and Facilities

414 pages, 250 photos and figures, tables, 6" x 9" hardcover, index.
ISBN 0-87201-173-9 #1173 \$79

Volume 2: Design of Gas-Handling Systems and Facilities

522 pages, photos, figures, tables, 6" x 9" hardcover, index.
ISBN 0-87201-175-5 #1175 \$79

Order directly from:



Gulf Publishing Company
P.O. Box 2608 • Dept. IE
Houston, Texas 77252-2608
713-520-4444 • FAX: 713-525-4647
E-Mail: ezorder@gulfpub.com

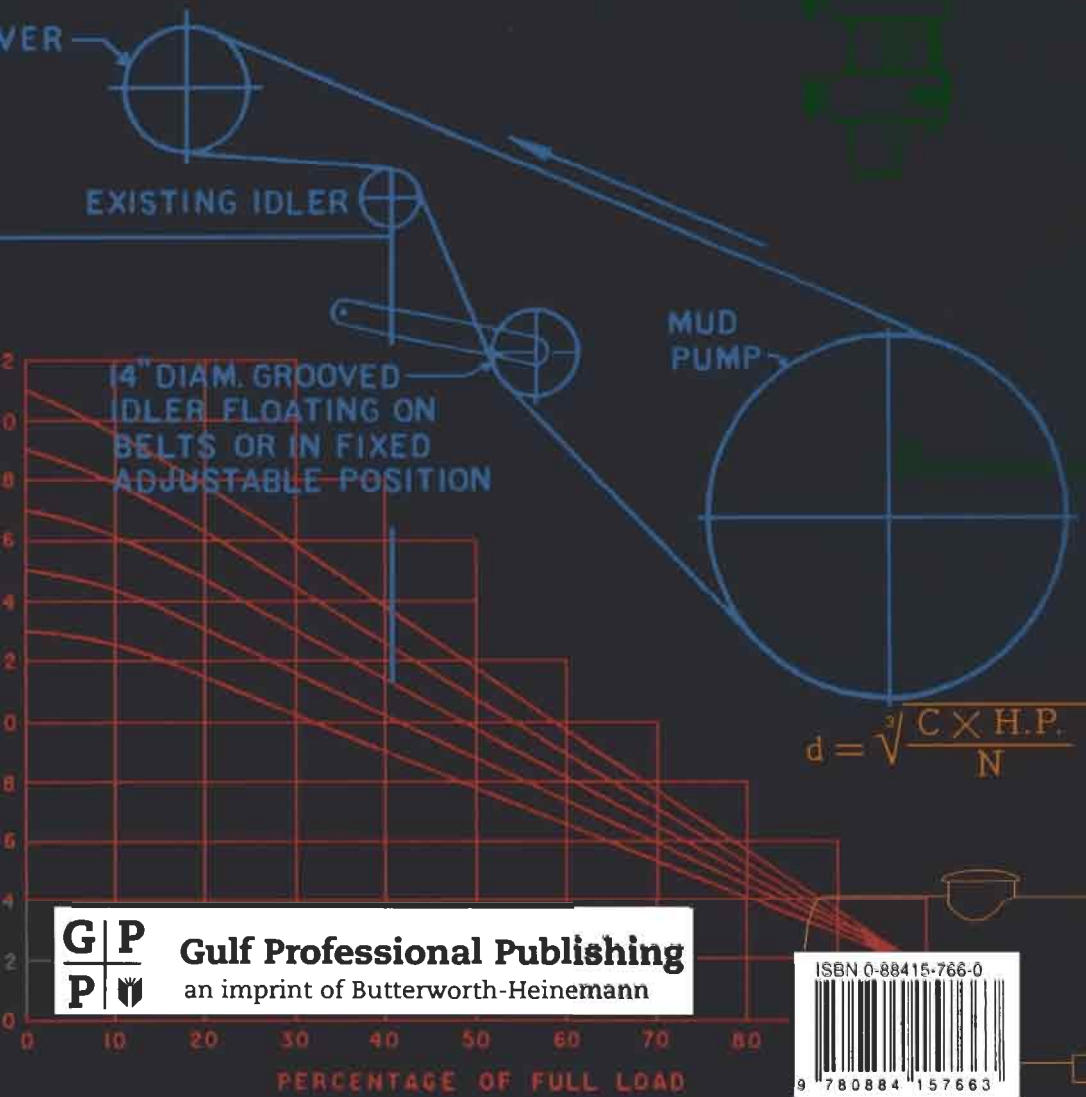
VISIT YOUR FAVORITE BOOKSTORE

Send payment plus \$9.95 (\$11.55 if the order is \$75+, \$17.15 if the order is \$150 or more) shipping and handling or credit card information. CA, IL, NJ, PA, and TX residents must add sales tax on books and shipping total. Prices subject to change without notice.

Thank you for your order!

$$\int \sqrt{u^2 \pm a^2} \cdot du = \frac{1}{2} \left[u \sqrt{u^2 \pm a^2} \pm a^2 \log \left(u + \sqrt{u^2 \pm a^2} \right) \right]$$

Volume 2 presents the industry standards and practices for reservoir engineering and production engineering. This second volume also looks at all aspects of petroleum economics and shows how to estimate oil and gas reserves.



Gulf Professional Publishing
an imprint of Butterworth-Heinemann

